

Rida T. Farouki

Pythagorean-Hodograph Curves

Algebra and Geometry Inseparable

Geometry and Computing

Series Editors

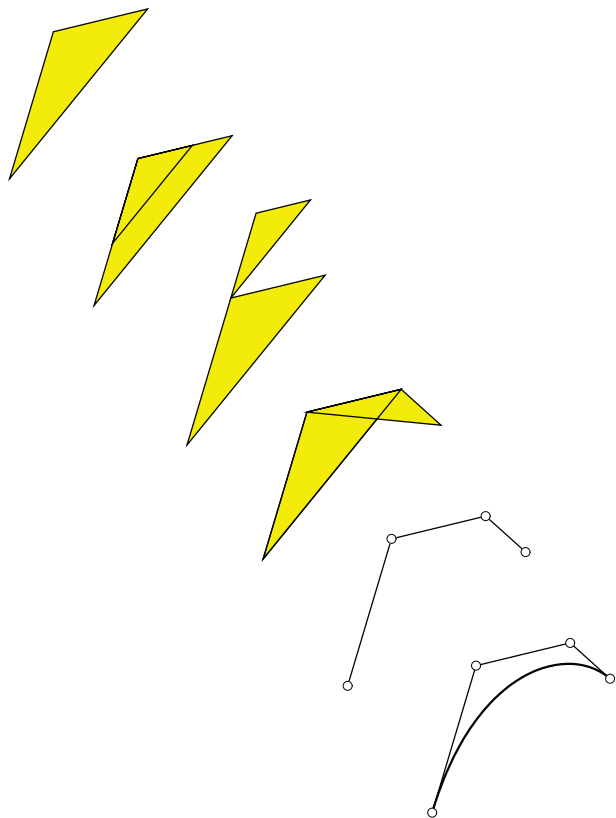
Herbert Edelsbrunner

Leif Kobbelt

Konrad Polthier

There is no excellent beauty that hath not
some strangeness in the proportion.

Francis Bacon (1561–1626)



Rida T. Farouki

Pythagorean-Hodograph Curves: Algebra and Geometry Inseparable

With 204 Figures and 15 Tables



Springer

Rida T. Farouki

Department of Mechanical and Aeronautical Engineering
University of California
Davis, CA 95616, USA
farouki@ucdavis.edu

Library of Congress Control Number: 2007932296

Mathematics Subject Classification: 51N20, 53A04, 65D17, 68U07

ISBN 978-3-540-73397-3 Springer Berlin Heidelberg New York

This work is subject to copyright. All rights are reserved, whether the whole or part of the material is concerned, specifically the rights of translation, reprinting, reuse of illustrations, recitation, broadcasting, reproduction on microfilm or in any other way, and storage in data banks. Duplication of this publication or parts thereof is permitted only under the provisions of the German Copyright Law of September 9, 1965, in its current version, and permission for use must always be obtained from Springer. Violations are liable for prosecution under the German Copyright Law.

Springer is a part of Springer Science+Business Media
springer.com
© Springer-Verlag Berlin Heidelberg 2008

The use of general descriptive names, registered names, trademarks, etc. in this publication does not imply, even in the absence of a specific statement, that such names are exempt from the relevant protective laws and regulations and therefore free for general use.

Typesetting by the author and SPi using a Springer L^AT_EX macro package

Printed on acid-free paper SPIN: 12081448 46/SPi/3100 5 4 3 2 1 0

Preface

Pythagorean-hodograph curves are characterized by the special property that their “parametric speed” — i.e., the derivative of the arc length with respect to the curve parameter — is a polynomial (or rational) function of the parameter. This distinctive attribute, achieved by *a priori* construction of the hodograph (derivative) components of polynomial or rational curves in \mathbb{R}^n as elements of *Pythagorean $(n+1)$ -tuples*, endows the Pythagorean–hodograph (PH) curves with many computationally attractive features. For example, it is possible to compute their arc lengths, bending energies, and offset (parallel) curves in an essentially exact manner, without recourse to approximations; and they are exceptionally well-suited to problems of real-time motion control and spatial path planning based on the use of rotation-minimizing frames.

This study surveys and assesses the considerable body of research on PH curves that has accumulated since their inception in 1990. As indicated by the Contents, this research spans a spectrum of topics ranging from elucidation of the basic mathematical theory of PH curves, through development of practical algorithms for their construction and analysis, to the demonstration of their use in computer-aided design and manufacturing applications.

In contrast to the traditional (Bézier/B-spline) schemes of computer-aided geometric design, the PH curves require models that are inherently *non-linear* in nature. However, by use of appropriate algebraic tools — *complex numbers* and *quaternions* for planar and spatial PH curves, and *Clifford algebra* for the most general setting — their construction and analysis is greatly facilitated. The investigation of PH curves thus offers an excellent context and motivation for exploring the pervasive ties between *algebra* and *geometry*.

For ease of access, the material has been organized into seven parts, each comprising a number of chapters. Parts I through III are expository in nature, and serve to establish the required mathematical background. The core theory of planar and spatial PH curves is then developed in Parts IV and V, while Parts VI and VII present practical details on their construction, analysis, and applications. A more detailed synopsis of contents may be found in Chapter 1.

It is inevitable that a study of this nature will lean toward greater emphasis on the author's own contributions, if only because they shape his perspective on the subject matter. Nevertheless, an effort has been made to summarize the key ideas (if not the technical details) of all the most significant developments in the field, and give pointers to many others. The subject matter originated in papers co-authored with Takis Sakkalis in 1990. Subsequently, the author has been fortunate to have the opportunity to pursue related research with many other distinguished colleagues — including Gudrun Albrecht, Hyeong In Choi, Paolo Costantini, Carlotta Giannelli, Chang Yong Han, Sung Chul Jee, Song Hwa Kwon, Jairam Manjunathaiah, Carla Manni, Hwan Pyo Moon, Andy Neff, Lyle Noakes, Francesca Pelosi, Christian Perwass, Jörg Peters, Helmut Pottmann, Kazuhiro Saitou, Lucia Sampoli, Thomas Sederberg, Alessandra Sestini, and Tait Smith, and also a number of graduate students (Mohammad al-Kandari, Bryan Feldman, Bethany Kuspa, David Nicholas, Sagar Shah, Sebastian Timar, Yi-Feng Tsai, and Guo-Feng Yuan). Much of the material presented in Parts IV through VII is a direct outcome of these enlightening, fruitful, and always enjoyable collaborations.

The author is grateful for financial support from a number of NSF grants (CCR-0202179, DMS-0138411, CCR-9902669, DMI-9908525, CCR-9530741) that have been directly or indirectly related to the subject matter of this book. Thanks are also due to a number of experts, whose suggestions have greatly improved portions of the book: Eleanor Robson, of the Department of History and Philosophy of Science, Cambridge University, and Colin Wakefield of the Bodleian Library, Oxford University (Chapter 2), and Peter Plaßmeyer, of the Mathematisch–Physikalischer Salon, Staatliche Kunstsammlungen Dresden — Chapter 18. Finally, the patience and encouragement of Martin Peters and Ute McCrory of Springer–Verlag helped guide this project to a conclusion.

Since a perusal of the Table of Contents may leave the reader wondering as to whether this volume was intended as a textbook, research monograph, or historical treatise, some explanatory remarks are perhaps in order. There was, in fact, no conscious intent to aim for any of these — but what has transpired seems, in part, each of them. In the pursuit of research and scholarly endeavor, there is nothing remiss in simply pursuing one's intuition — on the contrary, this often proves the most enjoyable and rewarding *modus operandi*.

Davis, California, June 2007

Rida T. Farouki

*Some books are to be tasted, others to be swallowed,
and some few are to be chewed and digested; that is
some books are to be read only in parts; others to be
read but not curiously; and some few to be read wholly,
and with diligence and attention. Some books also may
be read by deputy, and extracts of them made by others.*

Francis Bacon (1561–1626)

Contents

1	Introduction	1
1.1	The Lure of Analytic Geometry	1
1.2	Symbiosis of Algebra and Geometry	3
1.3	Computer-aided Geometric Design	4
1.4	Pythagorean-hodograph Curves	6
1.5	Algorithms and Applications	7

Part I Algebra

2	Preamble	11
2.1	A Historical Enigma	11
2.2	Theorem of Pythagoras	17
2.3	Al-Jabr wa'l-Muqabala	22
2.4	Fields, Rings, and Groups	25
3	Polynomials	29
3.1	Basic Properties	29
3.2	Polynomial Bases	31
3.3	Roots of Polynomials	36
3.4	Resultants and Discriminants	38
3.5	Rational Functions	41
4	Complex Numbers	45
4.1	Caspar Wessel	45
4.2	Elementary Properties	48
4.3	Functions of Complex Variables	49
4.4	Differentiation and Integration	51
4.5	Geometry of Conformal Maps	54
4.6	Harmonic Functions	56

VIII Contents

4.7	Conformal Transplants	56
4.8	Some Simple Mappings	58
5	Quaternions	61
5.1	Multi-dimensional Numbers	61
5.2	No Three-dimensional Numbers	64
5.3	Sums and Products of Quaternions	64
5.4	Quaternions and Spatial Rotations	67
5.5	Rotations as Products of Reflections	69
5.6	Families of Spatial Rotations	70
5.7	Four-dimensional Rotations	74
6	Clifford Algebra	79
6.1	Clifford Algebra Bases	79
6.2	Algebra of Multivectors	80
6.3	The Geometric Product	82
6.4	Reflections and Rotations	85

Part II Geometry

7	Coordinate Systems	89
7.1	Cartesian Coordinates	91
7.2	Barycentric Coordinates	93
7.2.1	Barycentric Coordinates on Intervals	94
7.2.2	Barycentric Coordinates on Triangles	95
7.2.3	Transformation of the Domain	98
7.2.4	Barycentric Points and Vectors	98
7.2.5	Directional Derivatives	100
7.2.6	Polynomial Bases Over Triangles	101
7.2.7	Un-normalized Barycentric Coordinates	102
7.2.8	Three or More Dimensions	103
7.3	Curvilinear Coordinates	104
7.3.1	One-to-one Correspondence	105
7.3.2	Distance and Angle Measurements	106
7.3.3	Jacobian of the Transformation	109
7.3.4	Example: Plane Polar Coordinates	110
7.3.5	Three or More Dimensions	111
7.4	Homogeneous Coordinates	112
7.4.1	The Projective Plane	113
7.4.2	Circular Points and Isotropic Lines	114
7.4.3	The Principle of Duality	116
7.4.4	Projective Transformations	118
7.4.5	Invariance of the Cross Ratio	122
7.4.6	Geometrical Figures and their Shadows	123
7.4.7	Projective Geometry of Three Dimensions	127

8 Differential Geometry	131
8.1 Intrinsic Geometry of Plane Curves	133
8.1.1 Tangent and Curvature	133
8.1.2 The Circle of Curvature	135
8.1.3 Vertices of Plane Curves	137
8.1.4 The Intrinsic Equation	137
8.2 Families of Plane Curves	138
8.2.1 Envelopes of Curve Families	139
8.2.2 Families of Implicit Curves	140
8.2.3 Families of Parametric Curves	142
8.2.4 Families of Lines and Circles	144
8.3 Evolutes, Involutes, Parallel Curves	144
8.3.1 Tangent Line and Osculating Circle.....	144
8.3.2 Evolutes and Involutes	146
8.3.3 The <i>Horologium Oscillatorium</i>	154
8.3.4 Families of Parallel (Offset) Curves	161
8.3.5 Trimming the Untrimmed Offset	167
8.4 Intrinsic Geometry of Space Curves	178
8.4.1 Curvature and Torsion	178
8.4.2 The Frenet Frame	180
8.4.3 Inflections of Space Curves	181
8.4.4 Intrinsic Equations	181
8.5 Intrinsic Geometry of Surfaces	183
8.5.1 First Fundamental Form	183
8.5.2 Second Fundamental Form	184
8.5.3 Curves Lying on a Surface	185
8.5.4 Normal Curvature of a Surface	186
8.5.5 Principal Curvatures and Directions	186
8.5.6 Local Surface Shape	188
8.5.7 Gauss Map of a Surface	190
8.5.8 Lines of Curvature.....	191
8.5.9 Geodesics on a Surface	193
9 Algebraic Geometry	197
9.1 Parametric and Implicit Forms	198
9.2 Plane Algebraic Curves	199
9.2.1 Singular Points.....	201
9.2.2 Intersections with a Straight Line	202
9.2.3 Double Points of Algebraic Curves.....	202
9.2.4 Higher-order Singular Points	204
9.2.5 Genus of an Algebraic Curve.....	204
9.2.6 Resolution of Singularities	208
9.2.7 Birational Transformations	211
9.2.8 Plücker Relations.....	212

9.2.9	Bézout's Theorem	214
9.2.10	Implicitization and Parameterization	216
9.3	Algebraic Surfaces	219
9.3.1	Singular Points and Curves	220
9.3.2	Rationality of Algebraic Surfaces	221
9.4	Algebraic Space Curves	222
9.4.1	Composite Surface Intersections	223
9.4.2	Plane Projections of a Space Curve	226
9.4.3	Genus of an Algebraic Space Curve	227
9.4.4	Singularities of Space Curves	228
10	Non-Euclidean Geometry	231
10.1	The Metric Tensor	232
10.2	Contravariant and Covariant Vectors	233
10.3	Methods of Tensor Algebra	235
10.4	The Geodesic Equations	240
10.5	Differentiation of Tensors	241
10.6	Parallel Transport of Vectors	243

Part III Computer Aided Geometric Design

11	The Bernstein Basis	249
11.1	Theorem of Weierstrass	250
11.2	Bernstein-form Properties	252
11.3	The Control Polygon	254
11.4	Transformation of Domain	254
11.5	Degree Operations	255
11.6	de Casteljau Algorithm	256
11.7	Arithmetic Operations	258
11.8	Computing Roots on $(0, 1)$	259
11.9	Numerical Condition	260
12	Numerical Stability	261
12.1	License to Compute	261
12.2	Characterization of Errors	262
12.3	Floating-point Computations	263
12.3.1	Floating-point Numbers	264
12.3.2	Floating-point Arithmetic	266
12.3.3	Dangers of Digit Cancellation	267
12.3.4	Models for Error Propagation	270
12.4	Stability and Condition Numbers	271
12.4.1	Condition of a Polynomial Value	272
12.4.2	Condition of a Polynomial Root	275
12.4.3	Wilkinson's Polynomial	277

12.4.4	Vector and Matrix Norms	281
12.4.5	Condition of a Linear Map	285
12.4.6	Basis Transformations	287
12.4.7	Subdivision Processes	289
12.4.8	Ill-posed Problems	289
12.5	Backward Error Analysis	290
12.5.1	Equivalent Input Errors	290
12.5.2	Example: Horner's Method	291
13	Bézier Curves and Surfaces	295
13.1	Convex-hull Confinement	296
13.2	Variation-diminishing Property	298
13.3	Degree Elevation	298
13.4	de Casteljau Algorithm	300
13.5	Bézier Curve Hodographs	301
13.6	Rational Bézier Curves	303
13.7	Conics as Bézier Curves	309
13.8	Tensor-product Surface Patches	312
13.9	Triangular Surface Patches	320
14	C^2 Cubic Spline Curves	323
14.1	Mechanical Splines	324
14.2	Elastic Bending Energy	325
14.3	Polynomial Interpolation	326
14.3.1	The Lagrange Basis	326
14.3.2	Convergence Behavior	327
14.4	C^2 Cubic Spline Functions	328
14.4.1	Cubic Hermite Form	328
14.4.2	C^2 Continuity Equations	329
14.4.3	Choice of End Conditions	330
14.4.4	Solution of Tridiagonal Systems	332
14.4.5	Minimum Energy Property	333
14.4.6	Spline Approximation Convergence	336
14.5	C^2 Cubic Spline Curves	336
14.5.1	Choice of Knot Sequence	337
14.5.2	Parametric or Geometric Continuity	338
14.5.3	Geometric Hermite Interpolation	339
14.5.4	Elastica or "Non-linear" Splines	341
15	Spline Basis Functions	345
15.1	Bases for Spline Functions	345
15.2	The Cardinal Basis	346
15.2.1	Construction of Cardinal Basis	346
15.2.2	Bivariate Spline Functions	348
15.2.3	Tensor-product Spline Surfaces	351

15.3	The B-spline Basis	353
15.3.1	The Knot Vector	356
15.3.2	Cox–de Boor Algorithm	361
15.3.3	Tensor–product B-spline Surfaces	361
15.3.4	Rational B-spline Curves and Surfaces	362
15.3.5	Bézier and B-spline Forms Compared	362
15.4	Spline Basis Conversion	364
15.4.1	Cardinal to B-spline Form	364
15.4.2	Basis Conversion Matrix	365

Part IV Planar Pythagorean–hodograph Curves

16	Arc-length Parameterization	369
16.1	In Search of an Elusive Ideal	370
16.2	The Rectification of Curves	374
16.3	Polynomial Parametric Speed	377
16.4	Algebraically–rectifiable Curves	378
16.5	Unit Speed Approximations	379
17	Pythagorean–hodograph Curves	381
17.1	Planar Pythagorean Hodographs	381
17.2	Bézier Control Points of PH Curves	384
17.3	Parametric Speed and Arc Length	386
17.4	Differential and Integral Properties	388
17.5	Rational Offsets of PH Curves	389
18	Tschirnhausen’s Cubic	393
18.1	Ehrenfried Walther von Tschirnhaus	393
18.2	Tschirnhaus and Caustic Curves	396
18.3	Unique Pythagorean–hodograph Cubic	400
18.4	You Mean we Pay you to do <i>That!</i> ?	404
19	Complex Representation	407
19.1	Complex Curves and Hodographs	408
19.2	One-to-one Correspondence	409
19.3	Rotation Invariance of Hodographs	414
19.4	Pythagorean–hodograph Cubics Revisited	414
19.5	Characterization of the PH Quintics	415
19.6	Geometry of the Control Polygon	419
19.7	Intrinsic Features of Corresponding Curves	422

20 Rational Pythagorean–hodograph Curves	427
20.1 Construction of Rational PH Curves	428
20.2 Dual Bézier Curve Representation	433
20.3 Relation to Polynomial PH Curves	437
20.4 Rational Arc Length Functions	438
20.5 Geometrical Optics Interpretation	439
20.6 Laguerre Geometry Formulation	444
20.7 Improper Rational Parameterizations	446
20.8 Rational Surfaces with Rational Offsets	449
20.9 Minkowski Isoperimetric–hodograph Curves	451

Part V Spatial Pythagorean–hodograph Curves

21 Pythagorean Hodographs in \mathbb{R}^3	455
21.1 Geometry of Spatial PH Cubics	456
21.2 Spatial Pythagorean Hodographs	462
21.3 Bézier Control Polygons	464
21.4 Differential Properties	465
22 Quaternion Representation	469
22.1 Pythagorean Condition in \mathbb{R}^3	469
22.2 Degeneration of Spatial PH Curves	472
22.3 Rotation Invariance of Hodographs	476
22.4 Reflection Form of Hodographs	480
22.5 One-to-one Correspondence?	483
23 Helical Polynomial Curves	485
23.1 Helical Curves and PH Curves	486
23.2 Morphology of Helical PH Quintics	488
23.3 Monotone–helical PH Quintics	490
23.4 General Helical PH Quintics	492
23.5 Sufficient and Necessary Conditions	497
24 Minkowski Pythagorean Hodographs	507
24.1 The Minkowski Metric	508
24.2 Medial Axis Transform	510
24.3 Minkowski PH Curves in $\mathbb{R}^{2,1}$	512
24.4 Clifford Algebra Representation	515
24.5 MAT Approximation by MPH Curves	516
24.6 Generalization to the Space $\mathbb{R}^{3,1}$	519

Part VI Algorithms

25 Planar Hermite Interpolants	523
25.1 Hermite Interpolation Problem	524
25.2 Solution in Complex Representation	527
25.3 The Absolute Rotation Index	531
25.4 Comparison with “Ordinary” Cubics	535
25.5 Higher-order Hermite Interpolants	537
25.6 Monotone Curvature Segments	539
26 Elastic Bending Energy	543
26.1 Complex Form of the Integrand	544
26.2 Energy of Tschirnhaus Segments	545
26.3 Bending Energy of PH Quintics	546
26.4 The “Gracefulness” of PH Quintics	550
26.5 Minimal-energy Hermite Interpolants	552
27 Planar C^2 PH Quintic Splines	555
27.1 Construction of PH Splines	555
27.1.1 C^2 PH Quintic Spline Equations	556
27.1.2 End Conditions for PH Splines	558
27.1.3 Number of Distinct Interpolants	560
27.2 Solution by Homotopy Method	561
27.2.1 Choice of Initial System	561
27.2.2 Predictor–corrector Procedure	562
27.2.3 Empirical Results and Examples	565
27.3 Solution by Iterative Methods	572
27.3.1 Choice of Starting Approximation	572
27.3.2 Functional Iteration and Relaxation	574
27.3.3 Newton–Raphson Method	576
27.3.4 Computed Examples	579
27.4 Generalizations of PH Splines	582
27.4.1 Non-uniform Knot Sequences	582
27.4.2 Shape-preserving PH Splines	586
27.5 Control Polygons for PH Splines	587
27.5.1 Equivalent Interpolation Problem	588
27.5.2 Inclusion of Multiple Knots	589
27.5.3 Emulating B-spline Curve Properties	590
27.5.4 Illustrative Examples	591
28 Spatial Hermite Interpolants	595
28.1 G^1 Interpolation by Cubics	595
28.2 C^1 Hermite Interpolation Problem	596
28.3 Rotation Invariance of Interpolants	598
28.4 Residual Degrees of Freedom	600

28.5 Integral Measures of Shape	600
28.6 Clifford Algebra Formulation.....	604
28.7 Helical PH Quintic Interpolants	605
28.8 Higher-order Hermite Interpolants.....	613
28.9 Spatial C^2 PH Quintic Splines	613

Part VII Applications

29 Real-time CNC Interpolators.....	619
29.1 Digital Motion Control	619
29.2 Taylor Series Interpolators	621
29.3 PH Curve Interpolators	623
29.3.1 Constant Feedrate	624
29.3.2 Curvature-dependent Feedrate	625
29.3.3 Offset Curve Interpolator	626
29.4 Feedrate in Terms of Arc Length	627
29.4.1 Linear Dependence on Arc Length	628
29.4.2 Quadratic Dependence on Arc Length.....	628
29.5 Time-dependent Feedrate	630
29.5.1 Polynomial Time Dependence	631
29.5.2 Acceleration/Deceleration Profiles	632
29.5.3 Traversing a Single PH Curve	634
29.5.4 Experimental Results	635
29.6 Constant Material Removal Rate	642
29.6.1 Form of Feedrate Function.....	643
29.6.2 Interpolator Algorithm	644
29.6.3 Experimental Results	647
29.7 Contour Machining of Surfaces	651
29.7.1 Tool Path Generation	651
29.7.2 Optimal Contour Orientations	653
30 Rotation-minimizing Frames	661
30.1 Introduction and Motivation	661
30.2 Adapted Frames on Space Curves	664
30.3 Euler–Rodrigues Frame for PH Curves	666
30.4 Rotation-minimizing Frames	667
30.5 Energy of Framed Space Curves	668
30.6 Exact RMFs on PH Curves	670
30.6.1 Integration of Rational Functions.....	672
30.6.2 Frames for PH Cubics and Quintics	674
30.7 Rational RMF Approximations	677
30.7.1 Rational Hermite Interpolation.....	679
30.7.2 Computed Examples	685
30.8 Parameterization of Canal Surfaces	689

XVI Contents

31 Closure	693
References	697
Index	719

1

Introduction

As long as algebra and geometry were separated, their progress was slow and their uses limited; but once these sciences were united, they lent each other mutual support and advanced rapidly together towards perfection.

Joseph-Louis Lagrange (1736–1813)

1.1 The Lure of Analytic Geometry

The use of coordinates to describe and analyze geometrical configurations has undoubtedly been one of the most pervasive and productive developments in the entire history of mathematics, science, and engineering. This seminal idea — from which the field of *analytic geometry* arose — was first systematically expounded by René Descartes in his 1637 treatise *La Géométrie*. The immense appeal of analytic geometry derives from its intuitive visual aspect; from its remarkable success in applying algebra and analysis to geometrical problems; and from the ubiquity of such problems in science and technology.

In the relentless endeavor to further expand the frontiers of knowledge, a tendency to neglect (or take for granted) established or “traditional” subjects often arises. This is not so much an indication of their diminished importance, but rather of the pressures to “make room” for novel methods, theories, and perhaps even *fashions*. A related phenomenon is the tendency for a discipline, once regarded as an organic whole, to fragment under intensive investigation into specialized sub-disciplines that communicate only infrequently, if at all. Analytic geometry is a notable victim of these trends. Of course, they are not new — the poet Alexander Pope (1688–1744), a contemporary and erstwhile critic of Isaac Newton, lamented them eloquently in his *Essay on Man*:

Trace science then, with modesty thy guide;
First strip off all her equipage of pride,
Deduct what is but vanity, or dress,

Or learning's luxury, or idleness;
 Or tricks to show the stretch of human brain,
 Mere curious pleasure, or ingenious pain:
 Expunge the whole, or lop th'excrescent parts
 Of all, our vices have created arts:
 Then see how little the remaining sum,
 Which served the past, and must the times to come!

Fortunately, a counter-trend has begun to emerge in recent decades, motivated by the desire to employ digital computers for the construction, analysis, and display of geometrical configurations in fields such as *computational geometry*, *computer-aided design*, *computer graphics*, and *scientific visualization*.

Apart from their practical importance, the emergence of these disciplines is perhaps the expression of a latent desire to restore the foundations of analytic geometry as a subject in which *computation*¹ is the principal tool employed in geometrical deductions. Certainly, the efficiency, infallibility, and memory of computers, and their ability to organize complicated data, permit geometrical computations that would formerly have been deemed impossible. At the same time, efforts to implement basic geometrical functions of practical importance — such as surface intersections — highlight the inadequacy of existing theory as a basis for “robust” computations, and thus prompt new research.

This study is nominally concerned with a novel family of parametric curves — the *Pythagorean-hodograph curves* — that were introduced [186] to provide simple closed-form solutions to elementary computational problems, such as *arc length measurement* and *offset* (parallel) *curve* constructions. In fact, the key idea of constructing curves in \mathbb{R}^n from hodographs (derivatives) defined by *Pythagorean* $(n+1)$ -*tuples of polynomials* arose serendipitously in a different context: a proof that no curve, other than a straight line, can be parameterized by rational functions of its arc length [187]. Subsequent to these initial studies, it became increasingly apparent that the Pythagorean-hodograph (PH) curves also satisfy a useful converse purpose — the wealth of basic ideas from algebra and geometry that their investigation entails makes them a natural setting in which to survey these two fields, and their diverse connections.

For ease of assimilation and organizational convenience, the contents of this study are divided into seven principal parts, each comprising several chapters. Some effort was expended on molding each chapter into a reasonably brief and self-contained unit, with appropriate pointers to other chapters or published papers for further details. Essentially, Parts I through III furnish the requisite background in algebra, geometry, and computer aided geometric design; Parts IV and V elucidate the rather distinct theories of planar and spatial PH curves; and, finally, Parts VI and VII present the practical details of algorithms for their construction, analysis, and applications. But the reader must not expect

¹ As distinct from *synthetic* geometry, in which “ruler-and-compass” constructions (and their generalizations) predominate. A liberal interpretation of *computation* is imputed here — it might be symbolic, rather than numeric, in nature.

rigid adherence to such “jurisdictional” boundaries: some mingling of subject matter is inevitable, perhaps even desirable. Likewise, uniformity in the nature or difficulty of the subject matter was relinquished in favor of a frankly eclectic admixture of expository or tutorial material, historical or anecdotal interludes, and mathematical derivations, algorithm descriptions, and technical details of particular applications. It is hoped that this approach will render the material more palatable, and also highlight its interconnections, to a broader audience of potential readers (it certainly made the author’s task more enjoyable).

1.2 Symbiosis of Algebra and Geometry

To elucidate the basic theory of Pythagorean–hodograph curves, and develop algorithms that facilitate their use in various practical applications, we must deploy a remarkably diverse array of ideas and methods from the most ancient and fundamental of quantitative sciences, *algebra* and *geometry*. Whereas PH curve constructions are motivated by the practical requirements of “free–form” *geometric* design, it is the special *algebraic* structures they embody that endow them with uniquely advantageous computational properties.

A comprehensive review of the relevant ideas from algebra and geometry is provided in Parts I and II, respectively. While algebra is primarily concerned with finite computations on numeric or symbolic quantities, and geometry is basically the study of spatial relationships, the historical development of these disciplines has revealed a rich web of useful and insightful connections between them. Algebraic methods offer powerful tools for the quantitative specification and analysis of geometrical configurations. Conversely, geometrical models of increasingly abstract algebraic entities (complex numbers, quaternions, etc.) yield fruitful and intuitive perspectives on their “meaning” and manipulation. Thus, our philosophy here is to treat these pillars of mathematics as different facets of a single “grand scheme” — the sequestration of algebra and geometry into Parts I and II is nominal rather than categorical.

The survey of algebra in Part I begins with a review of the historical origins of key ideas for the theory of Pythagorean–hodograph curves (see Chap. 2), including the first known study of Pythagorean triples of integers, documented in Plimpton 322 (a cuneiform tablet from ancient Mesopotamia); the rigorous proof, attributed to the mystical Pythagorean school, that the sides a , b , c of all right triangles satisfy the celebrated relation $a^2 + b^2 = c^2$; the etymological origins of the terms *algebra* and *algorithm*, in the works of the medieval author Muhammad ibn Musa al–Khwarizmi of Baghdad; and finally the classification of algebraic systems as fields, rings, or groups (with many finer distinctions) in terms of the rules that govern combinations of their elements.

Since digital computers are only capable of finite sequences of arithmetic operations, computer descriptions of geometrical loci usually employ functions amenable to evaluation by such arithmetic sequences, namely, *polynomials* and *rational functions* (ratios of polynomials). Chap. 3 reviews basic properties

and algorithms for polynomials and rational functions — their representation in different bases, the computation of their roots, the elimination of variables between polynomial equations, the division of polynomials, greatest common divisors, and the partial fraction expansions of rational functions.

Chapters 4 and 5 review *complex numbers* and *quaternions*, which provide concise algebraic characterizations for the hodographs of planar and spatial PH curves, respectively. These hodograph formulations can be interpreted in terms of continuous families of scalings and rotations of vectors in \mathbb{R}^2 and \mathbb{R}^3 — with the non-commutative nature of the quaternion product reflecting the dependence of the final outcome of successive spatial rotations on the *order* in which they are performed. For involved calculations, such as the construction of PH spline curve interpolants, the complex number and quaternion models prove to be indispensable, and they offer new insights into the basic properties and capabilities of PH curves. Complex numbers and quaternions are examples of “higher-dimensional number systems” — namely, dimension 2 and 4. The most general framework for the study of higher-dimensional number systems, *Clifford algebra* (or *geometric algebra*), is reviewed in Chap. 6. This provides a means of categorizing the structure of Pythagorean hodographs in spaces of various dimensions, under both the Euclidean and Minkowski metrics.

The survey of geometry in Part II begins with a discussion of alternatives to the familiar Cartesian coordinates (see Chap. 7) — barycentric coordinates for the specification of position within a finite domain; curvilinear coordinates (mandatory in non-Euclidean spaces); and homogeneous coordinates, which provide a rigorous description of behavior “at infinity” and reveal the elegant *principal of duality* that characterizes projective geometry.

Chapters 8 and 9 provide, respectively, surveys of differential geometry and algebraic geometry. The former covers the intrinsic shape properties of plane curves, space curves, and surfaces, and also discusses families of plane curves and various “derived” curves: evolutes, involutes, and parallel (offset) curves. The latter discusses planar algebraic curves, algebraic surfaces, and algebraic space curves as point sets on which one or more polynomials in the Cartesian coordinate variables vanish. The singularities of these loci, and conditions for their irreducibility and rationality, are addressed. Finally, Chap. 10 provides a brief synopsis of some basic ideas from non-Euclidean geometry.

1.3 Computer-aided Geometric Design

The representation of *free-form* curves and surfaces — i.e., loci not describable in terms of “simple” geometrical parameters such as axes, centers, radii, etc. — is a core problem of computer-aided geometric design. In general, parametric rather than implicit curve and surface equations are preferred, and they must be of sufficiently simple functional form to yield efficient and robust algorithms for downstream applications, while providing the shape flexibility required to design complicated shapes such as ship hulls, turbine blades, and automobile

body parts. Such requirements have led to widespread adoption of (piecewise) *polynomial* and *rational* parametric curve and surface representations.

The manner in which the *degrees of freedom* associated with such forms are expressed is also an important issue — i.e., a *basis* that spans the space of the chosen functions must be specified. A suitable basis offers the design engineer a geometrically intuitive (and numerically stable) approach to specifying and manipulating curves and surfaces. These issues were independently addressed in the early 1960s by two French engineers working in the automotive industry: Paul de Faget de Casteljau of Citroën and Pierre Bézier of Renault.

They developed essentially equivalent schemes, that subsequently evolved into industry standards. Though not initially recognized as such, these curve and surface design schemes are intimately related to the elegant properties of a polynomial basis first introduced by S. N. Bernstein fifty years earlier, in a proof of the *Weierstrass approximation theorem*. For polynomials defined on a finite interval, the *Bernstein form* is superior in many respects to the *power* or “monomial” form. The Bernstein coefficients of a vector-valued polynomial define the *control points* of a parametric curve — they form the vertices of a polygon that is a “caricature” of the curve, embodying basic shape information and providing an intuitive means to interactively modify it.

Whereas Renault allowed Bézier considerable freedom to disseminate his work in conferences and publications [35–41], the ideas of de Casteljau were regarded as proprietary by Citroën, and hence they remained sequestered in unpublished Company reports [118] for two decades [119, 120]. Consequently, the Bernstein-form representation of parametric curves and surfaces is now named after Bézier, although the most fundamental algorithm associated with such representations (see §13.4) honors de Casteljau.

Part III reviews these basic ideas from computer-aided geometric design, and their extensions to *spline* curves and surfaces, to provide the context for the subsequent formulation of PH curves and splines. Chapter 11 describes the basic properties of polynomials in Bernstein form on the interval $[0, 1]$ while Chap. 12 extends this discussion to highlight the extraordinary stability of this representation. A comprehensive survey of the Bézier form of parametric curves and surfaces is then presented in Chap. 13.

Since individual curve segments or surface patches offer only limited shape flexibility, the preferred means of introducing further shape freedoms is by the use of piecewise-polynomial forms — i.e., *splines*. Chapter 14 summarizes the classical problem of smooth interpolation by C^2 cubic splines. In Chap. 15 the notion of *spline bases* (for a given sequence of knots and end conditions) is introduced, and is used to construct bivariate tensor-product spline bases. The B-spline basis — a fundamental concept in the theory of splines — is also defined, and is seen to be a natural generalization of the Bernstein polynomial basis on $[0, 1]$ when a partition of this domain is imposed. The basic properties of B-spline curves and surfaces are also summarized in this chapter.

1.4 Pythagorean–hodograph Curves

Parametric curves, which are essentially just vector-valued functions $\mathbf{r}(t)$ of a real variable or “parameter” t , are the preferred means of specifying planar or spatial loci in most practical applications. However, the practice of introducing a curve parameter is not without shortcomings. Although it plays a key role in allowing us to plot a curve, and analyze its intrinsic properties, the parameter is completely unrelated to the curve geometry — a defect apparent in the fact that there are *infinitely many* different parameterizations of a curve.

In differential geometry, a unique “natural” parameterization is identified — namely, that for which the parameter t coincides with *arc length* measured along the curve from a chosen initial point. Although this seems geometrically a natural and reasonable choice, it transpires algebraically to be an alarmingly *unnatural* circumstance. Our foray into the theory of PH curves commences in Chap. 16 by showing that, except in the trivial case of straight lines, planar or spatial curves can never have natural parameterizations that are *rational* (i.e., admit evaluation by a finite number of arithmetic operations).

The categorically negative nature of this result is mitigated by the fact that it suggests an alternative, more fruitful avenue of investigation — namely, the formulation of polynomial or rational curves whose *hodograph* (i.e., derivative) components satisfy a *Pythagorean condition* in \mathbb{R}^2 or \mathbb{R}^3 — from which arise many attractive and advantageous properties. Because of their rather different formulations, planar and spatial PH curves are treated separately in Parts IV and V, respectively. Chap. 17 is a gentle introduction to planar PH curves and their properties, using only real-variable methods, and in Chap. 18 we focus on the uniqueness of the planar PH cubic and its historical significance, concluding with a sociological interlude. It is possible to achieve much faster progress with the PH curves if we relinquish our attachment to real variables. Chapter 19 introduces a complex-variable model, in which planar curves are viewed as complex-valued functions of a real parameter: the PH property then arises through a simple squaring process. This model proves so propitious that it becomes the basis for all subsequent treatment of planar PH curves. Finally, Chap. 20 treats the generalization from polynomial to *rational* PH curves, and describes a remarkable connection to classical geometrical optics.

Upon proceeding to spatial PH curves in Part V, a new characterization of the Pythagorean condition for polynomial hodographs in \mathbb{R}^3 is required, and this is best characterized by means of a *quaternion* model — the counterpart of the complex-variable description of planar PH curves. Chapter 21 introduces spatial PH curves, and gives a complete analysis of the cubics purely in terms of their Bézier control polygons (this subsumes the characterization of planar PH cubics in Chap. 18). Chapter 22 treats the quaternion model for spatial PH curves in detail, and highlights its property of *invariance* under any spatial rotation. A special form of the spatial PH curves is addressed in Chap. 23 — namely, the *helical* PH curves (every helix with a polynomial parameterization is a PH curve). Finally, Part V concludes with a discussion of spatial PH curves

specified under the *Minkowski* (rather than Euclidean) metric in Chap. 24. This definition is motivated by the problem of reconstruction of the boundary of a planar domain from its *medial axis transform* (MAT). Specifying the MAT segments as *Minkowski PH* (MPH) *curves* permits an exact description of the domain boundary as a piecewise-rational curve.

1.5 Algorithms and Applications

In order to make the PH curves useful for practical applications, algorithms to construct or modify them in accordance with specified geometrical constraints are required. In Part VI we shall see that, because of the inherently non-linear dependence of PH curves on the coefficients of their defining polynomials, such algorithms incur systems of quadratic equations, and thus yield a multiplicity of formal solutions. Chapter 25 treats the problem of interpolating first-order Hermite data by planar PH quintics, using the complex-variable formulation. In general this yields four distinct solutions, and the *absolute rotation index* is introduced as a quantitative means for identifying the “good” interpolant among them. The evaluation of a further important shape measure for planar PH curves, the *bending energy* (i.e., the integral of the square of the curvature with respect to arc length) is then described in Chap. 26.

To obtain more shape flexibility than single PH quintic segments can offer, Chap. 27 introduces planar C^2 PH quintic spline curves. Like the system that governs “ordinary” C^2 cubic splines, the defining equations for PH splines involve only three consecutive variables — but the variables are *complex* rather than real, and the equations are *quadratic* rather than linear. Efficient schemes for numerical solution of the PH spline equations under various end conditions are proposed, and a control-polygon approach to designing PH splines is also described. Chapter 28 addresses the Hermite interpolation problem for spatial PH curves, using the quaternion model. This problem admits a *two-parameter family* of formal solutions, rather than a finite multiplicity, and the “optimal” choice of the free parameters remains an open problem. The generalization to spatial C^2 PH quintic splines is correspondingly a more challenging task, that is only briefly touched upon at the conclusion of Chap. 28.

Part VII brings the theory and algorithms for PH curves, developed thus far, to bear on selected practical applications. The focus is on a comprehensive treatment of two technical problems, rather than a superficial survey of many possible applications. Chapter 29 treats the problem of *real-time interpolator* algorithms for PH curves, a fundamental component of the motion controllers for computer numerical control (CNC) machines. Although more emphasis is given here to planar PH curves, the methods extend in a fairly straightforward manner to the spatial PH curves. The role of the interpolator algorithm is to compute a stream of reference points, one per sampling interval (~ 0.001 sec.), from the commanded path geometry and speed variation, for comparison with

actual machine positions as measured by encoders on its axes. This is a task for which the PH curves transpire to be eminently well-suited.

Chapter 30 describes an application for spatial PH curves — namely, the computation of *rotation-minimizing frames* (RMFs), which are advantageous in prescribing a “natural” variation of the orientation for a rigid body, as its center of mass executes a given spatial trajectory. Such frames are used in, for example, animation, robot path planning, and swept surface constructions. Algorithms for computing both exact RMFs on spatial PH curves (which incur transcendental terms), and rational RMF approximations, are developed.

Finally, Chap. 31 gives an assessment of the current state of development of PH curve theory and algorithms, identifies some important open problems that deserve further attention, and suggests possibilities for new applications.

Preamble

I was unable to devote myself to the learning of this al-jabr and the continued concentration upon it, because of obstacles in the vagaries of Time which hindered me; for we have been deprived of all the people of knowledge save for a group, small in number, with many troubles, whose concern in life is to snatch the opportunity, when Time is asleep, to devote themselves meanwhile to the investigation and perfection of a science; for the majority of people who imitate philosophers confuse the true with the false, and they do nothing but deceive and pretend knowledge, and they do not use what they know of the sciences except for base and material purposes; and if they see a certain person seeking for the right and preferring the truth, doing his best to refute the false and untrue and leaving aside hypocrisy and deceit, they make a fool of him and mock him.

Omar Khayyam,
Risala fi'l-barahin 'ala masa'il al-jabr wa'l-muqabala

2.1 A Historical Enigma

Figure 2.1 shows cuneiform tablet no. 322 in the Plimpton Collection of the Rare Book and Manuscript Library at Columbia University. This compilation of sexagesimal (base 60) numbers¹ is believed to originate from the ancient Mesopotamian city Larsa (Tell Senkereh in modern Iraq) and has been dated to the period 1820–1762 BC. It was discovered in the 1920s and acquired in a market by the antiquities dealer Edgar A. Banks, who then sold it for \$10 to George A. Plimpton, a New York publisher and a collector of mathematical artifacts. Plimpton bequeathed his entire collection to Columbia University in 1936, but the significance of the tablet was not fully appreciated until a

¹ Our modern use of *minutes* and *seconds* as measures of time and angle can be traced back to the Mesopotamian sexagesimal number system.



Fig. 2.1. Plimpton 322, the “Pythagorean triples” cuneiform tablet from the ancient city of Larsa in Mesopotamia (~1820–1762 BC). Reproduced with permission from the Plimpton Collection, Rare Book and Manuscript Library, Columbia University.

thorough transcription and analysis of its contents was published [344] in 1945 by Otto Neugebauer and Abraham Sachs at Brown University.

Of all existing cuneiform mathematical tablets, Plimpton 322 has been the subject of the most intense scholarly research [65, 66, 72, 128, 205, 344, 377, 378, 393]. While its numerical content (and even the correction of calculation and transcription errors therein) is no longer in doubt, the interpretation of its mathematical significance and its “purpose” are still the subject of lively debate and reassessment, some 60 years after its initial decipherment.

The tablet measures approximately $5 \times 3\frac{1}{2}$ inches, but is incomplete — a portion has broken off at the left edge, while parts of the available fragment are damaged and hence illegible. Traces of modern glue have been identified along the broken edge, suggesting that the tablet may have been broken after its modern discovery. The available portion, though incomplete, nevertheless reveals a profound degree of numeracy and algebraic sophistication.

The fragment lists fifteen rows of sexagesimal numbers arranged in four columns, with the last column being simply a counter for the rows. A clearer impression may be gained from the drawing by Eleanor Robson [377] shown in Fig. 2.2. Table 2.1 presents a transcription of Plimpton 322 in modern Indo-Arabic numerals [343], with commas employed to separate the coefficients for successive powers of 60. In the second and third columns, it is assumed that the right-most entries are the coefficients of unity — for example, the quantity 3,31,49 in the fourth row, second column is interpreted as

$$3 \times (60)^2 + 31 \times 60 + 49,$$

or 12,709 in familiar decimal notation. However, the quantities in the first column apparently all begin with 1, suggesting a different interpretation with



Fig. 2.2. A scale drawing by Eleanor Robson, clarifying the cuneiform sexagesimal numbers tabulated in Plimpton 322 — reproduced with permission from [377].

Table 2.1. Left: the transcription of Plimpton 322 by Neugebauer and Sachs [344], including interpolated missing or corrected values in square brackets. Right: deduced integers p and q that generate the values in the four columns of Plimpton 322.

$f = [(p^2 + q^2)/2pq]^2$	$a = p^2 - q^2$	$c = p^2 + q^2$	#	p	q
[1;59,0.]15	1,59	2,49	1	12	5
[1;56,56.]58,14,50,6,15	56,7	1,20,25	2	1,4	27
[1;55,7.]41,15,33,45	1,16,41	1,50,49	3	1,15	32
[1;]5[3,1]0,29,32,52,16	3,31,49	5,9,1	4	2,5	54
[1;]48,54,1,40	1,5	1,37	5	9	4
[1;]47,6,41,40	5,19	8,1	6	20	9
[1;]43,11,56,28,26,40	38,11	59,1	7	54	25
[1;]41,33,59,3,45	13,19	20,49	8	32	15
[1;]38,33,36,36	8,1	12,49	9	25	12
1;35,10,2,28,27,24,26,40	1,22,41	2,16,1	10	1,21	40
1;33,45	45,0	1,15,0	11	1,0	30
1;29,21,54,2,15	27,59	48,49	12	48	25
[1;]27,0,3,45	2,41	4,49	13	15	8
1;25,48,51,35,6,40	29,31	53,49	14	50	27
[1;]23,13,46,40	56	1,46	15	9	5

the left-most entries as the coefficients of unity.² The quantity 1;48,54,1,40 in the fifth row, first column is thus interpreted as

² Mesopotamian numbers do not use a “sexagesimal point” to separate whole and fractional parts, and are thus indeterminate by a power of 60 (although this is often resolved by the context). Following Robson [377] we employ semi-colons to denote the putative position of such points.

$$1 + \frac{48}{60} + \frac{54}{(60)^2} + \frac{1}{(60)^3} + \frac{40}{(60)^4}.$$

The parentheses [] in Table 2.1 indicate illegible entries that were “restored” by Neugebauer and Sachs, who also corrected several apparent transcription or calculation errors (where the listed values are inconsistent with the overall structure apparent in the tabulation).

From a modern viewpoint, this structure is that the first three columns can be generated from appropriately-selected integers p and q by the expressions

$$f = \left[\frac{p^2 + q^2}{2pq} \right]^2, \quad a = p^2 - q^2, \quad c = p^2 + q^2. \quad (2.1)$$

Deduced values for p and q are appended on the right in Table 2.1, where it can be seen that $1 < q < 60$, $q < p$, and the ratio p/q is steadily decreasing — which also implies that the first-column entries steadily decrease. The column headings in Table 2.1 are repeated here from (2.1) for convenience, and are *not* transcriptions from the original tablet — it must be emphasized that the manipulation of symbolic notations in mathematics was not widely practiced prior to the Renaissance, and was certainly unknown in ancient Mesopotamia.

Neugebauer [343] observed that the values in columns two and three, and also the denominators of the squares of the rational numbers in column one, are intimately connected to a well-known procedure from number theory that generates *Pythagorean triples* of integers (a, b, c) satisfying

$$a^2 + b^2 = c^2, \quad (2.2)$$

where a, b, c denote the three sides of a right triangle (see Fig. 2.3). Namely, when p and q range over all pairs of positive integers such that: (i) $q < p$; (ii) p and q are not both odd; and (iii) p and q have no common factor other than 1; then the expressions

$$a = p^2 - q^2, \quad b = 2pq, \quad c = p^2 + q^2 \quad (2.3)$$

yield *all* primitive integer solutions to (2.2) without repetition (a “primitive” triple is one in which a, b, c have no common factor other than 1 — i.e., we exclude solutions that are merely of the form $(a', b', c') = (ka, kb, kc)$ where (a, b, c) is an integer solution and k is an integer greater than 1).

Mathematicians who have studied Plimpton 322 were tempted to regard it as an exercise in number theory, in which their Mesopotamian predecessors were engaged in computing Pythagorean triples by means of the generating functions (2.3) — or alternatively as a trigonometric table, since the entries in the first column amount to $\sec^2 \theta$ (where θ is the angle between the triangle

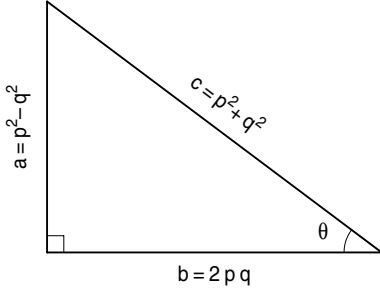


Fig. 2.3. Right triangle with integer sides generated by expressions (2.3).

sides b and c , as in Fig. 2.3) and the resulting θ values decrease in an orderly progression from just under 45° to just over 30° .

However, Robson [377, 378] argues convincingly that such “internalized” mathematical interpretations are unduly colored by the modern perspectives of their authors, and do not adequately take account of the historical, cultural, and linguistic milieu of the tablet’s creation. For example, the theory that the Pythagorean generating functions (2.3) were *directly* employed in calculating the column entries contradicts the typical orderly left-to-right calculational progression seen on contemporaneous tablets: one would expect each line to begin explicitly with p and q , and proceed to subsequent derived quantities towards the right. Similarly, a trigonometric reading contradicts the absence of a well-developed notion of angle measure in Mesopotamian mathematics. Robson illustrates this by contrasting the Mesopotamian perspective on the area of a circle with the modern view. The modern formula $A = \pi r^2$ derives from the genesis of a circle by the angular rotation of a vector of length r , the radius. In Mesopotamian thought, however, the circumference C (which we know to be $C = 2\pi r$) is predominant: they expressed the area as $A = C^2/4\pi$ — with, of course, an approximate π value — i.e., they conceived of the circle as the locus of given length C that bounds a symmetric area.

The explication of the *purpose* of Plimpton 322 currently considered most likely [65, 66, 205, 377, 378, 393] is that it represents a “school text” employed to train scribes to perform computations concerned with reciprocal numbers. In Mesopotamian mathematics, the division p/q of two numbers p and q is accomplished by first computing the reciprocal $1/q$ of the denominator, and then multiplying it with the numerator p . The *regular* sexagesimal numbers — i.e., those whose reciprocals have finite sexagesimal expressions — are of particular importance in this regard (such numbers possess factorizations of the form $2^\alpha 3^\beta 5^\gamma$ for positive integers α, β, γ). Lists of regular reciprocal pairs are common among mathematical cuneiform tablets, and presumably served as aides to routine computations.

Now if p/q and q/p are a regular reciprocal pair (i.e., two numbers with finite sexagesimal representations whose product is unity), the Plimpton 322 entries can be readily computed from them using the formulae

$$f = \frac{1}{4} \left(\frac{p}{q} + \frac{q}{p} \right)^2, \quad a = pq \left(\frac{p}{q} - \frac{q}{p} \right), \quad c = pq \left(\frac{p}{q} + \frac{q}{p} \right). \quad (2.4)$$

Such numbers occur in the solution of an equation of the form

$$x = \frac{1}{x} + h \quad (2.5)$$

for a regular reciprocal pair, x and $1/x$, where the former exceeds the latter by some integer amount h . The motivation for this is a “cut-and-paste” geometry problem of the following form: given a rectangle of area $A = 1$ with sides x and $1/x$, the former exceeding the latter by h , we wish to determine x and $1/x$ from this data. We cut off a portion of width $\frac{1}{2}h$ along the side x of the rectangle, and affix it to the top to form an L shape, as shown in Fig. 2.4. The L shape is contained within a square of side $1/x + \frac{1}{2}h$, and its area $A = 1$ must equal the area of this square, minus the area of the smaller shaded square shown in Fig. 2.4, of side $\frac{1}{2}h$. Thus

$$1 = (1/x + \frac{1}{2}h)^2 - (\frac{1}{2}h)^2,$$

and multiplying both sides by x yields equation (2.5). Now writing $x = p/q$, the quantities $\frac{1}{2}h$ and $1/x + \frac{1}{2}h$ arising in this construction become

$$\frac{1}{2} \left(\frac{p}{q} - \frac{q}{p} \right) \quad \text{and} \quad \frac{1}{2} \left(\frac{p}{q} + \frac{q}{p} \right),$$

and if we scale them by $2pq$ to obtain integers, they agree precisely with the quantities a and c in (2.4), while the quantity f represents the (unscaled) area of the square that contains the L shape.

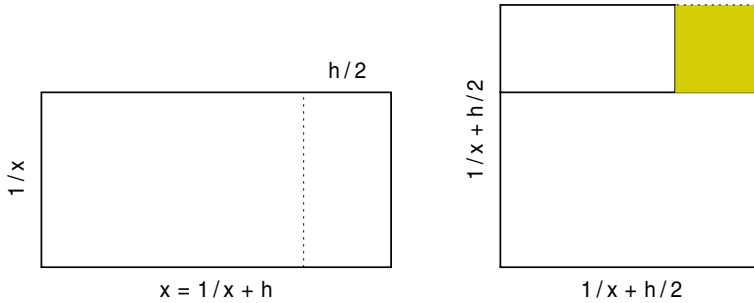


Fig. 2.4. Interpretation of Plimpton 322 in terms of a “cut-and-paste” geometry problem. Left: a rectangle of unit area with reciprocal sides, x and $1/x$, the former exceeding the latter by an integer amount h . Right: cutting off width $\frac{1}{2}h$ and placing it on top produces an L shape within a square of side $1/x + \frac{1}{2}h$. The area of this square minus that of the smaller shaded square, of side $\frac{1}{2}h$, must be equal to 1.

The interpretation of Plimpton 322 as a compilation of “cut-and-paste” geometry exercises involving regular reciprocal pairs is perhaps more mundane (but more credible) than “number theory” or “trigonometry” interpretations. Even as a humble pedagogical tool, however, it suggests at least an *implicit* familiarity with the concept of Pythagorean triples, and imparts respect for the thoroughness of Mesopotamian scribal training. A sense of the dedication and professional pride that Mesopotamian scribes possessed, as the vanguard of human literacy and numeracy, is apparent in the following passage from “In praise of the scribal art,” translated [417] by Åke W. Sjöberg:

*The scribal art is the mother of orators, the father of masters,
 The scribal art is delightful, it never satiates you,
 The scribal art is not (easily) learned, (but) he who has learned it
 need no longer be anxious about it,
 Strive to master the scribal art and it will enrich you,
 Be industrious in the scribal art
 and it will provide you with wealth and abundance,
 Do not be careless about the scribal art, do not neglect it ...*

2.2 Theorem of Pythagoras

Pythagoras of Samos (~580–500 BC) is credited with the famous theorem

$$a^2 + b^2 = c^2 \quad (2.6)$$

that relates the hypotenuse length c of a right triangle to the lengths a, b of the other sides. On account of its simplicity and profundity, and its archetypal role in the emerging concept of *proof*, this mathematical theorem has acquired the unusual distinction of universal recognition. However, modern scholarship — exemplified by the exhaustive treatise of W. Burkert [74] — has demolished the legendary and heroic stature of Pythagoras (concerning his mathematical achievements, at least). According to M. F. Burnyeat [76]:

It is hard to let go of Pythagoras. He has meant so much to so many for so long. I can with confidence say to readers of this essay: most of what you believe, or think you know, about Pythagoras is fiction, much of it deliberately contrived.

The “traditional lore” concerning Pythagoras goes as follows. He is thought to have travelled to Egypt and perhaps Mesopotamia, acquiring scientific and mathematical knowledge there before founding a secretive society called the “Pythagorean school” in Crotone on the south coast of modern Italy — part of *Magna Graecia* in the time of Pythagoras. The Pythagorean school’s secretive nature, and the fact that no contemporary biography of Pythagoras survives, have only served to enhance his legendary standing and near-apotheosis. The

followers of Pythagoras supposedly shunned individuality, and believed that the discovery and stewardship of knowledge should be a communal endeavor: it was their custom to credit all discoveries to their leader.

The Pythagorean school was ultimately destroyed in a political upheaval, possibly engendered by external suspicion of their secret and elitist practices. Pythagoras himself fled Crotone but was pursued and killed in Metapontum. The Pythagoreans left no written documents — what we know of their ideas and accomplishments comes from others. It is usually claimed, however, that they were the first intellectual society, pursuing philosophy and mathematics for their own sake,³ and as a medium for moral advancement. Their putative motto — *All is number* — expresses their faith in the unity of nature’s latent mathematical structure, with its diverse manifestations in musical harmony, the planetary motions, and other natural phenomena.⁴

The Pythagoreans pursued a fruitful mixture of algebra and geometry, in which the emphasis was on securing the certainty and universality of results by *rigorous proof*, based upon logical argument, rather than the case-by-case examples that characterized most prior mathematics. Although commonly attributed to Pythagoras, it has not been possible to establish with certainty that he was the first to prove the right-triangle theorem (2.6). The form of the proof is unknown, but is likely to have followed an intuitive geometrical argument, such as that suggested [61] in Fig. 2.5. Four copies of a right-triangle tile are positioned adjacent to each other, so the long side indicates the four compass directions — north, east, south, west. Adding a small square tile (shaded) in the center then yields the square on the hypotenuse. By a simple re-arrangement of these tiles, it is evident that the area of this square equals the areas of the squares on the long and short triangle sides.

The legend that Pythagoras sacrificed a hundred oxen for the Muses, to celebrate his proof of the theorem, is likely apocryphal in view of the strict vegetarianism of the Pythagorean school — motivated by their beliefs in the transmigration of souls and other mystical views. Having established the basic relation (2.6) that governs all right triangles, the Pythagoreans were naturally interested in examples for which it is satisfied by “whole numbers” (a, b, c) — i.e., in *Pythagorean triples of integers*. They were familiar with the simplest triple $(3, 4, 5)$ employed by the Egyptians in the construction of the pyramids, and probably many others transmitted from Mesopotamia or discovered by themselves. But they also devised a procedure to *construct* such triples, by inserting odd numbers m into the expressions

$$a = \frac{1}{2}(m^2 - 1), \quad b = m, \quad c = \frac{1}{2}(m^2 + 1).$$

³ Pythagoras himself supposedly coined the terms *philosophy* for “love of wisdom” and *mathematics* for “that which is learned” to describe the goals of his school.

⁴ In medieval times, the *quadrivium* or “four paths” (arithmetic, geometry, music, astronomy) complemented the *trivium* (grammar, dialectic, rhetoric) to form the *seven liberal arts*. Arithmetic was the study of *pure number*; geometry of *number in space*; music of *number in time*; and astronomy of *number in space and time*.

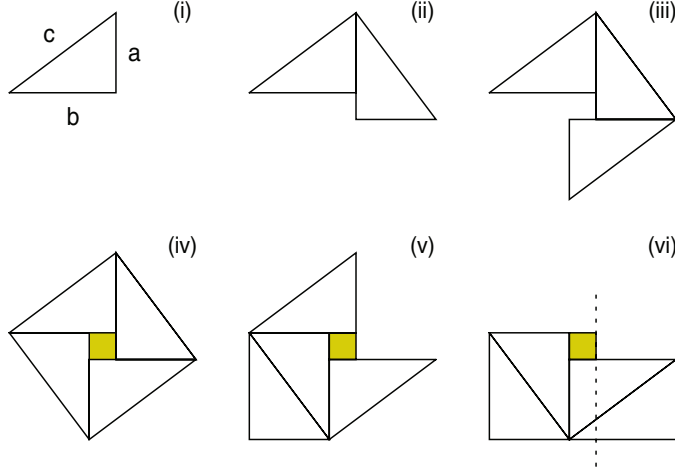


Fig. 2.5. By four-fold replication of the triangle in (i), and addition of the central shaded square of side $b - a$, we obtain the square of area c^2 on the hypotenuse in (iv). This can be re-arranged and divided, as indicated by the dashed line in (vi), into squares of areas a^2 and b^2 — hence, the Pythagorean theorem $a^2 + b^2 = c^2$.

This was subsequently generalized in Euclid's *Elements* — where it is shown that, for integers u and v , the formulae

$$a = u^2 - v^2, \quad b = 2uv, \quad c = u^2 + v^2 \quad (2.7)$$

yield all Pythagorean triples. If u, v have no common factor ($\gcd(u, v) = 1$), expressions (2.7) define a *primitive* Pythagorean triple in which a, b, c have no common factors. Of course, it is possible to generate other Pythagorean triples by simply multiplying expressions (2.7) by any integer $h > 1$.

But the Pythagorean theorem also proved to be a source of consternation to the Pythagoreans — a severe blow to their belief that *all is number* (where “number” connotes a *whole* number or, at most, a *ratio* of whole numbers). If we choose $a = b = 1$ in (2.6) the resulting value for c , which nowadays we denote by $\sqrt{2}$ and recognize to be irrational, is not a whole number nor a ratio p/q of whole numbers p, q . The Pythagoreans knew this, by one of the first recorded cases of “proof by contradiction” or *reductio ad absurdum*. The argument is as follows: suppose that $\sqrt{2} = p/q$, where p and q are integers with no common factors (and hence not both even). Then

$$p^2 = 2q^2, \quad (2.8)$$

so p^2 is even, and p must also be even, since only the squares of even numbers are even. Thus, $p = 2r$ for some integer r , and substituting into (2.8) gives

$$4r^2 = 2q^2 \quad \text{or} \quad q^2 = 2r^2.$$

So q^2 must be even, and q must also be even. The conclusion that p, q must both be even contradicts the supposition that $\sqrt{2} = p/q$, with p and q not both even, and hence this supposition must be false.

The discovery of “incommensurable” lengths in elementary geometrical configurations incurred a crisis of confidence for the Pythagorean school and subsequent Greek geometers. Their response was to retreat within the safety of intuitive geometrical constructions by straight-edge and compass, a strategy that allowed them to circumvent algebraic confrontations with values that are not exactly expressible as whole-number ratios. As with other mathematical stumbling blocks, the ultimate solution to this impasse was to regard it as an opportunity to define a richer and more general mathematical structure, the continuum of *real numbers*, based on experience in the natural world.

The significance of the Pythagorean theorem, which has been deemed the most fundamental result in all of mathematics, is that it lies at the foundation of *distance measurement*. The use of Cartesian coordinates (x, y) to describe the position of any point \mathbf{p} corresponds to specifying its distances from two orthogonal lines, the *coordinate axes*. The distance

$$d = \sqrt{(x_2 - x_1)^2 + (y_2 - y_1)^2}$$

between points (x_1, y_1) and (x_2, y_2) is then obtained by applying the theorem to a triangle with horizontal and vertical sides $x_2 - x_1$ and $y_2 - y_1$.

With the advent of calculus, it became possible to precisely define not only the straight-line distance between two points, but also the distance along a curved path, i.e., to *rectify*⁵ (compute the arc length of) curves. Applying the Pythagorean theorem to an infinitesimal segment $d\xi$ of a differentiable parametric curve $\mathbf{r}(\xi) = (x(\xi), y(\xi))$ allows us to express its arc length as

$$ds = \sqrt{x'^2(\xi) + y'^2(\xi)} d\xi,$$

and the total arc length S of a finite segment $\xi \in [a, b]$ is thus given by the integral

$$S = \int_a^b \sqrt{x'^2(\xi) + y'^2(\xi)} d\xi.$$

Under what circumstances can we consider this integral exactly computable? To obtain a closed-form reduction of the integral, the integrand must admit an indefinite integral — or “anti-derivative” — expressible in terms of known analytic functions, i.e., we must be able to identify a function $s(\xi)$ such that

$$\frac{d}{d\xi} s(\xi) = \sqrt{x'^2(\xi) + y'^2(\xi)}.$$

⁵ The term *rectification* connotes the “straightening out” a curve, as though it were a piece of string, so it can be compared with straight lines of known length.

It is instructive to consider a sequence of progressively more difficult cases:

- if $x(\xi), y(\xi)$ are linear polynomials — i.e., $\mathbf{r}(\xi)$ is a straight line — then $\sqrt{x'^2(\xi) + y'^2(\xi)}$ is a constant, and $s(\xi)$ is linear in ξ ;
- if $x(\xi) = r \cos \xi, y(\xi) = r \sin \xi$ — i.e., $\mathbf{r}(\xi)$ is a circle of radius r — then $\sqrt{x'^2(\xi) + y'^2(\xi)} = r$ and $s(\xi)$ is again linear in the angular variable ξ ;
- if $x(\xi), y(\xi)$ are quadratic, $\mathbf{r}(\xi)$ defines a parabola, and $\sqrt{x'^2(\xi) + y'^2(\xi)}$ is the square root of a quadratic in ξ — a closed-form expression for $s(\xi)$ involving a logarithmic terms is possible;
- when $x(\xi), y(\xi)$ are cubic, $\sqrt{x'^2(\xi) + y'^2(\xi)}$ is the square root of a quartic in ξ , and $s(\xi)$ can be expressed in terms of *incomplete elliptic integrals* — the same is true for the ellipse and hyperbola.

For higher degree curves, the arc length integral $s(\xi)$ does not, in general, admit a closed-form expression. Even in the cases where such an expression is possible, but involves transcendental functions, its cumbersome nature may compromise its practical value.⁶ However, the qualification *in general* suggests a possible means to ameliorate this problem: if the argument $x'^2(\xi) + y'^2(\xi)$ of the square root happens to be the *exact square* of some polynomial $\sigma(\xi)$ — i.e., $x'(\xi), y'(\xi), \sigma(\xi)$ constitute a *Pythagorean triple of polynomials* satisfying

$$x'^2(\xi) + y'^2(\xi) \equiv \sigma^2(\xi)$$

— then $s(\xi)$ is just the indefinite integral of the polynomial $\sigma(\xi)$, and is thus itself a polynomial (of degree one higher). To make this a viable scheme, we cannot depend on the Pythagorean nature of the triple $x'(\xi), y'(\xi), \sigma(\xi)$ to arise serendipitously — rather, we must ensure that we explicitly incorporate this structure into the polynomials $x'(\xi), y'(\xi)$ that represent the hodograph (derivative) components of a planar curve $\mathbf{r}(\xi) = (x(\xi), y(\xi))$.

Like the integers, polynomials with coefficients in any given field (e.g., the rational, real, or complex numbers) constitute a *unique factorization domain* (UFD). A UFD is, essentially, a set closed under addition or subtraction and (commutative) multiplication, whose members admit unique decompositions into products of *prime* or “irreducible” factors. In the case of integers, these factors are of course the prime numbers. In the case of degree- n polynomials, they are polynomials of degree $\leq n$ with coefficients in the prescribed field that admit no further reduction into products of lower-degree factors with coefficients in that field (we first factor out the highest-order coefficient, to obtain a *monic* polynomial whose irreducible factors are also monic).

Euclid’s characterization (2.7) of Pythagorean triples of *integers* may be generalized [292] to the members of *any* unique factorization domain. Thus, three polynomials $a(t), b(t), c(t)$ with coefficients in the field of real numbers and no non-constant common factors will satisfy the Pythagorean condition

$$a^2(t) + b^2(t) \equiv c^2(t)$$

⁶ See §16.2 for a historical perspective on the curve rectification problem.

if and only if they can be written in terms of two real polynomials $u(t)$, $v(t)$ in the form

$$a(t) = u^2(t) - v^2(t), \quad b(t) = 2u(t)v(t), \quad c(t) = u^2(t) + v^2(t).$$

Note that, for polynomials with real coefficients, the roles of $a(t)$ and $b(t)$ are essentially interchangeable since we can obtain the same triple from

$$a(t) = 2\tilde{u}(t)\tilde{v}(t), \quad b(t) = \tilde{u}^2(t) - \tilde{v}^2(t), \quad c(t) = \tilde{u}^2(t) + \tilde{v}^2(t),$$

where $\tilde{u}(t) = [u(t) + v(t)]/\sqrt{2}$ and $\tilde{v}(t) = [u(t) - v(t)]/\sqrt{2}$. By considering curves defined by hodographs (derivatives) defined in terms of relatively prime polynomials $u(t)$, $v(t)$ in the form

$$x'(t) = u^2(t) - v^2(t), \quad y'(t) = 2u(t)v(t)$$

we resolve the difficulty of rectification. For such *Pythagorean-hodograph* (PH) curves, the arc length can be exactly computed through just a few arithmetic operations on the curve coefficients, and we shall find that they possess many other interesting and useful attributes. For space curves, the three hodograph components $x'(t)$, $y'(t)$, $z'(t)$ must be specified in terms of *four* polynomials $u(t)$, $v(t)$, $p(t)$, $q(t)$ in order to satisfy a Pythagorean condition.

To facilitate their construction and analysis, it is advantageous to employ PH curve formulations based on appropriate algebras — the complex numbers and quaternions for planar and spatial PH curves, and Clifford algebra in an even broader setting — this is the motivation for our present survey of algebra. The treatment of PH curves begins in earnest in Part IV.

2.3 Al-Jabr wa'l-Muqabala

The etymological origins of the term *algebra*, as the descriptor of a particular style of mathematical methodology, can be traced to the *Kitab al-mukhtasar fi hisab al-jabr wa'l-muqabala* [273,380], a treatise in Arabic by the 9th-century Persian mathematician Muhammad ibn Musa al-Khwarizmi (or Muhammad, son of Moses, of Khwarizm). A copy of this manuscript, dated A. H. 743 (A. D. 1342), is housed in the Bodleian Library of Oxford University: see Fig. 2.6.

In rough translation, the phrase *al-jabr wa'l-muqabala* means “restoration and balancing” — in reference to the rearrangements of terms in an equation, so as to determine its solution.⁷ Khwarizmi’s book was translated into Latin in 1145 by the Englishman Robert of Chester, while living in Segovia (Spain), as the *Liber algebrae et almucabola* — hence the discipline *algebra*. The term

⁷ Another use of *algebra* was in the sense of “reunion of broken parts,” in reference to the surgical process of setting fractured bones. According to a 1565 quotation in the *Oxford English Dictionary*, “This Araby worde Algebra sygnifyeth as well fractures of bones, etc. as sometyme the restauration of the same.”



Fig. 2.6. Opening page (folio 1a) of MS. Huntington 214 in the Bodleian Library, University of Oxford — a compilation of mathematical treatises including the *Kitab al-mukhtasar fi hisab al-jabr wa'l-muqabala* by Muhammed ibn Musa al-Khwarizmi and several related works by other authors. Reproduced with permission.

algorithm, prevalent in modern computer science, arose from a corruption of al-Khwarizmi's name through the title of the translation⁸ of another treatise, dealing with the Hindu numeral system: the *Algoritmi de numero Indorum*.

Another famous medieval Persian algebraist (but more famous as a poet) was Omar Khayyam (1048–1131), or Ghiyath al-Din Abu'l-Fath Umar ibn Ibrahim al-Nisaburi al-Khayyami to be more precise, where the moniker al-Nisaburi identifies his place of origin as the town of Nishapur in Khurasan, and al-Khayyami reveals the family profession, namely, tent-makers. Among his diverse mathematical, astronomical, musical, and poetical writings is the *Risala fil-barahin 'ala masa'il al-jabr wa'l-muqabala* (or *Treatise on Proofs in Problems of Algebra*) written c. 1070 under, by his own account, difficult circumstances of political upheaval [274]. In it he proclaims

I say, with God's help and good guidance, that the art of al-jabr and al-muqabala is a mathematical art, whose subject is pure number and measurable quantities in as far as they are unknown, added to a known thing with the help of which they may be found; and that

⁸ Possibly by Adelard of Bath [75] c. 1130: the translation was discovered by Baron Baldassarre Boncompagni in Cambridge, and published in 1857 — see [420].

thing is either a quantity or a ratio, so that no other is like it, and the thing is revealed to you by thinking about it. And what is required in it are the coefficients which are attached to its subject-matter in the manner stated above. And the perfection of the art is knowing the mathematical methods by which one is led to the manner of extracting the numerical and mensurable unknowns.⁹

This has been regarded as one of the first definitions of *algebra*, as a clearly-identified and articulated field of mathematical study [478].

Among his diverse scientific accomplishments, Khayyam was engaged in a refinement of the calendar by measuring the length of the year in days to an accuracy of five decimal places (the true value actually varies in the sixth decimal place over a human lifespan), and he also developed methods to solve specific types of cubic equations “geometrically” in terms of the intersections of conic curves. For example, he solved cubics of the form

$$x^3 + a^2x = a^2b \quad \text{and} \quad x^3 + ax^2 = b^3 \quad (2.9)$$

in terms of the intersections of conics (see Fig. 2.7). In the former case, he drew the parabola $x^2 = ay$ and the circle $x^2 + y^2 - bx = 0$. If P is their point of intersection (other than the origin), and we drop a perpendicular from it to the point Q on the x -axis, the unique real root is given by OQ . In the latter case, he invoked the parabola $y^2 = b(x + a)$ and rectangular hyperbola $xy = b^2$. Dropping a perpendicular from P (their intersection point in the right half-plane) to Q on the x -axis, the desired positive root is OQ .

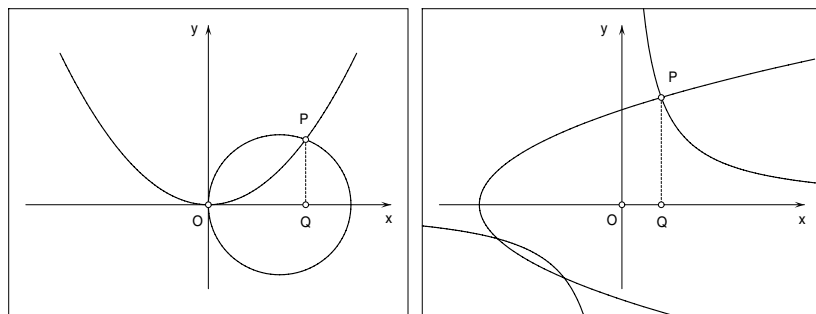


Fig. 2.7. Omar Khayyam’s solution of the cubic equations (2.9), in terms of the parabola $x^2 = ay$ and circle $x^2 + y^2 - bx = 0$ on the left, and the parabola $y^2 = b(x + a)$ and hyperbola $xy = b^2$ on the right. In each case, the length OQ is the desired root.

Khayyam knew that some cubics possess more than one real root, and he aspired to a method for solving general cubics. But this was not achieved until more than 400 years later, using complex numbers, in Renaissance Italy. Today, he is more renowned as a poet, for his famous *Ruba‘iyat* (quatrains),

⁹ As translated in S. H. Nasr, *Science and Civilization in Islam* [341].

popularized by Edward FitzGerald's translation/interpretation of 1859. These stanzas — alternately mystical and sensual, optimistic and fatalistic — offer a fascinating glimpse into the complexity and subtlety of Khayyam's mind:

*The moving finger writes, and, having writ,
Moves on: nor all thy piety nor wit
Shall lure it back to cancel half a line,
Nor all thy tears wash out a word of it.*

It has been said of the *Ruba'iyat* that “No other book of poetry has appeared in so many guises, from the edition de luxe to the penny pamphlet” [121] — it has even been rendered as a musical score, for voice and orchestra, by the composer Alan Hovhaness in 1975 (opus 282).

Of course, in the time of al-Khwarizmi and Khayyam, algebraic deductions were conducted entirely in prose: the use of symbolic methods in algebra came much later. The universal symbol x for the unknown quantity in an algebraic equation is thought to be derived through Spanish from the Arabic word *shay'* for “thing” — by which al-Khwarizmi and Khayyam referred to the unknown.

2.4 Fields, Rings, and Groups

Beginning with the “natural” numbers (i.e., the positive integers), which arise directly from physical experience, the development of algebra is characterized by a steadily increasing level of abstraction in the concept of *number*. Despite the absurdity of a negative number of cows or sheep, the *negative numbers* are simply too useful in calculations to be disqualified on philosophical grounds. Elementary geometrical problems soon lead to confrontations with *irrational numbers*, such as $\sqrt{2}$, and even *transcendental numbers* like π . The desire to systematically solve non-linear algebraic equations obliges us to introduce the “two-dimensional” *complex numbers* $a + i b$, where $i = \sqrt{-1}$. Despite lingering doubts over their “existence,” the complex numbers prove immensely valuable in contexts that greatly exceed their original purpose (see Chap. 4).

The quaternions, which resulted from Hamilton's attempt to construct a “three-dimensional number” system, are a turning point in this development: aspects of the familiar rules of arithmetic, formerly considered inviolable, were for the first time relinquished — the result of multiplying two or more of these entities depends on the *order* in which they are specified. This led to a certain loss of inhibition among algebraists: the laws of algebra were no longer viewed as immutable expressions of the natural order that governs the physical world, but as more-or-less arbitrary rules (or *axioms*) that one can posit at will, in order to investigate their logical consequences. Although this has incurred an explosion in the variety and complexity of algebraic systems that have been subject to detailed scrutiny, it has been convincingly argued by Morris Kline [282] that the resulting detachment of mathematics from the “natural world” has not been an unequivocally beneficial development.

Since we will be working with algebraic systems such as the real numbers, complex numbers, quaternions, polynomials, and rational functions, it is useful to briefly review some of the basic principles used to categorize them. Suppose a, b, c are elements of some set S , and let $+$ and \times be two binary operations that, acting on any pair of elements from S , generate another element of S . We postulate a set of possible rules for these operations, as follows:

- A₁. $a + b = b + a$
- A₂. $(a + b) + c = a + (b + c)$
- A₃. there exists $z \in S$ such that $a + z = a$ for all $a \in S$
- A₄. for all $a \in S$ there exists $-a \in S$ such that $(-a) + a = z$
- M₁. $a \times b = b \times a$
- M₂. $(a \times b) \times c = a \times (b \times c)$
- M₃. there exists $u \in S$ such that $a \times u = a$ for all $a \in S$
- M₄. for all $a \in S$, except z , there exists $a^{-1} \in S$ such that $a^{-1} \times a = u$
- D₁. $a \times (b + c) = (a \times b) + (a \times c)$

The binary operations $+$ and \times on pairs of elements in S are called *addition* and *multiplication*. Rules A₁ and M₁ specify the *commutative law* for sums and products, which requires the result to be independent of the *order* of the two operands. Similarly, A₂ and M₂ specify the *associative law* for sums and products: this states that the result is independent of the *grouping* of terms in a sum or product of three (or more) elements. Rules A₃ and M₃ guarantee that an *additive identity* and *multiplicative identity* exist as elements of S . In all the sets that interest us, these elements of are simply $z = 0$ and $u = 1$. Furthermore, rules A₄ and M₄ ensure that each element of S has an *additive inverse* and (except z) a *multiplicative inverse*. Finally, the *distributive law* D₁ states that the product of an element with a sum equals the sum of the products of that element with each of the summands.

Rules A₄ and M₄ allow us to introduce *inverses* – and \div to the operations $+$ and \times . Specifically, we set $a - b = a + (-b)$ and $a \div b = a \times (b^{-1})$, and the existence of the additive and multiplicative inverse for every element of S ensures *closure* under these operations, called *subtraction* and *division*.

A *field* is a set S whose elements are subject to a pair of operations $+, \times$ that satisfy *all* of the rules A₁–A₄, M₁–M₄, and D₁. Some familiar fields are the rational numbers (i.e., fractions) \mathbb{Q} , real numbers \mathbb{R} , complex numbers \mathbb{C} , and rational functions (i.e., ratios of polynomials) with real coefficients $\mathbb{R}(t)$. All these sets exhibit closure under the operations of addition, subtraction, multiplication, and division. Moreover, sums and products in these systems are commutative and associative, and they obey the distributive law.

A *ring* is a set S whose elements are subject to a pair of operations $+, \times$ that satisfy the rules A₁–A₄, M₂, and D₁. Rule M₁ may or may not be also satisfied — if it is, we have a *commutative ring*, otherwise a *non-commutative ring*. In other words, addition, subtraction, and multiplication (which may or

may not be commutative) are always possible within S , although division is not. Familiar examples of rings are the integers \mathbb{Z} , and the polynomials $\mathbb{R}[t]$ with real coefficients in some variable t . We can add, subtract, and multiply integers or polynomials, and the result is always an integer or polynomial. However, we cannot in general divide integers or polynomials, and expect the result to always be an integer or polynomial.

The integers and polynomials are commutative rings, in which the order of terms in a product does not matter. An example of a non-commutative ring is $\mathbb{R}^{n \times n}$, the set of $n \times n$ matrices with real entries. Matrix products do not, in general, commute — $BA \neq AB$ for general matrices $A, B \in \mathbb{R}^{n \times n}$ so M_1 is not satisfied. Also, matrices must be non-singular to have an inverse, so in general they do not satisfy M_4 (although M_3 is satisfied).

Some systems that concern us lie “between” a ring and a field in terms of their algebraic structure — i.e., they obey all the laws of a ring, but not quite all the laws of a field. Many commutative rings that interest us also satisfy M_3 but not M_4 . A system that obeys all the laws of a field *except* M_4 is an *integral domain*. The integers \mathbb{Z} are, of course, the archetypal example of such systems. Another example is the polynomials with real coefficients $\mathbb{R}[t]$ in a variable t . We can construct a field from an integral domain by extending membership of the set S to include all ratios a/b of elements a and $b \neq z$. Such *quotient fields* include the rational numbers (obtained from the integers) and rational functions (obtained from the polynomials).

A system that obeys all the laws of a field except M_1 is a *division ring* (or a *skew field* or *non-commutative field*). The example of primary interest to us here is the *quaternions* \mathbb{H} . We defer a detailed treatment of them to Chap. 5 and simply observe now that, although every quaternion has a multiplicative inverse, the non-commutative nature of quaternion products requires us to make a careful distinction between the processes of “left-multiplication” and “right-multiplication” in manipulating quaternion expressions.

Table 2.2 summarizes these classifications. However, not every system with the two binary operations $+$ and \times will fall neatly into one of these categories. Consider, for example, the case of *interval arithmetic* — which is concerned [332, 333] with sets of real values t , of the form $[a, b] = \{t \mid a \leq t \leq b\}$. The result of an arithmetic operation $* \in \{+, -, \times, \div\}$ on interval operands $[a, b]$ and $[c, d]$ is the set of values obtained by applying $*$ to pairs of values drawn from each of the two intervals:

$$[a, b] * [c, d] = \{x * y \mid x \in [a, b] \text{ and } y \in [c, d]\}.$$

From this definition, one may infer that

$$\begin{aligned} [a, b] + [c, d] &= [a + c, b + d], \\ [a, b] - [c, d] &= [a - d, b - c], \\ [a, b] \times [c, d] &= [\min(ac, ad, bc, bd), \max(ac, ad, bc, bd)], \\ [a, b] \div [c, d] &= [a, b] \times [1/d, 1/c], \end{aligned} \tag{2.10}$$

Table 2.2. Summary of rules observed (*) or not observed (–) by the two binary operations + and \times in canonical algebraic systems, together with some examples.

	ring	commutative ring	integral domain	division ring	field
A ₁	*	*	*	*	*
A ₂	*	*	*	*	*
A ₃	*	*	*	*	*
A ₄	*	*	*	*	*
M ₁	–	*	*	–	*
M ₂	*	*	*	*	*
M ₃	–	–	*	*	*
M ₄	–	–	–	*	*
D ₁	*	*	*	*	*
example	$\mathbb{R}^{n \times n}$	$\mathbb{Z}, \mathbb{R}[t]$	$\mathbb{Z}, \mathbb{R}[t]$	\mathbb{H}	$\mathbb{R}, \mathbb{C}, \mathbb{R}(t)$

where division is usually defined only for denominators such that $0 \notin [c, d]$. This system may be employed to model the propagation of errors in numerical computations, or calculations with uncertain input values (see §12.3.4).

It can be verified that addition and multiplication are commutative and associative, and the degenerate¹⁰ intervals $[0, 0]$ and $[1, 1]$ define the additive and multiplicative identities. However, non-degenerate intervals $[a, b]$ do not have additive or multiplicative inverses ($–$, \div are *not* the inverses to $+$, \times). Furthermore, multiplication does not in general distribute over addition — instead, we have the *sub-distributive law*

$$[a, b] \times ([c, d] + [e, f]) \subseteq ([a, b] \times [c, d]) + ([a, b] \times [e, f]).$$

Thus, interval arithmetic has a rather unusual algebraic structure — it obeys the rules A₁–A₃ and M₁–M₃, but not A₄, M₄, and D₁.

We conclude by briefly mentioning the simpler algebraic structure known as a *group*. This is a set S equipped with just a single binary operation. This operation obeys the associative law, and the set exhibits closure under it — if the group operation also obeys the commutative law, we have a *commutative* (or *Abelian*) group, otherwise a *non-commutative* group. S also includes an identity element with respect to the group operation, and each element of S has a corresponding inverse in S . An important example is SO(n), the set of *special orthogonal* real $n \times n$ matrices. A matrix is *orthogonal* if its inverse is identical to its transpose, and it is *special* if its determinant is unity. Since the product of two special orthogonal matrices is always a special orthogonal matrix, such matrices constitute a (non-commutative) group under matrix multiplication. The geometrical significance of the matrices in the group SO(n) is that they describe *rotations* in the Euclidean space \mathbb{R}^n (see §5.7).

¹⁰ By including degenerate elements, interval arithmetic subsumes the real numbers.

3

Polynomials

The more it approaches intuition, the more reliable is the deduction. Intuition has two distinctive features — it is an instantaneous act, and it consists of clear grasp of an idea. Intuition and deduction should be trustworthy processes which we can use to lead to genuine knowledge.

René Descartes

A polynomial $p(t)$ in the variable t is a finite sum of products of a sequence of constants or *coefficients* a_0, a_1, \dots, a_n with powers $1, t, \dots, t^n$ of the variable,

$$p(t) = a_0 + a_1 t + \cdots + a_n t^n = \sum_{k=0}^n a_k t^k. \quad (3.1)$$

Any function of t that can be evaluated by a *finite* sequence of the arithmetic operations $+, -, \times$ (but not \div) amounts to a polynomial in t . The number n is the *degree* of the polynomial, and polynomials of degree $n = 0, 1, 2, 3, 4 \dots$ are called constant, linear, quadratic, cubic, quartic … polynomials.

3.1 Basic Properties

Polynomials have the algebraic structure of a *ring*. This means that we may add, subtract, and multiply polynomials — and their scalar multiples — in any combination we choose, and the end result will always be a polynomial, i.e., the set of polynomials is *closed* under the operations of addition/subtraction, multiplication, and scaling. However, we cannot *divide* two polynomials and expect the result to be, in general, a polynomial: the division of polynomials yields, in general, a *rational function* (see §3.5) — just as the division of two integers typically yields a rational number (fraction).

The set of polynomials is also closed under *differentiation* and *integration* — for example, the derivative $p'(t)$ of the polynomial (3.1) of degree n is the polynomial of degree $n - 1$ defined by

$$p'(t) = a_1 + 2a_2 t + \cdots + n a_n t^{n-1} = \sum_{k=0}^{n-1} (k+1) a_{k+1} t^k.$$

Higher-order derivatives $p''(t), \dots, p^{(m)}(t)$ are defined similarly. Note that all derivatives of order $> n$ vanish identically: $p^{(m)}(t) \equiv 0$ if $m > n$ — this can be regarded as the *defining property* of degree- n polynomials.

Horner's method, or “nested multiplication,” is an efficient procedure for evaluating a degree- n polynomial $p(t)$ that requires just n multiplications and n additions. Given the coefficients a_0, a_1, \dots, a_n and a t value, we set $p_0 = a_n$ and recursively compute a sequence of values p_1, p_2, \dots, p_n as follows:

$$\begin{aligned} p_1 &= p_0 \times t + a_{n-1}, \\ p_2 &= p_1 \times t + a_{n-2}, \\ &\dots \\ p_k &= p_{k-1} \times t + a_{n-k}, \\ &\dots \\ p_n &= p_{n-1} \times t + a_0. \end{aligned}$$

Each step consists of multiplying the outcome of the preceding step by t , and adding the next “unused” coefficient as we proceed through them in reverse order: a_n, \dots, a_1, a_0 . The final step then yields the value of the polynomial: $p(t) = p_n$. Horner's method amounts to writing

$$p(t) = ((\cdots (a_n \times t + a_{n-1}) \times t \cdots + a_2) \times t + a_1) \times t + a_0.$$

We can *homogenize* the polynomial (3.1) by substituting $t = T/U$ and then multiplying by U^n . This yields the corresponding *homogeneous polynomial*

$$P(T, U) = a_0 U^n + a_1 T U^{n-1} + \cdots + a_n T^n = \sum_{k=0}^n a_k T^k U^{n-k}, \quad (3.2)$$

where each term is of total degree n in T and U . The *homogeneous variables* (T, U) are not independent, since we are interested only in their *ratios* $T : U$. Each distinct ratio defines a unique value T/U of the *inhomogeneous variable* t . For example, we do not distinguish the (T, U) pairs $(3, 1)$ and $(6, 2)$: both identify $t = 3$. For any $k \neq 0$, the pair $(0, k)$ identifies the origin, and $(k, 0)$ identifies the *point at infinity*. The pair $(0, 0)$ is excluded from consideration: it does not identify any point. The homogeneous form allows us to describe the behavior of a polynomial “at infinity” in a rigorous manner.

3.2 Polynomial Bases

Let $\phi_0(t), \phi_1(t), \dots, \phi_n(t)$ be a set of $n + 1$ polynomials, each of degree $\leq n$. These polynomials are *linearly independent* if the identity

$$c_0\phi_0(t) + c_1\phi_1(t) + \dots + c_n\phi_n(t) \equiv 0$$

can only be satisfied by choosing $c_0 = c_1 = \dots = c_n = 0$ (the identity sign “ \equiv ” means that the equation holds for *every value of t*).

Any set $\phi_0(t), \phi_1(t), \dots, \phi_n(t)$ of $n + 1$ linearly independent polynomials forms a *basis* for all polynomials of degree $\leq n$. This means we can *uniquely* express any polynomial $p(t)$ of degree $\leq n$ in the form

$$p(t) = c_0\phi_0(t) + c_1\phi_1(t) + \dots + c_n\phi_n(t) = \sum_{k=0}^n c_k\phi_k(t),$$

c_0, c_1, \dots, c_n being the *coefficients* of $p(t)$ in the basis $\phi_0(t), \phi_1(t), \dots, \phi_n(t)$. In any basis, different polynomials always have different coefficients, and we can obtain the coefficients in one basis from those in any other basis through a linear transformation (i.e., a matrix multiplication).

The *monomial* or *power* basis used above, $\phi_k(t) = t^k$ for $k = 0, \dots, n$, is the most familiar and the most commonly seen in “theoretical” treatments of the properties of polynomials. However, it is often not the most convenient nor the most numerically-stable basis for practical computations. Since we are concerned with polynomials over finite intervals — usually, $t \in [0, 1]$ — we shall make extensive use of the *Bernstein basis* defined by

$$b_k^n(t) = \binom{n}{k}(1-t)^{n-k}t^k, \quad k = 0, \dots, n.$$

This employs the *barycentric coordinates* t and $1 - t$ to specify the position of a point symmetrically with respect to the interval end-points. A thorough discussion of the properties and advantages of the Bernstein form is deferred to Chap. 13. For now, we briefly review a few other useful bases.

The *Hermite basis* is convenient for interpolation of end-point values and derivatives on a finite interval, typically $[0, 1]$. For example, given function values f_0, f_1 and derivatives f'_0, f'_1 at $t = 0, 1$ the unique cubic polynomial that interpolates these values can be written as

$$p(t) = f_0\alpha_0(t) + f_1\alpha_1(t) + f'_0\beta_0(t) + f'_1\beta_1(t),$$

where the cubic Hermite basis functions are defined by

$$\begin{aligned} \alpha_0(t) &= 1 - 3t^2 + 2t^3, & \alpha_1(t) &= 3t^2 - 2t^3, \\ \beta_0(t) &= t - 2t^2 + t^3, & \beta_1(t) &= -t^2 + t^3. \end{aligned} \tag{3.3}$$

The α functions have vanishing *derivatives* at both interval end points, while their *values* are unity at one end and zero at the other. Conversely, the β

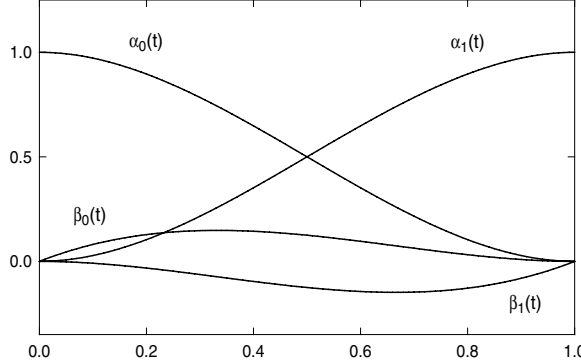


Fig. 3.1. The cubic Hermite basis on the interval $t \in [0, 1]$.

functions have vanishing *values* at both end points, and their *derivatives* are unity at one end and zero at the other. Thus, we have

$$\begin{bmatrix} \alpha_0(0) & \alpha_0(1) & \alpha'_0(0) & \alpha'_0(1) \\ \alpha_1(0) & \alpha_1(1) & \alpha'_1(0) & \alpha'_1(1) \\ \beta_0(0) & \beta_0(1) & \beta'_0(0) & \beta'_0(1) \\ \beta_1(0) & \beta_1(1) & \beta'_1(0) & \beta'_1(1) \end{bmatrix} = \begin{bmatrix} 1 & 0 & 0 & 0 \\ 0 & 1 & 0 & 0 \\ 0 & 0 & 1 & 0 \\ 0 & 0 & 0 & 1 \end{bmatrix},$$

where primes denote derivatives with respect to t . Figure 3.1 shows the cubic Hermite basis on $[0, 1]$. Note that $\alpha_0(t) \equiv \alpha_1(1-t)$ and $\beta_0(t) \equiv -\beta_1(1-t)$. Bases of higher (odd) degree n may be similarly defined, in terms of end-point values and derivatives to order $\frac{1}{2}(n-1)$.

In algorithms for computer-aided curve and surface design, we are often concerned with transformations between cubic Hermite and Bernstein bases. One can easily verify that these transformation have the matrix forms

$$\begin{bmatrix} b_0^3(t) \\ b_1^3(t) \\ b_2^3(t) \\ b_3^3(t) \end{bmatrix} = \begin{bmatrix} 1 & -3 & 0 & 0 \\ 0 & 3 & 0 & 0 \\ 0 & 0 & -3 & 0 \\ 0 & 0 & 3 & 1 \end{bmatrix} \begin{bmatrix} \alpha_0(t) \\ \beta_0(t) \\ \beta_1(t) \\ \alpha_1(t) \end{bmatrix}, \quad (3.4)$$

and

$$\begin{bmatrix} \alpha_0(t) \\ \beta_0(t) \\ \beta_1(t) \\ \alpha_1(t) \end{bmatrix} = \begin{bmatrix} 1 & 1 & 0 & 0 \\ 0 & \frac{1}{3} & 0 & 0 \\ 0 & 0 & -\frac{1}{3} & 0 \\ 0 & 0 & 1 & 1 \end{bmatrix} \begin{bmatrix} b_0^3(t) \\ b_1^3(t) \\ b_2^3(t) \\ b_3^3(t) \end{bmatrix}. \quad (3.5)$$

The *Legendre basis* is suited to problems of *least-squares approximation* of functions by polynomials over finite domains [113, 256]. It is usually defined on the interval $[-1, +1]$ to emphasize certain symmetry properties, but it is more convenient for us to define it on $[0, 1]$. The Legendre polynomials $L_k(t)$ on $t \in [0, 1]$ can be generated by the recurrence relation

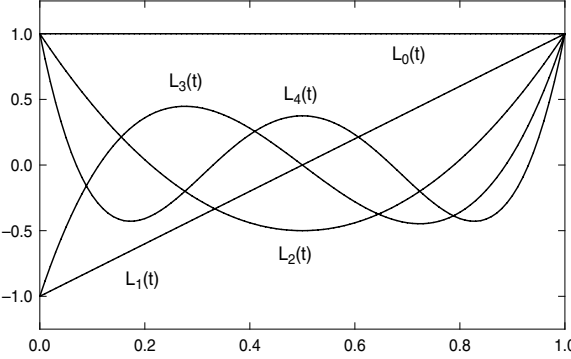


Fig. 3.2. The first five Legendre polynomials on the interval $t \in [0, 1]$.

$$(k+1)L_{k+1}(t) = (2k+1)(2t-1)L_k(t) - kL_{k-1}(t) \quad (3.6)$$

for $k = 1, 2, \dots$, commencing with $L_0(t) = 1$ and $L_1(t) = 2t - 1$. This gives

$$L_2(t) = 6t^2 - 6t + 1, \quad L_3(t) = 20t^3 - 30t^2 + 12t - 1, \quad \dots \text{ etc.}$$

Figure 3.2 illustrates the behavior of $L_0(t)$ through $L_5(t)$.

The Legendre polynomials possess the orthogonality property defined by

$$\int_0^1 L_j(t) L_k(t) dt = \begin{cases} 0 & \text{if } j \neq k, \\ \frac{1}{2k+1} & \text{if } j = k. \end{cases} \quad (3.7)$$

This allows us to determine the coefficients of the degree- n least-squares polynomial approximant

$$p_n(t) = \sum_{k=0}^n c_k L_k(t)$$

to a given function $f(t)$, that minimizes the “error integral”

$$E = \int_0^1 [p_n(t) - f(t)]^2 dt,$$

by means of the formulae

$$c_k = (2k+1) \int_0^1 L_k(t) f(t) dt, \quad k = 0, \dots, n.$$

Moreover, the Legendre form of the approximating polynomial $p_n(t)$ exhibits *permanence of coefficients*, i.e., the values c_0, \dots, c_n remain unchanged if we wish to increase the degree of the approximant to $n+1$ by the introduction

of an additional term $c_{n+1}L_{n+1}(t)$ — only c_{n+1} requires computation. There is an elegant relation between the Legendre and Bernstein bases on $[0, 1]$ — namely, the Bernstein coefficients of the k^{th} Legendre polynomial are simply the binomial coefficients of order k , taken with alternating signs:

$$L_k(t) = \sum_{i=0}^k (-1)^{k+i} \binom{k}{i} b_i^k(t).$$

Transformations between the Bernstein and Legendre forms of a polynomial on $[0, 1]$ are comparatively stable [154].

Finally, we consider a basis useful in “min–max approximation” problems and the best approximation of polynomials by polynomials of lower degree — the *Chebyshev basis*. The Chebyshev¹ polynomials (of the first kind) are also conventionally defined on the interval $[-1, +1]$ by the formula

$$T_k(t) = \cos(k \cos^{-1} t) = \sum_{i=0}^{\lfloor \frac{1}{2}k \rfloor} \binom{k}{2i} (t^2 - 1)^i t^{k-2i}$$

for $k = 0, 1, 2, \dots$, where the “floor” function $\lfloor x \rfloor$ denotes the largest integer not exceeding x . In other words, $T_k(t)$ is just the polynomial in t obtained by expanding $\cos(k\theta)$ in powers of $\cos \theta$, and setting $t = \cos \theta$. The first few Chebyshev polynomials are

$$T_0(t) = 1, \quad T_1(t) = t, \quad T_2(t) = 2t^2 - 1, \quad T_3(t) = 4t^3 - 3t, \quad \text{etc.}$$

Beginning with $T_0(t) = 1$ and $T_1(t) = t$, they may also be generated by the recurrence relation

$$T_{k+1}(t) = 2tT_k(t) - T_{k-1}(t), \quad k = 1, 2, \dots$$

Chebyshev polynomials on $[0, 1]$ can be obtained by replacing t with $2t - 1$, giving $1, 2t - 1, 8t^2 - 8t + 1, 32t^3 - 48t^2 + 18t - 1$, etc. The first few Chebyshev polynomials on $[-1, +1]$ are illustrated in Fig. 3.3.

The Chebyshev polynomials exhibit the orthogonality property

$$\int_{-1}^{+1} \frac{T_j(t)T_k(t)}{\sqrt{1-t^2}} dt = \begin{cases} 0 & \text{if } j \neq k, \\ \pi & \text{if } j = k = 0, \\ \frac{1}{2}\pi & \text{if } j = k > 0, \end{cases}$$

with respect to the “weight function” $1/\sqrt{1-t^2}$ on $t \in [-1, +1]$. Note that $T_k(t)$ has the k real roots $t_k = \cos(i - \frac{1}{2})\pi/k$, $i = 1, \dots, n$ on $[-1, +1]$ and these roots separate the alternating extremal values -1 and $+1$.

¹ Named for the Russian mathematician Pafnuty Lvovich Chebyshev (1821–1894), who contributed to number theory, orthogonal polynomials, and probability. The polynomials are denoted T after an alternative transliteration — Tschebyscheff.

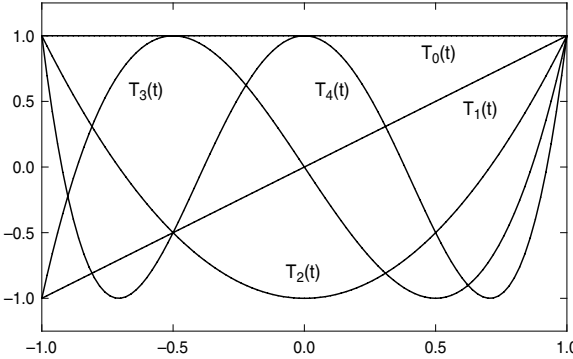


Fig. 3.3. The first five Chebyshev polynomials on the interval $[-1, +1]$.

Another interpretation of $T_k(t)$ is as follows. Let Π_k denote the set of all polynomials $p(t)$ of degree $\leq k$. Suppose we seek the polynomial $\hat{p}(t) \in \Pi_k$ that exhibits the least possible absolute difference

$$\epsilon_k = \min_{p(t) \in \Pi_k} \max_{t \in [-1, +1]} |p(t) - t^{k+1}|$$

from the monomial t^{k+1} over the interval $[-1, +1]$. The error of this best “min–max” polynomial approximant $\hat{p}(t)$ of degree $\leq k$ to t^{k+1} proves to be a multiple of the Chebyshev polynomial $T_{k+1}(t)$ — namely,

$$t^{k+1} - \hat{p}(t) = 2^{-k} T_{k+1}(t),$$

and since $|T_{k+1}(t)| \leq 1$ for $t \in [-1, +1]$, the value of the minimum possible error is $\epsilon_k = 2^{-k}$. This leads to the method of *Chebyshev economization* for polynomials — i.e., best min–max approximation of a given polynomial by polynomials of lower degree. If a polynomial $p(t) = a_0 + a_1 t + \cdots + a_{k+1} t^{k+1}$ of degree $k+1$ is given, and we wish to determine the polynomial $\hat{p}(t)$ of degree $\leq k$ with the least absolute difference from $p(t)$ over $[-1, +1]$, we can immediately identify this best approximating polynomial as

$$\hat{p}(t) = p(t) - a_{k+1} 2^{-k} T_{k+1}(t),$$

since $\hat{p}(t)$ can agree *exactly* with $p(t)$ in all terms up to $a_k t^k$. Furthermore, the approximation error will satisfy $|\hat{p}(t) - p(t)| \leq 2^{-k} a_{k+1}$, and this error bound is attained at the extrema of $T_{k+1}(t)$. Clearly, this process can be repeated to obtain best approximants of successively lower degree.

The Chebyshev polynomials have many other useful applications: least-squares approximation, expansion of functions, power series economization, etc. For a thorough treatment of their properties and applications, see [376]. The Legendre and Chebyshev bases are actually special instances of a more general class of orthogonal polynomials, the *Jacobi polynomials* [113, 434].

3.3 Roots of Polynomials

A *simple root* of the polynomial $p(t)$ is a value τ of the variable t such that $p(\tau) = 0 \neq p'(\tau)$. A *multiple root* is a value τ such that $p(\tau) = 0$ and one or more successive derivatives of $p(t)$ vanish at $t = \tau$. Specifically, if

$$p(\tau) = p'(\tau) = \cdots = p^{(m-1)}(\tau) = 0 \neq p^{(m)}(\tau),$$

we call τ an *m -fold root*, or a *root of multiplicity m* . In the cases $m = 2, 3, \dots$ we speak of double, triple, \dots roots. The roots of a polynomial may be *real* or *complex*. When the coefficients a_0, a_1, \dots, a_n are real numbers, complex roots must occur in *conjugate pairs*, i.e., if $t = \alpha + i\beta$ is a root, $t = \alpha - i\beta$ must also be a root (of the same multiplicity).

The vanishing of successive low-order coefficients a_0, a_1, \dots or high-order coefficients a_n, a_{n-1}, \dots of $p(t)$ indicates the presence of certain special roots. To identify them, we employ the homogeneous form (3.2) — for which roots correspond to distinct ratios $T : U$. Note that multiplying both T and U by a constant $k \neq 0$ gives

$$P(kT, kU) = k^n P(T, U),$$

so $P(T, U) = 0 \iff P(kT, kU) = 0$. If $a_0 = 0$, we evidently have $P(0, U) = 0$, i.e., there is a root at the origin. On the other hand, if $a_n = 0$ but we formally consider the polynomial as being of degree n , then $P(T, 0) = 0$, i.e., there is a root at infinity. If m consecutive low- or high-order coefficients vanish, we have an m -fold root at the origin or at infinity, respectively.

The *Fundamental Theorem of Algebra* states that a degree- n polynomial $p(t)$ has *exactly n roots*, if we count both real and complex roots, and each distinct root is counted according to its multiplicity. This is equivalent to the property that $p(t)$ can be expressed in *factored form* as

$$p(t) = a_n(t - r_1)(t - r_2) \cdots (t - r_n) = a_n \prod_{k=1}^n (t - r_k)$$

where the n roots r_1, r_2, \dots, r_n are not necessarily real or distinct. Combining factors that correspond to complex conjugate roots, it is always possible to decompose a real polynomial into *real* factors that are (powers of) linear or quadratic terms. On multiplying out the factored form, we see that the sum $r_1 + \cdots + r_n$ of the roots equals $-a_{n-1}/a_n$, while the product $r_1 \cdots r_n$ of the roots equals $(-1)^n a_0/a_n$. In general, the sum of the $\binom{n}{k}$ products of roots, taken k at a time, is equal to $(-1)^k a_{n-k}/a_n$. These sums of products of the roots are called the *symmetric functions* of the roots.

Descartes' Law of Signs gives basic information on polynomial real roots, without calculation. According to this law, the number N of *positive* real roots of the polynomial $p(t)$ — each counted according to its multiplicity — is less than the number $V(a_0, a_1, \dots, a_n)$ of *sign variations* in the ordered sequence of its coefficients by an even amount:

$$N = V(a_0, a_1, \dots, a_n) - 2K,$$

where K is a non-negative integer. We ignore coefficients that are zero when counting the coefficient sign variations — for example, $V(-3, 2, 5, -1, 4) = 3$ and $V(-7, 0, 2, -6, -8, 3, 0, -1, 9) = 5$.

This provides, by mere inspection, a *bound* on the number of positive real roots of $p(t)$. In particular, if a_0, a_1, \dots, a_n are all of like sign, there are no positive roots. By the change of variables $t \rightarrow -t$, we can also bound the number of negative real roots in terms of the sign variations in the sequence $a_0, -a_1, a_2, -a_3, \dots$ (where only odd-power coefficients are negated). One may also bound the number of real roots on a finite interval $t \in (a, b)$ by considering the Bernstein form of the polynomial on that interval (see §11.2).

The *linear* polynomial $a_0 + a_1 t$ obviously has the single root $t = -a_0/a_1$. *Quadratic*, *cubic*, and *quartic* equations admit a *solution by radicals*, i.e., their roots can be expressed in terms of their coefficients using just a finite sequence of *arithmetic operations* and *root extractions*. For the quadratic equation

$$a_0 + a_1 t + a_2 t^2 = 0,$$

for example, the roots are given by the well-known formula

$$t = \frac{-a_1 \pm \sqrt{a_1^2 - 4a_2 a_0}}{2a_2}.$$

Similarly, *Cardano's method* [452] can be used to solve for the roots of the cubic equation

$$a_0 + a_1 t + a_2 t^2 + a_3 t^3 = 0.$$

Set

$$p = \frac{3a_1 a_3 - a_2^2}{9a_3^2}, \quad q = \frac{9a_1 a_2 a_3 - 27a_0 a_3^2 - 2a_2^3}{54a_3^3}, \quad \delta = p^3 + q^2,$$

and let r be any of the three complex values specified by

$$r^3 = q + \sqrt{\delta}. \tag{3.8}$$

Then the roots of the cubic equation are given by

$$t = \begin{cases} -\frac{a_2}{3a_3} + r - \frac{p}{r}, \\ -\frac{a_2}{3a_3} - \frac{1}{2}\left(r - \frac{p}{r}\right) + \frac{\sqrt{3}}{2}i\left(r + \frac{p}{r}\right), \\ -\frac{a_2}{3a_3} - \frac{1}{2}\left(r - \frac{p}{r}\right) - \frac{\sqrt{3}}{2}i\left(r + \frac{p}{r}\right). \end{cases} \tag{3.9}$$

One of the roots (3.9) is real and the other two are complex conjugates when $\delta > 0$; all three roots are real and distinct when $\delta < 0$; and there is a

multiple root when $\delta = 0$. Note that, even if all three roots are real, complex arithmetic is generally required to evaluate the quantities (3.8)–(3.9).

When $\delta < 0$ (in which case p must be negative), it is possible to solve the cubic equation exclusively in real arithmetic, by appealing to trigonometric functions. Namely, if the angle θ is defined by

$$\cos \theta = \frac{q}{\sqrt{-p^3}},$$

the three (real) solutions can be expressed as

$$t = -\frac{a_2}{3a_3} + 2\sqrt{-p} \cos\left(\theta + \frac{k2\pi}{3}\right), \quad k = 0, 1, 2.$$

Finally, the four roots of the quartic equation

$$a_0 + a_1 t + a_2 t^2 + a_3 t^3 + a_4 t^4 = 0$$

may be computed by *Ferrari's method* [452]. Namely, let z be a real root of the *resolvent* cubic equation

$$z^3 + c_2 z^2 + c_1 z + c_0 = 0$$

with

$$c_2 = -\frac{a_2}{a_4}, \quad c_1 = \frac{a_1 a_3 - 4a_0 a_4}{a_4^2}, \quad c_0 = \frac{4a_0 a_2 a_4 - a_1^2 a_4 - a_0 a_3^2}{a_4^3},$$

and let s be either of the complex values defined by

$$s^2 = a_3^2 - 4a_4^2 z - 4a_2 a_4.$$

Then the roots of the quartic are the same as the roots of the two *quadratic* equations

$$t^2 + \left(\frac{a_3 \pm s}{2a_4}\right)t + \frac{1}{2}\left(z \pm \frac{a_3 z - 2a_1}{s}\right) = 0. \quad (3.10)$$

Again, even if all the roots are real, complex arithmetic is in general required to obtain the root z of the resolvent cubic, and to solve the two quadratics.

Galois theory reveals that polynomial equations of degree $n \geq 5$ do not, in general, admit a solution by radicals — we are obliged to invoke iterative “numerical methods” to *approximate* their roots.

3.4 Resultants and Discriminants

Given two polynomials

$$p(t) = a_0 + a_1 t + \cdots + a_n t^n \quad \text{and} \quad q(t) = b_0 + b_1 t + \cdots + b_m t^m,$$

one might ask: “do they have a common root?” In other words, does a value τ exist such that $p(\tau) = q(\tau) = 0$? This question can, in fact, be answered

without knowing the roots. There exists a function $f(a_0, \dots, a_n, b_0, \dots, b_m)$ of the coefficients — the *resultant* of $p(t)$ and $q(t)$ with respect to t — such that

$$f(a_0, \dots, a_n, b_0, \dots, b_m) = 0 \iff p(\tau) = q(\tau) = 0 \text{ for some } \tau.$$

Informally, the resultant is the expression in the coefficients one obtains upon “eliminating” the variable t from the equations $p(t) = 0$, $q(t) = 0$.

The vanishing of the resultant indicates the existence of common roots, but gives no information on their numerical values, their number, or whether they are real or complex conjugates. We use the notation $\text{Resultant}_t(p, q)$ for the resultant of $p(t)$ and $q(t)$ with respect to t , so that

$$\text{Resultant}_t(p, q) = f(a_0, \dots, a_n, b_0, \dots, b_m).$$

The resultant may be compactly expressed as a determinant, whose entries depend upon the coefficients a_0, \dots, a_n and b_0, \dots, b_m of $p(t)$ and $q(t)$. The Sylvester determinant [452], defined by

$$\text{Resultant}_t(p, q) = \begin{vmatrix} a_0 & a_1 & a_2 & \cdots & a_n \\ a_0 & a_1 & a_2 & \cdots & a_n \\ \cdot & \cdot & \cdot & \cdot & \cdot \\ & a_0 & a_1 & a_2 & \cdots & a_n \\ b_0 & b_1 & b_2 & \cdots & b_m \\ b_0 & b_1 & b_2 & \cdots & b_m \\ \cdot & \cdot & \cdot & \cdot & \cdot \\ b_0 & b_1 & b_2 & \cdots & b_m \end{vmatrix}, \quad (3.11)$$

is perhaps the simplest formulation — it is of dimension $(n+m) \times (n+m)$, and contains m rows of the coefficients a_0, \dots, a_n followed by n rows of the coefficients b_0, \dots, b_m , successive rows being displaced one space to the right — all of the “empty space” in (3.11) is filled in with zeros.

Another useful form is the Bézout resultant. Expressed as a determinant, this form is of smaller dimension than the Sylvester form, although its entries are correspondingly more complicated. Consider the polynomial

$$f(t, \alpha) = \frac{p(t)q(\alpha) - p(\alpha)q(t)}{t - \alpha} = \sum_k r_k(t) \alpha^k$$

in t and a new variable α (since $p(t)q(\alpha) - p(\alpha)q(t)$ vanishes for $t = \alpha$, it must contain the factor $t - \alpha$ divided out above). The coefficients of the polynomials $r_k(t)$ are quadratic expressions in the coefficients of $p(t)$, $q(t)$ and the Bézout resultant is the determinant of the array formed by those coefficients [212].

Resultants are also useful in answering the question: “does the polynomial $p(t) = a_0 + a_1 t + \cdots + a_n t^n$ possess any *multiple* roots?” As previously stated, a multiple root τ satisfies $p(\tau) = p'(\tau) = 0$, so this question is equivalent to asking if the polynomial has any roots in common with its derivative, and this

can be answered by forming the resultant of $p(t)$ and $p'(t)$. The *discriminant* of the polynomial $p(t)$ is an expression in its coefficients a_0, a_1, \dots, a_n that is conventionally defined by

$$\Delta(a_0, \dots, a_n) = (-1)^{\frac{1}{2}n(n-1)} \frac{1}{a_n} \text{Resultant}_t(p, p') ,$$

and we have

$$\Delta(a_0, \dots, a_n) = 0 \iff p(\tau) = p'(\tau) = 0 \text{ for some } \tau .$$

For example, the discriminants of the quadratic $a_0 + a_1 t + a_2 t^2$ and the cubic $a_0 + a_1 t + a_2 t^2 + a_3 t^3$ are given by

$$\begin{aligned} \Delta &= a_1^2 - 4a_0a_2 , \\ \Delta &= 18a_0a_1a_2a_3 + a_1^2a_2^2 - 4a_0a_2^3 - 4a_1^3a_3 - 27a_0^2a_3^2 . \end{aligned}$$

The vanishing of the discriminant indicates only the *presence* of one or more multiple roots: it yields no information on their number, their multiplicities, or whether they are real or complex. However, a sign change of the discriminant is (usually) accompanied by a change in the number of real roots. For example, a quadratic polynomial has two real roots when $\Delta > 0$ and none when $\Delta < 0$, as is evident from the familiar solution formula. Similarly, a cubic polynomial has three real roots when $\Delta > 0$ and just one when $\Delta < 0$.

Resultants can be used to reduce the dimension of systems of polynomial equations in two or more variables, by successively eliminating variables (this may be regarded as the non-linear generalization of the *Gaussian elimination* procedure commonly used when solving systems of *linear* equations). Suppose, for example, that

$$f(x, y) = g(x, y) = 0 \tag{3.12}$$

are a pair of bivariate polynomial equations in x, y . The system of equations defines two plane algebraic curves, and its solutions are the intersection points (real or complex) of these two curves. If we regard $f(x, y)$ and $g(x, y)$ as (say) polynomials in y , whose coefficients are polynomials in x , we can eliminate y between them by forming their resultant with respect to y . This yields a polynomial in x only,

$$p(x) = \text{Resultant}_y(f(x, y), g(x, y)) ,$$

since the entries in the Sylvester determinant (3.11) are now polynomials in x . The roots of $p(x)$ define the x -coordinates of all the intersection points of the two curves $f(x, y) = 0$ and $g(x, y) = 0$. By computing these roots and substituting their values into the original equations we can, in principle, find the corresponding y -coordinates of the intersection points.

However, resultants are more often employed as theoretical tools rather than for practical computations, except in small problems. *Bézout's theorem*

(see §9.2.9) states that two algebraic curves of degree m and n intersect in mn points, so we can expect the resultant of the polynomials (3.12) with respect to x or y to be, in general, of this degree. For higher-dimensional problems, the growth of the resultant degree can be even more alarming.

3.5 Rational Functions

A *rational function* $r(t)$ of the variable t is the quotient of two polynomials, $p(t)$ and $q(t)$, in t :

$$r(t) = \frac{p(t)}{q(t)},$$

where $p(t) = a_0 + a_1 t + \dots + a_n t^n$ and $q(t) = b_0 + b_1 t + \dots + b_m t^m$. Any function of t that can be evaluated by a *finite* sequence of the arithmetic operations $+, -, \times, \div$ amounts to a rational function in t .

Rational functions possess the algebraic structure of a *field* — this means that we may add/subtract and multiply/divide rational functions, and their scalar multiples, in any way we like, and the result will always be a rational function: it can always be expressed in the form $p(t)/q(t)$, and thus requires (in principle) only a single division for its evaluation.

The values of t at which $p(t)$ and $q(t)$ vanish are called, respectively, the *roots* and *poles* of the rational function $r(t)$: they may be *simple* or *multiple*. We assume that the *numerator* and *denominator* polynomials, $p(t)$ and $q(t)$, are *relatively prime* (i.e., they have no roots in common, otherwise we could cancel the terms in their factored forms corresponding to those roots).

If $m \leq n$, we can decompose $p(t)/q(t)$ into a *quotient* polynomial $f(t)$ of degree $n - m$ and a *remainder* polynomial $h(t)$ of degree $< m$, such that

$$\frac{p(t)}{q(t)} = f(t) + \frac{h(t)}{q(t)}.$$

The coefficients of $f(t)$ and $h(t)$ are uniquely determined by equating like terms on either side of

$$p(t) = q(t)f(t) + h(t),$$

which yields a system of $n + 1$ linear equations² for these coefficients. When $m > n$, we have $f(t) \equiv 0$ and $h(t) = p(t)$. The division of polynomials is analogous to the problem of expressing the ratio of two integers in terms of integral and fractional parts, e.g.,

$$\frac{11}{3} = 3 + \frac{2}{3}.$$

² The method of *synthetic division* [452] can also be used to compute $f(t)$ and $h(t)$.

The *greatest common divisor* of two given polynomials $p(t)$ and $q(t)$ is a polynomial, denoted by $\gcd(p(t), q(t))$, each root of which is also a root of $p(t)$ and $q(t)$. The multiplicity of a root τ of $\gcd(p(t), q(t))$ is the *smaller* of the multiplicities of τ as a root $p(t)$ and $q(t)$. Of course, $\gcd(p(t), q(t))$ is defined only up to a non-zero constant factor. If $\gcd(p(t), q(t)) = \text{constant}$, we say that $p(t)$ and $q(t)$ are *relatively prime* — they have no common roots.

We can compute $\gcd(p(t), q(t))$ without explicitly factorizing $p(t)$ and $q(t)$, or knowing their roots, through a sequence of polynomial divisions called the *Euclidean algorithm*. We set $\phi_0(t) = p(t)$, $\phi_1(t) = q(t)$, and then recursively define $\phi_{k+1}(t)$ as the remainder on dividing $\phi_{k-1}(t)$ by $\phi_k(t)$, so that

$$\begin{aligned}\phi_0(t) &= \phi_1(t)f_1(t) + \phi_2(t), \\ \phi_1(t) &= \phi_2(t)f_2(t) + \phi_3(t), \\ &\dots \\ \phi_{r-2}(t) &= \phi_{r-1}(t)f_{r-1}(t) + \phi_r(t), \\ \phi_{r-1}(t) &= \phi_r(t)f_r(t).\end{aligned}$$

We continue until a zero remainder is encountered, $\phi_{r+1}(t) \equiv 0$, and we then have $\phi_r(t) = \gcd(p(t), q(t))$. See [452] for a more thorough description.

A slight modification of the Euclidean algorithm provides a powerful tool for counting real roots of a polynomial on a finite interval. A *Sturm sequence* for the polynomial $p(t)$ is constructed by choosing $\phi_0(t) = p(t)$, $\phi_1(t) = p'(t)$, and then executing the Euclidean algorithm but with $\phi_2(t), \phi_3(t), \dots$ taken to be the *negation* of the remainder at each step [452]:

$$\begin{aligned}\phi_0(t) &= \phi_1(t)f_1(t) - \phi_2(t), \\ \phi_1(t) &= \phi_2(t)f_2(t) - \phi_3(t), \\ &\dots \\ \phi_{r-2}(t) &= \phi_{r-1}(t)f_{r-1}(t) - \phi_r(t), \\ \phi_{r-1}(t) &= \phi_r(t)f_r(t).\end{aligned}$$

The Sturm sequence $\phi_0(t), \dots, \phi_r(t)$ allows us to determine the *exact* number (not just a bound, as in Descartes' Law) of *distinct* real roots of $p(t)$ on any interval $t \in (a, b)$ such that $p(a) \neq 0, p(b) \neq 0$. On evaluating the members of this sequence at $t = a$ and $t = b$, the number N of distinct roots on (a, b) is given in terms of the numbers of sign variations in the resulting values by

$$N = V(\phi_0(a), \phi_1(a), \dots, \phi_r(a)) - V(\phi_0(b), \phi_1(b), \dots, \phi_r(b)).$$

Each distinct real root on (a, b) contributes *once* to N here — not according to its multiplicity, as in Descartes' Law.

Finally, we discuss the *partial fraction decomposition* of rational functions. The problem is to express a given rational function $r(t) = p(t)/q(t)$ as the sum of certain “simpler” rational functions, with denominators of lower degree.

To accomplish this, the denominator $q(t)$ must first be factorized. We may seek irreducible real factors (linear or quadratic) or complex factors (linear), and these factors may be simple or multiple. It is simpler in certain respects to use the factorization over complex numbers, which has the form

$$q(t) = \prod_{j=1}^N (t - r_j)^{m_j}$$

where r_1, \dots, r_N are the N distinct roots of $q(t)$, real or complex conjugate pairs, and m_1, \dots, m_N are their respective multiplicities.

The partial fraction decomposition can then be written in the form

$$\frac{p(t)}{q(t)} = \sum_{j=1}^N \sum_{k=1}^{m_j} \frac{C_{jk}}{(t - r_j)^k}. \quad (3.13)$$

Each root r_j of multiplicity m_j contributes terms $1/(t - r_j), \dots, 1/(t - r_j)^{m_j}$ to (3.13). Multiplying both sides of (3.13) by $(t - r_j)^{m_j}$ and differentiating $m_j - k$ times, one can verify that the coefficients C_{jk} are given by

$$C_{jk} = \frac{1}{(m_j - k)!} \left. \frac{d^{m_j - k}}{dt^{m_j - k}} (t - r_j)^{m_j} \frac{p(t)}{q(t)} \right|_{t=r_j}$$

for $j = 1, \dots, N$ and $k = 1, \dots, m_j$, where a derivative of order 0 is simply the function itself. Thus, for a simple root r_j with $m_j = 1$, we have

$$C_{j1} = \left. (t - r_j) \frac{p(t)}{q(t)} \right|_{t=r_j}.$$

Partial fraction expansions of rational functions play an important role in algorithms for their systematic integration. In this context, the coefficients C_{11}, \dots, C_{N1} have a special significance — they are called the *residues* of the rational function $p(t)/q(t)$ at its distinct poles r_1, \dots, r_N . We will encounter them again in Chaps. 4 and 16.

4

Complex Numbers

Wessel’s development [of complex numbers] proceeded rather directly from geometric problems, through geometric–intuitive reasoning, to an algebraic formula. Argand began with algebraic quantities and sought a geometric representation for them. . . . Wessel’s initial formulation was remarkably clear, direct, concise and modern. It is regrettable that it was not appreciated for nearly a century and hence did not have the influence it merited.

Phillip S. Jones, “Caspar Wessel,” *Dictionary of Scientific Biography*

Complex numbers are indispensable tools for modern science and technology, and the emergence of fields such as quantum mechanics, signal processing, and control theory is inconceivable without a complete theory of complex variables. Nonetheless, complex numbers were slow to secure widespread acceptance, due to persistent philosophical concerns over the “existence” of $i = \sqrt{-1}$.

It was the *geometrical interpretation* of complex numbers as points in the Euclidean plane, coupled with their remarkable *utility* in diverse contexts, that ultimately won their universal recognition. This utility becomes apparent once again in Chap. 19, where the complex numbers offer a compact and elegant model for planar Pythagorean–hodograph curves, that greatly facilitates the formulation of algorithms for the construction and analysis of these curves.

4.1 Caspar Wessel

It has been recognized since antiquity that not all quadratic equations admit real solutions. During the Renaissance, the Italian mathematicians Scipione del Ferro (1465–1526), Niccolo Fontana (1500–1577) — commonly known as Tartaglia, “the stammerer” — and Girolamo Cardano (1501–1576) found the solution to cubic equations, and discovered that it required intermediate use of complex numbers even in cases where all three roots are real (see §3.3).

In that era, such discoveries were often held as closely-guarded secrets, to ward off potential competitors for patronage or academic positions.

Caspar Wessel (1745–1818), a little-known Norwegian surveyor, was the first to propose the idea that complex numbers may be described graphically as points in the Euclidean plane \mathbb{R}^2 , and their sums and products then admit intuitive geometrical interpretations that instill a greater degree of comfort in their use. He propounded these ideas in his paper *Om directionens analytiske betegning, et forsøg, anvendt fornemmelig til plane og sphæriske polygoners oplosning* (On the analytical representation of direction: an attempt, applied chiefly to the solution of plane and spherical polygons), presented in March 1797 to the Royal Danish Academy by Johannes Nicolaus Tetens, Professor of Mathematics and Philosophy in Copenhagen, and published [465] in the Academy's *Mémoires* for 1799 (see Fig. 4.1). Sadly, his efforts were largely ignored, and the geometrical interpretation of complex numbers is commonly known as the *Argand diagram* or the *Gaussian plane* after later investigations by the Swiss book-keeper Jean Robert Argand (1768–1822) and the German mathematician Karl Friedrich Gauss (1777–1855).

Wessel's modest yet remarkable paper provides the first clear exposition of vector addition, and of the multiplication of complex numbers by taking the product of the magnitudes and the sum of the polar angles. After lapsing into obscurity for a century, it was re-published by his compatriot Sophus Lie

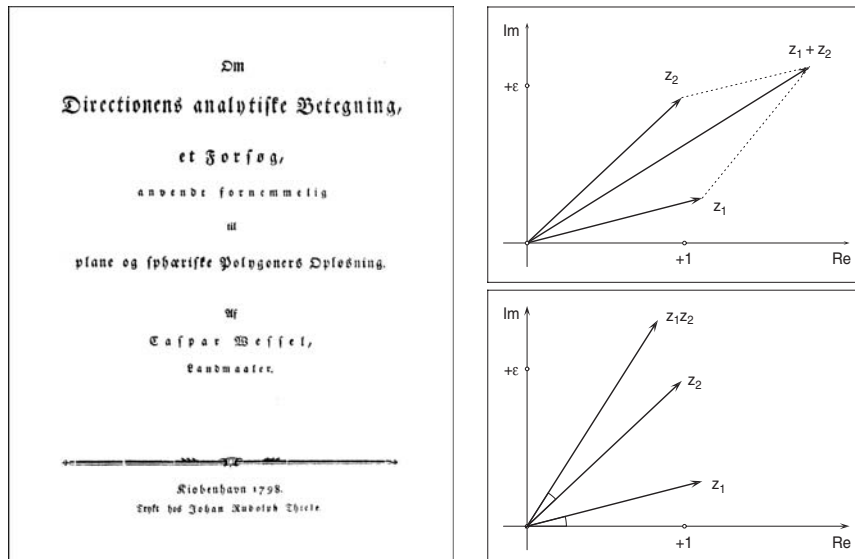


Fig. 4.1. Left: Wessel's paper *Om Directionens analytiske Betegning* (reproduced with permission from the Special Collections Library, University of Michigan). Right: Wessel's proposals for the addition and multiplication of directed line segments.

in 1895, and translated into French in 1897 (a complete English translation appeared only in 1999). Wessel begins [465] by posing the question:

... how may we represent direction analytically; that is, how shall we express right lines so that in a single equation involving one unknown line and others known, both the length and direction of the unknown line may be expressed?

Concerning the addition of directed line segments, he says:

Two right lines are added if we unite them in such a way that the second line begins where the first one ends, and then pass a right line from the first to the last point of the united lines.

For the product of directed line segments, he first multiplies their lengths to obtain its magnitude, while for its direction he proposes a logical extension of common experience with positive and negative real numbers, considered to make angles 0 and π with the real axis:

Firstly, the factors shall have such a direction that they both can be placed in the same plane with the positive unit.

Secondly, as regards length, the product shall be to one factor as the other factor is to the unit.

Finally, if we give the positive unit, the factors, and the product a common origin, the product shall, as regards its direction, lie in the plane of the unit and the factors and diverge from the one factor as many degrees, and on the same side, as the other factor diverges from the unit, so that the direction angle of the product, or its divergence from the positive unit, is equal to the sum of the direction angles of the factors.

Wessel suggests that “it seems not only permissible, but actually profitable, to make use of operations that apply to other lines than the equal (those of the same direction) and the opposite.” To represent directed line segments he uses numbers of the form $a + \epsilon b$, where ϵ denotes a unit that is orthogonal to the real axis. Then, from the above prescription for products of lines, he infers algebraically that ϵ must be the imaginary unit:

Let +1 designate the positive rectilinear unit and $+\epsilon$ a certain other unit perpendicular to the positive unit and having the same origin; then the direction angle of +1 is equal to 0° , that of -1 to 180° , that of $+\epsilon$ to 90° , and that of $-\epsilon$ to 270° . By the rule that the direction angle of a product equals the sum of the angles of the factors, we have $(+1)(+1) = +1$; $(+1)(-1) = -1$; ... $(+\epsilon)(+\epsilon) = -1$; ... it is seen that ϵ is equal to $\sqrt{-1}$...

Wessel's aspirations to explore geometrical algebras beyond complex numbers — e.g., lines in space — are apparent in his paper, although these ideas were not elaborated upon, since he "... accepted the advice of men of judgement, that in this paper both the nature of the contents and plainness of exposition demand that the reader be not burdened with concepts so abstract." Further background on the development of complex numbers may be found in [339].

Wessel's purpose was to employ complex numbers as tools in the solution of practical geometry problems, such as those encountered in surveying. But the converse view now predominates — i.e., the geometrical interpretation of complex numbers is used to obtain insight into problems of complex analysis. One of the few books that has championed the solution of analytic geometry problems using complex variables, Zwikker [480], is now out of print.

4.2 Elementary Properties

We assume the reader is familiar with the basic properties of complex numbers expressed in Cartesian and polar form, $\mathbf{z} = x + iy = r e^{i\theta} = r(\cos \theta + i \sin \theta)$. Here $x = \text{Re}(\mathbf{z})$ and $y = \text{Im}(\mathbf{z})$ are the *real* and *imaginary* parts of \mathbf{z} , while $r = |\mathbf{z}| = \sqrt{x^2 + y^2}$ and $\theta = \arg(\mathbf{z}) = \tan^{-1} y/x$ are its *modulus* and *argument*. The symbol i represents $\sqrt{-1}$. The Cartesian form is better suited to addition,

$$\mathbf{z}_1 + \mathbf{z}_2 = (x_1 + iy_1) + (x_2 + iy_2) = (x_1 + x_2) + i(y_1 + y_2),$$

while the polar form gives a more intuitive perspective on multiplication

$$\mathbf{z}_1 \mathbf{z}_2 = (r_1 e^{i\theta_1})(r_2 e^{i\theta_2}) = r_1 r_2 e^{i(\theta_1 + \theta_2)},$$

in accordance with Wessel's geometrical prescriptions. Using the property that $i^2 = -1$, multiplication in the Cartesian form is straightforward,

$$\mathbf{z}_1 \mathbf{z}_2 = (x_1 + iy_1)(x_2 + iy_2) = (x_1 x_2 - y_1 y_2) + i(x_1 y_2 + x_2 y_1),$$

but addition in the polar form is cumbersome and unenlightening. Thus, it is profitable to employ both forms, and switch between them as appropriate.

The polar form leads to *de Moivre's theorem*,

$$(\cos \theta + i \sin \theta)^n = \cos n\theta + i \sin n\theta,$$

and hence to identification of the n^{th} roots of a complex number $\mathbf{z} = r e^{i\theta}$ as

$$\mathbf{z}_k = r^{1/n} \left[\cos \left(\frac{\theta + k2\pi}{n} \right) + i \sin \left(\frac{\theta + k2\pi}{n} \right) \right], \quad k = 0, \dots, n-1.$$

For $\mathbf{z} = 1$, in particular, we obtain the n^{th} roots of unity as

$$\cos \left(\frac{k2\pi}{n} \right) + i \sin \left(\frac{k2\pi}{n} \right), \quad k = 0, \dots, n-1.$$

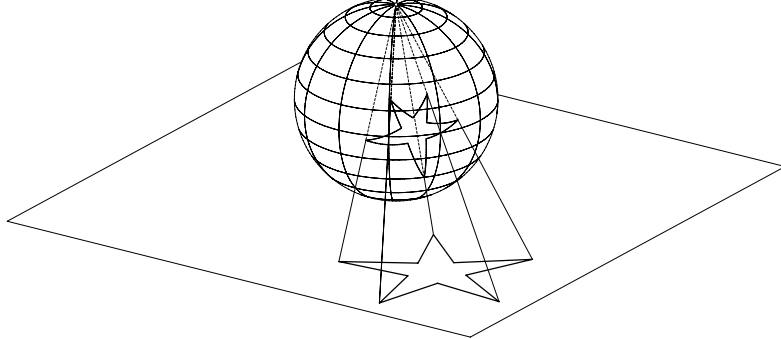


Fig. 4.2. Visualization of the “extended” complex plane by *stereographic projection* from the north pole of a sphere S whose south pole touches the complex plane at $\mathbf{z} = 0$. This mapping is one-to-one — except that all “infinitely distant points” are mapped, regardless of direction, to a single point on S (namely, the north pole).

Any complex number $\mathbf{z} = x + iy = r e^{i\theta}$ has a *conjugate*, $\bar{\mathbf{z}} = x - iy = r e^{-i\theta}$, so that $\mathbf{z}\bar{\mathbf{z}} = |\mathbf{z}|^2$. Using the conjugate, we can express the ratio $\mathbf{z}_1/\mathbf{z}_2$ as

$$\frac{\mathbf{z}_1}{\mathbf{z}_2} = \frac{\mathbf{z}_1\bar{\mathbf{z}}_2}{|\mathbf{z}_2|^2} = \frac{(x_1x_2 + y_1y_2) + i(x_2y_1 - x_1y_2)}{x_2^2 + y_2^2} = \frac{r_1}{r_2} e^{i(\theta_1 - \theta_2)}.$$

We can even define division in the case $\mathbf{z}_2 = 0$ upon introducing the *extended complex plane*, by appending the single value ∞ to the finite complex numbers. The *stereographic projection* offers an intuitive way of visualizing the extended complex plane. Consider a sphere S whose “south pole” touches the complex plane at $\mathbf{z} = 0$. Rays that connect the “north pole” to any point \mathbf{z} of the plane will pierce S at a *unique* location, except that all infinite points \mathbf{z} correspond to the *same* location — namely, the north pole — on S . Thus, the points of S provide a *representation* for the extended complex plane (see Fig. 4.2).

The complex numbers have the algebraic structure of a field, and obey all the familiar rules of real arithmetic. In fact, they are the *only* example of “higher-dimensional” numbers with this property. On progressing to the four-dimensional *quaternions* in Chap. 5, we must relinquish the commutative nature of products: the *order* of the terms in a product influences its value.

4.3 Functions of Complex Variables

We are familiar with the process of graphing a real-valued function $f(x)$ of a real variable x — i.e., drawing the locus of a point with Cartesian coordinates (x, y) where x is the independent variable or *abscissa*, and $y = f(x)$ is the corresponding function value or *ordinate*. If we substitute a *complex* number \mathbf{z} in the function f , the value $\mathbf{w} = f(\mathbf{z})$ is, in general, also a complex number. The problem of defining a “graph” for such a complex-valued function of a

complex variable is not so simple: expressing the independent and dependent variables in terms of real and imaginary parts as $\mathbf{z} = x + iy$ and $\mathbf{w} = u + iv$, we see that the perspective of a *four*-dimensional real Euclidean space — with axes labelled x, y, u, v — is required to “visualize” this function.

Since humans possess limited ability to perceive, sketch, or analyze four-dimensional configurations, a different interpretation of the equation $\mathbf{w} = f(\mathbf{z})$ is appropriate. Namely, we regard this relation as *a mapping of the Euclidean plane into itself*, that takes each point with Cartesian coordinates $(x, y) = (\text{Re}(\mathbf{z}), \text{Im}(\mathbf{z}))$ to an *image point* with coordinates $(u, v) = (\text{Re}(\mathbf{w}), \text{Im}(\mathbf{w}))$. Thus, a curve or region in the plane will be mapped by f to an image curve or region that has, in general, a different shape and location.

To aid in visualization, any given geometrical configuration and its image may be drawn in two “separate” planes, using Cartesian coordinates labelled (x, y) and (u, v) respectively. Of special interest are those curves in the (u, v) plane that are the images of the coordinate lines $x = \text{constant}$, $y = \text{constant}$ — and, conversely, those curves in the (x, y) plane that map into the lines $u = \text{constant}$, $v = \text{constant}$. These families of *level curves* convey some idea of the correspondence between points in the \mathbf{z} and \mathbf{w} planes — see Fig. 4.3 (note that, in general, the correspondence is *not* one-to-one).

For the preceding interpretation, the coordinates (x, y) and (u, v) in the \mathbf{z} -plane and \mathbf{w} -plane are both *Cartesian* coordinates. Since a point \mathbf{z} and its image \mathbf{w} are usually distinct, they typically have *different* numerical values

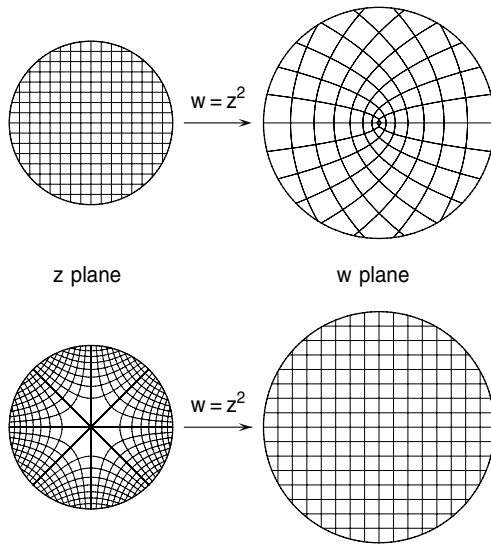


Fig. 4.3. The map $\mathbf{w} = \mathbf{z}^2$, with $\mathbf{z} = x + iy$ and $\mathbf{w} = u + iv$. Lines of constant x and y in the \mathbf{z} plane map into two families of confocal parabolae in the \mathbf{w} plane. Conversely, the images of the two families of rectangular hyperbolae asymptotic to $x = 0$, $y = 0$ or $x = \pm y$ in the \mathbf{z} plane are lines of constant u and v in the \mathbf{w} plane.

for their Cartesian coordinates (x, y) and (u, v) . An alternative geometrical interpretation of the map $\mathbf{w} = f(\mathbf{z})$ is to regard the real and imaginary parts of $f(\mathbf{z}) = u(x, y) + i v(x, y)$ as defining a transformation $(x, y) \rightarrow (\zeta, \eta)$ from Cartesian to curvilinear coordinates according to

$$\zeta = u(x, y) \quad \text{and} \quad \eta = v(x, y). \quad (4.1)$$

Then \mathbf{w} is the image of \mathbf{z} if the *curvilinear* coordinates (ζ, η) of the latter, as obtained from its Cartesian coordinates (x, y) by expressions (4.1), have the same numerical values as the *Cartesian* coordinates (u, v) of the former.

Consider, for example, the simple function

$$\mathbf{w} = f(\mathbf{z}) = \mathbf{z}^2, \quad (4.2)$$

which corresponds to the mapping

$$(x, y) \rightarrow (u, v) = (x^2 - y^2, 2xy).$$

Interpreting both (x, y) and (u, v) as Cartesian coordinates, we see that the point $(x, y) = (2, 1)$ is mapped to the point $(u, v) = (3, 4)$. However, we may also consider the system of curvilinear coordinates defined by

$$\zeta = u(x, y) = x^2 - y^2 \quad \text{and} \quad \eta = v(x, y) = 2xy.$$

As seen in Fig. 4.3, the level curves $\zeta = \text{constant}$ and $\eta = \text{constant}$ in the \mathbf{z} -plane then correspond to two families of rectangular hyperbolae. We note that the point \mathbf{z} has *curvilinear* coordinates $(\zeta, \eta) = (3, 4)$ that are identical to the *Cartesian* coordinates $(u, v) = (3, 4)$ of its image point \mathbf{w} . Note that the mapping (4.2) is not one-to-one since, if \mathbf{w}_* is the image of \mathbf{z}_* , it is also the image of $-\mathbf{z}_*$. In fact, the entire \mathbf{w} -plane can be obtained from just the half-plane lying to one side of any line through $\mathbf{z} = 0$. If we do not restrict \mathbf{z} , the map (4.2) gives a “double covering” of the \mathbf{w} plane.

4.4 Differentiation and Integration

If the function $f(\mathbf{z})$ is *analytic*, i.e., its derivative with respect to the complex variable \mathbf{z} is defined at each point and satisfies

$$\frac{df}{d\mathbf{z}} \neq 0$$

for (almost) all \mathbf{z} , the mapping defined by $\mathbf{w} = f(\mathbf{z})$ exhibits some attractive geometrical properties, and thus merits a special name — it is known as a *conformal map*. Exceptionally, cases where $df/d\mathbf{z}$ vanishes at certain points or loci may also be allowed, and special care must be exercised in considering such locations. To properly appreciate these ideas, we must first review the concept of differentiation for a function of a complex variable.

To differentiate a function $f(x)$ of a real variable, we compute the limit of the ratio of corresponding increments $\Delta f = f(x) - f(x_0)$ and $\Delta x = x - x_0$ in the function value and independent variable at a given point x_0 . This limit may be obtained with x approaching x_0 from either *smaller* or *larger* values, and it should not matter which we choose if $f(x)$ is to be considered differentiable at x_0 — both should give the same derivative value there.

For a function $f(\mathbf{z})$ of a *complex* variable, an extra complication arises in defining its derivative: we may approach a given complex value $\mathbf{z}_0 = x_0 + i y_0$ of the independent variable along *infinitely many directions* in the complex plane — not just from the “left” or “right” as in the real-variable case. If the function does not satisfy certain criteria, the limiting ratio of corresponding (complex) increments in f and in \mathbf{z} may depend upon the direction in which we approach \mathbf{z}_0 . Such behavior is unacceptable — for the function $f(\mathbf{z})$ to be considered *differentiable with respect to its complex argument* at the point \mathbf{z}_0 of interest, the ratio

$$\frac{f(\mathbf{z}) - f(\mathbf{z}_0)}{\mathbf{z} - \mathbf{z}_0} \quad (4.3)$$

must have a finite (complex) limiting value as $\mathbf{z} \rightarrow \mathbf{z}_0$ that is *independent* of the particular direction along which \mathbf{z} approaches \mathbf{z}_0 .

A sufficient and necessary condition for such direction-independence of the complex derivative is that the real and imaginary parts of $f(\mathbf{z})$, regarded as bivariate real functions $u(x, y)$ and $v(x, y)$, should satisfy a system of partial differential equations known as the *Cauchy–Riemann equations*¹

$$\frac{\partial u}{\partial x} = \frac{\partial v}{\partial y} \quad \text{and} \quad \frac{\partial u}{\partial y} = -\frac{\partial v}{\partial x}. \quad (4.4)$$

The complex function $f(\mathbf{z})$ is said to be *analytic* at each point \mathbf{z}_0 where the Cauchy–Riemann relations are satisfied, and the unique limit of the ratio (4.3) as \mathbf{z} approaches \mathbf{z}_0 along any direction is then its *complex derivative* $d\mathbf{f}/d\mathbf{z}$ at that point. Implicit in this definition is the requirement that the partial derivatives of u and v in equation (4.4) be defined at \mathbf{z}_0 .

Note that when conditions (4.4) are satisfied, the complex-derivative of f may be written in terms of partial derivatives with respect to only the real part x or the imaginary part y of \mathbf{z} , as

$$\frac{d\mathbf{f}}{d\mathbf{z}} = \frac{\partial u}{\partial x} + i \frac{\partial v}{\partial x} = \frac{\partial v}{\partial y} - i \frac{\partial u}{\partial y}. \quad (4.5)$$

We say $f(\mathbf{z})$ is analytic in a region Ω of the complex plane if it is analytic at each point $\mathbf{z} \in \Omega$. If Ω is the entire complex plane, we simply say that “ $f(\mathbf{z})$ is analytic” (*holomorphic* is also used as a synonym for analytic). Most “elementary” (polynomial, rational, trigonometric, hyperbolic, exponential,

¹ Named for the founders of the theory of functions of a complex variable, Augustin–Louis Cauchy (1789–1857) and Georg Friedrich Bernhard Riemann (1826–1866).

logarithmic, etc.) functions we are familiar with in the real-variable context prove to be analytic at nearly all points, on substituting a complex argument $\mathbf{z} = x + iy$ in lieu of the real variable (verify this for some simple examples).

Suppose now we wish to integrate a function $f(\mathbf{z})$ between specified limits \mathbf{a} and \mathbf{b} of the complex variable \mathbf{z} . The two-dimensional nature of complex variables permits an infinitude of paths from \mathbf{a} to \mathbf{b} , other than the straight line between them, along which the integration may be performed. However, if $f(\mathbf{z})$ is analytic in a subset Ω of the complex plane containing \mathbf{a} and \mathbf{b} , this freedom of choice does not matter — all integration paths C within Ω yield *exactly the same complex value* for the integral of $f(\mathbf{z})$ from \mathbf{a} to \mathbf{b} .

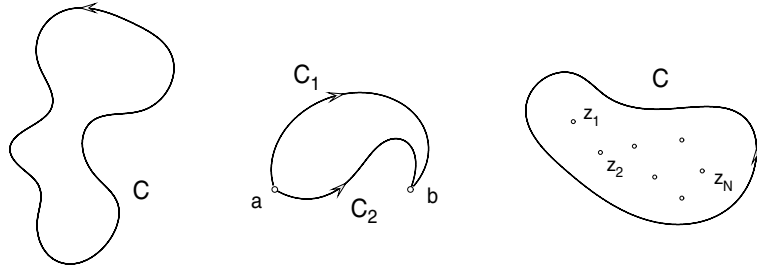


Fig. 4.4. Left: the integral of a function $f(\mathbf{z})$ around a closed path C in the complex plane is zero if $f(\mathbf{z})$ is analytic in a domain Ω containing C . Center: the integral of $f(\mathbf{z})$ between two points \mathbf{a} and \mathbf{b} is independent of the integration path within Ω between them. Right: the integral of a rational function $f(\mathbf{z})$ around a closed path C depends only on the behavior of $f(\mathbf{z})$ at its poles $\mathbf{z}_1, \dots, \mathbf{z}_N$ that lie within C .

This property of *path independence* of the integral of an analytic function $f(\mathbf{z})$ between given points \mathbf{a} and \mathbf{b} in the complex plane is a consequence of *Cauchy's theorem*, which states that if $C \in \Omega$ is a *closed path*,² the integral of $f(\mathbf{z})$ along it (see Fig. 4.4) vanishes:

$$\oint_C f(\mathbf{z}) \, d\mathbf{z} = 0,$$

where the circle superposed on the integral indicates that integration occurs along a closed path. This is one of the most fundamental results in complex analysis, and is related to the fact that $f(\mathbf{z})$ must satisfy the Cauchy–Riemann relations within Ω . If we break the closed integration path into components P and Q at distinct points \mathbf{a} and \mathbf{b} on C , so that $C = P \cup Q$, we have

$$\oint_C f(\mathbf{z}) \, d\mathbf{z} = \int_P f(\mathbf{z}) \, d\mathbf{z} + \int_Q f(\mathbf{z}) \, d\mathbf{z} = 0,$$

P being a path from \mathbf{a} to \mathbf{b} , and Q a path from \mathbf{b} to \mathbf{a} . Now if \tilde{P} is the *reversal* of path Q — i.e., the same path traversed in the opposite sense — then \tilde{P} is

² We assume here that closed paths have an anti-clockwise orientation.

a path from \mathbf{a} to \mathbf{b} , and the integral along this path is the negative of that along Q . Therefore, Cauchy's theorem implies that

$$\int_{\tilde{P}} f(\mathbf{z}) \, d\mathbf{z} = \int_P f(\mathbf{z}) \, d\mathbf{z}$$

for any two paths P, \tilde{P} between \mathbf{a} and \mathbf{b} lying in the domain Ω within which $f(\mathbf{z})$ is analytic. An equivalent concept is the invariance of a complex integral under *deformation of the integration path* — namely, if P is a path with fixed end points \mathbf{a} and \mathbf{b} , we may deform it into any other path \tilde{P} from \mathbf{a} to \mathbf{b} within Ω , without altering the value of the integral of $f(\mathbf{z})$.

What happens if we integrate a function $f(\mathbf{z})$ around a closed path C , and that function is *not* analytic at every point within C ? A typical instance is the case of a *rational function* — i.e., the ratio of two polynomials (see §3.5). The roots of the denominator polynomial are called the *poles* of the rational function — it is not analytic at such points, since the complex ratio (4.3) does not have a finite limit as $\mathbf{z} \rightarrow \mathbf{z}_0$ when \mathbf{z}_0 is a pole. Suppose $f(\mathbf{z})$ has just a single pole \mathbf{z}_0 within Ω . We can form a new domain $\tilde{\Omega} = \Omega - \delta_0$ by removing a small disk δ_0 of radius r centered on \mathbf{z}_0 , and $f(\mathbf{z})$ is then analytic in $\tilde{\Omega}$. By the invariance under path deformation, we can shrink the path C around δ_0 without changing the integral, and we can also make r as small as we please. This means that the integral along any closed path within Ω that contains \mathbf{z}_0 depends only on the behavior of $f(\mathbf{z})$ at \mathbf{z}_0 .

The value of the integral about the pole \mathbf{z}_0 depends on what is called the *residue* of $f(\mathbf{z})$ at \mathbf{z}_0 — it corresponds to the coefficient of the $1/(\mathbf{z} - \mathbf{z}_0)$ term in the partial fraction expansion of $f(\mathbf{z})$. If \mathbf{z}_0 is of multiplicity m as a pole of $f(\mathbf{z})$, the residue may be computed (see §3.5) from the expression

$$\text{residue}_{\mathbf{z}=\mathbf{z}_0} f(\mathbf{z}) = \frac{1}{(m-1)!} \left. \frac{d^{m-1}}{d\mathbf{z}^{m-1}} (\mathbf{z} - \mathbf{z}_0)^m f(\mathbf{z}) \right|_{\mathbf{z}=\mathbf{z}_0}.$$

The integral along a closed contour C containing \mathbf{z}_0 is $2\pi i$ times the residue of $f(\mathbf{z})$ at that pole. This may be generalized (see Fig. 4.4) to the case where the contour C contains several poles $\mathbf{z}_1, \dots, \mathbf{z}_N$ of $f(\mathbf{z})$, to obtain

$$\oint_C f(\mathbf{z}) \, d\mathbf{z} = 2\pi i \sum_{k=1}^N \text{residue}_{\mathbf{z}=\mathbf{z}_k} f(\mathbf{z}),$$

a result known as *Cauchy's residue theorem*. This is an extremely powerful result, that can facilitate the calculation of definite integrals over the real line in cases where other methods fail. We will return to it in Chap. 16.

4.5 Geometry of Conformal Maps

The map $\mathbf{w} = f(\mathbf{z})$ is *conformal* at the point \mathbf{z}_0 if it is analytic at that point and its derivative there satisfies $d\mathbf{f}/d\mathbf{z} \neq 0$. Geometrically, this means that:

- (a) if two curves Z_1 and Z_2 intersect at an angle θ at the point \mathbf{z}_0 , the images $W_1 = f(Z_1)$ and $W_2 = f(Z_2)$ of these curves will intersect at the image point $\mathbf{w}_0 = f(\mathbf{z}_0)$ at angle θ also (*isogonality* property);
- (b) if ds_1 and ds_2 are the lengths of infinitesimal segments of Z_1 and Z_2 at the intersection point \mathbf{z}_0 , the lengths $d\ell_1$ and $d\ell_2$ of their image segments will satisfy $d\ell_1 : d\ell_2 = ds_1 : ds_2$ (*isometry* property).

In other words, *angles* and *relative sizes* are preserved “locally” by the map $\mathbf{w} = f(\mathbf{z})$, in a neighborhood of each point where f is conformal — i.e., any geometrical configuration in the \mathbf{z} -plane and its corresponding image in the \mathbf{w} -plane are *locally* “similar” to each other.

We may deduce the above properties as follows. Let $\mathbf{z}_1(t)$ and $\mathbf{z}_2(t)$ be two complex-valued differentiable functions of a real parameter t , that describe smooth loci Z_1 and Z_2 in the plane. We suppose these loci intersect at a point \mathbf{z}_* corresponding to values τ_1 and τ_2 of the parameter: $\mathbf{z}_* = \mathbf{z}_1(\tau_1) = \mathbf{z}_2(\tau_2)$. In order to analyze this intersection point, we express the curve parametric derivatives there in polar form as

$$\mathbf{z}'_1(\tau_1) = \sigma_1 \exp(i\theta_1) \quad \text{and} \quad \mathbf{z}'_2(\tau_2) = \sigma_2 \exp(i\theta_2).$$

Here σ_1 and σ_2 represent the *parametric speeds* (i.e., the rates of change of arc length with respect to the parameter t) of the two curves $\mathbf{z}_1(t)$ and $\mathbf{z}_2(t)$ at their point of intersection, while the angles θ_1 and θ_2 indicate the curve *tangent directions* at that point. Thus, the complex ratio

$$\mathbf{k} = \frac{\mathbf{z}'_1(\tau_1)}{\mathbf{z}'_2(\tau_2)} = \frac{\sigma_1}{\sigma_2} \exp(i(\theta_1 - \theta_2)) \quad (4.6)$$

incorporates the following information: (i) its *magnitude* indicates the ratio of arc lengths of infinitesimal segments — corresponding to a fixed parameter increment dt — of $\mathbf{z}_1(t)$ and $\mathbf{z}_2(t)$ about the intersection point; and (ii) its *argument* gives the angle between $\mathbf{z}_1(t)$ and $\mathbf{z}_2(t)$ at that point.

We now consider the mapping of the curves $\mathbf{z}_1(t)$ and $\mathbf{z}_2(t)$ by an analytic function $f(\mathbf{z})$. The image curves W_1 and W_2 are given by

$$\mathbf{w}_1(t) = f(\mathbf{z}_1(t)) \quad \text{and} \quad \mathbf{w}_2(t) = f(\mathbf{z}_2(t)),$$

and they evidently intersect at the image point $\mathbf{w}_* = f(\mathbf{z}_*)$. The parametric derivatives of these image curves at the point \mathbf{w}_* may be computed using the *chain rule* for differentiating a “function of a function” — namely:

$$\mathbf{w}'_1(\tau_1) = \left. \frac{df}{d\mathbf{z}} \right|_{\mathbf{z}_*} \mathbf{z}'_1(\tau_1) \quad \text{and} \quad \mathbf{w}'_2(\tau_2) = \left. \frac{df}{d\mathbf{z}} \right|_{\mathbf{z}_*} \mathbf{z}'_2(\tau_2).$$

If $df/d\mathbf{z} \neq 0$ at the intersection point \mathbf{z}_* , these derivatives clearly also have the complex ratio \mathbf{k} given by (4.6). Hence, the image curves intersect at the same angle as the original curves, and have the same ratio of parametric speeds.

4.6 Harmonic Functions

In two dimensions, the *Laplacian* is the differential operator

$$\Delta = \frac{\partial^2}{\partial x^2} + \frac{\partial^2}{\partial y^2},$$

which may be applied to any twice-differentiable bivariate function $\phi(x, y)$ of the Cartesian coordinates x and y . If such a function satisfies the equation

$$\Delta\phi \equiv 0, \tag{4.7}$$

it is known as a *harmonic* or *potential* function. The *Laplace equation* (4.7) is of fundamental importance in a variety of physical problems characterized by the fact that there is no net “flux” of a vector field through the boundary $\partial\Omega$ of any region Ω that does not contain *sources* or *sinks* of that flux.

Examples include the determination of velocity fields for incompressible, inviscid fluid flow and of electrostatic or gravitational force fields subject to specified conditions at the boundary $\partial\Omega$ of the volume Ω of interest. In these contexts, the function ϕ satisfying (4.7) is a *velocity* potential or *electrostatic* or *gravitational* potential, and its gradient $\nabla\phi$ is a velocity or force field.

By differentiating the Cauchy–Riemann relations (4.4) one can easily verify that the real and imaginary parts $u(x, y)$ and $v(x, y)$ of any analytic function $f(\mathbf{z})$ of a complex variable $\mathbf{z} = x + iy$ must be harmonic functions. Thus, complex-variable methods provide a rich class of “trial” harmonic functions, which we can form linear combinations of in attempting to satisfy prescribed boundary conditions. *Dirichlet* boundary conditions amount to specifying the value of the potential function ϕ on $\partial\Omega$, while *Neumann* boundary conditions involve specifying the normal component $\mathbf{n} \cdot \nabla\phi$ of the corresponding vector field (\mathbf{n} being the unit normal to $\partial\Omega$ at each point).

4.7 Conformal Transplants

Complex-variable methods can also be used to simplify the *geometry* of the region Ω of interest, facilitating satisfaction of constraints on solutions to (4.7) along the boundary $\partial\Omega$. This method, known as the *conformal transplantation* of harmonic functions, is based on the following reasoning.

Suppose $\mathbf{w} = f(\mathbf{z})$ specifies a conformal map between the complex planes $\mathbf{z} = x + iy$ and $\mathbf{w} = u + iv$, and let Π be the image in the \mathbf{w} -plane of a given domain Ω of interest in the \mathbf{z} -plane: $\Pi = f(\Omega)$. We are concerned here with cases in which the boundary curve $\partial\Pi$ of the image region is “simpler” than the original boundary curve $\partial\Omega$ and the desired boundary conditions are thus easier to impose in the \mathbf{w} -plane than in the \mathbf{z} -plane.

Suppose $\phi(x, y)$ and $\psi(u, v)$ are functions of the coordinates $x = \text{Re}(\mathbf{z})$, $y = \text{Im}(\mathbf{z})$ and $u = \text{Re}(\mathbf{w})$, $v = \text{Im}(\mathbf{w})$ in the \mathbf{z} and \mathbf{w} planes, respectively.

We call $\psi(u, v)$ the *conformal transplant* of $\phi(x, y)$ under the map $\mathbf{w} = f(\mathbf{z})$ if the functions ϕ and ψ have identical values at corresponding points \mathbf{z} and \mathbf{w} of this map. In other words, when a point is mapped according to $\mathbf{z} \rightarrow \mathbf{w}$ it “carries” the value of the function ϕ with it, and these redistributed ϕ -values then define the transplanted function ψ . We will demonstrate that, if $\phi(x, y)$ is a harmonic function of x and y , i.e., it satisfies

$$\Delta_{\mathbf{z}}\phi = 0,$$

where $\Delta_{\mathbf{z}} = \partial^2/\partial x^2 + \partial^2/\partial y^2$ denotes the Laplacian in the \mathbf{z} -plane, then its conformal transplant $\psi(u, v)$ is a harmonic function of u and v satisfying

$$\Delta_{\mathbf{w}}\psi = 0,$$

where $\Delta_{\mathbf{w}} = \partial^2/\partial u^2 + \partial^2/\partial v^2$ is the Laplacian in the \mathbf{w} -plane.

Writing the function f in terms of its real and imaginary parts as

$$f(\mathbf{z}) = u(x, y) + i v(x, y),$$

the condition for ψ to be the transplant of ϕ under f may be expressed as

$$\phi(x, y) \equiv \psi(u(x, y), v(x, y)).$$

Using standard rules for partial differentiation, we have

$$\frac{\partial \phi}{\partial x} = \frac{\partial u}{\partial x} \frac{\partial \psi}{\partial u} + \frac{\partial v}{\partial x} \frac{\partial \psi}{\partial v},$$

and upon further differentiation

$$\frac{\partial^2 \phi}{\partial x^2} = \left(\frac{\partial u}{\partial x} \right)^2 \frac{\partial^2 \psi}{\partial u^2} + 2 \frac{\partial u}{\partial x} \frac{\partial v}{\partial x} \frac{\partial^2 \psi}{\partial u \partial v} + \left(\frac{\partial v}{\partial x} \right)^2 \frac{\partial^2 \psi}{\partial v^2} + \frac{\partial^2 u}{\partial x^2} \frac{\partial \psi}{\partial u} + \frac{\partial^2 v}{\partial x^2} \frac{\partial \psi}{\partial v}.$$

Adding the above to the analogous expression for the second derivative of ϕ with respect to y then gives

$$\begin{aligned} \Delta_{\mathbf{z}}\phi &= \left[\left(\frac{\partial u}{\partial x} \right)^2 + \left(\frac{\partial u}{\partial y} \right)^2 \right] \frac{\partial^2 \psi}{\partial u^2} + \left[\left(\frac{\partial v}{\partial x} \right)^2 + \left(\frac{\partial v}{\partial y} \right)^2 \right] \frac{\partial^2 \psi}{\partial v^2} \\ &\quad + 2 \left[\frac{\partial u}{\partial x} \frac{\partial v}{\partial x} + \frac{\partial u}{\partial y} \frac{\partial v}{\partial y} \right] \frac{\partial^2 \psi}{\partial u \partial v} + \Delta_{\mathbf{z}}u \frac{\partial \psi}{\partial u} + \Delta_{\mathbf{z}}v \frac{\partial \psi}{\partial v}. \end{aligned}$$

Now since f is analytic, its real and imaginary parts are harmonic functions, and we have $\Delta_{\mathbf{z}}u = \Delta_{\mathbf{z}}v = 0$. We also note, by virtue of the Cauchy–Riemann relations (4.4), that the coefficient of the mixed second derivative $\partial^2 \psi / \partial u \partial v$ vanishes. Finally, from (4.5) we may write

$$\left(\frac{\partial u}{\partial x} \right)^2 + \left(\frac{\partial u}{\partial y} \right)^2 = \left(\frac{\partial v}{\partial x} \right)^2 + \left(\frac{\partial v}{\partial y} \right)^2 = \left| \frac{df}{d\mathbf{z}} \right|^2, \quad (4.8)$$

we hence deduce that the Laplacians of ϕ and of its conformal transplant ψ are related by

$$\Delta_{\mathbf{z}}\phi = \left| \frac{df}{d\mathbf{z}} \right|^2 \Delta_{\mathbf{w}}\psi.$$

Now the complex-derivative of f is non-vanishing if the map is conformal, and we therefore conclude that $\Delta_{\mathbf{z}}\phi = 0 \implies \Delta_{\mathbf{w}}\psi = 0$, i.e., the conformal transplant of a harmonic function is likewise a harmonic function.

Note that, by the Cauchy–Riemann equations (4.4), we can write (4.8) as

$$\left| \frac{df}{d\mathbf{z}} \right|^2 = \frac{\partial u}{\partial x} \frac{\partial v}{\partial y} - \frac{\partial u}{\partial y} \frac{\partial v}{\partial x},$$

which is simply the Jacobian (see §7.3.1) for the coordinate transformation (4.1) specified by the conformal map $\mathbf{w} = f(\mathbf{z})$. So the condition $df/d\mathbf{z} \neq 0$ guarantees that the map $(x, y) \rightarrow (u, v)$ is (locally) one-to-one.

Thus, conformal mapping allows us to solve two-dimensional potential problems by invoking a transformation that maps the domain of interest to one of simpler geometry, solving within that domain, and then mapping back to the original domain. A well-known example is the case of fluid flow around an airfoil, which may be regarded as a *Joukowski map* of a circle (see §4.8).

4.8 Some Simple Mappings

Given complex numbers $\mathbf{a}, \mathbf{b}, \mathbf{c}, \mathbf{d}$ such that $\mathbf{ad} - \mathbf{bc} \neq 0$, the mapping

$$\mathbf{w} = f(\mathbf{z}) = \frac{\mathbf{a}\mathbf{z} + \mathbf{b}}{\mathbf{c}\mathbf{z} + \mathbf{d}} \quad (4.9)$$

is known as a *Möbius transformation*, after the astronomer–mathematician³ August Ferdinand Möbius (1790–1868). It is also called a fractional linear (or bilinear) map. Since the derivative of f is

$$\frac{df}{d\mathbf{z}} = \frac{\mathbf{ad} - \mathbf{bc}}{(\mathbf{c}\mathbf{z} + \mathbf{d})^2},$$

the condition $\mathbf{ad} - \mathbf{bc} \neq 0$ ensures that the map (4.9) is conformal for all \mathbf{z} . If this condition is *not* satisfied, $f(\mathbf{z}) = \text{constant}$, since the numerator and denominator in (4.9) are then multiples of each other. The inverse

$$\mathbf{z} = f^{-1}(\mathbf{w}) = - \frac{\mathbf{d}\mathbf{w} - \mathbf{b}}{\mathbf{c}\mathbf{w} - \mathbf{a}},$$

³ Möbius, like his mentor Gauss, was a professor of *astronomy* [197]: “At that time, a mathematician was essentially a poor drudge whose time was spent pumping basic calculations into ill-prepared unmotivated pupils, or if more ambitious was at best an administrator, whereas an astronomer was a scientific professional.”

of the map (4.9) is evidently also a Möbius transformation. Moreover, one can verify that the successive application or “composition” of any two (or more) Möbius transformations yields a single overall Möbius transformation. Hence, the Möbius transformations have the algebraic structure of a *group*.

If $\mathbf{c} \neq 0$, the value $\mathbf{z} = -\mathbf{d}/\mathbf{c}$ is exceptional, since it is not mapped to a finite value by (4.9). To address this we invoke the extended complex plane, appending the value “ ∞ ” to the finite complex numbers (see §4.2) so that

$$f(-\mathbf{d}/\mathbf{c}) = \infty \quad \text{and} \quad \mathbf{a}/\mathbf{c} = f(\infty).$$

We may then regard (4.9) as defining a one-to-one mapping of the extended complex plane into itself. In fact, Möbius transformations are the *only* complex mappings that are one-to-one over the entire (extended) complex plane. To obtain one-to-one correspondence with any other form of f , it is necessary to restrict the domain of the independent variable \mathbf{z} .

The Möbius transformation maps the set of all straight lines and circles in the \mathbf{z} -plane into the set of all straight lines and circles in the \mathbf{w} -plane (note, however, that lines may be mapped into circles and vice-versa). In general, such a map has two *fixed points*, i.e., complex values \mathbf{z} such that $\mathbf{z} = f(\mathbf{z})$. They are the solutions of the quadratic equation

$$\mathbf{c}\mathbf{z}^2 + (\mathbf{d} - \mathbf{a})\mathbf{z} - \mathbf{b} = 0.$$

Möbius transformations encompass several simple mappings as special cases, including translations, rotations, scalings, and inversions.

We note that there are only *three* essential (complex) parameters in (4.9), since we can divide the numerator and denominator by any of the constants \mathbf{a} , \mathbf{b} , \mathbf{c} , \mathbf{d} (if non-zero) without changing $f(\mathbf{z})$. Correspondingly, a Möbius transformation can be found that maps any three specified points \mathbf{z}_1 , \mathbf{z}_2 , \mathbf{z}_3 to three other specified points \mathbf{w}_1 , \mathbf{w}_2 , \mathbf{w}_3 . The desired map is obtained by solving for \mathbf{w} in terms of \mathbf{z} from the “cross ratio” relation

$$\frac{(\mathbf{w} - \mathbf{w}_1)(\mathbf{w}_2 - \mathbf{w}_3)}{(\mathbf{w} - \mathbf{w}_3)(\mathbf{w}_2 - \mathbf{w}_1)} = \frac{(\mathbf{z} - \mathbf{z}_1)(\mathbf{z}_2 - \mathbf{z}_3)}{(\mathbf{z} - \mathbf{z}_3)(\mathbf{z}_2 - \mathbf{z}_1)}.$$

As another example, consider the *Joukowski transformation* defined by

$$\mathbf{w} = f(\mathbf{z}) = \mathbf{z} + \frac{1}{\mathbf{z}}. \quad (4.10)$$

As noted in §4.7, this maps a circle through one of the points $\mathbf{z} = \pm 1$ into an airfoil shape (Fig. 4.5). This map is conformal everywhere, except the two points $\mathbf{z} = \pm 1$. Without restrictions on \mathbf{z} , it gives a *double covering* of the \mathbf{w} -plane, since if \mathbf{w}_* is the image of \mathbf{z}_* , it is also the image of $1/\mathbf{z}_*$. For a one-to-one map, we must restrict \mathbf{z} to either of the domains $|\mathbf{z}| \leq 1$ or $|\mathbf{z}| \geq 1$.

With the polar form $\mathbf{z} = r \exp(i\theta)$ one can verify that the loci $r = \text{constant}$ and $\theta = \text{constant}$ (circles centered on the origin and radial lines through it) are

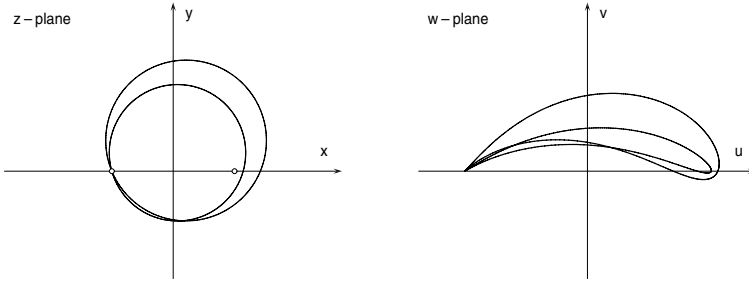


Fig. 4.5. The Joukowski map defined by equation (4.10) transforms any circle that passes through either of the points $\mathbf{z} = -1$ or $\mathbf{z} = +1$ into a cuspidal “airfoil” shape.

respectively mapped⁴ to families of confocal ellipses and hyperbolae that are mutually orthogonally. The circle $r = 1$ and the radial lines $\theta = 0, \theta = \pi/2$ are exceptions: they map to (portions of) the axes $\text{Im}(\mathbf{w}) = 0$ and $\text{Re}(\mathbf{w}) = 0$. The image in the \mathbf{w} -plane of a smooth curve in the \mathbf{z} -plane that passes through either of the points $\mathbf{z} = \pm 1$ is not, in general, a smooth curve.

Thus, using the method of conformal transplantation as described in §4.7, we can employ the Joukowski map to determine the nature of incompressible, inviscid flow over an airfoil section from the known solution to the simpler problem of such flow over a cylinder. In addition to the boundary condition $\mathbf{n} \cdot \nabla \phi = 0$ at the boundary, one usually makes the assumption that $\nabla \phi$ is constant (i.e., the flow is uniform) far from the body in question.

⁴ See [21] for an interesting discussion of the implications of this fact for the orbits of particles determined by power-law central force fields.

5

Quaternions

A school of “quaternionists” developed, which was led after Hamilton’s death by Peter Tait of Edinburgh and Benjamin Pierce of Harvard. Tait wrote 8 books on the quaternions, emphasizing their applications to physics. When Gibbs invented the modern notation for the dot and cross product, Tait condemned it as a “hermaphrodite monstrosity.” A war of polemics ensued, with luminaries such as Kelvin and Heaviside writing some devastating invective against quaternions. Ultimately the quaternions lost, and acquired a slight taint of disgrace from which they have never fully recovered.

John C. Baez, *The Octonions* [23]

The methods of three-dimensional vector analysis — *dot* and *cross* products, and the differential operators such as the *gradient*, *divergence*, and *curl* — are fundamental to modern science. It is not commonly appreciated, however, that these methods are actually a rather late development in mathematics: they devolved from a more-sophisticated theory, the algebra of the *quaternions*. We present here a brief introduction to quaternions and their use in describing an important set of geometrical transformations — namely, rotations in \mathbb{R}^3 . As we shall see in Chap. 22, this property of quaternions proves invaluable in the formulation of a sufficient-and-necessary characterization for Pythagorean hodographs in \mathbb{R}^3 , that is invariant under arbitrary spatial rotations.

5.1 Multi-dimensional Numbers

We noted in §4.2 that real and complex numbers are equivalent with regard to the rules for their algebraic manipulation: any result derived by algebraic operations on an expression in which the symbols represent real numbers will be equally true if, instead, we interpret them as complex numbers.

The Irish mathematician Sir William R. Hamilton (1805–1865) observed that, since the quantities “1” and “i” are qualitatively different in nature,

adding multiples of them to form $x + iy$ is like adding apples and oranges. To emphasize that $\mathbf{z} = x + iy$ is really a kind of “two-dimensional number,” he preferred to regard it as an *ordered pair* (x, y) of real numbers, the sums and products of such pairs being defined by the rules

$$(x_1, y_1) + (x_2, y_2) = (x_1 + x_2, y_1 + y_2),$$

$$(x_1, y_1)(x_2, y_2) = (x_1x_2 - y_1y_2, x_1y_2 + x_2y_1).$$

This purely formal interpretation — which defines a two-dimensional number system that mimics the one-dimensional real numbers in its behavior — also bypassed the controversy over the “existence” of $i = \sqrt{-1}$ that persisted¹ for years after the use of complex numbers became commonplace.

This “theory of algebraic couples” naturally motivated Hamilton to seek an algebra of *three*-dimensional numbers (i.e., triples of real numbers) whose sums are performed component-wise, and whose products are formulated so as to obey the commutative, associative, and distributive laws satisfied by the real and complex numbers. Hamilton devoted many years to this search and, although unsuccessful, his efforts revealed instead that an algebraic system of four-dimensional numbers — namely, the *quaternions* — can be constructed if one is willing to relinquish the commutative law for products.

Hamilton was a child prodigy, who reputedly attained varying degrees of familiarity with thirteen different languages. Like his German contemporary Möbius, he was appointed a professor of astronomy (in Trinity College, Dublin, at age 22) rather than of mathematics. The inspiration for the multiplication rules governing the quaternion basis elements $1, i, j, k$ came to him suddenly [108] while walking with his wife to a meeting of the Royal Irish Academy, and he carved the equations

$$i^2 = j^2 = k^2 = ijk = -1 \quad (5.1)$$

embodying those rules into a stone of Brougham Bridge in Dublin, which he happened to be crossing (here “1” is the usual real unit: its product with the other basis elements leaves them unchanged). Preserving the order of terms in products, one may deduce from the above that

$$ij = -ji = k, \quad jk = -kj = i, \quad ki = -ik = j. \quad (5.2)$$

Thus, the products of the basis elements are evidently non-commutative.

Hamilton is best known² nowadays for his studies in optics and mechanics, which paved the way towards the development of quantum mechanics. The

¹ Even as late as 1831, Augustus De Morgan (1806–1871), professor of mathematics at University College, London, wrote that “We have shown the symbol $\sqrt{-a}$ to be void of meaning, or rather self-contradictory and absurd. Nevertheless, by means of such symbols, a part of algebra is established which is of great utility.”

² His name also arises in graph theory: a *Hamiltonian* graph contains a path that starts and ends at a specific vertex, and visits each other vertex exactly once.

initial step in the study of complex physical systems is typically to formulate the *Hamiltonian*, which expresses the total energy of the system in terms of its degrees of freedom, thus allowing a systematic derivation of the equations governing the system dynamics. Hamilton secured international fame as early as 1832 by predicting theoretically a phenomenon known as *conical refraction*, associated with biaxial crystals, that was experimentally verified in the same year by his Trinity College colleague, the Rev. Humphrey Lloyd.

However, the majority of Hamilton's scientific career was preoccupied with the algebra of quaternions and its use in describing physical and geometrical phenomena. Insofar as modern physics and geometry rarely employ quaternion formulations, this endeavor — culminating in *Lectures on Quaternions* (1853) and the posthumous *Elements of Quaternions* (1866) — was hardly a success. These monumental treatises were considered by contemporaries to be virtually impenetrable: concerning the former, the astronomer Sir John Herschel (who discovered of the planet Uranus) solemnly declared it would “take any man a twelvemonth to read, and near a lifetime to digest ...” [108].

E. T. Bell's *Men of Mathematics* [32] characterizes Hamilton's latter years under the title “An Irish Tragedy.” The role that Hamilton sought to secure for the quaternions was occupied instead by three-dimensional vector analysis, a subject now familiar to every mathematician, scientist, and engineer. The main concepts of vector analysis in \mathbb{R}^3 — namely, the dot and cross products, and the vector differential operators (gradient, divergence, curl) — appear as sub-components of the quaternion algebra. As emphasized by Crowe [108], the real tragedy is perhaps the prevailing ignorance of the extent to which vector analysis was extracted from the theory of quaternions, by the physicists James Clerk Maxwell (1831–1879) and Josiah Willard Gibbs (1839–1903), and the engineer Oliver Heaviside (1850–1925). The struggle between quaternions and vectors for supremacy in scientific and mathematical discourse is described by Crowe [108] as follows:

A high level of intensity and a certain fierceness characterized much of the debate and must have led many readers to follow it with interest.

... Gibbs and Heaviside must have appeared to the quaternionists as unwelcome intruders who had burst in upon the developing dialogue between the quaternionists and the scientists of the day to arrive at a moment when success seemed not far distant. Charging forth, these two vectorists, the one brash and sarcastic, the other spouting historical irrelevancies, had promised a bright new day for any who would accept their overtly pragmatic arguments for an algebraically crude and highly arbitrary system. And worst of all, the system they recommended was, not some new system ... but only a perverted version of the quaternion system. Heretics are always more hated than infidels, and these two heretics had, with little understanding and less acknowledgement, wrenching major portions from the Hamiltonian system and then claimed that these parts surpassed the whole.

Because of the familiarity of modern readers with vector concepts, we opt below to express the basic quaternion operations in terms of them, although it should be recognized that this practice is anachronistic.

5.2 No Three-dimensional Numbers

Before proceeding to the quaternions, we briefly demonstrate why Hamilton's search for a three-dimensional number system was unsuccessful. Suppose we attempt to extend the complex numbers $x + iy$ by introducing a new unit j — i.e., we postulate three-dimensional numbers of the form $x + iy + jz$ that are presumed to exhibit closure under addition, subtraction, multiplication, and division, and also obey the commutative and associative rules for sums and products. Closure under multiplication implies that the product ij must be expressible as $x + iy + jz$ for real values x, y, z . Then multiplying by i and expanding $i(ij) = i(x + iy + jz)$ using $i^2 = -1$ and $ij = x + iy + jz$ gives

$$-j = zx - y + i(x + yz) + jz^2.$$

This equation is linear in j , and can be solved to obtain

$$j = \frac{y - zx - i(x + yz)}{1 + z^2}.$$

But since x, y, z are real numbers, this implies that j is just a complex number — contradicting the supposition that it is a fundamentally new unit, linearly independent of 1 and i . Therefore, the hypothesis that we can create a three-dimensional number system, that is a formal extension of the real and complex numbers, and obeys all the rules of a field (see §2.4), must be false.

5.3 Sums and Products of Quaternions

We employ calligraphic letters $\mathcal{A}, \mathcal{B}, \dots$ etc., to denote quaternions, which are “four-dimensional numbers” of the form

$$\mathcal{A} = a + a_x\mathbf{i} + a_y\mathbf{j} + a_z\mathbf{k} \quad \text{and} \quad \mathcal{B} = b + b_x\mathbf{i} + b_y\mathbf{j} + b_z\mathbf{k}. \quad (5.3)$$

In honor of Hamilton, the system of quaternions is denoted \mathbb{H} . The quaternion “basis elements” 1, \mathbf{i} , \mathbf{j} , \mathbf{k} are governed by the relations (5.1) and (5.2). Since the products of the basis elements are non-commutative, we have $\mathcal{A}\mathcal{B} \neq \mathcal{B}\mathcal{A}$ in general. Quaternion multiplication is associative,³ however — one may verify that $(\mathcal{A}\mathcal{B})\mathcal{C} = \mathcal{A}(\mathcal{B}\mathcal{C})$ for any three quaternions $\mathcal{A}, \mathcal{B}, \mathcal{C}$.

³ In fact, the adjective *associative* was introduced by Hamilton to describe precisely this property of the quaternions.

The sum of the two quaternions (5.3) is performed component-wise

$$\mathcal{A} + \mathcal{B} = (a + b) + (a_x + b_x)\mathbf{i} + (a_y + b_y)\mathbf{j} + (a_z + b_z)\mathbf{k}, \quad (5.4)$$

and using relations (5.2), the product is given by

$$\begin{aligned} \mathcal{A}\mathcal{B} &= (ab - a_x b_x - a_y b_y - a_z b_z) \\ &\quad + (ab_x + ba_x + a_y b_z - a_z b_y)\mathbf{i} \\ &\quad + (ab_y + ba_y + a_z b_x - a_x b_z)\mathbf{j} \\ &\quad + (ab_z + ba_z + a_x b_y - a_y b_x)\mathbf{k}. \end{aligned} \quad (5.5)$$

The notations of three-dimensional vector analysis offer a useful shorthand for quaternion operations. Regarding \mathbf{i} , \mathbf{j} , \mathbf{k} as unit basis vectors in a Cartesian coordinate system, we may consider \mathcal{A} as comprising “scalar” and “vector” parts,⁴ a and $\mathbf{a} = a_x\mathbf{i} + a_y\mathbf{j} + a_z\mathbf{k}$, and we write $\mathcal{A} = (a, \mathbf{a})$. Real numbers and three-dimensional vectors are subsumed as “pure scalar” and “pure vector” quaternions, of the form $(a, \mathbf{0})$ and $(\mathbf{0}, \mathbf{a})$, respectively — for brevity, we often denote such quaternions by simply a and \mathbf{a} .

Writing $\mathcal{A} = (a, \mathbf{a})$ and $\mathcal{B} = (b, \mathbf{b})$ in lieu of (5.3), the sum (5.4) and the product (5.5) may be more compactly expressed as

$$\mathcal{A} + \mathcal{B} = (a + b, \mathbf{a} + \mathbf{b}), \quad \mathcal{A}\mathcal{B} = (ab - \mathbf{a} \cdot \mathbf{b}, a\mathbf{b} + b\mathbf{a} + \mathbf{a} \times \mathbf{b}),$$

where the usual rules for vector sums and dot and cross products apply (the $\mathbf{a} \times \mathbf{b}$ term is responsible for the non-commutative nature of the product).

Hamilton also considered the quaternion differential operator

$$\triangleleft = \mathbf{i} \frac{\partial}{\partial x} + \mathbf{j} \frac{\partial}{\partial y} + \mathbf{k} \frac{\partial}{\partial z},$$

which we recognize as the *gradient* (denoted by ∇), and its negated square

$$-\triangleleft^2 = \frac{\partial^2}{\partial x^2} + \frac{\partial^2}{\partial y^2} + \frac{\partial^2}{\partial z^2},$$

which defines the *Laplacian* Δ . Taking the quaternion product of ∇ with a vector function $\mathbf{v} = v_x\mathbf{i} + v_y\mathbf{j} + v_z\mathbf{k}$ of (x, y, z) yields a quaternion

$$(-\nabla \cdot \mathbf{v}, \nabla \times \mathbf{v})$$

in which the now-familiar *divergence* $\nabla \cdot \mathbf{v}$ and *curl* $\nabla \times \mathbf{v}$ of the vector field \mathbf{v} are apparent in the scalar and vector parts. These operators are crucial to the modern formulations of mathematical physics — Maxwell’s equations of electromagnetism, the Navier–Stokes equation of fluid mechanics, etc.

⁴ Also called the “real” and “imaginary” parts of a quaternion, since the square of a “pure imaginary” (vector) quaternion is always negative. The terms *scalar* and *vector* were introduced by Hamilton in an 1846 *Philosophical Magazine* article.

Each quaternion $\mathcal{A} = (a, \mathbf{a})$ has a *conjugate* $\mathcal{A}^* = (a, -\mathbf{a})$ and a *magnitude* equal to the non-negative real number $|\mathcal{A}|$ defined by

$$|\mathcal{A}|^2 = \mathcal{A}^*\mathcal{A} = \mathcal{A}\mathcal{A}^* = a^2 + |\mathbf{a}|^2. \quad (5.6)$$

One can easily verify that the conjugates of quaternion products satisfy

$$(\mathcal{A}\mathcal{B})^* = \mathcal{B}^*\mathcal{A}^*. \quad (5.7)$$

In terms of the conjugate and magnitude, we can specify an *inverse*

$$\mathcal{A}^{-1} = \frac{\mathcal{A}^*}{|\mathcal{A}|}$$

for each quaternion $\mathcal{A} \neq 0$, so that $\mathcal{A}^{-1}\mathcal{A} = \mathcal{A}\mathcal{A}^{-1} = 1$. Using the inverse, one can define the *left division* or *right division* of \mathcal{B} by \mathcal{A} as $\mathcal{A}^{-1}\mathcal{B}$ or $\mathcal{B}\mathcal{A}^{-1}$ (due to the non-commutative nature of the product these results are, in general, distinct). Since the quaternions satisfy all the properties of a field except the commutative law M_1 for the product (see §2.4), they constitute a *division ring*. Alternatively, the quaternion algebra is sometimes called a *division algebra*.

When $|\mathcal{A}| = 1$, \mathcal{A} is a *unit* quaternion. In fact, we may identify the unit quaternions with the points of the unit “3–sphere” defined by

$$p^2 + p_x^2 + p_y^2 + p_z^2 = 1 \quad (5.8)$$

in the Euclidean space \mathbb{R}^4 with coordinates (p, p_x, p_y, p_z) . Now if \mathcal{A}, \mathcal{B} are unit quaternions (i.e., their components are coordinates of points on the 3–sphere) then $\mathcal{C} = \mathcal{A}\mathcal{B}$ is also unit, and identifies another point on (5.8). Thus, points on the 3–sphere have the structure of a *group*⁵ under quaternion multiplication.

As an alternative to the scalar/vector model, the quaternion algebra can be realized by various matrix models. For example, making the identifications

$$1 \rightarrow \begin{bmatrix} 1 & 0 \\ 0 & 1 \end{bmatrix}, \quad \mathbf{i} \rightarrow \begin{bmatrix} 0 & 1 \\ -1 & 0 \end{bmatrix}, \quad \mathbf{j} \rightarrow \begin{bmatrix} 0 & i \\ i & 0 \end{bmatrix}, \quad \mathbf{k} \rightarrow \begin{bmatrix} i & 0 \\ 0 & -i \end{bmatrix},$$

gives a representation for the quaternions in terms of complex 2×2 matrices. It is easy to verify that these matrices satisfy the relationships (5.1) and (5.2) characterizing the quaternion basis elements. Alternatively, quaternions can be represented by real skew-symmetric 4×4 matrices of the form

$$A = \begin{bmatrix} a & -a_x & -a_y & -a_z \\ a_x & a & -a_z & a_y \\ a_y & a_z & a & -a_x \\ a_z & -a_y & a_x & a \end{bmatrix}.$$

⁵ This is not true of the familiar “2–sphere” in \mathbb{R}^3 . In fact, the only other generalized spheres whose points admit such a group structure are the “0–sphere” in \mathbb{R}^1 (comprising the two points ± 1) and the “1–sphere” in \mathbb{R}^2 (the unit circle).

If A and B are two such matrices, representing the quaternions (5.3), one can readily check that their matrix product yields a 4×4 skew-symmetric matrix of the same form, with elements defined by the components of $\mathcal{A}\mathcal{B}$, as given in (5.5). Note that the transpose A^T represents \mathcal{A}^* and $\det(A) = |\mathcal{A}|^4$. Thus, the *unit* quaternions are defined by matrices of the above form with $\det(A) = 1$.

5.4 Quaternions and Spatial Rotations

As noted in §2.4, the algebra of quaternions forms a *division ring* (or *skew field* or *non-commutative field*), since they satisfy all the laws of a field except the commutative law of multiplication. Non-observance of this commutative law was an impediment to the acceptance of quaternions, but in fact this property is essential for the description of concatenated geometrical transformations in which the final outcome depends upon the *order* of the operations. Of primary interest to us here is the case of *spatial rotations* — see Fig. 5.1.

Unit quaternions offer a concise and elegant means of describing rotations of vectors about arbitrary axes in \mathbb{R}^3 , a geometrical transformation that can otherwise be quite cumbersome to manipulate. Since both terms on the right-hand side of (5.6) are non-negative, unit quaternions necessarily have the form $\mathcal{U} = (\cos \frac{1}{2}\theta, \sin \frac{1}{2}\theta \mathbf{n})$ for some angle $\frac{1}{2}\theta$ and unit vector \mathbf{n} .

If $\mathcal{V} = (0, \mathbf{v})$ is any pure vector, the quaternion product $\mathcal{U}\mathcal{V}\mathcal{U}^*$ also defines a pure vector, corresponding to a rotation of \mathbf{v} through angle θ about an axis defined by \mathbf{n} . This can be verified by carrying out the multiplication: using standard expansions for scalar and vector triple products, one obtains

$$\mathcal{U}\mathcal{V}\mathcal{U}^* = (0, (\mathbf{n} \cdot \mathbf{v})\mathbf{n} + \sin \theta \mathbf{n} \times \mathbf{v} + \cos \theta (\mathbf{n} \times \mathbf{v}) \times \mathbf{n}). \quad (5.9)$$

Now prior to the rotation, \mathbf{v} can be expressed as

$$\mathbf{v} = (\mathbf{n} \cdot \mathbf{v})\mathbf{n} + (\mathbf{n} \times \mathbf{v}) \times \mathbf{n}, \quad (5.10)$$

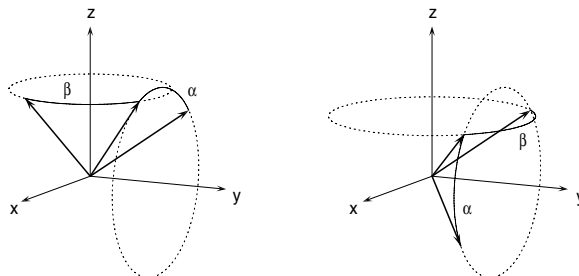


Fig. 5.1. Illustration of the non-commutative nature of spatial rotations. Left: a vector is rotated by angle α about the y -axis followed by angle β about the z -axis. Right: the same vector is rotated by angle β about the z -axis followed by angle α about the y -axis. These different orderings obviously produce disparate end results.

the terms on the right being the components of \mathbf{v} parallel and perpendicular to \mathbf{n} . As expected, the rotation leaves the parallel component unchanged, while the orthogonal component becomes $\sin \theta \mathbf{n} \times \mathbf{v} + \cos \theta (\mathbf{n} \times \mathbf{v}) \times \mathbf{n}$. Note that the correspondence between unit quaternions and spatial rotations is not quite one-to-one — one can easily verify that both $\mathcal{U} = (\cos \frac{1}{2}\theta, \sin \frac{1}{2}\theta \mathbf{n})$ and $-\mathcal{U} = (-\cos \frac{1}{2}\theta, -\sin \frac{1}{2}\theta \mathbf{n})$ describe exactly the same rotation.

Since (5.9) is linear in \mathbf{v} , the rotated vector can also be characterized by a matrix multiplication $\mathbf{M}\mathbf{v}$, where the elements m_{jk} of the 3×3 matrix \mathbf{M} are given in terms of θ and the components (n_x, n_y, n_z) of \mathbf{n} by

$$\begin{aligned} m_{11} &= n_x^2 + (1 - n_x^2) \cos \theta, \\ m_{12} &= n_x n_y (1 - \cos \theta) - n_z \sin \theta, \\ m_{13} &= n_z n_x (1 - \cos \theta) + n_y \sin \theta, \\ m_{21} &= n_x n_y (1 - \cos \theta) + n_z \sin \theta, \\ m_{22} &= n_y^2 + (1 - n_y^2) \cos \theta, \\ m_{23} &= n_y n_z (1 - \cos \theta) - n_x \sin \theta, \\ m_{31} &= n_z n_x (1 - \cos \theta) - n_y \sin \theta, \\ m_{32} &= n_y n_z (1 - \cos \theta) + n_x \sin \theta, \\ m_{33} &= n_z^2 + (1 - n_z^2) \cos \theta. \end{aligned}$$

The form $\cos \phi + \sin \phi \mathbf{n}$ of a unit quaternion (where $|\mathbf{n}| = 1$), regarded as a sum of scalar and vector parts rather than an ordered pair, is reminiscent of Euler's formula $\exp(i\phi) = \cos \phi + \sin \phi i$ for a unit complex number. Moreover, one can verify that unit quaternions satisfy an analog of de Moivre's theorem,

$$(\cos \phi + \sin \phi \mathbf{n})^k = \cos k\phi + \sin k\phi \mathbf{n}$$

for integer k . Thus, the quaternion $\mathcal{U} = (\sin \phi, \cos \phi \mathbf{n})$ is sometimes written in "exponential form" as $\exp(\phi \mathbf{n})$. One must be cautious, however, with the usual rules for the exponential function: if $\mathcal{U}_1 = \exp(\phi_1 \mathbf{n})$ and $\mathcal{U}_2 = \exp(\phi_2 \mathbf{n})$, we can write $\mathcal{U}_1 \mathcal{U}_2 = \exp((\phi_1 + \phi_2)\mathbf{n})$, but there is no simple exponential form for $\mathcal{U}_1 \mathcal{U}_2$ when $\mathcal{U}_1 = \exp(\phi_1 \mathbf{n}_1)$ and $\mathcal{U}_2 = \exp(\phi_2 \mathbf{n}_2)$ with $\mathbf{n}_1 \neq \mathbf{n}_2$.

Any number of successive spatial rotations, specified by arbitrary angles and axes, can be replaced by a single "equivalent" rotation corresponding to a unique angle and axis. The quaternion representation of rotations provides an elegant illustration of this fact — the result of consecutively applying the rotations defined by $\mathcal{U}_1 = (\cos \frac{1}{2}\theta_1, \sin \frac{1}{2}\theta_1 \mathbf{n}_1)$ and $\mathcal{U}_2 = (\cos \frac{1}{2}\theta_2, \sin \frac{1}{2}\theta_2 \mathbf{n}_2)$ to $\mathcal{V} = (0, \mathbf{v})$ is represented by

$$\mathcal{U}_2 (\mathcal{U}_1 \mathcal{V} \mathcal{U}_1^*) \mathcal{U}_2^*.$$

Now since $\mathcal{U}_1^* \mathcal{U}_2^* = (\mathcal{U}_2 \mathcal{U}_1)^*$ this can also be written as

$$\mathcal{U} \mathcal{V} \mathcal{U}^*,$$

where $\mathcal{U} = \mathcal{U}_2 \mathcal{U}_1$. Thus, the outcome of applying the rotation \mathcal{U}_1 followed by the rotation \mathcal{U}_2 is equivalent to a single rotation represented by $\mathcal{U} = \mathcal{U}_2 \mathcal{U}_1$. The non-commutative nature, $\mathcal{U}_2 \mathcal{U}_1 \neq \mathcal{U}_1 \mathcal{U}_2$, of quaternion products reflects the fact that the final outcome of a sequence of rotations depends explicitly on the *order* in which they are applied.

Now if $\mathcal{U} = (\cos \frac{1}{2}\theta, \sin \frac{1}{2}\theta \mathbf{n})$ is the product of $\mathcal{U}_2 = (\cos \frac{1}{2}\theta_2, \sin \frac{1}{2}\theta_2 \mathbf{n}_2)$ and $\mathcal{U}_1 = (\cos \frac{1}{2}\theta_1, \sin \frac{1}{2}\theta_1 \mathbf{n}_1)$ one may verify that the equivalent angle θ and axis \mathbf{n} for the compound rotation are given by

$$\begin{aligned}\frac{1}{2}\theta &= \pm \cos^{-1}(\cos \frac{1}{2}\theta_1 \cos \frac{1}{2}\theta_2 - \sin \frac{1}{2}\theta_1 \sin \frac{1}{2}\theta_2 \cos \alpha), \\ \mathbf{n} &= \pm \frac{\sin \frac{1}{2}\theta_1 \cos \frac{1}{2}\theta_2 \mathbf{n}_1 + \cos \frac{1}{2}\theta_1 \sin \frac{1}{2}\theta_2 \mathbf{n}_2 - \sin \frac{1}{2}\theta_1 \sin \frac{1}{2}\theta_2 \mathbf{n}_1 \times \mathbf{n}_2}{\sqrt{1 - (\cos \frac{1}{2}\theta_1 \cos \frac{1}{2}\theta_2 - \sin \frac{1}{2}\theta_1 \sin \frac{1}{2}\theta_2 \cos \alpha)^2}},\end{aligned}$$

where we set $\mathbf{n}_1 \cdot \mathbf{n}_2 = \cos \alpha$ (a sign ambiguity arises since rotations by θ about \mathbf{n} and by $-\theta$ about $-\mathbf{n}$ are equivalent). These formulae were first obtained, three years prior to Hamilton's discovery of quaternions, by the rather obscure French mathematician Olinde Rodrigues⁶ (1794–1851), who became wealthy through a career in banking and was a supporter of the socialist reform ideas of Claude Henri de Rouvroy, the Comte de Saint-Simon.

The algebra of unit quaternions allows us to compound spatial rotations without being explicitly concerned with ferocious formulae, such as the above expressions for θ and \mathbf{n} in terms of θ_1 , θ_2 and \mathbf{n}_1 , \mathbf{n}_2 . Quaternions have been employed in motion planning and attitude control for aircraft, spacecraft, and robots, and in defining spatial motions for computer graphics, animation, and “virtual reality” by smoothly interpolating discrete orientation sequences for rotating objects: see, for example, [28, 262, 278, 293, 410, 463]. They have also been used as a basis for alternative formulations of physical theories, such as quantum mechanics and the special and general theories of relativity.

5.5 Rotations as Products of Reflections

A plane Π in \mathbb{R}^3 is the set of points $\mathbf{p} = (x, y, z)$ satisfying the equation

$$\mathbf{n} \cdot \mathbf{p} = d,$$

where \mathbf{n} is a unit vector specifying the orientation of Π , and d is its distance from the origin. A *reflection* in the plane Π is a one-to-one mapping of \mathbb{R}^3 that takes each point \mathbf{p} to the image point $R(\mathbf{p})$ defined by

$$R(\mathbf{p}) = \mathbf{p} + 2(d - \mathbf{n} \cdot \mathbf{p})\mathbf{n}. \quad (5.11)$$

⁶ Another well-known mathematical result of Rodrigues is the recurrence relation (3.6) for the Legendre polynomials.

Geometrically, \mathbf{p} and $R(\mathbf{p})$ are on opposite sides of (and equidistant from) the plane Π , and the line joining them crosses this plane orthogonally. Note that $R(\mathbf{p}) = \mathbf{p} \iff \mathbf{p} \in \Pi$. Consider now successive reflections R_1, R_2 in distinct non-parallel planes Π_1, Π_2 with $L = \Pi_1 \cap \Pi_2$ as their line of intersection. Clearly, each point of L remains fixed under the compounded reflections R_2R_1 , and one can verify that the images of the points of each plane Π orthogonal to the line L amount to rotations about the point $\mathbf{c} = L \cap \Pi$ where L crosses Π . Thus, *a sequence of reflections in two distinct, non-parallel planes corresponds to a rotation in \mathbb{R}^3 about their line of intersection*.

The characterization of spatial rotations as products of reflections can be expressed in terms of a quaternion model [107]. Let $\mathcal{V} = (0, \mathbf{v})$ be a pure vector quaternion. Then for any pure vector quaternion $\mathcal{A} = (0, \mathbf{a})$ with $|\mathbf{a}| = 1$, the product

$$\mathcal{A}\mathcal{V}\mathcal{A} = (0, \mathbf{v} - 2(\mathbf{a} \cdot \mathbf{v})\mathbf{a})$$

yields a pure vector quaternion, and from (5.11) we recognize its vector part to be the *reflection* of \mathbf{v} in the plane $\mathbf{a} \cdot \mathbf{p} = 0$ through the origin. A sequence of two reflections, defined by pure vector quaternions $\mathcal{A} = (0, \mathbf{a})$ with $|\mathbf{a}| = 1$ and $\mathcal{B} = (0, \mathbf{b})$ with $|\mathbf{b}| = 1$, transforms \mathcal{V} into the pure vector quaternion

$$\mathcal{B}(\mathcal{A}\mathcal{V}\mathcal{A})\mathcal{B},$$

and one can easily verify that this is equivalent to the rotation $\mathcal{U}\mathcal{V}\mathcal{U}^*$, where the unit quaternion $\mathcal{U} = (\cos \frac{1}{2}\theta, \sin \frac{1}{2}\theta \mathbf{n})$ is defined by

$$\cos \frac{1}{2}\theta = -\mathbf{a} \cdot \mathbf{b} \quad \text{and} \quad \sin \frac{1}{2}\theta \mathbf{n} = \mathbf{b} \times \mathbf{a}.$$

Hence, if $\mathbf{a} \cdot \mathbf{b} = \cos \phi$, the angle of rotation is $2(\phi \pm \pi)$ and the axis of rotation is in the direction of the cross product $\mathbf{b} \times \mathbf{a}$.

We can invert the above reasoning and ask: for a spatial rotation specified by a unit quaternion $\mathcal{U} = (\cos \frac{1}{2}\theta, \sin \frac{1}{2}\theta \mathbf{n})$, what pairs of reflections in planes are equivalent to it? To address this we choose unit vectors $\mathbf{e}_1, \mathbf{e}_2$ orthogonal to \mathbf{n} , such that $(\mathbf{e}_1, \mathbf{e}_2, \mathbf{n})$ is an orthonormal triad. Then, for any α , successive reflections in the two planes through the origin with the normals

$$\cos \alpha \mathbf{e}_1 + \sin \alpha \mathbf{e}_2 \quad \text{and} \quad -\cos(\alpha + \frac{1}{2}\theta) \mathbf{e}_1 - \sin(\alpha + \frac{1}{2}\theta) \mathbf{e}_2$$

are equivalent to the specified rotation. Thus, there is a *one-parameter family* of pairs of reflections equivalent to any given spatial rotation — the reflection planes are members of the pencil of planes having the line through the origin along \mathbf{n} as their common line, with angular separation $\frac{1}{2}\theta \pm \pi$ of their normals.

5.6 Families of Spatial Rotations

Given distinct unit vectors in the plane, the problem of finding the rotation that maps one into the other is trivial: if θ is the clockwise angle between them, we can either rotate clockwise by angle θ or anti-clockwise by $2\pi - \theta$.

The equivalent problem in \mathbb{R}^3 is more subtle. The “obvious” solution is to rotate within the plane defined by the two vectors, in which case the solution to the planar problem holds (this corresponds to motion along a *great circle* on the unit sphere in \mathbb{R}^3). However, there is also a *one-parameter family* of spatial rotations that achieve the desired result, for which the motion of one vector into the other departs from their common plane — these correspond to motions along *small circles* of the unit sphere. Unit quaternions provide an elegant means of characterizing such families of spatial rotations.

Suppose, for simplicity, we choose coordinates so that the first unit vector coincides with \mathbf{i} . The second unit vector \mathbf{v} has a general orientation. We are then interested in the quaternion solutions \mathcal{U} to the equation

$$\mathcal{U}\mathbf{i}\mathcal{U}^* = \mathbf{v}, \quad (5.12)$$

that specifies⁷ a spatial rotation of \mathbf{i} into \mathbf{v} . Writing $\mathcal{U} = u_0 + u_x\mathbf{i} + u_y\mathbf{j} + u_z\mathbf{k}$ and $\mathbf{v} = \lambda\mathbf{i} + \mu\mathbf{j} + \nu\mathbf{k}$, equation (5.12) is equivalent to the system of three quadratic scalar equations

$$u_0^2 + u_x^2 - u_y^2 - u_z^2 = \lambda, \quad 2(u_0u_z + u_xu_y) = \mu, \quad 2(u_xu_z - u_0u_y) = \nu$$

in the four unknowns u_0, u_x, u_y, u_z . Note that summing the squares on both sides gives $(u_0^2 + u_x^2 + u_y^2 + u_z^2)^2 = \lambda^2 + \mu^2 + \nu^2 = 1$, so the condition that \mathcal{U} be a *unit* quaternion is automatically satisfied. Since we have *three* equations in *four* unknowns, the solutions to (5.12) possess one degree of freedom.

A particular (pure vector) solution, with $u_0 = 0$, is easily seen to be

$$\mathcal{U} = \pm\sqrt{\frac{1}{2}(1+\lambda)} \left(\mathbf{i} + \frac{\mu}{1+\lambda}\mathbf{j} + \frac{\nu}{1+\lambda}\mathbf{k} \right). \quad (5.13)$$

Moreover, if \mathcal{Q} is any quaternion satisfying the equation

$$\mathcal{Q}\mathbf{i}\mathcal{Q}^* = \mathbf{i}, \quad (5.14)$$

then $\mathcal{U}\mathcal{Q}$ must also be a solution of (5.12), since

$$(\mathcal{U}\mathcal{Q})\mathbf{i}(\mathcal{U}\mathcal{Q})^* = \mathcal{U}(\mathcal{Q}\mathbf{i}\mathcal{Q}^*)\mathcal{U}^* = \mathcal{U}\mathbf{i}\mathcal{U}^*.$$

The quaternions satisfying (5.14) are necessarily of the form

$$\mathcal{Q} = \cos\phi + \sin\phi\mathbf{i},$$

as can be deduced from the component equations of (5.14), namely

$$q_0^2 + q_x^2 - q_y^2 - q_z^2 = 1, \quad 2(q_0q_z + q_xq_y) = 0, \quad 2(q_xq_z - q_0q_y) = 0$$

⁷ For any vector \mathbf{v} and quaternion \mathcal{A} , the form $\mathcal{A}\mathbf{v}\mathcal{A}^*$ always yields a pure vector.

where we take $\mathcal{Q} = q_0 + q_x \mathbf{i} + q_y \mathbf{j} + q_z \mathbf{k}$. The most general solution to equation (5.12) can thus be parameterized in terms of the variable ϕ as

$$\begin{aligned}\mathcal{U}(\phi) = & \sqrt{\frac{1}{2}(1+\lambda)} \left(-\sin \phi + \cos \phi \mathbf{i} + \frac{\mu \cos \phi + \nu \sin \phi}{1+\lambda} \mathbf{j} \right. \\ & \left. + \frac{\nu \cos \phi - \mu \sin \phi}{1+\lambda} \mathbf{k} \right). \end{aligned}\quad (5.15)$$

Since $\sin(\phi + \pi) = -\sin \phi$ and $\cos(\phi + \pi) = -\cos \phi$, the above embodies the sign ambiguity in (5.13). Thus, on proceeding from the special solution (5.13) to the general solution (5.15), we may omit the \pm sign.

We can gain better geometrical insight by writing $\mathcal{U} = (\cos \frac{1}{2}\theta, \sin \frac{1}{2}\theta \mathbf{n})$. The rotation axis $\mathbf{n} = (n_x, n_y, n_z)$ and angle θ must then satisfy

$$\begin{aligned}n_x^2(1-\cos \theta) + \cos \theta &= \lambda, \\ n_x n_y(1-\cos \theta) + n_z \sin \theta &= \mu, \\ n_z n_x(1-\cos \theta) - n_y \sin \theta &= \nu.\end{aligned}$$

Writing $\alpha = \cos^{-1} \lambda$, this has (for $\alpha \leq \theta \leq 2\pi - \alpha$) the general solution

$$\begin{aligned}n_x &= \frac{\pm \sqrt{\cos^2 \frac{1}{2}\alpha - \cos^2 \frac{1}{2}\theta}}{\sin \frac{1}{2}\theta}, \\ n_y &= \frac{\pm \mu \sqrt{\cos^2 \frac{1}{2}\alpha - \cos^2 \frac{1}{2}\theta} - \nu \cos \frac{1}{2}\theta}{(1+\lambda) \sin \frac{1}{2}\theta}, \\ n_z &= \frac{\pm \nu \sqrt{\cos^2 \frac{1}{2}\alpha - \cos^2 \frac{1}{2}\theta} + \mu \cos \frac{1}{2}\theta}{(1+\lambda) \sin \frac{1}{2}\theta}.\end{aligned}$$

This parameterizes the family of spatial rotations that map the unit vector \mathbf{i} into another unit vector \mathbf{v} by specifying the rotation axis as a function $\mathbf{n}(\theta)$ of the rotation angle θ , over the restricted domain $\theta \in [\alpha, 2\pi - \alpha]$ where α is the angle between \mathbf{i} and \mathbf{v} (measured in their common plane).

We define a unit vector \mathbf{e}_\perp orthogonal to the common plane of \mathbf{i} and \mathbf{v} , and a unit vector \mathbf{e}_0 in its plane, by

$$\mathbf{e}_\perp = \frac{\mathbf{i} \times \mathbf{v}}{|\mathbf{i} \times \mathbf{v}|} \quad \text{and} \quad \mathbf{e}_0 = \frac{\mathbf{i} + \mathbf{v}}{|\mathbf{i} + \mathbf{v}|}.$$

Note that \mathbf{e}_0 corresponds to the (unit) bisector of \mathbf{i} and \mathbf{v} . The rotation axis lies in the plane spanned by these vectors, and may be written as

$$\mathbf{n}(\theta) = \frac{\sin \frac{1}{2}\alpha \cos \frac{1}{2}\theta \mathbf{e}_\perp \pm \sqrt{\cos^2 \frac{1}{2}\alpha - \cos^2 \frac{1}{2}\theta} \mathbf{e}_0}{\cos \frac{1}{2}\alpha \sin \frac{1}{2}\theta}. \quad (5.16)$$

The \pm sign in (5.16) indicates that for each $\theta \in (\alpha, 2\pi - \alpha)$ there are two axes \mathbf{n} about which a rotation by angle θ maps \mathbf{i} to \mathbf{v} . These axes lie in the plane of $\mathbf{e}_\perp, \mathbf{e}_0$ and have equal inclinations with \mathbf{e}_\perp . Some noteworthy special cases of expression (5.16) are as follows:

- (a) when $\theta = \alpha$, we have $\mathbf{n}(\alpha) = \mathbf{e}_\perp$, and the rotation is along the great circle between \mathbf{i} and \mathbf{v} ;
- (b) when $\theta = \pi$, we have $\mathbf{n}(\pi) = \pm \mathbf{e}_0$, so \mathbf{i} executes either a clockwise or anti-clockwise half-rotation about \mathbf{e}_0 onto \mathbf{v} ;
- (c) when $\theta = 2\pi - \alpha$, we have $\mathbf{n}(2\pi - \alpha) = -\mathbf{e}_\perp$, and the rotation is again along the great circle between \mathbf{i} and \mathbf{v} , in the opposite sense to case (a).

Figure 5.2 illustrates these ideas. The axes \mathbf{n} for all possible rotations of \mathbf{i} onto \mathbf{v} lie in the plane Π spanned by $\mathbf{e}_\perp, \mathbf{e}_0$. The smallest and largest rotation angles, $\theta = \alpha$ and $2\pi - \alpha$, correspond to the axes $\mathbf{n} = \mathbf{e}_\perp$ and $-\mathbf{e}_\perp$, respectively.

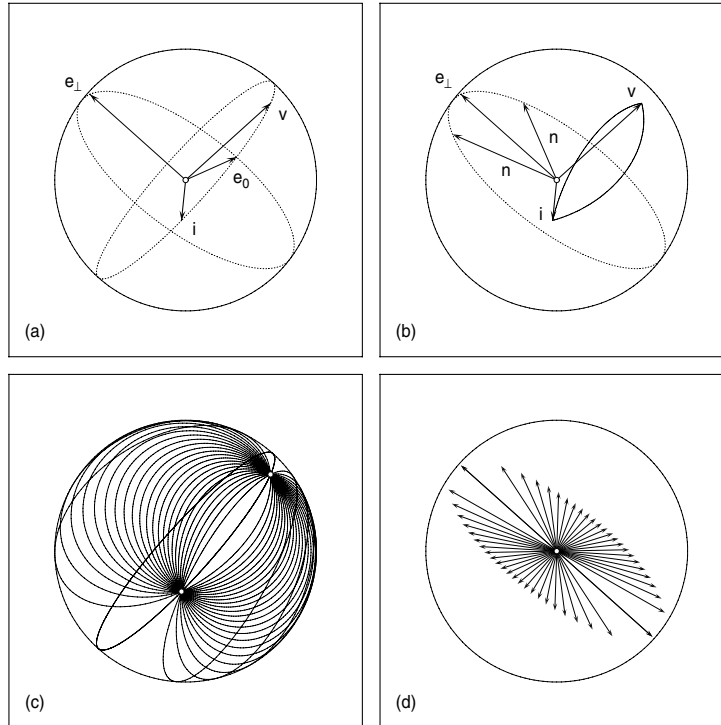


Fig. 5.2. Spatial rotations of a unit vector \mathbf{i} onto a unit vector \mathbf{v} . (a) Unit vectors \mathbf{e}_\perp (orthogonal to \mathbf{i} and \mathbf{v}) and \mathbf{e}_0 (the bisector of \mathbf{i} and \mathbf{v}) — the plane Π spanned by $\mathbf{e}_\perp, \mathbf{e}_0$ is orthogonal to that of \mathbf{i} and \mathbf{v} . (b) For any rotation angle $\theta \in (\alpha, 2\pi - \alpha)$, where $\alpha = \cos^{-1}(\mathbf{i} \cdot \mathbf{v})$, there are two possible rotations, with axes \mathbf{n} inclined equally to \mathbf{e}_\perp in the plane Π . (c) Sampling of the family of rotations of \mathbf{i} onto \mathbf{v} , shown as loci on the unit sphere. (d) Axes \mathbf{n} for the rotations in (c), lying in the plane Π .

These cases correspond to motions along the great circle of the unit sphere containing \mathbf{i} and \mathbf{v} . Intermediate rotation angles θ admit two distinct rotation axes, on either side of \mathbf{e}_\perp , and correspond to motions along small circles of the unit sphere, with the special case $\theta = \pm\pi$ arising when \mathbf{n} lies in the plane of \mathbf{i} and \mathbf{v} . Taken altogether, these motions describe a *coaxal system of circles* (see §8.2.2) on the unit sphere.

By comparing (5.15) with the solution giving \mathbf{n} in terms of θ , of the form

$$\mathcal{U}(\theta) = \cos \frac{1}{2}\theta + \sin \frac{1}{2}\theta (n_x \mathbf{i} + n_y \mathbf{j} + n_z \mathbf{k}),$$

we find the relationship between the angular variables ϕ and θ to be

$$\phi = -\sin^{-1} \frac{\cos \frac{1}{2}\theta}{\cos \frac{1}{2}\alpha} \in [-\frac{1}{2}\pi, +\frac{1}{2}\pi] \quad \text{for } \theta \in [\alpha, 2\pi - \alpha].$$

Although the parameter θ has a clearer geometrical interpretation (the angle of rotation from \mathbf{i} to \mathbf{v} about the corresponding axis \mathbf{n}), the parameterization (5.15) in terms of ϕ is simpler to use in practice. The special solution (5.13) corresponds to the case $\theta = \pi$, for which \mathbf{n} lies in the plane of \mathbf{i} and \mathbf{v} .

5.7 Four-dimensional Rotations

Quaternions live in \mathbb{R}^4 , a realm which admits possibilities that appear to defy our “common sense” geometrical intuition based on experience in \mathbb{R}^2 and \mathbb{R}^3 . In \mathbb{R}^4 one discovers [318] that, for example, a sphere made of flexible material may be turned inside out without tearing the material; a prisoner in a locked cell may escape without penetrating its walls; and a knot in a length of string may be untied without moving its ends. Such possibilities arise from the extra “maneuvering freedom” afforded by the additional dimension.

Our concern here is specifically with *rotations* in \mathbb{R}^4 — in Chap. 22 we shall employ quaternion polynomials (equivalent to parametric curves in \mathbb{R}^4) to generate Pythagorean hodographs in \mathbb{R}^3 through a continuous sequence of scalings/rotations applied to a unit “reference” vector. It transpires, however, that such a specification is not unique — there exists a *one-parameter family* of quaternion polynomials that specify a given Pythagorean hodograph, and we shall see that they correspond to rotations of each other in \mathbb{R}^4 .

Quaternions can be employed to describe rotations in \mathbb{R}^4 , as well as in \mathbb{R}^3 . If we regard a given quaternion \mathcal{A} as a vector in \mathbb{R}^4 , the most general rotation of it is specified [135, 310] using two unit quaternions $\mathcal{U}_1, \mathcal{U}_2$ by the map⁸

$$\mathcal{A} \rightarrow \mathcal{U}_1 \mathcal{A} \mathcal{U}_2^*. \tag{5.17}$$

⁸ This defines a linear transformation of the components of \mathcal{A} by a 4×4 orthogonal matrix of determinant 1, i.e., a member of $\text{SO}(4)$. Since $\mathcal{U}_1, \mathcal{U}_2$ are independently chosen, taking the conjugate of the latter in (5.17) is purely conventional.

The correspondence between pairs of unit quaternions and rotations in \mathbb{R}^4 is not one-to-one, however, since $-\mathcal{U}_1, -\mathcal{U}_2$ define the same rotation as $\mathcal{U}_1, \mathcal{U}_2$ — as with the description of rotations in \mathbb{R}^3 by a single unit quaternion. The special instances of (5.17) defined by

$$\mathcal{A} \rightarrow \mathcal{U}\mathcal{A} \quad \text{and} \quad \mathcal{A} \rightarrow \mathcal{A}\mathcal{U},$$

that involve multiplying a given quaternion by a single unit quaternion \mathcal{U} on the left or right, are known as a *right screw* and *left screw*, respectively [135]. Such quaternion mappings will play an important role in the theory of spatial Pythagorean–hodograph curves (see Chap. 22).

A rotation in \mathbb{R}^2 can be specified by a unit complex number $e^{i\theta}$ and has a single free parameter, the rotation angle θ . A rotation in \mathbb{R}^3 , being specified by a unit quaternion $\mathcal{U} = \cos \frac{1}{2}\theta + \sin \frac{1}{2}\theta \mathbf{n}$, exhibits three degrees of freedom — the rotation angle θ , and the direction cosines of the rotation axis \mathbf{n} . Since a general rotation in \mathbb{R}^4 is specified by two unit quaternions $\mathcal{U}_1, \mathcal{U}_2$ it exhibits *six* degrees of freedom [135, 310]. To understand the geometrical significance of this, we must review some ideas from the geometry of \mathbb{R}^4 [137, 319].

A *line*, *plane*, and *hyperplane* in \mathbb{R}^4 are respectively the point sets linearly dependent on two, three, and four points “in general position” — alternately, they are the sets of points that satisfy three, two, and one linear equations in the four Cartesian coordinates of \mathbb{R}^4 . A hyperplane in \mathbb{R}^4 is just a copy of the familiar three-dimensional Euclidean space \mathbb{R}^3 , but there are infinitely many such copies in \mathbb{R}^4 . A hyperplane divides \mathbb{R}^4 into two disjoint regions: it is not possible to move from one to the other without crossing the hyperplane — as is true for a plane in \mathbb{R}^3 , and a line in \mathbb{R}^2 . The following incidence relations⁹ follow directly from the preceding definitions:

1. two hyperplanes intersect in a plane;
2. three hyperplanes intersect in a line;
3. four hyperplanes intersect in a point.

Case (1) amounts to two linear equations in four unknowns, thus leaving two degrees of freedom. Case (2) yields three linear equations in four unknowns, leaving one degree of freedom — equivalently, one can say that “a plane and a hyperplane intersect in a line.” Case (3) corresponds to four linear equations in four unknowns, and thus admits a single point as its solution — one can say that “two planes intersect in a point” as an alternative phrasing.

Consider two planes Π_1, Π_2 in \mathbb{R}^4 with \mathbf{p} as their intersection point. These planes are said to be *absolutely perpendicular* if each line through \mathbf{p} on Π_1 is orthogonal to each line through \mathbf{p} on Π_2 . This is a strictly four-dimensional phenomenon, with no analog in \mathbb{R}^3 — in dealing with \mathbb{R}^4 , we must suppress our intuition concerning the behavior of planes in \mathbb{R}^3 (for example, it is possible to circumnavigate a plane in \mathbb{R}^4 without crossing it, just as it is possible to

⁹ These hold for hyperplanes in “general position” — or we can dispense with this qualification with homogeneous coordinates in *projective* four-dimensional space.

circumnavigate a line in \mathbb{R}^3 but not in \mathbb{R}^2). At each point of a given plane in \mathbb{R}^4 , there is a *unique* plane absolutely perpendicular to it.

A key geometrical feature of a general rotation in \mathbb{R}^n is its *stationary set*, i.e., the set of points that do not move under the rotation. In \mathbb{R}^2 the stationary set is a point (the *center* of the rotation), while in \mathbb{R}^3 it is a line (the *axis line* of the rotation). These are examples of *simple* rotations, characterized by the property that in \mathbb{R}^n the stationary set has dimension $n - 2$. Now in \mathbb{R}^4 , one of two absolutely perpendicular planes may rotate on itself about their common point while the other remains stationary. This is a simple rotation in \mathbb{R}^4 — the stationary set, the stationary *axis plane*, is of dimension $n - 2$.

However, a new possibility — a *double rotation* — arises for the first time in \mathbb{R}^4 . This involves both of the planes absolutely perpendicular to each other rotating on themselves about their common point. Such rotations of absolutely perpendicular planes are *commutative*, i.e., the outcome is independent of the order in which they are performed, and the stationary set comprises just the common point of the two absolutely perpendicular planes.

The six parameters associated with a general (double) rotation in \mathbb{R}^4 can be understood geometrically as follows. Without loss of generality, take the origin of \mathbb{R}^4 as the common point of the two absolutely perpendicular planes. We need only specify one of these planes, and the other will then be uniquely determined. Each plane has a rotation angle associated with it, accounting for two parameters. The remaining four parameters specify one of the two planes: the plane is determined by two additional points, not collinear with the origin — each point has four coordinates, but also two freedoms of motion within the plane, so only four essential parameters are required to fix the plane.

Under a continuous rotation at angular speed ω in \mathbb{R}^2 or \mathbb{R}^3 , every point (other than points of the stationary set) executes a periodic path — namely, a circle — and will return to its initial position, at time $t = 0$, every integer multiple of the motion period $T = 2\pi/\omega$. In \mathbb{R}^4 , however, we first encounter the strange phenomenon of rotations incurring *non-periodic motions* of points. Consider a double rotation involving angular velocities ω_1 and ω_2 about two absolutely perpendicular planes Π_1 and Π_2 with common point \mathbf{p} . As noted above, these two rotations commute, and their angular velocities ω_1 and ω_2 are therefore completely independent. If a point in \mathbb{R}^4 is to return exactly to its initial position at $t = 0$, there must be a precise coincidence of multiples $jT_1 = j2\pi/\omega_1$ and $kT_2 = k2\pi/\omega_2$ of the rotation periods for integers j and k , i.e., the angular velocity ratio must be a *rational number*, $\omega_2/\omega_1 = j/k$. If the ratio ω_2/ω_1 is irrational, the motions of points in \mathbb{R}^4 induced by the double rotation are non-periodic — their paths are not closed curves!

Another perspective on the nature of rotations in \mathbb{R}^n comes from studying the eigenvalues of their representation by the $n \times n$ *special orthogonal matrices*, $\text{SO}(n)$. These eigenvalues are necessarily of modulus 1. The matrices of $\text{SO}(2)$, describing rotations in \mathbb{R}^2 , always have two complex conjugate eigenvalues — because there are no real eigenvectors, no point other than the origin remains stationary. The matrices of $\text{SO}(3)$, specifying rotations in \mathbb{R}^3 , have one real

and two complex conjugate eigenvalues. The eigenvector that corresponds to the real eigenvalue identifies a stationary line through the origin — namely, the axis of the rotation. Finally, the matrices of $\text{SO}(4)$ may possess either two pairs of complex conjugate eigenvalues, or one complex conjugate pair and one real pair of eigenvalues. In the former case, the stationary set is just the origin, since there are no real eigenvectors. In the latter case, the eigenvectors corresponding to the two real eigenvalues span a plane through the origin that remains stationary under the rotation.

6

Clifford Algebra

We may always depend on it that algebra, which cannot be translated into good English and sound common sense, is bad algebra.

William Kingdon Clifford

Clifford algebra (also known as *geometric algebra*) is named after the English mathematician William Kingdon Clifford (1845–1879), who made significant contributions to algebra and geometry¹ in a brilliant but tragically brief career (he died of tuberculosis, possibly exacerbated by his rigorous work schedule). Clifford algebra provides a systematic framework for generalizing the known algebras of complex numbers and quaternions to any number of dimensions. For a more comprehensive discussion of its methods and diverse applications in science and engineering, see [30, 133, 134, 238, 310].

6.1 Clifford Algebra Bases

Consider an “ n –dimensional number” of the form

$$\mathbf{x} = x_1 \mathbf{e}_1 + \cdots + x_n \mathbf{e}_n, \quad (6.1)$$

where $x_1, \dots, x_n \in \mathbb{R}$ and $\mathbf{e}_1, \dots, \mathbf{e}_n$ form an orthonormal basis in \mathbb{R}^n . Such numbers are added component–wise, but to determine their products we must specify the results of the products of (ordered) combinations of two or more of the “units” $\mathbf{e}_1, \dots, \mathbf{e}_n$. The convention of Clifford algebra is to take

$$\mathbf{e}_i \mathbf{e}_i = \sigma_i, \quad (6.2)$$

where $\sigma_i = \pm 1$ for $i = 1, \dots, n$, and

$$\mathbf{e}_j \mathbf{e}_k = -\mathbf{e}_k \mathbf{e}_j \quad \text{if } j \neq k. \quad (6.3)$$

¹ He also presaged the general theory of relativity, by suggesting that gravity is a manifestation of the curvature of space–time.

This ensures that the square of (6.1) is the real number defined by

$$\mathbf{x}^2 = \sigma_1 x_1^2 + \cdots + \sigma_n x_n^2. \quad (6.4)$$

As a consequence of (6.3), the Clifford algebra product is not commutative — but it does obey the associative and distributive laws.

The signs σ_i specify the *signature* of the quadratic form (6.4). For example, the special theory of relativity makes use of 4-vectors with three spatial and one temporal components, and the appropriate signature is² (+++−). Two “events” (x_1, y_1, z_1, ct_1) and (x_2, y_2, z_2, ct_2) , where c is the speed of light, are separated by the 4-vector $(x_2 - x_1, y_2 - y_1, z_2 - z_1, c(t_2 - t_1))$. Such vectors are said to be *space-like* or *time-like* according to whether the quantity

$$d^2 = (x_2 - x_1)^2 + (y_2 - y_1)^2 + (z_2 - z_1)^2 - c^2(t_2 - t_1)^2$$

is positive or negative (and *light-like* when it is zero). The event (x_1, y_1, z_1, ct_1) may influence the event (x_2, y_2, z_2, ct_2) only if their separation is time-like.

The set of all products of k distinct vectors selected from $\mathbf{e}_1, \dots, \mathbf{e}_n$ for $0 \leq k \leq n$ forms a basis for the Clifford algebra over \mathbb{R}^n . This algebra is thus of dimension

$$\sum_{k=0}^n \binom{n}{k} = 2^n.$$

Note that, by means of relations (6.2)–(6.3), the product of any k of the vectors $\mathbf{e}_1, \dots, \mathbf{e}_n$ can be reduced to a product of $\leq k$ vectors in some canonical order. Thus, for example, the $n = 3$ basis can be written in the canonical form

$$\{1, \mathbf{e}_1, \mathbf{e}_2, \mathbf{e}_3, \mathbf{e}_2\mathbf{e}_3, \mathbf{e}_3\mathbf{e}_1, \mathbf{e}_1\mathbf{e}_2, \mathbf{e}_1\mathbf{e}_2\mathbf{e}_3\}, \quad (6.5)$$

where 1 is the *grade zero* element (i.e., the scalar unit); $\mathbf{e}_1, \mathbf{e}_2, \mathbf{e}_3$ are *grade one* elements (vectors); $\mathbf{e}_2\mathbf{e}_3, \mathbf{e}_3\mathbf{e}_1, \mathbf{e}_1\mathbf{e}_2$ are *grade two* elements (bivectors); and the unique element $\mathbf{e}_1\mathbf{e}_2\mathbf{e}_3$ of the *highest grade* is known as the “pseudoscalar.” Writing $\boldsymbol{\omega} = \mathbf{e}_1\mathbf{e}_2\mathbf{e}_3$, one can easily verify that

$$\boldsymbol{\omega} \mathbf{e}_i = \mathbf{e}_i \boldsymbol{\omega}, \quad i = 1, 2, 3$$

— i.e., the pseudoscalar commutes with each of the basis elements $\mathbf{e}_1, \mathbf{e}_2, \mathbf{e}_3$ and consequently with *all* the basis elements (6.5).

6.2 Algebra of Multivectors

Because of their inherently different nature, we say that the basis elements (6.5) of different grade define a *graded* algebra. The most general element of the Clifford algebra over \mathbb{R}^3 is an eight-dimensional *multivector* of the form

$$a_0 + a_1\mathbf{e}_1 + a_2\mathbf{e}_2 + a_3\mathbf{e}_3 + a_{23}\mathbf{e}_2\mathbf{e}_3 + a_{31}\mathbf{e}_3\mathbf{e}_1 + a_{12}\mathbf{e}_1\mathbf{e}_2 + a_{123}\mathbf{e}_1\mathbf{e}_2\mathbf{e}_3,$$

² Some authors use the signature (−−+) instead.

where the coefficients a_0, \dots, a_{123} are real numbers (adding different “types” of entities should cause no consternation, since we are already familiar with it in the context of complex numbers and quaternions — it is really a short-hand notation for manipulating multivectors as ordered 2^n -tuples).

If we introduce an ordering in which $\sigma_i = +1$ for $i = 1, \dots, p$ and $\sigma_i = -1$ for $i = p+1, \dots, p+q$ where $p+q = n$, the Clifford algebra over \mathbb{R}^n under this signature is denoted by $\mathcal{C}\ell_{p,q}$. In the common case $p = n, q = 0$ we may simply write $\mathcal{C}\ell_n$. The sub-space of all the grade k elements in $\mathcal{C}\ell_n$, of dimension $\binom{n}{k}$, is denoted by $\mathcal{C}\ell_n^k$. Also, the sub-space of *even* grade multivectors in $\mathcal{C}\ell_n$ comprise a sub-algebra, denoted by $\mathcal{C}\ell_n^+$ (the relations (6.2)–(6.3) ensure that a product contains only even grade components if the factors have this property).

The algebra of the complex numbers \mathbb{C} is isomorphic to the even Clifford algebra $\mathcal{C}\ell_2^+$ whose basis comprises the scalar unit 1 and the single bivector $\mathbf{i} = \mathbf{e}_1\mathbf{e}_2$, which we identify with the imaginary unit since it satisfies $\mathbf{i}^2 = -1$. Hence, general elements of this algebra are of the form $a + bi$ for $a, b \in \mathbb{R}$, and the square of any pure imaginary element is non-positive. Alternatively, the complex numbers are isomorphic to the Clifford algebra $\mathcal{C}\ell_{0,1}$ with basis 1 and the single vector $\mathbf{i} = \mathbf{e}_1$. On account of the signature $(-)$, the square of any pure imaginary element is again non-positive.

The algebra of the quaternions \mathbb{H} is isomorphic to the even Clifford algebra $\mathcal{C}\ell_3^+$, whose basis comprises the scalar unit 1 and three bivectors — identified with elements of the quaternion basis according to

$$\mathbf{e}_2\mathbf{e}_3 = \mathbf{i}, \quad \mathbf{e}_1\mathbf{e}_2 = \mathbf{j}, \quad \mathbf{e}_3\mathbf{e}_1 = \mathbf{k}.$$

To justify this identification we note, for example, that

$$\mathbf{i}^2 = (\mathbf{e}_2\mathbf{e}_3)(\mathbf{e}_2\mathbf{e}_3) = -\mathbf{e}_2\mathbf{e}_3\mathbf{e}_3\mathbf{e}_2 = -\mathbf{e}_2\mathbf{e}_2 = -1$$

and

$$\mathbf{i}\mathbf{j} = (\mathbf{e}_2\mathbf{e}_3)(\mathbf{e}_1\mathbf{e}_2) = -\mathbf{e}_3\mathbf{e}_2\mathbf{e}_1\mathbf{e}_2 = \mathbf{e}_3\mathbf{e}_1\mathbf{e}_2\mathbf{e}_2 = \mathbf{e}_3\mathbf{e}_1 = \mathbf{k}.$$

Alternatively, the quaternion algebra is also isomorphic to $\mathcal{C}\ell_{0,2}$ with signature $(--)$, the basis elements $\mathbf{e}_1, \mathbf{e}_2, \mathbf{e}_1\mathbf{e}_2$ being identified with $\mathbf{i}, \mathbf{j}, \mathbf{k}$.

As an example of a higher algebra subsumed by the multivector framework, Clifford demonstrated that the eight-dimensional system of “biquaternions” or *octonions*, discovered independently by Hamilton’s friend John T. Graves in 1843 and Arthur Cayley in 1845, is isomorphic to $\mathcal{C}\ell_{0,3}$. The algebra of the octonions — denoted by \mathbb{O} and sometimes also called “Cayley numbers” — is even more remote from the real numbers \mathbb{R} and complex numbers \mathbb{C} than the quaternions \mathbb{H} , because the octonion product is neither commutative nor associative³ (see [23, 99] for a detailed treatment).

³ According to *Hurwitz’s Theorem*, the 1, 2, 4, and 8-dimensional number systems $\mathbb{R}, \mathbb{C}, \mathbb{H}$, and \mathbb{O} are the only possible “composition algebras” — in which the norm of a product equals the product of the individual norms of the factors.

6.3 The Geometric Product

The products of vectors $\mathbf{a}, \mathbf{b} \in \mathbb{R}^3$ familiar to most mathematicians, scientists, and engineers are the *dot product* $\mathbf{a} \cdot \mathbf{b}$, and *cross product* $\mathbf{a} \times \mathbf{b}$. If $\theta \in [0, \pi]$ is the angle between \mathbf{a} and \mathbf{b} , the dot product is the *scalar* with the real value $|\mathbf{a}| |\mathbf{b}| \cos \theta$. The cross product, however, is a *vector* that is orthogonal to the plane of \mathbf{a} and \mathbf{b} — it has magnitude $|\mathbf{a}| |\mathbf{b}| \sin \theta$, and its sense is such that $\mathbf{a}, \mathbf{b}, \mathbf{a} \times \mathbf{b}$ form a right-handed triad (when $\theta \neq 0$ or π).

It is not widely appreciated that $\mathbf{a} \times \mathbf{b}$ is actually a different *type* of vector than \mathbf{a} and \mathbf{b} . If we write the latter in terms of components as $\mathbf{a} = (a_x, a_y, a_z)$ and $\mathbf{b} = (b_x, b_y, b_z)$ in a specific (right-handed) Cartesian coordinate system, then the change of coordinates $(x, y, z) \rightarrow (-x, -y, -z)$ evidently transforms these vectors to $-\mathbf{a} = (-a_x, -a_y, -a_z)$ and $-\mathbf{b} = (-b_x, -b_y, -b_z)$. Under such a reversal of the coordinate directions, the right-handed Cartesian system will become a left-handed system, and the components of vectors must be negated. Vectors that behave in this manner are called “true” vectors, or *polar* vectors. However, the vector $\mathbf{a} \times \mathbf{b}$ behaves differently — its components are evidently *unchanged* by the transformation $(x, y, z) \rightarrow (-x, -y, -z)$. Consequently, such vectors are called “pseudovectors” or *axial* vectors (they are closely associated with rotations). A triple cross product $(\mathbf{a} \times \mathbf{b}) \times \mathbf{c}$, corresponding to the cross product of an axial vector $\mathbf{a} \times \mathbf{b}$ and a polar vector \mathbf{c} , yields a true vector.

There is a similar distinction [80] between true scalars and pseudoscalars.⁴ The dot product of two vectors is a true scalar, if they are either both polar or both axial, since it does not change sign under a reversal of the coordinate axes. However, the dot product of a polar vector with an axial vector does change sign under such reversal, and is therefore deemed a *pseudoscalar* — a familiar example is the triple product $(\mathbf{a} \times \mathbf{b}) \cdot \mathbf{c}$ of three polar vectors $\mathbf{a}, \mathbf{b}, \mathbf{c}$.

As remarked in Chap. 5, vector analysis arose as an eclectic distillation of those parts of the quaternion algebra deemed most “practical” for applications and the formulation of physical theories.⁵ But the relationship between them is fraught with pitfalls. Whereas “ordinary” vectors are *polar* vectors, the vector parts of quaternions are inherently *axial* vectors. The uncritical identification of “pure vector” quaternions with ordinary vectors in \mathbb{R}^3 invites trouble, since the quaternion product of two “pure vector” quaternions is *not* a vector. Also, since the *dot* product is a dimension-reducing operation, it would seem more natural for the *cross* product to be a dimension-raising operation, rather than producing an entity of the *same* dimension. Among other quibbles concerning vector analysis, we just mention that it is specific to \mathbb{R}^3 , with neither a natural specialization to \mathbb{R}^2 nor a convincing generalization to \mathbb{R}^n for $n > 3$.

⁴ The term “pseudoscalar” is used here in a different sense than that of §6.1, where it represents the highest-grade element of a Clifford algebra. The intended sense should be clear from the prevailing context.

⁵ A key impetus was the theory of electromagnetism, as exemplified by Maxwell’s *Treatise on Electricity and Magnetism* (1873). The problematic relations between quaternions and modern vector analysis are documented in [20, 54, 108, 412, 428].

Contemporaneous with Hamilton's pursuit of the quaternion algebra, the German school teacher Hermann Günther Grassmann (1809–1877) proposed a systematic new approach to vector multiplications in his treatise *Die lineale Ausdehnungslehre, ...*⁶ (The linear extension theory) of 1844. In it he develops the *inner product* and *outer product* of two vectors. The former is essentially the familiar scalar (dot) product, but the latter yields a “higher-order” entity — namely, an *oriented area* — and outer products of any number of vectors may be formed to generate entities of successively higher dimension.

In view of the fact that Grassmann had little mathematical training, and was “only” a teacher at the *Gymnasium* in Stettin — now Szczecin, Poland — his ideas are remarkable for their sweeping generality and elegant hierarchical structure. However, they were not well received by his contemporaries: August Ferdinand Möbius (1790–1868) judged them to be too abstract, and an essay he submitted, in connection with his aspiration for a university position, was summarized by Ernst Eduard Kummer (1810–1893) as “commendably good material expressed in a deficient form.” A large fraction of the original printing of the *Ausdehnungslehre* remained unsold, and was eventually recycled.

In addition to subsuming the algebra of complex numbers and quaternions, Clifford algebra invokes Grassmann's inner and outer products and combines them into a new kind of “universal” vector product — the *geometric product*. For vectors \mathbf{a}, \mathbf{b} the inner product is defined by $\mathbf{a} \cdot \mathbf{b} = |\mathbf{a}| |\mathbf{b}| \cos \theta$, where θ is the angle between \mathbf{a} and \mathbf{b} . Although this coincides with the “scalar product” in the case of two vectors, we avoid using this term since the inner product can be applied to higher-grade elements — for which the result is *not*, in general, a scalar. The outer product $\mathbf{a} \wedge \mathbf{b}$ defines a bivector representing an *oriented area element* with magnitude $|\mathbf{a}| |\mathbf{b}| \sin \theta$, the area of the parallelogram with sides \mathbf{a} and \mathbf{b} , and orientation described by tracing these sides in that order. This orientation property implies that \wedge is anti-commutative

$$\mathbf{a} \wedge \mathbf{b} = -\mathbf{b} \wedge \mathbf{a} \quad (6.6)$$

(see Fig. 6.1) but it is associative and distributive. A direct consequence of (6.6) is that $\mathbf{a} \wedge \mathbf{b} = 0$ if $\mathbf{b} = \lambda \mathbf{a}$ for any scalar λ .

An ordered outer product of k vectors

$$\mathbf{x}_1 \wedge \mathbf{x}_2 \wedge \cdots \wedge \mathbf{x}_k$$

defines a *blade* of grade k , but it vanishes if the vectors are linearly dependent. Hence, the highest non-vanishing blade that can be defined in \mathbb{R}^n is of grade n . In \mathbb{R}^3 , for example, the trivector $\mathbf{a} \wedge \mathbf{b} \wedge \mathbf{c}$ is an *oriented volume element* (defined by the parallelepiped with edges $\mathbf{a}, \mathbf{b}, \mathbf{c}$). Inner and outer products can be

⁶ In full, *Die lineale Ausdehnungslehre, ein neuer Zweig der Mathematik dargestellt und durch Anwendungen auf die übrigen Zweige der Mathematik, wie auch auf die Statik, Mechanik, die Lehre vom Magnetismus und die Krystallonomie erläutert*.

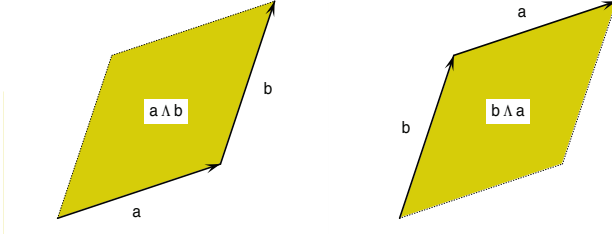


Fig. 6.1. Interpretation of the outer products $\mathbf{a} \wedge \mathbf{b}$ and $\mathbf{b} \wedge \mathbf{a}$ as oriented areas.

combined in various ways. For example, the inner product of a bivector and a vector defines a *vector*, given by the rule

$$(\mathbf{a} \wedge \mathbf{b}) \cdot \mathbf{c} = (\mathbf{c} \cdot \mathbf{b}) \mathbf{a} - (\mathbf{c} \cdot \mathbf{a}) \mathbf{b} = -\mathbf{c} \cdot (\mathbf{a} \wedge \mathbf{b}). \quad (6.7)$$

In $\mathcal{C}\ell_n$, the *geometric product* $\mathbf{a}\mathbf{b}$ of vectors \mathbf{a} and \mathbf{b} is defined to be the sum of the inner product and outer product of those vectors,

$$\mathbf{a}\mathbf{b} = \mathbf{a} \cdot \mathbf{b} + \mathbf{a} \wedge \mathbf{b}. \quad (6.8)$$

This is, in general, a multivector comprising the sum of a scalar and a bivector. Because of the commutative nature of $\mathbf{a} \cdot \mathbf{b}$ and anti-commutative nature of $\mathbf{a} \wedge \mathbf{b}$, the inner and outer products can be expressed as

$$\mathbf{a} \cdot \mathbf{b} = \frac{1}{2}(\mathbf{ab} + \mathbf{ba}) \quad \text{and} \quad \mathbf{a} \wedge \mathbf{b} = \frac{1}{2}(\mathbf{ab} - \mathbf{ba}),$$

i.e., they constitute the *symmetric* and *antisymmetric* parts of the geometric product \mathbf{ab} . The expressions $\frac{1}{2}(\mathbf{ab} - \mathbf{ba})$ and $\frac{1}{2}(\mathbf{ab} + \mathbf{ba})$ are also called the *commutator* and *anti-commutator* products for the vectors \mathbf{a} and \mathbf{b} .

Although the geometric product definition (6.8) is specifically for vectors, it can be extended in a systematic manner to blades and multivectors in $\mathcal{C}\ell_n$. In the latter context, however, its behavior differs from our usual notion of a product. For given vectors $\mathbf{a} \neq 0$ and \mathbf{b} , one can uniquely solve the equation

$$\mathbf{ax} = \mathbf{b}$$

for an unknown vector \mathbf{x} by defining the *inverse* $\mathbf{a}^{-1} = \mathbf{a}/|\mathbf{a}|^2$ of \mathbf{a} , such that $\mathbf{a}^{-1}\mathbf{a} = \mathbf{aa}^{-1} = 1$ (since $\mathbf{a} \wedge \mathbf{a} = 0$). We can also define an inverse for a blade $\mathbf{a}_1 \wedge \mathbf{a}_2 \wedge \dots \wedge \mathbf{a}_k$ as $\mathbf{a}_k \wedge \dots \wedge \mathbf{a}_2 \wedge \mathbf{a}_1 / |\mathbf{a}_1|^2 |\mathbf{a}_2|^2 \dots |\mathbf{a}_k|^2$ — i.e., it is the *reverse* of the blade, divided by the squared norms of the vectors defining it.

When we proceed to multivectors (i.e., sums of blades of different grade), however, it is no longer possible to always define an inverse, since the product of two multivectors may vanish even when they are individually non-zero. For example, in $\mathcal{C}\ell_{0,3}$ one can easily verify that

$$(\mathbf{e}_2 + \mathbf{e}_3\mathbf{e}_1)(\mathbf{e}_3 + \mathbf{e}_2\mathbf{e}_1) = 0,$$

and thus neither $\mathbf{e}_2 + \mathbf{e}_3\mathbf{e}_1$ nor $\mathbf{e}_3 + \mathbf{e}_2\mathbf{e}_1$ admits an inverse, since the existence of an inverse for either would imply that the other is 0. Non-zero elements for which the product with some other non-zero element vanishes, and hence no inverse exists, are called *zero divisors* (this is a new algebraic phenomenon — not evident⁷ among the real numbers, complex numbers, or quaternions). On the other hand, those elements that do have inverses are called *units*, and the set of all units forms a group: the product of two units is always a unit.

6.4 Reflections and Rotations

Any vector \mathbf{a} can be resolved into components parallel and perpendicular to a given unit vector \mathbf{n} . Namely, $\mathbf{a} = \mathbf{a}_{\parallel} + \mathbf{a}_{\perp}$ with $\mathbf{a}_{\parallel} = (\mathbf{n} \cdot \mathbf{a})\mathbf{n}$ and $\mathbf{a}_{\perp} = \mathbf{a} - \mathbf{a}_{\parallel}$. The *reflection* of \mathbf{a} by \mathbf{n} is defined to be the vector $\mathbf{a}_{\parallel} - \mathbf{a}_{\perp}$ that preserves the parallel component of \mathbf{a} , but reverses its perpendicular component.

The reflection of \mathbf{a} by \mathbf{n} can be concisely expressed as a geometric product, $\mathbf{n} \mathbf{a} \mathbf{n}$. To verify this, we expand the product using (6.8) to obtain

$$\mathbf{n} \mathbf{a} \mathbf{n} = (\mathbf{n} \cdot \mathbf{a})\mathbf{n} + (\mathbf{n} \wedge \mathbf{a}) \cdot \mathbf{n} + (\mathbf{n} \wedge \mathbf{a}) \wedge \mathbf{n}.$$

The third term on the right vanishes, since the three vectors are not linearly independent. Also, the first is evidently just \mathbf{a}_{\parallel} . Thus, it remains to show that the second term $(\mathbf{n} \wedge \mathbf{a}) \cdot \mathbf{n}$ equals $-\mathbf{a}_{\perp}$. Using (6.7), we obtain

$$(\mathbf{n} \wedge \mathbf{a}) \cdot \mathbf{n} = (\mathbf{n} \cdot \mathbf{a})\mathbf{n} - (\mathbf{n} \cdot \mathbf{n})\mathbf{a} = \mathbf{a}_{\parallel} - \mathbf{a} = -\mathbf{a}_{\perp}.$$

To obtain a vector \mathbf{b} by the reflection of a vector \mathbf{a} in a unit vector \mathbf{n} , where $|\mathbf{b}| = |\mathbf{a}|$, we use the (unit) *bisector* of \mathbf{a} and \mathbf{b} ,

$$\mathbf{n} = \frac{\mathbf{a} + \mathbf{b}}{|\mathbf{a} + \mathbf{b}|}. \quad (6.9)$$

The description of the reflection of \mathbf{a} by \mathbf{n} as $\mathbf{n} \mathbf{a} \mathbf{n}$ holds in \mathbb{R}^n for all n .

If we successively apply two reflections to a vector \mathbf{a} , specified by the unit vectors \mathbf{n} and \mathbf{m} , the result

$$\mathbf{m} \mathbf{n} \mathbf{a} \mathbf{n} \mathbf{m}$$

corresponds to a *rotation* of the vector \mathbf{a} . The plane of rotation is specified by the bivector $\mathbf{m} \wedge \mathbf{n}$, and the angle of rotation is 2θ where $\theta \in [0, \pi]$ is defined by $\cos \theta = \mathbf{m} \cdot \mathbf{n}$. Thus, the geometric product

$$\mathbf{R} = \mathbf{m} \mathbf{n} = \mathbf{m} \cdot \mathbf{n} + \mathbf{m} \wedge \mathbf{n} \quad (6.10)$$

⁷ The algebra of $n \times n$ matrices is a familiar context in which zero divisors arise — the zero divisors are precisely the (non-vanishing) *singular* matrices.

of two unit vectors is said to define a *rotor* in \mathbb{R}^n . By introducing the *reverse* of this rotor as $\tilde{\mathbf{R}} = \mathbf{n} \mathbf{m}$, the rotation of \mathbf{a} can be expressed as $\mathbf{R} \mathbf{a} \tilde{\mathbf{R}}$. A rotor and its reverse satisfy $\mathbf{R} \tilde{\mathbf{R}} = 1$, consistent with the fact that a rotation of \mathbf{a} changes its *orientation*, but not its *magnitude*.

By the definitions of $\mathbf{m} \cdot \mathbf{n}$ and $\mathbf{m} \wedge \mathbf{n}$, the rotor (6.10) can be written as

$$\mathbf{R} = \cos \theta + \sin \theta \frac{\mathbf{m} \wedge \mathbf{n}}{|\mathbf{m} \wedge \mathbf{n}|}. \quad (6.11)$$

This may be regarded as generalizing the unit complex number $\cos \theta + \sin \theta i$, which defines a rotation operator in \mathbb{R}^2 , and unit quaternion $\cos \theta + \sin \theta \mathbf{n}$ — a rotation operator in \mathbb{R}^3 . By replacing the imaginary unit “ i ” or unit vector \mathbf{n} appropriate to these contexts by a *unit bivector*, the formula (6.11) furnishes a “universal” rotation operator — valid in \mathbb{R}^n for any n . Furthermore, it can be applied to entities of *any grade*, not just grade one vectors.

Consider the rotation of a vector \mathbf{a} onto another vector \mathbf{b} , where $|\mathbf{b}| = |\mathbf{a}|$. Among all possible rotors that accomplish this, the “simplest” is the one for which \mathbf{a} is transformed into \mathbf{b} by a motion in their common plane, i.e., along a *great circle*. The rotor that accomplishes this can be specified as

$$\mathbf{R} = \frac{\mathbf{a} + \mathbf{b}}{|\mathbf{a} + \mathbf{b}|} \frac{\mathbf{a}}{|\mathbf{a}|}.$$

We recognize the first term as the vector (6.9) that reflects \mathbf{a} onto \mathbf{b} , and the second term simply serves to convert this vector into a bivector (note that the reflection of any vector in itself is the identity operation).

As with the quaternion rotation operators, the rotor (6.11) can be written in exponential form as $\exp(\theta \mathbf{b})$, where $\mathbf{b} = (\mathbf{m} \wedge \mathbf{n})/|\mathbf{m} \wedge \mathbf{n}|$ is the unit bivector that specifies the plane of rotation. Note that the *plane of rotation* is a valid concept in \mathbb{R}^n for any n — as distinct from the *center of rotation* in \mathbb{R}^2 or the *axis of rotation* in \mathbb{R}^3 . The rotors defined by (6.10) or (6.11) constitute a *group* under the geometric product operation. Thus, the outcome of applying rotor \mathbf{R}_1 then rotor \mathbf{R}_2 is equivalent to that of applying the single rotor $\mathbf{R} = \mathbf{R}_2 \mathbf{R}_1$. The reverse of this compound rotor is defined by $\tilde{\mathbf{R}} = \tilde{\mathbf{R}}_1 \tilde{\mathbf{R}}_2$.

Coordinate Systems

... the knowledge at which geometry aims is knowledge of the eternal, and not of aught perishing and transient.

Plato (ca. 427–347 BC), *The Republic*, Book VII [261]

Geometry enlightens the intellect, and sets one's mind right. All its proofs are very clear and orderly. It is hardly possible for errors to enter into geometrical reasoning, because it is so well arranged and orderly. Thus, the mind that constantly applies itself to geometry is not likely to fall into error. In this convenient way, the person who knows geometry acquires intelligence.

Ibn Khaldûn (1332–1406), *The Muqaddimah*

Coordinates may be regarded as a powerful and versatile means whereby the tools of algebra and analysis can be brought to bear upon various geometrical problems — constructions, transformations, analysis of shape and incidence relationships, etc. They are obviously crucial to the computer implementation of geometrical algorithms and the visualization of their results.

To many readers, the term “coordinates” is doubtless synonymous with *Cartesian* coordinates. Our concern here, however, is with a much broader and more fruitful interpretation of this term. For example, the formulation and solution of many scientific and engineering problems may be facilitated by invoking appropriate *curvilinear* coordinates in lieu of a Cartesian system. Proficiency in the problems of mensuration (measuring angles, lengths, areas, volumes, etc.) and the manipulation of vectors and tensors within curvilinear coordinate systems is thus invaluable in scientific computations.

In two dimensions, the Cartesian coordinates of a point may be identified with the real and imaginary parts of a complex number. *Conformal mapping* (i.e., the geometrical study of analytic functions of a complex variable) offers a

powerful and elegant approach to the construction and analysis of curvilinear coordinate systems (see Chap. 4). Such methods are also valuable in solving two-dimensional physical problems governed by Laplace's equation (electrostatic potentials, incompressible fluid flow, etc.) by simplifying the loci along which the boundary conditions hold. Although the complex numbers cannot be extended to a “three-dimensional number” system, the (non-commutative) algebra of *four*-dimensional numbers known as *quaternions* (see Chap. 5) is useful in describing the coordinate transformations associated with rotations in \mathbb{R}^3 . As noted in Chap. 5, the now-familiar concepts of three-dimensional vector analysis were distilled from the algebra of quaternions.

It is often desirable in geometrical problems to provide a rigorous means of describing and analyzing behavior “at infinity.” This need is satisfied by using *homogeneous coordinates* — the natural language of *projective geometry*. By eliminating certain “exceptional” geometrical situations, projective geometry offers an elegant unifying perspective — many formerly disparate results are seen to be different facets of a smaller system of fundamental relations.

On the other hand, in many geometrical problems we must focus on just a finite region, and it then becomes desirable to have a more “balanced” system than Cartesian coordinates for specifying location within that region. Here, the use of *barycentric coordinates* is recommended — barycentric formulations do not rely on the arbitrary choice of a special point as origin, and can often be expected to yield deeper geometrical insight and better numerical stability over the domain of interest than Cartesian formulations.

Finally, problems arise in which use of Cartesian coordinates is *impossible*, namely, geometrical configurations in *non-Euclidean spaces*. Suppose we are concerned with analyzing geometrical configurations “in” a curved surface \mathcal{S} . By this we mean that the curved surface is considered as a two-dimensional space in its own right, within which any motions or measurements are confined — we make no reference to the three-dimensional Euclidean space containing \mathcal{S} , that provides a perspective from which we can “see” the surface curvature. A curved (i.e., non-Euclidean) space such as \mathcal{S} does not admit construction of a Cartesian coordinate system. Correspondingly, in such a space, familiar notions — such as *distance*, *straight line*, or *parallelism* — acquire subtle new interpretations in terms of curvilinear coordinates that span the space.

We examine these coordinate schemes in greater detail below. Our goal is not to present a rigorous and exhaustive discussion, which would consume more space than we can afford, but rather to impart basic knowledge of the main concepts (references are provided so the reader can further investigate each approach in detail). One should bear in mind that *any* coordinate system is merely an artifact imposed on a geometrical problem by the human mind — it has no “real” existence, being merely an intermediary aid to visualization, analysis, and computation. Familiarity with a variety of coordinate methods helps instill a detached perspective — encouraging one to seek out the most propitious system of coordinates for the problem at hand.

7.1 Cartesian Coordinates

The first systematic use of coordinates may be traced to the year 1637 in which René Descartes (1596–1650) published his *Discours de la méthode pour bien conduire sa raison et chercher la vérité dans les sciences* (Discourse on the Method of Rightly Conducting the Reason and Seeking Truth in the Sciences). The third Appendix, *La géométrie*, of the *Discours* introduces the notion that a point P in the plane may be uniquely represented as an ordered pair (x, y) of real numbers. This is accomplished by choosing a distinguished point O as the *origin*, and two directed orthogonal lines OX and OY through O defining the *coordinate axes*. The numbers x and y then measure the (signed) distances of P from OY and OX (see Fig. 7.1) — they are the *Cartesian coordinates* of P . The generalization to three or more dimensions is straightforward.

Seminal ideas often emerge independently among the great thinkers of a given epoch, and the concept of coordinate representation of points is implicit in contemporaneous (though unpublished) correspondence of Pierre de Fermat (1601–1665). In the coordinate-based approach, the distance d between two points $P_1 = (x_1, y_1)$ and $P_2 = (x_2, y_2)$ is computed from the relation

$$d^2 = (x_2 - x_1)^2 + (y_2 - y_1)^2, \quad (7.1)$$

which we recognize as an expression of the Pythagorean theorem for a right triangle of hypotenuse d and sides $x_2 - x_1$, $y_2 - y_1$ parallel to the coordinate axes. Of course, the Pythagorean theorem predates Descartes and Fermat by two millenia, but coordinate methods confer a different *interpretation* on this ancient result. Instead of regarding (7.1) as a purely geometrical relationship (to the ancient Greek geometers, the “squares” literally meant the *areas* of the squares erected on the sides of a triangle — see §2.2) the Cartesian method transforms this relation into an *algebraic equation* from which numerical values for d can be computed once values for (x_1, y_1) and (x_2, y_2) are given.

Whereas classical Euclidean geometry was confined to “simple” forms — lines, circles, conics, etc. — specified by intuitive definitions or constructions, the Cartesian approach allowed a wealth of new shapes to be introduced and studied by regarding the coordinates as variables that satisfy prescribed rules. The powerful techniques of *algebra* and *analysis* are thus brought to bear on

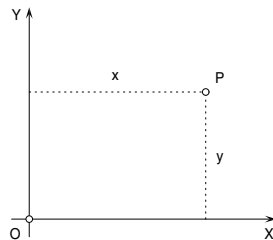


Fig. 7.1. Cartesian coordinates (x, y) of a point P .

geometry problems. Descartes described the awkwardness characterizing prior use of algebraic methods in geometry as follows [127]:

... I beg you to observe in passing that the considerations that forced ancient writers to use arithmetical terms in geometry, thus making it impossible for them to proceed beyond a point where they could see clearly the relation between the two subjects, caused much obscurity and embarrassment, in their attempts at explanation.

Suppose, for example, we stipulate the coordinates to be functions

$$x(t) \quad \text{and} \quad y(t) \tag{7.2}$$

of some independent variable or *parameter* t . This pair of functions defines a *parametric curve*: as t varies, the point $(x(t), y(t))$ traces a locus in the plane. Assuming the functions (7.2) are differentiable, the analysis of such parametric forms using the differential calculus is the foundation of *differential geometry* — i.e., the study of “intrinsic” properties (tangents, curvatures, etc.) that are *independent* of the parameterization and the chosen coordinate system. We shall survey the methods of differential geometry in Chap. 8.

Alternately, we may impose mutual constraints on Cartesian coordinates in the plane, typically expressed by an equation of the form

$$f(x, y) = 0. \tag{7.3}$$

A curve that is represented in the form (7.3) is usually called an *implicit curve* — it is much more difficult to trace the curve from such a representation than from the parametric representation (7.2). When f is a *polynomial* in x and y , the curve defined by (7.3) is a *plane algebraic curve*. The study of such curves, and of analogously-defined space curves and surfaces, is the domain of a profound and beautiful theory known as *algebraic geometry* — an introduction to its key ideas and methods is presented in Chap. 9.

Descartes called loci that can be described by finite algebraic expressions of the form (7.2) or (7.3) *geometrical curves*. On the other hand, loci that do not admit such definitions, but may otherwise be described in terms of a kinematical or similar construction, he considered to be *mechanical curves*. We now call the former *algebraic*, and the latter *transcendental*, curves.

Prior to the advent of coordinates, the relation of geometry and algebra in mathematical thought was converse to our modern view: a kind of *geometrical algebra* — i.e., the solution of algebraic equations by geometrical methods — prevailed. For example, Euclid used arguments concerning the areas of plane figures to solve quadratic equations, while Omar Khayyam solved certain cubic equations in terms of the intersections of conic curves (see §2.3). This mode of thought was predominant until the era of Leibniz and Newton.

7.2 Barycentric Coordinates

Given a function $f(x)$ of a variable x , we are often interested in its variation over only a finite interval I in that variable. Choosing a fixed point as origin, we may interpret x as a one-dimensional Cartesian coordinate, and depending on whether the origin is to the left of, to the right of, or within the interval I , the value of x is positive, negative, or of non-constant sign over I . This arbitrariness in the choice of origin is not a mere curiosity: it may also have important consequences for practical computations.

Consider, for example, the case where f is a degree- n polynomial

$$f(x) = \sum_{k=0}^n a_k x^k, \quad (7.4)$$

and the origin is to the left of I , at a distance large compared to its width. Then x has a large positive value within I , and if the coefficients a_0, \dots, a_n are of alternating sign, computing values for $f(x)$ incurs addition of quantities of large magnitude but opposite signs — a circumstance that, in floating-point arithmetic, can incur catastrophic loss of accuracy (see Chap. 12).



Fig. 7.2. *Der barycentrische Calcul* by A. F. Möbius (1827) — from the Special Collections, Science Library, University of Michigan (reproduced with permission).

Even if we take an endpoint of the interval I as origin, use of the Cartesian coordinate x yields an “unbalanced” representation of $f(x)$ over the entire interval — its values (or roots) near the other endpoint are more difficult to compute as accurately. A related problem is that the coefficients a_0, \dots, a_n in (7.4) do not convey much useful insight concerning the variation of $f(x)$ over the interval I ($r! a_r$ is the r -th derivative of f at $x = 0$). Clearly, it would be advantageous to have a representation from which useful information about the variation of f can be gleaned by merely inspecting its coefficients.

Such a representation is based on the “barycentric coordinates” proposed by A. F. Möbius¹ in his 1827 treatise *Der barycentrische Calcul: Ein neues Hülfsmittel zur analytischen Behandlung der Geometrie* (see Fig. 7.2). As we shall see, the term “barycentric” arises from a simple concept in mechanics — namely, the *center of mass* of a system of particles.

7.2.1 Barycentric Coordinates on Intervals

Consider first one-dimensional barycentric coordinates on an interval I that corresponds to Cartesian coordinates $x \in [a, b]$ referred to some origin. If we imagine I to be a rigid rod, with masses v and u attached to its left and right ends, we may ask: what values should these masses have, such that the rod will balance about point x without tilting to the left or right (Fig. 7.3)?

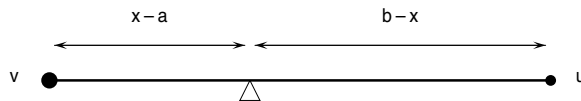


Fig. 7.3. One-dimensional barycentric coordinates — masses u and v given by (7.6) yield equilibrium about point x when placed at the endpoints of the interval $[a, b]$.

We call u and v the *barycentric coordinates* of point x with respect to the interval $[a, b]$. Taking moments about the pivot point, we must have

$$(x - a)v = (b - x)u,$$

i.e., x must be the *center of mass* for u and v . This allows to infer only the *ratio* $u : v$ — to obtain definite values for these masses, we impose the additional “normalization” constraint

$$u + v = 1, \tag{7.5}$$

i.e., the total mass is unity. We then have the explicit formulae

¹ Möbius, whom we met in the context of conformal maps, is perhaps best known as the discoverer of the *Möbius band* — a “non-orientable” or one-sided surface obtained by glueing together the ends of a twisted strip of paper — although this honor may properly belong to his contemporary, Johann Benedict Listing [197].

$$u = \frac{x-a}{b-a} \quad \text{and} \quad v = \frac{b-x}{b-a} \quad (7.6)$$

for the barycentric coordinates of x with respect to $[a, b]$.

To obtain a degree- n basis for polynomials on the interval I , we perform a binomial expansion of the left-hand side of (7.5) raised to the n -th power:

$$(u+v)^n = \sum_{k=0}^n \binom{n}{k} u^k v^{n-k} = 1.$$

The $n+1$ terms in this expansion, which we denote by

$$b_k^n(u, v) = \binom{n}{k} u^k v^{n-k}, \quad (7.7)$$

are linearly independent. Hence, by a suitable choice of the coefficients c_k , any polynomial given in the power form (7.4) may be cast in the barycentric form

$$P(u, v) = \sum_{k=0}^n c_k b_k^n(u, v). \quad (7.8)$$

Some noteworthy properties of the barycentric polynomials (7.7) are: they are homogeneous in u and v ; they are non-negative over the domain I ; and they sum to unity. Many useful features of barycentric forms, and algorithms for manipulating them, result from these simple facts — see Chap. 11 for a detailed discussion. Writing both u and v as arguments in (7.8) emphasizes the symmetry of the barycentric form, even though these variables are redundant and one of them can be eliminated by use of (7.5). For example, the barycentric form of a polynomial $P(t)$ on the interval $t \in [0, 1]$ can be expressed in an explicitly univariate manner as

$$P(t) = \sum_{k=0}^n c_k b_k^n(t), \quad \text{where } b_k^n(t) = \binom{n}{k} (1-t)^{n-k} t^k.$$

The functions $b_k^n(t)$, $k = 0, \dots, n$ constitute the *Bernstein basis* for degree- n polynomials on $[0, 1]$. We shall explore them further in Chap. 11.

7.2.2 Barycentric Coordinates on Triangles

Given a rectangular domain $D \subset \mathbb{R}^2$ of the form $(x, y) \in [a, b] \times [c, d]$ we may define barycentric coordinates on each of the intervals $x \in [a, b]$, $y \in [c, d]$ as described above, and use them to specify location within D . A basis for “tensor-product” bivariate polynomials may then be constructed from the products of the Bernstein basis functions on the two intervals.

A more fundamental approach, however, is based on a triangular (simplex) domain in \mathbb{R}^2 . Let T be a *reference triangle* in the plane, defined by its vertices $\mathbf{p}_k = (x_k, y_k)$ for $k = 1, 2, 3$. If T is a proper triangle — i.e., the vertices are not collinear — the value of the determinant

$$\Delta = \begin{vmatrix} 1 & 1 & 1 \\ x_1 & x_2 & x_3 \\ y_1 & y_2 & y_3 \end{vmatrix} \quad (7.9)$$

is non-zero, and the *signed area* of T is given by $A = \frac{1}{2} \Delta$, with the convention that A is positive or negative according to whether the vertices of T have been labelled in a counter-clockwise or clockwise sense.

Now for any point $\mathbf{p} = (x, y)$ in the plane, consider the triangles T_1, T_2, T_3 subtended there by the three sides of the reference triangle (see Fig. 7.4). We order the vertices of these triangles as follows:

$$(\mathbf{p}, \mathbf{p}_2, \mathbf{p}_3), \quad (\mathbf{p}_1, \mathbf{p}, \mathbf{p}_3), \quad (\mathbf{p}_1, \mathbf{p}_2, \mathbf{p}) \quad (7.10)$$

and define their signed areas $A_1 = \frac{1}{2} \Delta_1$, $A_2 = \frac{1}{2} \Delta_2$, $A_3 = \frac{1}{2} \Delta_3$ in terms of the determinants

$$\Delta_1 = \begin{vmatrix} 1 & 1 & 1 \\ x & x_2 & x_3 \\ y & y_2 & y_3 \end{vmatrix}, \quad \Delta_2 = \begin{vmatrix} 1 & 1 & 1 \\ x_1 & x & x_3 \\ y_1 & y & y_3 \end{vmatrix}, \quad \Delta_3 = \begin{vmatrix} 1 & 1 & 1 \\ x_1 & x_2 & x \\ y_1 & y_2 & y \end{vmatrix}. \quad (7.11)$$

The barycentric coordinates (u, v, w) of the point $\mathbf{p} = (x, y)$ with respect to the reference triangle T are then defined by the area-ratios

$$u = \frac{\Delta_1}{\Delta}, \quad v = \frac{\Delta_2}{\Delta}, \quad w = \frac{\Delta_3}{\Delta}. \quad (7.12)$$

The barycentric coordinates (u, v, w) have two important features: (a) they satisfy the normalization condition

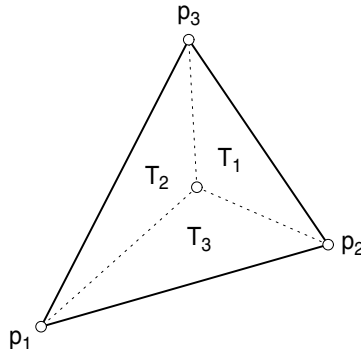


Fig. 7.4. Geometry of two-dimensional barycentric coordinates.

$$u + v + w = 1, \quad (7.13)$$

and (b) they are all non-negative if and only if the point \mathbf{p} lies inside, or on the boundary of, the reference triangle T . Note that property (a) follows from the interpretation of u, v, w as area ratios, while (b) is a consequence of the specific vertex orderings (7.10) we chose for the triangles T_1, T_2, T_3 .

Expressions (7.9)–(7.12) defining the barycentric coordinates (u, v, w) in terms of the Cartesian coordinates (x, y) can be written in matrix form as

$$\begin{bmatrix} u \\ v \\ w \end{bmatrix} = \frac{1}{\Delta} \begin{bmatrix} y_2 - y_3 & x_3 - x_2 & x_2y_3 - x_3y_2 \\ y_3 - y_1 & x_1 - x_3 & x_3y_1 - x_1y_3 \\ y_1 - y_2 & x_2 - x_1 & x_1y_2 - x_2y_1 \end{bmatrix} \begin{bmatrix} x \\ y \\ 1 \end{bmatrix}. \quad (7.14)$$

On inverting the above, we find that Cartesian coordinates are recovered from barycentric coordinates according to

$$\begin{bmatrix} x \\ y \\ 1 \end{bmatrix} = \begin{bmatrix} x_1 & x_2 & x_3 \\ y_1 & y_2 & y_3 \\ 1 & 1 & 1 \end{bmatrix} \begin{bmatrix} u \\ v \\ w \end{bmatrix}, \quad (7.15)$$

which can be more concisely expressed in the vector form

$$\mathbf{p} = u \mathbf{p}_1 + v \mathbf{p}_2 + w \mathbf{p}_3.$$

Thus u, v, w can be regarded as masses placed at the vertices $\mathbf{p}_1, \mathbf{p}_2, \mathbf{p}_3$ of T , subject to the normalization (7.13), with point \mathbf{p} as their center of mass.

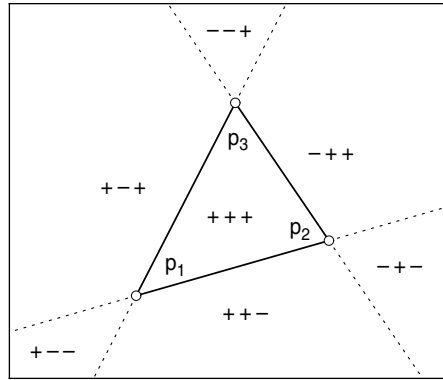


Fig. 7.5. Signature of barycentric coordinates over the entire plane.

The vertices $\mathbf{p}_1, \mathbf{p}_2, \mathbf{p}_3$ of T have barycentric coordinates $(1, 0, 0), (0, 1, 0), (0, 0, 1)$ while its *barycenter* $\frac{1}{3}(\mathbf{p}_1 + \mathbf{p}_2 + \mathbf{p}_3)$ has coordinates $(\frac{1}{3}, \frac{1}{3}, \frac{1}{3})$. Note also that u, v, w remain constant along lines parallel to the three sides $\mathbf{p}_2 - \mathbf{p}_3, \mathbf{p}_3 - \mathbf{p}_1, \mathbf{p}_1 - \mathbf{p}_2$ of T , respectively. In particular, $u = 0$ along $\mathbf{p}_2 - \mathbf{p}_3, v = 0$

along $\mathbf{p}_3 - \mathbf{p}_1$, and $w = 0$ along $\mathbf{p}_1 - \mathbf{p}_2$. Also, on each side of T the two non-zero members of (u, v, w) specialize to the *univariate* barycentric coordinates appropriate to that side (e.g., along $w = 0$, the coordinates u and v represent the fractional distances of a point \mathbf{p} from the vertices \mathbf{p}_2 and \mathbf{p}_1).

By extending the sides of T indefinitely, we divide its exterior into the six regions shown in Fig. 7.5. In the three regions adjacent to the sides of T , two of the barycentric coordinates are positive and the third is negative, while in the three wedge-shaped regions emanating from the vertices of T , only one is positive and the other two are negative.

7.2.3 Transformation of the Domain

Suppose (u, v, w) are the barycentric coordinates of \mathbf{p} relative to a triangle T with vertices $\mathbf{p}_1, \mathbf{p}_2, \mathbf{p}_3$ and we wish to determine the barycentric coordinates (u', v', w') of \mathbf{p} relative to another triangle T' with vertices $\mathbf{p}'_1, \mathbf{p}'_2, \mathbf{p}'_3$, so that

$$\mathbf{p} = u\mathbf{p}_1 + v\mathbf{p}_2 + w\mathbf{p}_3 = u'\mathbf{p}'_1 + v'\mathbf{p}'_2 + w'\mathbf{p}'_3. \quad (7.16)$$

Let α_{jk} for $1 \leq j, k \leq 3$ be the k -th barycentric coordinate of the vertex \mathbf{p}_j of T with respect to T' — i.e.,

$$\mathbf{p}_j = \alpha_{j1}\mathbf{p}'_1 + \alpha_{j2}\mathbf{p}'_2 + \alpha_{j3}\mathbf{p}'_3, \quad j = 1, 2, 3. \quad (7.17)$$

Substituting (7.17) into (7.16) and equating coefficients of $\mathbf{p}'_1, \mathbf{p}'_2, \mathbf{p}'_3$ we obtain

$$[u' \ v' \ w'] = [u \ v \ w] \begin{bmatrix} \alpha_{11} & \alpha_{12} & \alpha_{13} \\ \alpha_{21} & \alpha_{22} & \alpha_{23} \\ \alpha_{31} & \alpha_{32} & \alpha_{33} \end{bmatrix}.$$

Conversely, if β_{jk} for $1 \leq j, k \leq 3$ is the k -th barycentric coordinate of the vertex \mathbf{p}'_j of T' with respect to T , then

$$[u \ v \ w] = [u' \ v' \ w'] \begin{bmatrix} \beta_{11} & \beta_{12} & \beta_{13} \\ \beta_{21} & \beta_{22} & \beta_{23} \\ \beta_{31} & \beta_{32} & \beta_{33} \end{bmatrix}.$$

Clearly, the matrices \mathbf{A} and \mathbf{B} with elements α_{jk} and β_{jk} are inverses of each other: $\mathbf{AB} = \mathbf{I}$, the identity matrix.

7.2.4 Barycentric Points and Vectors

In Cartesian coordinates, we are accustomed to freely “adding” points, so that if $\mathbf{p}_a = (x_a, y_a)$ and $\mathbf{p}_b = (x_b, y_b)$, when we write $\mathbf{p}_c = \mathbf{p}_a + \mathbf{p}_b$ we mean that the Cartesian coordinates of \mathbf{p}_c are given by $x_c = x_a + x_b$ and $y_c = y_a + y_b$. Actually, we are not adding points here, but rather the *vectors* from the origin $(0, 0)$ to the prescribed points (x_a, y_a) and (x_b, y_b) .

How do we “add” two points \mathbf{p}_a and \mathbf{p}_b specified in terms of barycentric, rather than Cartesian, coordinates? Clearly, we cannot simply add the triples (u_a, v_a, w_a) and (u_b, v_b, w_b) component-wise to obtain (u_c, v_c, w_c) since then $u_c + v_c + w_c = 2$, which violates the normalization condition (7.13). In fact, the transformation (7.14) indicates that the proper barycentric coordinates for the point $(x_c, y_c) = (x_a + x_b, y_a + y_b)$ are given by

$$(u_c, v_c, w_c) = (u_a, v_a, w_a) + (u_b, v_b, w_b) - \frac{(x_2y_3 - x_3y_2, x_3y_1 - x_1y_3, x_1y_2 - x_2y_1)}{\Delta}, \quad (7.18)$$

so the problem is not simply one of re-normalizing after adding component-wise. Thus, points in a barycentric system are *not* equivalent to vectors (since there is no origin) and the formulae (7.18) must be invoked to “add” points — in the vectorial sense — specified by barycentric coordinates.

Consider now the *difference* of the barycentric coordinates of two points $\mathbf{p}_a = (u_a, v_a, w_a)$ and $\mathbf{p}_b = (u_b, v_b, w_b)$. Writing

$$(\lambda, \mu, \nu) = (u_a - u_b, v_a - v_b, w_a - w_b), \quad (7.19)$$

and noting that $u_a + v_a + w_a = u_b + v_b + w_b = 1$, we see that

$$\lambda + \mu + \nu = 0. \quad (7.20)$$

Furthermore, if $(\lambda_1, \mu_1, \nu_1)$ and $(\lambda_2, \mu_2, \nu_2)$ are any two triples that satisfy (7.20), and we add them component-wise to give

$$(\lambda_3, \mu_3, \nu_3) = (\lambda_1 + \lambda_2, \mu_1 + \mu_2, \nu_1 + \nu_2),$$

it is clear that $(\lambda_3, \mu_3, \nu_3)$ will also satisfy (7.20). Finally, any triple (λ, μ, ν) satisfying (7.20) may be scaled by a non-zero constant c to yield a new triple $(c\lambda, c\mu, c\nu)$ that also satisfies (7.20).

Thus, we regard any triple (λ, μ, ν) satisfying (7.20) as specifying a *vector* in barycentric form, just as any triple (u, v, w) satisfying (7.13) defines a point. Thus, for example, if we wish to parameterize the line between the two points (u_a, v_a, w_a) and (u_b, v_b, w_b) , we may write

$$(u(t), v(t), w(t)) = (u_a + \lambda t, v_a + \mu t, w_a + \nu t),$$

with (λ, μ, ν) given by (7.19), and it is then guaranteed that

$$u(t) + v(t) + w(t) \equiv 1.$$

We define the *norm* $\|\mathbf{v}\|$ of the barycentric vector $\mathbf{v} = (\lambda, \mu, \nu)$ by means of a symmetric quadratic form in its components:

$$\|\mathbf{v}\|^2 = [\lambda \mu \nu] \begin{bmatrix} M_{11} & M_{12} & M_{13} \\ M_{21} & M_{22} & M_{23} \\ M_{31} & M_{32} & M_{33} \end{bmatrix} \begin{bmatrix} \lambda \\ \mu \\ \nu \end{bmatrix}. \quad (7.21)$$

The matrix \mathbf{M} in (7.21) may be interpreted as a “metric” for measuring the lengths of barycentric vectors: its elements are given by

$$M_{ij} = M_{ji} = x_i x_j + y_i y_j \quad \text{for } i, j = 1, 2, 3. \quad (7.22)$$

The reason for this choice is that if the vector \mathbf{v} corresponds to the difference of two points $\mathbf{p}_a = (x_a, y_a)$ and $\mathbf{p}_b = (x_b, y_b)$ with barycentric coordinates (u_a, v_a, w_a) and (u_b, v_b, w_b) , we have

$$x_a - x_b = \lambda x_1 + \mu x_2 + \nu x_3, \quad y_a - y_b = \lambda y_1 + \mu y_2 + \nu y_3, \quad (7.23)$$

and by squaring and adding the above expressions, we see that

$$\|\mathbf{v}\|^2 = (x_a - x_b)^2 + (y_a - y_b)^2,$$

— i.e., the norm of the barycentric vector \mathbf{v} is simply the Euclidean distance between the points \mathbf{p}_a and \mathbf{p}_b . The norm defined by (7.21) exhibits the usual properties of a vector norm, namely $\|\mathbf{v}\| \geq 0$ for all \mathbf{v} ; $\|\mathbf{v}\| = 0 \iff \mathbf{v} = \mathbf{0}$; $\|k\mathbf{v}\| = |k| \|\mathbf{v}\|$; and the “triangle inequality” $\|\mathbf{v}_1 + \mathbf{v}_2\| \leq \|\mathbf{v}_1\| + \|\mathbf{v}_2\|$.

By the same reasoning behind equations (7.23), we can write the *Cartesian* components v_x and v_y of the barycentric vector $\mathbf{v} = (\lambda, \mu, \nu)$ as

$$v_x = \lambda x_1 + \mu x_2 + \nu x_3, \quad v_y = \lambda y_1 + \mu y_2 + \nu y_3. \quad (7.24)$$

Thus, to compute the barycentric vector (λ, μ, ν) corresponding to a Cartesian vector (v_x, v_y) we consider (7.24) together with the normalization condition (7.20) as a system of linear equations for λ, μ, ν . The solution is

$$\lambda = \frac{(y_2 - y_3)v_x - (x_2 - x_3)v_y}{\Delta}, \quad \mu = \frac{(y_3 - y_1)v_x - (x_3 - x_1)v_y}{\Delta}, \quad (7.25)$$

and $\nu = -(\lambda + \mu)$. The quadratic form (7.21) can be generalized to define the *dot product* $\mathbf{u} \cdot \mathbf{v}$ of two barycentric vectors $\mathbf{u} = (\alpha, \beta, \gamma)$ and $\mathbf{v} = (\lambda, \mu, \nu)$. To obtain the value of $\mathbf{u} \cdot \mathbf{v}$, we simply contract the matrix with elements (7.22) on the left and right with the sets of barycentric–vector components (α, β, γ) and (λ, μ, ν) . It is not difficult to verify that this gives results in accordance with the usual Cartesian interpretation of dot products.

7.2.5 Directional Derivatives

In Cartesian coordinates, we are familiar with the gradient ∇f of a bivariate function $f(x, y)$. When \mathbf{v} is a unit (Cartesian) vector, the *directional derivative* $\nabla_{\mathbf{v}} f = \mathbf{v} \cdot \nabla f$ is the rate of change of f along \mathbf{v} . We can adapt these ideas to functions $f(u, v, w)$ and vectors $\mathbf{v} = (\lambda, \mu, \nu)$ specified in barycentric form.

Let f_u, f_v, f_w be the partial derivatives of a homogeneous polynomial $f(u, v, w)$ of degree n . By Euler’s theorem for homogeneous functions, these derivatives satisfy at each point (u, v, w) the relation

$$uf_u + vf_v + wf_w = nf,$$

and hence they are not independent. To deduce the barycentric form of $\nabla_{\mathbf{v}} f$, suppose that the Cartesian components of \mathbf{v} are (v_x, v_y) . Expressing these components in terms of the barycentric form by means of (7.24), we have

$$\begin{aligned}\nabla_{\mathbf{v}} f &= v_x f_x + v_y f_y = (\lambda x_1 + \mu x_2 + \nu x_3) f_x + (\lambda y_1 + \mu y_2 + \nu y_3) f_y \\ &= \lambda (x_1 f_x + y_1 f_y) + \mu (x_2 f_x + y_2 f_y) + \nu (x_3 f_x + y_3 f_y).\end{aligned}$$

Now we note that

$$f_u = \frac{\partial f}{\partial u} = \frac{\partial x}{\partial u} \frac{\partial f}{\partial x} + \frac{\partial y}{\partial u} \frac{\partial f}{\partial y} = x_1 f_x + y_1 f_y$$

and likewise for f_v and f_w (the last step follows from equation (7.15)). Thus, on substitution, we find that

$$\nabla_{\mathbf{v}} f = \lambda f_u + \mu f_v + \nu f_w.$$

Note that the individual partial derivatives f_u , f_v , f_w of f with respect to the barycentric coordinates are *not* directional derivatives, since the triples $(1, 0, 0)$, $(0, 1, 0)$, $(0, 0, 1)$ are not barycentric vectors.

Using expressions (7.25) with $(v_x, v_y) = (1, 0)$ and $(0, 1)$, we can easily recover the partial derivatives of f with respect to the Cartesian coordinates:

$$\begin{aligned}f_x &= \frac{(y_2 - y_3)f_u + (y_3 - y_1)f_v + (y_1 - y_2)f_w}{\Delta}, \\ f_y &= \frac{(x_3 - x_2)f_u + (x_1 - x_3)f_v + (x_2 - x_1)f_w}{\Delta}.\end{aligned}$$

7.2.6 Polynomial Bases Over Triangles

We now consider the construction of a *basis* for bivariate polynomials of total degree n on a given triangular domain T . In Cartesian coordinates (x, y) one would ordinarily express such polynomials as

$$P(x, y) = \sum_{j=0}^n \sum_{k=0}^{n-j} a_{jk} x^j y^k \quad (7.26)$$

once a choice for the origin $(x, y) = (0, 0)$ has been made.

To construct a barycentric polynomial basis over the triangle T , we raise the left-hand side of the normalization relation (7.13) to the n -th power and use the *trinomial expansion formula* to obtain:

$$(u + v + w)^n = \sum_{\substack{0 \leq i, j, k \leq n \\ i+j+k=n}} \frac{n!}{i! j! k!} u^i v^j w^k = 1. \quad (7.27)$$

The individual terms of this expansion define the *bivariate barycentric basis functions* of degree n on the chosen reference triangle — we denote them by

$$b_{ijk}^n(u, v, w) = \frac{n!}{i! j! k!} u^i v^j w^k, \quad \text{where } i + j + k = n. \quad (7.28)$$

The total number of these linearly-independent basis functions is

$$\binom{n+2}{2} = \frac{1}{2}(n+1)(n+2),$$

namely, 6 for quadratics, 10 for cubics, etc. The identity (7.27) expresses the *partition of unity* property for the barycentric basis of degree n over T .

Under the mapping (7.14) from Cartesian to barycentric coordinates, the bivariate polynomial (7.26) can be expressed in the form

$$P(u, v, w) = \sum_{\substack{0 \leq i, j, k \leq n \\ i+j+k=n}} c_{ijk} b_{ijk}^n(u, v, w). \quad (7.29)$$

Although P has three arguments, it is really a bivariate polynomial in view of the constraint (7.13) on the barycentric coordinates. Note also the redundancy of the indices in the above expression: in some cases we may prefer to re-write the basis functions in a non-redundant manner as

$$b_{ij}^n(u, v) = \binom{n}{i, j} u^i v^j (1 - u - v)^{n-i-j},$$

where $0 \leq i \leq n$, $0 \leq j \leq n - i$, and the trinomial coefficients are defined by

$$\binom{n}{i, j} = \frac{n!}{i! j! (n - i - j)!}.$$

The bivariate basis (7.28) has the same homogeneity, non-negativity over T , and partition-of-unity properties as in the univariate case. Each basis function $b_{ijk}^n(u, v, w)$ has a single extremum value over T , at the point with barycentric coordinates $(u, v, w) = (i/n, j/n, k/n)$.

7.2.7 Un-normalized Barycentric Coordinates

Thus far, our barycentric formulations have relied upon normalizations such as (7.5) or (7.13) to ensure a *unique* correspondence between (affine) points and barycentric coordinate values. However, such normalizations are not essential. In the plane, for example, we may consider all sets of ratios $u : v : w$ as defining a barycentric coordinate system. As with homogeneous *Cartesian* coordinates (see §7.4), barycentric coordinates of the form (u, v, w) and $(\alpha u, \alpha v, \alpha w)$ with $\alpha \neq 0$ identify exactly the same point. In particular, if we no longer enforce condition (7.13) in the plane, we may admit sets of coordinates satisfying

$$u + v + w = 0,$$

which are impossible in the normalized system. In fact, this relation identifies a *point at infinity* in the un-normalized system. To verify this, we introduce homogeneous Cartesian coordinates into equation (7.15) by multiplying both sides by k ($\neq 0$) and setting $(W, X, Y) = (k, kx, ky)$. It is then apparent that

$$W = 0 \iff u + v + w = 0.$$

Hence, we may regard un-normalized barycentric coordinates as representing the *projective plane* (see §7.4) rather than just the affine plane.

7.2.8 Three or More Dimensions

The construction of barycentric coordinate systems, and of polynomial bases defined in terms of them, can be readily generalized from the one- and two-dimensional cases discussed above to an arbitrary number of dimensions. Any $d+1$ linearly-independent points $\mathbf{p}_0, \dots, \mathbf{p}_d$ in \mathbb{R}^d can be regarded as vertices of a d -dimensional *simplex* \mathcal{S} , defined as the point set

$$\{ \mathbf{p} = \mu_0 \mathbf{p}_0 + \dots + \mu_d \mathbf{p}_d \mid \mu_0 + \dots + \mu_d = 1 \text{ and } \mu_i \geq 0 \} \quad (7.30)$$

— i.e., the set of all points in \mathbb{R}^d that are *convex combinations* of $\mathbf{p}_0, \dots, \mathbf{p}_d$. We define the *faces* $\mathcal{F}_0, \dots, \mathcal{F}_d$ of the simplex \mathcal{S} to be the $d+1$ linear subspaces spanned by convex combinations of the vertices $\mathbf{p}_0, \dots, \mathbf{p}_d$ taken d at a time. Thus, for example, the face \mathcal{F}_k may be defined by omitting the vertex \mathbf{p}_k and its corresponding “weight” μ_k from expression (7.30).

Given any point \mathbf{p} , we construct the $d+1$ simplices $\mathcal{S}_0, \dots, \mathcal{S}_d$ subtended at \mathbf{p} by each face of \mathcal{S} — e.g., \mathcal{S}_k has vertices $\mathbf{p}_0, \dots, \mathbf{p}_{k-1}, \mathbf{p}, \mathbf{p}_{k+1}, \dots, \mathbf{p}_d$. We note that, if \mathbf{p} lies inside \mathcal{S} , these $d+1$ simplices form a *partition* of \mathcal{S} ,

$$\mathcal{S} = \bigcup_{k=0}^d \mathcal{S}_k.$$

The signed volume of \mathcal{S} is given by the $(d+1) \times (d+1)$ determinant

$$\text{vol}(\mathcal{S}) = \begin{vmatrix} 1 & 1 & \cdots & 1 \\ x_0 & x_1 & \cdots & x_d \\ y_0 & y_1 & \cdots & y_d \\ z_0 & z_1 & \cdots & z_d \\ \vdots & \vdots & \ddots & \vdots \\ \vdots & \vdots & \ddots & \vdots \end{vmatrix},$$

where (x_k, y_k, z_k, \dots) are the Cartesian coordinates of vertex \mathbf{p}_k . Similarly, the volume of each subsimplex \mathcal{S}_k is obtained by replacing the column with

entries $1, x_k, y_k, z_k, \dots$ in this determinant by the entries $1, x, y, z, \dots$ (where x, y, z, \dots are the coordinates of the chosen point \mathbf{p}).

The barycentric coordinates of \mathbf{p} with respect to the “reference simplex” \mathcal{S} are then defined to be the $d + 1$ values

$$(u_0, \dots, u_d) = \left(\frac{\text{vol}(\mathcal{S}_0)}{\text{vol}(\mathcal{S})}, \dots, \frac{\text{vol}(\mathcal{S}_d)}{\text{vol}(\mathcal{S})} \right).$$

The division by $\text{vol}(\mathcal{S})$ yields *normalized* barycentric coordinates, that satisfy $u_0 + \dots + u_d = 1$. To obtain a representation of d -dimensional *projective* space, we may omit this division and simply regard the ratios $\text{vol}(\mathcal{S}_0) : \dots : \text{vol}(\mathcal{S}_d)$ as specifying un-normalized barycentric coordinates.

A basis for polynomials of degree n within the domain \mathcal{S} is then given by the terms of the multinomial formula

$$1 \equiv (u_0 + \dots + u_d)^n = \sum_{\substack{0 \leq e_0, \dots, e_d \leq n \\ e_0 + \dots + e_d = n}} \frac{n!}{e_0! \dots e_d!} u_0^{e_0} \cdots u_d^{e_d}.$$

These basis functions are linearly independent, and there are altogether

$$\binom{n+d}{d} = \frac{(n+d)(n+d-1)\cdots(n+1)}{d!}$$

of them. Any degree- n homogeneous polynomial $f(u_0, \dots, u_d)$ can then be described by associating a coefficient $f_{e_0 \dots e_d}$ with each basis function.

One can easily verify that this general scheme is consistent with the lower-dimension cases already discussed. In one dimension, a simplex is just a line segment connecting two points, which are the faces of the simplex, and by its “volume” we mean the (directed) length of that segment. A two-dimensional simplex is a triangle defined by three points; the faces are the triangle edges, and by “volume” we mean its (oriented) area. Finally, in three dimensions, a simplex is a tetrahedron defined by four vertices; its faces are the triangular facets bounding it, and its “volume” is the (signed) spatial volume enclosed by those facets. An elegant property of this barycentric-coordinates hierarchy is that, if we confine our attention to some boundary element of the reference simplex \mathcal{S} by setting one or more of the coordinates to 0 or 1, the remaining “free” coordinates coincide with the barycentric system obtained by regarding that element as a lower-dimension simplex in its own right. In \mathbb{R}^3 , for example, each face of the reference tetrahedron inherits a two-dimensional barycentric system, and each edge a one-dimensional barycentric system.

7.3 Curvilinear Coordinates

Curvilinear coordinates were first systematically developed by the physicist, mathematician, and engineer Gabriel Lamé (1795–1870) in his treatise *Leçons*

sur les coordonnées curvilignes et leurs diverses applications of 1859. He used transformations to curvilinear coordinates in solving certain problems of heat conduction and elasticity. This proved to be a powerful idea: many problems in geometry, partial differential equations, multiple integrals, etc., become much simpler when cast in coordinate systems that reflect their symmetries.

In general, a *coordinate representation* of the Euclidean plane specifies a one-to-one correspondence between its points and pairs of real numbers (ζ, η) . The uniqueness of this correspondence may be contingent on restricting the values of the “coordinates” (ζ, η) . Exceptionally, representations in which the one-to-one correspondence between points and coordinates fails at certain points, or along certain loci, may also be admitted.

Cartesian coordinates are characterized by the property that the loci along which ζ and η remain constant are two families of parallel lines, orthogonal to each other. In this case we use the usual notation (x, y) where x and y are *unrestricted* real values. The distance d between two points is then defined by equation (7.1). By relaxing the requirement that the families of parallel lines be orthogonal, we obtain *oblique coordinates* — for which the distance relation (7.1) must be modified. Employing Cartesian coordinates as a “reference” we consider *curvilinear coordinates* to be defined by pairs of non-linear functions of the Cartesian coordinates

$$\zeta(x, y) \quad \text{and} \quad \eta(x, y) \tag{7.31}$$

that specify a map $(x, y) \rightarrow (\zeta, \eta)$. Whereas x, y are *unrestricted* real variables, the values that ζ, η take on are determined by the range of the functions (7.31).

7.3.1 One-to-one Correspondence

Assuming that the functions (7.31) are differentiable with respect to x and y , a *local* condition for them to define a valid curvilinear coordinate system may be phrased as follows. At any point $P = (x, y)$ we form the *Jacobian*²

$$J(x, y) = \frac{\partial(\zeta, \eta)}{\partial(x, y)} = \begin{vmatrix} \frac{\partial\zeta}{\partial x} & \frac{\partial\zeta}{\partial y} \\ \frac{\partial\eta}{\partial x} & \frac{\partial\eta}{\partial y} \end{vmatrix} \tag{7.32}$$

of the map $(x, y) \rightarrow (\zeta, \eta)$ defined by (7.31). Then, in some neighborhood of P , there will be a unique correspondence between the Cartesian and curvilinear coordinates of each pair of distinct points $P_1 \neq P_2$ — i.e.,

² Named for Carl Gustav Jacob Jacobi (1804–1851), a renowned champion of pure mathematics in 19th-century Germany. At a conference in Manchester in 1842, he reportedly “...had the courage to make the valid point that it is the great glory of science to be of no use” [197]. “This caused a vehement shaking of heads.”

$$(x_1, y_1) \neq (x_2, y_2) \iff (\zeta_1, \eta_1) \neq (\zeta_2, \eta_2)$$

— if and only if the condition

$$0 < |J(x, y)| < \infty \quad (7.33)$$

is satisfied at $P = (x, y)$. The satisfaction of this condition guarantees the existence of functions

$$x(\zeta, \eta) \quad \text{and} \quad y(\zeta, \eta) \quad (7.34)$$

that define the *inverse map* $(\zeta, \eta) \rightarrow (x, y)$ in some neighborhood of P .

When the Jacobian (7.32) is non-zero and finite at every point $P = (x, y)$, the inverse map (7.34) will hold for all pairs (ζ, η) of curvilinear coordinates. In the Cartesian coordinate system, the loci corresponding to constant values of ζ and η are then the curves described parametrically by equations (7.34) on substituting a fixed numerical value for one of the curvilinear coordinates, and allowing the other one to vary as a free parameter.

We emphasize that the condition (7.33) ensures only a “local” one-to-one correspondence between the Cartesian coordinates (x, y) and the curvilinear coordinates (ζ, η) — i.e., within a small neighborhood of each point where this condition is satisfied. Such local one-to-one correspondence does *not* ensure a “global” one-to-one correspondence: even if (7.33) is satisfied for all (x, y) , the inverse map (7.34) — considered for unrestricted (ζ, η) values — may be many-to-one, so that two (or more) distinct pairs (ζ_1, η_1) and (ζ_2, η_2) yield the *same* point (x, y) upon substitution into (7.34). To avoid the problem of a point having more than one set of curvilinear coordinates, it is often necessary — in addition to ensuring the satisfaction of (7.33) — to restrict the range of ζ and η , such that the inverse map (7.34) generates each Cartesian point (x, y) once and only once as (ζ, η) vary over their allowed values.

In the theory of plane algebraic curves, an important family of (almost) one-to-one coordinate transformations are those for which the map (7.31) and its inverse (7.34) are both specified by *rational functions*. Such *birational transformations* are used, for example, to “resolve” singular points of curves — we shall defer discussion of them to §9.2.6 and §9.2.7.

7.3.2 Distance and Angle Measurements

While curvilinear coordinates serve to simplify certain problem formulations, they necessitate a more involved machinery for basic angle, length, and area measurements. For example, the distance d between two points (ζ_1, η_1) and (ζ_2, η_2) specified by curvilinear coordinates cannot, in general, be determined directly from a simple algebraic expression such as (7.1). We examine here the problems of distance and angle measurement in curvilinear coordinates, and defer area determination to §7.3.3. Consider the functions (7.34) that specify the Cartesian coordinates in terms of the curvilinear coordinates. If \mathbf{i} and \mathbf{j} are orthogonal unit vectors in the Cartesian system, the expression

$$\mathbf{r}(\zeta, \eta) = \mathbf{i}x(\zeta, \eta) + \mathbf{j}y(\zeta, \eta) \quad (7.35)$$

amounts to a vector parameterization of the plane. Infinitesimal increments $(d\zeta, d\eta)$ in the coordinates (ζ, η) then yield a geometrical displacement

$$d\mathbf{r} = \mathbf{r}_\zeta d\zeta + \mathbf{r}_\eta d\eta \quad (7.36)$$

of the point $\mathbf{r}(\zeta, \eta)$, where

$$\mathbf{r}_\zeta = \mathbf{i} \frac{\partial x}{\partial \zeta} + \mathbf{j} \frac{\partial y}{\partial \zeta} \quad \text{and} \quad \mathbf{r}_\eta = \mathbf{i} \frac{\partial x}{\partial \eta} + \mathbf{j} \frac{\partial y}{\partial \eta} \quad (7.37)$$

are the partial derivatives of (7.35). The infinitesimal distance between points with coordinates (ζ, η) and $(\zeta + d\zeta, \eta + d\eta)$ is then $ds^2 = |d\mathbf{r}|^2$, and by use of (7.36) this can be expressed as the symmetric quadratic form

$$ds^2 = [d\zeta \ d\eta] \begin{bmatrix} \mathbf{r}_\zeta \cdot \mathbf{r}_\zeta & \mathbf{r}_\zeta \cdot \mathbf{r}_\eta \\ \mathbf{r}_\zeta \cdot \mathbf{r}_\eta & \mathbf{r}_\eta \cdot \mathbf{r}_\eta \end{bmatrix} \begin{bmatrix} d\zeta \\ d\eta \end{bmatrix} \quad (7.38)$$

in $d\zeta$ and $d\eta$. Now in order to determine the distance between $P_1 = (\zeta_1, \eta_1)$ and $P_2 = (\zeta_2, \eta_2)$, we must first specify how ζ and η vary between these two points — unlike the Cartesian case, a linear variation of the coordinates does not, in general, correspond to a straight-line path from P_1 to P_2 .

If we specify this variation parametrically, by functions $\zeta(t)$ and $\eta(t)$ for $t \in [t_1, t_2]$, the distance between P_1 and P_2 can be expressed as the integral

$$d = \int_{t_1}^{t_2} \sqrt{\mathbf{r}_\zeta \cdot \mathbf{r}_\zeta \zeta'^2 + 2 \mathbf{r}_\zeta \cdot \mathbf{r}_\eta \zeta' \eta' + \mathbf{r}_\eta \cdot \mathbf{r}_\eta \eta'^2} dt, \quad (7.39)$$

where primes denote derivatives with respect to t . The 2×2 matrix in (7.38), whose elements appear in the above integral, is called the *metric tensor*³ for the curvilinear system. As suggested by its name, it serves as the basis for *mensuration* of lengths and angles in non-Cartesian coordinates.

Expression (7.39) specifies the length of *any* curved path from P_1 to P_2 , defined by differentiable functions $\zeta(t)$ and $\eta(t)$ — not just the straight-line distance between these two points. Of course, if the functions (7.34) are known, and we are interested *only* in the straight-line distance between P_1 and P_2 , we could simply insert (ζ_1, η_1) and (ζ_2, η_2) into (7.34) and then use equation (7.1), instead of determining the appropriate path description, $\zeta(t)$ and $\eta(t)$, for a straight line and then evaluating the integral (7.39). The real advantage of the integral distance formulation (7.39) will become apparent in Chap. 10, in the context of *non-Euclidean geometry* — where only the metric tensor is known, and the introduction Cartesian coordinates is fundamentally *impossible*.

Consider now the measurement of angles. We construct unit vectors

$$\mathbf{e}_\zeta = \frac{\mathbf{r}_\zeta}{|\mathbf{r}_\zeta|} \quad \text{and} \quad \mathbf{e}_\eta = \frac{\mathbf{r}_\eta}{|\mathbf{r}_\eta|} \quad (7.40)$$

³ We shall elaborate on the meaning of a “tensor” in Chap. 10.

in the direction of the partial derivatives (7.37). These two unit vectors are linearly independent at each point where the Jacobian (7.32) is non-zero, and they specify a *local basis* at such points. We say “local” because, in general, the vectors (7.40) depend explicitly on the location (ζ, η) — i.e., they have a different orientation at each position (\mathbf{e}_ζ and \mathbf{e}_η are, respectively, everywhere tangent to the loci defined by $\eta = \text{constant}$ and $\zeta = \text{constant}$).

Now let \mathbf{v} be a vector at a particular point (ζ, η) that has “components” v^ζ and v^η with respect to the curvilinear coordinate system,⁴ so that

$$\mathbf{v} = v^\zeta \mathbf{e}_\zeta + v^\eta \mathbf{e}_\eta. \quad (7.41)$$

In Cartesian coordinates, we are accustomed to moving vectors around freely — i.e., we do not consider them to be “attached” to specific points. However, in curvilinear coordinates, there are no “free” vectors: one can meaningfully describe a vector in terms of its curvilinear-coordinate components only at a definite point. Merely stating that \mathbf{v} has components v^ζ and v^η is insufficient: since the basis vectors \mathbf{e}_ζ , \mathbf{e}_η change from point to point, we must also state the *location* at which these components are measured.

The magnitude of the vector (7.41) is evidently given by

$$|\mathbf{v}| = \sqrt{(v^\zeta)^2 + (v^\eta)^2 + 2v^\zeta v^\eta \mathbf{e}_\zeta \cdot \mathbf{e}_\eta}. \quad (7.42)$$

Note the “cross term” above involving the scalar product of the basis vectors. It is only in the special case of an *orthogonal* coordinate system — for which \mathbf{e}_ζ and \mathbf{e}_η are everywhere mutually perpendicular — that this term is absent (the simplest example is, of course, Cartesian coordinates).

Similarly, given two vectors \mathbf{u} and \mathbf{v} with curvilinear components (u^ζ, u^η) and (v^ζ, v^η) at a prescribed point (ζ, η) , we can form their dot product

$$\mathbf{u} \cdot \mathbf{v} = u^\zeta v^\zeta + u^\eta v^\eta + (u^\zeta v^\eta + u^\eta v^\zeta) \mathbf{e}_\zeta \cdot \mathbf{e}_\eta,$$

and thus determine the angle θ between them from

$$\cos \theta = \frac{\mathbf{u} \cdot \mathbf{v}}{|\mathbf{u}| |\mathbf{v}|}, \quad (7.43)$$

where $|\mathbf{u}|$ is given in terms of (u^ζ, u^η) by an expression analogous to (7.42). We can also avoid the normalization (7.40) and use the metric tensor directly to compute angles between vectors: we replace the numerator in (7.43) by

$$\begin{bmatrix} u^\zeta & u^\eta \end{bmatrix} \begin{bmatrix} \mathbf{r}_\zeta \cdot \mathbf{r}_\zeta & \mathbf{r}_\zeta \cdot \mathbf{r}_\eta \\ \mathbf{r}_\zeta \cdot \mathbf{r}_\eta & \mathbf{r}_\zeta \cdot \mathbf{r}_\eta \end{bmatrix} \begin{bmatrix} v^\zeta \\ v^\eta \end{bmatrix},$$

and similarly $|\mathbf{u}|$ and $|\mathbf{v}|$ are replaced by the square roots of the scalar values obtained by multiplying the metric on the left and right by the components of \mathbf{u} and \mathbf{v} , respectively.

⁴ Here vector components are indicated by superscripts, rather than subscripts, for reasons explained in §10.2 — they should not be confused with exponents.

7.3.3 Jacobian of the Transformation

The Jacobian (7.32) for the transformation $(x, y) \rightarrow (\zeta, \eta)$ from Cartesian to curvilinear coordinates has a simple geometrical interpretation. In Cartesian coordinates, the gradient operator

$$\nabla = \mathbf{i} \frac{\partial}{\partial x} + \mathbf{j} \frac{\partial}{\partial y} \quad (7.44)$$

acting on a differentiable function $\psi(x, y)$ yields a vector field $\nabla\psi(x, y)$. At each point, the orientation of the vector $\nabla\psi$ indicates the direction in which ψ experiences the greatest rate of increase, while the magnitude of this vector indicates the value of this maximum rate of increase.

Applying (7.44) to the curvilinear coordinate functions (7.31), we obtain vector fields $\nabla\zeta$ and $\nabla\eta$ that describe the “flow” of ζ and η with respect to Cartesian coordinates. The loci defined by

$$\zeta(x, y) = \text{constant} \quad \text{and} \quad \eta(x, y) = \text{constant}$$

are everywhere orthogonal to these vector fields. If we now take a point on the intersection of two such curves, and measure an infinitesimal distance ds in the $\nabla\zeta$ and $\nabla\eta$ directions from it, we obtain the sides of an infinitesimal parallelogram whose area is given by

$$|\nabla\zeta \times \nabla\eta| ds^2.$$

This may be compared with the area ds^2 of the square obtained by moving a distance ds in the x and y directions from the chosen point. The factor

$$|\nabla\zeta \times \nabla\eta| = \left| \frac{\partial\zeta}{\partial x} \frac{\partial\eta}{\partial y} - \frac{\partial\eta}{\partial x} \frac{\partial\zeta}{\partial y} \right|$$

by which these two areas differ is just the absolute value of the Jacobian (7.32) for the Cartesian-to-curvilinear coordinate transformation.

Hence, we may interpret the condition (7.33) as requiring the area ratio of the infinitesimal parallelogram and square, defined above, to be non-zero and finite. Equivalently, this condition may be interpreted as requiring the vectors $\nabla\zeta$ and $\nabla\eta$ to be linearly independent and of finite magnitude.

We can also define a Jacobian for the inverse map $(\zeta, \eta) \rightarrow (x, y)$ defined by (7.34) — i.e., the transformation *from* curvilinear *to* Cartesian coordinates. Writing this as

$$J(\zeta, \eta) = \frac{\partial(x, y)}{\partial(\zeta, \eta)} = \begin{vmatrix} \frac{\partial x}{\partial \zeta} & \frac{\partial x}{\partial \eta} \\ \frac{\partial y}{\partial \zeta} & \frac{\partial y}{\partial \eta} \end{vmatrix} \quad (7.45)$$

and invoking the representation (7.35), we observe that $|J(\zeta, \eta)| = |\mathbf{r}_\zeta \times \mathbf{r}_\eta|$. Now the area dA of an infinitesimal parallelogram with sides $\mathbf{r}_\zeta d\zeta$ and $\mathbf{r}_\eta d\eta$

— corresponding to increments $d\zeta$ and $d\eta$ in the curvilinear coordinates at the point $\mathbf{r}(\zeta, \eta)$ — is just the magnitude of the cross product $(\mathbf{r}_\zeta d\zeta) \times (\mathbf{r}_\eta d\eta)$, and hence we see that

$$dA = |J(\zeta, \eta)| d\zeta d\eta. \quad (7.46)$$

This allows us to formulate the integral of a function $F(\zeta, \eta)$ of the curvilinear coordinates over the area of any domain Ω with boundary specified in terms of ζ and η as

$$I = \int_{\Omega} F(\zeta, \eta) |J(\zeta, \eta)| d\zeta d\eta.$$

In particular, when $F \equiv 1$, we obtain the total area A of the region Ω . Note that if the Jacobian changes sign within Ω , it is necessary to break up this domain into subregions over which $J(\zeta, \eta)$ is of constant sign, to evaluate I .

7.3.4 Example: Plane Polar Coordinates

To illustrate the above points, consider the familiar case of *polar coordinates* (ρ, ϕ) defined by the functions

$$\rho(x, y) = \sqrt{x^2 + y^2} \quad \text{and} \quad \phi(x, y) = \tan^{-1}(x, y). \quad (7.47)$$

Here ρ is the distance of the point $P = (x, y)$ from the origin O , while ϕ is the counter-clockwise angle⁵ that the line OP makes with the positive x axis. From (7.47) we obtain the Jacobian for the transformation $(x, y) \rightarrow (\rho, \phi)$ as

$$J(x, y) = \begin{vmatrix} \frac{\partial \rho}{\partial x} & \frac{\partial \rho}{\partial y} \\ \frac{\partial \phi}{\partial x} & \frac{\partial \phi}{\partial y} \end{vmatrix} = \sqrt{x^2 + y^2}.$$

The origin is a *singular point* of the polar coordinate system, since $J(x, y) \rightarrow 0$ as $(x, y) \rightarrow (0, 0)$. The one-to-one correspondence between Cartesian and polar coordinates breaks down at $(x, y) = (0, 0)$: we clearly have $\rho = 0$ there, but ϕ is *indeterminate* — it may have any value between 0 and 2π .

The use of polar rather than Cartesian coordinates can greatly simplify problems involving rotational symmetry or functions of an angular variable. On account of this, the breakdown of one-to-one correspondence at the origin is considered a minor defect, which can be managed by special treatment of that point. In general, a *perfect* one-to-one correspondence between Cartesian and curvilinear coordinates is too restrictive a requirement for practical use — one should not discount curvilinear systems in which a unique correspondence breaks down at discrete points or on certain loci, provided such singularities

⁵ Here the arctangent function $\tan^{-1}(x, y)$ has range is $0 \leq \phi < 2\pi$, the value being determined from the *individual* signs of x and y , not just the ratio y/x .

are properly identified and treated. We insist, however, that no breakdown of one-to-one correspondence occurs over any finite *area* of the plane.

Apart from the origin, polar coordinates satisfy everywhere the condition (7.33) for a “local” one-to-one correspondence with Cartesian coordinates. However, the map $(x, y) \rightarrow (\rho, \phi)$ also illustrates the need to restrict the range of curvilinear coordinates to ensure “global” one-to-one correspondence. The value of ρ in (7.47) is evidently non-negative, and we have stipulated that the range of the function $\tan^{-1}(x, y)$ be such that $0 \leq \phi < 2\pi$. Any point (x, y) other than $(0, 0)$ will then have *unique* polar coordinates (ρ, ϕ) . We relinquish this uniqueness, however, if we regard ρ and ϕ as *unrestricted* variables with arbitrary values between $-\infty$ and $+\infty$. This can be seen from the inverse

$$x(\rho, \phi) = \rho \cos \phi \quad \text{and} \quad y(\rho, \phi) = \rho \sin \phi \quad (7.48)$$

to the transformation (7.47) — if (ρ, ϕ) corresponds to (x, y) , then so also do $(\rho, 2k\pi + \phi)$ and $(-\rho, (2k+1)\pi + \phi)$ for all integers k .

Substituting (7.48) into (7.35) we obtain $\mathbf{r}(\rho, \phi) = \mathbf{i}\rho \cos \phi + \mathbf{j}\rho \sin \phi$, and by differentiation we deduce the local basis (7.40) to be

$$\mathbf{e}_\rho = \mathbf{i} \cos \phi + \mathbf{j} \sin \phi \quad \text{and} \quad \mathbf{e}_\phi = -\mathbf{i} \sin \phi + \mathbf{j} \cos \phi. \quad (7.49)$$

Although they depend on the point under consideration, these vectors clearly form an orthogonal basis everywhere, i.e., $\mathbf{e}_\rho \cdot \mathbf{e}_\phi = 0$ for all (ρ, ϕ) . This fact is also evident from the metric, which is seen to be a *diagonal* matrix:

$$\mathbf{M}(\rho, \phi) = \begin{bmatrix} 1 & 0 \\ 0 & \rho \end{bmatrix}.$$

Hence the distance element (7.38) reduces to $ds = \sqrt{d\rho^2 + \rho^2 d\phi^2}$, while the area element (7.46) is given by $dA = \rho d\rho d\phi$.

7.3.5 Three or More Dimensions

Our discussion has been confined to two-dimensional curvilinear coordinates, but the ideas generalize in a fairly straightforward manner to three (or more) dimensions. Thus, three non-linear functions

$$\zeta(x, y, z), \quad \eta(x, y, z), \quad \theta(x, y, z)$$

of the spatial Cartesian coordinates x, y, z will, in general, describe a three-dimensional curvilinear coordinate system. We require the Jacobian

$$J(x, y, z) = \frac{\partial(\zeta, \eta, \theta)}{\partial(x, y, z)} = \begin{vmatrix} \frac{\partial \zeta}{\partial x} & \frac{\partial \zeta}{\partial y} & \frac{\partial \zeta}{\partial z} \\ \frac{\partial \eta}{\partial x} & \frac{\partial \eta}{\partial y} & \frac{\partial \eta}{\partial z} \\ \frac{\partial \theta}{\partial x} & \frac{\partial \theta}{\partial y} & \frac{\partial \theta}{\partial z} \end{vmatrix}$$

of the transformation $(x, y, z) \rightarrow (\zeta, \eta, \theta)$ to be of non-zero, finite magnitude to ensure local one-to-one correspondence. Moreover, it is often necessary to restrict the range of ζ, η, θ for a global one-to-one correspondence.

Using the inverse map $(\zeta, \eta, \theta) \rightarrow (x, y, z)$, defined by functions

$$x(\zeta, \eta, \theta), \quad y(\zeta, \eta, \theta), \quad z(\zeta, \eta, \theta), \quad (7.50)$$

we may define a local basis $\mathbf{e}_\zeta, \mathbf{e}_\eta, \mathbf{e}_\theta$ from the normalized partial derivatives of $\mathbf{r}(\zeta, \eta, \theta) = \mathbf{i}x(\zeta, \eta, \theta) + \mathbf{j}y(\zeta, \eta, \theta) + \mathbf{k}z(\zeta, \eta, \theta)$ in a manner analogous to equations (7.40). The metric tensor in three dimensions defines the distance element ds corresponding to coordinate increments $d\zeta, d\eta, d\theta$, namely

$$ds^2 = [d\zeta \ d\eta \ d\theta] \begin{bmatrix} \mathbf{r}_\zeta \cdot \mathbf{r}_\zeta & \mathbf{r}_\zeta \cdot \mathbf{r}_\eta & \mathbf{r}_\zeta \cdot \mathbf{r}_\theta \\ \mathbf{r}_\zeta \cdot \mathbf{r}_\eta & \mathbf{r}_\eta \cdot \mathbf{r}_\eta & \mathbf{r}_\eta \cdot \mathbf{r}_\theta \\ \mathbf{r}_\zeta \cdot \mathbf{r}_\theta & \mathbf{r}_\eta \cdot \mathbf{r}_\theta & \mathbf{r}_\theta \cdot \mathbf{r}_\theta \end{bmatrix} \begin{bmatrix} d\zeta \\ d\eta \\ d\theta \end{bmatrix},$$

and is used to measure angles and distances in three dimensions by methods analogous to those described above for the two-dimensional case.

Volume integrals of a function $F(\zeta, \eta, \theta)$ are computed by using the volume element $dV = |J(\zeta, \eta, \theta)| d\zeta d\eta d\theta$, where $J(\zeta, \eta, \theta)$ denotes the Jacobian of the inverse map (7.50) — note that $|J(\zeta, \eta, \theta)|$ corresponds to the magnitude of scalar triple product $(\mathbf{r}_\zeta \times \mathbf{r}_\eta) \cdot \mathbf{r}_\theta$ of the partial derivatives of $\mathbf{r}(\zeta, \eta, \theta)$.

Some familiar examples of three-dimensional curvilinear coordinates are the *cylindrical* (ρ, ϕ, z) and *spherical* (r, ϕ, θ) polar systems defined by

$$\rho = \sqrt{x^2 + y^2}, \quad \phi = \tan^{-1}(x, y), \quad z,$$

and

$$r = \sqrt{x^2 + y^2 + z^2}, \quad \phi = \tan^{-1}(x, y), \quad \theta = \sin^{-1} \frac{z}{\sqrt{x^2 + y^2 + z^2}}$$

with $0 \leq \phi < 2\pi$ and $-\pi/2 \leq \theta \leq +\pi/2$ (where $\tan^{-1}(x, y)$ denotes the angle that a radius vector from the origin to (x, y) makes with the positive x -axis).

7.4 Homogeneous Coordinates

In the Euclidean plane, any two lines that we choose will (ordinarily) intersect in a single point. We are obliged to include a qualification of this statement to allow for exceptional pairs of lines — namely, *parallel* lines — that, according to Euclidean precepts, do not intersect at all.

If we draw a pair of lines ℓ_1 and ℓ_2 intersecting at some point \mathbf{p} and then imagine rotating one of the lines about a chosen point $\mathbf{q} (\neq \mathbf{p})$ on it, we will observe that the point of intersection \mathbf{p} recedes arbitrarily far along the lines ℓ_1 and ℓ_2 as they approach parallelism. This behavior suggests the intuitive notion that ℓ_1 and ℓ_2 intersect “at infinity” when they are parallel.

Homogeneous coordinates, and the theory of projective geometry founded upon them, are a rigorous means of quantifying and analyzing such intuitive notions. By dealing systematically with “behavior at infinity,” they eliminate the exceptional nature of instances such as parallel lines, and they also furnish an elegant *principle of duality*, whereby any given algebraic condition admits two complementary geometrical interpretations. A brief survey of these ideas is presented below — for a comprehensive treatment, see [396, 472].

7.4.1 The Projective Plane

The *projective plane* is the familiar set of all points (x, y) with finite Cartesian coordinates, augmented by a family of special “points at infinity.” To describe all (finite or infinite) projective points, we use *homogeneous coordinate* triples (W, X, Y) subject to the following conventions:

- the triple $(0, 0, 0)$ is excluded — it does not represent any valid point;
- two triples (W, X, Y) and $(\alpha W, \alpha Y, \alpha X)$ differing by only a non-zero factor α are not distinguished — they identify the *same* point.

If $W \neq 0$, the triple (W, X, Y) corresponds to a finite (or *affine*) point, whose Cartesian coordinates are given by

$$x = \frac{X}{W} \quad \text{and} \quad y = \frac{Y}{W}. \quad (7.51)$$

If $W = 0$, on the other hand, (W, X, Y) represents a *point at infinity*.

Let us return to the problem of two intersecting lines. We may represent ℓ_1 and ℓ_2 by the implicit equations

$$K_1 + L_1 x + M_1 y = 0, \quad K_2 + L_2 x + M_2 y = 0, \quad (7.52)$$

and provided that $L_1 M_2 \neq L_2 M_1$ — i.e., ℓ_1 and ℓ_2 are non-parallel — the Cartesian coordinates of their intersection point are given by

$$x = \frac{M_1 K_2 - M_2 K_1}{L_1 M_2 - L_2 M_1}, \quad y = \frac{L_2 K_1 - L_1 K_2}{L_1 M_2 - L_2 M_1}.$$

To treat the singular case $L_1 M_2 = L_2 M_1$, we *homogenize* the line equations (7.52) by substituting from (7.51) and multiplying through by W , giving

$$K_1 W + L_1 X + M_1 Y = 0, \quad K_2 W + L_2 X + M_2 Y = 0. \quad (7.53)$$

It is then easily seen that equations (7.53) are simultaneously satisfied by the homogeneous coordinate triple

$$(W, X, Y) = (0, M_1 K_2 - M_2 K_1, L_2 K_1 - L_1 K_2)$$

which identifies a point at infinity. In other words, we have found a means of formally expressing the fact that “parallel lines intersect at infinity” without actually having to introduce the daunting symbol “ ∞ ” at any time.

Points at infinity may be regarded as specifying *directions* in the plane. In this interpretation, however, one should not distinguish between a particular direction and its reverse: although we may travel to the “left” or to the “right” along any line, if we persevere we will arrive in either case at one and the same point at infinity.⁶ This conclusion is necessitated by the indistinguishability of homogeneous coordinates that differ by only a constant factor — the triples $(0, X, Y)$ and $(0, -X, -Y)$ identify exactly the same point.

Consider again the homogeneous equation of a straight line,

$$KW + LX + MY = 0. \quad (7.54)$$

We are free to choose the constants K, L, M in any way we please (except for making them all zero); we obtain in each case a *projective line*. In particular, if we choose $L = M = 0$ and $K \neq 0$, the equation becomes simply

$$W = 0.$$

Since it consists of all points at infinity, this special projective line is known as *the line at infinity* — in projective geometry, it has the same stature as the x and y axes, whose equations are $Y = 0$ and $X = 0$ respectively.

To help visualize the projective plane, it is useful to consider mapping it to a sphere. For a unit sphere whose south pole touches the plane at the origin, we consider a *gnomonic projection*, in which rays are drawn connecting each point of the plane to the center of the sphere and beyond. Such rays will pierce the northern and southern hemispheres in “antipodal” points, and lines in the plane will project to *great circles* on the sphere. Hence, the entire (finite) plane is mapped one-to-one onto the northern and southern hemispheres, but the *points at infinity* of the projective plane are mapped to equatorial points of the sphere, and the *line at infinity* corresponds to the entire equator.

The gnomonic projection employed here should not be confused with the *stereographic projection* used in §4.2 to visualize the “extended” complex plane — the stereographic projection takes rays through the north pole of the sphere, rather than the center, and thus identifies just a single infinite point.

7.4.2 Circular Points and Isotropic Lines

We can also homogenize the equations of higher-order curves. Consider an *algebraic curve*, defined by an implicit polynomial equation

$$f(x, y) = 0$$

of degree n . By substituting from (7.51) into this equation, and multiplying through by W^n , we obtain the corresponding *homogeneous* curve equation

⁶ Unlike affine lines, projective lines are “unordered” point sets: they are equivalent topologically to a circle. Given three distinct points A, B, C on a projective line, we cannot uniquely identify one of them as lying “between” the other two.

$$F(W, X, Y) = 0 \quad (7.55)$$

wherein each term will be of total degree n in the homogeneous coordinates W, X, Y . The behavior of the curve “at infinity” may then be determined by setting $W = 0$ in this equation. For example,

$$x^2 + y^2 - 2ax - 2by + a^2 + b^2 - r^2 = 0$$

defines a circle of radius r with center at the point (a, b) . The corresponding homogeneous equation is

$$X^2 + Y^2 - 2aWX - 2bWY + (a^2 + b^2 - r^2)W^2 = 0, \quad (7.56)$$

and setting $W = 0$ in the above gives the equation $X^2 + Y^2 = 0$. The latter has only complex solutions⁷ — namely, values having the ratio $X : Y = 1 : \pm i$, and therefore the points at infinity on the locus (7.56) are identified by the two triples $(0, 1, \pm i)$. Note that these two points are *independent* of (a, b) and r — i.e., all circles have the same points at infinity. For this reason, the points $(0, 1, \pm i)$ are called the *circular points at infinity*.

Lines that pass through either of the circular points at infinity are known as *isotropic lines*. Their coefficients have the form $(K, L, M) = (k, \pm i, 1)$ for any real value $k \neq 0$, and they exhibit rather non-intuitive properties if we apply familiar ideas concerning real, affine lines to them. Consider, for example, the “orientation” of isotropic lines. Since the line $KW + LX + MY = 0$ has slope $s = -L/M$, the isotropic lines with $(K, L, M) = (k, \pm i, 1)$ have slope $s = \mp i$. Now the coordinate transformation $(W, X, Y) \rightarrow (W', X', Y')$ defined by

$$W = W', \quad X = X' \cos \theta + Y' \sin \theta, \quad Y = -X' \sin \theta + Y' \cos \theta,$$

corresponds to a rotation of the plane through angle θ . It transforms the line $KW + LX + MY = 0$ into $K'W' + L'X' + M'Y' = 0$, whose coefficients

$$K' = K, \quad L' = L \cos \theta - M \sin \theta, \quad M' = L \sin \theta + M \cos \theta$$

are obtained by substituting for W, X, Y into the former equation. Taking $(K, L, M) = (k, \pm i, 1)$, the slope of the isotropic line $kW \pm iX + Y = 0$ in the rotated coordinate system is then

$$s' = -\frac{L'}{M'} = -\frac{\pm i \cos \theta - \sin \theta}{\pm i \sin \theta + \cos \theta} = \mp i \frac{\cos \theta \pm i \sin \theta}{\cos \theta \mp i \sin \theta} = \mp i,$$

which is exactly the same as before the rotation. Thus, we have shown that *rotations do not alter the slopes of isotropic lines!*

⁷ The complex points of an algebraic curve $f(x, y) = 0$ are a natural generalization of the complex roots of a univariate polynomial $f(x) = 0$. Just as the introduction of complex values in the latter case allows us to say that $f(x)$ has precisely n (not necessarily distinct) roots, the study of the complex locus of $f(x, y) = 0$ also leads to elegant simplifications. The real locus is a special subset of its complex locus.

Another unusual property concerns the distance of points from isotropic lines. Ordinarily, the distance d between the point (W_0, X_0, Y_0) and the line $KW + LX + MY = 0$ can be written as

$$d = \frac{KW_0 + LX_0 + MY_0}{W_0\sqrt{L^2 + M^2}}$$

if $W_0 \neq 0$ and $(L, M) \neq (0, 0)$, i.e., we are speaking of affine points and lines. But, according to this formula, d is *infinite* for any affine point (W_0, X_0, Y_0) if the line is isotropic, with $(K, L, M) = (k, \pm i, 1)$! These and other “strange” properties of the isotropic lines highlight the danger of carrying our intuition, developed from real affine geometry, into the complex projective domain.

7.4.3 The Principle of Duality

Equation (7.54) exhibits a striking symmetry between the point coordinates W, X, Y and the line coefficients K, L, M . We usually regard the latter as fixed numerical values, and the former as variables — there is then a singly-infinite family of solutions (W, X, Y) to (7.54) that describe all the points lying on a fixed line. However, there is no reason why we should not regard W, X, Y in equation (7.54) as being fixed values, and allow K, L, M to vary instead: the equation then has a singly-infinite family of solutions (K, L, M) that identify all the lines passing through a fixed point. These alternative interpretations of the linear equation (7.54) are illustrated in Fig. 7.6.

Such observations illustrate the so-called *duality* of points and lines in the projective plane — for any statement concerning points, we can construct a “dual” statement in terms of lines, by appropriate transposition of the words. For example, we have the dual statements:

two distinct points define a line ... two distinct lines define a point.

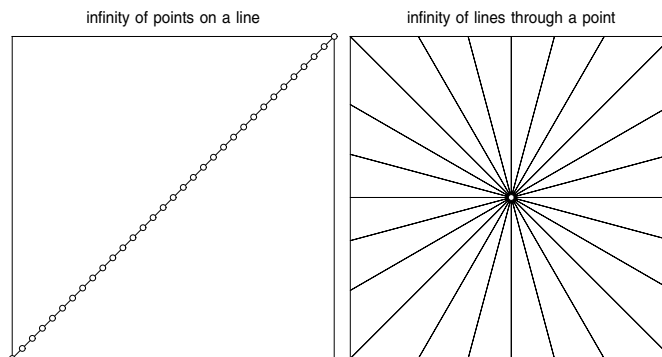


Fig. 7.6. Dual interpretations of equation (7.54). Left: the set of points on a given line (K, L, M fixed). Right: the set of lines through a given point (W, X, Y fixed).

Note that the statements encompass points at infinity and the line at infinity: indeed, these infinite elements *must* be included for the principle of duality to hold in complete generality. The point–line duality offers an interesting new perspective in the study of higher–order curves. At each smooth point of the curve (7.55) the *tangent* is the unique line that most closely approximates the curve in a neighborhood of the chosen point: the tangent “touches” the curve, rather than crossing it.⁸ This unique correspondence between the *points* and *tangents* of a plane curve allows us to think of the curve as a *continuous family of lines* (its tangents) rather than a continuous family of points.

Indeed, we can derive a dual *line equation* for the curve (7.55) — i.e., a polynomial equation of the form

$$G(K, L, M) = 0, \quad (7.57)$$

such that each set of values K, L, M satisfying this equation identifies a line that is tangent to the curve (one may consider K, L, M to be *line coordinates*, just as W, X, Y are *point coordinates*). Each set of values K, L, M satisfying (7.57) identifies a line that is tangent to the point locus defined by (7.55).

Consider, for example, an ellipse centered on the origin with semi–axes a and b . We will show how to derive its line equation from the point equation

$$b^2X^2 + a^2Y^2 - a^2b^2W^2 = 0. \quad (7.58)$$

If $M \neq 0$, we can identify points where the line $KW + LX + MY = 0$ meets the ellipse by substituting $Y = -(KW + LX)/M$ into the above to obtain

$$(L^2a^2 + M^2b^2)X^2 + 2a^2KLWX + (K^2 - M^2b^2)a^2W^2 = 0,$$

which may be regarded as a quadratic equation for the ratio $W : X$. In order for the line $KW + LX + MY = 0$ to touch the ellipse, this quadratic must indicate two “coincident” intersections, i.e., it must have a double root.

The condition for this to occur is that the discriminant of the quadratic must vanish. After simplifying and discarding constant factors, this yields $M^2(K^2 - a^2L^2 - b^2M^2) = 0$. Omitting the factor M^2 , since we assumed that $M \neq 0$ in the derivation, we obtain the homogeneous line equation

$$K^2 - a^2L^2 - b^2M^2 = 0 \quad (7.59)$$

of the ellipse. Thus, all lines whose coefficients or “coordinates” K, L, M satisfy (7.59) are tangent to the ellipse. The same arguments applied to the cubic

$$X^3 - W^2Y = 0 \quad (7.60)$$

yield its line equation as

$$4L^3 + 27K^2M = 0. \quad (7.61)$$

⁸ There are some technical qualifications to this characterization.

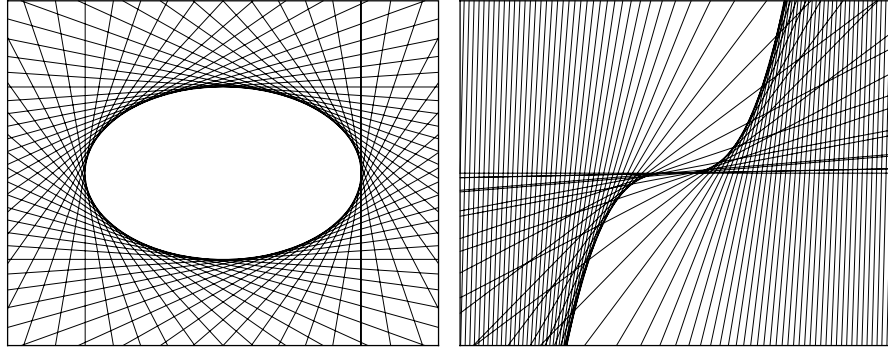


Fig. 7.7. Line representation of an ellipse (left) and the cubic $y = x^3$ (right).

Figure 7.7 shows the families of lines defined by equations (7.59) and (7.61). Note that, although we assumed $M \neq 0$ in the derivations, the equations (7.59) and (7.61) also encompass tangent lines with $M = 0$ as the limiting instances of tangent lines with $M \neq 0$ (namely, the two vertical lines $X = \pm aW$ for the ellipse, and the line at infinity $W = 0$ for the cubic $y = x^3$).

For the ellipse (7.58) and cubic (7.60), we observe that the line equations (7.59) and (7.61) are of the same degree as the point equations in the respective coordinates W, X, Y and K, L, M . However, this is not true for all curves — the degree of the line equation may, in general, be lower or higher than that of the point equation. To differentiate between the two,⁹ the degree of the point equation is called the *order* of the curve, while the degree of the line equation is known as its *class*. For a curve that is of lower class than order, the line representation is simpler to analyze and compute with (see also §9.2.8).

One can also describe curves *parametrically* in terms of line coordinates. If the points of a curve are specified by homogeneous-coordinate polynomials $W(t)$, $X(t)$, $Y(t)$ in some parameter t , the corresponding homogeneous line coordinate polynomials $K(t)$, $L(t)$, $M(t)$ — which describe all tangent lines to the curve — are given by

$$K = XY' - X'Y, \quad L = YW' - Y'W, \quad M = WX' - W'X.$$

This can be verified by regarding the tangent as the limit of the chord joining points $(W(t), X(t), Y(t))$ and $(W(t + \Delta t), X(t + \Delta t), Y(t + \Delta t))$ as $\Delta t \rightarrow 0$.

7.4.4 Projective Transformations

Our discussion of projective geometry originated with the homogenization of a Cartesian coordinate system, which may be recovered from the homogeneous coordinates (W, X, Y) by the relations (7.51). Actually, there is no uniqueness

⁹ If we just say *degree*, it is understood that we refer to the *order* of the curve.

about this homogeneous coordinate system — we can define an infinite number of such systems through mappings of the form

$$\begin{bmatrix} \tilde{W} \\ \tilde{X} \\ \tilde{Y} \end{bmatrix} = \begin{bmatrix} m_{00} & m_{01} & m_{02} \\ m_{10} & m_{11} & m_{12} \\ m_{20} & m_{21} & m_{22} \end{bmatrix} \begin{bmatrix} W \\ X \\ Y \end{bmatrix}. \quad (7.62)$$

If the matrix in (7.62) is non-singular, it defines a *projective transformation* from the coordinates (W, X, Y) to new coordinates $(\tilde{W}, \tilde{X}, \tilde{Y})$.

To elucidate the geometrical meaning of the 3×3 matrix that defines a two-dimensional projective transformation, we note that it can be factorized into the product of four matrices of the form

$$\begin{bmatrix} 1 & \lambda & \mu \\ 0 & 1 & 0 \\ 0 & 0 & 1 \end{bmatrix} \begin{bmatrix} k & 0 & 0 \\ 0 & 1 & 0 \\ 0 & 0 & 1 \end{bmatrix} \begin{bmatrix} 1 & 0 & 0 \\ \Delta x & 1 & 0 \\ \Delta y & 0 & 1 \end{bmatrix} \begin{bmatrix} 1 & 0 & 0 \\ 0 & m_{11} & m_{12} \\ 0 & m_{21} & m_{22} \end{bmatrix}, \quad (7.63)$$

where $\Delta x = m_{10}$, $\Delta y = m_{20}$, $\lambda = (m_{22}m_{01} - m_{21}m_{02})/(m_{11}m_{22} - m_{12}m_{21})$, $\mu = (m_{11}m_{02} - m_{12}m_{01})/(m_{11}m_{22} - m_{12}m_{21})$, and $k = m_{00} - (\lambda\Delta x + \mu\Delta y)$. Working from right to left — i.e., in the order in which they are successively applied — we now explain the significance of each matrix in (7.63).

The first matrix specifies an *affine transformation*, under which no affine point is mapped to a point at infinity, nor vice-versa. The coordinates (\tilde{x}, \tilde{y}) of the image of each affine point (x, y) are defined by the homogeneous linear combinations $\tilde{x} = m_{11}x + m_{12}y$ and $\tilde{y} = m_{21}x + m_{22}y$. Important cases of such maps are those in which the lower-right 2×2 sub-matrix is *orthogonal* — i.e., its inverse equals its transpose. In general, such a matrix has the form

$$\begin{bmatrix} \cos \phi & -\sin \phi \\ \sin \phi & \cos \phi \end{bmatrix} \quad \text{or} \quad \begin{bmatrix} \cos 2\alpha & \sin 2\alpha \\ \sin 2\alpha & -\cos 2\alpha \end{bmatrix}, \quad (7.64)$$

or is the product of such forms. The first form defines a *rotation* by an angle ϕ about the origin, the second a *reflection* in a line through the origin at angle α to the x -axis. These are *shape-preserving* transformations. If the lower-right 2×2 sub-matrix is *not* orthogonal, the affine transformation does not preserve shape — it involves a “shear” effect (the collinearity of points and parallelism of lines are maintained, but angles are altered).

The second and third matrices in (7.63) also incur no swapping of affine points with points at infinity. They define, respectively, a *translation* and a *uniform scaling* in the affine plane: the former simply shifts the affine point (x, y) to $(x + \Delta x, y + \Delta y)$, while the latter moves (x, y) along a ray through the origin to $(x/k, y/k)$. These are also clearly shape-preserving transformations. The most general shape-preserving transformation has the form

$$\begin{bmatrix} \tilde{W} \\ \tilde{X} \\ \tilde{Y} \end{bmatrix} = \begin{bmatrix} k & 0 & 0 \\ \Delta x \cos \phi - \sin \phi & \Delta y \sin \phi & \cos \phi \end{bmatrix} \begin{bmatrix} W \\ X \\ Y \end{bmatrix},$$

obtained by multiplying the right-most three matrices in (7.63), where the first matrix is assumed to be orthogonal: specifically, a rotation, although any combination of rotations and reflections is allowed. Each affine point (x, y) is first rotated by angle ϕ about the origin, then translated by amounts Δx , Δy parallel to the axes, and finally its distance from the origin is scaled by $1/k$ to yield the image point (\tilde{x}, \tilde{y}) . The *order* of these operations is important since, in general, the matrices do not commute under multiplication.

The left-most matrix in (7.63) is perhaps the most interesting. It defines a “perspectivity” under which — unlike the first three matrices — affine points may be mapped to infinity and, conversely, points at infinity may be mapped into the affine plane. Hence, parallel lines may become intersecting lines, and vice-versa, under such transformations. We see, in fact, that the affine line

$$W + \lambda X + \mu Y = 0$$

in the (W, X, Y) coordinates is mapped to the line at infinity, $\tilde{W} = 0$, in the $(\tilde{W}, \tilde{X}, \tilde{Y})$ coordinates by the left-most matrix in (7.63). Conversely, the line at infinity, $W = 0$, in the (W, X, Y) coordinates becomes the affine line

$$\tilde{W} - \lambda \tilde{X} - \mu \tilde{Y} = 0$$

in the $(\tilde{W}, \tilde{X}, \tilde{Y})$ coordinates. This phenomenon is best understood in terms of an intuitive geometrical model, which we discuss in §7.4.6 below.

The mapping of affine points to points at infinity, and vice-versa, has a dramatic effect on the appearance of curves. Consider mapping the unit circle

$$X^2 + Y^2 - W^2 = 0$$

by the transformation $(\tilde{W}, \tilde{X}, \tilde{Y}) = (W - Y, X, Y)$ corresponding to the choices $\lambda = 0$ and $\mu = -1$. The equation of the transformed curve is then

$$\tilde{X}^2 - 2\tilde{W}\tilde{Y} - \tilde{W}^2 = 0,$$

which represents a parabola symmetric about the \tilde{y} -axis, and crossing it at the point $(0, -\frac{1}{2})$. In fact, any conic can be mapped into any other by means of a projective transformation. This projective equivalence of the conics was first recognized by the astronomer Johannes Kepler (1571–1630), famous for his empirical laws of planetary motion. Rather than distinguishing between different types of conics, he imagined them to form a continuous family that can be characterized by the relative position of their two foci.

Starting with the degenerate case of two lines that intersect at the origin (both foci coincident at that point), one observes a sequence of hyperbolae as one focus moves to the right while the other one remains fixed at the origin. Eventually, in the limiting case of the moving focus infinitely far on the right, one has a parabola. As the moving focus reappears infinitely far on the left, and begins to approach the origin again, the parabola “closes” and one passes

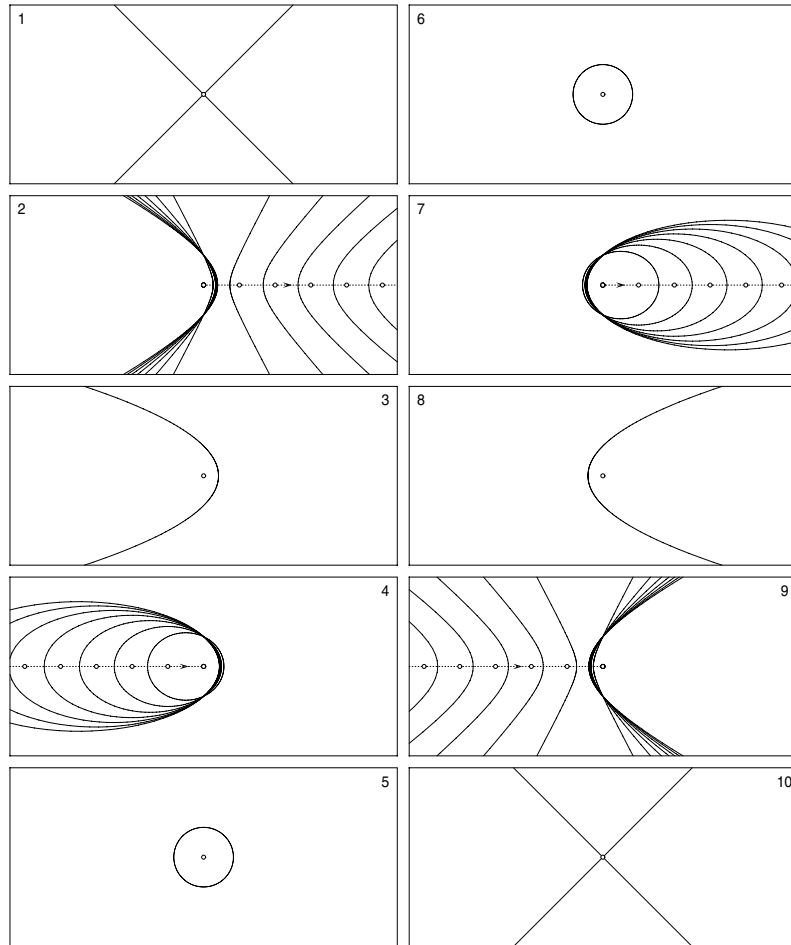


Fig. 7.8. Kepler's view of the conics as a continuum. With one fixed and one moving focus, we pass on the left from the degenerate case of intersecting lines (1) through a sequence of hyperbolae (2) to the transitional case of a parabola (3), with the moving focus "at infinity." As this focus reappears on the other side of the affine plane, we have a family of ellipses (4) culminating in a circle (5). With further motion of this focus, the entire sequence is repeated, but in reversed order (6)–(10), on the right.

through a sequence of increasingly round ellipses, finally arriving at a circle when the two foci are again coincident at the origin (see Fig. 7.8).

Kepler's notion of the parabola as a conic that has one focus "at infinity" heralded the beginning of projective geometry. The subject was then pursued by Girard Desargues (1591–1661), a French architect and military engineer, although his writings were rather obscure and apparently not well-received by contemporaries. It was the 1822 *Traité des Propriétés Projectives des Figures*

of Jean Victor Poncelet¹⁰ (1788–1867) that established projective geometry as an independent and rigorous discipline in its own right.

7.4.5 Invariance of the Cross Ratio

Projective transformations preserve the *incidence relations* among geometrical figures, but not angles, lengths, or ratios of lengths in those figures. Thus, they are the most basic or “primitive” of geometrical transformations, and subsume other important transformations (e.g., shape-preserving and affine mappings) as special instances. The English mathematician Arthur Cayley (1821–1895) thus remarked that “All geometry is projective geometry.”

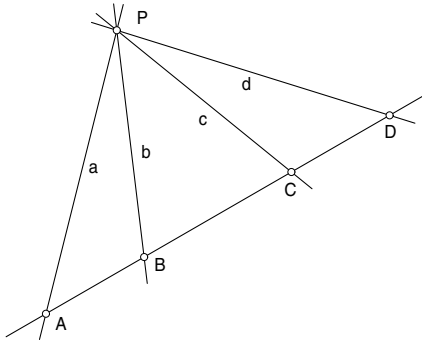


Fig. 7.9. The invariance of the cross ratio for four collinear points A, B, C, D is characterized by equation (7.65), while the dual invariance of the cross ratio of four concurrent lines a, b, c, d (through a common point P) is defined by equation (7.66).

Although, in general, projective transformations alter lengths and ratios of lengths, they do preserve a special quantity defined for sets of four collinear points, called the *cross ratio* — or “double ratio” — of those points. Namely, if A, B, C, D are four distinct collinear points, their images A', B', C', D' under a general projective transformation are also collinear, and the invariance of the cross ratio is defined by the equation

$$\frac{AB}{AD} \frac{CD}{CB} = \frac{A'B'}{A'D'} \frac{C'D'}{C'B'}, \quad (7.65)$$

where AB denotes the *signed* distance from A to B (i.e., $BA = -AB$), and likewise for $A'B'$, etc. This holds even if one of A, B, C, D or A', B', C', D' is a point at infinity, with the convention that we cancel the two terms involving

¹⁰ Poncelet is reputed to have developed many ideas for his *Traité* while incarcerated as a prisoner-of-war following Napoleon’s invasion of Russia. He also introduced the term *fatigue* to describe the sudden failure of materials under cyclical stress.

that point from the numerators and denominators. The definition of the cross ratio may also be extended to accommodate coincident points.

In accordance with the principle of duality, we can also define a cross ratio for any *four concurrent lines* (passing through a common point), as the dual to that for *four collinear points*, and this cross ratio for lines is also invariant under a general projective transformation. Namely, if a, b, c, d are four distinct lines concurrent at some point P , and a', b', c', d' are the images of these lines under a general projective transformation, we have

$$\frac{\sin(\angle ab)}{\sin(\angle ad)} \frac{\sin(\angle cd)}{\sin(\angle cb)} = \frac{\sin(\angle a'b')}{\sin(\angle a'd')} \frac{\sin(\angle c'd')}{\sin(\angle c'b')}, \quad (7.66)$$

where $\angle ab$ is the *oriented angle* at P between a, b — similarly for $\angle a'b'$, etc. Fig. 7.9 illustrates the dual cross ratios of points and lines.

7.4.6 Geometrical Figures and their Shadows

A deeper insight into projective transformations of the plane can be obtained from an elegant geometrical model that intuitively explains how parallel lines may be transformed into intersecting lines, or vice-versa. Consider a three-dimensional Euclidean space in which two non-parallel planes — an “object” plane O and “image” plane I — are chosen together with a point “light source” or *center of projection* c that does not lie on O or I (see Fig. 7.10).

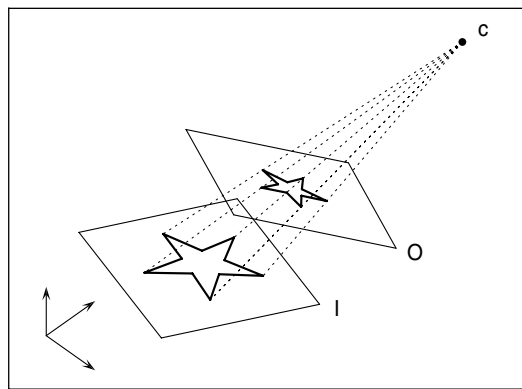


Fig. 7.10. Visualization of a plane projective transformation by means of a central projection of an object plane O to an image plane I from a center of projection c .

We imagine the object plane O to be translucent, with a geometrical figure A drawn on it in black ink. The point light source at c then casts a shadow A' of A onto the image plane I , such that the finite points of A and A' exhibit an (almost) one-to-one correspondence. The mapping of A to A' is called a *central projection*, and we are obliged to say “almost” for the following reasons.

Consider the plane I_{\parallel} through the center of projection \mathbf{c} that is parallel to the *image* plane I . This plane cuts the *object* plane O in a certain (affine) line ℓ_O . Clearly, no point of the line ℓ_O on O casts a finite shadow point on I , since rays from \mathbf{c} to each point of this line are all parallel to I . Thus, we say that the affine line ℓ_O on O is mapped¹¹ to the *line at infinity* on I .

Conversely, consider the plane O_{\parallel} through \mathbf{c} that is parallel to the *object* plane. It cuts the image plane in a certain (affine) line ℓ_I , and we ask: what points of the object plane are mapped to this line ℓ_I on the image plane? If we consider a point \mathbf{p} on I that approaches ℓ_I , the location at which the ray from \mathbf{c} to \mathbf{p} pierces the object plane recedes indefinitely along that plane, since this ray approaches parallelism with O . Thus, we say that the line ℓ_I on I is the “shadow” of the *line at infinity* on O .

Figure 7.11 illustrates these concepts. From the above reasoning, it should be evident that almost all intersecting lines on O are mapped to intersecting lines on I . However, when two lines on O happen to intersect at a point on ℓ_O , they will be mapped to *parallel lines* on I . Conversely, parallel lines on O are mapped to *intersecting lines* on I — their intersections lie on the line ℓ_I .

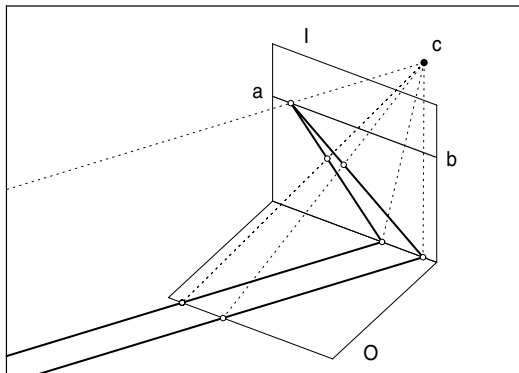


Fig. 7.11. Parallel lines on the object plane O , extended indefinitely, meet at a point on the line ab when projected from the center \mathbf{c} onto the image plane I . The line ab , defined by the intersection of I with a plane O_{\parallel} through \mathbf{c} that is parallel to O , is the image on I of the “line at infinity” on O .

A central projection of an object plane O from a finite center \mathbf{c} onto a non-parallel image plane I defines the most general form of two-dimensional projective transformation. When \mathbf{c} recedes to infinity, the rays connecting it to points of O become parallel, and we then have a *parallel projection* — which corresponds to an *affine* transformation of the plane, since points at infinity

¹¹ For obvious reasons, the line ℓ_O is often called the “vanishing line” on O .

on O are then mapped¹² to points at infinity on I . Finally, the case in which the image plane I and object plane O are parallel defines a shape-preserving affine transformation, namely, a simple *scaling* of the plane.

The model described above offers an intuitive geometrical understanding of the projective transformations that were introduced in purely algebraic terms in §7.4.4. It should be apparent that, in general, such transformations preserve the *incidence relations* (intersections, tangencies, etc.) in a geometrical figure — but they alter its size and shape. This can be seen, for example, in the case of the conics in Fig. 7.12, which imparts an intuitive interpretation to the statement that “the parabola is tangent to the line at infinity.”

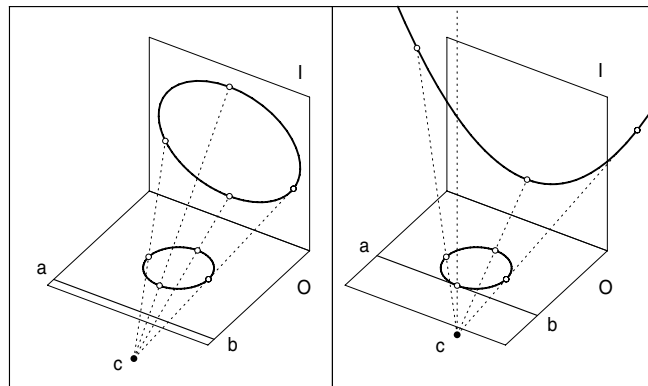


Fig. 7.12. Projective image of a circle. The “vanishing line” ab is the intersection of the object plane O with a plane through c that is parallel to the image plane I . The circle is mapped into an ellipse or a parabola according to whether ab lies outside the circle or touches it (not shown is the case where the vanishing line ab cuts the circle into two segments, which are mapped into the two branches of a hyperbola).

The equivalence of higher-order curves under projective transformations was perhaps first recognized by Sir Isaac Newton. In his *Enumeratio linearum tertii ordinis*, concerned with the classification of cubic curves (see also §9.2) he includes [432] the following paragraphs on *genesis curvarum per umbras* — i.e., the generation of curves by shadows:

“If the shadows of curves caused by a luminous point, be projected on an infinite plane, the shadows of conic sections will always be conic sections; those of curves of the second genus will always be of the second genus; those of the third genus will always be of the third genus; and so on *ad infinitum* . . . And in the same manner as the circle, projecting its shadow, generates all the conic sections, so the

¹² Unlike general projective transformations, this implies that parallel lines remain parallel under affine transformations.

five divergent parabolas, by their shadows, generate all other curves of the second genus. And thus some of the more simple curves of other genera might be found, which would form all curves of the same genus by the projection of their shadows on a plane."

In Newton's terminology¹³ (borrowed from Descartes) conics are curves of the "first genus" while cubics are of the "second genus." His "divergent parabolas" are cubics described by an equation of the form

$$y^2 = ax^3 + bx^2 + cx + d,$$

and he identifies five different types according to the root structure of the cubic on the right (namely: three simple real roots; a double root and a simple root either greater or smaller than it; one triple root; and one real root with two complex conjugate roots). Thus, Newton is claiming that *any* cubic may be regarded as the projective image of a curve of the above type.

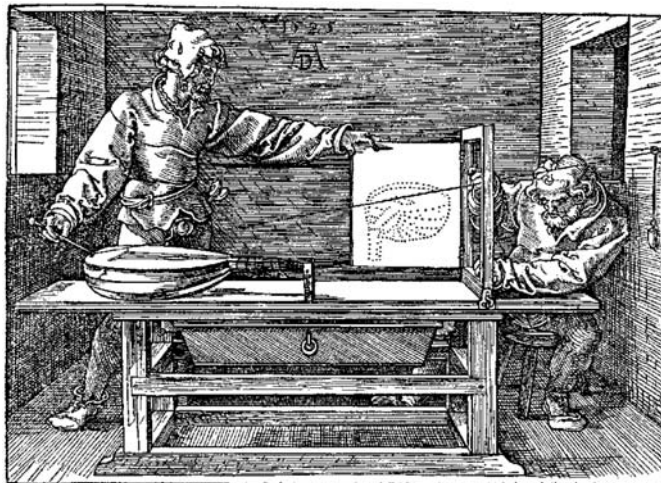


Fig. 7.13. Procedure for perspective drawing of a lute, from the *Unterweisung der Messung mit dem Zirkel und Rechtscheit* by the artist Albrecht Dürer (1471–1528).

The desire of Renaissance artists for greater "realism" in their paintings was the cultural pretext for the development of projective geometry. This led to a deeper grasp of the "perspective" projection of a three-dimensional scene onto a plane (the canvas) from a specified point (eye position), as seen in Fig. 7.13. Paolo Uccello (1379–1435) of Florence was perhaps the first to fully master the method — his perspective rendering of a chalice appears on the cover of the journal *Computer Aided Geometric Design*.

¹³ This should not be confused this with the modern concept of genus (see §9.2.5), that determines whether an algebraic curve admits a rational parameterization.

7.4.7 Projective Geometry of Three Dimensions

The ideas discussed above generalize readily to three dimensions, using the homogeneous coordinates (W, X, Y, Z) of three-dimensional projective space. A duality between *points* and *planes* is suggested by the equation

$$KW + LX + MY + NZ = 0, \quad (7.67)$$

which may be interpreted as defining either the set of points on a fixed plane, or the set of planes through a fixed point, depending on whether we consider (K, L, M, N) or (W, X, Y, Z) to be held constant. The equation $W = 0$ defines the *plane at infinity*. One can then form dual statements such as

three distinct points define a plane ... three distinct planes define a point.

Every pair of planes is considered to intersect in a line, either a line at infinity or an affine line according to whether or not those planes are parallel. In three dimensions, lines are considered to be *self-dual* — we do not change the word “line” when forming the dual of a statement. Thus we have

two distinct points define a line ... two distinct planes define a line.

as dual results, in which the words *point* and *plane* have been swapped, but *line* is unaltered. Similarly, dualizing “a point and a line define a plane” we obtain “a plane and a line define a point” — note that the validity of these statements is contingent on taking into account not only affine elements, but also points, lines, and the plane at infinity. As the dual of the *point* equation $F(W, X, Y, Z) = 0$ of a surface, we have the *plane* equation

$$G(K, L, M, N) = 0.$$

Each plane (7.67) whose coefficients K, L, M, N satisfy the above equation is tangent to the surface; the surface may be regarded as the *envelope* of this two-parameter family of tangent planes.

The homogeneous representation of *lines* in space is rather more subtle than that of points or planes. In three dimensions, there exist triply-infinite sets of both points and planes, and we can specify a particular point or plane by the ratios of *four* homogeneous coordinates: (W, X, Y, Z) or (K, L, M, N) . Now three-dimensional lines have four essential degrees of freedom,¹⁴ but it is not possible to give a “symmetrical” representation with five homogeneous coordinates. Thus, it is customary to employ a redundant set of *six* variables, known as *Plücker line coordinates*, to describe lines in space. Choosing distinct points (W_0, X_0, Y_0, Z_0) and (W_1, X_1, Y_1, Z_1) on any line ℓ in space, we may form the quantities defined by

$$(A_x, A_y, A_z) = (W_0X_1 - W_1X_0, W_0Y_1 - W_1Y_0, W_0Z_1 - W_1Z_0),$$

$$(B_x, B_y, B_z) = (Y_0Z_1 - Y_1Z_0, Z_0X_1 - Z_1X_0, X_0Y_1 - X_1Y_0).$$

¹⁴ Any line can be mapped to (say) the x -axis by two rotations and two translations.

One can then verify that the ratios $A_x : A_y : A_z : B_x : B_y : B_z$ are actually *independent* of the chosen points on ℓ — i.e., *any* points $(W_\lambda, X_\lambda, Y_\lambda, Z_\lambda)$ and $(W_\mu, X_\mu, Y_\mu, Z_\mu)$ given by distinct values $t = \lambda, \mu$ in $W = (1-t)W_0 + tW_1$, $X = (1-t)X_0 + tX_1, \dots$ etc., will yield the same ratios.

The above expressions may be simplified by using vector notations. Writing $\mathbf{P}_0 = (X_0, Y_0, Z_0)$, $\mathbf{P}_1 = (X_1, Y_1, Z_1)$ and $\mathbf{A} = (A_x, A_y, A_z)$, $\mathbf{B} = (B_x, B_y, B_z)$ we obtain

$$\mathbf{A} = W_0\mathbf{P}_1 - W_1\mathbf{P}_0 \quad \text{and} \quad \mathbf{B} = \mathbf{P}_0 \times \mathbf{P}_1.$$

Clearly, the components of \mathbf{A} and \mathbf{B} are not independent — they satisfy

$$\mathbf{A} \cdot \mathbf{B} = A_x B_x + A_y B_y + A_z B_z = 0.$$

This, together with the fact that only the ratios $A_x : A_y : A_z : B_x : B_y : B_z$ are significant, means that among the six line coordinates (\mathbf{A}, \mathbf{B}) there are only four degrees of freedom. Conversely, the (ratios of) components for any pair of vectors (\mathbf{A}, \mathbf{B}) that satisfy $\mathbf{A} \cdot \mathbf{B} = 0$ identify a unique line ℓ in space — note that ℓ is a line at infinity if and only if $\mathbf{A} = (0, 0, 0)$.

One can also formulate a dual system of line coordinates, by regarding ℓ as the intersection of distinct planes (K_0, L_0, M_0, N_0) and (K_1, L_1, M_1, N_1) , that is analogous to the above scheme. In fact, by writing $\mathbf{Q}_0 = (L_0, M_0, N_0)$ and $\mathbf{Q}_1 = (L_1, M_1, N_1)$, one can deduce that the intersection of these planes has line coordinates (\mathbf{A}, \mathbf{B}) given by

$$\mathbf{A} = \mathbf{Q}_0 \times \mathbf{Q}_1 \quad \text{and} \quad \mathbf{B} = K_0 \mathbf{Q}_1 - K_1 \mathbf{Q}_0.$$

Two arbitrary lines ℓ_1, ℓ_2 in space are ordinarily *skew* (i.e., non-intersecting). The condition for them to intersect can be expressed in terms of their Plücker coordinates $(\mathbf{A}_1, \mathbf{B}_1)$ and $(\mathbf{A}_2, \mathbf{B}_2)$ as

$$\mathbf{A}_1 \cdot \mathbf{B}_2 + \mathbf{A}_2 \cdot \mathbf{B}_1 = 0.$$

In three-dimensional projective geometry, the *circle at infinity* (also known as the *absolute circle*) assumes the role of the circular points at infinity in the two-dimensional case. This locus may be regarded as the intersection of any sphere with the plane at infinity. It is defined by the equations

$$W = X^2 + Y^2 + Z^2 = 0,$$

and thus comprises only complex points. Alternately, we may parameterize it using the rational form

$$W(t) : X(t) : Y(t) : Z(t) = 0 : 1 - t^2 : 2t : i(1 + t^2).$$

Each plane may be regarded as possessing two circular points at infinity: the circle at infinity is the locus of such points for planes of all orientations.

Three-dimensional projective transformations between two homogeneous coordinate systems (W, X, Y, Z) and $(\tilde{W}, \tilde{X}, \tilde{Y}, \tilde{Z})$ can be described by a non-singular 4×4 matrix:

$$\begin{bmatrix} \tilde{W} \\ \tilde{X} \\ \tilde{Y} \\ \tilde{Z} \end{bmatrix} = \begin{bmatrix} m_{00} & m_{01} & m_{02} & m_{03} \\ m_{10} & m_{11} & m_{12} & m_{13} \\ m_{20} & m_{21} & m_{22} & m_{23} \\ m_{30} & m_{31} & m_{32} & m_{33} \end{bmatrix} \begin{bmatrix} W \\ X \\ Y \\ Z \end{bmatrix}. \quad (7.68)$$

This matrix has a factorization analogous to (7.63), into an affine mapping (three-dimensional rotations/reflections, if the lower-right 3×3 sub-matrix is orthogonal), a translation, a scaling, and a three-dimensional perspectivity. The latter admits a geometrical interpretation similar to that discussed above in §7.4.6 for the two-dimensional case, although the visualization is now more difficult because it is based on a projection between three-dimensional subsets of a *four-dimensional* Euclidean space. In three dimensions, the most general shape-preserving transformation has the form

$$\begin{bmatrix} \tilde{W} \\ \tilde{X} \\ \tilde{Y} \\ \tilde{Z} \end{bmatrix} = \begin{bmatrix} k & 0 & 0 & 0 \\ \Delta x & \cos \phi \cos \theta & -\sin \phi & \cos \phi \sin \theta \\ \Delta y & \sin \phi \cos \theta & \cos \phi & \sin \phi \sin \theta \\ \Delta z & -\sin \theta & 0 & \cos \theta \end{bmatrix} \begin{bmatrix} W \\ X \\ Y \\ Z \end{bmatrix}.$$

Here we assume that the lower-right 3×3 sub-matrix represents a rotation, although any combination of rotations/reflections is allowed — the indicated form corresponds to rotation by a *polar* angle θ about the y -axis, followed by rotation by an *azimuthal* angle ϕ about the z -axis.

Differential Geometry

Let us therefore consider as differential geometry that branch of the subject which is based on ... the infinitesimal calculus ... The first writer we should consider in this connection actually did not use the calculus at all, for it was not invented in his time, Christiaan Huygens. He deserves to rank as a forerunner, however, owing to his interest in curvature and evolutes. He was led to this, strangely enough, from his interest in pendulums and clocks.

J. L. Coolidge, *A History of Geometrical Methods*

It is commonly believed that the invention of calculus was motivated by the desire to formulate and solve differential equations, especially the equations of motion of Newtonian dynamics. In fact, purely geometrical problems, such as the determination of tangents and curvatures, feature prominently among its earliest applications. The first calculus textbook, the *Analyse des infiniment petits, pour l'intelligence des lignes courbes* (see Fig. 8.1), published in 1696 by the French aristocrat Guillaume François Antoine de l'Hôpital (1661–1704), is an exposition on the elementary differential geometry of plane curves.¹

Differential geometry is primarily concerned with the *local intrinsic shape* properties of curves and surfaces. To characterize these properties, a curve or surface is first represented by a vector-valued function of “auxiliary variables” or *parameters* — one for a curve, and two for a surface. By *local* we mean that the curve or surface geometry in the neighborhood of a particular point is characterized in terms of its parametric derivatives *at that point*. By *intrinsic* we mean that, although the curve or surface representation is not unique, the shape measures formulated in terms of its derivatives have the same values regardless of the chosen parameterization (or coordinate system).

¹ It might seem that modesty dissuaded de l'Hôpital from having his name printed on the cover sheet, although it appears “pencilled in” on many copies. This is, in fact, more an indication of the limits to his audacity: the text is a near-verbatim translation [443], by an unknown hand, of earlier Latin notes by Johann Bernoulli!

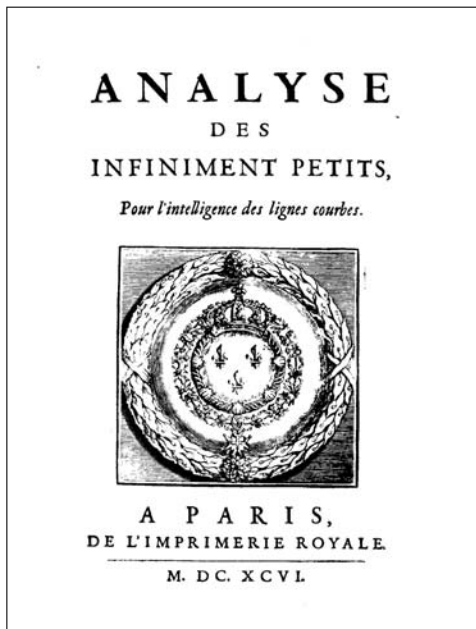


Fig. 8.1. The Marquis de l'Hôpital's *Analyse des infiniment petits* (1696), from the Special Collections Library, University of Michigan — reproduced with permission.

The *tangent* and *curvature* are the principal intrinsic shape properties of a plane curve — they characterize the “best” linear and circular approximants to the curve at each point. A plane curve is completely defined, modulo rigid motions, by specifying curvature as a function of position (arc length) along it. To describe a space curve an additional intrinsic property, the *torsion*, is required: this specifies the amount of “twisting” of the curve out of the plane that most nearly contains it in the neighborhood of each point.

At each point of a smooth surface the *tangent plane* — orthogonal to the *normal vector* at that point — identifies the “best” linear approximation to the surface. Since a surface is a two-dimensional locus, the characterization of its intrinsic shape properties is more subtle than for one-dimensional loci (curves). To elucidate the concept of surface curvature, we may appeal to the established concept of curvature for plane curves. The family of planes that contain the normal at a given point cut the surface in (planar) *normal section curves*, each with a well-defined curvature there. These “normal curvatures” exhibit minimum and maximum values, known as *principal curvatures* of the surface at that point, corresponding to orthogonal orientations of the section plane, which define the local *principal directions* for the surface. The surface shape in the vicinity of a point is like that of a “cup” or a “saddle” according to whether the principal curvatures there are of like or unlike sign.

Besides intrinsic shape properties (tangents and curvatures) at any fixed point, the freedoms of motion on a surface — as compared to a curve — allow the identification of *continuous loci* on the surface that are also expressions of its intrinsic geometry. The *lines of curvature*, for example, are an orthogonal network of curves on a surface that are everywhere tangential to the principal directions. For any two points, one may also consider the *geodesic* — or path of least length — on the surface between those points. Such “intrinsic loci” of a surface do not, in general, admit simple closed-form representations: they are the solutions to systems of non-linear differential equations.

8.1 Intrinsic Geometry of Plane Curves

A plane curve may be defined by an ordered pair of functions of a “parameter” ξ , the values of these functions being interpreted as the Cartesian coordinates of points along the curve: $\mathbf{r}(\xi) = (x(\xi), y(\xi))$. Actually, many different pairs of functions can exactly describe a given geometrical locus — i.e., there are many *different parameterizations* of a curve. However, assuming that $x(\xi)$ and $y(\xi)$ are at least twice-differentiable, we can identify certain expressions in their derivatives that are *independent* of the parameterization, and thus correspond to “intrinsic” geometrical properties of the curve.

8.1.1 Tangent and Curvature

The *tangent* and the *curvature* of a plane curve are its fundamental intrinsic geometrical properties. We say that the curve $\mathbf{r}(\xi)$ is *regular* if its derivative satisfies $\mathbf{r}'(\xi) \neq \mathbf{0}$ for each value of ξ in the parameter domain that concerns us. The derivative of a regular curve may be written in the form

$$\mathbf{r}'(\xi) = \sigma(\xi) \mathbf{t}(\xi), \quad (8.1)$$

i.e., as the product of a scalar function — the *parametric speed*

$$\sigma(\xi) = |\mathbf{r}'(\xi)| = \sqrt{x'^2(\xi) + y'^2(\xi)} = \frac{ds}{d\xi}, \quad (8.2)$$

which corresponds to the local rate of change of the curve arc length s with respect to the parameter ξ — and the unit *tangent vector*

$$\mathbf{t}(\xi) = \frac{\mathbf{r}'(\xi)}{|\mathbf{r}'(\xi)|} \quad (8.3)$$

to the curve. Under a differentiable transformation $\xi \rightarrow \zeta$ of the parameter, such that $d\zeta/d\xi \neq 0$ over the domain of interest, the tangent vector changes by at most a reversal in its sense. Thus, although (8.3) is not always invariant under re-parameterization, the *tangent line* (i.e., the line through any curve

point that contains the tangent vector) is an intrinsic property, and so is the *normal line* (the line orthogonal to the tangent line at each point).

By differentiating equation (8.1) again, we obtain

$$\mathbf{r}''(\xi) = \sigma'(\xi) \mathbf{t}(\xi) + \sigma(\xi) \mathbf{t}'(\xi). \quad (8.4)$$

Now $\mathbf{t}(\xi)$ is by definition a *unit* vector, and by differentiation of $|\mathbf{t}(\xi)|^2 \equiv 1$ we see that $\mathbf{t}'(\xi) \cdot \mathbf{t}(\xi) \equiv 0$, i.e., $\mathbf{t}'(\xi)$ is always perpendicular to $\mathbf{t}(\xi)$. Thus, introducing the unit *normal vector*

$$\mathbf{n}(\xi) = \mathbf{t}(\xi) \times \mathbf{z}, \quad (8.5)$$

where \mathbf{z} is a unit vector orthogonal to the plane of the curve, we may write

$$\mathbf{t}'(\xi) = -\sigma(\xi)\kappa(\xi) \mathbf{n}(\xi) \quad (8.6)$$

where $\kappa(\xi)$ is a scalar function, the *curvature* of $\mathbf{r}(\xi)$, that we shall presently determine (we introduce the factor $\sigma(\xi)$ to ensure that κ has a geometrical meaning independent of the curve parameterization). Through equations (8.3) and (8.5) we adopt the convention that $\mathbf{n}(\xi)$, $\mathbf{t}(\xi)$, \mathbf{z} form a right-handed orthonormal triad at each point of the curve, and $\mathbf{n}(\xi)$ points locally to the *right* of the curve $\mathbf{r}(\xi)$ as we traverse it in the sense of increasing ξ .

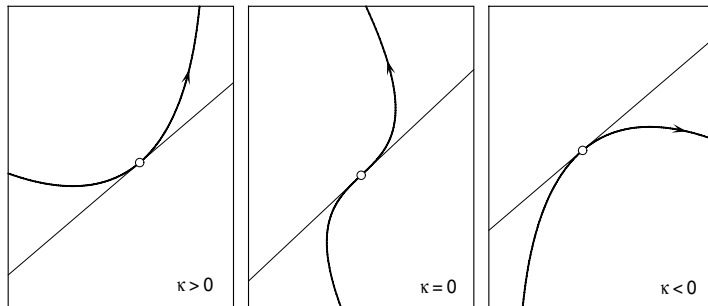


Fig. 8.2. Local behavior of a plane curve, relative to its tangent line, at points of positive, zero, and negative curvature. The arrows indicate the sense of the curve parameterization, and in the $\kappa = 0$ case we assume that $\kappa' \neq 0$, yielding an inflection.

Substituting (8.6) into (8.4), and taking the cross product of both sides with $\mathbf{r}'(\xi)$, we find that the curvature is given by

$$\kappa(\xi) = \frac{[\mathbf{r}'(\xi) \times \mathbf{r}''(\xi)] \cdot \mathbf{z}}{|\mathbf{r}'(\xi)|^3}. \quad (8.7)$$

It is not difficult to verify that, although it is expressed in terms of the first and second parametric derivatives of $\mathbf{r}(\xi)$, the value of $\kappa(\xi)$ is *independent* of the curve parameterization. Note that $\kappa(\xi)$ may assume both negative and

positive values, according to the orientations of $\mathbf{r}'(\xi)$ and $\mathbf{r}''(\xi)$ relative to \mathbf{z} . The vector $\mathbf{t}(\xi)$ defines the orientation of the tangent line at each point, and the curve lies locally to the *left* or *right* of this line according to whether $\kappa(\xi)$ is *positive* or *negative*. At points where $\kappa(\xi) = 0$, however, the curve *crosses* its tangent line² — we then have an *inflection* point (see Fig. 8.2).

8.1.2 The Circle of Curvature

We now define the *radius of curvature* to be the reciprocal of the curvature: $\rho(\xi) = 1/\kappa(\xi)$. Then, for each ξ , the point

$$\mathbf{e}(\xi) = \mathbf{r}(\xi) - \rho(\xi) \mathbf{n}(\xi) \quad (8.8)$$

is the *center of curvature*³ corresponding to the curve point $\mathbf{r}(\xi)$. The circle with center $\mathbf{e}(\xi)$ and radius $|\rho(\xi)|$ is called the *osculating circle* at that point: it is the circle that most closely “nestles” against the curve there. As ξ varies, equation (8.8) defines a parametric curve “derived” from the given curve $\mathbf{r}(\xi)$, namely, the locus of its centers of curvature — known as the *evolute* of that curve. We defer a more detailed discussion of evolutes to §8.3.

To quantitatively express the idea that the osculating circle “nestles” more closely against the curve at a given point than any other circle passing through that point consider, for a given scalar value R and fixed point \mathbf{c} , the function

$$f(\mathbf{p}) = |\mathbf{p} - \mathbf{c}|^2 - R^2$$

of the variable point $\mathbf{p} = (x, y)$. Clearly, the locus of points satisfying $f(\mathbf{p}) = 0$ is a circle of radius R with center \mathbf{c} . If we now choose a fixed parameter value ξ_* and take $\mathbf{c} = \mathbf{r}(\xi_*) - R \mathbf{n}(\xi_*)$, the equation

$$f(\mathbf{p}) = |\mathbf{p} - \mathbf{r}(\xi_*) + R \mathbf{n}(\xi_*)|^2 - R^2 = 0 \quad (8.9)$$

represents a circle passing through $\mathbf{r}(\xi_*)$ whose center lies on the normal line to the curve at that point, at distance R from it. To study how closely this circle conforms to the curve, we imagine that the variable point \mathbf{p} moves along the curve $\mathbf{r}(\xi)$. Taking $\mathbf{r}(\xi)$ as the argument of f yields the univariate function

$$F(\xi) = f(\mathbf{r}(\xi)) = |\mathbf{r}(\xi) - \mathbf{r}(\xi_*) + R \mathbf{n}(\xi_*)|^2 - R^2, \quad (8.10)$$

whose roots identify points ξ of the curve that lie on the circle (8.9).

Clearly ξ_* is such a root, because the point $\mathbf{r}(\xi_*)$ lies on the circle (8.9) by construction. In fact, differentiating (8.10) yields

$$F'(\xi) = 2 \mathbf{r}'(\xi) \cdot [\mathbf{r}(\xi) - \mathbf{r}(\xi_*) + R \mathbf{n}(\xi_*)], \quad (8.11)$$

² Provided that $\kappa'(\xi) \neq 0$, i.e., the value 0 is not a local extremum of the curvature.

³ Note that, according to the adopted sign convention, $\kappa(\xi)$ is positive when $\mathbf{n}(\xi)$ points *away* from the center of curvature.

and we see that $F'(\xi_*) = 0$, since $\mathbf{r}'(\xi_*)$ and $\mathbf{n}(\xi_*)$ are orthogonal. Hence, ξ_* is actually a *double root* of (8.10) for *all* values of R . Geometrically, this reflects the fact that, by construction, the circles defined by (8.9) all share the same tangent line with the curve at the point $\mathbf{r}(\xi_*)$ — these circles are said to have *first-order contact*⁴ with the curve at that point.

Among the family of circles (8.9), however, there is a unique member that is an even better local approximation to the curve at the point $\mathbf{r}(\xi_*)$ than all the others: this circle has *second-order contact* with the curve. To find the value of R identifying this special circle, we differentiate (8.11) again to obtain

$$F''(\xi) = 2 \mathbf{r}''(\xi) \cdot [\mathbf{r}(\xi) - \mathbf{r}(\xi_*) + R \mathbf{n}(\xi_*)] + 2 \mathbf{r}'(\xi) \cdot \mathbf{r}'(\xi), \quad (8.12)$$

and if ξ_* is to be a *triple root* of the function (8.10), we must have $F''(\xi_*) = 0$. Solving this equation for R gives

$$R = \frac{|\mathbf{r}(\xi_*)|^3}{[\mathbf{r}'(\xi_*) \times \mathbf{r}''(\xi_*)] \cdot \mathbf{z}} = \rho(\xi_*),$$

where $\rho(\xi_*)$ is the radius of curvature at $\mathbf{r}(\xi_*)$. Thus, $\mathbf{c} = \mathbf{r}(\xi_*) - \rho(\xi_*) \mathbf{n}(\xi_*) = \mathbf{e}(\xi_*)$, and we identify the circle that has second-order contact with the curve as the *osculating circle*, defined above. The point $\mathbf{r}(\xi_*)$ can be regarded as a *three-fold intersection* of the curve with its osculating circle, and the fact that osculating circle has *odd* intersection multiplicity with the curve implies that, in general, it *crosses* the curve at $\mathbf{r}(\xi_*)$. All other circles of radius $R \neq \rho(\xi_*)$ in the family (8.9), which are tangent to the curve at $\mathbf{r}(\xi_*)$, lie *locally on one side of the curve* in a neighborhood of that point (see Fig. 8.3).

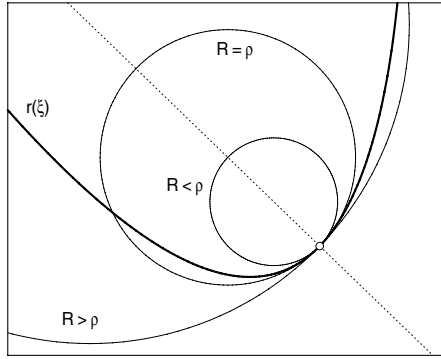


Fig. 8.3. Among all circles tangent to a curve at a generic point (with centers on the normal line there), those with radii R smaller or larger than the radius of curvature ρ lie locally to one side of the curve: the *osculating circle* with $R = \rho$ cuts the curve.

⁴ The *order of contact* at a common point of two curves is conventionally defined [383] to be one less than their intersection multiplicity at that point.

8.1.3 Vertices of Plane Curves

We have observed that, for any point of non-zero curvature on a regular plane curve $\mathbf{r}(\xi)$, there is a unique circle having second-order contact with the curve at that point. Higher-order contacts of circles with a curve are possible, but only at certain special points of the curve. By further differentiation of (8.12), for example, one can show that ξ_* is a four-fold root of $F(\xi)$ when $R = \rho(\xi_*)$ and this value also corresponds to a (local) *extremum* of $\rho(\xi)$.

A point where the radius of curvature (or curvature) of a curve attains a local extremum value is called a *vertex* of that curve. The osculating circle at a vertex has (at least) third-order contact with the curve, and it lies locally to one side of the curve. Thus an ellipse, for example, has four vertices — two of minimum and two of maximum curvature, on its minor and major axes, respectively. This is perhaps the simplest illustration of a “global” intrinsic property of closed plane curves, known as the *four-vertex theorem*:

Theorem 8.1 *A smooth closed plane curve has at least four vertices.*

The theorem may be proved by considering the curvature variation between points of contact of the curve with the circle circumscribed about it [352].

8.1.4 The Intrinsic Equation

The curvilinear distance s or *arc length* of the curve $\mathbf{r}(\xi)$, as measured from the point $\xi = 0$, is given by the function

$$s(\xi) = \int_0^\xi \sigma(t) dt \quad (8.13)$$

of the parameter ξ . Unfortunately, the radical in (8.2) precludes a resolution of this integral into elementary functions of ξ for even the “simplest” curves (i.e., those parameterized by polynomial or rational functions).

We shall demonstrate in §16.1 below that arc-length parameterizations in terms of rational functions are, in fact, *impossible* — except in the trivial case of a straight line. It is nevertheless advantageous, for theoretical purposes, to consider the parameter transformation $\xi \rightarrow s$ defined formally by (8.13). The distinguishing property of the arc-length or “natural” parameterization $\mathbf{r}(s)$ of a curve is that its parametric speed satisfies⁵ $\sigma(s) = |\dot{\mathbf{r}}(s)| \equiv 1$; hence this is often also called the “unit-speed” parameterization.

In terms of the arc-length parameterization, the tangent and normal are $\mathbf{t}(s) = \dot{\mathbf{r}}(s)$ and $\mathbf{n}(s) = \mathbf{t}(s) \times \mathbf{z}$, while the curvature is $\kappa(s) = [\dot{\mathbf{r}}(s) \times \ddot{\mathbf{r}}(s)] \cdot \mathbf{z}$. The variation of \mathbf{t} and \mathbf{n} along the curve is described by the *Frenet equations*

$$\frac{d\mathbf{t}}{ds} = -\kappa \mathbf{n} \quad \text{and} \quad \frac{d\mathbf{n}}{ds} = \kappa \mathbf{t}. \quad (8.14)$$

⁵ We employ dots to denote derivatives with respect to s , and primes for derivatives with respect to a general parameter ξ .

Now since the tangent and normal are orthogonal unit vectors, we may write $\mathbf{t}(s) = (\cos \theta(s), \sin \theta(s))$ and $\mathbf{n}(s) = (\sin \theta(s), -\cos \theta(s))$, $\theta(s)$ being the angle between the x -axis and the tangent to $\mathbf{r}(s)$. Substituting these expressions into (8.14) we observe that the curvature has the interpretation

$$\kappa = \frac{d\theta}{ds},$$

i.e., it is *derivative of the tangent-angle θ with respect to the arc length s* .

The function $\kappa(s)$ specifying the curvature in terms of arc length along a plane curve is called the *intrinsic equation* of that curve — apart from a rigid motion, it uniquely defines the curve. Given a start point $\mathbf{r}_0 = (x_0, y_0)$ and direction $\mathbf{t}_0 = (\cos \theta_0, \sin \theta_0)$ at $s = 0$, we have the explicit representation

$$x(s) = x_0 + \int_0^s \cos \theta(t) dt, \quad y(s) = y_0 + \int_0^s \sin \theta(t) dt \quad (8.15)$$

of the curve, where

$$\theta(s) = \theta_0 + \int_0^s \kappa(t) dt. \quad (8.16)$$

Of course, the possibility of resolving these integrals in terms of elementary functions depends on the functional form of $\kappa(s)$. In cases where an analytic reduction is impossible, numerical quadrature must be used to trace $\mathbf{r}(s)$.

Similarly, knowing the value and derivatives $\kappa_0, \dot{\kappa}_0, \dots$ of $\kappa(s)$ at the point \mathbf{r}_0 where $s = 0$, we can develop $\mathbf{r}(s)$ in a power series about that point,

$$\mathbf{r}(s) = \mathbf{r}_0 + \left(s - \frac{\kappa_0^2}{6} s^3 + \dots \right) \mathbf{t}_0 + \left(-\frac{\kappa_0}{2} s^2 - \frac{\dot{\kappa}_0}{6} s^3 + \dots \right) \mathbf{n}_0, \quad (8.17)$$

where \mathbf{t}_0 and \mathbf{n}_0 are the tangent and normal at \mathbf{r}_0 , and only cubic or lower-order terms in s are shown. We see that, referred to the tangent and normal as local axes, the curve at \mathbf{r}_0 looks “locally” like a parabola if $\kappa_0 \neq 0$, and like an inflectional cubic if $\kappa_0 = 0 \neq \dot{\kappa}_0$ (see Fig. 8.2).

8.2 Families of Plane Curves

Consider a one-parameter family of plane curves $\mathcal{C}(\lambda)$, where the parameter λ varies over a given interval. $\mathcal{C}(\lambda)$ may be specified by a polynomial equation $f(x, y, \lambda) = 0$ as a family of implicit algebraic curves, or by a vector polynomial or rational function $\mathbf{r}(\xi, \lambda)$ as a family of parametric curves — where ξ is the curve parameter, as distinct from the “family parameter” λ . These two forms evidently specify *differentiable* families of curves. The members of the family $\mathcal{C}(\lambda)$ may be all of the same size and shape, differing only in location and/or orientation, or they may change continuously in size and shape as λ varies. The former case arises naturally in describing the motion of a rigid body.

8.2.1 Envelopes of Curve Families

The most interesting feature of a differentiable family of plane curves $\mathcal{C}(\lambda)$ is its *envelope* [52]. An intuitive feel for the envelope can be obtained by plotting a discrete sample $\mathcal{C}(\lambda_1), \dots, \mathcal{C}(\lambda_N)$ of the family members (see Fig. 8.4) — typically, the curves occupy a subset of the plane, and they “nestle” against a certain locus that bounds the region occupied by the entire family: this locus is (a subset of) the envelope.⁶ However, some families of curves may have no envelope at all — e.g., families of parallel lines or concentric circles.

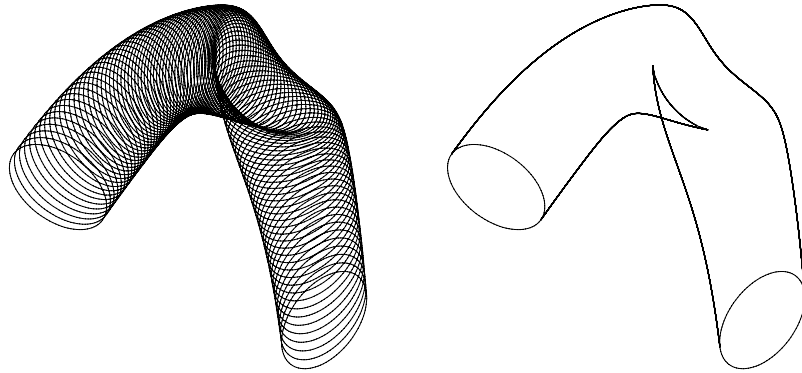


Fig. 8.4. Left: discrete sampling of a one-parameter family of curves $\mathcal{C}(\lambda)$, $\lambda \in [0, 1]$ generated by the motion (translation and rotation) of an ellipse. Right: envelope of the curve family $\mathcal{C}(\lambda)$ together with the initial and final instances, $\mathcal{C}(0)$ and $\mathcal{C}(1)$.

There are several alternative approaches to defining the envelope \mathcal{E} of the curve family $\mathcal{C}(\lambda)$ quantitatively, and in certain situations they incur technical differences in terms of what is considered to belong to the envelope. We briefly address some of these differences below — see [62, 63, 203] for details.

Definition 8.1 The envelope \mathcal{E} is a curve that is tangent at some point to each member of the curve family $\mathcal{C}(\lambda)$.

Definition 8.2 The envelope \mathcal{E} is the locus of intersections of “neighboring” curves, $\mathcal{C}(\lambda)$ and $\mathcal{C}(\lambda + \Delta\lambda)$, in the limit $\Delta\lambda \rightarrow 0$.

Definition 8.3 If \mathcal{S} is the surface defined by “stacking” each curve $\mathcal{C}(\lambda)$ at height $z = \lambda$ above the (x, y) plane, the envelope Γ is the *critical set* of the projection of \mathcal{S} onto this plane (or the *silhouette* of \mathcal{S} viewed along the z -axis).

We focus on the envelopes of *smooth* (tangent-continuous) curve families, for which it is possible to identify the points of each curve $\mathcal{C}(\lambda)$ that lie on the

⁶ Not all segments of the envelope separate regions occupied by the curve family from “empty space” — parts of the envelope may lie *within* the former regions.

envelope \mathcal{E} . Curves with tangent discontinuities incur further complications in the envelope formulation — each tangent-discontinuous point is a potential contributor to the envelope (for example, the envelope of a moving polygon is generated entirely by its vertices, unless there are instances where the motion is instantaneously parallel to one side of the polygon).

8.2.2 Families of Implicit Curves

If $\mathcal{C}(\lambda)$ is specified as a family of algebraic curves, by a polynomial equation of the form $f(x, y, \lambda) = 0$, its envelope \mathcal{E} is also an algebraic curve. Writing $f_\lambda = \partial f / \partial \lambda$, the equation of the envelope curve is obtained by eliminating λ among the equations⁷ $f = f_\lambda = 0$ — i.e.,

$$e(x, y) = \text{Resultant}_\lambda(f(x, y, \lambda), f_\lambda(x, y, \lambda)) = 0. \quad (8.18)$$

This may be understood in terms of Definition 8.3 as follows. Identifying λ with the Cartesian coordinate z in \mathbb{R}^3 , consider the silhouette of the algebraic surface $f(x, y, z) = 0$, viewed along the z -axis. A point of this surface belongs to the silhouette if the surface normal, in the direction of $\nabla f = (f_x, f_y, f_z)$, is orthogonal to the z -axis, i.e., if $f_z = 0$. The locus of points on $f(x, y, z) = 0$ satisfying $f_z(x, y, z) = 0$ is an algebraic space curve. The envelope \mathcal{E} of the curve family is just the (parallel) *projection* of that space curve onto the (x, y) plane — it may be regarded as the locus of points in the plane such that the equations $f = 0$ and $f_z = 0$ are simultaneously satisfied for *some* value of z . With $z = \lambda$, this interpretation yields (8.18) as the envelope equation.

In a number of exceptional circumstances, special factors may arise in the envelope equation (8.18) — depending on the particular context, these factors may or may not be regarded as defining parts of the desired envelope:

- (a) if the value $\lambda = \lambda_*$ identifies a “stationary” curve in the family, such that $f_\lambda(x, y, \lambda_*) \equiv 0$, then $f(x, y, \lambda_*)$ appears as a factor of $e(x, y)$;
- (b) conversely, if λ_* identifies a “vacuous” member, so that $f(x, y, \lambda_*) \equiv 0$, then $f_\lambda(x, y, \lambda_*)$ appears as a factor of $e(x, y)$;
- (c) if $g(x, y) = \text{gcd}(f(x, y, \lambda_*), f_\lambda(x, y, \lambda_*))$ is a non-constant common factor of f and f_λ for $\lambda = \lambda_*$, then $g(x, y)$ appears as a factor of $e(x, y)$;
- (d) if the family $f(x, y, \lambda)$ has a *locus of singular points* — i.e., there exists a curve $\sigma(x, y) = 0$ such that, as λ varies, $f = f_x = f_y = 0$ on this curve — $\sigma(x, y)$ also appears as a factor of $e(x, y)$.

Perhaps the simplest example is a linear family, or *pencil*, of curves:

$$f(x, y, \lambda) = (1 - \lambda) f_0(x, y) + \lambda f_1(x, y) = 0. \quad (8.19)$$

Since f_λ is *independent* of λ , the envelope equation (8.18) becomes

⁷ This method was first proposed [281] in the *Acta Eruditorum* of 1692 and 1694, by Gottfried Wilhelm von Leibniz (1646–1716).

$$e(x, y) = f_1(x, y) - f_0(x, y) = 0.$$

For example, the envelope of a pencil of conics is (in general) a conic itself.

Example 8.1 A pencil of circles — also called a *coaxal system of circles* — has one of the following three forms (see Fig. 8.5):

- the *common points* or “elliptic” system;
- the *tangential* or “parabolic” system;
- the *limiting points* or “hyperbolic” system.

The tangential system is a transitional case between the common and limiting points systems. If $f_0(x, y) = 0, f_1(x, y) = 0$ are the equations of distinct circles in a coaxal system, with the same coefficient for $x^2 + y^2$, the line defined by

$$\ell(x, y) = f_1(x, y) - f_0(x, y) = 0 \quad (8.20)$$

is known as the *radical axis* of that system. From the preceding discussion, we might expect this line to be the envelope of the coaxal system. However, the geometrical perspectives of Definitions 8.1–8.3 suggest that the envelope is at most a set of discrete points, rather than a locus — namely, the common points (elliptic system); the tangency point (parabolic system); and the empty set (hyperbolic system). Actually, $\ell(x, y)$ is one of the “extraneous” factors, discussed above, that may arise in the envelope formulation (8.18). When the coaxal system is expressed in the form (8.19), the value⁸ $\lambda = \pm\infty$ identifies the circle of “infinite radius” in the system, i.e., the radical axis (8.20). Since f and f_λ both reduce to $\ell(x, y)$ at $\lambda = \pm\infty$, we expect from case (c) that this factor will appear in (8.18).

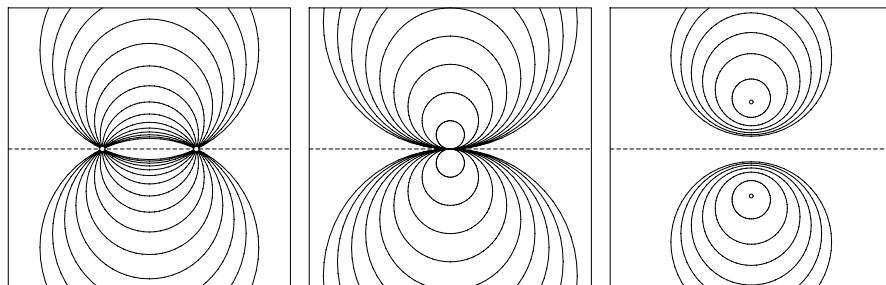


Fig. 8.5. Common points (left), tangent (center), and limiting points (right) coaxal circle systems: the dashed line indicates the radical axis. There is no envelope curve.

⁸ We may define $f(x, y, \pm\infty)$ as a formal limit — alternately, we may regard λ as being defined over the projective line by introducing a homogenizing variable.

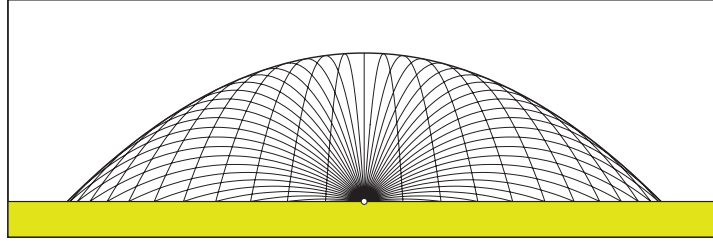


Fig. 8.6. Envelope of projectile trajectories or “parabola of safety” (Example 8.2).

Example 8.2 The trajectory of a projectile launched from the origin with speed v , at an angle $\theta = \tan^{-1} \lambda$ to the ground, has the equation

$$f(x, y, \lambda) = k(1 + \lambda^2)x^2 - \lambda x + y = 0, \quad (8.21)$$

where $k = g/2v^2$ and g is the gravitational acceleration. As seen in Fig. 8.6, for all λ this defines a *family of parabolas*. Taking the resultant of (8.21) and

$$f_\lambda = 2k\lambda x^2 - x \quad (8.22)$$

with respect to λ , we obtain the equation

$$e(x, y) = kx^4(4k^2x^2 + 4ky - 1) = 0.$$

The x^4 term arises because (8.21) and (8.22) have the common factor x^2 when $\lambda = \pm\infty$ (corresponding to a vertical trajectory). Discarding this term, we see that the envelope⁹

$$4k^2x^2 + 4ky - 1 = 0 \quad (8.23)$$

of the family of parabolas (8.21) is itself a parabola. Note that *every* member of the family (8.21) is tangent to the envelope (8.23), although for $|\lambda| < 1$ (i.e., $|\theta| < \pi/4$) the point of tangency lies below the ground, $y = 0$. As is well known, the maximum range at $y = 0$, $x_{\max} = v^2/g$, is obtained with $|\theta| = \pi/4$. Since the projectile cannot intercept any object that remains outside the locus (8.23), it is called the “parabola of safety” — see [52] for further details.

8.2.3 Families of Parametric Curves

Consider the envelope of a family $\mathcal{C}(\lambda)$ of *parametric* curves, specified by

$$\mathbf{r}(\xi, \lambda) = (X(\xi, \lambda), Y(\xi, \lambda)), \quad (8.24)$$

where X, Y are given (typically, polynomial or rational) functions of ξ and λ . In this case, the surface \mathcal{S} of Definition 8.3 can be parameterized as

⁹ This problem was first studied [281] by Torricelli and Bernoulli.

$$x = X(\xi, \lambda), \quad y = Y(\xi, \lambda), \quad z = \lambda.$$

We express this in vector form $\mathbf{s}(\xi, \lambda)$ where \mathbf{s} denotes a vector in \mathbb{R}^3 , and we regard ξ and λ as surface parameters. The unit normal to \mathcal{S} is given by

$$\mathbf{n} = \frac{\mathbf{s}_\xi \times \mathbf{s}_\lambda}{|\mathbf{s}_\xi \times \mathbf{s}_\lambda|},$$

where $\mathbf{s}_\xi = (\partial X / \partial \xi, \partial Y / \partial \xi, 0)$ and $\mathbf{s}_\lambda = (\partial X / \partial \lambda, \partial Y / \partial \lambda, 1)$. The condition that the surface normal \mathbf{n} be orthogonal to the z -axis thus amounts to

$$\frac{\partial X}{\partial \xi} \frac{\partial Y}{\partial \lambda} - \frac{\partial Y}{\partial \xi} \frac{\partial X}{\partial \lambda} = 0, \quad (8.25)$$

which may be cast in terms of the original specification (8.24) as $\mathbf{r}_\xi \times \mathbf{r}_\lambda = \mathbf{0}$. Note that the left-hand side of (8.25) is the *Jacobian*, $\partial(X, Y) / \partial(\xi, \lambda)$, of the bivariate functions $X(\xi, \lambda)$ and $Y(\xi, \lambda)$.

The condition (8.25) may be interpreted geometrically as follows. Provided that \mathbf{r}_ξ and \mathbf{r}_λ are non-vanishing, the former specifies the *tangent direction* for a fixed curve λ of the family, whereas the latter gives the instantaneous *direction of motion* for a point of fixed parameter value ξ as we pass through successive curves of the family — i.e., as we increase the family parameter λ . Thus, we may identify the points on each member of (8.24) that contribute to the envelope as those points where the curve tangent coincides with the direction of motion as we pass through successive curves in the family.

Equation (8.25) identifies, for each λ , the ξ value(s) corresponding to the point(s) that the curve $\mathbf{r}(\xi, \lambda)$ contributes to the envelope \mathcal{E} . If this equation can be solved in closed form to yield a symbolic expression $\lambda(\xi)$ for the family parameter in terms of the curve parameter, an explicit parameterization of the envelope is obtained by substituting this expression into (8.24):

$$\boldsymbol{\epsilon}(\xi) = \mathbf{r}(\xi, \lambda(\xi)). \quad (8.26)$$

In general, however, equation (8.25) does not admit closed-form solutions for λ in terms of ξ (moreover, the number of such solutions may vary with ξ). A particularly simple instance is that of a pencil of parametric curves,

$$\mathbf{r}(\xi, \lambda) = (1 - \lambda) \mathbf{r}_0(\xi) + \lambda \mathbf{r}_1(\xi).$$

In this case, equation (8.25) has the unique real solution

$$\lambda(\xi) = \frac{([\mathbf{r}_1(\xi) - \mathbf{r}_0(\xi)] \times \mathbf{r}'_0(\xi)) \cdot \mathbf{z}}{([\mathbf{r}'_1(\xi) - \mathbf{r}'_0(\xi)] \times [\mathbf{r}_1(\xi) - \mathbf{r}_0(\xi)]) \cdot \mathbf{z}},$$

\mathbf{z} being a unit vector orthogonal to the plane of $\mathbf{r}_0(\xi)$, $\mathbf{r}_1(\xi)$. Substituting this into expression (8.26) will yield, in general, a *rational* parameterization of the envelope $\boldsymbol{\epsilon}(\xi)$ when $\mathbf{r}_0(\xi)$ and $\mathbf{r}_1(\xi)$ are polynomial or rational curves.

8.2.4 Families of Lines and Circles

The envelopes of families of certain “simple” curves (namely, lines and circles) are of particular importance. We have already encountered, in our discussion of *dual representations* in § 7.4, the notion that a plane curve may be regarded as the envelope of its tangent lines (see Fig. 7.7). In some situations, the dual form is more useful than the customary point equation of a curve.

One might also postulate that a given family of lines are *normals*, rather than tangents, to a plane curve. Whereas a given family of tangents identifies a *unique* curve, a family of normals is compatible with an *infinity* of curves: these curves are “offsets” or “parallels” to each other (see §8.3.4). The envelope of the family of normal lines to a given curve is the *evolute* of that curve — it corresponds to the locus of its centers of curvature. All members of a sequence of offset curves share the same evolute — they are its *involutes*.

One family of circles associated with a sufficiently smooth curve is the set of *osculating circles* (see §8.1.2). These circles have centers on the evolute of the given curve, and radii given by its radius of curvature at each point. For $d > 0$, one may also consider the families of circles of fixed radius d whose centers lie on a given curve — the envelopes of such families correspond to the offset (parallel) curves at each distance d from the given curve. In geometrical optics, offset curves describe the propagation of a wavefront through a homogeneous medium. They are employed in computer-aided design to describe tool paths and tolerance zones, and they specify dilation and erosion operations for image processing. The following section explores the intimate relationships between evolutes, involutes, and offset curves in greater detail.

8.3 Evolutes, Involutes, Parallel Curves

For any given planar curve, several “derived” curves may be associated with it by means of intuitive geometrical constructions. Perhaps the most important examples are the intimately-connected *evolute*, *involutes*, and *parallel* (offset) *curves*. The first investigations of such loci were conducted, prior to the formal development of calculus, by Christiaan Huygens (1629–1695) in the context of his design of an ingenious pendulum clock (*Horologium Oscillatorium*, 1673) and his wave theory of light propagation (*Traité de la Lumière*, 1690).

To elucidate the properties of the evolute, involutes, and offset curves, it is instructive to begin by re-visiting the tangent line and osculating circle from a geometrical perspective (as distinct from the analytic arguments of §8.1) — this approach is closer in spirit to the original treatment by Huygens.

8.3.1 Tangent Line and Osculating Circle

Lines and circles are the first loci encountered in the study of geometry, and throughout history they have been universally regarded as the most “perfect”

curves. This is, no doubt, due to the geometric intuition we develop for them, and the rigor and ease with which “ruler and compass” configurations can be generated and analyzed. The notion of *tangent line* and *osculating circle* offer a bridge to carry this intuition over to the realm of higher-order curves.

At any point P on a smooth planar curve, the *tangent line* T_P embodies the most basic information concerning the location of nearby curve points. A “highly magnified” view of the curve, in a sufficiently small neighborhood of P , looks almost identical to T_P . If we desire an even better local approximation (one that better describes the curve shape at lower magnification), we employ the *circle of curvature* or *osculating¹⁰ circle* C_P — the circle that most closely “nestles” against the curve at P . The tangent line T_P is specified by a single number, its orientation at P , but the circle of curvature C_P requires two: the *direction* and *distance* to its center from the curve point P . This reflects the fact that C_P is a “higher-order” description of local curve shape than T_P .

The orientation of the tangent line at a point P of a smooth curve can be determined by a geometrical limit process. Consider an infinite sequence of points P_1, P_2, \dots progressing systematically toward P along the curve,

$$\lim_{k \rightarrow \infty} P_k = P.$$

In this progression, one finds that while the *length* of the chord $\overline{PP_k}$ shrinks, its orientation approaches, asymptotically, a definite direction. This limiting direction defines the tangent line T_P . The center of the osculating circle C_P (i.e., the *center of curvature* for the curve point P) can also be determined by a geometrical limit process. We assume the ability, as described, to determine the tangent lines T_1, T_2, \dots at each of an infinite sequence of points P_1, P_2, \dots that progress toward P . We define the *normal line* N_P to be the line through P that is perpendicular to T_P — similarly, the normals N_1, N_2, \dots are lines through P_1, P_2, \dots that are perpendicular to the tangents T_1, T_2, \dots . Then if Q_k denotes the *intersection point* of the normal lines N_P and N_k for $k = 1, 2, \dots$, one finds that the points Q_1, Q_2, \dots converge to a definite limit,

$$\lim_{k \rightarrow \infty} Q_k = Q.$$

This limit point Q is the *center of curvature* for the point P of the curve, and the distance $\rho = \overline{QP}$ is the *radius of curvature* there. Exceptionally, Q is a *point at infinity* (and ρ becomes infinite) if the curve is locally “flat” at P . Clearly, determining the center of curvature involves taking a “limit of limits” — i.e., it is a *second-order property* of the curve.

The existence of the tangent line T_P and osculating circle C_P is contingent on the curve being “sufficiently smooth” at the point P . A curve for which T_P exists at each point has first-order geometric (G^1) continuity. If, in addition, C_P exists at each point, the curve has second-order geometric (G^2) continuity. Figure 8.7 illustrates the two limit processes that determine tangent lines and

¹⁰ The adjective *osculating* comes from the Latin verb *osculare*, “to kiss.”

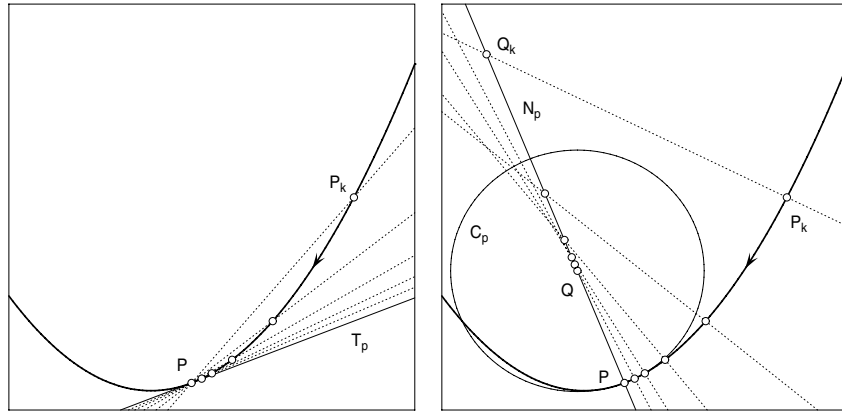


Fig. 8.7. Geometrical construction of tangent line T_P and osculating circle C_P at a curve point P . Left: the tangent at P is the limit of lines that connect it to curve points P_k , with $\lim_{k \rightarrow \infty} P_k = P$. Right: the center Q of the osculating circle at P is the limiting intersection of the normals at the points P_k with the normal N_P at P .

osculating circles through purely geometrical constructions. As seen here, the curve usually lies on one side of the tangent line T_P in a neighborhood of P — except when P is an *inflection* (a point where the center of curvature jumps from one side of the curve to the other), in which case the curve crosses T_P at P . On the other hand, the curve generally cuts its circle of curvature C_P at P , unless it is a *vertex* (a point where the radius of curvature is an extremum), in which case the curve lies on one side of C_P in a neighborhood of P .

8.3.2 Evolutes and Involutes

A smooth plane curve \mathcal{C} may be described by a continuous family of lines — namely, as the *envelope of its tangents*. We have already discussed this point of view in § 7.4.3, in the context of the point/line duality associated with the use of homogeneous coordinates in projective geometry. If the curve is sufficiently smooth, it may also be described by a continuous family of circles — as the *envelope of its osculating circles*. When \mathcal{C} has the parametric representation $\mathbf{r}(\xi)$, the latter description typically comprises two parts: (i) the locus $\mathbf{e}(\xi)$ of the centers of curvature; and (ii) the scalar function $\rho(\xi) = 1/\kappa(\xi)$ specifying the (signed) radius of curvature at each center of curvature.

The locus $\mathbf{e}(\xi)$ of centers of curvature of a curve $\mathbf{r}(\xi)$ is called the *evolute* of that curve. Another interpretation of it arises from our observation that the centers of curvature of $\mathbf{r}(\xi)$ correspond to the limiting intersections of normal lines at “neighboring” curve points that approach each other. This leads us to interpret $\mathbf{e}(\xi)$ as the *envelope of normal lines* to $\mathbf{r}(\xi)$ — see Fig. 8.8.

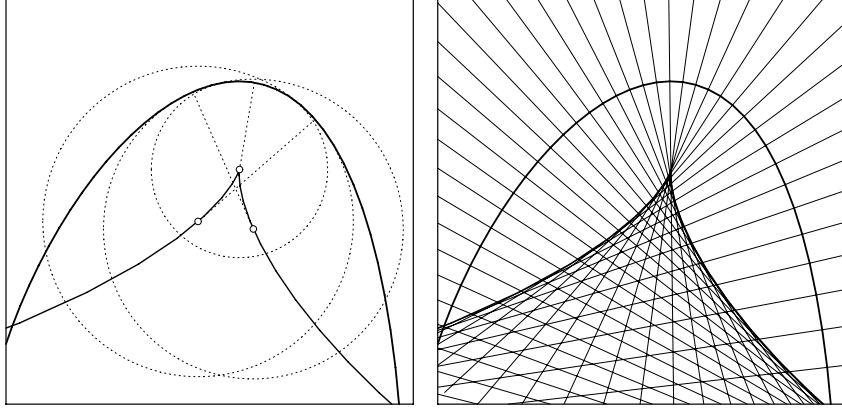


Fig. 8.8. Equivalent interpretations of the evolute of a smooth plane curve. Left: the locus of centers of curvature. Right: the envelope of the family of normal lines.

Point and Line Equations of Evolutes

Let $\mathbf{r}(\xi) = (x(\xi), y(\xi))$ be a degree- n curve, with unit tangent and normal

$$\mathbf{t}(\xi) = \frac{(x'(\xi), y'(\xi))}{\sqrt{x'^2(\xi) + y'^2(\xi)}}, \quad \mathbf{n}(\xi) = \frac{(y'(\xi), -x'(\xi))}{\sqrt{x'^2(\xi) + y'^2(\xi)}},$$

and (signed) curvature

$$\kappa(\xi) = \frac{x'(\xi)y''(\xi) - x''(\xi)y'(\xi)}{[x'^2(\xi) + y'^2(\xi)]^{3/2}},$$

which is negative or positive according to whether $\mathbf{n}(\xi)$ points toward or away from the center of curvature.¹¹ Interpreted as the *locus of centers of curvature* of $\mathbf{r}(\xi)$, the evolute $\mathbf{e}(\xi)$ is defined by

$$\mathbf{e}(\xi) = \mathbf{r}(\xi) - \rho(\xi) \mathbf{n}(\xi), \quad (8.27)$$

$\rho(\xi) = 1/\kappa(\xi)$ being the *radius of curvature*. The square root $\sqrt{x'^2(\xi) + y'^2(\xi)}$ evidently cancels in the product of $\rho(\xi)$ with $\mathbf{n}(\xi)$ above, and the evolute to a polynomial curve $\mathbf{r}(\xi)$ is thus a *rational* curve. Writing

$$\mathbf{e}(\xi) = \left(\frac{X_e(\xi)}{W_e(\xi)}, \frac{Y_e(\xi)}{W_e(\xi)} \right),$$

its homogeneous point coordinates are specified by

¹¹ Or, equivalently, whether the center of curvature lies to the right or left as we traverse the curve in the sense of increasing ξ .

$$\begin{aligned} W_e(\xi) &= x'(\xi)y''(\xi) - x''(\xi)y'(\xi), \\ X_e(\xi) &= [x'(\xi)y''(\xi) - x''(\xi)y'(\xi)]x(\xi) - [x'^2(\xi) + y'^2(\xi)]y'(\xi), \\ Y_e(\xi) &= [x'(\xi)y''(\xi) - x''(\xi)y'(\xi)]y(\xi) + [x'^2(\xi) + y'^2(\xi)]x'(\xi). \end{aligned} \quad (8.28)$$

From the above expressions it can be verified¹² that the evolute of a degree- n polynomial curve is of order $3n - 3$ (this is the degree of $X_e(\xi)$ and $Y_e(\xi)$ — the denominator polynomial $W_e(\xi)$ is of lower degree, namely, $2n - 4$).

The dual form of the evolute — in terms of homogeneous *line* rather than *point* coordinates — is actually much simpler than (8.28). In other words, the *class* of the evolute (i.e., the degree of its line equation) is lower than its *order* (the degree of its point equation). To demonstrate this, we use the alternate definition of the evolute as the *envelope of normal lines* of $\mathbf{r}(\xi)$ — each normal of the given curve is a tangent of its evolute. Writing the evolute tangent line corresponding to point ξ in terms of free coordinates (W, X, Y) as

$$K_e(\xi)W + L_e(\xi)X + M_e(\xi)Y = 0, \quad (8.29)$$

the dual — or homogeneous line — representation of the evolute is specified by the three polynomials $K_e(\xi), L_e(\xi), M_e(\xi)$.

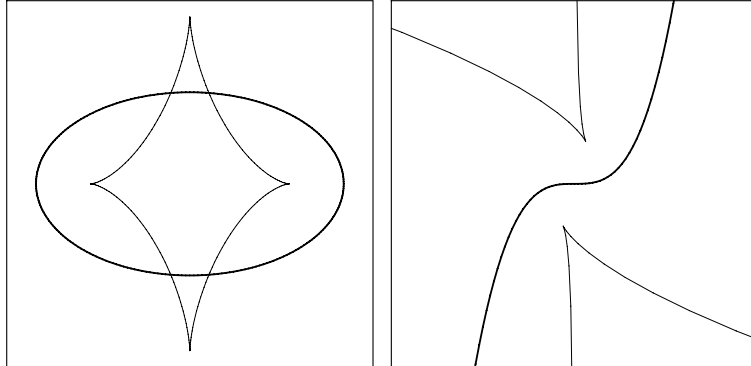


Fig. 8.9. Evolutes to an ellipse (left) and the inflectional cubic $y = x^3$ (right).

Now any point \mathbf{p} on the normal line to $\mathbf{r}(\xi)$ must satisfy

$$[\mathbf{p} - \mathbf{r}(\xi)] \cdot \mathbf{t}(\xi) = 0$$

i.e., the vector $\mathbf{p} - \mathbf{r}(\xi)$ must be orthogonal to the curve tangent $\mathbf{t}(\xi)$. Setting $\mathbf{p} = (X/W, Y/W)$ and multiplying through by W , this reduces to

$$[X - Wx(\xi)]x'(\xi) + [Y - Wy(\xi)]y'(\xi) = 0$$

¹² Due to cancellation of leading terms, $x'(\xi)y''(\xi) - x''(\xi)y'(\xi)$ is generally of degree $2n - 4$ for a degree- n curve.

or

$$-[x(\xi)x'(\xi) + y(\xi)y'(\xi)]W + x'(\xi)X + y'(\xi)Y = 0.$$

Since the normals to $\mathbf{r}(\xi)$ are tangents to its evolute $\mathbf{e}(\xi)$, we may identify the coefficients of W, X, Y above with the evolute line coordinates in (8.29),

$$K_e(\xi) = -[x(\xi)x'(\xi) + y(\xi)y'(\xi)], \quad L_e(\xi) = x'(\xi), \quad M_e(\xi) = y'(\xi). \quad (8.30)$$

The degree of this line representation (i.e., the *class* of the evolute) is seen to be $2n - 1$, which is lower than the degree $3n - 3$ of the point representation (8.28) when $n \geq 3$. For example, the evolute to a cubic is of order 6 and class 5, while for a quartic the order and class are 9 and 7, respectively. A similar analysis may be performed for the evolute of a *rational* degree- n curve $\mathbf{r}(\xi)$ — one finds that the evolute is again generically a rational curve, though of higher order and class than in the case of a polynomial curve. Examples of the evolutes to some simple curves are shown in Fig. 8.9.

A Physical Model for Involutes

Given a smooth plane curve \mathcal{C} , we have seen how to determine its evolute as either the locus of centers of curvature of \mathcal{C} or the envelope of the normal lines to \mathcal{C} . We now invert this problem and ask: if a given curve \mathcal{C} is known to be the evolute of some other curve, how can we determine that curve? In other words — which curve has the property that its centers of curvature precisely define the given curve \mathcal{C} ? Or, equivalently, which curve has the property that its normal lines coincide precisely with the set of all tangents to \mathcal{C} ? We shall see that there is actually an *infinite family* of curves for which the given curve \mathcal{C} is the evolute — these curves are known as the *involutes* of \mathcal{C} .

A simple “physical” model provides a good intuitive understanding of the involutes to a given curve \mathcal{C} . Suppose \mathcal{C} is specified parametrically as $\mathbf{r}(\xi)$. We imagine that a length of string is attached at one end to some distant curve point — i.e., at large positive ξ — and wrapped around the curve so that its free end coincides with the curve point $\xi = \tau$. As we unwrap this string from the curve (keeping it taut at each instant) its free end, originally at $\mathbf{r}(\tau)$, will trace out a certain locus.¹³ We call this locus the *involute of the curve* $\mathbf{r}(\xi)$, *corresponding to the point* $\xi = \tau$. Figure 8.10 illustrates this concept when \mathcal{C} is a circle (circle involutes are of fundamental importance in engineering, since they define the shape of gear teeth that ensures *conjugate action* of meshing gears [73] — i.e., a precisely constant ratio of angular speeds).

When the string has been unwrapped up to position ξ on the curve $\mathbf{r}(\xi) = (x(\xi), y(\xi))$, the unwrapped length corresponds to the total arc length

$$s_\tau(\xi) = \int_\tau^\xi \sqrt{x'^2(t) + y'^2(t)} dt \quad (8.31)$$

¹³ Alternatively, one may interpret the involute as the locus traced by the end of a straight rod that rolls without slipping around the given curve.

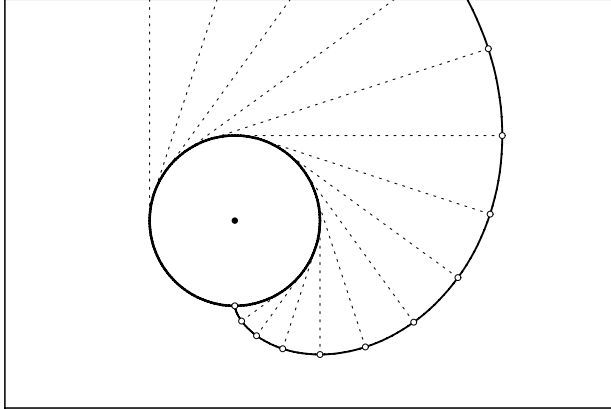


Fig. 8.10. Construction of an involute to a circle by the unwrapping of a taut string.

of the curve segment between parameter values τ and ξ . Since the string is kept taut, the sense of motion of its free end is orthogonal to its free length: we may consider the free end to be *instantaneously rotating*¹⁴ about the point $\mathbf{r}(\xi)$ in an arc of radius $s_\tau(\xi)$. In other words, the curve points $\mathbf{r}(\xi)$ are centers of curvature, and the arc lengths $s_\tau(\xi)$ are radii of curvature, for the trajectory of the free end of the string as we continuously unwrap it from the curve.

Hence $\mathbf{r}(\xi)$ is the evolute for the trajectory of the free end of the string — i.e., that trajectory is an *involute* of the curve $\mathbf{r}(\xi)$. We say here “an” involute, rather than “the” involute, because choosing different parameter values τ at which the unwrapping of the string begins will, in general, produce different trajectories for its free end. A parameterization for the involute $\mathbf{i}_\tau(\xi)$ can be formulated in terms of the integral (8.31) as

$$\mathbf{i}_\tau(\xi) = \mathbf{r}(\xi) - s_\tau(\xi) \mathbf{t}(\xi), \quad (8.32)$$

where $\mathbf{t}(\xi)$ is the unit tangent to $\mathbf{r}(\xi)$. This equation simply expresses the fact that the free end of the string is distance $s_\tau(\xi)$ from the curve point $\mathbf{r}(\xi)$ up to which it has been unwound, measured in a direction *opposite* to the curve tangent $\mathbf{t}(\xi)$ at that point.¹⁵ Each value τ yields, in general, a distinct curve: there is an *infinite family* of involutes to any specified curve $\mathbf{r}(\xi)$. As we shall see in §8.3.4, these involutes are nevertheless intimately related to each other. Note also that, even if $\mathbf{r}(\xi)$ is a “simple” (polynomial or rational) curve, the arc length (8.31) cannot in general be resolved into a polynomial or rational function of ξ . Hence, the involutes to polynomial or rational curves are not ordinarily themselves polynomial or rational curves.

¹⁴ This interpretation, in terms of instantaneous centers of rotation, is the basis of the first investigation of evolutes and their first practical use — see §8.3.3.

¹⁵ The minus sign in (8.32) arises since we measure “backward” along the string — opposite to the direction of the curve tangent $\mathbf{t}(\xi)$ in which $s_\tau(\xi)$ is increasing.

It can be verified that the dual form for the involute (8.32) to the curve $\mathbf{r}(\xi) = (x(\xi), y(\xi))$ is defined by the homogeneous line coordinates

$$\begin{aligned} K_{i,\tau}(\xi) &= \sigma(\xi)s_\tau(\xi) - x(\xi)x'(\xi) - y(\xi)y'(\xi), \\ L_{i,\tau}(\xi) &= x'(\xi), \quad M_{i,\tau}(\xi) = y'(\xi), \end{aligned} \quad (8.33)$$

where

$$\sigma(\xi) = s'_\tau(\xi) = \sqrt{x'^2(\xi) + y'^2(\xi)}$$

is the parametric speed of $\mathbf{r}(\xi)$. Note the similarity of (8.33) to the dual form (8.30) of the evolute — in fact, the evolute and all the involutes to $\mathbf{r}(\xi)$ have *parallel tangents* at corresponding points. Unlike the evolute, however, the line representation (8.33) of the involutes is not rational, because of the presence of the radical $\sigma(\xi)$ and the irreducible integral $s_\tau(\xi)$.

Thus far, the “string model” for involutes has assumed that the curve $\mathbf{r}(\xi)$ has curvature of constant sign, and the string is wrapped around its *convex* side — otherwise, we could not maintain the string taut: it would “fall off” the curve as we begin to unwrap! Nevertheless, equation (8.32) may be regarded as formally defining involutes to arbitrary smooth curves $\mathbf{r}(\xi)$, including those with *inflections*, i.e., points where the curvature changes sign. For inflectional curves, the string model can be salvaged — in our imagination, at least — as follows. At each inflection point, we imagine that the string “passes through” the curve, so as to always lie on the locally convex side. This ensures that the string will remain taut at all times (it is understood here that portions of the curve from which the string has already been unwrapped do not obstruct its subsequent motion). As we shall see below, this incurs a peculiar behavior of the involute at points corresponding to the inflections of $\mathbf{r}(\xi)$.

Reciprocal Nature of Evolutes and Involutes

We have presented an intuitive model, culminating in equation (8.32), for the involute $\mathbf{i}_\tau(\xi)$ corresponding to the point $\xi = \tau$ of the curve $\mathbf{r}(\xi)$. It is not difficult to verify formally that, for each τ , the curves specified by equation (8.32) are indeed involutes of the given curve $\mathbf{r}(\xi)$ — i.e., they all have $\mathbf{r}(\xi)$ as their evolute (or locus of centers of curvature). Hence, on taking the evolute of any of the involutes of a given curve $\mathbf{r}(\xi)$, we *uniquely* recover the original curve $\mathbf{r}(\xi)$. Reversing the order of these operations, however, does not yield a unique result — by taking an involute of the evolute of a given curve $\mathbf{r}(\xi)$, we obtain either the original curve or an *offset* to it. We elaborate on these relationships in §8.3.4 below — for now we focus on verifying that the involutes (8.32) have the curve $\mathbf{r}(\xi)$ as their locus of centers of curvature.

Now the derivatives of the tangent $\mathbf{t}(\xi)$ and normal $\mathbf{n}(\xi)$ to the curve $\mathbf{r}(\xi)$ satisfy the Frenet equations

$$\mathbf{t}'(\xi) = -\sigma(\xi)\kappa(\xi)\mathbf{n}(\xi) \quad \text{and} \quad \mathbf{n}'(\xi) = \sigma(\xi)\kappa(\xi)\mathbf{t}(\xi), \quad (8.34)$$

$\sigma(\xi)$ and $\kappa(\xi)$ being its parametric speed and curvature. Using the above, and the fact that $\mathbf{r}'(\xi) = \sigma(\xi) \mathbf{t}(\xi)$, the first and second derivatives of the involute (8.32) can be expressed in terms of properties of the curve $\mathbf{r}(\xi)$ as

$$\mathbf{i}'_\tau = s_\tau \sigma \kappa \mathbf{n}, \quad \mathbf{i}''_\tau = [s_\tau(\sigma' \kappa + \sigma \kappa') + \sigma^2 \kappa] \mathbf{n} + s_\tau \sigma^2 \kappa^2 \mathbf{t}. \quad (8.35)$$

We can then determine the normal and curvature of the involute $\mathbf{i}_\tau(\xi)$ from $\mathbf{n}_{i,\tau} = \mathbf{i}'_\tau \times \mathbf{z} / |\mathbf{i}'_\tau|$ and $\kappa_{i,\tau} = (\mathbf{i}'_\tau \times \mathbf{i}''_\tau) \cdot \mathbf{z} / |\mathbf{i}'_\tau|^3$ as

$$\mathbf{n}_{i,\tau}(\xi) = -\operatorname{sign}(\kappa(\xi)s_\tau(\xi)) \mathbf{t}(\xi) \quad \text{and} \quad \kappa_{i,\tau}(\xi) = \frac{\operatorname{sign}(\kappa(\xi))}{|s_\tau(\xi)|}. \quad (8.36)$$

These equations express formally what was stated intuitively above, namely: (i) the radius of curvature of the involute is equal in magnitude to the length of unwound string; and (ii) the *normal* line to the involute is *tangent* to the given curve at the point where the string separates from the curve — this tangent defines the orientation of the unwound length of string, and the instantaneous motion of the free end is perpendicular to this length.

The evolute of the locus (8.32) is the curve $\mathbf{i}_\tau(\xi) - \rho_{i,\tau}(\xi) \mathbf{n}_{i,\tau}(\xi)$, where $\rho_{i,\tau}(\xi) = 1/\kappa_{i,\tau}(\xi)$ is its radius of curvature, and on substituting from (8.32) and (8.36) one finds that this expression reduces to just $\mathbf{r}(\xi)$. Thus, for each τ , the loci defined by (8.32) are indeed involutes of $\mathbf{r}(\xi)$.

Equation (8.32) may be taken to define the involute of $\mathbf{r}(\xi)$ corresponding to the curve point τ for *all* values of the parameter ξ , greater than and less than τ . For $\xi < \tau$, the arc length (8.31) is negative, and the interpretation of the physical model is that the string is attached to the curve at a large *negative* value of ξ and unwound from it in the sense of decreasing ξ . Figure 8.11 shows a sampling of the infinite family of involutes to an ellipse and an inflectional cubic, as defined by expression (8.32) for $-\infty < \xi < +\infty$.

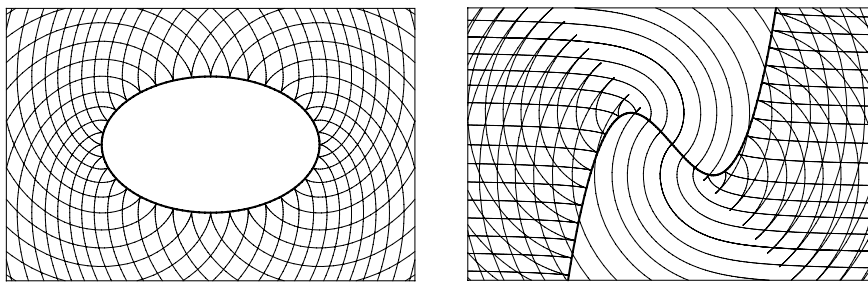


Fig. 8.11. Left: sampling of the family of involutes to an ellipse — note the cusps at the “points of attachment” to the curve. Right: involutes to an inflectional curve also exhibit (ramphoid) cusps where they meet the tangent line at the inflection.

Singularities of Evolutes and Involutes

As is evident from Figs. 8.9 and 8.11, the evolutes and involutes of a smooth plane curve are not, in general, themselves smooth curves. We shall examine here the nature of the geometric conditions under which singular points arise on the evolute and involutes of a given plane curve $\mathbf{r}(\xi)$.

We have noted that the evolute has a *point at infinity* when the curvature κ vanishes (or the radius of curvature ρ becomes infinite), i.e., when $\mathbf{r}(\xi)$ has an inflection. When $\kappa \neq 0$, differentiating the parametric form (8.27) gives

$$\mathbf{e}'(\xi) = \mathbf{r}'(\xi) - \rho'(\xi) \mathbf{n}(\xi) - \rho(\xi) \mathbf{n}'(\xi).$$

Now $\mathbf{r}' = \sigma \mathbf{t}$, and by the Frenet equations (8.34) we have $\rho \mathbf{n}' = \rho \sigma \kappa \mathbf{t} = \sigma \mathbf{t}$, so the first and third terms above cancel and we deduce that

$$\mathbf{e}'(\xi) = -\rho'(\xi) \mathbf{n}(\xi). \quad (8.37)$$

Hence the unit tangent to the evolute is given by

$$\mathbf{t}_e(\xi) = \frac{\mathbf{e}'(\xi)}{|\mathbf{e}'(\xi)|} = -\text{sign}(\rho'(\xi)) \mathbf{n}(\xi). \quad (8.38)$$

If $\rho'(\xi)$ changes sign at the point $\xi = t$, so that

$$\rho'(t) = 0 \neq \rho''(t), \quad (8.39)$$

then the evolute exhibits a *cusp*, or sudden tangent reversal, at that point:

$$\lim_{\Delta\xi \rightarrow 0} \mathbf{t}_e(t - \Delta\xi) = -\lim_{\Delta\xi \rightarrow 0} \mathbf{t}_e(t + \Delta\xi).$$

Condition (8.39) identifies points of *extremum* — minimum or maximum — *curvature* on the curve $\mathbf{r}(\xi)$, and such points are known as its *vertices*. Thus, a vertex (of non-zero curvature) on $\mathbf{r}(\xi)$ induces a cusp at the corresponding point of the evolute $\mathbf{e}(\xi)$, as seen in the examples of Fig. 8.9.

Consider now the involute $\mathbf{i}_\tau(\xi)$ corresponding to a parameter value τ on $\mathbf{r}(\xi)$. Assuming that $\mathbf{r}(\xi)$ is a regular curve — i.e., $\sigma(\xi) \neq 0$ for all ξ — we find from (8.35) that the tangent to the involute is given by

$$\mathbf{t}_{i,\tau}(\xi) = \frac{\mathbf{i}'_\tau(\xi)}{|\mathbf{i}'_\tau(\xi)|} = \text{sign}(s_\tau(\xi)\kappa(\xi)) \mathbf{n}(\xi).$$

We see that $\mathbf{t}_{i,\tau}(\xi)$ suddenly reverses, and the involute exhibits a cusp, when either $s_\tau(\xi)$ or $\kappa(\xi)$ changes sign. From (8.31) we note that the former occurs only once, namely, at the point $\xi = \tau$ where we begin¹⁶ “unwrapping” $\mathbf{i}_\tau(\xi)$ from $\mathbf{r}(\xi)$. Thus, the involute $\mathbf{i}_\tau(\xi)$ meets the curve $\mathbf{r}(\xi)$ in a cusp at the point $\xi = \tau$. Points where $\kappa(\xi)$ changes sign correspond to *inflections* of the curve $\mathbf{r}(\xi)$ — each of these also induces a cusp on the involute (see Fig. 8.11).

¹⁶ As noted above, we imagine the involute to be unwrapped from $\mathbf{r}(\xi)$ in opposite senses according to whether $\xi > \tau$ or $\xi < \tau$.

The Arc Length of an Evolute

By regarding any curve as an involute of its evolute, we can deduce a simple relation between the curvature of the given curve $\mathbf{r}(\xi)$ and the arc length of its evolute $\mathbf{e}(\xi)$. As noted previously, if we imagine $\mathbf{r}(\xi)$ to be traced by the free end of a piece of string that we unwrap from $\mathbf{e}(\xi)$, the radius of curvature of $\mathbf{r}(\xi)$ at each instant is equal to the total length of unwound string.

Consider two corresponding segments $\xi \in [a, b]$ on $\mathbf{r}(\xi)$ and $\mathbf{e}(\xi)$, such that the radius of curvature $\rho(\xi)$ of $\mathbf{r}(\xi)$ is finite, positive, and monotone-increasing between $\xi = a$ and $\xi = b$. If the string has free length ℓ_a when unwrapped up to the point $\xi = a$ of the evolute $\mathbf{e}(\xi)$, and upon further unwrapping it up to $\xi = b$ the free length becomes ℓ_b , we must have $\rho(a) = \ell_a$ and $\rho(b) = \ell_b$. Furthermore, the change $L = \ell_b - \ell_a = \rho(b) - \rho(a)$ in the unwrapped length corresponds to the arc length of the segment $\xi \in [a, b]$ on $\mathbf{e}(\xi)$.

Hence, *the arc length between two points of the evolute $\mathbf{e}(\xi)$ is the difference in radius of curvature between the corresponding points of the given curve $\mathbf{r}(\xi)$* . We may verify this conclusion analytically — and also remove the restrictions on the variation of $\rho(\xi)$ — as follows. Using expression (8.37), we write

$$L = \int_a^b |\mathbf{e}'(\xi)| d\xi = \int_a^b |\rho'(\xi)| d\xi,$$

and if $\rho'(\xi)$ is of constant sign for $\xi \in [a, b]$ this reduces to $L = |\rho(b) - \rho(a)|$. On the other hand, if there are values $\xi_1, \dots, \xi_N \in [a, b]$ where $\rho'(\xi)$ vanishes, the domain of integration must be broken up at these points, and on setting $\xi_0 = a$ and $\xi_{N+1} = b$ we obtain

$$L = \sum_{k=1}^{N+1} |\rho(\xi_k) - \rho(\xi_{k-1})|.$$

The significance of the values ξ_1, \dots, ξ_N is that they identify the vertices of the curve $\mathbf{r}(\xi)$, which incur cusps on its evolute (as noted above). As we unwrap the string from $\mathbf{e}(\xi)$, we can imagine it being “temporarily attached” to each cusp — once the point of separation of the string from $\mathbf{e}(\xi)$ reaches a cusp, we “detach” it at that point and proceed to unwrap up to the next cusp. The above expression for L then gives the total arc length of the evolute as the sum of arc lengths of its smooth segments between cusps.

8.3.3 The *Horologium Oscillatorium*

The earliest systematic investigation of evolutes and involutes was motivated by the invention of an “isochronous” pendulum clock by the Dutch physicist and mathematician Christiaan Huygens (1629–1695), described in his treatise *Horologium Oscillatorium* of 1673 (see Fig. 8.12). This treatise exemplifies a “golden era” of scientific research, in which new developments could — and, in fact, were even *expected* — to simultaneously elucidate novel mathematical or physical principles *and* serve practical applications.

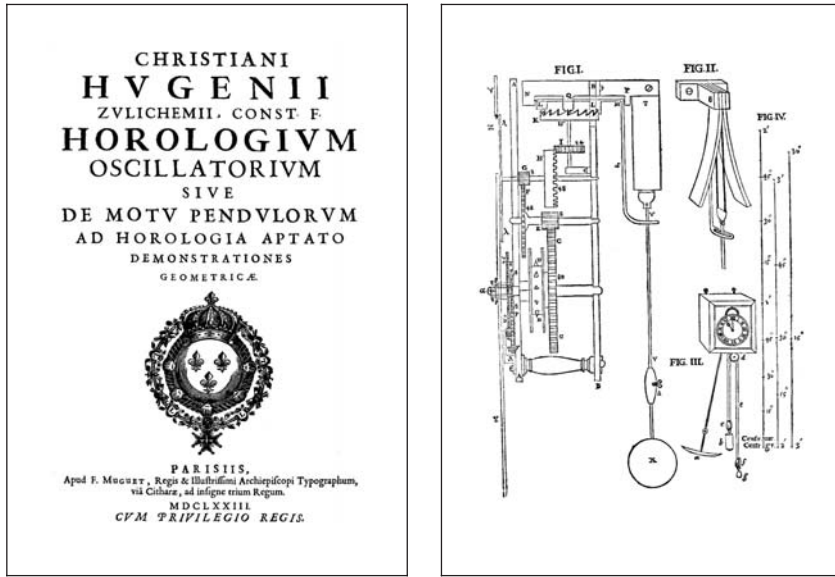


Fig. 8.12. Left: title page of Huygens' *Horologium Oscillatorium* of 1673. Right: sketch of Huygens' isochronous pendulum clock — the cycloidal “jaws” that serve to constrain the motion of the bob to a cycloidal trajectory may be seen in FIG. II.

The Problem of Isochronous Oscillation

An *isochronous pendulum* has an oscillation period that is *exactly* independent of the amplitude of its swing — not just in the limit of small oscillations. Recall that elementary dynamics yields the equation of motion

$$\frac{d^2\theta}{dt^2} + \frac{g}{\ell} \sin \theta = 0 \quad (8.40)$$

for the angular displacement θ of a simple pendulum, comprising a “bob” of mass m suspended from a string of length ℓ , where g is the acceleration due to gravity (see Fig. 8.13). Although equation (8.40) ignores the mass of the string, and the effects of air resistance and friction at the pivot, it nevertheless cannot be solved *exactly* in terms of “elementary” functions.¹⁷

Consequently, one typically resorts to the *small-amplitude approximation* — if $\theta \ll 1$, substituting $\sin \theta \approx \theta$ into (8.40) yields the solution

$$\theta(t) \approx \alpha \cos \omega t, \quad (8.41)$$

where α is the amplitude, $\omega = \sqrt{g/\ell}$, and the time t is measured from the instant of maximum excursion. The corresponding oscillation period

$$T_0 = 2\pi/\omega = 2\pi \sqrt{\ell/g} \quad (8.42)$$

¹⁷ The exact solution involves the *Jacobian elliptic functions* — see [299].

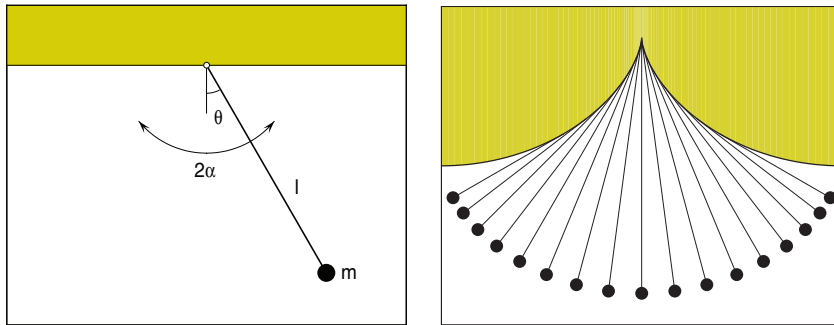


Fig. 8.13. Left: the “simple” pendulum, whose bob follows a circular path — the period depends on the amplitude. Right: Huygens’ isochronous involute pendulum, whose bob follows a cycloidal path with a period precisely independent of amplitude.

is *independent of the oscillation amplitude α* (and the mass m of the bob) if α is sufficiently small. This is a very desirable feature: to calibrate the pendulum clock, we need only know the length ℓ to high accuracy: the mass of the bob, and the magnitude of the “kick” that sets it in motion, are immaterial.

The departure of a simple pendulum from isochronous oscillation at finite amplitude α can be precisely quantified in terms of *elliptic integrals*. Energy conservation gives the angular velocity at position θ as

$$\frac{d\theta}{dt} = \pm \omega \sqrt{2(\cos \theta - \cos \alpha)},$$

and the exact period $T(\alpha)$ for an arbitrary amplitude of oscillation α may be obtained by integrating the above. Considering just the first quadrant of the oscillation, with θ increasing from 0 to α as t increases from 0 to $\frac{1}{4}T$, we may take the positive sign above to obtain

$$\frac{1}{4} T(\alpha) = \frac{1}{\omega} \int_0^\alpha \frac{d\theta}{\sqrt{2(\cos \theta - \cos \alpha)}}.$$

Introducing the change of variables defined by

$$\sin \frac{1}{2}\theta = \sin \frac{1}{2}\alpha \sin \phi,$$

so that ϕ increases from 0 to $\pi/2$ as θ increases from 0 to α , allows the above integral expression for $T(\alpha)$ to be reduced to a standard form:

$$T(\alpha) = \frac{4K(\alpha)}{\omega}, \quad \text{where } K(\alpha) = \int_0^{\pi/2} \frac{d\phi}{\sqrt{1 - \sin^2 \frac{1}{2}\alpha \sin^2 \phi}}. \quad (8.43)$$

$K(\alpha)$ is a *complete elliptic integral of the first kind*. Its value as a function of α may be found in standard mathematical tables, or it may be computed to any desired accuracy from the power series

$$K = \frac{\pi}{2} \left[1 + \left(\frac{1}{2} \right)^2 k^2 + \left(\frac{1 \cdot 3}{2 \cdot 4} \right)^2 k^4 + \left(\frac{1 \cdot 3 \cdot 5}{2 \cdot 4 \cdot 6} \right)^2 k^6 + \dots \right],$$

where we set $k = \sin \frac{1}{2}\alpha$. The ratio of the true (finite-amplitude) period to the nominal value defined by (8.42) is thus

$$\frac{T(\alpha)}{T_0} = \frac{2}{\pi} K(\alpha) = 1 + \left(\frac{1}{2} \right)^2 \sin^2 \frac{1}{2}\alpha + \left(\frac{1 \cdot 3}{2 \cdot 4} \right)^2 \sin^4 \frac{1}{2}\alpha + \dots,$$

and representative values for this ratio are enumerated in Table 8.1.

Table 8.1. Deviation of a simple pendulum from isochronicity at amplitude α .

α	2°	5°	10°	20°	30°	45°	60°	90°
$k = \sin \frac{1}{2}\alpha$	0.0175	0.0436	0.0872	0.1736	0.2588	0.3827	0.5000	0.7071
$T(\alpha)/T_0$	1.0001	1.0005	1.0019	1.0077	1.0174	1.0400	1.0732	1.1803

The formula (8.42) is clearly unsatisfactory for accurate time-keeping — if $\alpha = 10^\circ$, for example, the calibration error of $\sim 0.2\%$ amounts to a discrepancy of about 3 minutes per day, and this increases to nearly 30 minutes per day for $\alpha = 30^\circ$. Even if expression (8.43) rather than (8.42) is used for calibration, dissipative effects can be expected to induce a systematic decay of α , and a corresponding error in the cumulative indicated time.

Properties of the Cycloid Curve

In designing an isochronous clock, Huygens was aware that the oscillation of a pendulum of length ℓ is equivalent to the motion of a small particle that rolls on the inside of a spherical bowl of radius ℓ — both motions are determined simply by the exchange between potential and kinetic energy along a *circular* path. Recognizing that this principle will generalize to other paths, Huygens sought shapes of bowls that would cause a particle to exhibit an isochronous rolling motion — i.e., the time taken to reach the bottom of the bowl would be *independent* of the point from which the particle is first released.

At that time, the *cycloid* was a curve that enjoyed great interest — due, in part, to a competition to demonstrate certain of its properties sponsored by Blaise Pascal¹⁸ (1623–1662). The cycloid is the locus traced by a point on the circumference of a circle that rolls without slipping along a straight line (see Fig. 8.14). For a circle of radius ℓ , the cycloid has the parameterization

¹⁸ Pascal abandoned science in favor of theology in 1654. His interest was revived in 1658 when, on a sleepless night brought on by toothache, he occupied himself with investigations of the cycloid. Besides proving several new properties, this seems [56] to have cured his ailment (the dental profession, however, has subsequently been loath to prescribe mathematical exertions in lieu of fillings and extractions).

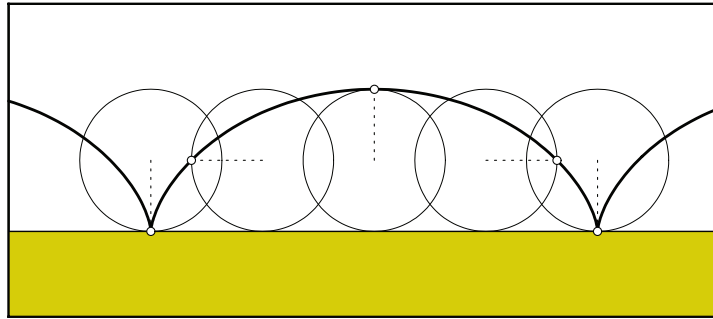


Fig. 8.14. Generation of the cycloid curve by a fixed point on a rolling circle.

$$x(\phi) = \ell(\phi - \sin \phi), \quad y(\phi) = \ell(1 - \cos \phi) \quad (8.44)$$

where ϕ is the angle of revolution of the circle about its center — the motion amounts to superposing a translation $\ell\phi$ in the x -direction and a rotation ϕ about the center. The cycloid was actually known long before Pascal: perhaps the earliest study was by Nicholas of Cusa (1401–1464). Note that, because ϕ appears both as the argument of trigonometric functions and on its own, the cycloid is a *transcendental* (i.e., non-algebraic) curve.

Huygens made the felicitous discovery that a particle rolling on the inside of an “inverted” cycloid — obtained by reversing the sign of $y(\phi)$ above — will exhibit the desired isochronous behavior. The question was thus: how can one construct a “variable-length” pendulum, whose bob executes a cycloidal trajectory? Huygens conjured up a remarkable answer — namely, use another cycloid¹⁹ to continuously adjust the length of the pendulum!

Consider the two cycloids $\mathbf{r}_1(\phi)$ and $\mathbf{r}_2(\phi)$ defined for $0 \leq \phi \leq 2\pi$ by

$$\begin{aligned} x_1(\phi) &= \ell(\phi - \sin \phi), & y_1(\phi) &= \ell(\cos \phi - 1), \\ x_2(\phi) &= \ell(\phi + \sin \phi), & y_2(\phi) &= \ell(1 - \cos \phi). \end{aligned} \quad (8.45)$$

Actually, these two loci are just appropriately-positioned segments of a *unique* (infinitely extended) cycloid. Figure 8.15 illustrates their generation by circles C_1 and C_2 of radius ℓ rolling from left to right in contact with and below the lines $y = 0$ and $y = 2\ell$. The initial common point $(x, y) = (0, 0)$ of the circles, considered as a fixed point of each, traces out the cycloids $\mathbf{r}_1(\phi)$ and $\mathbf{r}_2(\phi)$.

Huygens found that the cycloids (8.45) satisfy an involute-evolute relation: for each ϕ , the point $\mathbf{r}_2(\phi)$ is the *center of curvature* for the corresponding point on $\mathbf{r}_1(\phi)$. Conversely, the point $\mathbf{r}_1(\phi)$ may be regarded as the *end of a taut string “unwrapped” from the curve $\mathbf{r}_2(\phi)$* up to the corresponding point.

¹⁹ This solution to the problem is also discussed in Book I of Newton’s *Principia*.

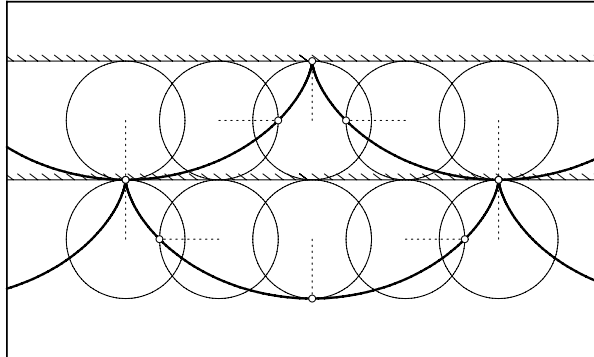


Fig. 8.15. Generation of cycloids $\mathbf{r}_1(\phi)$ and $\mathbf{r}_2(\phi)$ with an involute–evolute relation.

The Horologium Oscillatorium

Huygens' idea, then, was to employ the profile $\mathbf{r}_2(\phi)$ as a “cycloidal jaw” with the pendulum suspended from its cusp at $\phi = \pi$. As the pendulum oscillates, the string alternately wraps and unwraps about the left and right sides of this jaw (see Fig. 8.13) and the trajectory of the bob is the involute of the jaw profile, i.e., the cycloid $\mathbf{r}_1(\phi)$. By the isochronicity of cycloidal motion, this ensures an oscillation period that is *precisely* independent of the amplitude.

Considering the cycloidal trajectory $\mathbf{r}_1(\phi)$ as the envelope of its circles of curvature, one may interpret the bob motion as a succession of instantaneous circular motions, whose radii and centers are determined by the point along $\mathbf{r}_2(\phi)$ to which the string has unwrapped. Figure 8.12 is convincing evidence that Huygens was as concerned with the practical details of a viable clock as with the theory of evolutes and involutes. However, the tools and materials at his disposal could not match the precision of his mathematical arguments, and the “cycloidal clocks” he constructed were of scarcely better accuracy than simple pendulum clocks confined to small-amplitude oscillations.

The Problem of the Brachistochrone

The cycloid had further fascinating properties waiting to be discovered by 17th century mathematicians. In 1696, Johann Bernoulli sponsored an international competition involving a problem whose solution requires what we now call the *calculus of variations*, i.e., methods for finding a function $y(x)$ on $x \in [x_0, x_1]$ that minimizes an integral typically of the form

$$I = \int_{x_0}^{x_1} F(x, y, y') \, dx,$$

where $y' = dy/dx$ and F is a (differentiable) function of x , y , and y' . It can be shown [45] that the desired function $y(x)$ satisfies the *Euler–Lagrange equation*

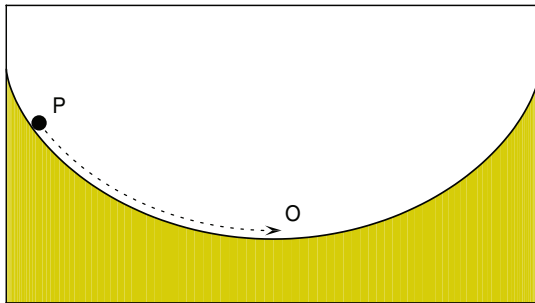


Fig. 8.16. The brachistochrone problem: a particle rolls from P to O .

$$\frac{\partial F}{\partial y} - \frac{d}{dx} \frac{\partial F}{\partial y'} = 0, \quad (8.46)$$

which is generally a second-order (non-linear) ordinary differential equation for $y(x)$, subject to the boundary conditions $y(x_0) = y_0$ and $y(x_1) = y_1$.

Bernoulli's problem was again concerned with a small particle rolling inside a smooth bowl, as follows: the particle is released from a point P at height h relative to, but not directly above, the lowest point O of the bowl (Fig. 8.16). The problem is to find the cross-sectional shape of the bowl that minimizes the time taken for the particle to roll from point P to point O . The desired curve was designated the *brachistochrone* — from the Greek for “least time.” Bernoulli and Leibniz both managed to deduce that the brachistochrone is, in fact, an inverted cycloid! The period of a particle that executes a cycloidal trajectory²⁰ is thus not only independent of amplitude — it is also the *least possible time* among all smooth trajectories between the points P and O .

At this point, Bernoulli and Leibniz saw a golden opportunity to confound Sir Isaac Newton — with whom a feud had developed over precedence in the invention of the calculus. So the challenge was sent to Newton, then Master of the Royal Mint in London. Although he had largely abandoned scientific matters, Newton nevertheless felt compelled to defend his honor — by staying up all night upon returning from his official duties, he succeeded in finding the correct solution. Bernoulli and Leibniz were no doubt chastened on promptly receiving an elegant anonymous solution in English! Bernoulli is reported [473] to have said *ex ungue Leonem*, “from the claw (one recognizes) the Lion.”

Interestingly, Bernoulli approached the brachistochrone problem through an ingenious physical analogy, rather than a “frontal assault” by the methods of variational calculus. Noting that the speed v of the particle at a point (x, y) depends only on the potential energy released in reaching it — i.e., on the local y coordinate but *not* on the actual shape of its path up to that point —

²⁰ The cycloid was first studied in detail by Galileo, but in his celebrated *Dialogue* [207] championing the heliocentric solar system theory, he mistakenly identifies the *circle* as the trajectory that yields isochronous oscillations of minimum period.

he recognized [366] that light propagation in a stratified medium, such as the atmosphere, is governed by a similar principle.

By reasoning that the variation of the speed of a light ray with the density (actually, the refractive index) of the medium causes it to follow a curved path, Bernoulli was able to derive and solve the differential equation defining the shape of the brachistochrone. He published his result in the *Acta Eruditorum* of May 1697, with the title “*Curvatura radii in diaphanis non uniformibus . . .*” (The curvature of a ray in a non-uniform medium . . .), saying:

... We have a just admiration for Huygens, because he was the first to discover that a heavy point on an ordinary cycloid falls in the same time, whatever the position from which the motion begins. But the reader will be greatly amazed, when I say that exactly this cycloid, or *tautochrone* of Huygens, is our required *brachistochrone* . . . I have discovered a wondrous agreement between the curved path of a light ray in a continuously varying medium and our *brachistochrone*.

The same issue of *Acta Eruditorum* contains Jakob Bernoulli’s contribution “*Solutio problematum fraternorum . . .*” (Solution of my brother’s problem) and the correct solutions by Leibniz, Newton, and Tschirnhaus — as well as an erroneous attempt by de l’Hôpital.

8.3.4 Families of Parallel (Offset) Curves

For a smooth curve $\mathbf{r}(\xi)$ with unit normal $\mathbf{n}(\xi)$, the offset at (signed) distance d is the locus defined by

$$\mathbf{r}_d(\xi) = \mathbf{r}(\xi) + d \mathbf{n}(\xi). \quad (8.47)$$

The offset is not in general a polynomial or rational curve — even if $\mathbf{r}(\xi)$ is — since unitization of $\mathbf{n}(\xi)$ incurs the square root of a polynomial. For a given sign of the offset distance d , the expression (8.47) defines a *one-sided* offset. The offset to a curve $\mathbf{r}(\xi) = (X(\xi), Y(\xi))$ can also be defined as the *envelope* (see §8.2) of the one-parameter family of circles

$$f_d(x, y, \lambda) = [x - X(\lambda)]^2 + [y - Y(\lambda)]^2 - d^2 = 0,$$

of fixed (positive) radius d centered on each point of $\mathbf{r}(\xi)$ — this specifies the *two-sided* offset, corresponding to replacement of d by $\pm d$ in (8.47). Using the methods of §8.2, one can verify that the two-sided offset is always an algebraic curve (of higher degree) when $\mathbf{r}(\xi)$ is a polynomial or rational curve.

The offsets to a given curve $\mathbf{r}(\xi)$ are also known [386] as its *parallel* curves: we can interpret $\mathbf{r}_d(\xi)$ as the locus of a point that (locally) maintains a fixed distance d from the given curve $\mathbf{r}(\xi)$, or alternatively as a curve whose tangents are parallel to those of $\mathbf{r}(\xi)$ at corresponding points (on common normal lines). Christiaan Huygens (1629–1695) used parallel curves in his wave theory for light propagation in a uniform medium, described in his *Traité de la Lumière*

(written before 1678, but published later in 1690). Given an “initial” wavefront $W(t)$ at time t , the wavefront $W(t + \Delta t)$ at time Δt later was described as the envelope of a family of spherical “wavelets” of radius $c\Delta t$ (c being the speed of light) centered on $W(t)$ — i.e., it is the parallel curve at distance $d = c\Delta t$. Huygens explained the known laws of reflection and refraction of light rays (the normals to the wavefronts) by this model, although the wavelets define a two-sided offset, predicting that light would travel in both the “forward” and “backward” directions, contrary to physical experience.

Offset curves are of great practical importance in contemporary computer aided design and manufacturing applications. If $\mathbf{r}(\xi)$ specifies a desired curve to be machined by the cylindrical cutter of a milling machine, the cutter must follow a center-line trajectory specified by the offset curve $\mathbf{r}_d(\xi)$, where d is the cutter radius. Similarly, one may imagine $\mathbf{r}(\xi)$ to be a desired profile subject to geometrical uncertainties due to manufacturing errors. If each point of $\mathbf{r}(\xi)$ is known only to some *tolerance* or dimensional accuracy d , the actual profile lies in the region delineated by the two-sided offset $\mathbf{r}(\xi) \pm d\mathbf{n}(\xi)$, which we regard as a “tolerance zone” of half-width d . Overlap of tolerance zones signals possible interference problems with manufactured components that are to be assembled together. In such applications, it is often necessary to generalize the definition (8.47) to piecewise-smooth curves, with tangent discontinuities at the junctures of their smooth segments. This can be accomplished by inserting a circular arc into the offset for each tangent discontinuity: the angular extent of such arcs is defined by the two normal orientations at these points.

Figure 8.17 illustrates this for a piecewise-linear/circular curve (these are the *only* curves that exhibit closure under offset operations). The form (8.47) — augmented by circular arcs at tangent discontinuities if necessary — defines the *untrimmed* offset $\mathbf{r}_d(\xi)$ at distance d from the curve $\mathbf{r}(\xi)$. Corresponding

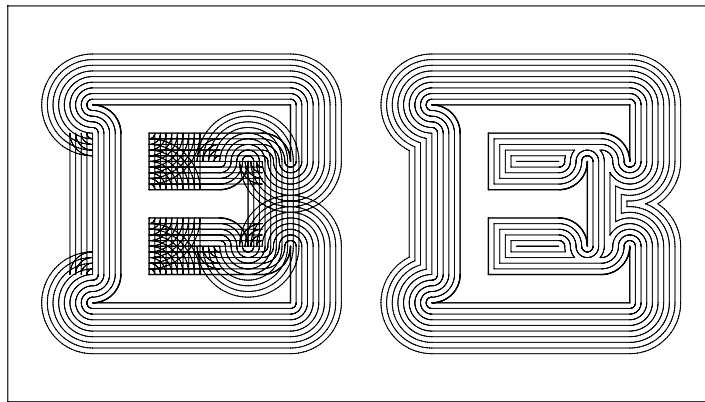


Fig. 8.17. Left: the one-sided (untrimmed) offsets at successive distances d from a piecewise-linear/circular curve with tangent discontinuities. Right: the trimmed offsets are obtained from the untrimmed offsets using an *offset trimming procedure*.

points $\mathbf{r}(\xi_*)$ and $\mathbf{r}_d(\xi_*)$ of the curve and its untrimmed offset clearly satisfy $|\mathbf{r}_d(\xi_*) - \mathbf{r}(\xi_*)| = |d|$, but this does not guarantee that a chosen point $\mathbf{r}_d(\xi_*)$ of the untrimmed offset is (at least) distance $|d|$ from *every* point of $\mathbf{r}(\xi)$. The locus satisfying the latter property is called the *trimmed* offset at distance d , since it obtained by deleting certain segments of the untrimmed offset, namely, those that come “too close” to $\mathbf{r}(\xi)$. Figure 8.17 illustrates the outcome of the *trimming procedure*, whereby the trimmed offsets are identified as subsets of the untrimmed offsets (this will be described quantitatively below).

Singular Points on Offset Curves

The untrimmed offset (8.47) is *not*, in general, a smooth curve — even if the given curve $\mathbf{r}(\xi)$ is smooth. The derivatives of (8.47) may be written as

$$\mathbf{r}'_d(\xi) = [1 + \kappa(\xi) d] \mathbf{r}'(\xi), \quad \mathbf{r}''_d(\xi) = [1 + \kappa(\xi) d] \mathbf{r}''(\xi) + \kappa'(\xi) d \mathbf{r}'(\xi)$$

where $\kappa = |\mathbf{r}'|^{-3} (\mathbf{r}' \times \mathbf{r}'') \cdot \mathbf{z}$ is the curvature of $\mathbf{r}(\xi)$. Substituting into the expressions $\mathbf{t}_d = \mathbf{r}'_d / |\mathbf{r}'_d|$ and $\kappa_d = |\mathbf{r}'_d|^{-3} (\mathbf{r}'_d \times \mathbf{r}''_d) \cdot \mathbf{z}$ for the tangent and curvature of the untrimmed offset, these quantities may be expressed as

$$\mathbf{t}_d(\xi) = \frac{1 + \kappa(\xi) d}{|1 + \kappa(\xi) d|} \mathbf{t}(\xi) \quad \text{and} \quad \kappa_d(\xi) = \frac{\kappa(\xi)}{|1 + \kappa(\xi) d|} \quad (8.48)$$

in terms of the tangent and curvature, \mathbf{t} and κ , of the given curve $\mathbf{r}(\xi)$ and the offset distance d . Thus, the tangent and/or curvature of the untrimmed offset evidently exhibits a singular behavior at those parameter values ξ where the curvature $\kappa(\xi)$ attains the “critical” value $-1/d$.

If $\kappa(\xi_*) = -1/d$ and $\kappa'(\xi_*) \neq 0$ — i.e., the curvature attains the critical value at $\xi = \xi_*$ without being an extremum there — the factor multiplying \mathbf{t} in equation (8.48) is a “step function” that changes abruptly from -1 to $+1$, or vice-versa, at that point. This incurs a sudden reversal of the tangent \mathbf{t}_d , corresponding to a *cusp* on the untrimmed offset. On the other hand, when $\kappa(\xi_*) = -1/d$ and $\kappa'(\xi_*) = 0 \neq \kappa''(\xi_*)$ — i.e., on attaining the critical value the curvature *is* an extremum — the factor that multiplies \mathbf{t} in (8.48) does not change sign on traversing $\xi = \xi_*$, but $|\kappa_d(\xi)| \rightarrow \infty$ as $\xi \rightarrow \xi_*$. This defines a *tangent-continuous point of infinite curvature* on the untrimmed offset.

Example 8.3 For the parabola $\mathbf{r}(\xi) = (\xi, \xi^2)$ the curvature

$$\kappa(\xi) = 2(4\xi^2 + 1)^{-3/2}$$

is non-negative for all ξ , and it attains its greatest value at the vertex $\xi = 0$. All of the exterior offsets (positive d) are smooth. The “interior” untrimmed offsets (negative d) are also smooth for $0 \geq d > -\frac{1}{2}$, since within this range $1 + \kappa(\xi)d > 0$ for all ξ . When $d = -\frac{1}{2}$, however, the offset exhibits a tangent-continuous point of infinite curvature at $\xi = 0$, since then $\kappa(0) = -1/d$ and

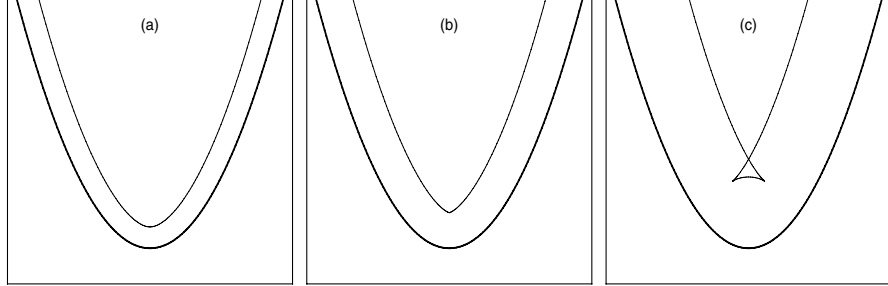


Fig. 8.18. Singularities on the interior offset to a parabola: (a) when $|d| < \frac{1}{2}$, the offset is smooth; (b) when $|d| = \frac{1}{2}$, there is a tangent-continuous point of infinite curvature; and (c) when $|d| > \frac{1}{2}$, there are two cusps and also a self-intersection.

$\kappa'(0) = 0 \neq \kappa''(0)$. Finally, when $d < -\frac{1}{2}$, there are two symmetric values, $\xi = \pm \frac{1}{2} [(-2d)^{2/3} - 1]$, that induce cusps ($\kappa = -1/d$ and $\kappa' \neq 0$). Figure 8.18 illustrates the singularities on the offsets to a parabola.

The occurrence of singular points has a simple geometrical interpretation: they arise when a point of $\mathbf{r}_d(\xi)$ coincides with the *center of curvature* for the corresponding point on the curve $\mathbf{r}(\xi)$. If $\kappa(\xi_*) = -1/d$ we have $d = -\rho(u_*)$, where $\rho(\xi) = 1/\kappa(\xi)$ is the (signed) *radius of curvature* of $\mathbf{r}(\xi)$, so that

$$\mathbf{r}_d(\xi_*) = \mathbf{r}(\xi_*) - \rho(\xi_*) \mathbf{n}(\xi_*)$$

from (8.47). This expression also identifies the center of curvature for $\xi = \xi_*$ (note that κ is positive when \mathbf{n} points *away* from the center of curvature).

As discussed in §8.3, the centers of curvature for every point of a smooth curve $\mathbf{r}(\xi)$ form a locus known as the *evolute* of that curve. Hence, the cusps of the untrimmed offsets at each distance d lie on the evolute to $\mathbf{r}(\xi)$. This observation yields a further interpretation of the evolute $\mathbf{e}(\xi)$ of a given curve $\mathbf{r}(\xi)$ — namely, it is the *locus of cusps on successive offsets* $\mathbf{r}_d(\xi)$ to that curve as the offset distance d increases (compare Fig. 8.19 with Fig. 8.8).

There is a pronounced similarity between Fig. 8.11, illustrating a family of involutes to a given curve, and Fig. 8.19 showing a family of offsets to a curve together with its evolute. This is not coincidental. In fact, the family of offsets $\mathbf{r}_d(\xi)$ to a given curve $\mathbf{r}(\xi)$ is precisely the *family of involutes to the evolute* $\mathbf{e}(\xi)$ of that curve. It is not difficult to see why this is so.

For simplicity, consider a curve $\mathbf{r}(\xi)$ whose curvature is positive, monotone, and finite.²¹ Its evolute is $\mathbf{e}(\xi) = \mathbf{r}(\xi) - \rho(\xi) \mathbf{n}(\xi)$, where $\rho(\xi)$ and $\mathbf{n}(\xi)$ are the radius of curvature and unit normal of $\mathbf{r}(\xi)$. Since $\rho'(\xi) \neq 0$ by assumption, we see from (8.38) that tangent to the evolute is $\mathbf{t}_e(\xi) = -\mathbf{n}(\xi)$. Moreover, we know that the arc length $s_{e,\tau}(\xi)$ of the evolute between τ and ξ is simply

²¹ The arguments can readily be extended to accommodate curves with inflections and vertices, although they are then considerably more cumbersome.

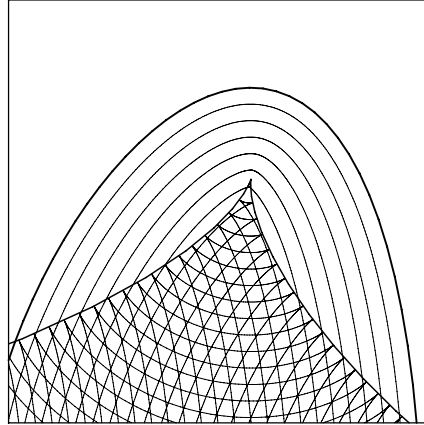


Fig. 8.19. Evolute of a given curve as the locus of cusps on its untrimmed offsets (compare with Fig. 8.8). Note that the cusp of the evolute coincides with the tangent–continuous point of infinite curvature on the offset at distance $d = -\frac{1}{2}$.

$\rho(\xi) - \rho(\tau)$. Hence, the expression $\mathbf{e}(\xi) - s_{e,\tau}(\xi) \mathbf{t}_e(\xi)$ for the involute of the evolute corresponding to parameter value τ reduces to

$$\mathbf{r}(\xi) - \rho(\tau) \mathbf{n}(\xi),$$

and we recognize this as the offset to $\mathbf{r}(\xi)$ at the distance $d = -\rho(\tau)$. Involutes corresponding to successive τ values thus generate a family of offsets to $\mathbf{r}(\xi)$.

One can also argue in purely geometrical terms. We know that the normals to $\mathbf{r}(\xi)$ are tangents to its evolute $\mathbf{e}(\xi)$. Furthermore, we also know that these tangents to $\mathbf{e}(\xi)$ are normals to each of its involutes. Hence, $\mathbf{r}(\xi)$ shares the same normal lines at corresponding points with every involute of its evolute, and this implies that the former and latter have parallel tangent lines at corresponding points. In other words, the involutes of the evolute of $\mathbf{r}(\xi)$ are all *parallel to* — i.e., offset from — that curve. Involutes of $\mathbf{e}(\xi)$ corresponding to parameter values τ_1 and τ_2 are a fixed distance $\rho(\tau_2) - \rho(\tau_1)$ apart (if we assume that $\rho(\xi)$ is monotone increasing).

Offsets to Tangent-discontinuous Curves

Many applications are concerned not only with smooth (G^1) curves, but also *piecewise-smooth* curves that exhibit only *point* continuity at the junctures of successive smooth segments. Since the order of continuity of the untrimmed offset $\mathbf{r}_d(\xi)$ is one less than that of the given curve $\mathbf{r}(\xi)$ — the former depends on the *derivative* of the latter — a curve with tangent discontinuities exhibits “gaps” in its untrimmed offset if we simply use (8.47) for each segment. Most often, this is not the desired result — the offset should be a *continuous* curve. Consistent with the property that the untrimmed offset is (locally) distance d

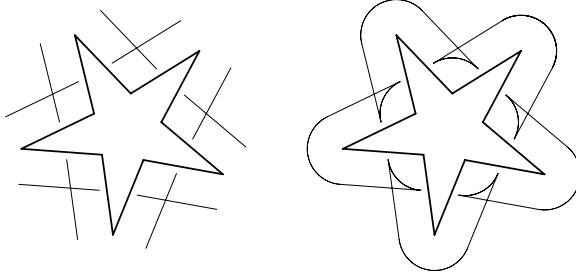


Fig. 8.20. Closure of the untrimmed offset to a polygonal curve by circular fillets.

from the given curve, the remedy is simple: we introduce circular “fillet” arcs of radius d centered on each tangent discontinuity. Depending on whether the tangent discontinuity is concave or convex relative to the offset direction, such arcs yield either a “swallowtail” or smooth closure of gaps in the untrimmed offset — Fig. 8.20 illustrates this in the case of a polygonal curve.

Suppose the given curve \mathcal{C} consists of one or more oriented, nested loops — each loop is a sequence of parametric segments that meet end-to-end with (at least) G^0 continuity, to form a closed curve free of self-intersections. The outermost loop is assumed to be parameterized in an anti-clockwise sense, and the orientation of the other loops reverses²² with successive nesting levels.

Definition 8.4 At each tangent-discontinuity \mathbf{q} of the curve \mathcal{C} we introduce a *cone of normals*, defined to be the continuous family of unit vectors with orientations between the limiting curve normals, \mathbf{n}_- and \mathbf{n}_+ , immediately before and after \mathbf{q} as we traverse \mathcal{C} in the sense of its parameterization.

The cone of normals is taken in the *clockwise* or *anticlockwise* sense between \mathbf{n}_- to \mathbf{n}_+ according to whether $(\mathbf{n}_- \times \mathbf{n}_+) \cdot \mathbf{z}$ is *negative* or *positive*, where \mathbf{z} is the vector orthogonal to the plane.

Definition 8.5 A point $\mathbf{p} = \mathbf{q} + d \mathbf{n}$ is a *generalized normal displacement* by distance d from a point \mathbf{q} on the curve \mathcal{C} if either: (a) \mathbf{q} is a smooth point of \mathcal{C} , and \mathbf{n} is the *unique* normal there; or (b) \mathbf{q} is a tangent-discontinuity, and \mathbf{n} is *any* member of the cone of normals there.

Definition 8.6 The *untrimmed offset* $\tilde{\mathcal{C}}_d$ at signed distance d from the curve \mathcal{C} is the locus of points corresponding to all generalized normal displacements by distance d from each point of \mathcal{C} .

Now $\tilde{\mathcal{C}}_d$ has the same number of loops as \mathcal{C} , but these loops may exhibit self-intersections or may intersect each other. Each smooth segment $\mathbf{r}(\xi)$ on \mathcal{C} generates a (not necessarily smooth) offset segment on $\tilde{\mathcal{C}}_d$, given by (8.47).

²² With this convention, the area enclosed by \mathcal{C} lies always to the *left* as we traverse any of its loops in the sense of increasing parameter ξ .

Furthermore, each tangent-discontinuous juncture \mathbf{q} of consecutive smooth segments on \mathcal{C} induces a circular “fillet” arc of radius $|d|$ on $\tilde{\mathcal{C}}_d$, centered on \mathbf{q} , whose angular extent is determined by the cone of normals there.

Definition 8.7 We say that $\mathbf{q} \in \mathcal{C}$ and $\mathbf{p} \in \tilde{\mathcal{C}}_d$ are *corresponding points* of a curve and its untrimmed offset if the latter may be obtained from the former through a generalized normal displacement by distance d . A point $\mathbf{p} \in \tilde{\mathcal{C}}_d$ that has two (or more) distinct corresponding points $\mathbf{q}_1, \mathbf{q}_2 \in \mathcal{C}$, with non-parallel normals \mathbf{n}_1 and \mathbf{n}_2 , is a *self-intersection* of the untrimmed offset.

8.3.5 Trimming the Untrimmed Offset

We now study in detail the problem of determining the “trimmed” offset from the “untrimmed” offset. Consider a piecewise-smooth curve \mathcal{C} , corresponding to the boundary $\partial\mathcal{D}$ of a connected domain $\mathcal{D} \subset \mathbb{R}^2$. This curve may consist of several loops, each parameterized so that its start and end points coincide. The sense of parameterization is such that the normal \mathbf{n} to \mathcal{C} points locally to the exterior of \mathcal{D} . Also, to ensure one-to-one correspondence between the points of \mathcal{C} and its untrimmed offset, we regard tangent-discontinuities on \mathcal{C} as “degenerate” circular arcs of zero radius but non-zero angular extent, defined by their normal cones (i.e., the curve parameter increases on these degenerate arcs, but the geometrical location does not). We denote the untrimmed and trimmed offsets at distance d from \mathcal{C} by $\tilde{\mathcal{C}}_d$ and \mathcal{C}_d , respectively.

The untrimmed offset $\mathbf{r}_d(\xi)$ is *locally* at distance $|d|$ from the curve $\mathbf{r}(\xi)$ — i.e., *corresponding points* of these loci satisfy $|\mathbf{r}_d(\xi) - \mathbf{r}(\xi)| = |d|$. However, the untrimmed offset does not necessarily maintain distance $|d|$ from the given curve in a *global* sense: for any given ξ , there may be values $\tau \neq \xi$ such that $|\mathbf{r}_d(\xi) - \mathbf{r}(\tau)| < |d|$. By the true or “trimmed” offset \mathcal{C}_d , we mean the locus of points at distance $\geq |d|$ from *every* point of \mathcal{C} — and *exactly* distance $|d|$ from at least one point (on the appropriate side, indicated by the sign of d). The true offset is actually a *subset* of the untrimmed offset: we may obtain \mathcal{C}_d from $\tilde{\mathcal{C}}_d$ by deleting a certain (possibly null) set of continuous segments from the latter. This process is called the *trimming* of the untrimmed offset.

The offset trimming problem is fundamentally *global* in nature: the parts of the untrimmed offset to be “trimmed away” cannot be identified by purely local considerations. As illustrated by Fig. 8.21, complicated structures can arise on the untrimmed offset due to *interference* of the offsets to “unrelated” portions of the given curve \mathcal{C} . This phenomenon may arise even if the entire untrimmed offset $\tilde{\mathcal{C}}_d$ is smooth (i.e., free of cusps), since it may self-intersect in a manner that is apparent only through consideration of the entire curve. Before describing the trimming procedure in detail, we must first quantify the notion of “distance” between a point and a curve, and between two curves.

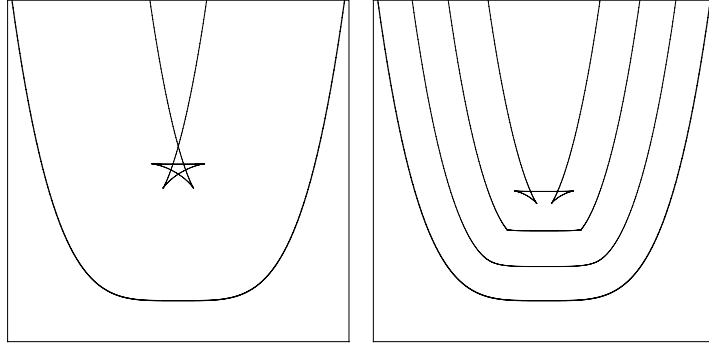


Fig. 8.21. Left: structure of the interior untrimmed offset at distance $|d| = 1$ to the curve $y = x^4$. Right: untrimmed offsets at distance less than, equal to, and greater than the smallest radius of curvature of $y = x^4$. As $|d|$ further increases, the overlap of the two “swallowtails” generates the five-point “star” configuration on the left.

Point/Curve Distance Function

The point/curve distance function “ $\text{distance}(\mathbf{p}, \mathcal{C})$ ” takes a point \mathbf{p} and a curve \mathcal{C} as its arguments — its value is a non-negative number, that vanishes only when \mathbf{p} lies on \mathcal{C} . It is defined in the most general terms (i.e., independent of the specification of \mathcal{C}) by the expression

$$\text{distance}(\mathbf{p}, \mathcal{C}) = \min_{\mathbf{q} \in \mathcal{C}} |\mathbf{p} - \mathbf{q}|. \quad (8.49)$$

Let $\mathbf{p} = (x, y)$, and \mathcal{C} be a parametric polynomial curve $\mathbf{r}(\xi) = (X(\xi), Y(\xi))$ defined on $\xi \in [0, 1]$. Then if ξ_1, \dots, ξ_N are the distinct (odd-multiplicity) roots of the polynomial

$$P_\perp(\xi) = X'(\xi)[x - X(\xi)] + Y'(\xi)[y - Y(\xi)] \quad (8.50)$$

on $\xi \in (0, 1)$, and we set $\xi_0 = 0$ and $\xi_{N+1} = 1$, we have

$$\text{distance}(\mathbf{p}, \mathcal{C}) = \min_{0 \leq k \leq N+1} |\mathbf{p} - \mathbf{r}(\xi_k)|. \quad (8.51)$$

The real roots of (8.50) identify those points on $\mathbf{r}(\xi)$ where a line drawn from \mathbf{p} meets the curve *orthogonally*. As we traverse the curve, the value of $|\mathbf{p} - \mathbf{r}(\xi)|$ attains a local extremum at ξ_1, \dots, ξ_N since

$$\frac{d}{d\xi} |\mathbf{p} - \mathbf{r}(\xi)| = - \frac{P_\perp(\xi)}{|\mathbf{p} - \mathbf{r}(\xi)|}.$$

The value of $\text{distance}(\mathbf{p}, \mathcal{C})$ is the smallest of these interior extremal distances and the distances to the endpoints of $\mathbf{r}(\xi)$. We consider only odd-multiplicity roots of (8.50) since even-multiplicity roots identify non-extremal stationary values of $|\mathbf{p} - \mathbf{r}(\xi)|$. The computation of $\text{distance}(\mathbf{p}, \mathcal{C})$ is easily extended to rational curves, and also piecewise polynomial or rational curves (in the latter context, we must include tangent discontinuities among the values ξ_1, \dots, ξ_N).

Example 8.4 For the parabola $\mathbf{r}(\xi) = (\xi, \xi^2)$ the polynomial (8.50) becomes

$$P_{\perp}(\xi) = -2\xi^3 + (2y - 1)\xi + x. \quad (8.52)$$

The *discriminant* (see §3.4) of the cubic $P_{\perp}(\xi)$ is

$$\Delta(x, y) = -108x^2 + 8(2y - 1)^3, \quad (8.53)$$

and it has either one or three distinct real roots, according to whether $\Delta < 0$ or $\Delta > 0$ (when $\Delta = 0$, there is a multiple real root). Figure 8.22 shows the two regions delimited by the algebraic curve²³ $\Delta(x, y) = 0$ — which have the property that *one* or *three* perpendiculars may be drawn from any point \mathbf{p} in them to the curve $\mathbf{r}(\xi)$. When $\Delta < 0$, $\text{distance}(\mathbf{p}, \mathcal{C})$ is the length of the unique perpendicular to \mathcal{C} from \mathbf{p} . When $\Delta > 0$, on the other hand, $\text{distance}(\mathbf{p}, \mathcal{C})$ is the *shortest* of the three perpendiculars from \mathbf{p} to \mathcal{C} .

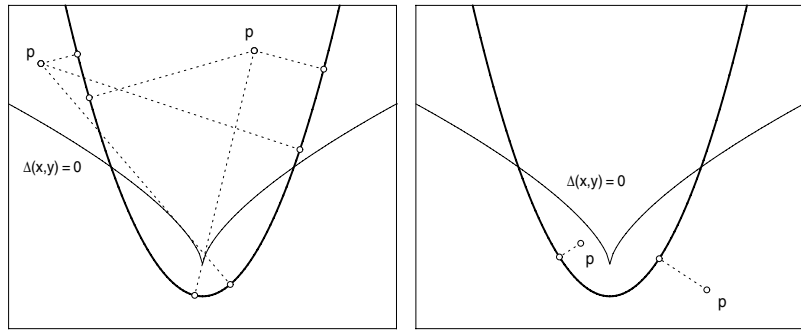


Fig. 8.22. Left: three distinct normals may be drawn to the parabola $\mathbf{r}(\xi) = (\xi, \xi^2)$ from any point \mathbf{p} above the curve $\Delta(x, y) = 0$ defined by (8.53), namely, the *evolute* of the parabola. Right: for any point \mathbf{p} below this curve, there is a unique normal.

Now for a given curve \mathcal{C} the function $\text{distance}(\mathbf{p}, \mathcal{C})$ is *continuous*, but not everywhere *differentiable*, with respect to the location of \mathbf{p} . A unit vector \mathbf{v} , defining a *direction of motion* for \mathbf{p} , must be specified to express the derivative of $\text{distance}(\mathbf{p}, \mathcal{C})$ with respect to \mathbf{p} as

$$\nabla_{\mathbf{v}} \text{distance}(\mathbf{p}, \mathcal{C}) = \mathbf{v} \cdot \left(\mathbf{i} \frac{\partial}{\partial x} + \mathbf{j} \frac{\partial}{\partial y} \right) \text{distance}(\mathbf{p}, \mathcal{C}),$$

where the partial derivatives are with respect to the coordinates (x, y) of \mathbf{p} . Clearly, these partial derivatives must exist at the point in question in order for $\nabla_{\mathbf{v}} \text{distance}(\mathbf{p}, \mathcal{C})$ to be defined. The non-differentiability of $\text{distance}(\mathbf{p}, \mathcal{C})$ may be understood as follows. As \mathbf{p} moves, the real roots ξ_1, \dots, ξ_N of (8.50)

²³ One can easily verify that this curve is actually the *evolute* of the parabola.

in expression (8.51) have, in general, an analytic dependence upon the location of \mathbf{p} . But the number of these roots may abruptly change at certain locations — since real roots may “appear” as double roots that subsequently bifurcate, or pairs of simple real roots may meet, coalesce, and “disappear” as complex conjugates. Even for a motion of \mathbf{p} such that (8.50) maintains a fixed number of real roots, the “identity” of the root yielding the smallest value in (8.51) may jump — from ξ_j to ξ_k , say — at some locations. At such jumps, whether due to the appearance/disappearance of real roots or otherwise, *continuity* of $\text{distance}(\mathbf{p}, \mathcal{C})$ is guaranteed by the fact that $|\mathbf{p} - \mathbf{r}(\xi_j)| = |\mathbf{p} - \mathbf{r}(\xi_k)|$. But these quantities have, in general, different rates of change with respect to the motion of \mathbf{p} , and hence $\text{distance}(\mathbf{p}, \mathcal{C})$ is non-differentiable at such points.

Curve/Curve Distance Function

The point/curve distance function may be used to define the *distance between two curves*. For given plane curves \mathcal{B} and \mathcal{C} , we denote this by $\text{distance}(\mathcal{B}, \mathcal{C})$. We have defined the distance between a point \mathbf{p} and a curve \mathcal{C} as the *smallest* distance from \mathbf{p} to each point $\mathbf{q} \in \mathcal{C}$. It may seem natural, when \mathbf{p} is allowed to traverse some curve \mathcal{B} , to define the distance between the curves \mathcal{B} and \mathcal{C} as the smallest value of $\text{distance}(\mathbf{p}, \mathcal{C})$ for each $\mathbf{p} \in \mathcal{B}$. This amounts to taking

$$\min_{\mathbf{p} \in \mathcal{B}} \min_{\mathbf{q} \in \mathcal{C}} |\mathbf{p} - \mathbf{q}| \quad (8.54)$$

for the value of $\text{distance}(\mathcal{B}, \mathcal{C})$. According to this rule, however, the distance between *any* two curves that intersect is zero — regardless of their behavior at points other than the intersections. This is not a satisfactory characterization of the “overall” distance between two curves. Clearly, it is preferable that the distance be zero only for *identical* curves:

$$\text{distance}(\mathcal{B}, \mathcal{C}) = 0 \iff \mathcal{B} \equiv \mathcal{C}. \quad (8.55)$$

One way to modify (8.54) so as to guarantee the property (8.55) is to take the “largest of the smallest” values, rather than the “smallest of the smallest” values, of the distance between pairs of points \mathbf{p} and \mathbf{q} on the two curves:

$$\rho(\mathcal{B}, \mathcal{C}) = \max_{\mathbf{p} \in \mathcal{B}} \min_{\mathbf{q} \in \mathcal{C}} |\mathbf{p} - \mathbf{q}|. \quad (8.56)$$

This corresponds to the *greatest* value of the point/curve distance function, $\text{distance}(\mathbf{p}, \mathcal{C})$, over all points $\mathbf{p} \in \mathcal{B}$. Expression (8.56) is also troublesome as a curve/curve distance function, however, since $\rho(\mathcal{B}, \mathcal{C}) \neq \rho(\mathcal{C}, \mathcal{B})$ in general — i.e., the distance from \mathcal{B} to \mathcal{C} is not the same as that from \mathcal{C} to \mathcal{B} !

In addition to satisfying (8.55), the following three features are generally required of any distance function (or *metric*):

- non-negativity: $\text{distance}(\mathcal{B}, \mathcal{C}) \geq 0$;

- symmetry: $\text{distance}(\mathcal{B}, \mathcal{C}) = \text{distance}(\mathcal{C}, \mathcal{B})$;
- satisfaction of the *triangle inequality*, namely:

$$\text{distance}(\mathcal{A}, \mathcal{B}) + \text{distance}(\mathcal{B}, \mathcal{C}) \geq \text{distance}(\mathcal{A}, \mathcal{C}).$$

These properties may be achieved by *symmetrizing* (8.56), i.e., by taking

$$\text{distance}(\mathcal{B}, \mathcal{C}) = \max(\rho(\mathcal{B}, \mathcal{C}), \rho(\mathcal{C}, \mathcal{B})). \quad (8.57)$$

This is known as the *Hausdorff distance* between the curves \mathcal{B} and \mathcal{C} . It can, in fact, be used for any two point sets — not just curves [230].

Example 8.5 Consider the problem of determining $\text{distance}(\mathcal{C}_1, \mathcal{C}_2)$ for two circles $\mathcal{C}_1, \mathcal{C}_2$ with centers $\mathbf{c}_1, \mathbf{c}_2$ and radii r_1, r_2 . If \mathbf{p} is a fixed point on \mathcal{C}_1 , the closest point \mathbf{q} to it on \mathcal{C}_2 is on the diametral line through \mathbf{p} and \mathbf{c}_2 . Thus, regardless of whether \mathbf{p} lies inside, on, or outside of \mathcal{C}_2 , we may write

$$\text{distance}(\mathbf{p}, \mathcal{C}_2) = | |\mathbf{p} - \mathbf{c}_2| - r_2 |.$$

To maximize this over all points $\mathbf{p} \in \mathcal{C}_1$ we assume, without loss of generality, that $\mathbf{c}_1 = (0, 0)$ and $\mathbf{c}_2 = (\ell, 0)$ where $\ell = |\mathbf{c}_2 - \mathbf{c}_1|$. Writing $\mathbf{p} = r_1(\cos \theta, \sin \theta)$ and substituting into $\text{distance}(\mathbf{p}, \mathcal{C}_2)$, we seek to maximize the quantity

$$| \sqrt{r_1^2 + \ell^2 - 2r_1\ell \cos \theta} - r_2 | \quad (8.58)$$

for $0 \leq \theta < 2\pi$. One can readily verify that extrema occur for $\theta = 0$ and π , and the Hausdorff distance between the two circles is given by

$$\text{distance}(\mathcal{C}_1, \mathcal{C}_2) = \max(|\ell + r_1 - r_2|, |\ell - r_1 + r_2|).$$

Note that for two concentric circles ($\ell = 0$), this reduces to $\text{distance}(\mathcal{C}_1, \mathcal{C}_2) = |r_1 - r_2|$, whereas for circles of equal radius, $\text{distance}(\mathcal{C}_1, \mathcal{C}_2) = \ell$.

Characterization of the Trimmed Offset

Each point \mathbf{p} of the untrimmed offset $\tilde{\mathcal{C}}_d$ clearly satisfies

$$\text{distance}(\mathbf{p}, \mathcal{C}) \leq |d|, \quad (8.59)$$

since it is obtained by a displacement d from some corresponding point $\mathbf{q} \in \mathcal{C}$. The equality holds in (8.59) if and only if \mathbf{q} is the *closest* point of \mathcal{C} to \mathbf{p} .

Definition 8.8 The “true” or *trimmed* offset \mathcal{C}_d at distance d from the curve \mathcal{C} is the subset $\mathcal{C}_d \subseteq \tilde{\mathcal{C}}_d$ of the untrimmed offset, such that the relation (8.59) holds with equality for each point $\mathbf{p} \in \mathcal{C}_d$.

We now show that the segments of the trimmed offset \mathcal{C}_d are delineated by the self-intersections of the untrimmed offset $\tilde{\mathcal{C}}_d$. Let ξ_1, \dots, ξ_N be the ordered parameter values on a single loop of $\tilde{\mathcal{C}}_d$ corresponding to self-intersections of the untrimmed offset (these may be either self-intersections of the loop under consideration, or its intersections with *other* loops of $\tilde{\mathcal{C}}_d$). Note that the values ξ_1, \dots, ξ_N are interpreted as a cyclical list.

Proposition 8.1 *Let S_k be a segment of the untrimmed offset $\tilde{\mathcal{C}}_d$ delineated by consecutive parameter values ξ_k and ξ_{k+1} on a single loop that correspond to self-intersections of $\tilde{\mathcal{C}}_d$. Then each interior point \mathbf{p} of S_k satisfies either*

$$\text{distance}(\mathbf{p}, \mathcal{C}) = |d|, \quad (8.60)$$

or

$$\text{distance}(\mathbf{p}, \mathcal{C}) < |d|. \quad (8.61)$$

Segments of $\tilde{\mathcal{C}}_d$ that satisfy (8.61) must be discarded. The remaining segments, satisfying (8.60), then constitute the trimmed offset \mathcal{C}_d .

Proof : Let C_p denote the circle of radius $|d|$ centered on any point \mathbf{p} of the untrimmed offset $\tilde{\mathcal{C}}_d$. Then there is a point $\mathbf{q} \in \mathcal{C}$ such that \mathbf{p} corresponds to a generalized normal displacement d from that point, and \mathbf{q} evidently lies on the circle C_p . Since, for each $\mathbf{p} \in \tilde{\mathcal{C}}_d$ there is (at least) one corresponding point $\mathbf{q} \in \mathcal{C}$ lying *on* C_p , the relation (8.59) is clearly satisfied. If all other points of \mathcal{C} lie *outside* — or, exceptionally, *on* — the circle C_p , we have equality in (8.59) and \mathbf{p} is then on a segment of $\tilde{\mathcal{C}}_d$ that should be retained. On the other hand, if other points of \mathcal{C} lie *inside* the circle C_p , the inequality in (8.59) holds and \mathbf{p} is then on a segment of $\tilde{\mathcal{C}}_d$ that must be discarded.

We will show that, as \mathbf{p} traverses the untrimmed offset $\tilde{\mathcal{C}}_d$, the locations incurring a change in status of the circle C_p from “empty” to “occupied” by some portion of \mathcal{C} — or vice-versa — correspond to *self-intersections* of $\tilde{\mathcal{C}}_d$. If $\mathbf{q} \in \mathcal{C}$ and $\mathbf{p} \in \tilde{\mathcal{C}}_d$ are two corresponding points, the circle C_p is tangent²⁴ to the curve \mathcal{C} at \mathbf{q} . We assume, at first, that no part of \mathcal{C} lies inside C_p — then, at the instant \mathcal{C} begins to enter C_p as \mathbf{p} traverses $\tilde{\mathcal{C}}_d$, this circle must become tangent to \mathcal{C} at some point \mathbf{q}_* that is, in general, distinct from \mathbf{q} . The point \mathbf{p} on $\tilde{\mathcal{C}}_d$ then arises through a generalized normal displacement d from two *distinct* points, \mathbf{q} and \mathbf{q}_* , on \mathcal{C} — i.e., we have

$$\mathbf{p} = \mathbf{q} + d \mathbf{n} = \mathbf{q}_* + d \mathbf{n}_* \quad (8.62)$$

\mathbf{n} and \mathbf{n}_* being, in general, distinct normals to \mathcal{C} at \mathbf{q} and \mathbf{q}_* . This identifies \mathbf{p} as a *self-intersection* of $\tilde{\mathcal{C}}_d$ (Definition 8.7) when the status of C_p changes from “empty” to “occupied” as \mathbf{p} traverses the untrimmed offset. Analogous arguments hold when C_p is initially “occupied” and becomes “empty.” ■

²⁴ We interpret tangency in a “generalized” sense here: if \mathbf{q} is a tangent discontinuity on the curve \mathcal{C} , we consider C_p to be tangent to \mathcal{C} there if the vector $\mathbf{p} - \mathbf{q}$ has the same orientation as any member of the cone of normals at \mathbf{q} .

Hence, each interval $\xi \in [\xi_k, \xi_{k+1}]$ between self-intersections identifies a segment of $\tilde{\mathcal{C}}_d$ that either belongs in its entirety to \mathcal{C}_d , or should be rejected in its entirety. Note that passing through a self-intersection is only a *necessary* condition for a change in status regarding membership in the trimmed offset as we traverse the untrimmed offset — not all self-intersections of the latter signal a transition from portions that are to be kept to those that are to be discarded, or vice-versa, as we move along $\tilde{\mathcal{C}}_d$.

In the proof of Proposition 8.1, we mentioned that the point \mathbf{q}_* at which the curve \mathcal{C} begins to enter the circle C_p of radius $|d|$ centered on a point \mathbf{p} traversing the untrimmed offset $\tilde{\mathcal{C}}_d$ is usually distinct from \mathbf{q} , the point that \mathbf{p} is obtained from by a generalized normal displacement. We now consider what happens in the exceptional cases where \mathcal{C} does enter C_p at \mathbf{q} .

Proposition 8.2 *If, as \mathbf{p} traces the untrimmed offset $\tilde{\mathcal{C}}_d$, the curve \mathcal{C} begins to enter the circle C_p of radius $|d|$ centered on \mathbf{p} at the corresponding point \mathbf{q} , rather than at some other point \mathbf{q}_* , then \mathbf{p} is a cusp on $\tilde{\mathcal{C}}_d$.*

Proof: Recall that \mathbf{p} is a cusp on $\tilde{\mathcal{C}}_d$ if it coincides with the *center of curvature* for the corresponding point \mathbf{q} on \mathcal{C} . We argue that, when the curve \mathcal{C} begins to enter C_p at the corresponding point \mathbf{q} , the circle C_p must be the *osculating circle* or “circle of curvature” to \mathcal{C} at \mathbf{q} . Among all circles tangent to \mathcal{C} at \mathbf{q} , only the osculating circle crosses²⁵ the curve there: tangential circles that are smaller or larger lie on one side of \mathcal{C} in the vicinity of \mathbf{q} (see §8.1.2). Hence, C_p must coincide with the osculating circle at \mathbf{q} when \mathcal{C} begins to enter it at that point, and \mathbf{p} is then a cusp on $\tilde{\mathcal{C}}_d$. ■

In the above proof we assume that \mathbf{q} is a smooth point on \mathcal{C} . One can easily verify that, if \mathbf{q} is a tangent discontinuity on \mathcal{C} , the offsets to the smooth segments meeting there connect in a cuspidal manner with the ends of the circular fillet arc associated with \mathbf{q} if this point is “concave” viewed from the side on which the offset is made — conversely, there is a smooth connection if it is “convex” (see Fig. 8.20). It might seem that the trimming procedure should involve splitting the untrimmed offset $\tilde{\mathcal{C}}_d$ at its cusps, as well as its self-intersections, since they also identify points where part of the curve \mathcal{C} begins to enter the circle C_p . We can show, in fact, that this is actually unnecessary.

Corollary 8.1 *No explicit consideration of the cusps on the untrimmed offset $\tilde{\mathcal{C}}_d$ is required in the trimming procedure.*

Proof: We argue that, if \mathcal{C} begins to enter C_p at the point \mathbf{q} corresponding to \mathbf{p} as the latter traces $\tilde{\mathcal{C}}_d$, then \mathcal{C} must already have crossed C_p before this occurs. For any \mathbf{p} , the circle C_p clearly has a two-fold intersection²⁶ with the curve \mathcal{C} at the corresponding point \mathbf{q} . Now by Proposition 8.2, C_p must be the *osculating circle* at \mathbf{q} when \mathbf{p} is a *cusp* on $\tilde{\mathcal{C}}_d$. The osculating circle differs from

²⁵ Except in the case that \mathbf{q} is a *vertex* (i.e., a point of extremum curvature) on \mathcal{C} .

²⁶ Actually, a “tangency” since C_p and \mathcal{C} do not, in general, cross at the point \mathbf{q} .

all other circles tangent to \mathcal{C} at \mathbf{q} in that it has a *three-fold* intersection²⁷ with the curve there (see §8.1.2). Now a two-fold intersection of C_p and \mathcal{C} can only become a three-fold intersection if it “meets” and “coalesces” with a formerly distinct, *simple* (i.e., transversal) intersection \mathbf{q}_* of C_p and \mathcal{C} . In other words, if \mathcal{C} begins to enter the circle C_p at the corresponding point \mathbf{q} , some portion of it must *previously* have entered that circle elsewhere. Similar arguments show, conversely, that if \mathcal{C} begins to exit from C_p at \mathbf{q} , some portion of it must *subsequently* vacate that circle elsewhere. Thus, cusps of $\tilde{\mathcal{C}}_d$ cannot alter the “empty/occupied” status of C_p established by self-intersections alone. ■

Again, the above argument applies to the case of a smooth point $\mathbf{q} \in \mathcal{C}$. It is not difficult to verify that, for a “concave” tangent-discontinuous point \mathbf{q} on \mathcal{C} , the cuspidal connections of the corresponding circular fillet arc with the offsets to the smooth segments that meet at \mathbf{q} will always lie within a self-intersection loop of $\tilde{\mathcal{C}}_d$ that must be discarded.

Example 8.6 A simple example may help clarify the above ideas. Consider an offset at distance $d < -\frac{1}{2}$ to the parabola \mathcal{C} defined by $\mathbf{r}(\xi) = (\xi, \xi^2)$. The untrimmed offset $\tilde{\mathcal{C}}_d$ is the locus

$$\mathbf{r}_d(\xi) = (\xi, \xi^2) + d \frac{(2\xi, -1)}{\sqrt{4\xi^2 + 1}}. \quad (8.63)$$

Let $\mathbf{q} = \mathbf{r}(\xi)$ and $\mathbf{p} = \mathbf{r}_d(\xi)$ be corresponding points on \mathcal{C} and $\tilde{\mathcal{C}}_d$. We wish to study the “occupancy status” of the circle C_p with radius $|d|$ and center \mathbf{p} . This circle has the implicit equation

$$\left[x - \xi - \frac{2d\xi}{\sqrt{4\xi^2 + 1}} \right]^2 + \left[y - \xi^2 + \frac{d}{\sqrt{4\xi^2 + 1}} \right]^2 - d^2 = 0$$

in free coordinates (x, y) . To identify the intersections of \mathcal{C} with C_p , we set $(x, y) = (\tau, \tau^2)$ in the above and thus obtain, for each ξ , the quartic equation

$$P(\tau) = (\tau - \xi)^2 \left[\tau^2 + 2\xi\tau + \frac{2d}{\sqrt{4\xi^2 + 1}} + \xi^2 + 1 \right] = 0$$

in τ , whose real roots describe the intersections of C_p and the parabola in terms of the parameter value on the latter.

The double root $\tau = \xi$ reflects the tangency of C_p to the parabola at \mathbf{q} . The other quadratic factor in $P(\tau)$ has no real roots, a double root, or two distinct real roots according to whether its discriminant $\Delta = -4 - 8d/\sqrt{4\xi^2 + 1}$ is negative, zero, or positive. Now as \mathbf{p} traverses $\tilde{\mathcal{C}}_d$ — i.e., as ξ increases from $-\infty$ to $+\infty$ — Δ first changes sign when

²⁷ Again we make the qualification that \mathbf{q} is a generic point, not a vertex, of \mathcal{C} .

$$\xi = -\sqrt{d^2 - \frac{1}{4}}. \quad (8.64)$$

Prior to reaching the value (8.64), we have $\Delta < 0$, and \mathcal{C} lies *outside* of C_p . On attaining the value (8.64), Δ vanishes, and \mathcal{C} is then *tangent* to C_p at a point $\mathbf{q}_* = (-\xi, \xi^2)$ other than the corresponding point $\mathbf{q} = (\xi, \xi^2)$, inducing a self-intersection of $\tilde{\mathcal{C}}_d$. Finally, when the value (8.64) is exceeded, we have $\Delta > 0$, and $P(\tau)$ has the two distinct real roots

$$\tau = -\xi \pm \sqrt{-1 - 2d/\sqrt{4\xi^2 + 1}},$$

indicating that a segment of \mathcal{C} must lie *inside* C_p .

As ξ is further increased, the intersection of C_p and \mathcal{C} identified by the smaller of these roots approaches the tangency point \mathbf{q} of C_p and \mathcal{C} . These points coalesce, causing C_p to be the circle of curvature to \mathcal{C} at \mathbf{q} , when

$$\xi = -\frac{1}{2} \sqrt{(-2d)^{2/3} - 1}$$

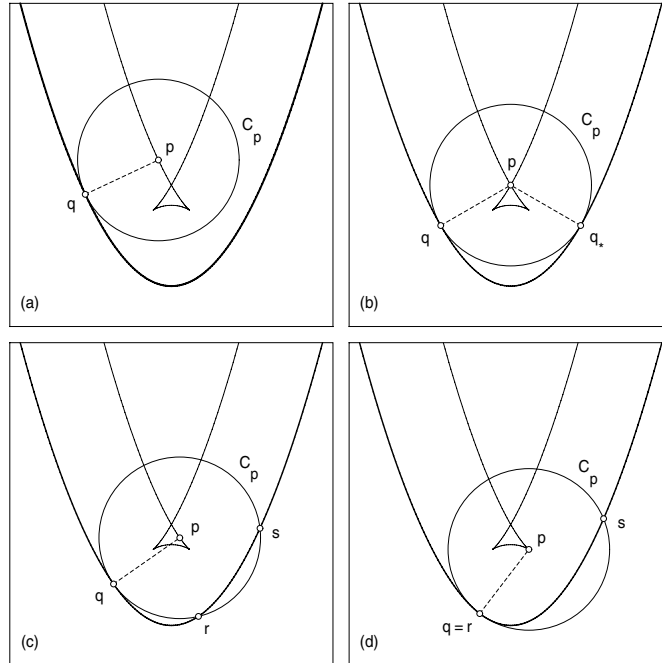


Fig. 8.23. The offset to a parabola \mathcal{C} : (a) before \mathbf{p} reaches the self-intersection, C_p contains no part of \mathcal{C} and \mathbf{p} belongs to the true offset; (b) when \mathbf{p} reaches the self-intersection, C_p is tangent to \mathcal{C} at some point \mathbf{q}_* other than the corresponding point \mathbf{q} ; (c) when \mathbf{p} moves through the self-intersection, the tangency \mathbf{q}_* splits into simple intersections, \mathbf{r} and \mathbf{s} , and \mathbf{p} no longer belongs to the true offset, since part of \mathcal{C} lies in C_p ; (d) when \mathbf{p} reaches the cusp, \mathbf{r} and \mathbf{q} coincide, and C_p becomes the *osculating circle*. Traversing the cusp does not alter the “occupancy status” of C_p .

— thereby inducing a cusp on $\tilde{\mathcal{C}}_d$. Note, however, that the occurrence of this cusp does not change the “occupancy status” of C_p with respect to \mathcal{C} .

Figure 8.23 illustrates this sequence of events, which evidently recurs in reverse order as ξ is increased through 0, on account of the symmetry of $\mathbf{r}(\xi)$. The true offset \mathcal{C}_d is the subset of the untrimmed offset $\tilde{\mathcal{C}}_d$, defined by (8.63), that corresponds to deleting the parameter interval

$$\xi \in \left[-\sqrt{d^2 - \frac{1}{4}}, +\sqrt{d^2 - \frac{1}{4}} \right]$$

delimited by the self-intersection of $\tilde{\mathcal{C}}_d$.

The Offset Trimming Procedure

We are now ready to describe the trimming procedure, whereby the true offset \mathcal{C}_d at distance d from a given curve \mathcal{C} is culled from the untrimmed offset $\tilde{\mathcal{C}}_d$. We assume that \mathcal{C} comprises one or more oriented, nested loops: the outermost loop has an anticlockwise parameterization, and the sense of parameterization reverses with successive nesting levels.

1. construct the untrimmed offset $\tilde{\mathcal{C}}_d$ at distance d , including circular fillet arcs to close the “gaps” incurred by tangent discontinuities of \mathcal{C} , so as to ensure that $\tilde{\mathcal{C}}_d$ is continuous;
2. compute all *self-intersections* of the untrimmed offset $\tilde{\mathcal{C}}_d$, and split it at these points into a collection of contiguous segments $\mathcal{S}_1, \dots, \mathcal{S}_N$;
3. select test points $\mathbf{p}_k \in \mathcal{S}_k$ on the *interior* of each segment and compute their distances from the given curve \mathcal{C} ;
4. for each segment, either $\text{distance}(\mathbf{p}_k, \mathcal{C}) < |d|$ or $\text{distance}(\mathbf{p}_k, \mathcal{C}) = |d|$ — those in the former category must be discarded, while those in the latter category are retained;
5. the retained segments, connected end-to-end, form zero or more oriented, nested loops that constitute the trimmed offset \mathcal{C}_d .

The given curve \mathcal{C} and its trimmed offset \mathcal{C}_d satisfy

$$\text{distance}(\mathcal{C}_d, \mathcal{C}) = |d|$$

in the sense of the curve/curve distance function defined by (8.56) and (8.57). Furthermore, \mathcal{C}_d lies (locally) to the *left* or *right* of \mathcal{C} according to whether d is *negative* or *positive* (note that the loops of the trimmed offset \mathcal{C}_d inherit the orientation convention of the original curve \mathcal{C}). Figure 8.24 illustrates the offset trimming procedure in the context of a piecewise-linear/circular curve.

Figure 8.25 shows a family of offsets at successive distances d to the curve in Fig. 8.24. By careful examination of Fig. 8.25 one can observe the locus of tangent discontinuities on the trimmed offsets, which exhibits a branching behavior at certain special points. These tangent discontinuities, generated by trimming the untrimmed offsets at self-intersections, are equidistant from (at

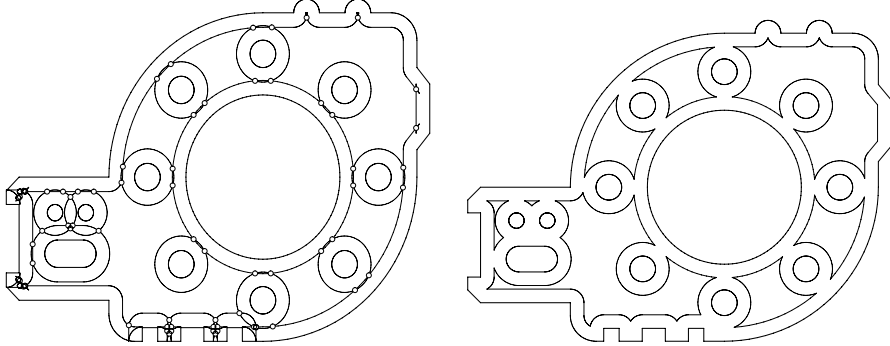


Fig. 8.24. Trimming the interior offset to a piecewise–linear/circular curve. Left: self–intersections of the untrimmed offset. Right: trimmed offset after distance tests.

least) two points of the curve \mathcal{C} , and are thus centers of *maximal disks* within the domain bounded by \mathcal{C} . The locus of centers of maximal disks inscribed in a planar domain is known as the *medial axis* of that domain [47, 49, 53, 83].

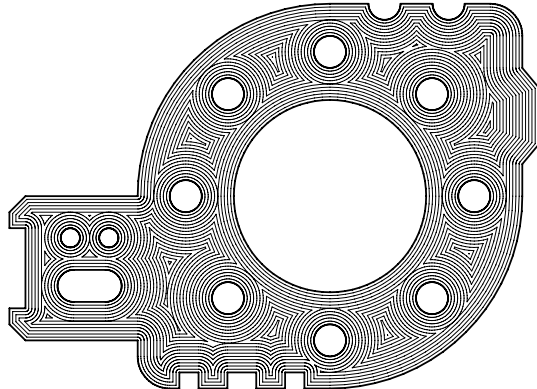


Fig. 8.25. A family of equidistant offsets to the piecewise–linear/circular boundary of a planar domain — the medial axis or “skeleton” of the domain is apparent upon squinting to bring into relief the locus of tangent–discontinuities on the offset curves.

The offset trimming problem can be simplified by computing *a priori* the medial axis of the domain bounded by the given curve \mathcal{C} [86, 90, 232]. Instead of constructing the entire untrimmed offset at distance d , and then trimming it, the offsets to each segment of \mathcal{C} can be directly trimmed against the medial axis edges as they are constructed — this eliminates the need for subsequent trimming operations. However, the medial axis computation is a substantial task in its own right [47, 87, 124, 375] and this approach is only advantageous when many offsets to the same boundary curve \mathcal{C} are to be computed.

8.4 Intrinsic Geometry of Space Curves

A space curve $\mathbf{r}(\xi) = (x(\xi), y(\xi), z(\xi))$ may be defined by three scalar functions of a parameter ξ . Henceforth \mathbf{r} and all other vectors we encounter (tangents, normals, etc.) are *three-dimensional* vectors; the preceding results are a special instance of the discussion that follows, corresponding to the choice $z(\xi) \equiv 0$. Equation (8.1) carries over to the present context, assuming the space curve is regular, but the parametric speed is now given by

$$\sigma(\xi) = |\mathbf{r}'(\xi)| = \sqrt{x'^2(\xi) + y'^2(\xi) + z'^2(\xi)}, \quad (8.65)$$

and the tangent (8.3) is a three-dimensional vector.

Now for a plane curve the normal $\mathbf{n}(\xi)$ is uniquely defined, up to a sign choice, by the fact it must lie in the plane of the curve and be perpendicular to the tangent $\mathbf{t}(\xi)$ — equation (8.5) fixes the sign ambiguity in a specific manner. In three dimensions, however, there is an infinity of vectors orthogonal to any tangent $\mathbf{t}(\xi)$, and a different approach is required to characterize them. We accomplish this by introducing two unit vectors — the *principal normal* $\mathbf{p}(\xi)$ and the *binormal* $\mathbf{b}(\xi)$ — that are orthogonal to $\mathbf{t}(\xi)$ and to each other. These vectors span the *normal plane* to the curve at each point.

8.4.1 Curvature and Torsion

The definition of $\mathbf{p}(\xi)$ and $\mathbf{b}(\xi)$ incurs the introduction of two functions, the *curvature* $\kappa(\xi)$ and *torsion* $\tau(\xi)$, identifying intrinsic geometrical properties of space curves.²⁸ The curvature of a space curve, unlike that of a plane curve, is by definition a *non-negative* quantity. Torsion is what distinguishes a true or “twisted” space curve: the torsion of a plane curve is identically zero.

Assuming $\mathbf{r}(\xi)$ is regular, its second derivative is again given by equation (8.4), and we introduce the curvature and the principal normal by writing the derivative of the tangent vector as

$$\mathbf{t}'(\xi) = \sigma(\xi)\kappa(\xi)\mathbf{p}(\xi) \quad (8.66)$$

with the stipulation that $\kappa(\xi) \geq 0$, i.e., $\mathbf{p}(\xi)$ is a unit vector in the direction of $\mathbf{t}'(\xi)$ — which is necessarily orthogonal to $\mathbf{t}(\xi)$ since this is a unit vector. From relations (8.1), (8.4), (8.66) and the fact that the tangent and principal normal are orthogonal, one may then deduce that κ and \mathbf{p} are given by

$$\kappa(\xi) = \frac{|\mathbf{r}'(\xi) \times \mathbf{r}''(\xi)|}{|\mathbf{r}'(\xi)|^3} \quad (8.67)$$

and

²⁸ The torsion is often called *second curvature* in early papers on the theory of space curves, consistent with the notion that they are “doubly curved” loci (see §9.4.2).

$$\mathbf{p}(\xi) = \frac{\mathbf{r}'(\xi) \times \mathbf{r}''(\xi)}{|\mathbf{r}'(\xi) \times \mathbf{r}''(\xi)|} \times \mathbf{t}(\xi). \quad (8.68)$$

We define the binormal to be the unit vector

$$\mathbf{b}(\xi) = \mathbf{t}(\xi) \times \mathbf{p}(\xi) = \frac{\mathbf{r}'(\xi) \times \mathbf{r}''(\xi)}{|\mathbf{r}'(\xi) \times \mathbf{r}''(\xi)|}, \quad (8.69)$$

so that \mathbf{t} , \mathbf{p} , \mathbf{b} form a right-handed orthonormal triad, the *Frenet frame*, at each point of the curve. Now if (8.69) were a constant vector (i.e., $\mathbf{b}'(\xi) \equiv \mathbf{0}$), $\mathbf{t}(\xi)$ and $\mathbf{p}(\xi)$ at each curve point would lie in a plane orthogonal to this fixed vector, and $\mathbf{r}(\xi)$ would necessarily be a *plane* curve. Therefore, to elucidate the essential three-dimensional nature of a “twisted” space curve, we need to study the variation of $\mathbf{b}(\xi)$ along the curve.

Differentiating the relation $\mathbf{b} = \mathbf{t} \times \mathbf{p}$, and noting that $\mathbf{t}' = \sigma\kappa \mathbf{p}$, we have $\mathbf{b}' = \mathbf{t} \times \mathbf{p}'$. Now since \mathbf{p} is a unit vector, its derivative \mathbf{p}' must lie in the plane orthogonal to it, spanned by \mathbf{b} and \mathbf{t} . Clearly, only the component of \mathbf{p}' along \mathbf{b} contributes to \mathbf{b}' , and hence we write

$$\mathbf{b}'(\xi) = \sigma(\xi) \tau(\xi) \mathbf{t}(\xi) \times \mathbf{b}(\xi) = -\sigma(\xi) \tau(\xi) \mathbf{p}(\xi). \quad (8.70)$$

Here $\sigma(\xi)\tau(\xi)$ represents the *magnitude* of $\mathbf{b}'(\xi)$. We write it in this manner to ensure that the function $\tau(\xi)$ — the *torsion* of $\mathbf{r}(\xi)$ — will be independent of the parameterization. To derive an expression for it, we write $\mathbf{r}' \times \mathbf{r}'' = \sigma^3 \kappa \mathbf{b}$ using (8.67) and (8.69). Differentiating this and invoking (8.70), we obtain

$$\mathbf{r}' \times \mathbf{r}''' = -\sigma^4 \kappa \tau \mathbf{p} + \sigma^2 (3\sigma' \kappa + \sigma \kappa') \mathbf{b},$$

and taking the dot product of this with the expression

$$\mathbf{r}'' = \sigma' \mathbf{t} + \sigma^2 \kappa \mathbf{p} \quad (8.71)$$

obtained from (8.4) and (8.6), we have

$$(\mathbf{r}' \times \mathbf{r}''') \cdot \mathbf{r}'' = -\sigma^6 \kappa^2 \tau,$$

where we make use of the fact that \mathbf{t} , \mathbf{p} , \mathbf{b} are mutually orthogonal. Thus, re-arranging the triple product and using (8.67), we deduce that

$$\tau(\xi) = \frac{[\mathbf{r}'(\xi) \times \mathbf{r}''(\xi)] \cdot \mathbf{r}'''(\xi)}{|\mathbf{r}'(\xi) \times \mathbf{r}''(\xi)|^2}. \quad (8.72)$$

The first, second, and third derivatives of $\mathbf{r}(\xi)$ must be linearly independent (an impossibility for a plane curve) for the torsion to be non-zero. Unlike the curvature, the torsion may assume both negative and positive values.

8.4.2 The Frenet Frame

At each point on a regular space curve with $\kappa \neq 0$, the vectors \mathbf{t} , \mathbf{p} , \mathbf{b} given by (8.3), (8.68), (8.69) define a right-handed system of orthogonal axes, called the *Frenet frame*, that offers a natural perspective on the local curve geometry (see Fig. 8.26). The mutually perpendicular planes through each curve point orthogonal to \mathbf{b} , \mathbf{t} , and \mathbf{p} are known as the *osculating*, *normal*, and *rectifying* planes. These planes are evidently spanned by the vector pairs (\mathbf{t}, \mathbf{p}) , (\mathbf{p}, \mathbf{b}) , and (\mathbf{b}, \mathbf{t}) . We may elucidate their geometrical significance as follows.

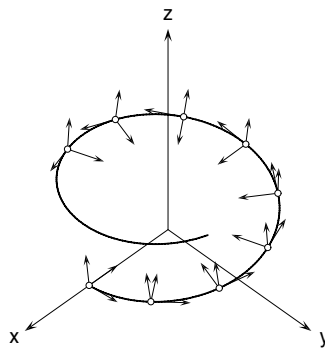


Fig. 8.26. The variation of the Frenet frame $(\mathbf{t}, \mathbf{p}, \mathbf{b})$ along a circular helix.

The normal plane is the easiest to visualize. It is simply the plane through each curve point that is orthogonal to the tangent (8.3) there — the normal plane “cuts the curve orthogonally” at each point. Now there are infinitely many planes that meet the curve tangentially at a given point (i.e., that have *first-order contact* with the curve there) — namely, the family or “pencil” of planes that contain the curve tangent at that point. If $\kappa \neq 0$, however, there is a *unique* member of this family, the osculating plane, that has *second-order* contact with the curve. Thus, the osculating plane at any point is the plane that “most nearly contains the curve” in a neighborhood of that point.

Finally, the rectifying plane has a more subtle geometrical significance. The *envelope* of the family of rectifying planes to a space curve — i.e., the surface that touches each rectifying plane — is known as the *rectifying developable* of that curve. The term “developable” is employed to describe a ruled surface, regarded as a thin material sheet, that we may flatten or *develop* onto a plane without “stretching” or “compressing” the material (see §8.5.6). A remarkable property of the rectifying developable is that, upon development onto a plane, the space curve embedded in it is transformed or “rectified” to a *straight line*. Since surface development incurs no dilation/compression, and thus preserves lengths, the arc length of any segment of the space curve is equal to that of the corresponding line segment after flattening its rectifying developable.

8.4.3 Inflections of Space Curves

At points where $\kappa = 0$, a space curve exhibits *second* — rather than first — order contact with its tangent line. We regard such points, where the normal (8.68) and binormal (8.69) are evidently indeterminate,²⁹ as the *inflections* of a space curve. Now for a regular space curve, the curvature vanishes only if (i) $\mathbf{r}'' = \mathbf{0}$, or (ii) \mathbf{r}' and \mathbf{r}'' are parallel. In either circumstance, \mathbf{p} and \mathbf{b} will ordinarily both suffer a sudden reversal on traversing the inflection.

This may be compared with our treatment of plane curves — where the fact that we defined κ to be a *signed* quantity allowed the normal \mathbf{p} to vary *continuously*, even through an inflection. One may, in principle, also define a signed curvature for space curves that yields continuous normal and binormal vectors through the curve inflections. The approach has the disadvantage that \mathbf{p} , \mathbf{b} , and κ are no longer determined by strictly “local” curve attributes as in (8.67)–(8.69). Instead, we must fix them at a specific curve point and then keep track of how many inflections we traverse to reach any point of interest.

8.4.4 Intrinsic Equations

The arc length of a space curve is given by the integral (8.13), with the speed (8.65) for a three-dimensional curve as integrand. In terms of the arc-length parameterization $\mathbf{r}(s)$, the Frenet frame may be expressed as

$$\mathbf{t}(s) = \dot{\mathbf{r}}(s), \quad \mathbf{p}(s) = \frac{\ddot{\mathbf{r}}(s)}{\kappa(s)}, \quad \mathbf{b}(s) = \mathbf{t}(s) \times \mathbf{p}(s).$$

Here the curvature is simply $\kappa(s) = |\ddot{\mathbf{r}}(s)|$, while the torsion $\tau(s)$ equals the triple product of the first three arc-length derivatives divided by $|\ddot{\mathbf{r}}(s)|^2$.

With the above definitions, the *Frenet–Serret equations*

$$\frac{d\mathbf{t}}{ds} = \kappa \mathbf{p}, \quad \frac{d\mathbf{p}}{ds} = -\kappa \mathbf{t} + \tau \mathbf{b}, \quad \frac{d\mathbf{b}}{ds} = -\tau \mathbf{p} \quad (8.73)$$

characterize the arc-length variation of the Frenet frame along a space curve. The French mathematician Jean Gaston Darboux (1842–1917) observed that, upon introducing the vector

$$\mathbf{d} = \kappa \mathbf{b} + \tau \mathbf{t}, \quad (8.74)$$

equations (8.73) can be cast in the more compact and enlightening form

$$\frac{d\mathbf{t}}{ds} = \mathbf{d} \times \mathbf{t}, \quad \frac{d\mathbf{p}}{ds} = \mathbf{d} \times \mathbf{p}, \quad \frac{d\mathbf{b}}{ds} = \mathbf{d} \times \mathbf{b}. \quad (8.75)$$

The *Darboux vector* (8.74) evidently lies in the rectifying plane at each point, and we may interpret its geometrical significance as follows.

²⁹ At an inflection, we may regard *any* two vectors in the normal plane that comprise a right-handed orthonormal system with the tangent \mathbf{t} as the Frenet frame.

Equations (8.75) indicate that the instantaneous rate of change of each of the vectors \mathbf{t} , \mathbf{p} , \mathbf{b} is orthogonal to itself *and* to the vector \mathbf{d} . This behavior characterizes an *instantaneous rotation* of the Frenet frame about the axis defined by (8.74): we may regard \mathbf{t} , \mathbf{p} , \mathbf{b} as instantaneously sweeping conical surfaces about \mathbf{d} as a common axis. If we describe the orientation of any of these vectors about \mathbf{d} by an azimuthal angle ϕ , the magnitude

$$\omega = |\mathbf{d}| = \sqrt{\kappa^2 + \tau^2}$$

of the Darboux vector corresponds to the instantaneous rotation rate, $d\phi/ds$. Thus ω is usually called the “total curvature” of a space curve.

Of course, \mathbf{d} varies in both magnitude and direction along a general space curve, and that is why we emphasize that it describes the “instantaneous” rate of rotation of the Frenet frame. Now if functions $\kappa(s)$ and $\tau(s)$ that specify the arc-length variation of curvature and torsion are given, together with an “initial” point \mathbf{r}_0 and corresponding frame $(\mathbf{t}_0, \mathbf{p}_0, \mathbf{b}_0)$ at $s = 0$, equations (8.73) may be integrated to yield $(\mathbf{t}, \mathbf{p}, \mathbf{b})$ as functions of s , and a space curve is then uniquely defined by

$$\mathbf{r}(s) = \mathbf{r}_0 + \int_0^s \mathbf{t}(u) du. \quad (8.76)$$

Thus, $\kappa(s)$ and $\tau(s)$ are known as the *intrinsic equations* of a space curve.

Unfortunately, except for trivial $\kappa(s), \tau(s)$ this integration does not yield closed-form expressions for the curve $\mathbf{r}(s)$ in terms of elementary functions (even a symbolic expression of the process, the generalization of (8.15)–(8.16) for plane curves, is rather involved). The equations (8.73) are not independent, since any solution $(\mathbf{t}, \mathbf{p}, \mathbf{b})$ to them must be an orthonormal frame. Thus, one could eliminate \mathbf{p} and \mathbf{b} among (8.73) to obtain a second-order (non-linear) equation for \mathbf{t} , whose solutions may be used directly in (8.76).

Knowing values and derivatives $\kappa_0, \dot{\kappa}_0, \dots$ and $\tau_0, \dot{\tau}_0, \dots$ of $\kappa(s)$ and $\tau(s)$ at an initial point \mathbf{r}_0 from which we measure s , the curve can be expressed as an infinite series for $\mathbf{r}(s) - \mathbf{r}_0$ of the form

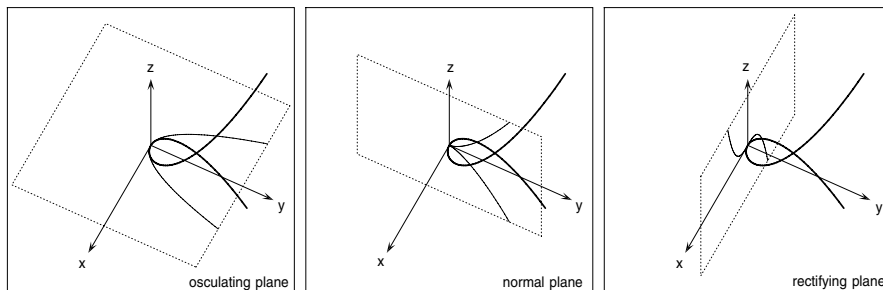


Fig. 8.27. Projections of the cubic $\mathbf{r}(\xi) = (\xi, \xi^2, \xi^3)$ onto its osculating, normal, and rectifying planes at the origin — these planes coincide with the coordinate planes.

$$\left(s - \frac{\kappa_0^2}{6} s^3 \dots \right) \mathbf{t}_0 + \left(\frac{\kappa_0}{2} s^2 + \frac{\dot{\kappa}_0}{6} s^3 \dots \right) \mathbf{p}_0 + \left(\frac{\kappa_0 \tau_0}{6} s^3 \dots \right) \mathbf{b}_0, \quad (8.77)$$

where $(\mathbf{t}_0, \mathbf{p}_0, \mathbf{b}_0)$ is the Frenet frame at \mathbf{r}_0 , and only cubic and lower-order terms are shown. We observe that, at a generic point with $\kappa_0 \neq 0$ and $\tau_0 \neq 0$, the projections of $\mathbf{r}(s)$ onto its osculating, normal, and rectifying planes at \mathbf{r}_0 look “locally” like a parabola, a cuspidal cubic, and an inflectional cubic, respectively — see, for example, Fig. 8.27.

8.5 Intrinsic Geometry of Surfaces

A parametric surface representation is specified by a vector function $\mathbf{r}(u, v)$ in \mathbb{R}^3 of two variables or *parameters*. Subscripts denote partial derivatives of this function with respect to the parameters. We confine our attention here to *regular* surfaces. As an immediate generalization of the curve case, this means that $\mathbf{r}_u \neq \mathbf{0}$ and $\mathbf{r}_v \neq \mathbf{0}$ — i.e., a change in either parameter induces a motion on the surface. But we also require such motions due to increments in u, v to be linearly independent: \mathbf{r}_u and \mathbf{r}_v should be non-parallel. Thus, the general regularity condition is that $\mathbf{r}_u \times \mathbf{r}_v \neq \mathbf{0}$ throughout the domain of interest.

Whereas non-regular points on curves are usually *geometrical singularities* (cusps), surfaces may have points that are geometrically smooth and singular only in the *parameterization* — e.g., the “poles” on a sphere described by lines of latitude and longitude. Another fundamental difficulty with surfaces is that there is no (global) equivalent to the “natural” or arc-length parameterization of curves, that serves to simplify the intrinsic geometry of surfaces.

8.5.1 First Fundamental Form

Consider the displacement $d\mathbf{r}$ between two points $\mathbf{r}(u, v)$ and $\mathbf{r}(u+du, v+dv)$ on a surface. Expanding in a bivariate Taylor series, we may write

$$\begin{aligned} d\mathbf{r} &= \mathbf{r}(u+du, v+dv) - \mathbf{r}(u, v) \\ &= \mathbf{r}_u du + \mathbf{r}_v dv + \frac{1}{2} (\mathbf{r}_{uu} du^2 + 2 \mathbf{r}_{uv} du dv + \mathbf{r}_{vv} dv^2) + \dots \end{aligned} \quad (8.78)$$

To first order in du and dv , the distance ds between these points is given by

$$ds^2 = |d\mathbf{r}|^2 = E du^2 + 2F du dv + G dv^2, \quad (8.79)$$

where we set

$$E = \mathbf{r}_u \cdot \mathbf{r}_u, \quad F = \mathbf{r}_u \cdot \mathbf{r}_v, \quad G = \mathbf{r}_v \cdot \mathbf{r}_v. \quad (8.80)$$

The quadratic expression (8.79) in the differentials du and dv is known as the *first fundamental form* of the surface, and the functions (8.80) of (u, v) are its

“first fundamental coefficients” (they define the *metric tensor* of the surface,³⁰ considered as a two-dimensional non-Euclidean space: see Chap. 10).

The quantities (8.80) are also employed in the computation of surface area. An area element dA corresponding to parameter increments du and dv may be written, by the parallelogram rule, as $|\mathbf{r}_u du \times \mathbf{r}_v dv|$. Noting that

$$|\mathbf{r}_u \times \mathbf{r}_v|^2 = |\mathbf{r}_u|^2 |\mathbf{r}_v|^2 - (\mathbf{r}_u \cdot \mathbf{r}_v)^2 = EG - F^2 > 0 \quad (8.81)$$

for a regular surface, we may write the surface area A corresponding to any parameter domain Ω as

$$A = \iint_{\Omega} \sqrt{EG - F^2} \, du \, dv.$$

8.5.2 Second Fundamental Form

The partial derivatives \mathbf{r}_u and \mathbf{r}_v at each point span the surface *tangent plane* at that point (if they are linearly independent). This plane is orthogonal to the unit *surface normal vector*, defined by

$$\mathbf{n} = \frac{\mathbf{r}_u \times \mathbf{r}_v}{|\mathbf{r}_u \times \mathbf{r}_v|}. \quad (8.82)$$

Now the first fundamental form (8.79) characterizes the distance ds between $\mathbf{r}(u, v)$ and $\mathbf{r}(u + du, v + dv)$ in terms of a local approximation of the surface by its tangent plane — i.e., only *linear* terms in (8.78) are retained — and hence it conveys no information about the *curvature* of the surface.

To characterize the deviation of the surface from its tangent plane in the vicinity of any point (i.e., its curvature at that point) we must examine the *quadratic* terms in (8.78). Taking the dot product of (8.78) with (8.82) yields the component d^2h of $d\mathbf{r}$ orthogonal to the tangent plane:

$$2d^2h = 2\mathbf{n} \cdot d\mathbf{r} = Ldu^2 + 2Mdudv + Ndv^2, \quad (8.83)$$

where we write

$$L = \mathbf{n} \cdot \mathbf{r}_{uu}, \quad M = \mathbf{n} \cdot \mathbf{r}_{uv}, \quad N = \mathbf{n} \cdot \mathbf{r}_{vv}. \quad (8.84)$$

Note that we express the height d^2h of the point $\mathbf{r}(u + du, v + dv)$ above the tangent plane at $\mathbf{r}(u, v)$ as a *second-order* differential since, to first order, this neighboring point lies *in* the tangent plane. The quadratic expression (8.83) is known as the *second fundamental form* of the surface, the three functions (8.84) of (u, v) being its “second fundamental coefficients.”

³⁰ We adopt the notation E, F, G — and L, M, N in the second fundamental form (8.83) below — employed by Gauss in his pioneering studies of surface differential geometry, rather than the more sophisticated tensor notations of Chap. 10.

Whereas E, F, G can not vanish simultaneously at any point of a regular surface, we may have $L = M = N = 0$ at exceptional surface points, namely, locations where the tangent plane has (at least) second-order contact with the surface. We confine our surface curvature analysis to the generic case, with at least one of L, M, N non-zero, since otherwise it becomes quite cumbersome.

8.5.3 Curves Lying on a Surface

A curve lying on the surface $\mathbf{r}(u, v)$ may be defined by functions $u(t)$ and $v(t)$, that specify the variation of the surface parameters in terms of a parameter t describing position on the curve. An explicit representation of the locus as a space curve is obtained by the composition of the surface equation with these functions: $\mathbf{r}(t) = \mathbf{r}(u(t), v(t))$. Differentiating $\mathbf{r}(t)$ by the chain rule then gives

$$\mathbf{r}' = u' \mathbf{r}_u + v' \mathbf{r}_v = \sigma \mathbf{t}, \quad (8.85)$$

where primes indicate derivatives with respect to t and it is understood that the surface partial derivatives $\mathbf{r}_u, \mathbf{r}_v$ have $u(t), v(t)$ as their arguments. Here \mathbf{t} denotes the unit tangent vector to the curve, and from (8.80) we see that its parametric speed $\sigma(t) = |\mathbf{r}'(t)|$ may be written as

$$\sigma = \sqrt{Eu'^2 + 2Fu'v' + Gv'^2}. \quad (8.86)$$

The length of a segment $t \in [a, b]$ of the curve $u(t), v(t)$ lying on the surface $\mathbf{r}(u, v)$ may be obtained by integrating (8.86) between $t = a$ and $t = b$.

We see from (8.85) that the tangent \mathbf{t} at any point of a curve on $\mathbf{r}(u, v)$ resides within the surface tangent plane, spanned by \mathbf{r}_u and \mathbf{r}_v , at that point. Provided they are linearly independent, we may regard \mathbf{r}_u and \mathbf{r}_v as defining axes and scale lengths for “local coordinates” in the tangent plane. A vector such as (8.85), expressible in terms of the local basis $(\mathbf{r}_u, \mathbf{r}_v)$ at each point, is considered to lie “in the surface” at that point. We regard u' and v' to be *components* of the vector (8.85); their ratio $u' : v'$ specifies a *direction* in the surface there. Note that the magnitude of this vector is given by (8.86), rather than $\sqrt{u'^2 + v'^2}$, since in general the local coordinates are oblique.

The coefficients (8.80) of the first fundamental form also allow us to define the *angle* between two vectors (considered as curve tangents) “in” the surface. If $u_1(s), v_1(s)$ and $u_2(t), v_2(t)$ describe curves that intersect at a point (u_*, v_*) , i.e., there exist values s_* and t_* such that $u_1(s_*) = u_2(t_*) = u_*$ and $v_1(s_*) = v_2(t_*) = v_*$, the angle α between the two curves $\mathbf{r}_1(s) = \mathbf{r}(u_1(s), v_1(s))$ and $\mathbf{r}_2(t) = \mathbf{r}(u_2(t), v_2(t))$ at their intersection is given by

$$\cos \alpha = \frac{\mathbf{r}'_1 \cdot \mathbf{r}'_2}{|\mathbf{r}'_1| |\mathbf{r}'_2|} = \frac{Eu'_1 u'_2 + F(u'_1 v'_2 + u'_2 v'_1) + Gv'_1 v'_2}{\sqrt{Eu'^2_1 + 2Fu'_1 v'_1 + Gv'^2_1} \sqrt{Eu'^2_2 + 2Fu'_2 v'_2 + Gv'^2_2}}$$

where primes indicate derivatives with respect to s or t , as appropriate, and E, F, G are evaluated at (u_*, v_*) .

8.5.4 Normal Curvature of a Surface

We now differentiate (8.85) again using the chain rule to obtain

$$\mathbf{r}'' = u'^2 \mathbf{r}_{uu} + 2u'v' \mathbf{r}_{uv} + v'^2 \mathbf{r}_{vv} + u'' \mathbf{r}_u + v'' \mathbf{r}_v = \sigma' \mathbf{t} + \sigma^2 \kappa \mathbf{p}, \quad (8.87)$$

where the final expression comes from equation (8.71) with κ and \mathbf{p} being the curvature and principal normal of the space curve $\mathbf{r}(t)$.

In order to determine κ from equation (8.87), we take the dot product of both expressions for \mathbf{r}'' with the surface normal \mathbf{n} defined by (8.82). Noting that \mathbf{n} is orthogonal to \mathbf{r}_u , \mathbf{r}_v , and \mathbf{t} , and using (8.84) and (8.86), this yields

$$\kappa \cos \psi = \frac{Lu'^2 + 2Mu'v' + Nv'^2}{Eu'^2 + 2Fu'v' + Gv'^2}, \quad (8.88)$$

where ψ is the angle between the unit vectors \mathbf{p} and \mathbf{n} . Note that expression (8.88) depends on the ratio $u' : v'$, though not on the individual magnitudes of these derivatives — i.e., it is determined only by the *direction* of the curve tangent \mathbf{t} in the surface tangent plane, together with the angle ψ .

Now the principal normal \mathbf{p} to an arbitrary curve on the surface $\mathbf{r}(u, v)$ and the surface normal \mathbf{n} are both orthogonal to the curve tangent \mathbf{t} at each point, but they may have any relative orientation in the plane perpendicular to it — i.e., for a given ratio $u' : v'$, the factor $\cos \psi$ in (8.88) can be made to assume *any* value between -1 and $+1$ by a suitable choice for $u(t)$, $v(t)$.

In order to extract from (8.88) an “intrinsic” measure of surface curvature — one that depends *only* on direction in the tangent plane at each point — we must be more restrictive about the curves on the surface that we consider. Specifically, suppose that $u(t)$ and $v(t)$ define a *normal section* of the surface at the point of interest, i.e., its intersection with any plane that contains the surface normal \mathbf{n} there. There is an infinite family or “pencil” of such planes, each associated with a unique direction or ratio $u' : v'$ of derivatives.

For a normal section, the curve principal normal \mathbf{p} and surface normal \mathbf{n} are identical or opposite, and thus $\cos \psi = \pm 1$. Adopting the convention for plane curves introduced in §8.1, that κ is positive when the curve normal points *away* from the center of curvature, amounts to choosing $\cos \psi = -1$. Thus, the curvature of the normal section in the direction $u' : v'$ is

$$\kappa = - \frac{Lu'^2 + 2Mu'v' + Nv'^2}{Eu'^2 + 2Fu'v' + Gv'^2}, \quad (8.89)$$

and we call this the *normal curvature* of the surface for that direction.

8.5.5 Principal Curvatures and Directions

Expression (8.89) gives the normal curvature as a rational quadratic function of the ratio $u' : v'$ that describes the orientation of the section plane about the

surface normal \mathbf{n} at each point. We will now see that, in general, this function exhibits unique minimum and maximum values, corresponding to orthogonal directions on the surface. Writing (8.89) in the form

$$(Eu'^2 + 2Fu'v' + Gv'^2)\kappa + (Lu'^2 + 2Mu'v' + Nv'^2) = 0,$$

and differentiating with respect to u' and v' , we set $\partial\kappa/\partial u' = \partial\kappa/\partial v' = 0$ to identify extrema. This gives the homogeneous system of equations

$$\begin{bmatrix} \kappa E + L & \kappa F + M \\ \kappa F + M & \kappa G + N \end{bmatrix} \begin{bmatrix} u' \\ v' \end{bmatrix} = \begin{bmatrix} 0 \\ 0 \end{bmatrix} \quad (8.90)$$

for u' and v' . Now in order for a non-trivial solution $(u', v') \neq (0, 0)$ to exist, the matrix on the left-hand side must be singular — i.e., κ must satisfy

$$(\kappa E + L)(\kappa G + N) - (\kappa F + M)^2 = 0 \quad (8.91)$$

when it is an extremum. Noting that $EG - F^2 > 0$ everywhere on a regular surface, we may write equation (8.91) for the extremum normal curvatures as

$$\kappa^2 - 2H\kappa + K = 0,$$

where we introduce the quantities

$$K = \frac{LN - M^2}{EG - F^2} \quad \text{and} \quad H = \frac{2FM - EN - GL}{2(EG - F^2)}, \quad (8.92)$$

known as the *Gaussian curvature* and *mean curvature* at each surface point. In terms of (8.92) the minimum and maximum normal curvatures are evidently

$$\kappa_{\min} = H - \sqrt{H^2 - K} \quad \text{and} \quad \kappa_{\max} = H + \sqrt{H^2 - K}, \quad (8.93)$$

and these values are called the surface *principal curvatures* at the point under consideration. The normal curvature κ for *any* surface direction at that point satisfies $\kappa_{\min} \leq \kappa \leq \kappa_{\max}$. Conversely, the Gaussian and mean curvatures (8.92) may be expressed in terms of the principal curvatures as

$$K = \kappa_{\min}\kappa_{\max} \quad \text{and} \quad H = \frac{1}{2}(\kappa_{\min} + \kappa_{\max}). \quad (8.94)$$

The Gaussian and mean curvature (and hence also the principal curvatures) are *intrinsic* properties of the surface at each point — they remain unchanged under any non-singular re-parameterization of the surface.

Having computed the principal curvatures (8.93), the directions in which they are attained (i.e., the *principal directions* of the surface at each point) can be deduced from equations (8.90) as

$$u' : v' = -(\kappa_p F + M) : \kappa_p E + L = -(\kappa_p G + N) : \kappa_p F + M, \quad (8.95)$$

where $\kappa_p = \kappa_{\min}$ or κ_{\max} — the equality of the above ratios follows from the fact that both principal curvatures satisfy equation (8.91).

The principal directions on a surface are always orthogonal — by setting $u'_1 : v'_1 = -(\kappa_{\min}F+M) : \kappa_{\min}E+L$ and $u'_2 : v'_2 = -(\kappa_{\max}F+M) : \kappa_{\max}E+L$ in the numerator of the expression for $\cos \alpha$, and using (8.92) and (8.94), one may verify that the angle α between them satisfies $\cos \alpha = 0$.

Equations (8.93) indicate that $\kappa_{\min} = \kappa_{\max}$ if the quantities (8.92) satisfy $K = H^2$. In this degenerate case the principal directions are undefined, since the normal curvature is *independent of direction* — the surface looks locally like a sphere in the neighborhood of such an *umbilic* point. Equations (8.90) must be vacuous at an umbilic, i.e., they must be satisfied by *any* ratio $u' : v'$, indicating that the derivatives of the normal curvature with respect to u' and v' vanish identically. This means that each entry of the 2×2 matrix in (8.90) must be zero at an umbilic, and the normal curvature at such a point is thus

$$\kappa_{\text{umbilic}} = -\frac{L}{E} = -\frac{M}{F} = -\frac{N}{G}.$$

Conversely, any point at which the first and second fundamental coefficients are in the same proportions, $E : F : G = L : M : N$, must be an umbilic with normal curvature given by the above formulae.

Exceptionally, one of the ratios (8.95) that define the principal directions at a point may assume the indeterminate form $0 : 0$. In such cases the other ratio, which is necessarily determinate and of the form $0 : 1$ or $1 : 0$ if the point is not an umbilic, must be used to identify the principal direction — which evidently coincides with one of the coordinate directions.

Since the principal directions are orthogonal, we can construct a locally orthogonal parameterization (u, v) aligned with them in the neighborhood of any non-umbilic point, such that $|\mathbf{r}_u| = |\mathbf{r}_v| = 1$, $\mathbf{r}_u \cdot \mathbf{r}_v = 0$, $\mathbf{r}_{uv} = \mathbf{0}$ there.³¹ We then have $E = G = 1$ and $F = M = 0$, and expression (8.89) becomes $\kappa = -(L \cos^2 \alpha + N \sin^2 \alpha)$ on setting $u' : v' = \cos \alpha : \sin \alpha$, where α is the angle that the direction $u' : v'$ makes with that of κ_{\min} (say). Hence, we must have $L = -\kappa_{\min}$ and $M = -\kappa_{\max}$, and the dependence of κ on α at any non-umbilic point has the form

$$\kappa(\alpha) = \kappa_{\min} \cos^2 \alpha + \kappa_{\max} \sin^2 \alpha. \quad (8.96)$$

This relation is usually known as *Euler's theorem*.

8.5.6 Local Surface Shape

The sign of the Gaussian curvature is an indicator of the surface “shape” in the neighborhood of each point. If $K > 0$, the principal curvatures (and hence the

³¹ This form of local parameterization is known as a system of *isothermal coordinates* at the given point. It plays an important role in the theory of *minimal surfaces*, i.e., surfaces of minimum area bounded by a given closed space curve [351].

normal curvatures in all directions) have the *same* sign — corresponding to a “cup” shape. If $K < 0$, the principal curvatures are of *opposite* signs, and the normal curvature must vanish for some intermediate direction — we then have a “saddle” shape. These cases identify *elliptic* and *hyperbolic* points on the surface. Finally, if $K = 0$, at least one of the principal curvatures vanishes — the surface has a locally “cylindrical” shape at such a *parabolic* point.

Planes, cylinders, and cones are examples of simple surfaces with $K \equiv 0$. In general, surfaces that exhibit this property are called *developables*, since — if we imagine them to be made of thin sheets of flexible material — they can be “developed” or “flattened” onto a plane without any stretching or compressing of the material. A surface with $H \equiv 0$ is called a *minimal surface*, since it can be shown that, given a closed space curve C , the surface patch of least area that has C as its boundary must satisfy this condition [351].

Every developable is a ruled surface (i.e., we can consider it as being swept out by the continuous motion of a straight line), though not all ruled surfaces are developable.³² We observe from (8.92) that a surface is developable if its second fundamental coefficients satisfy $LN - M^2 \equiv 0$, where the trivial case $L = M = N = 0$ yields a plane. In fact, developables are indistinguishable from planes in terms of their “intrinsic” geometry — we may regard them as being essentially “non-curved” surfaces (see also §10.6).

From expression (8.89), we observe that the normal curvature vanishes in the surface directions $u' : v'$ for which $Lu'^2 + 2Mu'v' + Nv'^2 = 0$. Since this is a homogeneous quadratic expression in u' and v' , it has two solution ratios $u' : v'$ — not necessarily real or distinct — which identify what are called the *asymptotic directions* at the given surface point. Alternately, using (8.96), we can identify these directions by $\tan \alpha = \pm \sqrt{\kappa_{\min}/\kappa_{\max}}$.

At an elliptic point, the asymptotic directions are complex conjugates, and the normal curvature is of the same sign for all directions. A parabolic point has a single (repeated) asymptotic direction — the normal curvature vanishes in this direction but is otherwise of constant sign. Finally, the two asymptotic directions at a hyperbolic point are real and distinct: the normal curvature changes sign as we pass through them.

The *Dupin indicatrix*³³ is an intuitive means of visualizing the dependence of normal curvature on direction at a surface point. If $r = 1/\kappa$ is the (signed) radius of curvature, this plot shows how $\sqrt{|r|}$ varies with the surface direction α . Introducing coordinates $x = \sqrt{|r|} \cos \alpha$ and $y = \sqrt{|r|} \sin \alpha$ in the tangent plane, equation (8.96) at an elliptic point can be expressed as

$$\frac{x^2}{|r_{\min}|} + \frac{y^2}{|r_{\max}|} = 1$$

³² A ruled surface is developable if and only if the surface normal (8.82) is constant along each line or “ruling” of that surface.

³³ The French engineer/mathematician Charles Dupin (1784–1873) made pioneering contributions to differential geometry and its applications — see also §8.5.8.

which is the equation of an ellipse, while at a hyperbolic point we obtain

$$\frac{x^2}{|r_{\min}|} - \frac{y^2}{|r_{\max}|} = \pm 1$$

which defines two hyperbolae that are asymptotic — on opposite sides — to lines along the asymptotic directions at that point (these hyperbolae indicate the variation of $\sqrt{|r|}$ in the regimes where $r > 0$ and $r < 0$). Finally, for a parabolic point with (say) $\kappa_{\min} = 0$, the Dupin indicatrix becomes

$$y^2 = |r_{\max}|,$$

which represents two lines parallel to the asymptotic direction at that point.

It can be shown that, when the surface is cut by a plane parallel to the tangent plane at some point, and slightly below or above it, the section curve approximates a conic with the same shape (locally) as the Dupin indicatrix (at an elliptic point, of course, the section plane should not lie on the convex side of the surface; and at a hyperbolic point we have one hyperbola or the other according to whether it is “above” or “below” the tangent plane).

8.5.7 Gauss Map of a Surface

Equation (8.82) defines the unit normal \mathbf{n} at each point of a regular surface. If we translate these vectors so that they emanate from a common origin, their tips will lie on the surface of the unit sphere. This correspondence between the points of a surface and points on the unit sphere, defined by the orientation of (8.82), is called the *Gauss map* or “spherical image” of the surface.

The Gauss map imparts an intuitive meaning to the Gaussian curvature of a surface. Consider an area δA about some point \mathbf{p} of a regular surface — the Gauss map of this area will, in general, cover some area δS on the unit sphere³⁴ about the location of the surface normal \mathbf{n} at \mathbf{p} . The area δS defines the *solid angle* subtended by the normals at each point within δA — it is a measure of the (angular) “spreading out” of those normals. It can be shown that the Gaussian curvature at \mathbf{p} can be interpreted as the limiting ratio

$$K = \lim_{\delta A \rightarrow 0} \frac{\delta S}{\delta A},$$

when $\delta A \rightarrow 0$ in such a manner that its boundary curve shrinks to zero length. Thus, K measures the “rate of angular divergence” of the surface normal \mathbf{n} with respect to the surface area A at each point.

For a general — i.e., “doubly-curved” — surface, the Gauss map covers an area on the unit sphere. For a developable surface, however, it degenerates to a curve — since the normal is constant along each ruling of the surface. Finally, for a plane, the Gauss map is a single point on the unit sphere.

³⁴ The Gauss map is one-to-one in a neighborhood of elliptic or hyperbolic points.

In general, the Gauss map of a surface is not one-to-one since there may be two or more distinct surface points that have parallel normals. In fact, the Gauss map “folds back” on itself along those loci on the unit sphere that are the images of the *parabolic lines* on the surface — i.e., curves comprising only parabolic surface points (of zero Gaussian curvature).

8.5.8 Lines of Curvature

At each point (other than the umbilics) of a smooth surface, the ratios defined by (8.95) with $\kappa_p = \kappa_{\min}$ and κ_{\max} identify orthogonal directions, in which the normal curvature of the surface attains its minimum and maximum values. The *lines of curvature* of a surface are two families of curves on the surface, each tangent to one of the principal directions at every point, that form an “orthogonal net” covering the surface. Choosing the first of equations (8.95), we may formulate it as the pair of first-order differential equations

$$\frac{du}{dt} = -\alpha(\kappa_p F + M) \quad \text{and} \quad \frac{dv}{dt} = \alpha(\kappa_p E + L), \quad (8.97)$$

where $\alpha(t)$ is an arbitrary non-vanishing function — this function determines the *parameterization* of the line of curvature. To specify this function, it is natural to consider the line of curvature parameterized in terms of arc length s along it. Substituting $du = -\alpha(\kappa_p F + M) dt$ and $dv = \alpha(\kappa_p E + L) dt$ in the first fundamental form (8.79), we may obtain the parametric speed $\sigma = ds/dt$ associated with the representation (8.97). Dividing both sides of equations (8.97) by σ then gives the equations

$$\frac{du}{ds} = -\beta(\kappa_p F + M) \quad \text{and} \quad \frac{dv}{ds} = \beta(\kappa_p E + L) \quad (8.98)$$

governing the arc-length parameterization of a line of curvature, where

$$\beta = \frac{\pm 1}{\sqrt{E(\kappa_p F + M)^2 - 2F(\kappa_p F + M)(\kappa_p E + L) + G(\kappa_p E + L)^2}}.$$

The sign ambiguity is resolved by fixing the sense in which s increases.

Now the other ratio in (8.95) could have been used to obtain the system

$$\frac{du}{ds} = -\beta(\kappa_p G + N) \quad \text{and} \quad \frac{dv}{ds} = \beta(\kappa_p F + M), \quad (8.99)$$

in lieu of equations (8.98), where β is now defined by

$$\beta = \frac{\pm 1}{\sqrt{E(\kappa_p G + N)^2 - 2F(\kappa_p G + N)(\kappa_p F + M) + G(\kappa_p F + M)^2}}.$$

In tracing a line of curvature, it may be necessary to switch between (8.98) and (8.99) when *both* right-hand sides in one system vanish. As noted above,

this occurs when a principal direction coincides with that of one of the surface parameters. When making such a switch, a change of sign in the appropriate β expression may be necessary to ensure that the line of curvature is traced in a consistent sense. Of course, this works only for a non-umbilic point; neither of the systems (8.98) and (8.99) can be integrated at an umbilic.

In equations (8.98) and (8.99) it is understood that κ_p is consistently set to either κ_{\min} or κ_{\max} , as determined from (8.93) and (8.92) — these choices yield lines of “minimum” and “maximum” curvature. Since the differential equations are of first order, the determination of lines of curvature is an *initial value problem*. A unique pair of lines of curvature pass orthogonally through any specified point (other than an umbilic) — it is meaningless to speak of a line of curvature between two generic points of a surface.

Figure 8.28 illustrates lines of curvature on a “triaxial” ellipsoid (all three semi-axes are of unequal length) — in this case, the lines of curvature are all closed loops. They form an orthogonal net, except at the umbilics situated on the section containing the smallest and largest semi-axes. These curves were first accurately drawn — in plane projection — by Gaspard Monge in his 1807 treatise *Application de l’Analyse à la Géometrié*. He also employed them in a 1795 architectural design for the ellipsoidal roof of a new High Court building — the surface “patches” delineated by the lines of curvature would define the shapes of the roof tiles, and he proposed that chandeliers be suspended from the two umbilical points — see [367, p. 269].

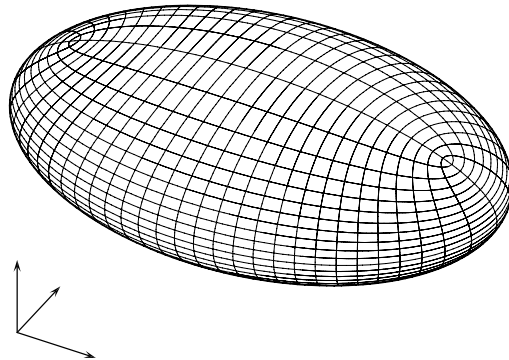


Fig. 8.28. Lines of curvature on a triaxial ellipsoid, forming an *orthogonal net* that divides the surface into 4-sided patches except at umbilic points (two are seen here).

The lines of curvature shown in Fig. 8.28 admit an elegant geometrical interpretation. For constants a, b, c and three different instances λ, μ, ν (such that $0 < \lambda < c^2 < \mu < b^2 < \nu < a^2$) of the parameter η in the equation

$$\frac{x^2}{a^2 - \eta} + \frac{y^2}{b^2 - \eta} + \frac{z^2}{c^2 - \eta} - 1 = 0, \quad (8.100)$$

we obtain three families of mutually orthogonal quadric surfaces with common foci: ellipsoids, hyperboloids of one sheet, and hyperboloids of two sheets. A unique member of each family passes through each point (x, y, z) and hence the parameters (λ, μ, ν) constitute a curvilinear coordinate system in \mathbb{R}^3 known as *confocal ellipsoidal coordinates*. In his *Développements de géométrie* of 1813 — with putative “applications to the stability of ships, excavation and fill, fortifications, optics, etc” — Charles Dupin, a student of Monge, demonstrated that if *any* three families of surfaces are mutually orthogonal, their pairwise intersection curves must be lines of curvature on each surface.³⁵ Hence, the curves in Fig. 8.28 are the intersections of the ellipsoid, defined by (8.100) with $\eta = \lambda$, with the hyperboloids defined by (8.100) with $\eta = \mu, \nu$.

In addition to the principal directions, identifying extrema of the normal curvature at each surface point, we also mentioned in §8.5.6 the asymptotic directions, in which the normal curvature vanishes. The *asymptotic lines* of a surface are defined, by analogy with the lines of curvature, to be those loci having the asymptotic directions as their tangents at each point. Unlike lines of curvature, however, real asymptotic lines exist only in regions of negative Gaussian curvature, and they are not orthogonal in general.

8.5.9 Geodesics on a Surface

The path of least length between distinct points in the plane is a straight line. *Geodesics* extend of this idea to curved surfaces — and, in general, curved or “non–Euclidean” spaces of any dimension (see Chap. 10). The geodesic corresponding to two distinct points (u_0, v_0) and (u_1, v_1) on a surface $\mathbf{r}(u, v)$ is the path *on the surface* that minimizes the distance

$$S = \int_0^1 \sqrt{E u'^2 + 2F u' v' + G v'^2} dt, \quad (8.101)$$

among differentiable functions $u(t), v(t)$ on $[0, 1]$ with $u(0) = u_0, v(0) = v_0$ and $u(1) = u_1, v(1) = v_1$. This is a problem in the *calculus of variations* [45]. Using arc length s along the geodesic as parameter, the path that minimizes (8.101) must satisfy the *Euler–Lagrange equations*

$$\begin{aligned} \frac{d^2u}{ds^2} + \Gamma_{uu}^u \left(\frac{du}{ds} \right)^2 + 2\Gamma_{uv}^u \frac{du}{ds} \frac{dv}{ds} + \Gamma_{vv}^u \left(\frac{dv}{ds} \right)^2 &= 0, \\ \frac{d^2v}{ds^2} + \Gamma_{uu}^v \left(\frac{du}{ds} \right)^2 + 2\Gamma_{uv}^v \frac{du}{ds} \frac{dv}{ds} + \Gamma_{vv}^v \left(\frac{dv}{ds} \right)^2 &= 0, \end{aligned} \quad (8.102)$$

where the *Christoffel symbols* are defined by

³⁵ Systems of mutually orthogonal surfaces are uncommon. In \mathbb{R}^2 we can construct a family of curves orthogonal to any given family, but two families of orthogonal surfaces in \mathbb{R}^3 do not, in general, admit a third family orthogonal to them.

$$\Gamma_{uu}^u = \frac{\mathbf{n} \cdot (\mathbf{r}_{uu} \times \mathbf{r}_v)}{|\mathbf{r}_u \times \mathbf{r}_v|}, \quad \Gamma_{uv}^u = \Gamma_{vu}^u = \frac{\mathbf{n} \cdot (\mathbf{r}_{uv} \times \mathbf{r}_v)}{|\mathbf{r}_u \times \mathbf{r}_v|}, \quad \Gamma_{vv}^u = \frac{\mathbf{n} \cdot (\mathbf{r}_{vv} \times \mathbf{r}_v)}{|\mathbf{r}_u \times \mathbf{r}_v|},$$

$$\Gamma_{uu}^v = \frac{\mathbf{n} \cdot (\mathbf{r}_u \times \mathbf{r}_{uu})}{|\mathbf{r}_u \times \mathbf{r}_v|}, \quad \Gamma_{uv}^v = \Gamma_{vu}^v = \frac{\mathbf{n} \cdot (\mathbf{r}_u \times \mathbf{r}_{uv})}{|\mathbf{r}_u \times \mathbf{r}_v|}, \quad \Gamma_{vv}^v = \frac{\mathbf{n} \cdot (\mathbf{r}_u \times \mathbf{r}_{vv})}{|\mathbf{r}_u \times \mathbf{r}_v|}.$$

The boundary value problem for the second-order system (8.102) between two points (u_0, v_0) and (u_1, v_1) does not necessarily have a unique solution. Also, its solutions identify all (local) *extrema* of the distance between these points, which may correspond to maxima as well as minima. To determine the true minimum-distance path in the case of multiple solutions, one must explicitly compute and compare the distance (8.101) for all the solutions.

Alternately, equations (8.102) may be regarded as defining an initial value problem — we specify a start point (u_0, v_0) and direction (\dot{u}_0, \dot{v}_0) satisfying

$$E_0 \dot{u}_0^2 + 2F_0 \dot{u}_0 \dot{v}_0 + G_0 \dot{v}_0^2 = 1$$

for arc-length parameterization, where the subscripts on the first fundamental coefficients indicate that they are evaluated at (u_0, v_0) — and there is then a unique geodesic emanating from this point in the specified direction.

Of course the geodesic equations (8.102), whether regarded as specifying an initial or a boundary value problem, rarely admit closed-form solutions. We must usually resort to numerical integration schemes to compute geodesics, and for this purpose it is more convenient to express (8.102) as a system of first-order equations in the unknowns $u, v, \dot{u} = du/ds, \dot{v} = dv/ds$:

$$\begin{aligned} \frac{du}{ds} &= \dot{u}, & \frac{d\dot{u}}{ds} &= -(\Gamma_{uu}^u \dot{u}^2 + 2\Gamma_{uv}^u \dot{u}\dot{v} + \Gamma_{vv}^u \dot{v}^2), \\ \frac{dv}{ds} &= \dot{v}, & \frac{d\dot{v}}{ds} &= -(\Gamma_{uu}^v \dot{u}^2 + 2\Gamma_{uv}^v \dot{u}\dot{v} + \Gamma_{vv}^v \dot{v}^2). \end{aligned} \quad (8.103)$$

Our discussion of geodesics thus far has been based upon purely analytical considerations: we shall now consider *geometrical* characterizations of these loci. One such characterization is based on the idea of “geodesic curvature” of curves on a surface. The geodesics on a surface are analogs of straight lines in the plane — we can regard them as the “straightest” curves that we can draw on the surface. While it may be difficult to visualize the “global straightness” of a curve on a surface, we can readily formulate *local* indicators of it. Namely, at each point of the curve we may perform an orthogonal projection onto the surface tangent plane. Then, as described in §8.1, the resulting plane curve has (modulo sign) a well-defined curvature — we call this the *geodesic curvature* of the given curve on the surface. Geodesics can then be identified as those curves on a surface whose geodesic curvature vanishes along their entire extent. In other words, geodesics are curves that appear “locally straight” viewed from the perspective of the surface tangent plane at each point along them. The following theorem gives another, closely-related, geometrical characterization:

Theorem 8.2 *The geodesics of a surface are those loci on the surface which, regarded as space curves, have a principal normal vector \mathbf{p} that coincides with the surface normal vector \mathbf{n} at each point.*

In other words the *rectifying plane* at every point of a geodesic, considered as an independent space curve, coincides with the surface *tangent plane*.

The above theorem can easily be verified by considering equation (8.87) for the second derivative of a curve on a surface, in the case of an arc-length parameterization. Since $\sigma \equiv 1$ and $\dot{\sigma} \equiv 0$, we have

$$\ddot{\mathbf{r}} = \dot{u}^2 \mathbf{r}_{uu} + 2\dot{u}\dot{v} \mathbf{r}_{uv} + \dot{v}^2 \mathbf{r}_{vv} + \ddot{u} \mathbf{r}_u + \ddot{v} \mathbf{r}_v = \kappa \mathbf{p},$$

where dots indicate arc-length derivatives. By considering a curve for which $\mathbf{p} \equiv \mathbf{n}$, and performing the following three steps: (a) take the cross product of this equation with \mathbf{r}_u and \mathbf{r}_v ; (b) dot the resulting equations with \mathbf{n} ; and (c) divide these equations by $|\mathbf{r}_u \times \mathbf{r}_v|$, we arrive at the geodesic differential equations (8.102) with the Christoffel symbols as given above.

The simplest non-trivial geodesics on a curved surface are, of course, the *great circles* of a sphere — i.e., its sections by those planes that pass through its center. In fact, it follows from Theorem 8.2 that if a surface is symmetrical about a plane, the section of the surface by that plane must be a geodesic. For example, the “profile” sections of a surface of revolution (by planes containing the axis of revolution) are geodesics. Note, however, that geodesics on closed surfaces are not always closed loci — Fig. 8.29 illustrates this for a torus.

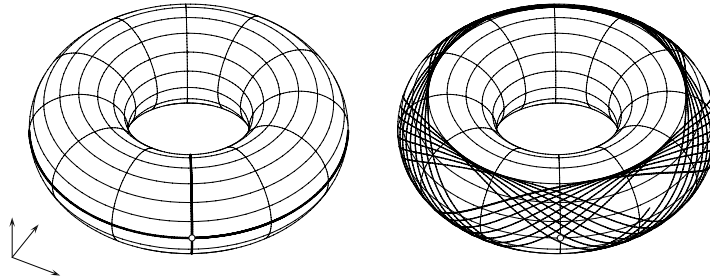


Fig. 8.29. Geodesics from a point on the “equatorial plane” of a torus. If the initial direction is in this plane or orthogonal to it, the geodesic is a closed path (left). For any other direction, the geodesic is a non-periodic path that “fills” a region (right).

The geodesic that passes through a given surface point (u_0, v_0) in a given direction (\dot{u}_0, \dot{v}_0) , corresponding to integration of (8.103) as an initial-value problem, is unique. However, equations (8.103) may have multiple solutions³⁶ if treated as a boundary value problem for the geodesic between two given

³⁶ Some of these may correspond to *maxima* of the distance S , since the derivation of (8.103) in §10.4 was based only on the condition that S be extremal.

points (u_0, v_0) and (u_1, v_1) . Examples in the case of two points on a torus are shown in Fig. 8.30. Ordinarily, the shortest of a family of multiple solution paths is taken as “the” geodesic — but even this may be non-unique (e.g., the infinitude of great-circle arcs between the “poles” of a sphere).

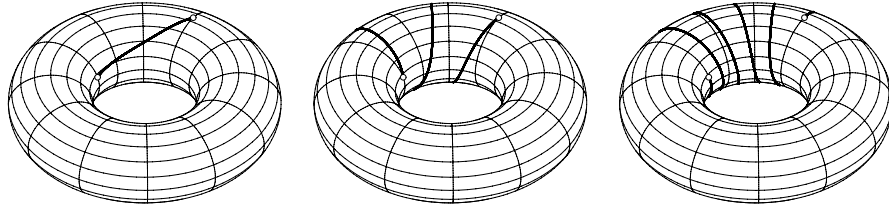


Fig. 8.30. Multiplicity of geodesic paths between two fixed points on a torus. There are actually infinitely-many such paths, corresponding to extrema (with respect to small path perturbations) of the total distance (8.101) between the specified points.

A physical model may help impart a better intuitive feel for the geodesic between specified points (for a surface of positive Gaussian curvature, at least). Imagine piercing the surface at the two points, and passing a thread through the holes so as to lie on the convex side. If the surface is frictionless, the thread slips across it and assumes the minimum-length shape of the geodesic path between those points, when pulled taut from the other side.

Although surfaces have no global “natural” parameterizations, analogous to arc-length parameterizations of curves, geodesics can be used to define such a parameterization *locally*, i.e., within the neighborhood of some chosen point (geodesic polar coordinates) or curve (geodesic parallel coordinates).

Geodesic polar coordinates are constructed by computing geodesics that emanate in all possible directions from a point P on the surface. The loci of points that lie at successive equal distances d from P along these geodesics are, for sufficiently small d , analogous to circles and they meet the geodesics orthogonally. However, distinct geodesics from P may intersect if extended too far, and the geodesic polar coordinates are then no longer valid.

Geodesic parallel coordinates are constructed by selecting a smooth curve C on the surface and computing geodesics orthogonal to this curve from each point on it. The loci of points that lie at successive equal distances d from the starting points on C of these geodesics meet the geodesics orthogonally, and thus form a system of “parallel” curves on the surface. Again, however, the coordinate system thus defined is only valid near C , since distinct geodesics orthogonal to C may intersect when extended too far.

Familiar examples of polar and parallel geodesic coordinate systems are the circles of latitude and longitude on a sphere, in the vicinity of its “poles” and its “equator,” respectively. Unfortunately, for more general surfaces, one cannot derive simple closed-form expressions for polar or parallel geodesic coordinate systems. Further details may be found in [290] and [433].

9

Algebraic Geometry

For the solution of any one of these problems of loci is nothing more than the finding of a point for whose complete determination one condition is wanting ... In every such case an equation can be obtained containing two unknown quantities.

René Descartes, *La Géométrie*

Algebraic geometry is the study of point sets satisfying polynomial equations in the Cartesian coordinates of two, three, or more dimensions. For example, a plane algebraic curve is just the set of points with two-dimensional Cartesian coordinates (x, y) on which some polynomial f vanishes: $f(x, y) = 0$. Similarly, an algebraic surface is the set of three-dimensional points (x, y, z) on which a polynomial g vanishes: $g(x, y, z) = 0$. These are examples of *implicit* curve and surface equations. They allow us to easily test whether a point lies on the curve or surface, but are not so convenient for generating points on it.

Whereas a plane algebraic curve is a one-dimensional locus, an algebraic surface is two-dimensional. Both are describable by a *single* equation since, in each case, the dimension of the locus is precisely one less than that of the Cartesian space in which it resides: we say that such loci are of *codimension* one. An algebraic space curve, on the other hand, is a one-dimensional locus residing in a three-dimensional space — it is of codimension two.

Hence, to describe an algebraic space curve, *two* polynomial equations $g(x, y, z) = h(x, y, z) = 0$ in the *three* Cartesian coordinates (x, y, z) must be specified. But this simply amounts to formulating the space curve as the set of points common to the two surfaces $g(x, y, z) = 0$ and $h(x, y, z) = 0$ — i.e., as the *intersection* of those surfaces. This fact incurs difficult theoretical issues, concerning the conditions under which two algebraic surfaces will intersect in a single “irreducible” space curve, or in a composite of such curves.

All of the (polynomial or rational) parametric curves and surfaces that are commonly used in computer-aided design fall within the realm of algebraic geometry, since the curve or surface parameters may always be “eliminated” to

obtain implicit polynomial equations in the Cartesian coordinates. However, the converse is *not* true: only a subset of all algebraic curves and surfaces are parameterizable using “simple” (polynomial or rational) functions.¹

The set of rational curves and surfaces is not flexible enough to encompass all loci that are needed in applications, especially those that are *derived* from rational loci through simple geometrical operations. We are thus often obliged to consider the full family of *algebraic* curves and surfaces. Our intent here is to impart a basic knowledge of their properties, the methods used to analyze them, and the conditions under which they are rational.

Although it admits a remarkable variety of curves and surfaces, there are loci of practical importance that lie beyond the scope of algebraic geometry — prominent examples of such “non–algebraic” or *transcendental* curves are the cycloid and the involute of a circle, discussed in §8.3 above.²

9.1 Parametric and Implicit Forms

We may regard a parametric representation of a plane curve as a description of its point set by *generating functions* $x(t)$ and $y(t)$ — to obtain an ordered sequence of points along the curve, we simply insert successive values of the parameter t into those functions. When an arbitrary point (x_0, y_0) is specified, however, the question — “does this point lie on the curve?” — is not so easy to address using a parametric representation; it amounts to determining whether the equations $x(t) = x_0$, $y(t) = y_0$ have a common root t .

An “implicit” representation $f(x, y) = 0$ of the curve, which amounts to a description of its point set by means of the *predicate function* $f(x, y)$, exhibits the opposite behavior. Determining whether (x_0, y_0) lies on the curve amounts to simply testing if $f(x_0, y_0)$ vanishes, but generating an ordered sequence of points along it from this representation is not a trivial matter.

In most computational contexts, parametric curve and surface forms are more convenient than implicit forms, and *ab initio* design is typically based on them. However, many “procedurally–defined” loci required in downstream applications, that are derived according to simple geometrical prescriptions from given (polynomial or rational) parametric curves and surfaces, belong to the realm of *non–rational* algebraic curves and surfaces. Examples include:

- the *offset* to a given curve or surface, i.e., the locus of a point that always maintains a *fixed distance* from that curve or surface;

¹ Since polynomial parameterizations are subsumed by rational parameterizations, we shall henceforth refer to such loci generically as *rational* curves and surfaces.

² Cartesian coordinates were criticized by Gilles Personne de Roberval (1602–1675), and subsequently also by Isaac Newton, on the grounds that the cycloid admits an elementary geometrical/kinematical description and analysis, but has no “simple” — i.e., algebraic — equation in Cartesian coordinates [219].

- the *bisector* of two given curves or surfaces, i.e., the locus of a point that remains *equidistant* with respect to those curves or surfaces;
- the *intersection* curve of two given surfaces, i.e., the locus of a point that lies *simultaneously* on both those surfaces.

As a practical necessity, such non-rational loci are usually approximated using (piecewise) rational forms by some numerical scheme. This often incurs severe penalties in terms of the accuracy, efficiency, memory requirements, and — most importantly — the *reliability* of the software system.

9.2 Plane Algebraic Curves

A plane algebraic curve of degree n is the locus of points (x, y) that satisfy an implicit polynomial equation of the form

$$f(x, y) = \sum_{j=0}^n \sum_{k=0}^{n-j} c_{jk} x^j y^k = 0. \quad (9.1)$$

In general, all terms of total degree $\leq n$ in x and y appear in this equation, and hence there are altogether

$$\binom{n+2}{2} = \frac{1}{2}(n+1)(n+2)$$

coefficients c_{jk} that define such a curve. The number of degrees of freedom of the curve is one less than this, however, since we may divide (9.1) through by any (non-zero) coefficient without altering the locus it defines.

The simplest non-trivial algebraic curves — the conics ($n = 2$) — were of course well-known to the ancient Greeks, although they treated these loci in purely geometrical terms. The introduction of Cartesian coordinates allowed a much richer class of higher-order algebraic curves to be studied, although at first Descartes did not fully comprehend the role of negative values of the coordinates. Thus, after drawing the “loop” of the cubic curve

$$x^3 + y^3 - 3xy = 0 \quad (9.2)$$

— known as the *folium of Descartes* — in the positive quadrant, he assumed that its form in the other three quadrants would simply be mirror images of this loop. The proper locus of the folium is shown in Fig. 9.1.

Newton subsequently made the same mistake, but soon corrected himself. Around 1670 he performed what was probably the first systematic study of higher-order algebraic curves [466] in his paper³ *Enumeratio curvarum trium*

³ An improved version, *Enumeratio linearum tertii ordinis*, identifying seventy-two different cubic curve types, was published in 1704 as an appendix to the *Opticks*.

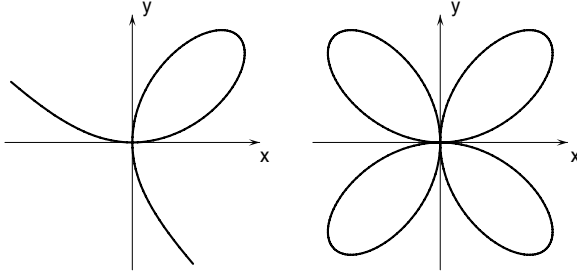


Fig. 9.1. Left: the correct geometry of the cubic curve (9.2) known as the folium of Descartes. Right: the erroneous four-fold symmetric form assumed by Descartes.

dimensionum (The enumeration of cubics), which attempts to determine an exhaustive taxonomy for the real loci defined by (9.1) when $n = 3$. Newton's scheme classified the cubics into nine cases, within which he identified sixteen "species" — these were further subdivided into "forms" and "grades" to yield a total of fifty-eight distinct types of cubic curve!

The intrinsic shape properties of the curve (9.1) may be determined from its implicit equation, although this is not as convenient as with the parametric equation. At a curve point (x_*, y_*) the vector $\nabla f = (f_x, f_y)$ defines the normal direction, and hence the equation of the tangent line is

$$f_x(x_*, y_*)(x - x_*) + f_y(x_*, y_*)(y - y_*) = 0. \quad (9.3)$$

By methods similar to those used in §8.1.2, one may verify that the curvature is given by the expression

$$\kappa = \frac{2f_x f_y f_{xy} - f_x^2 f_{yy} - f_y^2 f_{xx}}{(f_x^2 + f_y^2)^{3/2}} \quad (9.4)$$

evaluated at (x_*, y_*) — with the sign convention that $\kappa > 0$ when the center of curvature lies in the direction of ∇f and $\kappa < 0$ otherwise. However, equations (9.3) and (9.4) are not valid at a singular point, where $f_x = f_y = 0$.

The degree- n algebraic curve specified by (9.1) is said to be *irreducible* if the bivariate polynomial $f(x, y)$ does not factor into a product of lower-order (non-constant) polynomials, with real or complex coefficients,⁴ whose degrees sum to n . For a reducible curve, such that

$$f(x, y) = f_1(x, y) f_2(x, y) \cdots f_r(x, y), \quad (9.5)$$

the r lower-degree algebraic curves defined by $f_k(x, y) = 0$ for $k = 1, \dots, r$ are called the *components* of the curve $f(x, y) = 0$. Such a factorization⁵ of a

⁴ For example, $x^2 + y^2 = 0$ is reducible to the complex conjugate lines $x + iy = 0$, $x - iy = 0$. It has just one real point $(0, 0)$ — the intersection of those lines.

⁵ Whereas univariate polynomials can *always* be factorized into (possibly multiple) real or complex linear terms, the factorization (9.5) of a bivariate (or multivariate) polynomial into several non-constant terms is an exceptional circumstance.

reducible curve may exhibit squares, cubes, or higher powers of certain factors — these terms identify *multiple components* of the curve.

We confine our attention here to irreducible curves. In most applications, we are interested in only *finite real points* (x, y) of the locus defined by (9.1). However, to develop a comprehensive theory of such curves, we must broaden our perspective in two respects, to encompass: (i) *complex points* as well as real points; and (ii) *points at infinity* as well as finite points. In other words, we will need to consider the locus of the algebraic curve (9.1) over the entire *complex projective plane*, rather than just the real affine plane.

We are comfortable with the idea that a degree- n univariate polynomial $f(x)$ with real coefficients has, in general, both real and complex conjugate roots. Similarly, a degree- n algebraic curve $f(x, y) = 0$ with real coefficients — being the zero set of a bivariate polynomial — defines both a real and a complex locus, the latter comprising points with complex coordinates (x, y) that occur in conjugate pairs. Whereas the real locus may be drawn in the Cartesian plane, the complex locus is not so easy to visualize — it resides in a *four-dimensional* space, since x and y each have real and imaginary parts. Just as the univariate polynomial $f(x)$ has exactly n real or complex roots, we shall see that consideration of the both real and complex loci of the algebraic curve $f(x, y) = 0$ leads to important simplifications.

The behavior of the algebraic curve $f(x, y) = 0$ at infinity is determined by *homogenizing* equation (9.1): we substitute $x = X/W$, $y = Y/W$ and clear denominators by multiplying through by W^n to obtain an equation

$$F(W, X, Y) = W^n f(X/W, Y/W) = \sum_{j=0}^n \sum_{k=0}^{n-j} c_{jk} W^{n-j-k} X^j Y^k = 0 \quad (9.6)$$

where each term has total degree n in the homogeneous coordinates W, X, Y (see §7.4). Points at infinity of the curve (9.1) are then identified by triples of the form $(0, X, Y)$ that satisfy (9.6) for real or complex values X, Y .

9.2.1 Singular Points

In general, almost every point of the algebraic curve (9.1) is “regular” in the sense that we can identify a unique curve tangent, and a generic line through that point is considered to have a single intersection with the curve there.

However, irreducible curves of degree $n \geq 3$ may also have “exceptional” or *singular* points, where the curve has more than one tangent, and a generic line is regarded as intersecting the curve more than once. The singular points of algebraic curves are not merely mathematical curiosities: the analysis of such points allows us to address an important practical question, namely, whether or not such curves admit *rational parameterizations*.

Now the existence of singular points on an algebraic curve is actually an exceptional circumstance, requiring the satisfaction of *three* equations in *two* variables. Consequently, an algebraic curve of the form (9.1) of degree $n \geq 3$

with randomly-chosen coefficients c_{jk} has, in general, no singular points and cannot be parameterized in terms of rational functions. On the other hand, any rational curve that is specified by homogeneous-coordinate polynomials $W(t)$, $X(t)$, $Y(t)$ can always be described by an implicit polynomial equation of the form (9.1) by “elimination” of the parameter t from the two equations

$$x = \frac{X(t)}{W(t)} \quad \text{and} \quad y = \frac{Y(t)}{W(t)}$$

(see §9.2.10 below). Hence, the rational curves evidently form a *proper subset* of all algebraic curves.

9.2.2 Intersections with a Straight Line

Our analysis of singular points is based on examining the intersection points of a straight line with an algebraic curve. Suppose that (x_0, y_0) is a point on the curve (9.1). We consider the parametric equations

$$x(t) = x_0 + \lambda t, \quad y(t) = y_0 + \mu t \quad (9.7)$$

of a line through that point, with orientation specified by the direction cosines (λ, μ) . Substituting (9.7) into the curve equation (9.1) and expanding in a bivariate Taylor series about (x_0, y_0) yields the univariate function

$$\begin{aligned} F(t) &= f(x_0 + \lambda t, y_0 + \mu t) \\ &= [f_x^{(0)}\lambda + f_y^{(0)}\mu]t + [f_{xx}^{(0)}\lambda^2 + 2f_{xy}^{(0)}\lambda\mu + f_{yy}^{(0)}\mu^2]t^2 + \dots \end{aligned} \quad (9.8)$$

of t , where the superscripts on the partial derivatives of $f(x, y)$ indicate that they are evaluated at (x_0, y_0) . Note that (9.8) is a *polynomial of degree n* in t , since all the partial derivatives of $f(x, y)$ of order $> n$ vanish identically. Furthermore, it has no constant term since the point (x_0, y_0) lies on the curve by supposition, and therefore $f(x_0, y_0) = 0$. The roots of the polynomial (9.8) identify the locations along the line (9.7) where it intersects the algebraic curve (9.1). The Fundamental Theorem of Algebra indicates that $F(t)$ has precisely n real or complex roots (counted according to their multiplicities) and hence we infer that *a straight line intersects an irreducible degree-n algebraic curve in n points* (not necessarily all real, distinct, or affine).

9.2.3 Double Points of Algebraic Curves

Since it has no constant term, $t = 0$ is evidently a root of the polynomial (9.8) — corresponding to the fact that (x_0, y_0) lies on the curve (9.1). Ordinarily, $t = 0$ is a *simple* root of (9.8), but if the coefficient of the linear term vanishes, it becomes a *multiple* root — indicating that the line (9.7) has *more than one* intersection with the curve (9.1) at (x_0, y_0) . This may occur under two distinct circumstances:

- (a) If $f_x^{(0)}, f_y^{(0)}$ are not both zero, there is a *unique* line through (x_0, y_0) that causes the coefficient of the linear term in (9.8) to vanish, namely, the line whose orientation is specified by the particular ratio

$$\lambda : \mu = -f_y^{(0)} : f_x^{(0)}.$$

In this case (x_0, y_0) is a regular point of the curve, and the above direction identifies the unique *tangent* to the curve there. Thus, the tangent line at any curve point is considered to have, in general, a two-fold intersection with the curve at that point.⁶

- (b) If, on the other hand, $f_x^{(0)} = f_y^{(0)} = 0$, the coefficient of the linear term in (9.8) vanishes for *any* orientation $\lambda : \mu$ of the line through (x_0, y_0) — i.e., *every* line through that point has (at least) a two-fold intersection with the curve there. If the second derivatives of f are not all zero at (x_0, y_0) we call it a *double point* of the curve. Certain lines through a double point (x_0, y_0) actually have *more than two* intersections with the curve there — their orientations are such as to make the coefficient of the quadratic term in (9.8) vanish, i.e., (λ, μ) satisfy

$$f_{xx}^{(0)}\lambda^2 + 2f_{xy}^{(0)}\lambda\mu + f_{yy}^{(0)}\mu^2 = 0. \quad (9.9)$$

Since this is a homogeneous quadratic equation in λ and μ , it possesses two solutions for the ratio $\lambda : \mu$. The lines that these solutions identify are the *two tangents* to the curve at the double point.

A double point has one of three morphologies, according to the nature of its two tangents: (i) a *crunode*, or real self-intersection, if the tangent directions are real and distinct; (ii) a *cusp* if the tangent directions are coincident; and (iii) an *acnode*, or isolated real point, if the tangent directions are complex conjugates.⁷ These types may be illustrated by the cubics

$$f(x, y) = x^3 + kx^2 + y^2 = 0. \quad (9.10)$$

The origin $(0, 0)$ is a double point, because $f = f_x = f_y = 0 \neq f_{xx}, f_{yy}$ there. Equation (9.9) defining the tangents at this double point yields $k\lambda^2 + \mu^2 = 0$, and choosing $k = -1, 0, +1$ gives a double point with distinct real tangents, coincident tangents, and complex conjugate tangents, as shown in Fig. 9.2.

For the case of two coincident tangents, curves of degree > 3 may exhibit double point morphologies more involved than the cusp shown in Fig. 9.2 — we investigate some of them in §9.2.6 below (see Examples 9.2 and 9.3).

⁶ We assume that the point under consideration is not an inflection.

⁷ If the coefficients of (9.1) are real, its complex locus consists of conjugate point sets. An acnode, being a point common to conjugate portions of the curve, must be real — though no other real curve points exist in its immediate vicinity.

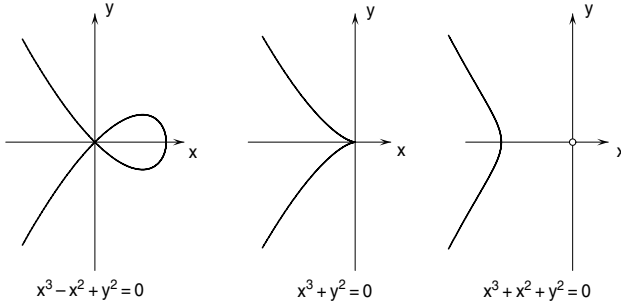


Fig. 9.2. The cubics (9.10) illustrating three possible morphologies of a double point — namely, a real self-intersection, a cusp, and an isolated real point (at the origin).

9.2.4 Higher-order Singular Points

We characterized (x_0, y_0) as a double point of the curve (9.1) by the property that lines of *any* orientation through that point have a two-fold intersection with the curve there — i.e., $t = 0$ is a double root of the polynomial (9.8) for arbitrary (λ, μ) . This idea may be easily extended to define triple, quadruple, and higher-order singular points. Thus (x_0, y_0) is said to be a singular point of *multiplicity m* (or an m -fold singular point) on the curve $f(x, y) = 0$ if all partial derivatives of f of order $\leq m - 1$ vanish at (x_0, y_0) but at least one of order m does not. This means that $t = 0$ is an m -fold root of the polynomial (9.8) for any (λ, μ) . The curve has m tangents (not necessarily real or distinct) at an m -fold point (x_0, y_0) , with orientations $\lambda : \mu$ given by the solutions of

$$\sum_{k=0}^m \binom{m}{k} \frac{\partial^m f^{(0)}}{\partial x^{m-k} \partial y^k} \lambda^{m-k} \mu^k = 0, \quad (9.11)$$

where again the partial derivatives are evaluated at (x_0, y_0) . The expression on the left is just the coefficient of the t^m term in equation (9.8).

We say that an m -fold singular point is *ordinary* if equation (9.11) has m distinct (real or complex) solutions $\lambda : \mu$, i.e., there are no multiple tangents. An ordinary m -fold point is considered to be the “equivalent” of $\frac{1}{2}m(m - 1)$ double points — an ordinary triple point, for example, may be considered as arising from a coalescence of three double points (see Example 9.1). However, a non-ordinary singular point requires a sophisticated analysis to determine its “equivalent” number of double points — see §9.2.6 below.

9.2.5 Genus of an Algebraic Curve

There are limits on the number and nature of singular points of an irreducible degree- n curve. For example, a conic ($n = 2$) cannot have *any* singular points: if one existed, a line drawn through it and any other point of the curve would

intersect the conic more than twice, which contradicts the conclusion of §9.2.2 that a straight line intersects a degree- n curve in exactly n points.

A cubic may have at most one double point — if any other singular point existed, a line drawn through it and the double point would have more than three intersections with the cubic. Similar arguments show that a quartic may have one triple point or up to three double points and, in general, a degree- n curve may have no individual singular point of multiplicity $> n - 1$, nor any combination of singular points equivalent to $> \frac{1}{2}(n - 1)(n - 2)$ double points.

The difference between the maximum possible number of double points for degree- n algebraic curves, and the actual number on a given degree- n curve, is known as the *genus* of that curve. Thus, if the curve (9.1) has r (ordinary) singular points with multiplicities m_1, \dots, m_r its genus g is given by

$$g = \frac{1}{2}(n - 1)(n - 2) - \sum_{k=1}^r \frac{1}{2}m_k(m_k - 1). \quad (9.12)$$

If a singular point of multiplicity m_k is *not* ordinary, its contribution to the sum in (9.12) that represents the “equivalent” number of double points may not be simply $\frac{1}{2}m_k(m_k - 1)$. The singularity must be *resolved* by the methods described in §9.2.6 to determine the appropriate contribution to this sum. The genus of an algebraic curve is invariant under projective transformations.

The significance of the genus is expressed in the following theorem.

Theorem 9.1 *An algebraic curve is rational if and only if it is of genus 0.*

In other words, if the curve (9.6) has $g = 0$, polynomials $W(t), X(t), Y(t)$ with $\gcd(W(t), X(t), Y(t)) = \text{constant}$ exist such that $F(W(t), X(t), Y(t)) \equiv 0$ and vice-versa. As the parameter t varies over all real values, the rational functions $x(t) = X(t)/W(t)$, $y(t) = Y(t)/W(t)$ describe the real locus of the curve.

A more general theorem states that, if a *birational correspondence* exists between the points of two algebraic curves (i.e., the coordinates of points on one curve can be expressed as rational functions of the coordinates of points on the other, and vice-versa) then those curves must be of the same genus.⁸ The proofs of these results are subtle and beyond our present scope: they may be found in standard texts on algebraic curves [101, 374, 406, 456].

Example 9.1 The quartic algebraic curve defined by

$$f(x, y) = x^4 + 2x^2y^2 + y^4 - x^3 + 3xy^2 = 0 \quad (9.13)$$

has a triple point at the origin, since $f = f_x = f_y = f_{xx} = f_{xy} = f_{yy} = 0$ for $(x, y) = (0, 0)$. Hence this curve must be rational, and in fact it is readily verified that the homogeneous coordinates

$$W(t) = (1 + t^2)^2, \quad X(t) = 1 - 3t^2, \quad Y(t) = t - 3t^3 \quad (9.14)$$

⁸ The converse of this statement, however, is not always true.

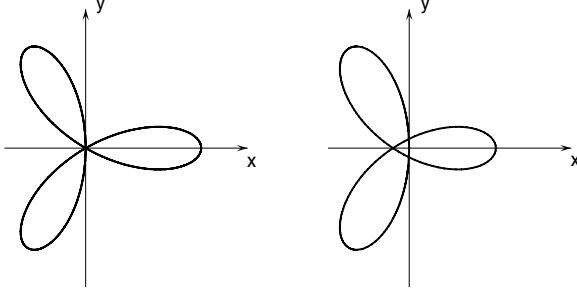


Fig. 9.3. A small perturbation to the rational quartic (9.13) with a triple point at the origin (left) causes that point to split into three distinct double points (right).

define a rational parameterization of it.⁹ In Fig. 9.3 we illustrate the effect of perturbing¹⁰ this curve by subtracting $\frac{1}{4}$ from $X(t)$ — the triple point is seen to split into three double points.

In the genus formula (9.12), it is understood that one must account for the contributions of both real and complex singular points — the latter occur in conjugate pairs if the curve coefficients are real — and also singular points *at infinity*. The discussion of §9.2.1 was implicitly phrased in terms of affine singular points, which are solutions to the system of equations

$$f(x, y) = f_x(x, y) = f_y(x, y) = 0.$$

Here $f = 0$ identifies a point of the curve, and $f_x = f_y = 0$ are the conditions for it to be singular. The generalization to the projective plane is obtained by substituting the parametric equations

$$W(t) = W_0 + \lambda t, \quad X(t) = X_0 + \mu t, \quad Y(t) = Y_0 + \nu t,$$

of a projective line into the homogeneous equation (9.6), and then expanding in a trivariate Taylor series about (W_0, X_0, Y_0) . The resulting polynomial has a multiple root at $t = 0$ for *arbitrary* ratios $\lambda : \mu : \nu$ if the conditions

$$F_W(W, X, Y) = F_X(W, X, Y) = F_Y(W, X, Y) = 0$$

are satisfied. These conditions amount to three equations in two unknowns, since only the *ratios* $W : X : Y$ matter. The curve equation does not appear explicitly above, but by Euler's theorem

$$WF_W + XF_X + YF_Y \equiv nF$$

⁹ This curve is the “three-leaved rose,” with polar-coordinate equation $r = \cos 3\theta$.

¹⁰ Note that we perturb the parametric, rather than implicit, equation. Perturbing the latter destroys the singularity (i.e., the curve is no longer rational), but small perturbations of the parametric form retain the equivalent of three double points.

for a degree- n homogeneous function, a point satisfying $F_W = F_X = F_Y = 0$ necessarily satisfies $F = 0$ also — i.e., that point *must* lie on the curve.

In terms of the homogeneous curve equation, the multiplicity of a singular point is m if every partial derivative of $F(W, X, Y)$ with respect to the three homogeneous coordinates of order $\leq m - 1$ vanishes, but at least one of order m does not. We have a double point, for example, when $F_W = F_X = F_Y = 0$ but at least one of $F_{WW}, F_{WX}, F_{XX}, F_{XY}, F_{YY}, F_{YW}$ is non-zero. The two tangent lines at that point may be identified by equating to zero the linear factors of the homogeneous quadratic form

$$F_{WW}W^2 + 2F_{WX}WX + F_{XX}X^2 + 2F_{XY}XY + F_{YY}Y^2 + 2F_{YW}YW. \quad (9.15)$$

The factors of an analogous degree- m homogeneous expression identify the m tangent lines at an m -fold point.

The term *genus*, from the field of topology, actually refers to the structure of the *complex locus* of an algebraic curve. This locus may be interpreted as a two-dimensional *surface* in \mathbb{R}^4 . To understand this, we express the Cartesian coordinates in terms of real and imaginary parts: $x = \alpha + i\beta$, $y = \gamma + i\delta$. The curve equation is then separable into real and imaginary parts

$$f(x, y) = p(\alpha, \beta, \gamma, \delta) + iq(\alpha, \beta, \gamma, \delta) = 0,$$

where p and q are real polynomials in their real arguments $\alpha, \beta, \gamma, \delta$. In the four-dimensional space with coordinates $(\alpha, \beta, \gamma, \delta)$, points of the complex locus are identified by the fact that these polynomials vanish *simultaneously*. This locus is thus of dimension 2 — and codimension 2 — in that space; it is a (real) surface residing in a (real) four-dimensional space.

Surfaces that can be “elastically deformed” into each other are considered equivalent in topology.¹¹ We distinguish among topologically distinct types by assigning a non-negative integer, the *genus*, to each surface. Surfaces of genus 0 and 1 are equivalent to a sphere and torus, respectively. Their distinct topology is apparent from the fact that cutting along any closed curve on the sphere always separates it into two pieces, but the torus remains in one piece when we cut along certain closed curves on it (alternately, every closed curve on the sphere can be continuously shrunk to a point, but this is not true of the torus). A surface of genus $g > 1$ is equivalent to a “sphere with g handles.” The quantity (9.12), expressed in terms of the degree and number and nature of the singular points of a curve, is exactly this topological property¹² of the surface defined in the four-dimensional space $(\alpha, \beta, \gamma, \delta)$ by the two equations $p(\alpha, \beta, \gamma, \delta) = q(\alpha, \beta, \gamma, \delta) = 0$.

¹¹ More precisely, two surfaces are considered topologically equivalent if there exists a *homeomorphism* (a continuous one-to-one mapping) between their points.

¹² This is by no means obvious, and even in the case of non-singular curves, a formal proof is non-trivial [275, 279]. The problem is further complicated by the fact that we need to consider the topology of a *projective*, rather than an affine, space.

9.2.6 Resolution of Singularities

A linear relation between two homogeneous coordinate systems (W, X, Y) and (W', X', Y') defines a one-to-one mapping of the projective plane. Since such maps preserve the degree and the number and nature of singular points on an algebraic curve, they cannot help resolve the ambiguity concerning the number of “equivalent” double points that a non-ordinary singular point contributes to the sum in the genus expression (9.12). To resolve a non-ordinary singular point, we need to invoke a non-linear map of the projective plane, known as a *standard quadratic transformation* (or s.q.t. for brevity).

It is convenient to consider a system of homogeneous coordinates as being specified by three (non-collinear) points A, B, C that form the vertices of a “reference triangle” — for example, if we take

$$A = (1, 0, 0), \quad B = (0, 1, 0), \quad C = (0, 0, 1),$$

the sides BC, CA, AB of the reference triangle correspond, respectively, to the three projective lines $W = 0, X = 0, Y = 0$. An s.q.t. defines an (almost) one-to-one correspondence between pairs of points with coordinates (W, X, Y) and (W', X', Y') in two projective planes \mathcal{P} and \mathcal{P}' , according to the relations

$$W = X'Y', \quad X = Y'W', \quad Y = W'X'. \quad (9.16)$$

The one-to-one nature of this map breaks down, however, at the vertices and along the sides of the two reference triangles ABC and $A'B'C'$ in the planes \mathcal{P} and \mathcal{P}' . From (9.16) it can be seen that the *points* A, B, C in \mathcal{P} “blow up” into the *lines* $B'C', C'A', A'B'$ in \mathcal{P}' and, conversely, the *lines* AB, BC, CA in \mathcal{P} “collapse” into the *points* C', A', B' in \mathcal{P}' . In other words, vertices of the triangle of reference are mapped into the opposite sides, and vice-versa. It is this property that makes the map (9.16) extremely useful for analyzing the “latent” structure of non-ordinary singular points.

Suppose $F(W, X, Y) = 0$ has a non-ordinary singular point that we wish to resolve. We begin by translating and orienting the curve such that this point is at A , and neither AB nor CA is tangent to the curve there. We then apply an s.q.t. of the form (9.16) to obtain the transformed curve equation, $F'(W', X', Y') = 0$. Nominally, the degree of the transformed curve is twice that of the original curve, although it may exhibit powers of W', X', Y' as factors that do not concern us and must be discarded.

Since the point A maps to the line $B'C'$, points of the transformed curve $F'(W', X', Y') = 0$ that lie on $B'C'$ — other than B' and C' — are said to be “in the first neighborhood” of the singular point of $F(W, X, Y) = 0$ at A . In general, the s.q.t. (9.16) maps an ordinary singular point at A into several *regular* points on $B'C'$. If the singular point is non-ordinary, however, the transformed curve may exhibit singularities on $B'C'$ — which are said to be “implicit” or “infinitely near” to the non-ordinary singular point at A — and they must also be taken into account in the genus formula (9.12).

Singularities in the first neighborhood that are themselves non-ordinary will require a second, third, ... s.q.t. to reduce them to ordinary singular points — such points are considered to be “in the second, third, ... neighborhood” of the non-ordinary singular point at A . We say that the singular point has been *resolved* when we encounter a neighborhood containing only ordinary singular points. A fundamental theorem of algebraic geometry guarantees that such a resolution is always possible.

Theorem 9.2 (Noether¹³) *The non-ordinary singular points of irreducible plane algebraic curves can be resolved by means of a finite sequence of standard quadratic transformations.*

For a proof of this theorem see, for example, Chap. 6 of [406].

Thus, to compute the genus of an arbitrary algebraic curve, we first resolve its non-ordinary singular points, noting the multiplicity of the singular points found in each neighborhood of those points. Then both the “explicit” singular points (apparent in the original curve) and “implicit” singular points (in the successive neighborhoods of non-ordinary singularities, that become apparent only through quadratic transformations) will contribute amounts $\frac{1}{2}m_k(m_k-1)$ — according to their multiplicities m_k — to the sum in (9.12).

Example 9.2 Consider the quartic curve defined by

$$f(x, y) = x^4 + y^4 - 2(x^2 + y^2) + 4xy = 0. \quad (9.17)$$

The origin is evidently a double point of this curve, since $f = f_x = f_y = 0$ and $f_{xx} = f_{yy} = -f_{xy} = -4$ there. Furthermore, the tangents at this double point both have the direction $\lambda : \mu = 1 : 1$, so it is non-ordinary. We now homogenize the curve equation to obtain

$$F(W, X, Y) = X^4 + Y^4 - 2W^2(X^2 + Y^2) + 4W^2XY = 0,$$

and, noting that the repeated tangent to the double point located at A does not lie along the lines AB or CA , we invoke the s.q.t. (9.16). Omitting a factor W'^2 that does not concern us, this yields the transformed curve

$$F'(W', X', Y') = W'^2(X'^4 + Y'^4) - 2X'^2Y'^2(X'^2 + Y'^2) + 4X'^3Y'^3 = 0$$

of degree 6. We now inspect the line $B'C'$ (i.e., $W' = 0$) for any “implicit” singular points. $(W', X', Y') = (0, 1, 1)$ is the only point of the transformed curve on this line other than B' and C' , and since $F'_{W'} = F'_{X'} = F'_{Y'} = 0$ but not all of the second derivatives vanish there, it is a double point. Expression (9.15) then factors to give two *distinct* tangent lines

$$W' - X' + Y' = 0 \quad \text{and} \quad W' + X' - Y' = 0$$

¹³ Max Noether (1844–1921) is often regarded as the “father of algebraic geometry.”

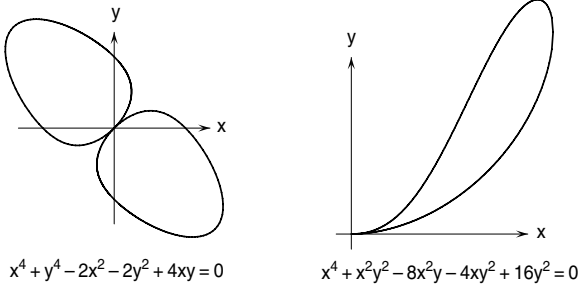


Fig. 9.4. Examples of quartic curves with non-ordinary double points — a *tacnode* on the left (see Example 9.2), and a *ramphoid cusp* on the right (see Example 9.3).

at this double point, which is thus a node, and the resolution is complete. The double point of (9.17) at the origin is known as a *tacnode* — it arises when two distinct branches of the curve are tangent to each other (see Fig. 9.4). Since the curve (9.17) has just one “explicit” double point, and one “implicit” double point in its first neighborhood, it is of genus 1.

Example 9.3 Consider the irreducible quartic

$$f(x, y) = x^4 + x^2y^2 - 8x^2y - 4xy^2 + 16y^2 = 0. \quad (9.18)$$

We have $f = f_x = f_y = 0$ and $f_{xx} = f_{xy} = 0 \neq f_{yy}$ at the origin, so it is again a non-ordinary double point, with the x -axis as its repeated tangent. Before invoking the s.q.t. (9.16), we must rotate the curve so its tangent at the double point does not lie along the coordinate axes. The substitution $W \rightarrow \sqrt{2}W$, $X \rightarrow X + Y$, $Y \rightarrow X - Y$ in the homogeneous equation

$$F(W, X, Y) = X^4 + X^2Y^2 - 8WX^2Y - 4WXY^2 + 16W^2Y^2 = 0$$

accomplishes this (we will omit the resulting equation, and subsequent details, since they are rather cumbersome). After the s.q.t., we observe a double point in the first neighborhood at $(W', X', Y') = (0, 1, 1)$ on the line $B'C'$. This also has a repeated tangent, although we find no further singular points in the second neighborhood. Figure 9.4 shows the double point of (9.18); it is called a *ramphoid cusp*. Whereas the tacnode of Example 9.2 has a node in its first neighborhood, the ramphoid cusp has an “ordinary” cusp (of the form shown in Fig. 9.2) there. Note that, unlike an ordinary cusp, both branches of the curve lie on the *same* side of the tangent at a ramphoid cusp.¹⁴

As an example of a double point with an even more intricate structure, we mention the offset to the parabola $y = kx^2$ (see §20.7) — a degree 6 rational curve. In addition to one affine node and six affine cusps, of which at most

¹⁴ The name is supposed to suggest the shape of a bird’s beak.

two are real, it can be shown [190] that $(W, X, Y) = (0, 0, 1)$ is a non-ordinary double point, with double points in its first and second neighborhoods. Thus, the curve has the ten double points required to ensure its rationality.

9.2.7 Birational Transformations

The s.q.t. (9.16) expresses one homogeneous coordinate system (W, X, Y) for the projective plane rationally in terms of another (W', X', Y') . Inverting the relations (9.16) we find that, conversely, the coordinates (W', X', Y') are given in terms of (W, X, Y) by the rational expressions¹⁵

$$W' = XY, \quad X' = YW, \quad Y' = WX. \quad (9.19)$$

As noted in §9.2.6, there is a one-to-one correspondence of points (W, X, Y) and (W', X', Y') except that certain points (lines) correspond to lines (points). The s.q.t. is an example of a *birational transformation* of the projective plane.

In general, the defining characteristics of birational plane transformations are: (i) the coordinates in each system are *rational functions* of those in the other; and (ii) there exists a one-to-one correspondence of points, except that finitely many points (loci) may correspond to loci (points). The “ordinary” projective transformations discussed in §7.4.4 are, of course, birational: their one-to-one nature and rational invertibility are immediate consequences of their *linearity*. The birationality of a *non-linear* transformation, on the other hand, is a rather special property. Birational transformations of the plane are often called *Cremona transformations* in honor of the Italian mathematician, Luigi Cremona (1830–1903), who first studied them in full generality.

Example 9.4 The earliest known (non-linear) birational transformation of the plane corresponds to *inversion* in a circle C . If C has radius R and center at the origin O , any affine point $P \neq O$ and its image P' under inversion in C lie on the same radial line through O , and their distances r and r' from O satisfy $rr' = R^2$. It is easily verified that the coordinates (x, y) and (x', y') of P and P' are related by the rational expressions

$$x' = \frac{R^2 x}{x^2 + y^2}, \quad y' = \frac{R^2 y}{x^2 + y^2} \quad \text{and} \quad x = \frac{R^2 x'}{x'^2 + y'^2}, \quad y = \frac{R^2 y'}{x'^2 + y'^2}. \quad (9.20)$$

Hence, inversion in C is one-to-one over the affine plane minus the origin.¹⁶ Points inside C are mapped to points outside, and vice-versa, while points on C are invariant. One may show that, under inversion in C , lines and circles

¹⁵ Equations (9.16) give $XY : YW : WX = W'^2 X' Y' : W' X'^2 Y' : W' X' Y'^2$. If $W', X', Y' \neq 0$, we can cancel the common factor $W' X' Y'$ to obtain (9.19). The validity of (9.19) when one or two of W', X', Y' vanish can also be easily verified.

¹⁶ One might think that the origin is mapped to the line at infinity, but introducing homogeneous coordinates for P and P' gives $W' : X' : Y' = X^2 + Y^2 : X : Y$, and hence $(W, X, Y) = (1, 0, 0)$ does not have a valid image in the projective plane.

passing through O have lines as their images, while lines and circles that do not pass through O have circles as their images.

Another fundamental theorem due to Max Noether states that any plane Cremona transformation can be interpreted as the composition of a sequence of “simple” — i.e., rational linear and quadratic — transformations. Moreover, any algebraic transformation (one defined by algebraic functions) of the plane must be a Cremona transformation if it is one-to-one.

The image C' of an algebraic curve C under any Cremona transformation will, in general, be an algebraic curve of higher order. Although the curve and its image have different degrees n and n' , and their geometrical loci are quite dissimilar, the birationality of the map guarantees that C and C' are of the same genus (see Fig. 9.5 for an elementary example).

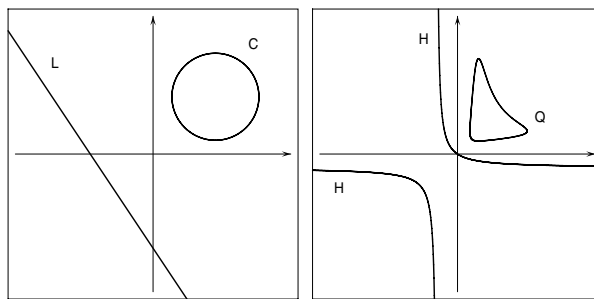


Fig. 9.5. The images of a line L and circle C under the s.q.t. (9.16) are, respectively, the hyperbola H and quartic Q (the coordinate axes are *not* images of each other).

Finally we note that, while a Cremona transformation defines a birational correspondence between the points of any curve and its image (since the map is birational over the entire projective plane), one may also have a birational correspondence between two curves that does not extend to the entire plane.

9.2.8 Plücker Relations

Our investigation of plane algebraic curves thus far has been based on their definition by an equation $F(W, X, Y) = 0$ in homogeneous point coordinates. As observed in §7.4.3, an algebraic curve can also be described by an equation $G(K, L, M) = 0$ in homogeneous line coordinates. Ratios $W : X : Y$ satisfying the former equation identify the curve points, while ratios $K : L : M$ satisfying the latter equation identify its tangent lines. The degree m of the line equation, known as the *class* of the curve, differs in general from the degree n of its point equation, which we refer to as the *order* of the curve.

We have seen that the order of a curve equals the number of points it has in common with an arbitrary fixed line. Similarly, the class of a curve equals

the number of its tangents that pass through an arbitrary fixed point.¹⁷ The dual representation of an algebraic curve may also exhibit *singular lines* that are analogs of the *singular points* discussed above. The singularity that is dual to a double point is a *double tangent*, i.e., a line that is tangent to the curve at two points. Ordinarily, a double point has two distinct tangents and is called a *node*, and a double tangent touches the curve at two distinct points and is called a *bitangent*. In the case of a double point with two coincident tangents we have a *cusp* — the dual to this is a line that is tangent to the curve at two coincident points, i.e., an *inflectional tangent* (see Fig. 9.6).

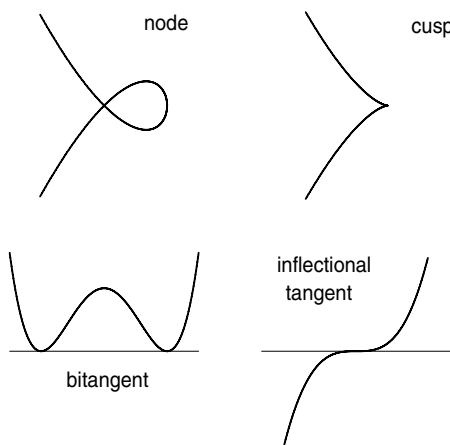


Fig. 9.6. Dual forms of the point and line singularities of algebraic curves.

Just as the order (n) and class (m) of an algebraic curve may be different, the number of nodes (δ) and bitangents (τ), and of cusps (κ) and inflectional tangents (ι), are also generally unequal. However, these six numbers are not unrelated — in fact, they must satisfy the three independent constraints

$$m = n(n - 1) - 2\delta + 3\kappa, \quad n = m(m - 1) - 2\tau + 3\iota, \quad 3(m - n) = \iota - \kappa$$

called the *Plücker equations*,¹⁸ so that only three of them may be freely chosen. The first two relations are dual to each other, i.e., we obtain one from the other by replacing n, δ, κ by m, τ, ι and vice-versa, while the third is self-dual.

¹⁷ Appropriate conventions apply here for counting both real and complex points and lines, according to their multiplicities, over the complex projective plane.

¹⁸ The German mathematician Julius Plücker (1801–1868) helped to unify algebraic and projective geometry — the Plücker relations first appeared in his *System der analytischen Geometrie* (1834) and *Theorie der algebraischen Kurven* (1839).

9.2.9 Bézout's Theorem

Two circles intersect in zero, one, or two real points, but two ellipses intersect in zero, one, two, three, or four real points. One can easily sketch examples that illustrate these possibilities (we do not distinguish between “proper” and “tangential” intersections). Because circles and ellipses are both second-order algebraic curves, the former being special instances of the latter, this apparent qualitative difference in behavior is perhaps unexpected.

Bézout's theorem resolves such discrepancies in the intersection behavior of algebraic curves of given degree, by considering intersections over the complex projective plane — rather than just the real affine plane — and by assigning an *intersection multiplicity* to each distinct intersection point.

Theorem 9.3 (Bézout¹⁹) *Two irreducible plane algebraic curves, of degree n_1 and n_2 , have exactly $n_1 n_2$ intersection points in the complex projective plane if each distinct point is counted according to its intersection multiplicity.*

This is basically just a generalization of the Fundamental Theorem of Algebra (see Chap. 3) for univariate polynomials to the case of *bivariate* polynomials. The theorem is vacuous, however, until we have a precise meaning for the idea of “intersection multiplicity.” As we shall presently see, this is a much more subtle issue than the root multiplicity of univariate polynomials.

Returning to the disparate intersection behavior of circles and ellipses, we may recall from §7.4.2 that the “circular points at infinity” with homogeneous coordinates $(W, X, Y) = (0, 1, \pm i)$ lie on *all* circles. Thus, any two circles may be considered to intersect at these complex points at infinity and hence — by Bézout's theorem — may exhibit at most two real affine intersections.

The simplest intersection of two algebraic curves occurs when the common point is *regular* on each curve, and the curves have *distinct* tangents there — the intersection multiplicity is then just 1. If the point is regular on each curve, but the curves have *coincident* tangents there, the intersection multiplicity is (at least) 2. A common point that is *singular* on either (or both) curves has a correspondingly higher intersection multiplicity: if the point is of multiplicity m_1 and m_2 on the two curves, the intersection multiplicity is at least $m_1 m_2$ — it is exactly $m_1 m_2$ if all m_1 tangents of the first curve at that point are distinct from all m_2 tangents of the second; otherwise it is higher.

Algebraic methods provide a rigorous means of determining intersection multiplicities in the most general case. Suppose

$$F_1(W, X, Y) = 0 \quad \text{and} \quad F_2(W, X, Y) = 0 \quad (9.21)$$

are the homogeneous equations of two curves, of degree n_1 and n_2 , and let (W_k, X_k, Y_k) for $k = 1, \dots, r$ be their distinct intersections with corresponding

¹⁹ Étienne Bézout (1730–1783) gave one of the first (not entirely rigorous) proofs of this theorem in 1779, but the result had been claimed in 1720 by Colin Maclaurin (1698–1746) in *Geometria organica sive descriptio linearum curvarum universalis*.

multiplicities m_k . Bézout's theorem states that $m_1 + \dots + m_r = n_1 n_2$. Since the ratios $W_k : X_k : Y_k$ simultaneously satisfy equations (9.21), we may eliminate $y = Y/W$ between them, i.e., we may take their *resultant* with respect to y , and thus obtain a univariate polynomial in $x = X/W$ whose (real or complex) roots identify the x -coordinates of the intersection points. This polynomial is, in general, of degree²⁰ $n_1 n_2$ in x . But the intersection multiplicities of the curves are not necessarily just the multiplicities of its roots, since there may be intersections with equal x -coordinates but different y -coordinates.

We circumvent this problem as follows. Distinct points with coordinates (W_a, X_a, Y_a) and (W_b, X_b, Y_b) define the projective line

$$KW + LX + MY = 0, \quad (9.22)$$

where $K : L : M = X_a Y_b - X_b Y_a : Y_a W_b - Y_b W_a : W_a X_b - W_b X_a$, and this line may also be represented by the parametric expressions

$$W(t) = (1-t)W_a + tW_b, \quad X(t) = (1-t)X_a + tX_b, \quad Y(t) = (1-t)Y_a + tY_b.$$

Suppose the values K, L, M are such that an intersection point of the curves (9.21) lies on the line (9.22), i.e., the polynomials defined by

$$P_1(t) = F_1(W(t), X(t), Y(t)) \quad \text{and} \quad P_2(t) = F_2(W(t), X(t), Y(t))$$

have a common root t . A sufficient and necessary condition for this is that the resultant of the above polynomials with respect to t vanishes. This resultant is evidently a polynomial of degree $n_1 n_2$ in K, L, M , and to ensure that it vanishes if and only if one of the intersection points (W_k, X_k, Y_k) lies on the line (9.22), it must have a factorization of the form

$$\text{Resultant}_t(P_1(t), P_2(t)) = C \prod_{k=1}^r (KW_k + LX_k + MY_k)^{m_k}, \quad (9.23)$$

where C is a non-zero constant, $m_k \geq 1$, and $m_1 + \dots + m_r = n_1 n_2$. The multiplicities of the linear terms in the above factorization are precisely the intersection multiplicities m_k that we seek, and the latter condition on their sum yields Bézout's theorem.

Example 9.5 Consider the intersection of the circle $x^2 + y^2 - x = 0$ and the quartic (9.13) of Example 9.1. To form the polynomials $P_1(t)$ and $P_2(t)$, we substitute the parametric line representation $W(t), X(t), Y(t)$ into the homogeneous curve equations

$$\begin{aligned} F_1(W, X, Y) &= X^2 + Y^2 - WX = 0, \\ F_2(W, X, Y) &= X^4 + 2X^2Y^2 + Y^4 - WX^3 + 3WXY^2 = 0. \end{aligned}$$

²⁰ If one or more consecutive highest-order coefficients of this polynomial vanish, the curves (9.21) intersect at the point at infinity on the x -axis.

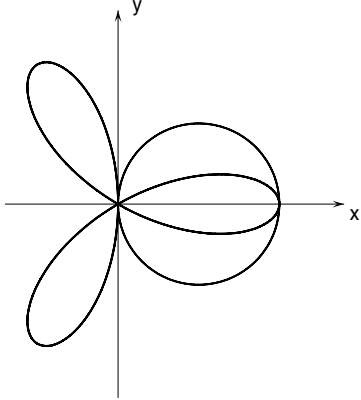


Fig. 9.7. A quartic and a circle with 4-fold and 2-fold real affine intersection points — the remaining two intersections coincide with the two circular points at infinity.

Upon writing $K = X_a Y_b - X_b Y_a$, $L = Y_a W_b - Y_b W_a$, $M = W_a X_b - W_b X_a$ we then find that the resultant with respect to t has the factorization

$$\text{Resultant}_t(P_1(t), P_2(t)) = 16 K^4 (K + L)^2 (L + iM)(L - iM).$$

Comparing with (9.23), we identify the following distinct intersection points of the two curves, and their respective multiplicities:

$$\begin{aligned} (W_1, X_1, Y_1) &= (1, 0, 0) & m_1 &= 4, & (W_3, X_3, Y_3) &= (0, 1, +i) & m_3 &= 1, \\ (W_2, X_2, Y_2) &= (1, 1, 0) & m_2 &= 2, & (W_4, X_4, Y_4) &= (0, 1, -i) & m_4 &= 1. \end{aligned}$$

Note that, in accordance with Bézout's theorem, we have $m_1 + m_2 + m_3 + m_4 = 2 \times 4$. Thus $(x, y) = (0, 0)$ is a four-fold intersection — it is a triple point on the quartic and a regular point on the circle, but the intersection multiplicity exceeds 3 since the circle is tangent to one branch of the quartic at that point; see Fig. 9.7. The point $(x, y) = (1, 0)$ is a double intersection: it is regular on both curves, but they share a common tangent there. The circular points at infinity account for the two remaining (simple) intersections.

9.2.10 Implicitization and Parameterization

The comparative merits of parametric and implicit representations of plane curves were discussed in §9.1. For the computation of intersections and other applications, it is useful to have a means of transforming (if possible) between these representations. We now turn our attention to this problem.

Implicitization of Rational Curves

As noted in the introduction to this chapter, the rational curves form a proper subset of all algebraic curves. A rational curve specified by three homogeneous

coordinate polynomials $W(t)$, $X(t)$, $Y(t)$ of degree n can always be alternately described by an implicit polynomial equation $f(x, y) = 0$, also of degree n . To obtain that equation, we form the polynomials

$$P(x, y, t) = W(t)x - X(t) \quad \text{and} \quad Q(x, y, t) = W(t)y - Y(t)$$

in terms of free Cartesian coordinates x, y and the curve parameter t . Now the point (x, y) lies on the curve if and only if there exists a value of t that causes the equations $P(x, y, t) = Q(x, y, t) = 0$ to be satisfied simultaneously, i.e., if and only if these polynomials have a common root t . A sufficient and necessary condition for such a root to exist is that the *resultant* of the polynomials with respect to t (see §3.4) should vanish. Thus, we have

$$f(x, y) = \text{Resultant}_t(P(x, y, t), Q(x, y, t)) = 0.$$

The resultant may be expressed as a *Sylvester determinant* (see §3.4), whose entries are the coefficients of P and Q , regarded as polynomials in t . Since each of these coefficients is evidently linear in x or y , expansion of the determinant gives a polynomial expression $f(x, y)$ that vanishes if and only if (x, y) is a point on the curve specified parametrically by $W(t)$, $X(t)$, $Y(t)$. Therefore, $f(x, y) = 0$ is the desired implicit equation of that curve.

Although the Sylvester determinant is of dimension $2n \times 2n$ with elements linear in x and y , its special structure yields an implicit equation $f(x, y) = 0$ of degree n upon expansion. A rational curve thus has the same degree whether we specify it by parametric²¹ or implicit equations. The implicitization scheme described above obviously applies also to planar curves specified by *polynomial* parameterizations, which correspond to the case $W(t) \equiv 1$.

There are more efficient and elegant approaches to curve implicitization than expansion of the Sylvester determinant, that also help to reveal when the implicit equation is of lower degree than the nominal value n , but a detailed discussion of them would take us too far astray — the interested reader may consult [212, 400, 401, 403] for an authoritative treatment of these issues.

Parameterization of Rational Curves

An algebraic curve, as specified by an implicit equation $f(x, y) = 0$, admits a parameterization in terms of rational functions if and only if it is genus zero. To construct the rational parameterization in such a case, we seek a means to uniquely associate each point of the curve with the values of a real variable t , such that the point coordinates depend rationally on t .

Suppose that $f(x, y) = 0$ is of degree n . We introduce a one-parameter family (or *pencil*) of curves $g(x, y, t) = 0$, of degree m in (x, y) and linear in the family parameter t , constructed in such a manner that $mn - 1$ of the mn

²¹ We assume a *proper* parameterization, with a one-to-one correspondence between parameter values and curve points except, possibly, at finitely many points.

intersections with $f(x, y) = 0$ occur at known fixed points. Then, as t varies, the remaining unaccounted-for intersection point traces out the curve — it corresponds to a linear factor of (9.23) in which W_k, X_k, Y_k are degree- n polynomials in t (all other factors, corresponding to fixed intersections, have known numerical values for W_k, X_k, Y_k). The polynomials $W(t), X(t), Y(t)$ thus identified define a rational parameterization of $f(x, y) = 0$.

To parameterize a conic $f(x, y) = 0$, we first choose coordinates in which it passes through the origin. Each member of the pencil of lines $y = tx$ through the origin then has one other intersection point with the conic, and solving for its (non-zero) coordinates x and y in terms of t among the equations $y = tx$ and $f(x, y) = 0$ yields a rational parameterization of the conic.

A cubic must have a double point in order to be rational. It is convenient to adopt coordinates with the double point at the origin (which may require a projective transformation). For our auxiliary family of curves, we may again take the pencil of lines $y = tx$ through the origin. Each line has a two-fold intersection with the cubic at the origin, and the residual intersection point traces the curve as we vary the slope t . Solving for (non-zero values) x, y in terms of t among the equations $f(x, y) = 0$ and $y = tx$ for the singular cubic (9.10), for example, we obtain the parameterization

$$x(t) = -k - t^2, \quad y(t) = -kt - t^3$$

of the curves in Fig. 9.2 (note that in the case $k = +1$, the “acnode” or isolated real point at the origin corresponds to the parameter values $t = \pm i$).

In general, any irreducible degree- n algebraic curve $f(x, y) = 0$ that has a singular point of maximum multiplicity, $m = n - 1$, is rational — it can be parameterized by placing the m -fold point at the origin, and introducing the auxiliary pencil of lines $y = tx$. Such curves are called *monoids*.

A quartic must have a triple point, or three double points, to be rational. In the former case, we place the triple point at the origin: Bézout’s theorem then indicates that each member of the pencil of lines $y = tx$ through the origin has one residual intersection with the quartic, whose coordinates can be expressed rationally in terms of t . The rational parameterization (9.14) of the quartic (9.13), for example, is obtained in this manner.

If the quartic has three double points, however, we cannot use a pencil of lines to construct the parameterization, since in this case we cannot identify a variable line that has three fixed intersections with the quartic. We therefore appeal to a pencil of *conics* drawn through the three double points and one additional fixed point of the quartic — this leaves one degree of freedom (since conics have five). The prescribed points account for seven of the total of eight intersections of the quartic and the conics — the remaining intersection point traces the quartic as we vary the pencil parameter t , and its coordinates can be expressed as rational functions of that variable.

The above parameterization procedures can, in principle, be generalized to accommodate rational curves of arbitrary degree — but they are evidently

rather involved for higher-order curves. Further details on the parametrization of rational curves may be found in [5–8].

Elliptic Curves

The “simplest” algebraic curves beyond rational curves are those of genus 1, known as *elliptic curves* since they can be parameterized using elliptic, rather than rational, functions. Elliptic functions²² [299] are generalizations of the trigonometric functions: they have two linearly-independent complex periods rather than one real period: see [136] for a comprehensive discussion. Examples of elliptic curves are the non-singular plane cubics (see [353] for details on their parameterization by elliptic functions), and the non-singular intersections of quadric surfaces, i.e., quartic algebraic space curves; see §9.4. As an alternative to elliptic functions, genus 1 curves can also be parameterized by rational functions of a variable t and the square root of a polynomial in t .

9.3 Algebraic Surfaces

An algebraic surface of degree n is the locus of points with three-dimensional Cartesian coordinates (x, y, z) that satisfy a polynomial equation of the form

$$g(x, y, z) = \sum_{i=0}^n \sum_{j=0}^{n-i} \sum_{k=0}^{n-i-j} c_{ijk} x^i y^j z^k = 0, \quad (9.24)$$

specified by

$$\binom{n+3}{3} = \frac{1}{6}(n+1)(n+2)(n+3)$$

coefficients. As in §9.2, the number of degrees of freedom is one fewer than the number of coefficients, and the surface is considered reducible if $g(x, y, z)$ can be factored into lower-order components with real or complex coefficients.

The algebraic surface (9.24) has the property that it is cut by any plane in a (possibly reducible) plane algebraic curve of degree n . A shape-preserving transformation that maps an arbitrary section plane $ax + by + cz + d = 0$ into the (x, y) -plane can be applied to equation (9.24) — the equation $f(x, y) = 0$ of the section as a degree- n plane algebraic curve is then obtained by merely substituting $z = 0$ into the transformed surface. Of course, these ideas may be generalized to three-dimensional projective space — setting $W = 0$ in the homogeneous equation $G(W, X, Y, Z) = W^n g(X/W, Y/W, Z/W) = 0$ of the surface, for example, defines its intersection with the *plane at infinity*.

²² So called because these functions arise in computing the cumulative arc length of an ellipse — note, however, that the ellipse is a rational (not an elliptic) curve!

9.3.1 Singular Points and Curves

As with algebraic curves, algebraic surfaces may have singular points. We can identify them, and analyze their properties, by methods similar to those used in §9.2. Consider the line $x(t) = x_0 + \lambda t$, $y(t) = y_0 + \mu t$, $z(t) = z_0 + \nu t$ passing through a point (x_0, y_0, z_0) of the surface (9.24), with orientation specified by direction cosines (λ, μ, ν) . Proceeding as in §9.2, we find that the intersections of this line with the surface (9.24) are identified by the roots of the polynomial

$$\begin{aligned} G(t) &= g(x_0 + \lambda t, y_0 + \mu t, z_0 + \nu t) = [g_x^{(0)}\lambda + g_y^{(0)}\mu + g_z^{(0)}\nu]t \\ &\quad + [g_{xx}^{(0)}\lambda^2 + 2g_{xy}^{(0)}\lambda\mu + g_{yy}^{(0)}\mu^2 + 2g_{yz}^{(0)}\mu\nu + g_{zz}^{(0)}\nu^2 + 2g_{zx}^{(0)}\nu\lambda]t^2 + \dots \end{aligned}$$

of degree n in t . Hence, a straight line intersects a degree- n algebraic surface in n points (counted according to multiplicity over complex projective space).

Clearly $t = 0$ is a *multiple* root of $G(t)$ — i.e., the point (x_0, y_0, z_0) counts as *more than one* intersection of the line with the surface — when

$$g_x^{(0)}\lambda + g_y^{(0)}\mu + g_z^{(0)}\nu = 0.$$

Now if $g_x^{(0)}$, $g_y^{(0)}$, $g_z^{(0)}$ are not all zero, this amounts to a linear constraint on the direction cosines, and since only their *ratios* $\lambda : \mu : \nu$ are significant, there is a singly-infinite family of lines through (x_0, y_0, z_0) satisfying it. These lines are all *tangent* to the surface (9.24) at (x_0, y_0, z_0) : they lie in the *tangent plane* at that point, defined by the equation

$$g_x^{(0)}(x - x_0) + g_y^{(0)}(y - y_0) + g_z^{(0)}(z - z_0) = 0.$$

When $g_x^{(0)} = g_y^{(0)} = g_z^{(0)} = 0$, however, $t = 0$ is a multiple root of $G(t)$ for lines of *any* orientation (λ, μ, ν) through (x_0, y_0, z_0) . This condition identifies a *singular point* of the algebraic surface — in particular, a *double point* if the second partial derivatives of g are not all zero at (x_0, y_0, z_0) . Any line through a double point has (at least) a two-fold intersection with the surface at that point. Further, lines whose direction cosines satisfy the quadratic equation

$$g_{xx}^{(0)}\lambda^2 + 2g_{xy}^{(0)}\lambda\mu + g_{yy}^{(0)}\mu^2 + 2g_{yz}^{(0)}\mu\nu + g_{zz}^{(0)}\nu^2 + 2g_{zx}^{(0)}\nu\lambda = 0 \quad (9.25)$$

have a three-fold intersection — such lines are *tangent* to the surface at the double point. The singly-infinite family of lines that satisfy equation (9.25) constitute the (quadric) *tangent cone* to the surface at the double point.

Singular points of higher multiplicity are defined by generalizing the above ideas: at an m -fold point, all partial derivatives of order $\leq m-1$ vanish, but at least one of order m does not. The family of tangent lines to the surface at such a point, whose direction cosines are solutions to the equation

$$\sum_{k=0}^m \sum_{j=0}^k \binom{m}{k} \binom{k}{j} \frac{\partial f^{(0)}}{\partial x^{m-k} y^{k-j} z^j} \lambda^{m-k} \mu^{k-j} \nu^j = 0,$$

make up the m -th order tangent cone at that singular point.

Now the singularities of an algebraic surface may be isolated points, or they may constitute a locus — i.e., a *singular curve* — on the surface. For example, a locus of double points along which the quadratic form (9.25) factors into two linear terms — i.e., the quadric tangent cone degenerates into two planes — corresponds to a *self-intersection* or a *cuspidal ridge* of the algebraic surface, according to whether those planes are distinct or coincident.

Whereas a plane algebraic curve of degree n may exhibit singular points of multiplicity up to $n - 1$ only, certain special algebraic surfaces of degree n may have an n -fold singular point. Such a surface is known as a *cone*, and its n -fold point is called the *vertex* of the cone: a line passing through the vertex must either lie entirely on the cone, or have no other intersections with it (in order to comply with Bézout's theorem). This agrees with our use of the term “tangent cone” to describe the set of tangent lines to a surface at each point, whether regular or singular (planes are the simplest type of cones).

A homogeneous degree- n equation $g(x, y, z) = 0$ in the *affine* coordinates defines a cone with vertex at the origin, since if the point (x_*, y_*, z_*) satisfies this equation, each point (kx_*, ky_*, kz_*) on the line joining it to the origin also satisfies the equation. Conversely, if $f(x, y) = 0$ is any degree- n plane curve, which we imagine to be situated in the plane $z = 1$, the cone defined by the family of lines that pass through the origin and each point of this curve has the homogeneous equation $g(x, y, z) = z^n f(x/z, y/z) = 0$.

9.3.2 Rationality of Algebraic Surfaces

An algebraic surface defined by the homogeneous equation $G(W, X, Y, Z) = 0$ is rational if there exist polynomials $W(u, v)$, $X(u, v)$, $Y(u, v)$, $Z(u, v)$ in two parameters, u and v , such that

$$G(W(u, v), X(u, v), Y(u, v), Z(u, v)) \equiv 0.$$

Clearly, the functions

$$x(u, v) = \frac{X(u, v)}{W(u, v)}, \quad y(u, v) = \frac{Y(u, v)}{W(u, v)}, \quad z(u, v) = \frac{Z(u, v)}{W(u, v)}$$

then define a rational parameterization of the surface.

The formulation of sufficient-and-necessary conditions for the rationality of algebraic surfaces is a much deeper problem than that for plane curves (see §9.2.5). Two kinds of genus are defined for a surface, an “arithmetic” genus and a “geometric” genus, and both must vanish for a rational surface. However, their vanishing is only a *necessary* condition for the rationality of a surface. *Castelnuovo's theorem* [407] gives a sufficient-and-necessary condition, but it requires rather sophisticated concepts that lie beyond our scope.

Nevertheless, algebraic surfaces of degree 1 (planes) and 2 — the *quadrics*, encompassing the “natural” shapes: spheres and right-circular cylinders and

cones, as well as ellipsoids, paraboloids, and hyperboloids [139] — are rational. To parameterize a (non-singular) quadric, we choose an origin at any point (x_0, y_0, z_0) on it, and consider a two-parameter family of lines passing through this point that assume all possible directions — for example, we could write

$$x = x_0 + \lambda \tau, \quad y = y_0 + \mu \tau, \quad z = z_0 + \nu \tau \quad (9.26)$$

where each set of ratios $\lambda : \mu : \nu$ identifies a distinct line, and τ specifies position on it. Setting²³ $u = \lambda/\nu$ and $v = \mu/\nu$, for example, the coordinates of the intersection point of the line and quadric other than (x_0, y_0, z_0) can then be expressed by rational functions $x(u, v)$, $y(u, v)$, $z(u, v)$ that comprise a parameterization of the surface. In fact, this method applies to any *monoid* (i.e., any degree- n surface with a singular point of multiplicity $n - 1$).

Furthermore, all cubic surfaces with singular points of multiplicity ≤ 2 are rational [4, 407, 423]. In the case of a monoidal cubic surface, we position the double point at the origin and proceed as described above, while for the non-singular cubic surfaces a somewhat more involved procedure is required [6]. A cubic surface with a triple point (a cubic cone) may or may not be rational. Placing its vertex at the origin (this may require a projective transformation) gives its homogeneous equation $g(x, y, z) = 0$. Dividing this by z^3 and setting $x/z \rightarrow x$ and $y/z \rightarrow y$ defines the cone “generating curve” $f(x, y) = 0$ in the plane $z = 1$; the cubic cone admits a rational parameterization if this plane cubic is a rational curve. A remarkable property of the general cubic surface is that it contains 27 (real or complex conjugate) straight lines [233] — their identification can be valuable [404] in formulating a parameterization.

The study of higher-order surfaces has not been as thorough as that of the quadrics and the cubics. One exception is the family of quartics known [260] as *Steiner surfaces*,²⁴ that exhibit three double lines meeting in a triple point. These monoidal surfaces have attracted some attention [51, 97, 123, 399] in computer-aided design, since they have *quadratic* rational parameterizations. In fact, the general rational quadratic triangular Bézier surface (see §13.9) is a portion of a Steiner surface; it encompasses the quadrics and certain cubics as special instances. Another attractive feature of the Steiner surfaces is that their plane sections are rational curves: every plane passes through the triple point, or has a double point where it meets the three double lines — possibly at infinity. In some cases, the section curve degenerates from a plane quartic to a composite of lower-order curves whose degrees sum to four.

9.4 Algebraic Space Curves

The intersection of two irreducible algebraic surfaces, of degree m and n , is in general an algebraic space curve of degree mn . Such a curve intersects any

²³ Note that this choice does not necessarily yield the “best” parameterization.

²⁴ Named after the German mathematician Jacob Steiner (1796–1863).

plane in mn points (not necessarily real, distinct, or affine). This observation is an immediate consequence of Bézout's theorem, and the fact that the plane cuts the surfaces in curves of degree m and n — the common points of these planar curves are evidently points where the space curve meets the plane.

Of course, if the surfaces are reducible, their intersection is a “composite” of lower-degree space curves — corresponding to pairwise intersections of the component surfaces — whose degrees sum to mn if counted with multiplicity over three-dimensional complex projective space. A fundamental difficulty in the theory of algebraic space curves is that the converse of this statement does not hold: even if the two given surfaces are *irreducible*, their intersection may nevertheless be a *composite* of several lower-order space curves whose degrees sum to mn , rather than a single space curve of degree mn .

9.4.1 Composite Surface Intersections

The problem of composite intersections can be illustrated by a simple example. The simplest non-planar algebraic curves are the cubics. Unlike plane cubics, every space cubic is a *rational curve*,²⁵ and may be regarded as a projective image of the “canonical” cubic defined by

$$W(t) = 1, \quad X(t) = t, \quad Y(t) = t^2, \quad Z(t) = t^3. \quad (9.27)$$

However, a space cubic cannot be the complete intersection of two algebraic surfaces. If we postulate that two surfaces $g(x, y, z) = 0$ and $h(x, y, z) = 0$, of degree m and n , have a space cubic as their entire intersection, then $mn = 3$, and hence $(m, n) = (3, 1)$ or $(1, 3)$ — i.e., one of the surfaces must be a plane, and hence the intersection must be a *planar* curve rather than a *space* curve.

The simplest specification for a space cubic \mathcal{C} is the *partial* intersection of two quadric surfaces, $q_0(x, y, z) = q_1(x, y, z) = 0$, that possess a straight line \mathcal{L} as their “residual” intersection component. To *uniquely* specify the cubic as the zero set of a system of polynomial equations, we must introduce a third quadric $q_2(x, y, z) = 0$ containing \mathcal{C} but not \mathcal{L} . Clearly, it cannot be a member of the one-parameter linear family or *pencil* of quadrics

$$(1 - \lambda) q_0(x, y, z) + \lambda q_1(x, y, z) = 0 \quad (9.28)$$

defined by the given quadrics, since any two members of this family have both \mathcal{C} and \mathcal{L} (which constitute the *base curve* of the pencil) as their intersection.

Example 9.6 Consider the quadrics defined by the homogeneous equations

$$Q_0(W, X, Y, Z) = XZ + WY = 0, \quad Q_1(W, X, Y, Z) = Y^2 - Z^2 + WY = 0.$$

Substituting into the above, we see that the rational cubic \mathcal{C} described by

²⁵ In general, any n -dimensional curve of degree $\leq n$ is rational.

$$W(t) = 1 - t^2, \quad X(t) = t^3 - t, \quad Y(t) = t^2, \quad Z(t) = t \quad (9.29)$$

lies on both quadrics, and is thus a component of their intersection. Clearly, the line \mathcal{L} defined by $Y = Z = 0$ (i.e., the x -axis) is the residual component. We now introduce a third quadric

$$Q_2(W, X, Y, Z) = XY + WX + WZ = 0, \quad (9.30)$$

that is linearly independent of the other two — and is thus not a member of the pencil they define — but also contains \mathcal{C} . The space cubic may then be identified with the zero-set of the system of equations

$$Q_0(W, X, Y, Z) = Q_1(W, X, Y, Z) = Q_2(W, X, Y, Z) = 0. \quad (9.31)$$

In the above example, we tacitly assumed that the third quadric does not intersect the line \mathcal{L} except at common points of \mathcal{C} and \mathcal{L} . Otherwise, there would be solutions to the system (9.31) that are *not* points of the space cubic. This assumption is actually valid for any quadric that contains \mathcal{C} and does not belong to the pencil (9.28). It can be shown [423] that, if the intersection of two quadrics comprises a cubic and a line, these loci must have two points in common,²⁶ and since the third quadric contains \mathcal{C} by supposition, these two common points of \mathcal{C} and \mathcal{L} account for all intersections of that quadric with the line \mathcal{L} — it cannot have other intersections, not on \mathcal{C} , with \mathcal{L} .

Finding sets of equations that define individual components of composite intersections among higher-order surfaces is not so straightforward, however. To isolate a component of the intersection of $f_0(x, y, z) = 0$ and $f_1(x, y, z) = 0$, for example, we might introduce a third surface $f_2(x, y, z) = 0$ that contains the desired component. But it is difficult to guarantee *a priori* that this surface does not intersect the residual intersection components, thereby introducing solutions to the system of equations $f_0(x, y, z) = f_1(x, y, z) = f_2(x, y, z) = 0$ that are extraneous to the desired space curve. To eliminate such points, *four* (or more) surface equations may be required. The question of the number of equations that suffice to specify a component of the composite intersection of two irreducible surfaces — and, especially, how to identify such equations — is intrinsically quite difficult. To quote from an authoritative source [3]:

The history of this problem goes back at least to Kronecker [291], who proved in 1882 that four equations are always enough to define a space curve set-theoretically, and shortly after, Vahlen [453] claimed to give an example for which three equations could not be sufficient. This remained the generally accepted status of the problem until 1942, when Perron [356] explicitly exhibited three polynomials giving Vahlen's curve. Finally, Kneser [284] proved in 1960 that all irreducible space curves can be set-theoretically defined by three equations.

²⁶ Or, exceptionally, one common point where they meet with tangency.

It should be noted that composite intersection curves are an exceptional occurrence — two irreducible surfaces of degree m and n in “general position” will intersect in a *single* space curve of degree mn . Nevertheless, the ability to recognize and process composite intersections is extremely important, since in practice surfaces are often positioned in the special relative orientations that incur this problem. An examination of its simplest non-trivial context — the intersections of quadrics — already suggests the rich variety of ways in which lower-order curves may combine to form composite intersections.

In general, two quadrics intersect in a non-singular quartic curve, but the following “degenerate” intersections may arise under special circumstances: a singular quartic; a cubic and a line; two irreducible conics; an irreducible conic and two lines; and four lines (Fig. 9.8). A more refined classification scheme for the projectively distinct forms of the *base curve* of the quadric pencil (9.28) differentiates between various incidence relations among the components: for example, two conic or linear components may be distinct or coincident.

Such a classification is codified [60, 423] by the *Segre characteristic* of the pencil. We may write the equation of a quadric in matrix form as

$$Q(W, X, Y, Z) = [W \ X \ Y \ Z] \begin{bmatrix} a & f & h & l \\ f & b & g & m \\ h & g & c & n \\ l & m & n & d \end{bmatrix} \begin{bmatrix} W \\ X \\ Y \\ Z \end{bmatrix} = 0,$$

and if \mathbf{Q}_0 and \mathbf{Q}_1 are symmetric 4×4 matrices of the above form that define a quadric pencil, the Segre characteristic is determined by examining the root structure of the determinantal equation

$$| (1 - \lambda) \mathbf{Q}_0 + \lambda \mathbf{Q}_1 | = 0,$$

and each of its minors, in the pencil parameter λ . The four roots identify *cones* of the pencil, and the generic case in which they are distinct corresponds to the generic base curve, a non-singular quartic. As indicated in Table 9.1 there are,

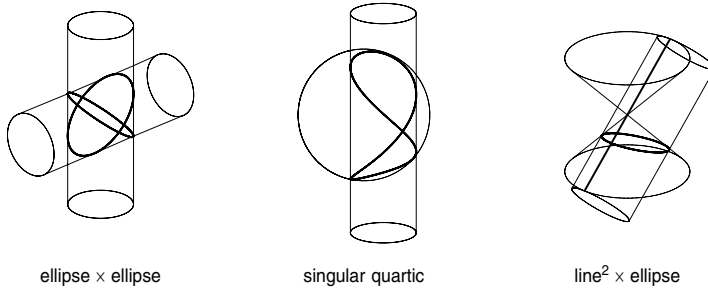


Fig. 9.8. Degenerate quadric intersections: two cylinders intersecting in a pair of ellipses (left); a cylinder and a sphere intersecting in a nodal space quartic (center); and a cylinder and a cone intersecting in an ellipse and a line counted twice (right).

Table 9.1. Segre characteristics and base curves for quadric pencils.

characteristic	base curve morphology
[1 1 1 1]	a non-singular quartic
[(1 1) 1 1]	two conics, intersecting in two distinct points
[(1 1) (1 1)]	four lines, intersecting in four non-coplanar points
[(1 1 1) 1]	a single conic, counted twice
[2 1 1]	a nodal quartic
[(2 1) 1]	two conics, touching at one point
[2 (1 1)]	a conic and two lines, intersecting in three points
[(2 1 1)]	two lines, each counted twice
[2 2]	a cubic and a line, intersecting in two distinct points
[(2 2)]	three lines, one counted twice
[3 1]	a cuspidal quartic
[(3 1)]	a conic and two lines, all intersecting in one point
[4]	a cubic and a line, touching at one point
[{3} 1]	a conic and a line counted twice

in addition, *thirteen* projectively distinct degenerate forms of the base curve (note that linear and conic intersection components may not be real or affine). A detailed explanation may be found in [60, 423] — see also [178].

9.4.2 Plane Projections of a Space Curve

A space curve of degree n defined by surfaces $g(x, y, z) = 0$ and $h(x, y, z) = 0$ may be projected onto the (x, y) plane by eliminating z from these equations — the projected curve then has the equation

$$f(x, y) = \text{Resultant}_z(g(x, y, z), h(x, y, z)) = 0, \quad (9.32)$$

which defines a planar algebraic curve, of the same degree as the space curve. When we do not confine our attention to the (x, y) plane, this equation can also be interpreted as defining a surface, namely, a *cylinder* with rulings parallel to the z -axis that pass through each point of the space curve.

Similarly, we can project the space curve onto the (y, z) and (z, x) planes (or, for that matter, planes of any orientation). We may regard a space curve as being described by any two of its projections on the three coordinate planes. This was, in fact, the perspective of the first systematic study of space curves, the 1731 treatise *Recherche sur les courbes à double courbure*²⁷ by the French mathematician Alexis-Claude Clairaut (1713–1765).

Note, however, that the space curve is *not* the complete intersection of just two of the cylindrical surfaces defined by such projections. Since each cylinder

²⁷ Each projection has its own (planar) curvature function, hence the notion that a three-dimensional locus has “double” curvature. Clairaut’s *Recherche* was written at age 16; he was admitted to the Paris Academy of Sciences the following year.

is of degree n , their pairwise intersections are space curves of total degree n^2 — they contain other space curves, whose degrees sum to $n^2 - n$, besides the original degree- n space curve. In order to uniquely describe the latter curve, the equations of *all three* cylinders must be specified.

A plane projection of a space curve exhibits singularities corresponding to each singular point of that space curve. In addition, the projection may incur singular points on the plane curve corresponding to *regular* points of the space curve. For example, distinct points (x, y, z_1) and (x, y, z_2) of the space curve, with $z_1 \neq z_2$, project to the *same* point of the curve (9.32) — and this point will, in general, be a *node* or self-intersection of that curve. And a point where the space curve tangent is parallel to the projection direction will typically incur a *cusp* or tangent-reversal on the plane curve.²⁸

Thus one cannot, in general, expect an exact one-to-one correspondence between the points of a space curve and its projection onto a plane — there are usually finitely many points where the correspondence is many-to-one. Exceptionally, the projection may be such that distinct *continuous segments* of the space curve possess identical images on the plane curve. The former and latter then exhibit a many-to-one correspondence at an infinite number of points. We usually wish to avoid such “degenerate” projections.

9.4.3 Genus of an Algebraic Space Curve

Fundamentally, an irreducible algebraic space curve is a locus of points whose Cartesian coordinates (x, y, z) satisfy two or more polynomial equations. As remarked in §9.4.1, two equations may not suffice to isolate the desired curve, and introducing further equations so as to specify only the desired curve, and exclude all points extraneous to it, is not a simple matter.

For applications, *parametric* representations of space curves are preferable to “implicit” ones, since they conveniently circumvent the uncertainty in the number of equations required to uniquely specify a space curve. However, we encounter the same problem that arose in the case of plane algebraic curves: although we are interested in the full set of algebraic space curves — arising, for example, as surface intersections — only a special subset of them can be parameterized in terms of “simple” (polynomial or rational) functions.

We may associate a non-negative integer with any algebraic space curve, the *genus*, and as in the planar case the curve is rational if and only if its genus is zero. The genus of a space curve may be determined by projecting it onto a plane, such that the points of the curve and its projection are in one-to-one correspondence (except, possibly, at finitely many points). The genus of the space curve is then equal to that of the *plane* algebraic curve, determined by the methods of §9.2.5, obtained by such a projection.

Example 9.7 Consider the intersection of the cylinder and sphere given by

²⁸ Consider, for example, the projection of the cubic (9.27) onto the (y, z) plane.

$$g(x, y, z) = x^2 + z^2 - 2z = 0, \quad h(x, y, z) = x^2 + y^2 + z^2 - 4 = 0. \quad (9.33)$$

The space curve thus defined is an irreducible quartic, and we project it onto the (x, y) plane to obtain

$$f(x, y) = \text{Resultant}_z(g(x, y, z), h(x, y, z)) = y^4 + 4x^2 - 4y^2 = 0. \quad (9.34)$$

Homogenizing this equation, we write

$$F(W, X, Y) = Y^4 + 4W^2X^2 - 4W^2Y^2 = 0,$$

and it is then clear that $(W, X, Y) = (1, 0, 0)$ and $(0, 1, 0)$ are double points, since $F_W = F_X = F_Y = 0$ there. The double point at the origin is ordinary, since it has distinct tangent lines $X \pm Y = 0$. But the double point at infinity is not ordinary, since it has the line at infinity $W = 0$ as a repeated tangent. Moving this non-ordinary double point to the origin and orienting the curve so the tangent does not coincide with $X = 0$ or $Y = 0$, we may apply a quadratic transformation to resolve the singularity. This reveals one (ordinary) double point in the first neighborhood. Thus, the plane quartic (9.34) has three double points altogether, and is of genus zero. Hence, the spatial quartic defined by (9.33) is a rational curve: it is the “figure eight” curve seen in Fig. 9.8.

A cubic space curve must be non-singular since, by postulating that it has a double point, we arrive at the contradiction that a plane through that point and two other curve points exhibits more than three intersection points with the cubic. As noted in §9.4.1, the space cubics are all rational. To construct the rational parameterization, consider the pencil of planes that have in common a line drawn between two fixed points of the curve. Each of these planes has just one other intersection with the cubic, and the coordinates of that point can be expressed rationally in terms of the pencil parameter.

Similar arguments show that a quartic space curve may have at most one double point; it is rational if the double point exists. To construct the rational parameterization of a singular quartic, consider the pencil of planes that have in common a line defined by the double point and any other curve point. Each plane has just one other intersection with the quartic, and the coordinates of that point are rational functions of the pencil parameter.

9.4.4 Singularities of Space Curves

We have investigated singular points of plane algebraic curves in §9.2.1, and in §9.4.2 we described how to project a space curve onto a plane. However, the projected curve may exhibit singular points that correspond to *regular* points of the space curve. Thus, in order to study the singularities of space curves, we must employ their three-dimensional representations.

Consider a space curve \mathcal{S} specified by the (non-composite) intersection of irreducible surfaces, $g(x, y, z) = 0$ and $h(x, y, z) = 0$, of degree m and n . The

degree $d = mn$ of this curve is the number of its intersection points with an arbitrary plane (counted with multiplicity over complex projective space).

Consider the plane \mathcal{P} with unit normal \mathbf{n} through a point $\mathbf{p}_0 = (x_0, y_0, z_0)$ of \mathcal{S} . If $\mathbf{e}_u, \mathbf{e}_v$ are unit vectors orthogonal to \mathbf{n} and to each other, then

$$\mathbf{r}(u, v) = \mathbf{p}_0 + \mathbf{e}_u u + \mathbf{e}_v v \quad (9.35)$$

defines a parameterization of this plane \mathcal{P} . It cuts the two surfaces in plane algebraic curves of degree m and n , whose equations in the coordinates (u, v) of \mathcal{P} are obtained by substituting the components $x(u, v), y(u, v), z(u, v)$ of (9.35) into $g(x, y, z) = 0$ and $h(x, y, z) = 0$ and performing Taylor expansions:

$$\begin{aligned} p(u, v) &= \nabla_u g^{(0)} u + \nabla_v g^{(0)} v \\ &\quad + \frac{1}{2} [\nabla_u^2 g^{(0)} u^2 + 2 \nabla_u \nabla_v g^{(0)} uv + \nabla_v^2 g^{(0)} v^2] + \dots = 0, \\ q(u, v) &= \nabla_u h^{(0)} u + \nabla_v h^{(0)} v \\ &\quad + \frac{1}{2} [\nabla_u^2 h^{(0)} u^2 + 2 \nabla_u \nabla_v h^{(0)} uv + \nabla_v^2 h^{(0)} v^2] + \dots = 0, \end{aligned} \quad (9.36)$$

where ∇_u, ∇_v are the dot products of $\mathbf{e}_u, \mathbf{e}_v$ with the gradient operator ∇ in \mathbb{R}^3 (the superscripts on the derivatives of g and h indicate evaluation at \mathbf{p}_0). Note that the plane section curves $p(u, v) = 0$ and $q(u, v) = 0$ are indeed of degree m and n , since partial derivatives of g and h of order greater than m and n , respectively, vanish identically. We also note that these equations both lack constant terms: $g^{(0)} = h^{(0)} = 0$, since \mathbf{p}_0 lies on \mathcal{S} by supposition, and hence on both the surfaces $g(x, y, z) = 0$ and $h(x, y, z) = 0$.

Now common points of the curves $p(u, v) = 0, q(u, v) = 0$ define locations where the space curve \mathcal{S} intersects the plane \mathcal{P} . Moreover, the *multiplicities* of such common points (see §9.2.9) of the plane section curves indicate how many times each distinct intersection of \mathcal{S} with \mathcal{P} must be counted in order to obtain the total of $d = mn$ intersections. Clearly $(u, v) = (0, 0)$ is a common point of $p(u, v) = 0, q(u, v) = 0$. Suppose this point is non-singular on each of these plane curves. If the curves have distinct tangents there, \mathbf{p}_0 counts as just one intersection of the space curve \mathcal{S} with the plane \mathcal{P} . However, if the plane section curves have a common tangent at $(0, 0)$ — i.e., if the condition

$$p_u(0, 0) : p_v(0, 0) = q_u(0, 0) : q_v(0, 0)$$

is satisfied — \mathbf{p}_0 counts for (at least) two intersections of \mathcal{S} with \mathcal{P} . Using (9.36) and the vector identity $(\mathbf{a} \times \mathbf{b}) \cdot (\mathbf{c} \times \mathbf{d}) = (\mathbf{a} \cdot \mathbf{c})(\mathbf{b} \cdot \mathbf{d}) - (\mathbf{a} \cdot \mathbf{d})(\mathbf{b} \cdot \mathbf{c})$, together with the fact that $\mathbf{e}_u \times \mathbf{e}_v = \mathbf{n}$, this condition can be expressed as

$$\mathbf{n} \cdot (\nabla g^{(0)} \times \nabla h^{(0)}) = 0. \quad (9.37)$$

Now if $\nabla g^{(0)}$ and $\nabla h^{(0)}$ are non-vanishing and non-parallel, we define

$$\mathbf{t} = \frac{\nabla g^{(0)} \times \nabla h^{(0)}}{|\nabla g^{(0)} \times \nabla h^{(0)}|} \quad (9.38)$$

to be the unit *tangent*²⁹ to the space curve \mathcal{S} at \mathbf{p}_0 . Thus, a (regular) point of a space curve amounts to a multiple intersection with a plane when the curve tangent \mathbf{t} lies in that plane (i.e., is orthogonal to its normal \mathbf{n}).

If $\nabla g^{(0)} \times \nabla h^{(0)} = \mathbf{0}$, on the other hand, the condition (9.37) is satisfied for planes of *any* orientation — i.e., the point \mathbf{p}_0 corresponds to a multiple intersection of the space curve with the plane for all choices of the normal \mathbf{n} . We then say that \mathbf{p}_0 is a *singular point* of the space curve \mathcal{S} . There are two circumstances under which this may arise: (i) either $\nabla g^{(0)}$ or $\nabla h^{(0)}$ is zero; or (ii) $\nabla g^{(0)}$ and $\nabla h^{(0)}$ are non-zero and parallel. For case (i), \mathbf{p}_0 is a singular point of the space curve because it is singular on either or both surfaces (the components of ∇g and ∇h are (g_x, g_y, g_z) and (h_x, h_y, h_z) — recall from §9.3.1 that a singular point of a surface arises if all three partial derivatives are zero). In case (ii), \mathbf{p}_0 is a *regular* point on both surfaces, and a singularity arises on the space curve because the surfaces have a *common tangent plane* at \mathbf{p}_0 .

We assumed above that $(u, v) = (0, 0)$ is a non-singular point on both the curves (9.36). If $\nabla g^{(0)} \neq \mathbf{0}$ and $\nabla h^{(0)} \neq \mathbf{0}$, we have $p_u(0, 0) = p_v(0, 0) = 0$ or $q_u(0, 0) = q_v(0, 0) = 0$ only if $\nabla g^{(0)}$ or $\nabla h^{(0)}$, respectively, is parallel to \mathbf{n} . This implies that condition (9.37) is met — i.e., that \mathbf{p}_0 is a *regular* point of the space curve \mathcal{S} , which has a multiple intersection with the plane \mathcal{P} there since its normal \mathbf{n} is orthogonal to the curve tangent \mathbf{t} . Thus, \mathbf{p}_0 is a singular point of the algebraic space curve defined by the intersection of two surfaces if and only if: (a) it is singular on either (or both) of the surfaces; or (b) the surfaces have a common tangent plane at \mathbf{p}_0 . Circumstances (a) and (b) may also arise *simultaneously*, and this greatly complicates determination of the multiplicity of a singular point on a space curve. However, it is not less than the product of the multiplicities of that point on the individual surfaces.

An r -fold point \mathbf{p}_0 of a space curve of degree d has the property that *any* plane through \mathbf{p}_0 must be counted as having (at least) r of its d intersections with the curve at that point. The curve tangent (9.38) is not uniquely defined at such a point: in fact, there are r tangent directions — not necessarily real or distinct — such that a plane whose normal is orthogonal to any of these directions has *more than* r intersections with the space curve at that point.

²⁹ Since the directions of $\nabla g^{(0)}$ and $\nabla h^{(0)}$ define the *surface normals* at the point \mathbf{p}_0 , the tangent of the space curve is orthogonal to both surface normals — it lies along the intersection of the surface tangent planes at that point.

10

Non-Euclidean Geometry

Out of nothing I have created a strange new universe.

János Bolyai (1802–1860)

I am convinced more and more that the necessary truth of our geometry cannot be demonstrated, at least not by the human intellect to the human understanding. Perhaps in another world, we may gain insights into the nature of space which at present are unattainable to us. Until then we must consider geometry as of equal rank not with arithmetic, which is purely a priori, but with mechanics.

Karl Friedrich Gauss (1777–1855)

Computing the distance between points on a plane is a trivial matter once we erect a Cartesian coordinate system on it — we simply use equation (7.1). Seen from a three-dimensional vantage point, the plane may have any position or orientation we like. If we choose to remain “in” the plane, we can regard it as a *two-dimensional space* in its own right: the possibility of erecting Cartesian coordinates upon it, and using equation (7.1) to measure distances between its points, characterizes it as a “flat” or *Euclidean* space.

Consider now a curved surface, upon which we choose two points, and we again wish to measure the distance between them. By this we mean not the length of the straight line “crossing through three-dimensional space” that connects these two points, but rather the length of the (shortest) curve *lying in the surface* between them. Here, again, we regard the curved surface as a two-dimensional space in its own right, and make no reference to the three-dimensional space in which it resides. No Cartesian coordinate system can cover the surface, and hence no simple algebraic relation such as (7.1) suffices for determining distances on it. Indeed, since it is a “curved” or *non-Euclidean* space, a sophisticated theory involving tensor algebra, non-linear differential

equations, and the calculus of variations must be invoked. In this chapter we review some basic concepts from the geometry of curved spaces, also known as *non-Euclidean* or *Riemannian* geometry (see §8.5 for a detailed treatment of the two-dimensional case, i.e., the intrinsic geometry of curved surfaces).

10.1 The Metric Tensor

In §7.3.2, we introduced the *metric tensor* as the basis for measuring angles and distances in plane curvilinear coordinates, as defined by the two functions (7.34) corresponding to the parameterization (7.35) of the plane. The methods discussed in §7.3.2 carry over directly to measurement of angles and distances *on a curved surface*, specified by the parametric representation

$$\mathbf{r}(\zeta, \eta) = \mathbf{i}x(\zeta, \eta) + \mathbf{j}y(\zeta, \eta) + \mathbf{k}z(\zeta, \eta), \quad (10.1)$$

where $\mathbf{i}, \mathbf{j}, \mathbf{k}$ are unit vectors along Cartesian axes in three dimensions. Here we regard the “surface parameters” ζ and η as *curvilinear coordinates* spanning the two-dimensional space defined by this surface.

The principal difference between the present context and §7.3.2 is that, in the case of the planar or “flat” space (7.35) one may opt for either Cartesian or curvilinear coordinates, but the “curved” space specified by (10.1) *does not admit Cartesian coordinates* and thus a more-complicated machinery for angle and distance measurements, based on the metric tensor, is *mandatory*. As in §7.3.2, the metric tensor elements are defined in terms of the dot products of the partial derivatives

$$\mathbf{r}_\zeta = \mathbf{i}\frac{\partial x}{\partial \zeta} + \mathbf{j}\frac{\partial y}{\partial \zeta} + \mathbf{k}\frac{\partial z}{\partial \zeta} \quad \text{and} \quad \mathbf{r}_\eta = \mathbf{i}\frac{\partial x}{\partial \eta} + \mathbf{j}\frac{\partial y}{\partial \eta} + \mathbf{k}\frac{\partial z}{\partial \eta} \quad (10.2)$$

of the surface (10.1), and the distance element ds between neighboring points (ζ, η) and $(\zeta + d\zeta, \eta + d\eta)$ is again given by expression (7.38). The length of a finite curve, defined by parametric surface-coordinate functions $\zeta(t), \eta(t)$ for $t \in [t_0, t_1]$, is determined by evaluating the integral (7.39).

We can also apply the angle-measurement procedure of §7.3.2 to curved surfaces by determining the basis vectors (7.40) from the surface derivatives (10.2) — which are assumed to be everywhere linearly independent. The basis $(\mathbf{e}_\zeta, \mathbf{e}_\eta)$ at any point spans the surface *tangent plane* at that point, and a vector is considered to be “in” the surface if it resides within this tangent plane.¹ Before we proceed to determine angles between vectors on a curved surface, however, it is prudent to examine some fundamental notions about how we specify such vectors in terms of their components.

¹ Recall from §7.3.2 that, in curvilinear coordinates, vectors are *attached to specific points*: there are no “free” vectors. We also caution against the temptation (which is second nature in Cartesian coordinates) to consider the *differences* between the coordinates of two points as components of a vector.

10.2 Contravariant and Covariant Vectors

The Cartesian components (v_x, v_y) of a prescribed vector \mathbf{v} at any point of the two-dimensional Euclidean space \mathbb{R}^2 are determined by drawing perpendicular axes OX and OY through that point as a local origin O . The component v_x of \mathbf{v} may then be defined as the directed length obtained by either (i) drawing a line from OY , parallel to OX , to the tip of \mathbf{v} , or (ii) measuring along OX to the point where a perpendicular drawn from the tip of \mathbf{v} meets that axis. The component v_y is defined analogously. It is the *orthogonality* of the coordinate axes that guarantees the equivalence of these “parallel” and “perpendicular” projection methods for measuring vector components.

Consider now how these concepts generalize to the problem of measuring the curvilinear-coordinate components of a vector \mathbf{v} at a given point (ζ, η) of a two-dimensional *non-Euclidean* space. The basis vectors \mathbf{e}_ζ and \mathbf{e}_η define “oblique coordinates” in the tangent plane: in general, they are not orthogonal, and hence the above prescriptions (i) and (ii) for the components of \mathbf{v} are *not* equivalent in this context (see Fig. 10.1). If v^ζ and v^η are the components of \mathbf{v} obtained by *parallel projection* onto the basis vectors, as in prescription (i), then by the familiar parallelogram rule for vector addition we may write

$$\mathbf{v} = v^\zeta \mathbf{e}_\zeta + v^\eta \mathbf{e}_\eta, \quad (10.3)$$

in agreement with the usual expression for a vector in terms of a unit basis. The scalar values v^ζ and v^η are called the *contravariant components* of \mathbf{v} .

If, on the other hand, we follow prescription (ii) and denote by v_ζ and v_η the lengths obtained by *perpendicular projection* of \mathbf{v} onto \mathbf{e}_ζ and \mathbf{e}_η , these *covariant components* may evidently be expressed as

$$v_\zeta = \mathbf{e}_\zeta \cdot \mathbf{v} = v^\zeta + v^\eta \cos \phi, \quad v_\eta = \mathbf{e}_\eta \cdot \mathbf{v} = v^\zeta \cos \phi + v^\eta, \quad (10.4)$$

with $\cos \phi = \mathbf{e}_\zeta \cdot \mathbf{e}_\eta$. Adding the products of the covariant components with the basis vectors \mathbf{e}_ζ and \mathbf{e}_η does *not*, however, produce the vector \mathbf{v} . We can

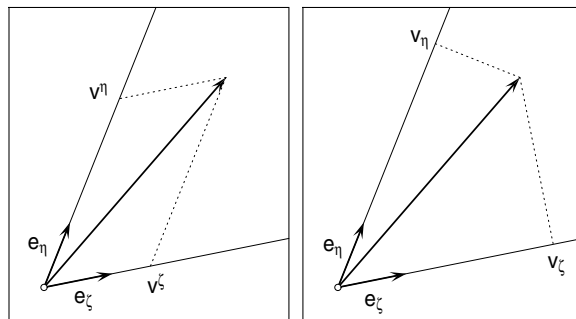


Fig. 10.1. Contravariant (left) and covariant (right) components of a vector.

interpret v_ζ and v_η as the components of \mathbf{v} in a different (non-unit) basis,² which we write with superscripts and define by

$$\begin{bmatrix} \mathbf{e}^\zeta \\ \mathbf{e}^\eta \end{bmatrix} = \frac{1}{\sin^2 \phi} \begin{bmatrix} 1 & -\cos \phi \\ -\cos \phi & 1 \end{bmatrix} \begin{bmatrix} \mathbf{e}_\zeta \\ \mathbf{e}_\eta \end{bmatrix}. \quad (10.5)$$

Geometrically, \mathbf{e}^ζ and \mathbf{e}^η are vectors of magnitude $|\sin \phi|^{-1}$ orthogonal to \mathbf{e}_η and \mathbf{e}_ζ , respectively. On account of the fact that

$$\mathbf{e}_\zeta \cdot \mathbf{e}^\zeta = \mathbf{e}_\eta \cdot \mathbf{e}^\eta = 1 \quad \text{and} \quad \mathbf{e}_\zeta \cdot \mathbf{e}^\eta = \mathbf{e}_\eta \cdot \mathbf{e}^\zeta = 0, \quad (10.6)$$

we say that the two bases $\mathbf{e}_\zeta, \mathbf{e}_\eta$ and $\mathbf{e}^\zeta, \mathbf{e}^\eta$ are “dual” to each other. Using (10.4) and (10.5), it is then easily verified that

$$\mathbf{v} = v_\zeta \mathbf{e}^\zeta + v_\eta \mathbf{e}^\eta. \quad (10.7)$$

In the special case of *orthogonal* coordinates³ — i.e., $\phi = \pi/2$ for all (ζ, η) — the distinction between contravariant and covariant components of a vector \mathbf{v} vanishes, as is evident from equations (10.4) and (10.5).

The use of *both* the contravariant and covariant representations of a vector in curvilinear coordinates may seem, at first, rather contrived or redundant. But it serves a very important purpose: it allows us to express the fact that vectors are “geometrical” entities, characterized by attributes — lengths and directions — *independent of the chosen coordinates*. Consider the problem of computing the length $|\mathbf{v}| = \sqrt{\mathbf{v} \cdot \mathbf{v}}$ of a vector. Depending on whether we choose the contravariant form (10.3) or covariant form (10.7), we obtain

$$\sqrt{(v^\zeta)^2 + (v^\eta)^2 + 2v^\zeta v^\eta \cos \phi} \quad \text{or} \quad \frac{\sqrt{(v_\zeta)^2 + (v_\eta)^2 - 2v_\zeta v_\eta \cos \phi}}{|\sin \phi|}. \quad (10.8)$$

The appearance of the angle ϕ between \mathbf{e}_ζ and \mathbf{e}_η in these expressions incurs an explicit dependence of $|\mathbf{v}|$ on *location* in the chosen coordinate system.

We would like to express the length of \mathbf{v} purely in terms of its components, without explicit reference to its location. This can be accomplished by using one contravariant and one covariant form in the dot product $\mathbf{v} \cdot \mathbf{v}$. We write

$$|\mathbf{v}| = \sqrt{(v^\zeta \mathbf{e}_\zeta + v^\eta \mathbf{e}_\eta) \cdot (v_\zeta \mathbf{e}^\zeta + v_\eta \mathbf{e}^\eta)} = \sqrt{v^\zeta v_\zeta + v^\eta v_\eta}, \quad (10.9)$$

where the final expression follows from the fact that $\mathbf{e}_\zeta \cdot \mathbf{e}^\eta = \mathbf{e}_\eta \cdot \mathbf{e}^\zeta = 0$ and $\mathbf{e}_\zeta \cdot \mathbf{e}^\zeta = \mathbf{e}_\eta \cdot \mathbf{e}^\eta = 1$, as may be verified from (10.5). From this expression we

² We must divide the components v_ζ and v_η obtained by perpendicular projection in Fig. 10.1 by $|\sin \phi|$ if we wish to unitize \mathbf{e}^ζ and \mathbf{e}^η . It is simplest to omit this: in curvilinear coordinates, the use of non-unit bases is common practice.

³ Cartesian coordinates are an obvious example, though curvilinear systems may also be orthogonal, as in the case of polar coordinates discussed in §7.3.4. General curved spaces, however, do not ordinarily admit orthogonal coordinate systems.

see that, by carrying both contravariant and covariant forms, we can directly compute the length of a vector without specifying its location.

Using relations (10.4) and (10.5), it can be seen that (10.9) is equivalent to the earlier formulations (10.8), expressed solely in terms of the contravariant and covariant components. We can also generalize this approach to define the dot product of *any* two curvilinear-coordinate vectors, $\mathbf{u} = u^\zeta \mathbf{e}_\zeta + u^\eta \mathbf{e}_\eta$ and $\mathbf{v} = v_\zeta \mathbf{e}^\zeta + v_\eta \mathbf{e}^\eta$, when one is given in contravariant and the other in covariant form (it does not matter which is which). Thus, we write

$$\mathbf{u} \cdot \mathbf{v} = u^\zeta v_\zeta + u^\eta v_\eta,$$

and the angle θ between \mathbf{u} and \mathbf{v} may be determined from $\mathbf{u} \cdot \mathbf{v} = |\mathbf{u}| |\mathbf{v}| \cos \theta$.

10.3 Methods of Tensor Algebra

Contravariant and covariant vectors are *first-order tensors*. They are defined, in a given curvilinear coordinate system, by specifying certain scalar functions — their “components” — of the coordinates. In a general n -dimensional space, a first-order tensor is described by n components — one associated with each of the coordinate directions. We may also define higher-order tensors. They are likewise specified in terms of sets of scalar components, associated with *combinations* of the coordinate directions. In n -dimensional space, a k^{th} -order tensor has n^k components, one for each ordered set of k coordinate directions.

A simple way to form higher-order tensors is to take the “tensor product” of two or more vectors. Multiplying each of the n components of one vector with each of those of another vector, for example, yields n^2 functions that can be regarded as the components of a second-order tensor. Not all higher-order tensors are of this “composite” form, however. An example is the 2nd-order *stress tensor* in \mathbb{R}^3 , whose components can be arranged in a matrix:

$$\begin{bmatrix} \sigma_{xx} & \sigma_{xy} & \sigma_{xz} \\ \sigma_{yx} & \sigma_{yy} & \sigma_{yz} \\ \sigma_{zx} & \sigma_{zy} & \sigma_{zz} \end{bmatrix}. \quad (10.10)$$

Each component represents a force per unit area: the first subscript gives the direction of the normal to the area, while the second indicates the direction of the force acting on it.⁴ Upon multiplying this tensor on the left and right by appropriate unit vectors, one may determine the force-per-unit-area in any direction acting on a plane of any orientation. In some problems, it is useful to express the stress tensor in cylindrical polar coordinates (ρ, ϕ, z) or spherical polar coordinates (r, ϕ, θ) . The tensor components in these systems may be obtained through systematic *transformation laws* that we describe below.

Now although a definite coordinate system is needed to specify a tensor, so as to give its component-functions concrete expression, all tensors embody

⁴ The diagonal and off-diagonal components are *direct* and *shear* stresses.

certain “intrinsic” features — computable from their components — that are *the same in all coordinate systems*. For first-order tensors these “invariants” are clearly vector magnitudes and directions. For second-order tensors, such as the stress tensor (10.10), the *eigenvalues* and *eigenvectors* are invariant.⁵

We now describe how the components of a tensor in one coordinate system are obtained from those in another, in the general context of an n -dimensional curved space. Let (ξ^1, \dots, ξ^n) and $(\bar{\xi}^1, \dots, \bar{\xi}^n)$ be curvilinear coordinates for such a space, the transformation from the latter to the former being defined by functions

$$\xi^k(\bar{\xi}^1, \dots, \bar{\xi}^n) \quad \text{for } k = 1, \dots, n, \quad (10.11)$$

and the converse transformation by the corresponding inverse functions

$$\bar{\xi}^k(\xi^1, \dots, \xi^n) \quad \text{for } k = 1, \dots, n. \quad (10.12)$$

By the chain rule, we may write the derivative operator with respect to ξ^j as

$$\frac{\partial}{\partial \xi^j} = \sum_{k=1}^n \frac{\partial \bar{\xi}^k}{\partial \xi^j} \frac{\partial}{\partial \bar{\xi}^k}, \quad (10.13)$$

and if we apply this to coordinate ξ^i , we obtain the important relation

$$\sum_{k=1}^n \frac{\partial \bar{\xi}^k}{\partial \xi^j} \frac{\partial \xi^i}{\partial \bar{\xi}^k} = \delta_j^i = \begin{cases} 1 & \text{if } i = j \\ 0 & \text{otherwise} \end{cases} \quad (10.14)$$

concerning derivatives of the coordinate transformations (10.11) and (10.12). Geometrically, $\partial \xi^i / \partial \xi^j$ vanishes when $i \neq j$ since the coordinate ξ^i remains constant on loci along which only ξ^j increases — otherwise we obviously have $\partial \xi^i / \partial \xi^j = 1$ if $i = j$ (δ_j^i is the Kronecker delta symbol). Equation (10.14) has a simple interpretation: it says that the *Jacobian matrices* for the coordinate functions (10.11) and (10.12) must be inverses of each other.

In expressions (10.13) and (10.14) the summation index k appears *twice* in the summands, and in tensor algebra it is typically true that a repeated index is associated with summation over that index. Thus, we shall henceforth use a convenient shorthand,⁶ known as the *summation convention*, in which we omit summation signs and interpret repeated indices as *implying* a summation from 1 to n . Such indices are called “dummy” indices (as distinct from unrepeated or “free” indices), since we can replace them by any unused index symbol without altering the meaning of an expression.

⁵ The eigenvectors of the stress tensor identify the *principal planes*, on which the shear stress is zero, and the eigenvalues give the corresponding *principal stresses* on those planes, which represent extremal values of the direct stress.

⁶ This scheme was popularized by Albert Einstein (1879–1955), who made extensive use of it in developing the general theory of relativity.

Now suppose the coordinates (10.11) are regarded as parametric variables that specify location on a curved “hypersurface” $\mathbf{r}(\xi^1, \dots, \xi^n)$ which resides⁷ in an $(n+1)$ -dimensional Euclidean space. Then the components of the metric tensor are given by

$$g_{ij}(\xi^1, \dots, \xi^n) = \frac{\partial \mathbf{r}}{\partial \xi^i} \cdot \frac{\partial \mathbf{r}}{\partial \xi^j}, \quad (10.15)$$

for $1 \leq i, j \leq n$, and the distance ds corresponding to coordinate increments $(d\xi^1, \dots, d\xi^n)$ about any point is expressed by the quadratic form

$$ds^2 = g_{ij} d\xi^i d\xi^j \quad (10.16)$$

(in the above, and henceforth, the summation convention is in effect). Also, if $G(\xi^1, \dots, \xi^n)$ denotes the determinant of the $n \times n$ array of metric elements (10.15), the n -dimensional “volume element” of our curved space, defined by a parallelepiped with coordinate increments $d\xi^1, \dots, d\xi^n$ for its sides, is

$$dV = \sqrt{G} d\xi^1 \cdots d\xi^n. \quad (10.17)$$

In the familiar case $n = 2$ of a curved surface — with $(\xi^1, \xi^2) = (\zeta, \eta)$ say — this reduces to the usual area-element expression $dA = |\mathbf{r}_\zeta \times \mathbf{r}_\eta| d\zeta d\eta$.

The metric elements $\bar{g}_{ij}(\bar{\xi}^1, \dots, \bar{\xi}^n)$ for $1 \leq i, j \leq n$, corresponding to the alternative coordinate system (10.12), may be defined analogously in terms of a re-parameterization $\bar{\mathbf{r}}(\bar{\xi}^1, \dots, \bar{\xi}^n)$ of the hypersurface. Distance and volume elements in this curved space, in terms of the alternative coordinates (10.12), are then given by expressions analogous to (10.16) and (10.17).

As local bases for vectors “in” our n -dimensional non-Euclidean space, we use the hypersurface partial derivatives

$$\mathbf{e}_j = \frac{\partial \mathbf{r}}{\partial \xi^j} \quad (10.18)$$

for $j = 1, \dots, n$, which we assume are everywhere linearly independent: these vectors span the *tangent hyperplane* to $\mathbf{r}(\xi^1, \dots, \xi^n)$ at each point. We do not bother to unitize these basis vectors. Consider now the transformation of the contravariant vector

$$\mathbf{v} = v^j \mathbf{e}_j, \quad (10.19)$$

as specified in the coordinate system (10.11), to the system (10.12). Applying (10.13) to $\bar{\mathbf{r}}(\bar{\xi}^1, \dots, \bar{\xi}^n)$, we observe that the basis (10.18) in the (ξ^1, \dots, ξ^n) coordinates is related to that $\bar{\mathbf{e}}_k = \partial \bar{\mathbf{r}} / \partial \bar{\xi}^k$ in the $(\bar{\xi}^1, \dots, \bar{\xi}^n)$ coordinates by

$$\mathbf{e}_j = \frac{\partial \bar{\xi}^k}{\partial \xi^j} \bar{\mathbf{e}}_k$$

⁷ Here \mathbf{r} is a Euclidean vector of dimension $n+1$, and the dot products in equation (10.15) are to be interpreted accordingly.

for $k = 1, \dots, n$. Hence, substituting into (10.19), we see that the contravariant components $(\bar{v}^1, \dots, \bar{v}^n)$ in the system $(\bar{\xi}^1, \dots, \bar{\xi}^n)$ are given by

$$\bar{v}^k = \frac{\partial \bar{\xi}^k}{\partial \xi^j} v^j \quad (10.20)$$

for $k = 1, \dots, n$. We may interpret (10.20) as the *definition* of a contravariant vector \mathbf{v} — namely, it is an infinite family of scalar n -tuples (v^1, \dots, v^n) , one associated with each curvilinear coordinate system (ξ^1, \dots, ξ^n) , such that the values or “contravariant components” in two different systems are related to each other by the transformation law (10.20).

We can also express the vector (10.19) in covariant form as

$$\mathbf{v} = v_j \mathbf{e}^j, \quad (10.21)$$

where the *dual* vector basis $\mathbf{e}^1, \dots, \mathbf{e}^n$ is completely specified by the conditions

$$\mathbf{e}^j \cdot \mathbf{e}_k = \delta_k^j \quad (10.22)$$

for $1 \leq j, k \leq n$, which define the n -dimensional generalization of expressions (10.6) in the case $n = 2$. Geometrically, \mathbf{e}^j is a vector that is orthogonal to the hyperplane spanned by all of the vectors $\mathbf{e}_1, \dots, \mathbf{e}_n$ *except* \mathbf{e}_j , and we require that the projection of \mathbf{e}^j onto \mathbf{e}_j be of unit length. Conditions (10.22) allow us to interpret the contravariant and covariant components of a vector \mathbf{v} as its dot products with appropriate basis vectors, namely:

$$v^k = \mathbf{v} \cdot \mathbf{e}^k \quad \text{and} \quad v_k = \mathbf{v} \cdot \mathbf{e}_k. \quad (10.23)$$

In §10.2 we saw in the two-dimensional case that, by taking one vector in contravariant form and the other in covariant form, we could express their dot product as an *invariant*, i.e., in a form independent of the chosen coordinates. In the general n -dimensional case, we require covariant vectors to transform in a manner, consistent with the established contravariant–vector transformation rule (10.20), such as to retain this property. Now the length $|\mathbf{v}|$ of any vector must be the same in all coordinates, and we express it in terms of contravariant and covariant components in the systems (ξ^1, \dots, ξ^n) and $(\bar{\xi}^1, \dots, \bar{\xi}^n)$ as

$$|\mathbf{v}|^2 = v^j v_j = \bar{v}^k \bar{v}_k. \quad (10.24)$$

Suppose that the covariant components obey the transformation law

$$\bar{v}_k = C_k^i v_i, \quad k = 1, \dots, n.$$

Substituting this and expression (10.20) into (10.24), we obtain the identity

$$v^j v_j = \frac{\partial \bar{\xi}^k}{\partial \xi^j} C_k^i v^j v_i,$$

which must hold for *all* corresponding n -tuples, (v^1, \dots, v^n) and (v_1, \dots, v_n) . The sum on the left comprises only “diagonal” terms $v^1 v_1 + \dots + v^n v_n$, while on the right we have a double-sum over all terms $v^j v_i$ for $1 \leq i, j \leq n$. Hence, the quantity $(\partial \bar{\xi}^k / \partial \xi^j) C_k^i$ must vanish unless $i = j$, in which case it must be unity. We can now infer from (10.14) that $C_k^i = \partial \xi^i / \partial \bar{\xi}^k$, and the fundamental transformation law characterizing covariant vectors may be written as

$$\bar{v}_k = \frac{\partial \xi^i}{\partial \bar{\xi}^k} v_i, \quad k = 1, \dots, n. \quad (10.25)$$

The contravariant and covariant transformation laws (10.20) and (10.25) for vectors can be readily extended to higher-order tensors. Thus, for example, if a^{ij} and b_{ij} are the components of contravariant and covariant second-order tensors in the coordinates (ξ^1, \dots, ξ^n) , their components in the coordinates $(\bar{\xi}^1, \dots, \bar{\xi}^n)$ are given by

$$\bar{a}^{kl} = \frac{\partial \bar{\xi}^k}{\partial \xi^i} \frac{\partial \bar{\xi}^l}{\partial \xi^j} a^{ij} \quad \text{and} \quad \bar{b}_{kl} = \frac{\partial \xi^i}{\partial \bar{\xi}^k} \frac{\partial \xi^j}{\partial \bar{\xi}^l} b_{ij} \quad (10.26)$$

for $1 \leq k, l \leq n$. One can also have higher-order tensors that are of “mixed” type, with both contravariant (superscript) and covariant (subscript) indices. For example, the mixed second-order tensor c^i_j transforms according to

$$\bar{c}_l^k = \frac{\partial \bar{\xi}^k}{\partial \xi^i} \frac{\partial \xi^j}{\partial \bar{\xi}^l} c^i_j. \quad (10.27)$$

Note that the *order* of indices is important, so we leave “blanks” among the superscripts or subscripts of mixed tensors to indicate proper positions.

The metric defined in (10.15) is a *covariant* second-order tensor. In terms of the basis vectors (10.18), it is given by $g_{ij} = \mathbf{e}_i \cdot \mathbf{e}_j$ for $1 \leq i, j \leq n$. By analogy, we now introduce the *contravariant* metric tensor

$$g^{ij} = \mathbf{e}^i \cdot \mathbf{e}^j, \quad 1 \leq i, j \leq n$$

defined by dot products of the *dual* basis vectors. Interpreted as matrices, the covariant and contravariant metrics are actually inverses of each other, i.e.,

$$g_{ij} g^{jk} = \delta_i^k, \quad 1 \leq i, k \leq n. \quad (10.28)$$

This can be seen as follows. Using relations (10.23) we note that any vector \mathbf{v} can be written as $\mathbf{v} = (\mathbf{v} \cdot \mathbf{e}_j) \mathbf{e}^j$. Thus, if we choose $\mathbf{v} = \mathbf{e}_i$, we find that

$$\mathbf{e}_i = (\mathbf{e}_i \cdot \mathbf{e}_j) \mathbf{e}^j = g_{ij} \mathbf{e}^j,$$

and on taking the dot product of the left- and right-hand sides with \mathbf{e}^k , and recalling the property (10.22) of the dual bases, we arrive at (10.28).

The contravariant and covariant metrics can be used to “raise” and “lower” indices — i.e., to convert covariant into contravariant components and vice-versa. Taking the dot products of $\mathbf{v} = v_j \mathbf{e}^j$ and $\mathbf{v} = v^j \mathbf{e}_j$ with \mathbf{e}^i and \mathbf{e}_i , respectively, we find that

$$v^i = g^{ij} v_j \quad \text{and} \quad v_i = g_{ij} v^j.$$

This raising/lowering “index mechanics” also applies to higher-order tensors.

The vector dot product (10.24) is the simplest example of a “contracted” tensor expression, in which all indices appear in contravariant and covariant (i.e., upper and lower) pairs, implying summation from 1 to n . We may also form contracted combinations of higher-order tensors, with no remaining free indices, such as

$$u^i a_{ij} b^{jk} v_k \quad \text{and} \quad a^i_i.$$

The significance of such tensor contractions, in which no free indices remain, is that they identify *invariants* — quantities that have the same value in *all* coordinate systems. The invariance of contracted tensor expressions follows from the contravariant/covariant transformation rules discussed above.

10.4 The Geodesic Equations

A path between two points $\mathbf{p}_0 = (\xi_0^1, \dots, \xi_0^n)$ and $\mathbf{p}_1 = (\xi_1^1, \dots, \xi_1^n)$ in a curved n -dimensional space may be described parametrically by n functions $\xi^k(t)$ of a parameter $t \in [0, 1]$ such that $\xi^k(0) = \xi_0^k$ and $\xi^k(1) = \xi_1^k$ for $k = 1, \dots, n$. We are concerned with identifying paths of least length, or *geodesics*, between the given points. These are the analogs of straight lines in Euclidean space.

Denoting the derivative of $\xi^k(t)$ with respect to t by $\dot{\xi}^k(t)$, we set $d\xi^k = \dot{\xi}^k dt$ in (10.16) and hence express the distance element as

$$ds = \sqrt{g_{ij} \dot{\xi}^i \dot{\xi}^j} dt.$$

The total distance between \mathbf{p}_0 and \mathbf{p}_1 is then

$$S = \int_0^1 \sqrt{g_{ij} \dot{\xi}^i \dot{\xi}^j} dt, \tag{10.29}$$

and we desire the path $\xi^1(t), \dots, \xi^n(t)$ that will minimize S . This is a standard problem in the calculus of variations [45], involving n unknown functions of a single independent variable. Regarding the integrand in (10.29) as a function $F(t, \xi^1, \dot{\xi}^1, \dots, \xi^n, \dot{\xi}^n)$ of the path parameter t and the n coordinates and their parametric derivatives, the solutions to the *Euler–Lagrange equations*

$$\frac{\partial F}{\partial \xi^k} - \frac{d}{dt} \frac{\partial F}{\partial \dot{\xi}^k} = 0$$

for $k = 1, \dots, n$ identify the sets of functions $\xi^1(t), \dots, \xi^n(t)$ that cause S to be an extremum value. In the reduction of these equations, the combinations

$$\Gamma_{ij}^k = \frac{1}{2} g^{kl} \left(\frac{\partial g_{jl}}{\partial \xi^i} + \frac{\partial g_{il}}{\partial \xi^j} - \frac{\partial g_{ij}}{\partial \xi^l} \right) \quad (10.30)$$

for $1 \leq i, j, k \leq n$ of the metric tensor derivatives occur. These quantities are called the *Christoffel symbols*.⁸ We have already encountered them (see §8.5.9) in our discussion of curved surfaces, $n = 2$, and we shall encounter them again in other contexts (see §10.5 and 10.6 below). Note that the Christoffel symbols are symmetric with respect to the lower indices: $\Gamma_{ij}^k = \Gamma_{ji}^k$.

Using the Christoffel symbols, the Euler–Lagrange equations become

$$\frac{d^2 \xi^k}{ds^2} + \Gamma_{ij}^k \frac{d\xi^i}{ds} \frac{d\xi^j}{ds} = 0, \quad k = 1, \dots, n, \quad (10.31)$$

s being the *arc length* along a geodesic. These *geodesic equations* comprise a system of n coupled, non-linear, second-order ordinary differential equations. They may be solved as a boundary value problem, as discussed above, or as an initial-value problem in which we specify a starting point and *direction* for the geodesic. In the former context, there may be more than one solution — possibly identifying *maxima*, as well as minima, of the integral (10.29).

Note that, in (10.30), the rather intimidating expression involving partial derivatives of the metric tensor (10.15) has a simpler vectorial interpretation in terms of the parameterized “hypersurface” representation $\mathbf{r}(\xi^1, \dots, \xi^n)$ of our curved space — it can be verified that

$$\frac{1}{2} \left(\frac{\partial g_{jl}}{\partial \xi^i} + \frac{\partial g_{il}}{\partial \xi^j} - \frac{\partial g_{ij}}{\partial \xi^l} \right) = \frac{\partial^2 \mathbf{r}}{\partial \xi^i \partial \xi^j} \cdot \frac{\partial \mathbf{r}}{\partial \xi^l}. \quad (10.32)$$

10.5 Differentiation of Tensors

The *gradient* $\nabla\phi$ of a scalar function $\phi(\xi^1, \dots, \xi^n)$ is an important example of a covariant vector. The components of $\nabla\phi$ are simply

$$\frac{\partial \phi}{\partial \xi^i}, \quad i = 1, \dots, n$$

and the fact that they obey the covariant–vector transformation law (10.25) follows directly from the chain rule for partial derivatives. A scalar function can be regarded as a “zeroth–order” tensor, and its gradient is a first–order tensor. However, when we proceed to vectors or tensors of order $k \geq 1$, we find that their “gradients” are *not* tensors of order $k + 1$.

⁸ Also called the “connection coefficients.” We do not call them Christoffel *tensors* since, in fact, they are not tensors: they do not obey the transformation rules (we shall see in §10.5 that derivatives of tensors are *not* ordinarily tensors themselves).

Consider, for example, the differentiation of a contravariant vector v^j . We will show that the quantities

$$c^j_i = \frac{\partial v^j}{\partial \xi^i}, \quad 1 \leq i, j \leq n$$

do *not* obey the transformation rule (10.27) that characterizes mixed second-order tensors. Applying the derivative

$$\frac{\partial}{\partial \bar{\xi}^l} = \frac{\partial \xi^i}{\partial \bar{\xi}^l} \frac{\partial}{\partial \xi^i}$$

to equation (10.20), we have

$$\bar{c}^k_l = \frac{\partial \xi^i}{\partial \bar{\xi}^l} \frac{\partial}{\partial \xi^i} \left(\frac{\partial \bar{\xi}^k}{\partial \xi^j} v^j \right) = \frac{\partial \xi^i}{\partial \bar{\xi}^l} \frac{\partial^2 \bar{\xi}^k}{\partial \xi^i \partial \xi^j} v^j + \frac{\partial \xi^i}{\partial \bar{\xi}^l} \frac{\partial \bar{\xi}^k}{\partial \xi^j} c^j_i.$$

In the expression on the right, the second term *alone* is what we expect from the transformation rule (10.27) — the presence of the “extra” first term means that the quantities c^j_i are not the components of a tensor.

However, it is possible to append “correction terms” to ordinary derivatives of contravariant and covariant vectors, so as to obtain a tensor result. This process is known as *covariant differentiation*, and it involves the Christoffel symbols (10.30). In the case of a *contravariant* vector v^k , the elements of its covariant derivative are defined to be

$$v^k_{,j} = \frac{\partial v^k}{\partial \xi^j} + \Gamma_{ij}^k v^i \quad (10.33)$$

for $1 \leq j, k \leq n$ — they define a mixed second-order tensor. On the other hand, the covariant derivative of a *covariant* vector v_k has elements

$$v_{k,j} = \frac{\partial v_k}{\partial \xi^j} - \Gamma_{jk}^i v^i \quad (10.34)$$

for $1 \leq j, k \leq n$, which define a covariant second-order tensor. Expressions (10.33) and (10.34) use the convention of denoting covariant derivatives with respect to ξ^j by a subscript j after a comma (following all other superscripts and subscripts of the given tensor).

A proof that the quantities (10.33) and (10.34) do transform properly as second-order tensors may be found in Chap. 7 of [290]. Covariant derivatives of higher-order tensors can also be formed: “correction” terms associated with each superscript or subscript of the given tensor must be included to ensure that the result transforms as a tensor — see [290] for further details.

An elementary example may help to elucidate the significance of covariant differentiation. Suppose a constant vector \mathbf{v} is assigned to each point of the Euclidean plane. When we describe location by Cartesian coordinates (x, y) , derivatives of the components of \mathbf{v} vanish, as expected for a constant vector.

If we use curvilinear coordinates (ζ, η) , however, the components of \mathbf{v} vary from point to point since the vector basis $(\mathbf{e}_\zeta, \mathbf{e}_\eta)$ is varying, and hence they have non-zero derivatives. The Christoffel symbols carry information on the variation of $(\mathbf{e}_\zeta, \mathbf{e}_\eta)$ enabling them, by the “correction” terms, to cancel out this effect and ensure that the *covariant* derivative of \mathbf{v} vanishes.

The process of forming covariant derivatives is sometimes called *absolute differentiation*, to emphasize that it always yields a tensor result. Although we express them using components in specific coordinate systems, tensors are essentially *independent* of all coordinates: they can be completely described by *intrinsic* or “geometrical” properties that are invariant under changes of coordinates (e.g., the eigenvalues and eigenvectors of second-order tensors).

10.6 Parallel Transport of Vectors

In any Euclidean space, endowed with Cartesian coordinates, moving a vector \mathbf{v} from an initial point \mathbf{p}_0 to a final point \mathbf{p}_1 so that it remains parallel to its initial instance is a trivial matter. One way to accomplish this is to simply “copy” the components of \mathbf{v} , given at \mathbf{p}_0 , to the location \mathbf{p}_1 . Another way is to imagine “sliding” the vector along the straight line between \mathbf{p}_0 and \mathbf{p}_1 , such that it always maintains a fixed angle with that line.

Suppose now that \mathbf{p}_0 and \mathbf{p}_1 are points in a *non-Euclidean* space, and we want to find at \mathbf{p}_1 a “parallel” copy of a vector \mathbf{v} specified at \mathbf{p}_0 . As noted in §7.3.2, the vector basis (10.18) in general curvilinear coordinates (ξ^1, \dots, ξ^n) varies from point to point, so it is not geometrically meaningful to just “copy” components with respect to it from one point to another. We can, however, give a sensible generalization for the second of the above methods for *parallel transport* of vectors. Namely, we replace the straight line of Euclidean space by the *geodesic path* between \mathbf{p}_0 and \mathbf{p}_1 in the curved space, and insist that \mathbf{v} *maintains a fixed angle with the geodesic* as it slides along that path.⁹

If coordinate functions $\xi^1(s), \dots, \xi^n(s)$ describe the geodesic between \mathbf{p}_0 and \mathbf{p}_1 , parameterized by arc length s , it can be shown that parallel transport of a vector $\mathbf{v} = (v^1, \dots, v^n)$ amounts to solving the initial-value problem posed by the coupled system of linear first-order differential equations

$$\frac{dv^k}{ds} + \Gamma_{ij}^k v^i \frac{d\xi^j}{ds} = 0, \quad k = 1, \dots, n. \quad (10.35)$$

This concept of “parallelism” of vectors in a curved space was introduced by the Italian mathematician Tullio Levi-Civita (1873–1941).

Actually, we can drop the stipulation that $\xi^1(s), \dots, \xi^n(s)$ be a geodesic, and regard these functions as describing an arbitrary differentiable locus C in the curved space. The solution to (10.35) then defines *parallel transport* of \mathbf{v}

⁹ Both \mathbf{v} and the tangent to the geodesic lie in the *tangent hyperplane* of the curved space at each point, and hence the angle between them is unambiguously defined.

with respect to the curve C . Invoking this concept, we can invert our reasoning above and define a geodesic to be any curve C having the property that its unit tangent vector is parallel-transported along it (note that equations (10.31) are automatically satisfied upon substituting $v^k = d\xi^k/ds$ in (10.35)). A vector that is parallel-transported with respect to a non-geodesic curve C , on the other hand, does not exhibit a fixed angle with the tangent to that curve.

In fact, the ideas of covariant differentiation and parallel transport are intimately related. For any path C with coordinate functions $\xi^1(s), \dots, \xi^n(s)$ of the arc length s , we can define the covariant derivative of a vector v^k along C by contracting the second-order tensor elements $v^k_{,j}$ given by (10.33) with the tangent vector $d\xi^j/ds$ to C . Identifying

$$\frac{d}{ds} = \frac{d\xi^j}{ds} \frac{\partial}{\partial \xi^j}$$

as the derivative operator along C , this yields the right-hand side of (10.35). Hence, a vector is parallel-transported with respect to a curve C if and only if its covariant derivative along that curve vanishes. Conversely, we may regard the covariant derivative of a vector along a path C as measuring the deviation of that vector from being parallel-transported with respect to C .

It is instructive to consider the above concepts in the context of a surface $\mathbf{r}(u, v)$. The geodesics are those curves on the surface along which the curve tangent vectors are parallel transports of each other. Consider a vector

$$\mathbf{a}(s) = a^u(s) \mathbf{r}_u + a^v(s) \mathbf{r}_v$$

defined along a curve $\mathbf{c}(s) = \mathbf{r}(u(s), v(s))$ on the surface by the (contravariant) components (a^u, a^v) specified as differentiable functions of arc length s . We can identify those vector fields $\mathbf{a}(s)$ that correspond to the parallel transport of an “initial” vector $\mathbf{a}(0)$ with respect to $\mathbf{c}(s)$ as follows.

Theorem 10.1 *The members of a vector field $\mathbf{a}(s)$ are parallel transports of each other with respect to the curve $\mathbf{c}(s)$ on the surface $\mathbf{r}(u, v)$ if and only if $d\mathbf{a}/ds$ is everywhere parallel to the surface normal \mathbf{n} .*

To verify Theorem 10.1 one must show that satisfaction of the condition stated therein is equivalent to solving equations (10.35) in the case of a surface.

Now since $\mathbf{a}(s)$ always lies in the local surface tangent plane, and $d\mathbf{a}/ds$ is perpendicular to it, a parallel-transported vector satisfies $|\mathbf{a}(s)| = \text{constant}$. Adopting the perspective of the three-dimensional Euclidean space in which the surface $\mathbf{r}(u, v)$ is embedded, we may regard any vector $\mathbf{a}(s)$ that is parallel-transported with respect to the curve $\mathbf{c}(s)$ as instantaneously rotating about a moving axis that lies in the surface tangent plane at each point of $\mathbf{c}(s)$.

We may elucidate this rotation as follows. Suppose $\mathbf{a}(s)$ and $\mathbf{a}(s+ds)$ are “neighboring” instances of the parallel-transported vector. If the latter were exactly parallel to the former, we would have $\mathbf{k} \cdot [\mathbf{a}(s+ds) - \mathbf{a}(s)] = 0$ for

any vector \mathbf{k} in the surface tangent plane at the point $\mathbf{c}(s)$. But $\mathbf{a}(s + ds)$ is confined to the surface tangent plane at $\mathbf{c}(s + ds)$, which has a somewhat different orientation than that at $\mathbf{c}(s)$, precluding an *exact* satisfaction of this condition for arbitrary curves on the surface. Hence, the rotation that defines $\mathbf{a}(s + ds)$ as an infinitesimal parallel transport of $\mathbf{a}(s)$ is such as to make the former “as parallel as possible” to the latter while still satisfying the constraint that these vectors must reside in their respective tangent planes. Namely, we require that $\mathbf{k} \cdot [\mathbf{a}(s + ds) - \mathbf{a}(s)]$ vanishes to first order in ds for all vectors \mathbf{k} in the surface tangent plane at the point $\mathbf{c}(s)$.

From the perspective of the Euclidean space \mathbb{R}^3 in which $\mathbf{r}(u, v)$ resides, a vector $\mathbf{a}(s)$ parallel-transported along a curve $\mathbf{c}(s)$ on this surface remains from point to point as parallel to itself as is compatible with the constraint of lying at all times in the surface tangent plane. If $\mathbf{t} = \dot{\mathbf{c}}(s)$ is the curve tangent, and \mathbf{n} is the surface normal, then from Theorem 8.2 the vectors \mathbf{t} , \mathbf{n} , $\mathbf{t} \times \mathbf{n}$ coincide with the Frenet frame of $\mathbf{c}(s)$ if this curve is a geodesic: in that case, $\mathbf{a}(s)$ maintains a fixed orientation relative to the vectors \mathbf{t} and $\mathbf{t} \times \mathbf{n}$ spanning the tangent plane. If $\mathbf{a}(s)$ is parallel-transported along an arbitrary curve, however, it exhibits a varying orientation with respect to these vectors.

Using these results, we can connect the “local” and “global” geometry of surfaces (with non-zero Gaussian curvature) in a manner that reveals their essential difference from two-dimensional Euclidean space. Suppose $\mathbf{c}(s)$ is a *closed* curve of total length S , so that $\mathbf{c}(S) = \mathbf{c}(0)$. If this curve resides in the Euclidean plane, and a vector \mathbf{a} is parallel-transported around it, we recover the initial instance upon completing the traversal, i.e., $\mathbf{a}(S) = \mathbf{a}(0)$. However, if $\mathbf{c}(s)$ lies on a curved surface and we parallel-transport \mathbf{a} around it we find that, in general, we end up with a different vector: $\mathbf{a}(S) \neq \mathbf{a}(0)$! Fig. 10.2 illustrates this phenomenon in the case of a sphere.

One may verify that any two vectors $\mathbf{a}(s)$ and $\mathbf{b}(s)$ parallel-transported along a curve $\mathbf{c}(s)$ on the surface $\mathbf{r}(u, v)$ maintain a constant (oriented) angle

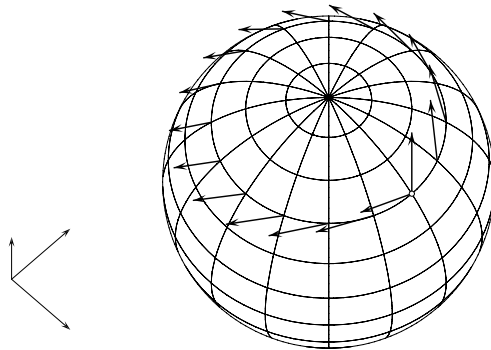


Fig. 10.2. Parallel transport of a vector around a small circle on the unit sphere. Upon returning to the start point, the vector is found to have suffered a net rotation about the surface normal there by the holonomy angle ϑ for the small-circle path.

relative to each other. Hence, the net change ϑ in the orientation of a vector that is parallel-transported around a closed curve $\mathbf{c}(s)$ depends only on the intrinsic geometry of the surface and the chosen path — this angle is called the *holonomy* of the path $\mathbf{c}(s)$ on the surface $\mathbf{r}(u, v)$. If the closed curve $\mathbf{c}(s)$ bounds a region Ω on the surface $\mathbf{r}(u, v)$, it can be shown that the holonomy ϑ of this path can be related (modulo 2π) to the surface curvature by either an area integral or a path integral:

$$\vartheta = \iint_{\Omega} K \, dA = \oint_{\mathbf{c}(s)} \kappa_g \, ds,$$

K and $dA = \sqrt{EG - F^2} \, du \, dv$ being the Gaussian curvature and area element of $\mathbf{r}(u, v)$, and κ_g the geodesic curvature (see §8.5.9) along $\mathbf{c}(s)$. We see that $\vartheta = 0$ for *any* closed path on a developable surface (since $K \equiv 0$), agreeing with the perception (see §8.5.5) that developables are essentially “flat” spaces. For more general surfaces, we have $\vartheta = 0$ for any closed path along which $\kappa_g \equiv 0$. As previously noted, the vanishing of the geodesic curvature along a path identifies it as a geodesic. Of course, we expect that $\vartheta = 0$ for any closed geodesic, since we have also characterized geodesics as those curves on the surface that exhibit parallel transport of their own tangent vectors.

11

The Bernstein Basis

... the Bézier methods emerge as an application of the Bernstein polynomial approximation operator to vector-valued functions.

W. J. Gordon and R. F. Riesenfeld [216]

Suppose we are concerned with a polynomial $p(t)$ over the interval $t \in [0, 1]$. At any point of this interval, the values t and $1-t$ represent the distances from the two interval end-points, $t = 0$ and $t = 1$. As in §7.2, we call t and $1-t$ the *barycentric coordinates* of a point with respect to the interval $t \in [0, 1]$ — if we imagine the interval to be a rigid rod, it will balance precisely about the chosen point when we place weights proportional to $1-t$ and t at the ends $t = 0$ and $t = 1$. The barycentric coordinates $(t, 1-t)$ of a point are evidently redundant, since $t + (1-t) \equiv 1$ for any t , but they provide a more symmetric or “balanced” specification of position on the interval $[0, 1]$.

Taking the identity $t + (1-t) \equiv 1$ and performing a binomial expansion of the expression on the left raised to the n^{th} power, we obtain

$$[t + (1-t)]^n = \sum_{k=0}^n \binom{n}{k} (1-t)^{n-k} t^k \equiv 1.$$

The $n+1$ terms

$$b_k^n(t) = \binom{n}{k} (1-t)^{n-k} t^k, \quad k = 0, \dots, n \quad (11.1)$$

appearing in the sum are linearly independent polynomials — they comprise the *Bernstein basis* for polynomials of degree n on $[0, 1]$.

We may also generate the Bernstein basis by a simple recursion. Starting with $b_0^0(t) \equiv 1$, and taking $b_k^r(t) \equiv 0$ if $k < 0$ or $k > r$, the basis of degree $r+1$ is obtained from that of degree r by

$$b_k^{r+1}(t) = t b_{k-1}^r(t) + (1-t) b_k^r(t) \quad (11.2)$$

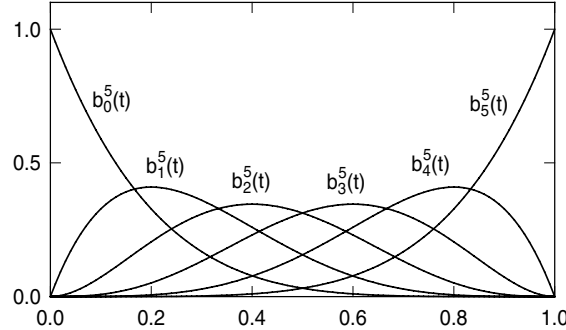


Fig. 11.1. Bernstein basis functions of degree 5 on the interval $t \in [0, 1]$.

for $k = 0, \dots, r + 1$. Figure 11.1 illustrates the basis functions for $n = 5$. Note that $b_k^n(t)$ and $b_{n-k}^n(t)$ are mirror images of each other about $t = \frac{1}{2}$, i.e.,

$$b_{n-k}^n(1-t) \equiv b_k^n(t).$$

Although we are mainly concerned with the Bernstein basis on $t \in [0, 1]$ here, it is understood that all the properties and algorithms associated with it will generalize to an arbitrary interval $t \in [a, b]$ if we systematically replace $u = t$ and $v = 1 - t$ by the barycentric coordinates $u = (t - a)/(b - a)$ and $v = (b - t)/(b - a)$ appropriate to that interval (see §11.4 below).

11.1 Theorem of Weierstrass

Polynomials are an attractive class of functions for use in various scientific and engineering computations. They are concisely represented by coefficients in a suitable basis, and are amenable to efficient evaluation by simple algorithms. The set of polynomials is closed under the arithmetic operations of addition, subtraction, and multiplication, and under differentiation, integration, and composition (i.e., substitution of one polynomial into another).

The approximative capabilities of polynomials are also of great practical interest in applications. Perhaps the most fundamental result in this context is the *theorem of Weierstrass*, which guarantees the existence of a polynomial $P_n(t)$ of a certain degree n that does not deviate anywhere over a specified domain $t \in [a, b]$ by more than a prescribed tolerance δ , however small, from a given function $f(t)$ that is merely *continuous* on that domain.

In 1912 the Russian mathematician S. N. Bernstein published an elegant constructive proof [34] of this theorem, in which the polynomial basis (11.1) was first introduced. The Bernstein polynomial approximation of degree n to any continuous function $f(t)$ on the interval $t \in [0, 1]$ is defined by sampling that function at the $n + 1$ equidistant positions $t_k = k/n$ for $k = 0, \dots, n$ and “blending” together the sampled values with the Bernstein basis functions:

$$P_n(t) = \sum_{k=0}^n f\left(\frac{k}{n}\right) b_k^n(t), \quad (11.3)$$

where $b_k^n(t)$ is defined by (11.1). The approximant (11.3) to the function $f(t)$ can be made to satisfy any prescribed accuracy by choosing a sufficiently high degree — i.e., for each $\delta > 0$ there exists an integer n_δ such that

$$|P_n(t) - f(t)| \leq \delta \quad \text{for all } t \in [0, 1] \quad \text{when } n \geq n_\delta.$$

Thus, we say that $P_n(t)$ converges uniformly to $f(t)$ as $n \rightarrow \infty$.

For each n , the Bernstein polynomial $P_n(t)$ is always “at least as smooth” as the function it approximates: if we know lower and upper bounds on the derivatives of $f(t)$ of each order over $[0, 1]$, the corresponding derivatives of $P_n(t)$ also observe those bounds [113]. This implies, for example, that if $f(t)$ is monotone or convex, $P_n(t)$ is correspondingly monotone or convex.

Note that, apart from $f(0)$ and $f(1)$, the Bernstein approximation (11.3) does not *interpolate* the values $f(k/n)$ sampled from the given function $f(t)$. Furthermore $P_n(t) \not\equiv f(t)$ even when $f(t)$ is itself a polynomial of degree $\leq n$. However, in contrast to the monotone convergence of (11.3) to $f(t)$ as $n \rightarrow \infty$, the degree- n polynomial that interpolates $n+1$ equidistant values $f(k/n)$ for $k = 0, \dots, n$ can exhibit wild oscillations as $n \rightarrow \infty$ (see §14.3).

The remarkable feature of the theorem of Weierstrass is that, although an *analytic* function can always be expanded in an infinite Taylor series about a point — and by truncating this series we obtain polynomial approximations of any desired precision within its radius of convergence — this theorem does not need to assume that $f(t)$ is *differentiable* to obtain such approximations over any finite interval. However, the orderly convergence of $P_n(t)$ to $f(t)$ as $n \rightarrow \infty$ comes at a rather severe price — as illustrated by the example shown in Fig. 11.2, it typically proceeds at a very leisurely pace.

In fact, it can be shown [113] that the error $|P_n(t) - f(t)|$ of the Bernstein approximation diminishes only in proportion to n^{-1} at any point where $f''(t)$ is defined and non-vanishing. This may be compared with, for example, the

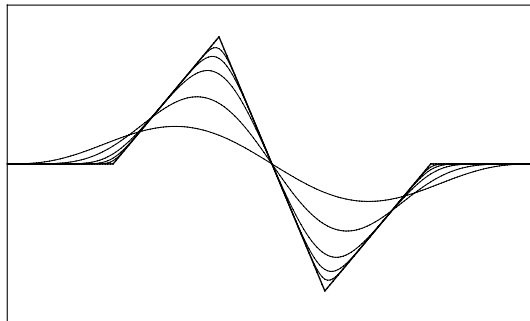


Fig. 11.2. The Bernstein polynomial approximants (11.3) of degree $n = 10, 30, 100, 300$, and 1000 to a continuous (but non-differentiable) piecewise-linear function $f(t)$.

n^{-4} convergence rate of the cubic spline interpolating $n+1$ equidistant values of a function with at least four-fold differentiability (see §14.4.6).

In his book *Interpolation and Approximation* [113], first published in 1963, P. J. Davis remarked on the slow convergence rate of Bernstein approximations to continuous functions:

“This fact seems to have precluded any numerical application of Bernstein polynomials from having been made. Perhaps they will find application when the properties of the approximant in the large are of more importance than the closeness of the approximation.”

Coincidentally, the increasing industrial use of computers gave rise to just such an application — namely, the need to provide a means of interactively defining curves and surfaces (i.e., vector-valued functions of one or two parameters) for design and manufacturing purposes. Although a continuous curve or surface has an infinity of points, its computer representation must obviously rely on just a *finite* set of data. The mapping from the finite set of input values to a continuous locus is accomplished by interpreting those values as coefficients for certain *basis functions* in the parametric variables.

Since the associated coefficients must serve as “shape handles” that allow manipulation of the curve or surface geometry to satisfy desired aesthetic or functional requirements, the choice of basis is fundamental to a viable design scheme. On account of the properties enumerated above, the Bernstein basis transpires to be an especially propitious choice for the computer description of (finite portions of) polynomial curves and surfaces.

11.2 Bernstein-form Properties

The convergence behavior of Bernstein polynomial approximations stems from certain intrinsic properties of the Bernstein basis functions, and consequent relations between the behavior over $t \in [0, 1]$ of the polynomial

$$p(t) = \sum_{k=0}^n c_k b_k^n(t) \quad (11.4)$$

and its Bernstein coefficients c_0, \dots, c_n . We now enumerate these properties.

1. **unimodality:** $b_k^n(t)$ has a single maximum, at $t = k/n$, on $t \in [0, 1]$.
2. **non-negativity property:** $b_k^n(t) \geq 0$ on $t \in [0, 1]$ for $k = 0, \dots, n$.
3. **partition of unity property:** since $b_0^n(t), \dots, b_n^n(t)$ are just the $n+1$ terms in the binomial expansion of $1 \equiv [t + (1-t)]^n$, we have

$$\sum_{k=0}^n b_k^n(t) \equiv 1.$$

Of course, this holds for *all* values of t , not just the interval $t \in [0, 1]$.

4. **lower & upper bounds:** from properties 2 and 3, we may infer that

$$\min_{0 \leq k \leq n} c_k \leq p(t) \leq \max_{0 \leq k \leq n} c_k \quad \text{for } t \in [0, 1].$$

5. **variation-diminishing property:** the number N of real roots of $p(t)$ on the open interval $t \in (0, 1)$ is less than the number $V(c_0, \dots, c_n)$ of sign variations in its Bernstein coefficients by an even amount:

$$N = V(c_0, \dots, c_n) - 2K, \quad (11.5)$$

K being a non-negative integer.¹ This is an expression of Descartes' Law of Signs (see Chap. 3), since the map $t \in (0, 1) \rightarrow u \in (0, \infty)$ defined by $t(u) = u/(1+u)$ transforms $p(t)$ into

$$q(u) = p(t(u)) = (1+u)^{-n} \sum_{k=0}^n a_k u^k, \quad \text{where } a_k = \binom{n}{k} c_k.$$

The coefficients a_0, \dots, a_n and c_0, \dots, c_n clearly have the same signs, and the roots of $q(u)$ on $u \in (0, \infty)$ are in one-to-one correspondence with the roots of $p(t)$ on $t \in (0, 1)$.

6. **derivatives and integrals** of $p(t)$ may be expressed as polynomials in Bernstein form of degree $n-1$ and $n+1$, respectively, with coefficients that are linear combinations of c_0, \dots, c_n . The relation

$$\frac{d}{dt} b_k^n(t) = n [b_{k-1}^{n-1}(t) - b_k^{n-1}(t)] \quad (11.6)$$

for $k = 0, \dots, n$ (where we take $b_{-1}^{n-1}(t) \equiv 0$ and $b_n^{n-1}(t) \equiv 0$) can be easily verified by direct differentiation. By setting $n \rightarrow n+1$, and adding up and integrating cases $k+1, \dots, n+1$ of the above equation, we obtain

$$\int b_k^n(t) dt = \frac{1}{n+1} \sum_{j=k+1}^{n+1} b_j^{n+1}(t) \quad (11.7)$$

for $k = 0, \dots, n$. This relation allows us to write the derivative of (11.4) as

$$\frac{dp}{dt} = \sum_{k=0}^{n-1} n(c_{k+1} - c_k) b_k^{n-1}(t)$$

(further derivatives can be written in terms of higher-order differences of the coefficients) and its indefinite integral as

$$\int p(t) dt = \text{constant} + \sum_{k=1}^{n+1} \left(\frac{1}{n+1} \sum_{j=0}^{k-1} c_j \right) b_k^{n+1}(t).$$

¹ It is understood that the roots are to be counted according to their multiplicities.

For definite integrals, we observe that the area contained under each basis functions $b_k^n(t)$, $k = 0, \dots, n$ over $t \in [0, 1]$ is the same,

$$\int_0^1 b_k^n(t) dt = \frac{1}{n+1} \quad \text{and hence} \quad \int_0^1 p(t) dt = \frac{1}{n+1} \sum_{k=0}^n c_k.$$

11.3 The Control Polygon

A *control polygon* may be associated with the graph of a degree- n polynomial $p(t)$ expressed in Bernstein form on $t \in [0, 1]$. The ordered sequence of vertices for this polygon are the points with coordinates $(k/n, c_k)$ for $k = 0, \dots, n$. Figure 11.3 illustrates such control polygons, which impart some idea of the shape of the graph of the polynomial on $[0, 1]$. In Chap. 13 we generalize the control polygon from scalar to *vector* polynomials, i.e., parametric curves.

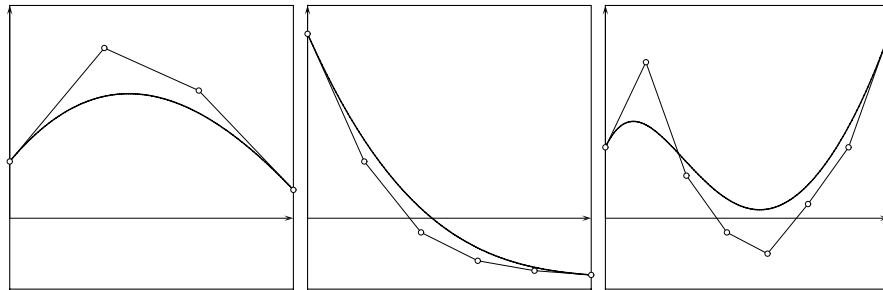


Fig. 11.3. Bernstein-form polynomials on $[0, 1]$ with control polygons. Left: a cubic with no roots on $[0, 1]$ because the Bernstein coefficients are all positive (the graph of the cubic is convex since the control polygon is convex). Center: a quintic with one root on $[0, 1]$ indicated by the single sign change in the coefficients (the graph is monotone since the control polygon is monotone). Right: a degree 7 polynomial — although there are two coefficient sign changes, it has no roots: $K = 1$ in (11.5).

11.4 Transformation of Domain

The properties of the degree- n Bernstein basis on $t \in [0, 1]$ described above carry over (with appropriate modifications) to the corresponding basis

$$b_k^n(t) = \binom{n}{k} \frac{(b-t)^{n-k}(t-a)^k}{(b-a)^n}, \quad k = 0, \dots, n \quad (11.8)$$

defined on an arbitrary interval $t \in [a, b]$. It is useful to have the capability of transforming the representation of a polynomial $p(t)$ among bases on different

intervals. If c_0, \dots, c_n are the Bernstein coefficients of $p(t)$ in the basis (11.8) on $t \in [a, b]$, its coefficients $\bar{c}_0, \dots, \bar{c}_n$ in the analogous basis $\bar{b}_k^n(t)$, $k = 0, \dots, n$ on a different interval $t \in [\bar{a}, \bar{b}]$ may be obtained from the given coefficients by a matrix multiplication,

$$\bar{c}_j = \sum_{k=0}^n M_{jk} c_k, \quad j = 0, \dots, n. \quad (11.9)$$

The matrix elements M_{jk} can be expressed [176] as sums of products of the basis functions (11.8), evaluated at the endpoints \bar{a}, \bar{b} of the new interval:

$$M_{jk} = \sum_{i=\max(0,j+k-n)}^{\min(j,k)} b_{k-i}^{n-j}(\bar{a}) b_i^j(\bar{b}), \quad 0 \leq j, k \leq n. \quad (11.10)$$

The matrix defined by (11.10) has the property that its elements sum to unity across each row. Moreover, the elements are all non-negative when $[\bar{a}, \bar{b}] \subset [a, b]$. These features are the defining characteristics of *stochastic matrices*, which play an important role in probability theory [198].

Two instances of the map (11.9) that are of special interest correspond to choosing $[a, b] = [0, 1]$ and $[\bar{a}, \bar{b}] = [0, \tau]$ or $[\tau, 1]$ for some value $\tau \in (0, 1)$. Since we have $b_{k-i}^{n-j}(0) \neq 0$ only when $i = k$, and $b_i^j(1) \neq 0$ only when $i = j$, it can be seen that the matrix elements (11.10) reduce to

$$M_{jk} = \begin{cases} b_k^j(\tau) & \text{if } k \leq j, \\ 0 & \text{if } k > j, \end{cases} \quad (11.11)$$

for $[\bar{a}, \bar{b}] = [0, \tau]$, and

$$M_{jk} = \begin{cases} 0 & \text{if } k < j, \\ b_{k-j}^{n-j}(\tau) & \text{if } k \geq j, \end{cases} \quad (11.12)$$

for $[\bar{a}, \bar{b}] = [\tau, 1]$. In these cases, instead of using the matrix multiplication (11.9), the Bernstein coefficients on the subintervals $[0, \tau]$ and $[\tau, 1]$ may be obtained simultaneously from the initial coefficients on $[0, 1]$ by means of the *de Casteljau algorithm*, discussed in §11.6 below.

11.5 Degree Operations

The *actual* degree of a polynomial $p(t)$ may be lower than the nominal degree n of the Bernstein basis in which it is expressed. Conversely, any polynomial $p(t)$ of true degree n admits a non-trivial representation in the Bernstein basis of degree $n+r$ for any $r \geq 1$. The process of raising the degree of the basis in which $p(t)$ is specified is called *degree elevation*, while the process of reducing the degree (when $p(t)$ is of true degree $< n$) is called *degree reduction*.

To express $b_k^n(t)$ in terms of the basis of degree $n+r$, we multiply by the binomial expansion of $[t + (1-t)]^r$ and collect like terms, to obtain

$$b_k^n(t) = \sum_{j=k}^{k+r} \frac{\binom{n}{k} \binom{r}{j-k}}{\binom{n+r}{j}} b_j^{n+r}(t), \quad k = 0, \dots, n.$$

On substituting this into (11.4) and re-arranging terms, we obtain the r -fold “degree-elevated” representation

$$p(t) = \sum_{k=0}^{n+r} c_k^{n+r} b_k^{n+r}(t),$$

of (11.4), the degree-elevated coefficients being given by

$$c_k^{n+r} = \sum_{j=\max(0, k-r)}^{\min(n, k)} \frac{\binom{r}{k-j} \binom{n}{j}}{\binom{n+r}{k}} c_j^n, \quad k = 0, \dots, n+r \quad (11.13)$$

where we have appended a superscript n to the coefficients c_0, \dots, c_n in (11.4). For the case $r = 1$, we have simply

$$c_k^{n+1} = \frac{k}{n+1} c_{k-1}^n + \left(1 - \frac{k}{n+1}\right) c_k^n, \quad k = 0, \dots, n+1.$$

A degree reduction, on the other hand, is possible only if $p(t)$ is of true degree $< n$. By expressing the power coefficients a_0, \dots, a_n (see §12.4.6) in terms of the Bernstein coefficients, the condition for (11.4) to be of true degree $n-r$ can be expressed as $a_n = a_{n-1} = \dots = a_{n-r+1} = 0 \neq a_{n-r}$. The representation

$$p(t) = \sum_{k=0}^{n-r} c_k^{n-r} b_k^{n-r}(t)$$

of degree $n-r$ is then defined by the coefficients

$$c_k^{n-r} = \sum_{j=0}^k (-1)^{k-j} \frac{\binom{k-j+r-1}{r-1} \binom{n}{j}}{\binom{n-r}{k}} c_j^n, \quad k = 0, \dots, n-r.$$

11.6 de Casteljau Algorithm

The *de Casteljau algorithm* is a fundamental computation for polynomials in Bernstein form on $t \in [0, 1]$. It serves a dual purpose — at a chosen point $t = \tau$ between 0 and 1, it computes the polynomial value $p(\tau)$, and it *subdivides* $p(t)$

at that point — i.e., it determines the Bernstein coefficients that describe the subsegments $t \in [0, \tau]$ and $t \in [\tau, 1]$ of $p(t)$ individually.

The algorithm proceeds as follows. Choosing $\tau \in (0, 1)$, we set $c_j^0 = c_j$ for $j = 0, \dots, n$, and then compute the triangular array of values

$$\begin{array}{ccccccc} c_0^0 & c_1^0 & c_2^0 & \cdot & \cdot & \cdot & c_n^0 \\ c_1^1 & c_2^1 & \cdot & \cdot & \cdot & c_n^1 \\ c_2^2 & \cdot & \cdot & \cdot & c_n^2 \\ & \cdot & \cdot & \cdot & \\ & & & c_n^n \end{array} \quad (11.14)$$

defined by the iterated linear interpolations

$$c_j^r = (1 - \tau) c_{j-1}^{r-1} + \tau c_j^{r-1} \quad (11.15)$$

for $j = r, \dots, n$ and $r = 1, \dots, n$. The final entry in this array is the polynomial value corresponding to the chosen parameter value,

$$p(\tau) = c_n^n. \quad (11.16)$$

The de Casteljau algorithm is an immediate consequence of the recursion relation (11.2) defining the Bernstein basis functions. From (11.2) and (11.15) one may easily verify by induction that the coefficients in row j of the array (11.14) are related to the initial coefficients $c_j^0 = c_j$ for $j = 0, \dots, n$ by

$$c_j^r = \sum_{k=0}^r c_{j-r+k} b_k^r(\tau) \quad (11.17)$$

for $j = r, \dots, n$ (bear in mind that we have $b_k^r(t) \equiv 0$ when $k < 0$ or $k > r$). In particular, taking $j = r = n$ in the above equation, we find that

$$c_n^n = \sum_{k=0}^n c_k b_k^n(\tau),$$

which corroborates the result in equation (11.16) that the apex of the array (11.14) corresponds to the value $p(\tau)$.

Consider now the sequences of $n + 1$ values on the left and right diagonal sides of the array (11.14), namely

$$c_0^0, c_1^1, c_2^2, \dots, c_n^n \quad \text{and} \quad c_n^n, c_n^{n-1}, c_n^{n-2}, \dots, c_n^0. \quad (11.18)$$

Using expression (11.17), with appropriate changes of the summation index, we can express these values for $j = 0, \dots, n$ in the form

$$c_j^j = \sum_{k=0}^j c_k b_k^j(\tau) \quad \text{and} \quad c_n^{n-j} = \sum_{k=j}^n c_k b_{k-j}^{n-j}(\tau).$$

But from (11.11) and (11.12) we notice that the factors multiplying c_0, \dots, c_n in these expressions are, respectively, the elements of the matrices that map the Bernstein coefficients on $[0, 1]$ to those on the intervals $[0, \tau]$ and $[\tau, 1]$. Thus, the values (11.18) define the coefficients for the “left” and “right” sub-segments — i.e., $t \in [0, \tau]$ and $t \in [\tau, 1]$ — of the polynomial $p(t)$ defined on $t \in [0, 1]$. In addition to computing the value $p(\tau)$ of the polynomial, we say that the de Casteljau algorithm *subdivides* it at $t = \tau$.

11.7 Arithmetic Operations

We are often concerned with performing the elementary arithmetic operations (addition, subtraction, multiplication, and division) on polynomials specified in Bernstein form. Suppose that $f(t)$ and $g(t)$ are polynomials of degree m and n with Bernstein coefficients a_0, \dots, a_m and b_0, \dots, b_n . If $m = n$, the Bernstein coefficients of the sum/difference polynomial $f(t) \pm g(t)$ are obtained by just adding/subtracting the corresponding coefficients. If $m \neq n$, however, we first need to degree-elevate the polynomial of lower degree, so as to express both polynomials in the Bernstein basis of the same degree. If $n < m$, for example, this gives [182] the coefficients of the sum/difference polynomial as

$$c_k = a_k \pm \sum_{j=\max(0, k-m+n)}^{\min(n, k)} \frac{\binom{m-n}{k-j} \binom{n}{j}}{\binom{m}{k}} b_j, \quad k = 0, \dots, m. \quad (11.19)$$

The product polynomial $f(t)g(t)$, of degree $m + n$, is specified [182] by the Bernstein coefficients

$$c_k = \sum_{j=\max(0, k-n)}^{\min(m, k)} \frac{\binom{m}{j} \binom{n}{k-j}}{\binom{m+n}{k}} a_j b_{k-j}, \quad k = 0, \dots, m+n. \quad (11.20)$$

This can be verified by explicitly multiplying out, and collecting like terms in $1-t$ and t . Finally, in performing the division $f(t)/g(t)$, we are concerned with determining the *quotient* and *remainder* polynomials, $q(t)$ and $r(t)$, defined by the identity

$$f(t) = q(t)g(t) + r(t),$$

where $\deg(q) = m - n$ and $\deg(r) = n - 1$ when $\deg(f) = m$ and $\deg(g) = n$. In this case, determining $q(t)$ and $r(t)$ amounts to solving a system of $m + 1$ linear equations in their Bernstein coefficients q_0, \dots, q_{m-n} and r_0, \dots, r_{n-1} . These equations are defined [182] for $k = 0, \dots, m$ by

$$\begin{aligned} & \sum_{j=\max(0,k-n)}^{\min(m-n,k)} \frac{\binom{m-n}{j} \binom{n}{k-j}}{\binom{m}{k}} b_{k-j} q_j \\ & + \sum_{j=\max(0,k-m+n-1)}^{\min(n-1,k)} \frac{\binom{m-n+1}{k-j} \binom{n-1}{j}}{\binom{m}{k}} r_j = a_k. \end{aligned}$$

An accurate and efficient means of computing the binomial coefficient terms in these operations is based [211] on decompositions into primes.

Other useful algorithms for Bernstein-form polynomials include resultants and greatest common divisor computations, and *composition* of polynomials — i.e., substituting one polynomial for the argument of another polynomial. For details on these algorithms and their implementation, see [182, 444].

11.8 Computing Roots on $(0, 1)$

Used in conjunction with the variation-diminishing property, the de Casteljau algorithm provides an efficient and numerically-stable means of isolating and approximating the (simple) real roots of the degree- n polynomial (11.4) on² $t \in (0, 1)$. The basic idea, suggested by J. M. Lane and R. F. Riesenfeld [296], is to recursively subdivide $t \in [0, 1]$ into contiguous subintervals characterized by the property that the Bernstein coefficients for each exhibit either zero or one sign variations. Then K in (11.5) must be zero and we have $N = 0$ or 1 , respectively, for the number of real roots on these subintervals.

Once the real roots are isolated, it is preferable to invoke approximation procedures with faster rates of convergence than further binary subdivision. The Newton-Raphson method, for example, gives “quadratic convergence” — the number of accurate digits in an approximate root roughly doubles with successive iterations — *if* we can be sure that the starting approximation is “sufficiently close” to the true root to guarantee convergence.

Fortunately, such a guarantee can be expressed in terms of the Bernstein form. If the Bernstein coefficients c_0, \dots, c_n of a polynomial $p(t)$ on $t \in [a, b]$ exhibit only one sign change, the following conditions suffice to guarantee that

² Roots at $t = 0$ or $t = 1$ are, of course, indicated by the vanishing of c_0 or c_n .

the Newton–Raphson iteration — see equation (12.1) below — will converge to the unique real root on that interval from *any* start point within it:

$$V(\Delta c_0, \dots, \Delta c_{n-1}) = 0, \quad (11.21)$$

$$V(\Delta^2 c_0, \dots, \Delta^2 c_{n-2}) = 0, \quad (11.22)$$

$$|c_0| \leq n |\Delta c_0| \quad \text{and} \quad |c_n| \leq n |\Delta c_{n-1}|. \quad (11.23)$$

Here $\Delta c_k = c_{k+1} - c_k$ and $\Delta^2 c_k = \Delta c_k - \Delta c_{k-1} = c_{k+2} - 2c_{k+1} - c_k$ denote the first and second forward-differences of the coefficients, and $V(\dots)$ equals the number of sign changes in the ordered sequence of its arguments.

Conditions (11.21) and (11.22) require the graph of $p(t)$ over $t \in [a, b]$ to be *monotone* and *convex* (its first and second derivatives must not vanish) while condition (11.23) guarantees that the tangent lines to $p(t)$ at $t = a$ and $t = b$ cross the t -axis within the interval $[a, b]$. For a proof of the sufficiency of these conditions for convergence of Newton's method from any starting value t_0 within $[a, b]$ to the unique root in that interval, see [234, p. 79].

Note that, in the presence of a real root of multiplicity m , the Bernstein coefficients for the subinterval containing that root will always exhibit at least m (rather than 0 or 1) sign changes in the limit under repeated subdivision. In principle, multiple real roots can be identified (within a given tolerance) by simultaneously applying the de Casteljau algorithm to the Bernstein form of $p(t)$ and its successive derivatives $p'(t), p''(t)$, etc.

11.9 Numerical Condition

The control polygon of a Bernstein-form polynomial $p(t)$ on $t \in [0, 1]$ provides useful insight concerning the behavior of the polynomial over that interval. In particular, the *shape* and *range* of the control polygon are closely correlated to the graph of the polynomial — especially if the degree is relatively low. By contrast, when we represent polynomials in the familiar “power” form (3.1), the coefficients a_0, \dots, a_n offer less insight into the behavior of the polynomial over a specified interval, and their values are more weakly correlated with the actual range of the polynomial over that interval. It is possible, for example, that the power coefficients may exceed the actual range of the polynomial on $[0, 1]$ by many orders of magnitude (see §12.4.3). These observations have an important practical consequence, which we elaborate on in the next chapter: the Bernstein form is numerically *more stable* than the power form.

12

Numerical Stability

The purpose of computing is insight, not numbers.

Richard W. Hamming (1962)

The purpose of computing numbers is not yet in sight.

Richard W. Hamming (1970)

12.1 License to Compute

The geometrical algorithms of computer-aided design systems usually employ *floating-point arithmetic* — a finite approximation to real-number arithmetic that sacrifices exactitude for computational efficiency and predictable memory requirements. In general, floating-point arithmetic incurs errors whenever real numbers must be stored in the computer memory, or arithmetic operations are performed on numbers already in memory. These errors are typically of small relative magnitude, but under certain circumstances they can be dramatically magnified, yielding numerical results that are essentially meaningless.

To operate a vehicle, one must obtain a *driver's license* by demonstrating knowledge of the rules of the road and practical skill in managing the vehicle controls in a manner that does not endanger oneself or others. On the other hand, although scientific and engineering calculations are typically performed in floating-point arithmetic, a medium that can often incur emotional or even physical danger, it is a sad fact that most scientists and engineers are set loose on computers without first having to earn a *license to compute*.¹

Such considerations are especially acute in the context of computer-aided design algorithms, which carry a higher premium on *reliability* or “robustness” than virtually any other kind of scientific or engineering computations. The output of a CAD system is rarely an end in itself — most often, it is routed

¹ Readers may wish to test themselves on the following representative problem from the *Computer's License* test: among the four floating-point arithmetic operations $+, -, \times, \div$ which is (a) the most *expensive*, and (b) the most *dangerous*?

more or less directly to some manufacturing or inspection process, or to finite-element analysis programs that require topologically valid and geometrically accurate three-dimensional shape descriptions. Examples include: numerical-control machining, rapid prototyping, and robot path-planning; inspection by coordinate measuring machines; and mesh generation from solid models for finite-element stress, heat transfer, or fluid flow analysis.

The consequences of feeding erroneous or inconsistent geometric data to such downstream applications is in some cases merely frustrating and wasteful of resources, and in others dangerous or disastrous. Moreover, since the volume of data involved can often be overwhelming, imposing a manual “sanity check” between the CAD system and the end application is neither a practical nor a humane remedy. The onus is therefore on the developers and the implementors of CAD system algorithms to remain vigilant of the pitfalls of floating-point arithmetic, to seek out numerically-stable formulations, and to incorporate internal checks on the accuracy and consistency of their calculations.

Do you ever want to kick the computer? Does it iterate endlessly on your newest algorithm that should have converged in three iterations? And does it finally come to a crashing halt with the insulting message that you divided by zero? These minor trauma are, in fact, the ways the computer manages to kick you and, unfortunately, you almost always deserve it! For it is a sad fact that most of us can more readily compute than think — which might have given rise to that famous definition, “Research is when you don’t know what you are doing.”

Forman S. Acton, *Numerical Methods that (Usually) Work* [9]

12.2 Characterization of Errors

It is important to distinguish between two types of errors that typically arise in geometrical computations. Many problems that concern us do not admit a closed-form solution, expressible in finite terms. For example, the roots of high-degree polynomials are often required in computing curve and surface intersections. As noted in §3.3, however, only polynomials of degree ≤ 4 allow a “solution by radicals” for their roots. For a polynomial $p(t)$ of degree > 4 , *numerical* methods, such as the Newton–Raphson iteration

$$t_{k+1} = t_k - \frac{p(t_k)}{p'(t_k)}, \quad k = 1, 2, \dots \quad (12.1)$$

must be used to approximate the roots. This yields a sequence t_1, t_2, \dots of root approximations that approach the exact (simple) root τ monotonically if the initial “guess” t_0 is sufficiently close to τ . Even with a hypothetical computer capable of *exact* real arithmetic, one can never obtain exact solutions by such methods. Clearly, the iterations must be halted after a finite number of steps, even if they are rapidly convergent. Similarly, when an analytic function is approximated by expanding it in a Taylor series about a given point, the need

to stop after a finite number of terms incurs a truncation error. We call such errors, due to the absence of a closed-form solution, *approximation errors* — they arise even in the hypothetical case of infinite-precision arithmetic.

On the other hand, even “simple” geometrical problems that nominally *do* admit closed-form solutions cannot be solved exactly in practice, because each arithmetic step of the solution procedure incurs a *rounding* or *truncation* error when real numbers are approximated by fixed-size words in the computer, i.e., one implements the solution in *floating-point arithmetic*. These errors, which we shall call *arithmetic errors*, are our main concern at present.

In general, combinations of approximation errors and arithmetic errors will arise in all but the very simplest calculations dealing with free-from curves and surfaces; it is not easy to separate or independently analyze the two. For example, since a root τ of the polynomial $p(t)$ satisfies $p(\tau) = 0$, one may plan to choose a small number ϵ and stop (12.1) at iteration r , such that

$$|p(t_r)| \leq \epsilon.$$

But this approach is only meaningful if the *arithmetic error* in computing the value of $p(t_r)$ is appreciably smaller than the chosen “tolerance” ϵ . One might think that, since iterative methods incur *approximation* errors, with which any *arithmetic* errors are inextricably mixed up, one should not worry unduly about the latter. But this kind of sloppy thinking is a recipe for trouble.

Many iterative methods are, in principle, capable of furnishing results that approach as close as we might practically desire to the exact solution — i.e., we can make the *approximation* error very small — *if* we formulate them in such a manner that the end result is not extremely sensitive to small perturbations in the input or intermediate values (i.e., to any arithmetic errors that occur). A problem formulation that has this property is said to be *well-conditioned*. In an *ill-conditioned* problem formulation, on the other hand, small input or intermediate perturbations may induce disproportionately large errors in the output — it is then impossible to compute accurate results in floating-point arithmetic, regardless of the iterative method employed.

It is only by detailed analysis of the influence of arithmetic errors — which may be viewed as perturbations of the input values in a hypothetical exact arithmetic computation — that we can quantify this notion of the *condition* of a problem formulation. We shall consider specific examples in due course: our purpose here has been merely to convince the reader that analyzing the effects of arithmetic error is an important issue, logically quite independent of the presence or absence of approximation errors.

12.3 Floating-point Computations

On account of its speed, convenience, and (in most cases) reasonable accuracy, scientific and engineering calculations almost invariably rely on floating-point arithmetic. However, the very speed of modern computers incurs greater risk

of encountering those seemingly–rare circumstances in which floating–point calculations yield miserable accuracy. By bringing these pitfalls to the reader’s attention, our intent here is to quell the usual temptation to rush to the computer and “repeat the classical blunders of generations past” [204].

12.3.1 Floating–point Numbers

A normalized floating–point number f in base b has the form

$$f = m b^e, \quad (12.2)$$

where e , the *exponent*, is an integer in a prescribed range $-E \leq e \leq +E$ and m , the *mantissa*, is a (signed) fractional real number that has exactly d digits in base b . By “normalized” we mean that the value of m satisfies

$$1/b \leq |m| < 1.$$

This ensures that all d digits of the mantissa convey useful information; there are no “wasted” leading zeros. Some examples of 4-digit decimal and 12-digit binary normalized floating–point numbers are:

$$0.3074 \times 10^3 \quad \text{and} \quad 0.101101000101 \times 2^7$$

(we express the mantissa m explicitly in base b , but the exponent is decimal).

The restriction on e means that no number of absolute value smaller than $1/b^{E+1}$ or greater than or equal to b^E is allowed — calculations that attempt to generate numbers outside this *dynamic range* will result in floating–point “underflow” or “overflow.” Also, restricting m to just d digits implies that the floating–point number system (12.2) is *discrete* rather than *continuous* — it encompasses only a *finite set* of distinct real values. Real numbers whose true values lie in between two consecutive floating–point numbers (which could be either initial input data, or values generated by arithmetic operations) must be *rounded* or *truncated* so as to have a mantissa of only d digits.²

For an arbitrary real value X within dynamic range, $1/b^{E+1} \leq |X| < b^E$, there exists an integer e and a real value μ having an *unrestricted* number of digits in base b , such that $X \equiv \mu b^e$ and $1/b \leq |\mu| < 1$. The floating–point approximation x of the real number X is then defined to be

$$x = \text{float}(X) = m b^e,$$

² Truncation incurs systematic errors. The steady erosion of the Vancouver Stock Exchange index to approximately half its value at inception in 1982, despite fair performance of its component securities, offers a humorous illustration of this. The “bear market” persisted for almost two years before being traced to minuscule truncation errors in the program that was used to periodically update the index!

where m is determined from μ by either rounding or truncation at the d -th digit. Hence, the value of $|\mu - m|$ cannot exceed $\frac{1}{2}b^{-d}$ (for rounding) or b^{-d} (for truncation), and the greatest *fractional* error arising in the floating-point approximation of a (non-zero) real number X is thus

$$\eta \equiv \max_{X \neq 0} \frac{|\text{float}(X) - X|}{|X|} = k b^{-(d-1)}, \quad (12.3)$$

where the quantity k is defined by

$$k = \begin{cases} \frac{1}{2} & \text{for rounding,} \\ 1 & \text{for truncation.} \end{cases}$$

The value η given by (12.3) is usually called the *machine unit*.

Even “innocuous” numbers may incur rounding errors merely on *input* to the computer. Consider, for example, the representation of the fraction $\frac{1}{10}$ in normalized binary floating point. In the exact value

$$(0.110011001100110011001100\dots) \times 2^{-3},$$

the bit-sequence “1100” is repeated *ad infinitum* in the mantissa — forcing us to round or truncate after d places. The IEEE standard for double-precision floating point [1], for example, employs a 53-bit binary mantissa³ together with rounding, giving a machine unit $\eta = \frac{1}{2}2^{-52} \approx 10^{-16}$. Thus, assigning the decimal value 0.1 to a floating-point variable incurs an immediate relative error of maximum magnitude η . While this may seem insignificant, there are circumstances under which it can be greatly “magnified” (see §12.4.3).

Humans are accustomed to the decimal numbers, while computers usually employ binary representations. Note that the choice of the parameters b and d , consistent with a specified word-size, has important practical consequences. Consider, for example, the case of single-precision arithmetic using a 32-bit word, of which 24 bits are reserved for the mantissa. If a binary representation and rounding are employed, then (12.3) with $b = 2$, $d = 24$, and $k = \frac{1}{2}$ gives

$$\eta = \frac{1}{2}2^{-23} \approx 6.0 \times 10^{-8}.$$

On the other hand, in a hexadecimal representation ($b = 16$), there is room for only $d = 6$ mantissa digits, and if truncation is employed ($k = 1$) we have

$$\eta = 16^{-5} \approx 9.5 \times 10^{-7}.$$

The latter use of the 32-bit word, common on mainframes, yields far larger errors in storing variables or executing arithmetic operations (see Fig. 12.1).

³ In normalized binary floating-point, the leading bit of the mantissa is known to be 1 and hence is not stored: it is used instead to indicate the *sign* of the number.

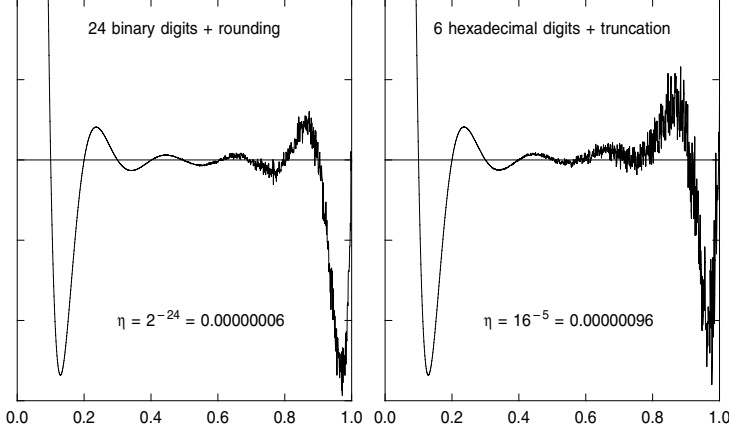


Fig. 12.1. The degree 10 polynomial $p(t) = (t - 0.1)(t - 0.2) \cdots (t - 1.0)$ evaluated by Horner's method in single-precision floating point using: binary arithmetic with rounding (on the left), and hexadecimal arithmetic with truncation (on the right). The latter gives arithmetic errors with both a greater spread *and* a systematic bias.

12.3.2 Floating-point Arithmetic

Let $*$ represent any of the four basic arithmetic operations $\{+, -, \times, \div\}$. Given two floating-point numbers x and y of the form (12.2), we denote the result of a floating-point arithmetic operation on them by $\text{float}(x * y)$. In general, this result differs from the *exact* result $x * y$, since the latter typically exceeds the constraint of d mantissa digits. However, virtually all modern computers⁴ have floating-point arithmetic processors designed [429] so as to ensure that the *fractional* error in each individual arithmetic step is also bounded by the machine unit:

$$\frac{|\text{float}(x * y) - x * y|}{|x * y|} \leq \eta, \quad (12.4)$$

where we assume that $x * y \neq 0$ (and $y \neq 0$ for the case of division). This seems, at first sight, like a very promising result: it indicates that the relative error incurred in each floating-point arithmetic operation is bounded by the small quantity η . On re-writing (12.4) in the form

$$(1 - \eta)x * y \leq \text{float}(x * y) \leq (1 + \eta)x * y, \quad (12.5)$$

⁴ RISC machines may have a floating-point multiply-and-add (FMA) instruction that allows the expression $(x \times y) + z$ to be evaluated in a single cycle, with lower error than sequential \times and $+$ operations incur. These machines may yield more accurate results than indicated by the analysis given below, although the ability to utilize such instructions can be algorithm- and compiler-dependent.

one might hope to apply bounds of the above form to each arithmetic step of an algorithm, and hence monitor the propagation of floating-point round-off error through any calculation of interest.

By way of example, consider evaluation of the polynomial (3.1) by Horner's method, which requires n multiplications and additions:

$$P_k = t \times P_{k-1} + a_{n-k} \quad \text{for } k = 1, \dots, n, \quad (12.6)$$

where $P_0 = a_n$, and the final step gives the value of the polynomial: $p(t) = P_n$. The additions and multiplications are performed in floating-point arithmetic, but for simplicity we assume a_n, \dots, a_0 and t are *a priori* allowable floating-point values (i.e., there is no floating-point conversion error on input).

Now let e_r be a bound on the absolute error in the r -th computed Horner term, i.e., this computed value equals $P_r + \Delta P_r$ with $-e_r \leq \Delta P_r \leq +e_r$. We can obtain a recursion relation for the error bounds e_0, e_1, \dots, e_n as follows. The outcome of the k -th floating-point Horner step will be

$$[t \times (P_{k-1} + \Delta P_{k-1})(1 + \delta) + a_{n-k}] (1 + \epsilon), \quad (12.7)$$

where δ and ϵ are the relative errors (no greater in magnitude than η) arising in the floating-point multiplication and addition that constitute step k . To first order in small quantities, the deviation of the computed value (12.7) from the exact one (12.6) is thus

$$\Delta P_k = t \Delta P_{k-1} + t P_{k-1} \delta + (t P_{k-1} + a_{n-k}) \epsilon.$$

Noting that the term in parentheses on the right-hand side is just the (exact) k -th Horner sum P_k , and that $-e_{k-1} \leq \Delta P_{k-1} \leq +e_{k-1}$ and $-\eta \leq \delta, \epsilon \leq +\eta$, the bound on the absolute value of the above error in P_k is

$$e_k = |t| e_{k-1} + (|t| |P_{k-1}| + |P_k|) \eta. \quad (12.8)$$

By running the recursion (12.8) starting with $e_0 = 0$, it would seem that we can determine a rigorous bound on the error e_n in the value P_n of $p(t)$, as computed by the Horner method (12.6). Such an approach, which attempts to estimate and propagate the errors incurred in each arithmetic operation of a calculation, is usually called *forward error analysis*. Despite its simplicity and intuitive appeal, forward error analysis embodies a basic flaw that can make it seriously underestimate the significance of arithmetic errors under certain circumstances. To understand the nature of this flaw, we must consider more carefully what we mean by the “error” in a computed value.

12.3.3 Dangers of Digit Cancellation

Basically, equation (12.4) says that the relative error incurred in each floating-point operation is bounded by a very small quantity η . However, caution must be urged in imputing a “practical” significance to this statement, since we have not yet given a precise meaning to the term *relative error*.

It is implicit in equation (12.4) that the two operands x and y are numbers that have *ab initio* exact floating-point representations. But this is hardly ever true! In practice, x and y usually represent *approximations* to arbitrary real numbers X and Y . At minimum, the approximate nature of x and y arises from the need to round X and Y on input (if x and y denote intermediate values in some calculation, they will often incorporate significantly larger *accumulated* round-off errors, compared to the exact values X and Y). For simplicity, we consider only the case where X and Y are input values, so that x and y suffer only initial round-off errors characterized by

$$\begin{aligned} (1 - \eta)X &\leq x = \text{float}(X) \leq (1 + \eta)X, \\ (1 - \eta)Y &\leq y = \text{float}(Y) \leq (1 + \eta)Y. \end{aligned} \quad (12.9)$$

In practice, of course, the error of interest incurred by the floating-point arithmetic operation $\text{float}(x * y)$ is not that expressed by equation (12.4), but instead *the error relative to an exact-arithmetic operation on the underlying real numbers, X and Y , that the floating-point numbers x and y approximate* — i.e., it is the quantity

$$\text{relative error} = \frac{|\text{float}(x * y) - X * Y|}{|X * Y|}. \quad (12.10)$$

In most cases the quantity (12.10) is, in agreement with intuition, no more than a few times η , and the model (12.4) thus provides a fairly reliable basis for analyzing error propagation and estimating the deviation of floating-point calculations from exact-arithmetic results — as in the discussion of Horner's method. However, there are situations in which (12.10) can exceed η by many orders of magnitude, and the model (12.4) fails dramatically in monitoring the true discrepancy between floating-point and exact-arithmetic results. These cases correspond to *subtraction of like-signed floating-point numbers x and y that have identical exponents and agree in many leading digits of the mantissas* (or, equivalently, the addition of such quantities of unlike sign).

In such situations, cancellation of the identical leading digits of x and y occurs, and hence the quantity $x * y$ actually needs no rounding for machine representation: $\text{float}(x * y) \equiv x * y$. The problem is thus not one of *arithmetic error* in the subtraction, but rather a *magnification of “pre-existing” errors incurred in the floating-point conversions $x = \text{float}(X)$ and $y = \text{float}(Y)$* . To illustrate this, we use (12.9) to write

$$x = (1 + \delta)X \quad \text{and} \quad y = (1 + \epsilon)Y,$$

where δ and ϵ are random numbers with $-\eta \leq \delta, \epsilon \leq +\eta$. We further suppose that X, Y are of like sign and agree in $r \geq 1$ of their leading binary digits. Noting again that $\text{float}(x * y) \equiv x * y$ in such a case, expression (12.10) becomes

$$\text{relative error} = \frac{|(1 + \delta)X - (1 + \epsilon)Y - (X - Y)|}{|X - Y|} = \frac{|\delta X - \epsilon Y|}{|X - Y|}.$$

Now the numerator of the right-hand side attains its largest value, namely

$$|\delta X - \epsilon Y| = \eta (|X| + |Y|),$$

when δ and ϵ both have absolute value η but unlike signs, and if X and Y have mantissas that agree in r leading bits, we have

$$|X| + |Y| \approx 2|X|,$$

and typically

$$|X - Y| \approx 2^{-r}|X|$$

(although $|X - Y|$ may actually be much smaller). Thus the magnitude of the error, *relative to exact arithmetic*, is approximately

$$\text{relative error} \approx 2^{r+1}\eta. \quad (12.11)$$

This error evidently becomes arbitrarily large as $r \rightarrow \infty$ (note that r is the number of identical bits in the real numbers X and Y — it is not bounded by d , the number of mantissa bits in the floating-point number system).

We emphasize again the nature of the phenomenon that gives rise to the error (12.11): it is not at all an “arithmetic error” but rather a *magnification* of the small relative errors incurred by the conversions⁵ $x = \text{float}(X)$ and $y = \text{float}(Y)$ that arises when $|X - Y| \ll |X|, |Y|$. A simple example serves to illustrate this point: consider the addition of the two numbers, $X = 0.275347$ and $Y = -0.275162$, in 4-digit decimal floating-point arithmetic. In exact arithmetic we obtain

$$\begin{array}{r} X = +0.275347 \\ Y = -0.275162 \\ \hline X + Y = +0.000185, \end{array}$$

whereas converting first to floating-point by rounding gives $x = \text{float}(X) = 0.2753$ and $y = \text{float}(Y) = -0.2752$, and hence

$$\begin{array}{r} x = +0.2753 \\ y = -0.2752 \\ \hline \text{float}(x + y) = +0.0001. \end{array}$$

Note that no rounding was necessary in the above floating-point calculation. However, the fractional error — *relative to the exact-arithmetic result* — is

$$\text{relative error} = \frac{|0.0001 - 0.000185|}{|0.000185|} \approx 0.46.$$

But the machine unit for 4-digit decimal floating-point is just $\frac{1}{2} \times 10^{-(4-1)} = 5 \times 10^{-4}$, and thus the above error exceeds η by about 3 orders of magnitude!

⁵ If X, Y were intermediate (rather than input) values, any *accumulated* error that x, y have relative to the exact values would be subject to the same amplification.

12.3.4 Models for Error Propagation

We may summarize the preceding discussion as follows. In the absence of digit cancellation effects, the accumulation of arithmetic errors in the execution of an algorithm — as compared to exact–arithmetic results — is reasonably well described by the formula (12.5), which indicates rather small relative errors in each step, and consequently fairly mild final errors in all but very lengthy calculations. When cancellations occur, however, the “forward error analysis” model based on (12.5) fails dramatically to provide a reliable indication of the deviation from exact–arithmetic results, and cannot be easily amended to do so. In such cases, the errors that arise are not actually *arithmetic* errors, but rather *magnifications* of pre-existing errors in the operands.

The potential for large relative errors to arise through cancellation effects — as expressed by the factor 2^{r+1} in equation (12.11) — seriously complicates the task of formulating systematic floating–point error propagation models. The amount of error amplification in each subtraction depends on the precise number of digits r that cancel in the operands. If the latter are intermediate values in a rather lengthy calculation, r would be virtually impossible to know other than through a tedious step–by–step examination of numerical values — which is clearly impractical for all but the most trivial calculations.

There is a systematic (though rather subtle) approach to floating–point error analysis that accommodates cancellation effects and avoids the tedium of a case–by–case inspection for each set of input parameters. Developed by the pioneering British numerical analyst James H. Wilkinson (1919–1986), this approach is based on computing a *condition number* for the given problem, coupled with a *backward error analysis* of it.

Instead of attempting to monitor the discrepancies between “exact” and “computed” results in a floating–point calculation, Wilkinson’s method has a radically different philosophy — it aims to show that the outcome of a finite–precision calculation on given input values is identical to what is obtained in an exact–arithmetic calculation, but with “perturbed” input values. Assessing the accuracy of floating–point calculations is then a two–stage process:

1. compute a *condition number* C for the given problem, which characterizes the sensitivity of the output values to perturbations in the input values;
2. perform a *backward error analysis* so as to determine the magnitude ϵ of the input perturbations that, in exact arithmetic, would be equivalent to the cumulative effects of round–off error during the calculation.

The product $C\epsilon$ of the condition number and “effective” input perturbations is then a measure of the floating–point error in the computed solution. These concepts will be explained in greater detail below. Although the backward error analysis method is quite general, it can become unwieldy in practice if the algorithm is not relatively simple. Quite often, just being able to compute (or estimate) the condition number gives a sufficient indication of whether or not the results of a calculation can be regarded as trustworthy.

An alternative approach to monitoring the propagation of rounding errors or other uncertainties during a calculation is by the use of *interval arithmetic* (see §2.4). Each variable is considered to identify a range of possible values, between specified lower and upper limits, and each value within this range is regarded equally likely as the value of the variable — there is no information on the relative *probabilities* of values within the specified range. If the arithmetic operations required to determine the lower and upper bounds of the resulting intervals on the right-hand side of expressions (2.10) are to be performed in floating point, it is possible to automatically adjust them to allow for the effect of round-off errors: this approach is known as “rounded” interval arithmetic. For a more detailed treatment of this topic, see [16, 226, 332, 333].

The interval widths need not necessarily reflect only round-off errors: they may also reflect inherent “physical” uncertainties associated with the variables — for example, interval arithmetic can be used to analyze the accumulation of tolerances in a mechanical assembly whose component parts have dimensional uncertainties due to manufacturing variations. Many familiar algorithms can be reformulated to accept interval operands — see, for example, [227, 228]. The use of interval arithmetic in the context of geometric modeling has been discussed in [286, 338, 402]. It should be noted, however, that “mindless” use of interval arithmetic can yield very pessimistic results — i.e., the interval width grows very large, whereas the true value is, with high probability, localized in a much narrower subset of the nominal interval.

12.4 Stability and Condition Numbers

Conceptually, we may regard a mathematical problem \mathcal{P} as receiving certain numerical values as its “input” and yielding other values as its “output” or solution — we assume the output to be an analytic function of the input, even if we cannot in general express that function in closed form. We say that \mathcal{P} is a *stable* or “well-conditioned” problem if input values that differ only slightly always define solutions that differ only slightly. If, on the other hand, input values that differ only slightly can incur dramatically different solutions, we say that \mathcal{P} is an *unstable* or “ill-conditioned” problem. Figure 12.2 gives a

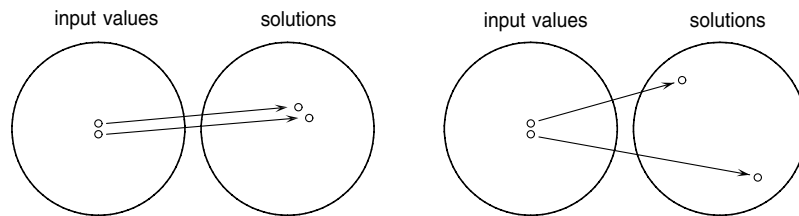


Fig. 12.2. The “distance” between solutions for two neighboring sets of input values distinguishes a well-conditioned problem (left) from an ill-conditioned one (right).

schematic illustration of this concept, which may be quantified by introducing suitable metrics for the sets of input values and solutions.

The *condition number* $C(\mathcal{P})$ of the problem \mathcal{P} is a quantitative measure of the sensitivity of its output to changes in its input. We are speaking here of the *intrinsic stability* of the input–output relationship for the specified problem \mathcal{P} . We make no reference to any particular algorithm or computational scheme whereby solutions are actually determined. The condition number $C(\mathcal{P})$ is an intrinsic property of the problem \mathcal{P} , independent of any solution method.

The typical approach to formulating a condition number $C(\mathcal{P})$ is as follows. We imagine that the input parameters to \mathcal{P} suffer random perturbations, of maximum relative magnitude ϵ , about their nominal values. Corresponding perturbations of the output values will then be induced, and we require the condition number to be such that the *greatest* of these output perturbations is bounded by the quantity $C(\mathcal{P})\epsilon$. Thus “well-conditioned” problems have condition numbers of order unity (i.e., the input and output perturbations are comparable) while “ill-conditioned” problems will have very large condition numbers. Although we have not yet discussed backward error analysis, it will be intuitively clear that high-accuracy solutions to ill-conditioned problems are extremely difficult to compute using floating-point arithmetic.

The study of condition numbers can be useful in identifying more-stable problem formulations, and thereby obtaining more-accurate computed results. We now examine in greater detail some condition number formulations for two important problems: *univariate polynomials* and *linear maps* (i.e., matrices). The condition numbers for polynomial values and roots used below are based upon the formulations of Gautschi [209, 210]. For linear maps, the condition numbers are based on standard vector and matrix norms: see §12.4.4.

12.4.1 Condition of a Polynomial Value

Consider the representation

$$p(t) = \sum_{k=0}^n c_k \phi_k(t) \quad (12.12)$$

of a degree- n polynomial $p(t)$ by its coefficients c_0, \dots, c_n in a specified basis $\phi_0(t), \dots, \phi_n(t)$. Suppose we are interested in evaluating $p(t)$, but we do not know its coefficients c_0, \dots, c_n precisely. Specifically, suppose that c_k is in error by δc_k for each k . Then the nominal value $p(t)$ is perturbed to

$$p(t) + \delta p(t) = \sum_{k=0}^n c_k \phi_k(t) + \sum_{k=0}^n \delta c_k \phi_k(t).$$

If the coefficient errors are assumed to be random and of a uniform relative magnitude ϵ , so that

$$-\epsilon \leq \delta c_k / c_k \leq +\epsilon \quad (12.13)$$

for $k = 0, \dots, n$ the perturbation δp in p evidently lies in the range

$$-\sum_{k=0}^n |\delta c_k \phi_k(t)| \leq \delta p(t) \leq +\sum_{k=0}^n |\delta c_k \phi_k(t)|, \quad (12.14)$$

and using (12.13) we may write

$$|\delta p(t)| \leq C_\phi(p(t)) \epsilon \quad \text{where} \quad C_\phi(p(t)) = \sum_{k=0}^n |c_k \phi_k(t)|. \quad (12.15)$$

We call $C_\phi(p(t))$ the *condition number for the value of $p(t)$* with respect to its coefficients in the basis $\phi_0(t), \dots, \phi_n(t)$. We append the subscript ϕ to this condition number to emphasize that it depends on the *choice of basis*, as well as on the polynomial $p(t)$ itself. Note that we make no assumption concerning the size of the fractional coefficient error ϵ in deducing the bound (12.15). Thus, the perturbation in the value of $p(t)$ satisfies this bound for *finite* (not just infinitesimal) relative errors in the coefficients. We now compare condition numbers for the value of a polynomial in different bases.

Definition 12.1 A basis $\phi_0(t), \dots, \phi_n(t)$ for polynomials of degree n is said to be *non-negative* on the interval $t \in [a, b]$ if

$$\phi_k(t) \geq 0 \quad \text{for all } t \in [a, b] \quad \text{and } k = 0, \dots, n. \quad (12.16)$$

Non-negative polynomial bases are of interest in the following context [181].

Theorem 12.1 Let $\psi_0(t), \dots, \psi_n(t)$ and $\phi_0(t), \dots, \phi_n(t)$ be two non-negative bases for polynomials of degree n on the interval $t \in [a, b]$, such that the former can be expressed as a non-negative combination of the latter, i.e.,

$$\psi_j(t) = \sum_{k=0}^n M_{jk} \phi_k(t), \quad j = 0, \dots, n, \quad (12.17)$$

$$\text{where } M_{jk} \geq 0 \quad \text{for } 0 \leq j, k \leq n. \quad (12.18)$$

Then the condition number for the value of any degree- n polynomial $p(t)$ at any point $t \in [a, b]$ in these bases satisfies the inequality

$$C_\phi(p(t)) \leq C_\psi(p(t)). \quad (12.19)$$

Proof : Let $p(t)$ have coefficients a_0, \dots, a_n in the basis $\psi_0(t), \dots, \psi_n(t)$:

$$p(t) = \sum_{j=0}^n a_j \psi_j(t). \quad (12.20)$$

On substituting (12.17) into (12.20), we see that the coefficients c_0, \dots, c_n of $p(t)$ in the basis $\phi_0(t), \dots, \phi_n(t)$ are given by

$$c_k = \sum_{j=0}^n a_j M_{jk} \quad \text{for } k = 0, \dots, n. \quad (12.21)$$

Since the bases $\psi_0(t), \dots, \psi_n(t)$ and $\phi_0(t), \dots, \phi_n(t)$ are both non-negative on $t \in [a, b]$, the condition numbers for the value of $p(t)$ may be written as

$$C_\phi(p(t)) = \sum_{k=0}^n |c_k| \phi_k(t) \quad \text{and} \quad C_\psi(p(t)) = \sum_{j=0}^n |a_j| \psi_j(t). \quad (12.22)$$

We now substitute (12.21) into $C_\phi(p(t))$ and use the triangle inequality

$$\left| \sum_{k=0}^n x_k \right| \leq \sum_{k=0}^n |x_k| \quad (12.23)$$

for any sequence x_0, \dots, x_n of real values, to obtain

$$C_\phi(p(t)) = \sum_{k=0}^n \left| \sum_{j=0}^n a_j M_{jk} \right| \phi_k(t) \leq \sum_{k=0}^n \left[\sum_{j=0}^n |a_j M_{jk}| \right] \phi_k(t). \quad (12.24)$$

Thus, setting $|a_j M_{jk}| = |a_j| M_{jk}$ (since $M_{jk} \geq 0$ for all j, k) and re-arranging the order of summation on the right-hand side of (12.24) we have

$$C_\phi(p(t)) \leq \sum_{j=0}^n |a_j| \sum_{k=0}^n M_{jk} \phi_k(t) = \sum_{j=0}^n |a_j| \psi_j(t) = C_\psi(p(t)), \quad (12.25)$$

where we make use of (12.17) in the second step. ■

We emphasize again the general nature of the inequality (12.19) — it holds for *every* polynomial $p(t)$ and for *each* value $t \in [a, b]$ if the non-negative bases $\phi_0(t), \dots, \phi_n(t)$ and $\psi_0(t), \dots, \psi_n(t)$ satisfy (12.17) and (12.18). The former basis then offers as a *systematically more stable representation* for evaluating polynomials at points $t \in [a, b]$ than the latter basis.

A trivial instance in which the relation (12.19) holds with equality is if we simply *scale* the basis functions, i.e., we set

$$\psi_k(t) = \lambda_k \phi_k(t) \quad \text{for } k = 0, \dots, n,$$

where $\lambda_0, \dots, \lambda_n$ are any (non-zero) constants. It is not difficult to see in this case that $C_\psi(p(t)) \equiv C_\phi(p(t))$, i.e., the condition number for the value of $p(t)$ is *independent of the scaling of the basis functions*. A non-trivial example is a comparison of the Bernstein basis

$$b_k^n(t) = \binom{n}{k} (1-t)^{n-k} t^k \quad \text{for } k = 0, \dots, n, \quad (12.26)$$

on which the Bézier curve and surface forms are based (see Chap. 13) with the monomial basis $1, t, \dots, t^n$. Since the polynomials (12.26) are non-negative for $t \in [0, 1]$ and the monomials are the non-negative combinations

$$t^j = \sum_{k=j}^n \frac{\binom{k}{j}}{\binom{n}{j}} b_k^n(t) \quad \text{for } j = 0, \dots, n \quad (12.27)$$

of them [181], the Bernstein representation

$$p(t) = \sum_{k=0}^n c_k b_k^n(t) \quad (12.28)$$

of a polynomial is systematically more stable on the interval $t \in [0, 1]$ than the “power” form (3.1). On the other hand, we note from the expression

$$b_j^n(t) = \sum_{k=j}^n (-1)^{k-j} \binom{n}{k} \binom{k}{j} t^k \quad \text{for } j = 0, \dots, n \quad (12.29)$$

for the Bernstein basis in terms of the monomial basis [181] that the former are *not* non-negative combinations of the latter.

In fact, it can be shown [161] that the Bernstein basis is “optimally stable” in the sense of Theorem 12.1 — it is *impossible* to construct a non-negative basis for degree- n polynomials on $t \in [0, 1]$, in terms of which the Bernstein basis can be expressed as a non-negative combination,⁶ so that this basis will yield systematically smaller condition numbers than the Bernstein form.

The transformation between two degree- n polynomial bases by means of a non-negative matrix establishes a *partial ordering* among the set of such bases that are non-negative over any specified interval, and the Bernstein basis is a *minimal element* of this partially-ordered set. No other commonly-used basis is known to have this property — see [161] for more complete details.

12.4.2 Condition of a Polynomial Root

We discussed above the stability of the *value* of a polynomial, with respect to perturbations of its coefficients. Many problems concerning curve and surface intersections, ray tracing of surfaces, etc., can be reduced to computing *roots* of polynomials, so we are also interested in analyzing their stability. Clearly, these problems are related, since a root is a point t where the value is zero.

Suppose τ is a simple real root of the polynomial $p(t)$, i.e., $p(\tau) = 0 \neq p'(\tau)$. We are interested in characterizing the sensitivity of τ to perturbations of the coefficients c_0, \dots, c_n of $p(t)$ in the basis $\phi_0(t), \dots, \phi_n(t)$. We consider first an infinitesimal perturbation δc_r in the coefficient c_r only, and suppose that the root τ is displaced to $\tau + \delta\tau$ when $p(t)$ is perturbed to $p(t) + \delta c_r \phi_r(t)$. Then we must have

$$p(\tau + \delta\tau) + \delta c_r \phi_r(\tau + \delta\tau) = 0.$$

⁶ We exclude, of course, the trivial case of scalar multiples of the Bernstein basis functions. The result can be easily generalized to an arbitrary interval $t \in [a, b]$.

Moving the second term to the right and expanding both sides in Taylor series gives

$$\sum_{k=1}^n \frac{p^{(k)}(\tau)}{k!} (\delta\tau)^k = -\delta c_r \sum_{k=0}^n \frac{\phi_r^{(k)}(\tau)}{k!} (\delta\tau)^k. \quad (12.30)$$

Note that there is no constant term on the left, since $p(\tau) = 0$, and the Taylor series are finite because $p(t)$ is just a polynomial.

Keeping only first-order terms in infinitesimal quantities, we find that

$$\lim_{\delta c_r \rightarrow 0} \frac{\delta\tau}{\delta c_r / c_r} = -\frac{c_r \phi_r(\tau)}{p'(\tau)}. \quad (12.31)$$

This expresses the sensitivity of τ to a perturbation in the coefficient c_r only. If we now imagine *every* coefficient to be subject to a random (infinitesimal) perturbation of maximum relative magnitude ϵ ,

$$|\delta c_k / c_k| \leq \epsilon \quad \text{for } k = 0, \dots, n, \quad (12.32)$$

the greatest overall root perturbation $\delta\tau$ will be achieved when $|\delta c_k| = \epsilon |c_k|$ for each k , and the signs of the δc_k 's are such as to make their contributions on the right-hand side of (12.31) add up in the same sense.

Thus, we deduce that the simple root τ of $p(t)$ will suffer a perturbation $\delta\tau$ satisfying the bound

$$|\delta\tau| \leq C_\phi(\tau) \epsilon \quad \text{where} \quad C_\phi(\tau) = \frac{1}{|p'(\tau)|} \sum_{k=0}^n |c_k \phi_k(\tau)| \quad (12.33)$$

when the coefficients c_0, \dots, c_n of $p(t)$ in the basis $\phi_0(t), \dots, \phi_n(t)$ are subject to random *infinitesimal* errors of maximum relative magnitude ϵ . We call the quantity $C_\phi(\tau)$ a *root condition number* for the polynomial $p(t)$.

Note that although $C_\phi(\tau)$ differs from $C_\phi(p(\tau))$ by only the factor $1/|p'(\tau)|$, the interpretation of the root condition number is rather different from that for the polynomial value. While (12.15) expresses a sharp bound on the change in the polynomial value for *arbitrary* coefficient perturbations, the bound (12.33) on the root displacement is valid only for *infinitesimal* perturbations: it is only by restricting to infinitesimal perturbations that we can omit the higher-order terms in (12.30) and thus proceed to equation (12.31) and hence (12.33).

Since the factor $|p'(\tau)|$ in $C_\phi(\tau)$ is evidently *independent of the basis* that we choose for the polynomial $p(t)$, the inequality of Theorem 12.1 with respect to condition numbers for the polynomial *value* in different non-negative bases applies equally to the *root* condition numbers. For example, if we are interested in the roots of a polynomial $p(t)$ on $t \in [0, 1]$, the Bernstein form is always a better-conditioned representation for computing them than the power form.

The root condition number (12.33) is formally *infinite* if $p'(\tau) = 0$ — i.e., when τ is a *multiple* root. This indicates that $|\delta\tau|$ actually has a *faster than linear* growth with ϵ . In order to characterize the dependence of $\delta\tau$ on ϵ in

such instances, we return to equation (12.30) and retain only the lowest-order non-vanishing term on the left-hand side. We thus find, at an m -fold root τ such that $p(\tau) = p'(\tau) = \dots = p^{(m-1)}(\tau) = 0 \neq p^{(m)}(\tau)$, that

$$|\delta\tau| \leq C_\phi^m(\tau) \epsilon^{1/m} \quad \text{with} \quad C_\phi^m(\tau) = \left[\frac{m!}{|p^{(m)}(\tau)|} \sum_{k=0}^n |c_k \phi_k(\tau)| \right]^{1/m}. \quad (12.34)$$

We may interpret $C_\phi^m(\tau)$ as a condition number for the m -fold root τ of $p(t)$ in the basis $\phi_0(t), \dots, \phi_n(t)$. Again, the above bound holds only in the limit $\epsilon \rightarrow 0$ — note that $\epsilon^{1/m} \gg \epsilon$ when $\epsilon \ll 1$.

12.4.3 Wilkinson's Polynomial

An (in)famous polynomial, first investigated by Wilkinson [468] in 1959, offers a vivid illustration of these ideas. In the course of testing newly-implemented software for floating-point arithmetic (only fixed-point arithmetic processors were available at that time), Wilkinson attempted to compute the roots of a degree 20 polynomial. Specifically, he chose a polynomial with 20 equidistant real roots,

$$p(t) = \prod_{k=1}^n (t - k/n), \quad n = 20, \quad (12.35)$$

so as not to encounter numerical difficulties (or so he thought) on account of closely-spaced or near-multiple roots.⁷ Wilkinson's approach was to multiply out expression (12.35), so as to determine the power coefficients a_0, \dots, a_n in the representation (3.1), and to use this representation in evaluating $p(t)$ and its derivative for Newton-Raphson iterations. He discovered, in fact, that he could find few of the roots of (12.35) to more than just a few accurate digits — if at all — and was at first convinced that his software implementation of floating-point arithmetic must be plagued by bugs.

It was only on verifying this was not the case that he discovered the true source of the problem, namely, the severe ill-conditioning of the roots of $p(t)$ with respect to its power coefficients a_0, \dots, a_n . He subsequently called this “the most traumatic experience in my career as a numerical analyst” [470].

We begin to understand why the roots of $p(t)$ are so difficult to determine in floating-point arithmetic when we compute their condition numbers in the power basis, as given by expression (12.33). Table 12.1 lists these condition numbers, which are found to be greater than 10^{13} in some instances. In other words, a minuscule coefficient perturbation of merely 1 part in 10^{13} may induce displacements of order unity in the roots! Perturbations of this magnitude might certainly be expected in computing the power coefficients a_0, \dots, a_{20} of $p(t)$ by multiplying out (12.35) in floating-point arithmetic.

⁷ Wilkinson actually used roots at $t = 1, \dots, 20$, which we scale down to the unit interval $t \in [0, 1]$ here — this does not alter the problem in any substantive way.

Table 12.1. Root condition numbers for Wilkinson's polynomial.

root	condition number in power basis	condition number in Bernstein basis
0.05	2.10×10^1	3.41×10^0
0.10	4.39×10^3	1.45×10^2
0.15	3.03×10^5	2.34×10^3
0.20	1.03×10^7	2.03×10^4
0.25	2.06×10^8	1.11×10^5
0.30	2.68×10^9	4.15×10^5
0.35	2.41×10^{10}	1.12×10^6
0.40	1.57×10^{11}	2.22×10^6
0.45	7.57×10^{11}	3.32×10^6
0.50	2.78×10^{12}	3.80×10^6
0.55	7.82×10^{12}	3.32×10^6
0.60	1.71×10^{13}	2.22×10^6
0.65	2.89×10^{13}	1.12×10^6
0.70	3.78×10^{13}	4.15×10^5
0.75	3.78×10^{13}	1.11×10^5
0.80	2.83×10^{13}	2.03×10^4
0.85	1.54×10^{13}	2.34×10^3
0.90	5.74×10^{12}	1.45×10^2
0.95	1.31×10^{12}	3.41×10^0
1.00	1.38×10^{11}	0.00×10^0

How do such enormous root condition numbers arise? The answer lies in that dreaded blight of all finite-precision calculations, discussed in §12.3.3 — namely, the problem of *error amplification through digit cancellation*. Suppose we try computing the value of $p(t)$ at the point $t = 0.525$, say, by enumerating the values of its 21 constituent terms $a_k t^k$ in the power form at that point (we choose a point *between* two roots since that value *at* a root is, of course, zero). The contributions of these terms, accurate to the number of digits shown, are found to be as follows:

$$\begin{aligned}
a_0 &= +0.000000023201961595 \\
a_1 t &= -0.000000876483482227 \\
a_2 t^2 &= +0.000014513630989446 \\
a_3 t^3 &= -0.000142094724489860 \\
a_4 t^4 &= +0.000931740809130569 \\
a_5 t^5 &= -0.004381740078100366 \\
a_6 t^6 &= +0.015421137443693244 \\
a_7 t^7 &= -0.041778345191908158 \\
a_8 t^8 &= +0.088811127150105239
\end{aligned}$$

$$\begin{aligned}
a_9 t^9 &= -0.150051459849195639 \\
a_{10} t^{10} &= +0.203117060946715796 \\
a_{11} t^{11} &= -0.221153902712311843 \\
a_{12} t^{12} &= +0.193706822311568532 \\
a_{13} t^{13} &= -0.135971108107894016 \\
a_{14} t^{14} &= +0.075852737479877575 \\
a_{15} t^{15} &= -0.033154980855819210 \\
a_{16} t^{16} &= +0.011101552789116296 \\
a_{17} t^{17} &= -0.002747271750190952 \\
a_{18} t^{18} &= +0.000473141245866219 \\
a_{19} t^{19} &= -0.000050607637503518 \\
a_{20} t^{20} &= +0.000002530381875176 \\
\hline p(t) &= 0.0000000000000003899 .
\end{aligned} \tag{12.36}$$

The actual value of $p(t)$, halfway between two consecutive roots, is seen to be just a tiny residual left over when relatively large terms of alternating sign are summed up. In fact, this value is ~ 13 orders of magnitude smaller than the largest of the individual terms $a_k t^k$. A perturbation of just a single coefficient coefficient a_k may thus be amplified as much as 10^{13} times in the value of $p(t)$! Since the roots are just the points at which the polynomial value vanishes, they suffer commensurate errors.

This example shows that error amplification due to cancellation need not be confined to individual arithmetic operations, as in the example of §12.3.3 — although no two consecutive terms in (12.36) have many digits in common, the relative accuracy of the final value is still extremely susceptible to individual arithmetic errors or small perturbations in the coefficients a_0, \dots, a_{20} .

We have observed that the Bernstein basis on $t \in [0, 1]$ is systematically better-conditioned than the power basis about $t = 0$. Table 12.1 compares the Bernstein-basis root condition numbers for (12.35) with the power-basis condition numbers — we see that, for the most unstable roots, they are about 7 orders of magnitude smaller. This means that, when using the Bernstein form (12.28), we can expect to compute the roots with about *seven more digits of accuracy* than when using then power form (assuming that the coefficients of both forms have relative errors of similar magnitudes).

This is dramatically illustrated in Table 12.2, where we show the result of a fractional perturbation $\epsilon \approx 5 \times 10^{-10}$ in the coefficients a_{19} and c_{19} of the power and Bernstein forms. The values shown are correct to the given number of digits — they indicate the *intrinsic sensitivity* of the roots to perturbations in a_{19} or c_{19} , rather than the effects of arithmetic or approximation errors in a numerical root-finding procedure. Whereas all the roots of the perturbed Bernstein form exhibit at least 8 accurate digits, many roots of the perturbed power form have *no* accurate digits at all — they become complex conjugate

Table 12.2. Perturbed roots of Wilkinson's polynomial.

exact root	perturbed root (power basis)	perturbed root (Bernstein basis)
0.05	0.05000000	0.05000000000
0.10	0.10000000	0.10000000000
0.15	0.15000000	0.15000000000
0.20	0.20000000	0.20000000000
0.25	0.25000000	0.25000000000
0.30	0.30000035	0.30000000000
0.35	0.34998486	0.35000000000
0.40	0.40036338	0.40000000000
0.45	0.44586251	0.45000000000
0.50	0.50476331±	0.50000000000
0.55	0.03217504 i	0.5499999997
0.60	0.58968169±	0.6000000010
0.65	0.08261649 i	0.6499999972
0.70	0.69961791±	0.7000000053
0.75	0.12594150 i	0.7499999930
0.80	0.83653687±	0.8000000063
0.85	0.14063124 i	0.8499999962
0.90	0.97512197±	0.9000000013
0.95	0.09701652 i	0.9499999998
1.00	1.04234541	1.0000000000

pairs! This provides an excellent illustration of the fact that the *formulation* of a problem can often exert a profound influence on the accuracy with which we can hope to compute the solutions of that problem.

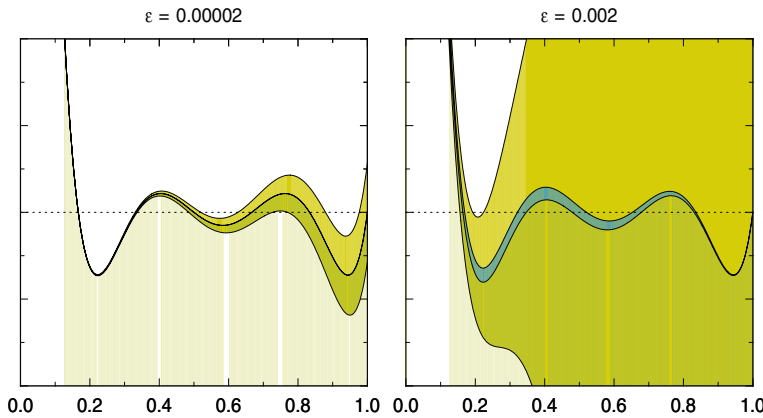


Fig. 12.3. Perturbation regions for the Bernstein (dark grey) and power (light grey) forms of a degree-6 Wilkinson polynomial with specified relative coefficient error ϵ .

Figure 12.3 shows the *perturbation regions* defined by (12.14) for the power and Bernstein forms of a polynomial of the Wilkinson form (12.35) with $n = 6$ and relative coefficient perturbations $\epsilon = 0.00002$ and 0.002 . The intervals defined by the intersections of these regions with the t -axis bound the values of the real roots. For the $\epsilon = 0.00002$ perturbation, the width of the Bernstein-form perturbation region is narrower than the line thickness in the plot, but the power-form perturbation region is already quite prominent. For $\epsilon = 0.002$, the Bernstein-form region becomes more apparent, but it is still possible to unambiguously distinguish the six real roots. However, the power-form region grows dramatically, and the identities of the original six roots are lost.

12.4.4 Vector and Matrix Norms

We have discussed above the stability of univariate polynomials, which may be regarded as non-linear maps from an independent variable x to a dependent variable, $y = p(x)$ — the *value* of the polynomial. The stability properties of maps between *several* variables are also important, but since the analysis is more difficult we confine our attention to *linear* multivariate maps, specified by *matrices*. In order to proceed, we need to introduce some basic concepts concerning the *norms* of vectors and matrices.

Let $\mathbf{v} = (v_0, \dots, v_n)^T$ be a column vector⁸ with $n + 1$ real elements. By a *norm* of \mathbf{v} , we mean a non-negative number that characterizes the “length” or “magnitude” of this vector. We are familiar with the *Euclidean* norm,

$$\|\mathbf{v}\|_2 = \sqrt{v_0^2 + \dots + v_n^2}, \quad (12.37)$$

which may be regarded as a special case of the p -norm defined by

$$\|\mathbf{v}\|_p = \left[\sum_{i=0}^n |v_i|^p \right]^{1/p}. \quad (12.38)$$

In the particular cases $p = 1$ and $p = \infty$, we have

$$\|\mathbf{v}\|_1 = \sum_{i=0}^n |v_i| \quad \text{and} \quad \|\mathbf{v}\|_\infty = \max_{0 \leq i \leq n} |v_i|. \quad (12.39)$$

The case $p = \infty$ is sometimes called the *maximum* or *uniform* norm. For all p , the norms defined by (12.38) satisfy the following conditions:

1. $\|\mathbf{v}\|_p \geq 0$ and $\|\mathbf{v}\|_p = 0 \iff \mathbf{v} = \mathbf{0}$;
2. $\|\alpha\mathbf{v}\|_p = |\alpha| \|\mathbf{v}\|_p$ for any scalar α ;
3. $\|\mathbf{v} + \mathbf{u}\|_p \leq \|\mathbf{v}\|_p + \|\mathbf{u}\|_p$ (the “triangle inequality”).

⁸ We use zero-indexed vectors here (likewise for matrices) since the vector elements will often be the coefficients of a polynomial of degree n in some basis.

The triangle inequality is a consequence of Minkowski's inequality [31]:

$$\left[\sum_{i=0}^n (x_i + y_i)^p \right]^{1/p} \leq \left[\sum_{i=0}^n x_i^p \right]^{1/p} + \left[\sum_{i=0}^n y_i^p \right]^{1/p}$$

(where $p \geq 1$) for sets of non-negative real numbers x_0, \dots, x_n and y_0, \dots, y_n . Note that $\|\mathbf{v} + \mathbf{u}\|_p = \|\mathbf{v}\|_p + \|\mathbf{u}\|_p$ if and only if the vectors \mathbf{u} and \mathbf{v} are *parallel*, i.e., $u_k = \alpha v_k$ for some scalar α and $k = 0, \dots, n$.

Because of the simplicity of the corresponding matrix norms, we shall use mostly the $\|\mathbf{v}\|_1$ and $\|\mathbf{v}\|_\infty$ vector norms. The following bounds indicate that the choice of p does not strongly influence the value of $\|\mathbf{v}\|_p$:

Lemma 12.1 *For all vectors \mathbf{v} , the norm $\|\mathbf{v}\|_p$ with $1 < p < \infty$ satisfies*

$$\frac{\|\mathbf{v}\|_1}{(n+1)^{1-1/p}} \leq \|\mathbf{v}\|_p \leq \|\mathbf{v}\|_1 \quad \text{and} \quad \|\mathbf{v}\|_\infty \leq \|\mathbf{v}\|_p \leq (n+1)^{1/p} \|\mathbf{v}\|_\infty.$$

These bounds may be verified by appealing to Hölder's inequality [31]:

$$\sum_{i=0}^n x_i y_i \leq \left[\sum_{i=0}^n x_i^p \right]^{1/p} \left[\sum_{i=0}^n y_i^q \right]^{1/q}$$

for non-negative real numbers x_0, \dots, x_n and y_0, \dots, y_n where p and q satisfy

$$\frac{1}{p} + \frac{1}{q} = 1 \quad \text{and} \quad 1 < p, q < \infty.$$

Since $\|\mathbf{v}\|_\infty \leq \|\mathbf{v}\|_p \leq \|\mathbf{v}\|_1$ for all \mathbf{v} and $1 < p < \infty$, we may regard $\|\mathbf{v}\|_\infty$ as the “smallest” of the vector norms (12.38), and $\|\mathbf{v}\|_1$ as the “largest.”

For any real $(n+1) \times (n+1)$ matrix \mathbf{M} , the matrix norm *subordinate to* or *induced by* the vector norm (12.38) is the non-negative number defined by

$$\|\mathbf{M}\|_p = \max_{\mathbf{v} \neq \mathbf{0}} \frac{\|\mathbf{M}\mathbf{v}\|_p}{\|\mathbf{v}\|_p}. \quad (12.40)$$

Informally, we may think of the matrix norm $\|\mathbf{M}\|_p$ as the greatest factor by which the “length” of any vector (as measured by the vector norm $\|\mathbf{v}\|_p$) is increased through the action of the linear map \mathbf{M} . From the scaling property $\|\alpha\mathbf{v}\|_p = |\alpha| \|\mathbf{v}\|_p$ of the vector norm, we also have the alternative definition

$$\|\mathbf{M}\|_p = \max_{\|\mathbf{v}\|_p = 1} \|\mathbf{M}\mathbf{v}\|_p.$$

Note that from (12.40) we may infer the inequality

$$\|\mathbf{M}\mathbf{v}\|_p \leq \|\mathbf{M}\|_p \|\mathbf{v}\|_p \quad \text{for all } \mathbf{v} \neq \mathbf{0}. \quad (12.41)$$

Furthermore, it can be shown [256] that the bound given in (12.41) is sharp, i.e., there exists a non-zero \mathbf{v} for which $\|\mathbf{M}\mathbf{v}\|_p = \|\mathbf{M}\|_p \|\mathbf{v}\|_p$. The following properties of the matrix norm (12.40) are easily verified:

1. $\|\mathbf{M}\|_p \geq 0$ and $\|\mathbf{M}\|_p = 0 \iff \mathbf{M} = \mathbf{0}$;
2. $\|\alpha\mathbf{M}\|_p = |\alpha| \|\mathbf{M}\|_p$ for any scalar α ;
3. $\|\mathbf{A} + \mathbf{B}\|_p \leq \|\mathbf{A}\|_p + \|\mathbf{B}\|_p$;
4. $\|\mathbf{AB}\|_p \leq \|\mathbf{A}\|_p \|\mathbf{B}\|_p$.

For general p , the matrix norm (12.40) can be quite difficult to compute, or even estimate. However, the cases $p = 1$ and $p = \infty$ are relatively simple.

Proposition 12.1 *Let M_{jk} for $0 \leq j, k \leq n$ be the matrix elements of \mathbf{M} . Then the norms $\|\mathbf{M}\|_1$ and $\|\mathbf{M}\|_\infty$ are given by*

$$\|\mathbf{M}\|_1 = \max_{0 \leq k \leq n} \sum_{j=0}^n |M_{jk}| \quad \text{and} \quad \|\mathbf{M}\|_\infty = \max_{0 \leq j \leq n} \sum_{k=0}^n |M_{jk}| \quad (12.42)$$

i.e., they are the greatest of the column sums and row sums of absolute values of the matrix elements M_{jk} , respectively.

Proof : First, for $\|\mathbf{M}\|_1$, we use the triangle inequality (12.23) to note that

$$\|\mathbf{Mv}\|_1 = \sum_{j=0}^n \left| \sum_{k=0}^n M_{jk} v_k \right| \leq \sum_{j=0}^n \sum_{k=0}^n |M_{jk}| |v_k| = \sum_{k=0}^n \left[\sum_{j=0}^n |M_{jk}| \right] |v_k|.$$

The term in parenthesis on the right is the sum of absolute values of matrix elements across column k . Replacing this by the greatest such sum, we have

$$\|\mathbf{Mv}\|_1 \leq \left[\max_{0 \leq k \leq n} \sum_{j=0}^n |M_{jk}| \right] \sum_{k=0}^n |v_k| = \left[\max_{0 \leq k \leq n} \sum_{j=0}^n |M_{jk}| \right] \|\mathbf{v}\|_1,$$

and if column m exhibits the greatest sum of absolute values, the above will hold with equality for the vector \mathbf{v} given by

$$v_k = \delta_{km} = \begin{cases} 1 & \text{if } k = m, \\ 0 & \text{otherwise.} \end{cases}$$

Thus, we have

$$\|\mathbf{M}\|_1 = \max_{\mathbf{v} \neq 0} \frac{\|\mathbf{Mv}\|_1}{\|\mathbf{v}\|_1} = \max_{0 \leq k \leq n} \sum_{j=0}^n |M_{jk}|.$$

The argument for $\|\mathbf{M}\|_\infty$ is quite similar:

$$\begin{aligned} \|\mathbf{Mv}\|_\infty &= \max_{0 \leq j \leq n} \left| \sum_{k=0}^n M_{jk} v_k \right| \\ &\leq \max_{0 \leq j \leq n} \sum_{k=0}^n |M_{jk}| |v_k| \leq \left[\max_{0 \leq j \leq n} \sum_{k=0}^n |M_{jk}| \right] \max_{0 \leq k \leq n} |v_k|. \end{aligned}$$

Thus, since $\|\mathbf{v}\|_\infty = \max_k |v_k|$, we may write

$$\|\mathbf{Mv}\|_\infty \leq \left[\max_{0 \leq j \leq n} \sum_{k=0}^n |M_{jk}| \right] \|\mathbf{v}\|_\infty,$$

and we note that if m is the row with the greatest sum of absolute values, the above holds with equality for the vector \mathbf{v} defined by

$$v_k = \text{sign}(M_{mk}) = \begin{cases} M_{mk}/|M_{mk}| & \text{if } M_{mk} \neq 0, \\ 0 & \text{if } M_{mk} = 0, \end{cases}$$

for $k = 0, \dots, n$. Hence we deduce that

$$\|\mathbf{Mv}\|_\infty = \max_{\mathbf{v} \neq \mathbf{0}} \frac{\|\mathbf{Mv}\|_\infty}{\|\mathbf{v}\|_\infty} = \max_{0 \leq j \leq n} \sum_{k=0}^n |M_{jk}|. \quad \blacksquare$$

From (12.42) it is clear that $\|\mathbf{M}\|_1 = \|\mathbf{M}^T\|_\infty$ for any real matrix \mathbf{M} and, in particular, that $\|\mathbf{M}\|_1 = \|\mathbf{M}\|_\infty$ when \mathbf{M} is a *symmetric* matrix.

The matrix norm subordinate to the $\|\cdot\|_2$ vector norm defined by (12.37) is somewhat more difficult to compute:

Proposition 12.2 *For any real $(n+1) \times (n+1)$ matrix \mathbf{M} , let $\lambda_0, \dots, \lambda_n$ be the $n+1$ eigenvalues of the symmetric matrix $\mathbf{M}^T \mathbf{M}$, and let*

$$\lambda_{\max} = \max_{0 \leq i \leq n} \lambda_i.$$

Then the $\|\cdot\|_2$ norm of the matrix \mathbf{M} is given by

$$\|\mathbf{M}\|_2 = \sqrt{\lambda_{\max}}.$$

Proof : For any real vector \mathbf{v} , we have $\mathbf{v}^T \mathbf{v} = \|\mathbf{v}\|_2^2$. Thus, by the definition of $\|\mathbf{M}\|_2$, we obtain

$$\|\mathbf{M}\|_2^2 = \max_{\mathbf{v} \neq \mathbf{0}} \frac{\|\mathbf{Mv}\|_2^2}{\|\mathbf{v}\|_2^2} = \max_{\mathbf{v} \neq \mathbf{0}} \frac{(\mathbf{Mv})^T \mathbf{Mv}}{\mathbf{v}^T \mathbf{v}} = \max_{\mathbf{v} \neq \mathbf{0}} \frac{\mathbf{v}^T (\mathbf{M}^T \mathbf{M}) \mathbf{v}}{\mathbf{v}^T \mathbf{v}}. \quad (12.43)$$

Now let $\mathbf{e}_0, \dots, \mathbf{e}_n$ be orthonormal eigenvectors for $\mathbf{M}^T \mathbf{M}$, corresponding to its eigenvalues $\lambda_0, \dots, \lambda_n$ (not necessarily all distinct), so that

$$\mathbf{M}^T \mathbf{M} \mathbf{e}_i = \lambda_i \mathbf{e}_i \quad \text{for } i = 0, \dots, n.$$

In this eigensystem, any non-zero vector \mathbf{v} has a representation of the form

$$\mathbf{v} = \sum_{i=0}^n c_i \mathbf{e}_i,$$

where the coefficients $\{c_i\}$ are not all zero. Since $\mathbf{e}_j \cdot \mathbf{e}_k = \delta_{jk}$, we note that

$$\mathbf{v}^T \mathbf{v} = \sum_{i=0}^n c_i^2 \quad \text{and} \quad \mathbf{v}^T (\mathbf{M}^T \mathbf{M}) \mathbf{v} = \sum_{i=0}^n c_i^2 \lambda_i, \quad (12.44)$$

and on substituting into (12.43) we have

$$\|\mathbf{M}\|_2^2 = \max_{(c_0, \dots, c_n) \neq (0, \dots, 0)} \frac{\sum c_i^2 \lambda_i}{\sum c_i^2} = \max_{0 \leq i \leq n} \lambda_i.$$

$\|\mathbf{M}\mathbf{v}\|_2^2 / \|\mathbf{v}\|_2^2$ attains its maximum value when $\mathbf{v} = \mathbf{e}_{\max}$, i.e., the eigenvector corresponding to the largest eigenvalue λ_{\max} . ■

The eigenvalues of $\mathbf{M}^T \mathbf{M}$ are called the *singular values* of the matrix \mathbf{M} (they are necessarily real and non-negative), and $\|\mathbf{M}\|_2$ is also known as the *spectral norm* of \mathbf{M} , since λ_{\max} is the *spectral radius* of $\mathbf{M}^T \mathbf{M}$ [471]. If \mathbf{M} is a symmetric matrix, we have $\mathbf{M}^T \mathbf{M} = \mathbf{M}^2$, and the eigenvalues $\lambda_0, \dots, \lambda_n$ of $\mathbf{M}^T \mathbf{M}$ are then just the squares of the eigenvalues μ_0, \dots, μ_n of \mathbf{M} . Thus, for a symmetric matrix we may write

$$\|\mathbf{M}\|_2 = \max_{0 \leq i \leq n} |\mu_i|.$$

12.4.5 Condition of a Linear Map

We are now ready to define the condition number of a linear map. Suppose \mathbf{M} is a non-singular matrix that maps $\mathbf{x} = (x_0, \dots, x_n)$ to $\mathbf{y} = (y_0, \dots, y_n)$:

$$\mathbf{y} = \mathbf{M}\mathbf{x}. \quad (12.45)$$

When the “input” vector \mathbf{x} suffers the perturbation $\delta\mathbf{x} = (\delta x_0, \dots, \delta x_n)$, a corresponding perturbation $\delta\mathbf{y} = (\delta y_0, \dots, \delta y_n)$ is induced in the “output” vector, given by

$$\delta\mathbf{y} = \mathbf{M}\delta\mathbf{x}. \quad (12.46)$$

We characterize these perturbations by scalar fractional measures of the form

$$\epsilon_{\mathbf{x}} = \frac{\|\delta\mathbf{x}\|_p}{\|\mathbf{x}\|_p} \quad \text{and} \quad \epsilon_{\mathbf{y}} = \frac{\|\delta\mathbf{y}\|_p}{\|\mathbf{y}\|_p}. \quad (12.47)$$

Now since \mathbf{M} is non-singular, the inverse map

$$\mathbf{x} = \mathbf{M}^{-1}\mathbf{y} \quad (12.48)$$

also exists. Applying the inequality (12.41) to (12.46) and (12.48), we obtain

$$\|\delta\mathbf{y}\|_p \leq \|\mathbf{M}\|_p \|\delta\mathbf{x}\|_p \quad \text{and} \quad \|\mathbf{x}\|_p \leq \|\mathbf{M}^{-1}\|_p \|\mathbf{y}\|_p.$$

Combining these inequalities, we see that ϵ_y is bounded in terms of ϵ_x by

$$\epsilon_y \leq C_p(\mathbf{M}) \epsilon_x, \quad (12.49)$$

where the p -norm *condition number* $C_p(\mathbf{M})$ of the matrix \mathbf{M} is defined by

$$C_p(\mathbf{M}) = \|\mathbf{M}\|_p \|\mathbf{M}^{-1}\|_p. \quad (12.50)$$

The condition number $C_p(\mathbf{M})$ gives a *sharp* bound on the error amplification in the linear map (12.45), i.e., there always exists a perturbation $\delta\mathbf{x}$ for which (12.49) holds with equality. Note also that (12.49) does not depend upon the assumption of infinitesimal perturbations. In terms of the amplification of the output error ϵ_y relative to the input error ϵ_x , the two factors in (12.50) can be interpreted as follows: $\|\mathbf{M}\|_p$ indicates how much *larger* the absolute output errors $\delta\mathbf{y}$ are than the absolute input errors $\delta\mathbf{x}$, while $\|\mathbf{M}^{-1}\|_p$ indicates how much *smaller* the nominal output \mathbf{y} is than the nominal input \mathbf{x} .

The following useful properties of the condition numbers of non-singular matrices are not difficult to verify:

1. $C_p(\mathbf{M}) \geq 1$;
2. $C_p(\mathbf{M}^{-1}) = C_p(\mathbf{M})$;
3. if $\mathbf{M} = \mathbf{M}_1 \mathbf{M}_2$ then $C_p(\mathbf{M}) \leq C_p(\mathbf{M}_1) C_p(\mathbf{M}_2)$;
4. $C_1(\mathbf{M}) = C_\infty(\mathbf{M})$ if \mathbf{M} is symmetric;
5. $C_2(\mathbf{M}) = \sqrt{\lambda_{\max}/\lambda_{\min}}$, where λ_{\min} and λ_{\max} are the smallest and largest eigenvalues of $\mathbf{M}^T \mathbf{M}$.

Property 1 implies that, in the linear map (12.45), the greatest relative error ϵ_y in the “output” \mathbf{y} will always exceed that ϵ_x in the “input” \mathbf{x} .

The condition number can also be used to characterize the sensitivity of \mathbf{x} to perturbations of \mathbf{M} , assuming \mathbf{y} is held constant in equation (12.45). It can be shown [364] that when \mathbf{M} suffers a perturbation $\delta\mathbf{M}$, with \mathbf{y} fixed, the induced relative uncertainty in \mathbf{x} is bounded by

$$\epsilon_x \leq \frac{C_p(\mathbf{M}) \epsilon_M}{1 - C_p(\mathbf{M}) \epsilon_M},$$

where $\epsilon_M = \|\delta\mathbf{M}\|_p / \|\mathbf{M}\|_p$ is assumed to be smaller than $1/C_p(\mathbf{M})$.

Matrix condition numbers for norms other than $p = 1, 2, \infty$ are, in general, quite difficult to compute. However, we can bound their values in terms of the “simple” instances $C_1(\mathbf{M})$ and $C_\infty(\mathbf{M})$ as follows. It can be shown⁹ that any square matrix \mathbf{M} satisfies the inequality

$$\|\mathbf{M}\|_p \leq \|\mathbf{M}\|_1^{1/p} \|\mathbf{M}\|_\infty^{1-1/p}.$$

⁹ This is an instance of the *Riesz convexity theorem* of functional analysis [105].

Now, since $\|\mathbf{M}\|_1$ and $\|\mathbf{M}\|_\infty$ are the greatest sums of absolute values across columns and rows, $\|\mathbf{M}\|_1 \leq (n+1) \|\mathbf{M}\|_\infty$ and $\|\mathbf{M}\|_\infty \leq (n+1) \|\mathbf{M}\|_1$. On substituting into the above inequality, and applying similar arguments to the inverse \mathbf{M}^{-1} , we obtain the relations

$$C_p(\mathbf{M}) \leq (n+1)^{2-2/p} C_1(\mathbf{M}) \quad \text{and} \quad C_p(\mathbf{M}) \leq (n+1)^{2/p} C_\infty(\mathbf{M}).$$

Since the condition numbers $C_1(\mathbf{M})$ and $C_\infty(\mathbf{M})$ are perhaps easiest to use in practice, it is useful to explicitly note the forms of the fractional error measures associated with them, namely

$$\epsilon_{\mathbf{x}} = \frac{|\delta x_0| + \cdots + |\delta x_n|}{|x_0| + \cdots + |x_n|} \quad \text{for } p=1, \quad (12.51)$$

and

$$\epsilon_{\mathbf{x}} = \frac{\max_k |\delta x_k|}{\max_k |x_k|} \quad \text{for } p=\infty. \quad (12.52)$$

Notwithstanding these different definitions, property 4 above indicates that, when \mathbf{M} is symmetric, its condition numbers in the two norms are identical.

12.4.6 Basis Transformations

Consider the matrix \mathbf{M} that maps the Bernstein coefficients $\mathbf{c} = (c_0, \dots, c_n)^T$ of a polynomial $p(t)$ to its power coefficients $\mathbf{a} = (a_0, \dots, a_n)^T$:

$$\mathbf{a} = \mathbf{M} \mathbf{c}, \quad \text{where } p(t) = \sum_{k=0}^n a_k t^k = \sum_{k=0}^n c_k b_k^n(t).$$

The elements of \mathbf{M} and its inverse \mathbf{M}^{-1} are given [147] by

$$M_{jk} = \begin{cases} (-1)^{j-k} \binom{n}{j} \binom{j}{k} & \text{if } j \geq k, \\ 0 & \text{if } j < k, \end{cases}$$

and

$$M_{jk}^{-1} = \begin{cases} \frac{\binom{j}{k}}{\binom{n}{k}} & \text{if } j \geq k, \\ 0 & \text{if } j < k. \end{cases}$$

It can be shown [147] that the condition number of this matrix in the $\|\cdot\|_1$ and $\|\cdot\|_\infty$ norms is

$$C_1(\mathbf{M}) = C_\infty(\mathbf{M}) = (n+1) \binom{n}{\nu} 2^\nu, \quad \text{where } \nu = \left\lfloor \frac{2(n+1)}{3} \right\rfloor$$

(the value of the “floor” function $\lfloor x \rfloor$ is the largest integer not exceeding x). For $n \geq 3$, a good approximation to the above [147] is given by

$$C_1(\mathbf{M}) = C_\infty(\mathbf{M}) \approx 3^{n+1} \sqrt{\frac{n+1}{4\pi}}.$$

Clearly, the condition number grows very rapidly with the polynomial degree n , and explicit conversions between the power and Bernstein bases are quite unstable for high-degree polynomials, e.g., $C \approx 10^{10}$ when $n = 20$ — see also [111]. In numerical analysis, as in all walks of life, *there is no free lunch*: if we wish to take advantage of the enhanced stability properties of the Bernstein representation discussed in §12.4.1–12.4.3, we must formulate the problem in Bernstein form *ab initio*. There is nothing to be gained from explicit floating-point conversions from the power to the Bernstein basis.

On the other hand, the transformation between the Bernstein basis and the Legendre basis on $[0, 1]$ — defined by the recurrence (3.6) with $L_0(t) = 1$ and $L_1(t) = 2t - 1$ — is relatively well-conditioned. It can be shown [154] that the elements of the matrix \mathbf{M} that transforms the Legendre coefficients of a degree- n polynomial into its Bernstein coefficients are given explicitly by

$$M_{jk} = \frac{1}{\binom{n}{j}} \sum_{i=\max(0,j+k-n)}^{\min(j,k)} (-1)^{k+i} \binom{k}{i} \binom{k}{i} \binom{n-k}{j-i},$$

while the elements of the inverse \mathbf{M}^{-1} are given by

$$M_{jk}^{-1} = \frac{2j+1}{n+j+1} \binom{n}{k} \sum_{i=0}^j (-1)^{j+i} \frac{\binom{j}{i} \binom{j}{i}}{\binom{n+j}{k+i}}$$

for $0 \leq j, k \leq n$. From these expressions one may easily deduce that

$$C_1(\mathbf{M}) = 2^n.$$

for the Legendre–Bernstein basis transformation. The dependence of $C_\infty(\mathbf{M})$ on n does not admit an elementary closed-form expression, but one can easily compute it for specific n values and deduce that, for all n ,

$$C_\infty(\mathbf{M}) < C_1(\mathbf{M}).$$

The growth of the condition number with n is appreciably milder than for the power–Bernstein transformation. The Legendre form is advantageous in least-squares approximation problems. Further discussion of condition numbers for the matrices that map polynomials between the power, Bernstein, and Hermite forms may be found in [236]. Figure 12.4 summarizes these results.

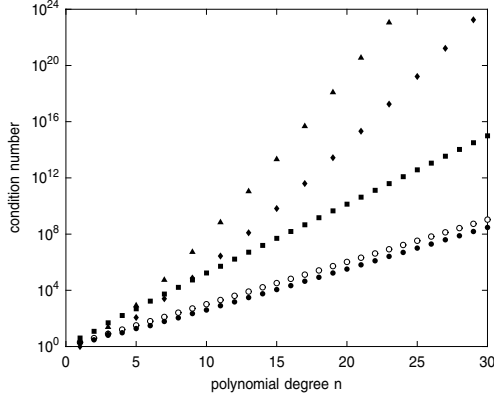


Fig. 12.4. Condition numbers C_p for basis transformations: Legendre–Bernstein — circles ($p = 1$) and dots ($p = \infty$); power–Bernstein — squares ($p = 1$ and ∞); Bernstein–Hermite — diamonds ($p = \infty$); and power–Hermite — triangles ($p = 1$).

12.4.7 Subdivision Processes

The relation between the Bernstein coefficients c_0, \dots, c_n and $\bar{c}_0, \dots, \bar{c}_n$ of a given polynomial $p(t)$ on an interval $[a, b]$ and a subinterval $[\bar{a}, \bar{b}]$ thereof is fundamental in the design of algorithms to isolate and approximate real roots on $t \in [a, b]$ — see §11.8. One may characterize the sensitivity of $\bar{c}_0, \dots, \bar{c}_n$ to perturbations of uniform relative magnitude ϵ in c_0, \dots, c_n by means of a condition number for the “subdivision matrix” \mathbf{M} defined by (11.10). In the $\|\cdot\|_\infty$ norm, this is given [176] by

$$C_\infty(\mathbf{M}) = [2f \max(u_{\bar{c}}, v_{\bar{c}})]^n$$

where $u_{\bar{c}} = (\bar{c} - a)/(b - a)$ and $v_{\bar{c}} = (b - \bar{c})/(b - a)$ denote the barycentric coordinates of the subinterval midpoint $\bar{c} = \frac{1}{2}(\bar{a} + \bar{b})$, $f = (b - a)/(\bar{b} - \bar{a})$ is the “zoom” factor of the subdivision map, and n is the degree of $p(t)$.

12.4.8 Ill-posed Problems

For certain special problems, we may find that the condition number is either infinite or undefined. Thus, for example, the root condition number (12.15) becomes formally infinite at a *multiple* root τ , since we then have $|p'(\tau)| = 0$. Similarly, for a linear map specified by a singular matrix \mathbf{M} , the condition number (12.50) is undefined, since the inverse \mathbf{M}^{-1} does not exist.

We call such “singular” cases *ill-posed* problems — they typically comprise a lower-dimension subset of the problem space under consideration. It may still be possible to characterize the sensitivity of the output to perturbations of the input in such cases, although the analysis will be somewhat different (as, for example, in the characterization (12.34) of the sensitivity of a multiple

root to perturbations in the polynomial coefficients). In fact, the magnitudes of the condition numbers for “regular” problems are closely correlated to their “distances” from the set of ill-posed problems [125].

12.5 Backward Error Analysis

We have seen how to characterize the sensitivity of the solution of a problem to perturbations of its input parameters by means of the condition number. The goal of *backward error analysis* is to interpret the cumulative effects of the roundoff errors incurred during a particular floating-point calculation as being “equivalent” to certain input perturbations.¹⁰

Knowing the condition number and these equivalent input perturbations then allows us to accurately estimate the “quality” of the computed solution. This approach, although rather more subtle than the *forward* error analysis method described in §12.3, circumvents the inability of that method to fully account for cancellation effects. In essence, backward error analysis converts a question of *error propagation* into one of *numerical stability*.

12.5.1 Equivalent Input Errors

The basic idea underlying backward error analysis is to note that the results of floating-point arithmetic operations on operands x and y satisfy

$$\begin{aligned}\text{float}(x \times y) &\equiv (1 + \delta) xy, \\ \text{float}(x \div y) &\equiv (1 + \delta) x/y, \\ \text{float}(x \pm y) &\equiv (1 + \delta)x \pm (1 + \epsilon)y,\end{aligned}\tag{12.53}$$

for some values $-\eta \leq \delta, \epsilon \leq +\eta$. Rather than furnishing bounds on the errors incurred in floating-point arithmetic operations, the relationships (12.53) are interpreted as stating that the outcome of such operations is identical to the result of *exact arithmetic operations on perturbed operands*. For multiplication and division, we associate a perturbation of relative magnitude $\leq \eta$ with just *one* of the two operands, whereas for addition and subtraction we must allow for such a perturbation in *both* operands [469].

Applying this idea to each arithmetic step of an algorithm, one can say that the final outcome of a floating-point computation is the *exact* result for some “neighboring” problem, corresponding to perturbed input values. The key requirement is to propagate the individual perturbations of operands in each step backward — in a symbolic, rather than numeric, manner — so as to obtain appropriate overall perturbations of the input values. These “effective”

¹⁰ Whereas the condition number is an intrinsic property of the problem formulation, independent of the particular algorithm used to solve it, backward error analysis is only meaningful in the context of a specific clearly-stated solution procedure.

perturbations, together with the problem condition number, yield a measure of the accuracy of a solution computed in floating-point arithmetic.

Thus, the method does not attempt a detailed step-by-step comparison of corresponding floating-point and exact-arithmetic calculations — rather, it says that the floating-point result *is* exact for some “nearby” problem (i.e., one with slightly different input data). Whether this hypothetical problem is sufficiently nearby to give an accurate answer depends, of course, on whether or not neighboring problems have neighboring results, i.e., on the *condition* of the problem. Unlike the forward error analysis approach described in §12.3.2, this method fully accommodates the possibility of cancellation effects.

12.5.2 Example: Horner’s Method

To illustrate the use of backward error analysis, consider the evaluation of the polynomial (3.1) by means of the Horner method (12.6). We assume again that a_n, \dots, a_0 and t are *ab initio* allowed floating-point values. The result of the k -th Horner term can then be written as

$$\begin{aligned} P_k &= \text{float}(\text{float}(t \times P_{k-1}) + a_{n-k}) \\ &\equiv (1 + \delta_k)(1 + \zeta_k) t P_{k-1} + (1 + \epsilon_k) a_{n-k}. \end{aligned} \quad (12.54)$$

Here ζ_k is the perturbation associated with the product, and δ_k and ϵ_k are the perturbations associated with the sum; these quantities are all of magnitude $\leq \eta$. We emphasize the intended interpretation of equation (12.54): it represents an *exact* execution of the Horner step (12.6), but with perturbed operands — for example

$$(1 + \zeta_k) t, \quad (1 + \delta_k) P_{k-1}, \quad \text{and} \quad (1 + \epsilon_k) a_{n-k}$$

— rather than the nominal operands t , P_{k-1} , and a_{n-k} .

We are interested here only in the final computed value $P_n = \text{float}(p(t))$ of the polynomial, i.e., the value produced by a floating-point computation. By carrying through the steps (12.54) for $k = 1, \dots, n$ it is possible to express this value in the form

$$\text{float}(p(t)) \equiv \sum_{j=0}^n a_j (1 + e_j) t^j, \quad (12.55)$$

i.e., the computed quantity represents the *exact* value of a polynomial with “perturbed” coefficients $a_n(1 + e_n), \dots, a_0(1 + e_0)$ in lieu of a_n, \dots, a_0 .

It is not difficult to derive closed-form expressions giving the “effective” coefficient perturbations e_n, \dots, e_0 in terms of the individual arithmetic-step perturbations $\delta_k, \epsilon_k, \zeta_k$ for $k = 1, \dots, n$. However, such expressions would in any case require simplification to be of practical use. This can be achieved, without formally writing down the expressions, as follows.

Upon executing (12.54) for $k = 1, \dots, n$, the term with nominal coefficient a_j in (12.55) participates in j floating-point multiplications and $j+1$ floating-point additions (except that the a_n term participates in n additions). If we imagine these steps to have executed in *exact* arithmetic, but on perturbed operands, we see that the perturbation factors in (12.55) will be of the form

$$1 + e_j = \langle 2j+1 \rangle \quad \text{for } j = 0, \dots, n-1 \quad \text{and} \quad 1 + e_n = \langle 2n \rangle$$

where, following Stewart [430], we introduce the notation

$$\langle m \rangle = \prod_{k=1}^m (1 + \lambda_k), \quad (12.56)$$

the λ_k 's denoting appropriate instances of the individual-step perturbations $\zeta_k, \delta_k, \epsilon_k$ (each bounded in magnitude by η).

We are thus interested in finding bounds on quantities of the form (12.56). If $\eta \ll 1$, we clearly have the *approximate* bound

$$1 - m\eta \lesssim \langle m \rangle \lesssim 1 + m\eta.$$

Assuming (as is reasonable in most practical circumstances) that $m\eta < 0.1$, more rigorous bounds may be derived [110, 469] as follows. Noting that¹¹

$$(1 + \eta)^m < \exp(m\eta)$$

we have

$$(1 + \eta)^m - 1 < \sum_{k=1}^{\infty} \frac{(m\eta)^k}{k!} < m\eta \sum_{k=0}^{\infty} \left(\frac{m\eta}{2}\right)^k,$$

where the second step follows from the fact that $r! \geq 2^{r-1}$ for $r \geq 1$. Now the infinite sum in the final expression is just $(1 - \frac{1}{2}m\eta)^{-1}$ and thus $(1 + \eta)^m - 1 < m\eta(1 - \frac{1}{2}m\eta)^{-1} \lesssim 1.053m\eta$ when $m\eta < 0.1$. Conventionally [469], we write

$$1 - 1.06m\eta < \langle m \rangle < 1 + 1.06m\eta.$$

This completes our backward error analysis, and we can state the result as follows. If a_n, \dots, a_0 are the monomial coefficients of a degree- n polynomial $p(t)$, the outcome $P_n = \text{float}(p(t))$ of the Horner algorithm (12.6) running in floating-point arithmetic is the *exact* value of a polynomial with coefficients $(1 + e_n)a_n, \dots, (1 + e_0)a_0$, where the perturbations e_j satisfy

$$|e_j| < 1.06(2j+1)\eta \quad \text{for } j = 0, \dots, n-1 \quad \text{and} \quad |e_n| < 1.06 2n\eta.$$

These uncertainties are evidently of non-uniform magnitude — higher-order terms participate in more floating-point operations, and consequently their coefficients exhibit larger “effective” perturbations.

¹¹ Since each term in the binomial expansion of the left-hand side is less than or equal to the corresponding term in the Taylor series for the right-hand side.

However, our condition numbers (12.15) and (12.33) for polynomial values and roots were based on the assumption of uniform error ϵ in the coefficients. As a conservative measure, one can multiply these condition numbers by $\epsilon = e_n$ (the largest perturbation) to estimate the effects of rounding errors on the computed value. Alternately, it is not too difficult to reformulate the condition numbers to allow for non-uniform coefficient perturbations.

Similar backward error analysis techniques can be applied to algorithms for systems of linear equations. For example, in the matrix equation

$$\mathbf{M}\mathbf{x} = \mathbf{y},$$

which we might solve by Gaussian elimination, the right-hand side vector \mathbf{y} is the “input” and the vector of unknowns \mathbf{x} is the “output.” A backward error analysis of Gaussian elimination (see, for example, Appendix 3 of [430]) then reveals that a floating-point solution to this system is equivalent to the *exact* solution of a perturbed system, with right-hand side $\mathbf{y} + \delta\mathbf{y}$. Knowing the condition number $C_p(\mathbf{M})$ of the matrix, and the relative magnitude $\epsilon_{\mathbf{y}} = \|\delta\mathbf{y}\|_p/\|\mathbf{y}\|_p$ of the “effective” input perturbations, then allows us to estimate the cumulative effects of the round-off errors during the solution procedure.

13

Bézier Curves and Surfaces

The polynomial functions were chosen according to the properties that were considered best: tangency, curvature, etc. Later it was discovered that they could be considered as sums of Bernstein's functions.

Pierre Bézier, *How a Simple System was Born*, in [144]

If we replace the scalar values c_0, \dots, c_n in (11.4) by points $\mathbf{p}_0, \dots, \mathbf{p}_n$ in the plane or in space, we obtain a degree- n Bézier curve,

$$\mathbf{r}(t) = \sum_{k=0}^n \mathbf{p}_k b_k^n(t). \quad (13.1)$$

The $n + 1$ points $\mathbf{p}_0, \dots, \mathbf{p}_n$ are called the *control points* for the curve $\mathbf{r}(t)$ — they define the vertices of its *control polygon*, obtained by connecting them in a piecewise-linear manner. The line segments that connect consecutive points \mathbf{p}_{k-1} and \mathbf{p}_k for $k = 1, \dots, n$ are the *legs* of the control polygon.

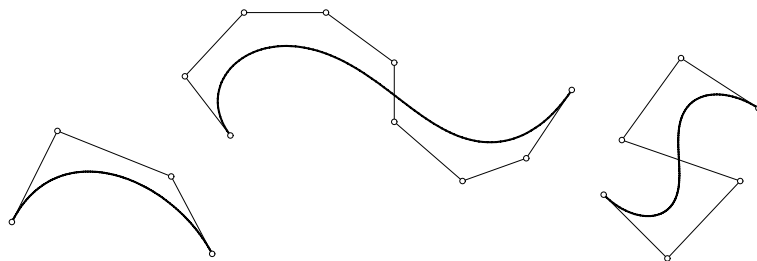


Fig. 13.1. Examples of planar Bézier curves with their control polygons.

Figure 13.1 shows some examples of plane Bézier curves and their control polygons. Two features that arise from the properties of the Bernstein basis

discussed in §11.2 are immediately apparent — namely, the curve end-points coincide with the initial and final control points,

$$\mathbf{r}(0) = \mathbf{p}_0 \quad \text{and} \quad \mathbf{r}(1) = \mathbf{p}_n,$$

and the curves are tangent to the initial and final legs of the control polygon, i.e., their unit end-tangents are given by

$$\mathbf{t}(0) = \frac{\mathbf{p}_1 - \mathbf{p}_0}{|\mathbf{p}_1 - \mathbf{p}_0|} \quad \text{and} \quad \mathbf{t}(1) = \frac{\mathbf{p}_n - \mathbf{p}_{n-1}}{|\mathbf{p}_n - \mathbf{p}_{n-1}|}.$$

By moving its control points, we can manipulate the shape of a Bézier curve in a geometrically intuitive manner (the control polygon may be regarded as a “caricature” of the curve it defines, i.e., it *exaggerates* the curve shape). More quantitative characterizations of the relation between a control polygon and the shape of the curve it defines will be described below.

As is evident from the examples of Fig. 13.1, however, the correlation between the shape of a Bézier curve and its control polygon becomes weaker as the curve degree n increases. Increasing the degree of a *single* curve segment to obtain more “shape flexibility” is not, in general, a recommended approach. For that purpose, a sequence of lower-degree curves “pieced together” in a smooth manner is usually preferred. The B-spline representation, described in Chap. 15 below, accomplishes this automatically and provides a control-polygon approach to manipulating the curve shape that inherits many of the attractive properties associated with the Bézier form.

13.1 Convex-hull Confinement

Given a discrete set of fixed points $\mathbf{p}_0, \mathbf{p}_1, \dots, \mathbf{p}_n$, we define their *convex hull* to be the set of all positions \mathbf{p} that can be expressed as convex combinations of those points, i.e., for which we can write

$$\mathbf{p} = \mu_0 \mathbf{p}_0 + \mu_1 \mathbf{p}_1 + \cdots + \mu_n \mathbf{p}_n, \quad (13.2)$$

where the scalar factors satisfy

$$\mu_0 + \mu_1 + \cdots + \mu_n = 1 \quad \text{and} \quad \mu_k \geq 0 \quad \text{for } k = 0, \dots, n. \quad (13.3)$$

When the given points lie in a plane, the convex hull is a convex polygon in that plane with a subset of $\mathbf{p}_0, \mathbf{p}_1, \dots, \mathbf{p}_n$ as its vertices. Thus, the problem of constructing the convex hull amounts to determining the identity and proper ordering of such “boundary points” that delineate a convex polygon within which all the other (non-boundary) points are contained.

The “gift-wrapping algorithm” offers a conceptually intuitive approach to identifying the vertices of the convex hull (see Fig. 13.2) — starting from the point with the smallest y (or x) coordinate, we rotate a line through the

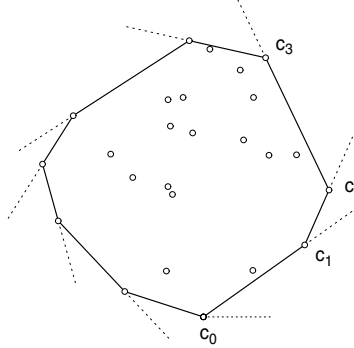


Fig. 13.2. Constructing the convex hull boundary for a random set of points in the plane by means of the “gift-wrapping” algorithm. The starting boundary vertex c_0 is the one with the smallest y -coordinate, say. Successive boundary vertices c_1, c_2, \dots are then identified through clockwise rotation of a line through the current vertex.

current vertex, aligned with the current edge, clockwise — the first point among $\mathbf{p}_0, \dots, \mathbf{p}_n$ this line encounters is the next vertex of the convex hull. Although this method is easy to implement, it has $O(n^2)$ computational cost — more efficient algorithms are available [349] when n is large.

In the three-dimensional case, the convex hull becomes a polyhedron with (generically) triangular faces — the vertices of these faces correspond to triples selected from the list $\mathbf{p}_0, \mathbf{p}_1, \dots, \mathbf{p}_n$. In this context, the identification of the boundary points and the construction of a datastructure that characterizes their topological relationships is a far more involved task.

Since (by virtue of properties 2 and 3 of §11.2) the values of the Bernstein basis functions $b_0^n(t), \dots, b_n^n(t)$ satisfy conditions (13.3) for each $t \in [0, 1]$, the Bézier curve (13.1) for $t \in [0, 1]$ evidently lies entirely within the convex hull of its control points. Thus, the convex hull offers a tighter localization of $\mathbf{r}(t)$ than the “bounding box” that would be obtained by applying property 4 of §11.2 separately to each coordinate component of the curve.

Expressions (13.2) and (13.3) admit the following physical interpretation: the convex hull is the set of all possible locations for the *center of mass* of a set of arbitrarily-chosen non-negative masses m_0, \dots, m_n situated at the points $\mathbf{p}_0, \dots, \mathbf{p}_n$ — note that the “normalized” masses $\mu_k = m_k / (m_0 + \dots + m_n)$, $k = 0, \dots, n$ automatically satisfy the conditions (13.3).

We can also interpret the Bézier curve (13.1) in terms of a center-of-mass paradigm. Imagine that the Bernstein basis functions $b_0^n(t), \dots, b_n^n(t)$ define certain “time-dependent” masses (as described, for example, by the graphs in Fig. 11.1 when $n = 5$) situated at the control points $\mathbf{p}_0, \dots, \mathbf{p}_n$. Then, on account of properties 2 and 3 of §11.2, the curve point $\mathbf{r}(t)$ identifies the corresponding center of mass at each instant t . As the “time” increases from $t = 0$ to $t = 1$, the center of mass traces out the curve (13.1).

13.2 Variation-diminishing Property

The variation-diminishing property of the Bernstein representation for scalar polynomials has already been mentioned in §11.2. This property, generalized to planar Bézier curves, may be phrased in geometrical terms as follows:

Proposition 13.1 *A straight line may never intersect a plane Bézier curve more often than it intersects the control polygon of that curve.*

The proof is elementary. If $\mathbf{r}(t) = (x(t), y(t))$ is the specified Bézier curve, with control points $\mathbf{p}_k = (x_k, y_k)$ for $k = 0, \dots, n$, there exists a shape-preserving coordinate transformation $(x, y) \rightarrow (\tilde{x}, \tilde{y})$ that maps any line L in the (x, y) -plane to the axis $\tilde{y} = 0$ of the (\tilde{x}, \tilde{y}) -plane. Intersections of L with $\mathbf{r}(t)$ then correspond to roots on $t \in (0, 1)$ of the scalar polynomial

$$\tilde{y}(t) = \sum_{k=0}^n \tilde{y}_k b_k^n(t),$$

where $\tilde{\mathbf{p}}_k = (\tilde{x}_k, \tilde{y}_k)$ are the mapped control points, while each intersection of L with the control polygon implies a sign change in the sequence $\tilde{y}_0, \dots, \tilde{y}_n$. By the results of §11.2, the latter cannot exceed the former in number.¹

Thus, in the above sense, a Bézier curve always exhibits a “simpler” shape than its control polygon. Curves defined by convex polygons, for example, are always convex (the converse, however, is not true). We may regard the control polygon as a “caricature” of the curve: it tends to *exaggerate* shape properties of the curve, an attribute that is valuable for design purposes.

For space curves, the variation-diminishing property is phrased in terms of intersections of an arbitrary *plane* with the curve and its control polygon. We argue along similar lines: there exists a shape-preserving transformation $(x, y, z) \rightarrow (\tilde{x}, \tilde{y}, \tilde{z})$ that maps an arbitrary plane to $\tilde{z} = 0$.

13.3 Degree Elevation

The degree elevation procedure, described in §11.2 for Bernstein-form scalar polynomials, can also be applied Bézier curves. Thus, upon multiplying the representation (13.1) by $t + (1 - t)$ and collecting like terms, we obtain

$$\mathbf{r}(t) = \sum_{k=0}^n \mathbf{p}_k b_k^n(t) = \sum_{k=0}^{n+1} \mathbf{p}'_k b_k^{n+1}(t),$$

where the control points for the degree-elevated representation are given by $\mathbf{p}'_0 = \mathbf{p}_0$, $\mathbf{p}'_{n+1} = \mathbf{p}_n$, and

¹ In fact, the difference must be even (taking multiple intersections into account).

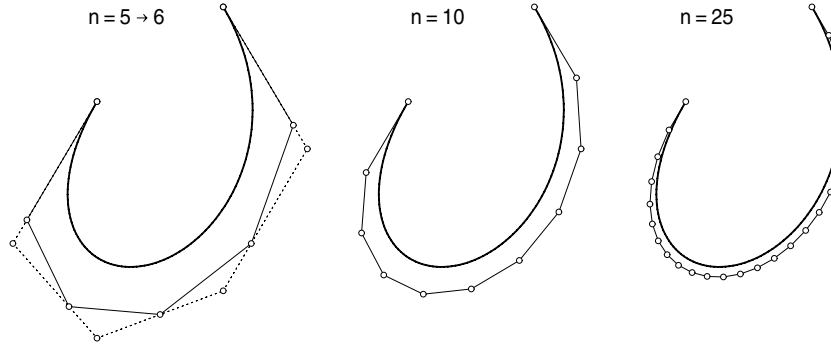


Fig. 13.3. Left: a single degree elevation, applied to a planar quintic Bézier curve (the original control polygon is indicated by the dotted lines). Center and right: the control polygon after repeated stages of degree elevation, to final degrees 10 and 25.

$$\mathbf{p}'_k = \frac{k}{n+1} \mathbf{p}_{k-1} + \left(1 - \frac{k}{n+1}\right) \mathbf{p}_k \quad (13.4)$$

for $k = 1, \dots, n$. Under iteration of this “degree elevation” procedure, one observes that the control polygons for representations of increasing degree converge monotonically to the curve $\mathbf{r}(t)$ itself — see Fig. 13.3.

Thus, repeated degree elevation offers a means of constructing piecewise-linear approximations of any prescribed accuracy to a given polynomial curve, although — as evident in the examples of Fig. 13.3 — the convergence of the control polygon to the curve is rather slow. This may be understood by interpreting degree elevation as the “converse” to the process of constructing Bernstein approximations of increasing degree to a continuous function. From §11.1 we know that, if $f(t)$ is continuous on $t \in [0, 1]$, the polynomial

$$P_n(t) = \sum_{k=0}^n c_k b_k^n(t)$$

converges monotonically to this function, $|P_n(t) - f(t)| \rightarrow 0$ for all $t \in [0, 1]$ as $n \rightarrow \infty$, if we choose its coefficients to be equidistant values sampled from the function: $c_k = f(k/n)$, $k = 0, \dots, n$. Conversely, if $f(t)$ is a polynomial of true degree n_* and the coefficients c_0, \dots, c_n are chosen so that $|P_n(t) - f(t)| \equiv 0$ for all $n \geq n_*$ — i.e., $P_n(t)$ is a degree-elevated representation of $f(t)$ — then $c_k \rightarrow f(k/n)$ for $k = 0, \dots, n$ as $n \rightarrow \infty$. This can be verified by invoking the Stirling approximation

$$m! \approx \sqrt{2\pi m} m^m e^{-m}$$

to the factorial function, when $m \gg 1$, to obtain

$$\binom{p}{q} \approx \sqrt{\frac{p}{2\pi(p-q)q}} \frac{1}{(1-q/p)^{p-q} (q/p)^q}$$

when $p, q \gg 1$. One can then check that, as $k \rightarrow \infty$ and $r \rightarrow \infty$ in expression (11.13), in such a manner that $k/r \rightarrow \tau$ with $0 < \tau < 1$, the degree-elevated coefficients have the limiting values

$$\lim_{\substack{k \rightarrow \infty, r \rightarrow \infty \\ k/r \rightarrow \tau}} c_k^{n+r} = \sum_{j=0}^n c_j^n \binom{n}{j} (1-\tau)^{n-j} \tau^j = p(\tau),$$

i.e., c_k^{n+r} approaches the value of the degree- n polynomial $p(t)$ with Bernstein coefficients c_0^n, \dots, c_n^n at the limit point $\tau = \lim k/r$ — note that, for fixed j , n we have $\lim k/(n+r) = \lim (k-j)/r = \lim k/r = \tau$.

13.4 de Casteljau Algorithm

The de Casteljau algorithm is perhaps the most fundamental computational procedure associated with the Bézier curve (13.1) defined on $t \in [0, 1]$. This algorithm serves a dual purpose — for a parameter value τ between 0 and 1, it computes the curve point $\mathbf{r}(\tau)$, and it *splits* the curve at that point — i.e., it determines the control points that describe the subsegments $t \in [0, \tau]$ and $t \in [\tau, 1]$ of $\mathbf{r}(t)$ individually, as Bézier curves in their own right.

The algorithm is the same as described in §11.6, except that we replace the scalar polynomial coefficients c_0, \dots, c_n with the control points $\mathbf{p}_0, \dots, \mathbf{p}_n$ (which may be points in \mathbb{R}^2 or \mathbb{R}^3). Choosing $\tau \in (0, 1)$, we set $\mathbf{p}_j^0 = \mathbf{p}_j$ for $j = 0 \dots, n$, and then compute the triangular array of points

$$\begin{array}{ccccccc} \mathbf{p}_0^0 & \mathbf{p}_1^0 & \mathbf{p}_2^0 & \cdot & \cdot & \cdot & \mathbf{p}_n^0 \\ \mathbf{p}_1^1 & \mathbf{p}_2^1 & \cdot & \cdot & \cdot & \mathbf{p}_n^1 \\ \mathbf{p}_2^2 & \cdot & \cdot & \cdot & \mathbf{p}_n^2 \\ & \cdot & \cdot & \cdot & & & \\ & & & & \mathbf{p}_n^n & & \end{array} \quad (13.5)$$

generated by the iterations

$$\mathbf{p}_j^r = (1-\tau) \mathbf{p}_{j-1}^{r-1} + \tau \mathbf{p}_j^{r-1} \quad (13.6)$$

for $j = r, \dots, n$ and $r = 1, \dots, n$. The final entry in this array is the curve point corresponding to parameter value τ ,

$$\mathbf{r}(\tau) = \mathbf{p}_n^n.$$

Starting from the original control polygon with $n+1$ vertices $\mathbf{p}_0, \dots, \mathbf{p}_n$, the algorithm (13.6) may be regarded as recursively generating a sequence of

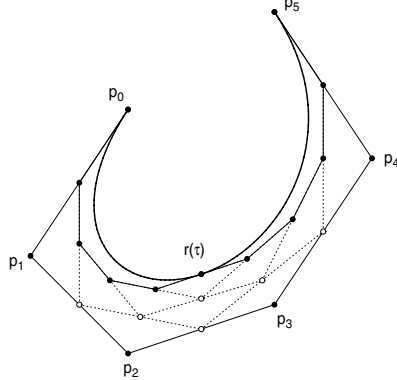


Fig. 13.4. Subdivision of a quintic Bézier curve $r(t)$ at the parametric midpoint $\tau = \frac{1}{2}$ by means of the de Casteljau algorithm. The initial control polygon, and the final control polygons of the left and right subsegments of $r(t)$, are indicated by solid lines, while intermediate constructions are shown as dotted lines and open circles.

new polygons for $r = 1, \dots, n$, each with one less vertex than its predecessor. The vertices of the r -th polygon are the points on the sides of the $(r - 1)$ -th polygon that divide those sides in the ratio $\tau : 1 - \tau$, since each step of (13.6) is simply a linear interpolation between the vertices $\mathbf{p}_{r-1}^{r-1}, \dots, \mathbf{p}_n^{r-1}$.

Figure 13.4 illustrates this process in the case $\tau = \frac{1}{2}$ for a quintic curve. The midpoints of the sides of the initial control polygon, with the six vertices $\mathbf{p}_0, \dots, \mathbf{p}_5$, define a new polygon with five vertices $\mathbf{p}_1^1, \dots, \mathbf{p}_5^1$. A subsequent polygon with four vertices $\mathbf{p}_2^2, \dots, \mathbf{p}_5^2$ is given by the midpoints of the sides of the latter, and this process is repeated until we finally obtain a single vertex \mathbf{p}_5^5 that coincides with the parametric midpoint $r(\frac{1}{2})$ of the curve.

Furthermore, the points $\mathbf{p}_0^0, \mathbf{p}_1^1, \mathbf{p}_2^2, \dots, \mathbf{p}_n^n$ and $\mathbf{p}_n^n, \mathbf{p}_n^{n-1}, \mathbf{p}_n^{n-2}, \dots, \mathbf{p}_n^0$ on the left and right diagonal sides of the array (13.5) define the control points for the left and right subsegments $t \in [0, \tau]$ and $t \in [\tau, 1]$ of the given curve $r(t)$ defined on $t \in [0, 1]$. In the interpretation of these control points, it is understood that the subintervals $[0, \tau]$ and $[\tau, 1]$ are both mapped to $[0, 1]$.

13.5 Bézier Curve Hodographs

Invoking the results of §11.2, consider now the vector-valued function

$$\mathbf{h}(t) = \sum_{k=0}^{n-1} n(\mathbf{p}_{k+1} - \mathbf{p}_k) b_k^{n-1}(t)$$

defined by the parametric derivative $\mathbf{r}'(t)$ of (13.1). We have introduced here a special notation $\mathbf{h}(t)$ for this function since we wish to regard it as a Bézier curve in its own right, of degree $n - 1$, that is “derived” from the curve (13.1):

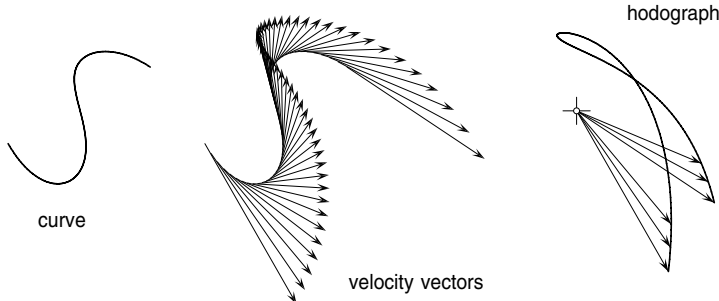


Fig. 13.5. A velocity vector may be specified at each point along a parametric curve $\mathbf{r}(t)$ by interpreting the parameter t as time — translating these vectors so that they emanate from a common origin, their tips will trace out the hodograph curve $\mathbf{r}'(t)$.

it is called the (polar) *hodograph* of that curve. See Fig. 13.5 for a kinematical interpretation of the hodograph² of a parametric curve.

A graphical inspection of the hodograph $\mathbf{h}(t)$ reveals valuable information concerning the intrinsic geometry and parameterization of the curve $\mathbf{r}(t)$. If $\mathbf{h}(t)$ passes through the origin, for example, a “stationary point” exists on the curve, where $\mathbf{r}'(t) = \mathbf{0}$. Ordinarily — i.e., if $\mathbf{r}''(t) \neq \mathbf{0}$ there — such a point is a *cusp*, since the sense of $\mathbf{r}'(t)$ reverses upon traversing it. In the exceptional case that $\mathbf{r}'(t) = \mathbf{r}''(t) = \mathbf{0}$, the hodograph exhibits a cusp at the origin, and this identifies a *tangent-continuous point of infinite curvature* on $\mathbf{r}(t)$.

Furthermore, if a tangent line of $\mathbf{h}(t)$ passes through the origin, it identifies a point of zero curvature on $\mathbf{r}(t)$, since $\mathbf{r}'(t)$ and $\mathbf{r}''(t)$ are collinear there, and hence (8.7) vanishes. Ordinarily, this identifies an *inflection* on $\mathbf{r}(t)$, but in the exceptional case that the point of tangency to $\mathbf{h}(t)$ is itself an inflection on the hodograph, the zero-curvature point on $\mathbf{r}(t)$ is a *vertex* — i.e., a point of extremum curvature. Cusps of the hodograph (not situated at the origin) also identify inflections on $\mathbf{r}(t)$, since they arise when $\mathbf{r}''(t) = \mathbf{0} \neq \mathbf{r}'''(t)$.

Figure 13.6 illustrates the identification of cusps and inflections on planar cubics from the geometry of their hodographs — the same principles also apply to twisted *space* curves. We may regard the successive higher derivatives $\mathbf{r}''(t)$, $\mathbf{r}'''(t)$, ... of a given curve $\mathbf{r}(t)$ as defining its second, third, ... hodographs, and the special points described above may be further elucidated by inspecting the geometrical loci of these higher-order hodographs.

We may also gain insight into the “quality” of parameterization of $\mathbf{r}(t)$ by an inspection of its hodograph $\mathbf{h}(t)$. For this purpose, it is convenient to consider the hodograph expressed in polar coordinates as $(\sigma(t), \theta(t))$ where $\sigma(t) = |\mathbf{r}'(t)|$ is the parametric speed of the curve, and $\theta(t)$ is the inclination of its tangent line with the x -axis. In the hypothetical “ideal” case of arc-length

² Hodographs were first introduced by Möbius in his *Mechanik des Himmels* (1843) and by Hamilton in his *Elements of Quaternions* (1846).

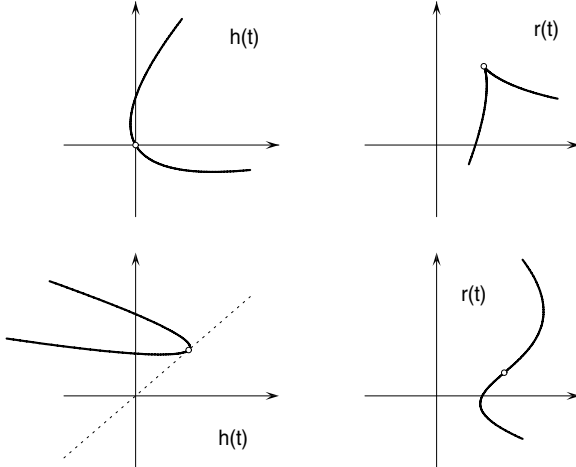


Fig. 13.6. A curve $\mathbf{r}(t)$ exhibits a *cusp* when its hodograph $\mathbf{h}(t)$ passes through the origin (upper), and an *inflection* point if a line through the origin is tangent to its hodograph (lower) — note that $\mathbf{r}(t)$ and $\mathbf{h}(t)$ are not drawn to the same scale here.

parameterization, one would have $\sigma(t) \equiv 1$, and hence $\mathbf{h}(t)$ would lie entirely on the unit circle centered on the origin.

For any polynomial or rational curve, however, $\sigma(t)$ is necessarily non-constant (except in the trivial case of a straight line — see §16.1), and large variations in its magnitude indicate an uneven parameter flow. The extremes $\sigma \rightarrow 0$ and $\sigma \rightarrow \infty$ identify, respectively, *cusps* and *points at infinity* on $\mathbf{r}(t)$ (the latter occur at finite t values only on *rational* curves — see below).

13.6 Rational Bézier Curves

So far we have confined our attention to *polynomial* Bézier curves, i.e., curves that are parameterized by polynomial functions of the parameter t . A planar Bézier curve $\mathbf{r}(t)$ of the form (13.1), for example, amounts to specifying *affine* coordinates in the plane by polynomial functions $x(t)$, $y(t)$.

Alternately, we can describe a plane curve $\mathbf{r}(t)$ by specifying *homogeneous* coordinates as polynomial functions $W(t)$, $X(t)$, $Y(t)$ — the affine locus of the curve is then generated by the rational functions

$$x(t) = \frac{X(t)}{W(t)}, \quad y(t) = \frac{Y(t)}{W(t)} \quad (13.7)$$

of t , and hence in this case we say that $\mathbf{r}(t)$ is a *rational* curve.

The polynomial curves are clearly a proper subset of the rational curves, corresponding to the choice $W(t) \equiv \text{constant}$, and in certain respects they are too restrictive to serve as the canonical curve representation scheme for CAD

systems. Thus, for example, a circular arc cannot be exactly represented as a polynomial curve — for a segment of the unit circle centered on the origin, this would require non-constant polynomials $x(t)$, $y(t)$ such that

$$x^2(t) + y^2(t) \equiv 1 \quad (13.8)$$

to exist, and one can easily verify that this is impossible. On the other hand, by choosing

$$W(t) = 1 + t^2, \quad X(t) = 1 - t^2, \quad Y(t) = 2t$$

we see that (13.8) is satisfied when $x(t)$, $y(t)$ are defined by (13.7).

In fact, the *only* conic that can be parameterized exactly as a polynomial curve is the parabola. As noted in §7.4.4, all conic curves are images of each other under projective transformations, and if $W(t) \equiv 1$, $X(t)$, $Y(t)$ represent a parabola, its image $\tilde{W}(t)$, $\tilde{X}(t)$, $\tilde{Y}(t)$ under the two-dimensional projective map (7.62), specified by a non-singular 3×3 matrix

$$\begin{bmatrix} \tilde{W}(t) \\ \tilde{X}(t) \\ \tilde{Y}(t) \end{bmatrix} = \begin{bmatrix} m_{00} & m_{01} & m_{02} \\ m_{10} & m_{11} & m_{12} \\ m_{20} & m_{21} & m_{22} \end{bmatrix} \begin{bmatrix} 1 \\ X(t) \\ Y(t) \end{bmatrix},$$

is seen to be *essentially* a rational curve, with $\tilde{W}(t) \not\equiv \text{constant}$. In general, the set of rational curves of fixed degree is closed under arbitrary projective transformations, whereas the set of polynomial curves is not.

In the Bézier representation of a degree- n rational curve segment, scalar values or “weights” w_0, \dots, w_n are assigned to each of the $n+1$ control points $\mathbf{p}_0, \dots, \mathbf{p}_n$, and we then write

$$\mathbf{r}(t) = \frac{\sum_{k=0}^n w_k \mathbf{p}_k b_k^n(t)}{\sum_{k=0}^n w_k b_k^n(t)}. \quad (13.9)$$

The Bernstein coefficients of the polynomials $W(t)$, $X(t)$, $Y(t)$ are thus given by w_k , $w_k x_k$, $w_k y_k$, where $\mathbf{p}_k = (x_k, y_k)$ for $k = 0, \dots, n$. Note that roots of the denominator polynomial $W(t)$ on $t \in [0, 1]$ incur *points at infinity* on the curve (13.9). A simple means of avoiding this undesirable circumstance is to ensure that all weights are of like sign; the variation-diminishing property then guarantees that $W(t)$ is root-free on $t \in [0, 1]$.

By the partition-of-unity property of the Bernstein basis, (13.9) reduces to the *polynomial* curve with control points $\mathbf{p}_0, \dots, \mathbf{p}_n$ if $w_0 = w_1 = \dots = w_n$. On the other hand, only the *ratios* $w_0 : w_1 : \dots : w_n$ matter when the weights are unequal. Thus, dividing w_0, \dots, w_n by any chosen (non-zero) weight w_r , we can always adopt a representation in which $w_r = 1$.

There is a further arbitrariness in the choice of weights, arising from the *parameterization freedoms* of rational curves. The polynomial curve (13.1) has no freedoms of re-parameterization when the interval $[0, 1]$ is to be retained as its parameter domain. The rational curve (13.9), on the other hand, admits fractional linear re-parameterizations $t \in [0, 1] \rightarrow u \in [0, 1]$ of the form³

$$t = \frac{(1 - \alpha)u}{\alpha(1 - u) + (1 - \alpha)u} \quad (13.10)$$

that preserve the curve degree. By substituting (13.10) into the rational Bézier curve (13.9), one obtains a re-parameterized version $\hat{\mathbf{r}}(u)$ that has the same control points, but new weights defined by

$$\hat{w}_k = c(1 - \alpha)^k \alpha^{n-k} w_k \quad (13.11)$$

for $k = 0, \dots, n$ with $c \neq 0$. In particular, the choices

$$\alpha = \frac{(w_n/w_0)^{1/n}}{1 + (w_n/w_0)^{1/n}} \quad \text{and} \quad c = \frac{[1 + (w_n/w_0)^{1/n}]^n}{w_n} \quad (13.12)$$

yield the “standard” parameterization, satisfying $\hat{w}_0 = \hat{w}_n = 1$.

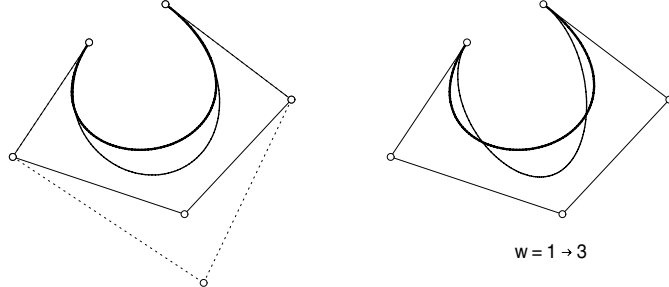


Fig. 13.7. Shape modification of a rational Bézier curve by: (left) the displacement of a single control point; and (right) an increase in the weight of that control point.

Hence it is always possible to take $w_0 = w_n = 1$ in (13.9) without altering the geometry of the curve thus defined — this choice defines the “standard” representation of a rational Bézier curve. The remaining weights w_1, \dots, w_{n-1} then offer additional “design handles” that can be employed to manipulate the curve shape. The variation of a single weight w_r exerts a somewhat different influence on the curve than movement of the control point \mathbf{p}_r (see Fig. 13.7).

One can show that, when a single control point \mathbf{p}_j is displaced an amount $\Delta\mathbf{p}_j$, each point of $\mathbf{r}(t)$ suffers a displacement parallel to $\Delta\mathbf{p}_j$, given by

³ This is a restriction of the Möbius transformation (see §4.8) to real variables.

$$\Delta \mathbf{r}(t) = \frac{w_j b_j^n(t)}{w(t)} \Delta \mathbf{p}_j,$$

where $w(t)$ is the polynomial with Bernstein coefficients w_0, \dots, w_n — i.e., the denominator of $\mathbf{r}(t)$. If, on the other hand, the control points are all held fixed and the single weight w_j is altered by Δw_j , each point of $\mathbf{r}(t)$ suffers a displacement toward \mathbf{p}_j , according to

$$\Delta \mathbf{r}(t) = \frac{\Delta w_j b_j^n(t)}{w(t) + \Delta w_j b_j^n(t)} [\mathbf{p}_j - \mathbf{r}(t)].$$

An intuitive geometrical model, based on the projective transformations discussed in §7.4.6, offers insight into what happens when we vary the weights of a plane rational Bézier curve such as (13.9). The homogeneous-coordinate polynomials $W(t)$, $X(t)$, $Y(t)$ that define (13.9) may also be interpreted as describing a three-dimensional *polynomial* curve $\mathbf{s}(t)$ residing in a space with axes labelled W , X , Y . The plane curve (13.7) then corresponds to a *central projection* of the spatial curve $\mathbf{s}(t)$ from the origin O onto the plane $W = 1$ (see Fig. 13.8) — i.e., the intersections of the lines drawn from O to each point of $\mathbf{s}(t)$ with the plane $W = 1$ trace out the rational curve $\mathbf{r}(t)$.

Imagine a line drawn from O through the control point $\mathbf{q}_r = (W_r, X_r, Y_r) = (w_r, w_r x_r, w_r y_r)$ of the space curve $\mathbf{s}(t)$. Then varying the single weight w_r in expression (13.9) evidently corresponds to a motion of the point \mathbf{q}_r along this line. Although the intersection of the line with the plane $W = 1$ at the control point $\mathbf{p}_r = (x_r, y_r)$ of (13.9) remains unchanged, the shape of the space curve $\mathbf{s}(t)$ has been altered by the displacement of \mathbf{q}_r , and this incurs a change of shape in its projected image $\mathbf{r}(t)$. An analogous model may be invoked for rational *space* curves, that involves the central projection of a *four-dimensional* curve onto the three-dimensional “hyperplane” $W = 1$ of the space with coordinates (W, X, Y, Z) .

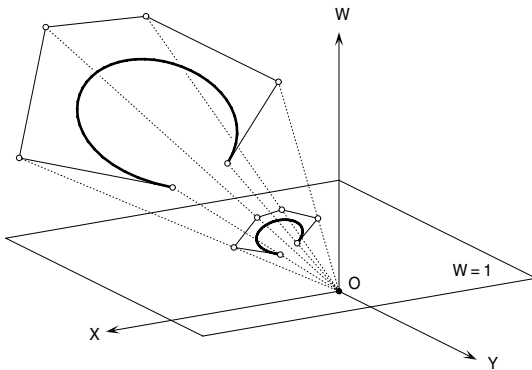


Fig. 13.8. A planar rational curve $\mathbf{r}(t)$ may be regarded as the image of a polynomial curve $\mathbf{s}(t)$ of equal degree in the three-dimensional space with Cartesian coordinates (W, X, Y) under a central projection from the origin O onto the plane $W = 1$.

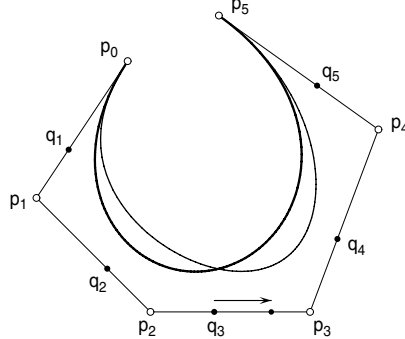


Fig. 13.9. A rational Bézier curve with control points $\mathbf{p}_0, \dots, \mathbf{p}_n$ and *weight points* $\mathbf{q}_1, \dots, \mathbf{q}_n$. The change in the curve induced by a displacement of \mathbf{q}_3 is illustrated.

A geometrical approach to the design of rational curves, that is equivalent to specifying a weight w_0, \dots, w_n for each control point $\mathbf{p}_0, \dots, \mathbf{p}_n$, has been suggested by Farin [142]. We introduce *weight points* (also called *Farin points*) on each leg of the control polygon, defined by

$$\mathbf{q}_k = \frac{w_{k-1}\mathbf{p}_{k-1} + w_k\mathbf{p}_k}{w_{k-1} + w_k} \quad \text{for } k = 1, \dots, n, \quad (13.13)$$

so that the location of \mathbf{q}_k on the line between \mathbf{p}_{k-1} and \mathbf{p}_k uniquely specifies the ratio $w_{k-1} : w_k$ — see also [143, 144]. Hence, the n points $\mathbf{q}_1, \dots, \mathbf{q}_n$ on the control-polygon legs determine the ratios $w_0 : w_1 : \dots : w_n$.

We may thus modify the curve shape by “sliding” the weight points along the control-polygon legs. For example, moving \mathbf{q}_k toward \mathbf{p}_k is equivalent to increasing w_k , with the effect of “pulling” the curve in the direction of the control point \mathbf{p}_k (see Fig. 13.9). As a “default” configuration, one may place $\mathbf{q}_1, \dots, \mathbf{q}_n$ at the midpoints of the control-polygon legs: this corresponds to the *polynomial* curve defined by $\mathbf{p}_0, \dots, \mathbf{p}_n$, since all weights are then equal. To ensure that $\mathbf{r}(t)$ has no points at infinity on the interval $t \in [0, 1]$, each weight point \mathbf{q}_k must lie strictly *between* the control points \mathbf{p}_{k-1} and \mathbf{p}_k .

Many properties of the polynomial Bézier curves, discussed above, carry over (with suitable qualifications and modifications) to rational Bézier curves. It is convenient to combine the control points $\mathbf{p}_k = (x_k, y_k)$ and weights w_k so as to form “projective” control points, with components

$$\mathbf{P}_k = (W_k, X_k, Y_k) = (w_k, w_k x_k, w_k y_k), \quad k = 0, \dots, n. \quad (13.14)$$

Just as one applies the degree elevation algorithm (13.4) and the de Casteljau algorithm (13.6) separately to the x, y components of the control points of a polynomial curve, these procedures are applied individually to the W, X, Y

components of the projective control points of a rational curve, to obtain the projective control points for the subdivided or degree-elevated curve.⁴

This approach amounts to performing a degree elevation or subdivision on the *polynomial* curve with control points (13.14) in the three-dimensional space (W, X, Y) — see Fig. 13.8 — and then making a central projection from the origin O back onto the plane $W = 1$, to recover the degree-elevated or subdivided rational plane curve. If one wishes to characterize the latter by (affine) control points $\mathbf{p} = (x, y)$ and weights w specified separately, they are obtained from the projective control points \mathbf{P} by making the identifications

$$x = \frac{X}{W}, \quad y = \frac{Y}{W}, \quad w = W.$$

The convex-hull property also holds for a rational Bézier curve *if* all the weights are positive, since then for each $t \in [0, 1]$ the quantities

$$\mu_k = \frac{w_k b_k^n(t)}{\sum_{k=0}^n w_k b_k^n(t)}, \quad k = 0, \dots, n$$

multiplying each of the control points \mathbf{p}_k in (13.9) satisfy (13.3). Similarly the variation-diminishing property, as stated in Proposition 13.1, carries over to rational Bézier curves if all weights are positive. To verify this, we again invoke a shape-preserving coordinate transformation $(x, y) \rightarrow (\tilde{x}, \tilde{y})$ that maps any given line L to the axis $\tilde{y} = 0$ of the (\tilde{x}, \tilde{y}) -plane. The intersections of L and $\mathbf{r}(t)$ then correspond to roots on $t \in (0, 1)$ of the rational function

$$\tilde{y}(t) = \frac{\sum_{k=0}^n w_k \tilde{y}_k b_k^n(t)}{\sum_{k=0}^n w_k b_k^n(t)},$$

where $\tilde{\mathbf{p}}_k = (\tilde{x}_k, \tilde{y}_k)$ are the mapped control points. When $w_0, \dots, w_n > 0$, this function is non-singular on $t \in [0, 1]$, and the number of its roots on that interval cannot exceed the number of sign variations in $w_0 \tilde{y}_0, \dots, w_n \tilde{y}_n$, which equals the number of sign variations in $\tilde{y}_0, \dots, \tilde{y}_n$. Since each intersection of L with the control polygon implies a sign change in $\tilde{y}_0, \dots, \tilde{y}_n$, Proposition 13.1 also holds for the rational curve (13.9) with arbitrary positive weights.

The hodographs of rational Bézier curves may also be regarded as rational Bézier curves — although, unlike the case of polynomial curves, the hodograph $\mathbf{h}(t) = \mathbf{r}'(t)$ of (13.9) is actually of *higher* degree than $\mathbf{r}(t)$ itself. Denoting the numerator and denominator of this curve by $\mathbf{R}(t)$ and $W(t)$, we have

$$\mathbf{h}(t) = \frac{W(t)\mathbf{R}'(t) - W'(t)\mathbf{R}(t)}{W^2(t)},$$

⁴ For brevity, we couch our discussion in terms of plane curves — the generalization to space curves is quite straightforward.

and hence $\mathbf{h}(t)$ has a numerator and denominator of degree $2n - 2$ and $2n$, respectively, when $\mathbf{r}(t)$ a degree- n rational curve. We may, in principle, express $\mathbf{h}(t)$ as a degree- $2n$ rational curve with control points $\mathbf{p}_0, \dots, \mathbf{p}_{2n}$ and weights w_0, \dots, w_{2n} , but the reduction to this form is rather involved — see [405] for further details. The geometrical methods for detecting exceptional points of polynomial curves by inspecting their hodographs, as discussed in §13.5, carry over to rational curves. For such curves, there is also the possibility — if the weights are not all positive — of the hodograph being unbounded in magnitude at finite t , corresponding to a *point at infinity* on the curve.

13.7 Conics as Bézier Curves

A rational quadratic Bézier curve in standard form is defined by

$$\mathbf{r}(t) = \frac{\mathbf{p}_0(1-t)^2 + w_1\mathbf{p}_12(1-t)t + \mathbf{p}_2t^2}{(1-t)^2 + w_12(1-t)t + t^2}, \quad (13.15)$$

corresponding to the choice $w_0 = w_2 = 1$ for the weights of \mathbf{p}_0 and \mathbf{p}_2 (when non-unit weights are specified for \mathbf{p}_0 and \mathbf{p}_2 , the curve can be reduced to standard form by replacing w_0, w_1, w_2 with $1, w_1/\sqrt{w_2w_0}, 1$).

The curves defined by (13.15) are all *conic segments*. In order to elucidate their nature, it is convenient to regard the three control points $\mathbf{p}_k = (x_k, y_k)$ for $k = 0, 1, 2$ as vertices of a reference triangle for a system (u_0, u_1, u_2) of barycentric coordinates (see §7.2.2) for a point $\mathbf{p} = (x, y)$, defined by

$$u_0 = \frac{\Delta_0}{\Delta}, \quad u_1 = \frac{\Delta_1}{\Delta}, \quad u_2 = \frac{\Delta_2}{\Delta}$$

where

$$\Delta = \begin{vmatrix} 1 & 1 & 1 \\ x_0 & x_1 & x_2 \\ y_0 & y_1 & y_2 \end{vmatrix},$$

and Δ_k is obtained from Δ by replacing the k -th column by elements 1, x , y . We then have (see §7.2.2):

$$\mathbf{p} = u_0 \mathbf{p}_0 + u_1 \mathbf{p}_1 + u_2 \mathbf{p}_2. \quad (13.16)$$

Suppose that $\mathbf{p} = \mathbf{r}(t)$ for some value t , i.e., the point \mathbf{p} lies on the conic. Comparing expressions (13.15) and (13.16), we observe that the barycentric coordinates of \mathbf{p} must be of the form

$$\begin{aligned} u_0 &= \frac{(1-t)^2}{(1-t)^2 + w_12(1-t)t + t^2}, \\ u_1 &= \frac{w_12(1-t)t}{(1-t)^2 + w_12(1-t)t + t^2}, \\ u_2 &= \frac{t^2}{(1-t)^2 + w_12(1-t)t + t^2}, \end{aligned} \quad (13.17)$$

for some t . We can eliminate the indeterminate value t by noting that *any* set of barycentric coordinates of the above form satisfy the equation

$$\phi(u_0, u_1, u_2) = u_1^2 - 4w_1^2u_0u_2 = 0. \quad (13.18)$$

This is, in fact, the *implicit equation* for the conic (13.15) in the barycentric coordinate system with \mathbf{p}_0 , \mathbf{p}_1 , \mathbf{p}_2 as vertices of the reference triangle. The satisfaction of this equation by values (u_0, u_1, u_2) , such that $u_0 + u_1 + u_2 = 1$, implies the existence of a t such that expressions (13.17) hold — i.e., \mathbf{p} given by (13.16) then coincides with the curve point $\mathbf{r}(t)$ defined by (13.15).

From the definitions of Δ_0 , Δ_1 , Δ_2 we can express the implicit equation in Cartesian coordinates as

$$f(x, y) = \begin{vmatrix} 1 & 1 & 1 \\ x_0 & x & x_2 \\ y_0 & y & y_2 \end{vmatrix}^2 - 4w_1^2 \begin{vmatrix} 1 & 1 & 1 \\ x & x_1 & x_2 \\ y & y_1 & y_2 \end{vmatrix} \begin{vmatrix} 1 & 1 & 1 \\ x_0 & x_1 & x \\ y_0 & y_1 & y \end{vmatrix} = 0. \quad (13.19)$$

Upon expanding out this equation in the customary form

$$f(x, y) = ax^2 + 2hxy + by^2 + 2fx + 2gy + c = 0, \quad (13.20)$$

one finds that the coefficients may be expressed in terms of the control-point coordinates and weights as

$$\begin{aligned} a &= (y_2 - y_0)^2 + 4(y_1 - w_1y_0)(y_1 - w_1y_2), \\ b &= (x_2 - x_0)^2 + 4(x_1 - w_1x_0)(x_1 - w_1x_2), \\ c &= (x_0y_2 - x_2y_0)^2 + 4(x_1y_0 - x_0y_1)(x_1y_2 - x_2y_1), \\ f &= 2w_1 [y_0(x_2y_1 - x_1y_2) + y_2(x_0y_1 - x_1y_0)] \\ &\quad + (y_2 - y_0)(x_2y_0 - x_0y_2) + 2y_1(x_1y_0 - x_0y_1 + x_1y_2 - x_2y_1), \\ g &= 2w_1 [x_0(x_1y_2 - x_2y_1) + x_2(x_1y_0 - x_0y_1)] \\ &\quad + (x_2 - x_0)(x_0y_2 - x_2y_0) + 2x_1(x_0y_1 - x_1y_0 + x_2y_1 - x_1y_2), \\ h &= -2w_1^2(x_0y_2 + x_2y_0) + 2w_1(x_0y_1 + x_1y_0 + x_1y_2 + x_2y_1) \\ &\quad - 4x_1y_1 - (x_2 - x_0)(y_2 - y_0). \end{aligned}$$

In the standard theory of conics [139], the curve (13.20) is identified to be an ellipse, a parabola, or a hyperbola according to whether the quantity $ab - h^2$ is positive, zero, or negative. From the above expressions, one may readily verify (preferably with the aid of a computer algebra system) that

$$ab - h^2 = 4(1 - w_1^2)[w_1(x_0y_2 - x_2y_0) + x_1y_0 - x_0y_1 + x_2y_1 - x_1y_2]^2.$$

Hence, we have the following observation.

Remark 13.1 The conic (13.15) represents an ellipse, parabola, or hyperbola segment according to whether w_1^2 is less than, equal to, or greater than unity.

Alternatively, one may simply note that real roots of the denominator in (13.15) correspond to *points at infinity* of the conic. The discriminant of this quadratic is $4(w_1^2 - 1)$, and hence there are no real points at infinity (an ellipse) if $w_1^2 < 1$, a tangency to the line at infinity (a parabola) if $w_1^2 = 1$, and two distinct real points at infinity (a hyperbola) if $w_1^2 > 1$.

The formulae (13.17) also furnish a solution to the problem of *inversion* for conics in rational Bézier form — i.e., given the Cartesian coordinates (x, y) of a point known to lie on the curve, determine its parameter value t . Recalling the definitions of Δ_0 , Δ_1 , Δ_2 we find, upon considering the ratios $u_0 : u_1$ and $u_1 : u_2$ in (13.17), that

$$\frac{1-t}{t} = 2w_1 \begin{vmatrix} 1 & 1 & 1 \\ x & x_1 & x_2 \\ y & y_1 & y_2 \\ 1 & 1 & 1 \\ x_0 & x & x_2 \\ y_0 & y & y_2 \end{vmatrix} = \frac{1}{2w_1} \begin{vmatrix} 1 & 1 & 1 \\ x_0 & x & x_2 \\ y_0 & y & y_2 \\ 1 & 1 & 1 \\ x_0 & x_1 & x \\ y_0 & y_1 & y \end{vmatrix}, \quad (13.21)$$

which amount to two equivalent linear equations for t when x and y have been specified — their equivalence follows from the fact that the point (x, y) must satisfy (13.20), and hence also (13.18).

Any conic segment is uniquely determined by five geometrical constraints. Suppose, for example, that end points $\mathbf{r}(0)$, $\mathbf{r}(1)$ and unit tangents $\mathbf{t}(0)$, $\mathbf{t}(1)$ are prescribed for (13.15). The first and last control points are then simply $\mathbf{p}_0 = \mathbf{r}(0)$ and $\mathbf{p}_2 = \mathbf{r}(1)$, while \mathbf{p}_1 is the intersection of lines through those points along $\mathbf{t}(0)$ and $\mathbf{t}(1)$ — it is given by either of the expressions

$$\mathbf{r}(0) + \frac{\mathbf{z} \cdot [\mathbf{r}(1) - \mathbf{r}(0)] \times \mathbf{t}(1)}{\mathbf{z} \cdot [\mathbf{t}(0) \times \mathbf{t}(1)]} \mathbf{t}(0) = \mathbf{r}(1) + \frac{\mathbf{z} \cdot [\mathbf{r}(1) - \mathbf{r}(0)] \times \mathbf{t}(0)}{\mathbf{z} \cdot [\mathbf{t}(0) \times \mathbf{t}(1)]} \mathbf{t}(1).$$

Assuming $w_0 = w_2 = 1$, one additional constraint must be imposed in order to determine the value of w_1 . Suppose we further require (13.15) to interpolate another point $\mathbf{p}_* = (x_*, y_*)$ — the implicit equation (13.19) must then satisfy $f(x_*, y_*) = 0$, and hence the weight is defined by⁵

$$w_1^2 = \frac{\begin{vmatrix} 1 & 1 & 1 \\ x_0 & x_* & x_2 \\ y_0 & y_* & y_2 \end{vmatrix}^2}{4 \begin{vmatrix} 1 & 1 & 1 \\ x_* & x_1 & x_2 \\ y_* & y_1 & y_2 \end{vmatrix} \begin{vmatrix} 1 & 1 & 1 \\ x_0 & x_1 & x_* \\ y_0 & y_1 & y_* \end{vmatrix}}.$$

⁵ Note that we do not specify the parameter value t_* such that $\mathbf{r}(t_*) = \mathbf{p}_*$ — this is not possible, since the parameterization is already fixed by the choice $w_0 = w_2 = 1$ (moreover, such a specification would amount to *two* constraints).

To obtain a real w_1 , the determinants in the denominator must be of the same sign. This holds when \mathbf{p}_* lies in either of the wedge-shaped regions between lines drawn through \mathbf{p}_1 along the directions $\mathbf{t}(0), \mathbf{t}(1)$. One then chooses the positive solution to ensure that (13.15) lies in the convex hull of $\mathbf{p}_0, \mathbf{p}_1, \mathbf{p}_2$.

Example 13.1 For a circular arc of radius R and center \mathbf{c} between end points \mathbf{p}_0 and \mathbf{p}_2 , one may easily verify that the middle control point is

$$\mathbf{p}_1 = \mathbf{c} + \frac{1}{2}(\mathbf{p}_0 + \mathbf{p}_2 - 2\mathbf{c}) \sec^2 \phi,$$

where $\phi = \cos^{-1}(\mathbf{p}_2 - \mathbf{c}) \cdot (\mathbf{p}_0 - \mathbf{c}) / R^2$ defines the angular extent of the arc, and with $w_0 = w_2 = 1$ the appropriate weight is

$$w_1 = \cos \frac{1}{2}\phi.$$

For further details on the rational Bézier form of conics, see [142, 144, 302].

13.8 Tensor–product Surface Patches

A surface patch is defined by a vector-valued function in \mathbb{R}^3 of two parameters, $\mathbf{r}(u, v)$, defined on a specified domain in the (u, v) -plane. The nature of the parameter domain determines the patch “type” — a triangular domain defines a three-sided patch, and a rectangular domain yields a four-sided patch.⁶

Three-sided patches are in certain respects more fundamental than four-sided patches. For example, any smooth closed surface of arbitrary topology may be completely covered by a network of contiguous three-sided patches, but a surface as basic as the sphere cannot be covered using only four-sided patches. Nevertheless, four-sided patches are often considered more “natural” for surface design applications, and are more widespread in practical use.

In this section, we describe properties of the so-called “tensor–product” formulation of rectangular Bézier surface patches — triangular patches will be discussed in §13.9 below. A tensor–product surface patch, of degree m in u and n in v , is defined by specifying a topologically rectangular $(m+1) \times (n+1)$ array of control points \mathbf{p}_{jk} for $0 \leq j \leq m$ and $0 \leq k \leq n$. As described in §7.2.2, we form bivariate basis functions through products of the univariate Bernstein basis functions of degree m in $u \in [0, 1]$ and n in $v \in [0, 1]$, and associate a control point with each of them in the double sum

$$\mathbf{r}(u, v) = \sum_{j=0}^m \sum_{k=0}^n \mathbf{p}_{jk} b_j^m(u) b_k^n(v), \quad (13.22)$$

defining a tensor–product Bézier patch for $(u, v) \in [0, 1] \times [0, 1]$.

⁶ Three-sided patches may be defined as images of rectangular parameter domains by forcing one of the patch boundaries to degenerate to a point. However, this has the disadvantage that the surface parameterization is singular at that point.

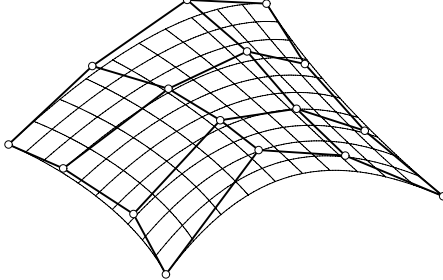


Fig. 13.10. A tensor–product bicubic patch and its Bézier control net.

By connecting each control point \mathbf{p}_{jk} to its four “neighbors” $\mathbf{p}_{j-1,k}$, $\mathbf{p}_{j+1,k}$, $\mathbf{p}_{j,k-1}$, $\mathbf{p}_{j,k+1}$ (if they exist) with a line segment, we obtain the *control net*⁷ for the tensor–product patch (13.22). As with Bézier curves, the surface patch mimics the shape properties of the control net that defines it.

Two commonly–used forms are the biquadratic ($m = n = 2$) and bicubic ($m = n = 3$) patches — Fig. 13.10 shows an example of the latter. We now highlight some key properties of the form (13.22):

- the surface patch lies within the convex hull of its control net;
- the patch interpolates the four corner points of the control net: $\mathbf{r}(0,0) = \mathbf{p}_{00}$, $\mathbf{r}(1,0) = \mathbf{p}_{m0}$, $\mathbf{r}(0,1) = \mathbf{p}_{0n}$, and $\mathbf{r}(1,1) = \mathbf{p}_{mn}$;
- the points $(\mathbf{p}_{00}, \mathbf{p}_{01}, \mathbf{p}_{10})$, $(\mathbf{p}_{m0}, \mathbf{p}_{m1}, \mathbf{p}_{m-1,0})$, $(\mathbf{p}_{0n}, \mathbf{p}_{1n}, \mathbf{p}_{0,n-1})$, and $(\mathbf{p}_{mn}, \mathbf{p}_{m-1,n}, \mathbf{p}_{m,n-1})$ define the tangent planes at the patch corners;
- the peripheral points $(\mathbf{p}_{00}, \dots, \mathbf{p}_{m0})$, $(\mathbf{p}_{0n}, \dots, \mathbf{p}_{mn})$, $(\mathbf{p}_{00}, \dots, \mathbf{p}_{0n})$, $(\mathbf{p}_{m0}, \dots, \mathbf{p}_{mn})$ of the control net define the four patch boundaries $\mathbf{r}(u,0)$, $\mathbf{r}(u,1)$, $\mathbf{r}(0,v)$, $\mathbf{r}(1,v)$ as independent Bézier curves.

Note, however, that the form (13.22) has no “simple” variation–diminishing property, bounding the complexity of the intersection of a line or plane with the surface in terms of its intersection with the control net.

We can regard the tensor–product patch (13.22) as being swept out by a curve that continuously moves and changes shape. Writing (13.22) in the form

$$\mathbf{r}(u, v) = \sum_{j=0}^m \mathbf{q}_j(v) b_j^m(u), \quad (13.23)$$

we interpret this to be a degree– m Bézier curve in the parameter $u \in [0, 1]$ with “variable control points”

$$\mathbf{q}_j(v) = \sum_{k=0}^n \mathbf{p}_{jk} b_k^n(v) \quad \text{for } j = 0, \dots, m \quad (13.24)$$

⁷ Note that this control net does *not* define a polyhedral surface, since each of its “facets” is defined by four control points that are not, in general, coplanar.

that each follow a degree- n Bézier curve as v increases from 0 to 1 (obviously, the roles of u and v can be swapped here).

Note that the degree-elevation and subdivision algorithms, as formulated in §13.3 and §13.4 for Bézier curves, can be directly applied to either the u or the v parameter of the surface patch (13.22). For example, to degree-elevate the patch with respect to v , or to subdivide it along the parameter line $v = \tau$, we apply (13.4) or (13.6) to *each* set of control points $j = 0, \dots, m$ in (13.24). The same method holds for degree-elevation or subdivision with respect to u .

The form (13.22) has an obvious generalization to rational tensor-product patches. Namely, we multiply each control point \mathbf{p}_{jk} in (13.22) by a weight w_{jk} and divide the resulting expression by the double-sum of the weights multiplied by the corresponding basis functions, $b_j^m(u)$ and $b_k^n(v)$. The rational form is essential for *exact* representation of general quadric-surface patches, patches on surfaces of revolution, and other important surface types.

Determining the control points and weights that define such surfaces can be laborious and error-prone if approached directly. However, *swept surface* methods can be invoked to accomplish this “automatically,” using only basic curve data. We may regard many important surfaces as being generated by the *continuous transformation* of a given “profile” curve. One may imagine, for example, the given curve to be continuously translated, rotated, or scaled — or any combination thereof — in some prescribed manner, such that its successive instances “sweep out” the desired surface. To incorporate such *swept surfaces* in CAD systems, it is necessary to derive explicit representations of them to ensure full compatibility with the surface algorithms of that system.

We describe here an elegant matrix algebra for the construction of swept surfaces, introduced [239, 240] by J. K. Hinds and L. P. Kuan, that furnishes CAD systems a powerful and intuitive framework for automatically generating the rational Bézier forms for a broad range of swept surface types. The basic paradigm may be phrased as follows. One selects two Bézier curves, a *profile curve* $\mathbf{p}(u)$ and a *sweep curve* $\mathbf{s}(v)$. Each point v of the sweep curve defines, according to some prescribed rule, a projective transformation that is specified by a 4×4 matrix $\mathbf{M}(v)$ — see §7.4.7. Then, as v increases from 0 to 1, the continuous action of $\mathbf{M}(v)$ on $\mathbf{p}(u)$ generates the desired swept surface $\mathbf{r}(u, v)$ in rational tensor-product Bézier form. The Bézier control points and weights of the swept surface $\mathbf{r}(u, v)$ are obtained from those of the profile and sweep curves, $\mathbf{p}(u)$ and $\mathbf{s}(v)$, through appropriate matrix multiplications.

To facilitate the use of matrices, we denote the homogeneous coordinates of a point by $\mathbf{P} = (P_0, P_1, P_2, P_3) = (W, X, Y, Z)$. A projective transformation $\mathbf{P} \rightarrow \tilde{\mathbf{P}}$ is defined by a non-singular 4×4 matrix \mathbf{M} , as in (7.68). Denoting the elements of this matrix by $M_{\alpha\beta}$ with $0 \leq \alpha, \beta \leq 3$, we may write

$$\tilde{P}_\alpha = \sum_{\beta=0}^3 M_{\alpha\beta} P_\beta, \quad \alpha = 0, \dots, 3.$$

In homogeneous coordinates, a rational cubic Bézier curve with control points $\mathbf{p}_i = (x_i, y_i, z_i)$ and weights w_i can be expressed as

$$\mathbf{P}(t) = \sum_{i=0}^3 \mathbf{p}_i b_i^3(t), \quad (13.25)$$

where $\mathbf{P}_i = (w_i, w_i x_i, w_i y_i, w_i z_i)$. The affine form $\mathbf{r}(t) = (x(t), y(t), z(t))$ is then $x(t) = P_1(t)/P_0(t)$, $y(t) = P_2(t)/P_0(t)$, $z(t) = P_3(t)/P_0(t)$, with $P_\alpha(t)$ being the components of $\mathbf{P}(t)$. Writing equation (13.25) in scalar form as

$$P_\alpha(t) = \sum_{i=0}^3 P_{\alpha i} b_i^3(t), \quad \alpha = 0, \dots, 3$$

we see that a rational cubic $\mathbf{r}(t)$ can be defined by a 4×4 matrix of the form

$$\begin{bmatrix} P_{00} & P_{01} & P_{02} & P_{03} \\ P_{10} & P_{11} & P_{12} & P_{13} \\ P_{20} & P_{21} & P_{22} & P_{23} \\ P_{30} & P_{31} & P_{32} & P_{33} \end{bmatrix}, \quad (13.26)$$

where $P_{\alpha i}$ is the α -th homogeneous coordinate of the i -th control point. We use Greek letters for *coordinate indices* and Roman letters for *basis function indices*. The former always run from 0 to 3. The latter coincidentally run from 0 to 3 because, for simplicity, we consider here only cubic curves.

Now the set of rational curves of a given degree is closed under projective maps — i.e., there is a matrix \mathbf{M} that transforms any rational curve $\mathbf{P}(t)$ into any other rational curve $\tilde{\mathbf{P}}(t)$ of the same degree. For cubics, the transformed curve is readily obtained from the given curve by the matrix multiplication

$$\tilde{P}_{\alpha i} = \sum_{\beta=0}^3 M_{\alpha\beta} P_{\beta i}.$$

This fact allows us to regard rational cubics as being essentially equivalent to projective transformations. Namely, if we introduce a “canonical” cubic⁸ $\mathbf{C}(t)$ defined by the homogeneous coordinate functions

$$C_0(t) = (1-t)^3, \quad C_1(t) = 3(1-t)^2 t, \quad C_2(t) = 3(1-t)t^2, \quad C_3(t) = t^3,$$

the matrix (13.26) that defines *any* rational cubic $\mathbf{P}(t)$ may be interpreted as a projective transformation, of the form (7.68), mapping $\mathbf{C}(t)$ to $\mathbf{P}(t)$.

⁸ The Bézier control points are $\mathbf{P}_0 = (1, 0, 0, 0)$, $\mathbf{P}_1 = (0, 1, 0, 0)$, $\mathbf{P}_2 = (0, 0, 1, 0)$, $\mathbf{P}_3 = (0, 0, 0, 1)$. Since \mathbf{P}_1 , \mathbf{P}_2 , \mathbf{P}_3 are points at infinity, the segment $t \in [0, 1]$ is semi-infinite, but its projective images may be *finite* segments. In algebraic geometry [407], it is customary to use $W(t) = 1$, $X(t) = t$, $Y(t) = t^2$, $Z(t) = t^3$ (the *rational normal curve* of order 3) as the “canonical” rational cubic.

We can also introduce a matrix representation for tensor–product surface patches. The rational bicubic surface patch

$$P_\alpha(u, v) = \sum_{i=0}^3 \sum_{j=0}^3 P_{\alpha ij} b_i^3(u) b_j^3(v), \quad \alpha = 0, \dots, 3$$

may be described by a $4 \times 4 \times 4$ matrix with elements $P_{\alpha ij}$. We enumerate this three-dimensional matrix in a “layer–by–layer” fashion as

$$\begin{aligned} & \left[\begin{matrix} P_{000} & P_{010} & P_{020} & P_{030} \\ P_{100} & P_{110} & P_{120} & P_{130} \\ P_{200} & P_{210} & P_{220} & P_{230} \\ P_{300} & P_{310} & P_{320} & P_{330} \end{matrix} \right] \\ & \left[\begin{matrix} P_{001} & P_{011} & P_{021} & P_{031} \\ P_{101} & P_{111} & P_{121} & P_{131} \\ P_{201} & P_{211} & P_{221} & P_{231} \\ P_{301} & P_{311} & P_{321} & P_{331} \end{matrix} \right] \\ & \left[\begin{matrix} P_{002} & P_{012} & P_{022} & P_{032} \\ P_{102} & P_{112} & P_{122} & P_{132} \\ P_{202} & P_{212} & P_{222} & P_{232} \\ P_{302} & P_{312} & P_{322} & P_{332} \end{matrix} \right] \\ & \left[\begin{matrix} P_{003} & P_{013} & P_{023} & P_{033} \\ P_{103} & P_{113} & P_{123} & P_{133} \\ P_{203} & P_{213} & P_{223} & P_{233} \\ P_{303} & P_{313} & P_{323} & P_{333} \end{matrix} \right]. \quad (13.27) \end{aligned}$$

The coordinate index α and basis function indices i, j define location in terms of row, column, and depth in this matrix. As in the curve case, transforming the surface by a projective map \mathbf{M} is simply a matter of matrix multiplication.

We wish to find the matrix (13.27) of a swept surface from given matrices of the form (13.26) defining profile and sweep curves, for a specified mode of sweeping. Let the sweep curve $\mathbf{s}(v)$ be defined by

$$S_\alpha(v) = \sum_{j=0}^3 S_{\alpha j} b_j^3(v), \quad \alpha = 0, \dots, 3. \quad (13.28)$$

To associate a 4×4 transformation matrix $\mathbf{M}(v)$ with each point v of the sweep curve, we invoke a $4 \times 4 \times 4$ *selector matrix* \mathbf{T} with suitably chosen elements $T_{\alpha\beta\gamma}$, $0 \leq \alpha, \beta, \gamma \leq 3$. Multiplying the row vector $[S_0(v) \ S_1(v) \ S_2(v) \ S_3(v)]$ defining $\mathbf{s}(v)$ by the $4 \times 4 \times 4$ selector matrix then yields a parameter-dependent 4×4 matrix with elements

$$M_{\beta\gamma}(v) = \sum_{\alpha=0}^3 S_\alpha(v) T_{\alpha\beta\gamma}, \quad 0 \leq \beta, \gamma \leq 3 \quad (13.29)$$

that describes a family of projective transformations, $\mathbf{M}(v)$. Consider now the mapping of the profile curve $\mathbf{p}(u)$, expressed in homogeneous form as

$$P_\gamma(u) = \sum_{i=0}^3 P_{\gamma i} b_i^3(u) \quad \text{for } \gamma = 0, \dots, 3, \quad (13.30)$$

by each instance of $\mathbf{M}(v)$ as v increases. This continuous mapping of $\mathbf{p}(u)$ by $\mathbf{M}(v)$ yields a parametric surface $\mathbf{r}(u, v)$ with the homogeneous representation

$$R_\beta(u, v) = \sum_{\alpha=0}^3 \sum_{\gamma=0}^3 S_\alpha(v) T_{\alpha\beta\gamma} P_\gamma(u), \quad \beta = 0, \dots, 3.$$

To determine the $4 \times 4 \times 4$ matrix of the form (13.27) describing this surface as a rational bicubic Bézier patch, we substitute expressions (13.28) and (13.30) into the above, and re-arrange the order of summation to obtain

$$R_\beta(u, v) = \sum_{i=0}^3 \sum_{j=0}^3 R_{\beta ij} b_i^3(u) b_j^3(v), \quad \beta = 0, \dots, 3,$$

where the homogeneous coordinates of the surface control points are given by

$$R_{\beta ij} = \sum_{\alpha=0}^3 \sum_{\gamma=0}^3 S_{\alpha j} T_{\alpha\beta\gamma} P_{\gamma i} \quad (13.31)$$

for $\beta = 0, \dots, 3$ and $0 \leq i, j \leq 3$. Equation (13.31) defines a direct construction of the swept surface matrix by a two-fold multiplication or “contraction” of the 4×4 profile and sweep curve matrices with the $4 \times 4 \times 4$ selector matrix — note that the row indices of the sweep and profile curve matrices contract with the *row* and *depth* indices of the selector matrix, respectively.

This describes the general procedure for constructing swept surfaces, given profile and sweep curve matrices and a selector matrix. To obtain a particular type of surface, the essence of the method lies in judicious choice of the selector matrix, so as to yield the desired sweeping mode of the profile curve. This is perhaps best understood in the context of some specific examples.

To define $\mathbf{r}(u, v)$ through a continuous translation of the profile curve $\mathbf{p}(u)$ by the coordinates of each point of the sweep curve $\mathbf{s}(v)$, we choose

$$T_{000} = T_{110} = T_{220} = T_{330} = T_{011} = T_{022} = T_{033} = 1, \quad (13.32)$$

with all other elements of the selector matrix \mathbf{T} set to zero. The multiplication (13.29) then defines the family of transformation matrices

$$\mathbf{M}(v) = w(v) \begin{bmatrix} 1 & 0 & 0 & 0 \\ x(v) & 1 & 0 & 0 \\ y(v) & 0 & 1 & 0 \\ z(v) & 0 & 0 & 1 \end{bmatrix},$$

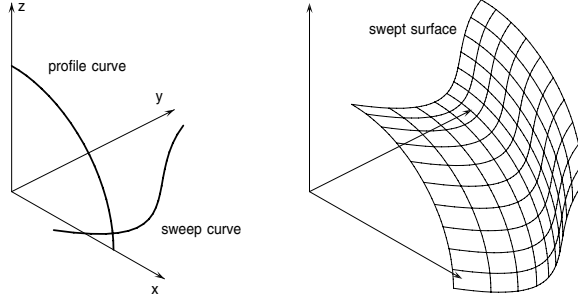


Fig. 13.11. A swept surface generated by the translation of a circular arc.

where we have set $w(v) = S_0(v)$ and $x(v) = S_1(v)/S_0(v)$, $y(v) = S_2(v)/S_0(v)$, $z(v) = S_3(v)/S_0(v)$. Note that, since only *ratios* of homogeneous coordinates matter, the factor $w(v)$ is immaterial and can be omitted. We know from §7.4.7 that a matrix of this form defines a translation by amounts $x(v)$, $y(v)$, $z(v)$ along the coordinate axes, i.e., by the vector $\mathbf{s}(v)$. Thus, the selector matrix (13.32) gives the surface defined by continuously translating $\mathbf{p}(u)$ along $\mathbf{s}(v)$:

$$\mathbf{r}(u, v) = \mathbf{p}(u) + \mathbf{s}(v).$$

The matrix representation (13.27) for $\mathbf{r}(u, v)$ is obtained by simply interposing the selector matrix \mathbf{T} defined by (13.32) between the profile and sweep curve matrices, according to the multiplication rule (13.31). Figure 13.11 shows an example of a translational sweep surface defined in this manner. Note that the profile curve maintains constant shape, size, and orientation as its motion sweeps out the surface. If the profile curve in its specified position is to form one side of the swept surface, the sweep curve must begin at the origin.

Consider now the case of a selector matrix with non-zero elements

$$T_{000} = T_{330} = T_{111} = T_{221} = T_{122} = -T_{212} = T_{033} = 1. \quad (13.33)$$

The multiplication (13.29) yields the family of transformation matrices

$$\mathbf{M}(v) = w(v) \begin{bmatrix} 1 & 0 & 0 & 0 \\ 0 & x(v) & -y(v) & 0 \\ 0 & y(v) & x(v) & 0 \\ z(v) & 0 & 0 & 1 \end{bmatrix}.$$

To elucidate their geometrical meaning, we define the quantities

$$\rho(v) = \sqrt{x^2(v) + y^2(v)}, \quad \cos \phi(v) = \frac{x(v)}{\rho(v)}, \quad \sin \phi(v) = \frac{y(v)}{\rho(v)}.$$

These functions define a parameterization of the sweep curve using cylindrical polar coordinates in \mathbb{R}^3 . Dropping the immaterial factor $w(v)$, we can write the transformations as

$$\mathbf{M}(v) = \begin{bmatrix} 1 & 0 & 0 & 0 \\ 0 & \rho(v) \cos \phi(v) & -\rho(v) \sin \phi(v) & 0 \\ 0 & \rho(v) \sin \phi(v) & \rho(v) \cos \phi(v) & 0 \\ z(v) & 0 & 0 & 1 \end{bmatrix}.$$

This defines a “generalized helical sweeping” of the profile curve. Specifically, each instance of the profile curve as it sweeps out $\mathbf{r}(u, v)$ amounts to:

1. rotating $\mathbf{p}(u)$ through the azimuthal angle $\phi(v)$ about the z -axis;
2. translating the rotated curve an amount $z(v)$ parallel to the z -axis;
3. and, finally, scaling the rotated and translated copy of $\mathbf{p}(u)$ parallel to the (x, y) -plane by a factor equal to the cylindrical radius $\rho(v)$.

Note that, when $\mathbf{s}(v)$ resides in the (x, y) -plane, the translational component of the sweep is suppressed. Moreover, when $\rho(v) \equiv 1$ the scaling component is also suppressed. These properties characterize $\mathbf{s}(v)$ as a portion of the unit circle, and $\mathbf{r}(u, v)$ is then a *surface of revolution* (about the z -axis).

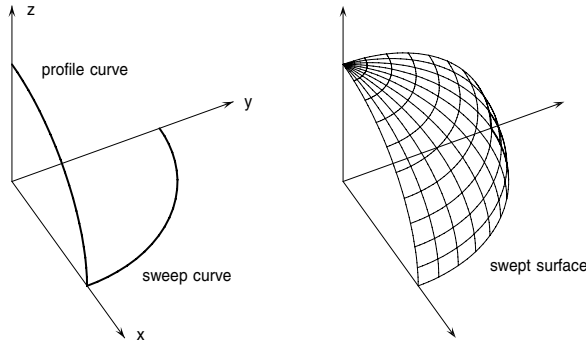


Fig. 13.12. An octant of the unit sphere generated as a rotational swept surface.

For example, it is a simple matter to obtain the rational Bézier form for an octant of the sphere, starting from the Bézier forms of two circular arcs, by means of the swept surface method⁹ — see Fig. 13.12. Obviously, patches on other quadrics of revolution, the torus, etc., can be automatically generated in an analogous manner. Attempting such constructions by other means incurs cumbersome manipulations and even embarrassing errors — see [96, 365].

When the sweep curve is not just a portion of the unit circle in the (x, y) plane, the selector matrix (13.33) generates a much broader family of swept surface forms that encompass the surfaces of revolution as a special instance — Fig. 13.13 gives an example of these more complex shapes.

In addition to generalized surfaces of extrusion and rotation, discussed above, a variety of other sweeping operations may be defined by appropriate

⁹ If represented as a tensor-product patch, the parameterization must be singular at one corner: for a non-degenerate representation as a triangular patch, see [145].

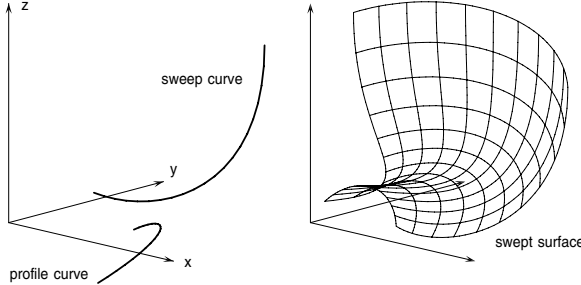


Fig. 13.13. An example of a swept surface for a more general selector matrix — corresponding to simultaneous rotation, translation, and scaling of a profile curve.

choice of the selector matrix. For example, if the only non-zero elements of \mathbf{T} are $T_{000} = T_{111} = T_{222} = T_{333} = 1$, we obtain the transformation matrix

$$\mathbf{M}(v) = w(v) \begin{bmatrix} 1 & 0 & 0 & 0 \\ 0 & x(v) & 0 & 0 \\ 0 & 0 & y(v) & 0 \\ 0 & 0 & 0 & z(v) \end{bmatrix},$$

which corresponds to a non-uniform scaling of the profile $\mathbf{p}(u)$ in the x , y , z directions by factors equal to the coordinates of the sweep curve $\mathbf{s}(v)$.

As another example, consider the choices $T_{000} = T_{330} = T_{311} = T_{322} = T_{033} = 1$, which yields the transformation matrix

$$\mathbf{M}(v) = w(v) \begin{bmatrix} 1 & 0 & 0 & 0 \\ 0 & z(v) & 0 & 0 \\ 0 & 0 & z(v) & 0 \\ z(v) & 0 & 0 & 1 \end{bmatrix}.$$

This corresponds to translating $\mathbf{p}(u)$ by the amount $z(v)$ in the z -direction, and also scaling it uniformly by a factor $z(v)$ parallel to the (x, y) plane — the resulting swept surfaces are thus generalized cones.

It should be noted that the swept surface procedure can also be applied to composite (spline) curves — each segment of the profile curve is transformed by each segment of the sweep curve, according to a single selector matrix, to yield a network of surface patches. The smoothness of this composite surface at patch boundaries is determined by the order of continuity of the composite profile and sweep curves at the junctures of their contiguous segments.

13.9 Triangular Surface Patches

A three-sided surface patch is defined by a vector mapping of a triangular two-dimensional parameter domain T to \mathbb{R}^3 . If (u, v, w) are barycentric coordinates over T , and we introduce the basis functions (7.28) for degree- n polynomials,

a control point \mathbf{p}_{ijk} may be associated with each of these functions. The triangular patch is then defined by

$$\mathbf{r}(u, v, w) = \sum_{\substack{0 \leq i, j, k \leq n \\ i+j+k=n}} \mathbf{p}_{ijk} b_{ijk}^n(u, v, w). \quad (13.34)$$

The *control net* for this patch is defined by connecting each point \mathbf{p}_{ijk} with its neighbors $\mathbf{p}_{i-1,j+1,k}$, $\mathbf{p}_{i+1,j-1,k}$, $\mathbf{p}_{i,j-1,k+1}$, $\mathbf{p}_{i,j+1,k-1}$, $\mathbf{p}_{i+1,j,k-1}$, $\mathbf{p}_{i-1,j,k+1}$ (if they exist) — it describes a polyhedral surface with triangular facets.

The surface patch (13.34) must lie within the convex hull of its control net, and it interpolates the corner points \mathbf{p}_{n00} , \mathbf{p}_{0n0} , \mathbf{p}_{00n} ; the tangent planes at these points are defined by $(\mathbf{p}_{n00}, \mathbf{p}_{n-1,1,0}, \mathbf{p}_{n-1,0,1})$, $(\mathbf{p}_{0n0}, \mathbf{p}_{0,n-1,1}, \mathbf{p}_{1,n-1,0})$, $(\mathbf{p}_{00n}, \mathbf{p}_{1,0,n-1}, \mathbf{p}_{0,1,n-1})$. Moreover, the peripheral control points define the patch boundaries as independent degree- n Bézier curves.

We can formulate a de Casteljau algorithm for subdividing (13.34) that is a natural two-dimensional generalization of the univariate method for curves described in §13.4. We choose a point (u_*, v_*, w_*) interior to T , and consider the three triangular subdomains T_1 , T_2 , T_3 subtended at that point by the sides $u = 0$, $v = 0$, $w = 0$ of T . Setting $\mathbf{p}_{ijk}^0 = \mathbf{p}_{ijk}$ for $0 \leq i, j, k \leq n$ (with $i + j + k = n$), we then compute the tetrahedral array of points defined by

$$\mathbf{p}_{ijk}^r = u_* \mathbf{p}_{i+1,j,k}^{r-1} + v_* \mathbf{p}_{i,j+1,k}^{r-1} + w_* \mathbf{p}_{i,j,k+1}^{r-1} \quad (13.35)$$

for $0 \leq i, j, k \leq n - r$ (with $i + j + k = n - r$) and $r = 1, \dots, n$. Figure 13.14 illustrates how the points generated by the algorithm (13.35) are interpreted as being arranged in a tetrahedral array. The apex \mathbf{p}_{000}^n of this array corresponds to the point $\mathbf{r}(u_*, v_*, w_*)$ on the surface (13.34), while the points on its three faces, identified by

$$\begin{aligned} \mathbf{p}_{0,j,n-r-j}^r &\quad \text{for } j = 0, \dots, n - r \quad \text{and } r = 0, \dots, n, \\ \mathbf{p}_{n-r-k,0,k}^r &\quad \text{for } k = 0, \dots, n - r \quad \text{and } r = 0, \dots, n, \\ \mathbf{p}_{i,n-r-i,0}^r &\quad \text{for } i = 0, \dots, n - r \quad \text{and } r = 0, \dots, n, \end{aligned}$$

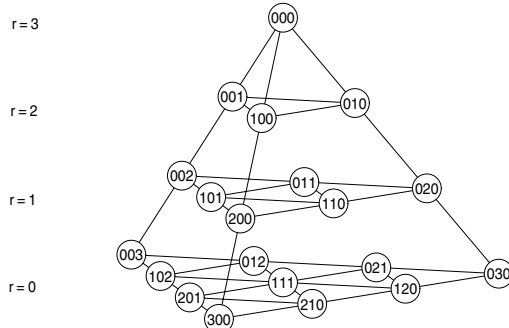


Fig. 13.14. Labelling of the points generated by successive stages $r = 0, 1, 2, 3$ of the bivariate de Casteljau algorithm (13.6), for the case of a cubic patch ($n = 3$).

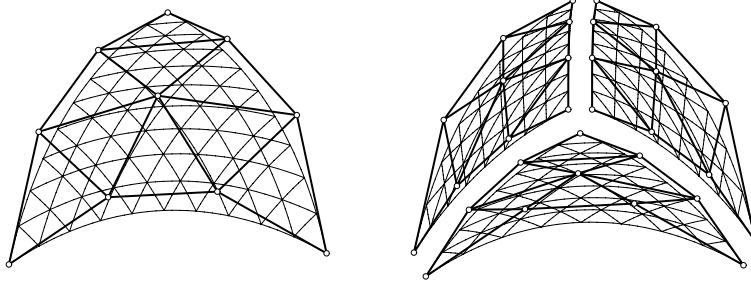


Fig. 13.15. A cubic triangular Bézier surface patch together with its control net, and its subdivision at an interior point using the de Casteljau algorithm (13.6).

define control nets for the sub-patches of (13.34) over the domains T_1, T_2, T_3 . Figure 13.15 gives an example of the subdivision of a cubic triangular patch.

We can also degree-elevate the patch (13.34), i.e., express it in the form

$$\mathbf{r}(u, v, w) = \sum_{\substack{0 \leq i, j, k \leq n+1 \\ i+j+k=n+1}} \mathbf{p}'_{ijk} b_{ijk}^{n+1}(u, v, w),$$

in terms of control points \mathbf{p}'_{ijk} for $0 \leq i, j, k \leq n+1$ (with $i+j+k=n+1$) in the bivariate barycentric basis of degree $n+1$ on the domain triangle T . Multiplying (13.34) by the identity $u+v+w=1$, and collecting like terms, one finds that the degree-elevated control points are given by

$$\mathbf{p}'_{ijk} = \frac{i \mathbf{p}_{i-1,j,k} + j \mathbf{p}_{i,j-1,k} + k \mathbf{p}_{i,j,k-1}}{n+1},$$

where terms on the right-hand side for which any of the indices is < 0 or $> n$ are ignored (this means that the three corner control points are unchanged, while other points along the periphery of the control net are generated by the univariate degree-elevation algorithm (13.4) for curves). Under repeated degree elevation, the control net converges to the surface patch it defines.

Of course, we may also generalize (13.34) to a *rational* triangular patch by associating a scalar weight with each control point. An octant of the sphere, for example, can be represented as a rational quartic triangular patch [145].

C^2 Cubic Spline Curves

The most illustrious and, in this sublime fashion of studying nature, most perspicacious man, Daniel Bernoulli, had pointed out to me that he could express in a single formula, which he calls the potential force, the whole force which inheres in a curved elastic strip, and that this expression must be a minimum in the elastic curve . . . if the strip be of uniform cross section and elasticity, and if it be straight, when in its natural position, the character of the curve will be such that in this case the expression $\int_0^s ds/R^2$ is an absolute minimum.

Leonhard Euler (1707–1783), as quoted in [440]

In the design of curves and surfaces subject to prescribed constraints, such as interpolation of a given set of points, the adopted representation must provide sufficient degrees of freedom to permit satisfaction of those constraints. If a *single* polynomial or rational form is employed, the only scope for introducing additional freedoms is to increase the degree. Unfortunately, interpolants of high degree often exhibit undesired oscillations that are incompatible with the “shape” of the given data, and can be difficult to suppress or control.

An alternative approach to providing additional degrees of freedom is to “piece together” segments of lower-degree polynomial or rational functions, defined on contiguous domains, in such a manner that they *appear* smooth — i.e., they have matched derivatives up to a certain order at their junctures or *knots*. There is actually an infinite variety of ways to do this, consistent with the prescribed constraints. The essence of a spline function is that it selects from among these possibilities the one that is *smoothest*, and best suppresses spurious oscillation, in a certain quantifiable sense (see §14.4.5).

The practical advantage of splines for the interpolation of discrete data is illustrated in Fig. 14.1. Perhaps the simplest imaginable interpolant is the polygonal *piecewise-linear* function. It is certainly faithful to the “shape” of the data (there are no spurious oscillations), but is only C^0 at the data points.

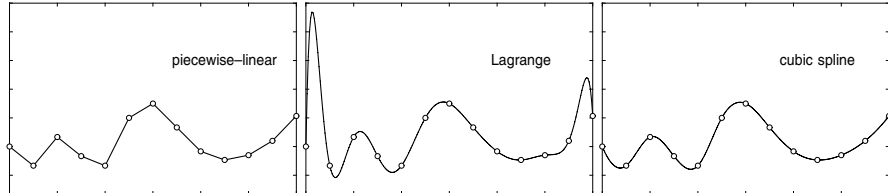


Fig. 14.1. While the piecewise–linear interpolant is not “locally smooth,” and the degree– N Lagrange polynomial interpolant is not “globally smooth,” the C^2 cubic spline exhibits acceptable behavior in terms of both *local* and *global* smoothness.

Its non-differentiable nature at these points disqualifies it from consideration in many applications. On the other hand, if we use a polynomial of degree N to interpolate $N + 1$ points, we are assured that the function is C^∞ everywhere. But, as can be seen in Fig. 14.1, this “local smoothness” does not guarantee global shape fidelity — the interpolant exhibits extrema that do not have any correlation with the discrete points. The cubic spline offers a happy medium between these extremes — it combines acceptable (C^2) “local smoothness” at the data points, while exhibiting “global smoothness” and good fidelity to the overall shape suggested by the discrete data points.

In this chapter we review the classical theory of “ordinary” C^2 cubic spline curves. In Chap. 27 we will describe how these ideas can be extended to the construction of C^2 *Pythagorean-hodograph quintic spline curves*.

14.1 Mechanical Splines

Although now commonly understood to mean piecewise-polynomial functions constructed according to certain principles, the term “spline” originates from a mechanical device formerly used in aircraft and ship design, and the layout of railway lines, to interpolate smooth curves through sequences of points.

Heavy weights called *ducks* were attached to a thin, flexible strip of wood or rubber (the *spline*), to bend it so as to pass through the prescribed points. The ducks constrain the *position* but not the *slope* of the spline, which “flexes” to as nearly straight a configuration as possible when loaded by the ducks — no energy is stored in the spline when in its unloaded (i.e., straight) state, and “as nearly straight as possible” means that the loaded spline has the shape of *minimum bending energy* consistent with the position constraints.

The “mathematical” spline reproduces this minimum-energy feature of the mechanical spline — for the small-deflection regime, at least. It is noteworthy that, although the mathematics involved in the construction and analysis of splines has long been known, they are a relatively recent development. Two papers by I. J. Schoenberg [394], published soon after the Second World War, are the first to specifically mention spline functions. The increasing availability of digital computers since the 1960s has provided the impetus for the practical use of splines, and the development of the underlying theory.

14.2 Elastic Bending Energy

When an elastic beam of uniform cross-sectional shape is bent from an initially straight configuration into a (planar) curved shape, the local curvature κ is related [126] to the bending moment M exerted across each beam section by

$$\kappa = \frac{M}{EI}, \quad (14.1)$$

where E is the modulus of elasticity for the material, and $I = \int y^2 dA$ is the second area-moment of the beam section about the “neutral axis.” This is a consequence of simple geometrical considerations and Hooke’s Law¹ $\sigma = E\epsilon$, relating stress σ and strain ϵ , under the following assumptions:

- transverse plane sections of the beam remain plane upon bending;
- the cross-sectional shape is symmetric about the plane of bending;
- the cross-sectional dimensions are small in comparison with the radius of curvature, $\rho = 1/\kappa$, at each position along the beam.

Suppose a moment M acts upon an infinitesimal element ds of the elastic beam, inducing a bending of this element through angle $d\theta$. The work done on this element is $\frac{1}{2}M d\theta$. Noting that the local curvature κ of the beam may be defined in terms of its slope θ and arc length s by $\kappa = d\theta/ds$, and using relation (14.1), we can express the work done as $\frac{1}{2}EI \kappa^2 ds$. Thus, under the stated assumptions, the work done in bending the beam to its curved configuration (i.e., the *strain energy* stored in the bent beam) is proportional to the integral

$$U = \int \kappa^2 ds. \quad (14.2)$$

If the beam is forced to satisfy certain geometrical constraints — e.g., passing through specified points, and perhaps assuming given slopes at the ends — it assumes the shape, consistent with those constraints, that minimizes U .

Curves that minimize (14.2) subject to geometrical constraints are known as *elastica*. They were first studied by the Bernoulli brothers and by Leonhard Euler. Such loci agree with our intuitive notions of “fair” or “smooth” curves: the curvature is no greater, and exhibits no more variation, than is necessary to accommodate the specified constraints. Unfortunately, exact solutions to the minimization of U under even simple constraints (e.g., specified end points and tangents) do not admit elementary closed-form representations.

The idea of minimizing an “energy integral” — actually, a much simpler version of (14.2) — as a paradigm for guaranteeing the overall smoothness of a

¹ Robert Hooke (1635–1703) was an accomplished scientist, who made many useful discoveries besides this law. A factor in our ignorance of his accomplishments was the antagonism of Isaac Newton, his successor as President of The Royal Society, who systematically destroyed all evidence of Hooke’s endeavors [21].

geometrically constrained locus carries over to the *spline curves* that we shall consider below. Splines offer great flexibility — while avoiding undesired shape variations, and remaining computationally tractable — by “piecing together” simple (usually cubic) segments, such that adjacent segments have derivatives in agreement (typically, to second order) at their junctures.

We begin by considering the problem of interpolating $N + 1$ scalar values f_0, \dots, f_N at specified points t_0, \dots, t_N by a “smooth” scalar function $f(t)$, and subsequently generalize this to the interpolation of geometrical points by vector-valued functions (i.e., parametric curves).

14.3 Polynomial Interpolation

One way to guarantee “local smoothness” throughout the domain $t \in [t_0, t_N]$ of interest is to interpolate the data using a *single* function that has continuous derivatives of arbitrary order. The obvious choice is a polynomial

$$f(t) = a_0 + a_1 t + a_2 t^2 + \cdots + a_N t^N$$

of degree N , since this has exactly $N + 1$ degrees of freedom and thus furnishes a *unique* interpolant. Evaluating $f(t)$ at t_0, \dots, t_N gives the linear system

$$\begin{bmatrix} 1 & t_0 & t_0^2 & \cdots & t_0^N \\ 1 & t_1 & t_1^2 & \cdots & t_1^N \\ \vdots & \vdots & \vdots & \ddots & \vdots \\ \vdots & \vdots & \vdots & \ddots & \vdots \\ \vdots & \vdots & \vdots & \ddots & \vdots \\ 1 & t_N & t_N^2 & \cdots & t_N^N \end{bmatrix} \begin{bmatrix} a_0 \\ a_1 \\ a_2 \\ \vdots \\ a_N \end{bmatrix} = \begin{bmatrix} f_0 \\ f_1 \\ f_2 \\ \vdots \\ f_N \end{bmatrix}.$$

for the coefficients a_0, \dots, a_N that define the desired interpolant. In principal this has a straightforward solution, but the matrix on the left-hand side — known as a *Vandermonde matrix* — is generally rather ill-conditioned, so this approach is not recommended in practice.

14.3.1 The Lagrange Basis

The unique polynomial interpolant can be determined immediately, without the need to solve a linear system of equations, by invoking the *Lagrange basis* for the nodes t_0, \dots, t_N . The Lagrange basis functions

$$L_j(t) = \prod_{\substack{k=0 \\ k \neq j}}^N \frac{t - t_k}{t_j - t_k} \tag{14.3}$$

for $j = 0, \dots, N$ are each polynomials of degree N , and they satisfy

$$L_j(t_i) = \delta_{ij} = \begin{cases} 1 & \text{if } i = j, \\ 0 & \text{otherwise.} \end{cases}$$

Hence, taking the values f_0, \dots, f_N to be interpolated as coefficients for these basis functions, the degree- N polynomial defined by

$$f(t) = \sum_{j=0}^N f_j L_j(t) \quad (14.4)$$

clearly fulfills the interpolation conditions $f(t_i) = f_i$ for $i = 0, \dots, N$.

14.3.2 Convergence Behavior

The degree- N polynomial interpolant (14.4) is “locally smooth” everywhere, since it is a C^∞ function. However, its global shape properties are often quite unacceptable — as is evident from the famous *Runge example* [141] illustrated in Fig. 14.2. Better results can be obtained by using the *Chebyshev nodes*, rather than uniformly-spaced nodes, when sampling the function $f(t)$. These are the projections onto the t -axis of $N + 1$ points distributed uniformly on a semi-circle constructed over the interval in t of interest. Nevertheless, the question of where a polynomial interpolant converges or diverges is a rather subtle problem in complex analysis — without such a convergence analysis, interpolation by high-degree polynomials is best avoided.

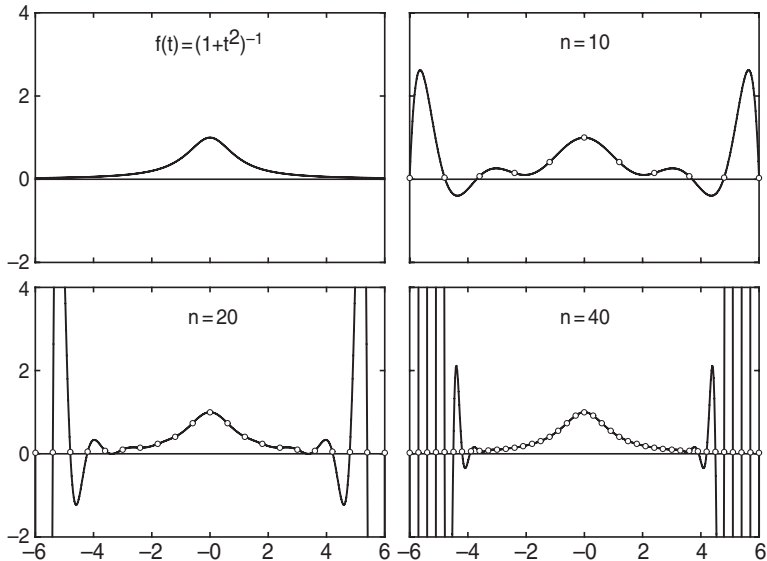


Fig. 14.2. Polynomial interpolants of degree $n = 10, 20, 40$ to equidistant points sampled from the smooth function $f(t) = 1/(1 + t^2)$. The interpolants converge in the interval $|t| < t_* \approx 3.63$, but exhibit increasingly wild oscillations when $|t| > t_*$.

14.4 C^2 Cubic Spline Functions

The basic idea of a spline function may be phrased as follows. Given a sequence of function values f_0, \dots, f_N that correspond to a monotone-increasing set of independent-variable values t_0, \dots, t_N , we seek to construct a function $f(t)$ that “smoothly” interpolates those values:

$$f(t_k) = f_k \quad \text{for } k = 0, \dots, N. \quad (14.5)$$

The values t_0, \dots, t_n are the spline *nodes* or *knots*. The requirement that $f(t)$ be “smooth” carries two connotations here (see Fig. 14.1) — (i) it should be *locally* smooth, in the sense that at each point $t \in [t_0, t_N]$ all derivatives up to some specified order are continuous; and (ii) it should be *globally* smooth, i.e., it should exhibit no undulations that are not implied by the data f_0, \dots, f_N . We shall impart more precise meanings to these stipulations below.

14.4.1 Cubic Hermite Form

A spline function is a composite of distinct polynomials “pieces” $p_k(t)$ defined over consecutive spans $t \in [t_{k-1}, t_k]$ of the interval $[t_0, t_N]$ in such a manner that they match smoothly — i.e., in their value and a prescribed number of derivatives — at the interior knots t_1, \dots, t_{N-1} . We shall be concerned mostly with *cubic* splines here, which exhibit C^2 continuity.

It is convenient to invoke a “local variable” τ for each span k , defined by

$$\tau = \frac{t - t_{k-1}}{t_k - t_{k-1}}, \quad (14.6)$$

such that the interval $t \in [t_{k-1}, t_k]$ is mapped to $\tau \in [0, 1]$. Derivatives with respect to t and τ are related by

$$\frac{d}{dt} = \frac{1}{\Delta t_k} \frac{d}{d\tau} \quad (14.7)$$

where the width of the k -th span is

$$\Delta t_k = t_k - t_{k-1}.$$

In terms of this local variable we can, in principle, choose any basis to represent the cubic $p_k(\tau)$ over the k -th span — for example, the power form about $\tau = 0$, or the Bernstein representation on $\tau \in [0, 1]$. The construction of the spline function is greatly simplified, however, by formulating the polynomials $p_k(\tau)$ in the cubic *Hermite basis* on $\tau \in [0, 1]$ consisting of the functions

$$\begin{aligned} \alpha_0(\tau) &= 1 - 3\tau^2 + 2\tau^3, & \alpha_1(\tau) &= 3\tau^2 - 2\tau^3, \\ \beta_0(\tau) &= \tau - 2\tau^2 + \tau^3, & \beta_1(\tau) &= -\tau^2 + \tau^3. \end{aligned} \quad (14.8)$$

Recall (see §3.2) that these are the *unique* cubics on $[0, 1]$ with the following properties. The “ α ” functions have zero *derivatives* at both end-points, and their *values* are unity at one end and zero at the other. Conversely, the “ β ” functions have vanishing *values* at both end-points, and their *derivatives* are unity at one end and zero at the other. Hence, a cubic with coefficients a_0, a_1 and b_0, b_1 in the Hermite basis,

$$p(\tau) = a_0\alpha_0(\tau) + a_1\alpha_1(\tau) + b_0\beta_0(\tau) + b_1\beta_1(\tau),$$

satisfies $p(0) = a_0, p(1) = a_1$ and $p'(0) = b_0, p'(1) = b_1$.

To take advantage of the Hermite basis (14.8) in the construction of spline functions, we express the polynomial over the k -th span in the form

$$p_k(\tau) = f_{k-1}\alpha_0(\tau) + f_k\alpha_1(\tau) + \Delta t_k [d_{k-1}\beta_0(\tau) + d_k\beta_1(\tau)] \quad (14.9)$$

in terms of the *given* values f_0, \dots, f_N and the *unknown* derivatives d_0, \dots, d_N at the knots (the factor Δt_k arises since d_0, \dots, d_N are derivatives *with respect to* t , which are related to τ -derivatives by equation (14.7)).

Comparing (14.9) with the analogous expression

$$p_{k+1}(\tau) = f_k\alpha_0(\tau) + f_{k+1}\alpha_1(\tau) + \Delta t_{k+1} [d_k\beta_0(\tau) + d_{k+1}\beta_1(\tau)], \quad (14.10)$$

for span $k+1$, we see that the C^0 and C^1 continuity conditions

$$p_k(1) = p_{k+1}(0) \quad \text{and} \quad \frac{p'_k(1)}{\Delta t_k} = \frac{p'_{k+1}(0)}{\Delta t_{k+1}} \quad (14.11)$$

are *automatically* satisfied. By also requiring continuity of *second* derivatives between spans k and $k+1$, we generate a system of linear equations for the unknown nodal derivatives d_0, \dots, d_N .

14.4.2 C^2 Continuity Equations

Equating second derivatives of expressions (14.9) and (14.10) with respect to t at their common juncture,

$$\frac{p''_k(1)}{(\Delta t_k)^2} = \frac{p''_{k+1}(0)}{(\Delta t_{k+1})^2}, \quad (14.12)$$

we obtain the C^2 continuity condition

$$\begin{aligned} & \Delta t_{k+1} d_{k-1} + 2(\Delta t_k + \Delta t_{k+1}) d_k + \Delta t_k d_{k+1} \\ &= 3 \left[\Delta t_k \frac{f_{k+1} - f_k}{\Delta t_{k+1}} + \Delta t_{k+1} \frac{f_k - f_{k-1}}{\Delta t_k} \right] \end{aligned} \quad (14.13)$$

at each “interior” node, $k = 1, \dots, N-1$. Since (14.13) involves only *three* consecutive unknowns d_{k-1}, d_k, d_{k+1} it defines a *tridiagonal system* of linear

equations for the derivatives d_0, \dots, d_N . The function values f_{k-1}, f_k, f_{k+1} and interval widths $\Delta t_k, \Delta t_{k+1}$ are given as part of the problem specification. For the case of uniform integer knots $t_0, \dots, t_N = 0, \dots, N$ the system (14.13) simplifies to

$$d_{k-1} + 4d_k + d_{k+1} = 3(f_{k+1} - f_{k-1}), \quad k = 1, \dots, N-1.$$

14.4.3 Choice of End Conditions

The tridiagonal system defined by (14.13) amounts to $N-1$ linear equations for the $N+1$ unknowns d_0, \dots, d_N , and is thus under-determined. To define a *unique* spline function, two additional (linear) constraints must be imposed on the nodal derivatives. These are called *end conditions*, since they are generally phrased in terms of the behavior of the spline over the first and last few spans — although their influence actually propagates throughout the entire domain $t \in [t_0, t_N]$ of the spline function.

specified end derivatives: d_0 and d_N are assigned values,² which may be directly substituted into the first and last of the equations (14.13). However, without *a priori* knowledge of appropriate end-derivatives (for example, when the spline is used to approximate a known differentiable function), one of the methods described below is preferable to just “guessing” such values.

quadratic end spans: Here, one assumes $p_1(\tau)$ and $p_N(\tau)$ are just *quadratic*, rather than cubic, functions of τ . The conditions $p_0'''(\tau) \equiv 0$ and $p_N'''(\tau) \equiv 0$ then yield the equations

$$d_0 + d_1 = 2 \frac{f_1 - f_0}{\Delta t_1} \quad \text{and} \quad d_{N-1} + d_N = 2 \frac{f_N - f_{N-1}}{\Delta t_N},$$

which are compatible with the tridiagonality of the system (14.13) since they involve only the first and last *two* unknowns — i.e., these end conditions and equations (14.13) taken together have the form

$$\begin{bmatrix} b_0 & c_0 & & & \\ a_1 & b_1 & c_1 & & \\ & a_2 & b_2 & c_2 & \\ & \ddots & \ddots & \ddots & \\ & & \ddots & \ddots & \\ & & & a_{N-1} & b_{N-1} & c_{N-1} \\ & & & & a_N & b_N \end{bmatrix} \begin{bmatrix} d_0 \\ d_1 \\ d_2 \\ \vdots \\ \vdots \\ d_{N-1} \\ d_N \end{bmatrix} = \begin{bmatrix} r_0 \\ r_1 \\ r_2 \\ \vdots \\ \vdots \\ r_{N-1} \\ r_N \end{bmatrix}. \quad (14.14)$$

The tridiagonal matrix coefficients a, b, c and the right-hand side values r are read off from equations (14.13) and the above end conditions.

² A spline interpolating nodal values and end-derivatives is called a *complete spline*.

not-a-knot condition: We impose C^3 continuity at the knots t_1 and t_{N-1} , which is equivalent to requiring that each of the two intervals $t \in [t_0, t_2]$ and $t \in [t_{N-2}, t_N]$ be covered by a *single* cubic, rather than two different cubics. The conditions

$$\frac{p_1'''(1)}{(\Delta t_1)^3} = \frac{p_2'''(0)}{(\Delta t_2)^3} \quad \text{and} \quad \frac{p_{N-1}'''(1)}{(\Delta t_{N-1})^3} = \frac{p_N'''(0)}{(\Delta t_N)^3}$$

then yield the equations

$$\begin{aligned} & (\Delta t_2)^2 d_0 + [(\Delta t_2)^2 - (\Delta t_1)^2] d_1 - (\Delta t_1)^2 d_2 \\ &= 2(\Delta t_2)^2 \frac{f_1 - f_0}{\Delta t_1} - 2(\Delta t_1)^2 \frac{f_2 - f_1}{\Delta t_2}, \\ & (\Delta t_N)^2 d_{N-2} + [(\Delta t_N)^2 - (\Delta t_{N-1})^2] d_{N-1} - (\Delta t_{N-1})^2 d_N \\ &= 2(\Delta t_N)^2 \frac{f_{N-1} - f_{N-2}}{\Delta t_{N-1}} - 2(\Delta t_{N-1})^2 \frac{f_N - f_{N-1}}{\Delta t_N}. \end{aligned}$$

To avoid compromising the tridiagonality of the system defined by the above in conjunction with (14.13) for $k = 1, \dots, N-1$, we need to remove d_2, d_{N-2} from these equations. This is accomplished by eliminating d_2, d_{N-2} between these equations and members $k = 1$ and $k = N-1$ of (14.13). We thus obtain

$$\begin{aligned} & (\Delta t_1 + \Delta t_2) \Delta t_2 d_0 + (\Delta t_1 + \Delta t_2)^2 d_1 \\ &= (3\Delta t_1 + 2\Delta t_2) \Delta t_2 \frac{f_1 - f_0}{\Delta t_1} + (\Delta t_1)^2 \frac{f_2 - f_1}{\Delta t_2}, \\ & (\Delta t_{N-1} + \Delta t_N)^2 d_{N-1} + \Delta t_{N-1} (\Delta t_{N-1} + \Delta t_N) d_N \\ &= (\Delta t_N)^2 \frac{f_{N-1} - f_{N-2}}{\Delta t_{N-1}} + \Delta t_{N-1} (2\Delta t_{N-1} + 3\Delta t_N) \frac{f_N - f_{N-1}}{\Delta t_N}. \end{aligned}$$

These two equations, together with (14.13) for $k = 1, \dots, N-1$, exhibit the tridiagonal form (14.14).

periodic end condition: Here we extend $f(t)$ to all values of t by regarding it as periodic, of period $T = t_N - t_0$, so that

$$f(t + mT) \equiv f(t)$$

for $t \in [t_0, t_N]$ and any integer m . By setting $f_N = f_0$ and $d_N = d_0$, we ensure C^1 continuity at the first/last knot, and we then have N (rather than $N+1$) unknown derivatives, d_0, \dots, d_{N-1} . The C^2 continuity condition

$$\frac{p_N''(1)}{(\Delta t_N)^2} = \frac{p_1''(0)}{(\Delta t_1)^2}$$

at the first/last knot then gives the equation

$$\Delta t_1 d_{N-1} + 2(\Delta t_N + \Delta t_1) d_0 + \Delta t_N d_1 = 3 \left[\Delta t_N \frac{f_1 - f_0}{\Delta t_1} + \Delta t_1 \frac{f_0 - f_{N-1}}{\Delta t_N} \right] \quad (14.15)$$

which is seen to be of the same form as (14.13) if we regard the derivatives as forming a cyclic array

$$\dots, d_{N-2}, d_{N-1}, d_0, d_1, \dots, d_{N-2}, d_{N-1}, d_0, d_1, \dots$$

(the values f_k and intervals Δt_k are regarded in the same manner). Appending (14.15) to members $k = 1, \dots, N-1$ of the system (14.13), we obtain a system of $N-1$ linear equations of the form

$$\begin{bmatrix} b_0 & c_0 & & a_0 \\ a_1 & b_1 & c_1 & \\ & a_2 & b_2 & c_2 \\ & \ddots & \ddots & \ddots \\ & & \ddots & \ddots \\ & & & a_{N-2} & b_{N-2} & c_{N-2} \\ c_{N-1} & & & a_{N-1} & b_{N-1} & \end{bmatrix} \begin{bmatrix} d_0 \\ d_1 \\ d_2 \\ \vdots \\ d_{N-2} \\ d_{N-1} \end{bmatrix} = \begin{bmatrix} r_0 \\ r_1 \\ r_2 \\ \vdots \\ r_{N-2} \\ r_{N-1} \end{bmatrix} \quad (14.16)$$

for the unknowns d_0, \dots, d_{N-1} (note that we must write member $k = N-1$ of (14.13) so as to refer to f_0 and d_0 , rather than f_N and d_N). Note that, because of the elements a_0 and c_{N-1} , the coefficient matrix is no longer tridiagonal.

One may also encounter the so-called “natural spline,” for which the end conditions correspond to the assumption that $f''(t_0) = f''(t_N) = 0$. In the analogy of bending an elastic beam discussed in §14.2, this corresponds (in the small slope regime; see §14.4.5 below) to a beam that is “pinned” at both ends — i.e., no bending moment is exerted at those ends. However, as in the case of arbitrarily choosing numerical values for the end-derivatives, this approach is not recommended unless there is *a priori* justification for it.

14.4.4 Solution of Tridiagonal Systems

Tridiagonal linear systems of the form (14.14) arise in the case of specified end-derivatives, quadratic end spans, and the not-a-knot condition. Such systems admit particularly simple, efficient solutions. We store the matrix coefficients a, b, c and the elements r of the right-hand-side vector in zero-indexed arrays of size $N+1$, and we create similar arrays β and ρ as work-spaces, and d for the solutions. The latter are obtained as follows:

forward elimination:

1. set $\beta_0 = b_0$ and $\rho_0 = r_0$
2. for $k = 0$ up to $N - 1$ set:

$$\begin{aligned} m &= a_{k+1}/\beta_k \\ \beta_{k+1} &= b_{k+1} - m c_k \\ \rho_{k+1} &= r_{k+1} - m \rho_k \end{aligned}$$

back substitution:

3. set $d_N = \rho_N/\beta_N$
4. for $k = N - 1$ down to 0 set:

$$d_k = (\rho_k - c_k d_{k+1})/\beta_k$$

Although the system (14.16) arising in the case of periodic end conditions is no longer tridiagonal, the above algorithm can be easily modified to compute its solution without invoking a general-purpose linear equations solver. The matrix elements a , b , c and right-hand-side values r are again stored in zero-indexed arrays of size N , and we create similar arrays β , ρ , ϵ as workspaces and d for the solutions, which are obtained as follows:

forward elimination:

1. set $\beta_0 = b_0$, $\rho_0 = r_0$, $\epsilon_0 = a_0$
2. for $k = 0$ up to $N - 3$ set:

$$\begin{aligned} m &= a_{k+1}/\beta_k \\ \beta_{k+1} &= b_{k+1} - m c_k \\ \rho_{k+1} &= r_{k+1} - m \rho_k \\ \epsilon_{k+1} &= -m \epsilon_k \end{aligned}$$

3. set $\epsilon_{N-2} = \epsilon_{N-2} + c_{N-2}$, $m = a_{N-1}/\beta_{N-2}$
4. set $\beta_{N-1} = b_{N-1} - m \epsilon_{N-2}$, $\rho_{N-1} = r_{N-1} - m \rho_{N-2}$
5. set $\theta = c_{N-1}$
6. for $k = 0$ up to $N - 2$ set:

$$\begin{aligned} m &= \theta/\beta_k \\ \beta_{N-1} &= \beta_{N-1} - m \epsilon_k \\ \rho_{N-1} &= \rho_{N-1} - m \rho_k \\ \theta &= -m c_k \end{aligned}$$

back substitution:

7. set $d_{N-1} = \rho_{N-1}/\beta_{N-1}$, $d_{N-2} = (\rho_{N-2} - \epsilon_{N-2} d_{N-1})/\beta_{N-2}$
8. for $k = N - 3$ down to 0 set:

$$d_k = (\rho_k - c_k d_{k+1} - \epsilon_k d_{N-1})/\beta_k$$

14.4.5 Minimum Energy Property

Our construction of the cubic spline $f(t)$ that interpolates values f_0, \dots, f_N at the points t_0, \dots, t_N was concerned mostly with issues of “local” smoothness, namely, ensuring that the constituent cubic segments of $f(t)$ have C^2 junctures at the nodes. It transpires, however, that this construction also gives functions with optimal “global” smoothness properties.

Theorem 14.1 Among all C^2 functions $f(t)$ interpolating values f_0, \dots, f_N at the positions t_0, \dots, t_N and given end-derivatives d_0 and d_N at t_0 and t_N , the cubic spline has the least value for the integral

$$\int_{t_0}^{t_N} f''^2(t) dt. \quad (14.17)$$

Proof: Suppose $g(t)$ is a C^2 function, distinct from the cubic spline $f(t)$, that satisfies the interpolation conditions $g(t_k) = f_k$, $k = 0, \dots, N$ and $g'(t_0) = d_0$, $g'(t_N) = d_N$. Writing $h(t) = f(t) - g(t)$, we see that $h(t_k) = 0$, $k = 0, \dots, N$ and $h'(t_0) = h'(t_N) = 0$. We then have

$$\begin{aligned} \int_{t_0}^{t_N} g''^2(t) dt &= \int_{t_0}^{t_N} [f''(t) - h''(t)]^2 dt \\ &= \int_{t_0}^{t_N} f''^2(t) dt + \int_{t_0}^{t_N} h''^2(t) dt - 2 \int_{t_0}^{t_N} f''(t) h''(t) dt, \end{aligned}$$

and the third term on the right can be integrated by parts as follows:

$$\begin{aligned} \int_{t_0}^{t_N} f''(t) h''(t) dt &= \left[f''(t) h'(t) \right]_{t_0}^{t_N} - \int_{t_0}^{t_N} f'''(t) h'(t) dt \\ &= - \sum_{k=1}^N f'''_k [h(t_k) - h(t_{k-1})] = 0. \end{aligned}$$

In deducing the above, we invoke the following facts: (i) $h'(t_0) = h'(t_N) = 0$; (ii) since $f(t)$ is piecewise-cubic, $f'''(t)$ is just piecewise-constant, with value f'''_k on the k -th span $t \in [t_{k-1}, t_k]$; and (iii) $h(t_k) = 0$ for $k = 0, \dots, N$. Finally, the integral of $h''^2(t)$ from t_0 to t_N must be a positive quantity, since $h(t) \not\equiv 0$, and hence we conclude that

$$\int_{t_0}^{t_N} g''^2(t) dt > \int_{t_0}^{t_N} f''^2(t) dt. \quad \blacksquare$$

This result — that the C^2 cubic spline yields the interpolant of best *global* smoothness, in the sense of minimizing the integral (14.17) — is really quite a surprise, considering that its construction was explicitly concerned with only *local* smoothness, i.e., with C^2 continuity at the knots! It should be noted, however, that the integral (14.17) is weakly related to the “bending energy” (14.2). The nature of this relationship may be understood as follows.

The graph of a scalar function $f(t)$ may be regarded as a parametric curve $\mathbf{r}(t) = (X(t), Y(t))$ upon taking $X(t) = t$ and $Y(t) = f(t)$. The infinitesimal arc length element along this curve is

$$ds = \sqrt{X'^2(t) + Y'^2(t)} dt = \sqrt{1 + f'^2(t)} dt,$$

while its curvature is given by

$$\kappa(t) = \frac{X'(t)Y''(t) - X''(t)Y'(t)}{[X'^2(t) + Y'^2(t)]^{3/2}} = \frac{f''(t)}{[1 + f'^2(t)]^{3/2}}.$$

Substituting into (14.2), we see that the bending energy integral becomes

$$U = \int_{t_0}^{t_N} \frac{f''^2(t)}{[1 + f'^2(t)]^{5/2}} dt.$$

Hence, the quantity (14.17) that the spline function $f(t)$ minimizes is a fair approximation of the true bending energy (14.2) only when the condition

$$|f'(t)| \ll 1 \quad \text{for } t \in [t_0, t_N]$$

holds. Functions satisfying this are said to be in the *small-slope regime*.

The fact that the C^2 cubic spline interpolates the prescribed data with the minimum possible value of (14.17) can also be deduced directly by variational arguments. A function $f(t)$ that minimizes an integral of the form

$$I = \int_a^b \Phi(t, f, f', f'') dt,$$

where Φ is a specified function of the independent variable t and the sought-after function f and its first and second derivatives f' , f'' must satisfy [45] the *Euler–Lagrange equation*

$$\frac{\partial \Phi}{\partial f} - \frac{d}{dt} \frac{\partial \Phi}{\partial f'} + \frac{d^2}{dt^2} \frac{\partial \Phi}{\partial f''} = 0,$$

which amounts to an ordinary differential equation for f . In the case of the integral (14.17) we evidently have $\partial \Phi / \partial f = \partial \Phi / \partial f' = 0$ and $\partial \Phi / \partial f'' = 2f''$, and hence this differential equation reduces to

$$\frac{d^4 f}{dt^4} = 0. \quad (14.18)$$

The most general solution to this equation is a piecewise-cubic function, and the requirement that f should interpolate the prescribed data and maintain C^2 continuity at the nodes identifies the cubic spline as the *unique* piecewise-cubic function minimizing (14.17). Equation (14.18) leads us back to our initial physical interpretation of spline functions, as characterizing the shape of bent elastic beams (in the regime of small deflections, at least). From elementary “strength of materials” [126] we know that this equation governs the shape of a beam whose ends are subject to certain constraints but has no other loading along its length, i.e., the “end conditions” completely determine the deflected beam shape. Actually, cubic splines describe a much broader class of beam bending problems, in which we allow “point loads” at discrete positions along the length of the beam, in addition to the end constraints.

14.4.6 Spline Approximation Convergence

In certain contexts one may be interested in a function $F(t)$ that is expensive to evaluate — e.g., it might be defined by a slowly-converging infinite series. Alternatively, values of $F(t)$ may be available only at discrete points, although it is known that the function varies smoothly between those points. In such instances, the use of a spline to *approximate* $F(t)$ may be contemplated.

Clearly, the question of the accuracy — and rate of convergence — of such spline approximations is of interest. We consider this only in the simplest case, namely, the use of a complete cubic spline $f(t)$ to approximate a function $F(t)$, defined on $t \in [0, 1]$ say, by interpolating equidistant values $f_k = F(k/N)$ for $k = 0, \dots, N$ and end-derivatives $d_0 = F'(0)$, $d_N = F'(1)$. In this case, it can be shown [116] that a bound on the approximation error may be expressed in terms of the largest magnitude of the fourth derivative of $F(t)$ as

$$\max_{t \in [0, 1]} |f(t) - F(t)| \leq \frac{5}{384} \frac{1}{(N-1)^4} \max_{t \in [0, 1]} |F^{(4)}(t)|.$$

Whether or not one can establish a reasonable bound on $|F^{(4)}(t)|$ depends on the specific context. The above formula does, however, illustrate the expected rate of convergence of the spline approximation to $F(t)$ as the number N of sample values increases — doubling N yields (at least) a 16-fold reduction in the maximum error.

14.5 C^2 Cubic Spline Curves

The ideas discussed above, in the context of scalar spline functions, extend in a straightforward manner to *parametric spline curves* in two, three, or more dimensions. One simply replaces the scalar function values f_0, \dots, f_N that are to be interpolated with points $\mathbf{q}_0, \dots, \mathbf{q}_N$. Thus, the C^2 continuity conditions (14.13) now become *vector* equations,

$$\begin{aligned} & \Delta t_{k+1} \mathbf{d}_{k-1} + 2(\Delta t_k + \Delta t_{k+1}) \mathbf{d}_k + \Delta t_k \mathbf{d}_{k+1} \\ &= 3 \left[\Delta t_k \frac{\mathbf{q}_{k+1} - \mathbf{q}_k}{\Delta t_{k+1}} + \Delta t_{k+1} \frac{\mathbf{q}_k - \mathbf{q}_{k-1}}{\Delta t_k} \right] \end{aligned}$$

for $k = 1, \dots, N-1$, where $\mathbf{d}_0, \dots, \mathbf{d}_N$ are unknown parametric derivatives — or “tangent vectors” — at the nodes. The various end conditions discussed in §14.4.3 are likewise interpreted as vector equations.

The system of vector linear equations that defines a parametric spline curve with given end conditions is solved component-wise. Thus, the interpolation of points $\mathbf{q}_0, \dots, \mathbf{q}_N$ at parameter values t_0, \dots, t_N by a spline curve amounts essentially to constructing independent scalar spline functions $x(t), y(t), \dots$ that interpolate the *coordinate components* $x_0, \dots, x_N, y_0, \dots, y_N, \dots$ of those

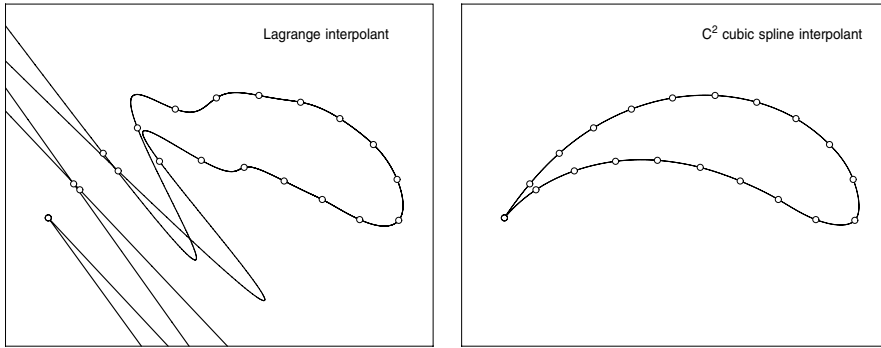


Fig. 14.3. Comparison of Lagrange polynomial and C^2 cubic spline (with quadratic end segments) interpolants to a sequence of points sampled from an airfoil section.

points. The “coupling” between the component spline functions $x(t), y(t), \dots$ is only through the parameter values t_0, \dots, t_N assigned to $\mathbf{q}_0, \dots, \mathbf{q}_N$. Once the derivative vectors $\mathbf{d}_0, \dots, \mathbf{d}_N$ are determined, each span k of the spline curve can be expressed as a cubic Hermite arc of the form

$$\mathbf{r}_k(\tau) = \mathbf{q}_{k-1}\alpha_0(\tau) + \mathbf{q}_k\alpha_1(\tau) + \Delta t_k [\mathbf{d}_{k-1}\beta_0(\tau) + \mathbf{d}_k\beta_1(\tau)] \quad (14.19)$$

in terms of the local parameter (14.6) on that span, for $k = 1, \dots, N$.

For 21 points $\mathbf{q}_0, \dots, \mathbf{q}_{20}$ sampled from an airfoil section, we compare in Fig. 14.3 the Lagrange polynomial interpolant of degree 20 and the C^2 cubic spline interpolant for the uniform knots $t_0, \dots, t_{20} = 0, \dots, 20$ and quadratic end spans (although a closed curve is indicated, with $\mathbf{q}_{20} = \mathbf{q}_0$, we do not use periodic end conditions, since a sharp trailing edge is desired). While the Lagrange interpolant exhibits the characteristic “wild oscillations,” the cubic spline yields a very smooth and plausible interpolant to the point data.

14.5.1 Choice of Knot Sequence

In the context of a parametric spline curve — as distinct from a scalar spline function — the choice of knot values t_0, \dots, t_N associated with the interpolant points $\mathbf{q}_0, \dots, \mathbf{q}_N$ is arbitrary. A specific choice must be made, however, and it can exert a significant influence on the “shape quality” of the resulting curve. If the data points have a roughly even geometric spacing, use of *uniform knots* $t_0, t_1, \dots, t_N = 0, 1, \dots, N$ generally gives satisfactory results.

For unevenly-spaced points, however, uniform knots will often give quite unacceptable results — poor shape (curvature distributions) or even “loops” between closely-spaced points.³ One approach to specifying non-uniform knot

³ These ill effects are less pronounced when there is a *gradual*, rather than sudden, change in the spacing of the interpolant points.

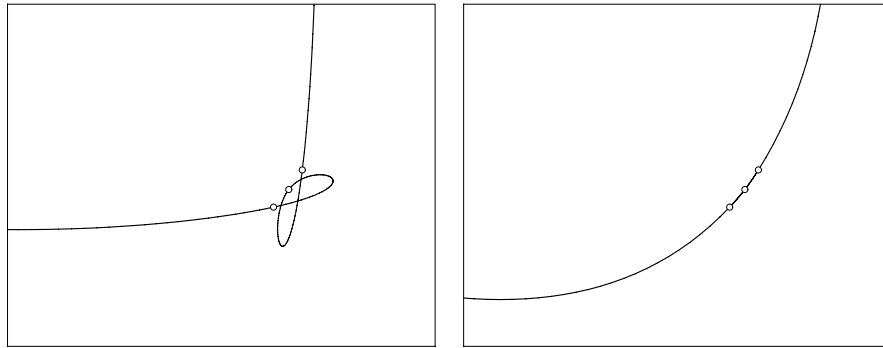


Fig. 14.4. Leading edge of the airfoil in Fig. 14.3, after introducing two closely-spaced points. The spline with uniform knots (left) incurs unacceptable loops, but using chord-length parameterization (right) yields an excellent smooth interpolant.

values t_0, \dots, t_N that offers significant improvements in such cases is the so-called *chord-length parameterization*, in which we set $t_0 = 0$ and

$$t_k = t_{k-1} + |\mathbf{q}_k - \mathbf{q}_{k-1}| \quad (14.20)$$

for $k = 1, \dots, N$ — i.e., the increment in the parameter t between successive points is equal to the straight-line distance between them. To illustrate the importance of choosing appropriate knots for non-uniformly spaced points, we introduce two additional points to the data shown in Fig. 14.3, on either side of (and very close to) the point at the leading edge, and re-compute the spline with both uniform knots and the chord-length parameterization. While the uniform knots incur an undesirable “looping” behavior, the chord-length parameterization still produces an excellent interpolant (see Fig. 14.4).

14.5.2 Parametric or Geometric Continuity

Our formulation of scalar C^2 cubic spline functions was based on guaranteeing continuity of the value and the first and second derivatives, as expressed by equations (14.11) and (14.12). A parametric spline curve can be regarded as a vector-valued spline function, and it is actually not essential that each of its coordinate components have precisely matched derivatives at every interior node in order for the curve to “appear” smooth — weaker conditions, which permit extra degrees of freedom, will suffice. Consider the case of a planar cubic spline curve. If $\mathbf{r}'_1, \mathbf{r}''_1$ and $\mathbf{r}'_0, \mathbf{r}''_0$ are the first and second parametric derivatives to the left and right of a given node, then the conditions

$$\mathbf{r}'_0 = \mathbf{r}'_1 \quad \text{and} \quad \mathbf{r}''_0 = \mathbf{r}''_1 \quad (14.21)$$

will certainly guarantee equality of the unit tangents $\mathbf{t}_i = \mathbf{r}'_i / |\mathbf{r}'_i|$ and signed curvatures $\kappa_i = (\mathbf{r}'_i \times \mathbf{r}''_i) \cdot \mathbf{z} / |\mathbf{r}'_i|^3$ to the left ($i = 1$) and right ($i = 0$) of that

node. The two conditions (14.21) are sufficient, but not necessary, for the unit tangent and signed curvature to be continuous across the node — which is all that is required for the curve to possess second-order “geometric” or “visual” (rather than *parametric*) continuity at this node.

In fact, if $\lambda (> 0)$ and μ are arbitrary real numbers, one can easily verify that conditions (14.21) may be generalized to

$$\mathbf{r}'_0 = \lambda \mathbf{r}'_1 \quad \text{and} \quad \mathbf{r}''_0 = \lambda^2 \mathbf{r}''_1 + \mu \mathbf{r}'_1 \quad (14.22)$$

without compromising the requirement that $\mathbf{t}_0 = \mathbf{t}_1$ and $\kappa_0 = \kappa_1$. Thus, we may associate “shape parameters” λ and μ with each node, that afford the possibility of manipulating the curve shape without affecting its intrinsic or *geometric* continuity. The exploitation of these additional degrees of freedom is the basis of the *beta splines* [29] introduced by B.J. Barsky.

A spline curve that satisfies the conditions (14.22), rather than (14.21), is said to exhibit G^2 — rather than C^2 — continuity. We can also generalize the idea of geometric continuity to higher orders, and to space curves in three or more dimensions. In the context of parametric surfaces, however, a complete characterization of the extra freedoms obtained by relaxing from parametric to geometric continuity is much harder to formulate.

14.5.3 Geometric Hermite Interpolation

There is a unique cubic $\mathbf{r}(t)$ that interpolates prescribed end points $\mathbf{r}(0)$, $\mathbf{r}(1)$ and parametric derivatives $\mathbf{r}'(0)$, $\mathbf{r}'(1)$ at those points. Such interpolants, in the form (14.19), are the basic elements of cubic splines. In constructing spline curves, the premise is that the points $\mathbf{q}_0, \dots, \mathbf{q}_N$ but no other geometrical data are specified. Nevertheless, as noted in §14.5.1, one must also define the knots t_0, \dots, t_N , which may significantly influence the shape of the spline.

In some applications, geometrical data in addition to the points $\mathbf{q}_0, \dots, \mathbf{q}_N$ — unit tangents, curvatures, etc. — may be available, that one also desires to interpolate. For example, one may need to approximate a non-rational curve (with a known analytic or procedural definition) by a piecewise-rational form for representation within a CAD system. Local schemes, based on the use of *geometric Hermite interpolants*, are suitable for such purposes.

Such interpolants match only *intrinsic geometrical data* sampled from the hypothetical underlying curve — all information about the *parameterization* of that curve is suppressed. For example, one may specify tangent *directions* but not tangent *vectors* (i.e., parametric derivatives with both direction and magnitude). For interpolants of a prescribed degree, this parameterization-independent approach releases further degrees of freedom in the interpolation process, yielding a faster (limiting) convergence to the underlying curve — but at the cost of requiring non-linear systems to be solved, with consequent issues concerning the existence and uniqueness of interpolants.

The simplest case is for G^1 interpolation of a sequence of points $\mathbf{q}_0, \dots, \mathbf{q}_N$ together with *unit* tangents $\mathbf{t}_0, \dots, \mathbf{t}_N$. In the planar case, piecewise-parabolic

curves suffice. Specifically, for the first parabolic segment, the Bézier control polygon has endpoints $\mathbf{p}_0 = \mathbf{q}_0$ and $\mathbf{p}_2 = \mathbf{q}_1$, while the middle point \mathbf{p}_1 is the intersection of lines through \mathbf{q}_0 and \mathbf{q}_1 along \mathbf{t}_0 and \mathbf{t}_1 , namely

$$\mathbf{p}_1 = \mathbf{q}_0 + \frac{\mathbf{t}_1 \times (\mathbf{q}_1 - \mathbf{q}_0) \cdot \mathbf{z}}{(\mathbf{t}_1 \times \mathbf{t}_0) \cdot \mathbf{z}} \mathbf{t}_0 = \mathbf{q}_1 - \frac{\mathbf{t}_0 \times (\mathbf{q}_1 - \mathbf{q}_0) \cdot \mathbf{z}}{(\mathbf{t}_0 \times \mathbf{t}_1) \cdot \mathbf{z}} \mathbf{t}_1,$$

where \mathbf{z} is a unit vector orthogonal to the plane. Clearly, when $\mathbf{t}_0 \times \mathbf{t}_1 \neq \mathbf{0}$, a unique interpolant exists. Each segment k interpolating the data $\mathbf{q}_{k-1}, \mathbf{t}_{k-1}$ and $\mathbf{q}_k, \mathbf{t}_k$ for $k = 1, \dots, N$ is constructed in a similar “local” fashion. Setting

$$h = \max_{1 \leq k \leq N} |\mathbf{q}_k - \mathbf{q}_{k-1}|,$$

it can be shown that, when the data are sampled from an analytic curve, the piecewise-parabolic approximant exhibits an $O(h^4)$ convergence to that curve. This is the same rate as given by a C^2 cubic spline curve, based on *parametric* Hermite interpolation of point data only (note also that constructing the latter is a global rather than a local “span-by-span” problem).

A more-challenging problem arises if we also append (signed) curvatures $\kappa_0, \dots, \kappa_N$ to the points/tangents, and seek a G^2 interpolant to the augmented data. Under suitable conditions, this can be achieved by piecewise-cubic loci [117] that have $O(h^6)$ convergence to an underlying analytic curve, from which the discrete data is sampled. Writing the Bézier control points $\mathbf{p}_0, \mathbf{p}_1, \mathbf{p}_2, \mathbf{p}_3$ of the cubic span interpolating the data $\mathbf{q}_0, \mathbf{t}_0, \kappa_0$ and $\mathbf{q}_1, \mathbf{t}_1, \kappa_1$ as

$$\mathbf{p}_0 = \mathbf{q}_0, \quad \mathbf{p}_1 = \mathbf{q}_0 + \ell_0 \mathbf{t}_0, \quad \mathbf{p}_2 = \mathbf{q}_1 - \ell_1 \mathbf{t}_1, \quad \mathbf{p}_3 = \mathbf{q}_1,$$

one finds that ℓ_0 and ℓ_1 must satisfy the system of quadratic equations

$$\begin{aligned} 3\kappa_0 \ell_0^2 + 2(\mathbf{t}_0 \times \mathbf{t}_1) \cdot \mathbf{z} \ell_1 - 2[\mathbf{t}_0 \times (\mathbf{q}_1 - \mathbf{q}_0)] \cdot \mathbf{z} &= 0, \\ 3\kappa_1 \ell_1^2 + 2(\mathbf{t}_0 \times \mathbf{t}_1) \cdot \mathbf{z} \ell_0 - 2[(\mathbf{q}_1 - \mathbf{q}_0) \times \mathbf{t}_1] \cdot \mathbf{z} &= 0. \end{aligned}$$

The solutions of these equations correspond to the intersection points of two parabolas in the (ℓ_0, ℓ_1) -plane, and only real solutions for ℓ_0 and ℓ_1 that are both positive define valid interpolants.

de Boor, Höllig, and Sabin [117] show that, when $\mathbf{t}_0 \times \mathbf{t}_1 \neq \mathbf{0}$, the number of such solutions can be characterized in terms of the parameters

$$R_0 = \frac{3}{2} \frac{\kappa_0 |(\mathbf{q}_1 - \mathbf{q}_0) \times \mathbf{t}_1|^2}{|\mathbf{t}_0 \times \mathbf{t}_1|^2 [\mathbf{t}_0 \times (\mathbf{q}_1 - \mathbf{q}_0)] \cdot \mathbf{z}}, \quad R_1 = \frac{3}{2} \frac{\kappa_1 |\mathbf{t}_0 \times (\mathbf{q}_1 - \mathbf{q}_0)|^2}{|\mathbf{t}_0 \times \mathbf{t}_1|^2 [(\mathbf{q}_1 - \mathbf{q}_0) \times \mathbf{t}_1] \cdot \mathbf{z}}.$$

If $[\mathbf{t}_0 \times (\mathbf{q}_1 - \mathbf{q}_0)] \cdot \mathbf{z}$, $[(\mathbf{q}_1 - \mathbf{q}_0) \times \mathbf{t}_1] \cdot \mathbf{z}$, and $(\mathbf{t}_0 \times \mathbf{t}_1) \cdot \mathbf{z}$ are all of the same sign, a sufficient criterion for a unique solution is that $R_0 > 1$ and $R_1 > 1$ — see [117] for further details.

Degen [122] has described a Hermite interpolant, based on rational cubics, that exhibits *third*-order geometric contact with a given curve at two points — giving $O(h^8)$ convergence to that curve under suitable conditions. In general, for approximants that have G^k contact at the endpoints of segments of length h of a given curve, the limiting convergence rate [122] is $O(h^{2k+2})$. Geometric Hermite interpolation schemes for space curves are also available [244].

In practice, the principal difficulty with higher-order geometric Hermite interpolation schemes is the necessity of solving coupled non-linear equations in their construction, and coping with the resulting possibility of an absence or multiplicity of real solutions under certain conditions.

14.5.4 Elastica or “Non-linear” Splines

In §14.4.5 we remarked that C^2 cubic spline curves minimize an *approximation* to the bending energy integral (14.2) — accurate in the “small slope” regime. For strongly-curved loci, however, this approximation may not be a reliable indicator of curve shape. It is therefore of interest to consider the construction of loci that minimize (14.2), subject to given interpolation constraints, from first principles. The first systematic treatment of this problem, by the Swiss mathematician Leonhard Euler (1707–1783), was presented in the appendix “*De curvis elasticis*” to *Methodus inveniendi lineas curvas maximi minimive proprietate gaudentes* (1744), a treatise on the calculus of variations.⁴

For brevity, we consider only the problem of constructing such an *elastica* between given end-points $\mathbf{q}_0, \mathbf{q}_1$ with end-tangent specified by angles θ_0, θ_1 at those points.⁵ If $\mathbf{r}(s)$ is the arc-length parameterization of such a curve, the first derivative is a unit vector,

$$\mathbf{r}'(s) = (\cos \theta(s), \sin \theta(s)) \quad (14.23)$$

where the angle function $\theta(s)$ represents the orientation of the curve tangent — its derivative is the curvature

$$\theta'(s) = \kappa(s)$$

of $\mathbf{r}(s)$. Our goal is to seek a differential equation for $\kappa(s)$, since this function (together with the end conditions) completely defines the desired curve.

We thus seek to minimize

$$U = \int_0^S \kappa^2 \, ds, \quad (14.24)$$

where S denotes the total (unconstrained) length of the curve, subject to the interpolation conditions $\mathbf{r}(0) = \mathbf{q}_0, \theta(0) = \theta_0$ and $\mathbf{r}(S) = \mathbf{q}_1, \theta(S) = \theta_1$. It is convenient to cast the constrained problem of minimizing (14.24) subject

⁴ For a summary of the rich history of “elastic curves” see Chap. 2 of [440].

⁵ For the case of non-linear splines interpolating a sequence of points, see [303].

to these conditions in terms of $\theta(s)$. Thus we set $\kappa(s) = \theta'(s)$ in (14.24) and, using (14.23), express the positional constraints in the integral form

$$\int_0^S \cos \theta(s) \, ds = \Delta x, \quad \int_0^S \sin \theta(s) \, ds = \Delta y,$$

where $\mathbf{q}_1 - \mathbf{q}_0 = \Delta \mathbf{q} = (\Delta x, \Delta y)$. Introducing the Lagrange undetermined multipliers λ and μ , we then seek the function $\theta(s)$ that minimizes

$$\int_0^S F(s, \theta, \theta') \, ds$$

with $\theta(0) = \theta_0$ and $\theta(S) = \theta_1$, where

$$F(s, \theta, \theta') = \theta'^2 + \lambda(\cos \theta - \Delta x/S) + \mu(\sin \theta - \Delta y/S).$$

With this integrand, the Euler–Lagrange equation

$$\frac{\partial F}{\partial \theta} - \frac{d}{ds} \frac{\partial F}{\partial \theta'} = 0$$

for the variational problem [45] yields

$$-\lambda \sin \theta + \mu \cos \theta - 2\theta'' = 0. \quad (14.25)$$

We can eliminate λ and μ from (14.25), and transform it into an equation for $\kappa(s)$, as follows. With $2\ell = \sqrt{\lambda^2 + \mu^2}$ and $\phi = \tan^{-1}(\mu/\lambda)$, we may write

$$\theta'' = -\ell \sin(\theta - \phi) = \kappa'. \quad (14.26)$$

Multiplying both sides by θ' and integrating with respect to s then gives

$$\theta'^2 = 2\ell \cos(\theta - \phi) + c = \kappa^2, \quad (14.27)$$

where c is an integration constant. Now by differentiating (14.26) we see that $\ell \cos(\theta - \phi) = -\kappa''/\kappa$, and substituting this into (14.27) gives the second-order non-linear differential equation

$$\kappa'' + \frac{1}{2} \kappa^3 - \frac{1}{2} c \kappa = 0 \quad (14.28)$$

for $\kappa(s)$. The appearance of the arbitrary constant c in this equation suggests the existence of a multiplicity of solutions to the elastica problem.

However, Brunnett [67] has shown that c must be set to zero for solutions of (14.28) to identify true minima of the integral (14.24): this condition arises from the fact that the domain of integration $[0, S]$ was not fixed *a priori*, but may also vary in the minimization of the energy integral. As noted by Birkhoff and de Boor [43], loci that minimize (14.24) need not be of finite length — one may have large “loops” of length $S \sim 2\pi r$ and curvature $\kappa \sim 1/r$ interpolating the given end points and slopes, such that $U \rightarrow 0$ as $r \rightarrow \infty$. One remedy for

this is to specify the total length S as an additional constraint in the energy minimization. Alternately, the energy integral (14.24) may be modified to

$$\tilde{U} = \int_0^S \kappa^2 + \sigma \, ds$$

where the positive constant σ is a “tension” parameter that may be regarded as representing an energy of “stretching” of the elastica — it penalizes loci of greater total length S . It can be shown [67] that minima of \tilde{U} are identified by solutions to equation (14.28) with $c = \sigma$.

Unfortunately the differential equation (14.28) does not, in general, admit elementary solutions compatible with the native polynomial/rational curves of most CAD systems. However, $\kappa(s)$ can be expressed in terms of the *Jacobian elliptic function* $\text{cn}(k, z)$ with modulus k and argument z , defined in terms of the incomplete elliptic integral of the first kind

$$z = \int_0^\phi \frac{d\theta}{\sqrt{1 - k^2 \sin^2 \theta}}$$

as follows [299]: for each $k \leq 1$ and z , its value is the cosine of the upper limit of integration ϕ that causes the above equation to hold:

$$\text{cn}(k, z) = \cos \phi.$$

The solutions $\kappa(s)$ to the elastica equation (14.28) with $c = 0$ may be expressed in the “implicit” form

$$\int_{\kappa_{\max}}^{\kappa} \frac{d\kappa}{\sqrt{1 - (\kappa/\kappa_{\max})^4}} = \pm \frac{\kappa_{\max}^2}{2} (s - s_{\max}),$$

κ_{\max} being the global maximum of $\kappa(s)$, at $s = s_{\max}$ (note that $\kappa'(s_{\max}) = 0$, and that κ must be real for all s). By substituting $\cos \theta = \kappa/\kappa_{\max}$ above, one can then write $\kappa(s)$ in the “explicit” form

$$\kappa(s) = \kappa_{\max} \text{cn}\left(\sqrt{\frac{1}{2}}, \sqrt{\frac{1}{2}} \kappa_{\max} (s - s_{\max})\right).$$

We refer the reader to the extensive literature on elastica [64, 68, 69, 257–259, 271, 303, 309, 316, 324] for further details.

Spline Basis Functions

The number of the dimensions of a linear system is the maximal number of linearly independent objects in the system.

Giuseppe Peano (1858–1932)

Constructing a spline curve that interpolates an ordered sequence of points is a relatively simple matter, involving only the solution of tridiagonal linear systems. Constructing a spline *surface* that interpolates an *array* of points is a much more challenging problem — such a surface comprises a network of “patches,” and we must guarantee second-order continuity along the common boundary curves of every pair of adjacent patches. Attempting to formulate and solve systems of equations that express these continuity constraints is an exceedingly cumbersome and unrewarding task. However, we shall see below that the expression of spline functions in terms of *spline bases* offers an elegant and easily-implemented solution to this problem.

15.1 Bases for Spline Functions

The set \mathcal{S} of all C^2 cubic spline functions with specified end conditions on a given knot sequence t_0, \dots, t_N forms a *vector space*¹ of dimension $N + 1$. This means that, if $f(t)$ and $g(t)$ are both members of \mathcal{S} , the linear combination

$$h(t) = \lambda f(t) + \mu g(t)$$

is also a member of \mathcal{S} , for any real numbers λ and μ . Further, if $f(t)$ and $g(t)$ interpolate f_0, \dots, f_N and g_0, \dots, g_N , then $h(t)$ interpolates the values

$$h_j = \lambda f_j + \mu g_j, \quad j = 0, \dots, N.$$

¹ Here “vector” is interpreted in the abstract sense of linear algebra [241], rather than the usual notion of a vector with Cartesian coordinate components.

The vector space \mathcal{S} is *spanned* by any set of $N+1$ *linearly independent* splines $f_0(t), \dots, f_N(t)$ — i.e., any spline $f(t) \in \mathcal{S}$ may be expressed in the form

$$f(t) = \sum_{j=0}^N c_j f_j(t)$$

by a suitable choice of coefficients c_0, \dots, c_N . Thus, we call $f_0(t), \dots, f_N(t)$ a *basis* for the spline space \mathcal{S} . The stipulation that the members of the basis be linearly independent means that

$$c_0 f_0(t) + \cdots + c_N f_N(t) \equiv 0 \iff c_0 = \cdots = c_N = 0. \quad (15.1)$$

There is a *one-to-one correspondence* between sets of coefficients (c_0, \dots, c_N) and spline functions $f(t) \in \mathcal{S}$, and we say that the coefficients (c_0, \dots, c_N) of $f(t)$ uniquely *represent* this spline function as a member of \mathcal{S} .

There are many possible bases for the set of spline functions on specified knots t_0, \dots, t_N that incorporate prescribed end conditions. Like the various *polynomial* bases that we have discussed (Bernstein, Lagrange, Hermite, etc.) the spline bases that are in widespread use offer special advantages in terms of simplifying problem formulations or facilitating computations.

We are concerned with just two spline bases here: the *B-spline basis* and the *cardinal basis* — which exhibit, respectively, many of the useful features associated with the Bernstein and Lagrange polynomial bases, in the context of *piecewise-polynomial* functions. We defer discussion of B-splines to §15.3 (see also §15.4 for details on converting between the two bases), and focus at present on using the cardinal basis in problems of spline interpolation.

15.2 The Cardinal Basis

Suppose we wish to interpolate many different data sets f_0, \dots, f_N using C^2 cubic splines $f(t)$ with specified end conditions. Clearly, we can just follow the methods of §14.4 for setting up and solving the appropriate system of linear equations with each new data set. But this seems quite wasteful, since the same types of calculations are performed repeatedly. The idea behind the cardinal basis is to *pre-compute* and store a set $\phi_0(t), \dots, \phi_N(t)$ of spline functions, with the desired end conditions, that will allow us to simply “write down” the spline interpolant for each new data set, without any further computation.

15.2.1 Construction of Cardinal Basis

For given end conditions, the cardinal spline basis functions $\phi_0(t), \dots, \phi_N(t)$ on the knots t_0, \dots, t_N are characterized by the following properties

$$\begin{aligned}
\phi_0(t) &\text{ interpolates } 1, 0, 0, \dots, 0 \text{ at } t_0, t_1, t_2, \dots, t_N \\
\phi_1(t) &\text{ interpolates } 0, 1, 0, \dots, 0 \text{ at } t_0, t_1, t_2, \dots, t_N \\
&\dots \\
\phi_N(t) &\text{ interpolates } 0, 0, 0, \dots, 1 \text{ at } t_0, t_1, t_2, \dots, t_N
\end{aligned} \tag{15.2}$$

— i.e., we have

$$\phi_j(t_k) = \delta_{jk} \quad \text{for } 0 \leq j, k \leq N. \tag{15.3}$$

Then for any data set f_0, \dots, f_N the unique C^2 cubic spline interpolant $f(t)$ can be immediately identified as

$$f(t) = \sum_{j=0}^N f_j \phi_j(t). \tag{15.4}$$

We observe that the conditions (15.2) guarantee that (15.1) is satisfied — the only way we can make $c_0\phi_0(t) + \dots + c_N\phi_N(t)$ vanish at *every* knot is to choose $c_0 = \dots = c_N = 0$. Hence, we can be sure that the splines $\phi_0(t), \dots, \phi_N(t)$ with the nodal values (15.2) do indeed form a basis. We shall call this basis the *cardinal basis*² for the nodes t_0, \dots, t_N and the given end conditions: it may be regarded as the spline analog of the Lagrange basis (14.3) for interpolation by degree- N polynomials at those nodes — see Fig. 15.1.

Note that the result (15.4) of expressing the spline interpolant in terms of the pre-computed cardinal basis is *exactly the same* as what would have been obtained by working through the procedure described in §14.4 with the given values f_0, \dots, f_N — the one-to-one correspondence of spline functions and their coefficients in a suitable basis guarantees this. Of course, this principle generalizes readily from the scalar function context to that of a parametric spline curve interpolating given points $\mathbf{q}_0, \dots, \mathbf{q}_N$:

$$\mathbf{r}(t) = \sum_{j=0}^N \mathbf{q}_j \phi_j(t). \tag{15.5}$$

We can also construct a cardinal basis for “complete” splines that permits interpolation of end-derivatives, d_0 and d_N , as well as the values f_0, \dots, f_N at t_0, \dots, t_N instead of incorporating given end conditions into the spline basis functions. In this context $\phi_0(t), \dots, \phi_N(t)$ again have the nodal values (15.2), but we now require that their end-derivatives vanish,

$$\phi'_j(t_0) = \phi'_j(t_N) = 0, \quad j = 0, \dots, N.$$

Two additional basis functions are needed, $\varphi_0(t)$ and $\varphi_N(t)$, characterized by the following properties. Both vanish at *every* knot t_0, \dots, t_N , and they have

² The term “cardinal” is used with a different connotation by some authors — for example, de Boor [116] refers to splines defined on *equidistant* knots, rather than those satisfying the interpolatory condition (15.3), as “cardinal splines.”

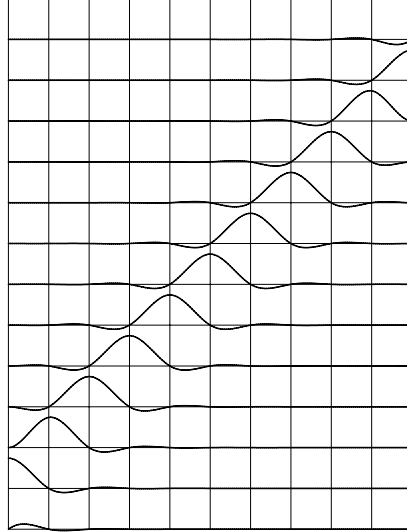


Fig. 15.1. Complete cardinal spline basis on a set of equidistant nodes. The first and last basis functions vanish at every node, and have unit derivative at one end-node and zero derivative at the other end-node. All the other functions are non-zero at just one distinct node, with zero derivatives at both the end-nodes.

the end-derivatives $\varphi'_0(t_0) = 1$, $\varphi'_0(t_N) = 0$ and $\varphi'_N(t_0) = 0$, $\varphi'_N(t_N) = 1$. The (unique) complete spline interpolant to the data f_0, \dots, f_N and d_0, d_N can then be expressed as

$$f(t) = d_0\varphi_0(t) + \sum_{j=0}^N f_j\phi_j(t) + d_N\varphi_N(t).$$

Note that the space of *complete* splines on the knots t_0, \dots, t_N has dimension $N + 3$ (rather than $N + 1$ for the case of prescribed end conditions).

The pre-computation of the cardinal basis amounts to working through the method of §14.4 with the values (15.2) appropriate to each basis function. Thus, the cost-effectiveness of this approach will be fully realized only when the number of data sets f_0, \dots, f_N to be interpolated exceeds N substantially. Actually, the advantage of the cardinal spline basis is not so much (as discussed above) one of computational efficiency — in practice the time saved is rather modest — but rather in providing an elegant conceptual framework for spline interpolation problems, and especially in formulating their generalization to the multivariate (tensor-product) case, as we shall now see.

15.2.2 Bivariate Spline Functions

We consider first the problem of interpolating an array of values in the scalar (bivariate function) context before turning to the vector (parametric surface)

case. A bivariate form of the spline interpolation problem discussed in §14.4 can be phrased as follows. Given sets of nodal values u_0, \dots, u_M and v_0, \dots, v_N defining a grid over the rectangular domain $(u, v) \in [u_0, u_M] \times [v_0, v_N]$ and a corresponding array of function values f_{jk} at the grid points (u_j, v_k) for $0 \leq j \leq M$ and $0 \leq k \leq N$, we seek a function $f(u, v)$ that will “smoothly” — in both the local and global sense — interpolate this data.

Attempting to accomplish this by means of a single bivariate polynomial usually leads, as in the univariate case, to unsatisfactory results in terms of the “global” smoothness. We therefore seek a method to smoothly piece together a set of $M \times N$ bivariate polynomial “patches”

$$p_{jk}(u, v) \quad \text{for } (u, v) \in [u_{j-1}, u_j] \times [v_{k-1}, v_k] \quad (15.6)$$

defined on each rectangular subregion of the complete domain, $j = 1, \dots, M$ and $k = 1, \dots, N$, such that the interpolation constraints are satisfied and the resulting piecewise-polynomial function $f(u, v)$ is globally smooth.

This problem is rather more subtle than univariate spline interpolation, as it involves matching values and partial derivatives of the polynomial pieces (15.6) along the *boundaries* of each subdomain, not just at discrete points. A naive direct formulation of the desired continuity conditions, for each of the $2MN - M - N$ “interior” boundaries between adjacent patches, leads to a very unwieldy and impractical system of linear equations. The cardinal-basis approach, however, yields a very simple and elegant solution.

Suppose that $\phi_0(u), \dots, \phi_M(u)$ and $\psi_0(v), \dots, \psi_N(v)$ are cardinal bases constructed on the knot sets u_0, \dots, u_M and v_0, \dots, v_N according to specified end conditions. Then, by virtue of the fact that

$$\phi_j(u_l) = \delta_{jl} \quad \text{and} \quad \psi_k(v_m) = \delta_{km}$$

for $0 \leq j, l \leq M$ and $0 \leq k, m \leq N$, the piecewise-polynomial function

$$f(u, v) = \sum_{j=0}^M \sum_{k=0}^N f_{jk} \phi_j(u) \psi_k(v) \quad (15.7)$$

clearly interpolates the given values: $f(u_j, v_k) = f_{jk}$. Expression (15.7) is the (unique) *tensor-product bicubic spline interpolant* to the given data.

The term “tensor-product” is widely used, although it has no connection with the definition and transformation properties of tensors (see Chap. 10). It refers merely to the fact that the quantities $\phi_j(u)\psi_k(v)$ in (15.7) may be regarded as a basis for the space of *bivariate* splines on the given grid, formed from the *products* of univariate spline basis functions on the knots u_0, \dots, u_M and v_0, \dots, v_N defining that grid. The spline function $f(u, v)$ is *bicubic* because each “patch” (15.6) is cubic in u and v individually — i.e., the highest-order terms are of the form $u^3 v^3$.

Since the bases $\phi_0(u), \dots, \phi_M(u)$ and $\psi_0(v), \dots, \psi_N(v)$ are both C^2 , each partial derivative $\partial^{r+s}f/\partial u^r\partial v^s$ of the function (15.7) with $r, s \leq 2$ is clearly continuous. We say that $f(u, v)$ is of continuity class C_2^4 — i.e., all its partial derivatives of order ≤ 4 involving no more than two-fold differentiation with respect to either variable are continuous. This ensures “local” smoothness of $f(u, v)$ across the boundaries of all adjacent patches. The interpolant (15.7) also exhibits “global” smoothness, in the sense of the following generalization of Theorem 14.1: among all C_2^4 functions that interpolate

- the function values f_{jk} at the grid points (u_j, v_k) of the domain $(u, v) \in [u_0, u_M] \times [v_0, v_N]$ for $j = 0, \dots, M$ and $k = 0, \dots, N$;
- cross-boundary derivatives at the boundary grid points of this domain, i.e., f_u values at (u_0, v_k) and (u_M, v_k) for $k = 0, \dots, N$, and f_v values at (u_j, v_0) and (u_j, v_N) for $j = 0, \dots, M$;
- and the mixed second derivative values f_{uv} at the four extreme corners $(u_0, v_0), (u_0, v_N), (u_M, v_0), (u_M, v_N)$ of the domain;

the bicubic tensor product spline (15.7) is the one that exhibits the lowest possible value of the integral

$$\int_{u_0}^{u_M} \int_{v_0}^{v_N} \left[\frac{\partial^4 f}{\partial u^2 \partial v^2} \right]^2 du dv. \quad (15.8)$$

It is convenient to use a matrix form for each patch of the tensor-product spline function $f(u, v)$. Defining “local” variables for patch (j, k) by

$$\mu = \frac{u - u_{j-1}}{u_j - u_{j-1}} \quad \text{and} \quad \nu = \frac{v - v_{k-1}}{v_k - v_{k-1}} \quad (15.9)$$

so $(\mu, \nu) \in [0, 1] \times [0, 1]$, this patch may be expressed in terms of the matrix

$$\mathbf{M}_{jk} = \begin{bmatrix} f(0, 0) & \Delta v_k f_v(0, 0) & \Delta v_k f_v(0, 1) & f(0, 1) \\ \Delta u_j f_u(0, 0) & \Delta u_j \Delta v_k f_{uv}(0, 0) & \Delta u_j \Delta v_k f_{uv}(0, 1) & \Delta u_j f_u(0, 1) \\ \Delta u_j f_u(1, 0) & \Delta u_j \Delta v_k f_{uv}(1, 0) & \Delta u_j \Delta v_k f_{uv}(1, 1) & \Delta u_j f_u(1, 1) \\ f(1, 0) & \Delta v_k f_v(1, 0) & \Delta v_k f_v(1, 1) & f(1, 1) \end{bmatrix}$$

and the cubic Hermite basis vectors $\mathbf{h}(\mu) = [\alpha_0(\mu) \ \beta_0(\mu) \ \beta_1(\mu) \ \alpha_1(\mu)]^T$ and $\mathbf{h}(\nu) = [\alpha_0(\nu) \ \beta_0(\nu) \ \beta_1(\nu) \ \alpha_1(\nu)]^T$ in these local variables as

$$p_{jk}(\mu, \nu) = \mathbf{h}^T(\mu) \mathbf{M}_{jk} \mathbf{h}(\nu). \quad (15.10)$$

The values of f and of the partial derivatives f_u, f_v, f_{uv} in the matrix \mathbf{M}_{jk} refer to the four corners of the (j, k) -th patch, in terms of its local coordinates (15.9). Note also that the factors

$$\Delta u_j = u_j - u_{j-1} \quad \text{and} \quad \Delta v_k = v_k - v_{k-1}$$

in \mathbf{M}_{jk} arise from the derivative relations

$$\frac{d}{d\mu} = \frac{1}{\Delta u_j} \frac{d}{du} \quad \text{and} \quad \frac{d}{d\nu} = \frac{1}{\Delta v_k} \frac{d}{dv}. \quad (15.11)$$

From expression (15.10) and the form of the matrix \mathbf{M}_{jk} for patch (j, k) we observe that to represent the spline function $f(u, v)$ it suffices to store the knot sequences u_0, \dots, u_M and v_0, \dots, v_N together with the (given) f values and the f_u, f_v, f_{uv} derivative values — computed from expression (15.7) — at each of the grid points. This approach is, in fact, the *preferred* representation for $f(u, v)$ since it facilitates very efficient repeated evaluation of the spline function at arbitrary (u, v) values. By contrast, evaluating all the individual basis functions $\phi_0(u), \dots, \phi_M(u)$ and $\psi_0(v), \dots, \psi_N(v)$ and then summing the products in expression (15.7) would be very inefficient.

A noteworthy feature of the bivariate tensor–product spline function (15.7) is that its restriction to a nodal value in either of the variables u or v yields *exactly the same univariate spline function* (using the prescribed knots and end conditions) as is obtained by fitting a univariate spline to the appropriate row or column from the array of values f_{jk} for $0 \leq j \leq M$ and $0 \leq k \leq N$.

When one performs N such univariate fits in the u direction, and M in the v direction, they furnish all the nodal first derivatives f_u and f_v needed by the bivariate spline representation. What this “network–of–curves” approach lacks is a means to specify nodal values for the *mixed* second derivative, f_{uv} . In essence, the significance of the tensor–product spline formulation (15.7) is that it provides such values so as to guarantee a “globally smooth” function — in the sense of minimizing expression (15.8), that is.

15.2.3 Tensor–product Spline Surfaces

The construction of a parametric surface smoothly interpolating a *topologically rectangular* array of points, \mathbf{q}_{jk} for $0 \leq j \leq M$ and $0 \leq k \leq N$, is a trivial extension of the method described above. One simply replaces the scalar values f_{jk} in expression (15.7) by the given points, and writes

$$\mathbf{r}(u, v) = \sum_{j=0}^M \sum_{k=0}^N \mathbf{q}_{jk} \phi_j(u) \psi_k(v). \quad (15.12)$$

This defines a piecewise–polynomial surface, which may be regarded as a network of bicubic patches having matched borders and continuity of parametric derivatives (up to second order in u and v individually) across those borders. The given points correspond to corners of these patches: $\mathbf{r}(u_j, v_k) = \mathbf{q}_{jk}$.

As in the scalar case (15.7), the form (15.12) is expensive to evaluate and it is advantageous to explicitly resolve it into the constituent surface patches

by evaluating (15.12) at its derivatives \mathbf{r}_u , \mathbf{r}_v , \mathbf{r}_{uv} at the nodes. The (j, k) -th patch, for example, is represented by a matrix of the form

$$\mathbf{M}_{jk} = \begin{bmatrix} \mathbf{r}(0,0) & \mathbf{r}_v(0,0) & \mathbf{r}_v(0,1) & \mathbf{r}(0,1) \\ \mathbf{r}_u(0,0) & \mathbf{r}_{uv}(0,0) & \mathbf{r}_{uv}(0,1) & \mathbf{r}_u(0,1) \\ \mathbf{r}_u(1,0) & \mathbf{r}_{uv}(1,0) & \mathbf{r}_{uv}(1,1) & \mathbf{r}_u(1,1) \\ \mathbf{r}(1,0) & \mathbf{r}_v(1,0) & \mathbf{r}_v(1,1) & \mathbf{r}(1,1) \end{bmatrix}$$

where the patch corners are identified in terms of the local parameters (15.9), and we assume that appropriate factors of Δu_j and Δv_k are absorbed into the derivatives \mathbf{r}_u , \mathbf{r}_v , \mathbf{r}_{uv} to allow for the scaling (15.11). The mixed derivatives \mathbf{r}_{uv} at the patch corners are sometimes called *twist vectors* — as noted above, they comprise the essential data furnished by the tensor–product formulation, that cannot be deduced from univariate (curve) spline interpolation.

In terms of the matrix \mathbf{M}_{jk} , surface patch (j, k) can be expressed as

$$\mathbf{r}_{jk}(\mu, \nu) = \mathbf{h}^T(\mu) \mathbf{M}_{jk} \mathbf{h}(\nu),$$

for $(\mu, \nu) \in [0, 1] \times [0, 1]$, where $\mathbf{h}(\mu) = [\alpha_0(\mu) \ \beta_0(\mu) \ \beta_1(\mu) \ \alpha_1(\mu)]^T$ and $\mathbf{h}(\nu) = [\alpha_0(\nu) \ \beta_0(\nu) \ \beta_1(\nu) \ \alpha_1(\nu)]^T$ are again the cubic Hermite basis vectors. Alternately, we can represent this patch by its Bézier control points

$$\mathbf{P}_{jk} = \begin{bmatrix} \mathbf{p}_{00} & \mathbf{p}_{01} & \mathbf{p}_{02} & \mathbf{p}_{03} \\ \mathbf{p}_{10} & \mathbf{p}_{11} & \mathbf{p}_{12} & \mathbf{p}_{13} \\ \mathbf{p}_{20} & \mathbf{p}_{21} & \mathbf{p}_{22} & \mathbf{p}_{23} \\ \mathbf{p}_{30} & \mathbf{p}_{31} & \mathbf{p}_{32} & \mathbf{p}_{33} \end{bmatrix}$$

as

$$\mathbf{r}_{jk}(\mu, \nu) = \mathbf{b}^T(\mu) \mathbf{P}_{jk} \mathbf{b}(\nu),$$

where $\mathbf{b}(\mu) = [b_0^3(\mu) \ b_1^3(\mu) \ b_2^3(\mu) \ b_3^3(\mu)]^T$, $\mathbf{b}(\nu) = [b_0^3(\nu) \ b_1^3(\nu) \ b_2^3(\nu) \ b_3^3(\nu)]^T$ are the cubic Bernstein basis vectors, and $\mathbf{P}_{jk} = Q^T \mathbf{M}_{jk} Q$ with Q being the matrix in (3.5) that maps the cubic Bernstein basis to the cubic Hermite basis.

We need to elaborate on the stipulation that the interpolant points form a “topologically rectangular” array. This simply means that they are doubly indexed, such that one index runs through exactly the same range of integer values for each successive fixed value of the other — i.e., the points can be regarded as entries in a rectangular table

$$\begin{array}{ccccccccc} \mathbf{q}_{00} & \mathbf{q}_{01} & \cdot & \cdot & \cdot & \mathbf{q}_{0N} & & & \\ \mathbf{q}_{10} & \mathbf{q}_{11} & \cdot & \cdot & \cdot & \mathbf{q}_{1N} & & & \\ \cdot & \cdot \\ \cdot & \cdot \\ \mathbf{q}_{M0} & \mathbf{q}_{M1} & \cdot & \cdot & \cdot & \mathbf{q}_{MN} & & & \end{array} \quad (15.13)$$

Although this imputes no restriction whatsoever on the relative positions of the points, there is typically some regularity in their geometrical distribution (or the manner in which they were generated) that suggests an appropriate assignment of indices. Indeed, if this is not the case, and one is left to “guess” how to arrange the points in an array of the form (15.13), it is improbable that (15.12) will give a satisfactory interpolating surface. In such circumstances, and in cases where the number of given points is actually incompatible with a rectangular array, the tensor-product formulation is inappropriate and we must appeal instead to methods for *scattered data interpolation*.

End conditions for the bases $\phi_0(u), \dots, \phi_M(u)$ and $\psi_0(v), \dots, \psi_N(v)$ may be independently chosen, to suit the context. For example, if the point data (15.13) is intended to be periodic with respect to the first index, as indicated by a coincidence of the first and last rows,

$$\mathbf{q}_{Mk} = \mathbf{q}_{0k} \quad \text{for } k = 0, \dots, N, \quad (15.14)$$

then using periodic end conditions for the u -basis yields a smooth “tube-like” surface (likewise regarding the second index and the v -basis). For data that is periodic in *both* indices, i.e., we have

$$\mathbf{q}_{jN} = \mathbf{q}_{j0} \quad \text{for } k = 0, \dots, N, \quad (15.15)$$

in addition to (15.14), periodic end conditions may be used for both bases — resulting in a smooth “doughnut-like” surface.

A noteworthy limitation of the tensor-product method is that it cannot be used to construct smooth “sphere-like” (genus zero) spline surfaces that are everywhere second-order differentiable. This is a basic topological constraint, a consequence of the fact it is impossible to define a differentiable map from a plane rectangular domain to the entire surface of a sphere.

15.3 The B-spline Basis

We have observed that the set of spline functions on a given sequence of knots constitutes a vector space, that may be spanned by many possible *spline bases*. The cardinal basis discussed in §15.2, for example, was designed to facilitate *interpolation* problems. However, splines are used not only to interpolate point data — we may wish to specify a set of points as *control points*, that provide “shape handles” for the *design* of spline curves and surfaces, with properties analogous to those associated with the Bézier control polygon.

Thus, we seek a set of basis functions $\{B_k^n(t)\}$ for degree- n splines on a given knot sequence $\{t_k\}$ such that, for a spline curve written in the form

$$\mathbf{r}(t) = \sum_k \mathbf{p}_k B_k^n(t), \quad (15.16)$$

the “control polygon” defined by the points $\{\mathbf{p}_k\}$ can be used to manipulate the curve shape in a natural and intuitive manner.³

In order to ensure that the curve $\mathbf{r}(t)$ lies within the *convex hull* of the control points $\{\mathbf{p}_k\}$, we require that the spline basis functions $\{B_k^n(t)\}$ inherit two properties from the Bernstein basis for polynomials, namely

- (a) the non-negativity property: $B_k^n(t) \geq 0$ for all t ;
- (b) the partition-of-unity property: $\sum_k B_k^n(t) \equiv 1$.

A feature of the cardinal basis functions that we wish to exclude from the new spline basis is their *global* nature (see Fig. 15.1) — i.e., moving a single point in the representation (15.5) alters the curve over its *entire* extent. To endow the form (15.16) with a “local shape modification” capability, we enforce

- (c) the compact support property: $B_k^n(t) \equiv 0$ if $t \notin [t_k, t_{k+n+1}]$.

This ensures that, when we move a single control point, at most n contiguous spans of the curve (15.16) are altered. Finally, we also introduce

- (d) the smoothness property: $B_k^n(t)$ is (usually) of class C^{n-1} .

By “usually” we mean in cases where the knots are all distinct: as we shall see below, introducing *multiple knots* allows us to reduce the order of continuity in a controlled manner. This flexibility of the form (15.16) permits an integrated representation of both smooth loci and those with sharp “corners.”

It transpires that properties (a)–(d) *uniquely* define a spline basis $\{B_k^n(t)\}$ on a given knot sequence, the *B-spline basis* of degree n . In the simplest case, with the infinite set of integers $\dots, -1, 0, 1, 2, \dots$ as knots, the B-spline basis may be defined by the recursion formula

$$B_k^r(t) = \frac{t - k}{r} B_k^{r-1}(t) + \frac{k + r + 1 - t}{r} B_{k+1}^{r-1}(t) \quad (15.17)$$

for $r = 1, \dots, n$, commencing with the piecewise-constant functions

$$B_k^0(t) = \begin{cases} 1 & \text{if } k \leq t < k + 1, \\ 0 & \text{otherwise.} \end{cases}$$

Due to the uniformity of the knots in this instance, the basis functions that correspond to different indices k are, for each degree r , just translated copies of each other. We note that they satisfy the *normalization* condition

$$\int_{-\infty}^{+\infty} B_k^r(t) dt = 1$$

for all k and r . Figure 15.2 shows examples of these functions for $r \leq 3$.

³ To avoid diversionary technicalities at this stage, we defer details concerning the range of the summation index k until later.

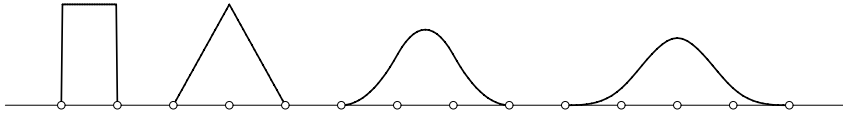


Fig. 15.2. B-spline basis functions $B_k^r(t)$ of degree $r = 0, 1, 2, 3$ on uniform knots — only one of each degree is shown: the others are simply translated copies of these functions. Note that the “support” of the basis function $B_k^r(t)$ is $k \leq t < k + r + 1$.

A more intuitive understanding of the shape of these basis functions may be obtained by considering their *centered forms*

$$\hat{B}_k^r(t) = B_k^r(t + w), \quad (15.18)$$

where $w = \frac{1}{2}(r + 1)$ is the half-width of the support of $B_k^r(t)$ — i.e., $\hat{B}_k^r(t)$ is simply $B_k^r(t)$ shifted to the left by w , so its support interval becomes

$$t \in [k - w, k + w]$$

of width $r + 1$ centered at $t = k$, rather than the interval $t \in [k, k + r + 1]$ after $t = k$. The centered B-spline basis functions of degree r can be expressed as the *convolutions*

$$\hat{B}_k^r(t) = \int_{-\infty}^{+\infty} \hat{B}_k^0(u - t) \hat{B}_k^{r-1}(u) du$$

of those of degree 0 and $r - 1$. This can be interpreted as follows: the center of the piecewise-constant function $\hat{B}_k^0(u - t)$ is imagined as moving along the u -axis, the variable t identifying its location at each instant. We observe at each t the area under $\hat{B}_k^{r-1}(u)$ that is “visible” through the *moving window* defined by $\hat{B}_k^0(u - t)$ — this area specifies the value of $\hat{B}_k^r(t)$. The above equation is actually a special instance of a more general convolution formula,

$$\hat{B}_k^r(t) = \int_{-\infty}^{+\infty} \hat{B}_k^i(u - t) \hat{B}_k^{r-i-1}(u) du.$$

The generalization of the recursion formula (15.17) to the B-spline basis for an arbitrary (non-decreasing) knot sequence $\dots, t_{k-1}, t_k, t_{k+1}, \dots$ is

$$B_k^r(t) = \frac{t - t_k}{t_{k+r} - t_k} B_k^{r-1}(t) + \frac{t_{k+r+1} - t}{t_{k+r+1} - t_{k+1}} B_{k+1}^{r-1}(t), \quad (15.19)$$

commencing with

$$B_k^0(t) = \begin{cases} 1 & \text{if } t_k \leq t < t_{k+1}, \\ 0 & \text{otherwise.} \end{cases}$$

Though it looks rather daunting, this formula is actually not too difficult to remember. The denominators of the factors multiplying $B_k^{r-1}(t)$ and $B_{k+1}^{r-1}(t)$

are the widths of the support intervals $[t_k, t_{k+r}]$ and $[t_{k+1}, t_{k+r+1}]$ for those functions, and the numerators are such that these linear factors increase from 0 to 1 and decrease from 1 to 0, respectively, over those intervals.

We note that the basis functions $B_k^r(t)$ have an $(r-1)$ -fold osculation to the t -axis at the end-points $t = t_k$ and $t = t_{k+r+1}$ of their support intervals (see Fig. 15.2). This is required to ensure a C^{r-1} connection of the non-zero part of $B_k^r(t)$ with $B_k^r(t) \equiv 0$ for $t < t_k$ and $t > t_{k+r+1}$.

15.3.1 The Knot Vector

We have been rather vague, thus far, about the sequence of knots on which the B-spline basis is defined — whether in the uniform or non-uniform case. In actual implementations, of course, we must prescribe a definite *finite* knot sequence, that will allow a sufficient number of linearly-independent B-spline basis functions to be constructed for the application at hand.

Suppose we want $N+1$ control points $\mathbf{p}_0, \dots, \mathbf{p}_N$ for the degree- n B-spline curve (15.16). Since each basis function $B_k^n(t)$ is defined for $t_k \leq t < t_{k+n+1}$, we require a total of $N+n+2$ knots — namely, t_0, \dots, t_{N+n+1} . In terms of the basis $B_0^n(t), \dots, B_N^n(t)$ defined on those knots, we can then express (15.16) in the more concrete form

$$\mathbf{r}(t) = \sum_{k=0}^N \mathbf{p}_k B_k^n(t). \quad (15.20)$$

The non-negativity and partition-of-unity properties of the basis functions ensure that the curve $\mathbf{r}(t)$, defined over the full interval $t \in [t_0, t_{N+n+1}]$, lies entirely within the convex hull of the B-spline control points $\mathbf{p}_0, \dots, \mathbf{p}_N$.

Moreover, on account of the “compact support” property, at most $n+1$ consecutive control points influence the shape of each span $t \in [t_k, t_{k+1}]$ of the curve — since, at each t , at most $n+1$ basis functions are non-zero. Conversely, if we move a single control point, it will alter at most $n+1$ consecutive spans of the curve, and the altered and unaltered portions are guaranteed to meet with C^{n-1} continuity. This “strictly local” shape-editing capability is a very useful feature of the B-spline representation — see Fig. 15.6 below.

All Knots Distinct

When the knots t_0, \dots, t_{N+n+1} are all distinct, we do not ordinarily employ the entire interval $t \in [t_0, t_{N+n+1}]$ as the domain of definition for the curve (15.20). In this case, there are fewer than $n+1$ non-zero basis functions over the first and last n spans, $t \in [t_0, t_n]$ and $t \in [t_{N+1}, t_{N+n+1}]$, and therefore the B-splines $\{B_k^n(t)\}$ do not form a basis capable of representing arbitrary degree- n spline functions over the full interval $t \in [t_0, t_{N+n+1}]$.

This problem is remedied by taking only the “middle” $N-n+1$ spans — corresponding to the interval $t \in [t_n, t_{N+1}]$ — as the parameter domain for $\mathbf{r}(t)$. Precisely $n+1$ of the basis functions $\{B_k^n(t)\}$ are non-zero over each span

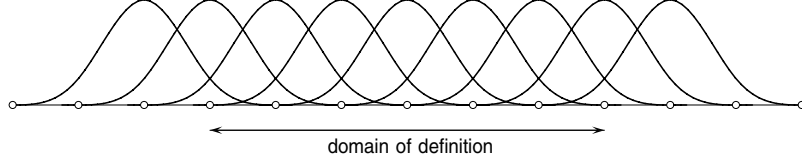


Fig. 15.3. Nine cubic B-splines on the uniform distinct knots $-3, -2, -1, \dots, 7, 8, 9$. They form a basis over the knot subset $0, 1, 2, 3, 4, 5, 6$ defined by deleting the first and last 3 knots, over each span of which precisely four basis functions are non-zero.

of this restricted domain (see Fig. 15.3), and these functions *do* constitute a basis for degree- n splines over $t \in [t_n, t_{N+1}]$. In this case, the actual choices for the knots t_0, \dots, t_{n-1} and $t_{N+2}, \dots, t_{N+n+1}$ do not affect the curve shape (over the domain of interest) at all — although we still need to specify them in order to define a complete B-spline basis.

Figure 15.3 illustrates the B-splines constructed on a set of distinct knots, and the restricted domain over which they constitute a basis. This approach is not often used in practice because the endpoints of the resulting curve, $\mathbf{r}(t_n)$ and $\mathbf{r}(t_{N+1})$, are “floating free” — they do not coincide with the initial and final control points, \mathbf{p}_0 and \mathbf{p}_N , as with a Bézier curve. Figure 15.4 shows a B-spline curve and its control polygon defined in this manner.

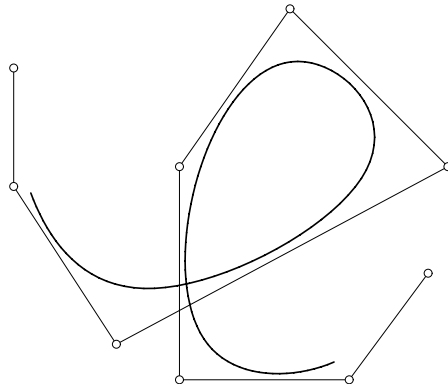


Fig. 15.4. Example of a B-spline curve defined on a knot sequence with all knots distinct: note that the curve does not interpolate the initial and final control points.

Multiple End-knots

The knots $\dots, t_{k-1}, t_k, t_{k+1}, \dots$ on which a set of B-splines are defined must be a *non-decreasing* sequence of values (i.e., $t_{k+1} \geq t_k$ for all k). Cases where two or more values coincide identify *multiple knots*. In particular, if

$$t_{k-1} \neq t_k = t_{k+1} = \dots = t_{k+m-1} \neq t_{k+m},$$

we have a *knot of multiplicity m*. An m -fold knot lying within the support of a basis function $B_k^n(t)$ has the effect of reducing its order of continuity at that point from C^{n-1} to C^{n-m} . Furthermore, the number of (non-degenerate) spans over which $B_k^n(t)$ is non-zero will be reduced from $n+1$ to $n-m+2$. In particular, an $(n+1)$ -fold knot induces a *discontinuity* in the basis function, and reduces its support interval to just *one* non-degenerate span.

We may continue to use the recursion formula (15.19) to compute B-spline bases for knot sequences incorporating multiplicities, provided we invoke the convention that the factors multiplying $B_k^{r-1}(t)$ and $B_{k+1}^{r-1}(t)$ are set equal to zero whenever — due to multiple knots — their denominators vanish.

Figure 15.5 illustrates a form commonly used in practice, namely, a cubic B-spline basis with 4-fold initial and final knots, and all other knots simple (this can be thought of as the outcome of coalescing the first and last 4 knots in the basis shown in Fig. 15.3). The knot vector is thus of the form

$$(a =) t_0 = t_1 = t_2 = t_3 < \cdots < t_{N+1} = t_{N+2} = t_{N+3} = t_{N+4} (= b). \quad (15.21)$$

The value a is a 4-fold knot for $B_0^3(t)$, 3-fold for $B_1^3(t)$, and 2-fold for $B_2^3(t)$ — similarly for the value b at the other end. We also see from Fig. 15.5 that $B_0^3(a) = 1$ and $B_N^3(b) = 1$, while all other basis functions vanish at the end points. Hence, using $(n+1)$ -fold initial and final knots gives a curve (15.20) that *interpolates the initial and final control points*, \mathbf{p}_0 and \mathbf{p}_N — as shown in the example of Fig. 15.6. We also use this example to illustrate the local “shape editing” capability of the B-spline form.

An important special form of the knot vector is the case where we employ just two distinct knots, 0 and 1 say, each of multiplicity $n+1$:

$$\overbrace{00 \cdots 00}^{n+1 \text{ times}} \overbrace{11 \cdots 11}^{n+1 \text{ times}}. \quad (15.22)$$

Here we have $N = n$, and it can be verified that the B-spline basis functions over the single non-degenerate interval $t \in [0, 1]$ become

$$B_k^n(t) = \binom{n}{k} (1-t)^{n-k} t^k,$$

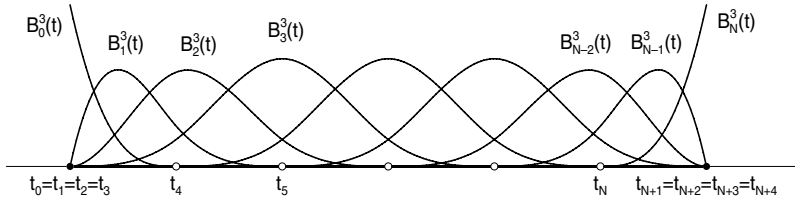


Fig. 15.5. Nine cubic B-splines on the knot sequence 0, 0, 0, 0, 1, 2, 3, 4, 5, 6, 6, 6 — i.e., the initial and final knots are each of multiplicity 4. They form a basis for cubic splines over the set of distinct knots 0, 1, 2, 3, 4, 5, 6 (compare with Fig. 15.3).

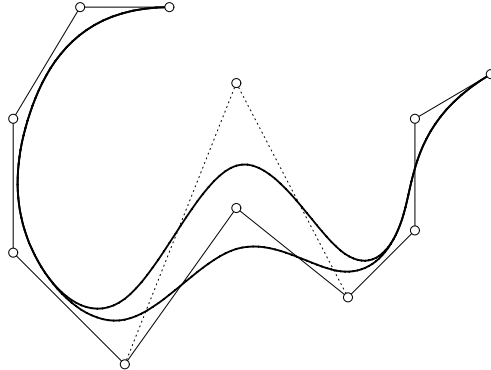


Fig. 15.6. A cubic B-spline curve with 4-fold initial and final knots, interpolating the initial and final control points. A local modification of this B-spline curve, by the displacement of a single control point, is also shown — note that smooth (C^2) connections between the modified and unmodified curve segments are maintained.

which we recognize as the *Bernstein basis* for polynomials of degree n on the unit interval. Thus, the Bézier representation of curves and surfaces may be considered a special instance of the B-spline representation.

Periodic Knot Sequences

In order for (15.20) to define a smooth *closed* B-spline curve, special treatment of the control points and knot sequence are required. The last n control points must coincide, in order, with the first n — i.e., we require

$$\mathbf{p}_{N-n+1} = \mathbf{p}_0, \quad \mathbf{p}_{N-n+2} = \mathbf{p}_1, \quad \dots, \quad \mathbf{p}_N = \mathbf{p}_{n-1}. \quad (15.23)$$

Furthermore, the knots t_0, \dots, t_{N+n+1} must be interpreted as forming a *cyclic array*. The interval $t \in [t_n, t_{N+1}]$ is again taken as the parameter domain for the curve (giving one complete traversal), and we require a C^{n-1} juncture of the coincident “end” points, $\mathbf{r}(t_n) = \mathbf{r}(t_{N+1})$.

Having chosen the knot values t_n, \dots, t_{N+1} , we consider $t_{N+1}, \dots, t_{N+n+1}$ to “overlap” t_n, \dots, t_{2n} , and similarly t_0, \dots, t_n overlap $t_{N-n+1}, \dots, t_{N+1}$. We can then obtain values for t_0, \dots, t_{n-1} and $t_{N+2}, \dots, t_{N+n+1}$ by equating the widths⁴ of corresponding intervals:

$$t_{N+k+1} - t_{N+k} = t_{n+k} - t_{n+k-1} \quad \text{and} \quad t_{N-n+k+1} - t_{N-n+k} = t_k - t_{k-1}$$

for $k = 1, \dots, n$. This is best understood by means of an example — the cubic B-splines, say (see Fig. 15.7). In that case, the above equations become

⁴ This is mainly of concern in the case of non-uniform knots, since for uniform knots $t_n, t_{n+1}, \dots, t_{N+1} = 0, 1, \dots, N - n + 1$ it gives the trivial results $t_0, \dots, t_{n-1} = -n, \dots, -1$ and $t_{N+2}, \dots, t_{N+n+1} = N - n + 2, \dots, N + 1$.

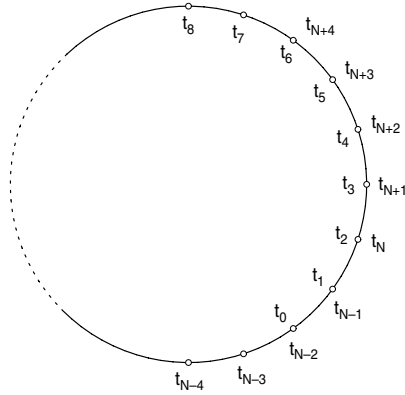


Fig. 15.7. Cyclic interpretation of knots for periodic cubic B-splines.

$$t_{N+2} - t_{N+1} = t_5 - t_4, \quad t_{N+3} - t_{N+2} = t_6 - t_5, \quad t_{N+4} - t_{N+3} = t_7 - t_6,$$

$$t_{N-1} - t_{N-2} = t_1 - t_0, \quad t_N - t_{N-1} = t_2 - t_1, \quad t_{N+1} - t_N = t_3 - t_2.$$

Knowing t_3, t_4, \dots, t_{N+1} , these equations allow us to determine the additional knots t_0, t_1, t_2 and $t_{N+2}, t_{N+3}, t_{N+4}$ needed to define a periodic B-spline basis.

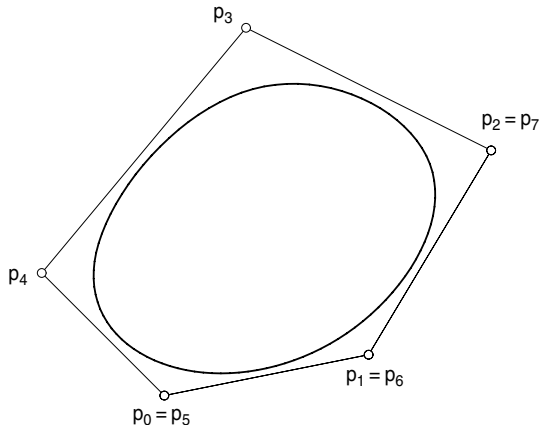


Fig. 15.8. A closed C^2 cubic B-spline curve, defined using a periodic knot sequence.

Figure 15.8 shows an example of a periodic C^2 cubic B-spline curve defined in this manner. Note that, although there are only five *distinct* control points, a total of eight are required — the first and last three being coincident.

15.3.2 Cox-de Boor Algorithm

We now describe a numerically-stable method, developed independently by M. G. Cox [106] and C. de Boor [115], to evaluate the B-spline curve (15.20). The algorithm is a consequence of the basic recursion relation (15.19), through which the B-spline basis was defined.

Given a value $t \in [t_j, t_{j+1}]$ within the j -th span,⁵ this algorithm computes the curve point $\mathbf{r}(t)$ using an iterated sequence of linear interpolations among the $n + 1$ consecutive control points $\mathbf{p}_{j-n}, \dots, \mathbf{p}_j$ as follows. We first set

$$\mathbf{p}_i^{(0)} = \mathbf{p}_i$$

for $i = j - n, \dots, j$. Then, for $r = 1, \dots, n$ and $i = j - n + r, \dots, j$, we compute the triangular array of quantities defined by

$$\mathbf{p}_i^{(r)} = (1 - \tau) \mathbf{p}_{i-1}^{(r-1)} + \tau \mathbf{p}_i^{(r-1)}, \quad (15.24)$$

where τ is defined by

$$\tau = \frac{t - t_i}{t_{i+n-r+1} - t_i}$$

(note that $1 - \tau$ and τ represent barycentric coordinates on the support interval $t \in [t_i, t_{i+n-r+1}]$ of the basis function $B_i^{n-r}(t)$). The final entry, at the apex of this triangular array, corresponds to the evaluated point on the curve:

$$\mathbf{r}(t) = \mathbf{p}_j^{(n)}.$$

The algorithm (15.24) is clearly analogous to the de Casteljau algorithm for evaluating a Bézier curve (see §13.4). In fact, it can be shown that in the special case of the knot sequence (15.22), the procedure (15.24) specializes to

$$\mathbf{p}_i^{(r)} = (1 - t) \mathbf{p}_{i-1}^{(r-1)} + t \mathbf{p}_i^{(r-1)}$$

for $r = 1, \dots, n$ and $i = r, \dots, n$, on choosing $t_i = 0$ for $0 \leq i \leq n$ and $t_i = 1$ for $n + 1 \leq i \leq 2n + 1$, $N = n$, and $j = n$ in (15.24). This is, in fact, just the familiar de Casteljau algorithm for a degree- n Bézier curve.

15.3.3 Tensor-product B-spline Surfaces

The principles described above have straightforward extensions to the design of tensor-product B-spline surfaces. Given a topologically rectangular array of control points \mathbf{p}_{jk} for $0 \leq j \leq M$ and $0 \leq k \leq N$, and knot sequences $u_0, u_1, \dots, u_{M+m+1}$ and $v_0, v_1, \dots, v_{N+n+1}$, we can form the B-spline surface

$$\mathbf{r}(u, v) = \sum_{j=0}^M \sum_{k=0}^N \mathbf{p}_{jk} B_j^m(u) B_k^n(v)$$

⁵ The standard domain $t \in [t_n, t_{N+1}]$ for the curve (15.20) then corresponds to the $N - n + 1$ spans identified by $j = n, n + 1, \dots, N$.

of degree (m, n) in (u, v) once we have constructed the appropriate B-spline bases $B_0^m(u), \dots, B_M^m(u)$ and $B_0^n(v), \dots, B_N^n(v)$ on the prescribed knots. The surface is considered to be defined on the parameter domain

$$(u, v) \in [u_m, u_{M+1}] \times [v_n, v_{N+1}],$$

and any of the conventions described in §15.3.1 can be used to assign the end-knots u_0, \dots, u_{m-1} ; $u_{M+2}, \dots, u_{M+m+1}$ and v_0, \dots, v_{n-1} ; $v_{N+2}, \dots, v_{N+n+1}$ to suit the particular application context.

15.3.4 Rational B-spline Curves and Surfaces

As with the Bézier curves and surfaces, we can generalize the B-spline form to *rational* curves and surfaces by associating a “weight” w with each control point. For example, given appropriate knots a rational B-spline curve with control points $\mathbf{p}_0, \dots, \mathbf{p}_N$ and weights w_0, \dots, w_N is defined by

$$\mathbf{r}(t) = \frac{\sum_{k=0}^N w_k \mathbf{p}_k B_k^n(t)}{\sum_{k=0}^N w_k B_k^n(t)}, \quad (15.25)$$

and rational tensor-product B-spline surfaces may be defined in an analogous manner. One of the principal advantages of such generalizations is to provide the capability for an *exact* description of conic curves and quadric surfaces in the same format as free-form curves and surfaces — and to ensure closure of the representation scheme under projective transformations.

In the most general case of rational B-splines defined on arbitrary knots — including, possibly, multiple knots — this approach has gained widespread acceptance in commercial CAD software, and is referred to by the acronym NURBS (non-uniform rational B-splines). By an appropriate choice of knots, weights, and control points, for example, a NURBS curve may incorporate both “simple” (linear/circular) and free-form segments — with either smooth connections or sharp corners at their junctures — in a single integrated format amenable to generic algorithms for rendering, intersections, etc.

15.3.5 Bézier and B-spline Forms Compared

From a designer’s perspective, both the Bézier and B-spline curve and surface formulations are based on specification and manipulation of control polygons. It is thus natural to enquire, for Bézier and B-spline geometries specified by identical control polygons,⁶ which properties they have in common, and which

⁶ For the B-spline forms we shall confine ourselves to the case of multiple end-knots or a periodic knot vector, as appropriate.

are disparate. Two important common features of these forms are that they both exhibit the *convex hull* and *variation diminishing* properties. They also admit similar algorithms, based on iterated sequences of linear interpolations among the control points, for evaluation and subdivision.

Perhaps the most fundamental difference is that, whereas for a Bézier curve the only scope for introducing extra degrees of freedom (i.e., control points) is to increase the degree n , for a B-spline curve one keeps n fixed (usually cubic) and instead increases the knot number N . As we increase n , the correlation between the shape of a Bézier curve and its control polygon becomes weaker. The reason for this is that the Bernstein basis functions of higher degree are more “spread out” — each control point exerts a more global influence on the curve shape. By contrast, the compact support of the B-spline basis ensures a localized influence of the control points on the shape of a B-spline curve. Thus, a B-spline curve tends to “hug” the control polygon more closely than its Bézier counterpart in cases with many control points (see Fig. 15.9).

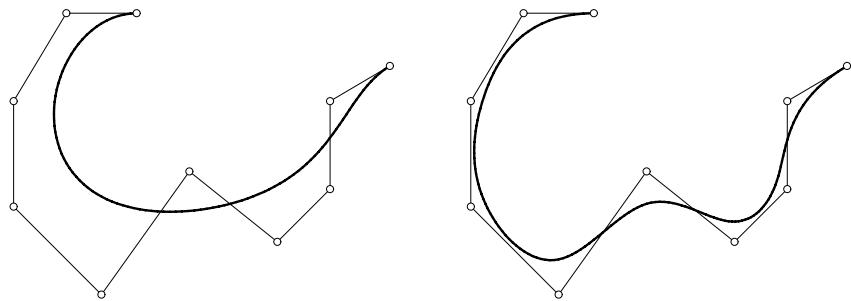


Fig. 15.9. Comparison of a degree-nine Bézier curve (left) and a cubic B-spline curve with multiple end-knots (right) that have identical control polygons — note that the latter conforms much more closely to the control polygon than the former.

In the cubic case, for example, any given control point influences no more than four contiguous spans of the curve — and, conversely, the shape of any span is determined by at most four consecutive control points.⁷ This provides an intuitive way to embed a *strictly linear* segment within a cubic B-spline curve, while maintaining C^2 continuity: if $r \geq 4$ control points are collinear, then the $r - 3$ spans they define must, by virtue of the convex hull property, degenerate to straight lines (see the example in Fig. 15.10). This is known as the *linear precision* property of B-spline curves.

A further important practical difference between the two forms is that a single Bézier curve *always*⁸ defines a smooth locus, while a B-spline curve

⁷ We make the qualifications “no more” and “at most” since, in the presence of multiple knots, the number will actually be less than 4.

⁸ We discount here the possibility of *cusps*, which arise only in exceptional instances.

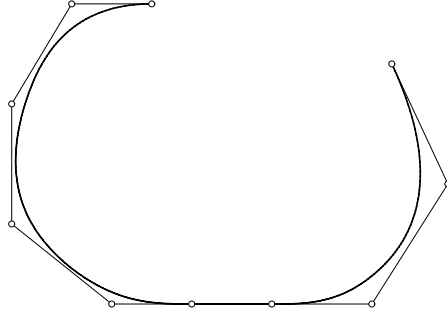


Fig. 15.10. A linear segment is embedded within a C^2 cubic B-spline curve when four or more consecutive control points are specified so as to lie on a straight line.

offers the possibility of incorporating discontinuities of (say) the curvature or tangent in a controlled manner, through the introduction of multiple knots.

15.4 Spline Basis Conversion

The cardinal basis and B-spline basis are just two among many possible sets of spline functions that span the linear space of spline functions of a given order on a given sequence of knots. We have emphasized them here because of their importance in interpolation and “design-with-local-control” applications. In this connection, *conversion* of spline curve or surface representations between different bases is an important practical requirement.

15.4.1 Cardinal to B-spline Form

Suppose, for example, we construct a C^2 cubic spline curve that interpolates points $\mathbf{q}_0, \dots, \mathbf{q}_N$ at the nodes t_0, \dots, t_N subject to specified end conditions, by invoking the appropriate cardinal basis

$$\mathbf{r}(t) = \sum_{j=0}^N \mathbf{q}_j \phi_j(t), \quad (15.26)$$

and we wish to determine the B-spline control points that define this curve, to permit local modifications of it. This problem, and the analogous problem for surfaces, can be reduced to certain matrix multiplications.

We confine our attention to the case of primary practical interest, namely, *cubic* splines. As noted in §15.3.1, the B-splines of degree n defined on a given sequence of knots do not form a basis over the entire interval delineated by those knots, but only over the subinterval defined by deleting the first and last n knots. In the present context this means that, in order to construct a set of cubic B-splines that form a complete basis over the interval $t \in [t_0, t_N]$, we

must *augment* the knot vector by three additional initial and final knots. We denote these “pseudoknots” by t_{-3}, t_{-2}, t_{-1} and $t_{N+1}, t_{N+2}, t_{N+3}$.

To obtain a symmetric notation, we prefer to employ the “centered” cubic B-splines, defined by (15.18) — this amounts to labelling each B-spline basis function by the knot identifying its maximum, rather than the left-most knot of its support interval. Since each centered basis function $\hat{B}_k^3(t)$ has support $t \in [t_{k-2}, t_{k+2}]$, we can define a total of $N + 3$ of them

$$\hat{B}_{-1}^3(t), \hat{B}_0^3(t), \dots, \hat{B}_N^3(t), \hat{B}_{N+1}^3(t) \quad (15.27)$$

on the augmented knot vector. Our problem is thus to compute the B-spline control points $\mathbf{p}_{-1}, \mathbf{p}_0, \dots, \mathbf{p}_N, \mathbf{p}_{N+1}$ in the representation

$$\mathbf{r}(t) = \sum_{k=-1}^{N+1} \mathbf{p}_k \hat{B}_k^3(t) \quad (15.28)$$

from the known interpolant points $\mathbf{q}_0, \dots, \mathbf{q}_N$.

Note that, whereas the cardinal representation (15.26) incorporates $N + 1$ terms, the B-spline form (15.28) has $N + 3$. Two more are needed in the latter case, since the curve (15.26) is not uniquely defined by the interpolant points $\mathbf{q}_0, \dots, \mathbf{q}_N$ alone — in addition, we must impose *end conditions*. Thus, the role of the two “extra” control points \mathbf{p}_{-1} and \mathbf{p}_{N+1} may be regarded as supplying the additional degrees of freedom needed to enforce the end conditions.⁹

15.4.2 Basis Conversion Matrix

To accomplish the basis conversion, we must express each of the cardinal basis functions $\phi_j(t)$ in terms of the B-spline basis (15.27),

$$\phi_j(t) = \sum_{k=-1}^{N+1} \lambda_{jk} \hat{B}_k^3(t) \quad (15.29)$$

for $j = 1, \dots, N$. Here, the quantities λ_{jk} may be regarded as the elements of an $N \times (N + 2)$ matrix, Λ . By substituting the above equation into (15.26), and re-arranging the order of summation, the B-spline control points in (15.28) can be written as

$$\mathbf{p}_k = \sum_{j=0}^N \mathbf{q}_j \lambda_{jk}$$

for $k = -1, \dots, N + 1$. This amounts to a left-multiplication of the matrix Λ by the row vector $[\mathbf{q}_0 \cdots \mathbf{q}_N]$ to yield the row vector $[\mathbf{p}_{-1} \cdots \mathbf{p}_{N+1}]$. Thus, if we have pre-computed the elements of Λ , we can obtain the desired basis conversion through a matrix multiplication.

⁹ Alternatively, we could have formulated (15.26) as a *complete* spline, interpolating end-derivatives \mathbf{d}_0 and \mathbf{d}_N in addition to the points $\mathbf{q}_0, \dots, \mathbf{q}_N$. In that case, we dispense with end conditions, and both (15.26) and (15.28) contain $N + 3$ terms.

The matrix elements are obtained as follows. We evaluate equation (15.29) at each of node t_l , obtaining

$$\begin{aligned}\phi_j(t_l) &= \sum_{k=-1}^{N+1} \lambda_{jk} \hat{B}_k^3(t_l) \\ &= \lambda_{j,l-1} \hat{B}_{l-1}^3(t_l) + \lambda_{jl} \hat{B}_l^3(t_l) + \lambda_{j,l+1} \hat{B}_{l+1}^3(t_l) = \delta_{jl}\end{aligned}\quad (15.30)$$

by the cardinality property of ϕ_j . For fixed j and $l = 0, \dots, N$ this amounts to an incomplete tridiagonal system of $N + 1$ linear equations for the $N + 3$ unknowns $\lambda_{j,-1}, \dots, \lambda_{j,N+1}$. The fact that there are only three non-zero terms in the sum over the centered cubic B-splines is a consequence of their compact support property. The required nodal values of the basis functions in (15.30) are readily obtained¹⁰ from the recursion formula (15.19).

Closure of the incomplete tridiagonal system (15.30) may be obtained by considering the end conditions imposed on $\phi_j(t)$. For example, using quadratic end-spans, the not-a-knot condition, or periodic end conditions yield linear equations that can be appended to (15.30) to close the system. Except in the periodic case, the additional equations are compatible with the tridiagonality of (15.30). As noted above in §14.4.4, tridiagonal systems can be solved very efficiently. To assemble the full matrix A , we need to solve a total of $N + 1$ such systems, defined by $j = 0, \dots, N$ in (15.30) together with the appropriate end-condition equations.

¹⁰ We employ $\hat{B}_k^3(t) = B_{k-2}^3(t)$ in this formula, since it is cast in terms of B-splines indexed by the first knot of the support interval, rather than centered B-splines.

16

Arc-length Parameterization

The fluxion of the Length is determin'd by putting it equal to the square-root of the sum of the squares of the fluxion of the Absciss and of the Ordinate.

Isaac Newton, *Fluxions* (1736)

For a differentiable plane curve $\mathbf{r}(t) = (x(t), y(t))$ the derivative of arc length s with respect to the parameter t is given by

$$\frac{ds}{dt} = |\mathbf{r}'(t)| = \sqrt{x'^2(t) + y'^2(t)}. \quad (16.1)$$

We call this function the *parametric speed* of the curve, and denote it by $\sigma(t)$. A regularly-parameterized curve has the property that $\sigma(t) \neq 0$ for all t — in general, a point where $\mathbf{r}'(t) = \mathbf{0}$ incurs a *cusp* (tangent reversal) on the curve. Ideally, we would like to study curves for which $\sigma(t) \equiv 1$ and hence $s \equiv t$, i.e., *curves parameterized by arc length*. We can easily achieve this for a straight line, and also for a circle (using trigonometric functions). But these “simple” examples are, unfortunately, exceptional — we shall see in §16.1 that no curve can be parameterized by rational functions of its arc length.

Failure to achieve the ideal of arc-length or “unit speed” parameterization should not be cause for complete despondency. If we cannot make $\sigma(t)$ equal to unity, we can at least try to make it something that can be easily integrated, so we can obtain a closed-form cumulative arc-length function $s(t)$ from (16.1). When $\mathbf{r}(t)$ is a degree n polynomial curve, the quantity on the right in (16.1) is the square root of a polynomial of degree $2(n - 1)$. The indefinite integral has a closed-form expression in the case $n = 2$ (a parabola), and also the case $n = 3$ of cubics if we appeal to *elliptic functions* [299]. For higher degrees n , however, a closed-form integration is, in general, no longer possible.

We can circumvent this difficulty by incorporating a special structure into the curve hodograph $\mathbf{r}'(t) = (x'(t), y'(t))$ which ensures that the argument of the square root in (16.1) is the *perfect square* of a polynomial. This property defines the *Pythagorean-hodograph curves* (see §16.3), a family of polynomial

curves that — among other attractive properties — admit *exact* measurement of their arc lengths by simply evaluating a polynomial. The remaining chapters of this book describe in detail the formulations and special properties of planar and spatial Pythagorean–hodograph curves, algorithms for their construction and manipulation, and some of their practical applications.

16.1 In Search of an Elusive Ideal

The differential geometer’s ideal is to parameterize a curve by its arc length s , measured from some fixed point. With this representation $\mathbf{r}(s) = (x(s), y(s))$ the intrinsic geometry becomes exceedingly simple: the tangent and curvature are $\mathbf{t} = d\mathbf{r}/ds$ and $\kappa = d\theta/ds$, where θ is the angle that \mathbf{t} makes with a fixed direction. However, this “natural” parameterization of a plane curve does not, in general, admit closed-form expression in terms of elementary functions. The algebraic geometer’s notion of an “ideal” parameterization is rather different. In algebraic geometry, curves that can be parameterized in terms of “simple” — i.e., *rational* — functions enjoy special distinction. Since any function that can be evaluated through a *finite* sequence of arithmetic operations is rational (see Chap. 3) such functions¹ are, in fact, the most general that computers can evaluate *exactly* (modulo round-off error — see Chap. 12).

For computer descriptions of geometrical loci, a reconciliation of these two perspectives (i.e., *curves parameterized by rational functions of the arc length*) would be extremely useful. A trivial example is the straight line

$$x(s) = x_0 + \lambda s, \quad y(s) = y_0 + \mu s$$

whose direction cosines satisfy $\lambda^2 + \mu^2 = 1$. Generalizing to curves defined by polynomials $x(s)$, $y(s)$ of degree $n \geq 2$ in s , it is obvious that

$$\sigma(s) = \sqrt{x'^2(s) + y'^2(s)} \tag{16.2}$$

cannot be identically equal to unity, since the argument of the square root is a non-constant polynomial of degree $2(n - 1) \geq 2$ in s . It is not so obvious, however, that the case where $x(s)$, $y(s)$ are *rational functions* in s does not allow arc length parameterizations either. Despite its innocuous appearance, the proof of this statement is rather subtle, involving ideas from integration theory and complex variables [187].

Theorem 16.1 *It is impossible to parameterize any plane curve, other than a straight line, by rational functions of its arc length.*

Proof : Consider a rational curve

¹ Trigonometric, exponential, logarithmic, and other “library” functions available in programming languages are actually rational *approximations* of those functions.

$$x(s) = \frac{X(s)}{W(s)}, \quad y(s) = \frac{Y(s)}{W(s)} \quad (16.3)$$

defined by polynomials $W(s), X(s), Y(s)$ with $\gcd(W, X, Y) = \text{constant}$ (since otherwise we would cancel their common factors). We assume the curve degree satisfies $n = \max(\deg(W), \deg(X), \deg(Y)) > 1$ so as to exclude straight lines. Differentiating (16.3) we see that, for the speed (16.2) to be identically equal to 1, the polynomials $U = WX' - W'X$, $V = WY' - W'Y$, W must satisfy

$$U^2 + V^2 \equiv W^4. \quad (16.4)$$

Clearly U, V, W^2 must comprise a *Pythagorean triple* of polynomials. As with the Pythagorean triples of integers (see Chap. 2), such an equation has only “special” solutions: we cannot freely choose two of the three polynomials and expect to find a polynomial solution for the third. Specifically, any polynomial solution to (16.4) must have the form [292]:

$$U = (a^2 - b^2)c, \quad V = 2abc, \quad W^2 = (a^2 + b^2)c \quad (16.5)$$

for three non-zero (real) polynomials a, b, c with $\gcd(a, b) = 1$. Furthermore, a and b cannot both be constants if the curve is not a straight line.

To define a “unit speed” curve, with arc-length parameterization, we must substitute (16.5) into $x' = U/W^2$, $y' = V/W^2$ and integrate this hodograph. However, this may not yield a *rational* curve, since the integrals of rational functions are not necessarily themselves rational. We will obtain a unit-speed rational curve only if we can find two real non-zero polynomials $a(t)$ and $b(t)$ — relatively prime and not both constants — such that

$$\begin{aligned} I_x(s) &= \int_0^s \frac{a^2(t) - b^2(t)}{a^2(t) + b^2(t)} dt = x(s) - x_0, \\ I_y(s) &= \int_0^s \frac{2a(t)b(t)}{a^2(t) + b^2(t)} dt = y(s) - y_0, \end{aligned} \quad (16.6)$$

are both rational functions of s , where (x_0, y_0) are integration constants.

We argue by contradiction. Suppose that two polynomials $a(t), b(t)$ with $\gcd(a, b) = \text{constant}$ and $\max(\deg(a), \deg(b)) \geq 1$ can be found, such that the integrals (16.6) are both rational. To integrate a rational function $p(t)/q(t)$, we must compute its *partial fraction decomposition* (see §3.5), of the form

$$\frac{p(t)}{q(t)} = \sum_{r=1}^k \sum_{s=1}^{m_r} \frac{C_{rs}}{(t - z_r)^s}, \quad (16.7)$$

where z_1, \dots, z_k are the distinct (real and complex) roots of the denominator, with multiplicities m_1, \dots, m_k . The integrals of the terms on the right in (16.7) are well known — those with $s > 1$ yield rational terms on integration,

while those with $s = 1$ incur transcendental (i.e., logarithmic or arc-tangent) expressions [199]. Thus if the integral of (16.7) is to be rational, we must have

$$C_{r1} = 0 \quad \text{for } r = 1, \dots, k.$$

The coefficients C_{r1} of the inverse linear terms in (16.7) are called the *residues* of the rational function $p(t)/q(t)$ at its poles z_r (see §3.5).

The residues also arise in computing the *definite* integral of $p(t)/q(t)$ over the entire real line — from the “calculus of residues” [235] we know that

$$\int_{-\infty}^{+\infty} \frac{p(t)}{q(t)} dt = 2\pi i \sum_{\text{Im}(z_r) > 0} C_{r1} \quad (16.8)$$

when $q(t)$ has no real roots and $\deg(q) - \deg(p) \geq 2$ (so the integrand decays sufficiently rapidly as $|t| \rightarrow \infty$). The sum in (16.8) is taken over all the poles of $p(t)/q(t)$ in the *upper half* of the complex plane.

Now for two relatively prime polynomials $a(t), b(t)$ we can always choose numbers λ and μ , not both zero, so that

$$\deg(\lambda a + \mu b) < \max(\deg(a), \deg(b)).$$

If we postulate that the integrals (16.6) are *both* rational functions, then

$$\begin{aligned} I(s) &= \int_0^s \frac{[\lambda a(t) + \mu b(t)]^2}{a^2(t) + b^2(t)} dt \\ &= \frac{1}{2}(\lambda^2 - \mu^2) I_x(s) + \lambda \mu I_y(s) + \frac{1}{2}(\lambda^2 + \mu^2) s \end{aligned}$$

is evidently also a rational function, and hence the residues of the integrand $(\lambda a + \mu b)^2/(a^2 + b^2)$ at each of its poles must be zero. But this integrand also satisfies the requirements for its definite integral to be given by (16.8) — since $\gcd(a, b) = 1$ by assumption, $a^2 + b^2$ has no real roots, and by our choice of λ, μ the integrand satisfies $\deg(a^2 + b^2) - \deg((\lambda a + \mu b)^2) \geq 2$. The vanishing of these residues implies that

$$\int_{-\infty}^{+\infty} \frac{[\lambda a(t) + \mu b(t)]^2}{a^2(t) + b^2(t)} dt = 0,$$

but this is clearly impossible, since the integrand has a positive value for all t when $a(t), b(t)$ are not both zero and $\gcd(a, b) = 1$.

Since the supposition that non-zero relatively prime polynomials $a(t), b(t)$ exist for which the integrals (16.6) are *both* rational incurs a contradiction, this supposition must be false — the integration of a unit-speed hodograph defined by rational functions will always lead us outside the realm of rational curves. We conclude that it is impossible to create a plane curve, other than a straight line, parameterized by rational functions of its arc length. ■

The above proof is specifically for planar curves, but can be extended [189] to space curves. Consider a rational space curve defined by four polynomials $W(s), X(s), Y(s), Z(s)$ with $n = \max(\deg(W), \deg(X), \deg(Y), \deg(Z)) > 1$ and $\gcd(W, X, Y, Z) = \text{constant}$. In order for the parametric speed to be unity, the four polynomials $WX' - W'X, WY' - W'Y, WZ' - W'Z, W^2$ must form a Pythagorean quartuple, and hence must be [130] of the form

$$\begin{aligned} WX' - W'X &= u^2 + v^2 - p^2 - q^2, \\ WY' - W'Y &= 2(uq + vp), \\ WZ' - W'Z &= 2(vq - up), \\ W^2 &= u^2 + v^2 + p^2 + q^2 \end{aligned}$$

(for more on Pythagorean quartuples of polynomials, see §22.1). We assume that these polynomials are relatively prime, since if

$$f = \gcd(WX' - W'X, WY' - W'Y, WZ' - W'Z, W^2) \neq \text{constant}$$

we can simply divide each of them by f — note that a curve is uniquely defined (modulo translations) by its hodograph, which remains unchanged under such division. We also assume that $(u(t), v(t)) \not\equiv (0, 0)$ and $(p(t), q(t)) \not\equiv (0, 0)$ since otherwise the hodograph components y', z' vanish identically and the curve degenerates to a straight line parallel to the x -axis.

The existence of curves in \mathbb{R}^3 parameterized by rational functions of the arc length is then transformed into the problem of finding four polynomials $u(t), v(t), p(t), q(t)$ such that all three of the integrals

$$\begin{aligned} I_x(s) &= \int_0^s \frac{u^2(t) + v^2(t) - p^2(t) - q^2(t)}{u^2(t) + v^2(t) + p^2(t) + q^2(t)} dt = x(s) - x_0, \\ I_y(s) &= \int_0^s \frac{2[u(t)q(t) + v(t)p(t)]}{u^2(t) + v^2(t) + p^2(t) + q^2(t)} dt = y(s) - y_0, \\ I_z(s) &= \int_0^s \frac{2[v(t)q(t) - u(t)p(t)]}{u^2(t) + v^2(t) + p^2(t) + q^2(t)} dt = z(s) - z_0, \end{aligned} \quad (16.9)$$

are rational. Suppose that such polynomials exist, with

$$m = \max(\deg(u), \deg(v), \deg(p), \deg(q)) \geq 1$$

(otherwise the curve defined by these integrals would be a straight line). Now we can always choose three numbers λ, μ, ν such that the polynomials

$$a(t) = \lambda u(t) + \mu p(t) + \nu q(t), \quad b(t) = \lambda v(t) + \nu p(t) - \mu q(t)$$

satisfy the conditions

$$\deg(a) < m, \quad \deg(b) < m \quad \text{and} \quad (a(t), b(t)) \not\equiv (0, 0).$$

Namely, let u_m, v_m, p_m, q_m be the t^m coefficients of $u(t), v(t), p(t), q(t)$. Then if $(p_m, q_m) = (0, 0)$ we take $\lambda = 0$, and $(a(t), b(t)) \not\equiv (0, 0)$ is easily satisfied by a suitable choice for μ, ν since $(p(t), q(t)) \not\equiv (0, 0)$. On the other hand, when $(p_m, q_m) \neq (0, 0)$ we can take

$$\lambda : \mu : \nu = p_m^2 + q_m^2 : -p_m u_m + q_m v_m : -q_m u_m - p_m v_m,$$

and the one remaining freedom allows us to ensure that $(a(t), b(t)) \not\equiv (0, 0)$.

Now if the three integrals (16.9) are all rational, the indefinite integral

$$\begin{aligned} I(s) &= \int_0^s \frac{a^2(t) + b^2(t)}{u^2(t) + v^2(t) + p^2(t) + q^2(t)} dt \\ &= \frac{1}{2}(\lambda^2 - \mu^2 - \nu^2) I_x(s) + \lambda\nu I_y(s) - \lambda\mu I_z(s) + \frac{1}{2}(\lambda^2 + \mu^2 + \nu^2) s \end{aligned}$$

must also be rational, and hence the residues at its poles must vanish. By the residue theorem, this implies that

$$\int_{-\infty}^{+\infty} \frac{a^2(t) + b^2(t)}{u^2(t) + v^2(t) + p^2(t) + q^2(t)} dt = 0,$$

a contradiction, since the integrand is positive for all t . Hence, the supposition that polynomials $u(t), v(t), p(t), q(t)$ can be found to make all three of the integrals (16.9) rational is false, and we conclude that no curve in \mathbb{R}^3 (except a straight line) can be parameterized by rational functions of its arc length.

16.2 The Rectification of Curves

The *rectification* (arc-length measurement) of curves has been a problematic issue from ancient times. The circumference of a circle of unit diameter, for example, is the transcendental² number π . The founding of analytic geometry by Descartes, in his 1637 treatise *La Géométrie*, did not resolve the problem. Descartes asserted [127] that:

... geometry should not include lines that are like strings, in that they are sometimes straight and sometimes curved, since the ratios between straight and curved lines are not known, and I believe cannot be discovered by human minds, and therefore no conclusion based upon such ratios can be accepted as rigorous and exact.

Descartes made a clear distinction between what he regarded as “geometrical” curves and “mechanical” curves (we now call the former *algebraic*, since they are definable by finite algebraic equations, and the latter *transcendental*, since they are not). However, his categorical rejection of the possibility of arc length measurement of curves was soon shown to be erroneous.

² The fact that π cannot be defined by any finite algebraic equation was proved by Johann Heinrich Lambert (1728–1777), a colleague of Leonhard Euler.

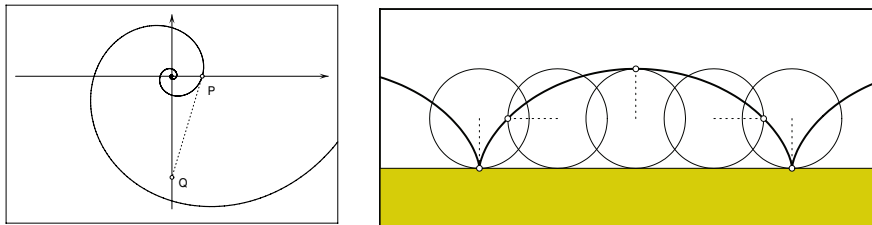


Fig. 16.1. Early curve rectifications. Left: the arc length of the logarithmic spiral (16.10) for $\theta \leq 0$ is equal to the length PQ on the tangent line. Right: the arc length of one arch of the cycloid (16.11) equals four times the diameter of the rolling circle.

Two of the earliest curves rectified are actually transcendental curves (see Fig. 16.1) — the *logarithmic spiral*, defined by the polar equation

$$r(\theta) = a e^{k\theta}, \quad (16.10)$$

and the *cycloid*, with the trigonometric parameterization

$$x(\theta) = a(\theta - \sin \theta), \quad y(\theta) = a(1 - \cos \theta). \quad (16.11)$$

In 1645 Evangelista Torricelli (1608–1647), a student of Galileo, rectified the logarithmic spiral (16.10) by the Archimedean “method of exhaustion” [56]: he showed that, for $-\infty < \theta \leq 0$, the arc length equals the length of the tangent at the point $P = (a, 0)$ defined by $\theta = 0$ extended to the point $Q = (0, -a/k)$ where it meets the y -axis — namely, $a\sqrt{1+k^2}$ (see Fig. 16.1). This result was quite remarkable, since the logarithmic spiral executes an *infinite* number of gyrations about the origin before (asymptotically) reaching it!

Galileo [207] observed that, if a body is dropped into a hole drilled through the center of the Earth, it will execute linear simple harmonic motion across the Earth diameter under the influence of gravity. Torricelli and Newton had conjectured that, if the initial tangential velocity due to the earth’s rotation is taken into account, the path will be a logarithmic spiral [21,466] — assuming the earth’s mass exerts gravitational attraction but does not otherwise impede the motion. This conjecture was wrong: the correct path, as argued by Robert Hooke, is an ellipse. The locus (16.10) is also known as the *equi-angular* spiral, since its tangent makes a fixed angle $\cot^{-1} k$ with the radius vector.

Another curve was subsequently rectified by Gilles Personne de Roberval (1602–1675) and Christopher Wren (1632–1723) — namely, the cycloid traced by a fixed point on a circle of radius a that rolls without slipping on a straight line (see Fig. 16.1). They showed that a single “arch” ($0 \leq \theta < 2\pi$) of this curve has length $8a$. Although it has now lapsed into obscurity, the cycloid was a “proving ground” for new mathematical methods and concepts in the mid-17th century: it caught the attention of all the leading scientists, and prompted international competitions and acrimonious controversies: see §8.3.3 for a discussion of its *tautochrone* and *brachistochrone* properties.

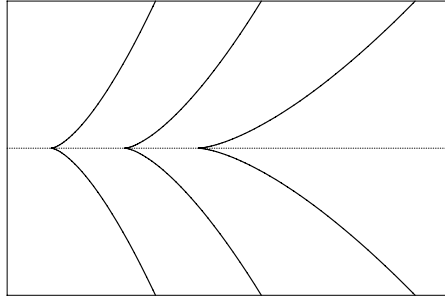


Fig. 16.2. The cubic (16.12) for various k values, with arc length given by (16.13).

It was not long before an algebraic curve succumbed to rectification, under the scrutiny of Pierre de Fermat (1601–1665), William Neil (1637–1670), and Hendrick van Heuraet (1633–1660). This was the cuspidal cubic defined by

$$x(t) = t^2, \quad y(t) = k t^3 \quad (16.12)$$

also known as the “semicubical parabola” (see Fig. 16.2). Its arc length s , measured from $t = 0$, is an *algebraic* function of the parameter:

$$s(t) = \frac{(9k^2t^2 + 4)^{3/2} - 8}{27k^2}. \quad (16.13)$$

Ironically, van Heuraet — an associate of Huygens — published his results in an appendix to van Schooten’s 1659 Latin version of Descartes, *Geometria a Renato Des Cartes*. Neil’s results also appeared in 1659, in the *Tractatus duo, prior de cycloide, posterior de cисsoide* published by John Wallis, and Fermat’s work followed in 1660 in *De linearum curvarum cum lineis rectis comparatione dissertatio geometrica* — an appendix to a treatise by de Lalouвre (this was the only publication by Fermat to appear during his lifetime).

Christiaan Huygens (1629–1695), in his *Horologium oscillatorium* of 1673, gave a historical account [254] of these rectifications that provoked arguments over the priority he attributed to van Heuraet and Wren for their discoveries — see Chap. 8 of [242]. This dispute reflects the philosophical importance of the problem of rectification, which had been considered impossible through long tradition that originated with Aristotle, was reinforced in the 11th century by Ibn Rushd (Averroes), and culminated in Descartes’ assertion quoted above. Huygens’ theory of evolutes and involutes, used in the design of his isochronous pendulum clock (see §8.3.3), offered profound new insights into this age-old problem. The cubic (16.12) was recognized as the evolute of a parabola, while the cycloid (8.44) has an identical (displaced) cycloid as its evolute.

All these results preceded the formal development of calculus. Although the theory of integration resolved the existential issue of curve arc length by defining it — for a (sufficiently smooth) parametric curve $(x(t), y(t))$ — as

$$s(t) = \int_0^t \sqrt{x'^2(\tau) + y'^2(\tau)} d\tau, \quad (16.14)$$

the awkward fact remained that this integral does not, in general, admit a closed-form reduction, even for curves with “simple” (polynomial or rational) parameterization. As the new field of differential geometry matured, it became customary in theoretical arguments to assume that $s \equiv t$, i.e., the integrand in (16.14) is unity. However, as demonstrated in §16.1, this *natural* or *arc-length* parameterization has only a hypothetical existence — it is incompatible with curves (other than straight lines) parameterized by simple functions.

16.3 Polynomial Parametric Speed

Although it is impossible for polynomial or rational curves (other than straight lines) to make the integrand in (16.14) identically equal to unity, a significant improvement can nevertheless be achieved for polynomial curves by requiring the argument of the square root to be the *perfect square* of a polynomial. Since the integrand will then be just a polynomial — rather than the square root of a polynomial — the expression (16.14) permits a closed-form reduction: the indefinite integral is just a polynomial of degree one higher.

This is the characteristic property of *Pythagorean-hodograph* (PH) curves, whose hodograph components $x'(t)$, $y'(t)$ satisfy the Pythagorean equation

$$x'^2(t) + y'^2(t) \equiv \sigma^2(t)$$

for some polynomial $\sigma(t)$, and are thus of the form

$$x'(t) = u^2(t) - v^2(t), \quad y'(t) = 2u(t)v(t), \quad \sigma(t) = u^2(t) + v^2(t)$$

where $u(t)$, $v(t)$ are relatively prime polynomials. The arc length function $s(t)$ obtained by integrating the parametric speed is *monotone increasing*, since it is the integral of a polynomial $\sigma(t) = u^2(t) + v^2(t)$ that is positive for all t . In motion control applications (e.g., driving a machine tool, robot end effector, or measurement probe at a prescribed speed along a curved path) the digital controller must repeatedly invert the function $s(t)$, i.e., for any given value s_* , the parameter value t_* defined by $s(t_*) = s_*$ must be accurately and efficiently computed. Although $s(t)$ does not in general admit a closed-form inversion, its monotonicity ensures that accurate and efficient numerical inversion can be performed using a few Newton–Raphson iterations (see Chap. 29 for a comprehensive discussion on the use of PH curves in this context). These ideas are also easily extended from planar curves to space curves.

The polynomial nature of their parametric speed endows PH curves with many other attractive features. For example, their unit tangents and normals are *rational* vector functions of the curve parameter. This means, for example, that the offset curves

$$\mathbf{r}_d(t) = \mathbf{r}(t) + d\mathbf{n}(t)$$

at distance d from a PH curve $\mathbf{r}(t)$ with unit normal $\mathbf{n}(t)$ are *rational curves* — they can be described *exactly* within the prevailing representation schemes of

CAD systems, without the need for heuristic numerical approximations [140]. Complete details concerning this property can be found in §17.5. In the case of spatial PH curves, one can define *rational adapted frames* and compute the “rotation–minimizing” frame (see Chap. 30). Planar and spatial PH curves also admit a closed–form evaluation of the energy integral (14.24), and in the interpolation of discrete data they typically yield *fairer loci* — with more even curvature distributions — than “ordinary” polynomial curves.

For efficient constructions of PH curves, and insight into their properties and behavior, the adoption of an appropriate computational model is critical. The methods of complex analysis provide such a model for planar PH curves, while for spatial PH curves we appeal to the algebra of quaternions.

16.4 Algebraically–rectifiable Curves

The arc length s of a parametric curve is said to be an *algebraic function* [46] of the parameter t if there exists a bivariate polynomial $F(\cdot, \cdot)$ such that

$$F(s, t) = 0.$$

This is clearly true of PH curves, since they have the property that s is just a *polynomial* in t . Curves for which s is a more general algebraic function of t were investigated in [385]. Although algebraic functions cannot, in general, be specified by simple closed–form expressions, it was shown in [385] that (16.14) is algebraic for a polynomial curve $\mathbf{r}(t) = (x(t), y(t))$ if and only if there exists a polynomial $h(t)$ such that

$$[x'^2(t) + y'^2(t)] h(t) \equiv h'^2(t). \quad (16.15)$$

As an immediate consequence, if the arc–length function (16.14) is algebraic, it must have the simple form

$$s(t) = 2\sqrt{h(t)} + \text{constant}.$$

Note that PH curves are subsumed as the special instance corresponding to

$$h(t) = \frac{1}{4} \left[\int_0^t u^2(\tau) + v^2(\tau) d\tau \right]^2.$$

In fact, the cuspidal cubic (16.12) studied by Fermat, Neil, and van Heuraet is the simplest (non–PH) case of such an *algebraically–rectifiable curve*, with

$$h(t) = \frac{(9k^2t^2 + 4)^3}{2916 k^4}.$$

Moreover, it is the *unique* non–PH cubic that is algebraically rectifiable [385].

It was further shown in [385] that the condition (16.15) is satisfied by non-constant polynomials $x'^2(t) + y'^2(t)$ and $h(t)$ if and only if they are expressible in terms of other polynomials $f(t)$ and $g(t)$ in the form

$$x'^2(t) + y'^2(t) = f(t) [3f'(t)g(t) + 2f(t)g'(t)]^2, \quad h(t) = f^3(t)g^2(t) \quad (16.16)$$

where $f(t)$ may be assumed square-free. In terms of $f(t)$ and $g(t)$, the most general form of the arc length function for algebraically rectifiable curves is

$$s(t) = 2g(t)\sqrt{f^3(t)}.$$

For further details on the nature of the solutions to (16.15), and examples of algebraically-rectifiable quartics and quintics, see [385].

16.5 Unit Speed Approximations

Since exact parameterizations of curves by rational functions of the arc length are impossible, it seems natural to enquire “how close” we can approximate this ideal. Consider, for example, a polynomial curve $\mathbf{r}(t)$ of degree n . With $0 < \alpha < 1$, the parameter transformation $t \in [0, 1] \rightarrow \tau \in [0, 1]$ defined by

$$t = \frac{(1 - \alpha)\tau}{\alpha(1 - \tau) + (1 - \alpha)\tau}$$

gives a rational representation of the same degree, and offers a single degree of freedom, α , to control the “parameter flow” over the curve. Using the integral

$$I = \int_0^1 (|\mathbf{r}'(\tau)| - 1)^2 d\tau \quad (16.17)$$

as a measure of “closeness” to arc-length parameterization (for which $I = 0$), the value of α that minimizes (16.17) can be found [151] as the unique root of a quadratic equation on $(0, 1)$ — see also [263]. Figure 16.3 shows the result of applying this method to a quadratic Bézier curve (i.e., a parabola segment). With the original parameterization, the parametric speed varies by a factor of ~ 2 below and above the desired unit speed, $\sigma = 1$. For the optimal rational parameterization, on the other hand, σ remains within $\sim 20\%$ of unity over the entire curve. In general, however, this “optimal parameterization” scheme offers rather limited scope for improvement, since fixing the curve degree n allows only one degree of freedom for the optimization process.

Another approach [154], based on the polynomial arc-length function $s(t)$ of PH curves, employs the Legendre series to compute a convergent sequence of (constrained) polynomial approximations $t_1(s), t_2(s), \dots$ to the *inverse* of this function [154], such that

$$\lim_{k \rightarrow \infty} t_k(s(t)) \equiv 1 \quad \text{for } t \in [0, 1],$$

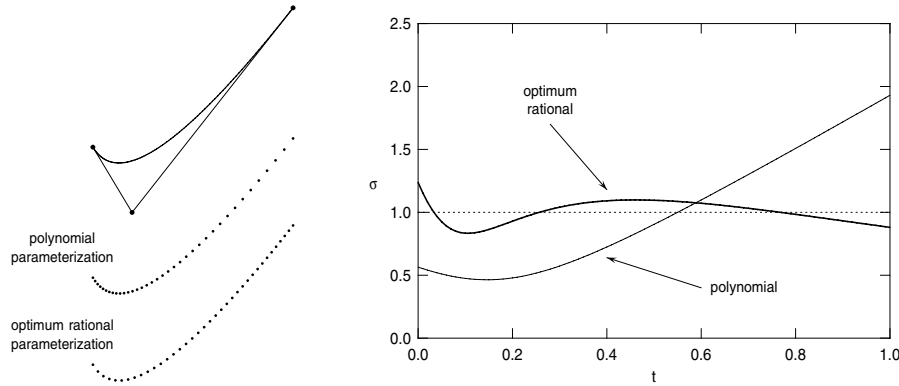


Fig. 16.3. Left: the parameter flow along a quadratic Bézier curve generated by the original polynomial parameterization and optimal rational parameterization of the same degree, minimizing (16.17). Right: comparison of parametric speed variations.

given the normalization $s \in [0, 1]$. The coefficients of $t_k(s)$ can be determined through closed-form reduction of certain integrals. For sufficiently high k , the re-parameterized version $\mathbf{r}_k(s) = \mathbf{r}(t_k(s))$ comes arbitrarily close to the exact arc-length parameterization, although it is formally of degree kn .

Methods for approximating arc-length parameterization based on the use of piecewise-polynomial re-parameterizations are described in [103, 237, 348].

Pythagorean–hodograph Curves

If the velocity vector of a particle is translated so as to start from the center of force, then the heads of the vectors trace out the particle’s hodograph, a locus of considerable antiquity in the history of mechanics.

H. Goldstein, *Classical Mechanics* [213]

The hodograph of a parametric curve $\mathbf{r}(t)$ in \mathbb{R}^n is just its derivative $\mathbf{r}'(t)$, regarded as a parametric curve in its own right. A polynomial curve $\mathbf{r}(t)$ in \mathbb{R}^n is a *Pythagorean-hodograph (PH) curve* if the n coordinate components of its hodograph are elements of a Pythagorean $(n+1)$ -tuple of polynomials — i.e., the sum of their squares coincides with the square of another polynomial $\sigma(t)$. Pythagorean-hodograph curves in \mathbb{R}^2 and \mathbb{R}^3 entail quite different approaches to their characterization, since Pythagorean polynomial triples and quartuples involve disparate algebraic structures. We are concerned here with just planar PH curves, and defer the treatment of spatial PH curves to Part V. A further extension, concerning PH curve formulations in Minkowski space $\mathbb{R}^{n,1}$ with n space-like and one time-like coordinates, is addressed in Chap. 24.

The definition, elementary properties, and Bernstein–Bézier representation of planar PH curves are presented below, exclusively in terms real variables. In Chap. 19 an alternative formulation is defined in terms of complex variables: the elegance and economy of expression this offers ensures its use as the basis for subsequent planar PH curve algorithms, such as construction of Hermite interpolants (Chap. 25), computation of the elastic bending energy integral (Chap. 26), and solution of the C^2 spline equations (Chap. 27).

17.1 Planar Pythagorean Hodographs

The key property that distinguishes a planar PH curve $\mathbf{r}(t) = (x(t), y(t))$ from an “ordinary” polynomial curve is the *a priori* incorporation of a Pythagorean

structure in its hodograph — namely, the components of $\mathbf{r}'(t) = (x'(t), y'(t))$ are required to satisfy the condition

$$x'^2(t) + y'^2(t) = \sigma^2(t) \quad (17.1)$$

for some polynomial $\sigma(t)$. This property is achieved by invoking the following characterization for Pythagorean triples of polynomials.

Theorem 17.1 *The Pythagorean condition*

$$a^2(t) + b^2(t) = c^2(t) \quad (17.2)$$

is satisfied by polynomials $a(t)$, $b(t)$, $c(t)$ if and only if they can be expressed in terms of other polynomials $u(t)$, $v(t)$, $w(t)$ in the form

$$\begin{aligned} a(t) &= [u^2(t) - v^2(t)] w(t), \\ b(t) &= 2u(t)v(t)w(t), \\ c(t) &= [u^2(t) + v^2(t)] w(t), \end{aligned} \quad (17.3)$$

where $u(t)$ and $v(t)$ are relatively prime.

Proof: That the form (17.3) is a *sufficient* condition for satisfaction of (17.2) follows immediately from substitution into this equation. To see that it is also *necessary*,¹ set $w(t) = \gcd(a(t), b(t), c(t))$ and consider the polynomials

$$\tilde{a}(t) = \frac{a(t)}{w(t)}, \quad \tilde{b}(t) = \frac{b(t)}{w(t)}, \quad \tilde{c}(t) = \frac{c(t)}{w(t)},$$

which are relatively prime and satisfy

$$\tilde{a}^2(t) + \tilde{b}^2(t) = \tilde{c}^2(t)$$

if $a(t)$, $b(t)$, $c(t)$ are a Pythagorean triple satisfying (17.2). Re-writing this as

$$\tilde{b}^2(t) = \tilde{c}^2(t) - \tilde{a}^2(t) = [\tilde{c}(t) + \tilde{a}(t)][\tilde{c}(t) - \tilde{a}(t)],$$

we note that $\tilde{c}(t) + \tilde{a}(t)$ and $\tilde{c}(t) - \tilde{a}(t)$ can have no common roots, since the existence of such roots would imply common roots of $\tilde{a}(t)$, $\tilde{b}(t)$, $\tilde{c}(t)$. Hence, every root of $\tilde{b}(t)$ must be a root of either $\tilde{c}(t) + \tilde{a}(t)$ or $\tilde{c}(t) - \tilde{a}(t)$, of even multiplicity, and without loss of generality we may write

$$\tilde{c}(t) + \tilde{a}(t) = 2u^2(t) \quad \text{and} \quad \tilde{c}(t) - \tilde{a}(t) = 2v^2(t)$$

for relatively prime polynomials $u(t)$ and $v(t)$, such that $\tilde{b}^2(t) = 4u^2(t)v^2(t)$. From these three equations, we may deduce that

$$\tilde{a}(t) = u^2(t) - v^2(t), \quad \tilde{b}(t) = 2u(t)v(t), \quad \tilde{c}(t) = u^2(t) + v^2(t),$$

and multiplying through by $w(t)$ yields the stated form (17.3). ■

¹ This argument is adapted from the well-known proof for integer Pythagorean triples: see, for example, [95]. For a more general proof, in the context of unique factorization domains of characteristic not equal to 2, see [292].

Remark 17.1 One can easily verify that solutions with $\gcd(a(t), b(t), c(t)) = \text{constant}$ correspond to taking $w(t) = \text{constant}$ and $\gcd(u(t), v(t)) = \text{constant}$ in (17.3). Such solutions are called *primitive* Pythagorean triples.

Thus, a planar PH curve $\mathbf{r}(t) = (x(t), y(t))$ is defined by substituting three polynomials $u(t)$, $v(t)$, $w(t)$ into the expressions

$$x'(t) = [u^2(t) - v^2(t)]w(t), \quad y'(t) = 2u(t)v(t)w(t) \quad (17.4)$$

and integrating. There is no loss of generality in identifying $x'(t)$ and $y'(t)$ with $a(t)$ and $b(t)$, respectively, in Theorem 17.1 — as noted in §2.2, alternatives to the polynomials $u(t)$ and $v(t)$ can always be obtained to satisfy the converse identification. Also, we assume in (17.4) that $u(t)$ and $v(t)$ are *relatively prime* — i.e., $\gcd(u(t), v(t)) = \text{constant}$ — since any non-constant common factor of $u(t)$ and $v(t)$ can be absorbed in $w(t)$. We must also discount certain choices for $w(t)$, $u(t)$, $v(t)$ that yield “degenerate” PH curves:

- (a) if $w(t) = 0$ or $u(t) = v(t) = 0$, the resulting hodograph $x'(t) = y'(t) = 0$ defines a *single point* rather than a continuous locus;
- (b) if $w(t)$, $u(t)$, $v(t)$ are all constants (with w and at least one of u , v non-zero) we obtain a uniformly-parameterized *straight line*, a trivial PH curve;
- (c) if $u(t)$ and $v(t)$ are constants, not both zero, and $w(t)$ is not a constant, the locus obtained by integrating (17.4) is again linear but its *parametric speed* is non-uniform — in general, it is *multiply-traced* over intervals delineated by odd-multiplicity roots of $w(t)$;
- (d) non-uniformly parameterized linear loci (parallel to the x -axis) also arise if $w(t) \neq 0$ and one of $u(t)$ and $v(t)$ is zero.

Henceforth we shall consider only cases where $w(t)$, $u(t)$, $v(t)$ are all non-zero, and $u(t)$, $v(t)$ are not *both* constants.

Remark 17.2 If $\lambda = \deg(w(t))$ and $\mu = \max(\deg(u(t)), \deg(v(t)))$, the PH curve obtained by integrating the hodograph (17.4) is of degree $n = \lambda + 2\mu + 1$.

Lemma 17.1 *PH curves of degree n have at most $n+3$ degrees of freedom, as compared to the $2(n+1)$ degrees of freedom associated with general polynomial curves of degree n .*

Proof: If $\mu = \max(\deg(u(t)), \deg(v(t)))$ the polynomials $u(t)$, $v(t)$ are each specified by at most $\mu + 1$ coefficients. If $\lambda = \deg(w(t))$ we associate only λ coefficients with $w(t)$, since without loss of generality we may assume its leading coefficient is unity. Hence, we may freely choose $\lambda + 2(\mu + 1)$ coefficients when specifying $u(t)$, $v(t)$, $w(t)$ and the integration constants provide two further freedoms, yielding a total of $\lambda + 2\mu + 4 = n + 3$ by the preceding remark. ■

However, these freedoms are not all available for manipulating the *intrinsic shape* of PH curves. Three of them are accounted for by choosing the origin and orientation of the coordinate axes, and another two correspond to freedoms of

parameterization — since the substitution $t \rightarrow at + b$ does not alter the shape or degree of the curve. Discounting these, we see that PH curves of degree n have $n - 2$ “shape freedoms” while general polynomial curves have $2n - 3$.

17.2 Bézier Control Points of PH Curves

We focus here primarily on hodographs of the form (17.4) with $w(t) = 1$ and $\gcd(u(t), v(t)) = \text{constant}$ — i.e., the *primitive* Pythagorean hodographs. Such hodographs define *regular* PH curves, satisfying $\mathbf{r}'(t) \neq \mathbf{0}$ for all t . A point on a parametric curve where $\mathbf{r}'(t)$ vanishes is a non-regular point — typically, a *cusp* or sudden tangent reversal. The use of a non-constant polynomial $w(t)$ in (17.4) incurs cusps (an undesirable feature) on the corresponding PH curve if $w(t)$ has real roots within the curve parameter domain. PH curves defined by integrating primitive hodographs are of *odd* degree, $n = 2\mu + 1$.

The simplest non-trivial PH curves arise from substituting $w(t) = 1$ and linear Bernstein-form polynomials

$$u(t) = u_0 b_0^1(t) + u_1 b_1^1(t), \quad v(t) = v_0 b_0^1(t) + v_1 b_1^1(t)$$

satisfying $u_0 v_1 - u_1 v_0 \neq 0$ and $(u_1 - u_0)^2 + (v_1 - v_0)^2 \neq 0$, so that $u(t), v(t)$ are relatively prime and not both constants, into (17.4) to obtain the hodograph

$$\begin{aligned} x'(t) &= (u_0^2 - v_0^2) b_0^2(t) + (u_0 u_1 - v_0 v_1) b_1^2(t) + (u_1^2 - v_1^2) b_2^2(t), \\ y'(t) &= 2u_0 v_0 b_0^2(t) + (u_0 v_1 + u_1 v_0) b_1^2(t) + 2u_1 v_1 b_2^2(t). \end{aligned}$$

Integrating this hodograph using (11.7) then yields a PH cubic with Bézier control points of the form

$$\begin{aligned} \mathbf{p}_1 &= \mathbf{p}_0 + \frac{1}{3} (u_0^2 - v_0^2, 2u_0 v_0), \\ \mathbf{p}_2 &= \mathbf{p}_1 + \frac{1}{3} (u_0 u_1 - v_0 v_1, u_0 v_1 + u_1 v_0), \\ \mathbf{p}_3 &= \mathbf{p}_2 + \frac{1}{3} (u_1^2 - v_1^2, 2u_1 v_1), \end{aligned} \tag{17.5}$$

the control point \mathbf{p}_0 , defined by the integration constants, being freely chosen.

Control polygons of the form (17.5) can also be characterized by intuitive geometrical constraints, that we derive in Chap. 18. Now according to the discussion of §17.1 the PH cubics possess just one “shape freedom,” and we show in Chap. 18 that this amounts to simply a *uniform scaling*. Hence, if we discount scaling as well as translation, rotation, and re-parameterization, the PH cubics are all segments of a *unique* curve, known (among other names) as *Tschirnhausen’s cubic*. A complete analysis of this curve, and a discussion of its many interesting properties, is deferred to Chap. 18.

Clearly, PH cubics are of limited value for free-form curve design due to their minimal shape flexibility — although a method for constructing Hermite

interpolants using “double” PH cubics (i.e., pairs of PH cubic segments with G^1 junctures) was described in [179]. From expressions (17.16) below we note that the curvature of PH cubic segments cannot change sign, i.e., they cannot exhibit inflections (since $uv' - u'v$ is simply a constant if $u(t), v(t)$ are linear). If we desire shape freedoms comparable to those of “ordinary” cubics, with a true inflectional capability, we must appeal to *quintic* PH curves.

To define quintic PH curves, we choose quadratic polynomials

$$u(t) = u_0 b_0^2(t) + u_1 b_1^2(t) + u_2 b_2^2(t), \quad v(t) = v_0 b_0^2(t) + v_1 b_1^2(t) + v_2 b_2^2(t)$$

in (17.4) and integrate, to obtain Bézier control points of the form

$$\begin{aligned} \mathbf{p}_1 &= \mathbf{p}_0 + \frac{1}{5}(u_0^2 - v_0^2, 2u_0v_0), \\ \mathbf{p}_2 &= \mathbf{p}_1 + \frac{1}{5}(u_0u_1 - v_0v_1, u_0v_1 + u_1v_0), \\ \mathbf{p}_3 &= \mathbf{p}_2 + \frac{2}{15}(u_1^2 - v_1^2, 2u_1v_1) + \frac{1}{15}(u_0u_2 - v_0v_2, u_0v_2 + u_2v_0), \\ \mathbf{p}_4 &= \mathbf{p}_3 + \frac{1}{5}(u_1u_2 - v_1v_2, u_1v_2 + u_2v_1), \\ \mathbf{p}_5 &= \mathbf{p}_4 + \frac{1}{5}(u_2^2 - v_2^2, 2u_2v_2), \end{aligned} \quad (17.6)$$

where \mathbf{p}_0 is again arbitrary. In this case, the condition for $u(t)$ and $v(t)$ to be relatively prime may be phrased as

$$(u_2v_0 - u_0v_2)^2 \neq 4(u_0v_1 - u_1v_0)(u_1v_2 - u_2v_1). \quad (17.7)$$

The PH quintics are in many respects analogous to the “ordinary” cubics — they may change their sense of curvature, and are capable of interpolating arbitrary first-order Hermite data, as described in Chap. 25. They are also the basic components of C^2 PH splines (see Chap. 27).

Lemma 17.2 *The PH quintic defined by (17.6) has either two real inflections or none, according to whether the quantity*

$$\Delta = (u_2v_0 - u_0v_2)^2 - 4(u_0v_1 - u_1v_0)(u_1v_2 - u_2v_1) \quad (17.8)$$

is positive or negative.

Proof : Substituting $u(t), v(t)$ into the numerator $k(t) = u(t)v'(t) - u'(t)v(t)$ of expression (17.16) below for the curvature, $k(t)$ is seen to be the quadratic with Bernstein coefficients

$$k_0 = 2(u_0v_1 - u_1v_0), \quad k_1 = -(u_2v_0 - u_0v_2), \quad k_2 = 2(u_1v_2 - u_2v_1).$$

Its discriminant $k_1^2 - k_0k_2$ is proportional to (17.8), and we observe that $\Delta \neq 0$ by virtue of the constraint (17.7). Thus, if $\Delta > 0$ there are two real t values for which κ vanishes, while if $\Delta < 0$ there are none. ■

The control point formulae (17.5) and (17.6) characterize PH cubics and quintics in terms of the coefficients of the two *real* polynomials $u(t)$ and $v(t)$. A significant economy of expression can be realized by interpreting them as the real and imaginary parts of a single *complex* polynomial, $\mathbf{w}(t) = u(t) + i v(t)$. This approach is developed in Chap. 19, and used extensively thereafter.

17.3 Parametric Speed and Arc Length

The parametric speed of a regular PH curve $\mathbf{r}(t) = (x(t), y(t))$ is given by

$$\sigma(t) = |\mathbf{r}'(t)| = \sqrt{x'^2(t) + y'^2(t)} = u^2(t) + v^2(t), \quad (17.9)$$

a *polynomial* in t . If $\mathbf{r}(t)$ is of (odd) degree n , $u(t)$ and $v(t)$ must be of degree $m = \frac{1}{2}(n - 1)$ and may be written in Bernstein form as

$$u(t) = \sum_{k=0}^m u_k b_k^m(t), \quad v(t) = \sum_{k=0}^m v_k b_k^m(t).$$

To express (17.9) in the Bernstein form

$$\sigma(t) = \sum_{k=0}^{n-1} \sigma_k b_k^{n-1}(t), \quad (17.10)$$

we invoke the multiplication rule (11.20) for Bernstein–form polynomials. This gives the coefficients of $\sigma(t)$ in terms of the coefficients of $u(t)$, $v(t)$ as

$$\sigma_k = \sum_{j=\max(0, k-m)}^{\min(m, k)} \frac{\binom{m}{j} \binom{m}{k-j}}{\binom{n-1}{k}} (u_j u_{k-j} + v_j v_{k-j}), \quad k = 0, \dots, n-1.$$

For the PH cubics, for example, $\sigma(t)$ is quadratic and has Bernstein coefficients

$$\sigma_0 = u_0^2 + v_0^2, \quad \sigma_1 = u_0 u_1 + v_0 v_1, \quad \sigma_2 = u_1^2 + v_1^2, \quad (17.11)$$

while for the PH quintics, $\sigma(t)$ is the quartic with Bernstein coefficients

$$\begin{aligned} \sigma_0 &= u_0^2 + v_0^2, & \sigma_1 &= u_0 u_1 + v_0 v_1, \\ \sigma_2 &= \frac{2}{3} (u_1^2 + v_1^2) + \frac{1}{3} (u_0 u_2 + v_0 v_2), \\ \sigma_3 &= u_1 u_2 + v_1 v_2, & \sigma_4 &= u_2^2 + v_2^2. \end{aligned} \quad (17.12)$$

In order to integrate $\sigma(t)$ and thus obtain the arc length s as a polynomial function of the parameter,

$$s(t) = \int_0^t \sigma(\tau) d\tau,$$

we use the integration rule (11.7) for the Bernstein basis functions. This gives

$$s(t) = \sum_{k=0}^n s_k \binom{n}{k} (1-t)^{n-k} t^k, \quad (17.13)$$

where

$$s_0 = 0 \quad \text{and} \quad s_k = \frac{1}{n} \sum_{j=0}^{k-1} \sigma_j, \quad k = 1, \dots, n.$$

Hence, the total arc length S is simply

$$S = s(1) = \frac{\sigma_0 + \sigma_1 + \dots + \sigma_{n-1}}{n}. \quad (17.14)$$

To compute the arc length of any PH curve segment $t \in [a, b]$ we need only take the difference $s(b) - s(a)$ of the polynomial (17.13) evaluated at a, b . The result is *exact* (modulo round-off errors if floating-point arithmetic is used), as distinct from arc length computations for “ordinary” polynomial curves — which require an inherently approximate numerical quadrature.

Similarly, it is much simpler to determine from (17.13) the parameter value t_* at which the arc length (measured from $t = 0$) has a given value s_* — i.e., to solve the equation

$$s(t_*) = s_*$$

for t_* . Consider, for example, the task of *uniform rendering* of a parametric curve. Typically, $\mathbf{r}(t)$ is rendered by evaluating at parameter values t_0, \dots, t_N corresponding to a uniform parameter increment $\Delta t = t_k - t_{k-1}$, $k = 1, \dots, N$. However, this yields an uneven spacing (by arc length) of the points $\mathbf{r}(t_k)$ on the curve, since the parametric speed $\sigma(t)$ is not, in general, constant.

Although the parametric speed of a PH curve is also non-constant, the simple form (17.13) of $s(t)$ allows us to easily compensate for its variation. Let t_0, \dots, t_N be the parameter values of the points uniformly spaced by an arc-length increment $\Delta s = S/N$, so that

$$s(t_k) = k \Delta s, \quad k = 1, \dots, N-1 \quad (17.15)$$

with $t_0 = 0$ and $t_N = 1$. Now since $\sigma(t) = ds/dt$ and $\sigma(t)$ is positive for all t when $\text{GCD}(u, v) = 1$, $s(t)$ is *monotone-increasing* with t , and hence for each k equation (17.15) has precisely one simple real root. Clearly, the root t_k of (17.15) lies between t_{k-1} and 1. As an initial approximation to it, we take

$$t_k^{(0)} = t_{k-1} + \frac{\Delta s}{\sigma(t_{k-1})}$$

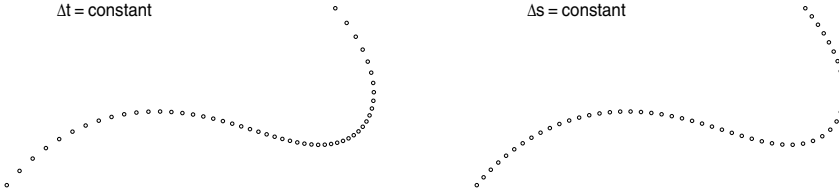


Fig. 17.1. Uniform increments in PH curve parameter (left) and arc length (right).

and obtain further refinements by applying the Newton–Raphson iteration

$$t_k^{(r)} = t_k^{(r-1)} - \frac{s(t_k^{(r-1)})}{\sigma(t_k^{(r-1)})}, \quad r = 1, 2, \dots$$

As is well known [110], such iterations are *quadratically convergent* for starting approximations sufficiently close to t_k , and in typical examples the parameter values t_k are obtained to an accuracy of 10^{-12} or better in just two or three iterations (see Fig. 17.1). Since *precise* uniformity by arc length is probably not crucial in many applications, a single iteration often suffices — typically, this gives uniform spacing to a relative accuracy of about 10^{-6} or better.

The problem of uniform arc-length rendering of a curve arises naturally in considering motion at *uniform speed* along a curve. This is the simplest case of a broader class of problems addressed by *real-time interpolator* algorithms for digital motion controllers. A comprehensive discussion of these problems, and the advantages of PH curves in solving them, can be found in Chap. 29.

17.4 Differential and Integral Properties

Since the parametric speed of the PH curve $\mathbf{r}(t)$ defined by integrating (17.4) is the *polynomial* (17.9) in t , its elementary differential properties — the unit tangent and normal, and the curvature — all have a *rational* dependence on the curve parameter. Specifically, they are defined in terms of the polynomials $u(t)$ and $v(t)$ by

$$\mathbf{t} = \frac{(u^2 - v^2, 2uv)}{\sigma}, \quad \mathbf{n} = \frac{(2uv, v^2 - u^2)}{\sigma}, \quad \kappa = 2 \frac{uv' - u'v}{\sigma^2}. \quad (17.16)$$

For a degree- n PH curve, \mathbf{t} and \mathbf{n} are rational functions of degree $n-1$, while κ is of degree $n-3$ in the numerator and $2n-2$ in the denominator.

The fact that the unit normal $\mathbf{n}(t)$ is a rational vector function on a PH curve $\mathbf{r}(t)$ means that its offsets $\mathbf{r}_d(t)$ at each distance d are *rational curves* — they admit exact representations in the standard rational Bézier form of CAD systems (see §17.5), eliminating the need for data-intensive and error-prone offset curve approximation schemes [140, 251, 252, 280, 362].

The rational curvature function is another advantage of PH curves over “ordinary” polynomial curves, since integrals of powers of the curvature with respect to the arc length $ds = \sigma dt$, defined by

$$I_n = \int_0^1 \kappa^n(t) \sigma(t) dt \quad \text{for } n = 0, 1, 2, \dots, \quad (17.17)$$

can be evaluated exactly by a partial fraction decomposition of the integrand (see §3.5). The case $n = 0$ gives the total arc length, discussed in §17.3 above. Since $\kappa = d\theta/ds$, where θ is the tangent angle with respect to a fixed direction, the integral I_1 defines the *net* rotation angle (i.e., with anti-clockwise rotation cancelling clockwise rotation) of the tangent along the curve. A modified form of I_1 is analyzed in §25.3, with $|\kappa|$ substituted for κ , defining the total *absolute* tangent rotation — this requires a subdivision of the parameter domain $[0, 1]$ at the t values that identify inflection points of the PH curve.

Finally, the integral I_2 is the *bending energy* of the curve — i.e., the strain energy stored in a thin, initially straight, elastic beam that is bent into the shape of the curve (see §14.2). Chapter 26 addresses the evaluation of I_2 for PH curves in detail. Note that evaluation of the integrals (17.17) by means of partial fraction decomposition requires a factorization of the parametric speed polynomial. Since, by construction, $\sigma(t)$ has no real roots, this factorization involves only terms that correspond to complex-conjugate root pairs (which may be combined into real quadratic factors).

17.5 Rational Offsets of PH Curves

The offsets at each distance d from a PH curve $\mathbf{r}(t)$, defined by

$$\mathbf{r}_d(t) = \mathbf{r}(t) + d \mathbf{n}(t), \quad (17.18)$$

admit *exact* representation as rational Bézier curves, because the unit normal $\mathbf{n}(t)$ has a rational dependence on the curve parameter t . In the case of cubics and quintics, the offset curves are of degree five and nine, respectively. Let the control points of the PH curve $\mathbf{r}(t)$ be written in homogeneous coordinates as

$$\mathbf{P}_k = (W_k, X_k, Y_k) = (1, x_k, y_k), \quad k = 0, \dots, n.$$

We define the forward differences of these coordinates by

$$\Delta \mathbf{P}_k = \mathbf{P}_{k+1} - \mathbf{P}_k = (0, \Delta x_k, \Delta y_k), \quad k = 0, \dots, n-1$$

where $\Delta x_k = x_{k+1} - x_k$, $\Delta y_k = y_{k+1} - y_k$, and we set $\Delta \mathbf{P}_k^\perp = (0, \Delta y_k, -\Delta x_k)$.

The offset at distance d from the PH curve $\mathbf{r}(t)$ is defined by (17.18), where the normal to $\mathbf{r}(t)$ is given by (17.16). The offset can be expressed as

$$\mathbf{r}_d(t) = \left(\frac{X(t)}{W(t)}, \frac{Y(t)}{W(t)} \right)$$

where $W(t)$, $X(t)$, $Y(t)$ are polynomials of degree $2n - 1$, whose coefficients

$$\mathbf{O}_k = (W_k, X_k, Y_k), \quad k = 0, \dots, 2n - 1$$

define the Bézier control points of the rational offset curve.

The homogeneous coordinates for the control points of the offset may be concisely expressed in terms of those of the original curve [148, 186] as

$$\mathbf{O}_k = \sum_{j=\max(0, k-n)}^{\min(n-1, k)} \frac{\binom{n-1}{j} \binom{n}{k-j}}{\binom{2n-1}{k}} (\sigma_j \mathbf{P}_{k-j} + d n \Delta \mathbf{P}_j^\perp), \quad k = 0, \dots, 2n-1.$$

Thus, for PH cubics, the control points of the rational quintic offsets are

$$\begin{aligned} \mathbf{O}_0 &= \sigma_0 \mathbf{P}_0 + 3d \Delta \mathbf{P}_0^\perp, \\ \mathbf{O}_1 &= \frac{1}{5} [2\sigma_1 \mathbf{P}_0 + 3\sigma_0 \mathbf{P}_1 + 3d(3\Delta \mathbf{P}_0^\perp + 2\Delta \mathbf{P}_1^\perp)], \\ \mathbf{O}_2 &= \frac{1}{10} [\sigma_2 \mathbf{P}_0 + 6\sigma_1 \mathbf{P}_1 + 3\sigma_0 \mathbf{P}_2 + 3d(3\Delta \mathbf{P}_0^\perp + 6\Delta \mathbf{P}_1^\perp + \Delta \mathbf{P}_2^\perp)], \\ \mathbf{O}_3 &= \frac{1}{10} [3\sigma_2 \mathbf{P}_1 + 6\sigma_1 \mathbf{P}_2 + \sigma_0 \mathbf{P}_3 + 3d(\Delta \mathbf{P}_0^\perp + 6\Delta \mathbf{P}_1^\perp + 3\Delta \mathbf{P}_2^\perp)], \\ \mathbf{O}_4 &= \frac{1}{5} [3\sigma_2 \mathbf{P}_2 + 2\sigma_1 \mathbf{P}_3 + 3d(2\Delta \mathbf{P}_1^\perp + 3\Delta \mathbf{P}_2^\perp)], \\ \mathbf{O}_5 &= \sigma_2 \mathbf{P}_3 + 3d \Delta \mathbf{P}_2^\perp. \end{aligned}$$

For PH quintics, the rational offsets are of degree 9 with control points

$$\begin{aligned} \mathbf{O}_0 &= \sigma_0 \mathbf{P}_0 + 5d \Delta \mathbf{P}_0^\perp, \\ \mathbf{O}_1 &= \frac{1}{9} [4\sigma_1 \mathbf{P}_0 + 5\sigma_0 \mathbf{P}_1 + 5d(5\Delta \mathbf{P}_0^\perp + 4\Delta \mathbf{P}_1^\perp)], \\ \mathbf{O}_2 &= \frac{1}{18} [3\sigma_2 \mathbf{P}_0 + 10\sigma_1 \mathbf{P}_1 + 5\sigma_0 \mathbf{P}_2 + 5d(5\Delta \mathbf{P}_0^\perp + 10\Delta \mathbf{P}_1^\perp + 3\Delta \mathbf{P}_2^\perp)], \\ \mathbf{O}_3 &= \frac{1}{42} [2\sigma_3 \mathbf{P}_0 + 15\sigma_2 \mathbf{P}_1 + 20\sigma_1 \mathbf{P}_2 + 5\sigma_0 \mathbf{P}_3 \\ &\quad + 5d(5\Delta \mathbf{P}_0^\perp + 20\Delta \mathbf{P}_1^\perp + 15\Delta \mathbf{P}_2^\perp + 2\Delta \mathbf{P}_3^\perp)], \\ \mathbf{O}_4 &= \frac{1}{126} [\sigma_4 \mathbf{P}_0 + 20\sigma_3 \mathbf{P}_1 + 60\sigma_2 \mathbf{P}_2 + 40\sigma_1 \mathbf{P}_3 + 5\sigma_0 \mathbf{P}_4 \\ &\quad + 5d(5\Delta \mathbf{P}_0^\perp + 40\Delta \mathbf{P}_1^\perp + 60\Delta \mathbf{P}_2^\perp + 20\Delta \mathbf{P}_3^\perp + \Delta \mathbf{P}_4^\perp)], \\ \mathbf{O}_5 &= \frac{1}{126} [5\sigma_4 \mathbf{P}_1 + 40\sigma_3 \mathbf{P}_2 + 60\sigma_2 \mathbf{P}_3 + 20\sigma_1 \mathbf{P}_4 + \sigma_0 \mathbf{P}_5 \\ &\quad + 5d(\Delta \mathbf{P}_0^\perp + 20\Delta \mathbf{P}_1^\perp + 60\Delta \mathbf{P}_2^\perp + 40\Delta \mathbf{P}_3^\perp + 5\Delta \mathbf{P}_4^\perp)], \end{aligned}$$

$$\begin{aligned}
\mathbf{O}_6 &= \frac{1}{42} [5\sigma_4 \mathbf{P}_2 + 20\sigma_3 \mathbf{P}_3 + 15\sigma_2 \mathbf{P}_4 + 2\sigma_1 \mathbf{P}_5 \\
&\quad + 5d(2\Delta\mathbf{P}_1^\perp + 15\Delta\mathbf{P}_2^\perp + 20\Delta\mathbf{P}_3^\perp + 5\Delta\mathbf{P}_4^\perp)], \\
\mathbf{O}_7 &= \frac{1}{18} [5\sigma_4 \mathbf{P}_3 + 10\sigma_3 \mathbf{P}_4 + 3\sigma_2 \mathbf{P}_5 + 5d(3\Delta\mathbf{P}_2^\perp + 10\Delta\mathbf{P}_3^\perp + 5\Delta\mathbf{P}_4^\perp)], \\
\mathbf{O}_8 &= \frac{1}{9} [5\sigma_4 \mathbf{P}_4 + 4\sigma_3 \mathbf{P}_5 + 5d(4\Delta\mathbf{P}_3^\perp + 5\Delta\mathbf{P}_4^\perp)], \\
\mathbf{O}_9 &= \sigma_4 \mathbf{P}_5 + 5d \Delta\mathbf{P}_4^\perp.
\end{aligned}$$

Figure 17.2 illustrates the control polygons specified by the above formulae, and the offset curves they define, for some PH quintics. Since the offsets are *rational* curves (each control point having, in general, a different weight W_k) the control polygons of the offsets are not necessarily intuitive indicators of the shape of the curves they define. Figure 17.3 shows that, as d increases, the offset curve control points move uniformly along straight lines.

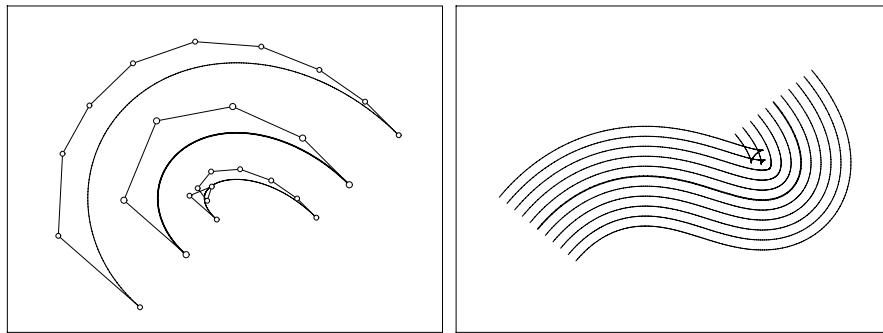


Fig. 17.2. Left: Bézier control polygons for degree 9 interior and exterior offsets to a PH quintic (note that each control point has a different weight). Right: the rational offsets are exact for every d — even when they develop cusps and self-intersections.

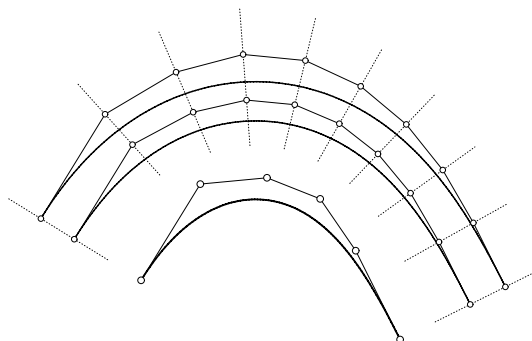


Fig. 17.3. Control polygons for offsets at two different distances d from a PH quintic: as d increases, the offset control points move uniformly along certain straight lines.

Tschirnhausen's Cubic

... I was very much pleased by his manners, and I recognize in that young man an outstanding and very promising talent. He showed me quite a number of [his] results (inventa), analytic as well as geometric and of reasonably good taste. From this I easily conclude how much can be expected from him ...

Gottfried Wilhelm Leibniz, letter to Henry Oldenburg
of December 28, 1675 — as quoted in [289]

18.1 Ehrenfried Walther von Tschirnhaus

The study of planar PH curves brings us to an unexpected acquaintance with Count Ehrenfried Walther von Tschirnhaus¹ (Fig. 18.1) — a less-prominent contemporary of Huygens, Leibniz, and Newton. Born on April 10, 1651 in Kieslingswalde (now Ślawnikowice in Poland), he was schooled privately and at Görlitz Gymnasium before entering the University of Leiden in 1668, where he studied philosophy, mathematics, and medicine. After completing his studies in Leiden, he travelled to England carrying a letter of recommendation from the philosopher Baruch Spinoza to Henry Oldenburg, Secretary of the newly-formed Royal Society of London for the Improvement of Natural Knowledge (and also editor of its *Philosophical Transactions*).

From Oldenburg, Tschirnhaus secured further letters of introduction to Huygens and Leibniz in Paris. During 1675–76, Tschirnhaus developed a close friendship with Leibniz and maintained regular correspondence with him after leaving Paris to visit Italy, where he became engaged in studying the use of mirrors to achieve very high temperatures by focusing sunlight. In this context,

¹ One occasionally sees [78] his name erroneously rendered as *Tschirnhausen*. The –en suffix is an antiquated genitive device in German, facilitating pronunciation of the possessive form of names ending with an “s”— as in *Tschirnhausen's cubic*.



Fig. 18.1. Left: portrait of Ehrenfried Walther von Tschirnhaus (1651–1708) from a small engraving. (Elke Estel, Kupferstich-Kabinett, Staatliche Kunstsammlungen Dresden). Right: example of a mirror used by Tschirnhaus to achieve temperatures up to 1500°C by focusing sunlight (Jürgen Karpinski, Mathematisch–Physikalischer Salon, Staatliche Kunstsammlungen Dresden). Reproduced with permission.

he became interested in *catacaustics* — i.e., the envelopes of parallel light rays reflected by a mirror. His knowledge of optics played an important role in his endeavor to develop the manufacture of hard-fired porcelain, in collaboration with Johann Friedrich Böttger (true porcelain had been produced in China for several centuries, but the materials and process remained unknown in Europe at that time). Böttger, an alchemist interested in transmutation of base metals into gold, was imprisoned in 1700 by Augustus the Strong, Elector of Saxony, who wished to be the exclusive beneficiary of his efforts. Tschirnhaus “saved” Böttger by suggesting they work together on production of porcelain instead, a collaboration that led to the now-famous *Meissen porcelain*.

Tschirnhaus died in Dresden on October 11, 1708. Although many — often tangential — accounts of his abilities, accomplishments, and his appreciation of contemporary scientific developments are unsympathetic, a less dismissive contrarian view of his contributions has begun to emerge [289]. By no means a leading figure in the scientific revolution engendered by the development of calculus, Tschirnhaus nevertheless bequeathed some noteworthy results that carry his name. In the theory of equations, *Tschirnhaus transformations* [77] are employed to eliminate certain lower-order terms from a polynomial $p(t)$ of degree n . Tschirnhaus proposed this method in his paper “Methodus auferendi omnes terminos intermedios ex data aequatione,” or Method of eliminating all intermediate terms from a given equation,² published in the *Acta Eruditorum*

² See [446] for an English translation.

of May 1683. Elimination of the t^{n-1} term from a given degree- n polynomial equation $p(t) = a_0 + \cdots + a_{n-1}t^{n-1} + a_nt^n = 0$ is easily accomplished by the change of variables $t = \tau - a_{n-1}/na_n$. This was already known to Descartes, and Tschirnhaus sought to remove successive lower-order terms.

He considered cubic equations of the form

$$t^3 = qt + r, \quad (18.1)$$

from which the quadratic term has been removed, and he sought to eliminate the linear term. He achieved this by a transformation $t \rightarrow \tau$ equivalent to

$$t = \frac{2qa - 3r + 3a\tau}{q - 3a^2 - 3\tau}, \quad (18.2)$$

where a is either root of the quadratic equation

$$3qa^2 - 9ra + q^2 = 0. \quad (18.3)$$

Substituting (18.2) into (18.1), clearing denominators, and using (18.3), one finds that the cubic is reduced to the desired form,

$$\tau^3 = \frac{(27r^2 - 4q^3)(2q^2 - 9ra)}{27q^2}. \quad (18.4)$$

Hence, by first solving a quadratic equation, the solutions to the cubic (18.1) can be obtained by cube root extractions. Of course, the right-hand side of (18.4) has a complex value if $27r^2 - 4q^3 < 0$ (since a is then complex).

Expression (18.2), extended to complex values of t and τ , defines a *Möbius transformation* (see §4.8) of the complex plane. Given a general cubic $p(t)$, elimination of the t^2 term is accomplished through a shift along the real axis, that positions the centroid of its three roots at the origin. The Tschirnhaus transform (18.2) then maps the complex plane in such a way that the roots lie symmetrically on a circle centered at the origin (as noted in §4.8, Möbius transformations can map any three points to any other three points).

Tschirnhaus falls short on the promise, in the title of his paper, to present a method that eliminates *all* intermediate terms from a polynomial equation $p(t) = 0$ of degree n , thus reducing it to the form $\tau^n = c$. Of course, we now know this is impossible using only arithmetic operations and root extractions — in 1824 the brilliant but tragically short-lived Norwegian mathematician Niels Henrik Abel (1802–1829) published a proof that “solution by radicals” is impossible for the quintic equation. Nevertheless, subsequent studies of the quintic by Hermite, Klein, and others often use the Bing–Jerrard “reduced” or “normal” form,

$$t^5 + at + b = 0,$$

obtained from a general quintic by means of Tschirnhaus transformations.

In 2003, the *Tschirnhaus Gesellschaft* was founded in Dresden as a society to help preserve and promote the achievements of E. W. von Tschirnhaus. The

society coordinates the activities of the Mathematisch–Physikalischer Salon at the Staatliche Kunstsammlungen Dresden (Dresden State Art Collections) — see http://www.tschirnhaus-gesellschaft.de/e_index.html.

18.2 Tschirnhaus and Caustic Curves

Tschirnhaus also contributed to the foundations of geometrical optics, through his studies of *caustic curves*. Two seminal texts on the geometrical treatment of light propagation are the *Traité de la Lumière* [255] published in 1690 by Christiaan Huygens, and the *Opticks* [346] of Isaac Newton, published in 1704. Huygens employed the *wave theory* of light, while Newton's exposition was based on *light rays* (regarded as the paths of discrete “particles” of light). In modern geometrical optics, descriptions of light propagation in terms of rays and wavefronts are regarded as equally valid, complementary, models.

A fundamental problem of geometrical optics is to describe what happens when a system of rays or wavefronts, emanating from a finitely or infinitely distant point source, is reflected or refracted by a mirror or a lens. Consider a wavefront W incident on a lens or mirror S (note that W is spherical or planar according to whether the point source is finitely or infinitely distant). Prior to reflection/refraction, *Huygens' Principle* describes the propagation of W — namely, at each subsequent time t , the shape of W is specified by the *offsets* (or *parallels*) to its initial shape. The incident rays are the normals to this family of parallel wavefronts, and the wavefronts corresponding to fixed time increments mark off equal distances along the rays.

Suppose W' is the new shape of the wavefront, after reflection/refraction by S . The propagation of W' is again governed by Huygens' Principle, and the reflected/refracted rays are the normals to the new system of wavefronts, all parallel to W' . These light rays appear to “concentrate” along a certain curve, that Tschirnhaus called the *caustic*,³ from the Greek for *burning*. The caustic C is the *envelope* of the family of reflected/refracted rays — i.e., the rays constitute the family of tangents to the caustic curve. Furthermore, since the rays are orthogonal to the reflected/refracted wavefront W' , the caustic is also the *evolute* — i.e., the locus of centers of curvature — of W' . The family of reflected/refracted wavefronts, parallel to W' , are the *involutes* of the caustic C — they all have C as their common locus of centers of curvature. See §8.3 for a review of the geometry of evolutes, involutes, parallel curves, and families of tangent and normal lines; a more detailed review of their significance in the context of geometrical optics may be found in [159].

Tschirnhaus first discusses caustics in a 1682 *Acta Eruditorum* paper, the text of his speech upon admission to the Royal Academy of Sciences in Paris. Specifically, he considers the caustic for reflection of parallel incident rays by

³ Distinct terms, *catacaustic* and *diacaustic*, were originally employed to distinguish between caustics by reflection and refraction, but are no longer in common use.

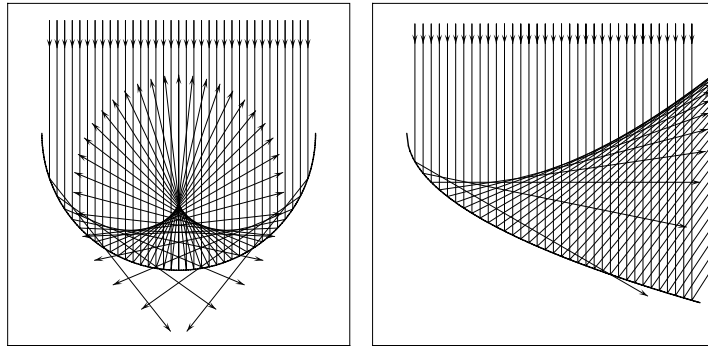


Fig. 18.2. Caustic curves studied by Tschirnhaus: reflection of parallel rays by a circle (left) and by a parabola (right). Only primary reflections are considered here.

a spherical mirror (Fig. 18.2). This curve had already been discussed before the Academy in 1678, when Huygens read his *Traité de la Lumière* — whose publication was delayed to 1690 — but the possibility that Tschirnhaus was guilty of plagiarism has been discounted in view of the fact that he was in Italy when Huygens read before the Academy, and his direct experience of caustics through experiments with burning mirrors [289, 390].

In a 1690 *Acta Eruditorum* paper, Tschirnhaus further elaborated upon caustics by reflection, apparently prompted by questions concerning his 1682 paper. He derived caustics for reflection by a circle, parabola, and hyperbola, referring to them as curves defined by “the crossing of the reflected rays,” an expression that presages the *dual form* of a curve, regarded as the envelope of a family of tangent lines rather than a locus of points. The envelope concept was more fully developed in a 1694 *Acta Eruditorum* paper by Leibniz, but the term was itself apparently first introduced [390] by Gaspard Monge in his *Application de l'analyse à la géométrie* (1795).

Figure 18.3 shows “completions” of the envelopes apparent in Fig. 18.2. In the case of reflection by a circle, the caustic is an *epicycloid* — i.e., the locus traced by a chosen point on the circumference of a circle that rolls without slipping on the exterior of a fixed circle. When the reflecting mirror is of unit radius, and the fixed and rolling circles have radii $\frac{1}{2}$ and $\frac{1}{4}$, respectively, the epicycloid is described for $\theta \in [0, 2\pi]$ by the parametric equations

$$x(\theta) = \frac{3 \cos \theta + \cos 3\theta}{4}, \quad y(\theta) = \frac{3 \sin \theta + \sin 3\theta}{4}.$$

In the case of reflection by the parabola $y^2 = 2px$, the completed caustic is the cubic curve defined by

$$16x^3 - 72x^2 - 108y^2 + 81x = 0,$$

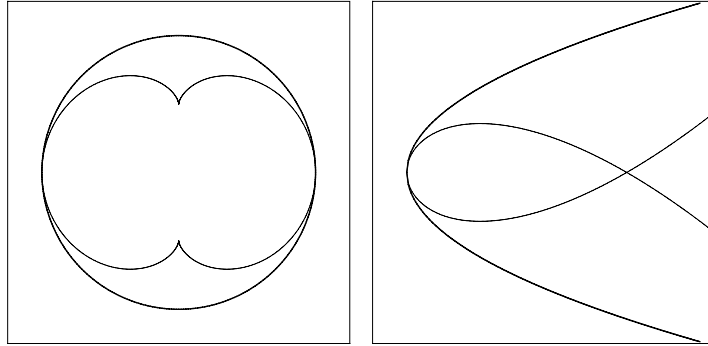


Fig. 18.3. Completions of the envelopes in Fig. 18.2 defining caustics for reflection by a circle and a parabola — left: an epicycloid, and right: Tschirnhausen's cubic.

which has the parameterization

$$x(t) = \frac{9}{4}t^2, \quad y(t) = \frac{3\sqrt{3}}{4}t(t^2 - 1). \quad (18.5)$$

This curve can be found (in slightly different variants) listed in most catalogs of special plane curves [300, 308] as *Tschirnhausen's cubic*⁴ — although it is also known as *l'Hôpital's cubic* and the *trisectrix of Catalan*. The Marquis de l'Hôpital (1661–1704) discussed it in his book *Analyse des infiniment petits, pour l'intelligence des lignes courbes* of 1696, commonly regarded as the first text on the calculus (see Chap. 8), and the Belgian mathematician Eugène Catalan (1814–1894) showed that it can be used to trisect angles.

To understand the latter use, we need to introduce *pedal curves*. Given a smooth curve C and a fixed point \mathbf{o} , the pedal curve C' of C with respect to \mathbf{o} is the locus of points where perpendiculars drawn from \mathbf{o} to the tangent lines of C meet those tangents. Conversely, given C' and \mathbf{p} , one may ask — which curve C has C' as its pedal curve with respect to \mathbf{o} ? We call C the *negative pedal* of C' with respect to \mathbf{o} , and we can construct C as follows. Through each point $\mathbf{p} \in C'$, we draw a line orthogonal to the line from \mathbf{o} to \mathbf{p} : these lines are the tangents to C , and we can recover C as their envelope.

Tschirnhausen's cubic can also be interpreted as the *negative pedal of a parabola with respect to its focus* — i.e., if \mathbf{f} is the focus and we construct lines through each point \mathbf{p} of the parabola that are orthogonal to the lines between \mathbf{f} and \mathbf{p} , the envelope of this family of lines is precisely the Tschirnhaus cubic. Figure 18.4 illustrates this for the parabola $y^2 = x$, with focus $\mathbf{f} = (\frac{1}{4}, 0)$.

The trisection property of Tschirnhausen's cubic arises from its negative pedal relation to the parabola (with respect to the focus), as illustrated in Fig. 18.5. To verify this property, it is convenient to use the polar form

⁴ Gomes Teixeira's *Traité des Courbes Spéciales Remarquables Planes et Gauches* cites the Strasbourg 1900 thesis of M. Archibald as establishing this name [214].

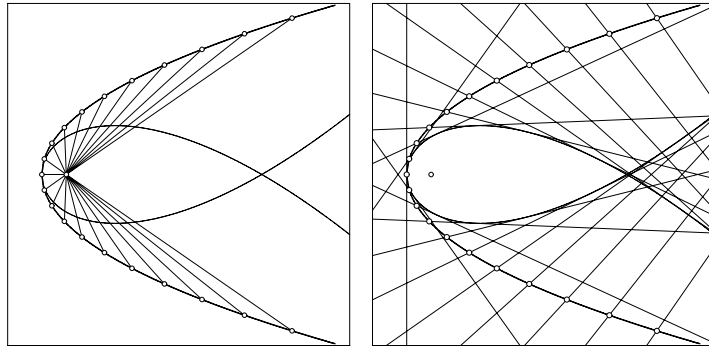


Fig. 18.4. Tschirnhausen's cubic interpreted as the negative pedal of the parabola $y^2 = x$ with respect to its focus. Left: radial lines drawn from the focus to points on the parabola. Right: a family of lines through each point on the parabola, orthogonal to the radial lines — Tschirnhausen's cubic is the envelope of this family of lines.

$$r(\theta) = \frac{1}{4} \sec^3\left(\frac{1}{3}\theta\right)$$

of the Tschirnhaus cubic, relative to the focus $(\frac{1}{4}, 0)$ as pole and the negative x -axis as the direction $\theta = 0$. The parameterization (18.5) can be recovered from this polar form by using the trigonometric identities

$$\sin \theta = 3 \sin \frac{1}{3}\theta - 4 \sin^3 \frac{1}{3}\theta, \quad \cos \theta = 4 \cos^3 \frac{1}{3}\theta - 3 \cos \frac{1}{3}\theta$$

in $x = \frac{1}{4} - r(\theta) \cos \theta$, $y = r(\theta) \sin \theta$ and setting $\tan(\frac{1}{3}\theta) = -\sqrt{3}t$.

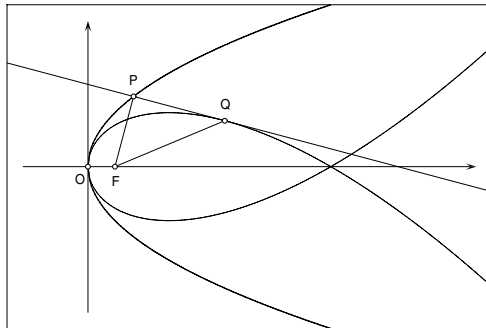


Fig. 18.5. Catalan's interpretation of the Tschirnhaus cubic as a trisectrix. Let O be the origin and F be the focus of the parabola. Also, let P be a generic point on the parabola, the line through P orthogonal to FP being tangent to the Tschirnhaus cubic at the point Q . Then $\angle PFQ = \frac{1}{3} \angle OFQ$ defines the angle trisection property.

18.3 Unique Pythagorean–hodograph Cubic

Straight lines are, trivially, PH curves. The simplest non-trivial PH curves are the cubics, with Bézier control points given in terms of the four parameters u_0, u_1 and v_0, v_1 by expressions (17.5). The Bézier representation of PH cubics is especially attractive because it admits intuitive constraints on the control-polygon geometry that serve to identify PH cubics within the set of all cubics (see Fig. 18.6). This structure reflects the fact that, as alluded to in §17.2, all PH cubics are actually segments of a unique curve, *Tschirnhausen's cubic*.

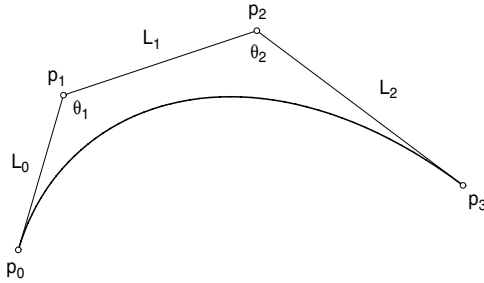


Fig. 18.6. The geometrical parameters defining a cubic Bézier control polygon — by Theorem 18.1, this cubic is a PH curve if and only if $L_1 = \sqrt{L_2 L_0}$ and $\theta_2 = \theta_1$.

Theorem 18.1 *For a plane cubic $\mathbf{r}(t)$ with control points $\mathbf{p}_0, \mathbf{p}_1, \mathbf{p}_2, \mathbf{p}_3$ let $L_0 = |\Delta\mathbf{p}_0| = |\mathbf{p}_1 - \mathbf{p}_0|$, $L_1 = |\Delta\mathbf{p}_1| = |\mathbf{p}_2 - \mathbf{p}_1|$, $L_2 = |\Delta\mathbf{p}_2| = |\mathbf{p}_3 - \mathbf{p}_2|$ be the lengths of the control polygon legs, and θ_1, θ_2 be the control polygon angles at the interior vertices $\mathbf{p}_1, \mathbf{p}_2$ as in Fig. 18.6. Then the conditions*

$$L_1 = \sqrt{L_2 L_0} \quad \text{and} \quad \theta_2 = \theta_1 \quad (18.6)$$

are sufficient and necessary for the hodograph $\mathbf{r}'(t)$ to be Pythagorean.

Proof : Consider a planar PH cubic with control points of the form (17.5). The lengths of the control-polygon legs are given by

$$\begin{aligned} L_0 &= |\Delta\mathbf{p}_0| = \frac{1}{3}(u_0^2 + v_0^2), \\ L_1 &= |\Delta\mathbf{p}_1| = \frac{1}{3}\sqrt{(u_0^2 + v_0^2)(u_1^2 + v_1^2)}, \\ L_2 &= |\Delta\mathbf{p}_2| = \frac{1}{3}(u_1^2 + v_1^2), \end{aligned}$$

and they clearly satisfy the condition $L_1 = \sqrt{L_2 L_0}$. Again using expressions (17.5), the sines and cosines of the angles θ_1, θ_2 are defined by

$$\begin{aligned}\sin \theta_1 &= \frac{(\Delta \mathbf{p}_1 \times \Delta \mathbf{p}_0) \cdot \mathbf{z}}{L_1 L_0} = \frac{u_1 v_0 - u_0 v_1}{\sqrt{(u_0^2 + v_0^2)(u_1^2 + v_1^2)}}, \\ \sin \theta_2 &= \frac{(\Delta \mathbf{p}_2 \times \Delta \mathbf{p}_1) \cdot \mathbf{z}}{L_2 L_1} = \frac{u_1 v_0 - u_0 v_1}{\sqrt{(u_0^2 + v_0^2)(u_1^2 + v_1^2)}},\end{aligned}$$

and

$$\begin{aligned}\cos \theta_1 &= -\frac{\Delta \mathbf{p}_1 \cdot \Delta \mathbf{p}_0}{L_1 L_0} = -\frac{u_0 u_1 + v_0 v_1}{\sqrt{(u_0^2 + v_0^2)(u_1^2 + v_1^2)}}, \\ \cos \theta_2 &= -\frac{\Delta \mathbf{p}_2 \cdot \Delta \mathbf{p}_1}{L_2 L_1} = -\frac{u_0 u_1 + v_0 v_1}{\sqrt{(u_0^2 + v_0^2)(u_1^2 + v_1^2)}},\end{aligned}$$

and since their sines and cosines are identical, we clearly have $\theta_2 = \theta_1$.

Conversely, suppose that $\mathbf{r}(t)$ is a plane cubic whose control polygon satisfies $L_1 = \sqrt{L_2 L_0}$ and $\theta_2 = \theta_1$ ($= \theta$, say). We can adopt a coordinate system in which the control-polygon legs have the form

$$\Delta \mathbf{p}_0 = L_0(1, 0), \quad \Delta \mathbf{p}_1 = \sqrt{L_2 L_0}(-\cos \theta, \sin \theta), \quad \Delta \mathbf{p}_2 = L_2(\cos 2\theta, -\sin 2\theta)$$

and the quartic polynomial

$$|\mathbf{r}'(t)|^2 = \left| \sum_{k=0}^2 \Delta \mathbf{p}_k b_k^2(t) \right|^2 = \sum_{k=0}^4 c_k b_k^4(t)$$

then has the Bernstein coefficients

$$\begin{aligned}c_0 &= 9L_0^2, \quad c_1 = -9L_0\sqrt{L_2} \cos \theta, \\ c_2 &= 3L_2 L_0(2 + \cos 2\theta), \\ c_3 &= -9L_2\sqrt{L_0} \cos \theta, \quad c_4 = 9L_2^2,\end{aligned}$$

and coincides precisely with the square of the quadratic polynomial

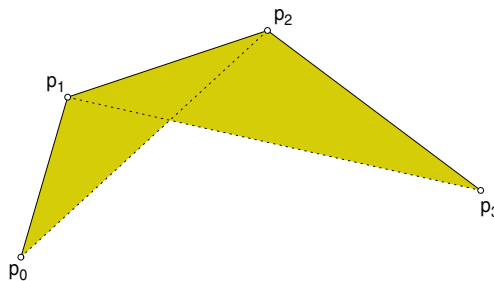


Fig. 18.7. The conditions (18.6) for a cubic Bézier curve to possess a Pythagorean hodograph are equivalent to similarity of the two triangles $\Delta \mathbf{p}_0 \mathbf{p}_1 \mathbf{p}_2$ and $\Delta \mathbf{p}_1 \mathbf{p}_2 \mathbf{p}_3$.

$$\sigma(t) = 3 [L_0 b_0^2(t) - \sqrt{L_2 L_0} \cos \theta b_1^2(t) + L_2 b_2^2(t)].$$

Hence, the hodograph of the cubic $\mathbf{r}(t)$ is Pythagorean. ■

One can easily verify that the Bézier control polygon constraints (18.6) are equivalent [355] to the requirement that the triangles with the control points $\mathbf{p}_0, \mathbf{p}_1, \mathbf{p}_2$ and $\mathbf{p}_1, \mathbf{p}_2, \mathbf{p}_3$ as vertices are similar — see Fig. 18.7. For an alternative characterization of the PH cubics, see [340].

Lemma 18.1 *PH cubics defined by the control points (17.5) exhibit a crunode (self-intersection) corresponding to the distinct parameter values*

$$t = \frac{(u_0^2 + v_0^2) - (u_0 u_1 + v_0 v_1) \pm \sqrt{3}(u_0 v_1 - u_1 v_0)}{(u_0 - u_1)^2 + (v_0 - v_1)^2}.$$

Proof : A self-intersection of the curve $\mathbf{r}(t) = (x(t), y(t))$ corresponds to a pair of parameter values $t, t + \tau$ such that $x(t + \tau) = x(t)$ and $y(t + \tau) = y(t)$ with $\tau \neq 0$. In other words, we require the two equations

$$\begin{aligned} p(t, \tau) &= \frac{x(t + \tau) - x(t)}{\tau} = \frac{1}{6} x'''(t) \tau^2 + \frac{1}{2} x''(t) \tau + x'(t) = 0, \\ q(t, \tau) &= \frac{y(t + \tau) - y(t)}{\tau} = \frac{1}{6} y'''(t) \tau^2 + \frac{1}{2} y''(t) \tau + y'(t) = 0, \end{aligned}$$

to have a common root τ for some value of t (the division by τ eliminates the solution $\tau = 0$). Now the condition for the two polynomials $p(t, \tau)$ and $q(t, \tau)$ to have a common root τ is that their *resultant* with respect to τ ,

$$r(t) = \text{Resultant}_\tau(p(t, \tau), q(t, \tau)),$$

must vanish. The resultant can be expressed as the Sylvester determinant

$$r(t) = \begin{vmatrix} \frac{1}{6} x'''(t) & \frac{1}{2} x''(t) & x'(t) & 0 \\ 0 & \frac{1}{6} x'''(t) & \frac{1}{2} x''(t) & x'(t) \\ \frac{1}{6} y'''(t) & \frac{1}{2} y''(t) & y'(t) & 0 \\ 0 & \frac{1}{6} y'''(t) & \frac{1}{2} y''(t) & y'(t) \end{vmatrix}.$$

Expanding the determinant reveals that, by a cancellation of leading terms, $r(t)$ is *quadratic* in t . We can write it as $r(t) = k(c_2 t^2 + 2c_1 t + c_0)$, where

$$\begin{aligned} k &= \frac{1}{9}(u_0 v_1 - u_1 v_0)^2, \\ c_2 &= [(u_1 - u_0)^2 + (v_1 - v_0)^2]^2, \\ c_1 &= [(u_1 - u_0)^2 + (v_1 - v_0)^2][u_0 u_1 + v_0 v_1 - u_0^2 - v_0^2], \\ c_0 &= [u_0 u_1 + v_0 v_1 - u_0^2 - v_0^2]^2 - 3(u_0 v_1 - u_1 v_0)^2. \end{aligned}$$

The discriminant of this quadratic is

$$\Delta = c_1^2 - c_0 c_2 = \frac{4}{27} [(u_1 - u_0)^2 + (v_1 - v_0)^2]^2 (u_0 v_1 - u_1 v_0)^6$$

and since by supposition $u_0 v_1 - u_1 v_0 \neq 0$ and $(u_1 - u_0)^2 + (v_1 - v_0)^2 \neq 0$ (see §17.2), this is positive and $r(t)$ has two distinct, real roots. ■

Definition 18.1 The *standard form* of a plane cubic $\mathbf{r}(t) = (x(t), y(t))$ with a crunode (real self–intersection) corresponds to a choice of coordinates and parameterization in which its components are of the form

$$x(t) = p(t^2 - 1), \quad y(t) = q(t - \alpha)(t^2 - 1). \quad (18.7)$$

The property $x(\pm 1) = y(\pm 1) = 0$ of the standard form implies that the crunode is situated at the origin, and corresponds to the two parameter values $t = \pm 1$. This fixes the position and parameterization of the curve, and we then fix the orientation by requiring $x(t)$ to be quadratic rather than cubic: this means that the curve tangent is asymptotically vertical as $|t| \rightarrow \infty$. A crunodal plane cubic in standard form has three remaining freedoms — the x and y scales p and q , and the parameter value α of the x -axis intercept.

Theorem 18.2 *In standard form, the Pythagorean–hodograph cubics are all instances of the Tschirnhaus cubic defined by*

$$x(t) = p(t^2 - 1), \quad y(t) = \frac{\pm p}{\sqrt{3}} t(t^2 - 1). \quad (18.8)$$

Proof : From the hodograph $x'(t) = 2pt$, $y'(t) = q(3t^2 - 2\alpha t - 1)$ of the standard–form crunodal cubic (18.7), we obtain

$$x'^2(t) + y'^2(t) = q^2 [9t^4 - 12\alpha t^3 + (4f^2 + 4\alpha^2 - 6)t^2 + 4\alpha t + 1]$$

where $f = p/q$. If this is to be the square of a quadratic $\sigma(t) = q(at^2 + bt + c)$, by comparing like terms we must have

$$a^2 = 9, \quad ab = -6\alpha, \quad 2ac + b^2 = 4f^2 + 4\alpha^2 - 6, \quad bc = 2\alpha, \quad c^2 = 1.$$

From the first three conditions, we deduce that $a = \pm 3$, $b = \mp 2\alpha$, and $c = \pm(\frac{2}{3}f^2 - 1)$. Substituting for b , c into the fourth then gives $-\alpha(\frac{2}{3}f^2 - 1) = \alpha$, and since $f \neq 0$ by assumption, this can be satisfied only if $\alpha = 0$. Finally, substituting for c in the last condition yields $\frac{2}{3}f^2(\frac{2}{3}f^2 - 2) = 0$, which implies that $f^2 = 3$, since $f \neq 0$. Thus $q = \pm\sqrt{3}p$ (the sign choice being immaterial, since it changes only the sense in which the parameter t increases along the curve), and for a PH cubic expressions (18.7) reduce to (18.8). ■

Figure 18.8 shows Tschirnhausen’s cubic in standard form, together with the Bézier control polygons for several finite segments, which all satisfy the geometrical constraints (18.6). As a consequence of these conditions we note that, unlike “ordinary” cubics, the PH cubics cannot inflect. By the variation–diminishing property of the Bézier form (see §13.2), a convex control polygon

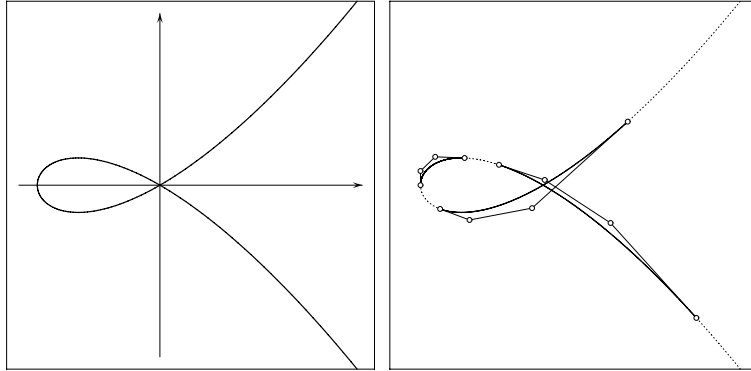


Fig. 18.8. Left: Tschirnhausen's cubic (18.8), expressed in standard form. Right: The Bézier control polygons for various finite segments of Tschirnhausen's cubic — the control polygon for any segment satisfies the two geometrical constraints (18.6).

implies a convex curve — i.e., the curvature cannot change sign. Evidently, the freedoms available for designing PH cubics amount to just scaling, rotating, and translating different portions of the curve defined by (18.8) for $-\infty < t < +\infty$. The elegant characterization (18.6) of PH cubics is mitigated by their inadequate shape freedoms for most practical design applications.

Pottmann [369] has noted that many of the properties of Tschirnhausen's cubic (including its interpretation as the caustic for reflection of parallel rays by a parabola) were discussed by W. Wunderlich [474] in a study of *curves of constant slope* in \mathbb{R}^3 . If we “lift” Tschirnhausen's cubic to \mathbb{R}^3 by taking its (polynomial) arc length function $s(t)$ as the z component, the tangent to the curve $\mathbf{r}(t) = (x(t), y(t), s(t))$ makes the fixed angle $\frac{1}{4}\pi$ with the (x, y) plane.

18.4 You Mean we Pay you to do *That!*?

While philosophers may argue over the *existence* of scientific facts or theories outside the minds of their discoverers and contemplators, it is incontrovertible that such facts and theories are *created* and *interpreted* by humans operating under specific social, cultural, and economic circumstances — see, for example, the discussion of the “meaning” of Plimpton 322 in §2.1.

Nevertheless, the accepted norm in scientific writing is to describe proofs, theories, discoveries, and inventions in the form of isolated and “impersonal” narratives that make little or no reference to the motivations, influences, and circumstances that may have directly or indirectly contributed to the genesis of an idea or its subsequent interpretation by others. However, one of the most profitable and enjoyable ways of approaching an unfamiliar topic is through a

study of its historical development,⁵ since the neophyte often faces conceptual difficulties and motivational doubts that closely mirror the initial stumbling steps, obstacles overcome, and social/cultural impetus through which the idea, theory, proof, or invention under consideration first came about.

Notwithstanding their high-minded tone, the intent of these philosophical circumlocutions is actually to excuse a brief indulgence in a favorite anecdote concerning the identification of Tschirnhausen's cubic as the unique planar PH cubic, that conveys some idea of the human dimension of scientific research. Of course, the reader who still prefers the "isolated and impersonal" style of presentation is at liberty to proceed directly to the next chapter.

The author's involvement with PH curves originated during employment in the Research Division of a large multi-national company — which, for the sake of anonymity, we shall refer to as the HAL Corporation. At that time, the HAL Research Division was a prestigious and world-renowned organization, credited with many fundamental advances in science and technology. But it was difficult to discern the direct relevance of much of its research activity to the Company's commercial interests. The author resided in the Manufacturing Research Department, which labored under persistent doubts as to whether it was more preoccupied with "manufacturing" research than with the study of manufacturing processes. But Manufacturing Research took solace in the fact that its activities seemed no less relevant than those of its sister departments: Mathematical Sciences, Physical Sciences, Computer Science, Semiconductor Technology, etc. The members of all these departments enjoyed virtually free rein in the pursuit of their individual research interests.

All good things come to an end. After some years, the Company was beset with dire financial circumstances, and the Research Division came under great pressure to prove its relevance and justify its existence. But it is not so easy to alter a deeply-ingrained culture overnight. As part of the endeavor to revamp Manufacturing Research, a new Department Director was appointed. The new Director hailed from a "shop floor" environment and, lacking a PhD, had little experience with (or tolerance for) high-falutin' research. And it was my fate to present one of the first weekly departmental seminars before the new Director. The subject of this seminar was, of course, *Pythagorean-hodograph curves* — it contained some theoretical results, including the proof that Tschirnhausen's cubic is the unique PH cubic, some historical connections, and some discussion of applications to CNC machining. Although I was confident of the seminar's success (it had been well received at a number of conferences) I was approached afterwards by a colleague, who quipped that he "really admired my courage." When I enquired what this meant, he expressed surprise that I had not noticed the manner in which the Director had *glared* at me throughout the seminar, as though he were about to lose control at any moment, jump out of his seat, and exclaim — "You mean we pay you to do *that!*?"

⁵ In the mathematical sciences, Morris Kline's *Mathematical Thought from Ancient to Modern Times* [281] is an excellent resource for this purpose.

Although this was a rather troubling development, one learns to take such things in stride. Just a few weeks later, however, we were greeted one morning by stunning tragic news: the new Director had succumbed to cardiac arrest in his office late the previous night — his soul had concluded its earthly sojourn. It was rumored that my seminar might have been the proximate cause of his untimely demise, but I vigorously repudiated these libelous allegations. In any case, a new Director of Manufacturing Research was appointed within a few months, and the department resumed its usual course of business.

Then one day there came an announcement of a most important “all-hands meeting,” at which the Vice President for Research would propound his vision for the complete overhaul and restructuring of the Research Division, to align its activities with the HAL Corporation’s business interests, and thus help to extricate the Company from its pecuniary woes. On the day of the momentous presentation, a great throng of the entire HAL Research Staff assembled with much anticipation and apprehension in the main lecture hall, to discover their fate. True to the promise for sweeping reforms, the Vice President announced that the current “traditional” departments — based on core disciplines such as Mathematical Sciences, Physical Sciences, Computer Science, Semiconductor Technology, etc. — did not adequately serve the Company’s business interests. He proposed, instead, a simplified, streamlined, and modernized departmental structure, motivated by four “core business principles” — namely,

- Department of Efficacy
- Department of Responsivity
- Department of Timeliness
- Department of ...

(I forgot the fourth, but it was very much in the same vein as the others). By way of elaboration, the Vice President explained that Efficacy was the science of minimizing wasted energy or materials, optimizing all operations, reducing manpower requirements, etc.; that Responsivity was the practice of sincerely listening to one’s customers, and acting on their feedback in the improvement of existing products or the introduction of new product lines; that Timeliness was the ability to reduce product design and development cycles, in order to beat the Company’s competitors to the marketplace, . . . etc., etc.

Needless to say, this *New Vision of Research* spawned much bewilderment, consternation, and incredulity among the assembled Research Staff, burdened as they were by “traditional” training as mathematicians, computer scientists, physicists, semiconductor technologists, etc. Nevertheless, it was greeted with dutiful silence and concealed skepticism — in the prevailing atmosphere of the HAL Corporation, there was an inverse relation between speaking one’s mind and one’s future career prospects. For my own part, I recall experiencing a very unusual sensation as the *New Vision of Research* unfolded, unlike anything I had experienced before. It was only later, on introspection, that I realized how narrowly I had managed to suppress a powerful urge to jump up and declaim to the Vice President of Research: “You mean we pay you to do *that!*?”

19

Complex Representation

The shortest path between two truths in the real domain passes through the complex domain.

Jacques Hadamard (1865–1963)

The recognition that complex numbers admit a geometrical interpretation, as points in the Euclidean plane, was a critical step in securing their widespread acceptance (see §4.1). The “geometric algebra” of points in \mathbb{R}^2 defined by the arithmetic rules for complex numbers allows us to *multiply* and *divide* points, as well as adding or subtracting them in the usual vector sense. However, the systematic use of complex numbers as a means of exploring analytic geometry in \mathbb{R}^2 has received less attention than it deserves — *The Advanced Geometry of Plane Curves and Their Applications*¹ by C. Zwikker [480] seems to be the only treatise that consistently employs this approach.

The complex representation of \mathbb{R}^2 is especially valuable in the analysis of planar PH curves, since it offers a simple and elegant characterization of the Pythagorean hodograph property. Any task performed in terms of the complex representation could, in principle, be accomplished using only real variables. However, on account of the useful geometrical insights it provides — and also significant savings in the cost of formulating and solving the systems of non-linear equations associated with interpolation problems (Chaps. 25 and 27) — we shall rely extensively on the complex representation of planar PH curves henceforth. An analogous representation for spatial PH curves (in terms of the *quaternions* rather than complex numbers) is developed in Chap. 22.

In this chapter, we use the complex formulation to establish a one-to-one correspondence between regular PH curves and “ordinary” polynomial curves in \mathbb{R}^2 , to characterize the control polygons of planar PH curves, and to verify their rotation invariance and study their intrinsic shape properties.

¹ Regrettably, this book has not survived even as a *Dover* reprint. Another useful source, though not directly concerned with the complex representation of plane curves, is Schwerdtfeger’s *Geometry of Complex Numbers* [397].

19.1 Complex Curves and Hodographs

Associating the point (x, y) of the Euclidean plane with the complex number $x + i y$, we regard these two quantities as interchangeable and use a single bold character \mathbf{z} to denote both. Expressions such as $\mathbf{z}_1 \pm \mathbf{z}_2$, $\mathbf{z}_1 \mathbf{z}_2$, $\mathbf{z}_1 / \mathbf{z}_2$ follow the usual rules of complex arithmetic (see §4.2), while $\mathbf{z}_1 \cdot \mathbf{z}_2$ and $\mathbf{z}_1 \times \mathbf{z}_2$ denote the scalar and vector products. Complex variables may also appear as arguments of transcendental functions — $\sin(\mathbf{z})$, $\cos(\mathbf{z})$, $\exp(\mathbf{z})$, $\log(\mathbf{z})$, etc.

A plane parametric curve can be specified by a complex-valued function $\mathbf{r}(t)$ defined on a given (possibly infinite) domain $t \in [a, b]$ of a real variable t . For example, $\mathbf{r}(t) = \mathbf{a}_1 t + \mathbf{a}_0$ and $\mathbf{r}(t) = \mathbf{a}_2 t^2 + \mathbf{a}_1 t + \mathbf{a}_0$ define a straight line and a parabola, respectively, while a circle with center \mathbf{c} and radius r can be written as $\mathbf{r}(t) = \mathbf{c} + r e^{it}$ for $0 \leq t < 2\pi$. Perhaps less obvious is the fact that circles may also be described by the fractional linear (Möbius) form

$$\mathbf{r}(t) = \frac{\mathbf{a}t + \mathbf{b}}{\mathbf{c}t + \mathbf{d}},$$

and that, for real α , the expressions

$$\mathbf{r}(t) = \cos(t + i\alpha) \quad \text{and} \quad \mathbf{r}(t) = \cos(\alpha + it)$$

define an ellipse and a hyperbola, respectively. See [480] for a wealth of further details on complex representations of plane curves and their properties.

For our purposes, the most interesting aspect of such representations is the ability to create new curves from any given curve by “distorting” the complex plane in which it resides using a *conformal map* defined by an analytic function of \mathbf{z} (see §4.5 for the definition and basic properties of such maps). Our concern here is more subtle than the *direct* deformation of planar curves by means of conformal maps. Instead, we introduce a mapping of the *hodograph plane* — the plane in which the derivative $\mathbf{r}'(t)$ of a parametric curve $\mathbf{r}(t)$ resides. By this scheme, we establish a one-to-one correspondence² between the sets of regular PH curves and of regular “ordinary” polynomial curves, which offers a framework for comparing and contrasting their properties.

Consider a polynomial curve in the complex plane specified in Bézier form

$$\mathbf{r}(t) = \sum_{k=0}^n \mathbf{p}_k \binom{n}{k} (1-t)^{n-k} t^k, \quad t \in [0, 1], \quad (19.1)$$

where the complex values $\mathbf{p}_k = x_k + i y_k$, $k = 0, \dots, n$ define the control points. The usual control polygon features — convex-hull confinement, the variation-diminishing property, and the subdivision and degree-elevation algorithms — carry over directly to the complex representation. The hodograph $\mathbf{w}(t) = \mathbf{r}'(t)$ of the curve (19.1) can be expressed as a complex Bézier curve of degree $n-1$,

² Note that $\mathbf{r}(t)$ is uniquely determined by $\mathbf{r}'(t)$, modulo a translation corresponding to the integration constant.

$$\mathbf{w}(t) = \sum_{k=0}^{n-1} \mathbf{w}_k \binom{n-1}{k} (1-t)^{n-1-k} t^k, \quad t \in [0, 1], \quad (19.2)$$

with control points given by

$$\mathbf{w}_k = n \Delta \mathbf{p}_k = n (\mathbf{p}_{k+1} - \mathbf{p}_k), \quad k = 0, \dots, n-1.$$

The forward differences $\Delta \mathbf{p}_k = \mathbf{p}_{k+1} - \mathbf{p}_k$ define the n directed “legs” of the control polygon. For clarity, we regard curves and their hodographs as residing in two separate complex planes, $\mathbf{z} = x + i y$ and $\mathbf{w} = u + i v$, respectively.

19.2 One-to-one Correspondence

Using \mathbb{C} as a representation for \mathbb{R}^2 , let Π be the set of all regular polynomial curves, and $\hat{\Pi}$ be the set of all regular PH curves. By a regular curve, we mean a *specific parameterization* of such a curve (see Remark 19.2). To assess how “flexible” PH curves are, it is useful to characterize the relationship between these two sets. Although Π and $\hat{\Pi}$ are both infinite sets — they include curves of *arbitrary* degree — it is clear that $\hat{\Pi} \subset \Pi$, since any regular PH curve is certainly a regular polynomial curve, but there are regular polynomial curves whose hodographs are *not* Pythagorean (e.g., the parabola $\mathbf{r}(t) = t + i t^2$). We introduce a simple three-stage procedure P that transforms any differentiable plane curve $\mathbf{r}(t)$ into a new curve $\hat{\mathbf{r}}(t)$.

procedure $P : \mathbf{r}(t) \rightarrow \hat{\mathbf{r}}(t)$

1. differentiate the given curve $\mathbf{r}(t)$
to obtain its hodograph $\mathbf{w}(t) = \mathbf{r}'(t)$;
2. apply the conformal map $\mathbf{w} \rightarrow \mathbf{w}^2$ to
the hodograph plane, giving $\hat{\mathbf{w}}(t) = \mathbf{w}^2(t)$;
3. integrate the transformed hodograph $\hat{\mathbf{w}}(t)$
to obtain the new curve $\hat{\mathbf{r}}(t) = \int \hat{\mathbf{w}}(t) dt$.

In this procedure, translational freedoms are fixed by taking $\mathbf{r}(0) = \hat{\mathbf{r}}(0) = 0$.

Proposition 19.1 P defines a bijective map, or one-to-one correspondence, between the sets Π and $\hat{\Pi}$ of regular polynomial curves and regular PH curves.

Proof : Let $\mathbf{r}(t) = x(t) + i y(t)$ be a regular polynomial curve with hodograph $\mathbf{w}(t) = u(t) + i v(t)$, where $u = x'$ and $v = y'$. Since $\mathbf{w}(t)$ does not pass through the origin, we must have $\gcd(u, v) = \text{constant}$. Step 2 gives

$$\hat{\mathbf{w}}(t) = \mathbf{w}^2(t) = u^2(t) - v^2(t) + i 2 u(t)v(t)$$

for the transformed hodograph, which is of Pythagorean form with u and v relatively prime. Integrating $\hat{\mathbf{w}}(t)$ then gives, modulo a translation, a unique

regular PH curve $\hat{\mathbf{r}}(t)$ corresponding to $\mathbf{r}(t)$. Conversely, let $\hat{\mathbf{r}}(t)$ be a regular PH curve. Its hodograph must be of the form $\hat{\mathbf{w}}(t) = u^2(t) - v^2(t) + i 2 u(t)v(t)$, where $\gcd(u, v) = \text{constant}$. The inverse to step 2 transforms $\hat{\mathbf{w}}(t)$ into

$$\mathbf{w}(t) = \sqrt{\hat{\mathbf{w}}(t)} = \pm [u(t) + i v(t)], \quad (19.3)$$

a hodograph that does not traverse the origin. Integrating $\mathbf{w}(t)$ gives, modulo translation, a unique regular polynomial curve $\mathbf{r}(t)$ corresponding to $\hat{\mathbf{r}}(t)$ — the *sense* of the parametric flow along $\mathbf{r}(t)$ is arbitrary, corresponding to the sign ambiguity on taking the complex square root. ■

Note that, in general, the inverse map $\mathbf{w} \rightarrow \sqrt{\mathbf{w}}$ in (19.3) does *not* yield a polynomial hodograph when applied to a general polynomial hodograph — in fact, it will give a polynomial hodograph only when applied to a *Pythagorean* hodograph. Thus, regarding P and its inverse P^{-1} as mappings between sets of *polynomial* curves, we have $P(\Pi) = \hat{\Pi}$ and $P^{-1}(\hat{\Pi}) = \Pi$.

We call a regular polynomial curve $\mathbf{r}(t)$ and a regular PH curve $\hat{\mathbf{r}}(t)$ a pair of *corresponding curves* if they are mapped into each other under the action of P and P^{-1} . Such pairs can be expressed explicitly as

$$\begin{aligned} \mathbf{r}(t) &= \int_0^t u(\tau) d\tau + i \int_0^t v(\tau) d\tau, \\ \hat{\mathbf{r}}(t) &= \int_0^t u^2(\tau) - v^2(\tau) d\tau + i \int_0^t 2 u(\tau)v(\tau) d\tau, \end{aligned} \quad (19.4)$$

where $u(t)$ and $v(t)$ are relatively prime polynomials, and we assume $\mathbf{r}(0) = \hat{\mathbf{r}}(0) = 0$ to fix translational freedoms.

Remark 19.1 The set $\hat{\Pi}$ of regular PH curves has the same “cardinality” or “power” as the set Π of regular polynomial curves.

The *cardinality* or *power* of an infinite set is a measure of its “size” [230] — specifically, two infinite sets have the same cardinality if we can establish a one-to-one correspondence between their members. Thus, in accordance with Proposition 19.1, we may say that there are “just as many” regular PH curves as there are regular polynomial curves in general.

Remark 19.2 The correspondence between the curves (19.4) refers not only to their geometrical loci, but also to the variation of the parameter t along those loci. Any polynomial curve $\mathbf{r}(t)$ may be re-parameterized by a linear transformation $t \rightarrow a + bt$ ($b \neq 0$) without altering its geometrical locus, its regularity, or its degree. However, if $\mathbf{r}(t)$ and $\hat{\mathbf{r}}(t)$ are corresponding curves, re-parameterizing the former does not simply yield a new parameterization of the latter as the corresponding PH curve. Fixing translational freedoms by always placing the point of zero parameter value at the origin, it is not difficult to verify that the sequence of PH curves corresponding to all linear re-parameterizations of a given curve $\mathbf{r}(t)$ are actually *uniform scalings* of a unique curve $\hat{\mathbf{r}}(t)$ by the factor b (see Fig. 19.1).

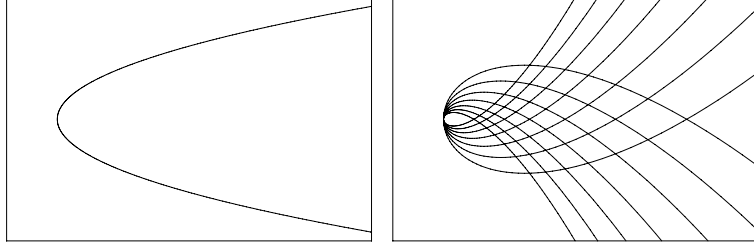


Fig. 19.1. Different parameterizations of a parabola (left) yield different scalings of a Tschirnhaus cubic (right) under the one-to-one correspondence of Proposition 19.1.

Now all linear re-parameterizations of a given PH curve are clearly also PH curves. Thus, if $\hat{\Pi}_*$ is a subset of the space $\hat{\Pi}$ of regular PH curves whose members are simply the various (fixed-degree) parameterizations of a unique locus, it follows from Remark 19.2 that the pre-image $\Pi_* = P^{-1}(\hat{\Pi}_*)$ of $\hat{\Pi}_*$ under the map P consists of *polynomial curves with mutually distinct loci*.

Example 19.1 The PH curve corresponding to the parabola $\mathbf{r}_1(t) = t + i t^2$ is the Tschirnhaus cubic $\hat{\mathbf{r}}_1(t) = t - \frac{4}{3}t^3 + i 2t^2$. Consider now the sequence of parabolae $\mathbf{r}_k(t) = kt + ik^3t^2$ for $0 < k < \infty$, any two members $k_1 \neq k_2$ of which are clearly of different shape. The PH curve corresponding to member k is easily verified to be $\hat{\mathbf{r}}_k(t) = k^2t - \frac{4}{3}k^6t^3 + i 2k^4t^2$. By setting $t = \tau/k^2$, however, we observe that $\hat{\mathbf{r}}_k(t) \equiv \hat{\mathbf{r}}_1(\tau)$ for all k . Thus, P maps the family of geometrically distinct parabolae $\mathbf{r}_k(t)$ into the different parameterizations of a geometrically unique cubic, $\hat{\mathbf{r}}_1(t)$ — see Fig. 19.2.

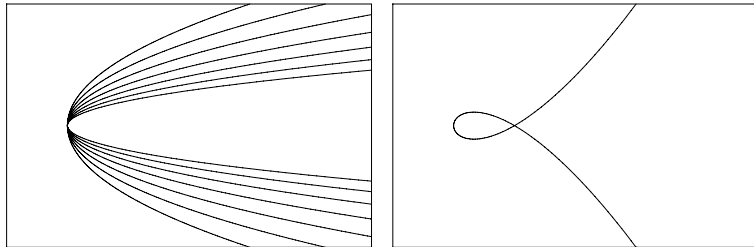


Fig. 19.2. Parabolae of different shape (left) yield different parameterizations of a Tschirnhaus cubic (right) under the one-to-one correspondence of Proposition 19.1.

Lemma 19.1 *The degrees n and \hat{n} of corresponding curves $\mathbf{r}(t)$ and $\hat{\mathbf{r}}(t)$ are related by $\hat{n} = 2n - 1$.*

Proof : Let $u(t)$ and $v(t)$ be two relatively prime polynomials, and let $m = \max(\deg(u), \deg(v))$. Integrating the hodograph $\mathbf{w}(t) = u(t) + i v(t)$ then gives

a polynomial curve $\mathbf{r}(t)$ of degree $n = m + 1$. Further, one can easily verify that $\max(\deg(u^2 - v^2), \deg(2uv)) = 2m$, so integrating $\hat{\mathbf{w}}(t) = u^2(t) - v^2(t) + i2u(t)v(t)$ gives a PH curve $\hat{\mathbf{r}}(t)$ of degree $\hat{n} = 2m + 1 = 2n - 1$. ■

Clearly, there are no *regular* PH curves of even degree. Straight lines in Π correspond to (different) straight lines in $\hat{\Pi}$, but P maps regular polynomial curves of degree ≥ 2 to regular PH curves of higher *odd* degree (see Table 19.1).

Table 19.1. Corresponding curves of low degree.

	polynomial curve $\mathbf{r}(t)$	PH curve $\hat{\mathbf{r}}(t)$
$n = 1$	straight lines	straight lines
$n = 2$	parabolae	Tschirnhaus cubics
$n = 3$	regular cubics	regular PH quintics
...

The properties of the map $\mathbf{w} \rightarrow \hat{\mathbf{w}} = \mathbf{w}^2$ are described in most textbooks on complex analysis — see, for example, [42, pp. 79–84]. As is well known [196] it takes the *Gaussian integers* or “grid points” $\alpha + i\beta$ (where $\alpha, \beta \in \mathbb{Z}$) of the complex plane into points $\alpha^2 - \beta^2 + i2\alpha\beta$ whose real and imaginary parts are members of *integer Pythagorean triples*. The map is conformal everywhere except $\mathbf{w} = 0$; this exceptional point need not concern us if we consider only regular curves. Note also that it gives a *double covering* of the complex plane, each point $\hat{\mathbf{w}}$ having two pre-images, $-\mathbf{w}$ and $+\mathbf{w}$. Writing $\mathbf{w} = u + iv$ and $\hat{\mathbf{w}} = \hat{u} + i\hat{v}$, the pre-images of the grid lines $u = \text{constant}$ and $v = \text{constant}$ of the $\hat{\mathbf{w}}$ plane are, respectively, the families of rectangular hyperbolae

$$u^2 - v^2 = \hat{u} \quad \text{and} \quad 2uv = \hat{v}$$

in the \mathbf{w} plane, with asymptotes $u = \pm v$ and $u = 0, v = 0$. On the other hand, the grid lines $u = \text{constant}$ and $v = \text{constant}$ of the \mathbf{w} plane are respectively mapped into the families of confocal parabolae

$$\hat{v}^2 + 4u^2\hat{u} = 4u^4 \quad \text{and} \quad \hat{v}^2 - 4v^2\hat{u} = 4v^4$$

in the $\hat{\mathbf{w}}$ plane, whose vertices lie along the positive and negative \hat{u} -axis. In the limits $u \rightarrow 0$ and $v \rightarrow 0$, we obtain the half-lines $\hat{u} < 0$ and $\hat{u} > 0$, doubly traced, as images of the imaginary and real axes (see Fig. 19.3).

In terms of the velocity vector $\mathbf{w}(t) = \mathbf{r}'(t) = \sigma(t)e^{i\psi(t)}$ at each point of a given curve $\mathbf{r}(t)$, describing motion with speed $\sigma(t)$ at an angle $\psi(t)$ relative to the real axis, the map $\mathbf{w} \rightarrow \mathbf{w}^2$ transforms this velocity (see Fig. 19.3) by *squaring* the speed and *doubling* the inclination angle,

$$\hat{\sigma}(t) = \sigma^2(t) \quad \text{and} \quad \hat{\psi}(t) = 2\psi(t).$$

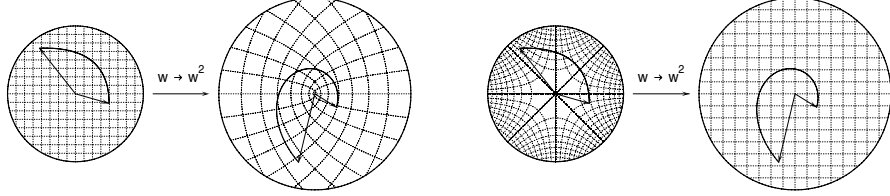


Fig. 19.3. The map $w \rightarrow \hat{w} = w^2$ of the hodograph plane squares the lengths of velocity vectors and doubles their inclination angles. Left: grid lines in the w plane are mapped to families of confocal parabolae in the \hat{w} plane. Right: the pre-images of grid lines in the \hat{w} plane are families of rectangular hyperbolae in the w plane.

Proposition 19.2 *The control points of a regular PH curve of degree $2n - 1$ are given in terms of n complex values w_0, \dots, w_{n-1} by the recursive formula*

$$\mathbf{p}_{k+1} = \mathbf{p}_k + \frac{1}{2n-1} \sum_{j=\max(0, k-n+1)}^{\min(k, n-1)} \frac{\binom{n-1}{j} \binom{n-1}{k-j}}{\binom{2n-2}{k}} \mathbf{w}_j \mathbf{w}_{k-j} \quad (19.5)$$

for $k = 0, 1, \dots, 2n - 2$, where \mathbf{p}_0 is arbitrary and w_0, \dots, w_{n-1} are such that the hodograph $w(t)$ defined by (19.2) does not traverse the origin.

Proof : The square of the complex hodograph (19.2) may be written as

$$\hat{w}(t) = \sum_{k=0}^{2n-2} \hat{w}_k \binom{2n-2}{k} (1-t)^{2n-2-k} t^k \quad (19.6)$$

where, making use of the product rule (11.20) for Bernstein-form polynomials, the coefficients \hat{w}_k are given in terms of w_0, \dots, w_{n-1} by

$$\hat{w}_k = \sum_{j=\max(0, k-n+1)}^{\min(k, n-1)} \frac{\binom{n-1}{j} \binom{n-1}{k-j}}{\binom{2n-2}{k}} \mathbf{w}_j \mathbf{w}_{k-j}, \quad k = 0, \dots, 2n - 2.$$

To integrate the hodograph (19.6), we employ property (11.7) of the Bernstein basis functions. This yields the quoted form (19.5) for the control points of a PH curve of degree $2n - 1$, with an arbitrary constant of integration \mathbf{p}_0 . ■

The requirement that the hodograph (19.2) defined by w_0, \dots, w_{n-1} must not pass through the origin for the control points (19.5) to define a *regular* PH curve does not, in general, have an intuitive geometrical interpretation in terms of the locations of w_0, \dots, w_{n-1} . This requirement amounts to the gcd of the real and imaginary parts of (19.2), $u(t)$ and $v(t)$, being a constant — or to their resultant with respect to t being non-zero. Criteria specific to the PH cubics and quintics are given in equations (19.10) and (19.13) below.

19.3 Rotation Invariance of Hodographs

The complex representation offers a simple proof for the *rotation invariance* of the sufficient-and-necessary form

$$x'(t) = u^2(t) - v^2(t), \quad y'(t) = 2u(t)v(t), \quad \sigma(t) = u^2(t) + v^2(t)$$

for primitive planar Pythagorean hodographs $\mathbf{r}'(t) = (x'(t), y'(t))$ satisfying

$$x'^2(t) + y'^2(t) = \sigma^2(t),$$

where $\gcd(u, v) = \text{constant} \Rightarrow \gcd(x', y') = \text{constant}$. On making a rotation

$$\begin{bmatrix} \tilde{x}'(t) \\ \tilde{y}'(t) \end{bmatrix} = \begin{bmatrix} \cos \theta & -\sin \theta \\ \sin \theta & \cos \theta \end{bmatrix} \begin{bmatrix} x'(t) \\ y'(t) \end{bmatrix}$$

through angle θ , we seek to express the rotated hodograph $\tilde{\mathbf{r}}'(t) = (\tilde{x}'(t), \tilde{y}'(t))$ in terms of two new polynomials $\tilde{u}(t), \tilde{v}(t)$ as

$$\tilde{x}'(t) = \tilde{u}^2(t) - \tilde{v}^2(t), \quad \tilde{y}'(t) = 2\tilde{u}(t)\tilde{v}(t). \quad (19.7)$$

One can easily see that the transformed hodograph,

$$\begin{aligned} \tilde{x}'(t) &= \cos \theta [u^2(t) - v^2(t)] - \sin \theta 2u(t)v(t), \\ \tilde{y}'(t) &= \sin \theta [u^2(t) - v^2(t)] + \cos \theta 2u(t)v(t), \end{aligned}$$

is obtained by substituting into (19.7) the polynomials

$$\tilde{u}(t) = \cos \frac{1}{2}\theta u(t) - \sin \frac{1}{2}\theta v(t), \quad \tilde{v}(t) = \sin \frac{1}{2}\theta u(t) + \cos \frac{1}{2}\theta v(t). \quad (19.8)$$

Using the complex representation $\mathbf{r}'(t) = \mathbf{w}^2(t)$ where $\mathbf{w}(t) = u(t) + i v(t)$, the rotation yields $\tilde{\mathbf{r}}'(t) = \exp(i\theta) \mathbf{w}^2(t) = \tilde{\mathbf{r}}'(t) = \tilde{\mathbf{w}}^2(t)$, the real and imaginary parts of $\tilde{\mathbf{w}}(t) = \exp(i\frac{1}{2}\theta) \mathbf{w}(t) = \tilde{u}(t) + i \tilde{v}(t)$ being defined by (19.8).

19.4 Pythagorean-hodograph Cubics Revisited

In the first non-trivial instance, that of the PH cubics, expression (19.5) yields control points of the form

$$\mathbf{p}_1 = \mathbf{p}_0 + \frac{1}{3} \mathbf{w}_0^2, \quad \mathbf{p}_2 = \mathbf{p}_1 + \frac{1}{3} \mathbf{w}_0 \mathbf{w}_1, \quad \mathbf{p}_3 = \mathbf{p}_2 + \frac{1}{3} \mathbf{w}_1^2. \quad (19.9)$$

Here, the complex values \mathbf{w}_0 and \mathbf{w}_1 must satisfy

$$\text{Im}(\overline{\mathbf{w}}_0 \mathbf{w}_1) \neq 0 \quad (19.10)$$

to obtain a regular curve. If $\mathbf{w}_0 = u_0 + i v_0$ and $\mathbf{w}_1 = u_1 + i v_1$, this amounts to $u_0 v_1 \neq u_1 v_0$ — i.e., the line from \mathbf{w}_0 to \mathbf{w}_1 should not pass through the origin.

The complex form offers a succinct expression of the sufficient-and-necessary conditions (18.6) characterizing PH cubics by the control-polygon geometry. Writing equations (19.9) in terms of the control-polygon legs as

$$3\Delta p_0 = w_0^2, \quad 3\Delta p_1 = w_0 w_1, \quad 3\Delta p_2 = w_1^2,$$

we may eliminate w_0 and w_1 to obtain the single complex constraint

$$(\Delta p_1)^2 = \Delta p_2 \Delta p_0, \quad (19.11)$$

whose satisfaction distinguishes the PH cubics from “ordinary” cubics. To see that the complex constraint (19.11) is equivalent to the two real constraints (18.6), we write the directed control-polygon legs in polar form as

$$\Delta p_0 = L_0 e^{i\xi_0}, \quad \Delta p_1 = L_1 e^{i\xi_1}, \quad \Delta p_2 = L_2 e^{i\xi_2}.$$

Substituting into (19.11), we obtain $L_1^2 = L_2 L_0$ and $2\xi_1 = \xi_0 + \xi_2$. In terms of the control polygon interior angles, $\theta_1 = \pi + \xi_1 - \xi_0$ and $\theta_2 = \pi + \xi_2 - \xi_1$, the latter condition implies that $\theta_2 = \theta_1$. Clearly, this derivation³ is much simpler than that given in §18.3 using only real variables.

We may regard general cubics as possessing eight degrees of freedom (the coordinates of their control points), although not all of them are intrinsic shape freedoms. Each cubic can be regarded as a point in a Euclidean space \mathbb{R}^8 with coordinates $(x_0, y_0, x_1, y_1, x_2, y_2, x_3, y_3)$, and the real and imaginary parts of (19.11) each define a degree 2 hypersurface (a *hyperquadric*) in this space. PH cubics lie on the intersection of the hyperquadrics, a locus of dimension 6.

19.5 Characterization of the PH Quintics

The PH quintics are of great practical interest, since they are the simplest PH curves that may inflect, and match first-order Hermite data (see Chap. 25). For regular curves, there is a unique correspondence between PH quintics and ordinary cubics, so we may expect similar “shape flexibility” among these two sets of curves. The control points (19.5) for PH quintics are of the form

$$\begin{aligned} p_1 &= p_0 + \frac{1}{5} w_0^2, \\ p_2 &= p_1 + \frac{1}{5} w_0 w_1, \\ p_3 &= p_2 + \frac{1}{5} \frac{2w_1^2 + w_0 w_2}{3}, \\ p_4 &= p_3 + \frac{1}{5} w_1 w_2, \\ p_5 &= p_4 + \frac{1}{5} w_2^2. \end{aligned} \quad (19.12)$$

³ The possibility of such a derivation was first noted by Professor Wendelin Degen.

Comparing (17.6) with (19.12) illustrates the economy of expression afforded by the complex representation. The constraint that ensures regularity of the PH curve defined by (19.12) may be written in the form

$$[\operatorname{Im}(\bar{\mathbf{w}}_0 \mathbf{w}_2)]^2 - 4 \operatorname{Im}(\bar{\mathbf{w}}_0 \mathbf{w}_1) \operatorname{Im}(\bar{\mathbf{w}}_1 \mathbf{w}_2) \neq 0, \quad (19.13)$$

or explicitly in terms of the real and imaginary parts of $\mathbf{w}_0, \mathbf{w}_1, \mathbf{w}_2$ as

$$(u_0 v_2 - u_2 v_0)^2 \neq 4(u_0 v_1 - u_1 v_0)(u_1 v_2 - u_2 v_1). \quad (19.14)$$

Although (19.13) does not have an intuitive geometrical meaning, we note as an immediate consequence that \mathbf{w}_0 and \mathbf{w}_2 must be non-zero, i.e., $\mathbf{p}_0 \neq \mathbf{p}_1$ and $\mathbf{p}_4 \neq \mathbf{p}_5$ (otherwise the parametric speed is zero at $t = 0$ or 1).

We now use the complex form to derive a characterization for PH quintics in terms of the control polygon geometry. We begin by re-writing equations (19.12) in terms of the directed control polygon legs $\Delta\mathbf{p}_k = \mathbf{p}_{k+1} - \mathbf{p}_k$ as

$$\begin{aligned} \Delta\mathbf{p}_0 &= \frac{\mathbf{w}_0^2}{5}, & \Delta\mathbf{p}_1 &= \frac{\mathbf{w}_0 \mathbf{w}_1}{5}, \\ \Delta\mathbf{p}_2 &= \frac{2\mathbf{w}_1^2 + \mathbf{w}_0 \mathbf{w}_2}{15}, \\ \Delta\mathbf{p}_3 &= \frac{\mathbf{w}_1 \mathbf{w}_2}{5}, & \Delta\mathbf{p}_4 &= \frac{\mathbf{w}_2^2}{5}. \end{aligned} \quad (19.15)$$

It is understood that, for a regular curve, $\Delta\mathbf{p}_0 \neq 0$ and $\Delta\mathbf{p}_4 \neq 0$.

Proposition 19.3 *Let the control-polygon legs of a regular quintic be defined by complex values $\Delta\mathbf{p}_0, \dots, \Delta\mathbf{p}_4$. Then the curve has a Pythagorean hodograph if and only if these values satisfy*

$$\Delta\mathbf{p}_0(\Delta\mathbf{p}_3)^2 = \Delta\mathbf{p}_4(\Delta\mathbf{p}_1)^2, \quad (19.16)$$

and are consistent with the following system of constraints:

$$\begin{aligned} 3\Delta\mathbf{p}_0\Delta\mathbf{p}_1\Delta\mathbf{p}_2 - (\Delta\mathbf{p}_0)^2\Delta\mathbf{p}_3 - 2(\Delta\mathbf{p}_1)^3 &= 0, \\ 3\Delta\mathbf{p}_4\Delta\mathbf{p}_3\Delta\mathbf{p}_2 - (\Delta\mathbf{p}_4)^2\Delta\mathbf{p}_1 - 2(\Delta\mathbf{p}_3)^3 &= 0, \\ 3\Delta\mathbf{p}_0\Delta\mathbf{p}_3\Delta\mathbf{p}_2 - \Delta\mathbf{p}_4\Delta\mathbf{p}_0\Delta\mathbf{p}_1 - 2(\Delta\mathbf{p}_1)^2\Delta\mathbf{p}_3 &= 0, \\ 3\Delta\mathbf{p}_4\Delta\mathbf{p}_1\Delta\mathbf{p}_2 - \Delta\mathbf{p}_0\Delta\mathbf{p}_4\Delta\mathbf{p}_3 - 2(\Delta\mathbf{p}_3)^2\Delta\mathbf{p}_1 &= 0, \\ 9\Delta\mathbf{p}_0(\Delta\mathbf{p}_2)^2 - 6(\Delta\mathbf{p}_1)^2\Delta\mathbf{p}_2 - 2\Delta\mathbf{p}_0\Delta\mathbf{p}_1\Delta\mathbf{p}_3 - (\Delta\mathbf{p}_0)^2\Delta\mathbf{p}_4 &= 0, \\ 9\Delta\mathbf{p}_4(\Delta\mathbf{p}_2)^2 - 6(\Delta\mathbf{p}_3)^2\Delta\mathbf{p}_2 - 2\Delta\mathbf{p}_4\Delta\mathbf{p}_3\Delta\mathbf{p}_1 - (\Delta\mathbf{p}_4)^2\Delta\mathbf{p}_0 &= 0. \end{aligned} \quad (19.17)$$

Before proceeding with the proof, some explanatory remarks are in order. Ordinarily, when $\Delta\mathbf{p}_1$ and $\Delta\mathbf{p}_3$ are both non-zero, equation (19.16) and *one* of the first four of equations (19.17) define sufficient-and-necessary conditions for a quintic to be a PH curve. If $\Delta\mathbf{p}_1 = \Delta\mathbf{p}_3 = 0$, however, (19.16) and the first four equations in (19.17) become identities, and we must take (a simplified form of) *either* of the last two of equations (19.17) as such a condition.

Proof of Proposition 19.3 : The necessity of *all* of the conditions in (19.16) and (19.17) follows from eliminating $\mathbf{w}_0, \mathbf{w}_1, \mathbf{w}_2$ from equations (19.15). For example, if we assume $\Delta\mathbf{p}_0, \dots, \Delta\mathbf{p}_4$ are of the form (19.15), we see from the first and last of these equations that $\mathbf{w}_0^2 : \mathbf{w}_2^2 = \Delta\mathbf{p}_0 : \Delta\mathbf{p}_4$, while from the second and fourth we have $\mathbf{w}_0 : \mathbf{w}_2 = \Delta\mathbf{p}_1 : \Delta\mathbf{p}_3$. From these expressions it is evident that condition (19.16) must be satisfied. Likewise, the necessity of the six conditions (19.17) is verified by substituting directly from (19.15).

Concerning the sufficiency of the stated conditions, we need to show that if equations (19.16) and (19.17) are satisfied, then $\Delta\mathbf{p}_0, \dots, \Delta\mathbf{p}_4$ must be of the form (19.15). Consider first equation (19.16). Without loss of generality, we may write $\Delta\mathbf{p}_0 = \mathbf{a}^2$ and $\Delta\mathbf{p}_4 = \mathbf{c}^2$ where, as noted above, \mathbf{a} and \mathbf{c} are *non-zero* complex numbers for a regular curve. Equation (19.16) then becomes

$$\mathbf{a}^2 (\Delta\mathbf{p}_3)^2 = \mathbf{c}^2 (\Delta\mathbf{p}_1)^2,$$

and if $\Delta\mathbf{p}_1$ and $\Delta\mathbf{p}_3$ are to satisfy the above, they must be of the form

$$\Delta\mathbf{p}_1 = \mathbf{ab} \quad \text{and} \quad \Delta\mathbf{p}_3 = \mathbf{bc}$$

for some complex number \mathbf{b} (not necessarily non-zero).

With these results, we may regard the six equations (19.17) as defining the value of $\Delta\mathbf{p}_2$. Specifically, on substituting into (19.17) we obtain

$$\begin{aligned} \mathbf{a}^3 \mathbf{b} [3\Delta\mathbf{p}_2 - \mathbf{ac} - 2\mathbf{b}^2] &= 0, \\ \mathbf{b}\mathbf{c}^3 [3\Delta\mathbf{p}_2 - \mathbf{ac} - 2\mathbf{b}^2] &= 0, \\ \mathbf{a}^2 \mathbf{bc} [3\Delta\mathbf{p}_2 - \mathbf{ac} - 2\mathbf{b}^2] &= 0, \\ \mathbf{abc}^2 [3\Delta\mathbf{p}_2 - \mathbf{ac} - 2\mathbf{b}^2] &= 0, \\ \mathbf{a}^2 [9(\Delta\mathbf{p}_2)^2 - 6\mathbf{b}^2 \Delta\mathbf{p}_2 - 2\mathbf{ab}^2 \mathbf{c} - \mathbf{a}^2 \mathbf{c}^2] &= 0, \\ \mathbf{c}^2 [9(\Delta\mathbf{p}_2)^2 - 6\mathbf{b}^2 \Delta\mathbf{p}_2 - 2\mathbf{ab}^2 \mathbf{c} - \mathbf{a}^2 \mathbf{c}^2] &= 0, \end{aligned}$$

and we must distinguish two cases, according to the value of \mathbf{b} .

Case (i) $\mathbf{b} \neq 0$: The first four equations above are obviously equivalent and yield the same solution

$$\Delta\mathbf{p}_2 = \frac{2\mathbf{b}^2 + \mathbf{ac}}{3},$$

for $\Delta\mathbf{p}_2$. The last two equations, on the other hand, give

$$\Delta\mathbf{p}_2 = \frac{2\mathbf{b}^2 + \mathbf{ac}}{3} \quad \text{or} \quad -\frac{\mathbf{ac}}{3}, \quad (19.18)$$

but the second solution must be discarded, since if $\mathbf{b} \neq 0$ it is inconsistent with the first four equations. Thus, equations (19.16) and (19.17) imply that $\Delta\mathbf{p}_0, \dots, \Delta\mathbf{p}_4$ can be expressed as

$$\Delta\mathbf{p}_0 = \mathbf{a}^2, \quad \Delta\mathbf{p}_1 = \mathbf{ab}, \quad \Delta\mathbf{p}_2 = \frac{2\mathbf{b}^2 + \mathbf{ac}}{3}, \quad \Delta\mathbf{p}_3 = \mathbf{bc}, \quad \Delta\mathbf{p}_4 = \mathbf{c}^2$$

which is clearly of the form (19.15) with $(\mathbf{w}_0, \mathbf{w}_1, \mathbf{w}_2) = \sqrt{5}(\mathbf{a}, \mathbf{b}, \mathbf{c})$.

Case (ii) $\mathbf{b} = 0$: The first four of equations (19.17) degenerate to identities and yield no information concerning $\Delta\mathbf{p}_2$, whereas the last two both simplify to $9(\Delta\mathbf{p}_2)^2 - \mathbf{a}^2\mathbf{c}^2 = 0$, giving solutions

$$\Delta\mathbf{p}_2 = \pm \frac{\mathbf{a}\mathbf{c}}{3}$$

that correspond to expressions (19.18) with $\mathbf{b} = 0$. Hence we have

$$\Delta\mathbf{p}_0 = \mathbf{a}^2, \quad \Delta\mathbf{p}_1 = 0, \quad \Delta\mathbf{p}_2 = \pm \frac{\mathbf{a}\mathbf{c}}{3}, \quad \Delta\mathbf{p}_3 = 0, \quad \Delta\mathbf{p}_4 = \mathbf{c}^2$$

which is also of the form (19.15), with $(\mathbf{w}_0, \mathbf{w}_1, \mathbf{w}_2) = \sqrt{5}(\pm\mathbf{a}, 0, \pm\mathbf{c})$. ■

Equations (19.16) and (19.17) were obtained by a Gröbner basis reduction on the system (19.15), employing a lexical ordering with $\mathbf{w}_0, \mathbf{w}_1, \mathbf{w}_2$ preceding $\Delta\mathbf{p}_0, \dots, \Delta\mathbf{p}_4$. Expressions (19.16) and (19.17) comprise all elements of the basis that do not depend on $\mathbf{w}_0, \mathbf{w}_1, \mathbf{w}_2$. We distinguish (19.16) from the other conditions (19.17) since: (i) it has a simple geometrical interpretation — see Remark 19.3; and (ii) among (19.16) and (19.17), it is the only condition that is *individually* invariant under reverse-ordering of the control-polygon legs. The significance of the latter point is that the substitution

$$\Delta\mathbf{p}_k \rightarrow -\Delta\mathbf{p}_{4-k} \quad k = 0, \dots, 4 \quad (19.19)$$

amounts to the re-parameterization $t \rightarrow 1 - t$, under which the Pythagorean nature of the hodograph must be preserved. While (19.16) is clearly unaltered by the substitution (19.19), the *individual* members of the system (19.17) are not (the entire system is invariant, however — the equations are grouped into pairs whose members clearly map into each other under (19.19)).

Additional necessary control-polygon constraints can be derived, that are symmetric with respect to the labelling of its legs. The quartic condition

$$9(\Delta\mathbf{p}_2)^2 \Delta\mathbf{p}_0 \Delta\mathbf{p}_4 = [2\Delta\mathbf{p}_1 \Delta\mathbf{p}_3 + \Delta\mathbf{p}_0 \Delta\mathbf{p}_4]^2, \quad (19.20)$$

for example, follows straightforwardly from expressions (19.15). In conjunction with (19.16), however, this does not amount to a *sufficient* condition for a PH curve, since if we choose $\Delta\mathbf{p}_0 = \mathbf{a}^2$, $\Delta\mathbf{p}_1 = \mathbf{ab}$, $\Delta\mathbf{p}_3 = \mathbf{bc}$, $\Delta\mathbf{p}_4 = \mathbf{c}^2$ then equation (19.20) gives two possibilities for the middle leg

$$\Delta\mathbf{p}_2 = \pm \frac{2\mathbf{b}^2 + \mathbf{a}\mathbf{c}}{3},$$

of which only the *positive* sign choice yields a Pythagorean hodograph.

Regarding quintics as residing in a 12-dimensional space defined by their control-point coordinates, the real and imaginary parts of equation (19.16) and of any one of the equations (19.17) define four cubic hypersurfaces in this space, on whose intersection — a locus of apparent dimension eight — the PH quintics lie (not all these dimensions correspond to intrinsic shape freedoms).

19.6 Geometry of the Control Polygon

As noted above, it is usually possible to take condition (19.16) and just *one* of the first four of conditions (19.17) as characterizing the PH quintics. We quote the entire system for completeness, and to highlight symmetry properties.

Remark 19.3 Condition (19.16) admits a simple geometrical interpretation. Expressing the control polygon legs in polar form $\Delta\mathbf{p}_k = L_k e^{i\xi_k}$, $k = 0, \dots, 4$ immediately gives $L_0 L_3^2 = L_4 L_1^2$ and $\xi_0 + 2\xi_3 = \xi_4 + 2\xi_1$. Re-phrasing the latter in terms of the four “interior” angles $\theta_i = \pi + \xi_i - \xi_{i-1}$ for $i = 1, \dots, 4$ we see that the geometry of the control polygon is constrained by the relations

$$\frac{L_1}{L_3} = \sqrt{\frac{L_0}{L_4}} \quad \text{and} \quad \theta_1 + \theta_4 = \theta_2 + \theta_3. \quad (19.21)$$

The remaining conditions (19.17) do not have geometrical interpretations as intuitive as (19.21). Assuming that $\Delta\mathbf{p}_0, \dots, \Delta\mathbf{p}_4 \neq 0$ we focus on the first of equations (19.17). Substituting $\Delta\mathbf{p}_k = L_k e^{i\xi_k}$ and $\theta_i = \pi + \xi_i - \xi_{i-1}$ as before, we obtain the equation

$$3 L_0 L_1 L_2 e^{i(2\theta_1 + \theta_2)} - L_0^2 L_3 e^{i(\theta_1 + \theta_2 + \theta_3)} - 2 L_1^3 e^{i3\theta_1} = 0.$$

This can be further simplified upon dividing by $e^{i2\theta_1}$ and using (19.21) to set $\theta_2 + \theta_3 - \theta_1 = \theta_4$ in the middle term. Hence we have

$$3 L_0 L_1 L_2 e^{i\theta_2} - L_0^2 L_3 e^{i\theta_4} - 2 L_1^3 e^{i\theta_1} = 0,$$

and the real and imaginary parts of this equation furnish two constraints

$$\begin{aligned} 3 L_0 L_1 L_2 \cos \theta_2 &= L_0^2 L_3 \cos \theta_4 + 2 L_1^3 \cos \theta_1, \\ 3 L_0 L_1 L_2 \sin \theta_2 &= L_0^2 L_3 \sin \theta_4 + 2 L_1^3 \sin \theta_1, \end{aligned} \quad (19.22)$$

which, together with (19.21), constitute sufficient and necessary conditions for a Pythagorean hodograph. Condition analogous to (19.22) result if we select instead the second, third, or fourth of the first four equations in (19.17).

Remark 19.4 The control polygons of PH quintics have *five* shape freedoms, since they are characterized by *four* constraints, equations (19.21) and (19.22), on the *nine* parameters L_0, \dots, L_4 and $\theta_1, \dots, \theta_4$. This is consistent with the fact that there are a finite number (four) of PH quintic solutions to the first-order Hermite interpolation problem, which corresponds to identifying PH quintics with specified control points $\mathbf{p}_0, \mathbf{p}_1$ and $\mathbf{p}_4, \mathbf{p}_5$. Fixing non-essential freedoms by taking $\mathbf{p}_0 = 0$ and $\mathbf{p}_1 = x_1$ (a real value), corresponding to a choice of the origin and orientation of the axes, this entails five free choices for the values $x_4 = \operatorname{Re}(\mathbf{p}_4)$, $y_4 = \operatorname{Im}(\mathbf{p}_4)$, $x_5 = \operatorname{Re}(\mathbf{p}_5)$, $y_5 = \operatorname{Im}(\mathbf{p}_5)$, and y_1 . As these requirements match the intrinsic freedoms of PH quintics, the Hermite interpolants cannot depend on any free parameters (see Chap. 25).

Remark 19.5 The control polygons of PH quintics may be generated from two complex “shape parameters” σ and τ , as follows:

- take points $\zeta_k = \sigma^k$ for $k = -2, -1, 0, 1, 2$ on a logarithmic spiral through $\zeta_0 = 1$, such that the angles between rays from the origin to these points are all equal, and set $\Delta\mathbf{p}_0 = \zeta_{-2}$ and $\Delta\mathbf{p}_4 = \zeta_2$;
- multiply ζ_{-1} and ζ_1 by τ to obtain $\Delta\mathbf{p}_1 = \tau\zeta_{-1}$ and $\Delta\mathbf{p}_3 = \tau\zeta_1$;
- and finally set $\Delta\mathbf{p}_2 = (2\tau^2 + 1)\zeta_0/3$.

This construction follows from the fact that multiplying the control polygon by any complex constant amounts to a *similarity transformation* — i.e., a scaling and rotation — under which its Pythagorean nature is preserved. In particular, expressions (19.15) are seen to be of the above form upon multiplying them by $(\mathbf{w}_0\mathbf{w}_2)^{-1}$ and taking $\sigma^2 = \mathbf{w}_2/\mathbf{w}_0$ and $\tau^2 = \mathbf{w}_1^2/(\mathbf{w}_0\mathbf{w}_2)$. Note that the constraints (19.21) follow directly from this construction.

The control points $\mathbf{p}_0, \dots, \mathbf{p}_5$ of PH quintics are usually distinct: for *regular* PH quintics, in particular, it follows from (19.13) that \mathbf{w}_0 and \mathbf{w}_2 are non-zero, and thus $\mathbf{p}_0 \neq \mathbf{p}_1$ and $\mathbf{p}_4 \neq \mathbf{p}_5$. By appropriately choosing \mathbf{w}_1 , however, it is possible to construct “degenerate” PH quintics that have coincident interior control points (see Fig. 19.4). These forms may be summarized as follows.

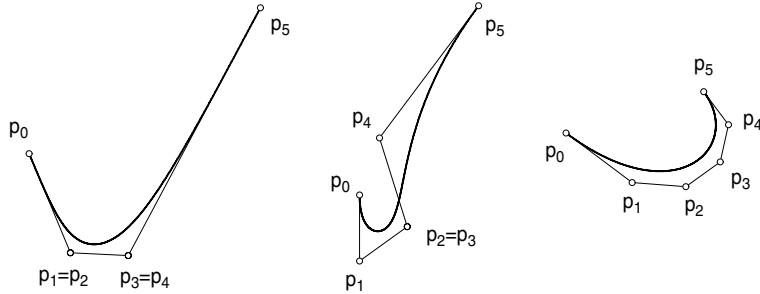


Fig. 19.4. Degenerate PH quintic control polygons — only 4 distinct control points (left); only 5 distinct control points (center); and a degree-elevated PH cubic (right).

Only Four Distinct Control Points

This case arises when we take $\mathbf{w}_1 = 0$ in (19.12), so that $\mathbf{p}_1 = \mathbf{p}_2$ and $\mathbf{p}_3 = \mathbf{p}_4$. The control polygon is then of the form

$$\Delta\mathbf{p}_0 = \frac{\mathbf{w}_0^2}{5}, \quad \Delta\mathbf{p}_1 = 0, \quad \Delta\mathbf{p}_2 = \pm \frac{\mathbf{w}_0\mathbf{w}_2}{15}, \quad \Delta\mathbf{p}_3 = 0, \quad \Delta\mathbf{p}_4 = \frac{\mathbf{w}_2^2}{5}.$$

Although there are only four distinct control points, this hodograph defines a true quintic PH, *not* a degree-elevated PH cubic (see below). Moreover, this curve is regular if $\mathbf{w}_0, \mathbf{w}_2 \neq 0$. As noted in the proof of Proposition 19.3, when

$\Delta\mathbf{p}_1 = \Delta\mathbf{p}_3 = 0$ the entire system of constraints (19.16) and (19.17) reduces to just $9(\Delta\mathbf{p}_2)^2 - \Delta\mathbf{p}_0\Delta\mathbf{p}_4 = 0$. Geometrically, this amounts to

$$3L_2 = \sqrt{L_0 L_4} \quad \text{and} \quad \theta_a = \theta_b, \quad (19.23)$$

where L_0, L_2, L_4 are lengths of the non-zero control polygon legs, and θ_a, θ_b are the interior angles at $\mathbf{p}_1 = \mathbf{p}_2$ and $\mathbf{p}_3 = \mathbf{p}_4$. Conditions (19.23) are clearly reminiscent of the geometrical constraints (18.6) for PH cubics.

Only Five Distinct Control Points

In this case, the value of \mathbf{w}_1 is chosen such that $2\mathbf{w}_1^2 + \mathbf{w}_0\mathbf{w}_2 = 0$, and hence $\mathbf{p}_2 = \mathbf{p}_3$. Thus, $\Delta\mathbf{p}_2 = 0$ and the other control polygon legs can be expressed in terms of \mathbf{w}_0 and \mathbf{w}_2 only:

$$\Delta\mathbf{p}_0 = \frac{\mathbf{w}_0^2}{5}, \quad \Delta\mathbf{p}_1 = \pm i \frac{\mathbf{w}_0}{5} \sqrt{\frac{\mathbf{w}_0\mathbf{w}_2}{2}}, \quad \Delta\mathbf{p}_3 = \pm i \frac{\mathbf{w}_2}{5} \sqrt{\frac{\mathbf{w}_0\mathbf{w}_2}{2}}, \quad \Delta\mathbf{p}_4 = \frac{\mathbf{w}_2^2}{5}.$$

For this degenerate form, conditions (19.16) and (19.17) may be reduced to

$$\Delta\mathbf{p}_0(\Delta\mathbf{p}_3)^2 = \Delta\mathbf{p}_4(\Delta\mathbf{p}_1)^2 \quad \text{and} \quad \Delta\mathbf{p}_0\Delta\mathbf{p}_4 + 2\Delta\mathbf{p}_1\Delta\mathbf{p}_3 = 0.$$

In terms of the lengths L_0, L_1, L_3, L_4 of the control polygon legs and interior angles $\theta_a, \theta_b, \theta_c$ at $\mathbf{p}_1, \mathbf{p}_2 = \mathbf{p}_3, \mathbf{p}_4$, we obtain the geometrical constraints

$$\frac{L_1}{L_3} = \sqrt{\frac{L_0}{L_4}}, \quad \frac{L_0}{L_1} = 2 \frac{L_3}{L_4}, \quad \theta_a - \theta_b + \theta_c = \pi, \quad \theta_a - \theta_c = \pm\pi.$$

Degree-elevated PH Cubics

It is possible to elevate the degree of any PH curve without compromising the Pythagorean nature of its hodograph, since degree elevation amounts merely to a redundant representation. Applying the degree elevation procedure (13.4) *twice* to the PH cubic control polygon (19.9) yields PH quintic control points

$$\begin{aligned} \mathbf{p}_1 &= \mathbf{p}_0 + \frac{1}{5}\mathbf{w}_0^2, \\ \mathbf{p}_2 &= \mathbf{p}_1 + \frac{1}{10}(\mathbf{w}_0^2 + \mathbf{w}_0\mathbf{w}_1), \\ \mathbf{p}_3 &= \mathbf{p}_2 + \frac{1}{30}(\mathbf{w}_0^2 + 4\mathbf{w}_0\mathbf{w}_1 + \mathbf{w}_1^2), \\ \mathbf{p}_4 &= \mathbf{p}_3 + \frac{1}{10}(\mathbf{w}_0\mathbf{w}_1 + \mathbf{w}_1^2), \\ \mathbf{p}_5 &= \mathbf{p}_4 + \frac{1}{5}\mathbf{w}_1^2. \end{aligned} \quad (19.24)$$

One can verify that expressions (19.24) are of the form (19.12) with $\mathbf{w}_0, \mathbf{w}_1, \mathbf{w}_2$ replaced by $\mathbf{w}_0, \frac{1}{2}(\mathbf{w}_0 + \mathbf{w}_1), \mathbf{w}_1$. Thus, it follows that whenever the value \mathbf{w}_1 in equations (19.12) is the *mean* of the values \mathbf{w}_0 and \mathbf{w}_2 , we have a PH cubic “masquerading” as a quintic, rather than a true PH quintic.

19.7 Intrinsic Features of Corresponding Curves

For a PH curve with complex hodograph $\mathbf{r}'(t) = \mathbf{w}^2(t)$, the parametric speed is evidently $\sigma(t) = |\mathbf{w}(t)|^2$. The unit tangent and normal may be expressed in terms of the complex polynomial $\mathbf{w}(t)$ as

$$\mathbf{t} = \mathbf{r}' / |\mathbf{r}'| = \mathbf{w} / \bar{\mathbf{w}} \quad \text{and} \quad \mathbf{n} = \mathbf{t} \times \mathbf{z} = \mathbf{w} / i \bar{\mathbf{w}}, \quad (19.25)$$

while the curvature is given by

$$\kappa = \frac{1}{|\mathbf{r}'|} \operatorname{Im}\left(\frac{\mathbf{r}''}{\mathbf{r}'}\right) = \frac{\operatorname{Im}(\bar{\mathbf{r}}' \mathbf{r}'')}{|\mathbf{r}'|^3} = 2 \frac{\operatorname{Im}(\bar{\mathbf{w}} \mathbf{w}')}{|\mathbf{w}|^4}. \quad (19.26)$$

In §19.2 a one-to-one correspondence between regular polynomial curves and regular PH curves was established by requiring the hodographs $\mathbf{w}(t)$ and $\hat{\mathbf{w}}(t)$ of corresponding curves $\mathbf{r}(t)$ and $\hat{\mathbf{r}}(t)$ to satisfy $\hat{\mathbf{w}}(t) = \mathbf{w}^2(t)$. We now compare the geometrical properties of corresponding curves.

Parametric Speed and Arc Length

The *unit-speed points* of a curve are identified by the t values (if any) where the parametric speed satisfies $\sigma(t) = 1$. In the vicinity of such points, the curve parameter t approximates the arc length s . Unit-speed points correspond to t values for which $\mathbf{r}'(t) = \mathbf{w}(t) = u(t) + i v(t)$ crosses or touches the unit circle $u^2 + v^2 = 1$ in the hodograph plane. For polynomial curves (except straight lines) the unit-speed points must be finite in number, since it is impossible to satisfy $u^2(t) + v^2(t) \equiv 1$ unless $u(t), v(t)$ are both constants — the hodograph then degenerates to just a single point, defining a straight line (the same is also true for *rational* curves: see §16.1).

Remark 19.6 The unit-speed points of a regular polynomial curve $\mathbf{r}(t)$ and its PH counterpart $\hat{\mathbf{r}}(t)$ are in one-to-one correspondence.

This follows from the fact that corresponding curves $\mathbf{r}(t)$ and $\hat{\mathbf{r}}(t)$, with hodographs $u(t) + iv(t)$ and $u^2(t) - v^2(t) + i2u(t)v(t)$, have speeds

$$\sigma(t) = \sqrt{u^2(t) + v^2(t)} \quad \text{and} \quad \hat{\sigma}(t) = u^2(t) + v^2(t). \quad (19.27)$$

Hence the unit-speed points of $\mathbf{r}(t)$ and $\hat{\mathbf{r}}(t)$ occur at identical values of t — namely, at the (real) roots of the polynomial

$$P(t) = u^2(t) + v^2(t) - 1. \quad (19.28)$$

For curves of degree n and $\hat{n} = 2n - 1$, there are at most $2n - 2$ of them. A unit-speed point is “simple” if it is not a multiple root of $P(t)$.

Definition 19.1 A segment $t \in [a, b]$ of a regular curve $\mathbf{r}(t)$ with no interior unit-speed points is “slow” or “fast” according to whether $\sigma(t) < 1$ or $\sigma(t) > 1$.

The (odd-multiplicity) unit-speed points of a curve delimit slow and fast segments of greatest extent on it. For corresponding curves $\mathbf{r}(t)$ and $\hat{\mathbf{r}}(t)$, the slow and fast segments are in one-to-one correspondence, and if $t = a$, $t = b$ are consecutive unit-speed points on $\mathbf{r}(t)$ and $\hat{\mathbf{r}}(t)$, then for $t \in (a, b)$ we have $\hat{\sigma}(t) < \sigma(t)$ for a slow segment, and $\hat{\sigma}(t) > \sigma(t)$ for a fast segment. In other words, compared to $\mathbf{r}(t)$, the PH curve $\hat{\mathbf{r}}(t)$ is *slower* on slow segments and *faster* on fast segments: the speed variations of $\hat{\mathbf{r}}(t)$ are “exaggerated” relative to those of $\mathbf{r}(t)$. Since the arc length of any segment $t \in [a, b]$ is the integral of the parametric speed over that interval, the lengths of such segments on corresponding curves satisfy the inequalities $\hat{S}_{\text{slow}} < S_{\text{slow}}$ and $\hat{S}_{\text{fast}} > S_{\text{fast}}$.

Tangents and Curvatures

For corresponding curves with hodographs $\mathbf{w} = u + iv$ and $\hat{\mathbf{w}} = u^2 - v^2 + i2uv$, we can write the tangent and curvature at points of equal parameter value as

$$\begin{aligned}\mathbf{t} &= \frac{(u, v)}{\sqrt{u^2 + v^2}} \quad \text{and} \quad \kappa = \frac{uv' - u'v}{(u^2 + v^2)^{3/2}}, \\ \hat{\mathbf{t}} &= \frac{(u^2 - v^2, 2uv)}{u^2 + v^2} \quad \text{and} \quad \hat{\kappa} = 2 \frac{uv' - u'v}{(u^2 + v^2)^2}.\end{aligned}\quad (19.29)$$

Now for each t , the tangent $\hat{\mathbf{t}}$ to $\hat{\mathbf{r}}(t)$ has an inclination angle *twice* that of the tangent \mathbf{t} to $\mathbf{r}(t)$: $\hat{\psi} = 2\psi$ (modulo 2π). Thus, horizontal *and* vertical tangents on $\mathbf{r}(t)$ are mapped to horizontal tangents of $\hat{\mathbf{r}}(t)$, while vertical tangents on $\hat{\mathbf{r}}(t)$ correspond to tangent angles $\psi = (2k+1)\pi/4$ for $k = 0, 1, 2, 3$ on $\mathbf{r}(t)$. Note also that the *rotation indices* of the curves

$$\mathcal{R} = \frac{1}{2\pi} \int_a^b \kappa \, ds \quad \text{and} \quad \hat{\mathcal{R}} = \frac{1}{2\pi} \int_a^b \hat{\kappa} \, d\hat{s} \quad (19.30)$$

satisfy $\hat{\mathcal{R}} = 2\mathcal{R}$ for any interval $t \in [a, b]$ — as can be verified from expressions (19.29) and the relations $ds = \sqrt{u^2 + v^2} dt$ and $d\hat{s} = (u^2 + v^2) dt$. These indices indicate the (net) fraction of a full circle that the curve tangent rotates through along $\mathbf{r}(t)$ and $\hat{\mathbf{r}}(t)$ — their evaluation is described in Chap. 25.

Lemma 19.2 *Inflections on $\mathbf{r}(t)$ and $\hat{\mathbf{r}}(t)$ are in one-to-one correspondence.*

Proof: Inflections are points where the curvature changes sign. From (19.29) the parameter values identifying inflections on $\mathbf{r}(t)$ and $\hat{\mathbf{r}}(t)$ must be roots of

$$u(t)v'(t) - u'(t)v(t) = 0. \quad (19.31)$$

To qualify as inflections, the first non-vanishing derivative of κ and $\hat{\kappa}$ at such values must be of *odd* order. Re-writing relations (19.29) as

$$\hat{\kappa} = \frac{2}{\sqrt{u^2 + v^2}} \kappa \quad \text{and} \quad \kappa = \frac{\sqrt{u^2 + v^2}}{2} \hat{\kappa} \quad (19.32)$$

and differentiating, the r -th derivative $\hat{\kappa}^{(r)}$ of the curvature of $\hat{\mathbf{r}}(t)$ is obtained as a homogeneous linear combination of the curvature κ of $\mathbf{r}(t)$ and its first r derivatives $\kappa', \dots, \kappa^{(r)}$ — and vice-versa. For $r = 1$, we have

$$\hat{\kappa}' = 2 \frac{(u^2 + v^2)\kappa' - (uu' + vv')\kappa}{(u^2 + v^2)^{3/2}}, \quad \kappa' = \frac{(u^2 + v^2)\hat{\kappa}' + (uu' + vv')\hat{\kappa}}{2\sqrt{u^2 + v^2}},$$

while higher derivatives incur more complicated expressions. Thus, at any root of equation (19.31), where $\kappa = \hat{\kappa} = 0$, we see that

$$\kappa = \kappa' = \dots = \kappa^{(r)} = 0 \iff \hat{\kappa} = \hat{\kappa}' = \dots = \hat{\kappa}^{(r)} = 0,$$

$\kappa^{(r+1)}$ and $\hat{\kappa}^{(r+1)}$ being non-zero. Inflections correspond to odd r values. ■

Corresponding points of $\mathbf{r}(t)$ and $\hat{\mathbf{r}}(t)$ where $\kappa = \hat{\kappa} = 0$ but the curvatures have even lowest-order non-vanishing derivatives are *vertices* of these curves, i.e., points where the curvature is a local extremum value (in this case, zero). However, vertices of non-zero curvature are *not* in simple correspondence, as can be seen by writing the derivatives κ' and $\hat{\kappa}'$ in terms of u and v :

$$\begin{aligned} \kappa' &= \frac{uv'' - u''v}{(u^2 + v^2)^{3/2}} - 3 \frac{(uu' + vv')(uv' - u'v)}{(u^2 + v^2)^{5/2}}, \\ \hat{\kappa}' &= 2 \frac{uv'' - u''v}{(u^2 + v^2)^2} - 8 \frac{(uu' + vv')(uv' - u'v)}{(u^2 + v^2)^3}, \end{aligned}$$

from which we see that κ' and $\hat{\kappa}'$ do not, in general, vanish simultaneously at points where $uv' - u'v \neq 0$ — i.e., where κ and $\hat{\kappa}$ are non-zero.

Remark 19.7 Inflections delineate corresponding maximal *convex segments* on $\mathbf{r}(t)$ and $\hat{\mathbf{r}}(t)$ — by “convex” we mean that the curvature is of constant sign (such segments may exhibit loops or spiral around themselves).

The correspondence of inflections on $\mathbf{r}(t)$ and $\hat{\mathbf{r}}(t)$ can also be understood geometrically. Consider a rotating line \mathbf{l} through the origin of the hodograph plane. If \mathbf{l} meets the hodograph $\mathbf{w}(t) = \mathbf{r}'(t)$ tangentially — and locally on one side — at $t = t_0$, the point $\mathbf{r}(t_0)$ is an inflection (see §13.5): interpreting $\mathbf{r}(t)$ vectorially, we note that $\mathbf{r}'(t_0)$ and $\mathbf{r}''(t_0)$ are parallel, and thus κ vanishes at t_0 . Since angles between loci are invariant under conformal maps (see §4.5), the line $\hat{\mathbf{l}} = \mathbf{l}^2$ meets the hodograph $\hat{\mathbf{w}}(t) = \mathbf{w}^2(t)$ tangentially at $t = t_0$. Thus, $\hat{\mathbf{r}}(t_0)$ is an inflection point of the PH curve corresponding to $\mathbf{r}(t)$.

Finally, we consider the *magnitudes* of the curvatures of $\mathbf{r}(t)$ and $\hat{\mathbf{r}}(t)$ at corresponding points. We have noted that the unit circle ($\sigma^2 = \hat{\sigma} = 1$) in the \mathbf{w} and $\hat{\mathbf{w}}$ hodograph planes plays an important role in determining the arc lengths of corresponding segments on $\mathbf{r}(t)$ and $\hat{\mathbf{r}}(t)$. In comparing curvatures, the circles $\sigma^2 = \hat{\sigma} = 4$ play a similar role — from (19.29) we have $|\hat{\kappa}(t)| > |\kappa(t)|$ when $\sigma^2(t) = \hat{\sigma}(t) < 4$ and $|\hat{\kappa}(t)| < |\kappa(t)|$ when $\sigma^2(t) = \hat{\sigma}(t) > 4$.

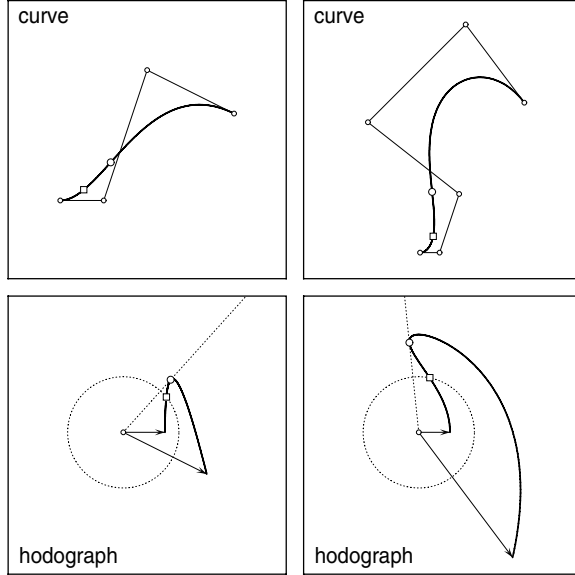


Fig. 19.5. Corresponding cubic (left) and PH quintic (right) for Example 19.2. Unit speed points (squares) arise when the hodograph crosses the circle $\sigma = 1$. Inflections (circles) arise when a radial line through the origin is tangent to the hodograph.

Example 19.2 Consider the regular cubic $\mathbf{r}(t)$ defined by control points $\mathbf{p}_0 = 0$, $\mathbf{p}_1 = \frac{1}{4}$, $\mathbf{p}_2 = \frac{1}{2} + \frac{3}{4}i$, $\mathbf{p}_3 = 1 + \frac{1}{2}i$. The corresponding PH quintic $\hat{\mathbf{r}}(t)$ has control points $\mathbf{p}_0 = 0$, $\mathbf{p}_1 = 9/80$, $\mathbf{p}_2 = (18 + 27i)/80$, $\mathbf{p}_3 = (-24 + 60i)/80$, $\mathbf{p}_4 = (21 + 105i)/80$, $\mathbf{p}_5 = (48 + 69i)/80$. The curves and their hodographs are illustrated in Fig. 19.5. Up to a constant factor, the polynomial (19.28) whose roots identify unit-speed points of $\mathbf{z}(t)$ and $\hat{\mathbf{z}}(t)$ is

$$P(t) = 550t^4 - 756t^3 + 342t^2 - 7,$$

and this has just one real root, $\alpha \approx 0.18$, on $t \in [0, 1]$. Thus, the subsegments $t \in [0, \alpha]$ and $t \in [\alpha, 1]$ are ‘‘slow’’ and ‘‘fast’’ on both $\mathbf{r}(t)$ and $\hat{\mathbf{r}}(t)$. For the PH quintic $\hat{\mathbf{r}}(t)$, the arc length of the slow/fast segment is smaller/greater than that of the cubic $\mathbf{r}(t)$. Both $\mathbf{r}(t)$ and $\hat{\mathbf{r}}(t)$ have just one real inflection for $t \in [0, 1]$, at $\beta \approx 0.37$, and since the hodographs $\mathbf{w}(t)$ and $\hat{\mathbf{w}}(t)$ lie inside the circles $\sigma^2 = \hat{\sigma} = 4$, we have $|\hat{\kappa}(t)| > |\kappa(t)|$ for all $t \in [0, 1]$ except $t = \beta$.

Rational Pythagorean–hodograph Curves

... I have succeeded in solving the following problem. If AEC (Fig. 20.1) is an arc of a circle and the lines DE signify the sun's rays and EF the reflected ones, the problem is to determine the curve FRC resulting from the crossing of the reflected rays.

E. W. von Tschirnhaus, *Acta Eruditorum* (1682), as quoted in [390]

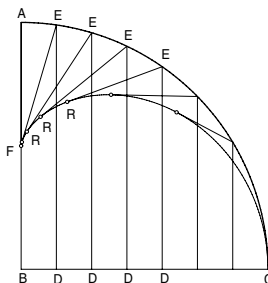


Fig. 20.1. Sketch of caustic by reflection from a circle (after Tschirnhaus).

Thus far, we have discussed only *polynomial* curves satisfying the Pythagorean hodograph condition (17.1). It is natural to also investigate the properties of *rational* curves characterized by this condition. Such curves were first studied by Fiorot and Gensane [202] and Pottmann [369], who gave elegant arguments for the *dual form* — in which curves are specified using line coordinates instead of point coordinates (see §7.4.3) — as the most natural representation for the study of such *rational PH curves*. Although polynomial and rational PH curves both have rational offsets, they differ significantly in terms of their arc-length functions. For polynomial PH curves, integrating the polynomial speed $\sigma(t)$ yields, with minimal effort, a polynomial arc length function $s(t)$. For rational PH curves, however, integration of the rational speed function $\sigma(t)$ requires a

partial fraction expansion and yields, in general, an arc length $s(t)$ comprising transcendental as well as rational terms. Thus, for applications such as motion control (see Chap. 29), polynomial PH curves are often preferable.

In Chap. 18 we observed that the simplest non-trivial planar PH curve, *Tschirnhausen's cubic*, was first studied as the caustic for reflection of parallel rays by a parabolic mirror. This optical interpretation is not just serendipitous — the study of *rational* PH curves (which subsume the polynomial PH curves) reveals that *all* PH curves can be interpreted as caustics by reflection, or their involutes (i.e., the curves that describe the reflected wavefronts) — see §20.5.

20.1 Construction of Rational PH Curves

To construct rational PH curves, Pottmann [369] notes that they must have unit normals of the form

$$n_x(t) = \frac{2a(t)b(t)}{a^2(t) + b^2(t)}, \quad n_y(t) = \frac{a^2(t) - b^2(t)}{a^2(t) + b^2(t)}, \quad (20.1)$$

for relatively prime polynomials $a(t)$ and $b(t)$, since the map $(a(t)/b(t), 0) \rightarrow (n_x(t), n_y(t))$ may be interpreted as the inverse stereographic projection of a rational parameterization of the projective real line to the unit circle.

Now in free coordinates (x, y) the tangent line at point t of a rational curve $\mathbf{r}(t) = (x(t), y(t))$ with the normal (20.1) has the implicit equation

$$\ell(x, y, t) = n_x(t)x + n_y(t)y - h(t) = 0, \quad (20.2)$$

and since $\mathbf{n}(t)$ is a unit vector, the function $h(t)$ specifies its (signed) distance from the origin. Furthermore, this must be a *rational* function, since the point $(x, y) = (x(t), y(t))$ satisfies equation (20.2) for each t , and we hence can write

$$h(t) = \frac{f(t)}{g(t)} \quad (20.3)$$

where $f(t)$ and $g(t)$ are relatively prime polynomials.

When we consider the curve $\mathbf{r}(t)$ as the envelope of its family of tangents (20.2), the curve points satisfy the simultaneous equations $\ell = \partial\ell/\partial t = 0$ — see §8.2.1. Denoting derivatives with respect to t by primes, we have

$$\frac{\partial\ell}{\partial t}(x, y, t) = n'_x(t)x + n'_y(t)y - h'(t) = 0. \quad (20.4)$$

Solving (20.2) and (20.4) for x, y then gives

$$x = \frac{hn'_y - h'n_y}{n_xn'_y - n'_xn_y}, \quad y = \frac{h'n_x - hn'_x}{n_xn'_y - n'_xn_y}, \quad (20.5)$$

where the derivatives of n_x, n_y, h can be written as

$$n'_x = -2 \frac{a'b - ab'}{a^2 + b^2} n_y, \quad n'_y = 2 \frac{a'b - ab'}{a^2 + b^2} n_x, \quad h' = \frac{f'g - fg'}{g^2},$$

and we note that

$$n_x n'_y - n'_x n_y = 2 \frac{a'b - ab'}{a^2 + b^2}.$$

Hence, setting $x = X(t)/W(t)$, $y = Y(t)/W(t)$ in (20.5) and substituting for n_x , n_y , h and n'_x , n'_y , h' we obtain

$$\begin{aligned} W &= (a^2 + b^2)(a'b - ab')g^2, \\ X &= 2ab(a'b - ab')fg - \frac{1}{2}(a^4 - b^4)(f'g - fg'), \\ Y &= (a^2 - b^2)(a'b - ab')fg + ab(a^2 + b^2)(f'g - fg'), \end{aligned} \quad (20.6)$$

as the homogeneous coordinate polynomials $W(t)$, $X(t)$, $Y(t)$ of $\mathbf{r}(t)$.

For pairs of relatively prime polynomials $a(t)$, $b(t)$ and $f(t)$, $g(t)$ equations (20.6) define the general form of the homogeneous point coordinates of rational curves with rational offsets. By choosing $a(t) = t$, $b(t) = 1$ and $f(t)/g(t) = \text{constant}$ ($= r$, say) we obtain the simplest example of such curves — a circle of radius r . Furthermore, if $h(t)$ in (20.2) is replaced by $h(t) + d$, the tangent line is simply displaced by distance d in the direction of the normal $\mathbf{n}(t)$. The envelope of a family of displaced tangent lines, each shifted by distance d in the associated normal direction $\mathbf{n}(t)$, defines the *offset* at distance d from the base curve $\mathbf{r}(t)$. Thus, simply replacing $f(t)$ by $f(t) + g(t)d$ in equations (20.6) gives the homogeneous coordinates of the rational offset, $\mathbf{r}(t) + d\mathbf{n}(t)$.

A form equivalent to (20.6) was also obtained by Fiorot and Gensane [202], through a similar approach. However, the point representation (20.6) seems unduly cumbersome compared to the simple forms of *polynomial* PH curves. Thus, Pottmann [369] has emphasized that the *dual form* of the rational curves (20.6) — in terms of *line coordinates* — is preferable. Recall (see §7.4) that the homogeneous line coordinates $K(t)$, $L(t)$, $M(t)$ of a rational parametric curve are simply the coefficients

$$K(t)W + L(t)X + M(t)Y = 0$$

in the tangent line equation at point t . We can ascertain the form of the line coordinates directly by inspection of (20.1)–(20.3) — namely,

$$K : L : M = -(a^2 + b^2)f : 2abg : (a^2 - b^2)g. \quad (20.7)$$

$K(t)$, $L(t)$, $M(t)$ are clearly simpler and of lower degree — for a given degree of the polynomials $a(t)$, $b(t)$ and $f(t)$, $g(t)$ — than $W(t)$, $X(t)$, $Y(t)$.

However, the polynomials (20.7) may not satisfy $\gcd(K(t), L(t), M(t)) = \text{constant}$, even if relatively prime pairs are chosen for $a(t)$, $b(t)$ and $f(t)$,

$g(t)$ — they will have a non-constant common factor if $a^2(t) + b^2(t)$ divides $g(t)$. This can be remedied by setting $g = -e(a^2 + b^2)$ to obtain

$$K : L : M = f : 2abe : (a^2 - b^2)e. \quad (20.8)$$

Then $K(t)$, $L(t)$, $M(t)$ will be relatively prime when $a(t)$, $b(t)$ and $e(t)$, $f(t)$ are relatively prime pairs, and the offset curve at distance d is obtained by replacing $f(t)$ with $f(t) - e(t)(a^2(t) + b^2(t))d$. After cancelling common factors, the corresponding point representation for this modified form becomes

$$\begin{aligned} W &= (a^2 + b^2)(a'b - ab')e^2, \\ X &= \frac{1}{2}(a^2 - b^2)(ef' - e'f) - (aa' - bb')ef, \\ Y &= (a'b + ab')ef - ab(ef' - e'f). \end{aligned} \quad (20.9)$$

For specified polynomials $a(t)$, $b(t)$ and $e(t)$, $f(t)$ expressions (20.8) and (20.9) permit a direct comparison of the *class* (degree of the line representation) and *order* (degree of the point representation) for rational PH curves.

Example 20.1 Consider the family of rational PH curves of class 3 defined by substituting linear polynomials $a(t)$, $b(t)$, $e(t)$ and a cubic polynomial $f(t)$ in (20.8). For the polynomials that parameterize the unit circle, we can choose $a(t) = t$ and $b(t) = 1$ without loss of generality, since this amounts to a specific choice among the family of re-parameterizations $t \rightarrow (\alpha t + \beta)/(\gamma t + \delta)$ that preserve the curve degree. Setting $e(t) = e_0 + e_1t$, $f(t) = f_0 + f_1t + f_2t^2 + f_3t^3$ we obtain homogeneous line coordinates of the form

$$K(t) : L(t) : M(t) = f_0 + f_1t + f_2t^2 + f_3t^3 : 2t(e_0 + e_1t) : (t^2 - 1)(e_0 + e_1t).$$

Taking $f_0 = f_1 = 0$ fixes the origin as the point, and the x -axis as the tangent, corresponding to the parameter value $t = 0$. Also, since only the ratios matter, we set $p = f_2/e_1$, $q = f_3/e_1$, $r = e_0/e_1$, leaving three degrees of freedom:

$$K(t) : L(t) : M(t) = t^2(p + qt) : 2t(r + t) : (t^2 - 1)(r + t). \quad (20.10)$$

From the corresponding homogeneous point coordinates

$$\begin{aligned} W(t) &= 2t^4 + 4rt^3 + 2(r^2 + 1)t^2 + 4rt + 2r^2, \\ X(t) &= (rq - p)t^4 - 2qt^3 - (3rq + p)t^2 - 2rpt, \\ Y(t) &= -2qt^4 - 4rqt^3 - 2rpt^2, \end{aligned} \quad (20.11)$$

we see that these expressions define quartic rational PH curves — an example of these curves is shown in Fig. 20.2.

The most striking feature of the example in Fig. 20.2 is, of course, the *cusp*. The occurrence of this cusp is not coincidental: we shall see in §20.4 and §20.5 that rational PH curves can be interpreted as the *involutes* of certain special curves, and an involute always has a cusp at the “point of attachment” to its

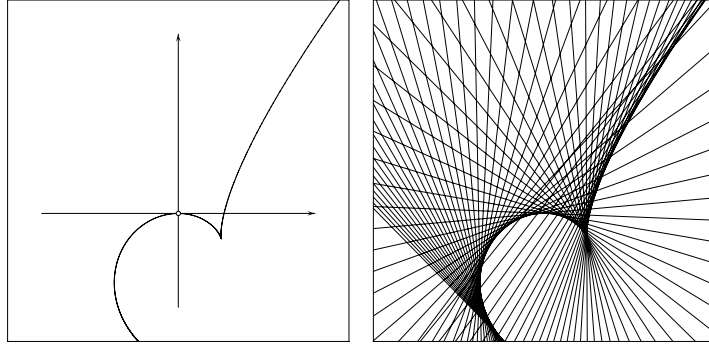


Fig. 20.2. Left: a quartic rational PH curve, defined by (20.11) with $p = 2$, $q = 1$, $r = 3$. Right: sampling of the system of tangents, defined by the dual form (20.10).

evolute (see §8.3.2). Note also that the curves defined by (20.11) always have a real point at infinity, since $W(t)$ has the factorization $2(1+t^2)(t+r)^2$. Of course, in practical applications one would need to choose the domain of the parameter t so as to exclude cusps and points at infinity.

Remark 20.1 For the parameterization of a rational PH curve specified by the choices $a(t) = t$, $b(t) = 1$ in (20.1), the curve tangent for parameter value t makes angle ϕ with the positive x -axis, where $t = \tan \frac{1}{2}\phi$, and for a convex curve segment there is a one-to-one correspondence between ϕ and t . Such a curve segment may be described [369, 370] in terms of the *support coordinates* $(\phi(t), h(t))$ where $h(t)$ gives the signed distance of the tangent from the origin. Equivalently, the curve may be described by the *support function* $h(\phi)$ defined by substituting t in terms of ϕ in h . A convex segment is free of inflections, and inflections are singularities of the line representation that are the duals of cusps in the point representation. The dual of the homogeneous coordinate condition $W' : W = X' : X = Y' : Y$ for a cusp becomes $K' : K = L' : L = M' : M$ for an inflection, and from (20.8) one can see that if $a(t)b'(t) - a'(t)b(t) \neq 0$ over an interval in t , the segment is free of inflections.

Regarding the inflectional ability of rational PH curves, we note from (20.9) that $W = 0$ at any root t_* of $a(t)b'(t) - a'(t)b(t)$. In order to obtain a (real) *affine* inflection, t_* must also be a common root of X and Y , so a factor $t - t_*$ can be cancelled¹ from all three polynomials. For further details on rational PH curve inflections, and their influence on the curve degree, see [180].

Methods to design rational PH curve segments by the interpolation of G^2 data (end points, tangents, and curvatures) are described by Pottmann [370]. These make use of the dual form (20.8) with either (i) $a(t)$, $b(t)$ linear and $e(t)$

¹ A parameter value t_* for which $W(t_*) = X(t_*) = Y(t_*) = 0$ identifies a *base point* of a rational curve, which allows a reduction in the curve degree by extraction of the common factor $t - t_*$ from $W(t)$, $X(t)$, $Y(t)$.

quadratic; or (ii) $a(t)$, $b(t)$ quadratic and $e(t)$ constant — in both cases, $f(t)$ is a quartic polynomial. These choices describe rational PH curves of *class 4*, i.e., four tangents can be drawn to the curve from a generic point in the plane, and the corresponding point equations are of degree 6 — although a reduction to degree 5 occurs if the curve has a real affine inflection. For complete details of the algorithms that determine coefficients for $a(t)$, $b(t)$ and $e(t)$, $f(t)$ so as to satisfy the G^2 interpolation constraints, we refer the reader to [370].

The above approach, in which rational PH curves are regarded as envelopes of the one-parameter families of lines (20.2) with rational coefficients, is much simpler and more intuitive than trying to construct them by integration. The parametric speed $\sigma(t)$ of a rational curve $\mathbf{r}(t) = (x(t), y(t))$ specified by the homogeneous coordinate polynomials $W(t)$, $X(t)$, $Y(t)$ is

$$\sigma = \frac{\sqrt{(WX' - W'X)^2 + (WY' - W'Y)^2}}{W^2},$$

and in order for $\sigma(t)$ to be a rational function, the polynomials $WX' - W'X$ and $WY' - W'Y$ must be components of a Pythagorean triple, and hence the hodograph must be of the form

$$x'(t) = \frac{[a^2(t) - b^2(t)] c(t)}{W^2(t)}, \quad y'(t) = \frac{2a(t)b(t)c(t)}{W^2(t)} \quad (20.12)$$

for polynomials $a(t)$, $b(t)$, $c(t)$ with $\gcd(a(t), b(t)) = \text{constant}$. This hodograph form is a necessary, but not sufficient, condition for a rational PH curve: one must also ensure that its integration does not incur transcendental terms.

Sufficient and necessary conditions for the integration of a hodograph of the form (20.12) to yield a *rational* curve were identified in [180] — namely, $W(t)$ and $c(t)$ must be expressible in terms of $a(t)$, $b(t)$ and another pair of relatively prime polynomials $e(t)$, $f(t)$ in the form

$$W = (a^2 + b^2)(a'b - ab')e^2,$$

$$\begin{aligned} c = & [(a^2 + b^2)^2(a''b' - a'b'') + (a'b - ab')(a'^2 + b'^2)] e^3 f \\ & - \frac{1}{2}(a^2 + b^2)[(a''b - ab'')(ef' - e'f) - (a'b - ab')(ef'' - e''f)] e^2 \\ & - (a'b - ab')(ef' - e'f) [(a^2 + b^2)g' + (aa' + bb')e] e. \end{aligned}$$

The cumbersome form of $c(t)$ makes this approach unattractive, but it serves a useful theoretical purpose. In general, roots of $c(t)$ identify *cusps* of rational PH curves, and since it is impossible to have $c(t) = \text{constant}$ — except in the trivial case of a circle — cusps are a generic feature² of rational PH curves. By contrast, it is easy to construct cusp-free polynomial PH curves, by simply choosing $\gcd(u(t), v(t)) = \text{constant}$ and $w(t) = \text{constant}$ in (17.4).

² This is consistent with the interpretation of rational PH curves as the *involutes* of certain curves — see §20.4 below.

20.2 Dual Bézier Curve Representation

Since the dual (line) representation of rational PH curves is simpler and more convenient to use than the customary point representation, we briefly review here some basic properties of the dual rational Bézier form of plane curves. This was first introduced and used by Hoschek [248, 249] and has subsequently been employed to great advantage by Pottmann [368, 369]. A recent study by Ait Haddou et al. [14] makes use of the dual form to construct and analyze *curves of constant width* in terms of piecewise-rational PH curves.

The dual Bézier form of a rational plane curve describes the one-parameter family of its tangent lines. To specify the dual form, a set of *control lines* with homogeneous line coordinates $\mathbf{L}_i = (K_i, L_i, M_i)$ for $i = 0, \dots, m$ is employed. However, since (K_i, L_i, M_i) and $\lambda(K_i, L_i, M_i)$ define the same line for every $\lambda \neq 0$, the dual Bézier form

$$\mathbf{L}(t) = \sum_{i=0}^m \mathbf{L}_i b_i^m(t), \quad (20.13)$$

where $b_i^m(t)$ are the Bernstein basis functions of degree m , requires additional parameters to uniquely specify a system of tangent lines. For the case of the rational point representation (see §13.6), this ambiguity is typically addressed by assigning a “weight” w_i to each control point (x_i, y_i) — uniquely fixing the homogeneous point coordinates $\mathbf{P}_i = (W_i, X_i, Y_i) = (w_i, w_i x_i, w_i y_i)$. However, as noted by Pottmann [368], the use of weights in the dual form is undesirable, since they are not independent of the chosen coordinate system. Instead, it is preferable to use analogs of the “weight points” or “Farin points” defined by (13.13). Specifying additional Farin lines $\hat{\mathbf{L}}_i = (\hat{K}_i, \hat{L}_i, \hat{M}_i)$ such that

$$\hat{\mathbf{L}}_i = \mathbf{L}_{i-1} + \mathbf{L}_i \quad \text{for } i = 1, \dots, n$$

amounts to fixing a definite scaling for each of the control lines \mathbf{L}_i . For further details on construction of the dual Bézier form of rational PH curves, see [369]. Methods for curve design using these forms are described in [370].

The de Casteljau algorithm for rational Bézier curves, used to evaluate and subdivide a curve at a chosen parameter value t , can be readily adapted to the dual form. Recall (see §13.4) that the standard de Casteljau algorithm employs an iterated sequence of linear interpolations of discrete points, starting with the curve control points. At each iteration stage, we have one point less than in the preceding stage, until ultimately we obtain a single point — the desired curve point $\mathbf{r}(t)$. Each linear interpolation corresponds to finding a new point on the line through two given points. With the dual form, on the other hand, each linear interpolation amounts to finding a new line through the common point of two given lines. Commencing with $\mathbf{L}_i^0(t) = \mathbf{L}_i$ for $i = 0, \dots, m$ the de Casteljau algorithm applied to the dual Bézier form (20.13) for a given t computes the triangular array of lines defined by

$$\mathbf{L}_i^r(t) = (1 - t) \mathbf{L}_{i-1}^{r-1}(t) + t \mathbf{L}_i^{r-1}(t) \quad (20.14)$$

for $i = r, \dots, m$ and $r = 1, \dots, m$. The final coefficients $\mathbf{L}_m^m(t)$ then define the *tangent line* to the curve for the given parameter value t .

For the homogeneous point representation of a degree– n curve with control points $\mathbf{P}_0, \dots, \mathbf{P}_n$ the last two points $\mathbf{P}_{n-1}^{n-1}(t)$ and $\mathbf{P}_n^{n-1}(t)$ generated by the de Casteljau algorithm define the *curve tangent* for parameter value t , namely, the line through them. Conversely, using the dual form (20.13), the last two lines $\mathbf{L}_{m-1}^{m-1}(t)$ and $\mathbf{L}_m^{m-1}(t)$ generated by the de Casteljau algorithm define the *curve point* for parameter t , namely, their intersection. The intersection point (W, X, Y) of two lines defined by homogeneous coordinates $\mathbf{L}_i = (K_i, L_i, M_i)$ and $\mathbf{L}_j = (K_j, L_j, M_j)$ may be specified [368] by the *exterior product*

$$\mathbf{L}_i \wedge \mathbf{L}_j = (L_i M_j - L_j M_i, M_i K_j - M_j K_i, K_i L_j - K_j L_i).$$

This prescription gives a simple, efficient means of generating points on curves defined in the dual form (20.13). In fact, we can express the homogeneous point representation $\mathbf{P}(t) = (W(t), X(t), Y(t))$ of the rational curve defined by the dual form (20.13) as the exterior product of the penultimate terms generated by the de Casteljau algorithm:

$$\mathbf{P}(t) = \mathbf{L}_{m-1}^{m-1}(t) \wedge \mathbf{L}_m^{m-1}(t), \quad (20.15)$$

from which we see that $\mathbf{P}(t)$ is generally of degree $2m - 2$, if $\mathbf{L}(t)$ is of degree m . Since the two terms in (20.15) can be written (see §11.6) in the form

$$\mathbf{L}_{m-1}^{m-1}(t) = \sum_{i=0}^{m-1} \mathbf{L}_i b_i^{m-1}(t) \quad \text{and} \quad \mathbf{L}_m^{m-1}(t) = \sum_{i=0}^{m-1} \mathbf{L}_{i+1} b_i^{m-1}(t),$$

the control points $\mathbf{P}_i = (W_i, X_i, Y_i)$ of (20.15) for $i = 0, \dots, 2m - 2$ can be expressed [370] in terms of the line coefficients $\mathbf{L}_i = (K_i, L_i, M_i)$ as

$$\mathbf{P}_i = \frac{1}{\binom{2m-2}{i}} \sum_{j=\max(0, i+2-m)}^{\min(m-1, i+1)} \binom{m-1}{j} \binom{m-1}{i-j} \mathbf{L}_j \wedge \mathbf{L}_{i-j+1}.$$

Since points on the envelope of a one-parameter family of plane curves satisfy the curve equation and its derivative with respect to the parameter (see §8.2), an alternative form of the point representation is given by

$$\mathbf{P}(t) = \mathbf{L}(t) \wedge \mathbf{L}'(t),$$

where the derivative $\mathbf{L}'(t)$ is of degree $m - 1$ with control lines $m(\mathbf{L}_{i+1} - \mathbf{L}_i)$, $i = 0, \dots, m - 1$. However, this expression is nominally of degree $2m - 1$, and gives a degree-elevated Bézier form of $\mathbf{P}(t)$ — an explicit degree reduction is required to extract the representation of the true degree, $2m - 2$.

Example 20.2 For the rational PH curves in Example 20.1, the cubic dual form (20.13) on $t \in [0, 1]$ has control lines $\mathbf{L}_i = (K_i, L_i, M_i)$ given by

$$\begin{aligned}\mathbf{L}_0 &= (0, 0, -r), \\ \mathbf{L}_1 &= \frac{1}{3}(0, 2r, -3r - 1), \\ \mathbf{L}_2 &= \frac{1}{3}(p, 4r + 2, -2r - 2), \\ \mathbf{L}_3 &= (p + q, 2r + 2, 0),\end{aligned}$$

while for the quartic point form, the control points $\mathbf{P}_i = (W_i, X_i, Y_i)$ are

$$\begin{aligned}\mathbf{P}_0 &= (2r^2, 0, 0), \\ \mathbf{P}_1 &= (r(1 + 2r), -\frac{1}{2}rp, 0), \\ \mathbf{P}_2 &= \frac{1}{6}(2 + 12r + 14r^2, -p - 6rp - 3rq, -2rp), \\ \mathbf{P}_3 &= ((1 + r)(1 + 3r), -\frac{1}{2}(1 + 3r)(p + q), -r(p + q)), \\ \mathbf{P}_4 &= (4(1 + r)^2, -2(1 + r)(p + q), -2(q + rp + 2rq)).\end{aligned}$$

The two alternative Bézier representations of the rational PH curve defined by the choices $p = 2, q = 1, r = 3$ are shown in Fig. 20.3.

Note that, since these are *rational* curves, the locations of the control lines or control points shown in Fig. 20.3 determine only the *ratios* $K_i : L_i : M_i$ and $W_i : X_i : Y_i$. To uniquely fix the *values*, further information must be given in the form of either weights, or the *auxiliary* or *Farin* points/lines.

The control lines for the offset at distance d from a rational PH curve are obtained by simply displacing each of the original control lines by d . However, this determines only the ratios $K_i : L_i : M_i$ of the offset curve line coefficients. As noted above, the offset at distance d is defined by replacing the polynomial

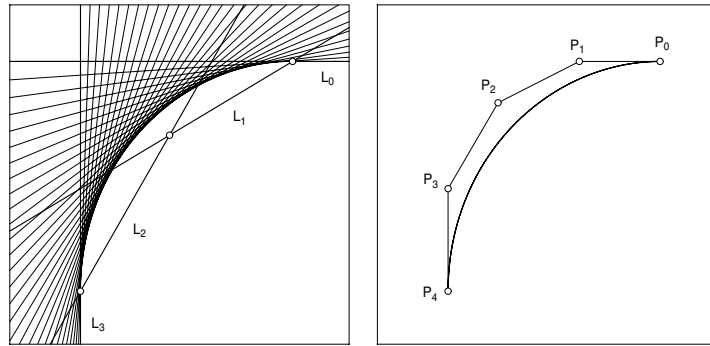


Fig. 20.3. Left: Bézier line representation of a rational PH curve of class 3 on the interval $t \in [0, 1]$ with control lines $\mathbf{L}_0, \mathbf{L}_1, \mathbf{L}_2, \mathbf{L}_3$ shown bold, and intersection points of consecutive control lines $\mathbf{L}_{i-1}, \mathbf{L}_i$ indicated. Right: corresponding Bézier point representation, of order 4, with control points $\mathbf{P}_0, \mathbf{P}_1, \mathbf{P}_2, \mathbf{P}_3, \mathbf{P}_4$ shown as dots and line segments connecting consecutive control points $\mathbf{P}_{i-1}, \mathbf{P}_i$ indicated.

$f(t)$ in (20.8) by $f(t) - e(t)(a^2(t) + b^2(t)) d$. To fix the proper scaling for each set of line coefficients, we must compute the Bernstein coefficients of the latter polynomial. This yields the homogeneous line representation defined by

$$\begin{aligned}\mathbf{L}_0 &= (-rd, 0, -r), \\ \mathbf{L}_1 &= \frac{1}{3}(-d - 3rd, 2r, -3r - 1), \\ \mathbf{L}_2 &= \frac{1}{3}(p - 2d - 4rd, 4r + 2, -2r - 2), \\ \mathbf{L}_3 &= (p + q - 2d - 2rd, 2r + 2, 0),\end{aligned}$$

for the offset at distance d , which is of the same class ($m = 3$) as the original curve. Likewise, replacing $f(t)$ with $f(t) - e(t)(a^2(t) + b^2(t)) d$ in (20.9), we find that the point representation of the offset at distance d can be obtained through the increments

$$\begin{aligned}\Delta\mathbf{P}_0 &= (0, 0, -2r^2) d, \\ \Delta\mathbf{P}_1 &= (0, r^2, -r(1 + 2r)) d, \\ \Delta\mathbf{P}_2 &= \frac{1}{6}(0, 4r(2 + 3r), -2(1 + r)(1 + 5r)) d, \\ \Delta\mathbf{P}_3 &= (0, (1 + r)(1 + 3r), -(1 + r)^2) d, \\ \Delta\mathbf{P}_4 &= (0, 4(1 + r)^2, 0) d,\end{aligned}$$

to the homogeneous coordinates $\mathbf{P}_0, \dots, \mathbf{P}_4$ given above. These line and point representations for the offset curve are illustrated in Fig. 20.4.

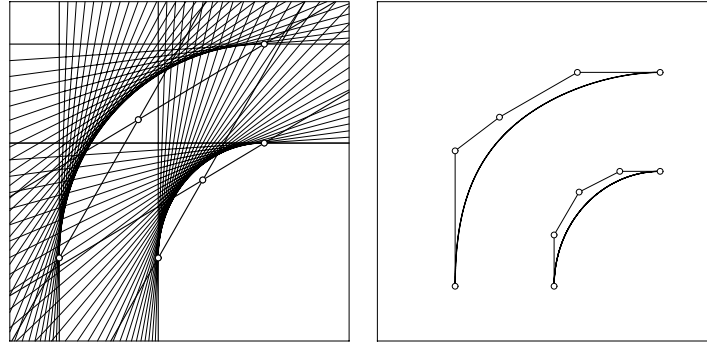


Fig. 20.4. The line and point representations of the offset to a rational PH curve.

In Fig. 20.5 we illustrate the dual de Casteljau algorithm applied to the curve in Example 20.2, for the parameter value $t = \frac{1}{2}$. As with the point form, the de Casteljau algorithm not only evaluates the tangent (and point) for the specified t value, but also subdivides the curve at that value, giving systems of control lines that define the segments $[0, t]$ and $[t, 1]$ mapped to $[0, 1]$.

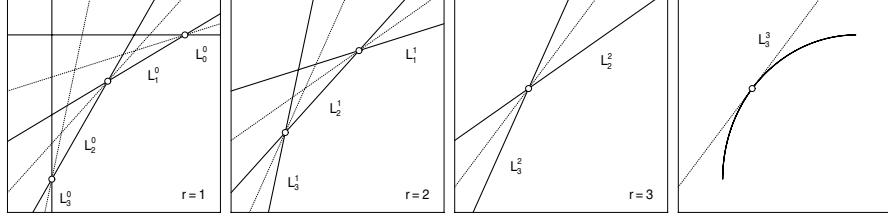


Fig. 20.5. Dual de Casteljau algorithm (20.14) applied to the curve in Example 20.2 with $t = \frac{1}{2}$. For each r , the lines \mathbf{L}_i^r are weighted averages of the lines \mathbf{L}_{i-1}^{r-1} , \mathbf{L}_i^{r-1} and pass through their intersection point. The final line \mathbf{L}_3^3 is the curve tangent for parameter value t , and the corresponding curve point is the intersection of \mathbf{L}_2^2 , \mathbf{L}_3^2 .

20.3 Relation to Polynomial PH Curves

Clearly, the polynomial PH curves must be subsumed as a proper subset of the rational PH curves defined by (20.9) — they correspond to special forms of the polynomials $e(t)$ and $f(t)$, which may be identified as follows.

Proposition 20.1 *The homogeneous coordinates (20.9) define a polynomial PH curve if and only if $e(t)$ and $f(t)$ are of the form*

$$e = \text{constant}, \quad f = 2ab \int (a^2 - b^2) k \, dt - (a^2 - b^2) \int 2ab k \, dt \quad (20.16)$$

for an arbitrary polynomial $k(t)$.

Proof : Suppose first that $e(t)$ and $f(t)$ have the form (20.16) where, without loss of generality, we may take $e = -1$. Substituting into (20.9) and cancelling common factors, the rational functions $X(t)/W(t)$ and $Y(t)/W(t)$ then reduce to the *polynomials*

$$x(t) = \int (a^2 - b^2) k \, dt, \quad y(t) = - \int 2ab k \, dt$$

which evidently describe a polynomial PH curve.

Conversely, suppose that expressions (20.9) define a *polynomial* PH curve. Then $W(t)$ must divide into $X(t)$ and $Y(t)$, i.e., $X(t) = W(t)x(t)$ and $Y(t) = W(t)y(t)$ for certain polynomials $x(t)$ and $y(t)$. Since equation (20.2) must be satisfied by each curve point $(x(t), y(t))$, and $g = -e(a^2 + b^2)$, we must have $e = \text{constant}$. Again, we take $e = -1$, and expressions (20.9) then reduce to

$$\begin{aligned} W &= (a^2 + b^2)(a'b - ab'), \\ X &= (aa' - bb')f - \frac{1}{2}(a^2 - b^2)f', \\ Y &= -(a'b + ab')f + abf'. \end{aligned} \quad (20.17)$$

Thus, if W divides X and Y , there exist polynomials $x(t)$ and $y(t)$ such that

$$\begin{aligned}(aa' - bb')f - \frac{1}{2}(a^2 - b^2)f' &= (a^2 + b^2)(a'b - ab')x, \\ -(a'b + ab')f + abf' &= (a^2 + b^2)(a'b - ab')y.\end{aligned}$$

Solving the above as simultaneous equations for f and f' gives

$$\begin{aligned}f &= 2abx + (a^2 - b^2)y, \\ f' &= 2(a'b + ab')x + 2(aa' - bb')y,\end{aligned}\tag{20.18}$$

and these expressions are consistent if and only if x and y satisfy the relation

$$2abx' + (a^2 - b^2)y' = 0.$$

The most general solution of this equation is

$$x = \int (a^2 - b^2)k \, dt \quad \text{and} \quad y = - \int 2abk \, dt,\tag{20.19}$$

where $k(t)$ is an arbitrary polynomial. Substituting the above into the first of the expressions (20.18), we obtain the form (20.16) for f . Thus, when (20.9) reduces to a *polynomial* PH curve, e and f must be of the form (20.16). ■

The dual form of polynomial PH curves can be deduced by substituting from (20.16) into (20.8), to obtain

$$K : L : M = (a^2 - b^2) \int 2abk \, dt - 2ab \int (a^2 - b^2)k \, dt : 2ab : a^2 - b^2.$$

Comparing with the homogeneous point representation

$$W : X : Y = 1 : \int (a^2 - b^2)k \, dt : - \int 2abk \, dt,$$

we see that the dual form is not advantageous for polynomial PH curves.

Polynomial PH curves of degree n generally have offsets of degree $2n - 1$. As noted above, however, the offsets at distance d to the rational PH curve defined by (20.6) are obtained by simply replacing $f(t)$ by $f(t) + g(t)d$, and hence they are generally the *same* degree as the original curve. This difference between polynomial and rational PH curves can be understood in terms of their cusps and behavior at infinity [180]. For a detailed comparison of the properties of polynomial and rational PH curves, and a reconciliation of their different formulations, see [180].

20.4 Rational Arc Length Functions

The parametric speed $\sigma(t) = \sqrt{x'^2(t) + y'^2(t)}$ of a rational PH curve must be a rational function of the curve parameter, to ensure that the unit normal $\mathbf{n}(t)$ is rational. In general, however, the indefinite integral of $\sigma(t)$ does not yield

a rational arc length function $s(t)$. In order for a rational function to possess a rational integral, the residues at its poles must vanish when it is expanded by partial fractions (see §3.5), because they incur transcendental terms in the integral. In general, integration of rational functions is a cumbersome process (compared to the ease with which $s(t)$ is obtained for polynomial PH curves) that requires factorization of the denominator polynomials.

Nevertheless, Pottmann [369] identified a special subset of the rational PH curves specified by (20.6) whose arc length functions are rational, and showed that these curves and their arc length functions can be determined by means of elegant geometrical arguments, without explicit integration. Moreover, these rational arc length curves play a key role in the theory of rational PH curves. The characterization given by Pottmann may be summarized as follows.

Theorem 20.1 *The rational curves $\mathbf{r}(t) = (x(t), y(t))$ that have rational arc length functions $s(t)$ are generated by relatively prime polynomials $a(t)$, $b(t)$ and a rational function $h(t)$ through the expressions*

$$x = \frac{b^2 - a^2}{a^2 + b^2} H - \frac{ab}{a'b - ab'} H', \quad y = \frac{2ab}{a^2 + b^2} H - \frac{a^2 - b^2}{2(a'b - ab')} H',$$

where the rational function $H(t)$ is defined by

$$H = \frac{a^2 + b^2}{2(a'b - ab')} h',$$

and their arc lengths $s(t)$ are given in terms of $a(t)$, $b(t)$, $h(t)$ by

$$s = h + \frac{a^2 + b^2}{2(a'b - ab)} H' + \text{constant}.$$

The rational arc length curves are the evolutes of rational curves with rational offsets — conversely, the rational curves with rational offsets are the involutes of rational arc length curves.

Proof : The proof is based on special properties of the *curve of constant slope* defined by “lifting” the curve $\mathbf{r}(t) = (x(t), y(t))$ from \mathbb{R}^2 to \mathbb{R}^3 , the arc length function $s(t)$ taken as the z coordinate. See [369] for complete details. ■

The identification of rational PH curves as the involutes of rational curves with rational arc lengths was independently deduced by Fiorot and Gensane [202] in the context of a classical geometrical optics problem, described below.

20.5 Geometrical Optics Interpretation

As observed in Chap. 18, the simplest PH curve — *Tschirnhausen’s cubic* — was first investigated in the context of a geometrical optics problem. However, the connection with optics is not peculiar to this specific curve. In fact, Fiorot

and Gensane [202] discovered a remarkable coincidence between curves known as *caustics* and *anticaustics* in classical geometrical optics, and the families³ of rational PH curves and rational curves with rational arc length functions. In order to elucidate this connection, we need to briefly review some concepts and terminology concerning the geometry of systems of reflected or refracted light rays — see [159] for a more comprehensive discussion.

Light propagation may be described in terms of conjugate families of *rays* and *wavefronts*. In a homogeneous medium, rays propagate as straight lines, namely, the normals to the curved wavefronts, which propagate as offsets in accordance with *Huygens' Principle*. When a system of rays is reflected by a mirror, the incident and reflected rays lie in a common plane with the normal vector to the mirror, being equally inclined to it, and the reflected wavefronts change shape so as to remain orthogonal to the reflected rays.

Consider a family of parallel rays incident upon a mirror, whose shape is specified by a plane⁴ rational curve $\mathbf{m}(t) = (m_x(t), m_y(t))$. Prior to reflection, the wavefronts will be parallel planes orthogonal to the rays. After reflection, the family of rays has an envelope along which the rays appear to concentrate, known as the *caustic* curve (see Figs. 18.2 and 18.3). The rays are tangents to the caustic, and normals to the reflected wavefronts. Hence, the caustic is the *evolute* — or locus of centers of curvature — of the reflected wavefronts, since the evolute of any curve can be equivalently interpreted as the envelope of its normal lines, and all offset curves share the same normal lines (see §8.3). Conversely, the reflected wavefronts can be viewed as *involutes* of the caustic, or “anticaustics” since the caustic is their evolute. Here we use a rather liberal connotation for the term *anticaustic*, to denote any of the reflected wavefronts: in geometrical optics, it is often used in the singular to identify an “archetypal” or “distinguished” wavefront, corresponding to *zero optical path length*. In the context of geometrical optics, the main results of Fiorot and Gensane [202] concerning rational PH curves may be summarized as follows.

Theorem 20.2 *Rational PH curves in \mathbb{R}^2 are the caustics and corresponding anticaustics for the reflection of parallel incident light rays by rational plane curves. Furthermore, the caustics constitute the set of rational curves with rational arc length functions.*

We refer the reader to [202] for complete details of the proof of this theorem, and describe below some of the main ideas using a different derivation.

Consider a mirror specified by a rational plane curve $\mathbf{m}(t) = (m_x(t), m_y(t))$ and a family of rays, parallel to the x -axis, incident on it. For a ray striking the mirror at the point $\mathbf{m}(t)$, where the normal has slope $\tan \theta = -m'_x/m'_y$, the reflected ray must have slope $\tan 2\theta = 2m'_x m'_y / (m'^2_x - m'^2_y)$, because the

³ Of course, these results also apply *a fortiori* to the polynomial PH curves, which are a proper subset of the rational PH curves.

⁴ Since we are considering a configuration in \mathbb{R}^3 that is rotationally symmetric, we can confine our attention to a plane containing the axis of symmetry.

incident and reflected rays make equal angles with the normal. Hence, the reflected ray is inclined in the direction of the rational unit vector

$$\mathbf{v}(t) = \frac{(m_x'^2(t) - m_y'^2(t), 2m_x'(t)m_y'(t))}{m_x'^2(t) + m_y'^2(t)}, \quad (20.20)$$

and we may parameterize the family of reflected rays as

$$\mathbf{r}(\xi, t) = (x(\xi, t), y(\xi, t)) = \mathbf{m}(t) + \xi \mathbf{v}(t),$$

where each t identifies a specific reflected ray, and ξ defines position along it. The caustic is the envelope of the reflected rays, and the condition (see §8.2.3) identifying the point ξ that each ray t contributes to this envelope is

$$\frac{\partial x}{\partial \xi} \frac{\partial y}{\partial t} - \frac{\partial y}{\partial \xi} \frac{\partial x}{\partial t} = 0.$$

This equation is linear in ξ , with the solution

$$\xi = \frac{[m_x'^2(t) + m_y'^2(t)] m_y'(t)}{2(m_x'(t)m_y''(t) - m_y'(t)m_x''(t))}. \quad (20.21)$$

Hence, the caustic has the parameterization

$$\mathbf{c}(t) = \mathbf{m}(t) + \frac{[m_x'^2(t) + m_y'^2(t)] m_y'(t)}{2(m_x'(t)m_y''(t) - m_y'(t)m_x''(t))} \mathbf{v}(t). \quad (20.22)$$

From (20.22) one can easily verify that the caustic $\mathbf{c}(t) = (c_x(t), c_y(t))$ has a hodograph of the form

$$\mathbf{c}'(t) = h(t) [m_x'^2(t) + m_y'^2(t)] \mathbf{v}(t), \quad (20.23)$$

where the rational function $h(t)$ is defined by

$$h = \frac{3m_y''(m_x'm_y'' - m_y'm_x'') - m_y'(m_x'm_y''' - m_y'm_x''')}{2(m_x'm_y'' - m_y'm_x'')^2}, \quad (20.24)$$

and hence it satisfies the Pythagorean condition

$$c_x'^2(t) + c_y'^2(t) = \sigma^2(t)$$

with the rational parametric speed

$$\sigma(t) = h(t) [m_x'^2(t) + m_y'^2(t)]. \quad (20.25)$$

Thus, for any rational mirror $\mathbf{m}(t) = (m_x(t), m_y(t))$ the caustic for reflection of parallel incident rays is clearly a rational PH curve. Moreover, from (20.24) and (20.25), the parametric speed can be written as

$$\sigma = h(m_x'^2 + m_y'^2) = \frac{d}{dt} \left[m_x + \frac{(m_x'^2 + m_y'^2)m_y'}{2(m_x'm_y'' - m_y'm_x'')} \right],$$

and hence the arc length of the caustic is given by the *rational* function

$$s(t) = \int \sigma(t) dt = m_x(t) + \frac{[m_x'^2(t) + m_y'^2(t)] m_y'(t)}{2[m_x'(t)m_y''(t) - m_y'(t)m_x''(t)]} + c, \quad (20.26)$$

where c is an integration constant. Hence, the caustic $\mathbf{c}(t)$ also has a *rational arc length function*. If $\sigma_m = ds_m/dt$ and $\kappa_m = (m_x'm_y'' - m_y'm_x'')/\sigma_m^3$ denote the parametric speed and curvature of the mirror, where s_m is the mirror arc length measured from some fixed point, we may cast the expression for the arc length of the caustic in a more geometrical form as

$$s(t) = m_x(t) + \frac{\sin \theta_m(t)}{2\kappa_m(t)} + c,$$

$\sin \theta_m = dm_y/ds_m$ being the sine of the mirror tangent angle θ_m .

The involutes to the caustic, which represent the reflected wavefronts, may be written (see §8.3.2) in the form

$$\mathbf{i}_c(t) = \mathbf{c}(t) - s(t) \frac{\mathbf{c}'(t)}{|\mathbf{c}'(t)|}, \quad (20.27)$$

where different integration constants c in (20.26) identify different involutes (different optical path lengths), and these involutes are all offsets of each other. Substituting from (20.22), (20.23), and (20.26) this simplifies to

$$\mathbf{i}_c(t) = \mathbf{m}(t) + (c - m_x(t)) \mathbf{v}(t).$$

Clearly, this defines a rational curve with *rational offsets*.

The simplest case corresponds to reflection by the parabola $\mathbf{m}(t) = (t, kt^2)$. In this instance, the direction of the reflected rays is given by the unit vector $\mathbf{v}(t) = (1 - 4k^2t^2, 4kt)/(1 + 4k^2t^2)$, and the parameter value (20.21) reduces to $\xi = \frac{1}{2}t(1 + 4k^2t^2)$. The rational parameterization (20.22) of the caustic is then $\mathbf{c}(t) = (\frac{3}{2}t - 2k^2t^3, 3kt^2)$ and under a suitable change of coordinates, this can be recognized as an instance of Tschirnhausen's cubic (18.8). The arc length (20.26) of the caustic is $s(t) = 2k^2t^3 + \frac{3}{2}t + c$, and hence its involutes (i.e., the reflected wavefronts) are the rational quartic curves defined by

$$\mathbf{i}_c(t) = \frac{(8k^2t^3, 4k^3t^4 - 3kt^2)}{1 + 4k^2t^2} + c \frac{(1 - 4k^2t^2, 4kt)}{1 + 4k^2t^2}.$$

Pottmann [369] calls these curves *Tschirnhausen quartics* — they are obtained by choosing linear polynomials in (20.9), and have one essential shape freedom. See [12] for an approximation scheme based on segments of these curves.

The above analysis holds for incident rays orthogonal to the parabola axis. For incident rays parallel to the axis, the caustic degenerates to just the single point $(1/4k, 0)$ — the *focus* of the parabola — in accordance with the familiar principle that parabolic telescope mirrors yield ideal on-axis star images.

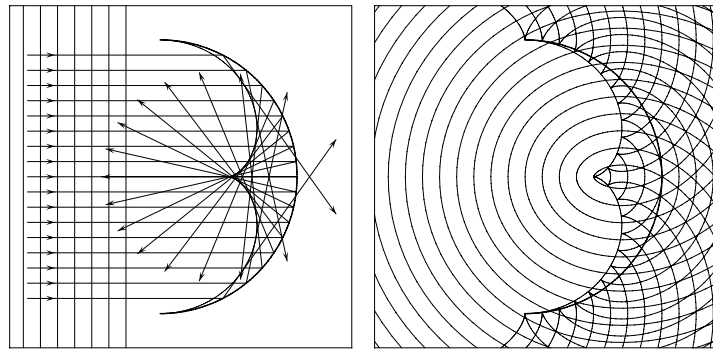


Fig. 20.6. Left: parallel rays (corresponding to planar wavefronts) incident upon a circular mirror, showing the caustic as the envelope of the reflected rays. Right: the corresponding reflected wavefronts — the involutes of the caustic — are rational PH curves of degree 6, with the reflected rays as their common normal lines. Note that the cusps of the involutes lie on their common evolute, i.e., the caustic (see §8.3.2).

Example 20.3 As a more challenging example, we consider a circular mirror (see Fig. 20.6) with the rational parameterization

$$\mathbf{m}(t) = (m_x(t), m_y(t)) = \left(\frac{1-t^2}{1+t^2}, \frac{2t}{1+t^2} \right).$$

The unit vector (20.20) defining the direction of the reflected rays is

$$\mathbf{v}(t) = \frac{(-t^4 + 6t^2 - 1, 4t^3 - 4t)}{(1+t^2)^2}$$

and the parameter value specifying the positions along the rays that identify points of the caustic becomes

$$\xi = \frac{1-t^2}{2(1+t^2)}.$$

Hence, the caustic (20.22) is the degree-6 rational curve defined by

$$\mathbf{c}(t) = \frac{(-t^6 - 9t^4 + 9t^2 + 1, 16t^3)}{2(1+t^2)^3}.$$

From (20.26) we obtain the arc length function for the caustic as

$$s(t) = \frac{3(1-t^2)}{2(1+t^2)} + c,$$

and the involutes (20.27), defining the reflected wavefronts, are thus given by

$$\mathbf{i}_c(t) = \frac{(-2t^6 + 6t^4 - 6t^2 + 2, 6t^5 - 4t^3 + 6t)}{(1+t^2)^3} + c \frac{(-t^4 + 6t^2 - 1, 4t^3 - 4t)}{(1+t^2)^2}.$$

For all values of c , this defines a family of rational PH curves of degree 6 that are offsets of each other, as illustrated in Fig. 20.6.

20.6 Laguerre Geometry Formulation

Peternell and Pottmann [361, 371] describe an elegant interpretation for the construction of rational curves and surfaces with rational offsets, in terms of the methods of *Laguerre geometry*.⁵ The basic elements of Laguerre geometry are oriented lines and circles in \mathbb{R}^2 , and oriented planes and spheres in \mathbb{R}^3 — the orientation of each element is fixed by associating a field of normal vectors with it. Points are subsumed as circles or spheres of zero radius (and hence indeterminate orientation). Oriented circles and spheres — and, in general, oriented hyperspheres in \mathbb{R}^n — are collectively called *cycles*.

Let \mathcal{L} and \mathcal{C} be the sets of oriented hyperplanes and hyperspheres in \mathbb{R}^n . Members of these sets are in *oriented contact* if they are tangent to each other, and have normals of the same sense at their point of tangency (point members of \mathcal{C} are considered to be in oriented contact with any member of \mathcal{L} on which they lie). Laguerre geometry is concerned with configurations invariant under *Laguerre transformations*, i.e., one-to-one mappings of the sets \mathcal{L} and \mathcal{C} onto themselves, that preserve oriented contact between their members.

The Laguerre transformation known as *dilatation* is intimately related to offset curves and surfaces. Dilatation by distance d shifts oriented hyperplanes by an amount d in the direction of their normals, and it increases the radius of oriented hypercycles by d . Here, hypercycles are considered to have negative or positive radii according to whether their normals point inward or outward. Hence, dilatation does not preserve points, or the orientation of hypercycles, but oriented contact of hyperplanes and hypercycles is preserved (Fig. 20.7). Regarding a hypersurface as the envelope of its oriented tangent hyperplanes, dilatation maps the surface to its (one-sided) offset at distance d .

The *cyclographic map* associates oriented hypercycles in \mathbb{R}^n with points in \mathbb{R}^{n+1} , and oriented hyperplanes in \mathbb{R}^n with hyperplanes in \mathbb{R}^{n+1} that make

⁵ The French mathematician Edmond Laguerre (1834–1886) made contributions to analysis and geometry, despite serious health problems. He is also known for the orthogonal *Laguerre polynomials*, used in approximation theory.

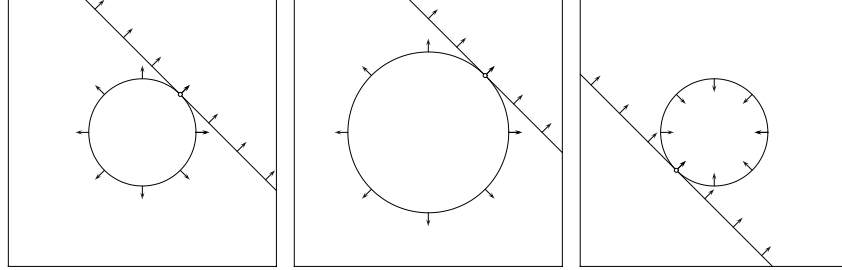


Fig. 20.7. The oriented contact between a line and a circle of radius $r > 0$ (left) is preserved under dilatation by any amount d , e.g., $d > 0$ (center) and $d < -r$ (right).

the angle $\gamma = \frac{1}{4}\pi$ with the particular hyperplane \mathbb{R}^n — such hyperplanes are called γ -planes in \mathbb{R}^{n+1} . When $n = 2$, for example, an oriented circle in \mathbb{R}^2 with center (x, y) and radius r — which may be negative, zero, or positive — is associated with the point $(x, y, r) \in \mathbb{R}^3$, and an oriented line in \mathbb{R}^2 defined by an equation $\lambda x + \mu y + \nu = 0$ and unit vector $\mathbf{n} = (\lambda, \mu)$ is associated with the γ -plane $\lambda x + \mu y + r + \nu = 0$ inclined at angle $\frac{1}{4}\pi$ to the (x, y) -plane in the space \mathbb{R}^3 with coordinates (x, y, r) . In the latter space, we use the *Minkowski* (or *pseudo-Euclidean*) norm for a vector $\mathbf{v} = (v_x, v_y, v_r)$ defined by

$$\|\mathbf{v}\| = \sqrt{v_x^2 + v_y^2 - v_r^2}.$$

According to whether $\|\mathbf{v}\|$ is real, zero, or imaginary, we say \mathbf{v} is a *space-like*, *light-like*, or *time-like* vector. To emphasize the different status of r , the space with coordinates (x, y, r) governed by this metric may be denoted⁶ $\mathbb{R}^{2,1}$.

Corresponding to each locus $\mathbf{p}(t) = (x(t), y(t), r(t))$ in $\mathbb{R}^{2,1}$ there is a one-parameter family of oriented circles in \mathbb{R}^2 . The envelope of this family of circles is known as the *cyclographic image* of the locus $\mathbf{p}(t)$. Peternell and Pottmann [361, 371] define a γ -curve in $\mathbb{R}^{2,1}$ by the property that its tangent lines define a rational γ -developable, i.e., a developable ruled surface that corresponds to the envelope of a one-parameter family of γ -planes. The significance of such curves is summarized in the following results [361, 371]:

Theorem 20.3 All rational PH curves in \mathbb{R}^2 are the cyclographic images of rational γ -curves $\gamma(t) = (x(t), y(t), r(t))$ in $\mathbb{R}^{2,1}$. Furthermore, the orthogonal projections $\mathbf{r}(t) = (x(t), y(t))$ of such curves onto \mathbb{R}^2 are rational plane curves with rational arc length functions $s(t)$.

Peternell and Pottmann use the cyclographic map to give another proof of the results (see Theorem 20.2) of Fiorot and Gensane [202], concerning the interpretation of rational PH curves as anticaustics for reflection of parallel

⁶ See also Chap. 24, which deals with very closely-related ideas, except that no consideration is given there to the *orientations* of cycles and planes.

rays by rational curves, with the caustics having rational arc lengths, and they give a generalization of these results to rational surfaces with rational offsets.

Besides its importance in elucidating the basic theory of rational curves and surfaces with rational offsets [361], the cyclographic map is useful [371] in developing deeper insight into many other contexts, such as *geometrical optics* problems based on Huygens' Principle (see §20.5); the *medial axis transforms* of planar domains (see §24.2); the rational parameterization of *canal surfaces* [360]; and the construction of *blend surfaces* using Dupin cyclides [50,372] — these topics lie beyond our present scope, however, and we refer the reader to the papers of Peternell and Pottmann [361,371] for complete details.

20.7 Improper Rational Parameterizations

The constructions of polynomial and rational PH curves described above yield curves with *proper* parameterizations — i.e., the parameter values t and curve points $\mathbf{r}(t)$ are in one-to-one correspondence for all⁷ real t . Furthermore, these proper parameterizations of PH curves induce proper parameterizations of the (one-sided) rational offset curves. Given a properly-parameterized curve, it is always possible to impose an improper parameterization by invoking a non-linear parameter transformation that compromises the unique correspondence between parameter values and curve points. The more-subtle task of detecting when a given parameterization is improper was first discussed, in the context of computer-aided design, by Sederberg [398]. It involves determining whether a given polynomial $p(t)$ is *composite*, i.e., it can be written in the form $f(g(t))$, where f and g are polynomials such that $\deg(p) = \deg(f) \cdot \deg(g)$.

W. Lü recognized [311,312] that possession of a Pythagorean hodograph is a sufficient, but not necessary condition, for a curve to admit rational offsets. He showed that the two-sided offsets to certain curves, whose hodographs are not nominally Pythagorean, can be rationally parameterized *if* an improper parameterization (a double tracing) is first imposed on them. The archetype of these (non-PH) “offset-rational” curves is, surprisingly, the *parabola*.

Example 20.4 A properly-parameterized quadratic curve $\mathbf{r}(t) = (x(t), y(t))$ is a parabola, which may be cast in the standard form

$$x(t) = t, \quad y(t) = kt^2 \quad (20.28)$$

by means of a rigid motion, uniform scaling, and linear re-parameterization. The (one-sided) offset at distance d to the parabola is the locus

$$\mathbf{r}_d(t) = \mathbf{r}(t) + d\mathbf{n}(t), \quad \text{where } \mathbf{n}(t) = \frac{(2kt, -1)}{\sqrt{1+4k^2t^2}}. \quad (20.29)$$

⁷ Except, possibly, for parameter values that identify self-intersections of $\mathbf{r}(t)$.

Because of the radical in the unit normal $\mathbf{n}(t)$, the representation (20.29) is not rational. To construct a rational parameterization of this locus, Lü introduces the rational parameter transformation $t \rightarrow s$ in (20.28) defined by

$$t(\xi) = \frac{\xi^2 - 16k^2}{16k^2\xi}. \quad (20.30)$$

The substitutions $x(t(\xi))$ and $y(t(\xi))$ yield a rational quartic parameterization $\mathbf{r}(\xi)$ of the parabola, defined by the homogeneous coordinate polynomials

$$W(\xi) = 256k^4\xi^2, \quad X(\xi) = 16k^2\xi^3 - 256k^4\xi, \quad Y(\xi) = k\xi^4 - 32k^3\xi^2 + 256k^5.$$

This parameterization is *improper*. There are two distinct parameter values, $\xi = 4k(2kt \pm \sqrt{4k^2t^2 + 1})$, corresponding to each point of the parabola. Note that, under the map (20.30), we have

$$\left. \begin{array}{l} \xi \in (-\infty, 0) \\ \xi \in (0, +\infty) \end{array} \right\} \rightarrow t \in (-\infty, +\infty),$$

so $\mathbf{r}(\xi)$ becomes *doubly traced* for $\xi \in (-\infty, +\infty)$ — it is traversed in *opposite senses* as ξ increases from $-\infty$ to 0 and from 0 to $+\infty$. With this improper parametrization, we have $x'^2(\xi) + y'^2(\xi) = \sigma^2(\xi)$, where

$$x'(\xi) = \frac{\xi^2 + 16k^2}{16k^2\xi^2}, \quad y'(\xi) = \frac{\xi^4 - 256k^4}{128k^3\xi^3}, \quad \sigma(\xi) = \frac{(\xi^2 + 16k^2)^2}{128k^3\xi^3},$$

and hence the unit normal

$$\mathbf{n}(\xi) = \frac{(\xi^2 - 16k^2, -8k\xi)}{\xi^2 + 16k^2}$$

depends *rationally* on ξ , and the offset

$$\mathbf{r}_d(\xi) = \mathbf{r}(\xi) + d\mathbf{n}(\xi)$$

is a rational curve. Its homogeneous coordinates are given explicitly by

$$\begin{aligned} W_d(\xi) &= 256k^3(\xi^2 + 16k^2)\xi^2, \\ X_d(\xi) &= 16k[\xi^4 + 16k^2d\xi^3 - 256k^4d\xi - 256k^4]\xi, \\ Y_d(\xi) &= \xi^6 - 16k^2\xi^4 - 2048k^4d\xi^3 - 256k^4\xi^2 + 4096k^6. \end{aligned} \quad (20.31)$$

Note that the offset $\mathbf{r}_d(\xi)$ is *not* doubly-traced — $\mathbf{n}(\xi)$ defines the “inward” or “outward” normal according to whether $\xi < 0$ or $\xi > 0$, so for $-\infty < \xi < +\infty$ equations (20.31) define a parameterization of the entire *two-sided* offset, at distance $\pm d$, to the parabola.

Pottmann [370] has noted that, in an appropriate coordinate system, the parabola (20.28) with $k = 1$ is compatible with the dual representation (20.8) for rational PH curves, through the choices

$$a(t) = t, \quad b(t) = 1, \quad e(t) = 2t, \quad f(t) = -(1+t^2)^2.$$

Again, this defines a double tracing — corresponding to each tangent line of the parabola there are two distinct t values, and this double-tracing yields a rational parameterization of the two-sided offset curve.

The two-sided offset to the parabola $\mathbf{r}(t) = (t, kt^2)$ forms an irreducible algebraic curve of degree 6, with the homogeneous implicit equation

$$\begin{aligned} F(W, X, Y) = & 16k^4 X^4 (X^2 + Y^2) - 8k^3 (5X^2 + 4Y^2) WX^2 Y \\ & - k^2 W^2 [(48k^2 d^2 - 1) X^4 + 32(k^2 d^2 - 1) X^2 Y^2 - 16 Y^4] \\ & + kW^3 [2(4k^2 d^2 - 1) X^2 - 8(4k^2 d^2 + 1) Y^2] Y \\ & + W^4 [4k^2 d^2 (12k^2 d^2 - 5) X^2 + (4k^2 d^2 - 1)^2 Y^2] \\ & + 8kd^2 W^5 (4k^2 d^2 + 1) Y - d^2 W^6 (4k^2 d^2 + 1)^2 = 0. \end{aligned}$$

In order to be rational, this curve must possess (see §9.2.5) the equivalent of 10 double points. They be accounted for as follows [190]. The offset has six affine cusps, of which at most two are real, defined by the curvature condition $\kappa(t) = -1/d$, and one affine node — a crunode (with distinct real tangents) or acnode (with complex conjugate tangents) according to whether d is larger or smaller than $1/2k$ (exceptionally, when $d = 1/2k$, two of the cusps coalesce with the node to produce an affine triple point). The remaining three double points are contributed by a non-ordinary double point at infinity, with double points in its first and second neighborhoods (see §9.2.5).

The parabola is the simplest example of a class of polynomial curves that, after a suitable (improper) rational parameter transformation, admit rational parameterization of their (two-sided) offsets. Lü [312] has provided a complete characterization⁸ of such “offset rational” polynomial curves, in terms of the complex representation (see Chap. 19), as follows.

Theorem 20.4 *The parametric speed of a properly parameterized polynomial curve specified in the complex form $\mathbf{r}(t) = x(t) + i y(t)$ can be transformed by a rational parameter transformation $t \rightarrow \xi$ into a rational function $\sigma(\xi)$ if and only if its hodograph can be written as*

$$\mathbf{r}'(t) = (\mathbf{k}t + 1) \mathbf{w}^2(t) p(t), \quad (20.32)$$

where \mathbf{k} is a complex constant, $\mathbf{w}(t) = u(t) + i v(t)$ is a complex polynomial with $\gcd(u(t), v(t)) = \text{constant}$, and $p(t)$ is a real polynomial.

Proof : See [312] — where it is also shown that, for curves with hodographs of the form (20.32), the parameter transformation $t \rightarrow \xi$ required to achieve a rational dependence of the speed σ on the new parameter ξ is defined by at most a quadratic rational function $t(\xi)$. ■

⁸ The same characterization was derived (without reference to Lü’s results) almost ten years later by Ahn and Kim [10] — this paper was subsequently retracted.

By writing $\mathbf{k} = \alpha + i\beta$, the components of the hodograph (20.32) can be expressed as the real polynomials

$$\begin{aligned} x'(t) &= [(\alpha t + 1)(u^2(t) - v^2(t)) - 2\beta t u(t)v(t)] p(t), \\ y'(t) &= [\beta t(u^2(t) - v^2(t)) + 2(\alpha t + 1)u(t)v(t)] p(t). \end{aligned}$$

Clearly, (20.32) subsumes the polynomial PH curves as the special case $\mathbf{k} = 0$. The simplest examples with $\mathbf{k} \neq 0$ are those for which $\mathbf{w}(t) = 1$ and $p(t)$ is a constant or linear polynomial: they define the parabola and the cuspidal cubic

$$x(t) = t^2, \quad y(t) = kt^3. \quad (20.33)$$

Both curves admit rational re-parameterizations that define double tracings: once in the “forward” direction, and once in “reverse.” With these improper parameterizations, the *two-sided offset curve* at distance $\pm d$ admits a rational parameterization (of degree 6 for the parabola and 8 for the cuspidal cubic). A class of offset-rational quartics defined by assuming $\mathbf{w}(t) = 1$ and a quadratic polynomial for $p(t)$ is described by Lü [312], having shape freedoms similar to those of the “ordinary” cubics and PH quintics — they may exhibit inflections, and are capable of interpolating first-order Hermite data. Note that, when the polynomial $p(t)$ is non-constant, its real roots incur cusps on $\mathbf{r}(t)$, although the curve parameter domain may be chosen so as to exclude them.

Remark 20.2 Recall from §16.4 that a polynomial curve $\mathbf{r}(t) = (x(t), y(t))$ is *algebraically rectifiable* if polynomials $f(t), g(t)$ exist such that

$$x'^2(t) + y'^2(t) = f(t)[3f'(t)g(t) + 2f(t)g'(t)]^2.$$

As noted by Lü [312], such curves also have rational offsets if $\deg(f(t)) \leq 2$. Taking $f(t) = |\mathbf{k}t + 1|^2$, the condition for algebraic rectifiability of the curve defined by (20.32) is that

$$[u^2(t) + v^2(t)]p(t) = 3f'(t)g(t) + 2f(t)g'(t)$$

must hold for some polynomial $g(t)$. The cuspidal cubic (20.33), for example, satisfies this condition with $u^2(t) + v^2(t) = 1$, $p(t) = 2t$, $f(t) = 1 + 9k^2t^2/4$, and $g(t) = 4/27k^2$, but the parabola does not.

A characterization of properly parameterized *rational* curves that permit a rational parameterization of their offsets, after imposing a suitable rational transformation of the parameter, is also given by Lü in [312].

20.8 Rational Surfaces with Rational Offsets

A key advantage of the dual approach introduced by Pottmann [369] is that it allows a simple and natural extension to constructions of rational *surfaces*

with rational offsets — a problem that seems intractable from the perspective of the usual point representation. In the dual approach, a surface is specified as the envelope of its two-parameter family of tangent planes

$$K(u, v)W + L(u, v)X + M(u, v)Y + N(u, v)Z = 0,$$

where the bivariate polynomials K, L, M, N define the *homogeneous plane coordinates* of a rational surface. By methods directly analogous to those used in the case of plane curves, Pottmann derives a characterization for rational surfaces with rational offsets as follows.

Theorem 20.5 *The homogeneous plane coordinates of all (non-developable) rational surfaces $\mathbf{r}(u, v)$ that have rational offsets $\mathbf{r}_d(u, v) = \mathbf{r}(u, v) + d\mathbf{n}(u, v)$, where $\mathbf{n}(u, v)$ is the unit surface normal, can be expressed in terms of three polynomials $a(u, v), b(u, v), c(u, v)$ with $\gcd(a, b, c) = \text{constant}$ and a rational function $h(u, v)$ in the form*

$$K : L : M : N = -(a^2 + b^2 + c^2)h : 2ac : 2bc : a^2 + b^2 - c^2. \quad (20.34)$$

Furthermore, the offset surface at distance d from $\mathbf{r}(u, v)$ is obtained by simply replacing $h(t)$ with $h(t) + d$ in the above expressions.

For the proof of this result, and an equivalent (but far more cumbersome) representation in homogeneous point coordinates, we refer the reader to [369]. The rational Bézier forms of rectangular (i.e., tensor-product) and triangular surface patches with rational offsets may be derived from (20.34). Note that the offset surfaces are of the same *class* (i.e., degree of the homogeneous plane representation) as the base surface, since they are obtained by simply adding the constant offset distance d to the rational function $h(t)$.

As noted by Pottmann [369], another advantageous property of the rational surfaces with rational offsets concerns their *isophotes*. For a specified direction of illumination \mathbf{l} , these are the loci on the surface $\mathbf{r}(u, v)$ along which the unit normal $\mathbf{n}(u, v)$ maintains a constant angle with respect to \mathbf{l} . The isophotes of rational-offset surfaces are *rational curves*, making them especially amenable to rendering by means of standard contouring algorithms.

The form (20.34) also applies to *developable* surfaces with rational offsets, with the simplification [369] that the polynomials a, b, c and rational function h now depend on only the single parameter u — assuming that the developable is parameterized in such a manner that its normal \mathbf{n} does not vary along the generators (rulings) with $u = \text{constant}$ and v varying.

Jüttler [265] and Jüttler and Sampoli [269] describe another approach to constructing (polynomial) surfaces that possess rational offsets. They consider triangular Bézier surface patches $\mathbf{r}(u, v, w)$ characterized by the property that a (non-unit) surface normal vector $\mathbf{N}(u, v, w)$ can be defined at each point as a linear combination

$$\mathbf{N}(u, v, w) = u\mathbf{n}_{(1,0,0)} + v\mathbf{n}_{(0,1,0)} + w\mathbf{n}_{(0,0,1)}$$

of given normals at the vertices of the triangular patch. This vector satisfies $\mathbf{N} \cdot \mathbf{r}_u = \mathbf{N} \cdot \mathbf{r}_v = \mathbf{N} \cdot \mathbf{r}_w = 0$ for all (u, v, w) — i.e., it is orthogonal to the surface tangent plane at each point. Such *LN surfaces* are shown, through a suitable re-parameterization, to possess rational offsets (this property may be regarded as a generalization to surfaces of the rational offsets to a parabola, discussed in §20.7). Methods for the construction of LN surfaces so as to match prescribed boundary data are developed in [265, 269] — see also [389].

Peternell and Pottmman [359, 361] use the methods of Laguerre geometry to systematically investigate families of “simple” surfaces with rational offsets. These include the envelopes of (real) rational one-parameter families of the “natural” quadric surfaces, i.e., spheres and cones/cylinders of revolution: such surfaces are generated by cutting tools commonly used in milling machines. Among the quadric surfaces, Lü [313] showed that ellipsoids, paraboloids, and hyperboloids always have rational offsets, and presented methods to compute their parameterizations. Cylinders/cones of revolution and parabolic cylinders also have rational offsets, but other cylinders/cones do not [313]. These results have been discussed from the perspective of Laguerre geometry in [361].

20.9 Minkowski Isoperimetric–hodograph Curves

The (two-sided) offset at distance $\pm d$ from a plane curve may be regarded as the boundary of the “convolution” — or *Minkowski sum* — of the curve with a circle of radius d . Ait Haddou et al. [13] have considered the generalization of this problem to the case where the circle is replaced by a convex, centrally-symmetric closed curve \mathcal{U} , called the *indicatrix*.

The indicatrix specifies a metric in the *Minkowski plane*⁹ as follows. If we consider \mathcal{U} to be defined in polar coordinates by a radius function $r(\theta)$, such that $r(\theta + \pi) = r(\theta)$, the Minkowski distance $m(\mathbf{p}_1, \mathbf{p}_2)$ between two points with Euclidean coordinates $\mathbf{p}_1 = (x_1, y_1)$ and $\mathbf{p}_2 = (x_2, y_2)$ is defined by

$$m(\mathbf{p}_1, \mathbf{p}_2) = \frac{|\mathbf{p}_2 - \mathbf{p}_1|}{r(\theta)}, \quad (20.35)$$

where $|\mathbf{p}_2 - \mathbf{p}_1| = \sqrt{(x_2 - x_1)^2 + (y_2 - y_1)^2}$ is the familiar Euclidean distance, and theta is the angle that the vector $\mathbf{p}_2 - \mathbf{p}_1$ makes with the x -axis. In other words, $m(\mathbf{p}_1, \mathbf{p}_2)$ is the Euclidean distance measured in terms of the radius vector of \mathcal{U} parallel to $\mathbf{p}_2 - \mathbf{p}_1$ as a unit of length (see Fig. 20.8). Thus, \mathcal{U} serves as an “anisotropic unit circle” in the Minkowski plane.

Ait Haddou et al. [13] discuss the differential geometry of curves defined in the Minkowski plane with the metric (20.35), including tangents, curvatures, evolutes, involutes, and offset curves. They also give conditions for a rational

⁹ This should not be confused with the “pseudo-Euclidean” Minkowski space used in §20.6 and Chap. 24 below. The latter space — denoted $\mathbb{R}^{n,1}$ — differs from \mathbb{R}^{n+1} only by the minus sign associated with one of the coordinates in the metric.

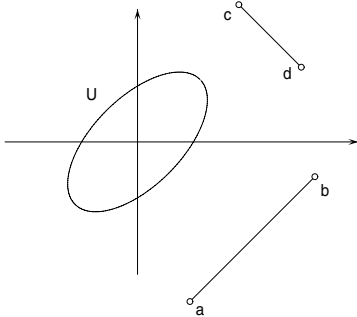


Fig. 20.8. Minkowski plane with the ellipse \mathcal{U} as indicatrix. The two line segments ab and cd are of equal length under the metric (20.35) associated with this indicatrix.

curve in the Minkowski plane (defined by a rational indicatrix) to have rational offsets under the Minkowski metric. Curves that satisfy these conditions are called *Minkowski isoperimetric-hodograph (IH) curves*. The definition of these curves is based on the dual (line) representation, similar to that used in the theory of Euclidean rational PH curves. Since we do not have room for a full account of these results, we refer the reader to [13] for the details.

21

Pythagorean Hodographs in \mathbb{R}^3

The extension of the Cartesian coordinate method to space of three dimensions was effected by the labors of Van Schooten, Parent, and Clairaut. Parent represented a surface by an equation involving the three coordinates of a point in space, and Clairaut perfected this new procedure in a most essential manner by a classic work upon curves of double curvature ... In a work of Pitot in 1724 (printed in 1726) upon the helix, we find for the first time the expression ligne à double courbure, line of double curvature, for a gauche curve.

Karl Fink, *A Brief History of Mathematics* [200]

Although the generalization of “ordinary” polynomial curves from \mathbb{R}^2 to \mathbb{R}^3 is a trivial matter, it is much more challenging to accomplish this generalization for PH curves. The problem lies in finding an appropriate characterization for polynomial solutions to the Pythagorean hodograph condition in \mathbb{R}^3 ,

$$x'^2(t) + y'^2(t) + z'^2(t) = \sigma^2(t). \quad (21.1)$$

Just as the complex–number model of Chap. 19 offers a concise and elegant description of solutions to the PH condition (17.1) in \mathbb{R}^2 , solutions to (21.1) can be succinctly expressed in terms of the algebra of *quaternions*. This model will be fully developed in Chap. 22 below. At present, we focus on some basic principles governing the construction and properties of spatial PH curves.

In §21.1 we give a thorough analysis of the spatial PH cubics, independent of any assumed characterization of the solutions to (21.1). The general form of solutions to (21.1) — in terms of four polynomials $u(t)$, $v(t)$, $p(t)$, $q(t)$ — is then described in §21.2. In §21.3 we discuss the structure of the Bézier control polygons of the spatial PH curves arising from these solutions, and in §21.4 we analyze some of their basic differential properties.

21.1 Geometry of Spatial PH Cubics

As in the planar case (Chap. 18), the simplest non-trivial spatial PH curves are cubics, and they admit characterization directly in terms of the geometry of their Bézier control polygons — without reference to the algebraic structure of the hodograph components. This is a consequence of the special intrinsic geometry of the spatial PH cubics: they are all *helical* curves.

Definition 21.1 A *helix* is a space curve whose curvature and torsion are in constant proportion, i.e., $\kappa(t) \equiv c\tau(t)$ with $c \neq 0$. The *pitch* angle of the helix is defined to be $\psi = \tan^{-1} c$.

We always take the pitch in the range $-\pi/2 \leq \psi \leq +\pi/2$. Geometrically, a helix can also be defined as a space curve whose tangent maintains the fixed angle ψ with respect to a given vector \mathbf{a} in \mathbb{R}^3 — the *axis* of the helix. The trivial case where $\kappa(t)$ and $\tau(t)$ maintain a constant proportion because they are individually (non-zero) constants defines the familiar *circular* helix, which has the property that its projection onto a plane perpendicular to the axis \mathbf{a} is a *circle*. The projection of a general helix is not an “elementary” curve.

Remark 21.1 The axis can be determined if the pitch angle ψ and the Frenet frame $(\mathbf{t}, \mathbf{p}, \mathbf{b})$ at any point are known. Suppose $\mathbf{a} = \lambda\mathbf{t} + \mu\mathbf{p} + \nu\mathbf{b}$ is a unit vector along the axis. Since $\mathbf{a} \cdot \mathbf{t} = \text{constant} (= \cos \theta$, say) differentiation with respect to t gives $\mathbf{a} \cdot \mathbf{t}' = \sigma\kappa \mathbf{a} \cdot \mathbf{p} = 0$ upon using the Frenet equations (8.73). Hence, we can infer that $\mu = 0$, since $\sigma \neq 0$ for a regular curve, and we assume $(\mathbf{t}, \mathbf{p}, \mathbf{b})$ are given at a “generic” point for which $\kappa \neq 0$. Now since $\lambda = \cos \theta$ and $|\mathbf{a}| = 1$, we can choose the sign of θ such that $\nu = \sin \theta$. Differentiating $\mathbf{a} = \cos \theta \mathbf{t} + \sin \theta \mathbf{b}$ and invoking equations (8.73) again, we then obtain

$$\mathbf{a}' = \sigma(\kappa \cos \theta - \tau \sin \theta) \mathbf{p} = \mathbf{0},$$

and hence $\kappa/\tau = \text{constant} = \tan \theta$. The fixed angle θ that \mathbf{t} makes with \mathbf{a} is thus the pitch angle $\psi = \tan^{-1}(\kappa/\tau)$, and the axis of the helix is given by

$$\mathbf{a} = \cos \psi \mathbf{t} + \sin \psi \mathbf{b}. \quad (21.2)$$

We now derive a characterization of the Pythagorean-hodograph property for all spatial cubics in terms of the geometry of their Bézier control polygons (which incorporates the planar PH cubics as a special case). For this purpose it will be convenient to use the control polygon legs $\mathbf{L}_k = \mathbf{p}_{k+1} - \mathbf{p}_k$, $k = 0, 1, 2$ — regarded as vectors emanating from a common origin.

Proposition 21.1 *A spatial cubic with Bézier control-polygon legs $\mathbf{L}_0, \mathbf{L}_1, \mathbf{L}_2$ has a Pythagorean hodograph if and only if \mathbf{L}_0 and \mathbf{L}_2 lie on a right-circular cone of some half-angle ϑ about \mathbf{L}_1 as axis, and their azimuthal separation φ on this cone is given in terms of the lengths L_0, L_1, L_2 by*

$$\cos \varphi = 1 - \frac{2L_1^2}{L_0 L_2}. \quad (21.3)$$

Proof : If the control polygon has the form specified in Proposition 21.1, we can adopt coordinate axes in which \mathbf{L}_1 points in the z direction and \mathbf{L}_0 is parallel to the z - x plane, so that

$$\begin{aligned}\mathbf{L}_0 &= L_0(\sin \vartheta, 0, \cos \vartheta), \quad \mathbf{L}_1 = L_1(0, 0, 1), \\ \mathbf{L}_2 &= L_2(\sin \vartheta \cos \varphi, \sin \vartheta \sin \varphi, \cos \vartheta).\end{aligned}\quad (21.4)$$

Now the hodograph of a cubic $\mathbf{r}(t)$ with control-polygon legs $\mathbf{L}_0, \mathbf{L}_1, \mathbf{L}_2$ is

$$\mathbf{r}'(t) = 3[\mathbf{L}_0(1-t)^2 + \mathbf{L}_1 2(1-t)t + \mathbf{L}_2 t^2], \quad (21.5)$$

and substituting from (21.4) gives the components

$$\begin{aligned}x'(t) &= 3L_0 \sin \vartheta (1-t)^2 + 3L_2 \sin \vartheta \cos \varphi t^2, \\ y'(t) &= 3L_2 \sin \vartheta \sin \varphi t^2, \\ z'(t) &= 3L_0 \cos \vartheta (1-t)^2 + 3L_1 2(1-t)t + 3L_2 \cos \vartheta t^2.\end{aligned}$$

Writing

$$x'^2(t) + y'^2(t) + z'^2(t) = \sum_{k=0}^4 c_k \binom{4}{k} (1-t)^{4-k} t^k,$$

the Bernstein coefficients of this quartic polynomial are given by

$$\begin{aligned}c_0 &= 9L_0^2, \quad c_1 = 9L_0 L_1 \cos \vartheta, \\ c_2 &= 3L_0 L_2 (\sin^2 \vartheta \cos \varphi + \cos^2 \vartheta) + 6L_1^2, \\ c_3 &= 9L_1 L_2 \cos \vartheta, \quad c_4 = 9L_2^2.\end{aligned}\quad (21.6)$$

Consider now the quadratic polynomial $\sigma(t) = \sigma_0(1-t)^2 + \sigma_1 2(1-t)t + \sigma_2 t^2$ with Bernstein coefficients

$$\sigma_0 = 3L_0, \quad \sigma_1 = 3L_1 \cos \vartheta, \quad \sigma_2 = 3L_2.$$

One can easily verify that the quartic polynomial defined by (21.6) coincides with the square of $\sigma(t)$ provided that $c_2 = (2\sigma_1^2 + \sigma_0 \sigma_2)/3$, i.e., the condition

$$3L_0 L_2 (\sin^2 \vartheta \cos \varphi + \cos^2 \vartheta) + 6L_1^2 = 6L_1^2 \cos^2 \vartheta + 3L_0 L_2$$

holds. Solving this for $\cos \varphi$, the result is found to be independent of ϑ , and is given by expression (21.3). Thus, satisfying the geometrical constraints of Proposition 21.1 implies that the hodograph is Pythagorean.

Conversely, suppose that the three control-polygon legs $\mathbf{L}_0, \mathbf{L}_1, \mathbf{L}_2$ define a Pythagorean hodograph. If $\theta_{01}, \theta_{12}, \theta_{20}$ (with $0 \leq \theta_{jk} \leq \pi$) are the pairwise angles between these vectors, we again choose coordinates with \mathbf{L}_1 in the z direction and \mathbf{L}_0 parallel to the z - x plane. We then have

$$\begin{aligned}\mathbf{L}_0 &= L_0(\sin \theta_{01}, 0, \cos \theta_{01}), \quad \mathbf{L}_1 = L_1(0, 0, 1), \\ \mathbf{L}_2 &= L_2(\sin \theta_{12} \cos \varphi, \sin \theta_{12} \sin \varphi, \cos \theta_{12}),\end{aligned}\quad (21.7)$$

where φ is the azimuthal angle of \mathbf{L}_2 about the z axis. Because the hodograph defined by (21.5) and (21.7) is Pythagorean, the quartic obtained by summing the squares of its components must coincide with the square of a quadratic, $\sigma_0(1-t)^2 + \sigma_1 2(1-t)t + \sigma_2 t^2$. Equating Bernstein coefficients, we thus have

$$\begin{aligned}\sigma_0^2 &= 9L_0^2, \quad \sigma_0\sigma_1 = 9L_0L_1 \cos\theta_{01}, \\ \sigma_2\sigma_0 + 2\sigma_1^2 &= 9L_0L_2(\sin\theta_{01}\sin\theta_{12}\cos\varphi + \cos\theta_{01}\cos\theta_{12}) + 18L_1^2, \\ \sigma_1\sigma_2 &= 9L_1L_2 \cos\theta_{12}, \quad \sigma_2^2 = 9L_2^2.\end{aligned}$$

According to the first and the last equations, $\sigma_0 = \pm 3L_0$ and $\sigma_2 = \pm 3L_2$ may be of like or unlike sign. Substituting into the second and fourth equations, the latter choice is seen to imply $\theta_{12} = \pi - \theta_{01}$, so that $\cos\theta_{12} = -\cos\theta_{01}$ and $\sin\theta_{12} = \sin\theta_{01}$. But then for non-zero L_0, L_1, L_2 the third equation is impossible to satisfy with a value of $|\cos\varphi|$ that does not exceed unity.

Therefore, σ_0 and σ_2 must be chosen to be of *like* sign, and from the second and fourth equations we infer that

$$\theta_{12} = \theta_{01} \quad (= \vartheta, \text{ say})$$

i.e., \mathbf{L}_0 and \mathbf{L}_2 lie on a cone of half-angle ϑ about \mathbf{L}_1 . Finally, setting $\cos\theta_{01} = \cos\theta_{12} = \cos\vartheta$ and $\sin\theta_{01} = \sin\theta_{12} = \sin\vartheta$ in the third equation and solving for $\cos\varphi$ yields the value (21.3). Thus, if the hodograph defined by $\mathbf{L}_0, \mathbf{L}_1, \mathbf{L}_2$ is Pythagorean, it must satisfy the constraints of Proposition 21.1. ■

As an immediate consequence of Proposition 21.1, we make the following observation concerning the control-polygon sides L_0, L_1, L_2 .

Corollary 21.1 *A spatial cubic can have a Pythagorean hodograph only when the lengths L_0, L_1, L_2 of its control-polygon legs satisfy the inequality*

$$L_1 \leq \sqrt{L_0L_2}. \quad (21.8)$$

Proof : Equation (21.3) admits a solution for the azimuthal separation φ of $\mathbf{L}_0, \mathbf{L}_2$ for given lengths L_0, L_1, L_2 only if the latter satisfy (21.8). ■

Remark 21.2 The constraints that identify *planar* PH cubics (see §18.3) in terms of the control-polygon sides L_0, L_1, L_2 and “interior” angles θ_1, θ_2 are

$$L_1 = \sqrt{L_0L_2} \quad \text{and} \quad \theta_1 = \theta_2.$$

These can be regarded as a specialization of the conditions in Proposition 21.1 for spatial PH cubics. For a cone of half-angle ϑ , a control polygon satisfying the constraints of Proposition 21.1 is planar when $\varphi = \pm\pi$. For such a polygon, we have $\theta_1 = \theta_2 = \vartheta$ and (21.3) reduces to $L_1 = \sqrt{L_0L_2}$ on setting $\cos\varphi = -1$ (the case $\varphi = 0$ may be discounted since it requires $L_1 = 0$ in (21.3) and gives $\theta_2 = 2\pi - \theta_1$, rather than $\theta_1 = \theta_2$).

Based on Proposition 21.1, a purely geometrical procedure for constructing Bézier control polygons of spatial PH cubics can be formulated as follows.

Algorithm. To construct a twisted Pythagorean–hodograph cubic:

- (a) choose lengths L_0, L_1, L_2 satisfying (21.8) for the control polygon legs;
- (b) choose a direction in \mathbb{R}^3 for the middle leg \mathbf{L}_1 , and construct a cone of any half-angle ϑ about this direction;
- (c) take outer legs \mathbf{L}_0 and \mathbf{L}_2 lying on this cone, with azimuthal separation φ given in terms of L_0, L_1, L_2 by (21.3);
- (d) the control points are $\mathbf{p}_{k+1} = \mathbf{p}_k + \mathbf{L}_k$ for $k = 0, 1, 2$ with \mathbf{p}_0 arbitrary.

Actually, one can consider *any three* of the quantities L_0, L_1, L_2 and φ as free parameters — subject to condition (21.8) — the fourth being fixed by (21.3). Note that the components of \mathbf{L}_0 and \mathbf{L}_2 along \mathbf{L}_1 must be of the *same* sign. Clearly, there are *four* free parameters (ϑ and three of L_0, L_1, L_2, φ) in the construction of spatial PH cubics, as compared to *three* in the planar case.

The parametric speed of a PH cubic constructed according to the above algorithm is the quadratic polynomial

$$\sigma(t) = |\mathbf{r}'(t)| = 3[L_0(1-t)^2 + L_1 \cos \vartheta 2(1-t)t + L_2 t^2]. \quad (21.9)$$

Invoking (21.8) we observe that the discriminant $\Delta = L_1^2 \cos^2 \vartheta - L_0 L_2$ of this polynomial is always non-positive, so $\sigma(t) \geq 0$ for all t .

Example 21.1 In the following examples we take $\mathbf{p}_0 = (0, 0, 0)$ as the initial control point upon integrating the hodograph.

- (a) Choosing $L_0 = \sqrt{2}$, $L_1 = 1$, $L_2 = \sqrt{2}$ and $\vartheta = \pi/4$, equation (21.3) gives $\cos \varphi = 0$ and thus $\varphi = \pm\pi/2$. Adopting the coordinate axes defined by (21.4) we obtain the control points

$$\mathbf{p}_1 = (1, 0, 1), \quad \mathbf{p}_2 = (1, 0, 2), \quad \mathbf{p}_3 = (1, \pm 1, 3).$$

The hodograph components are then

$$(x', y', z') = (3(1-t)^2, \pm 3t^2, 3)$$

and the parametric speed is given by $\sigma(t) = 3\sqrt{2}[(1-t)^2 + \frac{1}{2}2(1-t)t + t^2]$.

- (b) For $L_0 = 4$, $L_1 = 6$, $L_2 = 12$ and $\vartheta = \pi/3$, we have $\varphi = \pm 2\pi/3$. This gives the control points

$$\mathbf{p}_1 = (2\sqrt{3}, 0, 2), \quad \mathbf{p}_2 = (2\sqrt{3}, 0, 8), \quad \mathbf{p}_3 = (-\sqrt{3}, \pm 9, 14)$$

of the form (21.4). The Pythagorean hodograph is then

$$(x', y', z') = (2\sqrt{3}(1-t)^2 - 3\sqrt{3}t^2, \pm 9t^2, 2(1-t)^2 + 12(1-t)t + 6t^2)$$

and its magnitude is given by $\sigma(t) = 4(1-t)^2 + 6(1-t)t + 12t^2$.

(c) Finally, for $L_0 = 18$, $L_1 = 12$, $L_2 = 16$, and $\vartheta = 5\pi/6$ we have $\varphi = \pm\pi/2$ and hence

$$\mathbf{p}_1 = (9, 0, -9\sqrt{3}), \quad \mathbf{p}_2 = (9, 0, 12 - 9\sqrt{3}), \quad \mathbf{p}_3 = (9, \pm 8, 12 - 17\sqrt{3}).$$

The reader can easily verify that the corresponding hodograph is Pythagorean. Figure 21.1 illustrates these curves and their control polygons, as well as the conical surfaces that the control-polygon legs \mathbf{L}_0 and \mathbf{L}_2 lie on.

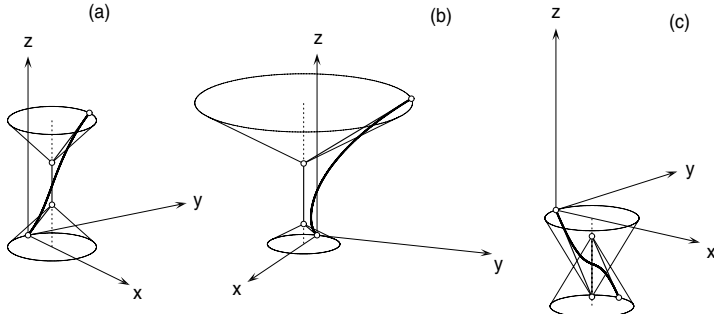


Fig. 21.1. Spatial PH cubics of Example 21.1, together with their control polygons.

The control-polygon structure that characterizes spatial PH cubics reflects the intrinsic geometrical nature of these curves, which we now elucidate.

Proposition 21.2 *Every spatial PH cubic is a helix, with pitch angle defined in terms of the parameters $L_0, L_1, L_2, \vartheta, \varphi$ described in Proposition 21.1 by*

$$\psi = \tan^{-1} \frac{-2L_1^2 |\sin \vartheta|}{L_0 L_2 \sin \varphi}. \quad (21.10)$$

Proof: We need to compute the curvature (8.67) and torsion (8.72) of cubics with Bézier control polygons of the form specified in Proposition 21.1. Again, we use coordinates in which this polygon has the form (21.4). Differentiating the hodograph (21.5) gives

$$\mathbf{r}''(t) = 6[(\mathbf{L}_1 - \mathbf{L}_0)(1-t) + (\mathbf{L}_2 - \mathbf{L}_1)t], \quad \mathbf{r}'''(t) = 6(\mathbf{L}_2 - 2\mathbf{L}_1 + \mathbf{L}_0)$$

and hence we infer that

$$\mathbf{r}'(t) \times \mathbf{r}''(t) = 18[\mathbf{L}_0 \times \mathbf{L}_1 (1-t)^2 - \mathbf{L}_2 \times \mathbf{L}_0 (1-t)t + \mathbf{L}_1 \times \mathbf{L}_2 t^2],$$

where, for the specific form (21.4), we have

$$\mathbf{L}_0 \times \mathbf{L}_1 = L_0 L_1 \sin \vartheta (0, -1, 0),$$

$$\mathbf{L}_2 \times \mathbf{L}_0 = L_2 L_0 \sin \vartheta (\cos \vartheta \sin \varphi, \cos \vartheta (1 - \cos \varphi), -\sin \vartheta \sin \varphi),$$

$$\mathbf{L}_1 \times \mathbf{L}_2 = L_1 L_2 \sin \vartheta (-\sin \varphi, \cos \varphi, 0).$$

Making use of (21.3), a straightforward but laborious calculation yields

$$|\mathbf{r}'(t) \times \mathbf{r}''(t)| = 6L_1 |\sin \vartheta| \sigma(t), \quad (21.11)$$

where the parametric speed is given by (21.9), and hence the curvature is

$$\kappa(t) = \frac{|\mathbf{r}'(t) \times \mathbf{r}''(t)|}{|\mathbf{r}'(t)|^3} = \frac{6L_1 |\sin \vartheta|}{\sigma^2(t)}. \quad (21.12)$$

To compute the torsion, we note that the scalar product of $\mathbf{r}' \times \mathbf{r}''$ and \mathbf{r}''' reduces to the constant

$$[\mathbf{r}'(t) \times \mathbf{r}''(t)] \cdot \mathbf{r}'''(t) = 108 (\mathbf{L}_0 \times \mathbf{L}_1) \cdot \mathbf{L}_2,$$

and for the form (21.4) we have $(\mathbf{L}_0 \times \mathbf{L}_1) \cdot \mathbf{L}_2 = -L_0 L_1 L_2 \sin^2 \vartheta \sin \varphi$. Thus, using (21.11), we obtain

$$\tau(t) = \frac{[\mathbf{r}'(t) \times \mathbf{r}''(t)] \cdot \mathbf{r}'''(t)}{|\mathbf{r}'(t) \times \mathbf{r}''(t)|^2} = \frac{-3L_0 L_2 \sin \varphi}{L_1 \sigma^2(t)}. \quad (21.13)$$

Since the curvature (21.12) and torsion (21.13) have a constant ratio, the PH cubic is a helix of pitch ψ given by (21.10) whose tangent is this constant. ■

Remark 21.3 Since $\sigma(t) \neq \text{constant}$ for any polynomial curve other than a straight line, we see from (21.12) and (21.13) that the curvature and torsion of PH space cubics are necessarily non-constant (assuming that $L_0, L_1, L_2, \vartheta, \varphi$ are all non-zero). Hence, these curves cannot be *circular* helices.

Remark 21.4 Assuming L_0, L_1, L_2 are all non-zero, two “degenerate” forms of spatial PH cubics can be identified from the curvature and torsion formulae (21.12) and (21.13) — (a) if $\sin \varphi = 0$ (or $L_1 = \sqrt{L_0 L_2}$) then $\tau(t) \equiv 0$, and we have a *plane* curve (see Remark 21.2); and (b) if $\sin \vartheta = 0$, then $\kappa(t) \equiv 0$ and we have a *straight line* — which is “twisted” if $\sin \varphi \neq 0$, i.e., the principal normal \mathbf{p} and binormal \mathbf{b} rotate about this line as we traverse it.

The helical axis \mathbf{a} of a spatial PH cubic can be determined from expression (21.2). In specific examples, the tangent \mathbf{t} and binormal \mathbf{b} at any point are easily determined and substituted into (21.2) together with $\cos \psi, \sin \psi$ values obtained from (21.10). To express \mathbf{a} symbolically for arbitrary orientations of the control polygon is more difficult. In the case of (21.4) we may write the condition $\mathbf{a} \cdot \mathbf{t} = \cos \psi$ as $\mathbf{a} \cdot \mathbf{r}'(t) = \cos \psi \sigma(t)$ and using (21.5) and (21.9) solve for the components of \mathbf{a} by equating Bernstein coefficients. This gives

$$\mathbf{a} = \frac{\cos \psi}{\sin \varphi} (\sin \vartheta \sin \varphi, \sin \vartheta (1 - \cos \varphi), \cos \vartheta \sin \varphi).$$

21.2 Spatial Pythagorean Hodographs

The first attempt at generalizing Pythagorean hodographs from \mathbb{R}^2 to \mathbb{R}^3 was described in [188], with the hodograph $\mathbf{r}'(t)$ assumed to be of the form

$$\begin{aligned} x'(t) &= h(t) [u^2(t) - v^2(t) - w^2(t)], \\ y'(t) &= 2h(t)u(t)v(t), \\ z'(t) &= 2h(t)u(t)w(t), \end{aligned} \quad (21.14)$$

for polynomials $h(t), u(t), v(t), w(t)$ so that $\sigma(t) = |h(t)| (u^2(t) + v^2(t) + w^2(t))$. The spatial PH quintics defined by taking $h(t) = 1$ and quadratic polynomials $u(t), v(t), w(t)$ were shown to be capable of interpolating arbitrary first-order Hermite data (with four distinct solutions), and the construction of *rational canal surfaces* based on such PH curves was discussed. Note that, if we choose $h(t) = 1$, then $\gcd(u, v, w) = \text{constant} \not\Rightarrow \gcd(x', y', z') = \text{constant}$ — consider the case $u(t) = t^2 + 1, v(t) = t^2, w(t) = t$ — but the hodograph components cannot have any common *real* roots if $\gcd(u, v, w) = \text{constant}$.

However, as noted in [188], being of the form (21.14) amounts to a *sufficient* but not *necessary* condition for a spatial hodograph $\mathbf{r}'(t) = (x'(t), y'(t), z'(t))$ to satisfy the Pythagorean equation (21.1). For example, the hodograph

$$x'(t) = (1-t)^2, \quad y'(t) = t^2, \quad z'(t) = 1,$$

satisfies (21.1) with $\sigma(t) = \sqrt{2}(t^2 - t + 1)$, but one can readily verify that it cannot be written in the form (21.14). A related problem is that (21.14) is not invariant with respect to re-labelling of the coordinates, or general rotations in \mathbb{R}^3 — i.e., a given hodograph may have this form in one coordinate system, but not in another (it is invariant under rotations about the x axis, but not about the y and z axes, or axes of arbitrary orientation in \mathbb{R}^3).

In a somewhat different context, Dietz, Hoschek, and Jüttler [130] gave a characterization for Pythagorean quartuples of polynomials, similar to results by V. A. Lebesgue (1868) and E. Catalan (1885) in number theory on sums of the squares of three integers — see Chap. VII of [129].

Theorem 21.1 *If relatively prime real polynomials $a(t), b(t), c(t), d(t)$ satisfy the Pythagorean condition*

$$a^2(t) + b^2(t) + c^2(t) = d^2(t), \quad (21.15)$$

they must be expressible in terms of other real polynomials $u(t), v(t), p(t), q(t)$ in the form¹

$$\begin{aligned} a(t) &= u^2(t) + v^2(t) - p^2(t) - q^2(t), \\ b(t) &= 2[u(t)q(t) + v(t)p(t)], \\ c(t) &= 2[v(t)q(t) - u(t)p(t)], \\ d(t) &= u^2(t) + v^2(t) + p^2(t) + q^2(t). \end{aligned} \quad (21.16)$$

¹ This form can be written in several different ways, corresponding to permutations of $a(t), b(t), c(t)$ and $u(t), v(t), p(t), q(t)$.

Proof : We re-write equation (21.15) as

$$b^2(t) + c^2(t) = d^2(t) - a^2(t),$$

which may be factorized to obtain

$$[b(t) + i c(t)][b(t) - i c(t)] = [d(t) - a(t)][d(t) + a(t)]. \quad (21.17)$$

If $w(t) = \gcd(b(t), c(t)) = \text{constant}$, the complex polynomials $b(t) + i c(t)$ and $b(t) - i c(t)$ cannot have common roots. Moreover, they cannot have any real roots, and the roots of one must be conjugates of the roots of the other. Since $d(t) - a(t)$ and $d(t) + a(t)$ are real polynomials, they must be decomposable into complex-conjugate pairs of linear factors, with one member of each pair from $b(t) + i c(t)$ and the other from $b(t) - i c(t)$. In other words, these latter polynomials must have factorizations of the form

$$b(t) + i c(t) = f(t) \bar{g}(t), \quad b(t) - i c(t) = \bar{f}(t) g(t), \quad (21.18)$$

where $f(t), g(t)$ are two complex polynomials such that

$$d(t) - a(t) = f(t) \bar{f}(t), \quad d(t) + a(t) = g(t) \bar{g}(t). \quad (21.19)$$

Writing the two complex polynomials in terms of real and imaginary parts as $f(t) = \sqrt{2}[p(t) + i q(t)]$ and $g(t) = \sqrt{2}[v(t) + i u(t)]$ where $p(t), q(t), v(t), u(t)$ are real polynomials, and substituting them into (21.18) and (21.19), these equations yield expressions (21.16) as solutions for $a(t), b(t), c(t), d(t)$.

If $w(t) = \gcd(b(t), c(t)) \neq \text{constant}$, we see from (21.17) that $w^2(t)$ must be a factor of either $d(t) - a(t)$ or $d(t) + a(t)$, but not the other — since a common root of $b(t), c(t), d(t) - a(t), d(t) + a(t)$ contradicts $a(t), b(t), c(t), d(t)$ being relatively prime. The preceding arguments can thus be invoked after dividing $w(t)$ out of $b(t) + i c(t)$ and $b(t) - i c(t)$, and $w^2(t)$ out of either $d(t) - a(t)$ or $d(t) + a(t)$, as appropriate. ■

Although expressions (21.16) may seem rather non-intuitive, we shall see in the next chapter that they admit a simple interpretation in terms of *products of quaternion polynomials*. Comparing Theorems 17.1 and 21.1, characterizing Pythagorean triples and quartuples of polynomials, respectively, we note some important differences. In Theorem 17.1 a *sufficient-and-necessary* condition for satisfaction of (17.2) is given by the form (17.3), and in Remark 17.1 it was noted that “primitive” triples, with $\gcd(a(t), b(t), c(t)) = \text{constant}$, are easily identified by the restrictions $w(t) = \text{constant}$ and $\gcd(u(t), v(t)) = \text{constant}$.

In Theorem 21.1, on the other hand, the form (21.16) is presented as only a *necessary* condition for a primitive Pythagorean quartuple, satisfying (21.15) with $\gcd(a(t), b(t), c(t), d(t)) = \text{constant}$. Although one can easily verify by substitution that the form (21.16) is also a *sufficient* condition for satisfaction of (21.15), it does not always yield primitive quartuples — even if we choose polynomials with $\gcd(u(t), v(t), p(t), q(t)) = \text{constant}$. In particular, we have $\gcd(a(t), b(t), c(t), d(t)) \neq \text{constant}$ whenever $\gcd(u^2(t) + v^2(t), p^2(t) + q^2(t)) \neq \text{constant}$. We will elaborate on this point in Chaps. 22 and 23.

21.3 Bézier Control Polygons

By Theorem 21.1, spatial Pythagorean hodographs must have components of the form

$$\begin{aligned} x'(t) &= u^2(t) + v^2(t) - p^2(t) - q^2(t), \\ y'(t) &= 2[u(t)q(t) + v(t)p(t)], \\ z'(t) &= 2[v(t)q(t) - u(t)p(t)], \end{aligned} \quad (21.20)$$

with parametric speed

$$\sigma(t) = u^2(t) + v^2(t) + p^2(t) + q^2(t). \quad (21.21)$$

When the polynomials $u(t)$, $v(t)$, $p(t)$, $q(t)$ are of degree μ at most, the spatial PH curve obtained by integration of this hodograph is evidently of *odd* degree, $n = 2\mu + 1$. Of course, it is always possible to multiply the components (21.20) by a common polynomial $h(t)$ and still satisfy (21.1) — but the hodograph is no longer primitive, and the resulting PH curve may exhibit cusps if $h(t)$ has real roots. As noted above, employing relatively prime polynomials $u(t)$, $v(t)$, $p(t)$, $q(t)$ in (21.20) does not *per se* guarantee $\gcd(x'(t), y'(t), z'(t)) = \text{constant}$ — but common factors of the hodograph components can have only complex conjugate roots, and thus cannot incur real cusps (see §23.3).

If the polynomials $u(t)$, $v(t)$, $p(t)$, $q(t)$ are specified in terms of Bernstein coefficients on $t \in [0, 1]$ the Bézier control points of the spatial PH curves they define can be expressed in terms of these coefficients, in a manner analogous to (17.5) and (17.6) for planar PH curves. For example, with $u(t) = u_0(1-t) + u_1t$ and similarly for $v(t)$, $p(t)$, $q(t)$, the control points of spatial PH cubics are found to be of the form

$$\begin{aligned} \mathbf{p}_1 &= \mathbf{p}_0 + \frac{1}{3}(u_0^2 + v_0^2 - p_0^2 - q_0^2, 2(u_0q_0 + v_0p_0), 2(v_0q_0 - u_0p_0)), \\ \mathbf{p}_2 &= \mathbf{p}_1 + \frac{1}{3}(u_0u_1 + v_0v_1 - p_0p_1 - q_0q_1, \\ &\quad u_0q_1 + u_1q_0 + v_0p_1 + v_1p_0, v_0q_1 + v_1q_0 - u_0p_1 - u_1p_0), \\ \mathbf{p}_3 &= \mathbf{p}_2 + \frac{1}{3}(u_1^2 + v_1^2 - p_1^2 - q_1^2, 2(u_1q_1 + v_1p_1), 2(v_1q_1 - u_1p_1)), \end{aligned} \quad (21.22)$$

the point \mathbf{p}_0 , corresponding to the integration constants, being freely chosen. However, the control point formulae for PH quintics become very cumbersome — see [158] — and it will be much more convenient to employ the quaternion expressions given in §22.1 below.

Since the four polynomials $u(t)$, $v(t)$, $p(t)$, $q(t)$ are each defined by $\mu + 1$ coefficients, and an additional three freedoms are associated with the control point \mathbf{p}_0 , degree- n spatial PH curves possess $4(\mu + 1) + 3 = 2n + 5$ degrees of freedom, compared to $3n + 3$ for “ordinary” polynomial curves of degree n . However, five of these freedoms correspond to a choice of origin and orientation

of the coordinate axes in \mathbb{R}^3 , and two amount to re-parameterization freedoms that do not alter the curve degree. Moreover, we shall see in §22.3 that, for the case of PH curves, choosing the polynomials $u(t)$, $v(t)$, $p(t)$, $q(t)$ involves one non-essential freedom — there is a *one-parameter family* of these polynomials whose members all generate the same hodograph. Thus, we can say that, while ordinary degree- n polynomial curves in \mathbb{R}^3 have $3n - 4$ “intrinsic” freedoms, degree- n spatial PH curves have $2n - 3$. This agrees with the conclusion of §21.1, that the Bézier control polygons of spatial PH cubics are characterized by just three independent parameters.

21.4 Differential Properties

The unit tangent to the spatial PH curve defined by the hodograph (21.20) is a *rational* function of the curve parameter, defined in terms of the polynomials $u(t)$, $v(t)$, $p(t)$, $q(t)$ by

$$\mathbf{t} = \frac{\mathbf{r}'}{|\mathbf{r}'|} = \frac{(u^2 + v^2 - p^2 - q^2, 2(uq + vp), 2(vq - up))}{\sigma}, \quad (21.23)$$

where σ is the parametric speed (21.21). However, the principal normal and binormal vectors \mathbf{p} and \mathbf{b} , as defined by (8.68) and (8.69), are not in general rational unit vectors. They are both dependent on the quantity $|\mathbf{r}' \times \mathbf{r}''|$, and by substituting from (21.20) into

$$|\mathbf{r}' \times \mathbf{r}''|^2 = (y'z'' - y''z')^2 + (z'x'' - z''x')^2 + (x'y'' - x''y')^2,$$

one can verify that

$$|\mathbf{r}'(t) \times \mathbf{r}''(t)|^2 = \sigma^2(t)\rho(t), \quad (21.24)$$

where the polynomial $\rho(t)$ is defined [164] by

$$\begin{aligned} \rho = 4 & [(up' - u'p)^2 + (uq' - u'q)^2 + (vp' - v'p)^2 + (vq' - v'q)^2 \\ & + 2(uv' - u'v)(pq' - p'q)]. \end{aligned} \quad (21.25)$$

This may be interpreted as the quantity

$$\rho(t) = |\mathbf{r}''(t)|^2 - \sigma'^2(t),$$

or as $|\mathbf{r}''(t)|^2 \sin^2 \psi(t)$, where $\psi(t)$ denotes the angle between $\mathbf{r}'(t)$ and $\mathbf{r}''(t)$. In fact, ρ can be written in terms of the four polynomials u , v , p , q and their derivatives u' , v' , p' , q' in a number of different ways. For example, it can be expressed [33] as a sum of squares,

$$\rho = 4 [(up' - u'p + vq' - v'q)^2 + (uq' - u'q - vp' + v'p)^2]. \quad (21.26)$$

The expressions for both $\mathbf{p}(t)$ and $\mathbf{b}(t)$ contain the radical term $\sqrt{\rho(t)}$ in their denominators. Similarly, the curvature (8.67) of a spatial PH curve, given by $\kappa(t) = \sqrt{\rho(t)/\sigma^2(t)}$, is not rational — although the torsion (8.72) is rational.

The spatial PH cubics (see §21.1), however, constitute a special case. Since they are defined by *linear* polynomials $u(t), v(t), p(t), q(t)$, all the polynomials of the form $up' - u'p, uq' - u'q$, etc. in (21.26) reduce to constants, and hence $\rho(t) = k^2$ for some real constant k . Thus, as observed by Wagner and Ravani [455], spatial PH cubics possess *rational Frenet frames*. For a spatial PH cubic $\mathbf{r}(t)$, the Frenet frame may be expressed in terms of $\mathbf{r}', \mathbf{r}''$ and the polynomial speed and its derivative σ, σ' in the evidently rational form

$$\mathbf{t} = \frac{\mathbf{r}'}{\sigma}, \quad \mathbf{p} = \frac{\sigma \mathbf{r}'' - \sigma' \mathbf{r}'}{k \sigma}, \quad \mathbf{b} = \frac{\mathbf{r}' \times \mathbf{r}''}{k \sigma},$$

where k^2 is determined by replacing $up' - u'p$ with $u_0 p_1 - u_1 p_0$ in (21.26), and similarly for the other terms $uq' - u'q$, etc. In Proposition 21.2 we noted that all spatial PH cubics are helical. In Chap. 23 we discuss helical curves in more general terms — we shall see that all helical polynomial curves are PH curves, with rational Frenet frames, curvature, and torsion. This is a consequence of the fact that, for helical curves, the polynomial $\rho(t)$ is a perfect square.

Although the principal normals and binormals of spatial PH curves (except cubics) are usually not rational unit vectors, it is possible to impose a rotation of them in the curve normal plane at each point that defines a rational orthonormal basis $(\mathbf{e}_1(t), \mathbf{e}_2(t))$ in this plane — $(\mathbf{t}, \mathbf{e}_1, \mathbf{e}_2)$ is then a *rational adapted frame* for the PH curve. Also, the fact that the torsion of a PH space curve is a rational function of the parameter allows us to compute *rotation-minimizing frames* on such curves. We elaborate on these topics in Chap. 30.

Integrating the hodograph (21.20) may also produce *linear* and *planar* PH curves as special cases, although the conditions that identify such degenerate curves in terms of $u(t), v(t), p(t), q(t)$ are not so simple. If all four polynomials are constants, the hodograph becomes a single point and its integration yields a (uniformly-parameterized) straight line. Moreover, straight lines with non-uniform parameterizations also arise when $x'(t), y'(t), z'(t)$ are non-constant, but exhibit constant ratios. This circumstance corresponds to the curvature $\kappa = |\mathbf{r}' \times \mathbf{r}''|/\sigma^3$ vanishing identically, and from (21.24) this is equivalent to the polynomial $\rho(t)$ vanishing identically, since $\sigma(t) \neq 0$ for a PH curve.

Now the polynomial $\rho(t)$ is of degree $2n - 6$ for a degree- n PH curve, and is thus a constant for PH cubics and a quartic for PH quintics. For PH cubics, the occurrence of straight lines coincides with vanishing of the constant

$$c = (u_0 p_1 - u_1 p_0 + v_0 q_1 - v_1 q_0)^2 + (u_0 q_1 - u_1 q_0 - v_0 p_1 + v_1 p_0)^2 \quad (21.27)$$

which corresponds geometrically to the control points (21.22) being collinear. In the case of PH quintics, vanishing of the quartic polynomial $\rho(t)$ yields five scalar conditions on the twelve coefficients of $u(t), v(t), p(t), q(t)$.

Planar degenerations of spatial PH curves correspond to vanishing of the torsion, and thus the polynomial $(\mathbf{r}'(t) \times \mathbf{r}''(t)) \cdot \mathbf{r}'''(t)$ — which can be written in terms of $u(t), v(t), p(t), q(t)$ and their first and second derivatives — must

be identically zero. For a PH curve of degree n , this polynomial is generally of degree $3n - 9$. For the PH cubics, in particular, it reduces to the constant

$$8c(u_0v_1 - u_1v_0 - p_0q_1 + p_1q_0). \quad (21.28)$$

Hence, for a planar PH cubic that is not simply a straight line, we have $c \neq 0$ and $u_0v_1 - u_1v_0 - p_0q_1 + p_1q_0 = 0$. For the PH quintics, $(\mathbf{r}'(t) \times \mathbf{r}''(t)) \cdot \mathbf{r}'''(t)$ is a polynomial of degree 6. Geometrically, planar degenerations of spatial PH curves correspond to coplanarity of the Bézier control points.

It is difficult to make much further progress in elucidating the nature of spatial PH curves, and devising algorithms for their construction and analysis, if we continue to regard the polynomials $u(t)$, $v(t)$, $p(t)$, $q(t)$ in the hodograph form (21.20) as a “loose association” — an algebraic language that embodies the structure (21.20) in a natural manner, and facilitates further calculations, is needed. As we shall see in the following chapter, the *quaternion formulation* for spatial PH curves addresses precisely these needs (this is the counterpart to the complex representation of planar PH curves, discussed in Chap. 19). For example, the circumstances for degeneration of spatial PH curves to straight lines and planar curves acquire quite simple expressions in terms of the linear dependence of certain quaternion coefficients (see §22.2).

Quaternion Representation

The algebraically real part may receive ... all values contained on the one scale of progression of number from negative to positive infinity; we shall call it therefore the scalar part, or simply the scalar ... On the other hand, the algebraically imaginary part, being geometrically constructed by a straight line or radius vector, which has, in general, for each determined quaternion, a determined length and direction in space, may be called the vector part, or simply the vector ...

William Rowan Hamilton, *Philosophical Magazine* (1846)

22.1 Pythagorean Condition in \mathbb{R}^3

An algebraic model for (primitive) planar Pythagorean hodographs, based on the properties of complex numbers, was proposed in Chap. 19. Namely, if $u(t)$ and $v(t)$ are real polynomials with $\gcd(u(t), v(t)) = \text{constant}$, the square $\mathbf{w}^2(t) = u^2(t) - v^2(t) + i 2u(t)v(t)$ of the complex polynomial $\mathbf{w} = u(t) + i v(t)$ has real and imaginary parts that correspond to the Cartesian components of a Pythagorean hodograph $\mathbf{r}'(t) = x'(t) + i y'(t)$ in \mathbb{R}^2 , identified with \mathbb{C} . For each t , the hodograph vector $\mathbf{r}'(t)$ is generated by rotating a unit vector along the x (real) axis by $\theta(t) = 2 \arg(\mathbf{w}(t))$ and scaling it by $\sigma(t) = |\mathbf{w}(t)|^2$.

Intuitively, it seems clear that this process of generating $\mathbf{r}'(t)$ through a continuous family of rotations and scalings of a unit “reference vector” should extend to \mathbb{R}^3 , and that it should be describable by a *quaternion* polynomial $\mathcal{A}(t)$ in lieu of the complex polynomial $\mathbf{w}(t)$, since quaternions are intimately related to spatial rotations — see Chap. 5. For each t , the expression for a spatial Pythagorean hodograph $\mathbf{r}'(t)$ in terms of $\mathcal{A}(t)$ must yield a pure vector

quaternion, so it cannot be simply the *square* $\mathcal{A}^2(t)$ — which has, in general, a non-zero scalar part. For a quaternion polynomial written as

$$\mathcal{A}(t) = u(t) + v(t)\mathbf{i} + p(t)\mathbf{j} + q(t)\mathbf{k}, \quad (22.1)$$

the appropriate quaternion form for the spatial Pythagorean hodograph with components (21.20) was identified¹ by Choi et al. [89] as

$$\begin{aligned} \mathbf{r}'(t) = \mathcal{A}(t)\mathbf{i}\mathcal{A}^*(t) &= [u^2(t) + v^2(t) - p^2(t) - q^2(t)]\mathbf{i} \\ &\quad + 2[u(t)q(t) + v(t)p(t)]\mathbf{j} \\ &\quad + 2[v(t)q(t) - u(t)p(t)]\mathbf{k}. \end{aligned} \quad (22.2)$$

Writing $\mathcal{A}(t) = |\mathcal{A}(t)|\mathcal{U}(t)$ where $\mathcal{U}(t) = (\cos \frac{1}{2}\theta(t), \sin \frac{1}{2}\theta(t)\mathbf{n}(t))$, this can be interpreted as generating $\mathbf{r}'(t)$ through a rotation of the unit vector \mathbf{i} by angle $\theta(t)$ about the axis $\mathbf{n}(t)$, together with a scaling by $|\mathcal{A}(t)|^2$. Here the choice of \mathbf{i} (rather than \mathbf{j} or \mathbf{k}) as the “reference vector” is merely conventional — by the *rotation invariance* (see §22.3) of the quaternion form of spatial Pythagorean hodographs, any unit vector could be used in place of \mathbf{i} . Expression (22.2) is an example of the *PH representation map* [89] proposed by Choi et al., which employs Clifford algebra methods to formulate Pythagorean $(n+1)$ -tuples of polynomials in n -dimensional Euclidean and Minkowski spaces.

To define spatial PH cubics, we begin with a linear quaternion polynomial

$$\mathcal{A}(t) = \mathcal{A}_0(1-t) + \mathcal{A}_1 t. \quad (22.3)$$

The control points of the cubic obtained by integrating the hodograph (22.2) are then given in terms of the quaternion coefficients $\mathcal{A}_0, \mathcal{A}_1$ by

$$\begin{aligned} \mathbf{p}_1 &= \mathbf{p}_0 + \frac{1}{3}\mathcal{A}_0\mathbf{i}\mathcal{A}_0^*, \\ \mathbf{p}_2 &= \mathbf{p}_1 + \frac{1}{6}(\mathcal{A}_0\mathbf{i}\mathcal{A}_1^* + \mathcal{A}_1\mathbf{i}\mathcal{A}_0^*), \\ \mathbf{p}_3 &= \mathbf{p}_2 + \frac{1}{3}\mathcal{A}_1\mathbf{i}\mathcal{A}_1^*, \end{aligned} \quad (22.4)$$

where \mathbf{p}_0 corresponds to a free integration constant (note that expressions of the form $\mathcal{A}_i\mathbf{i}\mathcal{A}_i^*$ and $\mathcal{A}_i\mathbf{i}\mathcal{A}_j^* + \mathcal{A}_j\mathbf{i}\mathcal{A}_i^*$ always have pure vector values).

Comparing with (21.22), we see that the quaternion representation offers a compact expression of the PH property, that is especially useful on proceeding to the quintics and higher-order PH curves. The results of §21.1 concerning spatial PH cubics can be alternatively derived using the form (22.4). For the cubic defined by (22.4), the parametric speed $\sigma(t)$ is quadratic, with Bernstein coefficients

¹ The quaternion form (22.2) — and its rotation invariance — were used by Wallner and Pottmann [457] in the context of blending surface constructions for quadrics. Ueda [448, 449] also proposed quaternion models for spatial PH curves, but they are based on the form (21.14) which is not invariant under spatial rotations.

$$\sigma_0 = |\mathcal{A}_0|^2, \quad \sigma_1 = \frac{1}{2}(\mathcal{A}_0\mathcal{A}_1^* + \mathcal{A}_1\mathcal{A}_0^*), \quad \sigma_2 = |\mathcal{A}_1|^2. \quad (22.5)$$

To obtain a spatial PH quintic, we substitute a quadratic polynomial

$$\mathcal{A}(t) = \mathcal{A}_0(1-t)^2 + \mathcal{A}_12(1-t)t + \mathcal{A}_2t^2 \quad (22.6)$$

with quaternion coefficients $\mathcal{A}_0, \mathcal{A}_1, \mathcal{A}_2$ into the hodograph form (22.2), and integrate. This gives the control points

$$\begin{aligned} \mathbf{p}_1 &= \mathbf{p}_0 + \frac{1}{5}\mathcal{A}_0 \mathbf{i} \mathcal{A}_0^*, \\ \mathbf{p}_2 &= \mathbf{p}_1 + \frac{1}{10}(\mathcal{A}_0 \mathbf{i} \mathcal{A}_1^* + \mathcal{A}_1 \mathbf{i} \mathcal{A}_0^*), \\ \mathbf{p}_3 &= \mathbf{p}_2 + \frac{1}{30}(\mathcal{A}_0 \mathbf{i} \mathcal{A}_2^* + 4\mathcal{A}_1 \mathbf{i} \mathcal{A}_1^* + \mathcal{A}_2 \mathbf{i} \mathcal{A}_0^*), \\ \mathbf{p}_4 &= \mathbf{p}_3 + \frac{1}{10}(\mathcal{A}_1 \mathbf{i} \mathcal{A}_2^* + \mathcal{A}_2 \mathbf{i} \mathcal{A}_1^*), \\ \mathbf{p}_5 &= \mathbf{p}_4 + \frac{1}{5}\mathcal{A}_2 \mathbf{i} \mathcal{A}_2^*, \end{aligned} \quad (22.7)$$

where \mathbf{p}_0 is again arbitrary. In this case, the parametric speed $\sigma(t)$ is defined by the quartic Bernstein coefficients

$$\begin{aligned} \sigma_0 &= |\mathcal{A}_0|^2, \quad \sigma_1 = \frac{1}{2}(\mathcal{A}_0\mathcal{A}_1^* + \mathcal{A}_1\mathcal{A}_0^*), \\ \sigma_2 &= \frac{1}{6}(\mathcal{A}_0\mathcal{A}_2^* + 4|\mathcal{A}_1|^2 + \mathcal{A}_2\mathcal{A}_0^*), \\ \sigma_3 &= \frac{1}{2}(\mathcal{A}_1\mathcal{A}_2^* + \mathcal{A}_2\mathcal{A}_1^*), \quad \sigma_4 = |\mathcal{A}_2|^2. \end{aligned} \quad (22.8)$$

Under special circumstances, the spatial PH cubics and quintics defined by the control points (22.4) and (22.7) may degenerate to straight lines, or planar curves other than straight lines, rather than true space curves. The conditions under which such degenerate forms occur are identified in §22.2. The *helical* curves are another “special” type of spatial PH curve. The cubic helices have already been comprehensively treated in §21.1, and conditions that identify the helical PH quintics will be presented in the following chapter.

Remark 22.1 As an alternative to the quaternion representation, Choi et al. [89] observe that the spatial Pythagorean hodograph (21.20) can be generated from two complex polynomials through the *Hopf map* $\mathbb{C} \times \mathbb{C} \rightarrow \mathbb{R}^3$. This map can be regarded as associating points $\mathbf{p} = (x, y, z) \in \mathbb{R}^3$ with complex number pairs $\boldsymbol{\alpha} = u + i v, \boldsymbol{\beta} = q + i p$ according to

$$\mathbf{p} = H(\boldsymbol{\alpha}, \boldsymbol{\beta}) = (|\boldsymbol{\alpha}|^2 - |\boldsymbol{\beta}|^2, 2\operatorname{Re}(\boldsymbol{\alpha}\bar{\boldsymbol{\beta}}), 2\operatorname{Im}(\boldsymbol{\alpha}\bar{\boldsymbol{\beta}})). \quad (22.9)$$

One can easily verify that the hodograph $\mathbf{r}'(t)$ specified by (21.20) is generated by the complex polynomials $\boldsymbol{\alpha}(t) = u(t) + i v(t), \boldsymbol{\beta}(t) = q(t) + i p(t)$ as

$$\mathbf{r}'(t) = H(\boldsymbol{\alpha}(t), \boldsymbol{\beta}(t)). \quad (22.10)$$

If we identify the complex-number imaginary unit i with the quaternion basis element \mathbf{i} , the quaternion polynomial $\mathcal{A}(t) = u(t) + v(t)\mathbf{i} + p(t)\mathbf{j} + q(t)\mathbf{k}$ can be related to the complex polynomials $\alpha(t)$ and $\beta(t)$ by

$$\mathcal{A}(t) = \alpha(t) + \mathbf{k}\beta(t).$$

When we restrict (22.9) to complex numbers satisfying $|\alpha|^2 + |\beta|^2 = 1$, it can be interpreted as a map between the “3-sphere” $S^3 : u^2 + v^2 + p^2 + q^2 = 1$ in the space \mathbb{R}^4 spanned by coordinates (u, v, p, q) , and the familiar “2-sphere” $S^2 : x^2 + y^2 + z^2 = 1$ in \mathbb{R}^3 with (x, y, z) as coordinates. Thus, for example, the great circles of S^3 are mapped to points of S^2 by (22.9). This map exhibits remarkable structural features that delight topologists [426, 438].

22.2 Degeneration of Spatial PH Curves

The quaternion form provides a more intuitive interpretation of the conditions, briefly discussed in §21.4, for spatial PH cubics and quintics to degenerate into straight lines and planar curves other than straight lines.

Lemma 22.1 *For any quaternion $\mathcal{A} \neq 0$, the four quaternions $\mathcal{A}, \mathcal{A}\mathbf{i}, \mathcal{A}\mathbf{j}, \mathcal{A}\mathbf{k}$ — interpreted as vectors in \mathbb{R}^4 — define an orthogonal basis, in terms of which any quaternion can be represented using four real values $\alpha, \beta, \gamma, \delta$ as a linear combination of the form*

$$\alpha\mathcal{A} + \beta\mathcal{A}\mathbf{i} + \gamma\mathcal{A}\mathbf{j} + \delta\mathcal{A}\mathbf{k} = \mathcal{A}(\alpha + \beta\mathbf{i} + \gamma\mathbf{j} + \delta\mathbf{k}). \quad (22.11)$$

Proof : If $\mathcal{A} = u + v\mathbf{i} + p\mathbf{j} + q\mathbf{k}$, taking the components of $\mathcal{A}, \mathcal{A}\mathbf{i}, \mathcal{A}\mathbf{j}, \mathcal{A}\mathbf{k}$ as columns of a 4×4 matrix gives

$$\begin{bmatrix} u & -v & -p & -q \\ v & u & -q & p \\ p & q & u & -v \\ q & -p & v & u \end{bmatrix}.$$

Since any two columns have zero dot product, this is an *orthogonal* matrix: it has determinant $|\mathcal{A}|^4 = (u^2 + v^2 + p^2 + q^2)^2$, and when $|\mathcal{A}| = 1$ we can regard it as defining a rotation in \mathbb{R}^4 . The linear independence of $\mathcal{A}, \mathcal{A}\mathbf{i}, \mathcal{A}\mathbf{j}, \mathcal{A}\mathbf{k}$ ensures that any quaternion can be expressed in the form (22.11), obtained by multiplying the above matrix with $(\alpha, \beta, \gamma, \delta)^T$. ■

The form (22.11) introduces special coordinates in \mathbb{R}^4 , relative to a given quaternion $\mathcal{A} \neq 0$, that simplify the identification of “degenerate” spatial PH curves. This can also be done by *left* multiplication of \mathcal{A} with $\mathbf{i}, \mathbf{j}, \mathbf{k}$, but the bases obtained by left and right multiplication are inherently different [345]: for simplicity, we use only the latter. Consider first the spatial PH cubics.

Proposition 22.1 Let \mathcal{A}_1 be expressed in terms of $\mathcal{A}_0 (\neq 0)$ as

$$\mathcal{A}_1 = \mathcal{A}_0 (\alpha + \beta \mathbf{i} + \gamma \mathbf{j} + \delta \mathbf{k}). \quad (22.12)$$

Then the spatial PH cubic defined by the control points (22.4) degenerates into a straight line if and only if $\gamma = \delta = 0$, and into a planar curve other than a straight line if and only if $\beta = 0$ and $(\gamma, \delta) \neq (0, 0)$.

Proof : Let $\mathcal{A}_r = u_r \mathbf{i} + v_r \mathbf{j} + p_r \mathbf{k}$ for $r = 0, 1$. Then the components of \mathcal{A}_1 expressed in the form (22.12) are given by

$$\begin{aligned} u_1 &= \alpha u_0 - \beta v_0 - \gamma p_0 - \delta q_0, \\ v_1 &= \alpha v_0 + \beta u_0 - \gamma q_0 + \delta p_0, \\ p_1 &= \alpha p_0 + \beta q_0 + \gamma u_0 - \delta v_0, \\ q_1 &= \alpha q_0 - \beta p_0 + \gamma v_0 + \delta u_0. \end{aligned} \quad (22.13)$$

A spatial PH cubic is a straight line if and only if the quantity (21.27) vanishes, i.e. — since the coefficients are real — if and only if

$$u_0 p_1 - u_1 p_0 + v_0 q_1 - v_1 q_0 = 0 \quad \text{and} \quad u_0 q_1 - u_1 q_0 - v_0 p_1 + v_1 p_0 = 0.$$

Substituting from (22.13) for u_1, v_1, p_1, q_1 into these equations, we obtain

$$\gamma (u_0^2 + v_0^2 + p_0^2 + q_0^2) = 0 \quad \text{and} \quad \delta (u_0^2 + v_0^2 + p_0^2 + q_0^2) = 0.$$

Hence, since $|\mathcal{A}_0|^2 = u_0^2 + v_0^2 + p_0^2 + q_0^2 \neq 0$ by assumption, the PH cubic is a straight line if and only if $\gamma = \delta = 0$ in expression (22.12) for \mathcal{A}_1 .

Also, a PH cubic is a planar curve (not a straight line) if and only if expression (21.28) vanishes, but (21.27) does not. Substituting u_1, v_1, p_1, q_1 into (21.27) and (21.28) and simplifying, these conditions amount to

$$\beta (u_0^2 + v_0^2 + p_0^2 + q_0^2) = 0 \quad \text{and} \quad (\gamma^2 + \delta^2)(u_0^2 + v_0^2 + p_0^2 + q_0^2)^2 \neq 0.$$

Hence, since $|\mathcal{A}_0| \neq 0$, the PH cubic is a planar curve (but not a straight line) if and only if $\beta = 0$ and $(\gamma, \delta) \neq (0, 0)$ in expression (22.12) for \mathcal{A}_1 . ■

Thus, viewing quaternions as vectors in \mathbb{R}^4 , a spatial PH cubic degenerates to a straight line if and only if \mathcal{A}_1 resides in the two-dimensional subspace spanned by $\mathcal{A}_0, \mathcal{A}_0 \mathbf{i}$ and to a plane curve (other than a line) if and only if \mathcal{A}_1 resides in the three-dimensional subspace spanned by $\mathcal{A}_0, \mathcal{A}_0 \mathbf{j}, \mathcal{A}_0 \mathbf{k}$.

For spatial PH quintics, the condition for degeneration to a straight line is a direct generalization of that for the spatial PH cubics, but a new consideration enters into the planarity condition. The following two propositions describe the conditions for degeneration of spatial PH quintics.

Proposition 22.2 Let $\mathcal{A}_1, \mathcal{A}_2$ be expressed in terms of $\mathcal{A}_0 (\neq 0)$ as

$$\mathcal{A}_r = \mathcal{A}_0 (\alpha_r + \beta_r \mathbf{i} + \gamma_r \mathbf{j} + \delta_r \mathbf{k}), \quad r = 1, 2. \quad (22.14)$$

Then the spatial PH quintic specified by the control points (22.7) degenerates into a straight line if and only if $\gamma_1 = \gamma_2 = \delta_1 = \delta_2 = 0$.

Proof : Let $\mathcal{A}_r = u_r + v_r \mathbf{i} + p_r \mathbf{j} + q_r \mathbf{k}$ for $r = 0, 1, 2$. Then when \mathcal{A}_1 and \mathcal{A}_2 are expressed in the form (22.14), their components are given for $r = 1, 2$ by

$$\begin{aligned} u_r &= \alpha_r u_0 - \beta_r v_0 - \gamma_r p_0 - \delta_r q_0, \\ v_r &= \alpha_r v_0 + \beta_r u_0 - \gamma_r q_0 + \delta_r p_0, \\ p_r &= \alpha_r p_0 + \beta_r q_0 + \gamma_r u_0 - \delta_r v_0, \\ q_r &= \alpha_r q_0 - \beta_r p_0 + \gamma_r v_0 + \delta_r u_0. \end{aligned} \quad (22.15)$$

Now a spatial PH quintic is a straight line if and only if the polynomial (21.26) vanishes identically, i.e., if and only if the two polynomials

$$\begin{aligned} f(t) &= 2[u(t)p'(t) - u'(t)p(t) + v(t)q'(t) - v'(t)q(t)], \\ g(t) &= 2[u(t)q'(t) - u'(t)q(t) - v(t)p'(t) + v'(t)p(t)], \end{aligned}$$

both vanish identically. For PH quintics, these polynomials are quadratic and have the Bernstein forms

$$\begin{aligned} f(t) &= 4(u_0 p_1 - u_1 p_0 + v_0 q_1 - v_1 q_0)(1-t)^2 \\ &\quad + 2(u_0 p_2 - u_2 p_0 + v_0 q_2 - v_2 q_0)2(1-t)t \\ &\quad + 4(u_1 p_2 - u_2 p_1 + v_1 q_2 - v_2 q_1)t^2, \\ g(t) &= 4(u_0 q_1 - u_1 q_0 - v_0 p_1 + v_1 p_0)(1-t)^2 \\ &\quad + 2(u_0 q_2 - u_2 q_0 - v_0 p_2 + v_2 p_0)2(1-t)t \\ &\quad + 4(u_1 q_2 - u_2 q_1 - v_1 p_2 + v_2 p_1)t^2. \end{aligned}$$

Substituting for u_1, v_1, p_1, q_1 and u_2, v_2, p_2, q_2 gives

$$\begin{aligned} f(t) &= 4|\mathcal{A}_0|^2 [f_0(1-t)^2 + f_1 2(1-t)t + f_2 t^2], \\ g(t) &= 4|\mathcal{A}_0|^2 [g_0(1-t)^2 + g_1 2(1-t)t + g_2 t^2], \end{aligned}$$

where

$$\begin{aligned} f_0 &= \gamma_1, \quad f_1 = \frac{1}{2}\gamma_2, \quad f_2 = \alpha_1\gamma_2 - \alpha_2\gamma_1 + \beta_1\delta_2 - \beta_2\delta_1, \\ g_0 &= \delta_1, \quad g_1 = \frac{1}{2}\delta_2, \quad g_2 = \alpha_1\delta_2 - \alpha_2\delta_1 - \beta_1\gamma_2 + \beta_2\gamma_1, \end{aligned} \quad (22.16)$$

and $|\mathcal{A}_0|^2 = u_0^2 + v_0^2 + p_0^2 + q_0^2$. Since $|\mathcal{A}_0| \neq 0$ by assumption, the polynomials $f(t)$ and $g(t)$ both vanish, and hence the PH quintic is a straight line, if and only if $\gamma_1 = \gamma_2 = \delta_1 = \delta_2 = 0$ in expression (22.14) for $\mathcal{A}_1, \mathcal{A}_2$. ■

When $\gamma_1 = \gamma_2 = \delta_1 = \delta_2 = 0$, one can verify that the hodograph (22.2) reduces to the form

$$\mathbf{r}'(t) = \sigma(t) \mathbf{t}_0,$$

where $\sigma(t) = |\mathbf{r}'(t)|$ is the parametric speed, and the unit vector

$$\mathbf{t}_0 = \frac{(u_0^2 + v_0^2 - p_0^2 - q_0^2, 2(u_0 q_0 + v_0 p_0), 2(v_0 q_0 - u_0 p_0))}{u_0^2 + v_0^2 + p_0^2 + q_0^2}$$

specifies the (constant) tangent direction. Since the direction of $\mathbf{r}'(t)$ does not vary, the locus is a (non-uniformly parameterized) straight line.

Proposition 22.3 *Let $\mathcal{A}_1, \mathcal{A}_2$ be expressed in terms of \mathcal{A}_0 ($\neq 0$) as in (22.14). Then the spatial PH quintic specified by the control points (22.7) degenerates into a planar curve, other than a straight line, if and only if $\beta_1 = \beta_2 = 0$ and $\gamma_1\delta_2 - \gamma_2\delta_1 = 0$ with $\gamma_1, \gamma_2, \delta_1, \delta_2$ not all zero, provided that the hodograph (22.2) is primitive — i.e., $\gcd(x', y', z') = \text{constant}$.*

Proof: We use the same notation as in Proposition 22.2. A spatial PH quintic degenerates to a plane curve if and only if the polynomial $(\mathbf{r}'(t) \times \mathbf{r}''(t)) \cdot \mathbf{r}'''(t)$ vanishes identically. For a spatial PH quintic, this polynomial is of degree six, with coefficients dependent on $\alpha_1, \beta_1, \gamma_1, \delta_1$ and $\alpha_2, \beta_2, \gamma_2, \delta_2$ when \mathcal{A}_1 and \mathcal{A}_2 are specified in terms of \mathcal{A}_0 in the form (22.14). Equating the coefficients of this degree six polynomial to zero furnishes a system of seven equations, to be satisfied by these variables, in the case of a planar curve. These equations are too cumbersome to derive by hand, and require the use of computer algebra software for their derivation and solution. Using MAPLE, we observe that the real solutions with $(\gamma_1, \gamma_2, \delta_1, \delta_2) \neq (0, 0, 0, 0)$ are characterized by $\beta_1 = \beta_2 = 0$ and $\gamma_1\delta_2 - \gamma_2\delta_1 = 0$, whenever $\gcd(x', y', z') = \text{constant}$.² ■

Thus, as with cubics, spatial PH quintics degenerate to straight lines when $\mathcal{A}_1, \mathcal{A}_2$ lie in the subspace of \mathbb{R}^4 spanned by $\mathcal{A}_0, \mathcal{A}_0\mathbf{i}$. For planar curves $\mathcal{A}_1, \mathcal{A}_2$ must lie in the subspace of \mathbb{R}^4 spanned by $\mathcal{A}_0, \mathcal{A}_0\mathbf{j}, \mathcal{A}_0\mathbf{k}$ (as with the cubics), but there is the additional requirement that $\gamma_1\delta_2 - \gamma_2\delta_1 = 0$ with $\gamma_1, \gamma_2, \delta_1, \delta_2$ not all zero. This implies that $\gamma_1 : \gamma_2 = \delta_1 : \delta_2$ so $\mathcal{A}_1, \mathcal{A}_2$ have the form

$$\mathcal{A}_1 = \alpha_1\mathcal{A}_0 + \gamma_1\mathcal{A}_0\mathbf{j} + \delta_1\mathcal{A}_0\mathbf{k}, \quad \mathcal{A}_2 = \alpha_2\mathcal{A}_0 + h(\gamma_1\mathcal{A}_0\mathbf{j} + \delta_1\mathcal{A}_0\mathbf{k}),$$

for some real value h . In other words, the components of $\mathcal{A}_1, \mathcal{A}_2$ in the subspace of \mathbb{R}^4 spanned by $\mathcal{A}_0\mathbf{j}, \mathcal{A}_0\mathbf{k}$ must be proportional. This means that, for planar PH quintics, the quaternions $\mathcal{A}_0, \mathcal{A}_1, \mathcal{A}_2$ are not linearly-independent — the combination $\lambda\mathcal{A}_0 + \mu\mathcal{A}_1 + \nu\mathcal{A}_2$ vanishes when $\lambda : \mu : \nu = \alpha_2 - h\alpha_1 : h : -1$.

One can verify that, when the conditions of Proposition 22.3 are met, the normal $\mathbf{n} = (n_x, n_y, n_z)$ to the plane in which the PH curve $\mathbf{r}(t)$ resides is defined by the ratios

$$\begin{aligned} n_x : n_y : n_z &= 2\gamma_2(u_0q_0 - v_0p_0) - 2\delta_2(u_0p_0 + v_0q_0) \\ &\quad : \gamma_2(v_0^2 + q_0^2 - u_0^2 - p_0^2) + 2\delta_2(u_0v_0 - p_0q_0) \\ &\quad : \delta_2(v_0^2 + p_0^2 - u_0^2 - q_0^2) - 2\gamma_2(u_0v_0 + p_0q_0). \end{aligned}$$

The expression of any quaternion in the form (22.11), relative to a specific non-zero quaternion \mathcal{A} , will be further invoked in §23.5 below to characterize another “degenerate” type of spatial PH curve: namely, the *helical* PH curves. Unlike the degenerate forms discussed above, these are true “twisted” space curves, but with certain distinctive geometrical features. In §21.1 we observed that spatial PH cubics are always helical, but we shall see that the helical PH

² Since the conditions under which $\gcd(x', y', z') \neq \text{constant}$ are rather technical in nature, we defer complete details of them to Chap. 23.

quintics form a proper subset of all spatial PH quintics. Propositions 23.3 and 23.4 give sufficient and necessary characterizations of helical PH quintics, in terms of the coefficients $\alpha_1, \beta_1, \gamma_1, \delta_1$ and $\alpha_2, \beta_2, \gamma_2, \delta_2$ in (22.14).

22.3 Rotation Invariance of Hodographs

In §21.2 we noted that a fundamental deficiency of the form (21.14) is its lack of invariance under arbitrary rotations in \mathbb{R}^3 — a hodograph constructed using the form (21.14) in one coordinate system might not admit representation by this form in a rotated coordinate system. We now show, using the quaternion representation, that the form (21.20) does exhibit rotation invariance. Note that (21.14) with $h(t) = 1$ is actually a special case of (21.20), corresponding to the replacement of $u(t), v(t), p(t), q(t)$ by 0, $u(t), v(t), w(t)$.

The rotation invariance property of spatial PH curves is of practical as well as theoretical concern. In §29.7.2, we shall consider the problem of finding the *optimal orientation* for a set of parallel section planes in the contour machining of free-form surfaces, with tool paths approximated by PH space curves. Since the milling machine has fixed axes, it is convenient to consider rotations of the surface relative to fixed sectioning planes, rather than vice-versa. It is then necessary to impose spatial rotations on the computed tool paths, to emulate section planes of varying orientations relative to a fixed workpiece.

A rotation in n -dimensional Euclidean space can be specified by an $n \times n$ orthogonal matrix with determinant +1. The set of all such matrices forms a group of dimension $\frac{1}{2}n(n-1)$, denoted by $\text{SO}(n)$, under matrix multiplication. Consider a three-dimensional rotation

$$\begin{bmatrix} \tilde{x}'(t) \\ \tilde{y}'(t) \\ \tilde{z}'(t) \end{bmatrix} = \begin{bmatrix} m_{11} & m_{12} & m_{13} \\ m_{21} & m_{22} & m_{23} \\ m_{31} & m_{32} & m_{33} \end{bmatrix} \begin{bmatrix} x'(t) \\ y'(t) \\ z'(t) \end{bmatrix} \quad (22.17)$$

of the hodograph (21.20), where m_{jk} are the elements of a matrix $\mathbf{M} \in \text{SO}(3)$. In the case of a rotation through angle θ about the unit vector $\mathbf{n} = (n_x, n_y, n_z)$, this matrix has [20] the elements

$$\begin{aligned} m_{11} &= n_x^2 + (1 - n_x^2) \cos \theta, \\ m_{12} &= n_x n_y (1 - \cos \theta) - n_z \sin \theta, \\ m_{13} &= n_z n_x (1 - \cos \theta) + n_y \sin \theta, \\ m_{21} &= n_x n_y (1 - \cos \theta) + n_z \sin \theta, \\ m_{22} &= n_y^2 + (1 - n_y^2) \cos \theta, \\ m_{23} &= n_y n_z (1 - \cos \theta) - n_x \sin \theta, \\ m_{31} &= n_z n_x (1 - \cos \theta) - n_y \sin \theta, \\ m_{32} &= n_y n_z (1 - \cos \theta) + n_x \sin \theta, \\ m_{33} &= n_z^2 + (1 - n_z^2) \cos \theta. \end{aligned} \quad (22.18)$$

Conversely, the rotation parameters θ and \mathbf{n} can be deduced from the elements m_{jk} of \mathbf{M} through

$$\begin{aligned}\theta &= \cos^{-1} \frac{1}{2}(m_{11} + m_{22} + m_{33} - 1), \\ \mathbf{n} &= \frac{(m_{32} - m_{23}, m_{13} - m_{31}, m_{21} - m_{12})}{2 \sin \theta}.\end{aligned}$$

Our intent is to show that the rotated hodograph $\tilde{\mathbf{r}}'(t) = (\tilde{x}'(t), \tilde{y}'(t), \tilde{z}'(t))$ can be written in terms of four new polynomials $\tilde{u}(t), \tilde{v}(t), \tilde{p}(t), \tilde{q}(t)$ as

$$\begin{aligned}\tilde{x}'(t) &= \tilde{u}^2(t) + \tilde{v}^2(t) - \tilde{p}^2(t) - \tilde{q}^2(t), \\ \tilde{y}'(t) &= 2[\tilde{u}(t)\tilde{q}(t) + \tilde{v}(t)\tilde{p}(t)], \\ \tilde{z}'(t) &= 2[\tilde{v}(t)\tilde{q}(t) - \tilde{u}(t)\tilde{p}(t)].\end{aligned}$$

Specifically, we desire closed-form expressions for $\tilde{u}(t), \tilde{v}(t), \tilde{p}(t), \tilde{q}(t)$ in terms of $u(t), v(t), p(t), q(t)$ and the rotation parameters θ and \mathbf{n} .

Consider the quaternion form (22.2) of a spatial Pythagorean hodograph. As a pure vector quaternion, $\mathbf{r}'(t)$ is amenable to the quaternion description of spatial rotations (see Chap. 5). Now the quaternion polynomial $\mathcal{A}(t)$ that generates a particular hodograph $\mathbf{r}'(t)$ through expression (22.2) is not unique. One can easily verify that, if \mathcal{Q} is any quaternion satisfying

$$\mathcal{Q} \mathbf{i} \mathcal{Q}^* = \mathbf{i}, \quad (22.19)$$

then the quaternion polynomial defined by $\hat{\mathcal{A}}(t) = \mathcal{A}(t)\mathcal{Q}$ generates precisely the same hodograph, since

$$\hat{\mathcal{A}}(t) \mathbf{i} \hat{\mathcal{A}}^*(t) = (\mathcal{A}(t)\mathcal{Q}) \mathbf{i} (\mathcal{A}(t)\mathcal{Q})^* = \mathcal{A}(t) \mathcal{Q} \mathbf{i} \mathcal{Q}^* \mathcal{A}^*(t) = \mathcal{A}(t) \mathbf{i} \mathcal{A}^*(t).$$

For example, the choice $\mathcal{Q} = \mathbf{i}$ satisfies (22.19), corresponding to a replacement of (22.1) by

$$\hat{\mathcal{A}}(t) = -v(t) + u(t)\mathbf{i} + q(t)\mathbf{j} - p(t)\mathbf{k}.$$

Writing $\mathcal{Q} = a + b\mathbf{i} + c\mathbf{j} + d\mathbf{k}$, condition (22.19) is equivalent to the system of equations

$$a^2 + b^2 - c^2 - d^2 = 1, \quad 2(ad + bc) = 0, \quad 2(bd - ac) = 0,$$

whose real solutions are necessarily of the form $(a, b, c, d) = (\cos \phi, \sin \phi, 0, 0)$. Hence, the totality of real solutions to (22.19) can be parameterized in terms of a real angular variable ϕ as

$$\mathcal{Q}(\phi) = \cos \phi + \sin \phi \mathbf{i}, \quad (22.20)$$

and as the most general alternative to $\mathcal{A}(t)$ we have

$$\begin{aligned}\hat{\mathcal{A}}(t) &= \hat{u}(t) + \hat{v}(t)\mathbf{i} + \hat{p}(t)\mathbf{j} + \hat{q}(t)\mathbf{k} \\ &= \cos \phi u(t) - \sin \phi v(t) + [\cos \phi v(t) + \sin \phi u(t)]\mathbf{i} \\ &\quad + [\cos \phi p(t) + \sin \phi q(t)]\mathbf{j} + [\cos \phi q(t) - \sin \phi p(t)]\mathbf{k}. \quad (22.21)\end{aligned}$$

The components of $\hat{\mathcal{A}}(t)$ depend linearly on those of $\mathcal{A}(t)$, through the matrix

$$\mathbf{Q}(\phi) = \begin{bmatrix} \cos \phi & -\sin \phi & 0 & 0 \\ \sin \phi & \cos \phi & 0 & 0 \\ 0 & 0 & \cos \phi & \sin \phi \\ 0 & 0 & -\sin \phi & \cos \phi \end{bmatrix}. \quad (22.22)$$

Thus, if we interpret $\mathcal{A}(t)$ and $\hat{\mathcal{A}}(t)$ as curves in \mathbb{R}^4 , the latter corresponds to a four-dimensional rotation of the former. Since the matrix $\mathbf{Q}(\phi)$ has no real eigenvectors, the origin is the only stationary point of \mathbb{R}^4 under this rotation — i.e., $\mathbf{Q}(\phi)$ defines a *double* rotation in \mathbb{R}^4 (see §5.7).

Now let the Pythagorean hodograph $\mathbf{r}'(t)$ be transformed to $\tilde{\mathbf{r}}'(t)$ under a rotation by angle θ about the unit vector $\mathbf{n} = (n_x, n_y, n_z)$. The unit quaternion $\mathcal{U} = (\cos \frac{1}{2}\theta, \sin \frac{1}{2}\theta \mathbf{n})$ represents this rotation, such that

$$\tilde{\mathbf{r}}'(t) = \mathcal{U} \mathbf{r}'(t) \mathcal{U}^*. \quad (22.23)$$

We wish to show that the transformed hodograph $\tilde{\mathbf{r}}'(t)$ can also be written as a “pure vector” quaternion, in the form

$$\begin{aligned} \tilde{\mathbf{r}}'(t) &= [\tilde{u}^2(t) + \tilde{v}^2(t) - \tilde{p}^2(t) - \tilde{q}^2(t)] \mathbf{i} \\ &\quad + 2[\tilde{u}(t)\tilde{q}(t) + \tilde{v}(t)\tilde{p}(t)] \mathbf{j} + 2[\tilde{v}(t)\tilde{q}(t) - \tilde{u}(t)\tilde{p}(t)] \mathbf{k}, \end{aligned}$$

and we wish to express the four polynomials $\tilde{u}(t), \tilde{v}(t), \tilde{p}(t), \tilde{q}(t)$ in terms of $u(t), v(t), p(t), q(t)$ and the rotation parameters θ and \mathbf{n} . To evaluate (22.23), we substitute for $\mathbf{r}'(t)$ from (22.2) and make use of relation (5.7) to obtain

$$\tilde{\mathbf{r}}'(t) = \mathcal{U} \mathcal{A}(t) \mathbf{i} \mathcal{A}^*(t) \mathcal{U}^* = \mathcal{U} \mathcal{A}(t) \mathbf{i} [\mathcal{U} \mathcal{A}(t)]^* = \tilde{\mathcal{A}}(t) \mathbf{i} \tilde{\mathcal{A}}^*(t), \quad (22.24)$$

where, in the last step, we set $\tilde{\mathcal{A}}(t) = \mathcal{U} \mathcal{A}(t)$. We see that the final expression above for the rotated hodograph $\tilde{\mathbf{r}}'(t)$ has the desired Pythagorean form (22.2), with the original quaternion polynomial $\mathcal{A}(t)$ replaced by a new quaternion polynomial, namely $\tilde{\mathcal{A}}(t) = \mathcal{U} \mathcal{A}(t)$. Thus, writing

$$\begin{aligned} \tilde{\mathcal{A}}(t) &= [\cos \frac{1}{2}\theta + \sin \frac{1}{2}\theta (n_x \mathbf{i} + n_y \mathbf{j} + n_z \mathbf{k})] [u(t) + v(t) \mathbf{i} + p(t) \mathbf{j} + q(t) \mathbf{k}] \\ &= \tilde{u}(t) + \tilde{v}(t) \mathbf{i} + \tilde{p}(t) \mathbf{j} + \tilde{q}(t) \mathbf{k}, \end{aligned}$$

one finds that the quaternion polynomial $\tilde{\mathcal{A}}(t)$ has the four components

$$\begin{aligned} \tilde{u}(t) &= \cos \frac{1}{2}\theta u(t) - \sin \frac{1}{2}\theta [n_x v(t) + n_y p(t) + n_z q(t)], \\ \tilde{v}(t) &= \cos \frac{1}{2}\theta v(t) + \sin \frac{1}{2}\theta [n_x u(t) + n_y q(t) - n_z p(t)], \\ \tilde{p}(t) &= \cos \frac{1}{2}\theta p(t) + \sin \frac{1}{2}\theta [n_y u(t) + n_z v(t) - n_x q(t)], \\ \tilde{q}(t) &= \cos \frac{1}{2}\theta q(t) + \sin \frac{1}{2}\theta [n_z u(t) + n_x p(t) - n_y v(t)]. \end{aligned} \quad (22.25)$$

A straightforward but laborious calculation confirms that these polynomials do indeed define the hodograph $\tilde{\mathbf{r}}'(t)$ obtained by rotating $\mathbf{r}'(t)$ through angle

θ about \mathbf{n} , i.e., using the matrix defined by (22.17) and (22.18) one may verify that the following relations hold (for brevity, we drop the dependence on t):

$$\begin{aligned}\tilde{x}' &= m_{11}x' + m_{12}y' + m_{13}z' \\ &= [n_x^2 + (1 - n_x^2)\cos\theta](u^2 + v^2 - p^2 - q^2) \\ &\quad + [n_x n_y(1 - \cos\theta) - n_x \sin\theta]2(uq + vp) \\ &\quad + [n_z n_x(1 - \cos\theta) + n_y \sin\theta]2(vq - up) \\ &= \tilde{u}^2 + \tilde{v}^2 - \tilde{p}^2 - \tilde{q}^2, \\ \tilde{y}' &= m_{21}x' + m_{22}y' + m_{23}z' \\ &= [n_x n_y(1 - \cos\theta) + n_x \sin\theta](u^2 + v^2 - p^2 - q^2) \\ &\quad + [n_y^2 + (1 - n_y^2)\cos\theta]2(uq + vp) \\ &\quad + [n_y n_z(1 - \cos\theta) - n_x \sin\theta]2(vq - up) \\ &= 2(\tilde{u}\tilde{q} + \tilde{v}\tilde{p}), \\ \tilde{z}' &= m_{31}x' + m_{32}y' + m_{33}z' \\ &= [n_z n_x(1 - \cos\theta) - n_y \sin\theta](u^2 + v^2 - p^2 - q^2) \\ &\quad + [n_y n_z(1 - \cos\theta) + n_x \sin\theta]2(uq + vp) \\ &\quad + [n_z^2 + (1 - n_z^2)\cos\theta]2(vq - up) \\ &= 2(\tilde{v}\tilde{q} - \tilde{u}\tilde{p}).\end{aligned}$$

By way of illustration, consider the case $\mathbf{n} = (0, 0, 1)$ and $\theta = \pi/2$, for which equations (22.25) give

$$\tilde{u} = \frac{u - q}{\sqrt{2}}, \quad \tilde{v} = \frac{v - p}{\sqrt{2}}, \quad \tilde{p} = \frac{v + p}{\sqrt{2}}, \quad \tilde{q} = \frac{u + q}{\sqrt{2}}.$$

As expected for a quarter-turn about the z -axis, we then obtain

$$\begin{aligned}\tilde{x}' &= \tilde{u}^2 + \tilde{v}^2 - \tilde{p}^2 - \tilde{q}^2 = -2(uq + vp) = -y', \\ \tilde{y}' &= 2(\tilde{u}\tilde{q} + \tilde{v}\tilde{p}) = u^2 + v^2 - p^2 - q^2 = x', \\ \tilde{z}' &= 2(\tilde{v}\tilde{q} - \tilde{u}\tilde{p}) = 2(vq - up) = z'.\end{aligned}$$

Note that relations (22.25) can be cast in matrix form as

$$\begin{bmatrix} \tilde{u} \\ \tilde{v} \\ \tilde{p} \\ \tilde{q} \end{bmatrix} = \begin{bmatrix} \cos \frac{1}{2}\theta & -n_x \sin \frac{1}{2}\theta & -n_y \sin \frac{1}{2}\theta & -n_z \sin \frac{1}{2}\theta \\ n_x \sin \frac{1}{2}\theta & \cos \frac{1}{2}\theta & -n_z \sin \frac{1}{2}\theta & n_y \sin \frac{1}{2}\theta \\ n_y \sin \frac{1}{2}\theta & n_z \sin \frac{1}{2}\theta & \cos \frac{1}{2}\theta & -n_x \sin \frac{1}{2}\theta \\ n_z \sin \frac{1}{2}\theta & -n_y \sin \frac{1}{2}\theta & n_x \sin \frac{1}{2}\theta & \cos \frac{1}{2}\theta \end{bmatrix} \begin{bmatrix} u \\ v \\ p \\ q \end{bmatrix}. \quad (22.26)$$

One can readily verify that the above 4×4 matrix, which we denote by \mathbf{N} , is orthogonal and has determinant +1. Hence $\mathbf{N} \in \text{SO}(4)$, and we can interpret it as a (special type of) four-dimensional rotation.

Since $n_x^2 + n_y^2 + n_z^2 = 1$, the characteristic equation of \mathbf{N} reduces to

$$(\lambda^2 - 2 \cos \frac{1}{2}\theta \lambda + 1)^2 = 0,$$

and thus it has two distinct (double) complex eigenvalues,

$$\lambda = \cos \frac{1}{2}\theta \pm i \sin \frac{1}{2}\theta = \exp(\pm i \frac{1}{2}\theta).$$

The eigenvectors are correspondingly complex, and hence no real point other than $(u, v, p, q) = (0, 0, 0, 0)$ remains fixed under this rotation.

It can be shown [135, 138, 245] that \mathbf{N} is orthogonally similar to the matrix

$$\begin{bmatrix} \cos \frac{1}{2}\theta & -\sin \frac{1}{2}\theta & 0 & 0 \\ \sin \frac{1}{2}\theta & \cos \frac{1}{2}\theta & 0 & 0 \\ 0 & 0 & \cos \frac{1}{2}\theta \sin \frac{1}{2}\theta & 0 \\ 0 & 0 & -\sin \frac{1}{2}\theta \cos \frac{1}{2}\theta & 0 \end{bmatrix}$$

— i.e., there exists a matrix $\mathbf{S} \in \text{SO}(4)$ such that $\mathbf{S}^T \mathbf{N} \mathbf{S}$ is of the above form. \mathbf{S} defines a change of orthonormal basis $(1, \mathbf{i}, \mathbf{j}, \mathbf{k}) \rightarrow (\mathbf{e}_1, \mathbf{e}_2, \mathbf{e}_3, \mathbf{e}_4)$ such that the planes spanned by $(\mathbf{e}_1, \mathbf{e}_2)$ and $(\mathbf{e}_3, \mathbf{e}_4)$ are “invariant subspaces” of the four-dimensional rotation — i.e., \mathbf{N} maps these planes into themselves.

The type of four-dimensional rotation corresponding to multiplication on the left by a unit quaternion is called a *right screw*, whereas multiplication on the right is a *left screw* [135]. An arbitrary four-dimensional rotation $\mathcal{A} \rightarrow \tilde{\mathcal{A}}$ can be described [135] in terms of two unit quaternions \mathcal{L} and \mathcal{R} in the form

$$\tilde{\mathcal{A}} = \mathcal{L} \mathcal{A} \mathcal{R}^*.$$

An interesting application [224, 315] of such quaternion rotations arises in the block-diagonalization of matrices.

Because of the inherent indeterminacy of the quaternion polynomial $\mathcal{A}(t)$ that generates a particular hodograph $\mathbf{r}'(t)$ — $\mathcal{A}(t)$ can be post-multiplied by any quaternion \mathcal{Q} satisfying (22.19) without altering $\mathbf{r}'(t)$ — equation (22.26) is not the *only* linear map between $u(t), v(t), p(t), q(t)$ and $\tilde{u}(t), \tilde{v}(t), \tilde{p}(t), \tilde{q}(t)$. In fact, we observe from (22.21) that a *one-parameter family* of such maps is defined by the products

$$\mathbf{N} \mathbf{Q}(\phi)$$

of the matrix \mathbf{N} in (22.26) with matrices of the form (22.22) for each real ϕ . We consider the case $\phi = 0$ to be the “canonical” transformation $u, v, p, q \rightarrow \tilde{u}, \tilde{v}, \tilde{p}, \tilde{q}$ for arbitrary spatial rotations of Pythagorean hodographs.

22.4 Reflection Form of Hodographs

In §5.5 we noted that a spatial rotation can be interpreted as a product of two reflections. This observation offers an alternative to the construction (22.2) of

a spatial Pythagorean hodograph $\mathbf{r}'(t)$ through a continuum of rotations and scalings of the unit “reference vector” \mathbf{i} — writing the quaternion polynomial (22.1) as $\mathcal{A}(t) = |\mathcal{A}(t)|(\cos \frac{1}{2}\theta(t), \sin \frac{1}{2}\theta(t)\mathbf{n}(t))$, we generate $\mathbf{r}'(t)$ for each t by rotating \mathbf{i} through $\theta(t)$ about $\mathbf{n}(t)$ and scaling it by $|\mathcal{A}(t)|^2$.

In the case of PH quintics, $\mathbf{r}'(t)$ can be alternatively generated through a continuum of *reflections* and scalings of \mathbf{i} , specified by a quadratic pure vector quaternion polynomial.³ Consider the spatial Pythagorean hodograph

$$\mathbf{r}'(t) = \hat{\mathcal{A}}(t)\mathbf{i}\hat{\mathcal{A}}^*(t),$$

$\hat{\mathcal{A}}(t) = \mathcal{A}(t)\mathcal{Q}(\phi)$ being the family (22.21) of quadratic quaternion polynomials that yield exactly the same hodograph, since (22.20) satisfies (22.19). Now let $\mathcal{B}(t) = (0, \mathbf{b}(t))$ and $\mathcal{C} = (0, \mathbf{c})$ be pure vector quaternions, the former having a quadratic vector part $\mathbf{b}(t)$ and the latter a constant vector part \mathbf{c} . We claim that for appropriate choices of ϕ , $\mathbf{b}(t)$, \mathbf{c} the hodograph can be expressed as

$$\mathbf{r}'(t) = \mathcal{B}(t)\mathcal{C}\mathbf{i}\mathcal{C}\mathcal{B}(t). \quad (22.27)$$

In this form, $\mathbf{r}'(t)$ is defined (see §5.5) for each t by reflecting \mathbf{i} in the planes through the origin that are orthogonal to \mathbf{c} and $\mathbf{b}(t)$ (in that order) and scaling by $|\mathbf{c}|^2|\mathbf{b}(t)|^2$. Without loss of generality, we henceforth assume $|\mathbf{c}| = 1$. Since $\mathcal{C}\mathcal{B}(t) = (-\mathcal{C})(-\mathcal{B}(t)) = \mathcal{C}^*\mathcal{B}^*(t) = (\mathcal{B}(t)\mathcal{C})^*$ it suffices to show that

$$\mathcal{B}(t)\mathcal{C} = \hat{\mathcal{A}}(t).$$

Writing $\hat{\mathcal{A}}(t) = \mathcal{A}(t)\mathcal{Q}(\phi)$, where $\mathcal{A}(t) = (A_0(t), \mathbf{A}(t))$ and $A_x(t), A_y(t), A_z(t)$ are the components of $\mathbf{A}(t)$, this is equivalent to

$$\mathbf{b}(t) \cdot \mathbf{c} = \sin \phi A_x(t) - \cos \phi A_0(t), \quad (22.28)$$

and

$$\mathbf{b}(t) \times \mathbf{c} = \sin \phi A_0(t)\mathbf{i} + \cos \phi \mathbf{A}(t) + \sin \phi \mathbf{A}(t) \times \mathbf{i}, \quad (22.29)$$

Taking the dot product of the latter equation with $\mathbf{c} = (c_x, c_y, c_z)$ gives

$$\begin{aligned} & (A_0(t) \sin \phi + A_x(t) \cos \phi) c_x \\ & + (A_y(t) \cos \phi + A_z(t) \sin \phi) c_y \\ & + (A_z(t) \cos \phi - A_y(t) \sin \phi) c_z \equiv 0. \end{aligned} \quad (22.30)$$

In order for this polynomial to vanish, each of its coefficients in the quadratic Bernstein basis must vanish. Writing $A_0(t) = A_{00}b_0^2(t) + A_{01}b_1^2(t) + A_{02}b_2^2(t)$, and likewise for $A_x(t)$, $A_y(t)$, $A_z(t)$, the vanishing of these coefficients can be viewed as a homogeneous system of linear equations

³ The reflection form of spatial Pythagorean hodographs was first proposed in [358], using the vector geometric product of Clifford algebra (see Chap. 6) — rather than the quaternion form employed here — to represent spatial reflections.

$$\begin{bmatrix} A_{00}\sin\phi + A_{x0}\cos\phi & A_{y0}\cos\phi + A_{z0}\sin\phi & A_{z0}\cos\phi - A_{y0}\sin\phi \\ A_{01}\sin\phi + A_{x1}\cos\phi & A_{y1}\cos\phi + A_{z1}\sin\phi & A_{z1}\cos\phi - A_{y1}\sin\phi \\ A_{02}\sin\phi + A_{x2}\cos\phi & A_{y2}\cos\phi + A_{z2}\sin\phi & A_{z2}\cos\phi - A_{y2}\sin\phi \end{bmatrix} \begin{bmatrix} c_x \\ c_y \\ c_z \end{bmatrix} = \begin{bmatrix} 0 \\ 0 \\ 0 \end{bmatrix}$$

for the components of \mathbf{c} . For a non-trivial solution to exist, the determinant of the matrix must vanish. This condition defines a homogeneous cubic equation in $\sin\phi$ and $\cos\phi$, which has at least one real root. On substituting such a root for ϕ in these equations, we may obtain the corresponding solution vectors \mathbf{c} , and for any such \mathbf{c} the solution of (22.28) and (22.29) for the quadratic vector function $\mathbf{b}(t)$ is given by

$$\sin\phi [A_0(t)\mathbf{c} \times \mathbf{i} + \mathbf{c} \times (\mathbf{A}(t) \times \mathbf{i}) + A_x(t)\mathbf{c}] + \cos\phi [\mathbf{c} \times \mathbf{A}(t) - A_0(t)\mathbf{c}].$$

Example 22.1 Consider the Pythagorean hodograph defined by a quadratic quaternion polynomial $\mathcal{A}(t) = (A_0(t), \mathbf{A}(t))$ where the Bernstein coefficients of $A_0(t)$ are $(A_{00}, A_{01}, A_{02}) = (0, 1, 0)$ and $\mathbf{A}(t)$ has control points $\mathbf{A}_0 = (1, 0, 0)$, $\mathbf{A}_1 = (0, 1, 0)$, $\mathbf{A}_2 = (0, 0, 1)$ — namely

$$\mathbf{r}'(t) = [b_0^4(t) - b_4^4(t)]\mathbf{i} + [b_1^4(t) + b_3^4(t)]\mathbf{j} - b_2^4(t)\mathbf{k},$$

which satisfies $|\mathbf{r}'(t)|^2 = \sigma^2(t)$, where

$$\sigma(t) = b_0^4(t) + \frac{4}{3}b_2^4(t) + b_4^4(t).$$

The equation determining the ϕ values for a reflection representation becomes

$$\begin{vmatrix} \cos\phi & 0 & 0 \\ \sin\phi & \cos\phi & -\sin\phi \\ 0 & \sin\phi & \cos\phi \end{vmatrix} = (\sin^2\phi + \cos^2\phi)\cos\phi = 0,$$

so $\phi = \frac{1}{2}\pi$ or $\frac{3}{2}\pi$. For the former choice, we obtain $\mathbf{c} = \frac{1}{\sqrt{2}}(1, 0, 1)$ and hence

$$\mathbf{b}(t) = \frac{1}{\sqrt{2}} [(b_0^2(t) - b_2^2(t))\mathbf{i} + 2b_1^2(t)\mathbf{j} + (b_0^2(t) + b_2^2(t))\mathbf{k}].$$

One can verify that the pure vector quaternions $\mathcal{B}(t) = (0, \mathbf{b}(t))$ and $\mathcal{C} = (0, \mathbf{c})$ satisfy $\mathcal{B}(t)\mathcal{C} = \mathcal{A}(t)\mathcal{Q}(\phi)$, where $\mathcal{Q}(\phi) = (\cos\phi, \sin\phi\mathbf{i})$ with $\phi = \frac{1}{2}\pi$.

Given a vector polynomial $\mathbf{b}(t)$ and fixed unit vector \mathbf{c} , expression (22.27) with $\mathcal{B}(t) = (0, \mathbf{b}(t))$ and $\mathcal{C} = (0, \mathbf{c})$ generates a Pythagorean hodograph $\mathbf{r}'(t)$ in \mathbb{R}^3 from the unit reference vector \mathbf{i} by first reflecting it in the plane through the origin with normal \mathbf{c} , followed by a reflection in the plane with normal $\mathbf{b}(t)$ and scaling by $|\mathbf{b}(t)|^2$. In general, however, this form is only possible for PH quintics (and *a fortiori* PH cubics) because the identity (22.30) cannot be satisfied if the quaternion polynomial $\mathcal{A}(t)$ is of degree > 2 .

Now when $|\mathbf{c}| = 1$, the product $\mathcal{C}\mathbf{i}\mathcal{C}$ in (22.27) simply maps the unit vector \mathbf{i} into another unit vector in \mathbb{R}^3 . If we write $\mathbf{b}(t) = u(t)\mathbf{i} + v(t)\mathbf{j} + w(t)\mathbf{k}$, the product (22.27) taken with $\mathcal{C} = 1$ yields

$$\mathcal{B}(t) \mathbf{i} \mathcal{B}(t) = -[(u^2(t) - v^2(t) - w^2(t)) \mathbf{i} + 2u(t)v(t)\mathbf{j} + 2u(t)w(t)\mathbf{k}],$$

which (apart from sign) is the same as the form (21.14) of spatial Pythagorean hodographs, in terms of *three* polynomials, introduced in [188]. As previously noted, this form is only *sufficient* for a Pythagorean hodograph — it cannot generate all such hodographs if we fix coordinates in \mathbb{R}^3 by the vectors $\mathbf{i}, \mathbf{j}, \mathbf{k}$. Thus, the role of the initial reflection $\mathbf{i} \rightarrow \mathcal{C} \mathbf{i} \mathcal{C}$, with \mathbf{c} computed as described above, is essentially to construct coordinate axes under which a given spatial Pythagorean hodograph *can* be obtained through the reflection/scaling action of a pure vector quaternion polynomial $\mathcal{B}(t) = (0, \mathbf{b}(t))$.

An alternative formulation [358] for the reflection characterization (22.27) of spatial Pythagorean hodographs can be expressed in terms of the geometric product of vectors in Clifford algebra (see §6.4). This was used [358] to derive a vector-based solution to the first-order Hermite interpolation problem, as a counterpart to the quaternion-based solution described in Chap. 28.

22.5 One-to-one Correspondence?

In §19.2 the complex representation of planar PH curves was used to establish a one-to-one correspondence between the sets of (regular) polynomial curves and PH curves in \mathbb{R}^2 . This shows that, in a certain sense, planar PH curves are just as flexible as the “ordinary” planar polynomial curves. The question naturally arises as to whether an analogous correspondence can be established between the sets of spatial PH curves and “ordinary” polynomial curves in \mathbb{R}^3 . However, this proves to be a more subtle problem.

In the first place, we note that choosing the basis vector \mathbf{i} in the quaternion hodograph expression (22.2) — rather than any other unit vector \mathbf{n} — entails no loss of generality. Any Pythagorean hodograph $\mathbf{r}'(t) = \mathcal{A}(t) \mathbf{i} \mathcal{A}^*(t)$ referred to \mathbf{i} as the unit reference vector can be equivalently expressed in terms of any other unit vector \mathbf{n} as $\mathbf{r}'(t) = \tilde{\mathcal{A}}(t) \mathbf{n} \tilde{\mathcal{A}}^*(t)$, where $\tilde{\mathcal{A}}(t) = \mathcal{A}(t) \mathcal{U}$ for any unit quaternion \mathcal{U} that maps \mathbf{n} to \mathbf{i} — i.e., $\mathbf{i} = \mathcal{U} \mathbf{n} \mathcal{U}^*$. Discounting translational freedoms that arise on integrating a hodograph, the quaternion representation defines a one-to-one correspondence between spatial PH curves of odd degree n , and the equivalence classes of quaternion polynomials that are of the form $\mathcal{A}(t) (\cos \phi + \sin \phi \mathbf{i})$, where $\mathcal{A}(t) = u(t) + v(t) \mathbf{i} + p(t) \mathbf{j} + q(t) \mathbf{k}$ for real degree $\frac{1}{2}(n-1)$ polynomials $u(t), v(t), p(t), q(t)$ and $0 \leq \phi < 2\pi$.

However, taking $\gcd(u(t), v(t), p(t), q(t)) = \text{constant}$ does not ensure that $\mathbf{r}'(t) = (x'(t), y'(t), z'(t)) = \mathcal{A}(t) \mathbf{i} \mathcal{A}^*(t)$ is a *primitive* Pythagorean hodograph — i.e., that $\gcd(x'(t), y'(t), z'(t)) = \text{constant}$. As we shall see in §23.3 below, $\mathbf{r}'(t)$ may have a factorization of the form $a(t) \mathcal{B}(t) \mathbf{i} \mathcal{B}^*(t)$, where $a(t)$ is a real polynomial of degree $2m$ and the degree of $\mathcal{B}(t)$ is less than that of $\mathcal{A}(t)$ by m , even when $u(t), v(t), p(t), q(t)$ are relatively prime. One can show (see §23.3) that the polynomial $a(t)$ cannot have real roots, so although the hodograph $\mathbf{r}'(t)$ is non-primitive, the PH curve is regular: $|\mathbf{r}'(t)| \neq 0$ for all real t .

Thus, to identify a correspondence between regular spatial PH curves and regular “ordinary” polynomial space curves, and investigate the properties of corresponding curves, we require a correspondence between the hodographs of general polynomial curves in \mathbb{R}^3 and the equivalence classes of curves in \mathbb{H} of the form $\mathcal{A}(t)(\cos \phi + \sin \phi \mathbf{i})$, where $\mathcal{A}(t) = u(t) + v(t)\mathbf{i} + p(t)\mathbf{j} + q(t)\mathbf{k}$ with $\gcd(u(t), v(t), p(t), q(t)) = \text{constant}$ and ϕ is a free angular parameter. The manner in which to best define such a correspondence — in order to obtain a useful and interesting relationship between spatial PH curves and “ordinary” polynomial curves in \mathbb{R}^3 — remains an open question. The Hopf map model (see Remark 22.1) or reflection model (see §22.4) may prove to be a more fruitful context in which to identify such a correspondence.

23

Helical Polynomial Curves

A necessary and sufficient condition that a curve be of constant slope is that the ratio of curvature to torsion be constant.

“Theorem of Lancret” (1802), as quoted in [433]

A *helix* — or “curve of constant slope” — is characterized by the property that its tangent maintains a constant inclination relative to a fixed direction — the *axis* of the helix. Equivalently, a helix exhibits a circular *tangent indicatrix*, and the ratio of curvature and torsion remains constant along its length [290, 307, 433]. Whereas all spatial PH cubics are helical (see §21.1), the helical PH quintics constitute a proper subset of the spatial PH quintics.

There is an intimate connection between helices and PH curves — namely, a helical curve that admits a polynomial parameterization *must be a PH curve*. Such curves have the further attractive property that their Frenet frames, and their curvature and torsion, are *rational functions* of the curve parameter. In this chapter, we employ the quaternion representation of spatial PH curves to characterize and construct helical curves. We give a complete characterization for helical PH quintics, which are of two basic non-degenerate¹ types: (i) the “monotone-helical” PH quintics, in which a scalar quadratic factors out of the hodograph, and the tangent exhibits a fixed sense of rotation about the axis; and (ii) the general helical PH quintics, which possess irreducible hodographs and may suffer reversals in the sense of their tangent rotation.

In Chap. 28 we consider first-order Hermite interpolation for both types of helical PH quintic — see §28.7. The helicity property offers a geometrically motivated means of fixing the two residual degrees of freedom that arise in the general first-order Hermite interpolation problem using spatial PH quintics.

¹ Straight lines and planar curves are trivially helical — the conditions under which they arise, in the context of the quaternion representation, were identified in §22.2.

23.1 Helical Curves and PH Curves

In general, a helix is a curve whose unit tangent \mathbf{t} makes a constant angle ψ with a fixed direction in space (the *axis*), specified by a unit vector \mathbf{a} . Namely,

$$\mathbf{t} \cdot \mathbf{a} = \cos \psi = \text{constant}, \quad (23.1)$$

and hence a helix is also called a “curve of constant slope.” Any *planar* curve is trivially a helix, with axis \mathbf{a} orthogonal to the plane and $\psi = \frac{1}{2}\pi$. Henceforth, when we speak of a helix, we mean a *spatial* curve. Invoking the Frenet–Serret equations, it can be shown [290, 433] that condition (23.1) is equivalent to the requirement that the curvature κ and torsion τ along a helix satisfy²

$$\frac{\kappa}{\tau} = \tan \psi = \text{constant}. \quad (23.2)$$

The familiar circular helix, which lies on a cylinder of revolution, corresponds to the case where (23.2) holds because κ and τ are *individually* constant.

The *tangent indicatrix* or “spherical image” of a curve — i.e., the locus on the unit sphere traced by the curve tangent \mathbf{t} , considered to emanate from the origin — offers another characterization. Any curve whose tangent indicatrix is a circle on the unit sphere is a helix [307], the axis vector \mathbf{a} corresponding to the center of the circular tangent indicatrix on the sphere. For a proper (spatial) helix, the tangent indicatrix must be a *small circle* on the unit sphere, since a *great circle* indicatrix corresponds to a planar curve.

Choosing coordinates with z along the axis \mathbf{a} and x, y perpendicular to it, a helix can be parameterized in the form

$$x = x(s), \quad y = y(s), \quad z(s) = s \cos \psi.$$

A further characterization for helices is expressed [307] by the condition

$$(\mathbf{r}^{(2)} \times \mathbf{r}^{(3)}) \cdot \mathbf{r}^{(4)} \equiv 0,$$

where $\mathbf{r}^{(k)}$ denotes the k^{th} arc-length derivative of the curve.

For any helix, the instantaneous motion of the unit tangent amounts to a rotation about the axis \mathbf{a} . For a general helix, the *sense* of this rotation may exhibit reversals at points that have “stationary” tangents, and the tangent indicatrix will be doubly-traced in the vicinity of such points. Hence, we define a *monotone-helical curve* as a helix that maintains a constant sense of tangent rotation, and a one-to-one correspondence between points and tangents — i.e., its tangent indicatrix is a singly-traced circle.

The familiar circular helix is a *transcendental* curve, since it can intersect certain planes in an infinite number of points. For practical applications, we are usually concerned with *polynomial* curves. There is an intimate connection between polynomial curves, helices, and PH curves.

² For spatial curves, κ is by definition non-negative, but τ is a signed quantity. Hence, the constant in (23.2) may change sign at special points where $\kappa = \tau = 0$.

Lemma 23.1 *If a polynomial space curve is helical, it must be a PH curve.*

Proof : The unit tangent to a space curve $\mathbf{r}(t)$ is given by $\mathbf{t} = \mathbf{r}' / |\mathbf{r}'|$, and hence the helix condition (23.1) may be written as

$$\mathbf{a} \cdot \mathbf{r}'(t) = \cos \psi |\mathbf{r}'(t)|.$$

The left-hand side of this equation is evidently a polynomial in t , if $\mathbf{r}(t)$ is a polynomial curve. However, the right-hand side is a polynomial only if $\mathbf{r}(t)$ is a PH curve, since only PH curves have a polynomial speed $|\mathbf{r}'(t)|$. ■

Although a polynomial curve *must* be a PH curve in order to be helical, not all PH curves are helical. The lowest-order PH curves that are not helices are quintics. An algebraic condition for the helicity of PH curves may be derived from the characterization (23.2). From the definitions (8.67) and (8.72) of the curvature and torsion, a helix must satisfy

$$|\mathbf{r}' \times \mathbf{r}''|^3 = \tan \psi \sigma^3 (\mathbf{r}' \times \mathbf{r}'') \cdot \mathbf{r}''', \quad (23.3)$$

where $\sigma = |\mathbf{r}'|$. Now a spatial PH curve satisfies the condition (21.24), where the polynomial ρ defined by (21.25) or (21.26) is of degree $2n-6$ for a degree- n PH curve. Hence, for a PH curve, the helicity condition (23.3) becomes

$$\rho^{3/2} = \tan \psi (\mathbf{r}' \times \mathbf{r}'') \cdot \mathbf{r}''',$$

and since the expression on the right is clearly a polynomial in t , we infer the following characterization.

Lemma 23.2 *If a spatial PH curve is helical, the polynomial $\rho(t)$ defined by (21.25) or (21.26) must be a perfect square.*

For PH cubics, this condition is trivially satisfied, since $(\mathbf{r}' \times \mathbf{r}'') \cdot \mathbf{r}'''$ is a constant. For PH quintics, it is a polynomial of degree 6, and satisfaction of the helicity condition requires that $\rho(t)$ be the square of a quadratic polynomial. Another proof [33] for Lemma 23.2 is similar to the argument in Lemma 23.1. In Remark 21.1 we derived the helix axis \mathbf{a} in terms of the pitch angle ψ and curve tangent \mathbf{t} and binormal \mathbf{b} at each point in the form (21.2). Thus, from expression (8.69) for the binormal, a helical curve must satisfy

$$\mathbf{a} \cdot [\mathbf{r}'(t) \times \mathbf{r}''(t)] = \sin \psi |\mathbf{r}'(t) \times \mathbf{r}''(t)|.$$

Since the quantity on the left is a polynomial in t , a helical curve must have the property that $|\mathbf{r}'(t) \times \mathbf{r}''(t)|$ is a polynomial in t . To be helical, $\mathbf{r}(t)$ must a PH curve satisfying (21.24), and hence $\rho(t)$ must be a perfect square.

For a helical PH curve with $\rho(t) = \omega^2(t)$, the form (21.26) of ρ indicates that the polynomials $2(up' - u'p + vq' - v'q)$, $2(uq' - u'q - vp' + v'p)$, ω must comprise [33] a Pythagorean triple, and are thus (Theorem 17.1) of the form

$$\begin{aligned} 2(up' - u'p + vq' - v'q) &= k(a^2 - b^2), \\ 2(uq' - u'q - vp' + v'p) &= 2kab, \\ \omega &= k(a^2 + b^2), \end{aligned} \quad (23.4)$$

for certain polynomials $k(t)$, $a(t)$, $b(t)$ with $\gcd(a(t), b(t)) = \text{constant}$. Hence, helical PH curves have *rational Frenet frames*, defined by

$$\mathbf{t} = \frac{\mathbf{r}'}{\sigma}, \quad \mathbf{p} = \frac{\sigma\mathbf{r}'' - \sigma'\mathbf{r}'}{\sigma\omega}, \quad \mathbf{n} = \frac{\mathbf{r}' \times \mathbf{r}''}{\sigma\omega},$$

and also *rational curvature and torsion functions*, namely

$$\kappa = \frac{\omega}{\sigma^2} \quad \text{and} \quad \tau = \frac{(\mathbf{r}' \times \mathbf{r}'') \cdot \mathbf{r}'''}{\sigma^2\omega^2}.$$

Substituting for κ and τ into (23.2) we find that, for a helical PH curve, the scalar triple product of \mathbf{r}' , \mathbf{r}'' , \mathbf{r}''' has the interesting form

$$[\mathbf{r}'(t) \times \mathbf{r}''(t)] \cdot \mathbf{r}'''(t) = \tan \psi \omega^3(t).$$

The polynomial $\omega(t)$ is of degree $n - 3$ for a degree- n helical PH curve $\mathbf{r}(t)$.

23.2 Morphology of Helical PH Quintics

We may classify the possible types of helical PH quintics as follows. Without loss of generality, we take the helical axis in the positive x -direction — i.e., $\mathbf{a} = (1, 0, 0)$. Let ψ be the constant angle that the curve tangent makes with this axis. Then the defining equation (23.1) of the helix becomes

$$u^2 + v^2 - p^2 - q^2 = \cos \psi (u^2 + v^2 + p^2 + q^2).$$

This is equivalent to

$$\frac{p^2 + q^2}{u^2 + v^2} = \frac{1 - \cos \psi}{1 + \cos \psi} = \tan^2 \frac{1}{2}\psi,$$

where $0 \leq \psi \leq \pi$, but we may exclude the degenerate cases $\psi = 0$, $\frac{1}{2}\pi$, or π . We can re-arrange this equation to obtain either

$$(p - u \tan \frac{1}{2}\psi)(p + u \tan \frac{1}{2}\psi) = (v \tan \frac{1}{2}\psi - q)(v \tan \frac{1}{2}\psi + q), \quad (23.5)$$

or

$$(p - v \tan \frac{1}{2}\psi)(p + v \tan \frac{1}{2}\psi) = (u \tan \frac{1}{2}\psi - q)(u \tan \frac{1}{2}\psi + q). \quad (23.6)$$

Since the analysis of these equations is essentially the same, we focus on the former. For a helical PH quintic u, v, p, q are real quadratic polynomials, and are thus members of the unique factorization domain (UFD) $\mathbb{R}[t]$.

Consider first the case where equation (23.5) is actually of the form $0 = 0$. This means that $p = \pm u \tan \frac{1}{2}\psi$ and $q = \pm v \tan \frac{1}{2}\psi$, and hence

$$\begin{aligned} x' &= u^2 + v^2 - p^2 - q^2 = (1 - \tan^2 \frac{1}{2}\psi)(u^2 + v^2), \\ y' &= 2(uq + vp) = 2 \tan \frac{1}{2}\psi(\pm uv \pm uv), \\ z' &= 2(vq - up) = 2 \tan \frac{1}{2}\psi(\mp u^2 \pm v^2), \\ \sigma &= u^2 + v^2 + p^2 + q^2 = (1 + \tan^2 \frac{1}{2}\psi)(u^2 + v^2). \end{aligned}$$

Note that all four sign combinations are possible in the expressions for y' , z' . The tangent indicatrix $\mathbf{t} = (x', y', z')/\sigma$ thus has the components

$$\frac{x'}{\sigma} = \cos \psi = \text{constant}, \quad \frac{y'}{\sigma} = \sin \psi \frac{\pm uv \pm uv}{u^2 + v^2}, \quad \frac{z'}{\sigma} = \sin \psi \frac{\mp u^2 \pm v^2}{u^2 + v^2}.$$

If we choose unlike signs in y'/σ and like signs in z'/σ , the tangent indicatrix becomes the single point $(\cos \psi, 0, \sin \psi)$. We discount this case, in which the PH quintic degenerates to a straight line. However, if we choose like signs in y'/σ and unlike signs in z'/σ , the tangent indicatrix is a circle, and this circle is doubly-traced, since u and v are quadratic polynomials.

Now suppose that each of the factors in (23.5) is non-zero and irreducible. Since $\mathbb{R}[t]$ is a UFD, we must have

$$p - u \tan \frac{1}{2}\psi = \pm(v \tan \frac{1}{2}\psi - q), \quad p + u \tan \frac{1}{2}\psi = \pm(v \tan \frac{1}{2}\psi + q),$$

or

$$p - u \tan \frac{1}{2}\psi = \pm(v \tan \frac{1}{2}\psi + q), \quad p + u \tan \frac{1}{2}\psi = \pm(v \tan \frac{1}{2}\psi - q).$$

One can easily verify that these equations also reduce to the previous case — i.e., the tangent indicatrix is a single point or a doubly-traced circle. Likewise, if the left- and right-hand sides of (23.5) each have just one irreducible factor ($p - u \tan \frac{1}{2}\psi$ and $v \tan \frac{1}{2}\psi - q$, say), we again obtain the above equations.

The remaining case is that in which all the terms in (23.5) are products of linear factors. Since $\mathbb{R}[t]$ is a UFD, there can be at most four distinct linear factors, which we denote by a, b, c, d . Suppose that

$$p - u \tan \frac{1}{2}\psi = ab, \quad p + u \tan \frac{1}{2}\psi = cd.$$

To obtain results that differ from the preceding cases, we must choose different combinations

$$v \tan \frac{1}{2}\psi - q = ad, \quad v \tan \frac{1}{2}\psi + q = bc,$$

say, for $v \tan \frac{1}{2}\psi \pm q$. The tangent indicatrix then becomes

$$\frac{x'}{\sigma} = \cos \psi = \text{constant}, \quad \frac{y'}{\sigma} = \sin \psi \frac{2bd}{b^2 + d^2}, \quad \frac{z'}{\sigma} = \sin \psi \frac{b^2 - d^2}{b^2 + d^2}.$$

Since b and d are real linear polynomials, this defines a singly-traced circle.

In summary, there are three classes of helical PH quintics. We discount the first, in which the tangent indicatrix degenerates to a single point and the PH quintic is a straight line. The second and third types, in which the tangent indicatrix is respectively a singly- and doubly-traced circle,³ will be treated in §23.3 and §23.4. The characterization of helical PH quintic types is evidently equivalent to determining the nature of the parameterization of circular arcs on the unit sphere. Rational representations of circular arcs in computer aided geometric design have been discussed in detail by many authors [26, 92, 201].

23.3 Monotone-helical PH Quintics

Consider first the helical PH quintics that have rational quadratic (rather than quartic) tangent indicatrices. This degree reduction arises from a cancellation of factors common to all the hodograph components (21.20)–(21.21). Now the tangent indicatrix of a degree- n PH curve is, in general, a rational curve of degree $n - 1$ on the unit sphere. When the PH curve is helical, this tangent indicatrix becomes a circle (possibly multiply-traced).

We usually take polynomials with $\gcd(u, v, p, q) = \text{constant}$ in (21.20) since common real roots of these polynomials incur cusps on the curve. However, we shall presently see that

$$\gcd(u, v, p, q) = \text{constant} \not\Rightarrow \gcd(x', y', z') = \text{constant}$$

in (21.20) — the hodograph components may have common quadratic factors, with complex conjugate roots, even if $\gcd(u, v, p, q) = \text{constant}$.

A PH quintic is said to be *monotone-helical* if x' , y' , z' , σ possess a non-constant common factor, whose cancellation causes the tangent indicatrix to become a rational quadratic on the unit sphere — i.e., a *singly-traced* circle. To identify the monotone-helical PH curves, we first express the hodograph components (21.20) in terms of complex polynomials $u \pm i v$ and $p \pm i q$ as

$$\begin{aligned} x' &= u^2 + v^2 - p^2 - q^2 = (u + i v)(u - i v) - (p + i q)(p - i q), \\ y' &= 2(uq + vp) = i [(u - i v)(p - i q) - (u + i v)(p + i q)], \\ z' &= 2(vq - up) = -[(u - i v)(p - i q) + (u + i v)(p + i q)]. \end{aligned} \quad (23.7)$$

Hence $y' = z' = 0 \iff (u - i v)(p - i q) = (u + i v)(p + i q) = 0$. Coupled with the condition $(u + i v)(u - i v) = (p + i q)(p - i q)$ from $x' = 0$, we deduce that

$$x' = y' = z' = 0 \iff u + i v = p - i q = 0 \quad \text{or} \quad u - i v = p + i q = 0.$$

³ The singly- or doubly-traced property refers to the *entire* tangent indicatrix, for $-\infty < t < +\infty$. A doubly-traced indicatrix may seem singly-traced if restricted, for example, to the standard parameter interval $t \in [0, 1]$.

Furthermore, one can verify that multiple roots of either $u + i v = p - i q = 0$ or $u - i v = p + i q = 0$ are also multiple roots of $x' = y' = z' = 0$, with the same multiplicity. This implies that

$$\gcd(x', y', z') = \gcd(u + i v, p - i q) \cdot \gcd(u - i v, p + i q).$$

When u, v, p, q are real polynomials, $\gcd(u + i v, p - i q)$ and $\gcd(u - i v, p + i q)$ are conjugates, and we may write

$$\gcd(x', y', z') = |\gcd(u + i v, p - i q)|^2.$$

Thus, $\gcd(x', y', z')$ is evidently a real polynomial of *even* degree, whose roots occur only in complex conjugate pairs.

In the case of PH quintics, $\gcd(x', y', z')$ may be of degree 0, 2, or 4. The degree 0 case is generic, and in the degree 4 case the tangent indicatrix is just a single point (the PH quintic becomes a straight line). It is the degree 2 case that concerns us: the tangent indicatrix reduces to a rational quadratic curve on the unit sphere — which is necessarily planar, and hence circular, so the degree 2 case *always* defines a monotone–helical PH quintic.

In view of the preceding arguments, $\gcd(x', y', z')$ will be quadratic for a PH quintic when we have polynomials (in the real variable t) of the form

$$\begin{aligned} u + i v &= \zeta(t - \alpha)(t - \beta), & p - i q &= \eta(t - \alpha)(t - \gamma), \\ u - i v &= \bar{\zeta}(t - \bar{\alpha})(t - \bar{\beta}), & p + i q &= \bar{\eta}(t - \bar{\alpha})(t - \bar{\gamma}), \end{aligned} \quad (23.8)$$

where $\alpha, \beta, \gamma, \zeta, \eta$ are complex values. Thus, to construct a monotone–helical PH quintic, we select $\alpha, \beta, \gamma, \zeta, \eta$ and substitute them into the expressions

$$\begin{aligned} u(t) &= \operatorname{Re}(\zeta)t^2 - \operatorname{Re}(\zeta(\alpha + \beta))t + \operatorname{Re}(\zeta\alpha\beta), \\ v(t) &= \operatorname{Im}(\zeta)t^2 - \operatorname{Im}(\zeta(\alpha + \beta))t + \operatorname{Im}(\zeta\alpha\beta), \\ p(t) &= \operatorname{Re}(\eta)t^2 - \operatorname{Re}(\eta(\alpha + \gamma))t + \operatorname{Re}(\eta\alpha\gamma), \\ q(t) &= -\operatorname{Im}(\eta)t^2 + \operatorname{Im}(\eta(\alpha + \gamma))t - \operatorname{Im}(\eta\alpha\gamma). \end{aligned}$$

Example 23.1 The four complex numbers $\alpha = 1 + 2i$, $\beta = 3 - i$, $\gamma = 2 + i$, $\zeta = 1 + i$, $\eta = -2 - i$ yield the quadratic polynomials

$$\begin{aligned} u(t) &= t^2 - 3t, & v(t) &= t^2 - 5t + 10, \\ p(t) &= -2t^2 + 3t + 5, & q(t) &= t^2 - 9t + 10, \end{aligned}$$

which define the Pythagorean hodograph

$$\begin{aligned} x'(t) &= -3t^4 + 14t^3 - 36t^2 + 50t - 25, \\ y'(t) &= -2t^4 + 2t^3 - 14t^2 - 50t + 100, \\ z'(t) &= 6t^4 - 46t^3 + 1386t^2 - 250t + 200, \\ \sigma(t) &= 7t^4 - 46t^3 + 144t^2 - 250t + 225. \end{aligned}$$

By construction, these hodograph components possess the common factor

$$\begin{aligned} \gcd(u + i v, p - i q) \cdot \gcd(u - i v, p + i q) \\ = (t - 1 - 2i)(t - 1 + 2i) = t^2 - 2t + 5, \end{aligned}$$

and hence the tangent indicatrix reduces to the rational quadratic curve

$$\mathbf{t} = \frac{(-3t^2 + 8t - 5, -2t^2 - 2t + 20, 6t^2 - 34t + 40)}{7t^2 - 32t + 45}.$$

Now setting $\zeta = r \exp(i\phi)$ and $\eta = s \exp(i\theta)$ in (23.8) and substituting into (23.7), it becomes apparent that the hodograph components depend only on the difference $\varphi = \phi - \theta$. Thus, we obtain

$$\begin{aligned} x' &= |t - \alpha|^2 [r^2|t - \beta|^2 - s^2|t - \gamma|^2], \\ y' &= 2rs|t - \alpha|^2 \operatorname{Im} [e^{i\varphi}(t - \beta)(t - \bar{\gamma})], \\ z' &= -2rs|t - \alpha|^2 \operatorname{Re} [e^{i\varphi}(t - \beta)(t - \bar{\gamma})], \end{aligned} \quad (23.9)$$

as the most general hodograph form for a monotone-helical PH quintic. The real values r, s, φ and complex values α, β, γ amount to 9 scalar freedoms, as compared to 12 for general PH quintics. Since interpolation of first-order spatial Hermite data involves the satisfaction of 9 scalar equations, we might expect the monotone-helical PH quintics to be capable of solving the general first-order Hermite interpolation problem — we address this in §28.7.

23.4 General Helical PH Quintics

Consider now helical PH quintics with $\gcd(x', y', z') = \text{constant}$. We call such curves “general helical PH quintics” (since the monotone-helical PH quintics comprise a lower-dimension subset of all helical PH quintics). To identify the general helical PH quintics, we examine the behavior of the tangent indicatrix.

For a spatial PH quintic defined by the quaternion polynomial (22.6), the tangent indicatrix may be expressed as the rational quartic

$$\frac{\mathbf{r}'(t)}{|\mathbf{r}'(t)|} = \frac{\sum_{k=0}^4 w_k \mathbf{t}_k \binom{4}{k} (1-t)^{4-k} t^k}{\sum_{k=0}^4 w_k \binom{4}{k} (1-t)^{4-k} t^k}, \quad (23.10)$$

with weights w_0, \dots, w_4 and control points $\mathbf{t}_0, \dots, \mathbf{t}_4$ given by

$$\begin{aligned}
w_0 &= \mathcal{A}_0 \mathcal{A}_0^*, \\
w_1 &= \frac{1}{2}(\mathcal{A}_0 \mathcal{A}_1^* + \mathcal{A}_1 \mathcal{A}_0^*), \\
w_2 &= \frac{1}{6}(\mathcal{A}_0 \mathcal{A}_2^* + 4\mathcal{A}_1 \mathcal{A}_1^* + \mathcal{A}_2 \mathcal{A}_0^*), \\
w_3 &= \frac{1}{2}(\mathcal{A}_1 \mathcal{A}_2^* + \mathcal{A}_2 \mathcal{A}_1^*), \\
w_4 &= \mathcal{A}_2 \mathcal{A}_2^*,
\end{aligned} \tag{23.11}$$

and

$$\begin{aligned}
w_0 \mathbf{t}_0 &= \mathcal{A}_0 \mathbf{i} \mathcal{A}_0^*, \\
w_1 \mathbf{t}_1 &= \frac{1}{2}(\mathcal{A}_0 \mathbf{i} \mathcal{A}_1^* + \mathcal{A}_1 \mathbf{i} \mathcal{A}_0^*), \\
w_2 \mathbf{t}_2 &= \frac{1}{6}(\mathcal{A}_0 \mathbf{i} \mathcal{A}_2^* + 4\mathcal{A}_1 \mathbf{i} \mathcal{A}_1^* + \mathcal{A}_2 \mathbf{i} \mathcal{A}_0^*), \\
w_3 \mathbf{t}_3 &= \frac{1}{2}(\mathcal{A}_1 \mathbf{i} \mathcal{A}_2^* + \mathcal{A}_2 \mathbf{i} \mathcal{A}_1^*), \\
w_4 \mathbf{t}_4 &= \mathcal{A}_2 \mathbf{i} \mathcal{A}_2^*.
\end{aligned} \tag{23.12}$$

In terms of the scalar and vector parts of the quaternion coefficients $\mathcal{A}_i = (a_i, \mathbf{a}_i)$ the control points of the tangent indicatrix are

$$\begin{aligned}
\mathbf{t}_0 &= \frac{(a_0^2 - |\mathbf{a}_0|^2) \mathbf{i} + 2a_{0x} \mathbf{a}_0 - 2a_0 \mathbf{i} \times \mathbf{a}_0}{a_0^2 + |\mathbf{a}_0|^2}, \\
\mathbf{t}_1 &= \frac{(a_0 a_1 - \mathbf{a}_0 \cdot \mathbf{a}_1) \mathbf{i} + a_{1x} \mathbf{a}_0 + a_{0x} \mathbf{a}_1 - \mathbf{i} \times (a_1 \mathbf{a}_0 + a_0 \mathbf{a}_1)}{a_0 a_1 + \mathbf{a}_0 \cdot \mathbf{a}_1}, \\
\mathbf{t}_2 &= 2 \frac{(a_1^2 - |\mathbf{a}_1|^2) \mathbf{i} + 2a_{1x} \mathbf{a}_1 - 2a_1 \mathbf{i} \times \mathbf{a}_1}{2(a_1^2 + |\mathbf{a}_1|^2) + a_2 a_0 + \mathbf{a}_2 \cdot \mathbf{a}_0} \\
&\quad + \frac{(a_2 a_0 - \mathbf{a}_2 \cdot \mathbf{a}_0) \mathbf{i} + a_{0x} \mathbf{a}_2 + a_{2x} \mathbf{a}_0 - \mathbf{i} \times (a_0 \mathbf{a}_2 + a_2 \mathbf{a}_0)}{2(a_1^2 + |\mathbf{a}_1|^2) + a_2 a_0 + \mathbf{a}_2 \cdot \mathbf{a}_0}, \\
\mathbf{t}_3 &= \frac{(a_1 a_2 - \mathbf{a}_1 \cdot \mathbf{a}_2) \mathbf{i} + a_{2x} \mathbf{a}_1 + a_{1x} \mathbf{a}_2 - \mathbf{i} \times (a_2 \mathbf{a}_1 + a_1 \mathbf{a}_2)}{a_1 a_2 + \mathbf{a}_1 \cdot \mathbf{a}_2}, \\
\mathbf{t}_4 &= \frac{(a_2^2 - |\mathbf{a}_2|^2) \mathbf{i} + 2a_{2x} \mathbf{a}_2 - 2a_2 \mathbf{i} \times \mathbf{a}_2}{a_2^2 + |\mathbf{a}_2|^2}.
\end{aligned} \tag{23.13}$$

Now for any $\mathcal{A}_0, \mathcal{A}_1, \mathcal{A}_2$ equations (23.10)–(23.12) define a rational quartic on the unit sphere. A rational quartic may be either the *complete* intersection of two quadric surfaces — in which case it is the *base curve* of a one-parameter family or “pencil” of quadrics — or one component of a composite intersection of a quadric with a higher-order surface [422, 423, 437]. Such curves are called *quartics of the first kind* and *quartics of the second kind*, respectively.

To identify the type of quartic specified by (23.10)–(23.12), consider the general quadric equation

$$[W \ X \ Y \ Z] \begin{bmatrix} a & f & h & k \\ f & b & g & l \\ h & g & c & m \\ k & l & m & d \end{bmatrix} \begin{bmatrix} W \\ X \\ Y \\ Z \end{bmatrix} = 0$$

in homogeneous coordinates (W, X, Y, Z) . Substituting the four polynomials $W(t), X(t), Y(t), Z(t)$ of degree 4 that define (23.10) into the above, we obtain a polynomial of degree 8 in t . This polynomial must vanish identically if the quartic curve lies on the quadric surface. Setting its coefficients equal to zero yields a system of nine homogeneous linear equations in the ten quantities a, \dots, m . There is a unique solution⁴ if the matrix of this system has rank 9, and the quartic is then of the second kind. If it is only of rank 8, however, a one-parameter family of solutions exists, and the quartic is then of the first kind — i.e., it is the base curve of a pencil of quadrics. By use of a computer algebra system, it can be verified that the matrix is generically of rank 8 and hence the quartic defined by (23.10)–(23.12) is of the first kind.

To be a rational curve, a quartic of the first kind must be singular — i.e., it must have a double point [422, 423, 437] which may be a self-intersection, cusp, or isolated real point [270]. The double point of the indicatrix indicates the existence of two distinct curve points with the same tangent (or a point with “stationary” tangent in the case of a cusp). A special case arises when the tangent indicatrix reduces to a planar curve — namely, a *doubly-traced circle*. This case, characterized by the fact that each curve point has a corresponding point with the same tangent, identifies the (general) helical PH quintics.

Proposition 23.1 *A sufficient condition for (22.2) to define a helical quintic is that the quaternions $\mathcal{A}_0, \mathcal{A}_1, \mathcal{A}_2$ in (22.6) are linearly dependent.*

Proof : If $\mathcal{A}_0, \mathcal{A}_1, \mathcal{A}_2$ are linearly dependent, we can write

$$\mathcal{A}_1 = c_0 \mathcal{A}_0 + c_2 \mathcal{A}_2. \quad (23.14)$$

for suitable scalars c_0, c_2 . Equations (23.11) and (23.12) then become

$$\begin{aligned} w_0 &= \mathcal{A}_0 \mathcal{A}_0^*, \\ w_1 &= c_0 \mathcal{A}_0 \mathcal{A}_0^* + \frac{1}{2} c_2 (\mathcal{A}_0 \mathcal{A}_2^* + \mathcal{A}_2 \mathcal{A}_0^*), \\ w_2 &= \frac{1}{6} [4c_0^2 \mathcal{A}_0 \mathcal{A}_0^* + (1 + 4c_0 c_2)(\mathcal{A}_0 \mathcal{A}_2^* + \mathcal{A}_2 \mathcal{A}_0^*) + 4c_2^2 \mathcal{A}_2 \mathcal{A}_2^*], \\ w_3 &= \frac{1}{2} c_0 (\mathcal{A}_0 \mathcal{A}_2^* + \mathcal{A}_2 \mathcal{A}_0^*) + c_2 \mathcal{A}_2 \mathcal{A}_2^*, \\ w_4 &= \mathcal{A}_2 \mathcal{A}_2^*, \end{aligned} \quad (23.15)$$

⁴ We consider all multiples of a given set of coefficients a, \dots, m as constituting a single unique solution, since such coefficients define the same quadric surface.

and

$$\begin{aligned}
 w_0 \mathbf{t}_0 &= \mathcal{A}_0 \mathbf{i} \mathcal{A}_0^*, \\
 w_1 \mathbf{t}_1 &= c_0 \mathcal{A}_0 \mathbf{i} \mathcal{A}_0^* + \frac{1}{2} c_2 (\mathcal{A}_0 \mathbf{i} \mathcal{A}_2^* + \mathcal{A}_2 \mathbf{i} \mathcal{A}_0^*), \\
 w_2 \mathbf{t}_2 &= \frac{1}{6} [4c_0^2 \mathcal{A}_0 \mathbf{i} \mathcal{A}_0^* + (1 + 4c_0 c_2)(\mathcal{A}_0 \mathbf{i} \mathcal{A}_2^* + \mathcal{A}_2 \mathbf{i} \mathcal{A}_0^*) + 4c_2^2 \mathcal{A}_2 \mathbf{i} \mathcal{A}_2^*], \\
 w_3 \mathbf{t}_3 &= \frac{1}{2} c_0 (\mathcal{A}_0 \mathbf{i} \mathcal{A}_2^* + \mathcal{A}_2 \mathbf{i} \mathcal{A}_0^*) + c_2 \mathcal{A}_2 \mathbf{i} \mathcal{A}_2^*, \\
 w_4 \mathbf{t}_4 &= \mathcal{A}_2 \mathbf{i} \mathcal{A}_2^*. \tag{23.16}
 \end{aligned}$$

Now each point of the tangent indicatrix (23.10) is generated by a weighted sum of the control points $\mathbf{t}_0, \dots, \mathbf{t}_4$ and thus it is a planar locus if and only if these five control points are coplanar. Specifically, it is a *circle* if they are coplanar, since circles are the only plane curves on the sphere. To demonstrate coplanarity of $\mathbf{t}_0, \dots, \mathbf{t}_4$ under the assumption (23.14), consider the volumes of the tetrahedra defined by taking two distinct subsets of four points. Writing $\mathbf{t}_r = (t_{rx}, t_{ry}, t_{rz})$ two such volumes are

$$\left| \begin{array}{cccc} t_{0x} & t_{0y} & t_{0z} & 1 \\ t_{1x} & t_{1y} & t_{1z} & 1 \\ t_{2x} & t_{2y} & t_{2z} & 1 \\ t_{3x} & t_{3y} & t_{3z} & 1 \end{array} \right| \quad \text{and} \quad \left| \begin{array}{cccc} t_{1x} & t_{1y} & t_{1z} & 1 \\ t_{2x} & t_{2y} & t_{2z} & 1 \\ t_{3x} & t_{3y} & t_{3z} & 1 \\ t_{4x} & t_{4y} & t_{4z} & 1 \end{array} \right|, \tag{23.17}$$

and using a computer algebra system, one can verify symbolically⁵ that these determinants vanish for arbitrary $\mathcal{A}_0, \mathcal{A}_2$ and c_0, c_2 . Hence, condition (23.14) yields a circular tangent indicatrix — i.e., a helical PH quintic. ■

Although Proposition 23.1 was proved solely on the basis of planarity of the tangent indicatrix, the curves that satisfy the linear dependence condition (23.14) are general helical PH quintics — the monotone-helical PH quintics discussed in §23.3 do not, in general, satisfy this condition.

Remark 23.1 Condition (23.14) can be interpreted geometrically in terms of the *generalized stereographic projection* [130], which maps a point of three-dimensional projective space with homogeneous coordinates (u, v, p, q) to the point on the unit sphere with coordinates

$$\left(\frac{u^2 + v^2 - p^2 - q^2}{u^2 + v^2 + p^2 + q^2}, \frac{2(uq + vp)}{u^2 + v^2 + p^2 + q^2}, \frac{2(vq - up)}{u^2 + v^2 + p^2 + q^2} \right).$$

Expression (22.6) defines a straight line when (23.14) holds, and we interpret the quaternion components as three-dimensional homogeneous coordinates. According to Lemma 3.5 of [130], the generalized stereographic projection maps lines in three-dimensional projective space to circles on the unit sphere.

⁵ An alternative proof, that does not rely on computer algebra, is given in [164].

The helical PH quintics defined by (23.14) for given quaternions $\mathcal{A}_0, \mathcal{A}_2$ and different scalars c_0, c_2 are closely related, as shown in the following result.

Proposition 23.2 For a helical PH quintic defined by quaternion coefficients $\mathcal{A}_0, \mathcal{A}_1, \mathcal{A}_2$ where $\mathcal{A}_1 = c_0\mathcal{A}_0 + c_2\mathcal{A}_2$, the helix axis \mathbf{a} and angle ψ in (23.1) are independent of c_0, c_2 and are given by

$$\mathbf{a} = \frac{a_0\mathbf{a}_2 - a_2\mathbf{a}_0 + \mathbf{a}_0 \times \mathbf{a}_2}{|a_0\mathbf{a}_2 - a_2\mathbf{a}_0 + \mathbf{a}_0 \times \mathbf{a}_2|}, \quad (23.18)$$

$$\cos \psi = \frac{a_0a_{2x} - a_2a_{0x} - a_{0y}a_{2z} + a_{0z}a_{2y}}{|a_0\mathbf{a}_2 - a_2\mathbf{a}_0 + \mathbf{a}_0 \times \mathbf{a}_2|}. \quad (23.19)$$

Proof : For the tangent indicatrix (23.10) with control points and weights given by (23.15) and (23.16), the condition (23.1) is equivalent to

$$\sum_{k=0}^4 w_k (\mathbf{t}_k \cdot \mathbf{a} - \cos \psi) \binom{4}{k} (1-t)^{4-k} t^k \equiv 0,$$

which implies that

$$w_k (\mathbf{t}_k \cdot \mathbf{a} - \cos \psi) = 0, \quad k = 0, \dots, 4. \quad (23.20)$$

This amounts to five homogeneous linear equations in four unknowns, namely, $\cos \psi$ and the components a_x, a_y, a_z of \mathbf{a} (which also satisfy $a_x^2 + a_y^2 + a_z^2 = 1$). By using a computer algebra system, one can verify that (23.18) and (23.19) define a solution of this system for any c_0 and c_2 . ■

Example 23.2 With the choices $\mathcal{A}_0 = 5 + \mathbf{i} - \mathbf{j} + 3\mathbf{k}$, $\mathcal{A}_2 = -2 - 3\mathbf{i} + 2\mathbf{j} - 4\mathbf{k}$ and $c_0 = 1, c_2 = -3$ in (23.14), we obtain the polynomials

$$u(t) = -19t^2 + 12t + 5, \quad v(t) = -22t^2 + 18t + 1,$$

$$p(t) = 15t^2 - 12t - 1, \quad q(t) = -31t^2 + 24t + 3,$$

which yield the Pythagorean hodograph

$$\begin{aligned} x'(t) &= -341t^4 + 600t^3 - 270t^2 - 12t + 16, \\ y'(t) &= 518t^4 - 588t^3 - 206t^2 + 252t + 28, \\ z'(t) &= 1934t^4 - 2988t^3 + 770t^2 + 300t + 16, \\ \sigma(t) &= 2031t^4 - 3096t^3 + 738t^2 + 324t + 36. \end{aligned}$$

Since $\gcd(x', y', z') = \text{constant}$, the tangent indicatrix $\mathbf{t} = (x', y', z')/\sigma$ is a rational quartic in this case, corresponding to a doubly-traced circle — from Proposition 23.2, we can verify that it lies in the plane defined by

$$15x'(t) - 3y'(t) + 15z'(t) = 11\sigma(t).$$

The sufficient condition of Proposition 23.1 on the quaternion coefficients $\mathcal{A}_0, \mathcal{A}_1, \mathcal{A}_2$ to define a general helical PH quintic is attractive, on account of its simplicity. In the following section we will see that, in the generic case, this condition is also necessary. We also present sufficient and necessary conditions on $\mathcal{A}_0, \mathcal{A}_1, \mathcal{A}_2$ for monotone–helical PH quintics. These conditions are deferred to the end of this chapter since they are rather technical, and more algebraic than geometric in nature, being based on the analysis of solutions to (23.4).

23.5 Sufficient and Necessary Conditions

In §23.1 we noted that a spatial PH curve is helical if and only if the polynomial ρ in the relation (21.24) is a perfect square: $\rho = \omega^2$ for some polynomial $\omega(t)$. This means that the helical PH curves in \mathbb{R}^3 are characterized by a “double” Pythagorean hodograph structure [33] — the components of the vectors $\mathbf{r}'(t)$ and $\mathbf{r}'(t) \times \mathbf{r}''(t)$ must both satisfy Pythagorean constraints, namely

$$x'^2 + y'^2 + z'^2 \equiv \sigma^2 \quad (23.21)$$

and

$$(y'z'' - y''z')^2 + (z'x'' - z''x')^2 + (x'y'' - x''y')^2 \equiv (\sigma\omega)^2, \quad (23.22)$$

where σ and ω are polynomials in t . The latter condition is equivalent to the requirement that the polynomials $2(up' - u'p + vq' - v'q), 2(uq' - u'q - vp' + v'p)$, ω comprise a Pythagorean triple, and are thus of the form (23.4).

For PH quintics u, v, p, q are quadratic, and to satisfy (23.4) we must have either (i) $\deg(k) = 2$ and $a, b = \text{constant}$ or (ii) $k = \text{constant}$ and $\deg(a, b) = 1$. We shall see below that these two cases correspond, respectively, to the general helical and monotone–helical PH quintics. For this purpose, it is convenient to use again the representation (22.14), invoked previously to characterize linear and planar degenerations of the spatial PH quintics.

Lemma 23.3 *Let $\mathbf{r}(t)$ be a spatial PH curve with hodograph $\mathbf{r}' = \mathcal{A} \mathbf{i} \mathcal{A}^*$ and parametric speed $\sigma = |\mathcal{A}|^2$ specified by the quaternion polynomial (22.1). Then the second derivative of $\mathbf{r}(t)$ can be expressed in the form*

$$\mathbf{r}'' = \sigma' \mathbf{t} + \mathbf{s} \times \mathbf{t}, \quad (23.23)$$

where $\mathbf{t} = \mathbf{r}'/\sigma$ is the unit tangent, and the function

$$\begin{aligned} \mathbf{s} = & 2 [(uv' - u'v + pq' - p'q) \mathbf{i} \\ & + (up' - u'p - vq' + v'q) \mathbf{j} \\ & + (uq' - u'q + vp' - v'p) \mathbf{k}] \end{aligned} \quad (23.24)$$

corresponds to twice the vector part of $\mathcal{A}' \mathcal{A}^*$.

Proof : This follows ideas from theoretical kinematics [55]. Introducing the unit quaternion function $\mathcal{U}(t) = \mathcal{A}(t)/|\mathcal{A}(t)|$, we may write

$$\mathbf{r}' = \mathcal{A} \mathbf{i} \mathcal{A}^* = \sigma \mathcal{U} \mathbf{i} \mathcal{U}^*, \quad (23.25)$$

and differentiation yields

$$\mathbf{r}'' = \sigma' \mathcal{U} \mathbf{i} \mathcal{U}^* + \sigma (\mathcal{U}' \mathbf{i} \mathcal{U}^* + \mathcal{U} \mathbf{i} \mathcal{U}'^*). \quad (23.26)$$

Multiplying equation (23.25) on the left and the right by \mathcal{U}^* and \mathcal{U} , and using $\mathcal{U} \mathcal{U}^* = \mathcal{U}^* \mathcal{U} = 1$, yields

$$\mathbf{i} = \frac{\mathcal{U}^* \mathbf{r}' \mathcal{U}}{\sigma} = \mathcal{U}^* \mathbf{t} \mathcal{U}.$$

Substituting this into (23.26) then gives

$$\mathbf{r}'' = \sigma' \mathbf{t} + \sigma (\mathcal{U}' \mathcal{U}^* \mathbf{t} + \mathbf{t} \mathcal{U} \mathcal{U}'^*). \quad (23.27)$$

Since $\mathcal{U} \mathcal{U}^* = 1$, we have $\mathcal{U}' \mathcal{U}^* + \mathcal{U} \mathcal{U}'^* = 0$, and hence $\mathcal{U}' \mathcal{U}^*$ is a pure vector quaternion, $\mathbf{v}(t)$ say, so the quaternion product rule gives

$$\sigma (\mathcal{U}' \mathcal{U}^* \mathbf{t} + \mathbf{t} \mathcal{U} \mathcal{U}'^*) = 2\sigma \mathbf{v} \times \mathbf{t}. \quad (23.28)$$

Setting $\mathcal{U} = \mathcal{A}/\sqrt{\sigma}$, we can evaluate $\mathbf{v} = \mathcal{U}' \mathcal{U}^*$ as

$$\mathbf{v} = \frac{\mathcal{A}' \mathcal{A}^* - \frac{1}{2} \sigma'}{\sigma},$$

where $\sigma = u^2 + v^2 + p^2 + q^2$, $\sigma' = 2(uu' + vv' + pp' + qq')$, and we have

$$\begin{aligned} \mathcal{A}' \mathcal{A}^* &= (uu' + vv' + pp' + qq') + (uv' - u'v + pq' - p'q) \mathbf{i} \\ &\quad + (up' - u'p - vq' + v'q) \mathbf{j} + (uq' - u'q + vp' - v'p) \mathbf{k}. \end{aligned}$$

Thus the vector function $\mathbf{s}(t)$ in (23.24) corresponds to $2\sigma(t)\mathbf{v}(t)$. Substituting from (23.28) into (23.27), we obtain the quoted form (23.23) for $\mathbf{r}''(t)$. ■

Taking the cross product of $\mathbf{r}' = \sigma \mathbf{t}$ with \mathbf{r}'' , the first term on the right in (23.23) makes no contribution, and since \mathbf{t} is a unit vector we have

$$\mathbf{r}' \times \mathbf{r}'' = \sigma \mathbf{t} \times (\mathbf{s} \times \mathbf{t}) = \sigma [\mathbf{s} - (\mathbf{t} \cdot \mathbf{s}) \mathbf{t}]. \quad (23.29)$$

The squared magnitude of $\mathbf{r}' \times \mathbf{r}''$ is then given by

$$|\mathbf{r}' \times \mathbf{r}''|^2 = \sigma^2 [|\mathbf{s}|^2 - (\mathbf{t} \cdot \mathbf{s})^2] = \sigma^2 |\mathbf{s} \times \mathbf{t}|^2. \quad (23.30)$$

Thus, comparing (23.30) with (21.24), we find that

$$\rho = |\mathbf{s}|^2 - (\mathbf{t} \cdot \mathbf{s})^2 = |\mathbf{s} \times \mathbf{t}|^2. \quad (23.31)$$

Since the dot product of (21.23) and (23.24) reduces to

$$\mathbf{t} \cdot \mathbf{s} = 2(uv' - u'v - pq' + p'q),$$

the first expression for the polynomial ρ in (23.30) gives

$$\begin{aligned}\rho = 4 & [(uv' - u'v + pq' - p'q)^2 + (up' - u'p - vq' + v'q)^2 \\ & + (uq' - u'q + vp' - v'p)^2 - (uv' - u'v - pq' + p'q)^2].\end{aligned}$$

Thus, we encounter the chameleon-like polynomial ρ — expressed in terms of u, v, p, q and their derivatives — in yet another guise! One may easily verify its equivalence to the forms (21.25) and (21.26) quoted previously. The second expression for ρ in (23.31) gives another formulation, but not as concise.

As observed in §21.4, a spatial PH curve has curvature $\kappa(t) = \sqrt{\rho(t)/\sigma^2(t)}$. Since the derivative of the unit tangent \mathbf{t} is given by $\mathbf{t}' = \sigma\kappa \mathbf{p}$, the function $\sqrt{\rho(t)/\sigma(t)}$ may be identified with the rotation rate of \mathbf{t} when we interpret the curve parameter t as time. We have already noted that the helical PH curves correspond to cases for which $\rho(t)$ is a perfect square — i.e., $\rho(t) = \omega^2(t)$ for some polynomial $\omega(t)$, and hence we obtain an alternative characterization.

Lemma 23.4 *A spatial PH curve is helical if and only if the rotation rate of its unit tangent \mathbf{t} is a rational function $\omega(t)/\sigma(t)$ of the curve parameter.*

The expression (21.26) for ρ as a sum of squares is the most convenient for further analysis. This particular form appears to be closely related to the Hopf map model (see Remark 22.1) for spatial Pythagorean hodographs. Namely, if $\alpha(t) = u(t) + i v(t)$ and $\beta(t) = q(t) + i p(t)$ are the two complex polynomials used to generate a hodograph $\mathbf{r}'(t)$ through (22.9) and (22.10), we have

$$\alpha\beta' - \alpha'\beta = (uq' - u'q - vp' + v'p) + i(up' - u'p + vq' - v'q),$$

and thus

$$\rho(t) = 4 |\alpha(t)\beta'(t) - \alpha'(t)\beta(t)|^2.$$

The form (21.26) indicates that, if ρ is to be a perfect square, the polynomials $f = 2(up' - u'p + vq' - v'q)$ and $g = 2(uq' - u'q - vp' + v'p)$ must be of the form (23.4). We shall see that the degrees of the polynomials k, a, b in (23.4) serve to distinguish between general helical and monotone-helical PH quintics [33].

Proposition 23.3 *Let $\mathcal{A}_1, \mathcal{A}_2$ be expressed in terms of $\mathcal{A}_0 (\neq 0)$ as in (22.14). Then the spatial PH quintic with the control points (22.7) is a helix satisfying (23.4) with $a, b = \text{constant}$ and $\deg(k) = 2$ if and only if*

$$\gamma_1 : \gamma_2 = \delta_1 : \delta_2 \quad \text{and} \quad \beta_1 : \beta_2 = (\gamma_1^2 + \delta_1^2) : (\gamma_1\gamma_2 + \delta_1\delta_2). \quad (23.32)$$

Proof : In the case $a, b = \text{constant}$ and $\deg(k) = 2$, we take

$$k(t) = k_0(1-t)^2 + k_12(1-t)t + k_2t^2.$$

Let $\mathcal{A}_1, \mathcal{A}_2$ be given in terms of \mathcal{A}_0 as in equation (22.14) of Proposition 22.2, with components given by (22.15) for $r = 1, 2$. Then the Bernstein forms of the quadratic polynomials $f = 2(up' - u'p + vq' - v'q)$, $g = 2(uq' - u'q - vp' + v'p)$ are as determined in Proposition 22.2. We combine $f(t), g(t)$ into the complex polynomial $f(t) + ig(t)$ and the constants a, b into the complex number $a + ib$. Then condition (23.4) is equivalent to

$$\begin{aligned} 4|\mathcal{A}_0|^2 & [(f_0 + ig_0)(1-t)^2 + (f_1 + ig_1)2(1-t)t + (f_2 + ig_2)t^2] \\ &= (a^2 - b^2 + i2ab)[k_0(1-t)^2 + k_12(1-t)t + k_2t^2]. \end{aligned} \quad (23.33)$$

Clearly, this is satisfied for suitable choices of a, b and k_0, k_1, k_2 if and only if

$$f_0 : g_0 = f_1 : g_1 = f_2 : g_2,$$

i.e., if and only if

$$f_0g_1 - f_1g_0 = f_0g_2 - f_2g_0 = 0.$$

Substituting from (22.16) into these equations and simplifying, we obtain

$$\gamma_1\delta_2 - \gamma_2\delta_1 = (\gamma_1^2 + \delta_1^2)\beta_2 - (\gamma_1\gamma_2 + \delta_1\delta_2)\beta_1 = 0,$$

and the solutions may be characterized by the equality of ratios in (23.32). ■

We may consider any four of $\beta_1, \gamma_1, \delta_1, \beta_2, \gamma_2, \delta_2$ as free parameters, and the relations (23.32) then determine the other two. Note that the conditions for linear or planar PH quintics (see §22.2) are subsumed by (23.32). In the linear case (Proposition 22.2) we have $\gamma_1 = \gamma_2 = \delta_1 = \delta_2 = 0$, and conditions (23.32) are trivially satisfied, since $\gamma_1 : \gamma_2 = \delta_1 : \delta_2 = (\gamma_1^2 + \delta_1^2) : (\gamma_1\gamma_2 + \delta_1\delta_2) = 0 : 0$. For the planar case (Proposition 22.3), we have $\beta_1 = \beta_2 = \gamma_1\delta_2 - \gamma_2\delta_1 = 0$, so the first condition in (23.32) holds, and the second is trivially satisfied because $\beta_1 : \beta_2 = 0 : 0$. One can verify that, for non-zero $\beta_1, \gamma_1, \delta_1, \beta_2, \gamma_2, \delta_2$ values, the conditions (23.32) are equivalent to

$$\beta_1 : \beta_2 = \gamma_1 : \gamma_2 = \delta_1 : \delta_2. \quad (23.34)$$

Remark 23.2 Proposition 23.1 identified linear dependence of $\mathcal{A}_0, \mathcal{A}_1, \mathcal{A}_2$ — expressed by the relation (23.14) with real coefficients c_0, c_2 — as a sufficient condition for a helical PH quintic. We can now ascertain that, for the generic case with non-zero values in (23.34), this condition is also necessary. Namely, if ℓ is the proportionality constant in (23.34), then (23.14) holds⁶ with $c_0 = \alpha_1 - \alpha_2/\ell$ and $c_2 = 1/\ell$ when $\mathcal{A}_1, \mathcal{A}_2$ are written in the form (22.14).

Corollary 23.1 *The spatial PH quintics with quaternion coefficients (22.14) satisfying (23.32), so that $a, b = \text{constant}$ and $\deg(k) = 2$ in (23.4), correspond to general helical PH quintics.*

⁶ Note that homogeneous parameters can be used to accommodate the case $\ell = 0$.

Proof: To avoid technical diversions concerning degenerate cases, the proof is based on the form (23.34) of the sufficient-and-necessary conditions, valid for non-zero $\beta_1, \gamma_1, \delta_1, \beta_2, \gamma_2, \delta_2$. In this case, for some proportionality constant ℓ we have

$$\mathcal{A}_1 = \mathcal{A}_0(\alpha_1 + \beta_1\mathbf{i} + \gamma_1\mathbf{j} + \delta_1\mathbf{k}), \quad \mathcal{A}_2 = \mathcal{A}_0(\alpha_2 + \ell\beta_1\mathbf{i} + \ell\gamma_1\mathbf{j} + \ell\delta_1\mathbf{k}).$$

The components of the quaternions $\mathcal{A}_0, \mathcal{A}_1, \mathcal{A}_2$, i.e., the Bernstein coefficients of the polynomials $u(t), v(t), p(t), q(t)$, are then given by

$$\begin{aligned} u_0, \quad u_1 &= \alpha_1 u_0 - \beta_1 v_0 - \gamma_1 p_0 - \delta_1 q_0, \quad u_2 = \alpha_2 u_0 - \ell\beta_1 v_0 - \ell\gamma_1 p_0 - \ell\delta_1 q_0, \\ v_0, \quad v_1 &= \alpha_1 v_0 + \beta_1 u_0 - \gamma_1 q_0 + \delta_1 p_0, \quad v_2 = \alpha_2 v_0 + \ell\beta_1 u_0 - \ell\gamma_1 q_0 + \ell\delta_1 p_0, \\ p_0, \quad p_1 &= \alpha_1 p_0 + \beta_1 q_0 + \gamma_1 u_0 - \delta_1 v_0, \quad p_2 = \alpha_2 p_0 + \ell\beta_1 q_0 + \ell\gamma_1 u_0 - \ell\delta_1 v_0, \\ q_0, \quad q_1 &= \alpha_1 q_0 - \beta_1 p_0 + \gamma_1 v_0 + \delta_1 u_0, \quad q_2 = \alpha_2 q_0 - \ell\beta_1 p_0 + \ell\gamma_1 v_0 + \ell\delta_1 u_0. \end{aligned}$$

In §23.3 we observed that, if the hodograph components x', y', z' have non-constant common factors, they are given by

$$\gcd(x', y', z') = \gcd(u + i v, p - i q) \cdot \gcd(u - i v, p + i q).$$

Using the above coefficients, we form the complex polynomials $u(t) \pm i v(t)$ and $p(t) \mp i q(t)$ in MAPLE, and take their resultant with respect to t , to obtain

$$\text{Resultant}_t(u(t) \pm i v(t), p(t) \mp i q(t)) = |\mathcal{A}_0|^4 (\ell^2 - 4\alpha_1\ell + 4\alpha_2)(\gamma_1 \mp i\delta_1)^2.$$

Now $|\mathcal{A}_0| \neq 0$ by assumption, and in the generic case with non-zero γ_1, δ_1 we have $\gamma_1 \mp i\delta_1 \neq 0$ since γ_1, δ_1 are real. Hence, except for the particular choice

$$\alpha_2 = \ell \left(\alpha_1 - \frac{\ell}{4} \right), \quad (23.35)$$

we see that $\gcd(u \pm i v, p \mp i q) = \text{constant}$, so the PH quintic has no common hodograph factors, and it is thus a general (non-monotone) helix. It can be verified (see Remark 23.3) that the singular choice (23.35) for α_2 in terms of ℓ and α_1 identifies a monotone-helical PH quintic. ■

Example 23.3 For the general helical PH quintic in Example 23.2, we have

$$(\alpha_1, \beta_1, \gamma_1, \delta_1) = \frac{(39, 11, -13, 13)}{12}, \quad (\alpha_2, \beta_2, \gamma_2, \delta_2) = \frac{(-27, -11, 13, -13)}{36}$$

when $\mathcal{A}_1, \mathcal{A}_2$ are specified in terms of \mathcal{A}_0 by (22.14). One can easily verify that these values satisfy conditions (23.34). Figure 23.1 shows another example.

We now turn our attention to case (ii) for the satisfaction of (23.4). As we shall presently see, this identifies monotone-helical PH quintics.

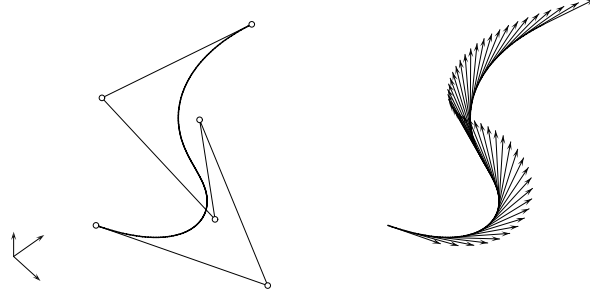


Fig. 23.1. Example of a general helical PH quintic, constructed in accordance with Proposition 23.3 using values $\mathcal{A}_0 = 1.6 - 0.4\mathbf{i} + 0.6\mathbf{j} + 1.0\mathbf{k}$, $\alpha_1 = -0.6$, $\beta_1 = -0.2$, $\gamma_1 = -0.4$, $\delta_1 = 0.4$, $\alpha_2 = 0.9$, and β_2 , γ_2 , δ_2 fixed by the proportionality constant $\ell = 0.5$ in (23.34). Left: PH curve and its Bézier control polygon. Right: the curve tangents exhibit a reversal in the sense of their rotation about the axis of the helix.

Proposition 23.4 Let $\mathcal{A}_1, \mathcal{A}_2$ be expressed in terms of \mathcal{A}_0 ($\neq 0$) as in (22.14). Then the spatial PH quintic with the control points (22.7) is a helix satisfying (23.4) with $\deg(a, b) = 1$ and $k = \text{constant}$ if and only if α_2, β_2 can be written in terms of $\alpha_1, \beta_1, \gamma_1, \delta_1$ and γ_2, δ_2 in the form

$$\alpha_2 = \frac{r\alpha_1 + s\beta_1}{\gamma_1^2 + \delta_1^2} + \frac{s^2 - r^2}{4(\gamma_1^2 + \delta_1^2)^2}, \quad \beta_2 = \frac{r\beta_1 - s\alpha_1}{\gamma_1^2 + \delta_1^2} + \frac{2rs}{4(\gamma_1^2 + \delta_1^2)^2} \quad (23.36)$$

where $r = \gamma_1\gamma_2 + \delta_1\delta_2$ and $s = \gamma_1\delta_2 - \gamma_2\delta_1$.

Proof : In the case $k = \text{constant}$ and $\deg(a, b) = 1$, we can take

$$k = 1, \quad a(t) = a_0(1-t) + a_1t, \quad b(t) = b_0(1-t) + b_1t$$

without loss of generality. Let $\mathcal{A}_1, \mathcal{A}_2$ be specified in terms of \mathcal{A}_0 as in equation (22.14) of Proposition 22.2, with components defined by (22.15) for $r = 1, 2$. Then the Bernstein forms of the polynomials $f = 2(up' - u'p + vq' - v'q)$ and $g = 2(uq' - u'q - vp' + v'p)$ are as given in Proposition 22.2. It is convenient to combine f, g and a, b into the complex polynomials $h(t) = f(t) + i g(t)$ and $c(t) = a(t) + i b(t)$, and (23.4) is then equivalent to $h(t) = c^2(t)$, where

$$c^2(t) = (a_0 + i b_0)^2(1-t)^2 + (a_0 + i b_0)(a_1 + i b_1)2(1-t)t + (a_1 + i b_1)^2t^2,$$

$$h(t) = 4|\mathcal{A}_0|^2[(f_0 + i g_0)(1-t)^2 + (f_1 + i g_1)2(1-t)t + (f_2 + i g_2)t^2].$$

Clearly, $h(t)$ coincides with $c^2(t)$ for suitable choices of a_0, a_1, b_0, b_1 if and only if its coefficients satisfy

$$(f_1 + i g_1)^2 = (f_0 + i f_0)(f_2 + i g_2)$$

or, equating real and imaginary parts, if and only if

$$f_1^2 - g_1^2 = f_0 f_2 - g_0 g_2 \quad \text{and} \quad 2f_1 g_1 = f_0 g_2 + f_2 g_0. \quad (23.37)$$

Substituting from (22.16) for the Bernstein coefficients⁷ of $f(t)$ and $g(t)$ into (23.37) gives two equations in the eight variables $\alpha_1, \beta_1, \delta_1, \gamma_1$ and $\alpha_2, \beta_2, \delta_2, \gamma_2$ which may be written as

$$\begin{aligned} 4(\gamma_1\gamma_2 - \delta_1\delta_2)\alpha_1 + 4(\gamma_1\delta_2 + \gamma_2\delta_1)\beta_1 - 4(\gamma_1^2 - \delta_1^2)\alpha_2 - 8\gamma_1\delta_1\beta_2 &= \gamma_2^2 - \delta_2^2, \\ 4(\gamma_1\delta_2 + \gamma_2\delta_1)\alpha_1 - 4(\gamma_1\gamma_2 - \delta_1\delta_2)\beta_1 - 8\gamma_1\delta_1\alpha_2 + 4(\gamma_1^2 - \delta_1^2)\beta_2 &= 2\gamma_2\delta_2. \end{aligned}$$

Now if $\gamma_1 = \delta_1 = 0$, all the terms on the left vanish, and then we must also have $\gamma_2 = \delta_2 = 0$ if these equations are to be satisfied. This circumstance identifies the degenerate case of a straight line (see Proposition 22.2). Discounting this case, we can be sure that $\gamma_1^2 + \delta_1^2 \neq 0$, and the real solutions of these equations for α_2, β_2 are then given in terms of $\alpha_1, \beta_1, \delta_1, \gamma_1, \delta_2, \gamma_2$ by expressions (23.36). Note that one could also solve for α_1, β_1 in terms of $\delta_1, \gamma_1, \alpha_2, \beta_2, \delta_2, \gamma_2$. ■

Corollary 23.2 *The spatial PH quintics with quaternion coefficients (22.14) satisfying (23.36), so that $\deg(a, b) = 1$ and $k = \text{constant}$ in (23.4), correspond to the monotone-helical PH quintics, and the quadratic common factor of their hodograph components is*

$$\gcd(x'(t), y'(t), z'(t)) = \omega(t),$$

where $\omega(t)$ is the polynomial defined in (23.4) by

$$\omega^2 = 4 [(up' - u'p + vq' - v'q)^2 + (uq' - u'q - vp' + v'p)^2] = (a^2 + b^2)^2.$$

Proof : We substitute from (23.36) into expressions (22.15) for $r = 1, 2$ and form the polynomials $u(t), v(t), p(t), q(t)$. Using MAPLE, we then obtain the quadratic polynomial

$$\begin{aligned} \gcd(u + i v, p - i q) \cdot \gcd(u - i v, p + i q) \\ = 4(\gamma_1^2 + \delta_1^2)(1-t)^2 + 2(\gamma_1\gamma_2 + \delta_1\delta_2)2(1-t)t + (\gamma_2^2 + \delta_2^2)t^2 \end{aligned}$$

as the common factor of all the hodograph components. Hence, the curve is a monotone-helical PH quintic. Furthermore, on forming the two polynomials $2(up' - u'p + vq' - v'q)$ and $2(uq' - u'q - vp' + v'p)$, we observe that the sum of their squares coincides (up to a constant factor) with the square of the above polynomial. Hence, for a monotone-helical PH curve, the common factor of the hodograph components is the polynomial ω defined by the helicity condition $\rho = 4 [(up' - u'p + vq' - v'q)^2 + (uq' - u'q - vp' + v'p)^2] = \omega^2$ (see §23.1). ■

Remark 23.3 For the generic case of helical PH quintics, characterized by equality of the ratios (23.34) with non-zero values, we have $r = \ell(\gamma_1^2 + \delta_1^2)$ and

⁷ Since equations (23.37) are homogeneous, we omit the common factor $4|\mathcal{A}_0|^2$.

$s = 0$ in Proposition 23.3 for a proportionality constant ℓ . Thus, substituting into (23.36), the conditions for a monotone–helical PH quintic become

$$\alpha_2 = \ell \left(\alpha_1 - \frac{\ell}{4} \right), \quad \beta_2 = \ell \beta_1.$$

This coincides with the singular case (23.35) of general helical PH quintics, for which the curve becomes monotone–helical, and the hodograph components may have a non–constant common factor. This factor proves to be a special quadratic polynomial — it is the perfect square of a linear polynomial, namely

$$\gcd(x'(t), y'(t), z'(t)) = [2(1-t) + \ell t]^2.$$

In Proposition 22.3, we specifically excluded curves with $\gcd(x', y', z') \neq$ constant from the quoted sufficient and necessary conditions for degeneration of spatial PH quintics into planar curves (other than straight lines). These cases correspond to the planar degenerations of monotone–helical PH quintics. Using MAPLE, we find that they correspond to solutions of either

$$\gamma_1 = 4\beta_1\delta_1 - \gamma_2 = 4\delta_1^2\beta_2 - 4\alpha_1\delta_1\gamma_2 + \gamma_2\delta_2 = 4\delta_1^2\alpha_2 - 4\alpha_1\delta_1\delta_2 + \delta_2^2 = 0$$

or

$$\begin{aligned} \beta_1\gamma_2 + \beta_2\gamma_1 - 4\alpha_1\beta_1\gamma_1 - 4\beta_1^2\delta_1 &= \gamma_1\delta_2 - \gamma_2\delta_1 + 4\beta_1\gamma_1^2 + 4\beta_1\delta_1^2 \\ &= 4\gamma_1^2\alpha_2 - 4\alpha_1\gamma_1\gamma_2 - 8\beta_1\delta_1\gamma_2 + 16\alpha_1\beta_1\gamma_1\delta_1 + 16\beta_1^2\delta_1^2 + \gamma_2^2 = 0. \end{aligned}$$

One may verify that such solutions are compatible with the forms (23.36) given in Proposition 23.4. They define planar curves whose hodograph components exhibit a common quadratic factor, that are not covered by the conditions of Proposition 22.3 for planar degeneration of spatial PH quintics.

Example 23.4 For the monotone–helical PH quintic curve in Example 23.1, the quaternion coefficients are

$$\mathcal{A}_0 = 10\mathbf{i} + 5\mathbf{j} + 10\mathbf{k}, \quad \mathcal{A}_1 = \frac{-3 + 15\mathbf{i} + 13\mathbf{j} + 11\mathbf{k}}{2}, \quad \mathcal{A}_2 = -2 + 6\mathbf{i} + 6\mathbf{j} + 2\mathbf{k}.$$

Expressing $\mathcal{A}_1, \mathcal{A}_2$ in terms of \mathcal{A}_0 in the form (22.14), we obtain

$$(\alpha_1, \beta_1, \gamma_1, \delta_1) = \frac{(13, 7, -1, -1)}{18} \quad \text{and} \quad (\alpha_2, \beta_2, \gamma_2, \delta_2) = \frac{(22, 14, -2, -2)}{45}.$$

One can easily verify that these coefficients satisfy the conditions (23.36) for a monotone–helical PH quintic. A further example of a monotone–helical PH curve, constructed using Proposition 23.4, is illustrated in Fig. 23.2.

We have remarked that helical PH curves are characterized by the “double” Pythagorean hodograph structure embodied in (23.21) and (23.22). This fact

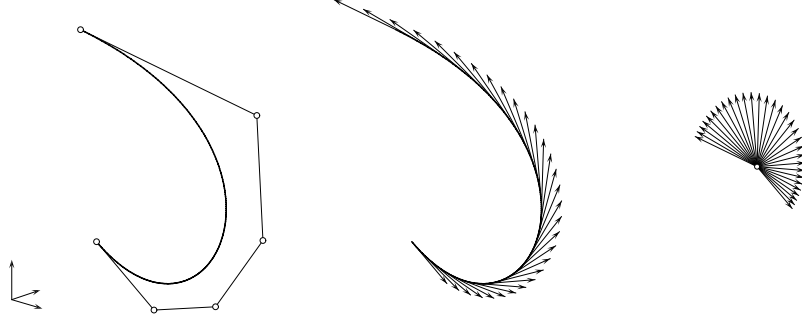


Fig. 23.2. Example of a monotone-helical PH quintic, constructed in accordance with Proposition 23.4 using values $\mathcal{A}_0 = 1.0 - 0.2\mathbf{i} + 0.6\mathbf{j} + 0.8\mathbf{k}$, $\alpha_1 = 0.6$, $\beta_1 = 0.2$, $\gamma_1 = -0.4$, $\delta_1 = 0.2$, $\gamma_2 = -0.8$, $\delta_2 = 1.0$, and α_2 , β_2 determined by (23.36). Left: PH curve with its Bézier control polygon. Center: the curve tangents exhibit a fixed sense of rotation about the helical axis. Right: when regarded as emanating from a common origin, the tangents all lie on the surface of a cone about the helical axis.

was independently deduced (and first published) by Beltran and Monterde [33] through somewhat different methods, and they also concluded that general helical and monotone-helical PH quintics correspond to a satisfaction of (23.4) with $\deg(k) = 2$ and $a, b = \text{constant}$, and $k = \text{constant}$ and $\deg(a, b) = 1$, respectively. Whereas all double PH cubics and quintics are helical, Beltran and Monterde identify a degree 7 double PH curve $\mathbf{r}(t)$, specified by

$$x(t) = \frac{1}{21} t^7 + \frac{1}{5} t^5 + t^3 - 3t, \quad y(t) = -\frac{1}{2} t^4 + 3t^2, \quad z(t) = -2t^3$$

with

$$|\mathbf{r}'(t)| = \frac{t^6 + 3t^4 + 9t^2 + 9}{3}$$

and

$$|\mathbf{r}'(t) \times \mathbf{r}''(t)| = 2(t^2 + 1)(t^6 + 3t^4 + 9t^2 + 9),$$

whose curvature/torsion ratio is non-constant — namely,

$$\frac{\kappa(t)}{\tau(t)} = -\frac{9(t^2 + 1)^2}{2t^6 + 9t^4 - 9}.$$

Thus, higher-order double PH curves exist that are *not* helical.

In general, the curvature/torsion ratio for a double PH curve is

$$\frac{\kappa(t)}{\tau(t)} = \frac{\omega^3(t)}{[\mathbf{r}'(t) \times \mathbf{r}''(t)] \cdot \mathbf{r}'''(t)}.$$

For PH cubics, the numerator and denominator are both constants, and hence they are all helices. For double PH quintics, the numerator and denominator

are constant multiples of each other, so all double PH quintics are helical. As seen in the above example, the lowest-order curves exhibiting the double PH structure that have a non-constant value for this ratio are of degree 7. For such curves, $2(up' - u'p + vq' - v'q)$ and $2(uq' - u'q - vp' + v'p)$ are degree 4, and they may satisfy (23.4) with either (i) $\deg(k) = 4$ and $a, b = \text{constant}$; or (ii) $\deg(k) = 2$ and $\deg(a, b) = 1$; or (iii) $k = \text{constant}$ and $\deg(a, b) = 2$.

24

Minkowski Pythagorean Hodographs

Henceforth space by itself, and time by itself, are doomed to fade away into mere shadows, and only a kind of union of the two will preserve an independent reality.

Hermann Minkowski (1908), as quoted in [327]

The *Minkowski Pythagorean hodograph curves* — or MPH curves for brevity — were first introduced by H. P. Moon¹ [328–330]. Their distinctive feature is that the hodographs satisfy a Pythagorean condition under the metric of the Minkowski space $\mathbb{R}^{2,1}$ with two “space-like” and one “time-like” coordinates, rather than the Euclidean metric of \mathbb{R}^3 with three space-like coordinates. The motivation for the definition of MPH curves is that they allow the *medial axis transform* of a planar domain to be specified in such a way that the domain boundary is exactly describable by rational curves. The medial axis transform (MAT) represents a planar domain as the union of a one-parameter family of variable-radius disks, and the problem of constructing the domain boundary from the MAT is a generalization of the problem of constructing offset curves, which correspond to envelopes of families of fixed-radius disks. Rationality of the domain boundary is ensured by requiring the components of a polynomial MAT to satisfy a Pythagorean condition under the metric of $\mathbb{R}^{2,1}$.

This chapter reviews the definitions and basic properties of MPH curves. Although the primary application of these curves is to the reconstruction of *planar* shapes in \mathbb{R}^2 from their medial axis transforms, the discussion of these curves is presented here since they are inherently *spatial* loci (although defined under a different metric). In §24.1 the Minkowski metric of $\mathbb{R}^{2,1}$ is introduced and its significance for medial axis transforms of planar domains is elucidated in §24.2. The polynomial solutions to a Pythagorean condition in $\mathbb{R}^{2,1}$ are then

¹ The fact that the acronym MPH is the mirror image of the inventor’s initials is, of course, purely coincidental. It is customary — even in Europe — to specify the parametric speed $\sigma(t)$ of MPH curves in miles per hour, not kilometers per hour.

characterized in §24.3, and are employed to construct MPH curves. A Clifford algebra model for these constructions is briefly described in §24.4. In §24.5 we survey the applications of MPH curves to boundary reconstruction of planar domains, through the approximation of smooth MAT segments. Finally, §24.6 discusses the extension of MPH curves to the Minkowski space $\mathbb{R}^{3,1}$.

24.1 The Minkowski Metric

In the special theory of relativity, time is regarded as a geometrical coordinate that augments the familiar spatial coordinates. However, as noted in §6.1, the temporal coordinate is treated differently from the spatial coordinates when computing the distance between points with given space–time coordinates: the squared difference of the time coordinates (multiplied by the speed of light) is *subtracted* from the sum of squared differences of the space coordinates. This imparts a fundamental distinction between space–time points or “events” that may influence each other (characterized by an imaginary distance or *time-like* separation), and those that may not (corresponding to a real distance or *space-like* separation). For zero distance, the points have *light-like* separation since they can be connected by signals propagating at the speed of light.

A space spanned by n “spatial” and one “temporal” coordinates, based on such a metric, is called the *Minkowski space* $\mathbb{R}^{n,1}$. Although its origins are in relativity, it also proves useful in many other contexts. Consider, for example, the *space of all circles* in the Euclidean plane \mathbb{R}^2 . A circle with center (x, y) and radius r can be represented by a point in a three-dimensional space with the coordinates (x, y, r) . To emphasize the different nature of the coordinates (x, y) and r — which we deem to be space–like and time–like, respectively — we shall identify this space² with $\mathbb{R}^{2,1}$ rather than \mathbb{R}^3 (the motivation for this will be apparent below). A family of circles with centers $(x(t), y(t))$ and radii $r(t)$ dependent on a real variable t corresponds to a curve in $\mathbb{R}^{2,1}$.

In accordance with the Minkowski metric, we define the distance $d(\mathbf{c}_1, \mathbf{c}_2)$ between two circles $\mathbf{c}_1 = (x_1, y_1, r_1)$ and $\mathbf{c}_2 = (x_2, y_2, r_2)$ in $\mathbb{R}^{2,1}$ by

$$d(\mathbf{c}_1, \mathbf{c}_2) = \sqrt{(x_1 - x_2)^2 + (y_1 - y_2)^2 - (r_1 - r_2)^2}. \quad (24.1)$$

The value of $d(\mathbf{c}_1, \mathbf{c}_2)$ is *real* or *imaginary* according to whether the distance $\sqrt{(x_1 - x_2)^2 + (y_1 - y_2)^2}$ between the two circle centers is greater than or less than the absolute value of the difference in their radii $|r_1 - r_2|$ (and zero when they are equal). Correspondingly, real and imaginary values of the distance (24.1) define *space-like* and *time-like* separation of the circles \mathbf{c}_1 and \mathbf{c}_2 , while zero distance corresponds to a *light-like* separation.

² In fact, we use only the subset of $\mathbb{R}^{2,1}$ specified by $r \geq 0$. In *Laguerre geometry* (see §20.6), a *signed* radius is invoked to distinguish between circles of clockwise and anti-clockwise orientation, but this is not needed in the present context.

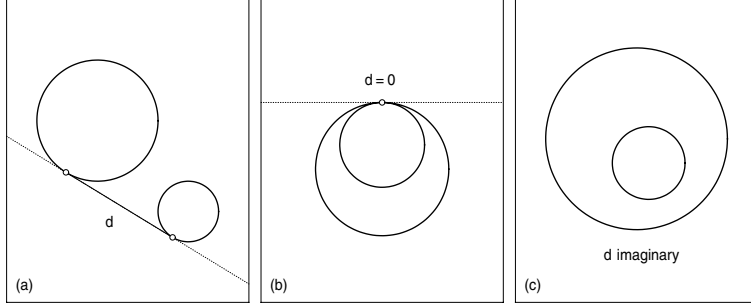


Fig. 24.1. Geometrical interpretation of the Minkowski distance (24.1) between two circles with coordinates (x_1, y_1, r_1) and (x_2, y_2, r_2) — (a) for circles with a common tangent, d is the distance between the points where it meets the two circles; (b) $d = 0$ for touching circles; and (c) for circles without a common tangent, d is imaginary.

The distance (24.1) between two circles can be interpreted geometrically as follows. If the two circles possess a common tangent, whose points of contact with the circles lie on the *same* side of the line that connects their centers, one can easily verify that the Minkowski distance is real and equal to the length of the tangent segment between these contact points.³ If the contact points of the common tangent coincide — i.e., the smaller circle is touching (and interior to) the larger circle — the Minkowski distance is zero. Finally, if the circles have no common tangent, the Minkowski distance becomes imaginary (this occurs when the distance between the centers is smaller than the absolute difference $|r_1 - r_2|$ of the radii). Figure 24.1 illustrates these possible configurations.

One can also define *vectors* in $\mathbb{R}^{2,1}$. For example, the separation between two points $\mathbf{p}_1 = (x_1, y_1, r_1)$ and $\mathbf{p}_2 = (x_2, y_2, r_2)$ is a vector. The *inner product* $\langle \mathbf{u}, \mathbf{v} \rangle$ of two vectors $\mathbf{u} = (u_x, u_y, u_r)$ and $\mathbf{v} = (v_x, v_y, v_r)$ is defined by

$$\langle \mathbf{u}, \mathbf{v} \rangle = u_x v_x + u_y v_y - u_r v_r.$$

Hence, the norm $|\mathbf{u}|$ of a single vector \mathbf{u} is given by $|\mathbf{u}|^2 = \langle \mathbf{u}, \mathbf{u} \rangle$. The vector \mathbf{u} is said to be *space-like*, *time-like*, or *light-like* according to whether $|\mathbf{u}|$ has a (positive) real, imaginary, or zero value — note that $|\mathbf{u}| = 0 \not\Rightarrow \mathbf{u} = (0, 0, 0)$. The set of light-like vectors defines the *light cone*, separating the sets of space-like and time-like vectors. The condition $\langle \mathbf{u}, \mathbf{v} \rangle = 0$ can be used to characterize *orthogonal* vectors in $\mathbb{R}^{2,1}$ — one of which must be space-like, and the other time-like (exceptionally, every light-like vector is self-orthogonal). Additional details on the geometry of Minkowski space can be found in [79].

Although the Minkowski distance violates the basic precepts of “ordinary” metric functions — its value is not always non-negative, it can vanish even if its arguments are distinct, and it does not satisfy the triangle inequality — it is nevertheless a useful tool for characterizing the behavior of one-parameter families of circles, in the context of medial axis transforms.

³ When $r_1 = r_2$, this length is simply the distance between the centers.

24.2 Medial Axis Transform

The *medial axis* of a planar domain is the locus of centers of maximal circles (touching the boundary in at least two⁴ points) inscribed within the domain: it provides a useful “shape abstraction” for planar domains. The medial axis transform (MAT) is defined by superposing a *radius function* on the medial axis, specifying the size of the maximal circles centered along it. The boundary of the domain can, in principle, be precisely re-constructed from its MAT [53]. Medial axes were originally proposed as a means of analyzing and comparing the morphological types of biological species [47–49]. The basic properties of MATs and algorithms for their construction have been discussed by many authors — see, for example, [83, 87, 301, 375, 408].

A closely-related idea is the *Voronoi diagram* of a planar domain bounded by N smooth curve segments, which partitions the plane into N regions such that every point of each Voronoi region is at least as close to its associated boundary segment as to all other segments. Whereas the medial axis depends only on the *geometry* of the boundary, the Voronoi diagram depends also on its *segmentation*. For example, the Voronoi diagram changes when a boundary segment is split in two, but the medial axis remains unaffected.

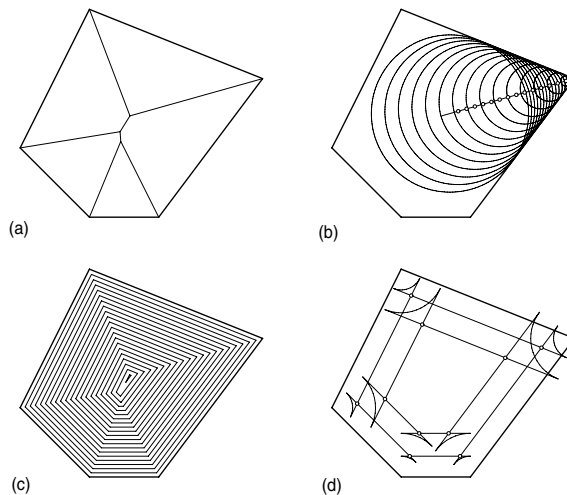


Fig. 24.2. (a) the medial axis of a convex polygon; (b) one segment of the medial axis as the locus of centers of maximal inscribed circles, defined by the radius function $r(t)$; (c) tangent discontinuities of the trimmed offset curves lie on the medial axis; and (d) they correspond to self-intersection points of the untrimmed offset curves.

⁴ For the limiting case in which the maximal circle osculates the boundary, it may be considered to have two *coincident* contact points with the domain boundary. The centers of maximal circles with $n \geq 3$ points of contact with the boundary identify *branch points*, from which n edges of the medial axis emanate.

The computation of medial axes or Voronoi diagrams can be a valuable pre-processing step in a variety of applications — such as tool path generation for NC machining [90, 232, 357]; finite element meshing [221, 425, 435]; font design [87]; surface fitting [218]; image compression [57]; pattern analysis and shape recognition [49, 53]; and determination of equivalent resistance networks for VLSI circuits [325]. The medial axis can greatly simplify [232, 357] the offset-trimming problem (see §8.3.5), since the self-intersection points — at which the untrimmed offsets should be trimmed — lie on the medial axis. Figure 24.2 illustrates this for the simple case of a convex polygonal boundary, for which the medial axis comprises only straight-line segments. In fact, by using the medial axis to restrict *a priori* the parameter domains of the (interior) offset curves at distance d from each boundary segment to those intervals for which $r(t) > d$, the trimming problem can be entirely circumvented.

The medial axis and Voronoi diagram of a planar domain may be regarded as graphs, whose edges are portions of *point/curve bisectors* and *curve/curve bisectors*, i.e., loci that are equidistant from certain points or curve segments of the domain boundary. For domains with piecewise-linear/circular boundaries, these bisectors are just conic arcs, and efficient algorithms have been developed [232, 278, 301, 373, 424, 476] that yield essentially *exact* Voronoi diagram and medial axis constructions. For domains bounded by free-form (polynomial or rational) curves, however, these constructions are more difficult⁵ — although point/curve bisectors are generically rational loci, curve/curve bisectors do not admit exact “simple” representations [165, 166, 183, 184] and approximations are therefore necessary [19, 83, 87, 91, 375]. By employing the Minkowski PH curves, described below, as approximants to curve/curve bisectors and their associated radius functions, we can guarantee that the reconstructed domain boundary consists of only *rational* curve segments.

Consider a one-parameter family of circles specified by centers $(x(t), y(t))$ and radii $r(t)$. Such a family may be parameterized by

$$\mathbf{r}(t, \theta) = (x(t) + r(t) \cos \theta, y(t) + r(t) \sin \theta) \quad (24.2)$$

where t is the family parameter and θ is the curve parameter. The relationship identifying the points θ of each circle t that contribute to the envelope of the family (see §8.2.3) is

$$\frac{\partial \mathbf{r}}{\partial t} \parallel \frac{\partial \mathbf{r}}{\partial \theta},$$

which yields the equation

$$x'(t) \cos \theta + y'(t) \sin \theta + r'(t) = 0.$$

Solving this simultaneously with $\cos^2 \theta + \sin^2 \theta = 1$ for $\cos \theta$ and $\sin \theta$ gives

⁵ Note that making a piecewise-linear approximation of a free-form boundary and invoking a polygonal algorithm is not, in general, a satisfactory approach, since it may generate results that are not even *topologically* correct.

$$\begin{aligned}\cos \theta &= -\frac{r'(t)x'(t) \pm \sqrt{x'^2(t) + y'^2(t) - r'^2(t)} y'(t)}{x'^2(t) + y'^2(t)}, \\ \sin \theta &= -\frac{r'(t)y'(t) \mp \sqrt{x'^2(t) + y'^2(t) - r'^2(t)} x'(t)}{x'^2(t) + y'^2(t)}.\end{aligned}\quad (24.3)$$

There are two solutions for every t since each circle contributes, in general, two distinct points to the envelope. Substituting these expressions into (24.2) then gives an explicit parameterization $\mathbf{e}(t) = (x_e(t), y_e(t))$ of the envelope as

$$\begin{aligned}x_e(t) &= x(t) - r(t) \frac{r'(t)x'(t) \pm \sqrt{x'^2(t) + y'^2(t) - r'^2(t)} y'(t)}{x'^2(t) + y'^2(t)}, \\ y_e(t) &= y(t) - r(t) \frac{r'(t)y'(t) \mp \sqrt{x'^2(t) + y'^2(t) - r'^2(t)} x'(t)}{x'^2(t) + y'^2(t)}.\end{aligned}\quad (24.4)$$

We note that $\mathbf{e}(t) = (x_e(t), y_e(t))$ is not, in general, a rational curve — even if $x(t), y(t), r(t)$ are rational functions — because of the presence of the radical $\sqrt{x'^2(t) + y'^2(t) - r'^2(t)}$. Note also that any MAT segment $(x(t), y(t), r(t))$ in $\mathbb{R}^{2,1}$ must be space-like — i.e., it must satisfy $x'^2(t) + y'^2(t) - r'^2(t) \geq 0$ — in order to generate a real segment of the envelope $\mathbf{e}(t)$.

Remark 24.1 When $r(t) = \text{constant} (= d, \text{say})$ the envelope equations (24.4) define the offsets at distance $\pm d$ from the medial axis curve $(x(t), y(t))$. Also, if we replace $r(t)$ by $r(t) \pm d$, these equations define the interior/exterior offsets at distance d from the domain boundary curve $\mathbf{e}(t)$.

24.3 Minkowski PH Curves in $\mathbb{R}^{2,1}$

The rationality of the fixed-distance offsets (17.18) to a (Euclidean) PH curve $\mathbf{r}(t) = (x(t), y(t))$ in \mathbb{R}^2 arises from the fact that its hodograph satisfies (17.1), and hence the radical term $\sqrt{x'^2(t) + y'^2(t)}$ incurred by the unit normal $\mathbf{n}(t)$ is simply a polynomial, $\sigma(t)$. In an analogous manner, Minkowski PH curves are based upon the requirement that the radical term $\sqrt{x'^2(t) + y'^2(t) - r'^2(t)}$ coincides with a polynomial $\sigma(t)$, ensuring that the envelope (24.4) of a family of variable-radius circles with centers $(x(t), y(t))$ and radii $r(t)$ is a rational locus. A characterization of curves in $\mathbb{R}^{2,1}$ that satisfy this requirement was first presented by H. P. Moon [328–330] as follows.

Theorem 24.1 *A polynomial curve $(x(t), y(t), r(t))$ in the Minkowski space $\mathbb{R}^{2,1}$ satisfies the Pythagorean condition*

$$x'^2(t) + y'^2(t) - r'^2(t) = \sigma^2(t)\quad (24.5)$$

for some polynomial $\sigma(t)$ if and only if $x'(t), y'(t), r'(t), \sigma(t)$ can be expressed in terms of four polynomials $u(t), v(t), p(t), q(t)$ in the form

$$\begin{aligned}x'(t) &= u^2(t) + v^2(t) - p^2(t) - q^2(t), \\y'(t) &= 2[u(t)p(t) - v(t)q(t)], \\r'(t) &= 2[u(t)v(t) - p(t)q(t)], \\\sigma(t) &= u^2(t) - v^2(t) + p^2(t) - q^2(t).\end{aligned}\quad (24.6)$$

Proof : The proof is adapted from [329]. The sufficiency of the form (24.6) for satisfying (24.5) follows from substituting into this equation. To see that the form (24.6) is also necessary, we re-write (24.5) as

$$y'^2(t) - r'^2(t) = \sigma^2(t) - x'^2(t),$$

which may be factorized to obtain

$$\frac{1}{2}[y'(t) + r'(t)]\frac{1}{2}[y'(t) - r'(t)] = \frac{1}{2}[\sigma(t) + x'(t)]\frac{1}{2}[\sigma(t) - x'(t)].$$

Since the four real polynomials above have unique real factorizations, they must be of the form

$$\frac{1}{2}[\sigma(t) + x'(t)] = a(t)b(t), \quad \frac{1}{2}[\sigma(t) - x'(t)] = c(t)d(t), \quad (24.7)$$

$$\frac{1}{2}[y'(t) + r'(t)] = a(t)c(t), \quad \frac{1}{2}[y'(t) - r'(t)] = b(t)d(t), \quad (24.8)$$

for certain real polynomials $a(t)$, $b(t)$, $c(t)$, $d(t)$. Writing

$$u(t) = \frac{1}{2}[a(t) + b(t)], \quad v(t) = \frac{1}{2}[c(t) - d(t)],$$

$$p(t) = \frac{1}{2}[c(t) + d(t)], \quad q(t) = \frac{1}{2}[b(t) - a(t)],$$

we have

$$u^2(t) - q^2(t) = a(t)b(t), \quad [u(t) - q(t)][p(t) + v(t)] = a(t)c(t),$$

$$p^2(t) - v^2(t) = c(t)d(t), \quad [u(t) + q(t)][p(t) - v(t)] = b(t)d(t).$$

Substituting into (24.7) and (24.8), we obtain expressions (24.6) upon solving for $x'(t)$, $y'(t)$, $r'(t)$, $\sigma(t)$. ■

For MPH curves, the envelope equations (24.4) reduce to the *rational* forms

$$\begin{aligned}x_e(t) &= x(t) - r(t) \frac{r'(t)x'(t) \pm \sigma(t)y'(t)}{x'^2(t) + y'^2(t)}, \\y_e(t) &= y(t) - r(t) \frac{r'(t)y'(t) \mp \sigma(t)x'(t)}{x'^2(t) + y'^2(t)},\end{aligned}\quad (24.9)$$

where $x(t)$, $y(t)$, $r(t)$ are defined by integrating $x'(t)$, $y'(t)$, $r'(t)$ with suitable integration constants. If the polynomials $u(t)$, $v(t)$, $p(t)$, $q(t)$ are of degree μ at most, then $(x(t), y(t), r(t))$ is a polynomial MAT of degree $n = 2\mu + 1$, and the envelope curve $(x_e(t), y_e(t))$ is a rational curve of degree $6\mu + 1 = 3n - 2$.

However, choosing relatively prime polynomials $u(t), v(t), p(t), q(t)$ in (24.6) does not guarantee $\gcd(x', y', r') = \text{constant}$ — one can easily verify that

$$\gcd(x', y', r') = \gcd(u + q, v + p) \cdot \gcd(u - q, v - p),$$

and only one of the terms on the right may be non-constant if $\gcd(u, v, p, q) = \text{constant}$. If $\gcd(x', y', r')$ is of degree ν ($\leq \mu$), the degree of the envelope curve is reduced by a cancellation of common factors to $3n - 2 - 2\nu$.

For a given MPH curve, the rational unit vectors

$$\mathbf{m}(t) = -\left(\frac{r'(t)x'(t) \pm \sigma(t)y'(t)}{x'^2(t) + y'^2(t)}, \frac{r'(t)y'(t) \mp \sigma(t)x'(t)}{x'^2(t) + y'^2(t)}\right)$$

define the direction of the two displacements by $r(t)$ from the point $(x(t), y(t))$ that identify envelope points contributed by a circle with the corresponding radius and center. Since $\mathbf{m}(t)$ depends only on the derivative $r'(t)$ of the radius function, it is unchanged if we add any constant d to $r(t)$ — which corresponds to specifying the *offset curve* at distance d from the nominal envelope [329]. Hence, MPH curves have the property that not only the envelope curve, but also *all its fixed-distance offsets*, are rational loci

In §22.3 we emphasized the importance of *rotation invariance* for PH curve representations in \mathbb{R}^3 . Orthogonal linear maps of the Minkowski space $\mathbb{R}^{2,1}$ are known as *Lorentz transformations* — they preserve the norms and inner products of vectors in this space. It can be shown [329] that the Pythagorean hodograph form (24.6) is invariant with respect to such transformations.

Example 24.1 Substituting the linear Bernstein-form polynomials

$$u(t) = 2(1-t) + 3t, \quad v(t) = (1-t), \quad p(t) = (1-t) - t, \quad q(t) = (1-t) - 2t$$

into (24.6) gives the quadratic Minkowski Pythagorean hodograph defined by

$$\begin{aligned} x'(t) &= 3(1-t)^2 + 9 \cdot 2(1-t)t + 4t^2, \\ y'(t) &= 2(1-t)^2 + 3 \cdot 2(1-t)t - 6t^2, \\ r'(t) &= 2(1-t)^2 + 6 \cdot 2(1-t)t - 4t^2, \\ \sigma(t) &= 3(1-t)^2 + 7 \cdot 2(1-t)t + 6t^2. \end{aligned}$$

Taking $(x_0, y_0, r_0) = (1, 1, 1)$ as integration constants, the MPH cubic defined by integrating this hodograph has the additional control points

$$(x_1, y_1, r_1) = \frac{(6, 5, 5)}{3}, \quad (x_2, y_2, r_2) = \frac{(15, 8, 11)}{3}, \quad (x_3, y_3, r_3) = \frac{(19, 2, 7)}{3}.$$

Figure 24.3 illustrates this MPH cubic for $t \in [0, 1]$ as a curve in $\mathbb{R}^{2,1}$ with the medial axis (i.e., locus of circle centers) obtained by projection onto the (x, y) plane. Also shown is a sampling of the one-parameter family of circles defined by the MPH curve, with its rational envelope defined by (24.9).

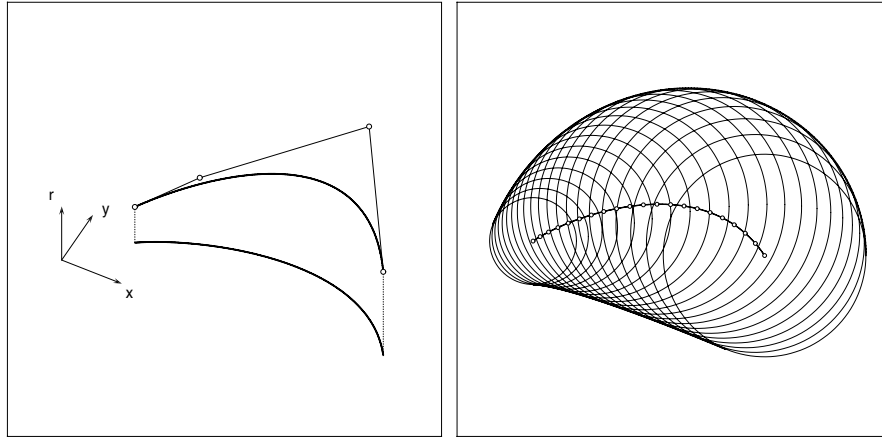


Fig. 24.3. The cubic Minkowski Pythagorean–hodograph curve from Example 24.1. Left: the cubic MPH curve shown in $\mathbb{R}^{2,1}$ with its medial axis curve projected onto the (x, y) plane. Right: The one–parameter family of circles specified by the cubic MPH curve, together with its medial axis and rational envelope curve (of degree 7).

In Example 24.1, the polynomial $\sigma(t)$ is clearly positive for $t \in [0, 1]$ since its Bernstein coefficients are all positive. In general, however, $\sigma(t)$ may have real roots and thus change sign over a given interval in t . Each segment of the MPH curve $(x(t), y(t), r(t))$ between such roots is space–like — i.e., it satisfies $x'^2(t) + y'^2(t) - r'^2(t) > 0$ — by virtue of condition (24.5). The significance of parameter values where $\sigma(t) = 0$ is seen by noting that, at such values, the two distinct boundary points defined by (24.9) coalesce into the *single* point

$$x_e(t) = x(t) - r(t) \frac{x'(t)}{r'(t)}, \quad y_e(t) = y(t) - r(t) \frac{y'(t)}{r'(t)}.$$

As remarked in §24.2, a point of the medial axis for which the maximal circle exhibits a coalescence of its two points of contact of with the domain boundary identifies the center of a circle that *osculates* the boundary. At such points, the MPH curve becomes “light–like” rather than “space–like” — they typically represent the termination of a medial axis edge.

24.4 Clifford Algebra Representation

In Chaps. 19 and 22 we have discussed how Pythagorean hodographs in the Euclidean spaces \mathbb{R}^2 and \mathbb{R}^3 admit simple algebraic formulations in terms of complex numbers and quaternions, respectively. It seems natural to enquire whether the hodograph form (24.6) appropriate to the Minkowski space $\mathbb{R}^{2,1}$ can also be interpreted as a kind of geometrical product.

This question was addressed by Choi et al. [89], who used Clifford algebra methods (see Chap. 6) to elucidate the algebraic structure of Pythagorean hodographs in Euclidean and Minkowski spaces of dimension two, three, and four. Specifically, it was shown in [89] that the forms (17.4), (21.20), and (24.6) can be viewed as particular instances of a *PH representation map*, defined by a polynomial expression in an appropriate Clifford algebra.

The Clifford algebras appropriate to \mathbb{R}^2 and \mathbb{R}^3 are the even sub-algebras $\mathcal{C}\ell_2^+$ and $\mathcal{C}\ell_3^+$ of $\mathcal{C}\ell_2$ and $\mathcal{C}\ell_3$ — and, as observed in §6.1, these are isomorphic to the complex numbers \mathbb{C} and quaternions \mathbb{H} . For $\mathbb{R}^{2,1}$ the appropriate setting is the even sub-algebra $\mathcal{C}\ell_{2,1}^+$ of $\mathcal{C}\ell_{2,1}$ — whose basis elements $\mathbf{e}_1, \mathbf{e}_2, \mathbf{e}_3$ are characterized by the properties

$$\mathbf{e}_1^2 = \mathbf{e}_2^2 = 1 = -\mathbf{e}_3^2 \quad \text{and} \quad \mathbf{e}_j \mathbf{e}_k = -\mathbf{e}_k \mathbf{e}_j \quad \text{if } j \neq k.$$

Consider a polynomial in the real parameter t of the form

$$P(t) = u(t) + v(t)\mathbf{e}_3\mathbf{e}_1 - p(t)\mathbf{e}_1\mathbf{e}_2 + q(t)\mathbf{e}_2\mathbf{e}_3$$

in the even sub-algebra $\mathcal{C}\ell_{2,1}^+$ with basis $1, \mathbf{e}_1\mathbf{e}_2, \mathbf{e}_2\mathbf{e}_3, \mathbf{e}_3\mathbf{e}_1$. The conjugate of this polynomial is defined by $P^*(t) = u(t) - v(t)\mathbf{e}_3\mathbf{e}_1 + p(t)\mathbf{e}_1\mathbf{e}_2 - q(t)\mathbf{e}_2\mathbf{e}_3$, and one can easily verify that the expression

$$\begin{aligned} P(t)\mathbf{e}_1P^*(t) &= [u^2(t) + v^2(t) - p^2(t) - q^2(t)]\mathbf{e}_1 \\ &\quad + 2[u(t)p(t) - v(t)q(t)]\mathbf{e}_2 + 2[u(t)v(t) - p(t)q(t)]\mathbf{e}_3, \end{aligned}$$

generates the components of the Pythagorean hodograph (24.6) in $\mathbb{R}^{2,1}$. Note that, as with (21.20), the form (24.6) can be written in different ways arising from permutations of $u(t), v(t), p(t), q(t)$ and sign changes for any of them.

24.5 MAT Approximation by MPH Curves

In computing the medial axis of a domain bounded by polynomial or rational curves, the edges that correspond to point/curve bisectors have exact rational representations, but those that correspond to curve/curve bisectors (or curve self-bisectors) do not, and must be approximated within a specified tolerance. Clearly, it is advantageous to use approximation elements that subsequently permit a piecewise-rational description of the reconstructed domain boundary — i.e., MPH curves. Typically, the approximation of smooth MAT segments (between medial axis bifurcations or end-points) is accomplished by Hermite interpolation of discrete data, sampled from the exact MAT. Such schemes have been developed by several authors [86, 277, 287, 288, 413].

Let $\mathbf{c} = (x, y)$ be a generic point on the medial axis, such that the maximal inscribed circle with center \mathbf{c} and radius r touches the domain boundary at the two *footpoints* \mathbf{p}_1 and \mathbf{p}_2 . Then if $\mathbf{t}_1, \mathbf{t}_2$ are unit tangents to the boundary

at $\mathbf{p}_1, \mathbf{p}_2$ (in the sense of increasing values of the parameter t), the medial axis unit tangent $\mathbf{t} = (\lambda, \mu)$ is defined by

$$\mathbf{t} = \frac{\mathbf{t}_1 + \mathbf{t}_2}{|\mathbf{t}_1 + \mathbf{t}_2|}, \quad (24.10)$$

i.e., it is just the *bisector* of \mathbf{t}_1 and \mathbf{t}_2 . Let ϕ be the angle between \mathbf{t}_1 and \mathbf{t} , and between \mathbf{t}_2 and \mathbf{t} . We take ϕ to be positive when \mathbf{t}_1 and \mathbf{t}_2 point into the half-planes separated by the medial axis tangent at \mathbf{c} that contain \mathbf{p}_1 and \mathbf{p}_2 , respectively, and otherwise it is negative (see Fig. 24.4).

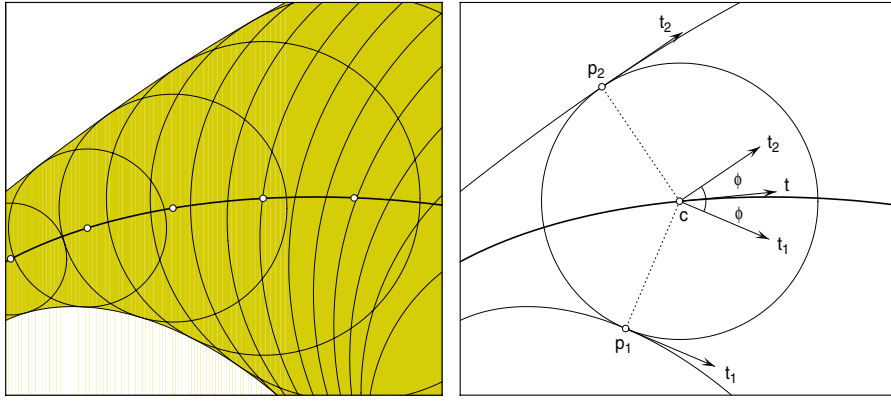


Fig. 24.4. Left: medial axis of a planar domain (shaded region) with several maximal inscribed circles shown. Right: a maximal circle centered at a point \mathbf{c} on the medial axis, with footpoints $\mathbf{p}_1, \mathbf{p}_2$ on the domain boundary. The medial axis tangent \mathbf{t} is given in terms of the boundary tangents $\mathbf{t}_1, \mathbf{t}_2$ at the footpoints $\mathbf{p}_1, \mathbf{p}_2$ by (24.10). The angle ϕ between \mathbf{t} and \mathbf{t}_1 or \mathbf{t}_2 defines the derivative of the circle radius r .

By considering neighboring elements $t, t + dt$ of the MAT $(x(t), y(t), r(t))$ one can deduce that its derivatives at each point have the ratios

$$x' : y' : r' = \lambda : \mu : \sin \phi, \quad (24.11)$$

specified by the geometry of the maximal inscribed circle — see Fig. 24.4. Choi et al. [86] proposed a scheme for approximating MATs using MPH cubic segments of the form

$$\gamma(t) = \mathbf{q}_0(1-t)^3 + \mathbf{q}_13(1-t)^2t + \mathbf{q}_23(1-t)t^2 + \mathbf{q}_3t^3$$

with control points $\mathbf{q}_k = (x_k, y_k, r_k) \in \mathbb{R}^{2,1}$ for $k = 0, \dots, 3$ and hodograph

$$\gamma'(t) = \mathbf{d}_0(1-t)^2 + \mathbf{d}_12(1-t)t + \mathbf{d}_2t^2,$$

where $\mathbf{d}_k = 3(\mathbf{q}_{k+1} - \mathbf{q}_k)$. This scheme is based directly on the Bézier control polygon in $\mathbb{R}^{2,1}$ rather than the hodograph form (24.6). To interpolate given

initial and final points (x_i, y_i, r_i) and (x_f, y_f, r_f) of a smooth MAT segment, and corresponding derivative ratios $(\lambda_i, \mu_i, \sin \phi_i)$ and $(\lambda_f, \mu_f, \sin \phi_f)$ of the form (24.11), $\gamma(t)$ must satisfy

$$\gamma(0) = \mathbf{q}_0 = (x_i, y_i, r_i), \quad \gamma'(0) = \mathbf{d}_0 = \delta_i(\lambda_i, \mu_i, \sin \phi_i), \quad (24.12)$$

$$\gamma(1) = \mathbf{q}_3 = (x_f, y_f, r_f), \quad \gamma'(1) = \mathbf{d}_2 = \delta_f(\lambda_f, \mu_f, \sin \phi_f), \quad (24.13)$$

and also the MPH condition

$$\langle \gamma'(t), \gamma'(t) \rangle \equiv [\sigma_0(1-t)^2 + \sigma_1 2(1-t)t + \sigma_2 t^2]^2 \quad (24.14)$$

for real values δ_i, δ_f and $\sigma_0, \sigma_1, \sigma_2$. The MPH condition is equivalent to the system of equations

$$\begin{aligned} \langle \mathbf{d}_0, \mathbf{d}_0 \rangle &= \sigma_0^2, & \langle \mathbf{d}_0, \mathbf{d}_1 \rangle &= \sigma_0 \sigma_1, \\ 2 \langle \mathbf{d}_1, \mathbf{d}_1 \rangle + \langle \mathbf{d}_2, \mathbf{d}_0 \rangle &= 2\sigma_1^2 + \sigma_2 \sigma_0, \\ \langle \mathbf{d}_1, \mathbf{d}_2 \rangle &= \sigma_1 \sigma_2, & \langle \mathbf{d}_2, \mathbf{d}_2 \rangle &= \sigma_2^2. \end{aligned} \quad (24.15)$$

Moreover, σ_0 and σ_2 must have the same sign, and σ_1 must satisfy $\sigma_1^2 < \sigma_0 \sigma_2$ if its sign differs from that of σ_0 and σ_2 , since otherwise the polynomial on the right in (24.14) vanishes at some t between 0 and 1, and $\gamma'(t)$ is not space-like for all t . By integrating $\gamma'(t)$, we also have

$$\mathbf{d}_0 + \mathbf{d}_1 + \mathbf{d}_2 = 3\Delta\mathbf{q} \quad (24.16)$$

where $\Delta\mathbf{q} = (x_f - x_i, y_f - y_i, r_f - r_i)$. Substituting for \mathbf{d}_1 from (24.16) into (24.15), the latter can be satisfied [86] by solving quadratic equations for δ_i, δ_f with coefficients dependent on the given end points (x_i, y_i, r_i) and (x_f, y_f, r_f) and derivative ratios $(\lambda_i, \mu_i, \sin \phi_i)$ and $(\lambda_f, \mu_f, \sin \phi_f)$.

The problem of identifying conditions on the data (24.12)–(24.13) for the existence of cubic MPH interpolants (and the choice of the “best” interpolant when a multiplicity of formal solutions exists) is rather involved. Choi et al. [86] noted that solutions exist for sufficiently mild variation of the Hermite data. Subsequently, Kosinka and Jüttler [287] performed a thorough analysis of the existence and number of space-like cubic MPH interpolants to given G^1 Hermite data, including singular cases, and showed that they achieve order 4 approximation of sufficiently smooth MAT segments. Another study [288] by the same authors is concerned with C^1 interpolation using MPH quintics.

Further approaches to Hermite interpolation of MAT data by MPH curves are described in studies by Kim and Ahn [277] and by Šír and Jüttler [413]. In the former, the problem of interpolation of C^1 Hermite end-point data by MPH quartics is considered — i.e., the *magnitudes* of the MAT derivatives $(x'(t), y'(t), r'(t))$ and not just their ratios (24.11) are specified. This method is based on characterizing the MPH property in terms of a certain root structure of the hodograph. The latter paper proposes a construction for spatial PH curves in \mathbb{R}^3 or $\mathbb{R}^{2,1}$ whose projections onto a prescribed plane coincide with a given “ordinary” planar cubic. The construction yields one residual degree of freedom, which can be used to interpolate a tangent at some chosen point.

24.6 Generalization to the Space $\mathbb{R}^{3,1}$

In general, the medial axis of a three-dimensional *volume* comprises a set of analytic surface segments that meet along certain branch curves and at certain branch points. By superposing a (bivariate) radius function on these surface segments, the boundary of the volume can be regarded as the envelope of a two-parameter family of maximal spheres centered on the medial axis.

The computation of the MAT for general volumes is a challenging problem, that incurs more intricate topological configurations than arise in the planar context. A much simpler three-dimensional problem concerns the envelopes of *one*-parameter families of spheres, which are known as *canal surfaces*. In the simplest case, i.e., spheres of constant radius centered on a given space curve, it was shown in [188] that the canal surface has a rational parameterization when the *spine curve* (i.e., the locus of centers) is a spatial PH curve. Subsequently, Peternell and Pottmann [360] showed that for *any* polynomial curve $\mathbf{r}(t) = (x(t), y(t), z(t))$ and radius function $r(t)$ satisfying

$$x'^2(t) + y'^2(t) + z'^2(t) - r'^2(t) \geq 0,$$

the corresponding canal surface is rational. However, determining its rational parameterization requires an algorithm to write the non-negative polynomial above as a sum of the squares of two real polynomials, and often yields poor quality parameterizations — the isoparametric curves may exhibit too much “unnecessary rotation” about the spine curve.

As an alternative, Choi et al. [89] formulate MPH curves in $\mathbb{R}^{3,1}$ using the even Clifford sub-algebra $\mathcal{C}\ell_{3,1}^+$ with eight independent basis elements. They show that the hodograph of a curve $(x(t), y(t), z(t), r(t)) \in \mathbb{R}^{3,1}$ satisfies

$$x'^2(t) + y'^2(t) + z'^2(t) - r'^2(t) = f^2(t) + g^2(t)$$

if its components can be expressed in terms of *eight* polynomials $p_k(t)$, $q_k(t)$ for $k = 0, \dots, 3$ in the form

$$\begin{aligned} x' &= p_0^2 + p_1^2 - p_2^2 - p_3^2 + q_0^2 + q_1^2 - q_2^2 - q_3^2, \\ y' &= 2(p_1 p_3 - p_0 p_2 + q_1 q_3 - q_0 q_2), \\ z' &= 2(p_1 p_2 + p_0 p_3 + q_1 q_2 + q_0 q_3), \\ r' &= 2(p_1 q_0 - p_0 q_1 + p_2 q_3 - p_3 q_2), \end{aligned}$$

and $f(t)$, $g(t)$ are then given by

$$\begin{aligned} f &= p_0^2 + p_1^2 + p_2^2 + p_3^2 - q_0^2 - q_1^2 - q_2^2 - q_3^2, \\ g &= 2(p_0 q_0 + p_1 q_1 + p_2 q_2 + p_3 q_3). \end{aligned}$$

By the result of Peternell and Pottmann, every space-like polynomial curve in $\mathbb{R}^{3,1}$ admits such a representation — i.e., every such curve is an MPH curve in $\mathbb{R}^{3,1}$ (unlike $\mathbb{R}^{2,1}$ where MPH curves comprise a proper subset of all space-like polynomial curves). The above approach essentially serves to furnish the desired decomposition of $x'^2 + y'^2 + z'^2 - r'^2$ into a sum of squares, $f^2 + g^2$.

Planar Hermite Interpolants

In theory there is no difference between theory and practice.

In practice there is.

Yogi Berra

Planar PH quintics offer sufficient shape flexibility for most practical design and manufacturing applications — they can inflect, and are in many respects similar in behavior to “ordinary” plane cubics (see §19.7). To construct planar PH quintics, a scheme that provides control over basic geometrical properties of a curve segment is required. Selecting numerical values for the coefficients u_0, u_1, u_2 and v_0, v_1, v_2 in (17.6) by “guesswork” clearly does not satisfy this need: we must develop algorithms that *determine* appropriate values for these coefficients, consistent with the specified geometrical constraints. Because the control points (17.6) have a non-linear dependence on u_0, u_1, u_2 and v_0, v_1, v_2 such algorithms incur non-linear equations with a multiplicity of solutions.

We consider here the *first-order Hermite interpolation* problem as a means of specifying planar PH quintics — namely, given end points $\mathbf{r}(0), \mathbf{r}(1)$ and end derivatives $\mathbf{r}'(0), \mathbf{r}'(1)$ in \mathbb{R}^2 , we wish to find a planar PH quintic $\mathbf{r}(t), t \in [0, 1]$ that matches this data. As is well-known, there is a *unique* “ordinary” cubic interpolant to such data — a fact that is of fundamental importance for the construction of C^2 cubic spline curves (Chap. 14). We shall see below that the construction of PH quintic Hermite interpolants involves solving a system of quadratic equations, generically yielding *four* distinct solutions. We first present a solution using only real variables, and then show that the complex representation discussed in Chap. 19 permits a simpler solution procedure, which is advantageous in terms of identifying the “good” interpolant through a shape measure known as the *absolute rotation index*.

25.1 Hermite Interpolation Problem

Discounting the arbitrary initial point \mathbf{p}_0 , the ten coordinates of the remaining control points $\mathbf{p}_1, \dots, \mathbf{p}_5$ defined by (17.6) depend on six quantities, u_0, u_1, u_2 and v_0, v_1, v_2 . Thus, there exist four “constraints relations” among the control points, whose satisfaction distinguishes PH quintics from quintic Bézier curves in general (see §19.5). However, unlike the case of PH cubics, they do not admit simple interpretations in terms of the control-polygon geometry.

Specifying end points $\mathbf{r}(0), \mathbf{r}(1)$ and end derivatives $\mathbf{r}'(0), \mathbf{r}'(1)$ of a quintic $\mathbf{r}(t)$ defined on $t \in [0, 1]$ is equivalent to fixing the first and last two Bézier control points $\mathbf{p}_0, \mathbf{p}_1$ and $\mathbf{p}_4, \mathbf{p}_5$. Thus, the first-order Hermite problem for planar PH quintics may be phrased as follows.

Problem 25.1 Given two pairs of distinct points $\mathbf{p}_0 \neq \mathbf{p}_1$ and $\mathbf{p}_4 \neq \mathbf{p}_5$ in the plane, can two additional points $\mathbf{p}_2, \mathbf{p}_3$ be found, such that all six points are expressible in the form (17.6) for real values of (u_0, u_1, u_2) and (v_0, v_1, v_2) ?

The stipulations $\mathbf{p}_0 \neq \mathbf{p}_1$ and $\mathbf{p}_4 \neq \mathbf{p}_5$ ensure that $\mathbf{r}'(0) \neq \mathbf{0}$ and $\mathbf{r}'(1) \neq \mathbf{0}$ (the interpolants should be *regular* curves). A solution to this problem offers a means of specifying or manipulating planar PH quintics by control polygons: the user freely chooses $\mathbf{p}_0, \mathbf{p}_1$ and $\mathbf{p}_4, \mathbf{p}_5$ while the algorithm “fills in” $\mathbf{p}_2, \mathbf{p}_3$. After solving the problem using only real variables, we show in §25.2 that the complex form of planar PH curves offers a simpler procedure — especially with regard to selecting the “good” interpolant among the four distinct solutions.

Lemma 25.1 *For all real values a and b , the real solutions to*

$$u^2 - v^2 = a \quad \text{and} \quad 2uv = b \tag{25.1}$$

may be expressed as

$$(u, v) = \pm \left(\sqrt{\frac{1}{2}(c+a)}, \operatorname{sign}(b) \sqrt{\frac{1}{2}(c-a)} \right), \tag{25.2}$$

where $c = \sqrt{a^2 + b^2}$ and we take $\operatorname{sign}(b) = \pm 1$ when $b = 0$.

Proof : Suppose first that $(a, b) \neq (0, 0)$. Then $u \neq 0$, and from the second equation we may substitute $v = b/2u$ into the first, giving the biquadratic

$$u^4 - au^2 - \frac{1}{4}b^2 = 0 \tag{25.3}$$

for u . Setting $c = \sqrt{a^2 + b^2}$ we have $u^2 = \frac{1}{2}(a \pm c)$, and since $a - c < 0$ and $a + c > 0$, the real solutions to (25.3) are seen to be

$$u = \pm \sqrt{\frac{1}{2}(c+a)}.$$

By substituting into $v = b/2u$ we obtain the corresponding values

$$v = \pm \frac{b}{2\sqrt{\frac{1}{2}(c+a)}} = \pm \text{sign}(b) \sqrt{\frac{1}{2}(c-a)}.$$

Thus, the real solutions agree with (25.2) when $(a, b) \neq (0, 0)$. We now show that (25.2) also gives the real solutions if a or b vanishes. First, if $a = b = 0$, the only solution is $(u, v) = (0, 0)$ which clearly agrees with (25.2). If $a = 0 \neq b$, the first equation yields $v = \pm u$. Together with the second equation this gives

$$(u, v) = \pm \left(\sqrt{\frac{1}{2}|b|}, \text{sign}(b) \sqrt{\frac{1}{2}|b|} \right),$$

consistent with (25.2). Finally, if $a \neq 0 = b$, either u or v must vanish and the solutions to (25.1) are thus of the form

$$(u, v) = \begin{cases} \pm(\sqrt{a}, 0) & \text{when } a > 0, \\ \pm(0, \sqrt{-a}) & \text{when } a < 0. \end{cases}$$

Taking $\text{sign}(b) = \pm 1$ when $b = 0$, the above is also a special case of (25.2). ■

Geometrically, the solutions to equations (25.1) are the intersection points of two rectangular hyperbolae in the (u, v) plane, with centers at the origin and asymptotes at 45° to each other — when $a = 0$ or $b = 0$, the corresponding hyperbola degenerates into the pair of lines defined by its asymptotes.

Proposition 25.1 *Problem 25.1 always has real solutions, given in terms of $\Delta\mathbf{p}_0 = (\Delta x_0, \Delta y_0) = \mathbf{p}_1 - \mathbf{p}_0$ and $\Delta\mathbf{p}_4 = (\Delta x_4, \Delta y_4) = \mathbf{p}_5 - \mathbf{p}_4$ by*

$$\begin{aligned} (u_0, v_0) &= \pm \sqrt{\frac{5}{2}} \left(\sqrt{|\Delta\mathbf{p}_0| + \Delta x_0}, \text{sign}(\Delta y_0) \sqrt{|\Delta\mathbf{p}_0| - \Delta x_0} \right), \\ (u_2, v_2) &= \pm \sqrt{\frac{5}{2}} \left(\sqrt{|\Delta\mathbf{p}_4| + \Delta x_4}, \text{sign}(\Delta y_4) \sqrt{|\Delta\mathbf{p}_4| - \Delta x_4} \right), \\ (u_1, v_1) &= -\frac{3}{4}(u_0 + u_2, v_0 + v_2) \pm \sqrt{\frac{1}{2}} \left(\sqrt{c+a}, \text{sign}(b) \sqrt{c-a} \right), \end{aligned} \quad (25.4)$$

where the quantities a , b , and $c = \sqrt{a^2 + b^2}$ are defined by

$$\begin{aligned} a &= \frac{9}{16}(u_0^2 - v_0^2 + u_2^2 - v_2^2) + \frac{5}{8}(u_0 u_2 - v_0 v_2) + \frac{15}{2}(x_4 - x_0), \\ b &= \frac{9}{8}(u_0 v_0 + u_2 v_2) + \frac{5}{8}(u_0 v_2 + u_2 v_0) + \frac{15}{2}(y_4 - y_0). \end{aligned} \quad (25.5)$$

Proof: Since $\mathbf{p}_0, \mathbf{p}_1$ and $\mathbf{p}_4, \mathbf{p}_5$ are specified, Lemma 25.1 can be immediately applied to the x and y components of the first and last equations in (17.6) with $(a, b) = (5\Delta x_0, 5\Delta y_0)$ and $(5\Delta x_4, 5\Delta y_4)$, respectively, to obtain expressions (25.4) for (u_0, v_0) and (u_2, v_2) , where $|\Delta\mathbf{p}_k| = \sqrt{(\Delta x_k)^2 + (\Delta y_k)^2}$. Writing $\mathbf{p}_4 - \mathbf{p}_1 = (\mathbf{p}_4 - \mathbf{p}_3) + (\mathbf{p}_3 - \mathbf{p}_2) + (\mathbf{p}_2 - \mathbf{p}_1)$ and substituting from (17.6) for the three terms on the right, we see that (u_1, v_1) must satisfy

$$\frac{15}{2}(x_4 - x_1) = u_1^2 - v_1^2 + \frac{3}{2}(u_0 + u_2)u_1 - \frac{3}{2}(v_0 + v_2)v_1 + \frac{1}{2}(u_0u_2 - v_0v_2),$$

$$\frac{15}{2}(y_4 - y_1) = 2u_1v_1 + \frac{3}{2}(v_0 + v_2)u_1 + \frac{3}{2}(u_0 + u_2)v_1 + \frac{1}{2}(u_0v_2 + u_2v_0),$$

and introducing the change of variables

$$\tilde{u}_1 = u_1 + \frac{3}{4}(u_0 + u_2) \quad \text{and} \quad \tilde{v}_1 = v_1 + \frac{3}{4}(v_0 + v_2)$$

the transformed equations for $(\tilde{u}_1, \tilde{v}_1)$ assume the form (25.1) with right-hand sides a and b given in terms of the known (u_0, v_0) and (u_2, v_2) values by (25.5). Thus, with $c = \sqrt{a^2 + b^2}$, the solutions to these equations have the form given in the last expression of (25.4). ■

Remark 25.1 Since three independent sign choices arise in equations (25.4), it might appear at first sight that there are *eight* PH quintics matching given end points and derivatives. However, if (u_0, u_1, u_2) and (v_0, v_1, v_2) are the coefficients for a particular choice of signs, careful inspection of (25.4) shows that the converse choice simply yields $(-u_0, -u_1, -u_2)$ and $(-v_0, -v_1, -v_2)$. Since expressions (17.6) involve only homogeneous quadratic forms in these coefficients, the control points they define are invariant under sign reversal of the coefficients. Thus, there are actually four *distinct* interpolants: they may be generated without replication by arbitrarily fixing the sign in any one of the three expressions (25.4) and exercising the sign freedoms of the other two.

Figure 25.1 shows examples of the four PH quintic interpolants that interpolate given first-order Hermite data — we take a fixed sign for the (u_1, v_1) expression in (25.4) and obtain the four distinct PH quintics from the sign choices $++, +-, -+, --$ in the expressions for (u_0, v_0) and (u_2, v_2) . The four interpolants are

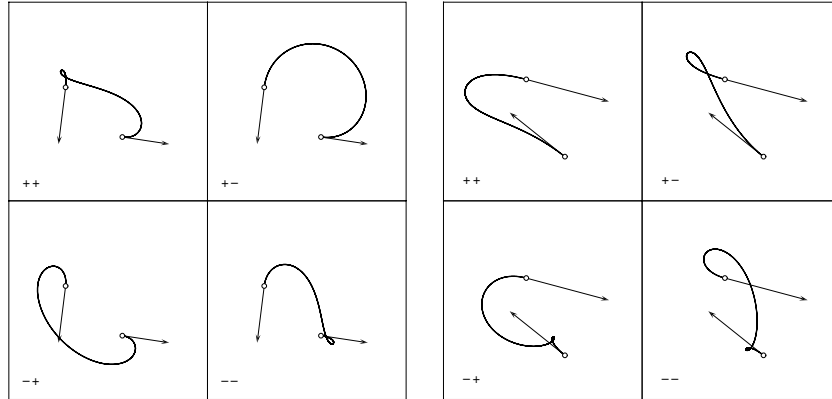


Fig. 25.1. Examples of the four distinct PH quintic interpolants defined by (25.4), for each of two different sets of first-order Hermite data $\mathbf{r}(0), \mathbf{r}(1)$ and $\mathbf{r}'(0), \mathbf{r}'(1)$.

all consistent with the Hermite data, but are otherwise markedly dissimilar. Typically, the shape of just one of the interpolants — the “good” solution — agrees with expectations for the specified Hermite data, while the other three exhibit undesirable loops. The problem of identifying the “good” interpolant *a posteriori*, or directly constructing it *a priori*, is of fundamental importance.

In view of their quite different shapes, the following feature of the four distinct PH quintic Hermite interpolants is perhaps rather surprising.

Corollary 25.1 *The four PH quintics interpolating given first-order Hermite data can be grouped into two pairs, such that the members of each pair have identical total arc lengths, given by*

$$S = \frac{5}{8} (|\Delta \mathbf{p}_0| + |\Delta \mathbf{p}_4|) - \frac{1}{12} (u_0 u_2 + v_0 v_2) + \frac{2}{15} c. \quad (25.6)$$

Proof : Substitute from (25.4) into the expressions (17.12) and (17.14) for the Bernstein coefficients of the parametric speed $\sigma(t)$ and the total arc length S in terms of u_0, u_1, u_2 and v_0, v_1, v_2 to obtain expression (25.6). It can then be verified from (25.6) that the value of S is unaltered upon reversing the choice of signs for both (u_0, v_0) and (u_2, v_2) in equations (25.4). ■

25.2 Solution in Complex Representation

To formulate a quantitative measure that helps identify the “good” PH quintic Hermite interpolant, we now solve the Hermite interpolation problem using the complex form of PH curves (see Chap. 19). Namely, a polynomial curve $\mathbf{r}(t) = (x(t), y(t))$ in \mathbb{R}^2 is regarded as a *complex-valued* polynomial $x(t) + i y(t)$ in the real parameter t . We use bold characters such as \mathbf{z} to denote complex numbers, and italics for explicitly real quantities. The former also define points or vectors in \mathbb{R}^2 , but products, quotients, radicals, etc., $(\mathbf{z}_1 \mathbf{z}_2, \mathbf{z}_1 / \mathbf{z}_2, \sqrt{\mathbf{z}}, \dots)$ must be evaluated using the algebra of complex numbers.

As observed in Chap. 19, regular PH curves in complex form correspond to those curves whose hodographs are perfect squares of complex polynomials that have relatively prime real and imaginary parts, i.e., $\mathbf{r}'(t) = \mathbf{w}^2(t)$, where $\mathbf{w}(t) = u(t) + i v(t)$ satisfies $\text{gcd}(u(t), v(t)) = \text{constant}$. Specifically, a quadratic polynomial $\mathbf{w}(t)$ yields a PH quintic on integrating the hodograph $\mathbf{r}'(t)$.

In the present context, it is convenient to express the hodographs that define PH quintics in the form

$$\mathbf{r}'(t) = \mathbf{k} [(t - \mathbf{a})(t - \mathbf{b})]^2 \quad (25.7)$$

for certain complex numbers $\mathbf{a}, \mathbf{b}, \mathbf{k}$. To ensure that $|\mathbf{r}'(t)| \neq 0$ for all real t , the numbers \mathbf{a} and \mathbf{b} should both have non-zero imaginary parts. Furthermore, \mathbf{a} and \mathbf{b} should not be conjugates, since the argument of $\mathbf{r}'(t)$ would then be independent of t , and $\mathbf{r}(t)$ degenerates to a straight line.

Remark 25.2 The correspondence between expression (25.7), and the form of PH quintics discussed in §19.5, amounts to identifying the Bernstein–form polynomial $\mathbf{w}_0(1-t)^2 + \mathbf{w}_1 2(1-t)t + \mathbf{w}_2 t^2$ with $\sqrt{\mathbf{k}}(t-\mathbf{a})(t-\mathbf{b})$. This gives

$$\mathbf{w}_0 = \sqrt{\mathbf{k}} \mathbf{a} \mathbf{b}, \quad \mathbf{w}_1 = -\sqrt{\mathbf{k}} \frac{1}{2} [\mathbf{a}(1-\mathbf{b}) + (1-\mathbf{a})\mathbf{b}], \quad \mathbf{w}_2 = \sqrt{\mathbf{k}} (1-\mathbf{a})(1-\mathbf{b}).$$

Now the shape of the Hermite interpolants depends only the magnitudes and orientations of the end derivatives $\mathbf{r}'(0)$ and $\mathbf{r}'(1)$ relative to the end-point displacement $\mathbf{r}(1) - \mathbf{r}(0)$. We therefore commence by eliminating non-essential freedoms from the Hermite data, as follows.

Definition 25.1 Arbitrary complex Hermite data $\mathbf{r}(0)$, $\mathbf{r}'(0)$ and $\mathbf{r}(1)$, $\mathbf{r}'(1)$ is reduced to the *standard form*

$$\mathbf{r}(0) = 0, \quad \mathbf{r}'(0) = \mathbf{d}_0 \quad \text{and} \quad \mathbf{r}(1) = 1, \quad \mathbf{r}'(1) = \mathbf{d}_1$$

by (i) subtracting $\mathbf{r}(0)$ from the end-points; and (ii) dividing the end-points and end-derivatives by $\mathbf{r}(1) - \mathbf{r}(0)$.

Since it is a trivial matter to transform to and from the original coordinate system by the appropriate complex arithmetic operations, we shall henceforth consider only the interpolation of Hermite data in standard form.

The following solution procedure is from [177]. By differentiation, one can easily verify that the PH quintic corresponding to the hodograph (25.7) may be expressed as

$$\mathbf{r}(t) = \frac{\mathbf{k}}{30} [(t-\mathbf{a})^5 - 5(t-\mathbf{a})^4(t-\mathbf{b}) + 10(t-\mathbf{a})^3(t-\mathbf{b})^2] + \mathbf{c} \quad (25.8)$$

where, in order to satisfy $\mathbf{r}(0) = 0$, the integration constant \mathbf{c} is given by

$$\mathbf{c} = \frac{\mathbf{k}}{30} (\mathbf{a}^5 - 5\mathbf{a}^4\mathbf{b} + 10\mathbf{a}^3\mathbf{b}^2). \quad (25.9)$$

Thus, in standard form, the problem of Hermite interpolation by PH quintics amounts to computing complex constants \mathbf{a} , \mathbf{b} , \mathbf{k} such that the curve defined by (25.8) and (25.9) satisfies $\mathbf{r}'(0) = \mathbf{d}_0$, $\mathbf{r}'(1) = \mathbf{d}_1$, and $\mathbf{r}(1) = 1$, and then deciding which of the resulting solutions gives the “best” curve.

Proposition 25.2 Let ρ be either of the two complex numbers defined by

$$\rho^2 = \frac{\mathbf{d}_0}{\mathbf{d}_1}, \quad (25.10)$$

and hence let α be either of the two solutions to the quadratic equation

$$\alpha^2 - 3(1+\rho)\alpha + 6\rho^2 + 2\rho + 6 - \frac{30}{\mathbf{d}_1} = 0. \quad (25.11)$$

Then, if μ_1 and μ_2 are the two roots of

$$\mu^2 - \alpha\mu + \rho = 0, \quad (25.12)$$

the values of \mathbf{a} and \mathbf{b} in (25.8) are given by

$$\mathbf{a} = \frac{\mu_1}{\mu_1 + 1} \quad \text{and} \quad \mathbf{b} = \frac{\mu_2}{\mu_2 + 1}. \quad (25.13)$$

The corresponding value of \mathbf{k} is

$$\mathbf{k} = \frac{\mathbf{d}_0}{\mathbf{a}^2 \mathbf{b}^2} = \frac{\mathbf{d}_1}{(1 - \mathbf{a})^2 (1 - \mathbf{b})^2}, \quad (25.14)$$

and \mathbf{c} is given in terms of \mathbf{a} , \mathbf{b} , \mathbf{k} by expression (25.9).

Proof : From (25.7) we have

$$\mathbf{k} \mathbf{a}^2 \mathbf{b}^2 = \mathbf{d}_0 \quad \text{and} \quad \mathbf{k} (1 - \mathbf{a})^2 (1 - \mathbf{b})^2 = \mathbf{d}_1, \quad (25.15)$$

while the condition $\mathbf{r}(1) = 1$ may be cast in the form

$$\begin{aligned} \mathbf{k} \{ & [6(1 - \mathbf{a})^2 - 3(1 - \mathbf{a})\mathbf{a} + \mathbf{a}^2] (1 - \mathbf{b})^2 \\ & + [-3(1 - \mathbf{a})^2 + 4(1 - \mathbf{a})\mathbf{a} - 3\mathbf{a}^2] (1 - \mathbf{b})\mathbf{b} \\ & + [(1 - \mathbf{a})^2 - 3(1 - \mathbf{a})\mathbf{a} + 6\mathbf{a}^2] \mathbf{b}^2 \} = 30. \end{aligned} \quad (25.16)$$

We begin by invoking expressions (25.15) to eliminate \mathbf{b} and \mathbf{k} from (25.16) — this is accomplished by substituting

$$\mathbf{b}^2 = \frac{\mathbf{d}_0}{\mathbf{k} \mathbf{a}^2}, \quad (1 - \mathbf{b})\mathbf{b} = \frac{\sqrt{\mathbf{d}_0 \mathbf{d}_1}}{\mathbf{k}(1 - \mathbf{a})\mathbf{a}}, \quad (1 - \mathbf{b})^2 = \frac{\mathbf{d}_1}{\mathbf{k}(1 - \mathbf{a})^2}.$$

The resulting equation depends only on \mathbf{d}_0 , \mathbf{d}_1 , and the ratio $\mu = \mathbf{a}/(1 - \mathbf{a})$,

$$\mathbf{d}_1(\mu^2 - 3\mu + 6) - \sqrt{\mathbf{d}_0 \mathbf{d}_1}(3\mu - 4 + 3\mu^{-1}) + \mathbf{d}_0(6 - 3\mu^{-1} + \mu^{-2}) = 30.$$

Defining $\rho^2 = \mathbf{d}_0/\mathbf{d}_1$, this may be further simplified to obtain the quadratic equation (25.11) by setting $\alpha = \mu + \rho\mu^{-1}$. Once a root α of (25.11) has been computed, the corresponding values of μ may be obtained by inverting the relation $\alpha = \mu + \rho\mu^{-1}$, i.e., by solving equation (25.12). Note here that, since equations (25.15) and (25.16) are symmetric in \mathbf{a} and \mathbf{b} , the two roots μ_1 and μ_2 of (25.12) must identify values of μ appropriate to *corresponding values* of \mathbf{a} and \mathbf{b} . The latter are obtained by inverting the relations $\mu_1 = \mathbf{a}/(1 - \mathbf{a})$ and $\mu_2 = \mathbf{b}/(1 - \mathbf{b})$, i.e., by expressions (25.13). Finally, knowing a pair of corresponding values for \mathbf{a} and \mathbf{b} , the appropriate value (25.14) for \mathbf{k} can be obtained by substituting $t = 0$ or $t = 1$ into (25.7). ■

The procedure of Proposition 25.2 yields four PH quintics — corresponding to distinct complex number pairs \mathbf{a} , \mathbf{b} — for any given complex values \mathbf{d}_0 , \mathbf{d}_1 . Four α values may occur in equation (25.12), since these values are roots of the quadratic (25.11), in which ρ assumes the two values defined by (25.10).

Compared to the real–arithmetic solution of Proposition 25.1, the complex form yields a more concise solution. More importantly, we shall see in §25.3 that the locations of \mathbf{a} and \mathbf{b} relative to the interval $[0, 1]$ of the real axis gives useful insight into the shape properties of the four distinct interpolants, and offers a simple quantitative basis for identifying the “good” solution.

Remark 25.3 Expressions (25.7) and (25.8) can be cast in Bernstein–Bézier form, to obtain control points for the hodograph and curve. Writing $t - \mathbf{a} = -\mathbf{a}(1-t) + (1-\mathbf{a})t$ in (25.7), and likewise for $t - \mathbf{b}$, and expanding gives

$$\begin{aligned}\mathbf{h}_0 &= \mathbf{k} \mathbf{a}^2 \mathbf{b}^2, \\ \mathbf{h}_1 &= -\frac{1}{2} \mathbf{k} \mathbf{a} \mathbf{b} (\mathbf{a} + \mathbf{b} - 2\mathbf{a}\mathbf{b}), \\ \mathbf{h}_2 &= \frac{1}{6} \mathbf{k} [(\mathbf{a} + \mathbf{b} - 2\mathbf{a}\mathbf{b})^2 + 2\mathbf{a}(1-\mathbf{a})\mathbf{b}(1-\mathbf{b})], \\ \mathbf{h}_3 &= -\frac{1}{2} \mathbf{k} (1-\mathbf{a})(1-\mathbf{b}) (\mathbf{a} + \mathbf{b} - 2\mathbf{a}\mathbf{b}), \\ \mathbf{h}_4 &= \mathbf{k} (1-\mathbf{a})^2 (1-\mathbf{b})^2,\end{aligned}$$

for the control points of the hodograph $\mathbf{r}'(t)$, and in terms of the above the control points for the PH quintic are

$$\mathbf{p}_k = \frac{1}{5} \sum_{j=0}^{k-1} \mathbf{h}_j, \quad k = 1, \dots, 5.$$

Here we take $\mathbf{p}_0 = 0$ as the integration constant: note also that $\mathbf{p}_5 = 1$ when $\mathbf{a}, \mathbf{b}, \mathbf{k}$ are computed according to Proposition 25.2. To restore these control points to the original coordinate system, the inverse of the transformations specified in Definition 25.1 should be applied.

Remark 25.4 In terms of the complex Bernstein–form hodograph

$$\mathbf{r}'(t) = [\mathbf{w}_0(1-t)^2 + \mathbf{w}_1 2(1-t)t + \mathbf{w}_2 t^2]^2, \quad (25.17)$$

rather than (25.7), the standardized Hermite interpolation problem amounts to solving the system of quadratic equations

$$\mathbf{w}_0^2 = \mathbf{d}_0, \quad \mathbf{w}_2^2 = \mathbf{d}_1, \quad \mathbf{w}_0^2 + \mathbf{w}_0 \mathbf{w}_1 + \frac{2\mathbf{w}_1^2 + \mathbf{w}_2 \mathbf{w}_0}{3} + \mathbf{w}_1 \mathbf{w}_2 + \mathbf{w}_2^2 = 5 \quad (25.18)$$

for the complex values $\mathbf{w}_0, \mathbf{w}_1, \mathbf{w}_2$.

This alternative formulation will be used extensively in constructing C^2 PH quintic spline curves (see Chap. 27). Although somewhat simpler, this approach does not directly yield information on the location of \mathbf{a} and \mathbf{b} in the complex plane, that will be used below to select the “best” solution.

25.3 The Absolute Rotation Index

For each solution $\mathbf{a}, \mathbf{b}, \mathbf{k}$ the form of the hodograph (25.7) indicates that the curve tangent at point t makes an angle

$$\theta(t) = \arg(\mathbf{k}) + 2\arg(\mathbf{a} - t) + 2\arg(\mathbf{b} - t) \quad (25.19)$$

with the positive real axis, where we take $-\pi < \arg(\mathbf{z}) \leq +\pi$. We will use the variation of $\theta(t)$ over $t \in [0, 1]$ to distinguish among the four solutions to the PH quintic Hermite interpolation problem.

Definition 25.2 *The rotation index R of a C^2 planar curve $\mathbf{r}(t)$, $t \in [0, 1]$ with curvature $\kappa(t)$ is defined by*

$$R = \frac{1}{2\pi} \int_0^1 \kappa(t) |\mathbf{r}'(t)| dt. \quad (25.20)$$

Rotation indices are a classical means [467] of characterizing global shape properties of curves. They indicate the fraction of a complete revolution that the curve tangent \mathbf{t} (or normal \mathbf{n}) executes on traversing a curve. This follows from the interpretation, $\kappa = d\theta/ds$, of the curvature as the derivative of the orientation angle θ of \mathbf{t} or \mathbf{n} with respect to arc length s . For simple (smooth) closed curves, for example, the “theorem of turning tangents” [132] states that $R = \pm 1$, depending upon the curve orientation. Here we are concerned with non-closed curves, for which R is generally not an integral value.

In Fig. 25.2 we illustrate the *Gauss maps* [326] for the curves in Fig. 25.1, describing the variation of the tangent \mathbf{t} as the curves are traversed. Since the initial and final tangent directions are determined by the Hermite data, the Gauss maps of the PH quintic interpolants differ from each other only

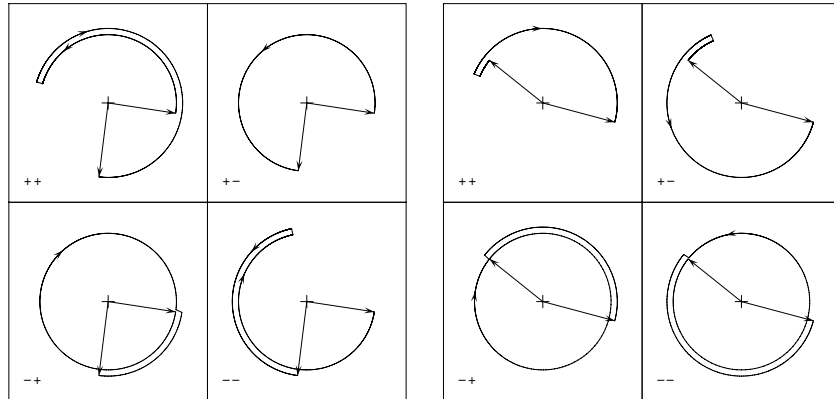


Fig. 25.2. Gauss maps for the PH quintic Hermite interpolants in Fig. 25.1. Note that reversals of the Gauss maps correspond to the inflection points of the curves.

in the manner in which they “wind” between these limits. Inflections, for example, correspond to sudden reversals of the Gauss map, and the tangent exhibits monotone turning between the two limits only for *convex* curves. The rotation index (25.20) describes the *net* amount of winding — i.e., clockwise turning of the tangent is cancelled by anti-clockwise turning.

As a first step, it might seem natural to compare the rotation indices of the PH quintic interpolants with that of the *unique* “ordinary” cubic as a basis for selecting the PH quintic with best shape properties. However, this approach may not be ideal, for a number of reasons [177]. Whereas the rotation indices of ordinary cubics must satisfy $-1 \leq R \leq +1$, the corresponding range for PH quintics is $-2 \leq R \leq +2$, and it can happen that *none* of the PH quintics has a rotation index in agreement with the ordinary cubic. Moreover, for certain Hermite data the ordinary cubic may exhibit an undesirable loop, while one of the corresponding PH quintics does not (see Fig. 25.3).

We will return to the issue of comparing PH quintic Hermite interpolants with their “ordinary” cubic counterparts in §25.4, but at present we prefer to adopt an *absolute* basis for selecting the “good” PH quintic. It seems obvious from the examples in Figs. 25.1 and 25.2 that minimizing the *net* variation of $\theta(t)$, expressed by the rotation index (25.20), is not a satisfactory criterion — cases in which large amounts of positive and negative rotation nearly cancel may be as undesirable as those that exhibit too much rotation of a fixed sense. Thus, we are motivated to introduce the *absolute rotation index*

$$R_{\text{abs}} = \frac{1}{2\pi} \int_0^1 |\kappa(t)| |\mathbf{r}'(t)| dt \quad (25.21)$$

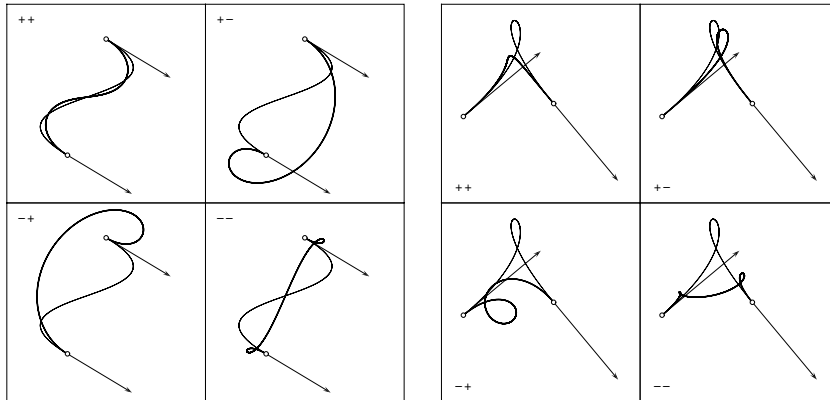


Fig. 25.3. Comparison of PH quintic Hermite interpolants (bold curves) with the corresponding “ordinary” cubic (light curve). Left: the ++ and -- PH quintics both have the same rotation index, $R = 0$, as the ordinary cubic. Right: the +- PH quintic has the same R as the ordinary cubic but the +- solution may be preferable.

as the quantity whose minimization will identify the “good” interpolant. R_{abs} measures the *total* amount — regardless of sense — of “winding” of the curve tangent. If κ is of constant sign over $t \in [0, 1]$ we simply have $R_{\text{abs}} = |R|$. If the curve has *inflections*, however, the integral (25.21) must be evaluated by breaking it up at the values $t_1, \dots, t_N \in (0, 1)$ where κ changes sign.

To compute R_{abs} , we appeal to expression (25.19) for the tangent angle of the PH quintic with the hodograph (25.7). Since (25.21) does not depend on the reference direction from which $\theta(t)$ is measured, we may drop the constant $\arg(\mathbf{k})$ and write $\theta(t) = 2[\arg(\mathbf{a} - t) + \arg(\mathbf{b} - t)]$. Note that for a regular curve, satisfying $\mathbf{r}'(t) \neq 0$ for all real t , \mathbf{a} and \mathbf{b} must have non-zero imaginary parts (and are not conjugates if the Hermite data is non-degenerate).

Proposition 25.3 *Let $\angle u \mathbf{z} v$ be the angle subtended at vertex \mathbf{z} of a triangle in the complex plane whose other vertices are at values u, v on the real axis. Then for the PH quintics constructed according to Proposition 25.2 we have*

$$R_{\text{abs}} = \frac{1}{\pi} (\angle 0 \mathbf{a} 1 + \angle 0 \mathbf{b} 1),$$

when \mathbf{a} and \mathbf{b} lie on the same side of the real axis, and

$$R_{\text{abs}} = \frac{1}{\pi} \sum_{k=0}^N |\angle t_k \mathbf{a} t_{k+1} - \angle t_k \mathbf{b} t_{k+1}|$$

where $t_0 = 0$, $t_{N+1} = 1$, and t_1, \dots, t_N ($N \leq 2$) are the ordered roots of

$$\text{Im}(\mathbf{a} + \mathbf{b}) t^2 - 2 \text{Im}(\mathbf{a}\mathbf{b}) t + \text{Im}(|\mathbf{a}|^2 \mathbf{b} + |\mathbf{b}|^2 \mathbf{a}) = 0 \quad (25.22)$$

on $t \in (0, 1)$ when \mathbf{a} and \mathbf{b} lie on opposite sides of the real axis.

Proof: If \mathbf{a} and \mathbf{b} lie on one side of the real axis, $\arg(\mathbf{a} - t)$ and $\arg(\mathbf{b} - t)$ are either both positive and monotone-increasing with t , or both negative and monotone-decreasing with t . Thus κ cannot vanish, and we may write

$$R_{\text{abs}} = \frac{2|\arg(\mathbf{a} - 1) - \arg(\mathbf{a})| + 2|\arg(\mathbf{b} - 1) - \arg(\mathbf{b})|}{2\pi} = \frac{\angle 0 \mathbf{a} 1 + \angle 0 \mathbf{b} 1}{\pi}.$$

If \mathbf{a} and \mathbf{b} lie on opposite sides of the real axis, there may be zero, one, or two inflections on $t \in (0, 1)$. The curvature can be expressed as

$$\kappa(t) = \frac{x'(t)y''(t) - x''(t)y'(t)}{[x'^2(t) + y'^2(t)]^{3/2}} = \frac{\text{Im}(\bar{\mathbf{r}}'(t)\mathbf{r}''(t))}{|\mathbf{r}'(t)|^3},$$

and by substituting from (25.7) we obtain

$$\kappa(t) = \frac{2}{|\mathbf{k}|} \frac{\text{Im}(\mathbf{b})|t - \mathbf{a}|^2 + \text{Im}(\mathbf{a})|t - \mathbf{b}|^2}{|(t - \mathbf{a})(t - \mathbf{b})|^4}.$$

The numerator of this expression is proportional to the quadratic (25.22), and hence its simple roots identify inflections. Geometrically, the parameter values t corresponding to inflections are points on the real axis from which the ratio of the distances to \mathbf{a} and \mathbf{b} has the fixed value

$$|\mathbf{a} - t| / |\mathbf{b} - t| = \sqrt{-\operatorname{Im}(\mathbf{a}) / \operatorname{Im}(\mathbf{b})}.$$

Note that the discriminant $\Delta = -4 \operatorname{Im}(\mathbf{a}) \operatorname{Im}(\mathbf{b}) |\bar{\mathbf{a}} - \bar{\mathbf{b}}|^2$ of (25.22) is positive in this case, so the number of inflections on $t \in (0, 1)$ equals the number of sign variations in its Bernstein coefficients. If there are inflections at t_1, \dots, t_N , and we set $t_0 = 0$ and $t_{N+1} = 1$, then

$$R_{\text{abs}} = \frac{1}{2\pi} \sum_{k=0}^N 2 |\arg(\mathbf{a} - t_{k+1}) - \arg(\mathbf{a} - t_k) + \arg(\mathbf{b} - t_{k+1}) - \arg(\mathbf{b} - t_k)|$$

and since $\arg(\mathbf{a} - t_{k+1}) - \arg(\mathbf{a} - t_k)$ and $\arg(\mathbf{b} - t_{k+1}) - \arg(\mathbf{b} - t_k)$ must be of opposite sign, and equal in absolute value to $\angle t_k \mathbf{a} t_{k+1}$ and $\angle t_k \mathbf{b} t_{k+1}$, we have

$$R_{\text{abs}} = \frac{1}{\pi} \sum_{k=0}^N |\angle t_k \mathbf{a} t_{k+1} - \angle t_k \mathbf{b} t_{k+1}|. \quad \blacksquare$$

Note that $\angle 0 \mathbf{a} 1$ and $\angle 0 \mathbf{b} 1$ correspond to $|\pi - \arg(\boldsymbol{\mu}_1)|$ and $|\pi - \arg(\boldsymbol{\mu}_2)|$, $\boldsymbol{\mu}_1$ and $\boldsymbol{\mu}_2$ being the roots of (25.12). Typically, configurations where \mathbf{a} and \mathbf{b} lie on opposite sides of the real axis and are not close to the interval $t \in (0, 1)$ generate the smallest values of R_{abs} — see the example shown in Fig. 25.4. The upper bound $R_{\text{abs}} = 2$ is approached when either: (i) \mathbf{a} and \mathbf{b} are near to and on the same side of $t \in (0, 1)$; or (ii) \mathbf{a} and \mathbf{b} are near to but on opposite sides of *distinct* subintervals $t \in (t_k, t_{k+1})$ delineated by the inflections.

The rotation index is the case $n = 1$ of the integral (17.17), and replacing $\kappa(t)$ with $|\kappa(t)|$ yields the absolute rotation index. The case $n = 0$ defines the total arc length, but this is not recommended as a measure for identifying the “good” interpolant — as seen in Fig. 25.1, it is possible for solutions of nominally smaller arc length to exhibit undesirable tight loops. The case $n = 2$

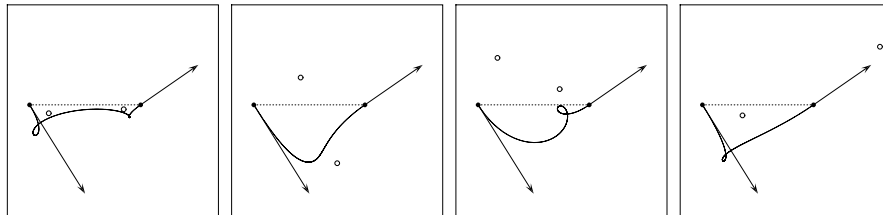


Fig. 25.4. Computation of the absolute rotation index R_{abs} from the locations of the roots \mathbf{a} , \mathbf{b} of the hodograph (25.7) relative to $t \in [0, 1]$. The best interpolant arises when \mathbf{a} and \mathbf{b} lie on opposite sides of (and are not too close to) this interval.

of (17.17) gives the *elastic bending energy* (see §14.2), which strongly penalizes curvature extremes. This is a viable alternative to the absolute rotation index, but its computation is significantly more involved — see Chap. 26.

25.4 Comparison with “Ordinary” Cubics

A comparison of the four PH quintic interpolants $\mathbf{r}(t)$ to given Hermite data with the corresponding “ordinary” cubic $\mathbf{c}(t)$, in terms of the Gauss maps and rotation indices, was first discussed in [177] but no simple and universal basis for selecting the “good” PH quintic emerged. This question was revisited in [331], using the Bernstein form (25.18) of the Hermite problem. The *absence of anti-parallel tangents* was introduced therein, as a qualitative measure of similarity between the PH quintic and ordinary cubic interpolants.

Definition 25.3 Two plane curves $\mathbf{c}(t)$ and $\mathbf{r}(t)$ interpolating given Hermite data on $t \in [0, 1]$ are said to be *free of anti-parallel tangents* if there exist no parameter values $\tau \in [0, 1]$ such that $\mathbf{r}'(\tau) = -k \mathbf{c}'(\tau)$ for positive real k .

In standard form (Definition 25.1) we consider Hermite data “reasonable” when the end derivatives $\mathbf{d}_0, \mathbf{d}_1$ lie in the complex-plane domain defined by

$$D = \{ \mathbf{d} \mid \operatorname{Re}(\mathbf{d}) > 0 \text{ and } |\mathbf{d}| < 3 \}. \quad (25.23)$$

The condition $\operatorname{Re}(\mathbf{d}) > 0$ requires that the derivatives be “forward-pointing” — i.e., in the direction of $\mathbf{r}(1) - \mathbf{r}(0)$ — while the restriction $|\mathbf{d}| < 3$ ensures that their magnitudes are commensurate with $|\mathbf{r}(1) - \mathbf{r}(0)|$. It is shown in [331] that, for reasonable Hermite data, the ordinary cubic and the ++ PH quintic¹ interpolant both have hodographs that lie entirely within the domain D , and hence these curves are free of anti-parallel tangents (since no two points of D identify anti-parallel tangents). As a corollary, both the cubic and ++ PH quintic interpolants of “reasonable” data are free of self-intersections.

A topological means of comparing PH quintic Hermite interpolants with the ordinary cubic was proposed in [331] and thoroughly analyzed in [84]. The hodographs are combined into a single curve $\gamma(t)$ defined on $t \in [0, 2]$ by

$$\gamma(t) = \begin{cases} \mathbf{r}'(t) & \text{for } 0 \leq t \leq 1, \\ \mathbf{c}'(2-t) & \text{for } 1 < t \leq 2. \end{cases} \quad (25.24)$$

Since $\gamma(2) = \mathbf{c}'(0) = \mathbf{d}_0 = \mathbf{r}'(0) = \gamma(0)$, this curve evidently defines a closed loop in the hodograph plane, for each of the PH quintic interpolants $\mathbf{r}(t)$. The adopted measure of similarity between $\mathbf{r}(t)$ and $\mathbf{c}(t)$ is the *winding number* of the composite hodograph curve with respect to the origin, defined [297] by

¹ In the context of the Bernstein formulation (25.18), the ++ solution is the one with $\operatorname{Re}(\mathbf{w}_0) \geq 0$ and $\operatorname{Re}(\mathbf{w}_2) \geq 0$.

$$\text{wind}(\gamma(t)) = \frac{1}{2\pi i} \int_{\gamma(t)} \frac{dz}{z} = \frac{1}{2\pi i} \int_0^2 \frac{\gamma'(t)}{\gamma(t)} dt.$$

Using (25.24), this integral can be decomposed [331] as

$$\text{wind}(\gamma(t)) = \frac{1}{2\pi i} \left[\int_0^1 \frac{\mathbf{r}''(t)}{\mathbf{r}'(t)} dt - \int_0^1 \frac{\mathbf{c}''(t)}{\mathbf{c}'(t)} dt \right] = R_{\mathbf{r}(t)} - R_{\mathbf{c}(t)}, \quad (25.25)$$

$R_{\mathbf{r}(t)}$ and $R_{\mathbf{c}(t)}$ being the rotation indices of the curves $\mathbf{r}(t)$ and $\mathbf{c}(t)$.

For closed curves, we can interpret $\text{wind}(\gamma(t))$ as the number of complete revolutions executed by a radius vector from the origin to points of $\gamma(t)$ during one full curve traversal — anti-clockwise rotation being counted positive, and clockwise negative. As noted in §25.3, $-2 \leq R_{\mathbf{r}(t)} \leq +2$ and $-1 \leq R_{\mathbf{c}(t)} \leq +1$, and since $\mathbf{r}'(0) = \mathbf{c}'(0)$ and $\mathbf{r}'(1) = \mathbf{c}'(1)$, the rotation indices $R_{\mathbf{r}(t)}$ and $R_{\mathbf{c}(t)}$ cannot be of opposite sign. Hence, the set of possible values for the winding number (25.25) is $\{-2, -1, 0, +1, +2\}$. In the present context, the significance of the composite hodograph winding number can be expressed [331] as follows.

Proposition 25.4 *If $\text{wind}(\gamma(t)) \neq 0$, it is impossible for the PH quintic $\mathbf{r}(t)$ and ordinary cubic $\mathbf{c}(t)$ to be free of anti-parallel tangents.*

Proof : If $\kappa_{\mathbf{r}}(t)$ and $\kappa_{\mathbf{c}}(t)$ are the curvatures of $\mathbf{r}(t)$ and $\mathbf{c}(t)$, we define the *angular phases* of these curves by

$$\theta_{\mathbf{r}}(t) = \arg(\mathbf{d}_0) + \int_0^t \kappa_{\mathbf{r}}(u) |\mathbf{r}'(u)| du, \quad \theta_{\mathbf{c}}(t) = \arg(\mathbf{d}_0) + \int_0^t \kappa_{\mathbf{c}}(u) |\mathbf{c}'(u)| du.$$

By definition, these are *continuous* functions: they are not reduced modulo 2π , like $\arg(\mathbf{r}'(t))$ and $\arg(\mathbf{c}'(t))$. Thus, in general, $\theta_{\mathbf{r}}(t) = \arg(\mathbf{r}(t)) + k\pi$ for integer k , and likewise for $\mathbf{c}(t)$. The angular phase difference $\Theta(t) = \theta_{\mathbf{r}}(t) - \theta_{\mathbf{c}}(t)$ is also a continuous function, with $\Theta(0) = 0$ and $\Theta(1) = 2\pi \text{wind}(\gamma(t))$. Thus, if $\text{wind}(\gamma(t)) \neq 0$, there must be a value t_* between 0 and 1 such that $\Theta(t_*) = \pm\pi$, and we have

$$\theta_{\mathbf{r}}(t_*) = \theta_{\mathbf{c}}(t_*) \pm \pi,$$

which implies that $\mathbf{r}(t)$ and $\mathbf{c}(t)$ have anti-parallel tangents at $t = t_*$. ■

Thus, if we desire a PH quintic free of anti-parallel tangents relative to the ordinary cubic, we must select an interpolant with $\text{wind}(\gamma(t)) = 0$. Figure 25.5 shows a typical example — for which the ++ solution is the unique PH quintic satisfying this condition. The questions of the existence and uniqueness of PH quintics satisfying $\text{wind}(\gamma(t)) = 0$ was thoroughly addressed in [84] — it was shown that, for generic data, such a solution always exists, although in certain cases there may be *two* such interpolants. A selection rule was formulated for such cases, to guide a choice among the two PH quintics free of anti-parallel tangents relative to the ordinary cubic. Since they are quite technical, we refer the reader to [84] for the precise statements and proofs of these results.

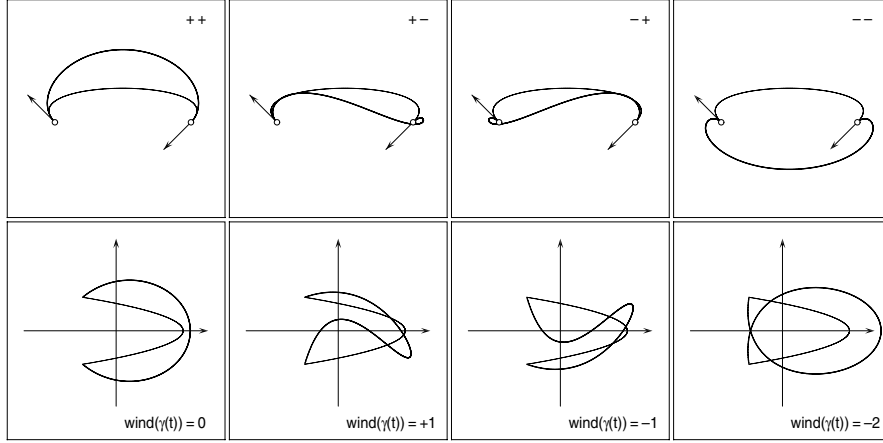


Fig. 25.5. Comparison of the four distinct PH quintic interpolants (thick curves) to given Hermite data with the corresponding ordinary cubic (thin curve). Also shown are the composite hodographs $\gamma(t)$, with values of their winding numbers indicated.

25.5 Higher-order Hermite Interpolants

The construction of second-order PH quintic Hermite interpolants, that match given end points and first and second derivatives, was considered in [168, 414]. These studies employ PH curves of degree 9, and generically yield four distinct C^2 interpolants for arbitrary Hermite data. A different approach was proposed in [266], using degree 7 PH curves to match end points, first derivatives, and curvatures. In this case, solutions may not exist for certain data.

The methods described in [168] are motivated by the design of cam profiles. Cams are typically used to transform continuous rotary motion into oscillatory linear motion of a follower. The follower should exhibit stationary “dwell”s of specified duration at the extremes of oscillation (corresponding, for example, to the open and closed positions of a valve), and the follower motion between the two dwells should be acceleration continuous. The dwells are generated by circular arcs of radii r_0 and r_1 on the cam, and these arcs must be connected by smooth curves — meeting them with C^2 continuity — that specify the “rise” and “return” segments of the cam profile (see Fig. 25.6).

A traditional approach to cam design is to specify (say) the rise portion of the follower motion by a suitable function of the cam rotation angle — for example, the *cycloidal rise function* defined over $\theta \in [\theta_0, \theta_1]$ by

$$h(\theta) = (r_1 - r_0) \left[\frac{\theta - \theta_0}{\theta_1 - \theta_0} - \frac{1}{2\pi} \sin 2\pi \frac{\theta - \theta_0}{\theta_1 - \theta_0} \right], \quad (25.26)$$

with $h(\theta_0) = 0$, $h(\theta_1) = r_1 - r_0$ and $h'(\theta_0) = h''(\theta_0) = 0$, $h'(\theta_1) = h''(\theta_1) = 0$. The actual shape of the cam profile for the angular extent $\theta \in [\theta_0, \theta_1]$ must

be deduced from the specified form (25.26) of the follower output.² However, the presence of θ alone and also as the argument of a trigonometric function in (25.26) implies that the cam shape is a *transcendental curve* — to describe it in a CAD system or cut it on a CNC machine, it must be approximated.

Rather than specifying the desired follower output and then determining the cam shape from it, the approach proposed in [168] employs PH curves to interpolate second-order Hermite data obtained from the end points of the circular dwell arcs. The follower motion is determined *a posteriori*, and can be fine-tuned using free parameters obtained by relaxing from C^2 to G^2 continuity. In [168] it is shown that second-order Hermite data $\mathbf{r}(0)$, $\mathbf{r}'(0)$, $\mathbf{r}''(0)$ and $\mathbf{r}(1)$, $\mathbf{r}'(1)$, $\mathbf{r}''(1)$ can always be interpolated by PH curves of degree 9 — as in the quintic case, there are four distinct interpolants and the “good” solution must be identified among them (an example is shown in Fig. 25.6). Relaxing from C^2 to G^2 continuity of the dwell and rise/return segments of the cam profile yields four free parameters for adjustment of the output motion. As seen in Fig. 25.6, excellent agreement with the displacement, velocity, and acceleration profiles of the cycloidal rise function (25.26) can be obtained.

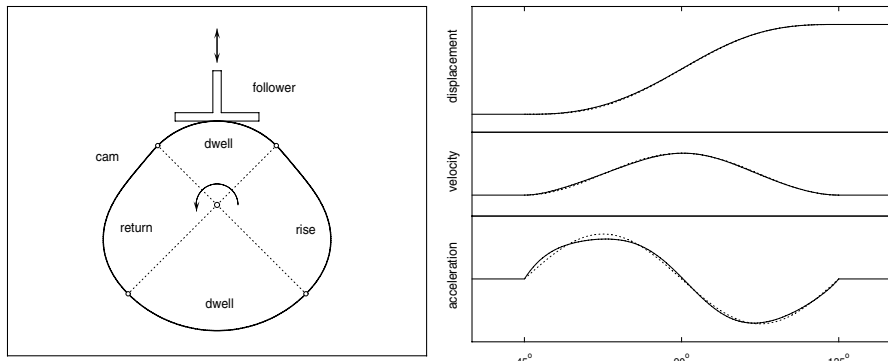


Fig. 25.6. Right: geometry of a rise–dwell–return–dwell cam/follower system. The dwell portions of the cam profile are circular arcs of radii r_0 , r_1 and the rise/return portions are specified by PH curves that meet these circular arcs with C^2 continuity. Left: follower displacement, velocity, and acceleration during the rise phase — the graphs for the cycloidal rise function (25.26) are also shown here, as dotted curves.

An important advantage of the PH curves in this context is their rational offset curves. If the cam is to be milled by a tool of radius d , the tool center must follow the offset at distance d from the cam profile. For cams defined by (25.26), on the other hand, both the cam and its offset are approximated, incurring compounded errors. For an analysis of the follower output motion, and more complete details on other aspects of this topic, see [168].

² The *dual form* (see §7.4.3) is convenient for this purpose, since (25.26) essentially specifies the cam *tangent line* for each angular position θ .

The solutions to the planar C^2 Hermite interpolation problem were further discussed in [414], and their rate of convergence to an underlying smooth curve (from which the Hermite data is sampled) was analyzed. The authors propose to use these interpolants for smoothing of piecewise-linear/circular “G code” paths for CNC machines, ensuring acceleration-continuous motions.

Jüttler [266] describes a scheme for interpolating data of the form

$$\mathbf{r}(0), \mathbf{r}'(0), \kappa(0) \quad \text{and} \quad \mathbf{r}(1), \mathbf{r}'(1), \kappa(1) \quad (25.27)$$

— i.e., first-order Hermite data augmented by end-point curvatures — using planar PH curves of degree 7. This is referred to as $G^2 [C^1]$ Hermite data. The construction of the interpolants involves computing the roots of two quartic equations, and yields as many as eight distinct curves (depending on the given data). As in the PH quintic case, a suitable shape measure must be invoked to select the “best” interpolant if a multiplicity of solutions exists.

However, for certain prescribed data of the form (25.27), there may be no PH interpolants of degree 7. An asymptotic analysis presented in [266] shows that, when such data is sampled sufficiently densely from an analytic curve, solutions exist under certain technical conditions, and the approximation order of the PH curves to the underlying analytic curve is determined — the reader should consult [266] for complete details.

25.6 Monotone Curvature Segments

In applications such as layout of highways, railways, and roller-coaster tracks, it is often necessary to construct G^2 blends between linear/circular loci. Such blends should be *spiral segments*, with monotone curvature variation between the limits imposed by the linear/circular loci they connect. The *Cornu spiral* or *clothoid*, characterized by a *linear* variation of its curvature with arc length, is often employed in this context [22, 229, 322, 323, 347].

The Cornu spiral or clothoid is defined in terms of the *Fresnel integrals*

$$\begin{aligned} C(t) &= \int_0^t \cos \frac{1}{2}\pi u^2 du = \sqrt{\frac{2}{\pi}} \sum_{k=0}^{\infty} (-1)^k \frac{t^{4k+1}}{(4k+1)(2k)!}, \\ S(t) &= \int_0^t \sin \frac{1}{2}\pi u^2 du = \sqrt{\frac{2}{\pi}} \sum_{k=0}^{\infty} (-1)^k \frac{t^{4k+3}}{(4k+3)(2k+1)!}, \end{aligned} \quad (25.28)$$

that are important for certain diffraction problems in optics (see Fig. 25.7). The eponymous spiral defined by $\mathbf{r}(t) = (C(t), S(t))$ was used by Marie-Alfred Cornu, Professor of Physics at the École Polytechnique, as a nomograph for diffraction calculations. The Italian mathematician Ernesto Cesàro proposed the more poetic name “clothoid” in reference to *Clotho* — daughter of Zeus and Themis, and one of three sisters known as the *Moirae* or “Fates” in Greek mythology. Clotho (the *spinner*) spun the metaphorical “thread of life” from a

distaff onto a spindle, while her sisters Lachesis (the *apportioner*) and Atropos (the *inevitable*) measured and cut it, fixing the life span and instant of death for each mortal. The aptness of the name *clothoid* is apparent in Fig. 25.7.

The clothoid was first studied in detail by Leonhard Euler in his treatise *Methodus inveniendi lineas curvas ...* (1744) on the calculus of variations. In the Additamentum I, *De curvis elasticis*, he considers the problem of a curved elastic beam with one end fixed and the other free end subject to a vertical point force F , and shows that the initial curved shape of the beam — prior to application of the force F — should be a segment of the clothoid if it is to bend into a precisely horizontal linear configuration under F .

The first two derivatives of the Cornu spiral are $\mathbf{r}'(t) = (\cos \frac{1}{2}\pi t^2, \sin \frac{1}{2}\pi t^2)$ and $\mathbf{r}''(t) = \pi t(-\sin \frac{1}{2}\pi t^2, \cos \frac{1}{2}\pi t^2)$. Hence $|\mathbf{r}'(t)| \equiv 1$ and $\kappa(t) = \pi t$, i.e., the parameter t coincides with the curve arc length s (measured from $t = 0$), and the curvature increases linearly with arc length. The point $t = 0$ (the origin) is an inflection, with $\kappa = 0$. The curve spirals with steadily increasing curvature (and infinite arc length) about the limit point $(\frac{1}{2}, \frac{1}{2})$ as $t \rightarrow +\infty$. For negative t , analogous behavior is observed in the negative quadrant (see Fig. 25.7).

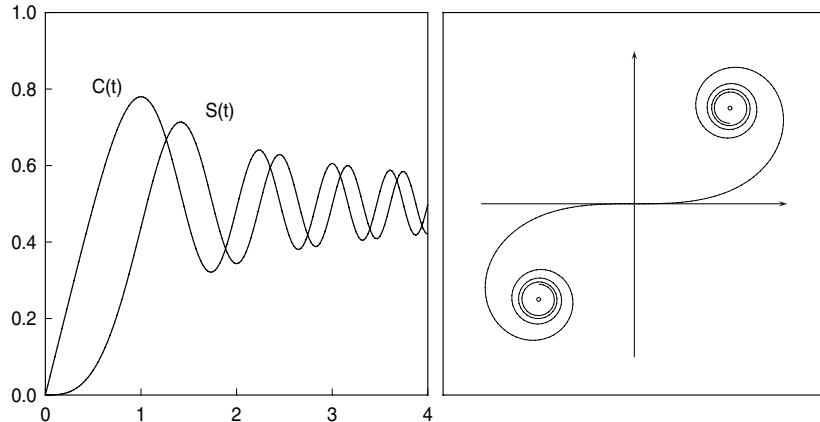


Fig. 25.7. Left: graphs of the Fresnel integrals (25.28) for $0 \leq t \leq 4$. Right: plot of the Cornu spiral or clothoid $\mathbf{r}(t) = (C(t), S(t))$ for $t \in [-4, +4]$. The parameter t coincides with the curve arc length measured from $t = 0$, and the curvature depends linearly on t . The limit points $(\pm \frac{1}{2}, \pm \frac{1}{2})$ of the curve as $t \rightarrow \pm\infty$ are also indicated.

Except when $|t| \ll 1$, the Taylor series expansions (25.28) of $C(t)$ and $S(t)$ are rather useless for numerical evaluation, since they involve terms of large magnitude and alternating signs, leading to serious error amplification through cancellation of significant digits — see §12.3.3. Alternative approaches, based on rational function approximations, are much preferred — Heald [231] gives coefficients for such approximants³ with errors as small as 4×10^{-8} .

³ There is a sign error in equation (3) of [231]: the + sign after $\frac{1}{2}$ should be -.

Meek and Walton [321–323] have developed algorithms for blending linear and circular segments using suitably positioned, oriented, and scaled clothoid arcs. The most general of these algorithms [323] yields G^2 clothoid spline interpolants matching specified end points, tangent directions, and curvatures (a clothoid spline is a G^2 piecewise-linear/circular/clothoid curve). However, these constructions are rather involved, and require careful analysis to ensure existence of interpolants. Since the clothoid is fundamentally a transcendental curve, any description of it in a CAD system must be approximate, and further operations (e.g., computing offsets) compound the approximation errors.

To circumvent these problems, Walton and Meek [458] proposed the use of PH curves as monotone-curvature elements. They showed that integrating the hodograph $\mathbf{r}'(t) = (u^2(t) - v^2(t), 2u(t)v(t))$ with certain special choices for the coefficients of the quadratic polynomials $u(t)$ and $v(t)$ yields PH quintics that have monotone curvature on $t \in [0, 1]$ and are capable of interpolating

- (a) an initial point \mathbf{p}_0 and tangent \mathbf{t}_0 with zero curvature, $\kappa(0) = 0$, at $t = 0$;
- (b) a final tangent \mathbf{t}_1 and extremal curvature, $\kappa(1) = 1/r$, $\kappa'(1) = 0$, at $t = 1$.

These PH quintics were used to define G^2 blends between linear and circular loci in various configurations. Subsequently, the problem was re-examined in [152] using the complex form, which revealed that the PH quintics defined by Walton and Meek are special cases of a one-parameter family of solutions. The availability of a free parameter relaxes constraints that are otherwise required to guarantee the existence of solutions, and offers the designer precise control over the length and curvature distribution of the blend (see Fig. 25.8).

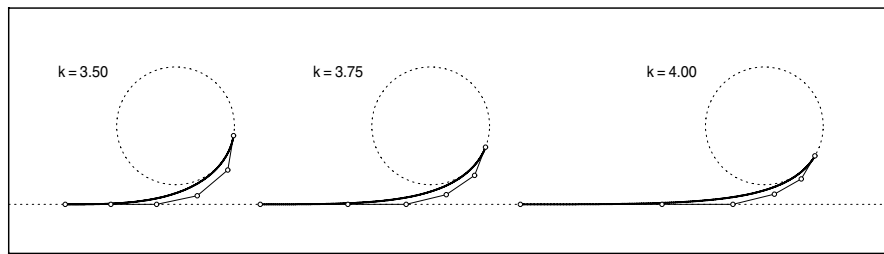


Fig. 25.8. G^2 blends between a line and a circle, defined by PH quintics of monotone curvature: the Bézier control polygons of the PH quintics are also shown. The free parameter k allows the user to control the rate of increase of the curvature [152].

Further studies concerning the use of the planar PH curves as monotone-curvature blends between linear/circular segments may be found in [222, 223, 459–462]. Related problems also occur in path planning for mobile robots — limitations on the steering mechanism range and rate require smooth paths with carefully controlled curvature profiles — see [70].

Elastic Bending Energy

Since the fabric of the universe is most perfect, and is the work of a most wise Creator, nothing whatsoever takes place in the universe in which some relation of maximum and minimum does not appear.

Leonhard Euler, *Methodus inveniendi lineas curvas ...* (1744)

In the Bernoulli–Euler theory of elastic beams, the strain energy contained in a thin beam, that is bent from an initially straight configuration into a curved (planar) shape, is proportional to the integral (14.2) of the squared curvature κ^2 with respect to the arc length s . The theory of (linear) *splines*, for example, deals with loci that interpolate prescribed data with a given order of continuity and minimize an *approximation* to the integral U — valid in the “small slope” regime (see §14.4.5). Curves that realize global minima of U under prescribed constraints (fixed arc length, interpolation of points, tangents, etc.) are known as *elastica* or “non-linear splines” (see §14.2). Unfortunately, they do not have elementary parametric representations. On the other hand, when one considers only the “simple” (polynomial or rational) curves $\mathbf{r}(t) = (x(t), y(t))$ commonly used in CAGD applications, one finds that the energy integral

$$U = \int \frac{(x'y'' - x''y')^2}{(x'^2 + y'^2)^{5/2}} dt \quad (26.1)$$

does not, in general, admit resolution in terms of elementary functions. In the case of “functional curves” — where we choose $t = x$ as the parameter — the integrand becomes $y''^2/(1 + y'^2)^{5/2}$ and for spline functions [116] one makes the further assumption that $|y'(t)| \ll 1$ to simplify this to just $y''^2(t)$.

The trouble with (26.1) stems from the radical $\sqrt{x'^2 + y'^2}$ in the integrand. For PH curves, however, the integrand becomes a *rational function* — which admits systematic integration through its partial fraction expansion (see §3.5). A resolution of (26.1) in terms of elementary analytic functions is thus feasible, offering the possibility of optimizing the “fairness” of PH curves with respect

to free parameters. While curves generated in this manner are not true *elastica*, they have the least energy — consistent with the given constraints — of curves in their class, and also have the virtue of exact representation in the standard Bernstein–Bézier form. In this chapter, we describe the analytic reduction of the energy (26.1) for planar PH cubics and quintics. Again, it is advantageous to employ the complex form of planar PH curves, and the factored hodograph form (25.7) is more convenient than the Bernstein form (25.17).

26.1 Complex Form of the Integrand

As noted in §19.7, the curvature of a plane curve $\mathbf{r}(t)$ specified in complex form is $\kappa(t) = |\mathbf{r}'(t)|^{-3} \operatorname{Im}(\bar{\mathbf{r}}'(t)\mathbf{r}''(t))$. For the PH curve specified by $\mathbf{r}'(t) = \mathbf{w}^2(t)$, where $\mathbf{w}(t) = u(t) + i v(t)$ is a complex polynomial, we thus have

$$\kappa(t) = 2 \frac{\operatorname{Im}(\bar{\mathbf{w}}(t)\mathbf{w}'(t))}{|\mathbf{w}(t)|^4} = 2 \frac{u(t)v'(t) - u'(t)v(t)}{[u^2(t) + v^2(t)]^2}, \quad (26.2)$$

and since $ds = \sigma(t) dt$, where $\sigma(t) = |\mathbf{w}(t)|^2 = u^2(t) + v^2(t)$, the integrand in (26.1) is a *rational* function of the curve parameter t , namely

$$4 \frac{\operatorname{Im}^2(\bar{\mathbf{w}}(t)\mathbf{w}'(t))}{|\mathbf{w}(t)|^6} = 4 \frac{[u(t)v'(t) - u'(t)v(t)]^2}{[u^2(t) + v^2(t)]^3}. \quad (26.3)$$

The indefinite integral of any rational function can be expressed in terms of rational functions, arctangents, and logarithms. It is determined by factoring the denominator into (at most quadratic) real or (linear) complex terms, and computing the *partial fraction decomposition* in terms of these factors — see §3.5 and [235]. We introduce the notation

$$h(t) = \operatorname{Im}(\bar{\mathbf{w}}(t)\mathbf{w}'(t)) = u(t)v'(t) - u'(t)v(t) \quad (26.4)$$

for the (real) polynomial occurring as the numerator in expression (26.2), and in doing so we call the reader's attention to a somewhat subtle point in order to avoid subsequent confusion or calculational errors.

Remark 26.1 In the complex representation, the parameter t is restricted to *real* values. Whereas a plane parametric curve $\mathbf{r}(t) = (x(t), y(t))$ — regarded as an ordered pair of real polynomials — may be evaluated at *complex* values of the parameter, to obtain “complex points” of the curve, this interpretation does *not* extend to the complex form $\mathbf{r}(t) = x(t) + i y(t)$. Nevertheless, we shall have occasion — in computing the partial fraction decomposition of (26.3) — to formally evaluate the polynomial $h(t)$ at complex values. This must be done by: (i) taking the imaginary part of $\bar{\mathbf{w}}(t)\mathbf{w}'(t)$, assuming the indeterminate t to be real; and (ii) *then* substituting the desired complex value into the real polynomial thus obtained. The converse order yields erroneous results.

For PH quintics, the *real* partial fraction decomposition of the integrand incurs the need to evaluate the indefinite integrals

$$I_n(t) = \int \frac{\ell(t)}{Q^n(t)} dt, \quad n = 1, 2, 3 \quad (26.5)$$

where, in Bernstein form,

$$\ell(t) = l_0(1-t) + l_1t, \quad Q(t) = q_0(1-t)^2 + q_12(1-t)t + q_2t^2,$$

and we assume that $Q(t)$ is monic (i.e., $q_2 - 2q_1 + q_0 = 1$). These are equivalent to standard forms [217], and can be concisely expressed as

$$\begin{aligned} I_1(t) &= \frac{2K}{\Delta} \tan^{-1} \frac{Q'(t)}{\Delta} + \frac{l_1 - l_0}{2} \ln Q(t), \\ I_2(t) &= \frac{4K}{\Delta^3} \tan^{-1} \frac{Q'(t)}{\Delta} + \frac{2}{\Delta^2} \frac{(q_1l_0 - q_0l_1)(1-t) + (q_2l_0 - q_1l_1)t}{Q(t)}, \\ I_3(t) &= \frac{12K}{\Delta^5} \tan^{-1} \frac{Q'(t)}{\Delta} - \frac{l_1 - l_0}{4Q^2(t)} + \frac{K}{2\Delta^2} \left[\frac{1}{Q(t)} + \frac{6}{\Delta^2} \right] \frac{Q'(t)}{Q(t)}, \end{aligned}$$

where $\Delta = 2\sqrt{q_0q_2 - q_1^2}$ and $K = (q_2 - q_1)l_0 - (q_1 - q_0)l_1$. These formulae are readily verified by differentiation. Note that each of the above integrals incurs transcendental terms — the *complex* partial fraction decomposition allows all the transcendental terms to be consolidated into a single expression.

26.2 Energy of Tschirnhaus Segments

As noted in Chap. 18, all PH cubics amount to suitably scaled, oriented, and parameterized segments of a unique curve — *Tschirnhausen's cubic*. Other than lines, circles, and parabolas, this is the simplest curve whose bending energy admits an elementary closed-form expression. Tschirnhaus segments are defined by substituting a linear complex polynomial

$$\mathbf{w}(t) = \mathbf{w}_0(1-t) + \mathbf{w}_1t$$

into $\mathbf{r}'(t) = \mathbf{w}^2(t)$, and integrating. It is convenient to write $\mathbf{w}(t)$ as

$$\mathbf{w}(t) = \mathbf{k}(t - \mathbf{a}),$$

where $\mathbf{k} = \mathbf{w}_1 - \mathbf{w}_0$ and $\mathbf{a} = \mathbf{w}_0/(\mathbf{w}_0 - \mathbf{w}_1) = a + i\alpha$, say. The polynomial (26.4) is then just the constant $|\mathbf{k}|^2\alpha$, and the parametric speed becomes

$$\sigma(t) = |\mathbf{k}|^2 (t^2 - 2at + a^2 + \alpha^2).$$

The indefinite energy integral

$$U(t) = \frac{4\alpha^2}{|\mathbf{k}|^2} \int \frac{dt}{(t^2 - 2at + a^2 + \alpha^2)^3}$$

amounts to a standard form [217], and can be concisely expressed as

$$U(t) = \left[\frac{|\mathbf{k}|^2}{\sigma(t)} + \frac{3}{2\alpha^2} \right] \frac{t-a}{\sigma(t)} + \frac{3}{2|\mathbf{k}|^2\alpha^3} \tan^{-1} \frac{t-a}{\alpha},$$

which may be verified by differentiation — there are no logarithmic terms in this case. The energy of a finite segment $t \in [t_0, t_1]$ is then $U(t_1) - U(t_0)$. In particular, for $t \in [0, 1]$ we may write¹

$$\begin{aligned} U = & \frac{1}{|\mathbf{k}|^2} \left\{ \frac{1-a}{|1-\mathbf{a}|^4} + \frac{a}{|\mathbf{a}|^4} + \frac{3}{2\alpha^2} \left[\frac{1-a}{|1-\mathbf{a}|^2} + \frac{a}{|\mathbf{a}|^2} \right] \right. \\ & \left. + \frac{3}{2\alpha^3} \left[\tan^{-1} \frac{1-a}{\alpha} + \tan^{-1} \frac{a}{\alpha} \right] \right\}. \end{aligned}$$

Tschirnhaus cubic segments have rather limited shape flexibility for free-form design, although G^1 interpolation schemes may be devised by doubling them up [179], and one may attempt to use the excess degrees of freedom incurred with this approach to minimize the above energy expression.

26.3 Bending Energy of PH Quintics

PH quintics are obtained by using a quadratic complex polynomial

$$\mathbf{w}(t) = \mathbf{w}_0(1-t)^2 + \mathbf{w}_12(1-t)t + \mathbf{w}_2t^2$$

in $\mathbf{r}'(t) = \mathbf{w}^2(t)$. In lieu of the Bernstein form, the factored expression

$$\mathbf{w}(t) = \mathbf{k}(t-\mathbf{a})(t-\mathbf{b})$$

is again more convenient, where $\mathbf{k} = \mathbf{w}_2 - 2\mathbf{w}_1 + \mathbf{w}_0$ and $\mathbf{a} = a + i\alpha$, $\mathbf{b} = b + i\beta$ are the roots of $\mathbf{w}(t)$ — namely

$$\mathbf{a}, \mathbf{b} = \frac{\mathbf{w}_0 - \mathbf{w}_1 \pm \sqrt{\mathbf{w}_1^2 - \mathbf{w}_0\mathbf{w}_2}}{\mathbf{w}_2 - 2\mathbf{w}_1 + \mathbf{w}_0}.$$

For a regular curve, we require $\alpha \neq 0$ and $\beta \neq 0$. The parametric speed is

$$\begin{aligned} \sigma(t) &= |\mathbf{k}|^2(t-\mathbf{a})(t-\mathbf{b})(t-\bar{\mathbf{a}})(t-\bar{\mathbf{b}}) \\ &= |\mathbf{k}|^2(t^2 - 2at + a^2 + \alpha^2)(t^2 - 2bt + b^2 + \beta^2), \end{aligned} \quad (26.6)$$

¹ We take $(-\pi/2, \pi/2]$ as the range of the arctangent function. The term in square parentheses involving arctangents may also be written as $\arg(1-\mathbf{a}) - \arg(-\mathbf{a})$.

and the polynomial (26.4) is given by

$$\begin{aligned} h(t) &= |\mathbf{k}|^2 \operatorname{Im} [(t - \bar{\mathbf{a}})(t - \bar{\mathbf{b}})(t - \mathbf{a} + t - \mathbf{b})] \\ &= |\mathbf{k}|^2 [\beta(t^2 - 2at + a^2 + \alpha^2) + \alpha(t^2 - 2bt + b^2 + \beta^2)]. \end{aligned} \quad (26.7)$$

Bearing in mind Remark 26.1, we take the second expression above as *defining* the polynomial $h(t)$ for all — real and complex — values of t .

In terms of $h(t)$ and the two *real* quadratic polynomials

$$A(t) = (t - \mathbf{a})(t - \bar{\mathbf{a}}) = |\mathbf{a}|^2(1 - t)^2 + (|\mathbf{a}|^2 - a)2(1 - t)t + |1 - \mathbf{a}|^2t^2,$$

$$B(t) = (t - \mathbf{b})(t - \bar{\mathbf{b}}) = |\mathbf{b}|^2(1 - t)^2 + (|\mathbf{b}|^2 - b)2(1 - t)t + |1 - \mathbf{b}|^2t^2,$$

the indefinite energy integral becomes

$$U(t) = \frac{4}{|\mathbf{k}|^6} \int \frac{h^2(t) dt}{A^3(t)B^3(t)}. \quad (26.8)$$

This integral may be resolved by forming the partial fraction decomposition

$$\frac{h^2(t)}{A^3(t)B^3(t)} = \frac{a_1(t)}{A(t)} + \frac{a_2(t)}{A^2(t)} + \frac{a_3(t)}{A^3(t)} + \frac{b_1(t)}{B(t)} + \frac{b_2(t)}{B^2(t)} + \frac{b_3(t)}{B^3(t)}, \quad (26.9)$$

of its integrand, where the numerators are (real) linear polynomials

$$a_k(t) = a_{k0}(1 - t) + a_{k1}t, \quad b_k(t) = b_{k0}(1 - t) + b_{k1}t.$$

Once the coefficients of these numerators have been computed, we can reduce the integrals of the terms on the right in (26.9) since they have the form (26.5).

The above approach employs a *real* factorization of the denominator of the integrand in (26.3) — so that each term in (26.9) is a *real* rational expression. However, one can also decompose a real rational function into *complex* partial fractions, and in practice this proves less cumbersome and yields more concise and manageable expressions. The integrand is expanded as

$$\begin{aligned} \frac{|\mathbf{k}|^{-4} h^2(t)}{(t - \mathbf{a})^3(t - \bar{\mathbf{a}})^3(t - \mathbf{b})^3(t - \bar{\mathbf{b}})^3} &= \\ \frac{\mathbf{a}_1}{t - \mathbf{a}} + \frac{\mathbf{a}_2}{(t - \mathbf{a})^2} + \frac{\mathbf{a}_3}{(t - \mathbf{a})^3} + \frac{\bar{\mathbf{a}}_1}{t - \bar{\mathbf{a}}} + \frac{\bar{\mathbf{a}}_2}{(t - \bar{\mathbf{a}})^2} + \frac{\bar{\mathbf{a}}_3}{(t - \bar{\mathbf{a}})^3} \\ + \frac{\mathbf{b}_1}{t - \mathbf{b}} + \frac{\mathbf{b}_2}{(t - \mathbf{b})^2} + \frac{\mathbf{b}_3}{(t - \mathbf{b})^3} + \frac{\bar{\mathbf{b}}_1}{t - \bar{\mathbf{b}}} + \frac{\bar{\mathbf{b}}_2}{(t - \bar{\mathbf{b}})^2} + \frac{\bar{\mathbf{b}}_3}{(t - \bar{\mathbf{b}})^3} \end{aligned} \quad (26.10)$$

where the numerators are now *complex constants* — the indicated conjugacies follow from the fact that the right-hand side must be a *real*-valued function of t . Once the complex values $\mathbf{a}_1, \mathbf{a}_2, \mathbf{a}_3$ and $\mathbf{b}_1, \mathbf{b}_2, \mathbf{b}_3$ have been determined, integrating (26.10) term-wise gives the indefinite energy integral

$$\begin{aligned}
U(t) = \frac{4}{|\mathbf{k}|^2} & \left[\mathbf{a}_1 \ln(t - \mathbf{a}) - \frac{\mathbf{a}_2}{t - \mathbf{a}} - \frac{\mathbf{a}_3}{2(t - \mathbf{a})^2} \right. \\
& + \mathbf{b}_1 \ln(t - \mathbf{b}) - \frac{\mathbf{b}_2}{t - \mathbf{b}} - \frac{\mathbf{b}_3}{2(t - \mathbf{b})^2} \\
& + \bar{\mathbf{a}}_1 \ln(t - \bar{\mathbf{a}}) - \frac{\bar{\mathbf{a}}_2}{t - \bar{\mathbf{a}}} - \frac{\bar{\mathbf{a}}_3}{2(t - \bar{\mathbf{a}})^2} \\
& \left. + \bar{\mathbf{b}}_1 \ln(t - \bar{\mathbf{b}}) - \frac{\bar{\mathbf{b}}_2}{t - \bar{\mathbf{b}}} - \frac{\bar{\mathbf{b}}_3}{2(t - \bar{\mathbf{b}})^2} \right]. \quad (26.11)
\end{aligned}$$

For real t this is a real-valued function, and can be explicitly written as such by combining the conjugate rational terms and writing the logarithmic terms in the form $\ln \mathbf{z} = \ln |\mathbf{z}| + i \arg(\mathbf{z})$ where $-\pi < \arg(\mathbf{z}) \leq \pi$, the appropriate quadrant being determined by the signs of $\text{Re}(\mathbf{z})$ and $\text{Im}(\mathbf{z})$. This gives

$$\begin{aligned}
U(t) = \frac{4}{|\mathbf{k}|^2} & \left\{ 2 \text{Re}(\mathbf{a}_1) \ln |t - \mathbf{a}| + 2 \text{Re}(\mathbf{b}_1) \ln |t - \mathbf{b}| \right. \\
& - 2 \text{Im}(\mathbf{a}_1) \arg(t - \mathbf{a}) - 2 \text{Im}(\mathbf{b}_1) \arg(t - \mathbf{b}) \\
& \left. - \text{Re} \left[\frac{2\mathbf{a}_2}{t - \mathbf{a}} + \frac{2\mathbf{b}_2}{t - \mathbf{b}} + \frac{\mathbf{a}_3}{(t - \mathbf{a})^2} + \frac{\mathbf{b}_3}{(t - \mathbf{b})^2} \right] \right\}. \quad (26.12)
\end{aligned}$$

To determine the coefficients of the partial fraction expansion, we multiply both sides of (26.10) by $(t - \mathbf{a})^3(t - \bar{\mathbf{a}})^3(t - \mathbf{b})^3(t - \bar{\mathbf{b}})^3$ to obtain

$$\begin{aligned}
|\mathbf{k}|^{-4} h^2(t) = & \left\{ [\mathbf{a}_1(t - \mathbf{a})^2 + \mathbf{a}_2(t - \mathbf{a}) + \mathbf{a}_3](t - \bar{\mathbf{a}})^3 \right. \\
& + [\bar{\mathbf{a}}_1(t - \bar{\mathbf{a}})^2 + \bar{\mathbf{a}}_2(t - \bar{\mathbf{a}}) + \bar{\mathbf{a}}_3](t - \mathbf{a})^3 \} (t - \mathbf{b})^3(t - \bar{\mathbf{b}})^3 \\
& + \left\{ [\mathbf{b}_1(t - \mathbf{b})^2 + \mathbf{b}_2(t - \mathbf{b}) + \mathbf{b}_3](t - \bar{\mathbf{b}})^3 \right. \\
& \left. + [\bar{\mathbf{b}}_1(t - \bar{\mathbf{b}})^2 + \bar{\mathbf{b}}_2(t - \bar{\mathbf{b}}) + \bar{\mathbf{b}}_3](t - \mathbf{b})^3 \right\} (t - \mathbf{a})^3(t - \bar{\mathbf{a}})^3.
\end{aligned}$$

The desired coefficients are then extracted by setting $t = \mathbf{a}$ and $t = \mathbf{b}$ in the above relation, and certain judiciously arranged derivatives of it, as follows:

$$\begin{aligned}
\mathbf{a}_3 &= \frac{|\mathbf{k}|^{-4} h^2(\mathbf{a})}{(\mathbf{a} - \mathbf{b})^3(\mathbf{a} - \bar{\mathbf{b}})^3(\mathbf{a} - \bar{\mathbf{a}})^3}, \\
\mathbf{b}_3 &= \frac{|\mathbf{k}|^{-4} h^2(\mathbf{b})}{(\mathbf{a} - \mathbf{b})^3(\bar{\mathbf{a}} - \mathbf{b})^3(\mathbf{b} - \bar{\mathbf{b}})^3}, \\
\mathbf{a}_2 &= \frac{\frac{d}{dt} [|\mathbf{k}|^{-4} h^2(t) - \mathbf{a}_3(t - \bar{\mathbf{a}})^3(t - \mathbf{b})^3(t - \bar{\mathbf{b}})^3]_{t=\mathbf{a}}}{(\mathbf{a} - \mathbf{b})^3(\mathbf{a} - \bar{\mathbf{b}})^3(\mathbf{a} - \bar{\mathbf{a}})^3}, \\
\mathbf{b}_2 &= \frac{\frac{d}{dt} [|\mathbf{k}|^{-4} h^2(t) - \mathbf{b}_3(t - \bar{\mathbf{b}})^3(t - \mathbf{a})^3(t - \bar{\mathbf{a}})^3]_{t=\mathbf{b}}}{(\mathbf{a} - \mathbf{b})^3(\bar{\mathbf{a}} - \mathbf{b})^3(\mathbf{b} - \bar{\mathbf{b}})^3},
\end{aligned}$$

$$\begin{aligned}\mathbf{a}_1 &= \frac{\frac{d^2}{dt^2} [|\mathbf{k}|^{-4} h^2(t) - (\mathbf{a}_2(t-\mathbf{a}) + \mathbf{a}_3)(t-\bar{\mathbf{a}})^3(t-\mathbf{b})^3(t-\bar{\mathbf{b}})^3]_{t=\mathbf{a}}}{2(\mathbf{a}-\mathbf{b})^3(\mathbf{a}-\bar{\mathbf{b}})^3(\mathbf{a}-\bar{\mathbf{a}})^3}, \\ \mathbf{b}_1 &= \frac{\frac{d^2}{dt^2} [|\mathbf{k}|^{-4} h^2(t) - (\mathbf{b}_2(t-\mathbf{b}) + \mathbf{b}_3)(t-\bar{\mathbf{b}})^3(t-\mathbf{a})^3(t-\bar{\mathbf{a}})^3]_{t=\mathbf{b}}}{2(\mathbf{a}-\mathbf{b})^3(\bar{\mathbf{a}}-\mathbf{b})^3(\mathbf{b}-\bar{\mathbf{b}})^3}.\end{aligned}$$

Note that these coefficients must be determined in the order indicated above.

From (26.7) we find that the values of $h(t)$ and its derivatives at $t = \mathbf{a}$ and $t = \mathbf{b}$, needed to evaluate the above expressions, may be written as

$$h(\mathbf{a}) = |\mathbf{k}|^2 \alpha (\mathbf{a} - \mathbf{b})(\mathbf{a} - \bar{\mathbf{b}}), \quad h'(\mathbf{a}) = 2|\mathbf{k}|^2 \alpha (\mathbf{a} - \bar{\mathbf{b}}),$$

$$h(\mathbf{b}) = |\mathbf{k}|^2 \beta (\mathbf{a} - \mathbf{b})(\bar{\mathbf{a}} - \mathbf{b}), \quad h'(\mathbf{b}) = -2|\mathbf{k}|^2 \beta (\bar{\mathbf{a}} - \mathbf{b}),$$

while $h''(t) \equiv 2|\mathbf{k}|^2(\alpha + \beta)$. Upon substituting, the most compact formulae for the coefficients are given recursively by

$$\begin{aligned}\mathbf{a}_3 &= \frac{i}{8\alpha(\mathbf{a}-\mathbf{b})(\mathbf{a}-\bar{\mathbf{b}})}, \\ \mathbf{b}_3 &= \frac{i}{8\beta(\mathbf{a}-\mathbf{b})(\bar{\mathbf{a}}-\mathbf{b})}, \\ \mathbf{a}_2 &= \left[\frac{3i}{2\alpha} + \frac{1}{\mathbf{a}-\mathbf{b}} - \frac{3}{\mathbf{a}-\bar{\mathbf{b}}} \right] \mathbf{a}_3, \\ \mathbf{b}_2 &= \left[\frac{3i}{2\beta} - \frac{1}{\mathbf{a}-\mathbf{b}} + \frac{3}{\bar{\mathbf{a}}-\mathbf{b}} \right] \mathbf{b}_3, \\ \mathbf{a}_1 &= \frac{3i}{2\alpha} \mathbf{a}_2 + \left[\frac{3}{4\alpha^2} - \frac{2}{(\mathbf{a}-\mathbf{b})^2} + \frac{6}{(\mathbf{a}-\bar{\mathbf{b}})^2} - \frac{1-2\beta/\alpha}{(\mathbf{a}-\mathbf{b})(\mathbf{a}-\bar{\mathbf{b}})} \right] \mathbf{a}_3, \\ \mathbf{b}_1 &= \frac{3i}{2\beta} \mathbf{b}_2 + \left[\frac{3}{4\beta^2} - \frac{2}{(\mathbf{a}-\mathbf{b})^2} + \frac{6}{(\bar{\mathbf{a}}-\mathbf{b})^2} - \frac{1-2\alpha/\beta}{(\mathbf{a}-\mathbf{b})(\bar{\mathbf{a}}-\mathbf{b})} \right] \mathbf{b}_3.\end{aligned}$$

The use of a computer algebra system is helpful in verifying the above.

Either (26.11) or (26.12), together with the above formulae for $\mathbf{a}_3, \mathbf{a}_2, \mathbf{a}_1$ and $\mathbf{b}_3, \mathbf{b}_2, \mathbf{b}_1$, amounts to a closed-form expression for the indefinite energy integral of PH quintics — if the curve is specified by the Bernstein coefficients $\mathbf{w}_0, \mathbf{w}_1, \mathbf{w}_2$ of $\mathbf{w}(t)$, the complex values $\mathbf{k}, \mathbf{a}, \mathbf{b}$ may be determined from them as described at the beginning of this section. The total energy $U = U(1) - U(0)$ of the segment $t \in [0, 1]$ may thus be expressed as

$$\begin{aligned}U &= \frac{4}{|\mathbf{k}|^2} \left\{ 2 \operatorname{Re}(\mathbf{a}_1) \ln \frac{|1-\mathbf{a}|}{|\mathbf{a}|} - 2 \operatorname{Im}(\mathbf{a}_1) [\arg(1-\mathbf{a}) - \arg(-\mathbf{a})] \right. \\ &\quad + 2 \operatorname{Re}(\mathbf{b}_1) \ln \frac{|1-\mathbf{b}|}{|\mathbf{b}|} - 2 \operatorname{Im}(\mathbf{b}_1) [\arg(1-\mathbf{b}) - \arg(-\mathbf{b})] \\ &\quad \left. - \operatorname{Re} \left[\frac{2\mathbf{a}_2}{\mathbf{a}(1-\mathbf{a})} + \frac{2\mathbf{b}_2}{\mathbf{b}(1-\mathbf{b})} + \frac{(2\mathbf{a}-1)\mathbf{a}_3}{\mathbf{a}^2(1-\mathbf{a})^2} + \frac{(2\mathbf{b}-1)\mathbf{b}_3}{\mathbf{b}^2(1-\mathbf{b})^2} \right] \right\}.\end{aligned}$$

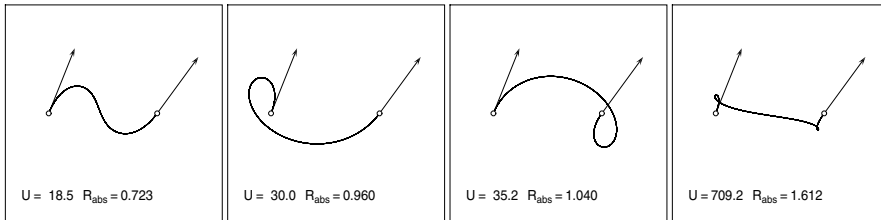


Fig. 26.1. The four PH quintic interpolants to given first-order Hermite data (the derivative vectors are shortened by a factor of 5 for clarity). The bending energy U and absolute rotation index R_{abs} agree in their identification of the “good” solution.

The explicit use of complex arithmetic and library functions, provided by most high-level languages, is clearly of great value in computing U .

The elastic energy U can be used as an alternative to the absolute rotation index (25.21), as the quantity whose minimum identifies the “good” Hermite interpolant among the four possible solutions — although it is obviously more costly to compute. For cases where the derivative magnitudes are not too large, these quantities usually indicate the same choice: see, for example, Fig. 26.1. When the derivatives are large, however, discrepancies may arise — as in the example of Fig. 26.2. Using R_{abs} penalizes interpolants that loop, but U is not averse to loops if regions of high curvature are thereby avoided.

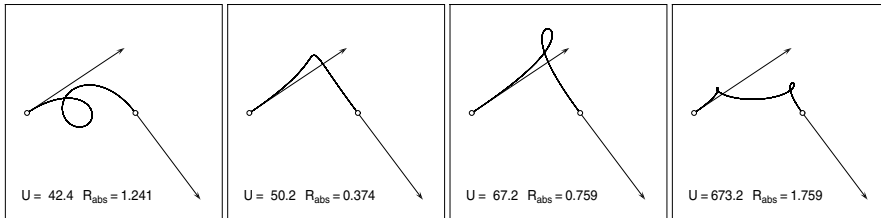


Fig. 26.2. An example with large derivatives, for which U and R_{abs} indicate *different* choices for the “good” solution (again, derivatives are shortened by a factor of 5) — R_{abs} favors the solution that avoids loops (but exhibits high curvature), while U selects the solution that performs a loop in order to avoid large curvature values.

26.4 The “Gracefulness” of PH Quintics

The good PH quintic interpolant to given first-order Hermite data is often a more aesthetically pleasing curve (with a more even curvature distribution) than its “ordinary” cubic counterpart. This observation is based on experience with numerous examples — due to the rather complicated form of the energy

of PH quintics, and the fact that ordinary cubics do not admit a closed-form energy expression, it would be difficult to verify analytically.

Quantitative empirical evidence for the statement comes from a numerical *Monte Carlo experiment* [150]. Fixing end-points $\mathbf{p}_0 = (0, 0)$ and $\mathbf{p}_1 = (1, 0)$ a total of 10^5 pairs of end-derivatives \mathbf{d}_0 and \mathbf{d}_1 were generated by randomly choosing orientations between 0 and 2π , and lengths between 0.3 and 3.0 — we exclude excessively small or large derivative magnitudes as “unrealistic” for practical use. The energies of the “good” PH quintic and ordinary cubic interpolants were computed for each data set (by numerical quadrature in the latter case). The resulting statistics may be summarized as follows.

The PH quintic was of lower energy than the ordinary cubic — often by a substantial factor — *for 99.7% of the data sets*. Moreover, in the very small fraction of instances where the PH quintic energy did exceed that of the cubic, the difference was barely significant — out of a total of 293 such cases, only 61 indicated a PH quintic energy more than 3% in excess of the cubic energy. All of these 61 cases were anomalous, in the sense that they corresponded to *a disparity of at least a factor of 4 in the derivative magnitudes*.

On the basis of this evidence, it seems safely established that for *reasonable* data — i.e., derivative magnitudes $|\mathbf{d}_0|$ and $|\mathbf{d}_1|$ commensurate with each other and with $|\mathbf{p}_1 - \mathbf{p}_0|$ — the PH quintics provide systematically better-shaped or “fairer” Hermite interpolants than the ordinary cubics. Thus, apart from their advantages in terms of computing offsets and arc lengths, PH quintics are worthy of consideration in design applications were the principal goal is to obtain as fair a curve as possible, consistent with interpolation constraints and compatibility with standard representation schemes.

Figure 26.3 illustrates the characteristic “gracefulness” of PH quintics, as compared to ordinary cubics. The bending energy offers a quantitative basis for this statement, but it is often also obvious merely from visual inspection. In Chap. 27 we shall see that this property of “shape elegance” extends to the comparison of planar C^2 PH quintic spline curves (that smoothly interpolate arbitrary sequences of points $\mathbf{p}_0, \dots, \mathbf{p}_N$) with “ordinary” C^2 cubic splines.

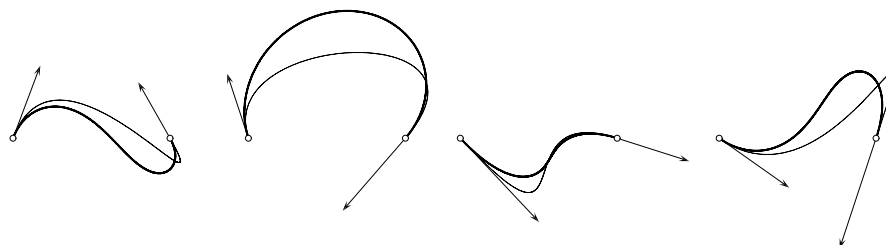


Fig. 26.3. Comparison of the “good” PH quintic (bold) and ordinary cubic (light) interpolants to four different first-order Hermite data sets. Clearly, the PH quintics are visually more pleasing or “fairer” curves, with less extreme curvature variations.

26.5 Minimal-energy Hermite Interpolants

From a strictly geometrical perspective, interpolation of tangent *vectors* (i.e., parametric derivatives), instead of just tangent *directions*, is a rather artificial requirement. We now relax the requirement to interpolate the magnitudes of the end derivatives \mathbf{d}_0 and \mathbf{d}_1 , and consider using the resulting freedoms to optimize the shape of G^1 (rather than C^1) PH quintic Hermite interpolants, by minimizing the energy U . Again, we fix $\mathbf{p}_0 = (0, 0)$ and $\mathbf{p}_1 = (1, 0)$ without loss of generality. The values \mathbf{a} , \mathbf{b} , \mathbf{k} appropriate to end-derivatives \mathbf{d}_0 , \mathbf{d}_1 are then (see §25.2) solutions to the system of quadratic equations

$$\begin{aligned} \mathbf{k}^2 \mathbf{a}^2 \mathbf{b}^2 &= \mathbf{d}_0 \quad \text{and} \quad \mathbf{k}^2 (1 - \mathbf{a})^2 (1 - \mathbf{b})^2 = \mathbf{d}_1, \\ \mathbf{k}^2 \left(\mathbf{a}^2 \mathbf{b}^2 - \mathbf{a}^2 \mathbf{b} - \mathbf{a} \mathbf{b}^2 + \frac{\mathbf{a}^2 + 4\mathbf{a}\mathbf{b} + \mathbf{b}^2}{3} - \frac{\mathbf{a} + \mathbf{b}}{2} + \frac{1}{5} \right) &= 1. \end{aligned}$$

The first two equations correspond to $\mathbf{r}'(0) = \mathbf{d}_0$ and $\mathbf{r}'(1) = \mathbf{d}_1$, while the third arises from the requirement that $\mathbf{r}(1) - \mathbf{r}(0) = 1$. These equations may, in principle, be solved for \mathbf{a} , \mathbf{b} , \mathbf{k} in terms of $\mathbf{d}_0 = d_0 \exp(i\theta_0)$, $\mathbf{d}_1 = d_1 \exp(i\theta_1)$. Substituting into the expressions for \mathbf{a}_k and \mathbf{b}_k for $k = 1, 2, 3$ and U for fixed θ_0 , θ_1 would then yield an expression $E(d_0, d_1)$ suitable for optimizing the energy with respect to the derivative magnitudes d_0 and d_1 .

However, solving for \mathbf{a} , \mathbf{b} , \mathbf{k} in terms of \mathbf{d}_0 , \mathbf{d}_1 involves a pair of nested quadratic equations (with four distinct solutions) and attempts to explicitly derive $U(d_0, d_1)$ prove unfruitful. In seeking to optimize it, we should regard U as a function that can be *evaluated* — by substituting into the expressions for \mathbf{a}_k , \mathbf{b}_k and U the \mathbf{a} , \mathbf{b} , \mathbf{k} values corresponding to the “good” interpolant for given d_0 and d_1 — but not easily *differentiated*. For optimization algorithms that do not require derivative information, see [58].

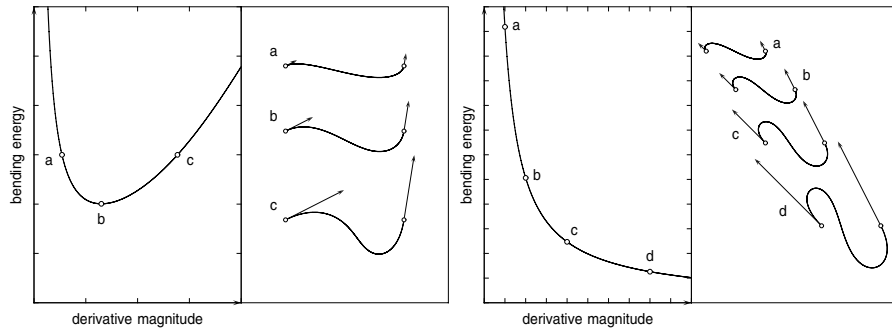


Fig. 26.4. Shape optimization of PH quintics with respect to derivative lengths. Left: a case with a clear optimum (b), of lower energy than the nearby curves (a) and (c). Right: a case in which the least energy curve is of infinite length — U declines monotonically with the magnitude of the two end derivatives from (a) through (d).

Figure 26.4 shows representative results, assuming $d_0 = d_1$ ($= d$ say). In the first example, $U(d)$ is a *convex* function with a global minimum identifying the “fairest” PH quintic with given end-slopes θ_0, θ_1 and derivatives of equal magnitude. In this case, for the entire range of d shown, the “good” interpolant corresponds to a unique choice of signs in the solution procedure for $\mathbf{a}, \mathbf{b}, \mathbf{k}$ in terms of $\mathbf{d}_0, \mathbf{d}_1$. However, this may not always be true: as d varies, the four continuous families of PH quintic interpolants may “cross” and the “good” interpolant then corresponds to *different* sign choices for different d values.

On the other hand, the second example in Fig. 26.4 shows a case where U apparently *has no minimum for finite d* (the computation was extended to values far greater than those shown). This illustrates a problem fundamental to the theory of *elastica*. As emphasized by Birkhoff and de Boor [43], curves that minimize the energy and interpolate given end-data, but are otherwise unconstrained, need not be of finite length — one may have loops of length $S \sim 2\pi r$ and curvature $\kappa \sim 1/r$, such that $\int \kappa^2 ds \rightarrow 0$ as $r \rightarrow \infty$.

In the theory of elastica, it is often posited that the total curve length S be specified as an *a priori* constraint (this is consistent with the physical model, in that U represents energy of *bending*, not axial extension or compression). For the PH quintics, S can be expressed in terms of $\mathbf{a}, \mathbf{b}, \mathbf{k}$ as

$$S = |\mathbf{k}|^2 \left(|\mathbf{a}|^2 |\mathbf{b}|^2 - |\mathbf{a}|^2 b - |\mathbf{b}|^2 a + \frac{|\mathbf{a}|^2 + 4ab + |\mathbf{b}|^2}{3} - \frac{a+b}{2} + \frac{1}{5} \right),$$

where $a = \text{Re}(\mathbf{a})$ and $b = \text{Re}(\mathbf{b})$. Assigning a fixed value to S as a constraint leaves one remaining degree of freedom with which to optimize U . However, this is a difficult problem, and fixing the length S may be an artificial condition in free-form design if there is no specific motivation for doing so.

It is also possible to define *unconstrained* optimization strategies that will circumvent the need to fix S , and still guarantee finite-length solutions. One possibility is to minimize the *product* SU of arc length and bending energy — this quantity is both *dimensionless* and *scale-invariant*, which are desirable characteristics for an “intrinsic shape” measure. Another is to include axial deformation in the elastic energy model — i.e., to minimize $\lambda U + \mu V$, where λ and μ are adjustable dimensionless weights, and $V = (S - S_0)^2 / S_0^3$ represents (for suitable S_0) the energy of tension or compression.

Planar C^2 PH Quintic Splines

There's always more room in the Spline Zoo!

Tom Lyche

In Chap. 14 we reviewed the classical (linear) theory of “ordinary” C^2 cubic splines. Having discussed how individual PH curve segments are constructed, we are now ready to address the more challenging problem of constructing C^2 PH quintic spline curves. Our focus at present is on *planar* PH splines, and we use the complex representation (Chap. 19) to facilitate their computation.

It should be noted that some authors use the term “spline” rather broadly to connote any piecewise-polynomial function or curve, with a given order of continuity at the junctures of adjacent segments. Such piecewise-polynomial functions or curves can easily be constructed in a purely *local* manner — e.g., Hermite interpolation of consecutive point/tangent pairs — but of course such “local” constructions cannot achieve the desired *global smoothness* emphasized in Chap. 14. Our intent here is to develop constructions for planar C^2 PH quintic splines that mirror, as closely as possible, the classical construction of C^2 “ordinary” cubic spline curves, as described in Chap. 14.

27.1 Construction of PH Splines

As will become apparent in this chapter, there are noteworthy similarities and differences in the constructions and properties of “ordinary” C^2 cubic splines and C^2 PH quintic splines. As an overview of what follows, we begin by briefly summarizing these common and disparate features.

1. Both involve, for their construction, the solution of a “global” system of equations, with only three consecutive unknowns in each equation.
2. Both require augmentation of the equations by suitable *end conditions*.

3. Whereas “ordinary” splines incur a *linear* system in *real* variables, for PH splines the equations are *quadratic* and the unknowns are *complex*.
4. With ordinary cubic splines, these equations arise from the C^2 continuity condition at interior nodes. For PH splines, they result from equating the integral of the hodograph to the displacement between successive points.
5. The linearity of ordinary splines guarantees uniqueness of the interpolant, and allows construction through vector space (spline basis) methods. The non-linear nature of PH splines yields a multiplicity of formal solutions, and precludes the possibility of linear superposition.
6. The coordinate components of ordinary splines are weakly coupled through the *a priori* specification of nodal parameter (knot) values. For PH splines, however, they are coupled in an essential and inextricable manner (namely, by the requirement that each segment have a Pythagorean hodograph).

To elaborate on point 6 above, note that an “ordinary” spline curve is a set of scalar spline *functions* $x(t), y(t), \dots$, one for each coordinate, constructed as described in §14.4. The only “communication” between these functions is through their common set of knot values t_0, \dots, t_N . Since the Pythagorean–hodograph nature of a curve corresponds to an algebraic coupling among its coordinate components, PH splines cannot be constructed in terms of scalar functions that are independent apart from common knots — the formulation must explicitly incorporate the PH property by regarding the PH spline curve as a single entity, rather than in a component-wise manner.

27.1.1 C^2 PH Quintic Spline Equations

The construction of a C^2 PH quintic spline curve, that interpolates an ordered set of $N + 1$ points $\mathbf{q}_0, \dots, \mathbf{q}_N$ and satisfies prescribed end conditions, entails the solution of a system of N quadratic equations in N complex unknowns, $\mathbf{z}_1, \dots, \mathbf{z}_N$. To formulate these equations, we begin by writing the hodograph of the PH quintic segment $\mathbf{r}_i(t)$, $t \in [0, 1]$ of the spline curve, between points \mathbf{q}_{i-1} and \mathbf{q}_i , as the square of a complex quadratic polynomial in the form

$$\mathbf{r}'_i(t) = [\frac{1}{2}(\mathbf{z}_{i-1} + \mathbf{z}_i)(1-t)^2 + \mathbf{z}_i 2(1-t)t + \frac{1}{2}(\mathbf{z}_i + \mathbf{z}_{i+1})t^2]^2. \quad (27.1)$$

This ensures that the spline segment $\mathbf{r}_i(t)$ obtained by integration of $\mathbf{r}'_i(t)$ is a PH quintic (see Chap. 19). Also, one can easily verify that the coefficients in (27.1) are written in such a manner as to guarantee that consecutive segments $\mathbf{r}_i(t)$ and $\mathbf{r}_{i+1}(t)$ exhibit continuity of first and second derivatives at their common juncture $\mathbf{q}_i = \mathbf{r}_i(1) = \mathbf{r}_{i+1}(0)$. Specifically, we have

$$\begin{aligned} \mathbf{r}'_i(1) &= \mathbf{r}'_{i+1}(0) = \frac{1}{4}(\mathbf{z}_i + \mathbf{z}_{i+1})^2, \\ \mathbf{r}''_i(1) &= \mathbf{r}''_{i+1}(0) = (\mathbf{z}_{i+1} - \mathbf{z}_i)(\mathbf{z}_i + \mathbf{z}_{i+1}). \end{aligned}$$

Having ensured continuity of first and second derivatives between adjacent segments, we now consider interpolation of the points $\mathbf{q}_0, \dots, \mathbf{q}_N$. Expanding (27.1) in the quartic Bernstein basis gives

$$\begin{aligned}\mathbf{r}'_i(t) = & \frac{1}{4} (\mathbf{z}_{i-1} + \mathbf{z}_i)^2 (1-t)^4 \\ & + \frac{1}{2} (\mathbf{z}_{i-1} + \mathbf{z}_i) \mathbf{z}_i 4(1-t)^3 t \\ & + \frac{1}{12} [8\mathbf{z}_i^2 + (\mathbf{z}_{i-1} + \mathbf{z}_i)(\mathbf{z}_i + \mathbf{z}_{i+1})] 6(1-t)^2 t^2 \\ & + \frac{1}{2} (\mathbf{z}_i + \mathbf{z}_{i+1}) \mathbf{z}_i 4(1-t)t^3 \\ & + \frac{1}{4} (\mathbf{z}_i + \mathbf{z}_{i+1})^2 t^4.\end{aligned}$$

Now each quartic Bernstein basis function has definite integral $\frac{1}{5}$ (see §11.2). Hence, on taking $\mathbf{r}_i(0) = \mathbf{q}_{i-1}$ as the integration constant and writing $\Delta\mathbf{q}_i = \mathbf{q}_i - \mathbf{q}_{i-1}$, the interpolation condition

$$\int_0^1 \mathbf{r}'_i(t) dt = \Delta\mathbf{q}_i$$

yields the equation

$$\begin{aligned}\mathbf{f}_i(\mathbf{z}_1, \dots, \mathbf{z}_N) = & 3\mathbf{z}_{i-1}^2 + 27\mathbf{z}_i^2 + 3\mathbf{z}_{i+1}^2 + \mathbf{z}_{i-1}\mathbf{z}_{i+1} \\ & + 13\mathbf{z}_{i-1}\mathbf{z}_i + 13\mathbf{z}_i\mathbf{z}_{i+1} - 60\Delta\mathbf{q}_i = 0\end{aligned}\quad (27.2)$$

relating the three unknowns \mathbf{z}_{i-1} , \mathbf{z}_i , \mathbf{z}_{i+1} to the known quantity $\Delta\mathbf{q}_i$. Such a condition must hold for each segment $\mathbf{r}_i(t)$, $i = 1, \dots, N$ of the spline curve, but the first and last equations, $\mathbf{f}_1(\mathbf{z}_1, \dots, \mathbf{z}_N) = 0$ and $\mathbf{f}_N(\mathbf{z}_1, \dots, \mathbf{z}_N) = 0$, should be modified by introducing “end conditions” in order to avoid reference to the undefined quantities \mathbf{z}_0 and \mathbf{z}_{N+1} . The modifications appropriate to (a) PH cubic (Tscheirnhaus) end segments; (b) periodic curves; and (c) prescribed end-derivatives \mathbf{d}_0 , \mathbf{d}_N at the points \mathbf{q}_0 , \mathbf{q}_N are described in §27.1.2.

As with the linear system for “ordinary” C^2 cubic splines (see §14.4), we observe that only three consecutive variables appear in each member of the system (27.2). Its non-linear nature, however, makes this system much more challenging to solve — in general, numerical methods must be invoked.

Two complementary approaches are described here. The *homotopy method* computes the entire set of solutions, allowing their geometrical properties to be systematically investigated. In general, there exists a unique “good” spline among the solutions: the others exhibit extreme curvature variations and/or undesired loops. Quantitative measures used to identify the “good” solution include the *absolute rotation index* and *elastic bending energy*. However, the homotopy method is very expensive for $N \gtrsim 10$. As an efficient alternative, the use of Newton–Raphson iterations to compute *only* the “good” PH spline, from an initial approximation close to the desired solution, is discussed.

Remark 27.1 The motivation for the chosen hodograph form (27.1) may be understood geometrically as follows. The points $\mathbf{z}_1, \dots, \mathbf{z}_N$ can be regarded as

vertices of a polygon in the complex plane, the polygon segment mid-points being $\frac{1}{2}(\mathbf{z}_{i-1} + \mathbf{z}_i)$, $\frac{1}{2}(\mathbf{z}_i + \mathbf{z}_{i+1})$, etc. Each triple of complex values

$$\frac{1}{2}(\mathbf{z}_{i-1} + \mathbf{z}_i), \quad \mathbf{z}_i, \quad \frac{1}{2}(\mathbf{z}_i + \mathbf{z}_{i+1})$$

defines a quadratic Bézier (i.e., parabola) segment, and these segments meet with C^1 continuity. The hodograph of the C^2 PH spline is the image of this C^1 quadratic spline under the map $\mathbf{z} \rightarrow \mathbf{z}^2$ of the complex plane (see Chap. 19).

Once the values $\mathbf{z}_1, \dots, \mathbf{z}_N$ are known, we can construct the Bézier form

$$\mathbf{r}_i(t) = \sum_{k=0}^5 \mathbf{p}_{i,k} \binom{5}{k} (1-t)^{5-k} t^k$$

for each PH quintic segment, $i = 1, \dots, N$. Specifically, the control points are obtained by integrating the hodograph (27.1), which gives

$$\begin{aligned} \mathbf{p}_{i,1} &= \mathbf{p}_{i,0} + \frac{1}{5} \mathbf{w}_{i,0}^2, \\ \mathbf{p}_{i,2} &= \mathbf{p}_{i,1} + \frac{1}{5} \mathbf{w}_{i,0} \mathbf{w}_{i,1}, \\ \mathbf{p}_{i,3} &= \mathbf{p}_{i,2} + \frac{2}{15} \mathbf{w}_{i,1}^2 + \frac{1}{15} \mathbf{w}_{i,0} \mathbf{w}_{i,2}, \\ \mathbf{p}_{i,4} &= \mathbf{p}_{i,3} + \frac{1}{5} \mathbf{w}_{i,1} \mathbf{w}_{i,2}, \\ \mathbf{p}_{i,5} &= \mathbf{p}_{i,4} + \frac{1}{5} \mathbf{w}_{i,2}^2, \end{aligned} \tag{27.3}$$

where $\mathbf{p}_{i,0} = \mathbf{q}_{i-1}$ and $\mathbf{w}_{i,0} = \frac{1}{2}(\mathbf{z}_{i-1} + \mathbf{z}_i)$, $\mathbf{w}_{i,1} = \mathbf{z}_i$, $\mathbf{w}_{i,2} = \frac{1}{2}(\mathbf{z}_i + \mathbf{z}_{i+1})$, with appropriate modifications for the end conditions.

27.1.2 End Conditions for PH Splines

The end conditions for C^2 PH quintic splines formulated below are analogs of those discussed in §14.4.3 for “ordinary” C^2 cubic splines, with one exception. In the latter context, the “not-a-knot” condition arose from equating *third* derivatives at the juncture of the initial two segments and final two segments. Since C^3 continuity of “ordinary” cubics implies that these cubics are actually identical, the first two and last two segments are then portions of single cubics. If we apply this strategy in the case of C^2 PH quintic splines, equating third derivatives at the first and last interior knots yields the undefined quantities \mathbf{z}_0 and \mathbf{z}_{N+1} as linear combinations of $\mathbf{z}_1, \mathbf{z}_2, \mathbf{z}_3$ and $\mathbf{z}_N, \mathbf{z}_{N-1}, \mathbf{z}_{N-2}$ respectively. However, the first two and last two segments are *not* portions of single PH quintics. Since this condition does not admit a meaningful interpretation in the context of PH splines, we omit it from consideration.

Cubic End Segments

A canonical end condition for ordinary C^2 cubic splines involves a reduction of degree, from cubic to quadratic, in the initial and final segments. Since regular PH curves are generated by integrating the squares of complex polynomials, they are necessarily of *odd* degree, and the analogous end conditions for C^2 PH quintic splines thus involve a degree reduction to *cubic* end segments. For cubic end spans, we replace equation (27.1) for $i = 1$ and $i = N$ by

$$\begin{aligned}\mathbf{r}'_1(t) &= [\frac{1}{2}(3\mathbf{z}_1 - \mathbf{z}_2)(1-t)^2 + \mathbf{z}_1 2(1-t)t + \frac{1}{2}(\mathbf{z}_1 + \mathbf{z}_2)t^2]^2, \\ \mathbf{r}'_N(t) &= [\frac{1}{2}(\mathbf{z}_{N-1} + \mathbf{z}_N)(1-t)^2 + \mathbf{z}_N 2(1-t)t + \frac{1}{2}(3\mathbf{z}_N - \mathbf{z}_{N-1})t^2]^2.\end{aligned}$$

The above quadratic forms are actually *degree-elevated linear polynomials*, so $\mathbf{r}_1(t)$ and $\mathbf{r}_N(t)$ are really *cubic* (Tscheirnhaus) PH curves, rather than quintics. The first and last equations in (27.2) then assume the form

$$\begin{aligned}\mathbf{f}_1(\mathbf{z}_1, \dots, \mathbf{z}_N) &= 13\mathbf{z}_1^2 + \mathbf{z}_2^2 - 2\mathbf{z}_1\mathbf{z}_2 - 12\Delta\mathbf{q}_1 = 0, \\ \mathbf{f}_N(\mathbf{z}_1, \dots, \mathbf{z}_N) &= 13\mathbf{z}_N^2 + \mathbf{z}_{N-1}^2 - 2\mathbf{z}_N\mathbf{z}_{N-1} - 12\Delta\mathbf{q}_N = 0.\end{aligned}\quad (27.4)$$

Periodic End Conditions

For the case of periodic end conditions, we assign $\mathbf{q}_N = \mathbf{q}_0$ to indicate that a smooth closed curve is desired, with $\mathbf{r}'_N(1) = \mathbf{r}'_1(0)$ and $\mathbf{r}''_N(1) = \mathbf{r}''_1(0)$. To achieve this, we interpret $\mathbf{z}_1, \dots, \mathbf{z}_N$ as a cyclical list, and for $i = 1$ and $i = N$ we replace (27.1) by

$$\begin{aligned}\mathbf{r}'_1(t) &= [\frac{1}{2}(\pm\mathbf{z}_N + \mathbf{z}_1)(1-t)^2 + \mathbf{z}_1 2(1-t)t + \frac{1}{2}(\mathbf{z}_1 + \mathbf{z}_2)t^2]^2, \\ \mathbf{r}'_N(t) &= [\frac{1}{2}(\mathbf{z}_{N-1} + \mathbf{z}_N)(1-t)^2 + \mathbf{z}_N 2(1-t)t + \frac{1}{2}(\mathbf{z}_N \pm \mathbf{z}_1)t^2]^2.\end{aligned}$$

The first and last members of the system (27.2) are then

$$\begin{aligned}\mathbf{f}_1(\mathbf{z}_1, \dots, \mathbf{z}_N) &= 3\mathbf{z}_N^2 + 27\mathbf{z}_1^2 + 3\mathbf{z}_2^2 \pm \mathbf{z}_N\mathbf{z}_2 \\ &\quad \pm 13\mathbf{z}_N\mathbf{z}_1 + 13\mathbf{z}_1\mathbf{z}_2 - 60\Delta\mathbf{q}_1 = 0, \\ \mathbf{f}_N(\mathbf{z}_1, \dots, \mathbf{z}_N) &= 3\mathbf{z}_{N-1}^2 + 27\mathbf{z}_N^2 + 3\mathbf{z}_1^2 \pm \mathbf{z}_{N-1}\mathbf{z}_1 \\ &\quad + 13\mathbf{z}_{N-1}\mathbf{z}_N \pm 13\mathbf{z}_N\mathbf{z}_1 - 60\Delta\mathbf{q}_N = 0.\end{aligned}\quad (27.5)$$

Note that the *same* sign choice must be employed in \mathbf{f}_1 and \mathbf{f}_N above — the “good” solution may occur for either. As with “ordinary” C^2 cubic splines, the system obtained with periodic end conditions is not strictly tridiagonal.

Specified End Derivatives

Finally, if derivatives $\mathbf{d}_0 = \mathbf{r}_1(0)$, $\mathbf{d}_N = \mathbf{r}_N(1)$ at \mathbf{q}_0 , \mathbf{q}_N are specified as end conditions, the first and last members of the system (27.2) become

$$\begin{aligned} \mathbf{f}_1(\mathbf{z}_1, \dots, \mathbf{z}_N) &= 12\mathbf{a}_0^2 + 17\mathbf{z}_1^2 + 3\mathbf{z}_2^2 + 12\mathbf{z}_1\mathbf{z}_2 \\ &\quad + 14\mathbf{a}_0\mathbf{z}_1 + 2\mathbf{a}_0\mathbf{z}_2 - 60\Delta\mathbf{q}_1 = 0, \\ \mathbf{f}_N(\mathbf{z}_1, \dots, \mathbf{z}_N) &= 12\mathbf{a}_N^2 + 17\mathbf{z}_N^2 + 3\mathbf{z}_{N-1}^2 + 12\mathbf{z}_N\mathbf{z}_{N-1} \\ &\quad + 14\mathbf{a}_N\mathbf{z}_N + 2\mathbf{a}_N\mathbf{z}_{N-1} - 60\Delta\mathbf{q}_N = 0, \end{aligned} \quad (27.6)$$

where the complex values \mathbf{a}_0 and \mathbf{a}_N satisfy

$$\mathbf{a}_0^2 = \mathbf{d}_0 \quad \text{and} \quad \mathbf{a}_N^2 = \mathbf{d}_N. \quad (27.7)$$

Imposing end derivatives is not recommended as a means of completing the system (27.2) without *a priori* knowledge of suitable values for \mathbf{d}_0 and \mathbf{d}_N . We focus henceforth on cubic end spans and periodic end conditions.

27.1.3 Number of Distinct Interpolants

The non-linear nature of the system of equations specified by (27.2) for $i = 2, \dots, N-1$ and any of the end conditions (27.4)–(27.6) implies a multiplicity of formal solutions, each defining a PH quintic spline curve that interpolates the given points $\mathbf{q}_0, \dots, \mathbf{q}_N$ and also exhibits C^2 continuity at the junctures of consecutive segments. To determine the number of C^2 PH splines for any given number of points N we may invoke *Bézout's theorem* (§9.2.9), but care must be exercised with regard to the treatment of end conditions and the identification of which formal solutions $\mathbf{z}_1, \dots, \mathbf{z}_N$ yield *distinct* PH splines.

We begin by noting that if $\mathbf{z}_1, \dots, \mathbf{z}_N$ is a solution of the spline equations, then so is $-\mathbf{z}_1, \dots, -\mathbf{z}_N$, and these two solutions define *exactly the same PH spline curve*, since they yield identical hodographs on substitution into (27.1). To avoid replication, we require that $\operatorname{Re}(\mathbf{z}_1) > 0$ — or, if $\operatorname{Re}(\mathbf{z}_1) = 0$, that $\operatorname{Re}(\mathbf{z}_\ell) > 0$ where ℓ is the least index satisfying $\operatorname{Re}(\mathbf{z}_\ell) \neq 0$.

For cubic end spans, the system specified by (27.2) for $i = 2, \dots, N-1$ augmented by (27.4) for $i = 1$ and N comprises N quadratic equations in N unknowns, so we may expect 2^N solutions $\mathbf{z}_1, \dots, \mathbf{z}_N$ from Bézout's theorem. Eliminating the immaterial sign ambiguity in these solutions by imposing the requirement that $\operatorname{Re}(\mathbf{z}_\ell) > 0$, as described above, we see that the number of *distinct* PH quintic splines with cubic end spans is 2^{N-1} .

The same analysis holds for the case of the periodic end conditions (27.5), except that the latter incorporate a single sign choice that must be exercised to obtain all distinct solutions. Hence, in the case of periodic end conditions, the number of distinct interpolants becomes 2^N . Finally, for the case (27.6) of specified end-derivatives, equations (27.7) incur *two* sign choices in (27.6), and hence the number of distinct interpolants is 2^{N+1} .

To summarize, the number of distinct C^2 PH quintic splines interpolating a sequence of $N+1$ points $\mathbf{q}_0, \dots, \mathbf{q}_N$ can be expressed as 2^{N+m} , where we take $m = -1$ for cubic end segments; $m = 0$ for periodic splines; and $m = +1$ for the case of specified end-derivatives \mathbf{d}_0 and \mathbf{d}_N .

27.2 Solution by Homotopy Method

The purpose of *homotopy* — or “continuation” or “embedding” — methods is to compute all solutions (real and complex) of a system of non-linear equations [17, 18, 335]. The equations are first “simplified” by omitting certain terms, or by other means, to obtain a system that has a *known* closed-form solution. A homotopy variable $\lambda \in [0, 1]$ is then introduced, to parameterize a continuous deformation of the simple system ($\lambda = 0$) into the given system ($\lambda = 1$). As λ is incremented from 0 to 1, the set of all (real and complex) solutions is tracked through the deformation process using a numerical (e.g., predictor–corrector) scheme with discrete steps.

27.2.1 Choice of Initial System

As the initial “simple” system, for $i = 2, \dots, N - 1$ we take

$$\mathbf{g}_i(\mathbf{z}_1, \dots, \mathbf{z}_N) = 27\mathbf{z}_i^2 - 60\Delta\mathbf{q}_i = 0, \quad (27.8)$$

obtained by deleting all terms in (27.2) that depend on variables other than \mathbf{z}_i . The solutions are obviously

$$\mathbf{z}_i = \pm \frac{2}{3} \sqrt{5\Delta\mathbf{q}_i}.$$

The $i = 1$ and $i = N$ equations depend on the adopted end conditions.

For cubic end spans, we delete all terms in (27.4) that depend on variables other than \mathbf{z}_1 and \mathbf{z}_N , respectively, to obtain

$$\begin{aligned}\mathbf{g}_1(\mathbf{z}_1, \dots, \mathbf{z}_N) &= 13\mathbf{z}_1^2 - 12\Delta\mathbf{q}_1 = 0, \\ \mathbf{g}_N(\mathbf{z}_1, \dots, \mathbf{z}_N) &= 13\mathbf{z}_N^2 - 12\Delta\mathbf{q}_N = 0,\end{aligned}$$

with solutions

$$\mathbf{z}_1 = \pm \sqrt{\frac{12}{13}\Delta\mathbf{q}_1}, \quad \mathbf{z}_N = \pm \sqrt{\frac{12}{13}\Delta\mathbf{q}_N}.$$

Since each variable has two different initial values, these expressions yield 2^N sets of starting values $\mathbf{z}_1, \dots, \mathbf{z}_N$. However, the requirement that $\text{Re}(\mathbf{z}_\ell) > 0$ reduces the number of initial-value sets to 2^{N-1} , in agreement with the known number of distinct PH splines with cubic end spans.

For periodic end conditions, we simplify equations (27.5) to

$$\begin{aligned}\mathbf{g}_1(\mathbf{z}_1, \dots, \mathbf{z}_N) &= 27\mathbf{z}_1^2 \pm 13\mathbf{z}_N\mathbf{z}_1 - 60\Delta\mathbf{q}_1 = 0, \\ \mathbf{g}_N(\mathbf{z}_1, \dots, \mathbf{z}_N) &= 27\mathbf{z}_N^2 \pm 13\mathbf{z}_N\mathbf{z}_1 - 60\Delta\mathbf{q}_N = 0.\end{aligned}$$

We retain the $\mathbf{z}_N\mathbf{z}_1$ “cross terms” and the sign freedoms associated with them, to ensure that the number of distinct solutions to the initial system is equal

to the number of distinct periodic PH splines. Eliminating \mathbf{z}_N among these equations, the sign choice disappears, and we obtain the biquadratic

$$252\mathbf{z}_1^4 - (1289\Delta\mathbf{q}_1 + 169\Delta\mathbf{q}_N)\mathbf{z}_1^2 + 1620(\Delta\mathbf{q}_1)^2 = 0$$

which has in general four distinct solutions for \mathbf{z}_1 . Substituting these solutions into $\mathbf{g}_1(\mathbf{z}_1, \dots, \mathbf{z}_N) = 0$ gives eight corresponding \mathbf{z}_N values. These eight pairs of \mathbf{z}_1 and \mathbf{z}_N values, taken in combination with the 2^{N-2} sets of solutions for $i = 1, \dots, N-1$ to (27.8), give 2^{N+1} initial value sets for $\mathbf{z}_1, \dots, \mathbf{z}_N$. Again the condition $\text{Re}(\mathbf{z}_\ell) > 0$ reduces this to 2^N sets, coinciding with the number of distinct PH splines that have periodic end conditions.

Finally, for specified end-derivatives, we again delete terms in (27.6) that depend on variables other than \mathbf{z}_1 and \mathbf{z}_N , respectively, to obtain

$$\begin{aligned}\mathbf{g}_1(\mathbf{z}_1, \dots, \mathbf{z}_N) &= 17\mathbf{z}_1^2 + 14\mathbf{a}_0\mathbf{z}_1 + 12\mathbf{a}_0^2 - 60\Delta\mathbf{q}_1 = 0, \\ \mathbf{g}_N(\mathbf{z}_1, \dots, \mathbf{z}_N) &= 17\mathbf{z}_N^2 + 14\mathbf{a}_N\mathbf{z}_N + 12\mathbf{a}_N^2 - 60\Delta\mathbf{q}_N = 0.\end{aligned}$$

These equations have the solutions

$$\begin{aligned}\mathbf{z}_1 &= \frac{-7\mathbf{a}_0 \pm \sqrt{1020\Delta\mathbf{q}_1 - 155\mathbf{a}_0^2}}{17}, \\ \mathbf{z}_N &= \frac{-7\mathbf{a}_N \pm \sqrt{1020\Delta\mathbf{q}_N - 155\mathbf{a}_N^2}}{17}.\end{aligned}$$

Since there are, in general, two distinct values for each of $\mathbf{z}_1, \dots, \mathbf{z}_N$ and also two for $\mathbf{a}_0, \mathbf{a}_N$ these expressions yield 2^{N+2} sets of starting values. Again, the requirement $\text{Re}(\mathbf{z}_\ell) > 0$ reduces this to 2^{N+1} , equal to the number of distinct PH splines incorporating prescribed end-derivatives.

27.2.2 Predictor–corrector Procedure

Having specified the initial systems and their closed-form solutions, we now define the homotopy system by

$$\mathbf{h}_i(\mathbf{z}_1, \dots, \mathbf{z}_N, \lambda) = (1-\lambda)e^{i\phi}\mathbf{g}_i(\mathbf{z}_1, \dots, \mathbf{z}_N) + \lambda\mathbf{f}_i(\mathbf{z}_1, \dots, \mathbf{z}_N) = 0 \quad (27.9)$$

for $i = 1, \dots, N$. The factor $e^{i\phi}$ guarantees that (for randomly-chosen ϕ) the solution paths $\mathbf{z}_1(\lambda), \dots, \mathbf{z}_N(\lambda)$ are regular [336, 337, 479] for $0 < \lambda < 1$ — i.e., the *Jacobian matrix* \mathbf{M} with elements

$$\mathbf{M}_{ij} = \frac{\partial \mathbf{h}_i}{\partial \mathbf{z}_j} \quad (27.10)$$

for $1 \leq i, j \leq N$ is non-singular at each point along these solution paths.

The advantage of the homotopy method is that it computes *all* solutions to (27.2), allowing the complete family of C^2 PH quintic splines interpolating $\mathbf{q}_0, \dots, \mathbf{q}_N$ to be investigated. Since the system (27.2) is well-conditioned, the

homotopy method typically yields convergence to machine precision. Except for modest N values, however, it is computationally very expensive. Among the totality of solutions computed by the homotopy method, we shall observe that there is typically a unique “good” interpolant (characterized by the least bending energy or absolute rotation index). In §27.3 we shall describe methods to compute this “good” solution directly, at reasonable cost.

We use a predictor–corrector path–following scheme based on constant, linear prediction steps $\Delta\lambda$ in the homotopy parameter, and Newton–Raphson correction iterations (the latter incur only tridiagonal linear equations). The method admits a compact implementation in complex arithmetic. It tracks the complete set of 2^{N+m} solution paths $\mathbf{z}_1(\lambda), \dots, \mathbf{z}_N(\lambda)$ to the system (27.9), as we continuously deform it, from the known solutions of the initial system (27.8) at $\lambda = 0$ to the desired solutions of the final system (27.2) at $\lambda = 1$.

For the functions (27.9), the $N \times N$ Jacobian matrix is tridiagonal (except for periodic end conditions). On rows $i = 2, \dots, N-1$ it has non–zero elements

$$\begin{aligned}\mathbf{M}_{i,i-1} &= \lambda(6\mathbf{z}_{i-1} + 13\mathbf{z}_i + \mathbf{z}_{i+1}), \\ \mathbf{M}_{ii} &= 13\lambda(\mathbf{z}_{i-1} + \mathbf{z}_{i+1}) + 54(\lambda + (1-\lambda)e^{i\phi})\mathbf{z}_i, \\ \mathbf{M}_{i,i+1} &= \lambda(\mathbf{z}_{i-1} + 13\mathbf{z}_i + 6\mathbf{z}_{i+1}).\end{aligned}$$

The non–zero elements on rows 1 and N depend on the end conditions. For cubic end segments, the non–zero elements are

$$\begin{aligned}\mathbf{M}_{11} &= 26(\lambda + (1-\lambda)e^{i\phi})\mathbf{z}_1 - 2\lambda\mathbf{z}_2, \\ \mathbf{M}_{12} &= 2\lambda\mathbf{z}_2 - 2\lambda\mathbf{z}_1, \\ \mathbf{M}_{N,N-1} &= 2\lambda\mathbf{z}_{N-1} - 2\lambda\mathbf{z}_N, \\ \mathbf{M}_{NN} &= 26(\lambda + (1-\lambda)e^{i\phi})\mathbf{z}_N - 2\lambda\mathbf{z}_{N-1}.\end{aligned}$$

For periodic end conditions we have

$$\begin{aligned}\mathbf{M}_{1N} &= 6\lambda\mathbf{z}_N \pm 13(\lambda + (1-\lambda)e^{i\phi})\mathbf{z}_1 \pm \lambda\mathbf{z}_2, \\ \mathbf{M}_{11} &= \pm 13(\lambda + (1-\lambda)e^{i\phi})\mathbf{z}_N + 54(\lambda + (1-\lambda)e^{i\phi})\mathbf{z}_1 + 13\lambda\mathbf{z}_2, \\ \mathbf{M}_{12} &= \pm \lambda\mathbf{z}_N + 13\lambda\mathbf{z}_1 + 6\lambda\mathbf{z}_2, \\ \mathbf{M}_{N1} &= 6\lambda\mathbf{z}_1 \pm 13(\lambda + (1-\lambda)e^{i\phi})\mathbf{z}_N \pm \lambda\mathbf{z}_{N-1}, \\ \mathbf{M}_{N,N-1} &= \pm \lambda\mathbf{z}_1 + 13\lambda\mathbf{z}_N + 6\lambda\mathbf{z}_{N-1}, \\ \mathbf{M}_{NN} &= \pm 13(\lambda + (1-\lambda)e^{i\phi})\mathbf{z}_1 + 54(\lambda + (1-\lambda)e^{i\phi})\mathbf{z}_N + 13\lambda\mathbf{z}_{N-1}.\end{aligned}$$

In this case, \mathbf{M} is no longer tridiagonal because \mathbf{M}_{1N} and \mathbf{M}_{N1} are non–zero. Finally, for specified end–derivatives, the non–zero elements on rows 1 and N of \mathbf{M} are

$$\begin{aligned}\mathbf{M}_{11} &= 12\lambda\mathbf{z}_2 + (\lambda + (1-\lambda)e^{i\phi})(34\mathbf{z}_1 + 14\mathbf{a}_0), \\ \mathbf{M}_{12} &= \lambda(12\mathbf{z}_1 + 6\mathbf{z}_2 + 2\mathbf{a}_0), \\ \mathbf{M}_{N,N-1} &= \lambda(6\mathbf{z}_{N-1} + 12\mathbf{z}_N + 2\mathbf{a}_N), \\ \mathbf{M}_{NN} &= 12\lambda\mathbf{z}_{N-1} + (\lambda + (1-\lambda)e^{i\phi})(34\mathbf{z}_N + 14\mathbf{a}_N).\end{aligned}$$

The predictor–corrector method is implemented as follows. For each step $\Delta\lambda$ in the homotopy parameter, the *prediction* stage consists of computing increments $\Delta\mathbf{z}_1, \dots, \Delta\mathbf{z}_N$ to the current $\mathbf{z}_1, \dots, \mathbf{z}_N$ values that correspond to a linear expansion of equations (27.9) about the current position. In other words, we step a distance $\Delta\lambda$ along the *tangent direction* to the one-dimensional locus in $\mathbb{C}^N \times \mathbb{R}$ defined by equations (27.9). This gives rise to the tridiagonal (linear) system of equations

$$\sum_{j=1}^N \mathbf{M}_{ij} \Delta\mathbf{z}_j = (e^{i\phi} \mathbf{g}_i - \mathbf{f}_i) \Delta\lambda, \quad i = 1, \dots, N \quad (27.11)$$

for the increments $\Delta\mathbf{z}_1, \dots, \Delta\mathbf{z}_N$, the Jacobian matrix elements \mathbf{M}_{ij} and the functions \mathbf{f}_i and \mathbf{g}_i being evaluated *at the current position* $(\mathbf{z}_1, \dots, \mathbf{z}_N, \lambda)$.

Due to the curvature of the solution locus, the prediction step generally incurs a deviation from the exact solution of (27.9) at $\lambda + \Delta\lambda$. To compensate for this, we employ Newton–Raphson *correction* iterations

$$\mathbf{z}_j^{(r+1)} = \mathbf{z}_j^{(r)} + \delta\mathbf{z}_j, \quad j = 1, \dots, N$$

for $r = 1, 2, \dots$, where the starting approximation $\mathbf{z}_1^{(0)}, \dots, \mathbf{z}_N^{(0)}$ corresponds to the outcome of the prediction step. At the r -th iteration, the increments $\delta\mathbf{z}_1, \dots, \delta\mathbf{z}_N$ are solutions to the tridiagonal system

$$\sum_{j=1}^N \mathbf{M}_{ij}^{(r)} \delta\mathbf{z}_j = -\mathbf{h}_i^{(r)}, \quad i = 1, \dots, N, \quad (27.12)$$

with the elements $\mathbf{M}_{ij}^{(r)}$ and functions $\mathbf{h}_i^{(r)}$ evaluated at $(\mathbf{z}_1^{(r)}, \dots, \mathbf{z}_N^{(r)}, \lambda + \Delta\lambda)$. The correction iterations proceed until the quantity

$$\epsilon_{\mathbf{h}}^{(r)} = \sqrt{\sum_{j=1}^N |\mathbf{h}_j(\mathbf{z}_1^{(r)}, \dots, \mathbf{z}_N^{(r)}, \lambda + \Delta\lambda)|^2} \quad (27.13)$$

diminishes below a prescribed tolerance. Typically, only a few iterations are needed if this value is $\sim 10^{-10}$ and $\Delta\lambda$ is not too large. Similar norms $\epsilon_{\mathbf{f}}, \epsilon_{\mathbf{g}}$ can be defined for the PH spline equations and initial equations individually.

For cubic end segments or specified end–derivatives, the prediction step (27.11) and correction iterations (27.12) incur only *tridiagonal linear systems*, which can be solved [110] with a cost of $3N - 3$ additions and multiplications and $2N - 1$ divisions. For periodic end conditions, the equations are no longer quite tridiagonal, but they can be solved at nominally higher cost using the modification to the tridiagonal solver described in §14.4.4.

The predictor–corrector scheme is run for each of the 2^{N+m} distinct sets of starting values in succession, and each yields a distinct solution $\mathbf{z}_1, \dots, \mathbf{z}_N$ to equations (27.2) for $i = 2, \dots, N - 1$ augmented by end conditions from

(27.4)–(27.6). From these solutions, the Bézier control points for each spline segment $\mathbf{r}_i(t)$ can be determined as described in §27.1.1. To fully exploit the advantages of PH curves, the quantities $\mathbf{w}_{i,0}$, $\mathbf{w}_{i,1}$, $\mathbf{w}_{i,2}$ associated with each segment $\mathbf{r}_i(t)$ should be stored (see §27.1.1), in addition to the control points, since they embody the Pythagorean nature of its hodograph.

27.2.3 Empirical Results and Examples

The homotopy method was coded in a double-precision, complex-arithmetic FORTRAN program. The use of complex arithmetic, and the fact that little more than a tridiagonal solver is needed allow a remarkably concise and robust implementation. Tests show that the homotopy system (27.9) is, in general, very well-conditioned, allowing PH splines to be computed to high precision (see the data in Table 27.2 below). Constant steps $\Delta\lambda = 0.02$ of the homotopy parameter were used for the examples below. This choice is quite conservative, and larger steps can often be safely employed. However, using very large steps ($\Delta\lambda > 0.1$) may incur “jumps” between the solution paths in the predictor–corrector scheme, causing some of the 2^{N+m} distinct splines to be missed on commencing with distinct solutions of the “start” system (27.8).

The well-conditioned nature of the system (27.9) allows a tight tolerance on the norm (27.13) that governs the Newton–Raphson correction iterations. We have consistently employed 10^{-12} for this value without encountering any convergence difficulties. Note that the transformation of the “initial” system (27.8) into the “desired” system (27.2) through the homotopy (27.9) is not necessarily a monotone process — Fig. 27.1 illustrates the variation of norms analogous to (27.13) for the \mathbf{f} and \mathbf{g} functions in a typical instance.

We find empirically that, among the 2^{N+m} distinct C^2 PH quintic spline curves interpolating given points $\mathbf{q}_0, \dots, \mathbf{q}_N$, all but one exhibit undesirable loops that do not agree with the intuitive “shape” of the data. The remaining

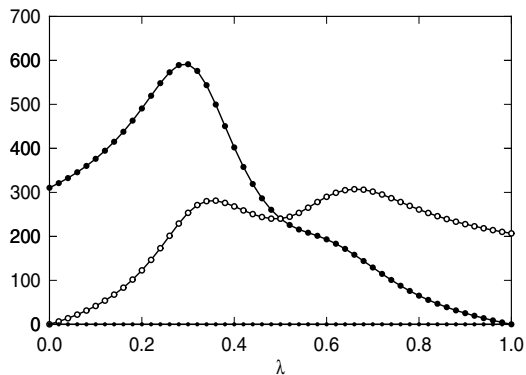


Fig. 27.1. Variation of the \mathbf{f} , \mathbf{g} , and \mathbf{h} function norms (indicated by solid dots, open dots, and smaller solid dots) during 50 equal steps of the continuation method.

“good” PH spline, however, is invariably a smoother or *fairer* locus than the “ordinary” C^2 cubic spline. To quantify this, certain integral shapes measures may be used to identify the “good” PH spline — including the *total arc length*, the *absolute rotation index*, and the *energy integral*,

$$S = \int ds, \quad R_{\text{abs}} = \frac{1}{2\pi} \int |\kappa| ds, \quad U = \int \kappa^2 ds, \quad (27.14)$$

where κ and s are the curvature and arc length. For PH curves, these integrals admit analytic reductions, as previously described — for the ordinary cubic spline, numerical quadrature must be invoked.

We shall see that the arc length S is not, alone, a good indicator of the best PH spline, but R_{abs} and U are. Typically, the spline with the least U also has the least R_{abs} , but there is no definitive guarantee that this is always so. In some cases, the user may be required to judge which of the two quantities identifies the best PH spline if they give conflicting recommendations.

Example 27.1 We wish to construct a C^2 PH quintic spline with cubic end spans, interpolating $\mathbf{q}_0 = (-2.1, 1.8)$, $\mathbf{q}_1 = (-3.1, 0.0)$, $\mathbf{q}_2 = (-0.3, -0.8)$, $\mathbf{q}_3 = (0.7, 2.2)$, $\mathbf{q}_4 = (3.4, 0.5)$, $\mathbf{q}_5 = (1.1, -0.6)$, and $\mathbf{q}_6 = (2.3, -2.4)$. The 32 solutions, computed by the homotopy method, are illustrated in Fig. 27.2.

Although they all interpolate the points and exhibit C^2 continuity between adjacent segments, it can be seen that the totality of solutions is quite a tangle! Table 27.1 lists values of the shape indicators (27.14) for each of the 32 distinct PH splines, ordered by U . The “good” solution is immediately identified as the one with the least values for R_{abs} and U (though not S). We see that U most strongly distinguishes the good spline, with $R_{\text{abs}} = 1.889$ and $U = 9.39$, from the next contender, with $R_{\text{abs}} = 2.189$ and $U = 21.55$. The “worst” case has the enormous energy $U = 385.74$, but its absolute rotation index is fairly

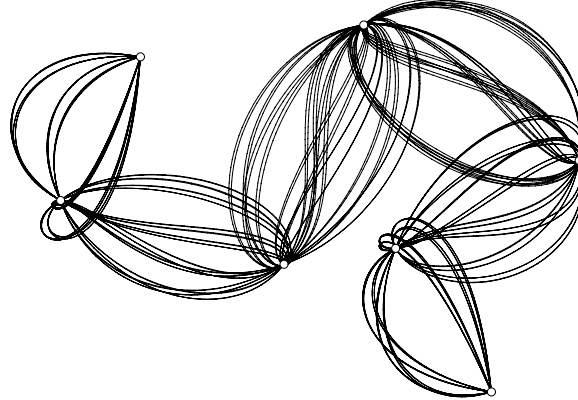


Fig. 27.2. The complete family of 32 distinct C^2 PH quintic splines with cubic end segments interpolating the sequence of points $\mathbf{q}_0, \dots, \mathbf{q}_6$ specified in Example 27.1.

Table 27.1. Values of the three integral shape measures (27.14) for the 32 distinct C^2 PH quintic splines in Example 1, ordered by increasing values of the energy U .

#	S	R_{abs}	U	#	S	R_{abs}	U
32	18.42	1.889	9.39	18	18.12	2.690	97.02
01	18.92	2.189	21.55	16	18.11	2.636	101.82
24	19.95	2.497	22.10	23	19.89	2.939	126.72
17	18.51	2.286	31.56	26	18.33	2.757	141.37
30	19.97	2.641	33.69	07	18.90	3.046	153.36
25	18.51	2.309	39.12	11	19.77	3.832	154.24
29	19.23	2.381	43.98	14	19.92	3.404	164.35
03	20.33	2.958	49.01	13	19.04	3.147	166.07
08	19.09	2.601	55.29	15	17.71	3.038	167.79
04	19.62	2.698	61.12	27	19.29	3.247	175.43
19	20.20	3.057	63.92	10	19.28	3.322	192.47
31	18.14	2.284	67.38	06	19.98	3.531	237.35
20	19.35	2.801	68.87	28	18.77	2.982	246.35
02	18.66	2.585	79.34	05	19.44	3.262	276.52
09	19.34	2.874	83.32	21	20.12	3.214	328.32
22	20.46	3.460	94.22	12	19.44	3.587	385.74

modest, at $R_{\text{abs}} = 3.587$. There is little correlation of S with R_{abs} and U , so we discount it from further consideration.

For comparison, the “ordinary” cubic spline¹ has $S = 17.09$, $R_{\text{abs}} = 1.744$, and $U = 13.40$ — i.e., slightly better for R_{abs} but worse for U . To gain insight into the geometrical significance of these values, in Fig. 27.3 we show (1) the “best” PH spline, with $U = 9.39$; (2) a “typical” PH spline, with $U = 154.24$; (3) a “bad” PH spline, with $U = 328.32$; and (4) the ordinary cubic spline, with $U = 13.40$. It is evident that large U values are associated with “looping” behavior of PH splines near some of the interpolation points. The tighter the loops, the higher the energy: the case with $U = 328.32$ has a loop near \mathbf{q}_2 so small, it is not discernible on the scale of the plot. The “good” solution, on the other hand, is characterized by an absence of such superfluous loops.

Comparing the “good” PH quintic spline and the “ordinary” cubic spline, the former evidently has a more pleasing or “fairer” shape, with a more even curvature variation over its extent. This is clearly apparent in the curvature profiles, shown in Fig. 27.4, and in the energy values: $U = 9.39$ for the PH quintic spline, and 13.40 for the ordinary cubic spline. Although both curves have continuous curvature κ , the cubic spline tends to exhibit “spikes” in κ near the interpolant points and “flat regions” in between. The PH spline gives a “rounder” shape, with a less severe κ variation.

We use Example 27.1 to illustrate the remarkable accuracy that is possible in the numerical construction of PH splines. Once the control points for each spline segment are computed, they can be used to test continuity of the left

¹ The ordinary cubic spline is based on quadratic end segments.

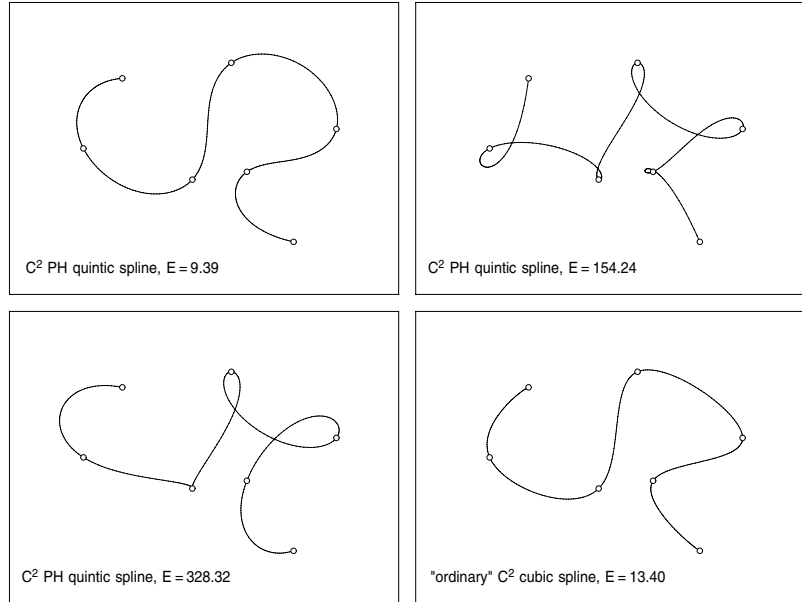


Fig. 27.3. A comparison of the “good” PH spline (top left) with a “typical” PH spline (top right); a “bad” PH spline (bottom left); and the “ordinary” cubic spline (bottom right). Tight loops in the PH splines incur large values for the energy U .

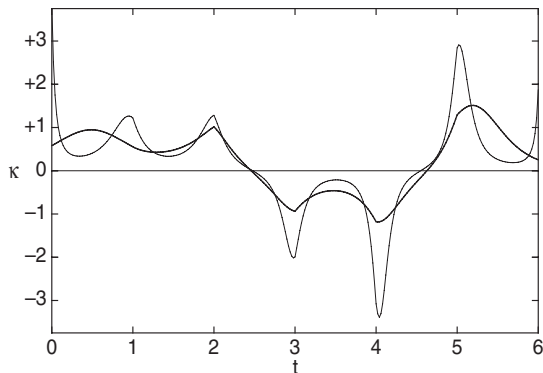


Fig. 27.4. Comparison of curvature profiles for the “good” PH quintic spline (bold) and the “ordinary” cubic spline (light) interpolating the point data of Example 27.1.

and right derivatives at the points \mathbf{q}_i for $i = 1, \dots, N - 1$, using the formulae

$$\mathbf{r}'_i(1) = 5(\mathbf{p}_{i,5} - \mathbf{p}_{i,4}), \quad \mathbf{r}'_{i+1}(0) = 5(\mathbf{p}_{i+1,1} - \mathbf{p}_{i+1,0})$$

for the first derivatives, and

Table 27.2. Comparison of nodal derivatives and “gaps” for Example 27.1.

q₁	$\Delta \mathbf{p}_1$	(-0.0000000000000000, 0.0000000000000000)
	$\mathbf{r}'_1(1)$	(1.360779002855208, -2.652974680926679)
	$\mathbf{r}'_2(0)$	(1.360779002855208, -2.652974680926679)
	$\mathbf{r}''_1(1)$	(5.632083355923054, -0.182314923482134)
	$\mathbf{r}''_2(0)$	(5.632083355923054, -0.182314923482134)
q₂	$\Delta \mathbf{p}_2$	(-0.0000000000000001, 0.0000000000000000)
	$\mathbf{r}'_2(1)$	(2.048883028548189, 2.211132842356474)
	$\mathbf{r}'_3(0)$	(2.048883028548189, 2.211132842356474)
	$\mathbf{r}''_2(1)$	(-7.081869673180421, 5.944174277861420)
	$\mathbf{r}''_3(0)$	(-7.081869673180421, 5.944174277861420)
q₃	$\Delta \mathbf{p}_3$	(0.0000000000000000, 0.0000000000000000)
	$\mathbf{r}'_3(1)$	(2.842303868097108, 1.968545850008491)
	$\mathbf{r}'_4(0)$	(2.842303868097108, 1.968545850008490)
	$\mathbf{r}''_3(1)$	(8.462769563261957, -7.740519332527053)
	$\mathbf{r}''_4(0)$	(8.462769563261962, -7.740519332527053)
q₄	$\Delta \mathbf{p}_4$	(0.0000000000000000, 0.0000000000000000)
	$\mathbf{r}'_4(1)$	(-0.755435263095192, -2.914313055871553)
	$\mathbf{r}'_5(0)$	(-0.755435263095192, -2.914313055871553)
	$\mathbf{r}''_4(1)$	(-9.583644688862023, 5.647009445446316)
	$\mathbf{r}''_5(0)$	(-9.583644688862023, 5.647009445446313)
q₅	$\Delta \mathbf{p}_5$	(0.0000000000000000, 0.0000000000000000)
	$\mathbf{r}'_5(1)$	(-1.735966775898855, -1.230156974065111)
	$\mathbf{r}'_6(0)$	(-1.735966775898856, -1.230156974065111)
	$\mathbf{r}''_5(1)$	(4.743411905896337, -3.811925035449617)
	$\mathbf{r}''_6(0)$	(4.743411905896337, -3.811925035449615)

$$\mathbf{r}''_i(1) = 20(\mathbf{p}_{i,5} - 2\mathbf{p}_{i,4} + \mathbf{p}_{i,3}), \quad \mathbf{r}''_{i+1}(0) = 20(\mathbf{p}_{i+1,2} - 2\mathbf{p}_{i+1,1} + \mathbf{p}_{i+1,0})$$

for the second derivatives. The results are enumerated in Table 27.2 — it can be seen that, despite the “numerical” nature of the solution method, the nodal derivatives agree to ~ 15 significant digits in all cases. For double-precision arithmetic with rounding and a mantissa of $d = 53$ bits, the *machine unit* is

$$\eta = \frac{1}{2} 2^{-(d-1)} \approx 1.1 \times 10^{-16},$$

and hence the computed solutions are accurate to within about one decimal digit of the theoretical limit imposed by the floating-point number system! As another measure of accuracy for the computed PH splines, we examine the magnitude of the “gaps”

$$\Delta \mathbf{p}_i = \mathbf{p}_{i+1,0} - \mathbf{p}_{i,5} \tag{27.15}$$

for $i = 1, \dots, N-1$ that may arise between consecutive segments — owing to the fact that the final control point $\mathbf{p}_{i,5}$ of segment i , as given by expressions

(27.3), need not coincide precisely with the initial control point $\mathbf{p}_{i+1,0}$ of segment $i + 1$. Again, we see that the effects of numerical errors are extremely subdued, and these gaps are insignificant. The data in Table 27.2 are by no means special: they are representative of what is observed in many examples.

Example 27.2 We wish to construct a periodic spline curve that interpolates the points $\mathbf{q}_0 = (-0.1, 3.2)$, $\mathbf{q}_1 = (2.5, 2.5)$, $\mathbf{q}_2 = (3.4, -0.1)$, $\mathbf{q}_3 = (5.2, 2.5)$, $\mathbf{q}_4 = (8.1, 4.4)$, $\mathbf{q}_5 = (5.2, 7.3)$, $\mathbf{q}_6 = (4.9, 4.4)$, $\mathbf{q}_7 = (2.6, 3.8)$, $\mathbf{q}_8 = (1.7, 5.7)$, $\mathbf{q}_9 = \mathbf{q}_0$. The “good” PH spline and the “ordinary” cubic spline are compared in Fig. 27.5, together with their curvature profiles. The discrepancy in the curvature variations is even more pronounced than before: the ordinary cubic spline has an extremum curvature more than 10 times that of the PH spline!

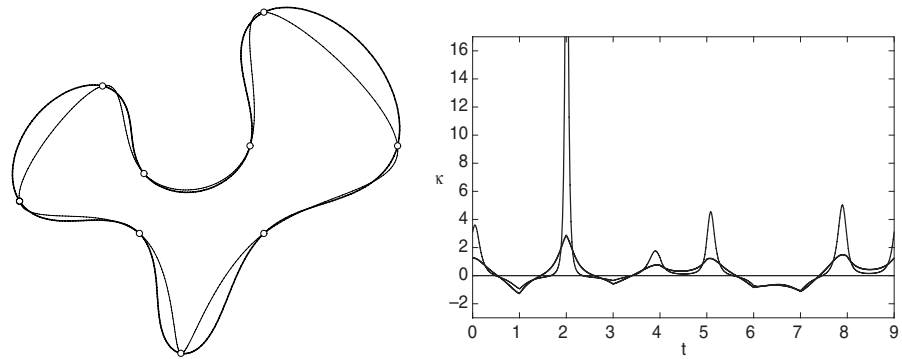


Fig. 27.5. Left: comparison of the “good” PH quintic spline (bold) and “ordinary” cubic spline (light), with periodic end conditions, for the point data of Example 27.2. Right: curvature profiles for the PH quintic spline and the “ordinary” cubic spline.

This discrepancy is apparent in the curve energies: $U = 15.76$ for the PH spline, whereas $U = 61.74$ for the ordinary cubic spline (although the latter has a somewhat smaller absolute rotation index: $R_{\text{abs}} = 2.653$ versus 2.806 for the PH spline). In this example, there are 512 distinct C^2 PH quintic splines interpolating the given points. Obviously, it is not instructive to plot them all — the behavior is qualitatively similar to that seen in Example 27.1.

Example 27.3 The final example calls for a periodic curve interpolating the points $\mathbf{q}_0 = (1, 0)$, $\mathbf{q}_1 = (0, 1)$, $\mathbf{q}_2 = (-1, 0)$, $\mathbf{q}_3 = (0, -1)$, $\mathbf{q}_4 = \mathbf{q}_0$ on the unit circle. The “good” PH spline is compared with the “ordinary” cubic spline in Fig. 27.6, together with their curvature plots. These plots indicate that the former is a much better approximation of the unit circle than the latter: for the ordinary cubic spline, the curvature varies between 0.84 and 1.33, while the PH spline has a narrower range of curvature, between 0.97 and 1.06. The energy integral for an exact circle is clearly $U = 2\pi$ — for the PH spline, we have $U/2\pi = 1.0034$, while the ordinary cubic spline gives $U/2\pi = 1.0376$.

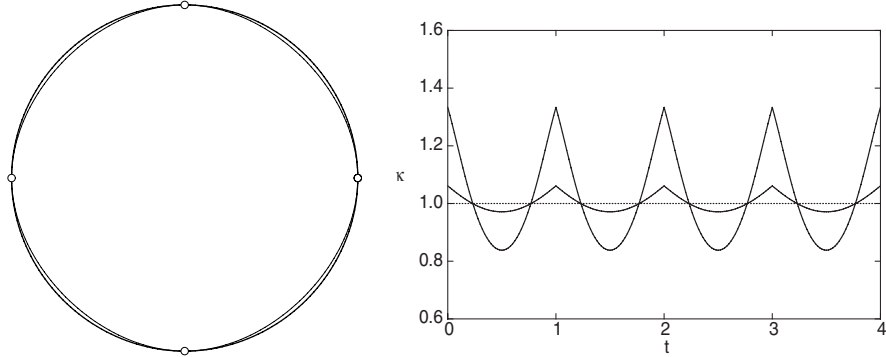


Fig. 27.6. Left: comparison of the periodic PH quintic spline (bold) and “ordinary” cubic spline (light) approximations to the unit circle — see Example 27.3. Right: curvature profiles for the PH spline and ordinary cubic spline circle approximations.

Although with $N = 4$ and periodic boundary conditions we might expect 16 distinct solutions, only six of them are actually of different shape owing to the symmetry of the data — see Fig. 27.7. Apart from the “good” solution, in the top left, all of these interpolants exhibit loops: in some cases, they are so “tight” as to be virtually hidden by the dots representing the data points. The energies of these other interpolants are correspondingly much higher than that of the “good” PH spline. The solutions may be categorized as follows:

- no loops (unique);
- one loop (four orientations);
- two loops, opposite (two orientations);
- two loops, adjacent (four orientations);
- three loops (four orientations);
- four loops (unique).

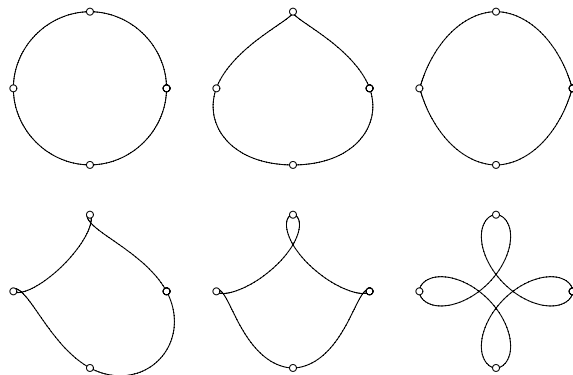


Fig. 27.7. The six different shapes among the total of 16 distinct C^2 PH quintic splines that interpolate four equally-spaced points on the unit circle (Example 27.3).

27.3 Solution by Iterative Methods

The homotopy method is useful in elucidating the nature of the complete space of solutions to the PH quintic spline interpolation problem, but for large N it is prohibitively expensive and impractical if our concern is to obtain *only* the “good” interpolant. Methods to directly construct the “good” PH quintic spline usually involve — (i) choosing initial values $\mathbf{z}_1^{(0)}, \dots, \mathbf{z}_N^{(0)}$ “close” to the good solution; and (ii) invoking an iterative method to recursively refine these values until they converge, within a prescribed tolerance, to the good solution. Careful consideration must be given to both the aspects (i) and (ii) to develop a scheme that reliably and efficiently converges to the good solution.

To formulate conditions for guaranteed convergence of iterative methods, we need to recall the definitions of vector and matrix norms (see §12.4.4). The p -norm of an N -dimensional vector $\mathbf{u} = (\mathbf{u}_1, \dots, \mathbf{u}_N)^T \in \mathbb{C}^N$ and subordinate norm of an $N \times N$ matrix $\mathbf{M} \in \mathbb{C}^N \times \mathbb{C}^N$ with elements \mathbf{M}_{jk} , are defined by

$$\|\mathbf{u}\|_p = \left[\sum_{i=1}^N |\mathbf{u}_i|^p \right]^{1/p} \quad \text{and} \quad \|\mathbf{M}\|_p = \sup_{\mathbf{u} \neq \mathbf{0}} \frac{\|\mathbf{M}\mathbf{u}\|_p}{\|\mathbf{u}\|_p}.$$

It will be convenient to work with the norm defined (in the limit $p \rightarrow \infty$) by $\|\mathbf{u}\|_\infty = \max_i |\mathbf{u}_i|$. The corresponding matrix norm is

$$\|\mathbf{M}\|_\infty = \max_{1 \leq i \leq N} \sum_{j=1}^N |\mathbf{M}_{ij}|,$$

i.e., the greatest sum of absolute values of the matrix elements across rows [430]. The norms of any given vector or matrix, for different p values, vary by factors that depend only weakly on N .

27.3.1 Choice of Starting Approximation

Iterative methods for solving the system (27.2) need a starting approximation

$$\mathbf{z}^{(0)} = (\mathbf{z}_1^{(0)}, \dots, \mathbf{z}_N^{(0)})$$

to the desired solution. The choice of initial values is critical in determining whether the iterations will converge and, if so, whether they converge to the “good” solution among the 2^{N+m} distinct solutions to the system defined by (27.2) for $k = 2, \dots, N-1$ together with appropriate end conditions.

As noted in §27.1.1, the values $\mathbf{z}_1, \dots, \mathbf{z}_N$ define a polygon in the complex plane, where each vertex and the mid-points of the two sides meeting at that vertex are interpreted as control points for a quadratic Bézier segment. The image of the C^1 piecewise-quadratic curve thus defined, under the conformal map $\mathbf{z} \rightarrow \mathbf{z}^2$, is the hodograph of the C^2 PH quintic spline curve.

For a smooth curve, we expect the values $\mathbf{z}_1, \dots, \mathbf{z}_N$ to exhibit a gradual variation (in the limiting case of a straight line, they are all equal). Hence, as a first attempt to estimate a starting approximation to the “good” solution, we set $\mathbf{z}_{i-1} = \mathbf{z}_i = \mathbf{z}_{i+1}$ in (27.2) to obtain

$$\mathbf{z}_i^2 = \Delta \mathbf{q}_i \quad (27.16)$$

for $i = 1, \dots, N$. This defines two choices for each \mathbf{z}_i — taking $\text{Re}(\mathbf{z}_1) > 0$, subsequent choices are made so as to minimize $|\mathbf{z}_i - \mathbf{z}_{i-1}|$.

If the points $\mathbf{q}_0, \dots, \mathbf{q}_N$ deviate significantly from a straight line, a more sophisticated method (taking the “shape” of the data into account) is needed to obtain a good starting approximation. One possible approach is based upon comparing derivative data for the PH quintic spline and the “ordinary” cubic spline interpolating the given points with analogous end conditions. Now the two splines may be expected to have similar shape only if the point data gives an unambiguous characterization of the desired shape, and this motivates us to impose mild constraints on the input data:

Definition 27.1 Points $\mathbf{q}_0, \dots, \mathbf{q}_N$ form a *reasonable* sequence if they satisfy

$$\Delta \mathbf{q}_i \cdot \Delta \mathbf{q}_{i+1} > 0 \quad \text{and} \quad \frac{1}{2} \leq \frac{|\Delta \mathbf{q}_{i+1}|}{|\Delta \mathbf{q}_i|} \leq 2, \quad (27.17)$$

for $i = 1, \dots, N-1$ (for an open curve) or $i = 1, \dots, N$ (for a closed curve, where $\mathbf{q}_N = \mathbf{q}_0$ and i is reduced modulo N).

The first condition ensures that \mathbf{q}_{i+1} lies in the “general direction” of $\Delta \mathbf{q}_i$, while the second precludes uneven spacing of the points. These conditions are satisfied by the data pertinent to most practical applications.

Now the nodal derivatives $\mathbf{d}_0, \dots, \mathbf{d}_N$ of an ordinary C^2 cubic spline satisfy the linear system

$$\mathbf{d}_{i-1} + 4\mathbf{d}_i + \mathbf{d}_{i+1} = 3(\mathbf{q}_{i+1} - \mathbf{q}_{i-1}) \quad (27.18)$$

for $i = 2, \dots, N-1$, augmented by two end-condition equations. On solving for $\mathbf{d}_0, \dots, \mathbf{d}_N$, each segment of the cubic spline can be expressed as

$$\mathbf{c}_i(t) = \mathbf{q}_{i-1} \alpha_0(t) + \mathbf{q}_i \alpha_1(t) + \mathbf{d}_{i-1} \beta_0(t) + \mathbf{d}_i \beta_1(t)$$

where $\alpha_0(t), \alpha_1(t), \beta_0(t), \beta_1(t)$ are the cubic Hermite functions (see §3.2).

Our first inclination might be to determine a starting approximation by equating the nodal derivatives of the PH quintic segments (27.1) with those of the ordinary cubic spline. For $i = 1, \dots, N-1$ this yields the equations

$$(\mathbf{z}_i + \mathbf{z}_{i+1})^2 = 4\mathbf{d}_i,$$

which must be augmented in the case of cubic end spans by

$$(3\mathbf{z}_1 - \mathbf{z}_2)^2 = 4\mathbf{d}_0 \quad \text{and} \quad (3\mathbf{z}_N - \mathbf{z}_{N-1})^2 = 4\mathbf{d}_N$$

while for periodic end conditions we use

$$(\pm \mathbf{z}_N + \mathbf{z}_1)^2 = 4\mathbf{d}_0 = 4\mathbf{d}_N.$$

This system may be linearized by taking the square root on both sides — we take a particular square root of \mathbf{d}_0 , and subsequent roots are chosen so as to minimize $|\sqrt{\mathbf{d}_i} - \sqrt{\mathbf{d}_{i-1}}|$. However, this approach is problematic: cubic end spans incur an over-determined system of $N+1$ equations in N unknowns, while for periodic end conditions the system is consistent only for one sign choice (which may not give a starting point close to the “good” solution).

To circumvent these difficulties, we need a scheme that imposes just one condition on $\mathbf{z}_1, \dots, \mathbf{z}_N$ per spline segment. We find that equating derivatives at the parametric mid-points of corresponding cubic and PH quintic segments, $\mathbf{r}'_i(\frac{1}{2}) = \mathbf{c}'_i(\frac{1}{2})$, gives good results. This yields the system of equations

$$\mathbf{z}_{i-1} + 6\mathbf{z}_i + \mathbf{z}_{i+1} = 4\sqrt{\mathbf{Q}_i}, \quad i = 2, \dots, N-1 \quad (27.19)$$

where we introduce the quantities

$$\mathbf{Q}_i = 6\Delta\mathbf{q}_i - (\mathbf{d}_{i-1} + \mathbf{d}_i), \quad i = 1, \dots, N. \quad (27.20)$$

For cubic end spans, this is augmented by

$$\mathbf{z}_1 = \frac{1}{2}\sqrt{\mathbf{Q}_1}, \quad \mathbf{z}_N = \frac{1}{2}\sqrt{\mathbf{Q}_N}, \quad (27.21)$$

and in the case of periodic end conditions we use

$$\pm \mathbf{z}_N + 6\mathbf{z}_1 + \mathbf{z}_2 = 4\sqrt{\mathbf{Q}_1}, \quad \mathbf{z}_{N-1} + 6\mathbf{z}_N \pm \mathbf{z}_1 = 4\sqrt{\mathbf{Q}_N}. \quad (27.22)$$

The square roots of the quantities (27.20) have two complex values. To obtain a starting approximation close to the “good” solution, we choose a particular value for $\sqrt{\mathbf{Q}_1}$, and for subsequent roots we take the value that has a positive dot product (regarding complex numbers as vectors) with the preceding root. In the case of periodic end conditions, the choice of sign to be used in (27.22) is determined by the sign of the dot product of $\sqrt{\mathbf{Q}_1}$ and $\sqrt{\mathbf{Q}_N}$.

To assess different methods of estimating a starting approximation $\mathbf{z}^{(0)} = (\mathbf{z}_1^{(0)}, \dots, \mathbf{z}_N^{(0)})$ to the “good” solution of the system (27.2), we need a measure of its distance from each of the solutions $\mathbf{z} = (\mathbf{z}_1, \dots, \mathbf{z}_N)$ of this system. We define this distance by the expression

$$\|\mathbf{z}^{(0)} - \mathbf{z}\|_\infty = \max_{1 \leq i \leq N} |\mathbf{z}_i^{(0)} - \mathbf{z}_i|.$$

27.3.2 Functional Iteration and Relaxation

In the functional iteration approach, we use (27.2) to express each variable as a function $\mathbf{z}_i = \phi_i(\mathbf{z}_1, \dots, \mathbf{z}_N)$ of all the variables [256]. This can be done in different ways: re-arranging (27.2), for example, yields the *rational* functions

$$\phi_i(\mathbf{z}_1, \dots, \mathbf{z}_N) = \frac{60\Delta\mathbf{q}_i - 3\mathbf{z}_{i-1}^2 - \mathbf{z}_{i-1}\mathbf{z}_{i+1} - 3\mathbf{z}_{i+1}^2}{13\mathbf{z}_{i-1} + 27\mathbf{z}_i + 13\mathbf{z}_{i+1}}.$$

Assembling the variables and functions into the vectors $\mathbf{z} = (\mathbf{z}_1, \dots, \mathbf{z}_N)$ and $\phi = (\phi_1, \dots, \phi_N)$, the system (27.2) may be expressed in the compact form $\mathbf{z} = \phi(\mathbf{z})$. Given an initial approximation $\mathbf{z}^{(0)} = (\mathbf{z}_1^{(0)}, \dots, \mathbf{z}_N^{(0)})$, we may then attempt to solve the system (27.2) by means of the functional iteration

$$\mathbf{z}^{(r+1)} = \phi(\mathbf{z}^{(r)}), \quad r = 0, 1, 2, \dots \quad (27.23)$$

Here the values $\mathbf{z}_1^{(r+1)}, \dots, \mathbf{z}_N^{(r+1)}$ at the $(r+1)$ -th iteration are to be updated *simultaneously*, based on the preceding values $\mathbf{z}_1^{(r)}, \dots, \mathbf{z}_N^{(r)}$.

With this method, the form of the functions $\phi(\mathbf{z})$ strongly influences the convergence behavior. Specifically, if $\mathcal{D} \subset \mathbb{C}^N$ is a domain such that $\mathbf{z} \in \mathcal{D} \implies \phi(\mathbf{z}) \in \mathcal{D}$ and

$$\|\phi(\mathbf{x}) - \phi(\mathbf{y})\|_p \leq L \|\mathbf{x} - \mathbf{y}\|_p$$

for all $\mathbf{x}, \mathbf{y} \in \mathcal{D}$ with $L < 1$, then the system exhibits a unique solution $\mathbf{z}^* \in \mathcal{D}$ and the iterations (27.23) will converge to \mathbf{z}^* from any point $\mathbf{z}^{(0)} \in \mathcal{D}$ [234]. These two properties characterize $\mathbf{z} \rightarrow \phi(\mathbf{z})$ as a *contraction mapping* over the domain \mathcal{D} . Now if $\mathbf{G}(\mathbf{z})$ is the Jacobian matrix for this map, with elements $\mathbf{G}_{ij} = \partial\phi_i/\partial\mathbf{z}_j$, the mean value theorem in several variables [71] gives

$$\phi(\mathbf{x}) - \phi(\mathbf{y}) = \mathbf{G}(\boldsymbol{\xi}) \cdot (\mathbf{x} - \mathbf{y})$$

with $\boldsymbol{\xi} = (1 - \lambda)\mathbf{x} + \lambda\mathbf{y}$ for some $0 < \lambda < 1$. Hence, for any two points \mathbf{x}, \mathbf{y} in a convex domain $\mathcal{D} \subset \mathbb{C}^N$, we have

$$\|\phi(\mathbf{x}) - \phi(\mathbf{y})\|_p \leq L \|\mathbf{x} - \mathbf{y}\|_p, \quad \text{with } L = \sup_{\mathbf{z} \in \mathcal{D}} \|\mathbf{G}(\mathbf{z})\|_p.$$

However, it may not be easy to identify a suitable domain \mathcal{D} over which the norm of the Jacobian $\mathbf{G}(\mathbf{z})$ is everywhere less than unity.

Relaxation methods [98] are closely related to functional iteration: rather than generating new $\mathbf{z}_1, \dots, \mathbf{z}_N$ values simultaneously by function evaluations, such a method visits each equation $\mathbf{f}_i(\mathbf{z}_1, \dots, \mathbf{z}_N) = 0$ individually, and *solves* it for a new \mathbf{z}_i to replace the value currently stored in a master list (initialized in a suitable manner). It is understood that, while solving $\mathbf{f}_i(\mathbf{z}_1, \dots, \mathbf{z}_N) = 0$ for \mathbf{z}_i , the variables $\mathbf{z}_1, \dots, \mathbf{z}_{i-1}, \mathbf{z}_{i+1}, \dots, \mathbf{z}_N$ are fixed at their current values. It is not essential to visit the equations in order — to accelerate convergence, they may be prioritized using the magnitudes $|\mathbf{f}_i(\mathbf{z}_1, \dots, \mathbf{z}_N)|$. Because of the tridiagonal nature of (27.2), only three of these residuals will change with each \mathbf{z}_i update. Note also that, since the equations (27.2) are quadratic, solving $\mathbf{f}_i(\mathbf{z}_1, \dots, \mathbf{z}_N) = 0$ for \mathbf{z}_i yields *two* complex values — among them, the one that is closest to the current \mathbf{z}_i is selected. Relaxation is essentially equivalent to functional iteration if we choose

$$\frac{-13(\mathbf{z}_{i-1} + \mathbf{z}_{i+1}) \pm \sqrt{6480\Delta\mathbf{q}_i - 155(\mathbf{z}_{i-1}^2 + \mathbf{z}_{i+1}^2) + 230\mathbf{z}_{i-1}\mathbf{z}_{i+1}}}{54}$$

for $\phi_i(\mathbf{z}_1, \dots, \mathbf{z}_N)$, and defer updating each \mathbf{z}_i until all these functions have been evaluated in order, using current \mathbf{z}_i values.

27.3.3 Newton–Raphson Method

Functional iteration and relaxation make no use of derivatives. Methods that use both function values *and* derivatives can, under suitable conditions, offer much faster rates of convergence. We now consider the multivariate Newton–Raphson iteration, and the Kantorovich theorem guaranteeing its quadratic convergence to a desired solution from any start point within a domain over which the derivatives of (27.2) satisfy certain conditions.

The Newton–Raphson method is based on a first–order Taylor expansion of equations (27.2). The *Jacobian matrix* \mathbf{M} for this system, with elements

$$\mathbf{M}_{ij} = \frac{\partial \mathbf{f}_i}{\partial \mathbf{z}_j}, \quad 1 \leq i, j \leq N \quad (27.24)$$

is tridiagonal: in rows $i = 2, \dots, N - 1$, the only non–zero elements are

$$\begin{aligned} \mathbf{M}_{i,i-1} &= 6\mathbf{z}_{i-1} + 13\mathbf{z}_i + \mathbf{z}_{i+1}, \\ \mathbf{M}_{ii} &= 13\mathbf{z}_{i-1} + 54\mathbf{z}_i + 13\mathbf{z}_{i+1}, \\ \mathbf{M}_{i,i+1} &= \mathbf{z}_{i-1} + 13\mathbf{z}_i + 6\mathbf{z}_{i+1}. \end{aligned}$$

Rows $i = 1$ and $i = N$ are modified to reflect the chosen end conditions.

By writing $\mathbf{z} = (\mathbf{z}_1, \dots, \mathbf{z}_N)^T$ and $\mathbf{f} = (\mathbf{f}_1, \dots, \mathbf{f}_N)^T$, we may express the Newton–Raphson iterations as

$$\mathbf{z}^{(r+1)} = \mathbf{z}^{(r)} + \delta\mathbf{z}^{(r)} \quad (27.25)$$

for $r = 0, 1, 2, \dots$, where the increment vectors $\delta\mathbf{z}^{(r)} = (\delta\mathbf{z}_1^{(r)}, \dots, \delta\mathbf{z}_N^{(r)})^T$ are given by the solutions of the linear systems

$$\mathbf{M}^{(r)} \delta\mathbf{z}^{(r)} = -\mathbf{f}^{(r)}. \quad (27.26)$$

The superscripts on the Jacobian matrix \mathbf{M} and the function vector \mathbf{f} indicate that their elements must be computed at $\mathbf{z}^{(r)} = (\mathbf{z}_0^{(r)}, \dots, \mathbf{z}_N^{(r)})$. The iterations commence with a suitable starting approximation $\mathbf{z}^{(0)} = (\mathbf{z}_1^{(0)}, \dots, \mathbf{z}_N^{(0)})$.

The tridiagonal nature of the Jacobian \mathbf{M} for the system (27.2) allows the increment $\delta\mathbf{z}^{(r)}$ in each Newton–Raphson step (27.26) to be directly computed in $O(N)$ arithmetic operations, as compared to the $O(N^3)$ cost of a general Gaussian elimination procedure. Coupled with the quadratic convergence of the Newton–Raphson method, we can expect this to be an extremely efficient

approach *provided* we choose the initial approximation $\mathbf{z}^{(0)} = (\mathbf{z}_1^{(0)}, \dots, \mathbf{z}_N^{(0)})$ close enough to the “good” solution to ensure convergence to it.

The Kantorovich theorem on convergence of the Newton–Raphson method is commonly expressed in terms of general norms in Banach spaces [272]. We are only interested in \mathbb{C}^N here, and to simplify the analysis we confine our attention to the $p = \infty$ norm: henceforth we just write $\|\cdot\|$ instead of $\|\cdot\|_\infty$. The following statement of the theorem is adapted from the formulations of Ortega [350] and Tapia [436] to the present context.

Theorem 27.1 (Kantorovich) *With $\mathbf{z} = (\mathbf{z}_1, \dots, \mathbf{z}_N)$ and $\mathbf{f} = (\mathbf{f}_1, \dots, \mathbf{f}_N)$, let $\mathbf{f}(\mathbf{z})$ denote the map $\mathbb{C}^N \rightarrow \mathbb{C}^N$ defined by equations (27.2), with Jacobian $\mathbf{M}(\mathbf{z})$ given by the matrix elements (27.24). For a starting approximation $\mathbf{z}^{(0)}$ within a domain $\mathcal{D}_0 \subset \mathbb{C}^N$, suppose that*

1. $\|\mathbf{M}^{-1}(\mathbf{z}^{(0)})\| \leq B$,
2. $\|\mathbf{M}^{-1}(\mathbf{z}^{(0)})\mathbf{f}(\mathbf{z}^{(0)})\| = \|\delta\mathbf{z}^{(0)}\| \leq \eta$,
3. $\|\mathbf{M}(\mathbf{x}) - \mathbf{M}(\mathbf{y})\| \leq K\|\mathbf{x} - \mathbf{y}\|$ for all $\mathbf{x}, \mathbf{y} \in \mathcal{D}_0$,

and define

$$h = BK\eta, \quad r = \frac{1 - \sqrt{1 - 2h}}{h} \eta.$$

Then, if the conditions

$$h \leq \frac{1}{2}, \quad \mathcal{S} = \{ \mathbf{z} \mid \|\mathbf{z} - \mathbf{z}^{(0)}\| \leq r \} \subset \mathcal{D}_0$$

hold, the Newton–Raphson iterations

$$\mathbf{z}^{(r+1)} = \mathbf{z}^{(r)} - \mathbf{M}^{-1}(\mathbf{z}^{(r)})\mathbf{f}(\mathbf{z}^{(r)}), \quad r = 1, 2, \dots$$

always remain inside the ball \mathcal{S} with center $\mathbf{z}^{(0)}$ and radius r , and converge to a solution $\mathbf{z}^* \in \mathcal{D}_0$ of $\mathbf{f}(\mathbf{z}) = 0$. Furthermore, the error bounds

$$\|\mathbf{z}^{(r)} - \mathbf{z}^*\| \leq \frac{(1 - \sqrt{1 - 2h})^{2^r}}{2^r} \frac{\eta}{h}$$

are satisfied for each r , indicating quadratic convergence to \mathbf{z}^* when $h < \frac{1}{2}$.

Proof : See [350] and [436]. ■

The conditions of Theorem 27.1 are remarkably easy to test in the context of the tridiagonal quadratic system (27.2). Condition 1 requires a bound for the norm of the inverse \mathbf{M}^{-1} of the Jacobian, at the start point $\mathbf{z}^{(0)}$. Actually, we can compute the *exact* value of this norm at reasonable cost, $O(N^2)$, since the Jacobian is tridiagonal. For any tridiagonal $N \times N$ matrix \mathbf{M} , one may consider the systems of equations

$$\mathbf{M}\mathbf{x}^{(j)} = \mathbf{r}^{(j)} \quad \text{for } j = 1, \dots, N, \quad (27.27)$$

with right-hand sides $\mathbf{r}^{(1)} = [1, 0, 0, \dots, 0]^T$, $\mathbf{r}^{(2)} = [0, 1, 0, \dots, 0]^T$, etc. The solutions $\mathbf{x}^{(1)}, \dots, \mathbf{x}^{(N)}$ are then simply the columns of the inverse \mathbf{M}^{-1} . Since each tridiagonal system in (27.27) can be solved with $O(N)$ cost, and there are N of them, the cost of computing \mathbf{M}^{-1} is $O(N^2)$ — for a general matrix, efficient algorithms for \mathbf{M}^{-1} typically have $O(N^3)$ cost [98].

In condition 2, the vector $\mathbf{M}^{-1}(\mathbf{z}^{(0)})\mathbf{f}(\mathbf{z}^{(0)})$ whose norm we wish to bound is simply the solution $\delta\mathbf{z}^{(0)}$ to the first Newton–Raphson step (27.26), $r = 0$. By solving the tridiagonal system (27.26), we can explicitly determine this vector and obtain its norm *exactly* with $O(N)$ cost. Finally, in condition 3 we need a Lipschitz constant K for the Jacobian over some domain $\mathcal{D}_0 \subset \mathbb{C}^N$ containing $\mathbf{z}^{(0)}$. The linear dependence of \mathbf{M} on \mathbf{z} makes this an easy task:

Lemma 27.1 *For the tridiagonal Jacobian defined by (27.24) we may take $K = 120$ with $\mathcal{D}_0 = \mathbb{C}^N$ in condition 3 of Theorem 27.1.*

Proof : For $\mathbf{x} = (\mathbf{x}_1, \dots, \mathbf{x}_N)$, $\mathbf{y} = (\mathbf{y}_1, \dots, \mathbf{y}_N)$, and the Jacobian defined by (27.10), the sum of absolute values across row i of $\mathbf{M}(\mathbf{x}) - \mathbf{M}(\mathbf{y})$ is

$$\begin{aligned} R_i &= |6(\mathbf{x}_{i-1} - \mathbf{y}_{i-1}) + 13(\mathbf{x}_i - \mathbf{y}_i) + (\mathbf{x}_{i+1} - \mathbf{y}_{i+1})| \\ &\quad + |13(\mathbf{x}_{i-1} - \mathbf{y}_{i-1}) + 54(\mathbf{x}_i - \mathbf{y}_i) + 13(\mathbf{x}_{i+1} - \mathbf{y}_{i+1})| \\ &\quad + |(\mathbf{x}_{i-1} - \mathbf{y}_{i-1}) + 13(\mathbf{x}_i - \mathbf{y}_i) + 6(\mathbf{x}_{i+1} - \mathbf{y}_{i+1})| \\ &\leq 20|\mathbf{x}_{i-1} - \mathbf{y}_{i-1}| + 80|\mathbf{x}_i - \mathbf{y}_i| + 20|\mathbf{x}_{i+1} - \mathbf{y}_{i+1}| \end{aligned}$$

for $2 \leq i \leq N - 1$, where we invoke the triangle inequality. Noting that

$$\|\mathbf{x} - \mathbf{y}\| = \max_{1 \leq i \leq N} |\mathbf{x}_i - \mathbf{y}_i|,$$

and checking also rows $i = 1$ and $i = N$ in the case of both cubic end-spans and periodic end conditions, we obtain the inequality

$$\|\mathbf{M}(\mathbf{x}) - \mathbf{M}(\mathbf{y})\| = \max_{1 \leq i \leq N} R_i \leq 120 \|\mathbf{x} - \mathbf{y}\|. \quad \square$$

Differentiating (27.10) again yields the $N \times N \times N$ Hessian \mathbf{H} with elements

$$\mathbf{H}_{ijk} = \frac{\partial^2 \mathbf{f}_i}{\partial \mathbf{z}_j \partial \mathbf{z}_k}, \quad 1 \leq i, j, k \leq N. \quad (27.28)$$

Now since equations (27.2) are quadratic, \mathbf{H} is *constant* — for each i , the only non-zero elements occur in the 3×3 sub-matrix

$$\begin{bmatrix} \mathbf{H}_{i,i-1,i-1} & \mathbf{H}_{i,i-1,i} & \mathbf{H}_{i,i-1,i+1} \\ \mathbf{H}_{i,i,i-1} & \mathbf{H}_{i,i,i} & \mathbf{H}_{i,i,i+1} \\ \mathbf{H}_{i,i+1,i-1} & \mathbf{H}_{i,i+1,i} & \mathbf{H}_{i,i+1,i+1} \end{bmatrix} = \begin{bmatrix} 6 & 13 & 1 \\ 13 & 54 & 13 \\ 1 & 13 & 6 \end{bmatrix}. \quad (27.29)$$

If we consider the bilinear form $\mathbf{x} = \mathbf{H} \mathbf{u} \mathbf{v}$ to be the vector with components

$$\mathbf{x}_i = \sum_{j=1}^N \sum_{k=1}^N \mathbf{H}_{ijk} \mathbf{u}_j \mathbf{v}_k, \quad i = 1, \dots, N,$$

we may define the norm of the Hessian by

$$\|\mathbf{H}\| = \sup_{\mathbf{u}, \mathbf{v} \neq \mathbf{0}} \frac{\|\mathbf{H} \mathbf{u} \mathbf{v}\|}{\|\mathbf{u}\| \|\mathbf{v}\|} = \max_{1 \leq i \leq N} \sum_{j=1}^N \sum_{k=1}^N |\mathbf{H}_{ijk}|.$$

We see from (27.29) that the Lipschitz constant in Lemma 27.1 is $K = \|\mathbf{H}\|$.

Since $\|\mathbf{M}(\mathbf{x}) - \mathbf{M}(\mathbf{y})\| \leq 120 \|\mathbf{x} - \mathbf{y}\|$ is a *global* property of the Jacobian (27.10) — i.e., $\mathcal{D}_0 = \mathbb{C}^N$ in condition 3 of Theorem 27.1 — the requirement $\mathcal{S} \subset \mathcal{D}_0$ is always satisfied, and we can guarantee convergence of the Newton–Raphson iterations from *any* start point $\mathbf{z}^{(0)} \in \mathbb{C}^N$ by the simple inequality

$$\|\mathbf{M}^{-1}(\mathbf{z}^{(0)})\| \|\delta \mathbf{z}^{(0)}\| \leq \frac{1}{240}.$$

As noted above, the quadratic tridiagonal nature of the system (27.2) ensures that evaluating the quantities on the left at any $\mathbf{z}^{(0)}$ incurs only $O(N^2)$ cost. As a measure of the convergence rate, we use the quantity

$$\epsilon_r = \sqrt{\sum_i |\mathbf{f}_i^{(r)}|^2}. \quad (27.30)$$

27.3.4 Computed Examples

The Newton–Raphson scheme was implemented in a double-precision complex arithmetic FORTRAN program, with starting approximations determined by comparing mid-point parametric derivatives with those of the “ordinary” C^2 cubic spline, as described in §27.3.1. The Kantorovich convergence test was also incorporated. The homotopy method was used to obtain comparison data on the complete set of PH splines interpolating the given points.

A variety of tests were run on both open and closed curves. Figure 27.8 shows typical examples of these test curves (in each case, the points satisfy the requirements of Definition 27.1). Convergence from the starting approximation to the “good” PH spline solution was observed in just 3 or 4 iterations in every instance.² Table 27.3 summarizes pertinent data for the examples shown in Fig. 27.8 — further examples may be found in [167].

In every case, the distance $\|\mathbf{z}^{(0)} - \mathbf{z}\|$ from the starting approximation to the “good” solution (in the ∞ norm) was 10–50 smaller than the distance to the next-closest solution, indicating that the method of §27.3.1 is very reliable. The conditions of Definition 27.1 are essential, however, to achieving this level of dependability: tests with very “sparse” point sets indicate that the starting

² In the tests we take the “good” PH spline to be the one of least bending energy.

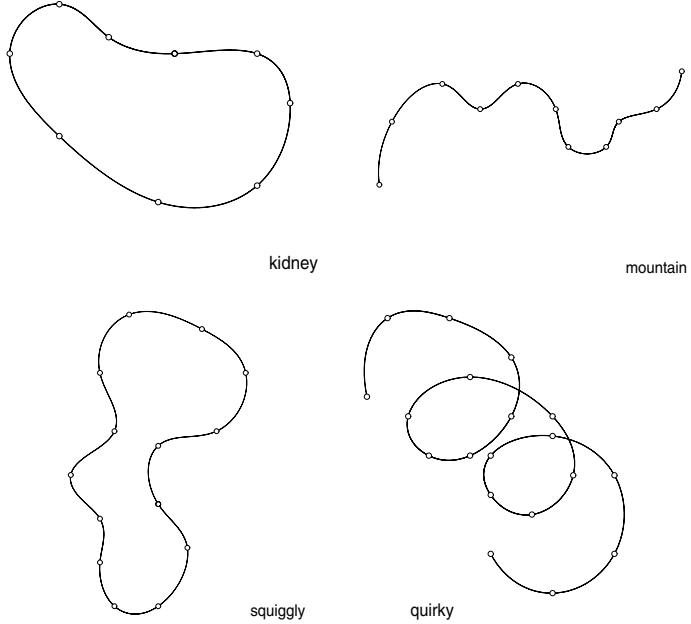


Fig. 27.8. Examples of C^2 PH quintic spline test curves (see Table 27.3).

approximation may not lie much closer to the “good” solution than to other solutions if the data is not “reasonable” in the sense of Definition 27.1.

In Table 27.3 the quantity h_0 gives the convergence parameter $h = BK\eta$ of Theorem 27.1, evaluated at the starting approximation. For B we use the exact inverse of the Jacobian, computed as described in §27.3.3, and for the Lipschitz constant we employ the global bound $K = 120$ determined in Lemma 27.1. The Kantorovich convergence condition $h_0 < \frac{1}{2}$ seems rather conservative — although rapid convergence to the good solution was observed in *all* the cases, some of them have h_0 values between about 1 and 2.

Table 27.3. Test data for splines in Fig. 27.8: the number of points $N + 1$; values of the Kantorovich parameter at the starting approximation h_0 , and after the first iteration h_1 ; estimate K_* for the local norm of the Hessian; and distance $\|\mathbf{z}^{(0)} - \mathbf{z}\|$ from start point to the good solution and next-closest solution (in the ∞ norm).

shape	$N + 1$	h_0	h_1	K_*	$\ \mathbf{z}^{(0)} - \mathbf{z}\ $ (good solution)	$\ \mathbf{z}^{(0)} - \mathbf{z}\ $ (next closest)
kidney	10	0.236	0.001	66.3	0.013	0.447
mountain	11	2.081	0.061	42.7	0.050	1.134
squiggly	15	0.749	0.009	91.0	0.029	0.391
quirky	19	1.891	0.070	30.0	0.068	1.141

This may be due, in part, to the loose global bound $K = 120$ on the norm of the Hessian (27.28). To test this hypothesis, we computed the values

$$K_* = \frac{\|\mathbf{M}(\mathbf{z}^{(0)}) - \mathbf{M}(\mathbf{z})\|}{\|\mathbf{z}^{(0)} - \mathbf{z}\|},$$

where $\mathbf{z}^{(0)}$ is the starting approximation and \mathbf{z} is the “good” solution, which give estimates of a suitable “local” Lipschitz constants. Table 27.3 shows that K_* is up to 4 times smaller than the nominal value $K = 120$. Thus, a sharper (local) Lipschitz constant might yield nominal satisfaction of the Kantorovich convergence condition at the starting approximation $\mathbf{z}^{(0)}$ in nearly all cases.

In Table 27.3 we also give the convergence parameter h_1 , computed *after* the first Newton iteration. In all cases, h_1 is dramatically smaller h_0 and easily satisfies the Kantorovich condition. We observe that, in all cases, h decreases to 0 in an essentially linear manner with distance from the good solution \mathbf{z} , as we approach it from the starting approximation $\mathbf{z}^{(0)}$. Since the method of §27.3.1 has proven very reliable in furnishing starting approximations close to the “good” solution, we adopt, as a practical convergence test, the conditions $h_1 < \frac{1}{2}$ and $h_1/h_0 < \alpha$ where a suitable α value is in the range 3–10.

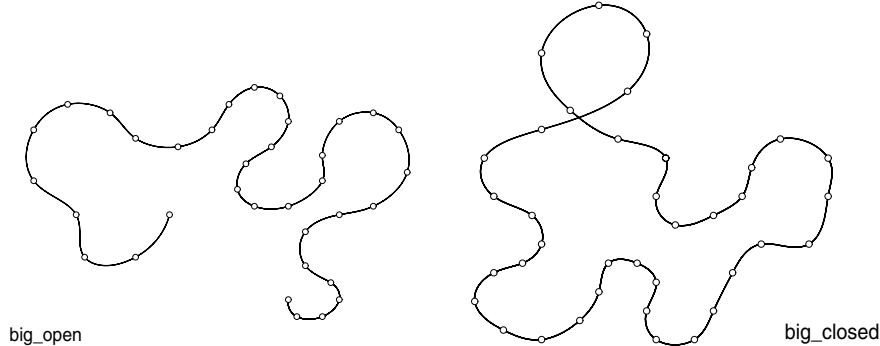


Fig. 27.9. Open and closed C^2 PH quintic splines interpolating large data sets, $N = 34$ and 37, computed in a fraction of a second by the Newton–Raphson method.

Using the Newton–Raphson method, it becomes feasible to compute PH splines interpolating large point sets ($N \gg 10$), a practical impossibility with the homotopy method. The examples in Fig. 27.9 were computed in just a fraction of a second, while the homotopy method would require hours to run to completion. Table 27.4 lists timing data³ for the test cases in Figs. 27.8 and 27.9: the alarming growth of the cpu time with N for the homotopy method, as compared to Newton–Raphson (with 6 iterations), is clearly apparent.

³ For the Newton–Raphson method, the times include constructing the “ordinary” cubic spline to obtain the starting approximation, and the Kantorovich tests.

Table 27.4. Timing comparisons for C^2 PH quintic spline test curves.

shape	$N + 1$	homotopy method	Newton–Raphson
mountain	11	2.44 s	0.13 s
kidney	10	8.09 s	0.11 s
squiggly	15	656.21 s	0.12 s
quirky	19	1128.97 s	0.23 s
big open	35	—	0.40 s
big closed	38	—	0.43 s

If the conditions of Definition 27.1 for “reasonable” data are satisfied, the good PH quintic spline and ordinary cubic spline are often virtually identical (the former usually has a somewhat better curvature profile). The cubic spline can thus be directly replaced by the PH quintic spline, allowing subsequent applications to exploit the unique computational advantages of PH curves.

27.4 Generalizations of PH Splines

The basic C^2 PH quintic spline problem is concerned with the interpolation of points $\mathbf{q}_0, \dots, \mathbf{q}_N$ associated with uniformly-spaced knots t_0, \dots, t_N using one of the three canonical end conditions described in §27.1.2. This formulation can be generalized in a number of useful ways, that incur modest modifications to the algorithm of §27.3. We describe some of these modifications below.

27.4.1 Non-uniform Knot Sequences

Thus far, we have considered only PH splines on uniform knots, i.e., the points $\mathbf{q}_0, \dots, \mathbf{q}_N$ correspond to integer parameter values, $t_k = k$ for $k = 0, \dots, N$. As noted in §14.5.1, non-uniform knots give better interpolants in the case of “ordinary” cubic splines if the points are unevenly spaced, and this is expected to be also true for PH splines. The generalization of the PH spline equations to non-uniform knots was developed in [167], and is briefly described below.

With $t_0 = 0$, let ℓ_1, \dots, ℓ_N be given non-uniform knot spacings, so that

$$t_i = t_{i-1} + \ell_i, \quad i = 1, \dots, N.$$

In the case of chord-length parameterization, for example, the values ℓ_i are determined by (14.20). The case where ℓ_1, \dots, ℓ_N are all identical corresponds to uniform knots. On each interval $t \in [t_{i-1}, t_i]$ we define a *local parameter*

$$\tau = \frac{t - t_{i-1}}{\ell_i} \in [0, 1],$$

and in terms of τ we re-write [167] the complex hodograph (27.1) as

$$\mathbf{r}'_i(\tau) = \left[\frac{\ell_i \mathbf{z}_{i-1} + \ell_{i-1} \mathbf{z}_i}{\ell_{i-1} + \ell_i} (1-\tau)^2 + \mathbf{z}_i 2(1-\tau)\tau + \frac{\ell_{i+1} \mathbf{z}_i + \ell_i \mathbf{z}_{i+1}}{\ell_i + \ell_{i+1}} \tau^2 \right]^2.$$

Since

$$\frac{d}{dt} = \frac{1}{\ell_i} \frac{d}{d\tau},$$

this form ensures satisfaction of the continuity conditions $\mathbf{r}'_i(1) = \mathbf{r}'_{i+1}(0)$ and $\mathbf{r}''_i(1) = \mathbf{r}''_{i+1}(0)$, where primes indicate derivatives with respect to the global parameter t . Integration of the hodograph $\mathbf{r}'_i(\tau)$ subject to the interpolation condition $\mathbf{r}_i(1) - \mathbf{r}_i(0) = \Delta \mathbf{q}_i$ then gives the equation

$$\begin{aligned} \mathbf{f}_i(\mathbf{z}_1, \dots, \mathbf{z}_N) &= \alpha_i \mathbf{z}_{i-1}^2 + \beta_i \mathbf{z}_i^2 + \gamma_i \mathbf{z}_{i+1}^2 + \delta_i \mathbf{z}_{i-1} \mathbf{z}_{i+1} \\ &\quad + \epsilon_i \mathbf{z}_{i-1} \mathbf{z}_i + \zeta_i \mathbf{z}_i \mathbf{z}_{i+1} - \eta_i \Delta \mathbf{q}_i = 0, \end{aligned} \quad (27.31)$$

incorporating the scalar factors

$$\begin{aligned} \alpha_i &= 3 \frac{\ell_i^2}{\ell_{i-1} \ell_{i+1}} \frac{\ell_i + \ell_{i+1}}{\ell_{i-1} + \ell_i}, \quad \gamma_i = 3 \frac{\ell_i^2}{\ell_{i-1} \ell_{i+1}} \frac{\ell_{i-1} + \ell_i}{\ell_i + \ell_{i+1}}, \\ \beta_i &= 1 + 2 \frac{\ell_{i-1} + \ell_i}{\ell_{i-1}} \frac{\ell_i + \ell_{i+1}}{\ell_{i+1}} \\ &\quad + 3 \frac{\ell_i + \ell_{i+1}}{\ell_{i+1}} \frac{2\ell_{i-1} + \ell_i}{\ell_{i-1} + \ell_i} + 3 \frac{\ell_{i-1} + \ell_i}{\ell_{i-1}} \frac{\ell_i + 2\ell_{i+1}}{\ell_i + \ell_{i+1}}, \\ \epsilon_i &= \frac{\ell_i}{\ell_{i-1}} \left[1 + 3 \frac{\ell_i + \ell_{i+1}}{\ell_{i+1}} \frac{3\ell_{i-1} + \ell_i}{\ell_{i-1} + \ell_i} \right], \\ \zeta_i &= \frac{\ell_i}{\ell_{i+1}} \left[1 + 3 \frac{\ell_{i-1} + \ell_i}{\ell_{i-1}} \frac{\ell_i + 3\ell_{i+1}}{\ell_i + \ell_{i+1}} \right], \\ \delta_i &= \frac{\ell_i^2}{\ell_{i-1} \ell_{i+1}}, \quad \eta_i = 15 \frac{(\ell_{i-1} + \ell_i)(\ell_i + \ell_{i+1})}{\ell_{i-1} \ell_i \ell_{i+1}}. \end{aligned} \quad (27.32)$$

In the case of uniform knots, the equations (27.31) reduce to (27.2), modulo a constant factor. As before, equation (27.31) holds for $i = 2, \dots, N-1$ but cases $i = 1$ and $i = N$ must be adjusted to reflect the end conditions.

For cubic end spans, $\mathbf{r}'_i(\tau)$ is modified when $i = 1$ and $i = N$ to the forms

$$\begin{aligned} &\left[\frac{(2\ell_1 + \ell_2) \mathbf{z}_1 - \ell_1 \mathbf{z}_2}{\ell_1 + \ell_2} (1-\tau)^2 + \mathbf{z}_1 2(1-\tau)\tau + \frac{\ell_2 \mathbf{z}_1 + \ell_1 \mathbf{z}_2}{\ell_1 + \ell_2} \tau^2 \right]^2, \\ &\left[\frac{\ell_N \mathbf{z}_{N-1} + \ell_{N-1} \mathbf{z}_N}{\ell_{N-1} + \ell_N} (1-\tau)^2 + \mathbf{z}_N 2(1-\tau)\tau + \frac{(\ell_{N-1} + 2\ell_N) \mathbf{z}_N - \ell_N \mathbf{z}_{N-1}}{\ell_{N-1} + \ell_N} \tau^2 \right]^2 \end{aligned}$$

and integrating these hodographs gives the equations

$$\begin{aligned} \mathbf{f}_1(\mathbf{z}_1, \dots, \mathbf{z}_N) &= \beta_1 \mathbf{z}_1^2 + \gamma_1 \mathbf{z}_2^2 + \zeta_1 \mathbf{z}_1 \mathbf{z}_2 - \eta_1 \Delta \mathbf{q}_1 = 0, \\ \mathbf{f}_N(\mathbf{z}_1, \dots, \mathbf{z}_N) &= \alpha_N \mathbf{z}_{N-1}^2 + \beta_N \mathbf{z}_N^2 + \epsilon_N \mathbf{z}_{N-1} \mathbf{z}_N - \eta_N \Delta \mathbf{q}_N = 0, \end{aligned}$$

where

$$\beta_1 = 6 + 4 \frac{\ell_1}{\ell_2} + 3 \frac{\ell_2}{\ell_1}, \quad \gamma_1 = \frac{\ell_1}{\ell_2}, \quad \zeta_1 = -2 \frac{\ell_1}{\ell_2}, \quad \eta_1 = 3 \frac{(\ell_1 + \ell_2)^2}{\ell_1^2 \ell_2},$$

and

$$\begin{aligned} \alpha_N &= \frac{\ell_N}{\ell_{N-1}}, & \beta_N &= 6 + 4 \frac{\ell_N}{\ell_{N-1}} + 3 \frac{\ell_{N-1}}{\ell_N}, \\ \epsilon_N &= -2 \frac{\ell_N}{\ell_{N-1}}, & \eta_N &= 3 \frac{(\ell_{N-1} + \ell_N)^2}{\ell_{N-1} \ell_N^2}. \end{aligned}$$

For the case of periodic end conditions, $\mathbf{r}'_i(\tau)$ for $i = 1$ and $i = N$ becomes

$$\begin{aligned} &\left[\frac{\pm \ell_1 \mathbf{z}_N + \ell_N \mathbf{z}_1}{\ell_N + \ell_1} (1 - \tau)^2 + \mathbf{z}_1 2(1 - \tau)\tau + \frac{\ell_2 \mathbf{z}_1 + \ell_1 \mathbf{z}_2}{\ell_1 + \ell_2} \tau^2 \right]^2, \\ &\left[\frac{\ell_N \mathbf{z}_{N-1} + \ell_{N-1} \mathbf{z}_N}{\ell_{N-1} + \ell_N} (1 - \tau)^2 + \mathbf{z}_N 2(1 - \tau)\tau + \frac{\ell_1 \mathbf{z}_N \pm \ell_N \mathbf{z}_1}{\ell_N + \ell_1} \tau^2 \right]^2 \end{aligned}$$

and hence the first and last equations are

$$\begin{aligned} \mathbf{f}_1(\mathbf{z}_1, \dots, \mathbf{z}_N) &= \alpha_1 \mathbf{z}_N^2 + \beta_1 \mathbf{z}_1^2 + \gamma_1 \mathbf{z}_2^2 \pm \delta_1 \mathbf{z}_N \mathbf{z}_2 \\ &\quad \pm \epsilon_1 \mathbf{z}_N \mathbf{z}_1 + \zeta_1 \mathbf{z}_1 \mathbf{z}_2 - \eta_1 \Delta \mathbf{q}_1 = 0, \\ \mathbf{f}_N(\mathbf{z}_1, \dots, \mathbf{z}_N) &= \alpha_N \mathbf{z}_{N-1}^2 + \beta_N \mathbf{z}_N^2 + \gamma_N \mathbf{z}_1^2 \pm \delta_N \mathbf{z}_{N-1} \mathbf{z}_1 \\ &\quad + \epsilon_N \mathbf{z}_{N-1} \mathbf{z}_N \pm \zeta_N \mathbf{z}_N \mathbf{z}_1 - \eta_N \Delta \mathbf{q}_N = 0, \end{aligned}$$

where the coefficients are obtained from expressions (27.32) by setting $\ell_0 = \ell_N$ when $i = 1$, and $\ell_{N+1} = \ell_1$ when $i = N$. Again, the *same* sign choice must be used in \mathbf{f}_1 and \mathbf{f}_N (the “good” solution may occur for either choice).

The solution procedure for the system (27.31), augmented by suitable end conditions, must also be modified. In the homotopy method described in §27.2, we take $\mathbf{g}_i(\mathbf{z}_1, \dots, \mathbf{z}_N) = \beta_i \mathbf{z}_i^2 - \eta_i \Delta \mathbf{q}_i$ as the “simple” initial system. For the Newton–Raphson method, noting that the coefficients (27.32) satisfy

$$\alpha_i + \beta_i + \gamma_i + \delta_i + \epsilon_i + \zeta_i = \eta_i \ell_i,$$

we replace equations (27.16) for the starting approximation by

$$\mathbf{z}_i^2 = \frac{\Delta \mathbf{q}_i}{\ell_i}.$$

Alternately, the method of equating derivatives of the “ordinary” cubic and PH quintic splines at their midpoints to estimate the starting approximation yields the system of equations

$$\frac{\ell_i}{\ell_{i-1} + \ell_i} \mathbf{z}_{i-1} + \left[\frac{\ell_{i-1}}{\ell_{i-1} + \ell_i} + 2 + \frac{\ell_{i+1}}{\ell_i + \ell_{i+1}} \right] \mathbf{z}_i + \frac{\ell_i}{\ell_i + \ell_{i+1}} \mathbf{z}_{i+1} = 2\sqrt{\mathbf{Q}_i}$$

for $i = 2, \dots, N - 1$, where we set $\mathbf{Q}_i = 6\Delta\mathbf{q}_i - \ell_i(\mathbf{d}_{i-1} + \mathbf{d}_i)$ for $i = 1, \dots, N$ and $\mathbf{d}_0, \dots, \mathbf{d}_N$ are the nodal derivatives of the non-uniform ordinary cubic spline. For cubic end spans, this system is augmented by

$$\mathbf{z}_1 = \frac{1}{2} \sqrt{\mathbf{Q}_1} \quad \text{and} \quad \mathbf{z}_N = \frac{1}{2} \sqrt{\mathbf{Q}_N},$$

while for the case of periodic end conditions we use

$$\begin{aligned} \pm \frac{\ell_1}{\ell_N + \ell_1} \mathbf{z}_N + \left[\frac{\ell_N}{\ell_N + \ell_1} + 2 + \frac{\ell_2}{\ell_1 + \ell_2} \right] \mathbf{z}_1 + \frac{\ell_1}{\ell_1 + \ell_2} \mathbf{z}_2 &= 2\sqrt{\mathbf{Q}_1}, \\ \frac{\ell_N}{\ell_{N-1} + \ell_N} \mathbf{z}_{N-1} + \left[\frac{\ell_{N-1}}{\ell_{N-1} + \ell_N} + 2 + \frac{\ell_1}{\ell_N + \ell_1} \right] \mathbf{z}_N \pm \frac{\ell_N}{\ell_N + \ell_1} \mathbf{z}_1 &= 2\sqrt{\mathbf{Q}_N}. \end{aligned}$$

For $2 \leq i \leq N - 1$, the elements of the Jacobian matrix (27.10) are now

$$\begin{aligned} \mathbf{M}_{i,i-1} &= 2\alpha_i \mathbf{z}_{i-1} + \delta_i \mathbf{z}_i + \epsilon_i \mathbf{z}_{i+1}, \\ \mathbf{M}_{ii} &= \delta_i \mathbf{z}_{i-1} + 2\beta_i \mathbf{z}_i + \zeta_i \mathbf{z}_{i+1}, \\ \mathbf{M}_{i,i+1} &= \epsilon_i \mathbf{z}_{i-1} + \zeta_i \mathbf{z}_i + 2\gamma_i \mathbf{z}_{i+1}. \end{aligned}$$

Correspondingly, the Lipschitz constant in Lemma 27.1 becomes

$$K = 30 \max_i \frac{\ell_{i-1} + \ell_i}{\ell_{i-1}} \frac{\ell_i + \ell_{i+1}}{\ell_{i+1}}.$$

Once the values $\mathbf{z}_1, \dots, \mathbf{z}_N$ are known, the construction of the Bézier form

$$\mathbf{r}_i(\tau) = \sum_{k=0}^5 \mathbf{p}_{i,k} \binom{5}{k} (1-\tau)^{5-k} \tau^k$$

for each segment $\mathbf{r}_i(\tau)$ is analogous to that described in §27.1.1. Since $\dot{\mathbf{r}}_i(\tau) = \ell_i \mathbf{r}'_i(\tau)$, where dots and primes indicate derivatives with respect to τ and t , respectively, we obtain the control points

$$\begin{aligned} \mathbf{p}_{i,1} &= \mathbf{p}_{i,0} + \ell_i \frac{1}{5} \mathbf{w}_{i,0}^2, \\ \mathbf{p}_{i,2} &= \mathbf{p}_{i,1} + \ell_i \frac{1}{5} \mathbf{w}_{i,0} \mathbf{w}_{i,1}, \\ \mathbf{p}_{i,3} &= \mathbf{p}_{i,2} + \ell_i \frac{2 \mathbf{w}_{i,1}^2 + \mathbf{w}_{i,0} \mathbf{w}_{i,2}}{15}, \\ \mathbf{p}_{i,4} &= \mathbf{p}_{i,3} + \ell_i \frac{1}{5} \mathbf{w}_{i,1} \mathbf{w}_{i,2}, \\ \mathbf{p}_{i,5} &= \mathbf{p}_{i,4} + \ell_i \frac{1}{5} \mathbf{w}_{i,2}^2. \end{aligned}$$

Here $\mathbf{p}_{i,0} = \mathbf{q}_{i-1}$, and $\mathbf{w}_{i,0} = (\ell_i \mathbf{z}_{i-1} + \ell_{i-1} \mathbf{z}_i) / (\ell_{i-1} + \ell_i)$, $\mathbf{w}_{i,1} = \mathbf{z}_i$, $\mathbf{w}_{i,2} = (\ell_{i+1} \mathbf{z}_i + \ell_i \mathbf{z}_{i+1}) / (\ell_i + \ell_{i+1})$ with appropriate modifications for the end spans.

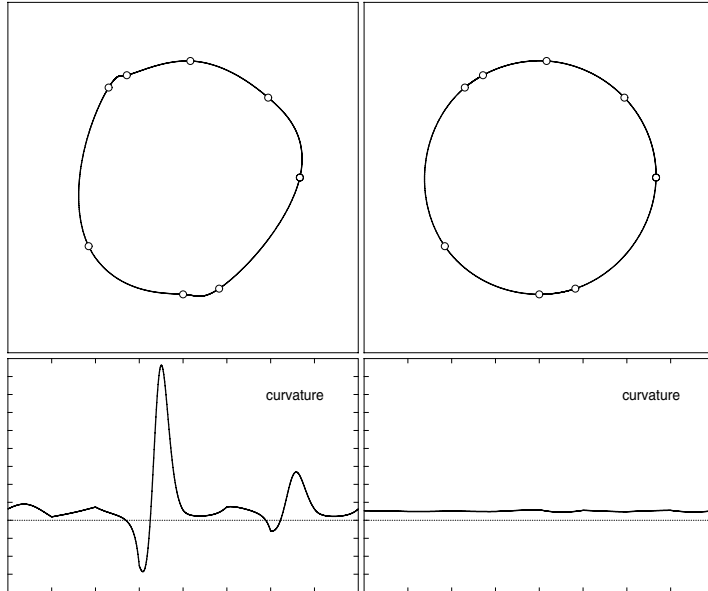


Fig. 27.10. Comparison of periodic C^2 PH quintic splines that interpolate a set of unevenly-sampled points from the unit circle, using: (left) uniform knots, and (right) the chordal parameterization (14.20). The curvature distributions indicate that the non-uniform knots provide a much better approximation to the circle.

Figure 27.10 compares the PH quintic splines that interpolate a sequence of unevenly-sampled points on the unit circle, using uniform knots and the chordal parameterization defined by (14.20). In this case, the deviation of the curvature from the nominal value $\kappa = 1$ gives a measure of “smoothness” of the two interpolants. For the PH spline with non-uniform knots, we have $0.91 \leq \kappa \leq 1.18$, while for the case of uniform knots, $-5.72 \leq \kappa \leq +17.26$. Note that use of the chordal parameterization (14.20) allows greater variations in the spacing of successive points than is indicated by the second condition in the characterization (27.17) of “reasonable” point sequences.

27.4.2 Shape-preserving PH Splines

With ordinary cubic splines and PH quintic splines there is no assurance that, if the data points $\mathbf{q}_0, \dots, \mathbf{q}_N$ have certain desired geometrical characteristics — such as monotonicity or convexity — the interpolating spline will exhibit the same property. The desire to provide smooth interpolation schemes that produce interpolants preserving such shape properties of the point data has prompted interest in *shape-preserving* splines. These are often based [102, 215, 294, 317] upon *tension methods*. The polynomial spline segments incorporate certain *tension parameters*, obtained by relaxing from parametric to geometric

continuity, that may be used to “stretch” them, and thereby ensure that the interpolant shape agrees with that of the discrete data.

An adaptation of the PH quintic spline equations to accommodate such tension parameters has been formulated in [172]. In the G^2 case, the PH spline construction is based on applying the Newton–Raphson iteration to a global system of equations, commencing with a suitable initialization strategy: this generalizes the construction of §27.3.3. As a simpler and cheaper alternative, a shape-preserving G^1 PH quintic spline scheme was also defined — although the order of continuity is lower, this has the advantage of allowing construction through purely local equations. We refer the reader to [172] for complete details of these shape-preserving PH spline schemes.

27.5 Control Polygons for PH Splines

The methods to construct PH spline curves discussed thus far are all based on *interpolation* of a set of points $\mathbf{q}_0, \dots, \mathbf{q}_N$ (with appropriate end conditions). Since a basic paradigm of computer-aided design is the use of *control polygons* as a means to define and manipulate shapes, a scheme that allows the designer to construct PH splines by sketching a polygon, as with the B-spline control polygons for “ordinary” C^2 cubic splines (see §15.3), seems desirable.

However, the non-linear nature of PH splines precludes the possibility of constructing a *basis* for them, and hence the principle of linear superposition cannot be invoked to characterize the complete space of PH splines. Although PH splines can always be represented in B-spline form, making any changes to their B-spline control polygons will invariably compromise their PH property. There are no simple and intuitive constraints on the control polygon geometry that will ensure preservation of the PH nature of a spline curve.

In view of these considerations, a “practical” approach to associating PH splines with control polygons seems best [355]. Namely, the control polygon is used to *define* a “hidden” PH spline interpolation problem, that can be solved by the methods of §27.3. Although an interpolation problem lurks within the algorithm, the user will manipulate the PH spline through the control polygon alone, and need not be concerned with — or even aware of — the underlying interpolation scheme. The interpolation points are defined as the nodal points of the corresponding “ordinary” C^2 cubic B-spline curve.

We outline here the algorithms developed in [355] based on this paradigm. The C^2 PH quintic spline curve associated with a given control polygon and knot sequence is defined to be the “good” interpolant to the nodal points of the ordinary C^2 cubic spline curve with the same B-spline control points, knot sequence, and end conditions — it may be computed to machine precision by just a few Newton–Raphson iterations. Multiple knots may be used to reduce the continuity to C^1 or C^0 at prescribed points, and by means of double knots the PH splines offer a *linear precision* and *local shape modification* capability.

27.5.1 Equivalent Interpolation Problem

Consider the cubic B-spline curve

$$\mathbf{c}(t) = \sum_{k=0}^N \mathbf{p}_k B_k^3(t) \quad (27.33)$$

with control points $\mathbf{p}_0, \dots, \mathbf{p}_N$ defined on a uniform knot sequence with 4-fold end knots, as appropriate for open curves (see §15.3.1): $t_0 = t_1 = t_2 = t_3 = 0$, $t_k = k$ for $k = 4, \dots, N$, and $t_{N+1} = t_{N+2} = t_{N+3} = t_{N+4} = N + 1$.

Our strategy for associating a C^2 PH spline curve with the control polygon defined by $\mathbf{p}_0, \dots, \mathbf{p}_N$ is as follows. First, we determine the *nodal points* \mathbf{q}_i of the cubic B-spline curve (27.33), i.e., the points that correspond to evaluating (27.33) at the distinct parameter values of the knot sequence: they identify the junctures of the cubic segments comprising the B-spline curve. These points, augmented with suitable end conditions, will serve as input to the algorithm of §27.3, which computes the “good” PH quintic spline interpolating them. We *define* the latter to be the C^2 PH quintic spline associated with the given control polygon $\mathbf{p}_0, \dots, \mathbf{p}_N$. In this manner, the “ordinary” cubic spline and the PH quintic spline associated with the polygon $\mathbf{p}_0, \dots, \mathbf{p}_N$ are both C^2 (assuming no interior multiple knots), and they exhibit the same nodal points and total number of segments. We shall see in the examples below that, for typical cases, these two spline curves are in very close agreement.

For the knot vector specified above, the non-zero nodal values of the basis functions are as follows. For the first three basis functions, we have

$$B_0(t_3) = 1, \quad B_1(t_4) = \frac{1}{4}, \quad B_2(t_4) = \frac{7}{12}, \quad B_2(t_5) = \frac{1}{6}.$$

The intermediate basis functions (which are simply translates of each other) have non-zero nodal values

$$B_k(t_{k+1}) = \frac{1}{6}, \quad B_k(t_{k+2}) = \frac{2}{3}, \quad B_k(t_{k+3}) = \frac{1}{6}$$

for $k = 3, \dots, N - 3$. Finally, for the last three basis functions, we have

$$B_{N-2}(t_{N-1}) = \frac{1}{6}, \quad B_{N-2}(t_N) = \frac{7}{12}, \quad B_{N-1}(t_N) = \frac{1}{4}, \quad B_N(t_{N+1}) = 1.$$

Thus, evaluating the B-spline curve at the distinct nodes t_3, \dots, t_{N+1} yields $N - 1$ points on the curve, which we label as follows

$$\begin{aligned} \mathbf{q}_0 &= \mathbf{c}(t_3) = \mathbf{p}_0, \\ \mathbf{q}_1 &= \mathbf{c}(t_4) = \frac{1}{12}(3\mathbf{p}_1 + 7\mathbf{p}_2 + 2\mathbf{p}_3), \\ \mathbf{q}_k &= \mathbf{c}(t_{k+3}) = \frac{1}{6}(\mathbf{p}_k + 4\mathbf{p}_{k+1} + \mathbf{p}_{k+2}), \quad k = 2, \dots, N - 4 \\ \mathbf{q}_{N-3} &= \mathbf{c}(t_N) = \frac{1}{12}(2\mathbf{p}_{N-3} + 7\mathbf{p}_{N-2} + 3\mathbf{p}_{N-1}), \\ \mathbf{q}_{N-2} &= \mathbf{c}(t_{N+1}) = \mathbf{p}_N. \end{aligned} \quad (27.34)$$

In the case of an open curve, we choose specified end-derivatives as the end conditions, since these derivatives can be computed directly from the definition of the B-spline curve (27.33). Specifically, we have

$$\mathbf{d}_0 = \mathbf{c}'(t_3) = 3\Delta\mathbf{p}_1 \quad \text{and} \quad \mathbf{d}_{N-2} = \mathbf{c}'(t_{N+1}) = 3\Delta\mathbf{p}_N,$$

where $\Delta\mathbf{p}_1 = \mathbf{p}_1 - \mathbf{p}_0$ and $\Delta\mathbf{p}_N = \mathbf{p}_N - \mathbf{p}_{N-1}$.

Thus, we define the C^2 PH quintic spline curve associated with the *open* control polygon specified by control points $\mathbf{p}_0, \dots, \mathbf{p}_N$ to be the “good” PH spline interpolant to the set of $N - 1$ points $\mathbf{q}_0, \dots, \mathbf{q}_{N-2}$ together with the end derivatives \mathbf{d}_0 and \mathbf{d}_{N-2} . It can be efficiently computed by the rapidly-convergent iterative methods described in §27.3. This PH spline replaces the “ordinary” cubic segments of the C^2 B-spline curve by PH quintic segments, on a one-for-one basis. These PH quintic segments meet with C^2 continuity at the same nodal points as the cubic segments they replace, and the initial/final tangents of the cubic B-spline curve are also preserved.

In the case of a closed polygon (with $\mathbf{p}_N = \mathbf{p}_0$, indicating that a periodic C^2 curve is desired), we do not employ the end derivatives. Instead, evaluating the periodic C^2 cubic B-spline curve in this context (assuming uniform knots) gives the nodal points

$$\mathbf{q}_k = \mathbf{c}(t_k) = \frac{1}{6}(\mathbf{p}_k + 4\mathbf{p}_{k+1} + \mathbf{p}_{k+2}) \quad (27.35)$$

for $k = 0, \dots, N - 2$. It is understood here that the control points $\mathbf{p}_0, \dots, \mathbf{p}_N$ follow the convention (15.23) for periodic B-spline curves — namely, the last n control points $\mathbf{p}_{N-n+1}, \dots, \mathbf{p}_N$ replicate the first n control points $\mathbf{p}_0, \dots, \mathbf{p}_{n-1}$ (here $n = 3$ for a cubic B-spline). The formula (27.35) then gives $N - 1$ points, at the junctures of the cubic segments of the B-spline curve, the last being coincident with the first, $\mathbf{q}_{N-2} = \mathbf{q}_0$, to indicate a closed curve. We pass these points to the algorithm of §27.3, with periodic end conditions specified, to be interpolated by a PH quintic spline. The result is defined to be the C^2 PH quintic spline associated with the closed control polygon $\mathbf{p}_0, \dots, \mathbf{p}_N$.

27.5.2 Inclusion of Multiple Knots

To define a PH spline with the control polygon $\mathbf{p}_0, \dots, \mathbf{p}_N$ and knots (15.21) containing the double knot $t_k = t_{k+1} = \tau$, we evaluate the nodal points

$$\mathbf{c}(t_3), \mathbf{c}(t_4), \dots, \mathbf{c}(t_{k-1}), \mathbf{c}(\tau), \mathbf{c}(t_{k+2}), \dots, \mathbf{c}(t_N), \mathbf{c}(t_{N+1})$$

of the corresponding B-spline curve (27.33), and also the three derivatives

$$\mathbf{d}_i = \mathbf{c}'(t_3), \quad \mathbf{d}_\tau = \mathbf{c}'(\tau), \quad \mathbf{d}_f = \mathbf{c}'(t_{N+1}).$$

Note that \mathbf{d}_τ is uniquely defined, since the cubic B-spline curve $\mathbf{c}(t)$ is C^1 at the double knot τ . We then compute two PH quintic splines: the “left” spline

interpolates the points $\mathbf{c}(t_3), \mathbf{c}(t_4), \dots, \mathbf{c}(t_{k-1}), \mathbf{c}(\tau)$ and has end derivatives \mathbf{d}_i and \mathbf{d}_τ , while the “right” spline interpolates $\mathbf{c}(\tau), \mathbf{c}(t_{k+2}), \dots, \mathbf{c}(t_N), \mathbf{c}(t_{N+1})$ and has end derivatives \mathbf{d}_τ and \mathbf{d}_f . The union of these left and right portions defines the PH quintic spline associated with the control polygon $\mathbf{p}_0, \dots, \mathbf{p}_N$ when the knot vector (15.21) contains a double knot $t_k = t_{k+1} = \tau$. It is (only) C^1 at $\mathbf{c}(\tau)$, since the left and right parts possess a common first derivative \mathbf{d}_τ there, but not a common second derivative. At all other nodes, it is C^2 .

The process for triple knots is similar. To define a PH spline corresponding to the control polygon $\mathbf{p}_0, \dots, \mathbf{p}_N$ and knot sequence (15.21) with a triple knot $t_k = t_{k+1} = t_{k+2} = \tau$, we evaluate the nodal points

$$\mathbf{c}(t_3), \mathbf{c}(t_4), \dots, \mathbf{c}(t_{k-1}), \mathbf{c}(\tau), \mathbf{c}(t_{k+3}), \dots, \mathbf{c}(t_N), \mathbf{c}(t_{N+1})$$

of the cubic B-spline curve. We also evaluate the four derivatives

$$\mathbf{d}_i = \mathbf{c}'(t_3), \quad \mathbf{d}_{\tau_-} = \mathbf{c}'(\tau_-), \quad \mathbf{d}_{\tau_+} = \mathbf{c}'(\tau_+), \quad \mathbf{d}_f = \mathbf{c}'(t_{N+1}).$$

Here \mathbf{d}_{τ_-} and \mathbf{d}_{τ_+} denote the left and right limits of $\mathbf{c}'(t)$, approaching $t = \tau$ from the left and right: note that $\mathbf{c}'(\tau)$ is undefined, since the B-spline is only C^0 there. The “left” PH spline now interpolates $\mathbf{c}(t_3), \mathbf{c}(t_4), \dots, \mathbf{c}(t_{k-1}), \mathbf{c}(\tau)$ and has end derivatives \mathbf{d}_i and \mathbf{d}_{τ_-} , while the “right” PH spline interpolates $\mathbf{c}(\tau), \mathbf{c}(t_{k+3}), \dots, \mathbf{c}(t_N), \mathbf{c}(t_{N+1})$ with end derivatives \mathbf{d}_{τ_+} and \mathbf{d}_f . The union of these portions defines the PH quintic spline associated with the control polygon $\mathbf{p}_0, \dots, \mathbf{p}_N$ when the knot vector contains the triple knot $t_k = t_{k+1} = t_{k+2} = \tau$. It is only C^0 at $\mathbf{c}(\tau)$, since the left and right parts have different derivatives there. At all the other nodes, it is C^2 .

The above discussion is for knot sequences corresponding to open curves, but similar methods can be defined for periodic splines with multiple knots.

27.5.3 Emulating B-spline Curve Properties

When four consecutive control points $\mathbf{p}_{k-3}, \mathbf{p}_{k-2}, \mathbf{p}_{k-1}, \mathbf{p}_k$ of a cubic B-spline curve are collinear, the curve segment $t \in [t_k, t_{k+1}]$ is precisely linear, and (for simple knots) it has C^2 junctures with the portions $t < t_k$ and $t > t_{k+1}$. This is known as the *linear precision* property of B-spline curves (see §15.3.5). The multiple knot capability of PH splines can be invoked to emulate this property of cubic B-splines. To accomplish this, we must accept C^1 (rather than C^2) connections of the linear segment with the remainder of the PH spline.

We assume a control polygon with $\mathbf{p}_{k-3}, \mathbf{p}_{k-2}, \mathbf{p}_{k-1}, \mathbf{p}_k$ collinear and the values t_k, t_{k+1} as double knots. The segment $[t_k, t_{k+1}]$ of the cubic B-spline defined by this polygon and knot sequence is precisely linear, and only C^1 at the double knots t_k and t_{k+1} . Nodal data from this cubic B-spline is used to construct a PH spline having the same control polygon and t_k, t_{k+1} as double knots. Since the point/tangent data for the interval $[t_k, t_{k+1}]$ are collinear, the PH spline will be precisely linear⁴ over this interval. One may generalize

⁴ A straight line is trivially a PH curve, and may be degree-elevated to a quintic.

to four or more collinear control points, and thus achieve linear precision over several consecutive intervals. Note that, without introducing the double knots, the PH spline would be only *approximately* linear over the relevant intervals when a sufficient number of consecutive control points are collinear.

The *local shape modification* capability of B-spline curves arises from the compact support of the basis functions. Moving control point \mathbf{p}_k , associated with basis function $B_k^n(t)$, influences the curve only on the interval $[t_k, t_{k+n+1}]$ since $B_k^n(t)$ vanishes outside this interval. The modified and unmodified parts of the curve still exhibit C^2 continuity at their junctures.

We can emulate this property for PH splines by introducing double knots, in a manner similar to that used for the linear precision property. With this method, the continuity between the modified and unmodified portions is C^1 rather than C^2 . Suppose control point \mathbf{p}_k is to be moved. We introduce double knots into the cubic B-spline at the values $a = t_k$ and $b = t_{k+n+1}$ *before* \mathbf{p}_k has been moved. With nodal data determined from the B-spline *after* \mathbf{p}_k has been moved, we then compute PH splines on the intervals $t \leq a$, $a \leq t \leq b$, $t \geq b$. The union of these three splines is defined to be the locally-modified PH spline corresponding to the control polygon with the new position of \mathbf{p}_k (and double knots at $t = a, b$). The locally-modified PH spline agrees exactly with the PH spline defined by the original control polygon over the intervals $t \leq a$ and $t \geq b$. Moreover, it coincides precisely, over its entire extent, with the PH spline defined by the modified polygon and a knot sequence with double knots at $t = a, b$. In this manner, we maintain one-to-one correspondence between PH splines and combinations of control polygons and knot sequences.

27.5.4 Illustrative Examples

Figure 27.11 illustrates the design of open and closed C^2 PH quintic splines by control polygons, using the above scheme. The control polygons are shown together with the PH splines (solid) and the “ordinary” cubic splines (dotted), and their common set of nodal points — i.e., the junctures of the “ordinary” cubic or PH quintic segments comprising these splines. In both examples, the PH quintic and “ordinary” cubic splines are evidently in excellent agreement — almost indistinguishable on the scale of the plots. The curvature profiles (which tend to exaggerate the shape differences) are compared in Fig. 27.12, and are also seen to be in excellent agreement.

The speed of convergence of the Newton–Raphson iterations to the “good” PH quintic spline in the open curve example is evident in the behavior of the quantity (27.30):

$$\epsilon_0 = 7.941, \quad \epsilon_1 = 0.05902, \quad \epsilon_2 = 0.000004387, \quad \epsilon_3 = 0.0000000000005872.$$

Of course, the PH splines constructed as described above also possess control polygons as quintic B-spline curves — but these polygons should not be made available for manipulation by the user, since alterations will generically yield “ordinary” quintic B-spline curves, that no longer possess the PH property.

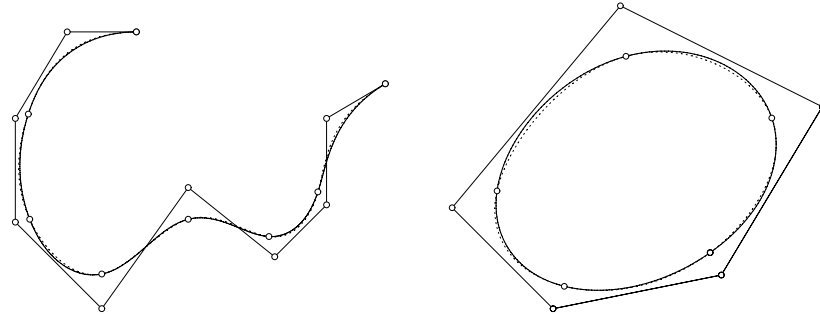


Fig. 27.11. Comparison of the “ordinary” cubic B-splines (dotted) and PH quintic splines (solid) associated with given control polygons: an open curve with multiple end knots (left), and a closed curve with periodic end conditions (right). The curves interpolate the same set of nodal points — and, in the case of the open curve, have the same end-derivatives. They are barely distinguishable on the scale of the plots.

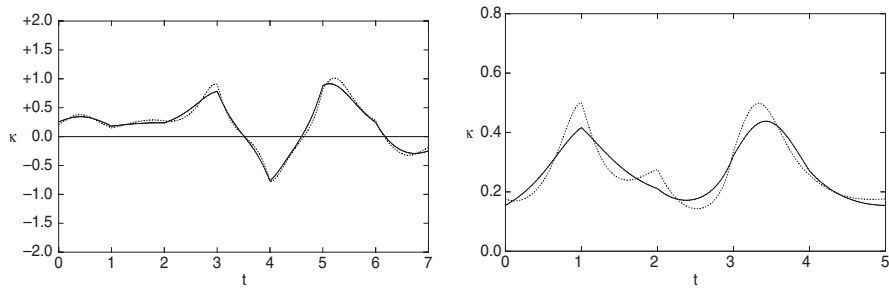


Fig. 27.12. Comparison of curvature profiles for the corresponding “ordinary” C^2 cubic B-splines (dotted) and C^2 PH quintic splines (solid), shown in Fig. 27.11.

Figure 27.13 shows the effect of a double knot on the cubic B-spline and the PH quintic spline defined by a control polygon with eight control points. The nodal point corresponding to the double knot lies on (and is tangent to) the control polygon. Because the curves are only C^1 at this point, there is a small discontinuity evident in the corresponding curvature profiles.

Fig. 27.14 illustrates the linear precision property for a polygon with four collinear control points. The knot vector has two double knots, corresponding to parameter values that delimit the linear segment. Fig. 27.14 also illustrates the local-shape modification capability, for a closed curve. Two double knots are inserted, prior to moving a single control point. Due to the presence of these double knots, two of the four intervals that will be influenced by the displacement of the chosen control point are degenerate, and hence only two non-degenerate segments of the spline curves are changed. The changes are thus even more localized than for splines with only simple knots. The nodal points corresponding to the two double knots, which separate the modified and unmodified portions of the curves, are shown as solid dots.

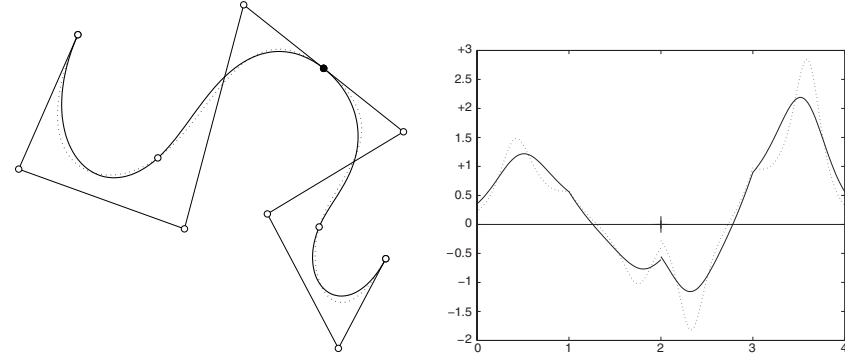


Fig. 27.13. Left: cubic B-spline and PH quintic spline incorporating a double knot — the solid dot indicates the nodal point corresponding to this knot. Right: the curvature profiles for these curves — although they are only C^1 at the double knot, the discontinuities in their curvatures at this point are nevertheless rather small.

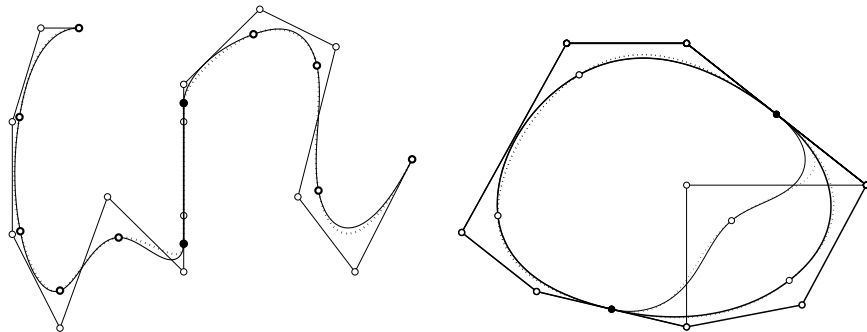


Fig. 27.14. Left: cubic B-spline and PH quintic spline defined by a control polygon with four collinear control points, and two double knots corresponding to the initial and final parameter values of the linear segment defined by them. The nodal points delineating the linear segment are indicated by solid dots. Right: local modification of corresponding cubic B-spline and PH quintic spline curves with two double knots and the same control polygon, by the displacement of just a single control point.

Although the non-linear nature of PH splines precludes formal proofs for certain features of cubic B-splines, such as convex-hull confinement and the variation-diminishing property, this is of little practical significance in view of the close agreement of the two curves in most cases — in fact, the PH spline typically exhibits a somewhat better curvature distribution.

Note that, since the Newton-Raphson method for constructing the C^2 PH spline associated with a given control polygon and knot sequence involves only tridiagonal linear systems, the computational cost is proportional to N . Even large examples ($N \sim 100$) can be computed in just a fraction of a second using modest processors, allowing for highly “interactive” design of PH splines.

The control polygon paradigm for PH splines has been described above in terms of uniform knots, but it can easily be extended to non-uniform knots. The formulae (27.34) and (27.35) that determine the nodal points of the cubic B-spline curve constructed on these non-uniform knots must be appropriately amended. Furthermore, we use the system of PH spline equations based on non-uniform knots, as described in §27.4.1. See [355] for further details.

Spatial Hermite Interpolants

I wish I had an answer to that because I'm tired of answering that question.

Yogi Berra

As with planar PH curves (see Chap. 25), first-order Hermite interpolation is a convenient approach to constructing spatial PH curves in a geometrically meaningful manner. The quaternion formulation introduced in Chap. 22 is useful in reducing the problem to a simple system of quadratic equations, but the nature of the solution space differs qualitatively from the planar case — instead of just a finite multiplicity of solutions, the spatial PH quintic Hermite interpolation problem admits a *two-parameter family* of solutions.

28.1 G^1 Interpolation by Cubics

We first briefly consider the suitability of spatial PH cubics for use as Hermite interpolants. As noted in §21.1, the spatial PH cubics are (non-circular) helices that admit a simple geometrical characterization in terms of the Bézier control polygon. The possibility of interpolating G^1 Hermite data — end points $\mathbf{p}_0, \mathbf{p}_1$ and unit tangent vectors $\mathbf{t}_0, \mathbf{t}_1$ — was first considered by Jüttler and Mäurer [267], in the context of modelling sweep surfaces. They showed algebraically that there may exist zero, one, or two spatial PH cubics interpolating such G^1 data. Subsequently, it was shown that a condition for existence of G^1 spatial PH cubic interpolants can be expressed [354] as the inequality

$$\cos \Delta\phi \leq -\frac{3}{4} + \frac{1}{8} \left(\frac{\tan \frac{1}{2}\theta_1}{\tan \frac{1}{2}\theta_0} + \frac{\tan \frac{1}{2}\theta_0}{\tan \frac{1}{2}\theta_1} \right),$$

where θ_0, θ_1 are the polar angles of $\mathbf{t}_0, \mathbf{t}_1$ relative to $\Delta\mathbf{p} = \mathbf{p}_1 - \mathbf{p}_0$, and $\Delta\phi$ is their azimuthal separation about $\Delta\mathbf{p}$. When this inequality is *not* satisfied, a “minimal adjustment” of $\mathbf{t}_0, \mathbf{t}_1$ was proposed in [354] to ensure its satisfaction.

A scheme for assigning suitable tangents $\mathbf{t}_0, \dots, \mathbf{t}_N$ to a sequence of points $\mathbf{p}_0, \dots, \mathbf{p}_N$ in \mathbb{R}^3 was also proposed in [354], to facilitate construction of a G^1 piecewise PH cubic curve that interpolates them. Because of their technical nature, we omit complete descriptions of the interpolation of G^1 Hermite data by spatial PH cubics here, and refer the reader to [267, 354] for details.

28.2 C^1 Hermite Interpolation Problem

Spatial PH quintics are generally preferred in free-form geometric design, since they offer greater shape flexibility. Regarded as a pure vector quaternion, the hodograph of spatial PH quintic

$$\begin{aligned}\mathbf{r}'(t) = & [u^2(t) + v^2(t) - p^2(t) - q^2(t)] \mathbf{i} \\ & + 2[u(t)q(t) + v(t)p(t)] \mathbf{j} + 2[v(t)q(t) - u(t)p(t)] \mathbf{k}\end{aligned}$$

can be concisely expressed (see Chap. 22) in the form

$$\mathbf{r}'(t) = \mathcal{A}(t) \mathbf{i} \mathcal{A}^*(t), \quad (28.1)$$

in terms of the quadratic polynomial

$$\mathcal{A}(t) = \mathcal{A}_0(1-t)^2 + \mathcal{A}_1 2(1-t)t + \mathcal{A}_2 t^2 \quad (28.2)$$

with quaternion coefficients $\mathcal{A}_r = u_r \mathbf{i} + v_r \mathbf{j} + q_r \mathbf{k}$. We wish to determine these coefficients by solving a first-order Hermite interpolation problem. Once $\mathcal{A}_0, \mathcal{A}_1, \mathcal{A}_2$ are known, the Bézier control points of the PH quintic interpolant (considered as pure vector quaternions) are given by expressions (22.7), where $\mathbf{p}_0 = \mathbf{p}_i$ and we have $\mathbf{p}_5 = \mathbf{p}_f$ by construction.

The problem of Hermite interpolation by spatial PH quintics often requires the quaternion solutions \mathcal{A} to equations of the form

$$\mathcal{A} \mathbf{i} \mathcal{A}^* = \mathbf{c}, \quad (28.3)$$

where $\mathbf{c} = c_x \mathbf{i} + c_y \mathbf{j} + c_z \mathbf{k}$ is a given vector. This equation defines a mapping of the unit basis vector \mathbf{i} to a general vector \mathbf{c} in \mathbb{R}^3 , through a spatial rotation and a scaling by the factor $|\mathbf{c}| = |\mathcal{A}|^2$. From §5.6, we know that there exists a *one-parameter family* of appropriate spatial rotations. Writing $\mathbf{c} = |\mathbf{c}|(\lambda, \mu, \nu)$ where $\lambda^2 + \mu^2 + \nu^2 = 1$, the solutions to (28.3) can be expressed in terms of an angular parameter ϕ as

$$\begin{aligned}\mathcal{A}(\phi) = & \sqrt{\frac{1}{2}(1+\lambda)|\mathbf{c}|} \left(-\sin \phi + \cos \phi \mathbf{i} \right. \\ & \left. + \frac{\mu \cos \phi + \nu \sin \phi}{1+\lambda} \mathbf{j} + \frac{\nu \cos \phi - \mu \sin \phi}{1+\lambda} \mathbf{k} \right). \quad (28.4)\end{aligned}$$

Suppose the Hermite data $\mathbf{r}(0) = \mathbf{p}_i$, $\mathbf{r}'(0) = \mathbf{d}_i$ and $\mathbf{r}(1) = \mathbf{p}_f$, $\mathbf{r}'(1) = \mathbf{d}_f$ are expressed as pure vector quaternions — namely, $\mathbf{p}_i = x_i \mathbf{i} + y_i \mathbf{j} + z_i \mathbf{k}$,

$\mathbf{d}_i = d_{ix} \mathbf{i} + d_{iy} \mathbf{j} + d_{iz} \mathbf{k}$ and $\mathbf{p}_f = x_f \mathbf{i} + y_f \mathbf{j} + z_f \mathbf{k}$, $\mathbf{d}_f = d_{fx} \mathbf{i} + d_{fy} \mathbf{j} + d_{ fz} \mathbf{k}$. Interpolation of the end-derivatives then yields the equations

$$\mathcal{A}_0 \mathbf{i} \mathcal{A}_0^* = \mathbf{d}_i \quad \text{and} \quad \mathcal{A}_2 \mathbf{i} \mathcal{A}_2^* = \mathbf{d}_f \quad (28.5)$$

for \mathcal{A}_0 and \mathcal{A}_2 . Moreover, with \mathbf{p}_i as the integration constant, interpolation of the end points gives the condition

$$\begin{aligned} \int_0^1 \mathcal{A}(t) \mathbf{i} \mathcal{A}^*(t) dt &= \mathbf{p}_f - \mathbf{p}_i \\ &= \frac{1}{5} \mathcal{A}_0 \mathbf{i} \mathcal{A}_0^* \\ &\quad + \frac{1}{10} (\mathcal{A}_0 \mathbf{i} \mathcal{A}_1^* + \mathcal{A}_1 \mathbf{i} \mathcal{A}_0^*) \\ &\quad + \frac{1}{30} (\mathcal{A}_0 \mathbf{i} \mathcal{A}_2^* + 4 \mathcal{A}_1 \mathbf{i} \mathcal{A}_1^* + \mathcal{A}_2 \mathbf{i} \mathcal{A}_0^*) \\ &\quad + \frac{1}{10} (\mathcal{A}_1 \mathbf{i} \mathcal{A}_2^* + \mathcal{A}_2 \mathbf{i} \mathcal{A}_1^*) \\ &\quad + \frac{1}{5} \mathcal{A}_2 \mathbf{i} \mathcal{A}_2^*. \end{aligned} \quad (28.6)$$

Since equations (28.5) are of the form (28.3), they can be solved directly to obtain \mathcal{A}_0 and \mathcal{A}_2 as

$$\begin{aligned} \mathcal{A}_0 &= \sqrt{\frac{1}{2}(1+\lambda_i)|\mathbf{d}_i|} \left(-\sin \phi_0 + \cos \phi_0 \mathbf{i} \right. \\ &\quad \left. + \frac{\mu_i \cos \phi_0 + \nu_i \sin \phi_0}{1+\lambda_i} \mathbf{j} + \frac{\nu_i \cos \phi_0 - \mu_i \sin \phi_0}{1+\lambda_i} \mathbf{k} \right), \end{aligned} \quad (28.7)$$

$$\begin{aligned} \mathcal{A}_2 &= \sqrt{\frac{1}{2}(1+\lambda_f)|\mathbf{d}_f|} \left(-\sin \phi_2 + \cos \phi_2 \mathbf{i} \right. \\ &\quad \left. + \frac{\mu_f \cos \phi_2 + \nu_f \sin \phi_2}{1+\lambda_f} \mathbf{j} + \frac{\nu_f \cos \phi_2 - \mu_f \sin \phi_2}{1+\lambda_f} \mathbf{k} \right), \end{aligned} \quad (28.8)$$

where $(\lambda_i, \mu_i, \nu_i)$ and $(\lambda_f, \mu_f, \nu_f)$ are the direction cosines of \mathbf{d}_i and \mathbf{d}_f , and ϕ_0, ϕ_2 are free angular variables. Knowing \mathcal{A}_0 and \mathcal{A}_2 , the solution of (28.6) for \mathcal{A}_1 may appear, at first sight, more difficult. However, by using (28.5) and making appropriate re-arrangements, this equation can be written as

$$\begin{aligned} (3\mathcal{A}_0 + 4\mathcal{A}_1 + 3\mathcal{A}_2) \mathbf{i} (3\mathcal{A}_0 + 4\mathcal{A}_1 + 3\mathcal{A}_2)^* \\ = 120(\mathbf{p}_f - \mathbf{p}_i) - 15(\mathbf{d}_i + \mathbf{d}_f) + 5(\mathcal{A}_0 \mathbf{i} \mathcal{A}_2^* + \mathcal{A}_2 \mathbf{i} \mathcal{A}_0^*), \end{aligned} \quad (28.9)$$

which has the form (28.3) with $\mathcal{A} = 3\mathcal{A}_0 + 4\mathcal{A}_1 + 3\mathcal{A}_2$. Note that the quantity on the right in (28.9) is a known pure vector — since $\mathcal{A}_2 \mathbf{i} \mathcal{A}_0^* = (\mathcal{A}_0 \mathbf{i} \mathcal{A}_2^*)^*$ we see that $\mathcal{A}_0 \mathbf{i} \mathcal{A}_2^* + \mathcal{A}_2 \mathbf{i} \mathcal{A}_0^*$ is twice the vector part of $\mathcal{A}_0 \mathbf{i} \mathcal{A}_2^*$. From (28.7) and (28.8) we may write

$$\mathcal{A}_0 \mathbf{i} \mathcal{A}_2^* + \mathcal{A}_2 \mathbf{i} \mathcal{A}_0^* = \sqrt{(1+\lambda_i)|\mathbf{d}_i|(1+\lambda_f)|\mathbf{d}_f|} (a_x \mathbf{i} + a_y \mathbf{j} + a_z \mathbf{k}),$$

where

$$\begin{aligned} a_x &= \cos(\phi_2 - \phi_0) - \frac{(\mu_i\mu_f + \nu_i\nu_f)\cos(\phi_2 - \phi_0) + (\mu_i\nu_f - \mu_f\nu_i)\sin(\phi_2 - \phi_0)}{(1 + \lambda_i)(1 + \lambda_f)}, \\ a_y &= \frac{\mu_i \cos(\phi_2 - \phi_0) - \nu_i \sin(\phi_2 - \phi_0)}{1 + \lambda_i} + \frac{\mu_f \cos(\phi_2 - \phi_0) + \nu_f \sin(\phi_2 - \phi_0)}{1 + \lambda_f}, \\ a_z &= \frac{\nu_i \cos(\phi_2 - \phi_0) + \mu_i \sin(\phi_2 - \phi_0)}{1 + \lambda_i} + \frac{\nu_f \cos(\phi_2 - \phi_0) - \mu_f \sin(\phi_2 - \phi_0)}{1 + \lambda_f}. \end{aligned}$$

Writing $\mathbf{c} = c_x \mathbf{i} + c_y \mathbf{j} + c_z \mathbf{k}$ for the right-hand side of (28.9), we deduce from (28.3) the solution

$$\begin{aligned} \mathcal{A}_1 &= -\frac{3}{4}(\mathcal{A}_0 + \mathcal{A}_2) + \frac{\sqrt{\frac{1}{2}(1+\lambda)|\mathbf{c}|}}{4} \left(-\sin \phi_1 + \cos \phi_1 \mathbf{i} \right. \\ &\quad \left. + \frac{\mu \cos \phi_1 + \nu \sin \phi_1}{1+\lambda} \mathbf{j} + \frac{\nu \cos \phi_1 - \mu \sin \phi_1}{1+\lambda} \mathbf{k} \right), \quad (28.10) \end{aligned}$$

where (λ, μ, ν) are the direction cosines of \mathbf{c} , and ϕ_1 is another free angular variable. Note that \mathcal{A}_1 depends on ϕ_0, ϕ_2 as well as ϕ_1 , due to the dependence of $\mathcal{A}_0, \mathcal{A}_2, \lambda, \mu, \nu, |\mathbf{c}|$ on those variables.

28.3 Rotation Invariance of Interpolants

As observed in §22.3, the quaternion formulation (28.1) of spatial Pythagorean hodographs is *rotation invariant*. Namely, if

$$\mathcal{U} = \cos \frac{1}{2}\theta + \sin \frac{1}{2}\theta \mathbf{n} \quad (28.11)$$

is the unit quaternion specifying a rotation by angle θ about a unit vector \mathbf{n} , the rotated hodograph can be written in the form

$$\tilde{\mathbf{r}}'(t) = \tilde{\mathcal{A}}(t) \mathbf{i} \tilde{\mathcal{A}}^*(t),$$

where we define $\tilde{\mathcal{A}}(t) = \mathcal{U}\mathcal{A}(t)$. When $\mathcal{A}(t)$ is the quadratic (28.2), for example, $\tilde{\mathcal{A}}(t)$ has the Bernstein coefficients $\tilde{\mathcal{A}}_r = \mathcal{U}\mathcal{A}_r$ for $r = 0, 1, 2$.

In this connection, a subtle issue arises concerning the role of the ϕ_0, ϕ_1, ϕ_2 parameters in the Hermite interpolation algorithm. Consider the pure vector quaternion \mathbf{c} — under the rotation defined by (28.11), it becomes the vector

$$\tilde{\mathbf{c}} = \mathcal{U} \mathbf{c} \mathcal{U}^*.$$

Now suppose the Hermite data $\mathbf{p}_i, \mathbf{d}_i$ and $\mathbf{p}_f, \mathbf{d}_f$ is rotated to

$$\tilde{\mathbf{p}}_i = \mathcal{U} \mathbf{p}_i \mathcal{U}^*, \quad \tilde{\mathbf{d}}_i = \mathcal{U} \mathbf{d}_i \mathcal{U}^* \quad \text{and} \quad \tilde{\mathbf{p}}_f = \mathcal{U} \mathbf{p}_f \mathcal{U}^*, \quad \tilde{\mathbf{d}}_f = \mathcal{U} \mathbf{d}_f \mathcal{U}^*.$$

One can easily verify that, if $\mathcal{A}_0, \mathcal{A}_1, \mathcal{A}_2$ are a solution to the Hermite system (28.5)–(28.6), then the quaternions

$$\tilde{\mathcal{A}}_0 = \mathcal{U}\mathcal{A}_0, \quad \tilde{\mathcal{A}}_1 = \mathcal{U}\mathcal{A}_1, \quad \tilde{\mathcal{A}}_2 = \mathcal{U}\mathcal{A}_2 \quad (28.12)$$

also solve the system (28.5)–(28.6), when we substitute $\tilde{\mathbf{p}}_i, \tilde{\mathbf{d}}_i$ and $\tilde{\mathbf{p}}_f, \tilde{\mathbf{d}}_f$ for $\mathbf{p}_i, \mathbf{d}_i$ and $\mathbf{p}_f, \mathbf{d}_f$. The interpolant defined by (28.12) is precisely the image of the original interpolant, under a rotation by angle θ about \mathbf{n} .

However, the quaternions (28.12) do *not* correspond to solving the Hermite interpolation problem for the rotated data, using the same values of ϕ_0, ϕ_1, ϕ_2 in the algorithm of §28.2 — *different* values $\tilde{\phi}_0, \tilde{\phi}_1, \tilde{\phi}_2$ must be used to obtain the solution (28.12). Consider, for example, the choice $\phi_0 = \phi_1 = \phi_2 = 0$ in (28.7), (28.8), (28.10). This yields pure vectors for *any* Hermite data, but the quaternions (28.12) are not, in general, pure vectors if $\theta \neq k\pi$ for integer k .

To find the correspondence between ϕ_0, ϕ_1, ϕ_2 and $\tilde{\phi}_0, \tilde{\phi}_1, \tilde{\phi}_2$ that ensures rotation invariance of the interpolation algorithm (i.e., that the interpolant to rotated Hermite data coincides precisely with the rotated copy of the original interpolant), we invoke the solution (28.4) to equation (28.3).

If $\mathbf{v} = \lambda \mathbf{i} + \mu \mathbf{j} + \nu \mathbf{k}$ is a unit vector in the direction of \mathbf{c} , we can express (28.4) in terms of the solutions (22.20) to equation (22.19) in the form

$$\mathcal{A}(\phi) = \sqrt{|\mathbf{c}|} \frac{\mathbf{i} + \mathbf{v}}{|\mathbf{i} + \mathbf{v}|} \mathcal{Q}(\phi). \quad (28.13)$$

Similarly, if the rotated vector $\tilde{\mathbf{c}} = \mathcal{U}\mathbf{c}\mathcal{U}^*$ has direction cosines $(\tilde{\lambda}, \tilde{\mu}, \tilde{\nu})$, the solutions to

$$\tilde{\mathcal{A}}\mathbf{i}\tilde{\mathcal{A}}^* = \tilde{\mathbf{c}}$$

can be expressed in terms of the unit vector $\tilde{\mathbf{v}} = \tilde{\lambda}\mathbf{i} + \tilde{\mu}\mathbf{j} + \tilde{\nu}\mathbf{k}$ as

$$\tilde{\mathcal{A}}(\tilde{\phi}) = \sqrt{|\tilde{\mathbf{c}}|} \frac{\mathbf{i} + \tilde{\mathbf{v}}}{|\mathbf{i} + \tilde{\mathbf{v}}|} \mathcal{Q}(\tilde{\phi}).$$

The correspondence between the free parameters ϕ and $\tilde{\phi}$ is then established by the requirement that $\tilde{\mathcal{A}}(\tilde{\phi}) = \mathcal{U}\mathcal{A}(\phi)$. Since $|\tilde{\mathbf{c}}| = |\mathbf{c}|$, this yields (after some manipulation) the condition

$$\mathcal{Q}(\tilde{\phi}) \mathcal{Q}^*(\phi) = \cos(\tilde{\phi} - \phi) + \sin(\tilde{\phi} - \phi) \mathbf{i} = \frac{(\mathbf{i} + \tilde{\mathbf{v}})^* \mathcal{U}(\mathbf{i} + \mathbf{v})}{|\mathbf{i} + \tilde{\mathbf{v}}| |\mathbf{i} + \mathbf{v}|}.$$

The quantity on the right is a unit quaternion with zero \mathbf{j} and \mathbf{k} components. By evaluating it, we can unambiguously determine the difference $\tilde{\phi} - \phi$ for a given rotation \mathcal{U} . Since all the equations arising in Hermite interpolation have the form (28.3), this approach can be applied to find each of $\tilde{\phi}_0, \tilde{\phi}_1, \tilde{\phi}_2$.

Because of the complicated nature of the relationships among ϕ_0, ϕ_1, ϕ_2 and $\tilde{\phi}_0, \tilde{\phi}_1, \tilde{\phi}_2$, the preferred means of rotating Hermite interpolants is clearly to first perform the interpolation for data in some “canonical” orientation, and then effect the rotation by pre-multiplying $\mathcal{A}_0, \mathcal{A}_1, \mathcal{A}_2$ with \mathcal{U} . This ensures rotation-invariance without consideration of the appropriate $\tilde{\phi}_0, \tilde{\phi}_1, \tilde{\phi}_2$ values that arises when the Hermite data is rotated *prior* to interpolation.

28.4 Residual Degrees of Freedom

As observed in §5.6, the parameters ϕ_0, ϕ_1, ϕ_2 may be restricted to the interval $[-\frac{1}{2}\pi, +\frac{1}{2}\pi]$ without loss of generality. However, these three variables do not identify independent degrees of freedom. This can be demonstrated as follows. The control points (22.7) depend only on products of the form

$$\mathcal{P}_{rs} = \mathcal{A}_r \mathbf{i} \mathcal{A}_s^* \quad \text{for } r, s \in \{0, 1, 2\}. \quad (28.14)$$

Since $\mathcal{A}_r = \mathcal{A}_r(0) (\cos \phi_r + \sin \phi_r \mathbf{i})$, where $\mathcal{A}_r(0)$ is the value of \mathcal{A}_r for $\phi_r = 0$, and likewise for \mathcal{A}_s , the quantities (28.14) can be written in the form

$$\begin{aligned} \mathcal{P}_{rs} &= [\mathcal{A}_r(0) (\cos \phi_r + \sin \phi_r \mathbf{i})] \mathbf{i} [\mathcal{A}_s(0) (\cos \phi_s + \sin \phi_s \mathbf{i})]^* \\ &= \mathcal{A}_r(0) [(\cos \phi_r + \sin \phi_r \mathbf{i}) \mathbf{i} (\cos \phi_s - \sin \phi_s \mathbf{i})] \mathcal{A}_s^*(0) \\ &= \mathcal{A}_r(0) [\sin(\phi_s - \phi_r) + \cos(\phi_s - \phi_r) \mathbf{i}] \mathcal{A}_s^*(0). \end{aligned}$$

Clearly, they depend only on the *differences* of the angles ϕ_0, ϕ_1, ϕ_2 . Thus we may, without loss of generality, take $\phi_1 = -\frac{1}{2}\pi$ and specialize (28.10) to

$$\mathcal{A}_1 = -\frac{3}{4}(\mathcal{A}_0 + \mathcal{A}_2) + \frac{\sqrt{\frac{1}{2}(1+\lambda)|\mathbf{c}|}}{4} \left(1 - \frac{\nu}{1+\lambda} \mathbf{j} + \frac{\mu}{1+\lambda} \mathbf{k} \right). \quad (28.15)$$

With this choice for ϕ_1 , substituting expressions (28.7), (28.8), (28.15) into (22.7) specifies a *two-parameter family* of spatial PH quintic interpolants to given first-order Hermite data $\mathbf{p}_i, \mathbf{d}_i$ and $\mathbf{p}_f, \mathbf{d}_f$. Although they all match the given data, the shape of these interpolants also depends on the free parameters ϕ_0, ϕ_2 — as we exercise these degrees of freedom, the first and last two control points $\mathbf{p}_0, \mathbf{p}_1$ and $\mathbf{p}_4, \mathbf{p}_5$ will remain fixed, while $\mathbf{p}_2, \mathbf{p}_3$ vary.

In principle, we might try to exploit these remaining degrees of freedom to satisfy two additional (scalar) interpolation conditions. For example, we could attempt to interpolate end-point curvatures — in three dimensions, however, this would be of questionable value if we cannot also specify the corresponding principal normals (osculating planes). We propose instead to select ϕ_0, ϕ_2 so as to ensure desirable overall shape properties of the curves.

28.5 Integral Measures of Shape

In Chaps. 25 and 26 we discussed a number of integral shape measures for planar PH curves — including the total arc length, absolute rotation index, and elastic bending energy. For a spatial PH curve with the parametric speed $\sigma(t) = |\mathbf{r}'(t)|$, the equivalent shape measures are defined by

$$S = \int_0^1 \sigma(t) dt, \quad R_{\text{abs}} = \frac{1}{2\pi} \int_0^1 \omega(t) \sigma(t) dt, \quad U = \int_0^1 \kappa^2(t) \sigma(t) dt$$

where the curvature κ , torsion τ , and total curvature ω of $\mathbf{r}(t)$ are specified (see §8.4) in terms of its derivatives

$$\mathbf{r}' = \mathcal{A} \mathbf{i} \mathcal{A}^*, \quad \mathbf{r}'' = \mathcal{A}' \mathbf{i} \mathcal{A}^* + \mathcal{A} \mathbf{i} \mathcal{A}'^*, \quad \mathbf{r}''' = \mathcal{A}'' \mathbf{i} \mathcal{A}^* + 2\mathcal{A}' \mathbf{i} \mathcal{A}'^* + \mathcal{A} \mathbf{i} \mathcal{A}''^*$$

by

$$\kappa = \frac{|\mathbf{r}' \times \mathbf{r}''|}{|\mathbf{r}'|^3}, \quad \tau = \frac{(\mathbf{r}' \times \mathbf{r}'') \cdot \mathbf{r}'''}{|\mathbf{r}' \times \mathbf{r}''|^2}, \quad \omega = \sqrt{\kappa^2 + \tau^2}. \quad (28.16)$$

We recall from §8.4 that the instantaneous rotation of the Frenet frame on a space curve is specified by the *Darboux vector* $\mathbf{d} = \tau \mathbf{t} + \kappa \mathbf{b}$, whose magnitude $\omega = |\mathbf{d}|$ defines the rate of rotation — i.e., the total curvature. In the initial study [158] of spatial PH quintic Hermite interpolants, the energy U was taken as the integral of ω^2 with respect to arc length $ds = \sigma dt$. However, the use of κ^2 as the integrand for U is better, since it defines the *least possible* energy of bending/twisting of an initially-straight elastic rod into a given spatial shape — a detailed explanation of this is given in §30.5 below.

The arc length S is easily determined in terms of the quaternion coefficients $\mathcal{A}_0, \mathcal{A}_1, \mathcal{A}_2$ — it is simply $\frac{1}{5}(\sigma_0 + \sigma_1 + \sigma_2 + \sigma_3 + \sigma_4)$, the Bernstein coefficients of the parametric speed being given by (22.8). Likewise, the integrand for the energy U is a rational function of t and thus it can, in principle, be evaluated by methods analogous to those developed in Chap. 26 for planar PH curves. The absolute rotation index R_{abs} , however, is more problematic. Although ω is by definition a non-negative function, so we need not worry about breaking up the interval $[0, 1]$ at inflections, in general this function is not rational and numerical quadrature must be used to approximate it.

As a representative example, we consider interpolation of the Hermite data $\mathbf{p}_i = (0, 0, 0)$, $\mathbf{d}_i = (1, 0, 1)$ and $\mathbf{p}_f = (1, 1, 1)$, $\mathbf{d}_f = (0, 1, 1)$. Tables 28.1 and 28.2 list the values of R_{abs} and U obtained (by numerical quadrature) for this data, at a representative sampling of ϕ_0, ϕ_2 values. The case $\phi_0 = \phi_2 = -\frac{1}{2}\pi$ identifies a clearly-defined minimum for both shape measures, but this is not

Table 28.1. The absolute rotation index R_{abs} for PH quintic Hermite interpolants to the data $\mathbf{p}_i = (0, 0, 0)$, $\mathbf{d}_i = (1, 0, 1)$ and $\mathbf{p}_f = (1, 1, 1)$, $\mathbf{d}_f = (0, 1, 1)$ corresponding to various choices for the two free parameters ϕ_0, ϕ_2 and the fixed value $\phi_1 = -\frac{1}{2}\pi$.

	$\phi_0 = -\frac{\pi}{2}$	$\phi_0 = -\frac{\pi}{4}$	$\phi_0 = 0$	$\phi_0 = +\frac{\pi}{4}$	$\phi_0 = +\frac{\pi}{2}$
$\phi_2 = -\frac{\pi}{2}$	0.389	0.499	0.860	1.232	1.250
$\phi_2 = -\frac{\pi}{4}$	0.468	0.689	0.976	1.347	1.565
$\phi_2 = 0$	0.645	0.908	1.168	1.467	1.784
$\phi_2 = +\frac{\pi}{4}$	0.872	1.102	1.328	1.574	1.858
$\phi_2 = +\frac{\pi}{2}$	1.221	1.284	1.431	1.596	1.845

Table 28.2. Values of the energy U , corresponding to the R_{abs} values in Table 28.1.

	$\phi_0 = -\frac{\pi}{2}$	$\phi_0 = -\frac{\pi}{4}$	$\phi_0 = 0$	$\phi_0 = +\frac{\pi}{4}$	$\phi_0 = +\frac{\pi}{2}$
$\phi_2 = -\frac{\pi}{2}$	1.31	1.56	2.75	21.11	2965.95
$\phi_2 = -\frac{\pi}{4}$	1.45	2.04	3.37	32.09	7916.70
$\phi_2 = 0$	3.07	5.85	8.40	43.11	4725.39
$\phi_2 = +\frac{\pi}{4}$	24.26	79.83	116.44	111.92	3444.50
$\phi_2 = +\frac{\pi}{2}$	3718.88	1662.05	968.25	1287.51	3740.58

always the case. Because of the “implicit” — and highly non-linear — nature of the dependence of these integrals on ϕ_0 and ϕ_2 , an analytic minimization with respect to these parameters is not practically feasible.

The development of an efficient formal procedure to identify the “optimal” ϕ_0 , ϕ_2 choices (that does not depend upon numerical integration of the shape measures for many cases) remains an open problem. Clearly, this is a much more difficult problem than in the planar context. In §28.7 we impose a *helicity* condition on the PH quintic interpolants, and this reduces the solution space to a finite number of cases (typically four), rather than a two-fold infinity.

Figure 28.1 shows two spatial PH quintic interpolants, with their Bézier control polygons, corresponding to different sets of data. For both cases, the values $\phi_0 = \phi_2 = -\frac{1}{2}\pi$ were used. This yields curves of pleasing shape, although they do not correspond to global minima of R_{abs} or U . In [158] it was suggested, on the basis of empirical evidence, that these choices can be used as a default for curves of “reasonable” shape. From the discussion of §5.6, one can verify that they correspond to mappings of the basis vector \mathbf{i} onto the end derivatives \mathbf{d}_i and \mathbf{d}_f through scalings by $|\mathbf{d}_i|$ and $|\mathbf{d}_f|$ and rotations along *great circle arcs*. However, this suggestion needs a firmer theoretical basis.

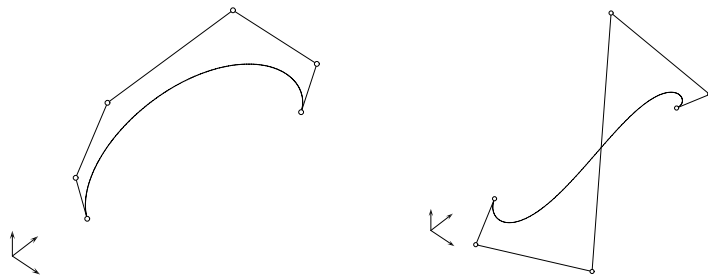


Fig. 28.1. Examples of spatial PH quintics that interpolate end points $\mathbf{p}_i = (0, 0, 0)$, $\mathbf{p}_f = (1, 1, 1)$ and end derivatives $\mathbf{d}_i = (-0.8, 0.3, 1.2)$, $\mathbf{d}_f = (0.5, -1.3, -1.0)$ and $\mathbf{d}_i = (0.4, -1.5, -1.2)$, $\mathbf{d}_f = (-1.2, -0.6, -1.2)$ on the left and the right, respectively. Both curves employ the choices $\phi_0 = \phi_1 = \phi_2 = -\frac{1}{2}\pi$.

The two-parameter family of spatial PH quintic interpolants to given first-order Hermite data has a remarkable structure¹ with respect to the total curve arc lengths, which can be regarded as a generalization of the pairing property of planar PH quintic Hermite interpolants (see Corollary 25.1).

Lemma 28.1 *The total arc length S of the PH quintic Hermite interpolants depends only on the difference $\phi_2 - \phi_0$ of the two angular degrees of freedom.*

Proof: By the arguments of §28.4, the vector \mathbf{c} defined by the right-hand side of equation (28.9) depends only on $\phi_2 - \phi_0$, rather than ϕ_0 and ϕ_2 individually. In solving this equation for \mathcal{A}_1 , we may always choose a solution of the form (28.15) without loss of generality — i.e., we assume $\phi_1 = -\frac{1}{2}\pi$ for the angular variable associated with the quaternion \mathcal{A}_1 . Now substituting from (22.8) into $S = \frac{1}{5}(\sigma_0 + \sigma_1 + \sigma_2 + \sigma_3 + \sigma_4)$ and making appropriate re-arrangements, the total arc length can be written as

$$\begin{aligned} S = & \frac{1}{120} [(3\mathcal{A}_0 + 4\mathcal{A}_1 + 3\mathcal{A}_0)(3\mathcal{A}_0 + 4\mathcal{A}_1 + 3\mathcal{A}_0)^* \\ & + 15(\mathcal{A}_0\mathcal{A}_0^* + \mathcal{A}_2\mathcal{A}_2^*) - 5(\mathcal{A}_0\mathcal{A}_2^* + \mathcal{A}_2\mathcal{A}_0^*)]. \end{aligned}$$

Since the right-hand side of (28.9) depends only on $\phi_2 - \phi_0$, and we always assume $\phi_1 = -\frac{1}{2}\pi$, the quaternion $3\mathcal{A}_0 + 4\mathcal{A}_1 + 3\mathcal{A}_2$ and its conjugate clearly depend only on $\phi_2 - \phi_0$. Also, we can replace the term $\mathcal{A}_0\mathcal{A}_0^* + \mathcal{A}_2\mathcal{A}_2^*$ by the constant $|\mathbf{d}_i| + |\mathbf{d}_f|$. Finally, using arguments analogous to those of §28.4, one can easily verify that $\mathcal{A}_0\mathcal{A}_2^* + \mathcal{A}_2\mathcal{A}_0^*$ depends only on $\phi_2 - \phi_0$. Thus, S depends on the difference $\phi_2 - \phi_0$, but not on ϕ_0 and ϕ_2 separately. ■

If we write $\phi_m = \frac{1}{2}(\phi_0 + \phi_2)$ and $\Delta\phi = \phi_2 - \phi_0$, so that $\phi_0 = \phi_m - \frac{1}{2}\Delta\phi$ and $\phi_2 = \phi_m + \frac{1}{2}\Delta\phi$, we can consider $\Delta\phi$ as specifying the arc length of the PH quintic Hermite interpolant (within a limited range), while changing ϕ_m with $\Delta\phi$ fixed yields curves of varying shape at fixed arc length (see Fig. 28.2) — a feature that can be quite useful in practical applications.

Table 28.3 gives the arc lengths S corresponding to the R_{abs} and U values listed in Tables 28.1 and 28.2 — the fact that S depends only on the difference $\phi_2 - \phi_0$ (see Lemma 28.1) is clearly apparent. A more detailed sampling shows that the arc lengths of the PH quintic Hermite interpolants lie in a relatively narrow range, $1.778 \leq S \leq 1.827$ — note that for the specified end points $\mathbf{p}_i = (0, 0, 0)$ and $\mathbf{p}_f = (1, 1, 1)$ we must have $S \geq \sqrt{3} \approx 1.732$.

Recent developments concerning the identification of “optimal” values for the free parameters ϕ_m , $\Delta\phi$ are reported in [160]. Three different criteria for selecting these free parameters are proposed, sharing the property that they produce a *cubic* PH interpolant whenever the Hermite data are compatible

¹ This was first observed by Alessandra Sestini, and was subsequently re-discovered in the context of the geometric product formulation [358] for spatial PH curves, which employs Clifford algebra methods to characterize them in terms of scaled reflection (rather than rotation) operations.

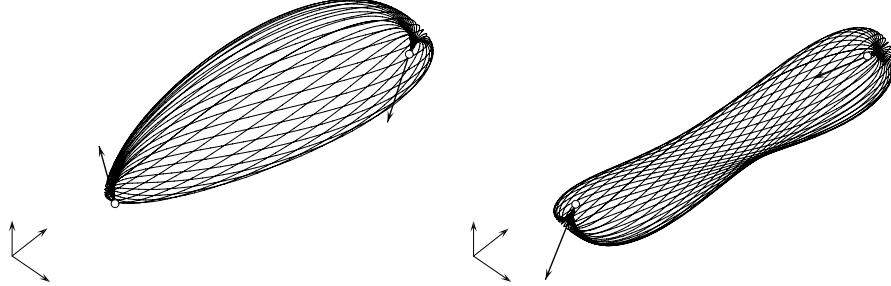


Fig. 28.2. Sampling of one-parameter families of spatial PH quintic interpolants, of identical arc length, to the Hermite data specified in Fig. 28.1 — these families are defined by keeping $\Delta\phi = \phi_2 - \phi_0$ constant, and varying only $\phi_m = \frac{1}{2}(\phi_0 + \phi_2)$.

with its existence. Numerical experiments indicate that all three criteria are capable of identifying spatial PH quintic interpolants with values of the energy U close to the absolute minimum, at relatively modest computational cost. For more complete details on these methods, see [160].

Table 28.3. Arc lengths S corresponding to R_{abs} and U values in Tables 28.1, 28.2.

	$\phi_0 = -\frac{\pi}{2}$	$\phi_0 = -\frac{\pi}{4}$	$\phi_0 = 0$	$\phi_0 = +\frac{\pi}{4}$	$\phi_0 = +\frac{\pi}{2}$
$\phi_2 = -\frac{\pi}{2}$	1.813	1.796	1.782	1.779	1.791
$\phi_2 = -\frac{\pi}{4}$	1.825	1.813	1.796	1.782	1.779
$\phi_2 = 0$	1.825	1.825	1.813	1.796	1.782
$\phi_2 = +\frac{\pi}{4}$	1.811	1.825	1.825	1.813	1.796
$\phi_2 = +\frac{\pi}{2}$	1.791	1.811	1.825	1.825	1.813

28.6 Clifford Algebra Formulation

An alternative approach to Hermite interpolation by spatial PH quintics was proposed in [358], based upon the reflection form of Pythagorean hodographs (§22.4) expressed by the *geometric product* of Clifford algebra (see Chap. 6) rather than quaternions. If $\mathbf{a}(t)$ is a vector polynomial and \mathbf{n} is a unit vector, the geometric product

$$\mathbf{r}'(t) = \mathbf{a}(t) \mathbf{n} \mathbf{a}(t) \quad (28.17)$$

specifies a spatial Pythagorean hodograph with components $x'(t)$, $y'(t)$, $z'(t)$ satisfying (21.1) with $\sigma(t) = |\mathbf{a}(t)|^2$. Taking $\mathbf{n} = \mathbf{i}$, for example, the hodograph

components can be expressed in terms of the components $a_x(t)$, $a_y(t)$, $a_z(t)$ of $\mathbf{a}(t)$ in the form (21.14) with $h(t) = 1$ as

$$x'(t) = a_x^2(t) - a_y^2(t) - a_z^2(t), \quad y'(t) = 2a_x(t)a_y(t), \quad z'(t) = 2a_x(t)a_z(t).$$

The geometrical meaning of (28.17) is that, for each t , the hodograph vector $\mathbf{r}'(t)$ is generated from the unit vector \mathbf{n} by reflecting it in $\mathbf{a}(t)$ and scaling it by $|\mathbf{a}(t)|^2$ — see §6.4. It was shown in [358] that the PH quintics obtained by integrating the hodograph form (28.17) are capable of interpolating general first-order Hermite data, provided the unit vector \mathbf{n} is not specified *a priori* — it should be regarded as a free parameter, a feasible instance of which is to be determined by the interpolation algorithm.

The free parameters ϕ_0 , ϕ_2 that arise in solving the Hermite interpolation problem using the quaternion form (28.1) are equivalent to the two degrees of freedoms associated with the unit vector \mathbf{n} in the reflection form (28.17). Varying the unit vector \mathbf{n} as a means of exploring the two-parameter family of PH quintic Hermite interpolants is perhaps a geometrically more-intuitive approach than varying ϕ_0 and ϕ_2 . For example, the fact that the arc lengths of the interpolants depend on only one parameter (Lemma 28.1) is more easily apparent [358] using the reflection form. Complete details on the construction of Hermite interpolants using the form (28.17) can be found in [358].

28.7 Helical PH Quintic Interpolants

As noted in Chap. 23, all helical polynomial curves (characterized by fixed curvature/torsion ratios) are PH curves. In Hermite interpolation, imposing a helicity condition offers a convenient means of fixing the two free parameters. We discuss here the spatial Hermite interpolation problem using monotone-helical PH quintics and general helical PH quintics. The former case is simpler than the latter, but does not admit solutions for arbitrary Hermite data.

Monotone Helical PH Quintics

Consider first Hermite interpolation by the monotone-helical PH quintics (see §23.3). The complex form (23.9) — used to elucidate the occurrence of factors common to x' , y' , z' when $\gcd(u, v, p, q) = \text{constant}$ — is rather inconvenient in this context. Knowing the circumstances that give $\gcd(x', y', z') \neq \text{constant}$, we will now derive an equivalent quaternion form.

Since the imaginary unit i and quaternion basis element \mathbf{i} are algebraically equivalent, we may use $\mathbf{i}\mathbf{j} = -\mathbf{j}\mathbf{i} = \mathbf{k}$ to write $\mathcal{A} = u + v\mathbf{i} + p\mathbf{j} + q\mathbf{k}$ and its conjugate in the form

$$\mathcal{A} = (u + v\mathbf{i}) + \mathbf{j}(p - q\mathbf{i}), \quad \mathcal{A}^* = (u - v\mathbf{i}) - (p + q\mathbf{i})\mathbf{j}. \quad (28.18)$$

Now suppose

$$\gcd(u + v \mathbf{i}, p - q \mathbf{i}) = f + g \mathbf{i} \quad \text{and} \quad \gcd(u - v \mathbf{i}, p + q \mathbf{i}) = f - g \mathbf{i}$$

are non-constant polynomials, so we can write

$$\begin{aligned} u + v \mathbf{i} &= (a + b \mathbf{i})(f + g \mathbf{i}), & p - q \mathbf{i} &= (c - d \mathbf{i})(f + g \mathbf{i}), \\ u - v \mathbf{i} &= (f - g \mathbf{i})(a - b \mathbf{i}), & p + q \mathbf{i} &= (f - g \mathbf{i})(c + d \mathbf{i}), \end{aligned}$$

for suitable polynomials $a \pm b \mathbf{i}$ and $c \pm d \mathbf{i}$ (note that, since they involve only the basis element \mathbf{i} , we are free to choose the ordering of the above products). Substituting these expressions into (28.18), we obtain

$$\mathcal{A} = [(a + b \mathbf{i}) + \mathbf{j}(c - d \mathbf{i})](f + g \mathbf{i}), \quad \mathcal{A}^* = (f - g \mathbf{i})[(a - b \mathbf{i}) - (c + d \mathbf{i})\mathbf{j}]$$

and forming the Pythagorean hodograph $\mathbf{r}' = \mathcal{A} \mathbf{i} \mathcal{A}^*$ yields

$$\mathbf{r}' = (a + b \mathbf{i} + c \mathbf{j} + d \mathbf{k})(f + g \mathbf{i})\mathbf{i}(f - g \mathbf{i})(a - b \mathbf{i} - c \mathbf{j} - d \mathbf{k}).$$

Since $(f + g \mathbf{i})\mathbf{i}(f - g \mathbf{i}) = (f^2 + g^2)\mathbf{i}$, this hodograph simplifies to

$$\mathbf{r}' = (f^2 + g^2)\mathcal{B}\mathbf{i}\mathcal{B}^*, \quad (28.19)$$

where the “reduced” quaternion polynomial

$$\mathcal{B} = a + b \mathbf{i} + c \mathbf{j} + d \mathbf{k}.$$

and its conjugate are defined by

$$\mathcal{B} = \frac{\mathcal{A}}{\gcd(u + v \mathbf{i}, p - q \mathbf{i})}, \quad \mathcal{B}^* = \frac{\mathcal{A}^*}{\gcd(u - v \mathbf{i}, p + q \mathbf{i})}.$$

The above divisions amount to extracting common factors from the terms in parentheses in (28.18) — on the right for \mathcal{A} , and on the left for \mathcal{A}^* .

In the case of a monotone-helical PH quintic, the polynomials f and g in (28.19) are linear, and so is the quaternion polynomial \mathcal{B} . Thus, the hodograph of a monotone-helical PH quintic is just the product of a non-negative scalar quadratic polynomial with the hodograph of a PH cubic. Monotone helicity is an intrinsic property of the latter — the non-negative quadratic polynomial simply serves to modulate the *magnitude* of the hodograph vector.

To perform Hermite interpolation with monotone-helical PH quintics, we consider a PH quintic with hodograph given by

$$\mathbf{r}'(\xi) = [b_0(1 - \xi)^2 + b_1 2(1 - \xi)\xi + b_2 \xi^2] \mathcal{B}(\xi) \mathbf{i} \mathcal{B}^*(\xi), \quad (28.20)$$

where

$$\mathcal{B}(\xi) = \mathcal{B}_0(1 - \xi) + \mathcal{B}_1 \xi$$

is a linear quaternion polynomial. Integrating (28.20) yields the control points

$$\begin{aligned}\mathbf{p}_1 &= \mathbf{p}_0 + \frac{1}{5} b_0 \mathcal{B}_0 \mathbf{i} \mathcal{B}_0^*, \\ \mathbf{p}_2 &= \mathbf{p}_1 + \frac{1}{20} [2b_1 \mathcal{B}_0 \mathbf{i} \mathcal{B}_0^* + b_0 (\mathcal{B}_0 \mathbf{i} \mathcal{B}_1^* + \mathcal{B}_1 \mathbf{i} \mathcal{B}_0^*)], \\ \mathbf{p}_3 &= \mathbf{p}_2 + \frac{1}{30} [b_2 \mathcal{B}_0 \mathbf{i} \mathcal{B}_0^* + 2b_1 (\mathcal{B}_0 \mathbf{i} \mathcal{B}_1^* + \mathcal{B}_1 \mathbf{i} \mathcal{B}_0^*) + b_0 \mathcal{B}_1 \mathbf{i} \mathcal{B}_1^*], \\ \mathbf{p}_4 &= \mathbf{p}_3 + \frac{1}{20} [b_2 (\mathcal{B}_0 \mathbf{i} \mathcal{B}_1^* + \mathcal{B}_1 \mathbf{i} \mathcal{B}_0^*) + 2b_1 \mathcal{B}_1 \mathbf{i} \mathcal{B}_1^*], \\ \mathbf{p}_5 &= \mathbf{p}_4 + \frac{1}{5} b_2 \mathcal{B}_1 \mathbf{i} \mathcal{B}_1^*. \end{aligned} \quad (28.21)$$

We wish to interpolate the first-order Hermite data

$$\mathbf{r}(0) = \mathbf{p}_i, \quad \mathbf{r}'(0) = \mathbf{d}_i \quad \text{and} \quad \mathbf{r}(1) = \mathbf{p}_f, \quad \mathbf{r}'(1) = \mathbf{d}_f \quad (28.22)$$

using such a curve. Interpolation of the end derivatives yields the equations

$$b_0 \mathcal{B}_0 \mathbf{i} \mathcal{B}_0^* = \mathbf{d}_i \quad \text{and} \quad b_2 \mathcal{B}_1 \mathbf{i} \mathcal{B}_1^* = \mathbf{d}_f \quad (28.23)$$

while the condition $\int_0^1 \mathbf{r}'(\xi) d\xi = \Delta \mathbf{p} = \mathbf{p}_f - \mathbf{p}_i$ gives

$$\begin{aligned}&(12b_0 + 6b_1 + 2b_2) \mathcal{B}_0 \mathbf{i} \mathcal{B}_0^* \\ &+ (3b_0 + 4b_1 + 3b_2) (\mathcal{B}_0 \mathbf{i} \mathcal{B}_1^* + \mathcal{B}_1 \mathbf{i} \mathcal{B}_0^*) \\ &+ (2b_0 + 6b_1 + 12b_2) \mathcal{B}_1 \mathbf{i} \mathcal{B}_1^* = 60\Delta \mathbf{p}. \end{aligned} \quad (28.24)$$

In (28.20) we may assume, without loss of generality, that the scalar quadratic is monic, so that $b_2 - 2b_1 + b_0 = 1$. Thus, eliminating b_1 and invoking (28.23), equation (28.24) may be re-written as

$$\begin{aligned}b_0 b_2 (5b_0 + 5b_2 - 2)(\mathcal{B}_0 \mathbf{i} \mathcal{B}_1^* + \mathcal{B}_1 \mathbf{i} \mathcal{B}_0^*) \\ = 60b_0 b_2 \Delta \mathbf{p} - b_2 (15b_0 + 5b_2 - 3)\mathbf{d}_i - b_0 (5b_0 + 15b_2 - 3)\mathbf{d}_f. \end{aligned} \quad (28.25)$$

With $\mathbf{d}_i = |\mathbf{d}_i|(\lambda_i, \mu_i, \nu_i)$ and $\mathbf{d}_f = |\mathbf{d}_f|(\lambda_f, \mu_f, \nu_f)$ in (28.23), these equations — which are of the form (28.3) — have the general solutions

$$\begin{aligned}\mathcal{B}_0 &= \sqrt{\frac{(1 + \lambda_i)|\mathbf{d}_i|}{2b_0}} \left(-\sin \phi_0 + \cos \phi_0 \mathbf{i} \right. \\ &\quad \left. + \frac{\mu_i \cos \phi_0 + \nu_i \sin \phi_0}{1 + \lambda_i} \mathbf{j} + \frac{\nu_i \cos \phi_0 - \mu_i \sin \phi_0}{1 + \lambda_i} \mathbf{k} \right), \end{aligned} \quad (28.26)$$

$$\begin{aligned}\mathcal{B}_1 &= \sqrt{\frac{(1 + \lambda_f)|\mathbf{d}_f|}{2b_2}} \left(-\sin \phi_1 + \cos \phi_1 \mathbf{i} \right. \\ &\quad \left. + \frac{\mu_f \cos \phi_1 + \nu_f \sin \phi_1}{1 + \lambda_f} \mathbf{j} + \frac{\nu_f \cos \phi_1 - \mu_f \sin \phi_1}{1 + \lambda_f} \mathbf{k} \right). \end{aligned} \quad (28.27)$$

Thus, with $\phi = \phi_1 - \phi_0$, we may write

$$\mathcal{B}_0 \mathbf{i} \mathcal{B}_1^* + \mathcal{B}_1 \mathbf{i} \mathcal{B}_0^* = \sqrt{\frac{|\mathbf{d}_i| |\mathbf{d}_f|}{b_0 b_2}} (c_x \mathbf{i} + c_y \mathbf{j} + c_z \mathbf{k}),$$

where

$$\begin{aligned} c_x &= \frac{[(1 + \lambda_i)(1 + \lambda_f) - (\mu_i \mu_f + \nu_i \nu_f)] \cos \phi - (\mu_i \nu_f - \mu_f \nu_i) \sin \phi}{\sqrt{(1 + \lambda_i)(1 + \lambda_f)}}, \\ c_y &= \frac{[(1 + \lambda_f)\mu_i + (1 + \lambda_i)\mu_f] \cos \phi + [(1 + \lambda_i)\nu_f - (1 + \lambda_f)\nu_i] \sin \phi}{\sqrt{(1 + \lambda_i)(1 + \lambda_f)}}, \\ c_z &= \frac{[(1 + \lambda_f)\nu_i + (1 + \lambda_i)\nu_f] \cos \phi + [(1 + \lambda_f)\mu_i - (1 + \lambda_i)\mu_f] \sin \phi}{\sqrt{(1 + \lambda_i)(1 + \lambda_f)}}. \end{aligned} \quad (28.28)$$

Substituting the above expressions into (28.25), we obtain

$$\begin{aligned} &\sqrt{b_0 b_2} (5b_0 + 5b_2 - 2) \sqrt{|\mathbf{d}_i| |\mathbf{d}_f|} (c_x \mathbf{i} + c_y \mathbf{j} + c_z \mathbf{k}) \\ &= 60b_0 b_2 \Delta \mathbf{p} - b_2 (15b_0 + 5b_2 - 3) \mathbf{d}_i - b_0 (5b_0 + 15b_2 - 3) \mathbf{d}_f. \end{aligned} \quad (28.29)$$

This vector condition is equivalent to three scalar equations in b_0 , b_2 , ϕ . Once these equations have been solved, we can obtain \mathcal{B}_0 and \mathcal{B}_1 by choosing ϕ_0 freely and setting $\phi_1 = \phi + \phi_0$ in (28.26) and (28.27). The control points of the monotone-helical PH quintic Hermite interpolant are then given by (28.21).

Now for the quadratic in (28.20) to be non-negative, the solution of (28.29) must yield positive values for b_0 , b_2 and also a negative discriminant. This is equivalent, under the assumption that it is monic, to the constraint

$$b_2^2 + b_0^2 - 2b_0 b_2 - 2b_0 - 2b_2 + 1 < 0. \quad (28.30)$$

This constraint excludes a small region of the positive quadrant in the (b_0, b_2) plane from consideration, bounded by a parabolic arc from $(1, 0)$ to $(0, 1)$ with vertex at $(\frac{1}{4}, \frac{1}{4})$. The following example shows that equation (28.29), subject to the constraint (28.30), does not always admit a solution.

Example 28.1 Consider the Hermite data

$$\Delta \mathbf{p} = \mathbf{p}_f - \mathbf{p}_i = (L, 0, 0), \quad \mathbf{d}_i = \frac{(0, 1, -1)}{\sqrt{2}}, \quad \mathbf{d}_f = \frac{(0, 1, 1)}{\sqrt{2}}.$$

From the z component of (28.29), we deduce that either $b_2 = b_0$ or $b_2 = \frac{3}{5} - b_0$. If $b_2 = b_0$, the x component of (28.29) gives

$$\cos \phi - \sin \phi = \frac{b_0}{5b_0 - 1} 30L.$$

This implies that, for large positive values of L , the quantity $b_0 = b_2$ can be made arbitrarily close to 0, which violates the constraint (28.30). Similarly, if $b_2 = \frac{3}{5} - b_0$, then (b_0, b_2) must approach $(\frac{3}{5}, 0)$ or $(0, \frac{3}{5})$ in order to satisfy the x component of (28.29) for large positive L — again, this violates (28.30).

Thus, the monotone-helical PH quintics do not appear to be sufficiently flexible to interpolate *arbitrary* Hermite data. We now turn our attention to the general helical PH quintics. In this case, interpolants to arbitrary data may be constructed with little more effort than the solution of a quartic equation.

General Helical PH Quintics

Interpolating the data (28.22) corresponds to solving the system of equations defined by (28.5) and (28.9) for the quaternions $\mathcal{A}_0, \mathcal{A}_1, \mathcal{A}_2$. For brevity, we set $\Delta\mathbf{p} = \mathbf{p}_f - \mathbf{p}_i$ in (28.9). On solving these equations, the control points of the interpolant are given by (22.7), where $\mathbf{p}_0 = \mathbf{p}_i$ (and $\mathbf{p}_5 = \mathbf{p}_f$ by construction).

With $\mathbf{d}_i = |\mathbf{d}_i|(\lambda_i, \mu_i, \nu_i)$ and $\mathbf{d}_f = |\mathbf{d}_f|(\lambda_f, \mu_f, \nu_f)$, the solutions of (28.5) are given by (28.7) and (28.8), where ϕ_0 and ϕ_2 are free angular variables. To obtain a helical PH quintic, we substitute (23.14) into (28.9), giving

$$\begin{aligned} & [1 + 3(c_0 + c_2) + 4c_0c_2] (\mathcal{A}_0 \mathbf{i} \mathcal{A}_2^* + \mathcal{A}_2 \mathbf{i} \mathcal{A}_0^*) \\ &= 30\Delta\mathbf{p} - (6 + 6c_0 + 4c_0^2)\mathbf{d}_i - (6 + 6c_2 + 4c_2^2)\mathbf{d}_f. \end{aligned} \quad (28.31)$$

Now from (28.7) and (28.8) we may write

$$\mathcal{A}_0 \mathbf{i} \mathcal{A}_2^* + \mathcal{A}_2 \mathbf{i} \mathcal{A}_0^* = \sqrt{|\mathbf{d}_i| |\mathbf{d}_f|} (c_x \mathbf{i} + c_y \mathbf{j} + c_z \mathbf{k}) \quad (28.32)$$

where, with $\phi = \phi_2 - \phi_0$, the vector (c_x, c_y, c_z) is again given by (28.28).

The vector condition (28.31) yields three scalar equations in c_0, c_2, ϕ . Once this system is solved, we can choose ϕ_0 or ϕ_2 arbitrarily, and fix the other from the difference $\phi = \phi_2 - \phi_0$. On substituting these values into (28.7)–(28.8), we can obtain \mathcal{A}_1 from (23.14) using the computed c_0, c_2 values.

To solve (28.31), we set $k_0 = c_0 + \frac{3}{4}$ and $k_2 = c_2 + \frac{3}{4}$, allowing us to express this equation in the simpler form

$$\mathbf{d}_i 16k_0^2 + \mathbf{d}_f 16k_2^2 + (\mathbf{u} \cos \phi + \mathbf{v} \sin \phi)(16k_0k_2 - 5) = \mathbf{h} \quad (28.33)$$

where $\mathbf{h} = 120\Delta\mathbf{p} - 15(\mathbf{d}_i + \mathbf{d}_f)$, and $\mathcal{A}_0 \mathbf{i} \mathcal{A}_2^* + \mathcal{A}_2 \mathbf{i} \mathcal{A}_0^* = \mathbf{u} \cos \phi + \mathbf{v} \sin \phi$, the vectors \mathbf{u} and \mathbf{v} being defined by (28.28) and (28.32).

Regarding the coordinate components of (28.33) as a system of three linear equations in $16k_0^2, 16k_2^2, 16k_0k_2 - 5$, Cramer's rule gives the solutions

$$16k_0^2 = \frac{(\mathbf{h}, \mathbf{d}_f, \mathbf{u} \cos \phi + \mathbf{v} \sin \phi)}{(\mathbf{d}_i, \mathbf{d}_f, \mathbf{u} \cos \phi + \mathbf{v} \sin \phi)}, \quad (28.34)$$

$$16k_2^2 = \frac{(\mathbf{d}_i, \mathbf{h}, \mathbf{u} \cos \phi + \mathbf{v} \sin \phi)}{(\mathbf{d}_i, \mathbf{d}_f, \mathbf{u} \cos \phi + \mathbf{v} \sin \phi)}, \quad (28.35)$$

$$16k_0 k_2 - 5 = \frac{(\mathbf{d}_i, \mathbf{d}_f, \mathbf{h})}{(\mathbf{d}_i, \mathbf{d}_f, \mathbf{u} \cos \phi + \mathbf{v} \sin \phi)}, \quad (28.36)$$

where $(\mathbf{a}, \mathbf{b}, \mathbf{c})$ denotes the scalar triple product $(\mathbf{a} \times \mathbf{b}) \cdot \mathbf{c}$. These solutions must satisfy the compatibility condition

$$(16k_0^2)(16k_2^2) = [(16k_0 k_2 - 5) + 5]^2.$$

By substituting into this condition and writing $\cos \phi = (1 - t^2)/(1 + t^2)$ and $\sin \phi = 2t/(1 + t^2)$, where $t = \tan \frac{1}{2}\phi$, we obtain a quartic equation

$$d_4 t^4 + d_3 t^3 + d_2 t^2 + d_1 t + d_0 = 0 \quad (28.37)$$

in t , with coefficients given by

$$\begin{aligned} d_4 &= (\mathbf{h}, \mathbf{d}_f, \mathbf{u})(\mathbf{d}_i, \mathbf{h}, \mathbf{u}) - (\mathbf{d}_i, \mathbf{d}_f, \mathbf{h} - 5\mathbf{u})^2, \\ d_3 &= -2(\mathbf{h}, \mathbf{d}_f, \mathbf{u})(\mathbf{d}_i, \mathbf{h}, \mathbf{v}) - 2(\mathbf{d}_i, \mathbf{h}, \mathbf{u})(\mathbf{h}, \mathbf{d}_f, \mathbf{v}) \\ &\quad - 20(\mathbf{d}_i, \mathbf{d}_f, \mathbf{v})(\mathbf{d}_i, \mathbf{d}_f, \mathbf{h} - 5\mathbf{u}), \\ d_2 &= -2(\mathbf{h}, \mathbf{d}_f, \mathbf{u})(\mathbf{d}_i, \mathbf{h}, \mathbf{u}) + 4(\mathbf{h}, \mathbf{d}_f, \mathbf{v})(\mathbf{d}_i, \mathbf{h}, \mathbf{v}) \\ &\quad - 100(\mathbf{d}_i, \mathbf{d}_f, \mathbf{v})^2 - 2(\mathbf{d}_i, \mathbf{d}_f, \mathbf{h} - 5\mathbf{u})(\mathbf{d}_i, \mathbf{d}_f, \mathbf{h} + 5\mathbf{u}), \\ d_1 &= 2(\mathbf{h}, \mathbf{d}_f, \mathbf{v})(\mathbf{d}_i, \mathbf{h}, \mathbf{u}) + 2(\mathbf{d}_i, \mathbf{h}, \mathbf{v})(\mathbf{h}, \mathbf{d}_f, \mathbf{u}) \\ &\quad - 20(\mathbf{d}_i, \mathbf{d}_f, \mathbf{v})(\mathbf{d}_i, \mathbf{d}_f, \mathbf{h} + 5\mathbf{u}), \\ d_0 &= (\mathbf{h}, \mathbf{d}_f, \mathbf{u})(\mathbf{d}_i, \mathbf{h}, \mathbf{u}) - (\mathbf{d}_i, \mathbf{d}_f, \mathbf{h} + 5\mathbf{u})^2. \end{aligned}$$

This quartic equation admits a closed-form solution by Ferrari's method (§3.3) — it may have either four, two, or zero real roots. For each real root t , we can evaluate the expressions on the right-hand sides of (28.34)–(28.36) by setting $\cos \phi = (1 - t^2)/(1 + t^2)$ and $\sin \phi = 2t/(1 + t^2)$. The expressions for $16k_0^2$ and $16k_2^2$ must both yield non-negative quantities for a valid solution. If they are both positive, they each yield two values of equal magnitude and opposite sign. However, not all four combinations of signs are permissible — compatibility with (28.36) allows pairs of like sign *or* unlike sign, but not both. Thus, each real root of (28.37) yields at most two feasible pairs of (k_0, k_2) values — and there is apparently an even number (between 0 and 8) of distinct helical PH quintic interpolants for given first-order Hermite data.

To construct the helical PH quintic that corresponds to a valid solution t , k_0 , k_2 , we take $\phi_0 = 0$ and $\phi_2 = 2 \tan^{-1} t$ in (28.7)–(28.8), and use $c_0 = k_0 - \frac{3}{4}$ and $c_2 = k_2 - \frac{3}{4}$ in (23.14) — the control points are then given by expressions (22.7). Because of the highly non-linear nature of the problem, it is difficult to derive *a priori* arguments concerning the number of distinct interpolants for a given set of Hermite data. However, we have observed empirically through numerous test cases that the quartic (28.37) generically has four real roots — of which two yield positive values for $16k_0^2$ and $16k_2^2$, and the other two yield

negative values. There are thus, in general, *four* distinct helical PH quintic interpolants to first-order spatial Hermite data, in agreement with the case of planar PH quintics — which are (trivially) helical. Furthermore, since the two helical PH quintics corresponding to a specific root t of (28.37) share the same angle ϕ , the quaternions (28.7) and (28.8) are identical for these two PH quintics: they differ only in A_1 . Hence, by Proposition 23.2, these two PH quintics share the same helical axis \mathbf{a} and angle ψ .

To choose among the helical PH quintic Hermite interpolants, we use the shape measures discussed in §28.5. This is much easier in the present context, since there are only four solutions rather than a two-parameter family.

Example 28.2 For the Hermite data $\mathbf{p}_i = (0, 0, 0)$, $\mathbf{d}_i = (1, 0, 1)$ and $\mathbf{p}_f = (1, 1, 1)$, $\mathbf{d}_f = (0, 1, 1)$ the quartic (28.37) has the four approximate roots

$$t_1 = -0.059419, \quad t_2 = -1.761857, \quad t_3 = 19.411014, \quad t_4 = 0.661850.$$

The roots t_1 and t_3 are rejected, since they do not yield non-negative values for k_0^2 and k_2^2 . Root t_2 yields the pair of feasible solutions

$$(k_0, k_2, \phi) = (\mp 1.705395, \pm 1.705395, -2.109108)$$

for which the helical axis and angle are given by

$$\mathbf{a} = (-0.309913, -0.309913, -0.898837), \quad \cos \psi = -0.854715.$$

The curvature/torsion ratio has magnitude $|\kappa/\tau| = 0.607333$ for both curves (κ/τ changes sign, since the curves have an inflection: see Fig. 28.3, upper). Similarly, root t_4 yields the pair of feasible solutions

$$(k_0, k_2, \phi) = (\mp 1.850380, \mp 1.850380, 1.169321)$$

for which the helical axis and angle are given by

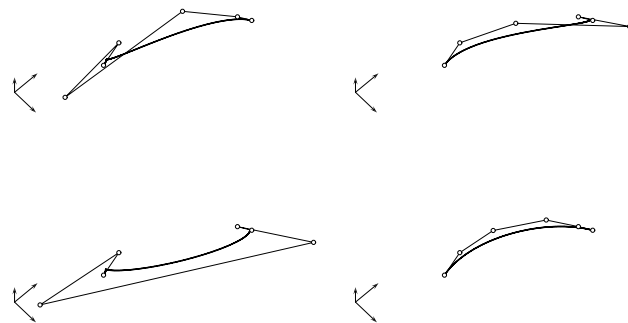


Fig. 28.3. The four distinct helical PH quintic Hermite interpolants for the data $\mathbf{p}_i = (0, 0, 0)$, $\mathbf{p}_f = (1, 1, 1)$ and $\mathbf{d}_i = (1, 0, 1)$, $\mathbf{d}_f = (0, 1, 1)$ of Example 28.2. Upper: the two curves defined by the root t_2 . Lower: the two curves defined by the root t_4 .

$$\mathbf{a} = (-0.354664, -0.354664, 0.865117), \quad \cos \psi = 0.862515.$$

These curves have no inflections (see Fig. 28.3, lower): the curvature/torsion ratio is $\kappa/\tau = -0.586692$ in the first case, and $\kappa/\tau = 0.586692$ in the second.

The four helical PH quintics have energy values $U = 322.3, 322.3, 89.60$, and 1.277 . As in the planar case (see Chap. 25), it is essential that the least-energy curve be chosen as the “good” solution, since the other three solutions may exhibit rather contorted shapes — see Fig. 28.3.

Figure 28.4 compares the “good” helical PH quintic interpolants with the solutions from §28.2 using the *ad hoc* choice $\phi_0 = \phi_2 = -\frac{1}{2}\pi$ in the general Hermite interpolation algorithm. Both examples have end points $\mathbf{p}_i = (0, 0, 0)$ and $\mathbf{p}_f = (1, 1, 1)$. The first example is for end derivatives $\mathbf{d}_i = (-0.8, 0.3, 1.2)$ and $\mathbf{d}_f = (0.5, -1.3, -1.0)$. In this case, the ad hoc solution is serendipitously quite good, and has an energy $U = 8.89$ only slightly greater than that of the helical interpolant, namely $U = 8.69$. The second example has end derivatives $\mathbf{d}_i = (0.4, -1.5, -1.2)$ and $\mathbf{d}_f = (-1.2, -0.6, -1.2)$. For this case, there is a more pronounced discrepancy between the helical and ad hoc solutions: the former has energy $U = 16.72$, the latter $U = 50.51$ — the “S” shape of this curve is clearly an extravagance not warranted by the Hermite data.

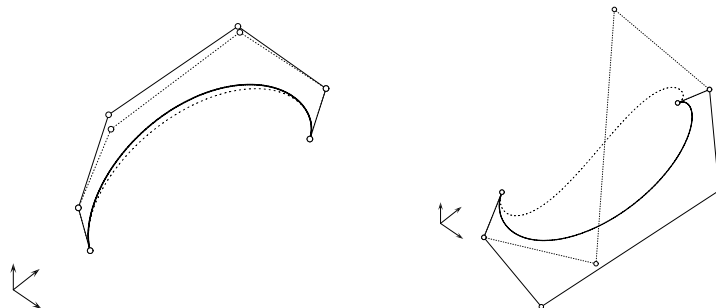


Fig. 28.4. PH quintics interpolating the end points $\mathbf{p}_i = (0, 0, 0)$ and $\mathbf{p}_f = (1, 1, 1)$. Left: end derivatives $\mathbf{d}_i = (-0.8, 0.3, 1.2)$ and $\mathbf{d}_f = (0.5, -1.3, -1.0)$. Right: end derivatives $\mathbf{d}_i = (0.4, -1.5, -1.2)$ and $\mathbf{d}_f = (-1.2, -0.6, -1.2)$. The solid curves and control polygons are the “good” helical PH quintics, while the dashed curves and control polygons correspond to the choice $\phi_0 = \phi_2 = -\frac{1}{2}\pi$ in the algorithm of §28.2.

The existence of general helical PH quintic interpolants for arbitrary first-order Hermite data, which remained an open question in the initial study [164], has recently been definitively answered in [160]. It was shown therein that four distinct general helical PH quintics always exist, which can be grouped into pairs of identical arc length. Moreover, it is shown that these general helical interpolants (but not the monotone helical interpolants) identify the minimum and maximum arc length among the two-parameter family of interpolants —

we recall from Lemma 28.1 that the arc length depends only on the difference $\Delta\phi = \phi_2 - \phi_0$. For complete details of these results, see [160].

28.8 Higher-order Hermite Interpolants

The problem of interpolating C^2 Hermite data (end points and derivatives of first and second order) using spatial PH curves of degree 9 was considered by Šir and Jüttler [416]. They show that the solutions to this problem comprise a four-parameter family of spatial PH curves, that agree with the four distinct solutions [168, 414] of the planar C^2 Hermite interpolation problem for certain special choices of the parameters. To identify a “best” Hermite interpolant in the four-parameter family of solutions, they analyze the convergence behavior of the interpolants to an analytic curve from which the data is sampled — it is shown that a unique choice of the parameters yields an $O(h^6)$ convergence rate (h being the sampling interval), while all other choices yield just an $O(h)$ rate. It is not clear that a selection criterion based on such asymptotic analysis will also hold for interpolants of *finite* extent, as required in most applications — see the example presented in [160].

28.9 Spatial C^2 PH Quintic Splines

A natural generalization of the Hermite interpolation problem discussed in this chapter is the construction of spatial C^2 PH quintic splines interpolating a sequence of points $\mathbf{q}_0, \dots, \mathbf{q}_N \in \mathbb{R}^3$ with given end conditions. For a variety of reasons, this is a much more challenging problem than the planar PH spline problem treated in Chap. 27. We confine our discussion here to a derivation of the general form for the system of quaternion equations that define spatial PH splines, and the nature of the difficulties that arise in its solution.

The hodograph of the spatial PH quintic segment $\mathbf{r}_k(t)$, between points \mathbf{q}_{k-1} and \mathbf{q}_k , is defined in terms of a quaternion polynomial $\mathcal{A}_k(t)$ in the form

$$\mathbf{r}'_k(t) = \mathcal{A}_k(t) \mathbf{i} \mathcal{A}_k^*(t). \quad (28.38)$$

To guarantee C^2 continuity of consecutive spatial PH quintic segments at each of the interior nodes $\mathbf{q}_1, \dots, \mathbf{q}_{N-1}$ we introduce $N+2$ quaternion coefficients $\mathcal{Z}_0, \dots, \mathcal{Z}_{N+1}$ and also two sets of $N+1$ real angular variables $\alpha_0, \dots, \alpha_N$ and β_0, \dots, β_N . In terms of these quantities, and the solutions (22.20) to equation (22.19), we write the quadratic polynomial $\mathcal{A}_k(t)$ in Bernstein form as

$$\begin{aligned} \mathcal{A}_k(t) = & \frac{1}{4} [\mathcal{Z}_{k-1} \mathcal{Q}(\alpha_{k-1}) + \mathcal{Z}_k] [1 + \mathcal{Q}(\beta_{k-1})] (1-t)^2 \\ & + \mathcal{Z}_k 2(1-t)t \\ & + \frac{1}{4} [\mathcal{Z}_k + \mathcal{Z}_{k+1} \mathcal{Q}(-\alpha_k)] [1 + \mathcal{Q}(\beta_k)] t^2. \end{aligned} \quad (28.39)$$

Note that the quaternions $\mathcal{Q}(\pm\theta)$ commute with \mathbf{i} , and in particular

$$\mathcal{Q}(+\theta) \mathbf{i} \mathcal{Q}(-\theta) = \mathcal{Q}(-\theta) \mathbf{i} \mathcal{Q}(+\theta) = \mathbf{i} \quad \text{for all } \theta.$$

The form (28.39) specified for $\mathcal{A}_k(t)$ ensures automatic satisfaction of the C^1 and C^2 continuity conditions at the juncture $\mathbf{r}_k(1) = \mathbf{r}_{k+1}(0) = \mathbf{q}_k$ of the consecutive spline segments k and $k+1$. Specifically, from (28.38) we have

$$\begin{aligned} \mathbf{r}'_k(1) &= \mathbf{r}'_{k+1}(0) = \\ &\frac{1}{8}(1 + \cos \beta_{k+1})[\mathcal{Z}_k + \mathcal{Z}_{k+1}\mathcal{Q}(-\alpha_k)]\mathbf{i}[\mathcal{Z}_k + \mathcal{Z}_{k+1}\mathcal{Q}(-\alpha_k)]^*, \end{aligned}$$

and differentiating (28.38) to obtain $\mathbf{r}''_k(t) = \mathcal{A}'_k(t)\mathbf{i}\mathcal{A}_k^*(t) + \mathcal{A}_k(t)\mathbf{i}\mathcal{A}'_k^*(t)$, a somewhat laborious calculation gives

$$\begin{aligned} \mathbf{r}''_k(1) &= \mathbf{r}''_{k+1}(0) = \\ &\frac{1}{2}(1 + \cos \beta_{k+1})[\mathcal{Z}_k + \mathcal{Z}_{k+1}\mathcal{Q}(-\alpha_k)]\mathbf{i}[\mathcal{Z}_k + \mathcal{Z}_{k+1}\mathcal{Q}(-\alpha_k)]^* \\ &- \frac{1}{2}\mathcal{Z}_k\mathbf{i}[(\mathcal{Z}_k + \mathcal{Z}_{k+1}\mathcal{Q}(-\alpha_k))(1 + \mathcal{Q}(\beta_k))]^* \\ &- \frac{1}{2}[(\mathcal{Z}_k + \mathcal{Z}_{k+1}\mathcal{Q}(-\alpha_k))(1 + \mathcal{Q}(\beta_k))]\mathbf{i}\mathcal{Z}_k^*. \end{aligned}$$

The angular variables α_k, β_k associated with each spline node \mathbf{q}_k arise from the non-uniqueness of the quaternion solutions (28.13) to equations of the form (28.3), when we match the first and second derivatives of the spatial PH quintic segments meeting at that node. The C^1 and C^2 continuity conditions are satisfied for arbitrary α_k, β_k values. As with single Hermite interpolants, their choice can significantly influence the shape of the spline segments. The case with $\alpha_k = \beta_k = 0$ for all k was discussed in the preliminary study² [173] — in this case, expression (28.39) reduces to

$$\mathcal{A}_k(t) = \frac{1}{2}(\mathcal{Z}_{k-1} + \mathcal{Z}_k)(1-t)^2 + \mathcal{Z}_k 2(1-t)t + \frac{1}{2}(\mathcal{Z}_k + \mathcal{Z}_{k+1})t^2,$$

which corresponds to just replacing the complex numbers \mathbf{z}_k in the form (27.1) used for planar C^2 PH quintic splines by the quaternions \mathcal{Z}_k .

For brevity, we write $\mathcal{U}_k = \frac{1}{4}[\mathcal{Z}_{k-1}\mathcal{Q}(\alpha_{k-1}) + \mathcal{Z}_k][1 + \mathcal{Q}(\beta_{k-1})]$ and $\mathcal{V}_k = \frac{1}{4}[\mathcal{Z}_k + \mathcal{Z}_{k+1}\mathcal{Q}(-\alpha_k)][1 + \mathcal{Q}(\beta_k)]$ in (28.39). Integration of the hodograph (28.38) then gives the end-point interpolation condition

$$\begin{aligned} \int_0^1 \mathcal{A}_k(t)\mathbf{i}\mathcal{A}_k^*(t)dt &= \frac{1}{5}\mathcal{U}_k\mathbf{i}\mathcal{U}_k^* + \frac{1}{10}(\mathcal{U}_k\mathbf{i}\mathcal{Z}_k^* + \mathcal{Z}_k\mathbf{i}\mathcal{U}_k^*) \\ &+ \frac{1}{30}(\mathcal{U}_k\mathbf{i}\mathcal{V}_k^* + 4\mathcal{Z}_k\mathbf{i}\mathcal{Z}_k^* + \mathcal{V}_k\mathbf{i}\mathcal{U}_k^*) \\ &+ \frac{1}{10}(\mathcal{Z}_k\mathbf{i}\mathcal{V}_k^* + \mathcal{V}_k\mathbf{i}\mathcal{Z}_k^*) + \frac{1}{5}\mathcal{V}_k\mathbf{i}\mathcal{V}_k^* = \Delta\mathbf{q}_k. \end{aligned}$$

where we set $\Delta\mathbf{q}_k = \mathbf{q}_k - \mathbf{q}_{k-1}$. These equations, corresponding to each span $k = 1, \dots, N$ of the spatial C^2 PH quintic spline curve, constitute a quadratic

² This study also presents the generalization to non-uniform knots.

“tridiagonal” system for the quaternion unknowns $\mathcal{Z}_0, \dots, \mathcal{Z}_{N+1}$ in which the angular variables $\alpha_0, \dots, \alpha_N$ and β_0, \dots, β_N appear as free parameters.

In Chap. 27 we found that the system of equations for planar C^2 PH quintic splines has approximately (depending on the specified end conditions) 2^N distinct solutions. For spatial C^2 PH quintic splines, the equations contain approximately $2N$ *free parameters*, and there will be a multiplicity of solutions for each numerical instance of these free parameters. Because of the non-linear nature of the equations, it is in general impossible to determine the solutions analytically in terms of the free parameters: a strategy for fixing them *a priori* must be found. A rigorous solution to the problem of fixing the ϕ_0, ϕ_2 variables in single-segment Hermite interpolation will likely shed light on this problem.

Even when appropriate values for $\alpha_0, \dots, \alpha_N$ and β_0, \dots, β_N are prescribed *a priori*, the task of solving the system of quaternion equations is more subtle than the complex equations for the planar case. The solution procedure must take account of the non-commutative nature of quaternion multiplication. For example, the Newton–Raphson method of §27.3 cannot be directly used, since it involves derivatives with respect to the unknowns, and the formulation of derivatives with respect to quaternion variables is a non-trivial matter.³ A “Newton–like” scheme was proposed in [173] to circumvent this difficulty.

Clearly, the problem of constructing spatial C^2 PH quintic splines offers scope for much further investigation into the basic nature of the solution space, and the formulation of efficient procedures for identifying “good” solutions.

³ In general, the limiting value of a quaternion expression is *not* independent of the direction from which a specific point of quaternion space is approached [114].

Real-time CNC Interpolators

When the cutting speed and feed are invariable during a cut, they must be chosen as a function of the most unfavorable conditions which can be met. If they are constantly adjusted to the real conditions and to the intended goal, there will be a resulting improvement in the output. This method is designated by the term “adaptive control.”

Pierre Bézier, *Numerical Control: Mathematics and Applications* [38]

29.1 Digital Motion Control

Multi-axis computer numerical control (CNC) machines use digital closed-loop feedback controllers to drive the individual machine axes so as to execute a given path at a specified (constant or variable) speed or *feedrate*. The digital *sampling frequency* of such controllers is typically $f = 1024$ Hz. Within each sampling interval $\Delta t = 1/f \approx 0.001$ second, the controller must compare the commanded machine position, computed from the specified path and feedrate, with the actual machine position, measured by encoders on the machine axes, in order to appropriately accelerate or decelerate the axis drive motors. Such “closed-loop” control is essential for accurate path traversals at the specified speeds under varying machine loads, external disturbances, etc.

Our interest here is in a particular component of the control algorithm, the *real-time interpolator*. The task of this function is to compute, from the given path geometry and speed variation, a stream of *reference points* with which the measured machine positions may be compared. This must be performed in *real time*, at the sampling frequency f (i.e., each reference-point computation should consume only a fraction of the sampling interval Δt). The interpolator algorithm must be *accurate*, to ensure faithful realization of the desired path and feedrate variation; it must be *efficient*, to permit real-time execution; and it should be *versatile* in terms of accommodating a variety of path geometries

and speed variations. Although a seemingly simple and modest component of the overall control algorithm, in practice the real-time interpolator may often be the limiting factor in the actual CNC machine performance.

CNC machines have traditionally relied on crude and data-intensive path descriptions — piecewise-linear/circular “G code” approximations [2] — due to the difficulty of formulating real-time interpolators that can accurately and efficiently compute reference points on free-form curves, traversed at varying feedrates. Any desired approximation accuracy can, in principle, be achieved by resorting to sufficiently small G code segments, but the discrete nature of such path descriptions compromises the ability of the interpolator to sustain smooth feedrate performance, especially at high speeds [445].

Several authors [93, 94, 253, 306, 409, 411, 475, 477] have recently proposed CNC interpolators for the standard (Bézier/B-spline) curves of CAD systems. However, the impossibility of *exact* arc length computation for such curves (see §16.1) makes these interpolators inherently approximate — even for constant feedrates — and frequently no attempt is made to estimate the approximation error, which may be significant for curves with strong curvature variations or uneven parameterization. By contrast, PH curves admit analytic reduction of the *interpolation integral*, yielding real-time interpolators that are essentially exact and remarkably versatile in terms of the repertoire of feedrate variations (with time, arc length, or curvature) they can accommodate.

Accurate feedrate performance becomes especially important in *high-speed machining* [285, 421, 441] where one requires extreme rates of feed acceleration and deceleration, and maintenance of very high feedrates. Moreover, failure of the interpolator to properly maintain the commanded feedrates may induce tool “chatter” or breakage through an inappropriate relationship between the spindle rotation speed and the path traversal rate. Reliable interpolators for time-dependent feedrates [445] are invaluable in this context.

Given a parametric curve¹ $\mathbf{r}(\xi)$, the variables that concern us in the context of real-time interpolator algorithms (with suitable *physical dimensions*) are:

- t = time (sec.),
- s = curve arc length (mm),
- ξ = curve parameter (dimensionless),
- $\sigma = ds/d\xi$ = “parametric speed” (mm),
- $V = ds/dt$ = feedrate along curve (mm sec.⁻¹),
- κ = curvature (mm⁻¹).

For a given sampling interval Δt , the function of the real-time interpolator is to compute a sequence reference points on the curve (identified by parameter values $\xi_0, \xi_1, \dots, \xi_N$) that correspond to a discrete sampling (at the instants $0, \Delta t, \dots, N\Delta t$) of a smooth traversal of the curve at the prescribed feedrate. The feedrate might be specified in number of different ways, such as

¹ Henceforth we use ξ as the curve parameter, since we reserve t for time.

- (a) a constant feedrate: V_0 ,
- (b) a function of the elapsed time: $V(t)$,
- (c) a function of the curve arc length: $V(s)$,
- (d) a function of the curve parameter: $V(\xi)$,
- (e) a function of the local curvature: $V(\kappa)$.

Case (a) is the simplest — it amounts to computing a sequence of points along the curve, spaced uniformly by the arc-length increment $\Delta s_0 = V_0 \Delta t$. Some authors have employed case (d) as a means of specifying variable feedrate along a curve [93, 94, 253, 475] — but this is a rather “artificial” approach, since the curve parameter ξ is unrelated to its *intrinsic geometry* (a re-parameterization of the curve yields a different physical realization of the feedrate variation).

Cases (c) and (e) are more “natural” ways to prescribe a variable feedrate, based on the curve geometry. For general polynomial or rational curves they are computationally more difficult, but the special algebraic structure of PH curves allows an analytic reduction of the interpolation integral (for cases of practical interest) in their implementation. Case (b) is useful in specifying the acceleration/deceleration phases of a motion that begins and ends at rest.

For each of the above modes (a)–(e) of feedrate specification, finding the desired sequence of parameter values $\xi_0, \xi_1, \dots, \xi_N$ amounts to integrating the differential equation

$$\frac{d\xi}{dt} = \frac{V}{\sigma} \quad (29.1)$$

from $t = 0$ (corresponding to $\xi_0 = 0$) to $t = \Delta t, 2\Delta t, \dots, N\Delta t$, where N is the smallest integer such that $\xi_N > 1$. When V is known — directly, or indirectly through s or κ — as a function of ξ , this may be cast in integral form as

$$\int_0^{\xi_k} \frac{\sigma}{V} d\xi = k\Delta t, \quad k = 1, 2, \dots, N, \quad (29.2)$$

where the unknown reference-point parameter values $\xi_0, \xi_1, \dots, \xi_N$ appear as *upper limits of integration*. For the formulation of real-time interpolators, the advantage of PH curves over general Bézier/B-spline curves derives from the feasibility of a *closed-form reduction* of the “interpolation integral” in (29.2), for a variety of useful feedrate functions V of the form (a)–(e) above.

29.2 Taylor Series Interpolators

Real-time interpolators for general Bézier/B-spline curves $\mathbf{r}(\xi)$ typically rely on Taylor series expansions to approximate the parameter values of successive reference points [93, 94, 253, 411, 475]. The reference-point parameter values correspond to a discrete sampling $\xi_k = \xi(k\Delta t)$ of the function $\xi(t)$ describing the variation of the curve parameter ξ with time t , according to the prescribed feedrate. We may expand $\xi(t)$ in a Taylor series about $t_k = k\Delta t$ to obtain

$$\xi_{k+1} = \xi_k + \dot{\xi}(t_k)\Delta t + \frac{\ddot{\xi}(t_k)}{2!}(\Delta t)^2 + \frac{\ddot{\dot{\xi}}(t_k)}{3!}(\Delta t)^3 + \dots, \quad (29.3)$$

where dots denote time derivatives. Now although $\xi(t)$ is not known explicitly, we can express its derivatives in terms of other (known) derivatives by noting that, from the definitions of the parametric speed σ and feedrate V , derivatives with respect to time t and the curve parameter ξ are related by

$$\frac{d}{dt} = \frac{ds}{dt} \frac{d\xi}{ds} \frac{d}{d\xi} = \frac{V}{\sigma} \frac{d}{d\xi}. \quad (29.4)$$

Applying this operator successively to $\xi(t)$, we obtain the recursive formulae

$$\dot{\xi} = \frac{V}{\sigma}, \quad \ddot{\xi} = \frac{\sigma V' - \sigma' V}{\sigma^2} \dot{\xi}, \quad \ddot{\dot{\xi}} = \frac{\sigma V' - 3\sigma' V}{\sigma^2} \ddot{\xi} + \frac{\sigma V'' - \sigma'' V}{\sigma^2} \dot{\xi}^2 \quad (29.5)$$

etc., where primes indicate derivatives with respect to ξ . The parametric speed σ and its derivatives, required in (29.5), can be expressed recursively as follows

$$\sigma = |\mathbf{r}'|, \quad \sigma' = \frac{\mathbf{r}' \cdot \mathbf{r}''}{\sigma}, \quad \sigma'' = \frac{\mathbf{r}' \cdot \mathbf{r}''' + |\mathbf{r}''|^2 - \sigma'^2}{\sigma}, \quad (29.6)$$

etc. If the feedrate V is given as a function of a physically significant variable, such as arc length, curvature, or time, derivatives with respect to that variable must be transformed into derivatives with respect to ξ for use in (29.5).

In practice, the custom has typically been to retain only the linear term in (29.3), with no attempt to estimate the truncation error, which may become significant whenever the curvature is high and/or the parametric speed is low. Improving the accuracy of this scheme by incorporating higher-order terms may incur significant computational cost, since the coefficients of the quadratic and subsequent terms become increasingly complicated in the case of variable feedrates. Yang and Kong [475] first proposed a variable-feedrate interpolator, based on a Taylor series truncated after the quadratic term. However, as noted in [191], their expansion contains an erroneous quadratic term (valid only for a *constant* feedrate, although a dependence on the curve parameter is explicitly indicated). This error was subsequently repeated by Yeh and Hsu [477].

A systematic derivation of the correct Taylor coefficients, up to third order in (29.3), was presented in [193] for the cases of constant feedrate and feedrates dependent on time, arc length, or curvature. For a constant feedrate, we simply set $V' = V'' = 0$ in (29.5). For a time-dependent feedrate, the recursive forms

$$\dot{\xi} = \frac{V}{\sigma}, \quad \ddot{\xi} = \frac{\dot{V}}{\sigma} - \frac{\sigma' V}{\sigma^2} \dot{\xi}, \quad \ddot{\dot{\xi}} = \frac{\ddot{V}}{\sigma} - \frac{3\sigma' V}{\sigma^2} \ddot{\xi} - \frac{\sigma'' V}{\sigma^2} \dot{\xi}^2.$$

are most convenient for implementation. The case of a feedrate dependent on arc length or curvature is more involved — details may be found in [193].

Taylor series interpolators inevitably incur *truncation errors*, through the omission of higher-order terms in the series (29.3). Since each reference-point

parameter value ξ_k is computed from a preceding value ξ_{k-1} that is itself only approximate, a significant *cumulative error* may arise in terms of the actual location along the curve at time $k\Delta t$ relative to the exact position according to the prescribed feedrate variation — see [193]. The PH curve interpolators, on the other hand, circumvent this error accumulation by relying on an analytic reduction of the integral form (29.2) of the interpolation equation.

29.3 PH Curve Interpolators

As noted in §29.1, CNC machine tool paths were traditionally approximated by linear/circular segments, due to the efficiency and exactitude of real-time interpolators for these “simple” curve types. General conic segments can also be accommodated in an essentially exact manner, by using the highly efficient arithmetic–geometric mean recursion to evaluate the elliptic integrals defining their arc lengths: see [171]. PH curves allow us to extend the scope of efficient and essentially exact real-time interpolators to accommodate “free-form” loci. A proposal for integrating PH curve tool paths with the established G code specifications for piecewise-linear/circular paths may be found in [170].

The special advantage of PH curves in the context of real-time interpolator algorithms is that, in most cases of practical interest, they admit a *closed-form reduction* of the integral in (29.2). This yields an equation specifying the value ξ_k as the unique real root of a monotone (usually polynomial) function, which can be computed to machine precision by a few Newton–Raphson iterations. This approach is much more accurate and efficient, and also more versatile, than reliance on a truncated series expansion such as (29.3).

For a (planar or spatial) PH curve, the parametric speed and arc length

$$\sigma(\xi) = |\mathbf{r}'(\xi)| \quad \text{and} \quad s(\xi) = \int_0^\xi \sigma(u) \, du,$$

are known explicitly as *polynomial* functions of ξ . This fact allows immediate reduction of (29.2) in the case $V = \text{constant}$. For a time-dependent feedrate, a different integration of (29.1) is appropriate, giving

$$s(\xi_k) = \int_0^{k\Delta t} V \, dt,$$

where we assume that the function $V(t)$ admits a straightforward integration. For any PH curve, we can transform feedrates V specified in terms of the arc length s or the curvature κ into functions of ξ by taking their composition with the arc-length polynomial $s(\xi)$ or curvature rational function $\kappa(\xi)$. We denote the resulting functions by

$$V_s(\xi) = V(s(\xi)) \quad \text{and} \quad V_\kappa(\xi) = V(\kappa(\xi)). \quad (29.7)$$

Note that, if $V(s)$ is a polynomial, then $V_s(\xi)$ is also a polynomial. However, $V_\kappa(\xi)$ is, in general, a rational function even when $V(\kappa)$ is just a polynomial. We address each of these cases in greater detail below.

For brevity, the interpolator algorithms described below are formulated mainly in the context of planar PH curves. In the case of a constant feedrate, or a feedrate dependent on elapsed time or arc length, the extension to spatial PH curves is straightforward. In other cases, they must be reworked to allow for inherent differences in the intrinsic geometry of planar and spatial paths. We do not address the computational efficiency of the algorithms here, since they are sufficiently simple to admit real-time execution on very modest processors. A basic analysis of the computational cost per reference point is given in [191].

29.3.1 Constant Feedrate

The simplest case is that of a constant feedrate, V_0 . Equation (29.2) then has an elementary reduction — namely, the values ξ_0, \dots, ξ_N are such that

$$s(\xi_k) = k \Delta s_0 \quad (29.8)$$

where $\Delta s_0 = V_0 \Delta t$. Now since the arc length polynomial $s(\xi)$ is the indefinite integral of a positive function, it is monotone-increasing, and equation (29.8) thus has a *unique* (simple) real root ξ_k . It may be efficiently computed by the Newton-Raphson iterations

$$\xi_k^{(r)} = \xi_k^{(r-1)} - \frac{s(\xi_k^{(r-1)}) - k \Delta s_0}{\sigma(\xi_k^{(r-1)})}, \quad r = 1, 2, \dots \quad (29.9)$$

from the starting approximation $\xi_k^{(0)} = \xi_{k-1} + \Delta s_0 / \sigma(\xi_{k-1})$, where ξ_{k-1} is the converged value from the preceding step (and $\xi_0 = 0$). Sufficient conditions for convergence of Newton's method from any point within a root isolating interval usually require, in addition to a non-vanishing first derivative, that the second derivative should not change sign in that interval [234]. Although

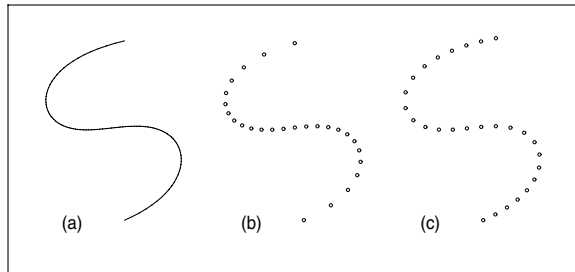


Fig. 29.1. A PH quintic (a), with points corresponding to: (b) a uniform parameter increment $\Delta\xi$, and (c) a uniform arc-length increment Δs (i.e., a constant feedrate).

the latter condition is not formally verified for equation (29.8), convergence problems have never been encountered in practice, owing to the availability of excellent starting approximations. In fact, two or three iterations are typically sufficient to ensure convergence to machine precision.

Figure 29.1 shows sequences of points on a PH quintic that correspond to uniform increments in the parameter ξ and arc length s . In the former case, the uneven distribution of points reflects the variation of the parametric speed σ along the curve. In the latter case, we use (29.9) with $V_0 = 4$ and $\Delta t = 0.02$ — the values ξ_1, \dots, ξ_N converge to machine precision in just three iterations.

29.3.2 Curvature-dependent Feedrate

Unlike general Bézier/B-spline curves, the curvature $\kappa(\xi)$ of a PH curve $\mathbf{r}(\xi)$ is a *rational* function of the curve parameter, and for any feedrate variation V specified by a rational expression in κ , the integrand in (29.2) is a rational function of ξ and therefore admits closed-form integration by a partial fraction decomposition if we can factor its denominator. We focus here on curvature-dependent feedrates for planar PH curves specified by hodographs of the form $\mathbf{r}'(\xi) = (u^2(\xi) - v^2(\xi), 2u(\xi)v(\xi))$ where $\gcd(u(\xi), v(\xi)) = \text{constant}$, for which the curvature is $\kappa(\xi) = 2(u(\xi)v'(\xi) - u'(\xi)v(\xi))/(u^2(\xi) + v^2(\xi))$.

Preliminary results on curvature-dependent feedrates for planar PH curves were reported in [191], which considered feedrates of the form

$$V(\kappa) = \frac{\kappa_*}{|\kappa|} V_* \quad \text{and} \quad V(\kappa) = \frac{\kappa_*}{|\kappa| + \kappa_*} V_{\max}, \quad (29.10)$$

where κ_* and V_* are specified “reference values” for the curvature and feedrate, while V_{\max} is an asymptotic bound on V . The absolute value of the curvature is used in the first expression, since the feedrate must be non-negative — this necessitates splitting the curve at its inflections, identified by odd-multiplicity roots of $u(\xi)v'(\xi) - u'(\xi)v(\xi)$. In terms of the composition (29.7) of $\kappa(\xi)$ with $V(\kappa)$, we can write the interpolation integral in the form

$$\int_{\xi_{k-1}}^{\xi_k} \frac{\sigma(\xi)}{V_\kappa(\xi)} d\xi = \frac{2}{\kappa_* V_*} \int_{\xi_{k-1}}^{\xi_k} \frac{u(\xi)v'(\xi) - u'(\xi)v(\xi)}{u^2(\xi) + v^2(\xi)} d\xi = \Delta t.$$

Although the first form in (29.10) is infinite at inflections, the integrand above remains regular at such points, and the substitution $\phi(\xi) = v(\xi)/u(\xi)$ allows a closed-form reduction yielding the polynomial equation

$$[c u(\xi_{k-1}) + v(\xi_{k-1})] u(\xi_k) - [u(\xi_{k-1}) - c v(\xi_{k-1})] v(\xi_k) = 0$$

for ξ_k , where we set $c = \tan(\frac{1}{2}\kappa_* V_* \Delta t)$ and ξ_{k-1} is known from the preceding step. Unlike equations (29.8), (29.14) and (29.16)–(29.18) for cases where V was given in terms s , the above polynomial in ξ_k for the case where V is given in terms of κ is not necessarily monotone. However, for a degree- n curve it is

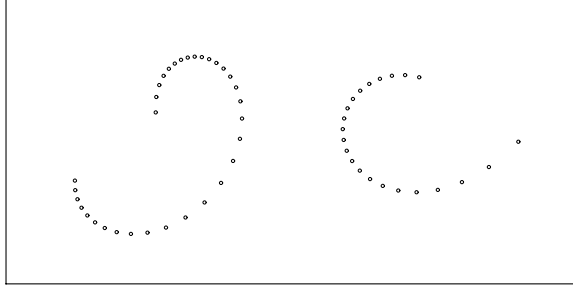


Fig. 29.2. Reference points on PH quintics determined by the first form in (29.10).

of degree $\frac{1}{2}(n - 1)$, rather than n as in these other cases. Figure 29.2 shows reference points on PH quintics determined by the first form in (29.10).

The second form in (29.10) is a modification of the first, that exhibits an asymptotic extremum feedrate value V_{\max} in regions of low curvature. In this case, evaluation of the interpolation integral yields the equation

$$2 \tan^{-1} \phi(\xi_k) + \kappa_* s(\xi_k) = 2 \tan^{-1} \phi(\xi_{k-1}) + \kappa_* s(\xi_{k-1}) + \kappa_* V_{\max} \Delta t$$

for ξ_k , where $\phi(\xi) = v(\xi)/u(\xi)$ (we assume a segment of positive curvature). Unlike the preceding cases, this cannot be reduced to a *polynomial* equation in ξ_k , although it can still be solved iteratively (at somewhat higher cost than in the other cases because of its more complicated form, and the appearance of transcendental functions in the unknown value ξ_k).

29.3.3 Offset Curve Interpolator

If a planar PH curve $\mathbf{r}(\xi)$ with the hodograph $\mathbf{r}'(\xi) = (u^2(\xi) - v^2(\xi), 2u(\xi)v(\xi))$ is the profile we wish to machine — with a cylindrical tool of radius d , say — the tool center must follow the *offset curve*

$$\mathbf{r}_d(\xi) = \mathbf{r}(\xi) + d \mathbf{n}(\xi)$$

at distance d from $\mathbf{r}(\xi)$, rather than $\mathbf{r}(\xi)$ itself. Note that the unit normal

$$\mathbf{n}(\xi) = \frac{(2u(\xi)v(\xi), v^2(\xi) - u^2(\xi))}{u^2(\xi) + v^2(\xi)}$$

to $\mathbf{r}(\xi)$ depends *rationally* on the parameter ξ , and the offset $\mathbf{r}_d(\xi)$ is thus a rational curve. Instead of explicitly constructing the offset curve, it is possible to formulate the interpolator algorithm so it accepts directly the profile $\mathbf{r}(\xi)$ to be machined, and performs the tool offset in real time.

Corresponding segments of the given curve $\mathbf{r}(\xi)$ and its offset $\mathbf{r}_d(\xi)$ will have, in general, different arc lengths and curvature distributions. The problem that concerns us here is to drive the tool *along the offset curve* at a feedrate

specified in terms of its intrinsic geometry. In general, construction of the offset curve involves “trimming away” portions of $\mathbf{r}_d(\xi)$ that will cause gouging of the desired curve $\mathbf{r}(\xi)$ by a tool of radius d — namely, “concave” regions of the curve with radius of curvature $< 1/d$ (see §8.3.4). We assume the relevant parameter intervals for the trimmed offset are pre-determined, and consider only the problem of driving the tool along them at a given feedrate.

The parametric speed $\sigma_d(\xi) = |\mathbf{r}'_d(\xi)|$ of the offset at distance d can be expressed (see §8.3.4) in terms of the speed $\sigma(\xi)$ and curvature $\kappa(\xi)$ of $\mathbf{r}(\xi)$ as

$$\sigma_d(\xi) = [1 + \kappa(\xi)d]\sigma(\xi).$$

To simplify matters, we assume that $\kappa(\xi)d > 0$ over the segment of interest.² It can then be shown [174] that the arc length S_d of an offset segment that corresponds to a segment of length S on the original curve is given by

$$S_d = S + d\Delta\theta,$$

where $\Delta\theta$ is the total rotation of the unit normal along the segment. Using this result, one can show that reference point locations for a uniform feedrate V_0 along the offset are obtained by solving the equation

$$2d \tan^{-1} \phi(\xi_k) + s(\xi_k) = 2d \tan^{-1} \phi(\xi_{k-1}) + s(\xi_{k-1}) + \Delta s_0, \quad (29.11)$$

where $\Delta s_0 = V_0 \Delta t$ and $\phi(\xi) = v(\xi)/u(\xi)$. This may be compared with the simpler constant-feedrate equation (29.8) for driving the tool along the curve $\mathbf{r}(\xi)$ itself. In fact, it is of precisely the same form as the equation obtained for the modified inverse-curvature feedrate function in (29.10). Other forms of feedrate variation along the offset may be analyzed using similar methods.

29.4 Feedrate in Terms of Arc Length

Consider the case in which we wish to specify the feedrate in terms of distance along the curve, i.e., as a function of the arc length s . It will be convenient to measure s as a fraction of the *total* arc length,

$$S = \int_0^1 \sigma(\xi) d\xi = s(1) - s(0).$$

From (29.1) we see that, knowing the value ξ_{k-1} , the succeeding value ξ_k is determined by the equation

$$\int_{\xi_{k-1}}^{\xi_k} \frac{\sigma(\xi)}{V_s(\xi)} d\xi = \Delta t.$$

Since $\sigma d\xi = ds$, the integral can be re-written in the simpler form

² In general, it is necessary to split the curve at inflections as a pre-processing step.

$$\int_{s_{k-1}}^{s_k} \frac{ds}{V(s)} = \Delta t, \quad (29.12)$$

where $s_{k-1} = s(\xi_{k-1})$, $s_k = s(\xi_k)$. When V is a polynomial or rational function of s , this integral always admits analytic reduction through a partial-fraction decomposition of the integrand. In the general case, however, the dependence of the reduced form on s_k may involve logarithmic, arctangent, and rational expressions. We focus here on two special cases of practical interest, in which the reduced form yields a *polynomial* equation for the determination of ξ_k — namely, a linear or quadratic dependence of V on s .

29.4.1 Linear Dependence on Arc Length

We express V as a function of the fractional arc length in Bernstein form:

$$V(s) = V_0 \left(1 - \frac{s}{S}\right) + V_1 \left(\frac{s}{S}\right). \quad (29.13)$$

Clearly, the initial and final feedrates, V_0 and V_1 , completely determine $V(s)$. Evaluating the integral (29.12) then gives rise to the equation

$$s(\xi_k) = \frac{V_s(\xi_{k-1}) e^{(V_1 - V_0)\Delta t/S} - V_0}{V_1 - V_0} S \quad (29.14)$$

for ξ_k , which is to be interpreted as follows. On the left-hand side, ξ_k appears as an *indeterminate* argument of the arc-length polynomial $s(\xi)$. Since ξ_{k-1} has already been computed, the right-hand side is a constant — which must, however, be re-evaluated at each step $k = 1, 2, \dots, N$.

Note again that the polynomial equation (29.14) for ξ_k has a unique real root, which may be determined to any desired accuracy by Newton-Raphson iteration. For the starting value, one takes $\xi_k^{(0)} = \xi_{k-1} + V_s(\xi_{k-1})\Delta t/\sigma(\xi_{k-1})$, where ξ_{k-1} denotes the preceding converged value.

In computing the constant on the right-hand side of (29.14) for each step, it is advisable to pre-compute and store the quantities

$$a = \frac{e^{(V_1 - V_0)\Delta t/S}}{V_1 - V_0} S \quad \text{and} \quad b = -\frac{V_0}{V_1 - V_0} S.$$

In addition to evaluating $V_s(\xi_{k-1})$, the determination of this constant then requires only one multiplication and one addition to form $a V_s(\xi_{k-1}) + b$.

29.4.2 Quadratic Dependence on Arc Length

Again, we express the feedrate variation in Bernstein form as

$$V(s) = V_0 \left(1 - \frac{s}{S}\right)^2 + V_1 2 \left(1 - \frac{s}{S}\right) \left(\frac{s}{S}\right) + V_2 \left(\frac{s}{S}\right)^2. \quad (29.15)$$

It is convenient to introduce also the polynomial

$$V'(s) = (V_1 - V_0) \left(1 - \frac{s}{S}\right) + (V_2 - V_1) \left(\frac{s}{S}\right).$$

In the analytic reduction of equation (29.12), it is necessary to employ separate treatment for the three cases where the discriminant of the quadratic $V(s)$ is less than, equal to, or greater than zero:

(i) $V_1^2 < V_2 V_0$ — setting $V_* = \sqrt{V_2 V_0 - V_1^2}$, the reduction of (29.12) yields

$$s(\xi_k) = \frac{V_* \Psi(\xi_{k-1}) - V_1 + V_0}{V_2 - 2V_1 + V_0} S \quad (29.16)$$

as the polynomial equation determining ξ_k , where we define

$$\Psi(\xi_{k-1}) = \frac{V'(s(\xi_{k-1})) + V_* \tan(V_* \Delta t / S)}{V_* - V'(s(\xi_{k-1})) \tan(V_* \Delta t / S)}.$$

Assuming the values V_* , $\tan(V_* \Delta t / S)$, $V_* \tan(V_* \Delta t / S)$ and the coefficients

$$a = \frac{V_*}{V_2 - 2V_1 + V_0} S \quad \text{and} \quad b = -\frac{V_1 - V_0}{V_2 - 2V_1 + V_0} S$$

are pre-computed, determining the constant on the right in (29.16) requires, in addition to evaluating $V'(s(\xi_{k-1}))$, one multiplication, two additions, and one division to compute $\Psi(\xi_{k-1})$, and then a further multiplication and addition to form $a\Psi(\xi_{k-1}) + b$.

(ii) $V_1^2 = V_2 V_0$ — in this case $V(s)$ is the square of a linear polynomial in s , and from (29.12) we obtain

$$s(\xi_k) = \frac{[S + (V_1 - V_0)\Delta t] s(\xi_{k-1}) + S V_0 \Delta t}{[S - (V_1 - V_0)\Delta t] S - (V_2 - 2V_1 + V_0)\Delta t s(\xi_{k-1})} S. \quad (29.17)$$

By pre-computing and storing the coefficients

$$a = S + (V_1 - V_0)\Delta t, \quad b = S V_0 \Delta t,$$

$$c = -(V_2 - 2V_1 + V_0)\Delta t / S, \quad d = S - (V_1 - V_0)\Delta t,$$

computation of the constant on the right in (29.17) requires, in addition to evaluating $s(\xi_{k-1})$, only two multiplications, two additions, and one division to form the quantity $(a s(\xi_{k-1}) + b) / (c s(\xi_{k-1}) + d)$.

(iii) $V_1^2 > V_2 V_0$ — setting $V_* = \sqrt{V_1^2 - V_2 V_0}$, we obtain

$$s(\xi_k) = \frac{V_* \Phi(\xi_{k-1}) - V_1 + V_0}{V_2 - 2V_1 + V_0} S \quad (29.18)$$

from equation (29.12), where we define

$$\Phi(\xi_{k-1}) = \frac{V'(s(\xi_{k-1})) - V_* \tanh(V_* \Delta t / S)}{V_* - V'(s(\xi_{k-1})) \tanh(V_* \Delta t / S)}.$$

Assuming the values V_* , $\tanh(V_* \Delta t / S)$, $V_* \tanh(V_* \Delta t / S)$ and the coefficients a and b defined in case **(i)** are pre-computed and stored, the cost of computing the constant on the right in (29.18) is identical to that of this earlier case. In fact, the outcome of the present case amounts to simply substituting iV_* for V_* in the results of case **(i)**.

Note that all three of the equations (29.16)–(29.18) are of the same form as equations (29.8) and (29.14) for the constant and linear feedrate cases — namely, the arc length polynomial with ξ_k as its indeterminate argument is set equal to some constant, dependent upon the preceding value ξ_{k-1} . Thus, equations (29.16)–(29.18) also have unique (simple) real roots, which can be accurately determined by just a few Newton–Raphson iterations.

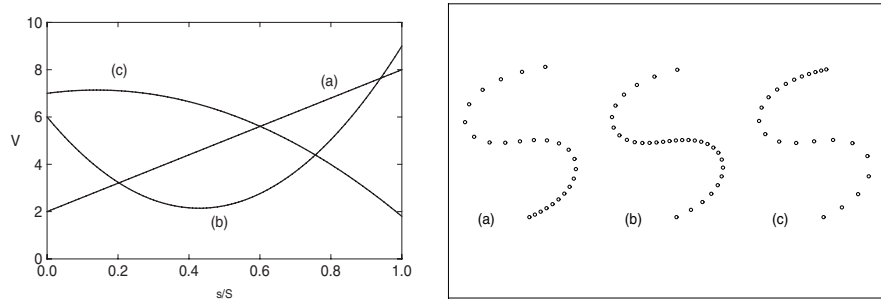


Fig. 29.3. Left: feedrate functions that vary (a) linearly, and (b)–(c) quadratically with arc length, as defined by expressions (29.13) and (29.15). Right: reference points on the PH curve of Fig. 29.1 generated in accordance with these feedrate functions.

Fig. 29.3 shows reference points on the PH quintic of Fig. 29.1, generated according to feedrates that depend linearly and quadratically on the arc length — case (a) is linear with $(V_0, V_1) = (2.0, 8.0)$, while (b) and (c) are quadratic with $(V_0, V_1, V_2) = (6.0, -3.0, 9.0)$ and $(7.0, 8.0, 1.8)$ respectively.

29.5 Time-dependent Feedrate

Real-time interpolators for time-dependent feedrates $V(t)$ on PH curves are easy to implement when the function $V(t)$ has a simple closed-form indefinite integral. In practice, they are useful in specifying the smooth feed accelerations and decelerations desired when the feedrate changes or the machine starts or stops. This section describes their implementation, and empirical results from runs on an open-architecture 3-axis CNC milling machine.

Consider a time-dependent feedrate function $V(t)$ for $t \in [0, T]$ imposed on the PH curve $\mathbf{r}(\xi)$, $\xi \in [0, 1]$. We require $V(t)$ to be non-negative and to have a simple expression $F(t)$ for its indefinite integral, such that $V(t) = \dot{F}(t)$. Since $V(t) \geq 0$, $F(t)$ is monotone-increasing over $t \in [0, T]$. Clearly, the value of $F(t)$ is simply the curvilinear distance travelled along $\mathbf{r}(\xi)$ in time t .

The function $\xi(t)$ that describes the variation of the parameter with time, when the curve is traversed in accordance with the feedrate function $V(t)$, is defined implicitly by the relation

$$s(\xi) = F(t).$$

Correspondingly, if $\mathbf{r}(\xi)$ has total arc length S , the traversal time T may be found *a priori* from

$$T = F^{-1}(S).$$

However, the inverse function F^{-1} cannot in general be expressed in closed form, and this equation may require an iterative solution for T .

For a sampling interval Δt , the real-time CNC interpolator must compute the parameter values ξ_1, ξ_2, \dots of reference points at times $\Delta t, 2\Delta t, \dots$ These values are roots of the polynomial equations

$$s(\xi_k) = F(k\Delta t) \quad \text{for } k = 1, 2, \dots \quad (29.19)$$

Since $s(\xi)$ is monotone, the above equation has a *unique* real root for each k . We may obtain ξ_k to machine precision by a few Newton–Raphson iterations,

$$\xi_k^{(r+1)} = \xi_k^{(r)} - \frac{s(\xi_k^{(r)}) - F(k\Delta t)}{\sigma(\xi_k^{(r)})} \quad r = 0, 1, \dots, \quad (29.20)$$

with starting approximation $\xi_k^{(0)} = \xi_{k-1}$ (i.e., the converged parameter value for the preceding point). These principles apply to *arbitrary* time-dependent feedrates $V(t)$ with closed-form indefinite integrals $F(t)$, allowing the right-hand side in (29.20) to be efficiently and precisely computed. Because of the uniqueness of the real root ξ_k of (29.19), and the availability of the parameter value ξ_{k-1} for the previous reference point as a good starting approximation, (29.20) usually converges to machine precision in a few iterations.

29.5.1 Polynomial Time Dependence

Specifying V as a *polynomial* in t provides a simple form of time-dependent feedrate, that proves very useful in achieving smooth feed accelerations from rest (or feed decelerations to rest). Of course, if $V(t)$ is a polynomial, $F(t)$ is also a polynomial, of degree one higher. It is convenient to express both in terms of the Bernstein basis in the “normalized” time variable $\tau = t/T$,

$$b_k^n(\tau) = \binom{n}{k} (1-\tau)^{n-k} \tau^k \quad \text{for } k = 0, \dots, n$$

on the unit interval $\tau \in [0, 1]$. Thus, if

$$V(\tau) = \sum_{k=0}^n V_k b_k^n(\tau), \quad (29.21)$$

its indefinite integral with respect to $t = T\tau$ is

$$F(\tau) = T \sum_{k=0}^{n+1} F_k b_k^{n+1}(\tau),$$

with Bernstein coefficients given by

$$F_0 = 0 \quad \text{and} \quad F_k = \frac{1}{n+1} \sum_{j=0}^{k-1} V_j \quad \text{for } k = 1, \dots, n+1.$$

29.5.2 Acceleration/Deceleration Profiles

Consider the problem of defining a *smooth* feedrate acceleration along a curved path — i.e., specifying how V should vary between some constant value V_i for $t < 0$ to another constant value V_f for $t > T$. Using a polynomial (29.21) of *odd* degree n , we can define a feedrate profile that matches $V = V_i$ for $t < 0$ and $V = V_f$ for $t > T$ with $C^{(n-1)/2}$ continuity. Specifically, we can achieve C^0 continuity if V is linear; C^1 continuity if V is cubic; and C^2 continuity if V is quintic. These instances are all compatible with the interpolation equation (29.19) — increasing n incurs only a slight additional expense in evaluating $F(k\Delta t)$, a polynomial of degree $n+1$, within each sampling interval.

Noting that the first and second time-derivatives of (29.21) are given by

$$\begin{aligned} \dot{V}(\tau) &= \frac{1}{T} \sum_{k=0}^{n-1} n \Delta V_k b_k^{n-1}(\tau), \\ \ddot{V}(\tau) &= \frac{1}{T^2} \sum_{k=0}^{n-2} n(n-1) \Delta^2 V_k b_k^{n-2}(\tau), \end{aligned} \quad (29.22)$$

where $\Delta V_k = V_{k+1} - V_k$ and $\Delta^2 V_k = \Delta V_{k+1} - \Delta V_k = V_{k+2} - 2V_{k+1} + V_k$, one can easily verify that the appropriate Bernstein coefficients are

$$V_0 = V_i, \quad V_1 = V_f \quad (29.23)$$

for a C^0 linear feed acceleration,

$$V_0 = V_1 = V_i, \quad V_2 = V_3 = V_f \quad (29.24)$$

for a C^1 cubic feed acceleration, and finally

$$V_0 = V_1 = V_2 = V_i, \quad V_3 = V_4 = V_5 = V_f \quad (29.25)$$

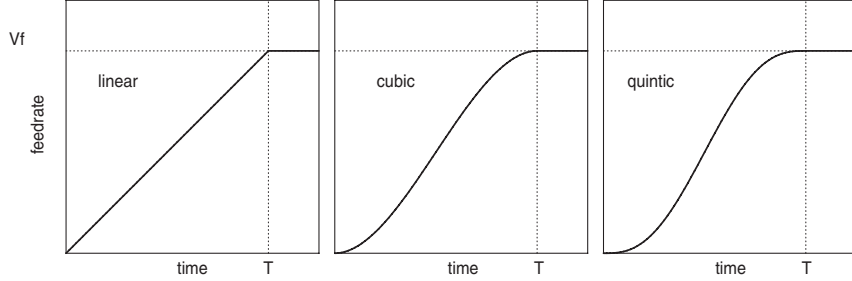


Fig. 29.4. Feed accelerations from $V = 0$ for $t \leq 0$ to $V = V_f$ for $t \geq T$ by means of C^0 linear, C^1 cubic, and C^2 quintic time-dependent feedrates defined by (29.21).

for a C^2 quintic feed acceleration. Figure 29.4 illustrates the feedrate profiles defined by (29.23)–(29.25) when $V_i = 0$. In each case, the distance travelled during the feed acceleration period $0 \leq t \leq T$ is simply $\frac{1}{2}V_f T$. For given V_f , the parameter T can be regarded as a measure of the rate of feed acceleration: decreasing T leads to a “steeper” feedrate change, and vice-versa.

The C^0 linear feedrate is not recommended, since it entails a discontinuous feed acceleration \dot{V} at times $t = 0$ and $t = T$. The axis motors cannot supply the instantaneous change of torque implied by such sudden jumps in \dot{V} . The “S-shaped” C^1 cubic and C^2 quintic profiles are far preferable — the latter, in particular, ensures continuity of both the feed acceleration \dot{V} and its time derivative (the “feed jerk” \ddot{V}), thus yielding very smooth transitions between different fixed-feedrate phases in the traversal of curved paths (even greater orders of smoothness in feedrate transitions are easily implemented, although their practical benefits become increasingly marginal).

Similar principles hold for a feed *deceleration*, from $V = V_i$ to $V = 0$ say, rather than a feed acceleration. The simplicity and versatility of interpolators for feedrates with polynomial time dependence is a very attractive feature. By defining $F(\tau)$ through a modular function call, one can achieve considerable flexibility in controlling the smoothness of a feedrate transition, the overall acceleration/deceleration rate, and the time or distance over which a feedrate transition is effected (by appropriate choice of the parameter T).

In fact, using the polynomial form (29.21) with odd n we can obtain a smooth match to *arbitrary* Hermite data of order $\frac{1}{2}(n-1)$ characterizing the feedrate for time $t < 0$ and $t > T$. The Bernstein coefficients of $V(\tau)$ are easily determined. For a C^0 linear profile with $V(0) = V_i$ and $V(T) = V_f$, we have

$$V_0 = V_i \quad \text{and} \quad V_1 = V_f.$$

For a C^1 cubic profile with $V(0) = V_i$, $\dot{V}(0) = \dot{V}_i$ and $V(T) = V_f$, $\dot{V}(T) = \dot{V}_f$, the coefficients are

$$V_0 = V_i, \quad V_1 = V_i + \frac{1}{3}T\dot{V}_i, \quad V_2 = V_f - \frac{1}{3}T\dot{V}_f, \quad V_3 = V_f.$$

Finally, for the C^2 quintic profile matching $V(0) = V_i$, $\dot{V}(0) = \dot{V}_i$, $\ddot{V}(0) = \ddot{V}_i$ and $V(T) = V_f$, $\dot{V}(T) = \dot{V}_f$, $\ddot{V}(T) = \ddot{V}_f$, we have

$$\begin{aligned} V_0 &= V_i, & V_1 &= V_i + \frac{1}{5}T\dot{V}_i, & V_2 &= V_i + \frac{2}{5}T\dot{V}_i + \frac{1}{20}T^2\ddot{V}_i, \\ V_3 &= V_f - \frac{2}{5}T\dot{V}_f + \frac{1}{20}T^2\ddot{V}_f, & V_4 &= V_f - \frac{1}{5}T\dot{V}_f, & V_5 &= V_f. \end{aligned}$$

These coefficients can be verified by inspecting the derivatives (29.22) of $V(\tau)$.

29.5.3 Traversing a Single PH Curve

As a test curve, we employ the PH quintic shown in Fig. 29.5, constructed as the interpolant to first-order Hermite data specified by the first and last two Bézier control points \mathbf{p}_0 , \mathbf{p}_1 and \mathbf{p}_4 , \mathbf{p}_5 . This curve, with total arc length $S = 12.812$ in, will be traversed by a motion comprising three phases:

1. acceleration from rest $V_i = 0$ to specified feedrate $V_f = V_m$;
2. maintenance of the specified feedrate — i.e., $V_i = V_f = V_m$;
3. deceleration from specified feedrate $V_i = V_m$ to rest $V_f = 0$.

By choosing appropriate (possibly zero) durations for each of the three phases, it is possible to use this basic structure to specify the feedrate variation across successive components of a multi-segment PH curve.

To compare the performance of PH curve interpolators with traditional G code interpolators, several piecewise-linear G code approximations to the test curve were generated — see Fig. 29.5. These approximations were computed by an adaptive algorithm that adjusts the segment lengths according to the curvature, so as to minimize the error for a prescribed number of segments. In Fig. 29.5 we see, for example, that relatively large segments are allowed near the “flat” (i.e., inflectional) region of the curve.

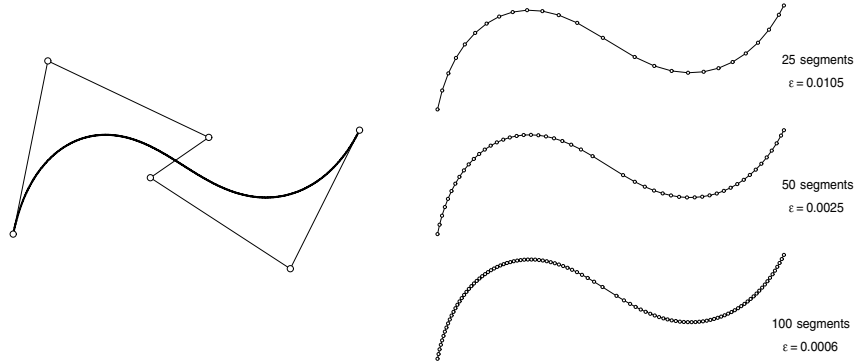


Fig. 29.5. Left: the PH quintic test curve, generated as the interpolant to Hermite data specified by initial and final pairs of control points \mathbf{p}_0 , \mathbf{p}_1 and \mathbf{p}_4 , \mathbf{p}_5 . Right: approximations to this PH quintic by 25, 50, and 100 linear G code segments. The geometrical tolerance ϵ for each of these G code approximations is also indicated.

For the feed acceleration/deceleration phases, a linear variation of feedrate with time is assumed as the default, since this is the method employed by the G code interpolator. Our main interest is in comparing the feedrate performance of the PH curve and G code interpolators. For the G code paths, we use the standard interpolator of a commercial CNC software controller (see §29.5.4). Since the error of the G code approximations is quite small, we do not expect significant differences in the geometrical (i.e., contour) accuracy. We shall see, however, that the “grainy” nature of the G code path description compromises the controller’s ability to maintain a steady feedrate.

29.5.4 Experimental Results

By a suitable choice of the coefficients V_0, \dots, V_n and time interval T , the feed acceleration, fixed feedrate, and feed deceleration phases can all be realized by a generic function $F(\tau)$ for $\tau = t/T \in [0, 1]$, where t is measured from the start of each phase (each phase spans a sub-interval of the parameter domain $\xi \in [0, 1]$). For greatest flexibility, we employ a quintic feedrate $V(\tau)$ as our generic function, with appropriate coefficients defining each phase.

The input to the interpolator comprises both *geometric* and *feedrate* data. The former consists of the curve end-point coordinates,³ and the Bernstein coefficients of the $u(\xi), v(\xi)$ polynomials. These coefficients also determine the parametric speed $\sigma(\xi)$ and arc length $s(\xi)$, required in the Newton iterations (29.20), and the curve coordinates $x(\xi), y(\xi)$ used to compute the reference points. Feedrate data includes the mode (constant, linear, cubic, or quintic) for each phase, the coefficients of $V(\tau)$ and its integral $F(\tau)$, and the overall duration T of the feedrate phase. As noted earlier, the parameter T is used to control the rate of feed acceleration/deceleration. Thus, once V_m is given, the durations T_{acc} and T_{dec} for the acceleration and deceleration phases can be simply assigned to achieve the desired rates. Alternatively, one may specify the arc length S_{acc} and S_{dec} over which these phases are to be accomplished, and the corresponding durations are then given by $T = 2S/V_m$.

With T_{acc} and T_{dec} specified, the duration T_{con} of the constant-feedrate phase is fixed by the requirement that the sum of the distances travelled in all three phases must equal the total curve arc length S . This gives

$$T_{\text{con}} = \frac{S}{V_m} - \frac{T_{\text{acc}} + T_{\text{dec}}}{2}. \quad (29.26)$$

It is convenient to specify T_{acc} and T_{dec} as integer multiples N_{acc} and N_{dec} of the servo sampling time Δt . The number of steps (servo updates) for the fixed-feedrate phase is then

$$N_{\text{con}} = \left[\frac{T_{\text{con}}}{\Delta t} \right], \quad (29.27)$$

³ The curve end point, rather than the start point, is chosen for consistency [170] with standard G code conventions.

where $[x]$ denotes the integer nearest to x . By suitable choices for N_{acc} , N_{dec} the basic three-phase motion can accommodate each segment of a smooth multi-segment (i.e., spline) curve. With a 3-segment curve, for example, we may take $N_{\text{acc}} \neq 0 = N_{\text{dec}}$ for the first segment; $N_{\text{acc}} = 0 = N_{\text{dec}}$ for the middle segment; and $N_{\text{acc}} = 0 \neq N_{\text{dec}}$ for the last segment.

These preparatory steps, and the computation of other required constants, are performed *a priori* by an (off-line) preprocessor, so the interpolator can focus on real-time computation of reference points. The desired acceleration or deceleration rates are achieved by simply supplying the interpolation scheme (29.20) with the function $F(t)$ appropriate to the desired feedrate variation. The simplicity and versatility of this approach may be contrasted with typical methods for handling accelerations/decelerations on G code paths, where the interpolator must attempt to “reason” in real time about how many segments will be needed to achieve a given change of feedrate, changes in path direction between successive segments, etc. The PH curve interpolators can also easily accommodate more complex feedrate variations, that may be used to maintain cutting forces within an acceptable range (see §29.6), prevent tool chatter, overload of the machine drives, etc. Such information is generated off-line by, for example, a simulation of the cutting process, and then passed to the PH curve interpolator in the form of appropriate feedrate functions.

The feedrate experiments were performed on a 3-axis CNC mill made by MHO Corp. of Oakland, California (Fig. 29.6). The machine axes are driven



Fig. 29.6. Experimental CNC system — MHO MillRight Series 18 3-axis mill, with MDSI OpenCNC software controller. Custom PH curve interpolators can be invoked (in lieu of G code interpolators) by the macro capability of the OpenCNC software.

by Yaskawa brushless motors and precision-ground ball screws, and the mill is controlled by the OpenCNC software from Manufacturing Data Systems, Inc. (MDSI) of Ann Arbor, Michigan. This is a true open-architecture controller, that provides complete variable specifications and programming interfaces for incorporating custom user functions (a macro capability at the part-program level is used to invoke such functions and communicate data to them).

It was thus a relatively easy task to link the PH curve interpolators into the OpenCNC system. A side-by-side comparison of machine performance can be made by switching between standard G code part programs, which cause the default G code interpolator to be invoked, and part programs with macros that invoke the PH curve interpolators. The basic real-time data, stored in memory for subsequent analysis, are the machine axis locations at the servo sampling frequency, $f_0 = 1024$ Hz. Feedrates and accelerations are obtained by first- and second-order differencing of this position data.

PH Curves versus G Codes

Figure 29.7 compares measured feedrates using the PH curve interpolator and G code interpolator, for commanded feedrates⁴ V_m of 100, 200, 400, 800 ipm.⁵ The axis feedrate components are obtained by differencing the real-time axis location data (stored in memory during a run); the overall feedrate is simply the magnitude of the vector sum of these axis feedrates. In Fig. 29.7 we see that the G code interpolator can accurately realize feedrates up to ~ 200 ipm on the multi-segment G code path by adjusting the x and y axis feedrates in a step-wise manner (consistent with the discrete changes in path direction at junctures of G code segments). The PH curve interpolator, on the other hand, traces a path by perfectly smooth motions of each axis.

Traversal of a polygonal path at a constant feedrate is actually a physical impossibility, since instantaneous changes of direction at finite speed amount to infinite accelerations — as reflected by the impulsive behavior of the axis feedrates seen for the G codes in Fig. 29.7. For low feedrates, the concern of “instantaneously changing direction at a finite speed” (between successive G code segments) is relatively insignificant. As the feedrate increases, however, the incompatibility of discrete G code approximations with smooth execution of a curved path becomes increasingly apparent.

In Fig. 29.7 we observe that, on increasing V_m from 200 to 400 ipm, the G code interpolator experiences great difficulty in achieving and maintaining the commanded feedrate. The PH curve interpolator, however, executes the commanded motion effortlessly. At $V_m = 400$ ipm, one can actually *hear* that the machine suffers a much more “jerky” motion with the G code interpolator

⁴ The data in Fig. 29.7 are based on the 50 G code approximation; qualitatively similar results were obtained when using the 25 and 100 G code approximations.

⁵ Specifying feedrates in the somewhat archaic units of inches-per-minute (ipm) is still common practice in machining applications.

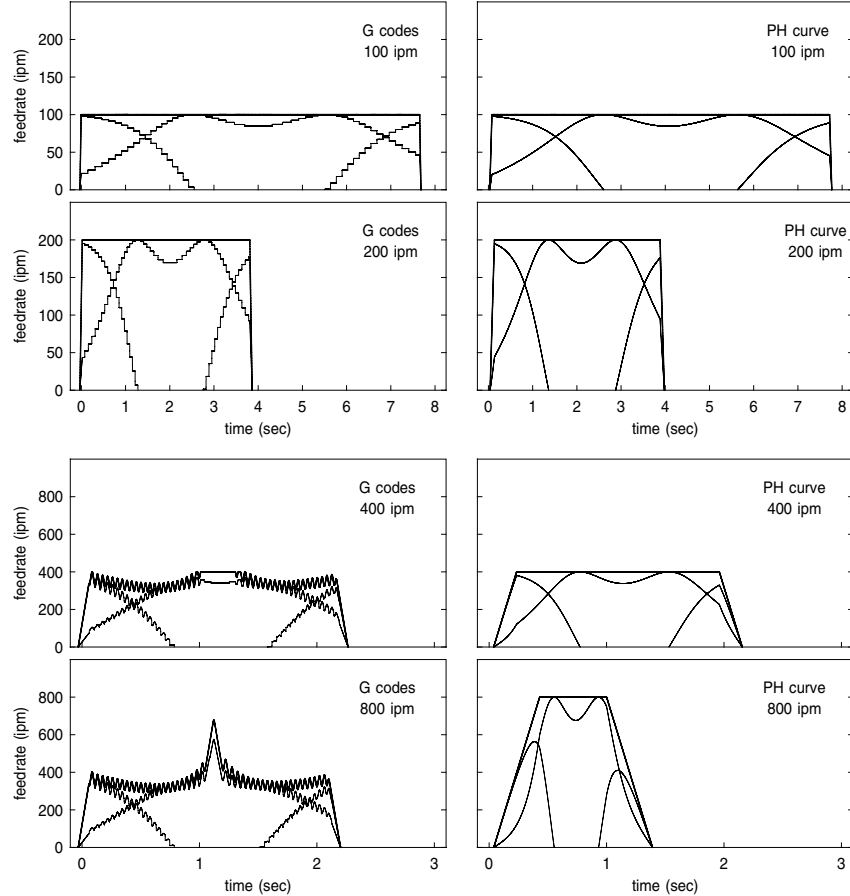


Fig. 29.7. Feedrate performance comparison for piecewise-linear G code (left) and PH curve (right) interpolators at feedrates of 100, 200, 400, and 800 ipm. The time and feedrate scales for the 400 & 800 ipm cases differ from those for 100 & 200 ipm. The x, y feedrate components are also shown (light curves), truncated below zero.

than with the PH curve interpolator! The degradation of performance with the G codes is even more pronounced at $V_m = 800$ ipm. Again, the PH curve interpolator easily attains and maintains the desired 800 ipm, but the G code interpolator can systematically sustain only about half this speed.⁶

In addition to the 50 G code part program, experiments were performed with the 25 and 100 G code approximations illustrated in Fig. 29.5. A steady deterioration of feedrate performance with the number of G code segments was apparent. Figure 29.8 compares the *average* feedrate achieved during the

⁶ The improved feedrate near the middle of the 800 ipm G code run correlates with the presence of a relatively long G code segment straddling the curve inflection.

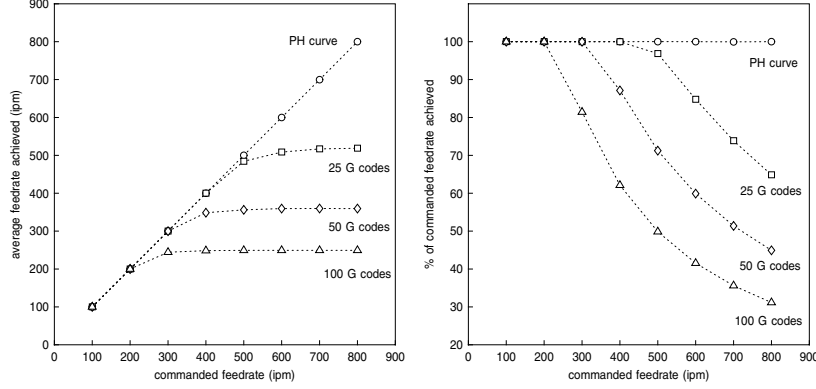


Fig. 29.8. Average feedrate achieved during the constant-feedrate phase of the curve traversal, using both the PH curve interpolator and G code interpolator with 25, 50, and 100 G code curve approximations. The mean achieved feedrate is plotted against the commanded feedrate on the left, while the plot on the right shows the mean achieved feedrate as a fraction of the commanded feedrate.

fixed-feedrate phase of the traversal for the PH curve interpolator and the G code interpolator with 25, 50, and 100 segments, at commanded feedrates V_m ranging from 100 to 800 ipm. Whereas the PH curve interpolator accurately maintains the desired feedrate in all circumstances, the G code interpolator exhibits an increasingly severe feedrate saturation as the number of segments grows. In the worst case (100 segments at 800 ipm), for example, the G code interpolator achieves only 31% of the commanded feedrate on average.

These results discredit the practice of setting tight geometrical tolerances when generating tool paths, thereby producing many short G code segments. Apart from producing huge part programs, this can severely compromise the feedrate performance of the machine. Thus, with G codes, there is evidently a fundamental conflict between the nominal geometrical accuracy of paths and the accurate maintenance of high feedrates along them.

Table 29.1. Feedrate standard deviations for V_m between 100 and 800 ipm.

V_m (ipm)	100	200	300	400	500	600	700	800
PH curve	0.03	0.03	0.03	0.03	0.03	0.03	0.03	0.03
25 G codes	0.03	0.05	0.07	0.12	22.1	52.3	72.2	78.5
50 G codes	0.03	0.03	0.38	32.3	50.9	64.8	66.6	66.1
100 G codes	0.03	0.03	27.1	40.5	45.3	45.3	45.3	45.3

Furthermore, in all cases where the G code interpolator exhibits feedrate saturation, this is accompanied by significant instantaneous fluctuations of the actual feedrate about the mean. Table 29.1 lists measured feedrate standard

deviations during the fixed-feedrate phase. Using the PH curve interpolator, the fluctuation is indistinguishable from measurement errors. However, the G code interpolator incurs fluctuations of some 10–20% about the mean realized feedrate, indicating a very “jerky” machine motion.

These experiments offer compelling evidence for the advantages of analytic real-time curve interpolators over traditional G codes when curved paths are to be traversed at very high speeds or with high acceleration and deceleration rates, as in high-speed machining applications. Apart from the fact that the commanded motion is more consistently realized to much higher feedrates,⁷ and rates of feedrate change, these motions become inherently much *smoother* and thus less demanding of (or potentially damaging to) the axis drives.

Due to the proprietary nature of OpenCNC algorithms, a specific cause for the performance limitations of the G code interpolator cannot be identified. However, it is not difficult to identify a variety of potential causes that, being intrinsic to the discrete nature of G code path descriptions, must inevitably contribute to degradation of feedrate performance at high speed.

These include: (i) the fact that short G code segments do not, in general, correspond to an integral number of sampling intervals Δt at a given feedrate V_m ; (ii) the need to reduce feedrates at appreciable changes of path direction between consecutive segments, to avoid imposing excessive torque demands on the motors; and (iii) the “block look-ahead” problem incurred when an acceleration/deceleration phase must span many G code segments.

In comparing the real-time machine location data, measured by encoders on the axes, with the reference points generated by the G code and PH curve interpolators, we make the remarkable observation that — apart from its more “noisy” nature — the former are virtually indistinguishable from the latter! This highlights the amazing capability of the machine hardware, which can execute virtually any commanded motion — even if, as in the case of G code paths, it is an extremely “jerky” motion. Thus, the poor feedrate performance evident with the G code paths in Figs. 29.7 and 29.8 is not a symptom of any *physical* machine limitations (motor torque capacity, backlash or inertia of the axes, etc.) or defects of the control algorithm, but a consequence of the real-time position data that the interpolator furnishes to the controller.

The ability to achieve dramatic improvements in feedrate performance by simply replacing a low-level module (the interpolator) in the control software illustrates the benefits of an open-architecture controller, such as OpenCNC. Since high-end CNC machines are major capital investments, throughput in machining operations is always of central concern. The ability to significantly improve machine performance by merely upgrading the control software can have a tremendous impact on manufacturing profitability.

⁷ Note also that, to maintain a safe *chip load* and avoid excessive frictional heating, the spindle speed must be coordinated with the feedrate — actual feedrates that are much lower than the commanded feedrate compromise this coordination.

Feed Acceleration/Deceleration

The preceding results used only linear time-dependent feedrate functions for the feed acceleration/deceleration phases at the start and end of the curve. To provide a smoother transition from or to rest and a given constant feedrate, we have also tested the cubic and quintic feedrate profiles discussed in §29.5.2 (in fact, we implement the quintic as the generic case, and specialize to linear or cubic profiles by the choice of appropriate coefficients). Figure 29.9 compares experimental results for feedrate and acceleration magnitude in accelerating from rest to a constant feedrate of 800 ipm (the acceleration magnitude plots are more “noisy” than the feedrate, since their computation involves second-order differencing of the axis positions).

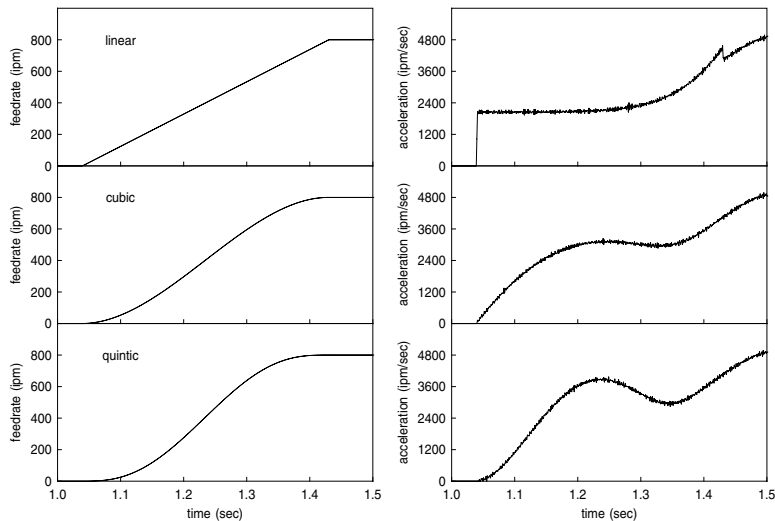


Fig. 29.9. Measurements of the acceleration magnitude for linear, cubic, and quintic feedrate profiles increasing from 0 to 800 ipm along the test curve in Fig. 29.5. Note the “jumps” in the acceleration magnitude incurred with the linear profile.

Arbitrary Time-dependent Feedrates

Although we have emphasized algorithms corresponding to a *polynomial* time dependence of the feedrate, the PH curve CNC interpolators are by no means limited to such functions. Provided the indefinite integral $F(\tau)$ of the feedrate $V(\tau)$ admits a simple closed-form expression, compatible with real-time evaluation, the updating (29.20) of the reference point parameter values poses no difficulty. To demonstrate this versatility in temporal feedrate variation, we consider the case of the sinusoidally-varying feedrate

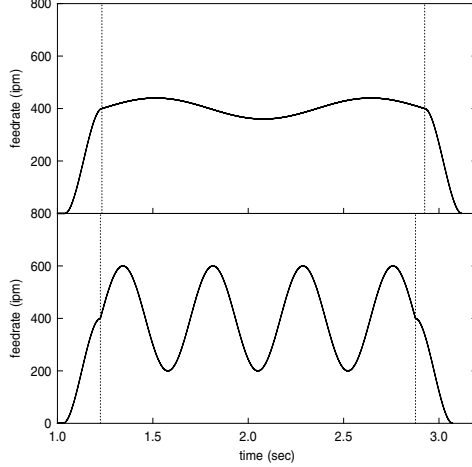


Fig. 29.10. Experimental results from the PH curve interpolators for the sinusoidal feedrate variation defined by (29.28), about the nominal value $V_0 = 400$ ipm. The two cases shown correspond to $a = 0.1$, $f_* \approx 1$ Hz and $a = 0.5$, $f_* \approx 2$ Hz. Cubic feedrate profiles are employed here for the feed acceleration and deceleration phases.

$$V(t) = V_0 [1 + a \sin(2\pi f_* t)], \quad (29.28)$$

where V_0 is a nominal feedrate, a is a fractional amplitude⁸ about this value, and f_* is the feedrate variation frequency. Figure 29.10 shows experimental results obtained for two different sets of a and f_* values. The accurate tracking of sinusoidal feedrate variations at different frequencies suggests the ability, by Fourier superposition, to generate any desired time dependence that does not contain too much high-frequency content (the highest frequency that can be achieved is limited by the machine structure and dynamics, and by aliasing effects when the quantity $f_* \Delta t$ is not small compared to unity).

29.6 Constant Material Removal Rate

We now consider a curvature-dependent feedrate form that addresses certain physical aspects of the machining process [169]. The curvature dependence is selected to yield, for a constant depth of cut, an (approximately) constant rate of volume removal. This is motivated by simple models of the milling process [206], in which the cutting force is proportional to the volume removal rate. Reduced cutting force variations can result in prolonged tool life and machined parts of enhanced dimensional accuracy and improved surface finish.

⁸ Normally, one would choose $a < 1$, but the algorithm can actually accommodate the direction reversals along a curved path that are incurred when $a > 1$.

It is perhaps not obvious that, for curved paths, a fixed feedrate and depth of cut do *not* imply a constant material removal rate (MRR) — in “concave” regions the remaining material strip curves around the tool, incurring higher MRR than for a linear cut, while in “convex” regions it curves away from the tool, causing a lower MRR.⁹ A quantitative description of this effect, which is primarily of interest for finish cuts on strongly-curved tool paths — i.e., the radius of curvature is comparable to the tool radius — is developed below.

29.6.1 Form of Feedrate Function

Consider a tool path defined by a plane PH curve $\mathbf{r}(\xi)$, with tangent $\mathbf{t} = \mathbf{r}' / |\mathbf{r}'|$, normal $\mathbf{n} = \mathbf{t} \times \mathbf{z}$, and curvature $\kappa = |\mathbf{r}'|^{-3} (\mathbf{r}' \times \mathbf{r}'') \cdot \mathbf{z}$, where \mathbf{z} is a unit vector orthogonal to the plane and κ is negative or positive according to whether \mathbf{n} points *towards* or *away from* the center of curvature. The desired part shape is described by the offset

$$\mathbf{r}_d(\xi) = \mathbf{r}(\xi) + d \mathbf{n}(\xi) \quad (29.29)$$

at distance d , the tool radius, from $\mathbf{r}(\xi)$. The material that is to be removed, at depth of cut δ , lies locally to the *right* of the curve (in the direction of \mathbf{n}) as we traverse it with ξ increasing. Thus, positive curvature corresponds to a “concave” cut, and negative curvature to a “convex” cut.

The curvature-dependent feedrate is based on the material removal rates along simple linear and circular paths (Fig. 29.11), and use of the osculating circle as an approximation to the actual tool path at each point along it.

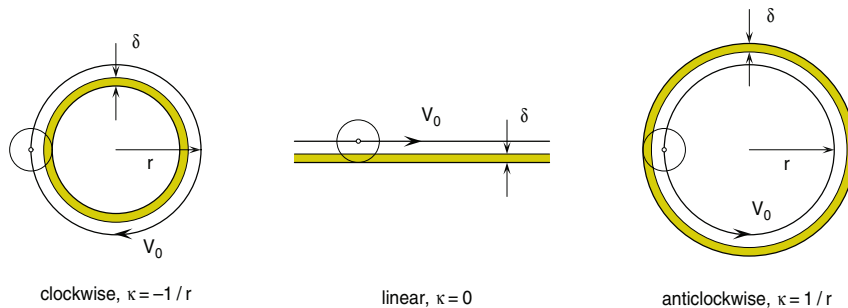


Fig. 29.11. Volume removed (shaded areas) by a cylindrical tool of radius d moving with feedrate V_0 through a depth of cut δ for: a clockwise circular path of radius r (left); a linear path (center); and an anti-clockwise circular path of radius r (right) — the material removal rate is given in terms of the path curvature κ by (29.30).

⁹ MRR variations incurred by tool path curvature are manifested by larger/smaller material chips issuing from concave/convex segments of the tool path, if all other machine parameters (feedrate, spindle speed, tool type, etc.) are fixed.

For feedrate V_0 and depth of cut δ , the volume removal rate along a linear path (assuming unit thickness) is just $V_0 \delta$. Now consider a clockwise circular path of radius r : the tool removes an annular volume $\pi(r - d + \delta)^2 - \pi(r - d)^2$ in time $2\pi r/V_0$ (see Fig. 29.11), and the rate of volume removal is therefore $V_0 \delta [1 - (d - \frac{1}{2}\delta)/r]$. Similarly, for an anti-clockwise circular path, an annular volume $\pi(r + d)^2 - \pi(r + d - \delta)^2$ is removed in time $2\pi r/V_0$, corresponding to a rate $V_0 \delta [1 + (d - \frac{1}{2}\delta)/r]$. Since κ is $-1/r$ for the clockwise circle and $1/r$ for the anti-clockwise circle (and zero for the linear path) we can express the material removal rate in all these cases as $V_0 \delta [1 + \kappa(d - \frac{1}{2}\delta)]$.

Thus, approximating a PH tool path $\mathbf{r}(\xi)$ with curvature function $\kappa(\xi)$ by its osculating circle at each point, we infer that the “curvature effect” incurs a varying volume removal rate $V_0 \delta [1 + \kappa(\xi)(d - \frac{1}{2}\delta)]$ when machining depth of cut δ with a tool of radius d . Conversely, to maintain an (approximately) *constant* volume removal rate, the feedrate V must be continuously varied in accordance with the curvature-dependent function

$$V(\xi) = \frac{V_0}{1 + \kappa(\xi)(d - \frac{1}{2}\delta)}. \quad (29.30)$$

Note that $0 < d - \frac{1}{2}\delta < d$, since $0 < \delta < 2d$ (the depth of cut cannot exceed the tool diameter). In order for the offset curve (29.29) to define a smooth shape without self-intersections (see §8.3.4), the curvature of $\mathbf{r}(\xi)$ must satisfy $\kappa(\xi) > -1/d$ for $\xi \in [0, 1]$. When this condition holds, equation (29.30) yields a finite positive feedrate along the entire curve.

The variable feedrate (29.30) deviates appreciably from the nominal value V_0 when $|\kappa(\xi)|(d - \frac{1}{2}\delta)$ is not small compared to 1 — i.e., when the (magnitude of the) radius of curvature of $\mathbf{r}(\xi)$ is not large compared to the tool radius d minus one-half of the depth of cut δ . Assuming that $\delta \ll 2d$, this occurs at tight “corners” in the tool path, of curvature magnitude comparable to $1/d$. Note also that when $\delta = 2d$, the tool is always fully immersed and expression (29.30) reduces to a constant feedrate.

29.6.2 Interpolator Algorithm

For the feedrate (29.30) and sampling interval Δt , the parameter value ξ_k that identifies the k -th reference point is determined by the condition

$$\int_0^{\xi_k} \frac{\sigma(\xi)}{V(\xi)} d\xi = k\Delta t. \quad (29.31)$$

Substituting (29.30) with $\kappa(\xi) = 2(u(\xi)v'(\xi) - u'(\xi)v(\xi))/(u^2(\xi) + v^2(\xi))$ into the above gives

$$(2d - \delta) \int_0^{\xi_k} \frac{u(\xi)v'(\xi) - u'(\xi)v(\xi)}{\sigma(\xi)} d\xi + \int_0^{\xi_k} \sigma(\xi) d\xi = kV_0\Delta t,$$

and by writing¹⁰ $\phi(\xi) = v(\xi)/u(\xi)$ and observing that $\sigma(\xi) = u^2(\xi) + v^2(\xi) = s'(\xi)$, these integrals can be resolved to obtain the equation

$$F(\xi_k) = (2d - \delta) [\tan^{-1} \phi(\xi_k) - \tan^{-1} \phi(0)] + s(\xi_k) - kV_0 \Delta t = 0. \quad (29.32)$$

This is a transcendental equation for ξ_k , that must be solved iteratively. The treatment of the arctangent function in (29.32) needs special attention. If F is to be continuous, we cannot simply take $-\pi/2 < \tan^{-1} \phi(\xi) \leq +\pi/2$ (say) for all ξ . Rather, we must add $j\pi$, where $j \in \{-1, 0, +1\}$ is chosen so as to minimize $|\tan^{-1} \phi(\xi_k) - \tan^{-1} \phi(\xi_{k-1}) + j\pi|$, to ensure the continuity of F (we assume here that $V_0 \Delta t$ is sufficiently small).

The integrand in (29.31) is positive when $\kappa(\xi) > -1/d$ for $\xi \in [0, 1]$ and F is then a *monotone* function, guaranteeing that equation (29.32) has a *unique* real root. The derivative of F can be written as

$$F'(\xi_k) = \sigma(\xi_k) [1 + \kappa(\xi_k) (d - \frac{1}{2}\delta)]$$

if, for example, Newton–Raphson iterations are used to determine its root. A good starting approximation for ξ_k is given by

$$\xi_k^{(0)} = \xi_{k-1} + \frac{V_0 \Delta t}{\sigma(\xi_{k-1}) [1 + \kappa(\xi_{k-1}) (d - \frac{1}{2}\delta)]}, \quad (29.33)$$

where ξ_{k-1} is the converged parameter value for the preceding reference point. Typically, a few iterations suffice for convergence of ξ_k to machine precision.

The total time T required to traverse the PH curve $\mathbf{r}(\xi)$ at the variable feedrate (29.30), obtained by integrating $\sigma(\xi)/V(\xi)$ from $\xi = 0$ to 1 , is

$$T = \frac{S + 2\pi(d - \frac{1}{2}\delta)R}{V_0}, \quad (29.34)$$

where the *rotation index* of $\mathbf{r}(\xi)$ is defined by

$$R = \frac{1}{2\pi} \int_0^1 \kappa(\xi) \sigma(\xi) d\xi = \frac{\tan^{-1} \phi(1) - \tan^{-1} \phi(0)}{\pi} - I_0^1 \phi(\xi).$$

The Cauchy index $I_0^1 \phi(\xi)$ of the rational function $\phi(\xi) = v(\xi)/u(\xi)$ on $[0, 1]$ is defined [235] to be the number of poles at which ϕ jumps from $-\infty$ to $+\infty$, minus the number at which it jumps from $+\infty$ to $-\infty$, as ξ increases from 0 to 1 . It can be computed by inspecting the sign of the quantity $v(\xi)/u'(\xi)$ at each odd-multiplicity root of u on $(0, 1)$. Now T is not, in general, an integer multiple N of the sampling interval Δt , but a traversal of the curve in a whole number of steps of duration Δt may be realized by modifying V_0 slightly — namely, we take

$$N_* = \left\lfloor \frac{S + 2\pi(d - \frac{1}{2}\delta)R}{V_0 \Delta t} + 0.5 \right\rfloor$$

¹⁰ Note that $2 \tan^{-1} \phi(\xi)$ is the tangent angle, relative to the x -axis, of $\mathbf{r}(\xi)$.

steps at the feedrate (29.30) with V_0 replaced by the slightly different value

$$\tilde{V}_0 = V_0 \frac{T}{N_* \Delta t}.$$

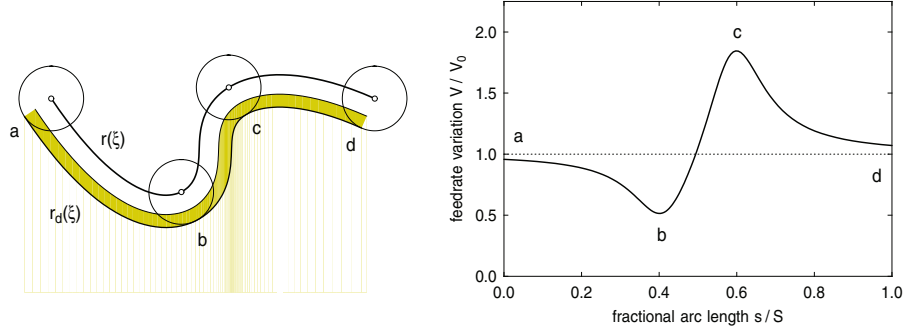


Fig. 29.12. Left: a PH curve tool path $\mathbf{r}(\xi)$ with depth of cut δ (shaded strip) above the offset $\mathbf{r}_d(\xi)$ at distance d , the tool radius. Right: the curvature-dependent feedrate (29.30) that yields an (approximately) constant material removal rate for this configuration. Corresponding tool positions and feedrate values are labelled a, b, c, d .

Figure 29.12 illustrates the feedrate function (29.30) for a single PH quintic segment — here we choose a tool radius $d = 0.1$ and depth of cut $\delta = 0.04$ (the distance between the curve endpoints is 1). The feedrate dips to $\sim 52\%$ of V_0 in the concave region, and then rapidly climbs to $\sim 185\%$ of V_0 in the convex region. Figure 29.13 shows the non-uniform sequence of reference points along this curve in accordance with the feedrate function (29.30) and a fixed Δt , as generated by the interpolator algorithm described above.

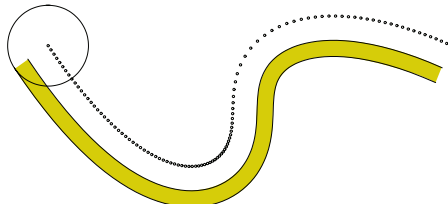


Fig. 29.13. Non-uniform distribution of reference points along the PH quintic tool path of Fig. 29.12, in accordance with the curvature-dependent feedrate (29.30).

The feedrate function (29.30) for constant material removal rate is based on a local approximation of the curve by its osculating circle, and is valid only if this approximation is sufficiently accurate over lengths comparable to the tool radius. We now derive a quantitative characterization of this condition.

An analytic plane curve can be developed as the power series (8.17) in its arc length s , measured from a given point \mathbf{r}_0 with tangent \mathbf{t}_0 and normal \mathbf{n}_0 , with κ_0 and $\dot{\kappa}_0$ being the curvature and its arc-length derivative at that point. Now the osculating circle at \mathbf{r}_0 has radius $\rho_0 = 1/\kappa_0$ and center $\mathbf{r}_0 - \rho_0\mathbf{n}_0$, and is thus described by the arc-length parameterization $\mathbf{c}(s) = \mathbf{r}_0 + \rho_0 \sin \theta \mathbf{t}_0 - \rho_0(1 - \cos \theta)\mathbf{n}_0$ with $\theta = s/\rho_0 = \kappa_0 s$. Expanding the trigonometric functions in power series gives

$$\mathbf{c}(s) = \mathbf{r}_0 + \left(s - \frac{\kappa_0^2}{6} s^3 + \dots \right) \mathbf{t}_0 - \left(\frac{\kappa_0}{2} s^2 - \frac{\kappa_0^3}{24} s^4 + \dots \right) \mathbf{n}_0, \quad (29.35)$$

and comparing (8.17) with (29.35), the discrepancy between points of equal arc length s from \mathbf{r}_0 along the given curve and its osculating circle is

$$\mathbf{c}(s) - \mathbf{r}(s) = \frac{\dot{\kappa}_0}{6} s^3 \mathbf{n}_0 + O(s^4). \quad (29.36)$$

Since the tool “samples” $\mathbf{r}(\xi)$ on a length scale $\sim d$, a rough criterion that the osculating circle approximates the curve satisfactorily at each point is that $|\mathbf{c}(s) - \mathbf{r}(s)| \ll d$ for $s \leq d$. This gives the condition

$$\frac{1}{6} |\dot{\kappa}_0| d^2 \ll 1, \quad (29.37)$$

where in terms of the polynomials $u(\xi)$, $v(\xi)$ defining the PH curve, we have

$$\dot{\kappa} = \frac{\kappa'}{\sigma} = \frac{2(u^2 + v^2)(uv'' - u''v) - 8(uu' + vv')(uv' - u'v)}{(u^2 + v^2)^4}. \quad (29.38)$$

Note, however, that at a *vertex* (a point of extremum curvature), $\dot{\kappa} = 0$ and the deviation of $\mathbf{r}(\xi)$ from its osculating circle is described by the higher-order terms in (29.36) — these are typically of much smaller magnitude.

To be confident that the feedrate function (29.30) yields an approximately constant volume removal rate along the PH curve tool path, one should check that the inequality (29.37) is satisfied along the curve. For the PH quintic in Fig. 29.12, the quantity $\frac{1}{6} |\dot{\kappa}_0| d^2$ has maximum magnitude ~ 0.2 over its entire extent, so this condition is nominally satisfied.

29.6.3 Experimental Results

The curvature-dependent feedrate (29.30) was implemented on a CNC milling machine with linear encoders and tachometers on each axis to provide position and motor speed feedback. The controller has a sampling interval of 0.01 sec., and the basic length unit (BLU), determined by the resolution of the position encoders, is 0.01 mm. The controller compares position measurements from the encoders with reference points generated by the real-time interpolator. To emphasize the influence of the interpolator (rather than the control algorithm)

on the machine performance, a simple proportional (P) controller was used in these experiments. At each sampling time, the actual feedrate along the curve is the magnitude of the velocity vector whose components are measured by the tachometers. To compare with the specified feedrate variation, we must express the latter as a function of the elapsed time t , rather than the curve parameter ξ , as in equation (29.30), or arc length s , as in Fig. 29.12. This is accomplished — for plotting purposes, at least — by noting that, with the feedrate function (29.30), t is given in terms of ξ by

$$t(\xi) = \frac{(2d - \delta) [\tan^{-1} \phi(\xi) - \tan^{-1} \phi(0)] + s(\xi)}{V_0}, \quad (29.39)$$

the arctangent function being computed according to the convention described in §29.6.2 above. In the interpolator, just two Newton–Raphson iterations from the starting approximation (29.33) were found to be more than adequate for real-time computation of the reference points to machine precision. Although (29.32) involves a transcendental function, the calculations are easily within the scope of the modest (33 MHz) CPU used to control the CNC machine.

Tachometer Measurements

Experiments were performed on the PH quintic curve shown in Fig. 29.12, the distance between the endpoints being scaled to 3600 BLU (36 mm). We take $V_0 = 4$ mm/sec., and for $(d, \delta) = (0.1, 0.04)$ we have $d - \frac{1}{2}\delta = 288$ BLU and the traversal time (29.34) is $T = 12.75$ sec. The size of the curve and the duration of the experiment were chosen to satisfy constraints on the memory available for real-time storage of the encoder and tachometer readings.

Figure 29.14 compares the actual feedrate, obtained from the tachometer readings, with the time-dependence of feedrate described by equations (29.30) and (29.39). The data shown is from a single run: a comparison of results from several independent runs suggests that the observed fluctuations are primarily measurement noise rather than physical variations. Although this case incurs

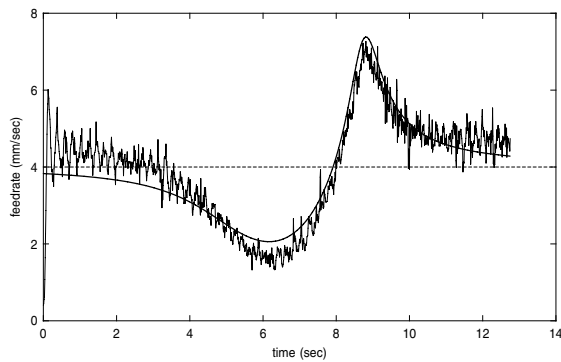


Fig. 29.14. Measured time variation of feedrate for the PH quintic in Fig. 29.12.

considerable acceleration between concave and convex parts of the curve, the controller accurately reproduces the prescribed feedrate. The *feed acceleration* $A = dV/dt$ can be obtained by applying (29.4) to (29.30) — this gives

$$A(\xi) = - \frac{V_0^2 \dot{\kappa}(\xi) (d - \frac{1}{2}\delta)}{[1 + \kappa(\xi) (d - \frac{1}{2}\delta)]^3}, \quad (29.40)$$

where $\dot{\kappa}$ is the arc-length derivative (29.38) of the curvature.

Dynamometer Measurements

To monitor machining force variations, a Kistler piezo-electric dynamometer was mounted on the machine table to measure the x and y force components while cutting 6061-aluminum. For these experiments, the PH quintic tool path shown in Fig. 29.12 was adopted, with the distance between the endpoints scaled to 2 inches (50.8 mm). The stock was initially rough-cut using a $\frac{1}{2}$ inch diameter tool, leaving a $\frac{3}{16}$ inch depth of cut ($\delta = 4.76$ mm) above the desired part shape. The part was then finish-cut using the same tool ($d = 6.35$ mm) and PH-curve CNC interpolators for both the variable feedrate (29.30) with $V_0 = 5$ mm/sec., and a constant 5 mm/sec. feedrate.

A two-flute cutter and a spindle speed of 1400 rpm were employed in these experiments, with an axial depth of cut ~ 3 mm into the aluminum stock.

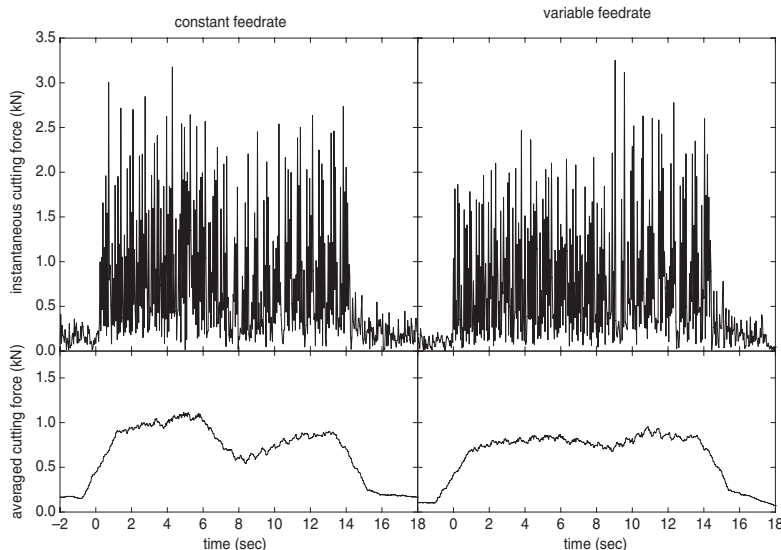


Fig. 29.15. Measured cutting force for the PH quintic in Fig. 29.12 using: (left) fixed feedrate and (right) the curvature-dependent feedrate function (29.30). The upper graphs show the instantaneous cutting-plane force, measured at a sampling frequency of 25 Hz, and the lower graphs are 1-second moving averages of the data.

Figure 29.15 shows the resultant force in the cutting plane, as measured by the dynamometer with a sampling frequency of 25 Hz. The spikes in these data represent successive engagements of the tool cutting edges with the workpiece. Since it is difficult to identify trends in the average cutting force from the raw measurements, we also present moving averages of them — obtained using a 1-second “smoothing window” — in Fig. 29.15.

In the smoothed data for the constant feedrate, an increase of the average cutting force on entering the “concave” region of the curve in Fig. 29.12, and a subsequent decrease when traversing the “convex” region, is apparent. In this case, the mean force varies by a factor of ~ 2 . In the run with the feedrate (29.30), on the other hand, these variations are almost precisely cancelled out, and systematic fluctuations of the mean force are no more than $\sim 10\%$ about the nominal value (note that the initial “rise” and final “decay” in the averaged graphs are artifacts of the smoothing process).

The two-flute cutter and 1400 rpm spindle speed correspond to a 46.7 Hz engagement frequency of the tool cutting edges with the workpiece. Since this exceeds the 25 Hz force-measurement frequency, one may be concerned that the data in Fig. 29.15 are influenced by aliasing effects. To verify that this is not so, the experiments were repeated using a 250 Hz sampling frequency. Figure 29.16 shows the averaged data (with 1-second smoothing) from these runs, excluding the initial and final 1-second intervals. The trend is identical to that seen in Fig. 29.15: the constant-feedrate run exhibits a substantial increase/decrease of mean cutting force in the concave/convex curve regions, while the variable feedrate (29.30) effectively cancels out these variations.

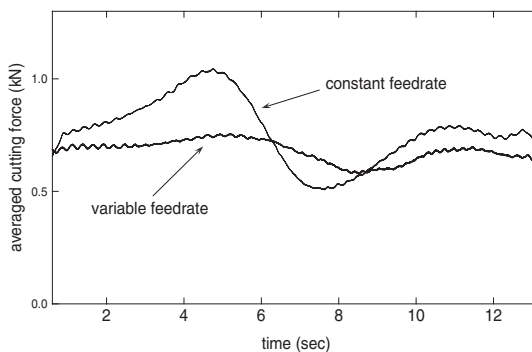


Fig. 29.16. Averaged cutting force for the curve in Fig. 29.12, based on a 250 Hz sampling frequency and 1-second smoothing interval, for both a fixed feedrate and the curvature-dependent feedrate (29.30) for a constant rate of material removal.

29.7 Contour Machining of Surfaces

The use of real-time CNC interpolators for PH curves in the context of path planning for free-form surface machining has been investigated in [194, 419]. These studies employ *contour machining*, in which the contact loci of the tool with the desired surface lie on equidistant parallel planes.

The generation of “part programs” for machining free-form surfaces is an inherently approximate process, whose accuracy and efficiency is constrained by several factors of a geometrical/kinematical nature [320]:

- (a) the surface is not, in general, exactly describable as the envelope of a finite sequence of motions by simple (cylindrical, spherical, or toroidal) tools — the need for an appreciable “stepover” between successive tool contact loci incurs *ridges* or *scallops* on the machined surface;
- (b) tool-center paths that correspond to desired geometrical properties of the surface contact loci (e.g., equidistant spacing on the surface, or relative to a coordinate axis) do not ordinarily admit exact rational representations, compatible with CAD systems;
- (c) commercial CNC machines have usually been restricted, by their software, to “simple” (linear/circular) motions: the necessity of using large numbers of such discrete motions to approximate complex paths incurs voluminous part programs and limits the “smoothness” (constancy or even variation of feedrate) with which tool paths can be executed.

Although problems (a) and (b) are inescapable in any path planning scheme, the use of PH curves (instead of linear/circular G code segments) to directly approximate the tool paths can significantly alleviate problem (c).

29.7.1 Tool Path Generation

Two approaches to surface contour machining using PH curve tool paths were described in [194]. For both methods, the loci of contact of the tool with the surface correspond to its planar sections at equidistant z heights. The first method, appropriate for machining of convex surfaces using a cylindrical tool, approximates plane sections of the surface by planar G^1 piecewise PH curves — the required tool paths are then the piecewise *rational* offsets (at distance d , the tool radius) to these loci, in the same plane. In fact, it is not necessary to explicitly construct the offset curves, since the offset displacements can be applied in the interpolator when computing the reference points.

The second method employs a spherical tool, and can be used to machine non-convex surfaces, if the least concave principal radius of curvature is larger than the tool radius d [146]. In this case, the tool center must be positioned at distance d from each point of the plane section curve, and in the direction of the *surface normal* \mathbf{n} . Since, in general, the orientation of \mathbf{n} varies along such curves, the desired tool center-line paths are *space curves* — even though the contact curves with the surface are planar. Thus, in this case, the approach is

to directly approximate the tool paths by interpolating exact point/tangent data sampled from them using *spatial* PH curves (these spatial tool paths lie on the offset surface at distance d from the desired surface).

When a spherical tool contacts a surface $\mathbf{r}(u, v)$ at some point on a planar section curve, its center is displaced from that point along the surface normal

$$\mathbf{n}(u, v) = \frac{\mathbf{r}_u \times \mathbf{r}_v}{|\mathbf{r}_u \times \mathbf{r}_v|}$$

by the tool radius d . For a plane section of the surface described by functions¹¹ $u(t), v(t)$ specifying the surface parameters in terms of an auxiliary parameter t , a vector representation of the section curve is given by $\mathbf{q}(t) = \mathbf{r}(u(t), v(t))$. If the tool is to maintain contact with the surface along the section curve, its center must trace the trajectory

$$\mathbf{q}_d(t) = \mathbf{r}(u(t), v(t)) + d \mathbf{n}(u(t), v(t)). \quad (29.41)$$

This defines a (non-planar) path on the *offset* $\mathbf{r}_d(u, v) = \mathbf{r}(u, v) + d \mathbf{n}(u, v)$ at distance d from the surface $\mathbf{r}(u, v)$ — it is generically a twisted (space) curve, since the surface normal \mathbf{n} has varying attitude along the section curve.

Discrete points on (29.41) are obtained by simply displacing points of the section curve by distance d along the surface normal \mathbf{n} . To determine tangents at these points, we differentiate (29.41) to obtain

$$\dot{\mathbf{q}}_d(t) = \dot{u}(t) [\mathbf{r}_u + d \mathbf{n}_u] + \dot{v}(t) [\mathbf{r}_v + d \mathbf{n}_v],$$

where the derivatives \mathbf{r}_u , \mathbf{r}_v and \mathbf{n}_u , \mathbf{n}_v of the surface and its normal are to be evaluated at the surface point under consideration (dots denote derivatives with respect to t). The surface normal derivatives can be written [146] as

$$\begin{aligned} \mathbf{n}_u &= \frac{\mathbf{r}_{uu} \times \mathbf{r}_v + \mathbf{r}_u \times \mathbf{r}_{uv} - \mathbf{n} \cdot (\mathbf{r}_{uu} \times \mathbf{r}_v + \mathbf{r}_u \times \mathbf{r}_{uv}) \mathbf{n}}{|\mathbf{r}_u \times \mathbf{r}_v|}, \\ \mathbf{n}_v &= \frac{\mathbf{r}_{uv} \times \mathbf{r}_v + \mathbf{r}_u \times \mathbf{r}_{vv} - \mathbf{n} \cdot (\mathbf{r}_{uv} \times \mathbf{r}_v + \mathbf{r}_u \times \mathbf{r}_{vv}) \mathbf{n}}{|\mathbf{r}_u \times \mathbf{r}_v|}. \end{aligned}$$

Note that, since \mathbf{n} is a unit vector, \mathbf{n}_u and \mathbf{n}_v are both orthogonal to it, i.e., they lie in the surface tangent plane.

If $z(u, v)$ is the z -component of $\mathbf{r}(u, v)$ the section curve has the implicit equation $F(u, v) = z(u, v) - z_* = 0$ for some fixed value z_* , and if F is to remain constant along this curve we must have $\dot{u}(t) : \dot{v}(t) = z_v : -z_u$. Thus, the unit tangent $\mathbf{t} = \dot{\mathbf{q}}_d / |\dot{\mathbf{q}}_d|$ to the tool-center trajectory (29.41) is

$$\mathbf{t} = \frac{z_v(\mathbf{r}_u + d \mathbf{n}_u) - z_u(\mathbf{r}_v + d \mathbf{n}_v)}{\sqrt{|\mathbf{r}_u + d \mathbf{n}_u|^2 z_v^2 - 2(\mathbf{r}_u + d \mathbf{n}_u) \cdot (\mathbf{r}_v + d \mathbf{n}_v) z_u z_v + |\mathbf{r}_v + d \mathbf{n}_v|^2 z_u^2}}.$$

¹¹ These functions do not, in general, admit elementary closed-form expressions (we do not need such expressions for our present purposes).

To approximate the tool paths, spatial PH quintic Hermite interpolants are fitted to consecutive pairs of points on (29.41) and corresponding tangents. If $\mathbf{p}_k, \mathbf{t}_k$ and $\mathbf{p}_{k+1}, \mathbf{t}_{k+1}$ are such data, we multiply the tangents by $|\mathbf{p}_{k+1} - \mathbf{p}_k|$ to obtain suitable derivative magnitudes for the Hermite interpolation.

The first stage in contour-machining tool path generation, whether for a cylindrical or spherical tool, is to generate approximations to the plane surface sections that satisfy a prescribed geometrical tolerance and faithfully describe their topological structure. This can be accomplished by sampling on a grid coupled with a curve-tracing scheme [194] or quadtree subdivision [387, 388]. To guarantee good approximations by Hermite interpolation, it is important to ensure that the tangents $\mathbf{t}_k, \mathbf{t}_{k+1}$ at consecutive sample points do not exhibit large variations — in practice, the threshold $\mathbf{t}_k \cdot \mathbf{t}_{k+1} \geq \frac{1}{2}$ typically yields satisfactory results (these may be the tangents of the actual section curve or the offset path (29.41), depending on the context). Figure 29.17 shows sample contouring tool paths for both a cylindrical tool and a spherical tool.

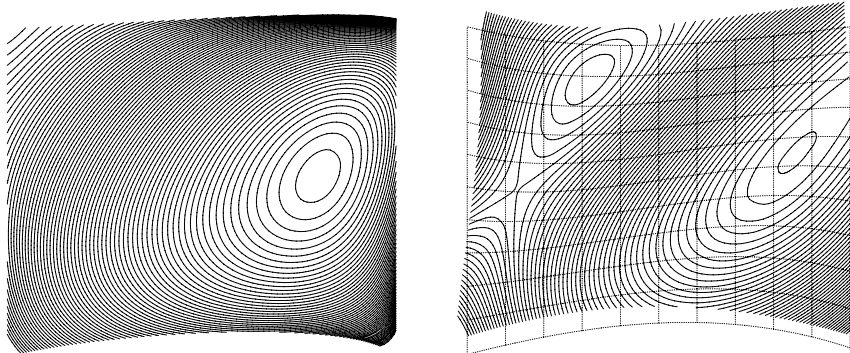


Fig. 29.17. Approximation of tool paths for contour machining by PH curves. Left: Plane sections of a convex surface for machining by a cylindrical tool (the offset by the tool radius is performed within the interpolator algorithm). Right: spatial tool paths on the offset to a non-convex surface, for machining using a spherical tool.

29.7.2 Optimal Contour Orientations

The methods described above utilize sets of planes of the form $z = k\Delta z$, for integer values k and a constant spacing Δz , to section surfaces in the context of contour machining. As seen in Fig. 29.17, however, this approach incurs widely-spaced contours and hence prominent “scallops” or ridges in regions of the machined surface where the surface normal vector \mathbf{n} is nearly aligned with the z axis — adjacent passes of a spherical tool remove tubular volumes (bounded by *canal surfaces*) from the workpiece, and the scallops arise from the intersection of these volumes. These scallops represent excess material left

by the machining process (the tool coincides precisely with the desired surface only along their planar contact locus), which must subsequently be removed by a time-consuming grinding and polishing process.

Contour machining may be performed using *any* set of equidistant parallel planes to define the tool contact loci as sections of a surface, and in [419] the problem of identifying the *optimal orientation* of such planes (that minimizes the maximum scallop height over the entire surface) was addressed. Consider the family of planes defined for integer k values by

$$\mathbf{N} \cdot \mathbf{r} = k\Delta, \quad (29.42)$$

where \mathbf{r} is a point in space, \mathbf{N} is a given unit vector (the normal to the planes), and Δ is a fixed spacing — $k\Delta$ is the distance of the plane from the origin. We use these planes to section the given surface. On a given section curve, the surface has a normal \mathbf{n} that, in general, varies with position along this curve. At each point the surface normal \mathbf{n} is typically distinct¹² from the normal \mathbf{N} of the planes, and if Δ is small compared to the magnitudes of the surface principal curvatures at that point, the quantity

$$\ell \approx \frac{\Delta}{\sqrt{1 - (\mathbf{N} \cdot \mathbf{n})^2}} \quad (29.43)$$

gives an estimate of the distance between the k^{th} and $(k+1)^{\text{th}}$ section curves, in the plane spanned by \mathbf{N} and \mathbf{n} . For example, consider a sphere of radius R sectioned by equidistant planes parallel to the equator with $\Delta \ll R$. At the equator, the spacing between section curves is $\ell \approx \Delta$ because \mathbf{N} and \mathbf{n} are orthogonal, but ℓ increases monotonically without bound as we approach the north pole and \mathbf{n} becomes more nearly parallel with \mathbf{N} .

In contour machining a surface with a spherical tool, the quantity ℓ — the (variable) “step-over” between toolpaths — is a key influence on the quality of the machined surface, since (for a fixed tool radius d) it determines the local scallop height. In the case of a plane surface machined using linear paths with equidistant spacing ℓ ($< 2d$), the scallop height is given [82, 320] by

$$h = d - \sqrt{d^2 - (\frac{1}{2}\ell)^2} \quad \left(\approx \frac{\ell^2}{8d} \text{ if } \ell \ll 2d \right).$$

For a general free-form surface, h is a rather complicated function of the local surface geometry, instantaneous tool-path direction on the surface, etc., that does not admit a simple closed-form expression.¹³ Nevertheless, it is obvious that h will always be a monotone-increasing function of ℓ . Hence, for a given surface, tool radius d , and contour spacing Δ , we can minimize the greatest scallop height over the machined surface by choosing an orientation \mathbf{N} for the

¹² In fact, the coincidence of \mathbf{n} and \mathbf{N} identifies a *singular point* of the section curve.

¹³ See, however, [276] for the case of cylindrical and spherical surfaces.

sectioning planes that is “as far as possible” from parallelism with the normal \mathbf{n} over the entire surface, so as to minimize (29.43).

To accomplish this, we must compute the *Gauss map* or “spherical image” (see §8.5.7) of the surface. For a surface $\mathbf{r}(u, v)$ with $\mathbf{r}_u \times \mathbf{r}_v \neq \mathbf{0}$ for $(u, v) \in [0, 1] \times [0, 1]$ the Gauss map associates, with each point of $\mathbf{r}(u, v)$, the point of the unit sphere \mathcal{S} in \mathbb{R}^3 identified by the surface normal \mathbf{n} . The Gauss map of a doubly-curved surface occupies a region $\Omega \subseteq \mathcal{S}$, but the correspondence between points of $\mathbf{r}(u, v)$ and Ω is not necessarily one-to-one, since distinct surface points may have identical normals. To determine the boundary $\partial\Omega$ of the Gauss map, we must consider the variation of \mathbf{n} along the boundary of the surface, and also along the singular loci of \mathbf{n} where the Gauss map “folds” [25] on itself — these are the *parabolic lines* of the surface, i.e., loci of zero Gaussian curvature separating “elliptic” regions of positive Gaussian curvature from “hyperbolic” regions of negative Gaussian curvature (see §8.5.7).

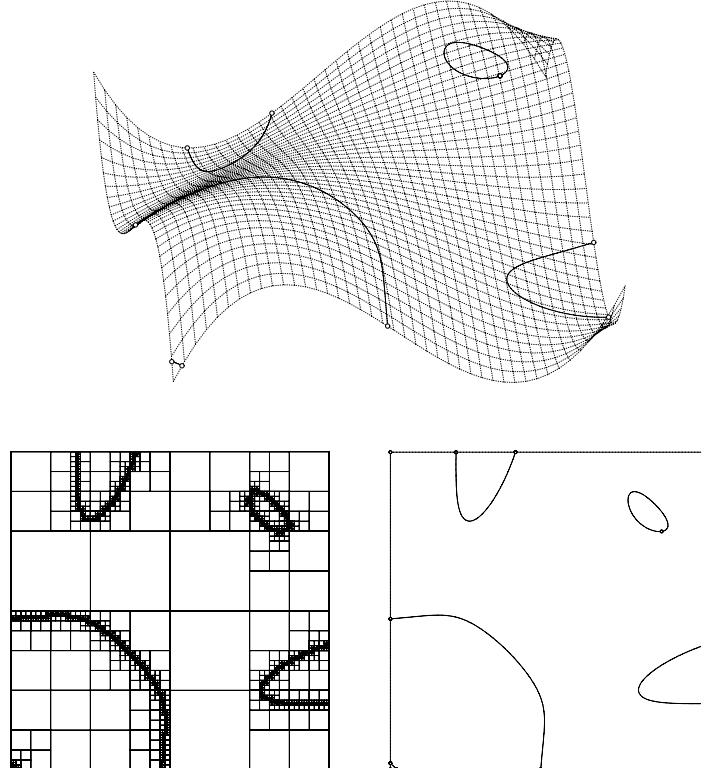


Fig. 29.18. Upper: the parabolic lines on a bicubic surface, comprising one closed loop and four loci terminating on the patch boundaries. Lower: quadtree localization (left) and approximation (right) of parabolic lines in the (u, v) parameter domain.

A systematic method to compute the Gauss map of a Bézier surface $\mathbf{r}(u, v)$ was presented in [418]. The parabolic lines are formulated as the zero-set of a bivariate polynomial $k(u, v)$ expressed in tensor-product Bernstein form¹⁴ on $[0, 1] \times [0, 1]$ and a quadtree subdivision [387, 388] of this domain, guided by the Bernstein coefficient signs, is then used to approximate these loci to any desired accuracy. The imaging of the Gauss map by a *stereographic projection* to the plane is also discussed in [418] — points $\mathbf{n} = (n_x, n_y, n_z) \in \mathcal{S}$ on the sphere are mapped to points $\mathbf{p} = (x, y)$ in the plane according to

$$(x, y) = \left(\frac{n_x}{1 - n_z}, \frac{n_y}{1 - n_z} \right), \quad (29.44)$$

for which the inverse map is given by

$$(n_x, n_y, n_z) = \left(\frac{2x}{x^2 + y^2 + 1}, \frac{2y}{x^2 + y^2 + 1}, \frac{x^2 + y^2 - 1}{x^2 + y^2 + 1} \right). \quad (29.45)$$

Figure 29.18 illustrates a representative computation of the parabolic lines on a bicubic surface patch, while Fig. 29.19 shows the computed Gauss map for this surface with its stereographic projection — see [418] for complete details.

As can be seen in Fig. 29.19, the parabolic lines and curves that describe the variation of the normal \mathbf{n} along the surface boundary often form a rather intricate tangle — a *boundary extraction algorithm* [418] must be invoked to determine the subset that constitutes the true Gauss map boundary.

In the context of finding the optimal orientation \mathbf{N} for contouring planes, we do not distinguish between a surface normal \mathbf{n} and its negation $-\mathbf{n}$, so we must consider a “symmetrized” version of the Gauss map — for each normal \mathbf{n} of an oriented surface, the symmetrized Gauss map also contains the antipodal point $-\mathbf{n}$ of \mathcal{S} . The stereographic projection of a symmetrized Gauss map has a special structure: for each \mathbf{n} , the antipodal normal $-\mathbf{n}$ has the image point

$$(x', y') = \left(\frac{-n_x}{1 + n_z}, \frac{-n_y}{1 + n_z} \right),$$

and hence the points (x, y) and (x', y') satisfy

$$(x', y') = \left(\frac{-x}{x^2 + y^2}, \frac{-y}{x^2 + y^2} \right).$$

This relation has the form (9.20) of an *inversion* in a circle with center at the origin, but R^2 is replaced by -1 , i.e., (x, y) and (x', y') lie on opposite sides of a line through the origin, and the product of their distances from the origin is unity (this is called [397] an *elliptic* inversion). Thus, to compute the stereographic projection of the symmetrized Gauss map, it suffices to consider the northern or southern hemisphere of \mathcal{S} only, the image of the other hemisphere being obtained by inversion in the unit circle — see Fig. 29.20.

¹⁴ This is the numerator of the expression $LN - M^2$ in the coefficients (8.84) of the *second fundamental form*. For a bicubic patch, it is degree 12 in each of u, v [418].

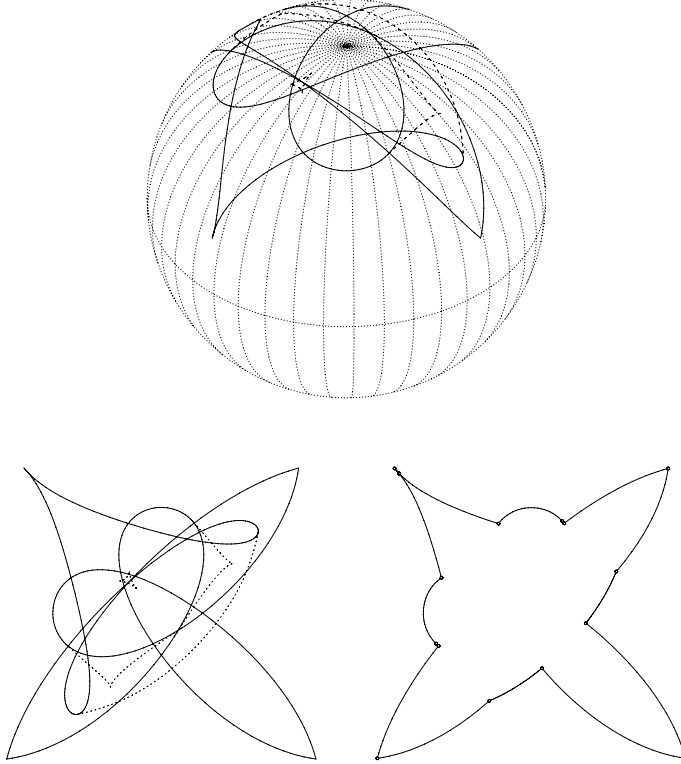


Fig. 29.19. Upper: images of parabolic lines (dotted) and patch boundaries (solid) on the Gauss sphere, for the surface in Fig. 29.18. Lower: stereographic projection of these curves onto the plane, and the Gauss map boundary extracted from them.

Now if Ω_s is the symmetrized Gauss map of the surface $\mathbf{r}(u, v)$, the optimal orientation \mathbf{N} of the contouring planes corresponds to the center of the largest circle in its *complement*, $\Omega_c = \mathcal{S} - \Omega_s$. To determine \mathbf{N} , we may compute the *medial axis transform* (see §24.2) of the domain Ω_c . The medial axis of a planar domain is the locus of centers of maximal circles (touching the boundary in at least two points) that can be inscribed within the domain. The medial axis transform (MAT) incorporates a radius function superposed upon the medial axis, specifying the size of the maximal circles centered on it.

By mapping Ω_c from the sphere \mathcal{S} to the plane through the stereographic projection (29.44), standard algorithms [83, 87, 301, 375, 408] for computing the MATs of planar domains can be applied, and the inverse map (29.45) can be used to transform the results back to \mathcal{S} . However, care must be exercised in identifying \mathbf{N} from a projection of Ω_c to the plane [419]. A circle $\mathbf{c} \cdot \mathbf{n} = \cos \alpha$ on \mathcal{S} with center $\mathbf{c} = (c_x, c_y, c_z)$ and angular radius α ($0 \leq \alpha \leq \frac{1}{2}\pi$) is mapped by (29.44) to a circle in the plane with center and radius given by

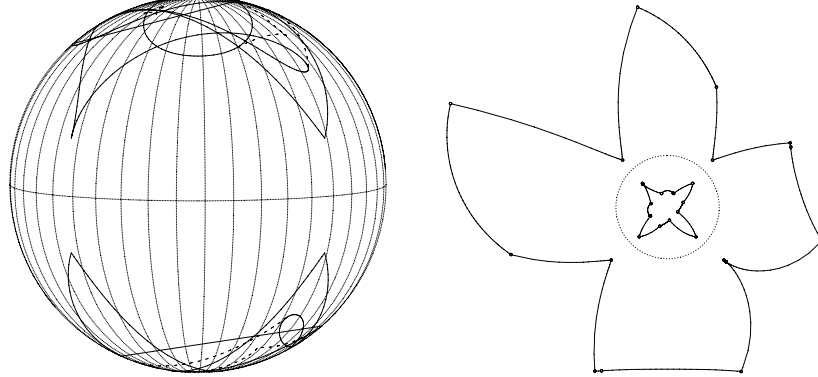


Fig. 29.20. Left: the “symmetrized” Gauss map for the surface in Fig. 29.18 — each point of the ordinary Gauss map is augmented by its antipodal image point. (b) Stereographic projection of the symmetrized Gauss map boundary onto the plane — note that the projections of the northern and southern hemispheres are images of each other under the complex inversion (9.20) in the unit circle.

$$\mathbf{p}_0 = (x_0, y_0) = \left(\frac{c_x}{\cos \alpha - c_z}, \frac{c_y}{\cos \alpha - c_z} \right) \quad \text{and} \quad R = \left| \frac{\sin \alpha}{\cos \alpha - c_z} \right|.$$

We note that: (a) \mathbf{p}_0 is not simply the image of \mathbf{c} under the map (29.44), and it becomes a “point at infinity” when $\cos \alpha = c_z$ (in which case the circle on \mathcal{S} passes through the north pole, and its image becomes a straight line); and (b) R is not a monotone-increasing function of α .

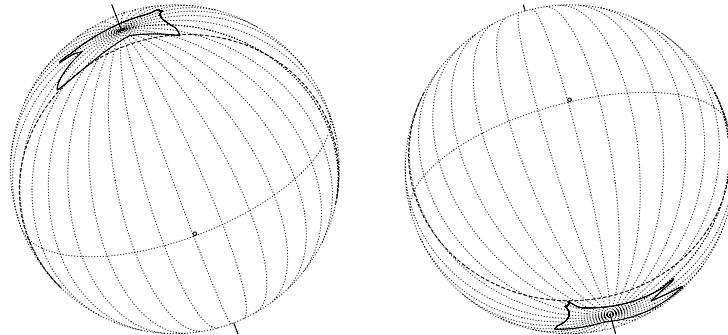


Fig. 29.21. Maximal circle in the complement of the symmetrized Gauss map for the surface in Fig. 29.22: its center identifies the optimal contour orientation \mathbf{N} . The circle touches the north and south “polar caps” of the symmetrized Gauss map.

Consider a circle in the plane with radius R and center at distance ρ from the origin. Choosing coordinates so that $(x_0, y_0) = (\rho, 0)$ it can be shown [419]

that this is the image under (29.44) of the circle on \mathcal{S} with angular radius α and center $\mathbf{c} = (\sin \theta, 0, \cos \theta)$ given by

$$\tan \alpha = \frac{2R}{\rho^2 - R^2 + 1} \quad \text{and} \quad \tan \theta = \frac{2\rho}{\rho^2 - R^2 + 1}.$$

Consequently, to identify the optimal contour orientation \mathbf{N} with the center of the circle of largest angular extent α in $\Omega_c \in \mathcal{S}$, we must find where the greatest value of the above expression for $\tan \alpha$ occurs along the edges of the medial axis of the stereographic projection of Ω_c onto the plane. This can be reduced to a polynomial root-finding problem — see [419] for further details. The determination of the optimal orientation \mathbf{N} for the section planes as the center of the largest circle within the complement of the symmetrized Gauss map is illustrated in Fig. 29.21 — it is nearly orthogonal to $(0, 0, 1)$.

Figure 29.22 illustrates contour-machining tool paths for a bicubic Bézier surface patch, corresponding to the nominal orientation $(0, 0, 1)$ of the contour planes, and the optimal orientation \mathbf{N} determined by the above method — to ensure a fair comparison, the spacing Δ of the contouring planes is adjusted so as to give an approximately equal total tool path length in these two cases.

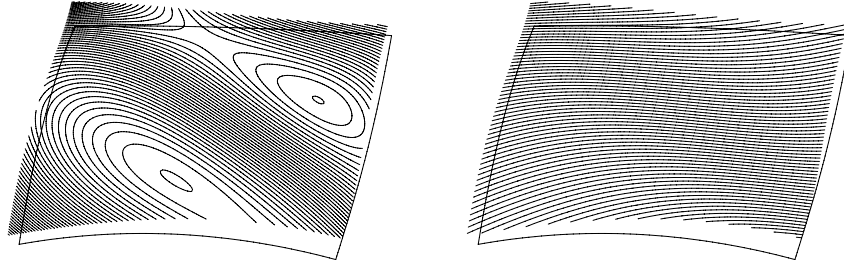


Fig. 29.22. Left: tool paths for contour machining of a bicubic surface with $(0, 0, 1)$ as the nominal orientation for the normal to the sectioning planes. Right: tool paths for the optimal orientation \mathbf{N} of the section planes, minimizing the maximum value of the dot product $\mathbf{N} \cdot \mathbf{n}$ over all the surface normals \mathbf{n} . The spacing Δ of the section planes is adjusted to give approximately equal total path lengths in the two cases.

Figure 29.23 illustrates the surfaces machined in wax, using the tool paths shown¹⁵ in Fig. 29.22. The difference between the quality of the machined surfaces is quite dramatic, with the optimal contouring paths yielding a much smoother finish with less prominent “scallops” incurred by successive passes of the spherical tool. This specific example is perhaps a little exaggerated, since it is evident *a priori* that $\mathbf{N} = (0, 0, 1)$ is a poor choice for the orientation of the section planes: there are surface points where it coincides with the normal

¹⁵ For clarity, Fig. 29.22 shows only the paths on alternate contouring planes used to machine the surfaces in Fig. 29.23, since the paths are rather dense.

n. For any given surface, it may often be possible to “intuitively” identify a better contouring orientation — without detailed calculations — than to rely on an arbitrary choice, such as $(0, 0, 1)$. Nevertheless, to minimize the expense of subsequent grinding and polishing processes (especially when many parts are to be manufactured), using the above algorithm to determine the optimum contouring orientation, in the sense of maximizing the smallest angle between \mathbf{N} and \mathbf{n} over the entire surface, can be well worthwhile.



Fig. 29.23. The bicubic surface machined using the two sets of tool paths shown in Fig. 29.22, corresponding to: section planes with the normal $(0, 0, 1)$ on the left, and the optimal normal \mathbf{N} identified on the unit sphere in Fig. 29.21 on the right.

In approximating the tool paths for surface contour machining by spatial PH curves, it is more convenient to always use constant- z planes, and obtain different relative contour orientations by rotating the surface. This approach requires the ability to impose compensating rotations on the PH space curve tool paths, which can be easily achieved by the rotation-invariance property of the quaternion formulation for spatial PH curves (see Chap. 22).

The optimal contour-orientation algorithm has useful applications in areas other than CNC machining. In *rapid prototyping* or “layered manufacturing” processes, for example, three-dimensional physical models are fabricated by bonding, curing, fusing, or depositing material in layers of finite thickness. The “stepped” nature of the fabricated model surface is especially pronounced in regions where the surface normal is nearly parallel to the build direction, and the use of optimal contouring orientations can be advantageous in minimizing such artifacts. Similar considerations apply in constructing three-dimensional computer models of physical objects from planar “slice” data, as obtained by a laser rangefinder, coordinate measuring machine, or medical imaging system. Such processes are collectively known as *reverse engineering*.

30

Rotation-minimizing Frames

There is more than one way to frame a curve.

R. L. Bishop [44]

30.1 Introduction and Motivation

To describe a general spatial motion of a rigid object, we must specify both its *position* and its *orientation* at each instant in time. The positional component amounts to specifying a space curve, parameterized by time, to be executed by some chosen point — e.g., the center of mass. In many applications, however, the orientational component is not precisely specified or constrained *a priori*. Instead, an algorithm must be formulated to determine a “natural” variation of orientation along the specified path, by aligning the body’s principal axes with an orthonormal frame defined at each point along the path.

The orthonormal frame most commonly associated with a space curve, the *Frenet frame* (see §8.4), is often not a suitable choice in this context. Although it is natural to take the tangent \mathbf{t} as one member of the orthonormal frame, the other Frenet frame members — the principal normal \mathbf{p} and binormal \mathbf{b} — may often appear to execute “unnecessary rotation” about the tangent in the context of rigid-body motion planning (see Fig. 30.1). This is a consequence of the fact that these vectors continuously re-orient themselves in the normal plane, so that \mathbf{p} points toward the center of curvature (see Fig. 30.2).

Another problem with using the Frenet frame to define orientation along a spatial path arises from the fact that \mathbf{p} and \mathbf{b} are *undefined* at the inflections of a space curve — where $\mathbf{r}' \times \mathbf{r}'' = \mathbf{0}$, and hence the curvature κ vanishes (see §8.4.3). Although it is possible to specify the principal normal and binormal at inflections by taking appropriate limits, great care is required to avoid sudden reversals of them on passing through the inflection point.

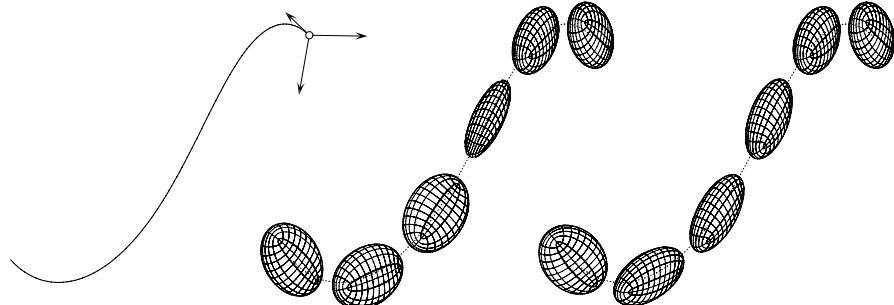


Fig. 30.1. A space curve (left) defining the center-line path for the motion of an ellipsoid (the initial orientation is specified by the Frenet frame at the start point). Sample orientations of the ellipsoid are shown along the path, in accordance with the Frenet frame (center), and rotation-minimizing frame (right). Careful comparison reveals that the Frenet frame motion incurs “unnecessary” rotation in the normal plane — a comparison of the total rotation rates is provided in Fig. 30.5 below.

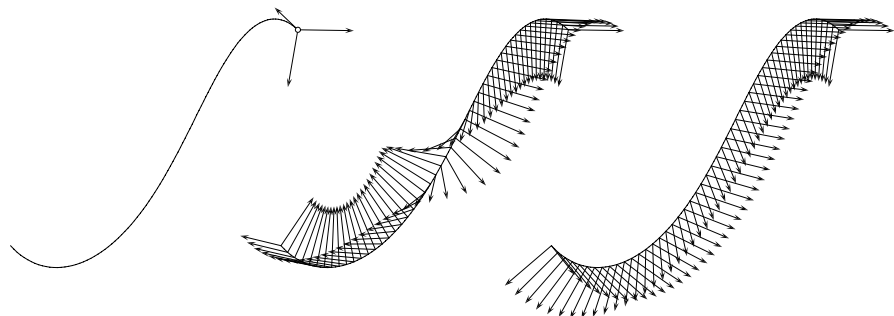


Fig. 30.2. Variation of Frenet frame (center) and rotation-minimizing frame (right) for the example in Fig. 30.1. These two frames have the same initial orientation, shown on the left. For clarity, the basis vector defined by the tangent (the same for both frames) is omitted: only the basis vectors in the curve normal plane are shown.

For a smooth space curve, it is possible to identify vectors \mathbf{u} and \mathbf{v} in the normal plane that comprise an orthonormal frame in conjunction with \mathbf{t} , and exhibit the “least possible” amount of rotation in that plane (consistent with the twisted nature of the curve) as we traverse the curve. Such vectors $(\mathbf{t}, \mathbf{u}, \mathbf{v})$ form a *rotation-minimizing frame* [283] on the given space curve. The vectors \mathbf{u}, \mathbf{v} can be defined in terms of \mathbf{p}, \mathbf{b} by rotating the latter about \mathbf{t} through an angle θ with a known dependence on position along the curve.

Determining the angular displacement θ of the rotation-minimizing frame (RMF) relative to the Frenet frame involves an integration of the curve *torsion* with respect to its arc length. For general polynomial or rational curves this requires numerical quadrature, but for spatial PH curves the integrand is a *rational* function of the curve parameter, and admits closed-form integration

by a partial fraction expansion (see §3.5). Thus, the spatial PH curves permit essentially *exact* RMF computations — a property that is useful in animation, robotics, motion planning, and other applications in which the orientation of a rigid body must be specified as its center of mass executes a given trajectory. Aligning the body’s principal axes with the RMF at each point offers a natural solution to this problem, that avoids the “unnecessary” normal–plane rotation and inflectional indeterminacies of the Frenet frame.

Another application in which rotation–minimizing frames are useful is the construction of “tube–like” surfaces, swept out by the motion of a plane profile curve as a specified reference point in its plane traverses a given sweep curve in \mathbb{R}^3 [283]. It is assumed that, during the sweep process, the plane of the profile coincides at each instant with the local normal plane of the sweep curve — i.e., the sweep curve tangent defines the normal to the plane of the profile curve. Again, using the Frenet frame to orient the profile curve within the sweep curve normal plane can yield a surface with an unreasonable “twisted” appearance (see Fig. 30.3). Using the RMF to define the profile curve orientation will invariably give surfaces of better shape. Even when the profile curve is just a circle, and thus apparently immune to orientational concerns, the RMF may be preferred to ensure better parameterization of the swept surface [88].

Finally, the RMF also plays an important role in defining an energy integral for space curves (see §30.5 below). Among all adapted frames for a space curve of prescribed shape, the RMF identifies the minimum possible elastic energy.

This chapter discusses the computation of RMFs for spatial PH curves. We begin in §30.2 with a review of the Frenet frame, and the Darboux vector that describes its rotation rate. The Frenet frame is just one example of the family of *adapted frames* on a space curve, for which one member is the curve tangent t , and the other two span the curve normal plane. It is shown in §30.4 that,

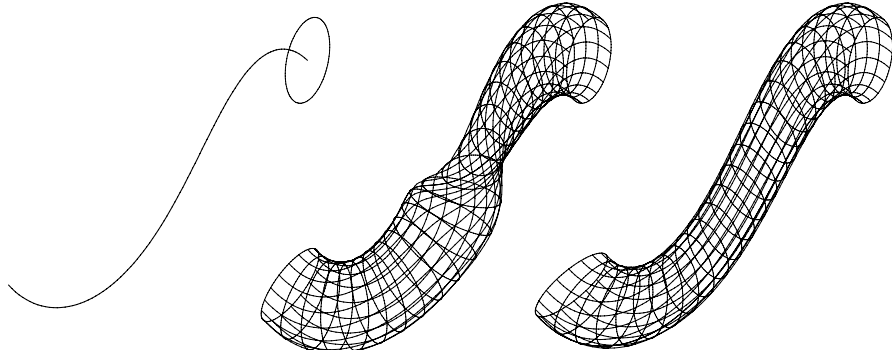


Fig. 30.3. A “tubular” surface swept by an ellipse whose center moves along a given space curve: at each instant, the ellipse is constrained to lie in the curve normal plane. Left: the given “spine” curve and initial orientation of the ellipse. Center: the surface obtained using the Frenet frame to orient the ellipse in the normal plane. Right: the surface generated using the rotation–minimizing frame to orient the ellipse.

among all adapted frames, the *rotation-minimizing frames* are the ones with no angular velocity component in the direction of the tangent \mathbf{t} . Furthermore, as shown in §30.5, RMFs specify the least possible value for the *elastic energy* among all adapted frames on a given space curve. Exact RMF computations for PH curves, by means of rational function integration, are discussed in §30.6. This typically incurs transcendental (logarithmic) terms, since the integral of a rational function is not generically rational. As an alternative, §30.7 presents a piecewise-rational RMF approximation scheme that yields high accuracy at low computational cost. Finally, the application of RMFs to the problem of rational parameterization of canal surfaces is treated in §30.8.

30.2 Adapted Frames on Space Curves

We recall from §8.4 that, at (almost) every point of a regular space curve $\mathbf{r}(\xi)$ — satisfying $\mathbf{r}'(\xi) \neq \mathbf{0}$ for all ξ — the *Frenet frame* specifies an orthonormal basis for \mathbb{R}^3 in terms of the local curve geometry. It comprises the tangent \mathbf{t} , principal normal \mathbf{p} , and binormal \mathbf{b} , defined by

$$\mathbf{t} = \frac{\mathbf{r}'}{|\mathbf{r}'|}, \quad \mathbf{p} = \frac{\mathbf{r}' \times \mathbf{r}''}{|\mathbf{r}' \times \mathbf{r}''|} \times \mathbf{t}, \quad \mathbf{b} = \mathbf{t} \times \mathbf{p}. \quad (30.1)$$

For polynomial or rational curves, the unit vectors (30.1) do not, in general, depend rationally¹ on the curve parameter ξ . For a regular curve, the tangent is defined at every point, but the principal normal and binormal are undefined at *inflection* points, where $\mathbf{r}''(\xi)$ becomes parallel to $\mathbf{r}'(\xi)$ or vanishes. In fact, \mathbf{p} and \mathbf{b} may experience sudden reversals on passing through inflections. At points where $\mathbf{r}' \times \mathbf{r}'' \neq \mathbf{0}$, the *osculating* plane is spanned by the vectors (\mathbf{t}, \mathbf{p}) , the *normal* plane by (\mathbf{p}, \mathbf{b}) , and the *rectifying* plane by (\mathbf{b}, \mathbf{t}) .

As noted in §8.4, the variation of the Frenet frame with curve arc length

$$s(\xi) = \int_0^\xi \sigma(t) dt,$$

where $\sigma(t) = |\mathbf{r}'(t)|$ is the parametric speed, is described by the equations

$$\frac{d\mathbf{t}}{ds} = \mathbf{d} \times \mathbf{t}, \quad \frac{d\mathbf{p}}{ds} = \mathbf{d} \times \mathbf{p}, \quad \frac{d\mathbf{b}}{ds} = \mathbf{d} \times \mathbf{b}, \quad (30.2)$$

where the *Darboux vector*

$$\mathbf{d} = \kappa \mathbf{b} + \tau \mathbf{t} \quad (30.3)$$

is defined in terms of the curvature and torsion, given by

$$\kappa = \frac{|\mathbf{r}' \times \mathbf{r}''|}{|\mathbf{r}'|^3} \quad \text{and} \quad \tau = \frac{(\mathbf{r}' \times \mathbf{r}'') \cdot \mathbf{r}'''}{|\mathbf{r}' \times \mathbf{r}''|^2}. \quad (30.4)$$

¹ A special class of curves with rational Frenet frames is discussed in Chap. 23.

These quantities are invariant under any (regular) curve re-parameterization. Equations (30.2) characterize the instantaneous variation of the Frenet frame as a rotation about the vector \mathbf{d} , at a rate given by the “total curvature”

$$\omega = |\mathbf{d}| = \sqrt{\kappa^2 + \tau^2}.$$

The Frenet frame is just one example of an *adapted frame* on a space curve $\mathbf{r}(\xi)$, i.e., a right-handed orthonormal system of vectors $\mathbf{t}(\xi)$, $\mathbf{u}(\xi)$, $\mathbf{v}(\xi)$ where $\mathbf{t}(\xi) = \mathbf{r}'(\xi)/|\mathbf{r}'(\xi)|$ is the tangent. There are infinitely many choices [44] for the unit vectors $\mathbf{u}(\xi)$, $\mathbf{v}(\xi)$ compatible with the requirement $\mathbf{t}(\xi) = \mathbf{u}(\xi) \times \mathbf{v}(\xi)$, and they are related to each other by rotations in the curve normal plane.

We use primes to denote derivatives with respect to the curve parameter ξ and dots for derivatives with respect to arc length s , connected by

$$\frac{d}{ds} = \frac{1}{\sigma(\xi)} \frac{d}{d\xi}.$$

Now the components of the frame vectors \mathbf{t} , \mathbf{u} , \mathbf{v} define an orthogonal matrix

$$\mathbf{A} = \begin{bmatrix} t_x & u_x & v_x \\ t_y & u_y & v_y \\ t_z & u_z & v_z \end{bmatrix},$$

and since these vectors form a basis for \mathbb{R}^3 , the arc-length derivative of \mathbf{A} must be expressible in the form

$$\dot{\mathbf{A}} = \mathbf{A} \mathbf{C}.$$

From the relations $|\mathbf{t}| = |\mathbf{u}| = |\mathbf{v}| = 1$ and $\mathbf{t} \cdot \mathbf{u} = \mathbf{u} \cdot \mathbf{v} = \mathbf{v} \cdot \mathbf{t} = 0$, one can easily see that the *Cartan connection matrix* has the skew-symmetric form

$$\mathbf{C} = \begin{bmatrix} 0 & -\gamma & \beta \\ \gamma & 0 & -\alpha \\ -\beta & \alpha & 0 \end{bmatrix},$$

where $\alpha = \dot{\mathbf{u}} \cdot \mathbf{v}$, $\beta = \dot{\mathbf{v}} \cdot \mathbf{t}$, $\gamma = \dot{\mathbf{t}} \cdot \mathbf{u}$. Equivalently, we may write

$$\dot{\mathbf{t}} = \boldsymbol{\omega} \times \mathbf{t}, \quad \dot{\mathbf{u}} = \boldsymbol{\omega} \times \mathbf{u}, \quad \dot{\mathbf{v}} = \boldsymbol{\omega} \times \mathbf{v}, \quad (30.5)$$

where the angular velocity vector $\boldsymbol{\omega}$ for the frame $(\mathbf{t}, \mathbf{u}, \mathbf{v})$ is defined by

$$\boldsymbol{\omega} = \alpha \mathbf{t} + \beta \mathbf{u} + \gamma \mathbf{v}. \quad (30.6)$$

For the Frenet frame, we have $\mathbf{u} = \mathbf{p}$, $\mathbf{v} = \mathbf{b}$ and $(\alpha, \beta, \gamma) = (\tau, 0, \kappa)$.

30.3 Euler–Rodrigues Frame for PH Curves

A *rational* adapted frame for spatial PH curves, the “Euler–Rodrigues frame” or ERF, was defined by Choi and Han [85] through the expressions

$$\mathbf{e}_1(\xi) = \frac{\mathcal{A}(\xi) \mathbf{i} \mathcal{A}^*(\xi)}{|\mathcal{A}(\xi)|^2}, \quad \mathbf{e}_2(\xi) = \frac{\mathcal{A}(\xi) \mathbf{j} \mathcal{A}^*(\xi)}{|\mathcal{A}(\xi)|^2}, \quad \mathbf{e}_3(\xi) = \frac{\mathcal{A}(\xi) \mathbf{k} \mathcal{A}^*(\xi)}{|\mathcal{A}(\xi)|^2}.$$

The existence of such rational frames on spatial PH curves was first noted by Jüttler [264]. Writing these three vectors explicitly in terms of the components $u(t)$, $v(t)$, $p(t)$, $q(t)$ of the quaternion polynomial (22.1) yields

$$\begin{aligned}\mathbf{e}_1 &= \frac{(u^2 + v^2 - p^2 - q^2) \mathbf{i} + 2(uq + vp) \mathbf{j} + 2(vq - up) \mathbf{k}}{u^2 + v^2 + p^2 + q^2}, \\ \mathbf{e}_2 &= \frac{2(vp - uq) \mathbf{i} + (u^2 - v^2 + p^2 - q^2) \mathbf{j} + 2(uv + pq) \mathbf{k}}{u^2 + v^2 + p^2 + q^2}, \\ \mathbf{e}_3 &= \frac{2(up + vq) \mathbf{i} + 2(pq - uv) \mathbf{j} + (u^2 - v^2 - p^2 + q^2) \mathbf{k}}{u^2 + v^2 + p^2 + q^2}.\end{aligned}$$

Taking the components of \mathbf{e}_1 , \mathbf{e}_2 , \mathbf{e}_3 as columns of a 3×3 matrix, we obtain

$$\frac{1}{u^2 + v^2 + p^2 + q^2} \begin{bmatrix} u^2 + v^2 - p^2 - q^2 & 2(vp - uq) & 2(up + vq) \\ 2(uq + vp) & u^2 - v^2 + p^2 - q^2 & 2(pq - uv) \\ 2(vq - up) & 2(uv + pq) & u^2 - v^2 - p^2 + q^2 \end{bmatrix}$$

and this is an orthogonal matrix of determinant 1, i.e., a member of the group $\text{SO}(3)$ that describes rotations in \mathbb{R}^3 . In fact, it can be shown that any member of the group $\text{SO}(3)$ can be written in the above form, with appropriate choices of u , v , p , q — the *Euler–Rodrigues parameters* [20, 55] of a spatial rotation.

By the choice of \mathbf{i} as a distinguished quaternion basis element in (22.2), the vector \mathbf{e}_1 is just the tangent to the spatial PH curve $\mathbf{r}(\xi)$ defined by integrating this hodograph, while \mathbf{e}_2 and \mathbf{e}_3 span the curve normal plane at each point. Unlike the Frenet frame, the ERF is uniquely defined at each point of a regular spatial PH curve (including inflections), and varies smoothly along the curve. Furthermore, the ERF components are *rational* functions, of degree $n - 1$ for a PH curve of degree n . Actually, the ERF is not uniquely defined for a given PH curve, because the quaternion representation of a PH curve is not unique (see §22.3). However, this ambiguity is immaterial, since any two ERFs always maintain a constant angular difference along the PH curve.

Choi and Han [85] characterized the angular velocity of the ERF relative to a rotation–minimizing frame, for spatial PH cubics and quintics. They showed that for the PH cubics, ERFs maintain a constant angle relative to the Frenet frame, and the ERF coincides with an RMF only if the cubic is planar,² i.e.,

² Han [225] has recently shown that no rational RMFs exist (regardless of whether or not they are also ERFs) on any spatial cubic.

a Tschirnhaus cubic (see Chap. 18). The planarity condition for coincidence of ERFs and RMFs extends to PH quintics, and the simplest non-planar PH curves with ERFs that can be RMFs are thus of degree 7. A characterization of such PH curves with rational RMFs is given in [85] — but there are currently no algorithms that facilitate intuitive geometrical constructions of them.

30.4 Rotation-minimizing Frames

For any adapted frame $(\mathbf{t}, \mathbf{u}, \mathbf{v})$ the angular velocity component $\alpha \mathbf{t}$ in (30.6) defines an instantaneous rotation of \mathbf{u} and \mathbf{v} in the normal plane of the curve. This component is not essential to the definition of an adapted frame: in fact, it is always possible to define an adapted frame that omits this “unnecessary” component. Such a frame, characterized by the property that $\alpha \equiv 0$, is called a *rotation-minimizing frame* (RMF). The angular velocity vector for an RMF can be written as

$$\boldsymbol{\omega} = \beta \mathbf{u} + \gamma \mathbf{v} = -(\dot{\mathbf{t}} \cdot \mathbf{v}) \mathbf{u} + (\dot{\mathbf{t}} \cdot \mathbf{u}) \mathbf{v}, \quad (30.7)$$

where we observe that $\dot{\mathbf{v}} \cdot \mathbf{t} = -\dot{\mathbf{t}} \cdot \mathbf{v}$, since $\mathbf{v} \cdot \mathbf{t} = 0$. Now $\dot{\mathbf{t}}$ lies in the normal plane spanned by \mathbf{u} and \mathbf{v} (since $|\dot{\mathbf{t}}| = 1$), and we can thus write $\dot{\mathbf{t}} = \mu \mathbf{u} + \nu \mathbf{v}$. By substituting into (30.7), we find that $\boldsymbol{\omega} = -\nu \mathbf{u} + \mu \mathbf{v}$ — i.e., for an RMF, $\boldsymbol{\omega}$ is just a rotation of \mathbf{t} by $\frac{1}{2}\pi$ in the normal plane. For the Frenet frame, on the other hand, the second basis vector \mathbf{p} is chosen so as to always lie in the direction of $\dot{\mathbf{t}}$, and this choice implies that $\alpha \not\equiv 0$.

Klok [283] invoked rotation-minimizing frames to construct swept surfaces, defined by translating a planar “profile” curve along a spatial “sweep” curve: the profile curve always resides within the normal plane of the sweep curve, but its orientation in that plane must be specified. In this context, the rotation-minimizing frame is preferable to the Frenet frame in the following sense. By substituting (30.3) into (30.2), we obtain

$$\begin{bmatrix} \dot{\mathbf{t}} \\ \dot{\mathbf{p}} \\ \dot{\mathbf{b}} \end{bmatrix} = \begin{bmatrix} 0 & \kappa & 0 \\ -\kappa & 0 & \tau \\ 0 & -\tau & 0 \end{bmatrix} \begin{bmatrix} \mathbf{t} \\ \mathbf{p} \\ \mathbf{b} \end{bmatrix}.$$

This reveals that \mathbf{t} changes at instantaneous rate κ in the direction of \mathbf{p} . The variation of \mathbf{p} has two components: rate $-\kappa$ in the direction of \mathbf{t} , and rate τ in the direction of \mathbf{b} . Finally, \mathbf{b} changes at the rate $-\tau$ in the direction of \mathbf{p} . Now changes in the direction of \mathbf{t} are unavoidable if $\kappa \not\equiv 0$. The change of \mathbf{p} in the direction of \mathbf{b} , and of \mathbf{b} in the direction of \mathbf{p} , however, correspond to a rotation of these vectors in the normal plane. We seek an orthonormal frame $(\mathbf{t}, \mathbf{u}, \mathbf{v})$ with (\mathbf{u}, \mathbf{v}) obtained from (\mathbf{p}, \mathbf{b}) by a rotation in the normal plane

$$\begin{bmatrix} \mathbf{u} \\ \mathbf{v} \end{bmatrix} = \begin{bmatrix} \cos \theta & \sin \theta \\ -\sin \theta & \cos \theta \end{bmatrix} \begin{bmatrix} \mathbf{p} \\ \mathbf{b} \end{bmatrix}, \quad (30.8)$$

$\theta(\xi)$ being defined so as to eliminate the “unnecessary” rotation of the Frenet frame. Klok [283] showed that the vectors \mathbf{u} and \mathbf{v} must satisfy

$$\mathbf{u}'(\xi) = - \frac{\mathbf{r}''(\xi) \cdot \mathbf{u}(\xi)}{|\mathbf{r}'(\xi)|^2} \mathbf{r}'(\xi), \quad \mathbf{v}'(\xi) = - \frac{\mathbf{r}''(\xi) \cdot \mathbf{v}(\xi)}{|\mathbf{r}'(\xi)|^2} \mathbf{r}'(\xi) \quad (30.9)$$

for $(\mathbf{t}, \mathbf{u}, \mathbf{v})$ to be a rotation-minimizing frame. Substituting from (30.8), this yields the differential equation

$$\frac{d\theta}{d\xi} = -\sigma\tau = -|\mathbf{r}'| \frac{(\mathbf{r}' \times \mathbf{r}'') \cdot \mathbf{r}'''}{|\mathbf{r}' \times \mathbf{r}''|^2} \quad (30.10)$$

for the angular function $\theta(\xi)$ that defines (\mathbf{u}, \mathbf{v}) in terms of (\mathbf{p}, \mathbf{b}) . Hence, as noted by Guggenheimer [220], this function has the form³

$$\theta(\xi) = \theta_0 - \int_0^\xi \tau(t) \sigma(t) dt, \quad (30.11)$$

Note that, since the determination of an RMF through expressions (30.8) and (30.11) amounts to solving an initial value problem, an infinite number of such frames exist (corresponding to different integration constants θ_0). Thus, an RMF is defined for any prescribed initial orientation of \mathbf{u} and \mathbf{v} at $\xi = 0$.

Unfortunately, the integral (30.11) does not, in general, admit closed-form reduction for the polynomial and rational curves employed in computer-aided design, computer graphics, robotics, and related applications. Consequently, a number of schemes have been proposed to approximate rotation-minimizing frames on a given curve, or to approximate curves by “simple” segments (e.g., circle arcs) with known rotation-minimizing frames [264, 267, 268, 464].

30.5 Energy of Framed Space Curves

In the theory of plane curves, the energy integral

$$E = \int_0^S \kappa^2 ds \quad (30.12)$$

is used as a measure of “fairness” for a curve of total length S . This integral is proportional to the strain energy stored in a thin elastic beam, bent from an initially-straight configuration into the shape of the curve [150]. Minimization of E subject to interpolation constraints (and possibly also $S = \text{constant}$) is a basic approach to the construction of “fair” curves (see §14.5.4).

Since curvature alone does not characterize the intrinsic geometry of space curves, the question arises as to how we can generalize the integral (30.12) to

³ An incorrect sign before the integral is given in [220].

obtain an appropriate fairness measure for space curves. The theory of non-planar elastic rods is more subtle [131, 295, 305, 309, 427] than that of planar beams. A basic difference is that, for the former, the “twist” of the elastic rod about its center line is an important contribution to the energy. This twist — which is distinct from and independent of the torsion in (30.4) — is specified by imposing an adapted frame on the curve. We shall see that the RMF plays a special role in formulating the energy of “framed space curves” [295].

Consider the deformation of a thin initially-straight elastic rod with total length S and circular cross section of radius $r \ll S$. The deformation includes bending and twisting of the rod, but the total length S remains unchanged. We define coordinates (ξ, ζ, η) in the deformed rod such that, in the undeformed state, they coincide with Cartesian coordinates (x, y, z) where the rod center line lies along the x -axis. After deformation, the orthonormal frame $(\mathbf{t}, \mathbf{u}, \mathbf{v})$ associated with the coordinates (ξ, ζ, η) rotates continuously along the length of the rod: \mathbf{t} is the tangent to the center-line, while \mathbf{u} and \mathbf{v} span the cross-sectional plane. This rotation is specified by the angular velocity vector

$$\boldsymbol{\omega} = \frac{d\phi}{ds} ,$$

where $d\phi$ is the (vector) infinitesimal frame rotation associated with arc length increment ds , through relations (30.5). Expressing the angular velocity vector $\boldsymbol{\omega}$ in terms of components as $\omega_\xi \mathbf{t} + \omega_\zeta \mathbf{u} + \omega_\eta \mathbf{v}$, the work done in deforming the rod from the initial straight configuration — i.e., the elastic strain energy stored in the deformed rod — can be written [295] as

$$U = \int_0^S \frac{1}{2} GJ \omega_\xi^2 + \frac{1}{2} EI(\omega_\zeta^2 + \omega_\eta^2) ds .$$

E and G are the Young’s modulus and shear modulus (modulus of rigidity) of the material and, for a circular cross section of radius r , the quantities

$$I = \frac{\pi r^4}{4} \quad \text{and} \quad J = \frac{\pi r^4}{2}$$

are the second moment of area about a diameter, and second polar moment of area about the center. The term $\frac{1}{2} EI(\omega_\zeta^2 + \omega_\eta^2)$ in the integrand represents the bending energy per unit length, while $\frac{1}{2} GJ \omega_\xi^2$ is the twisting energy per unit length. Introducing the material constitutive relation

$$G = \frac{E}{2(1+\nu)} ,$$

where ν is Poisson’s ratio, the energy integral may be expressed as

$$U = \frac{\pi r^4 E}{8} \int_0^S k \omega_\xi^2 + \omega_\zeta^2 + \omega_\eta^2 ds \quad (30.13)$$

where $k = 1/(1 + \nu)$. For most metals $\nu \approx 0.3$, and hence $k \approx 0.75$ can be used as a “canonical” value for this weight factor.

Clearly, we cannot speak of the energy of a space curve without specifying an adapted frame along the curve, to define the amount of “twisting” of the elastic rod about its center-line axis,⁴ which is an additional source of strain energy. Comparing with (30.6), we see that $\alpha = \omega_\xi$, $\beta = \omega_\zeta$, $\gamma = \omega_\eta$. Thus, if the twist is defined by the Frenet frame, the integrand in (30.13) is $k\tau^2 + \kappa^2$, and the twist of the rod evidently makes a non-zero contribution in this case. Now taking the cross product of the first equation in (30.5) with \mathbf{t} gives

$$\boldsymbol{\omega} = (\mathbf{t} \cdot \boldsymbol{\omega}) \mathbf{t} + \mathbf{t} \times \frac{d\mathbf{t}}{ds},$$

and since $\mathbf{t} \cdot \boldsymbol{\omega} = \omega_\xi$ and $d\mathbf{t}/ds = \kappa \mathbf{p}$, where κ is the curvature and \mathbf{p} is the principal normal vector, we obtain

$$\boldsymbol{\omega} = \omega_\xi \mathbf{t} + \kappa \mathbf{b},$$

where $\mathbf{b} = \mathbf{t} \times \mathbf{p}$ is the binormal vector. Thus, for *any* choice of \mathbf{u} and \mathbf{v} we always have $\omega_\zeta \mathbf{u} + \omega_\eta \mathbf{v} = \kappa \mathbf{b}$, and hence

$$\omega_\zeta^2 + \omega_\eta^2 = \kappa^2 = \left| \frac{d\mathbf{t}}{ds} \right|^2.$$

Hence, the integrand in (30.13) always has the form $k\omega_\xi^2 + \kappa^2$, and for a given curve its smallest value at each point will be realized when $\omega_\xi \equiv 0$ — i.e., the adapted frame chosen to specify the “twist” is an RMF.

Since choosing an RMF to specify the twist yields the least possible value for the integral (30.13), among all adapted frames, it is natural to adopt this choice in defining an “intrinsic” energy for space curves — that depends only on their shapes, and not the manner in which they are framed. Since $\omega_\xi \equiv 0$ for an RMF, and $\omega_\zeta^2 + \omega_\eta^2 = \kappa^2$ for any adapted frame, with this choice the energy integral (30.13) for space curves coincides (up to a multiplicative constant) with the energy integral (30.12) for planar curves.

30.6 Exact RMFs on PH Curves

For spatial PH curves, the integrand in (30.11) is always a *rational function*, and thus admits a closed-form integration. The integral of a rational function incurs, in general, both rational and transcendental (logarithmic) components. The rational terms require only arithmetic on polynomials, a greatest common divisor, and the solution of a linear system for their determination. Although the logarithmic terms cannot, in general, be determined without introducing

⁴ This twist is independent [309] of the torsion τ — the latter is determined by the intrinsic geometry of a space curve, but the twist ω_ξ can be imposed arbitrarily.

new algebraic constants, methods have been proposed [382, 442] that minimize the amount of polynomial root-solving required to obtain these constants.

Our present goal is to derive *exact* rotation-minimizing frames for spatial PH curves, defined by integrating hodographs of the form (22.2) for a given quaternion polynomial (22.1). For the present, we employ the Frenet frame as a reference, and seek to express the RMF in terms of it by the relation (30.8) with $\theta(\xi)$ defined by (30.11). Because of the indeterminacy of the Frenet frame at inflections, this may require us to identify these points on a given spatial PH curve *a priori*, and subdivide it at those points. This step can be circumvented by using a different adapted frame as a reference for the RMF — for example, the *Euler–Rodrigues frame* discussed in §30.7 below.

We begin by writing the relation (30.10) in the form

$$\frac{d\theta}{d\xi} = - \frac{p(\xi)}{q(\xi)}, \quad (30.14)$$

$$p(\xi) = |\mathbf{r}'(\xi)| [\mathbf{r}'(\xi) \times \mathbf{r}''(\xi)] \cdot \mathbf{r}'''(\xi), \quad q(\xi) = |\mathbf{r}'(\xi) \times \mathbf{r}''(\xi)|^2.$$

Now if $\mathbf{r}(\xi)$ is a polynomial curve of degree n , we have

$$\deg(\mathbf{r}' \times \mathbf{r}'') = 2n - 4 \quad \text{and} \quad \deg((\mathbf{r}' \times \mathbf{r}'') \cdot \mathbf{r}''') = 3n - 9$$

due to cancellation of highest-order terms, while $|\mathbf{r}'(\xi)|$ is the square root of a polynomial of degree $2n - 2$ in t . In general, the latter term precludes the possibility of a closed-form integration of equation (30.14).

For PH curves, however, some striking simplifications arise. First, we have $|\mathbf{r}'(\xi)| = \sigma(\xi) = u^2(\xi) + v^2(\xi) + p^2(\xi) + q^2(\xi)$, a *polynomial* of degree $n - 1$, and the right-hand side of (30.14) is thus a rational function. Moreover, using the factorization (21.24), where the polynomial $\rho(\xi)$ is specified by (21.25), a factor $\sigma(\xi)$ may be cancelled from $p(\xi)$ and $q(\xi)$ to obtain

$$\frac{d\theta}{d\xi} = - \frac{[\mathbf{r}'(\xi) \times \mathbf{r}''(\xi)] \cdot \mathbf{r}'''(\xi)}{\sigma(\xi) \rho(\xi)}. \quad (30.15)$$

Now for a degree- n PH curve, $\deg((\mathbf{r}' \times \mathbf{r}'') \cdot \mathbf{r}''') = 3n - 9$, $\deg(\sigma) = n - 1$, and $\deg(\rho) = 2n - 6$. Hence, the right-hand side is a *proper* rational fraction whose numerator is degree 2 less than the denominator. Specifically, for PH cubics $(\mathbf{r}' \times \mathbf{r}'') \cdot \mathbf{r}'''$ and ρ are constants, while σ is quadratic. For PH quintics, $(\mathbf{r}' \times \mathbf{r}'') \cdot \mathbf{r}'''$ is of degree 6, while σ and ρ are both quartic in t .

For $n \geq 5$, the partial fraction expansion of expression (30.15) is defined by polynomials $a(\xi)$, $b(\xi)$ with $\deg(a) \leq n - 2$ and $\deg(b) \leq 2n - 7$, such that

$$[\mathbf{r}'(\xi) \times \mathbf{r}''(\xi)] \cdot \mathbf{r}'''(\xi) = a(\xi) \rho(\xi) + b(\xi) \sigma(\xi). \quad (30.16)$$

This is an identity among polynomials of degree $3n - 8$. Equating coefficients of like terms yields $3n - 7$ linear equations for the $(n - 1) + (2n - 6) = 3n - 7$ unknown coefficients of $a(\xi)$ and $b(\xi)$. Solving for these coefficients, we have

$$\frac{[\mathbf{r}'(\xi) \times \mathbf{r}''(\xi)] \cdot \mathbf{r}'''(\xi)}{\sigma(\xi) \rho(\xi)} = \frac{a(\xi)}{\sigma(\xi)} + \frac{b(\xi)}{\rho(\xi)}. \quad (30.17)$$

With $\theta = \theta_0$ when $\xi = 0$, integration of (30.14) then yields

$$\theta(\xi) = \theta_0 - \int_0^\xi \frac{a(t)}{\sigma(t)} dt - \int_0^\xi \frac{b(t)}{\rho(t)} dt. \quad (30.18)$$

30.6.1 Integration of Rational Functions

For PH cubics, the integration of (30.15) is a trivial task, since the numerator is a constant and the denominator is quadratic. For PH quintics, we use (30.18), where $a(t)$, $b(t)$ are at most cubic and $\sigma(t)$, $\rho(t)$ are quartics. Before treating these specific cases in detail, we review some general principles governing the integration of rational functions in as exact a manner as possible.

In general, the indefinite integral of a rational function

$$\int \frac{p(t)}{q(t)} dt, \quad (30.19)$$

where $\gcd(p, q) = 1$ and $\deg(p) < \deg(q)$, yields a function with both rational and transcendental (logarithmic) terms. The naive approach is to attempt to completely factorize $q(t)$ into linear factors over \mathbb{C} , or into linear and quadratic factors over \mathbb{R} , and then perform a decomposition of the integrand into partial fractions. In general, however, such factorizations incur algebraic constants that can only be approximated in floating-point arithmetic, even though the final integral may not depend on all of them in an essential manner.

Research in the algorithmic integration of rational functions, with minimal introduction of algebraic constants, was motivated by the advent of computer algebra systems [112, 454]. The first step involves extracting the rational part of (30.19) through the method of Horowitz [246, 247]. Invoking the Euclidean algorithm [452] to compute $\gcd(q(t), q'(t))$, we define

$$q_1(t) = \gcd(q(t), q'(t)) \quad \text{and} \quad q_2(t) = \frac{q(t)}{\gcd(q(t), q'(t))}$$

so that

$$q(t) = q_1(t)q_2(t). \quad (30.20)$$

We assume, without loss of generality, that $q_2(t)$ is a monic polynomial — i.e., its highest-order coefficient is 1. Note that the roots of $q_1(t)$ are the *multiple* roots of $q(t)$. Specifically, if z is a root of q of multiplicity $m \geq 2$, then it is a root of q_1 of multiplicity $m - 1$. Moreover, each distinct (simple or multiple) root of $q(t)$ is a *simple* root of $q_2(t)$.

We seek polynomials $p_1(t)$, $p_2(t)$ such that $p(t)/q(t)$ can be expressed as

$$\frac{p(t)}{q(t)} = \left(\frac{p_1(t)}{q_1(t)} \right)' + \frac{p_2(t)}{q_2(t)} \quad (30.21)$$

Carrying out the differentiation and simplifying, we obtain the relation

$$p(t) = q_2(t)p'_1(t) - s(t)p_1(t) + q_1(t)p_2(t), \quad (30.22)$$

where

$$s(t) = \frac{q'_1(t)q_2(t)}{q_1(t)}.$$

By differentiating (30.20), we can re-write this as

$$s(t) = \frac{q'(t)}{\gcd(q(t), q'(t))} - q'_2(t),$$

and since $\gcd(q, q')$ divides q' without remainder, $s(t)$ must be a polynomial. Now since the polynomials $p(t)$, $q_1(t)$, $q_2(t)$, $s(t)$ are known, comparison of like terms in equation (30.22) yields a linear system of equations for the unknown coefficients of the polynomials $p_1(t)$, $p_2(t)$. Once these coefficients have been determined, we can express the integral of (30.21) as

$$\int \frac{p(t)}{q(t)} dt = \frac{p_1(t)}{q_1(t)} + \int \frac{p_2(t)}{q_2(t)} dt, \quad (30.23)$$

where $q_2(t)$ is “square-free” (i.e., it has no multiple roots).

The integral on the right in (30.23) is the transcendental part. If $\deg(q_2) = N$, then $q_2(t)$ has distinct roots z_1, \dots, z_N and the integrand has the complete partial fraction decomposition

$$\frac{p_2(t)}{q_2(t)} = \sum_{k=1}^N \frac{c_k}{t - z_k}, \quad (30.24)$$

and hence

$$\int \frac{p_2(t)}{q_2(t)} dt = \sum_{k=1}^N c_k \ln(t - z_k).$$

Since $p_2(t)$ and $q_2(t)$ are real, complex terms in this sum occur in conjugate pairs, and may be combined to yield explicitly real expressions.

In general, the roots z_1, \dots, z_N are algebraic numbers that do not have exact, finite decimal representations — in floating-point arithmetic, they must be approximated. A “defect” of the complete partial-fraction decomposition (30.24) is that it employs all these roots, although the integral may ultimately be expressible in a form that does not require all of them.

The following approach, due to Rothstein [382] and Trager [442], evaluates such integrals with a minimal algebraic extension of the set of constants. Let $f(t)$, $g(t)$ be polynomials satisfying $\deg(f) < \deg(g)$, $\gcd(f, g) = 1$, with $g(t)$ monic and square-free. Then if c_1, \dots, c_h are the distinct roots of

$$h(c) = \text{Resultant}_t(f(t) - cg'(t), g(t)) = 0 \quad (30.25)$$

we have

$$\int \frac{f(t)}{g(t)} dt = \sum_{k=1}^h c_k \ln \nu_k(t),$$

where the polynomials $\nu_1(t), \dots, \nu_h(t)$ are defined by

$$\nu_k(t) = \gcd(f(t) - c_k g'(t), g(t)).$$

Apart from the need for numerical determination of the roots of (30.25), this method is essentially exact for rational functions of arbitrary order.

30.6.2 Frames for PH Cubics and Quintics

In principle, the above procedure allows computation of rotation-minimizing frames for PH curves of arbitrary order. We now give more specific details for PH cubics and quintics. The former admit a particularly simple closed-form reduction, but in general PH cubics do not offer sufficient shape flexibility for free-form design applications. The PH quintics are somewhat more involved, but provide much greater geometrical versatility.

PH cubics are constructed by inserting four linear polynomials, expressed in the Bernstein form $u(\xi) = u_0(1-\xi) + u_1\xi$ and similarly for $v(\xi), p(\xi), q(\xi)$, into (22.2), and integrating the hodograph. In this case, $[\mathbf{r}'(\xi) \times \mathbf{r}''(\xi)] \cdot \mathbf{r}'''(\xi)$ and $\rho(\xi)$ are both constants, and their ratio is the quantity

$$k = 2(u_0v_1 - u_1v_0 - p_0q_1 + p_1q_0).$$

The orientation of the rotation-minimizing frame relative to the Frenet frame is thus defined by the function

$$\theta(\xi) = \theta_0 - k \int_0^\xi \frac{dt}{\sigma(t)},$$

where the parametric speed is the quadratic

$$\sigma(t) = \sigma_0(1-t)^2 + \sigma_1 2(1-t)t + \sigma_2 t^2$$

with Bernstein coefficients obtained from (22.5) as

$$\sigma_0 = u_0^2 + v_0^2 + p_0^2 + q_0^2, \quad \sigma_1 = u_0u_1 + v_0v_1 + p_0p_1 + q_0q_1, \quad \sigma_2 = u_1^2 + v_1^2 + p_1^2 + q_1^2.$$

Hence [217], according to whether $\sigma_1^2 - \sigma_0\sigma_2$ is positive or negative, we have

$$\theta(\xi) = \theta_0 + \frac{k}{\sqrt{\sigma_1^2 - \sigma_0\sigma_2}} \tanh^{-1} \frac{(\sigma_2 - 2\sigma_1 + \sigma_0)\xi + \sigma_1 - \sigma_0}{\sqrt{\sigma_1^2 - \sigma_0\sigma_2}},$$

or

$$\theta(\xi) = \theta_0 - \frac{k}{\sqrt{\sigma_0\sigma_2 - \sigma_1^2}} \tan^{-1} \frac{(\sigma_2 - 2\sigma_1 + \sigma_0)\xi + \sigma_1 - \sigma_0}{\sqrt{\sigma_0\sigma_2 - \sigma_1^2}}.$$

PH quintics are defined by inserting four quadratic polynomials, $u(\xi) = u_0(1-\xi)^2 + u_1 2(1-\xi)\xi + u_2 \xi^2$ and similarly for $v(\xi), p(\xi), q(\xi)$, into (22.2) and integrating. In this case $[\mathbf{r}'(\xi) \times \mathbf{r}''(\xi)] \cdot \mathbf{r}'''(\xi)$ is degree 6, while $\rho(\xi)$ and $\sigma(\xi)$ are quartics. We use the form (30.18), where $a(\xi)$ and $b(\xi)$ are determined by solving the linear system defined by equation (30.16).

We begin by dividing the numerator and denominator of the integrands in (30.18) by the highest-order coefficient of the denominator, so we can assume that $\sigma(t)$ and $\rho(t)$ are monic. These two quartics can be explicitly factorized by using Ferrari's method (see §3.3) to compute their roots. Denoting these roots by z_1, z_2, z_3, z_4 and w_1, w_2, w_3, w_4 respectively, the coefficients c_1, c_2, c_3, c_4 and d_1, d_2, d_3, d_4 in the partial fraction expansions

$$\frac{a(t)}{\sigma(t)} = \sum_{k=1}^4 \frac{c_k}{t - z_k} \quad \text{and} \quad \frac{b(t)}{\rho(t)} = \sum_{k=1}^4 \frac{d_k}{t - w_k}$$

are found by clearing the denominators, and equating t to each of the roots in succession, to obtain

$$c_k = \frac{a(z_k)}{\prod_{j \neq k} (z_k - z_j)} \quad \text{and} \quad d_k = \frac{b(w_k)}{\prod_{j \neq k} (w_k - w_j)} \quad (30.26)$$

for $k = 1, \dots, 4$. Integration then gives

$$\theta(t) = \theta_0 - \sum_{k=1}^4 c_k \ln(t - z_k) + d_k \ln(t - w_k).$$

Now since $\sigma(t)$ and $\rho(t)$ are real polynomials, their complex roots must occur as conjugate pairs, and the corresponding partial-fraction coefficients are also complex conjugates. Logarithmic terms that correspond to such pairs can be combined to give explicitly real expressions: for example, if z, \bar{z} and c, \bar{c} are conjugate roots and coefficients, we have

$$c \ln(t - z) + \bar{c} \ln(t - \bar{z}) = 2 [\operatorname{Re}(c) \ln |t - z| - \operatorname{Im}(c) \arg(t - z)].$$

Here $\arg(t - z)$ must be interpreted as a *continuous* function, i.e., it should not be reduced modulo 2π .

Example. Consider the PH quintic with Bernstein coefficients $(u_0, u_1, u_2) = (2, 0, 2)$, $(v_0, v_1, v_2) = (1, 1, 0)$, $(p_0, p_1, p_2) = (0, -2, 0)$, $(q_0, q_1, q_2) = (1, 2, 1)$ for the quadratic polynomials in (22.2). In this case,

$$\begin{aligned} [\mathbf{r}'(\xi) \times \mathbf{r}''(\xi)] \cdot \mathbf{r}'''(\xi) &= 16032 \xi^6 - 49152 \xi^5 + 74592 \xi^4 - 66560 \xi^3 \\ &\quad - 66560 \xi^3 + 32256 \xi^2 - 6912 \xi - 576 \end{aligned}$$

and

$$\begin{aligned}\sigma(\xi) &= 37\xi^4 - 72\xi^3 + 46\xi^2 - 12\xi + 6, \\ \rho(\xi) &= 80\xi^4 - 544\xi^3 + 3376\xi^2 - 2976\xi + 720.\end{aligned}$$

The partial fraction decomposition (30.17) is then defined by the polynomials

$$a(\xi) = 8\xi^2 - 8\xi \quad \text{and} \quad b(\xi) = 416\xi^2 - 384\xi - 96.$$

Ferrari's method (see §3.3) gives

$$z_1, \bar{z}_1 = 0.012018 \pm 0.394440i, \quad z_2, \bar{z}_2 = 0.960955 \pm 0.343344i$$

$$w_1, \bar{w}_1 = 0.493693 \pm 0.069303i, \quad w_2, \bar{w}_2 = 2.906307 \pm 5.269303i$$

for the roots of $\sigma(\xi)$ and $\rho(\xi)$. The corresponding partial fraction coefficients, obtained from (30.26), are

$$\begin{aligned}c_1, \bar{c}_1 &= -0.096100 \mp 0.030185i, \quad c_2, \bar{c}_2 = 0.096100 \mp 0.014590i \\ d_1, \bar{d}_1 &= \pm 0.5i, \quad d_2, \bar{d}_2 = \mp 0.5i.\end{aligned}$$

In terms of the above complex values, we now have

$$\begin{aligned}\theta(\xi) &= \theta_0 - 2 \sum_{k=1}^2 [\operatorname{Re}(c_k) \ln |\xi - z_k| - \operatorname{Im}(c_k) \arg(\xi - z_k)] \\ &\quad - 2 \sum_{k=1}^2 [\operatorname{Re}(d_k) \ln |\xi - w_k| - \operatorname{Im}(d_k) \arg(\xi - w_k)],\end{aligned}$$

with the integration constant θ_0 chosen so that $\theta(0) = 0$. Figure 30.4 compares the variation of the Frenet and rotation-minimizing frames along the example PH curve. A quantitative comparison is presented in Fig. 30.5, which shows the instantaneous rates of rotation for both frames — namely, $\omega = \sqrt{\kappa^2 + \tau^2}$ for the Frenet frame, and κ for the rotation-minimizing frame. It is apparent that, compared with the rotation-minimizing frame, the Frenet frame incurs a great deal of “unnecessary” rotation near the middle of the curve.

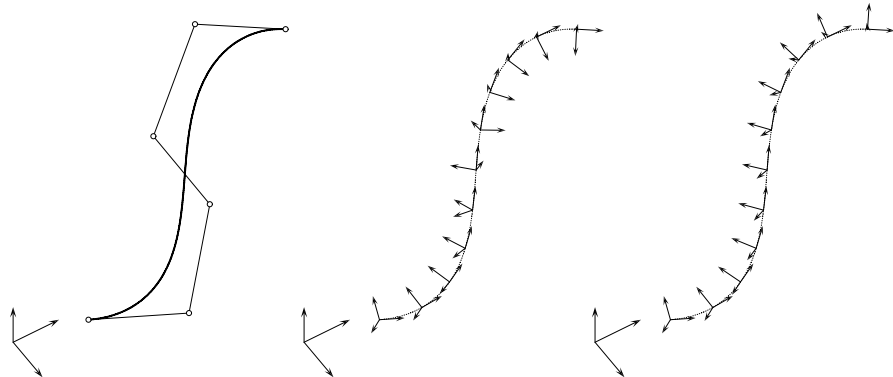


Fig. 30.4. A PH quintic space curve (left), with Bézier control polygon. Also shown is the variation of the Frenet frame (center) and rotation-minimizing frame (right).

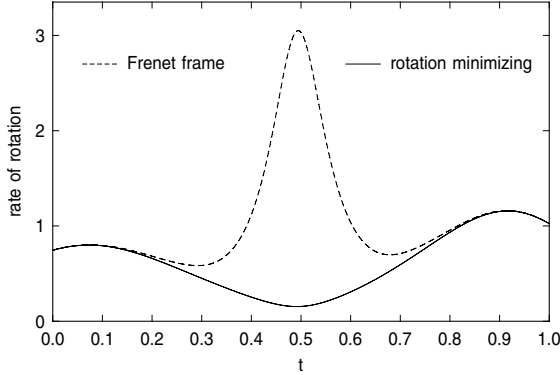


Fig. 30.5. Comparison of the instantaneous rates of rotation for the Frenet frame and the rotation-minimizing frame along the PH quintic illustrated in Fig. 30.4.

30.7 Rational RMF Approximations

Since rational forms are usually preferred in computer-aided design, we now consider the piecewise-rational approximation of RMFs on PH curves [162]. Instead of the Frenet frame, the *Euler–Rodrigues frame* (ERF) is employed here as a reference (see §30.3). The ERF is an adapted orthonormal frame with a rational dependence on the curve parameter, associated with the quaternion representation of spatial PH curves in a specific Cartesian coordinate system. The angular deviation of the RMF, relative to the ERF, is first derived as a transcendental function, and Padé (rational Hermite) approximations to this function are then constructed. For PH quintics, a rational rotation applied to the ERF furnishes very accurate approximations of the RMF.

Polynomial and rational curves do not, in general, admit rational RMFs, and approximations are thus necessary to conform to prevailing representation schemes in computer-aided design. For any adapted frame, exactitude of the curve tangent field $\mathbf{t}(\xi)$ is one attribute that should not be compromised by the approximation scheme. Since only the PH curves admit rational unit tangents, our focus here is on (piecewise) rational RMF approximations for spatial PH curves, using the quaternion representation (22.2).

Now the quantities (α, β, γ) in (30.6) were specified in terms of arc-length derivatives. It is convenient to define them here using parametric derivatives. These definitions differ only by a factor σ , the parametric speed of the curve. For the PH curve specified by (22.2), we have [85]:

$$\alpha = \mathbf{u}' \cdot \mathbf{v} = 2 \frac{uv' - u'v - pq' + p'q}{u^2 + v^2 + p^2 + q^2}.$$

A non-trivial PH curve that has $\alpha \equiv 0$ (i.e., the ERF and RMF are coincident) must be [85] of degree ≥ 7 . Since we prefer to work with lower-order PH curves

— specifically the quintics, for which many useful algorithms are available — we focus here on seeking rational rotations of the ERF about the tangent \mathbf{t} of PH quintics that will yield close approximations to an RMF.

Let $(\tilde{\mathbf{t}}, \tilde{\mathbf{u}}, \tilde{\mathbf{v}})$ be a rotation of the ERF about the tangent, such that

$$\tilde{\mathbf{t}}(\xi) = \mathbf{t}(\xi), \quad \begin{bmatrix} \tilde{\mathbf{u}}(\xi) \\ \tilde{\mathbf{v}}(\xi) \end{bmatrix} = \begin{bmatrix} \cos \theta(\xi) & \sin \theta(\xi) \\ -\sin \theta(\xi) & \cos \theta(\xi) \end{bmatrix} \begin{bmatrix} \mathbf{u}(\xi) \\ \mathbf{v}(\xi) \end{bmatrix}.$$

Then, as expected, we have

$$\tilde{\alpha} = \tilde{\mathbf{u}}' \cdot \tilde{\mathbf{v}} = \theta' + \alpha$$

i.e., the angular speed (about \mathbf{t}) of the rotated frame is its angular speed with respect to the reference frame, plus the angular speed of the reference frame itself. Hence, the rotated frame is an RMF if and only if $\theta(\xi)$ satisfies⁵

$$\theta' = -\alpha = 2 \frac{u'v - uv' - p'q + pq'}{u^2 + v^2 + p^2 + q^2}. \quad (30.27)$$

The exact computation of $\theta(\xi)$ entails integrating the above rational function. In general, this will incur transcendental terms in $\theta(\xi)$ — so we cannot expect $\cos \theta(\xi)$ and $\sin \theta(\xi)$, and the RMF, to be rational (see §30.6 above).

Instead of exact integration, we use rational approximation here. Let $\phi(\xi)$ be an approximation of $\theta(\xi)$, such that

$$\sin \phi(\xi) = \frac{a^2(\xi) - b^2(\xi)}{a^2(\xi) + b^2(\xi)}, \quad \cos \phi(\xi) = \frac{2a(\xi)b(\xi)}{a^2(\xi) + b^2(\xi)}$$

where $a(\xi)$ and $b(\xi)$ are polynomials. One can easily verify that

$$\frac{1}{2}\phi' = \frac{a'b - ab'}{a^2 + b^2} = \frac{d}{d\xi} \tan^{-1} \frac{a}{b},$$

and hence ϕ is a good approximation of θ if and only if a/b is a good rational approximation of the function

$$f(\xi) = \tan \frac{1}{2}\theta(\xi) = \tan \int \frac{g(\xi)}{h(\xi)} d\xi, \quad (30.28)$$

where

$$g(\xi) = u'(\xi)v(\xi) - u(\xi)v'(\xi) - p'(\xi)q(\xi) + p(\xi)q'(\xi), \quad (30.29)$$

$$h(\xi) = u^2(\xi) + v^2(\xi) + p^2(\xi) + q^2(\xi). \quad (30.30)$$

As a measure of the quality of approximation, we compare the exact function $\theta(\xi) = 2 \int g(\xi)/h(\xi) d\xi$ with the approximation $\phi(\xi) = 2 \tan^{-1} a(\xi)/b(\xi)$.

⁵ Since this is a differential constraint, there exists a one-parameter family of RMFs — corresponding to the choice of an initial orientation on integrating (30.27).

30.7.1 Rational Hermite Interpolation

The existence of rational adapted frames on space curves was first noted in the early study [149] of spatial PH curves, using a representation that is sufficient (but not necessary) for a Pythagorean hodograph. Jüttler and Mäurer [268] subsequently described RMF approximations for PH cubics. Since PH cubics have rather limited shape flexibility, we focus here on general rational RMF approximations for quintic or higher-order PH curves.

To approximate (30.28) by a rational function $a(\xi)/b(\xi)$ we use multi-point Padé approximation, equivalent to rational Hermite interpolation [24, 59, 109]. Consider a function $f(\xi)$ and a set of distinct nodes $\xi_0, \dots, \xi_r \in [0, 1]$ where, at each ξ_i , the function value and derivatives $f^{(k)}(\xi_i)$ for $k = 0, \dots, s_i - 1$ are given ($s_i \geq 1$). The rational Hermite interpolation problem of order (m, n) for $f(\xi)$ amounts to the construction of polynomials

$$a(\xi) = \sum_{i=0}^m a_i \xi^i \quad \text{and} \quad b(\xi) = \sum_{i=0}^n b_i \xi^i,$$

such that

$$\sum_{i=0}^r s_i = m + n + 1,$$

$$f^{(k)}(\xi_i) = \left(\frac{a}{b}\right)^{(k)}(\xi_i) \quad \text{for } k = 0, \dots, s_i - 1; \quad i = 0, \dots, r. \quad (30.31)$$

Note that the sum of degrees of a and b is minimal to satisfy the interpolation conditions. Instead of using (30.31) directly, we consider the conditions

$$(fb - a)^{(k)}(\xi_i) = 0 \quad \text{for } k = 0, \dots, s_i - 1; \quad i = 0, \dots, r. \quad (30.32)$$

These conditions define a homogeneous system of $m + n + 1$ linear equations in the $m + n + 2$ unknown coefficients a_i and b_i of $a(\xi)$ and $b(\xi)$, and hence they always admit at least one non-trivial solution. In fact, if $a_1(\xi), b_1(\xi)$ and $a_2(\xi), b_2(\xi)$ both satisfy (30.32) then we have $a_1(\xi)b_2(\xi) \equiv a_2(\xi)b_1(\xi)$, i.e., all rational solutions of (30.32) have the same irreducible form.

Having computed a rational interpolant a/b from the linear interpolation conditions (i.e., the conditions expressed in terms of $fb - a$ instead of $f - a/b$), it may happen exceptionally that an interpolation point is also a common root of a and b . At such points, the irreducible form of a/b may not interpolate the correct value. This problem may be remedied by checking for coincidence of the roots of $\gcd(a, b)$ with any of the nodes ξ_0, \dots, ξ_r . When such coincidences occur, a higher order (m, n) for the rational interpolant is needed in order to satisfy the prescribed interpolation conditions.

Now let x_0, \dots, x_{m+n} be a list of the distinct interpolation nodes ξ_0, \dots, ξ_r with each node repeated according to its multiplicity — i.e.,

$$\underbrace{x_0, \dots, x_{s_0-1}}_{= \xi_0}, \underbrace{x_{s_0}, \dots, x_{s_0+s_1-1}}_{= \xi_1}, \dots, \underbrace{x_{s_0+\dots+s_{r-1}}, \dots, x_{s_0+\dots+s_{r-1}+s_r-1}}_{= \xi_r}.$$

Then, for the specified set of nodes and multiplicities, the divided differences of $f(\xi)$ are defined [431] recursively by

$$f[x_i] = f(x_i),$$

and

$$f[x_i, \dots, x_{i+k}] = \begin{cases} \frac{f^{(k)}(x_i)}{k!} & \text{if } x_i = \dots = x_{i+k}, \\ \frac{f[x_{i+1}, \dots, x_{i+k}] - f[x_i, \dots, x_{i+k-1}]}{x_{i+k} - x_i} & \text{otherwise.} \end{cases}$$

It is convenient to introduce the more compact notation

$$c_{i,j} = \begin{cases} 0 & i > j, \\ f[x_i, \dots, x_j] & i \leq j. \end{cases}$$

If we then set

$$B_j(\xi) = \begin{cases} 1 & j = 0, \\ \prod_{k=1}^j (\xi - x_{k-1}) & \text{otherwise,} \end{cases}$$

and

$$F_{i,j}(\xi) = \begin{cases} 0 & i > j, \\ \sum_{k=i}^j c_{ik} B_k(\xi) & i \leq j, \end{cases}$$

the numerator and denominator of the rational interpolant $a(\xi)/b(\xi)$ can be formulated [109] as the determinants

$$a(\xi) = \begin{vmatrix} F_{0,m}(\xi) & F_{1,m}(\xi) & \dots & F_{n,m}(\xi) \\ c_{0,m+1} & c_{1,m+1} & \dots & c_{n,m+1} \\ c_{0,m+2} & c_{1,m+2} & \dots & c_{n,m+2} \\ \dots & \dots & \dots & \dots \\ c_{0,m+n} & c_{1,m+n} & \dots & c_{n,m+n} \end{vmatrix}, \quad b(\xi) = \begin{vmatrix} B_0(\xi) & B_1(\xi) & \dots & B_n(\xi) \\ c_{0,m+1} & c_{1,m+1} & \dots & c_{n,m+1} \\ c_{0,m+2} & c_{1,m+2} & \dots & c_{n,m+2} \\ \dots & \dots & \dots & \dots \\ c_{0,m+n} & c_{1,m+n} & \dots & c_{n,m+n} \end{vmatrix}.$$

An explicit expansion of the determinants is not necessarily a good approach to computing $a(\xi)$ and $b(\xi)$ — especially for large m and n . However, we are primarily interested in the low-degree case $m = n = 2$, for which we have the simple closed-form expressions

$$\begin{aligned} a(\xi) &= c_{0,0}[c_{1,4}c_{2,3} - c_{1,3}c_{2,4}] \\ &\quad + [c_{0,1}c_{1,4}c_{2,3} + c_{0,3}c_{1,1}c_{2,4} - c_{0,4}c_{1,1}c_{2,3} - c_{0,1}c_{1,3}c_{2,4}](\xi - x_0) \\ &\quad + [c_{0,2}c_{1,4}c_{2,3} + c_{0,3}c_{1,2}c_{2,4} + c_{0,4}c_{1,3}c_{2,2} \\ &\quad - c_{0,3}c_{1,4}c_{2,2} - c_{0,4}c_{1,2}c_{2,3} - c_{0,2}c_{1,3}c_{2,4}](\xi - x_0)(\xi - x_1), \end{aligned} \quad (30.33)$$

$$\begin{aligned} b(\xi) &= c_{1,4}c_{2,3} - c_{1,3}c_{2,4} + [c_{0,3}c_{2,4} - c_{0,3}c_{2,4}](\xi - x_0) \\ &\quad + [c_{0,4}c_{1,3} - c_{0,3}c_{1,4}](\xi - x_0)(\xi - x_1). \end{aligned} \quad (30.34)$$

To compute interpolant values and derivatives for the function (30.28) we wish to approximate, we note that since the denominator of the integrand in (30.28) is quartic, it can be factorized by using Ferrari's method (see §3.3) to compute its roots z_1, z_2, z_3, z_4 . In general, these roots are distinct, and we can use a partial fraction expansion to write the integrand as

$$\frac{g(\xi)}{h(\xi)} = \sum_{k=1}^4 \frac{c_k}{\xi - z_k},$$

the coefficients (residues) c_k being found by clearing denominators, and setting ξ equal to each root in succession, to obtain

$$c_k = \frac{g(z_k)}{\prod_{j \neq k} (z_k - z_j)}, \quad k = 1, \dots, 4.$$

Integration then gives

$$\int \frac{g(\xi)}{h(\xi)} d\xi = \theta_0 + \sum_{k=1}^4 c_k \ln(\xi - z_k),$$

where θ_0 is an integration constant. Assuming that $\gcd(u, v, p, q) = \text{constant}$, the roots of h must occur as complex conjugate pairs, and the corresponding residues are also complex conjugates. Logarithmic terms that correspond to such pairs can be combined to give explicitly real expressions — for example, if z, \bar{z} and c, \bar{c} are conjugate roots and residues, we have

$$c \ln(\xi - z) + \bar{c} \ln(\xi - \bar{z}) = 2 [\operatorname{Re}(c) \ln |\xi - z| - \operatorname{Im}(c) \arg(\xi - z)].$$

Denoting the other pair of roots and residues by w, \bar{w} and d, \bar{d} so that

$$\frac{g(\xi)}{h(\xi)} = \frac{c}{\xi - z} + \frac{\bar{c}}{\xi - \bar{z}} + \frac{d}{\xi - w} + \frac{\bar{d}}{\xi - \bar{w}}, \quad (30.35)$$

we have

$$\begin{aligned} \int \frac{g(\xi)}{h(\xi)} d\xi &= 2 [\operatorname{Re}(c) \ln |\xi - z| + \operatorname{Re}(d) \ln |\xi - w| \\ &\quad - \operatorname{Im}(c) \arg(\xi - z) - \operatorname{Im}(d) \arg(\xi - w)] + \theta_0. \end{aligned} \quad (30.36)$$

Since this integral is subject to evaluation by the tangent function, one must be careful to choose the integration constant θ_0 such that the integral does not cross $(n + \frac{1}{2})\pi$ in the interval $\xi \in [0, 1]$ of interest. This can be achieved by evaluating the extrema of the integral, which are located at the real roots of $g(\xi)$ on $\xi \in (0, 1)$ or at the interval endpoints $\xi = 0$ and $\xi = 1$. In case the range of values of the integral is not contained within an interval of the form $(n - \frac{1}{2})\pi < \xi < (n + \frac{1}{2})\pi$, a further subdivision of $\xi \in [0, 1]$ is necessary.

Example 30.1 Consider the general PH quintic defined by

$$\begin{aligned} u(\xi) &= 4.86877 + 4.78126\xi + 3.32330\xi^2, \\ v(\xi) &= -6.43321 + 5.52435\xi + 2.85747\xi^2, \\ p(\xi) &= 2.83170 - 9.98047\xi - 7.28976\xi^2, \\ q(\xi) &= -1.53492 - 2.73598\xi + 9.65593\xi^2. \end{aligned}$$

Forming the polynomials (30.29) and (30.30), we have

$$z, \bar{z} = -0.830350 \pm 0.828652i \quad \text{and} \quad c, \bar{c} = 0.0125113 \pm 0.219377i,$$

$$w, \bar{w} = 0.359226 \pm 0.449591i \quad \text{and} \quad d, \bar{d} = -0.0125113 \pm 0.312214i$$

in the partial fraction decomposition (30.35). The numerator $g(\xi)$ does not have real roots, and the right-hand side of (30.36) has values $0.561425\pi + \theta_0$ at $\xi = 0$ and $0.188488\pi + \theta_0$ at $\xi = 1$. Thus, by setting $\theta_0 = -0.374956\pi$, the integral remains in the range $\pm 0.186469\pi$.

As evident from the above example, additional structure can be discerned in the partial fraction decomposition (30.35) for general PH quintics.

Lemma 30.1 *For general PH quintics, the residues c and d in expression (30.36) satisfy $\operatorname{Re}(c) + \operatorname{Re}(d) = 0$.*

Proof : For general PH quintics, $\deg(g) = 2$ and $\deg(h) = 4$. Setting $h(\xi) = k(\xi - z)(\xi - \bar{z})(\xi - w)(\xi - \bar{w})$ and clearing denominators in (30.35) gives

$$g(\xi) = k(c + \bar{c} + d + \bar{d})\xi^3 + \text{lower order terms}.$$

Since $g(\xi)$ is just quadratic, we must have $c + \bar{c} + d + \bar{d} = 2\operatorname{Re}(c + d) = 0$, and hence $\operatorname{Re}(c) + \operatorname{Re}(d) = 0$. ■

Thus, expression (30.36) can be simplified somewhat to yield

$$\int \frac{g(\xi)}{h(\xi)} d\xi = 2 \left[\operatorname{Re}(c) \ln \left| \frac{\xi - z}{\xi - w} \right| - \operatorname{Im}(c) \arg(\xi - z) - \operatorname{Im}(d) \arg(\xi - w) \right] + \theta_0.$$

We now consider RMF approximations for *helical* PH quintics, which are characterized by the property that their tangents maintain a constant angle relative to a fixed direction (the axis of the helix) in space. If a polynomial curve is helical, it must be a PH curve (see §23.1).

As noted in Proposition 23.1, a sufficient condition for a general PH quintic to be helical is that the quaternion coefficients $\mathcal{A}_0, \mathcal{A}_1, \mathcal{A}_2$ of the quadratic polynomial (22.6) employed in (22.2) are linearly dependent.

Example 30.2 To define a helical PH quintic, we choose

$$\begin{aligned}\mathcal{A}_0 &= 1.098684\mathbf{i} + 0.455090\mathbf{k}, \\ \mathcal{A}_2 &= -0.774033 + 0.328603\mathbf{i} + 0.779681\mathbf{j} - 0.314967\mathbf{k}, \\ \mathcal{A}_1 &= 1.100380(\mathcal{A}_0 + \mathcal{A}_2).\end{aligned}$$

This corresponds to the “good” helical PH quintic interpolant to the Hermite data $\mathbf{r}(0) = (0, 0, 0)$, $\mathbf{r}'(0) = (1, 0, 1)$ and $\mathbf{r}(1) = (1, 1, 1)$, $\mathbf{r}'(1) = (0, 1, 1)$ — see Example 28.2. In the partial fraction expansion (30.35) we then have

$$\begin{aligned}z, \bar{z} &= -0.234351 \pm 0.356555\mathbf{i} \quad \text{and} \quad c, \bar{c} = \pm 0.431258\mathbf{i}, \\ w, \bar{w} &= 1.23435 \pm 0.356555\mathbf{i} \quad \text{and} \quad d, \bar{d} = \pm 0.431258\mathbf{i}.\end{aligned}$$

In this example, the structure of the roots z, \bar{z} and w, \bar{w} is a consequence of the symmetry of the Hermite data that define the curve. However, the fact that the residues c and d are pure imaginary numbers, of the same magnitude, is a generic property of helical PH quintics.

Lemma 30.2 *For general helical PH quintics, we have $\operatorname{Re}(c) = \operatorname{Re}(d) = 0$ and $|\operatorname{Im}(c)| = |\operatorname{Im}(d)|$.*

Proof : Any helical polynomial curve must be a PH curve (see Chap. 23), and without loss of generality we may choose the helical axis in the positive x -direction. The components of (22.1) then satisfy

$$u^2 + v^2 - p^2 - q^2 = \cos \psi(u^2 + v^2 + p^2 + q^2),$$

where ψ is the constant angle that the tangent makes with the axis. We can re-arrange the above equation to yield

$$(p - tu)(p + tu) = (tv - q)(tv + q) \quad \text{or} \quad (p - tv)(p + tv) = (tu - q)(tu + q),$$

where $t = \tan \frac{1}{2}\psi$. For a general PH quintic helix (i.e., with a doubly-traced tangent indicatrix), the above equations generate four pairs of solutions:

$$(p, q) = \pm t(u, v) \quad \text{or} \quad (p, q) = \pm t(-v, u). \quad (30.37)$$

Now since the function $g/h = -\frac{1}{2}\alpha$ is invariant under spatial rotations, we can rotate the curve such that the helical axis is aligned with the positive x -axis. Then the conditions (30.37) hold, and we have

$$\frac{g}{h} = \frac{1 - t^2}{1 + t^2} \frac{u'v - uv'}{u^2 + v^2} = \cos \psi \frac{d}{d\xi} \tan^{-1} \frac{u}{v}.$$

As in (30.35), we can write

$$\frac{c}{\xi - z} + \frac{\bar{c}}{\xi - \bar{z}} + \frac{d}{\xi - w} + \frac{\bar{d}}{\xi - \bar{w}} = \frac{g(\xi)}{h(\xi)} = \cos \psi \frac{d}{d\xi} \tan^{-1} \frac{u(\xi)}{v(\xi)},$$

and by the Residue Theorem, we have

$$c = \frac{1}{2\pi i} \oint_{\gamma} \frac{g}{h} d\xi = \frac{\cos \psi}{2\pi i} \oint_{\gamma} \frac{d}{d\xi} \tan^{-1} \frac{g}{h} d\xi$$

for a sufficiently small closed curve γ enclosing the point z (γ is parameterized on the interval $[0, 1]$ and has winding number 1 with respect to z).

Now since z, \bar{z} and w, \bar{w} are roots of h , we have $u^2/v^2 = -1$ at those points, and we may assume that

$$\frac{u(z)}{v(z)} = \frac{u(w)}{v(w)} = i \quad \text{and} \quad \frac{u(\bar{z})}{v(\bar{z})} = \frac{u(\bar{w})}{v(\bar{w})} = -i.$$

The arctangent function has poles at $\pm i$, and branch cuts from $+i$ to $+i\infty$ and from $-i$ to $-i\infty$. To apply the fundamental theorem of calculus

$$\oint_{\gamma} \frac{d}{d\xi} \tan^{-1} \frac{u}{v} d\xi = \tan^{-1} \frac{u(\gamma(1))}{v(\gamma(1))} - \tan^{-1} \frac{u(\gamma(0))}{v(\gamma(0))}, \quad (30.38)$$

the image of γ under the map u/v should not cross the branch cuts, i.e., we should choose the start and end points of γ such that u/v at those points lies on the branch cut from $+i$ to $+i\infty$. Then the images of $u(\gamma(1))/v(\gamma(1))$ and $u(\gamma(0))/v(\gamma(0))$ under the arctangent function are, respectively, on the lines $\operatorname{Re}(\xi) = +\frac{1}{2}\pi$ and $\operatorname{Re}(\xi) = -\frac{1}{2}\pi$ with the same height. Hence, the value of the integral (30.38) is π , and we obtain $c = -\frac{1}{2} \cos \psi i$. Identical arguments for the pole w yield $d = -\frac{1}{2} \cos \psi i$. ■

The above observation leads to the following interpretation for helical PH quintics. The quantity

$$\int \frac{g(\xi)}{h(\xi)} d\xi = -2 \operatorname{Im}(c) [\arg(\xi - z) \pm \arg(\xi - w)] + \theta_0$$

corresponds to half the angular displacement between the ERF and the RMF. As ξ traverses the real line from 0 to 1, the scaled sum (or difference) of the angular positions of z and w (the two independent complex roots of h) relative to ξ is just this angular difference.

Lemma 30.1 is a special case of the “sum of residues rule” for real rational functions with a numerator of degree two or more less than the degree of the denominator. For such rational functions, the residues always sum to zero. Lemma 30.2 is not so obvious — we are not aware of any simple geometrical interpretation or consequence of this lemma.

Once the rational approximation $a(\xi)/b(\xi)$ to (30.28) is computed, we can use the approximation $\phi(\xi) = 2 \tan^{-1} a(\xi)/b(\xi)$ to the angular deviation of the RMF from the ERF to construct the rational approximation

$$\begin{bmatrix} \hat{\mathbf{u}} \\ \hat{\mathbf{v}} \end{bmatrix} = \frac{1}{a^2 + b^2} \begin{bmatrix} b^2 - a^2 & 2ab \\ -2ab & b^2 - a^2 \end{bmatrix} \begin{bmatrix} \mathbf{u} \\ \mathbf{v} \end{bmatrix}$$

of the RMF. Since a, b are polynomials in ξ , and (\mathbf{u}, \mathbf{v}) depend rationally on ξ , it is clear that $(\hat{\mathbf{u}}, \hat{\mathbf{v}})$ have a rational dependence on ξ .

30.7.2 Computed Examples

In order to interpolate C^1 Hermite data at both $\xi = 0$ and 1 (four conditions), we must choose $a(\xi)$ linear and $b(\xi)$ quadratic, or vice-versa. Instead, we take both $a(\xi)$ and $b(\xi)$ quadratic, with an additional condition: interpolation at the midpoint, $\xi = \frac{1}{2}$. For the rational Hermite interpolation, we then have

$$\xi_0 = 0, \quad \xi_1 = \frac{1}{2}, \quad \xi_2 = 1, \quad x_0 = x_1 = 0, \quad x_2 = \frac{1}{2}, \quad x_3 = x_4 = 1,$$

and input data

$$f(0), \quad f'(0), \quad f\left(\frac{1}{2}\right), \quad f(1), \quad f'(1).$$

Note that $f^{(k)}(\xi_*)$ for $k = 0, 1, \dots$ can be computed *exactly* for any given ξ_* . Expressions (30.33) and (30.34) can then be written as

$$a(\xi) = c_{0,0}A + (c_{0,1}A + c_{1,1}B)\xi + (c_{0,2}A + c_{1,2}B + c_{2,2}C)\xi^2$$

and

$$b(\xi) = A + B\xi + C\xi^2,$$

where $A = c_{1,3}c_{2,4} - c_{1,4}c_{2,3}$, $B = c_{2,3}c_{0,4} - c_{2,4}c_{0,3}$, $C = c_{0,3}c_{1,4} - c_{0,4}c_{1,3}$.

Example 30.3 From Example 30.1, we have

$$\frac{g(\xi)}{h(\xi)} = \frac{-0.487492 - 0.231158\xi - 0.674078\xi^2}{0.455746 - 0.438713\xi + 0.514187\xi^2 + 0.942248\xi^3 + \xi^4},$$

and integration gives

$$\begin{aligned} \frac{1}{2}\theta(\xi) = 2 & \left[0.0125113 \ln \left| \frac{\xi + 0.830350 - 0.828652i}{\xi - 0.359226 - 0.449591i} \right| \right. \\ & - 0.219377 \arg(\xi + 0.830350 - 0.828652i) \\ & \left. - 0.312214 \arg(\xi - 0.359226 - 0.449591i) \right] - 0.374956\pi. \end{aligned}$$

We obtain the values $f(0) = +0.663502$, $f'(0) = -1.54056$, $f\left(\frac{1}{2}\right) = -0.112565$, $f(1) = -0.663502$, $f'(1) = -0.810949$, and the interpolant becomes

$$\frac{a(\xi)}{b(\xi)} = \frac{0.663502 - 1.37560 \xi - 0.468837 \xi^2}{1 + 0.248617 \xi + 0.531233 \xi^2}.$$

The error between the exact angle $\theta(\xi)$ and its rational approximation $\phi(\xi)$ is extremal at points where $\theta'(\xi) - \phi'(\xi) = 0$, which is equivalent to

$$\frac{g(\xi)}{h(\xi)} = \frac{a'(\xi)b(\xi) - a(\xi)b'(\xi)}{a^2(\xi) + b^2(\xi)}.$$

This is, in general, an algebraic equation of degree 6, which can be numerically solved to any desired accuracy. In this example, the roots on $[0, 1]$ are

$$\xi = 0, \quad 0.273067, \quad 0.662032, \quad 1$$

(where 0 and 1 appear by virtue of the fact that $\phi(\xi)$ is, by construction, a C^1 Hermite interpolant to $\theta(\xi)$ at these points). The error attains its maximum magnitude 0.013670 at $\xi = 0.273067$, corresponding to about 0.58% of the total variation of θ over the interval $\xi \in [0, 1]$ — in this case, $\theta(0) - \theta(1)$. The graphs of $\theta(\xi)$ and its rational approximant $\phi(\xi)$ are compared in Fig. 30.6 — they are virtually indistinguishable. To emphasize the approximation error, Fig. 30.6 also compares the derivatives of these functions.

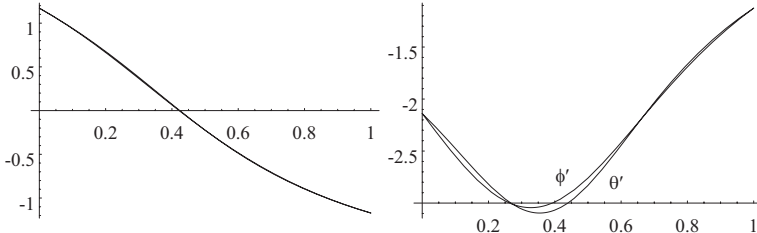


Fig. 30.6. Left: the exact angle function $\theta(\xi)$ and its rational approximation $\phi(\xi)$ in Example 30.3 — the two graphs are virtually indistinguishable at the scale shown. Right: comparison of the corresponding derivatives, $\theta'(\xi)$ and $\phi'(\xi)$.

Example 30.4 From Example 30.2 we have

$$\frac{g(\xi)}{h(\xi)} = \frac{-0.563650 + 0.615068 \xi - 0.615068 \xi^2}{0.300523 + 0.324281 \xi + 0.675719 \xi^2 - 2 \xi^3 + \xi^4},$$

and integration yields

$$\begin{aligned} \frac{1}{2}\theta(\xi) &= -2 \cdot 0.431258 [\arg(\xi + 0.234351 - 0.356555 i) \\ &\quad + \arg(\xi - 1.23435 - 0.356555 i)] + \theta_0. \end{aligned}$$

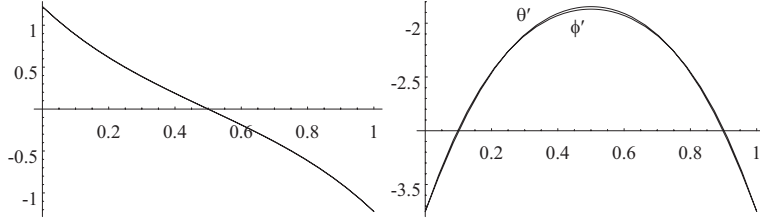


Fig. 30.7. Left: the exact angle function $\theta(\xi)$ and its rational approximation $\phi(\xi)$ in Example 30.4 — as before, the two graphs are virtually indistinguishable. Right: comparison of the corresponding derivatives, $\theta'(\xi)$ and $\phi'(\xi)$.

Again, by choosing $\theta_0 = -0.862515\pi$, the argument of the tangent function lies in the interval $\pm 0.194414\pi$, and we obtain the values $f(0) = +0.700063$, $f'(0) = -2.79476$, $f(\frac{1}{2}) = 0$, $f(1) = -0.700063$, $f'(1) = -2.79476$, for which the interpolant becomes

$$\frac{a(\xi)}{b(\xi)} = \frac{0.700063 - 1.40013\xi}{1 + 1.99215\xi - 1.99215\xi^2}.$$

In this case, the maximum error magnitude 0.003881 is about 0.16% of the total variation of θ over $\xi \in [0, 1]$, and occurs at $\xi = 0.250204$ and 0.749796 . Figure 30.7 compares $\theta(\xi)$ and $\phi(\xi)$, and their derivatives, for this example.

Figure 30.8 illustrates the Frenet frame, ERF, and rational approximation of the RMF along the curve of Example 30.4. The “unnecessary” rotation of the Frenet and Euler–Rodrigues frames, compared to the rotation–minimizing frame, is apparent. The RMF is clearly a superior choice for use in animation, motion planning, construction of swept surfaces, and similar applications.

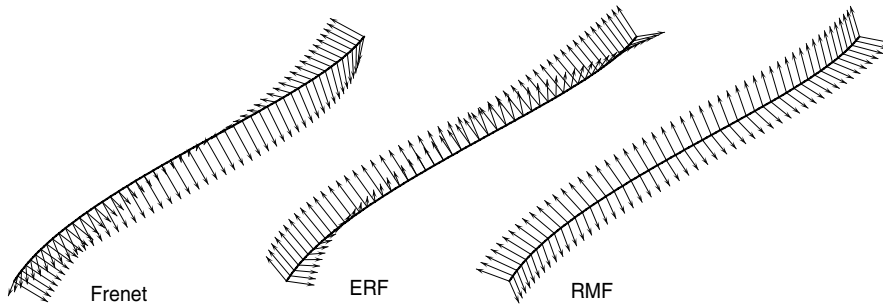


Fig. 30.8. Comparison of Frenet frame (left), Euler–Rodrigues frame (center), and the rational approximate rotation–minimizing frame (right) on the helical PH quintic of Example 30.4 (the tangent is omitted for clarity). The RMF approximation clearly provides the most “reasonable” basis in the curve normal plane at each point.

Example 30.5 As a final example, consider a PH quintic Hermite interpolant to the end points $\mathbf{p}_i = (-1, 0, 0)$, $\mathbf{p}_f = (1, 0, 0)$ and derivatives $\mathbf{d}_i = \mathbf{d}_f = (1, 1, 0)$. Choosing parameters $\phi_0 = \phi_2 = -\pi/4$ and $\phi_1 = -\pi/2$ in the Hermite interpolation algorithm (see Chap. 28) yields the quaternion coefficients

$$\mathcal{A}_0 = \mathcal{A}_2 = 0.776887 + 0.776887 \mathbf{i} + 0.321797 \mathbf{j} + 0.321797 \mathbf{k},$$

$$\mathcal{A}_1 = 2.54659 - 1.16533 \mathbf{i} - 0.482696 \mathbf{j} - 0.651072 \mathbf{k}.$$

The remaining Bézier control points are then $\mathbf{p}_1 = -\mathbf{p}_4 = (-0.8, 0.2, 0.0)$ and $\mathbf{p}_2 = -\mathbf{p}_3 = (-0.512415, 0.112735, -0.265059)$. This example is constructed specifically to exhibit an inflection: the curvature vanishes at $\xi = 0.5$.

In this case, we have

$$\frac{g(\xi)}{h(\xi)} = \frac{5.65912 - 11.3182 \xi}{1.41421 - 2.82390 \xi + 36.8149 \xi^2 - 67.9819 \xi^3 + 33.9910 \xi^4},$$

and integration gives

$$\begin{aligned} \frac{1}{2}\theta(\xi) &= 2 \cdot 0.416848 [\arg(\xi - 0.998568 + 0.200273 \mathbf{i}) \\ &\quad - \arg(\xi - 0.00143157 + 0.200273 \mathbf{i})] - 1.56041. \end{aligned}$$

The rational Hermite approximation to $f(\xi)$ is then

$$\frac{a(\xi)}{b(\xi)} = \frac{-0.448764 + 4.19880 \xi - 4.19880 \xi^2}{1 + 1.35636 \xi - 1.35636 \xi^2}.$$

Figure 30.9 compares $\theta(\xi)$ with its rational approximation $\phi(\xi)$, and also their derivatives, while Fig. 30.10 illustrates (from left to right) the Frenet frame, ERF, and rational RMF approximation. Note that the Frenet frame “flips” on passing through the inflection, at which point it is indeterminate.

The approximation scheme can achieve any prescribed accuracy by subdividing the $[0, 1]$ domain into sub-intervals, and constructing rational $(2, 2)$ approximants over those intervals — we have observed empirically that this approach often gives faster convergence to the exact RMF than higher-order

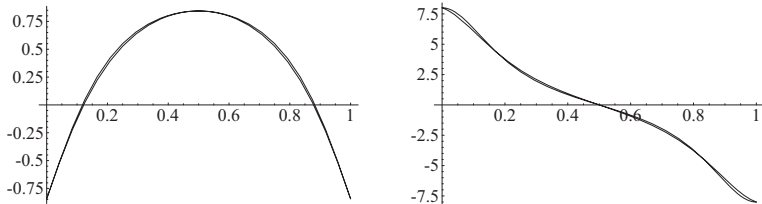


Fig. 30.9. Left: exact angle function $\theta(\xi)$ and its rational approximation $\phi(\xi)$ for Example 30.5. Right: comparison of the derivatives $\theta'(\xi)$ and $\phi'(\xi)$ of these functions.

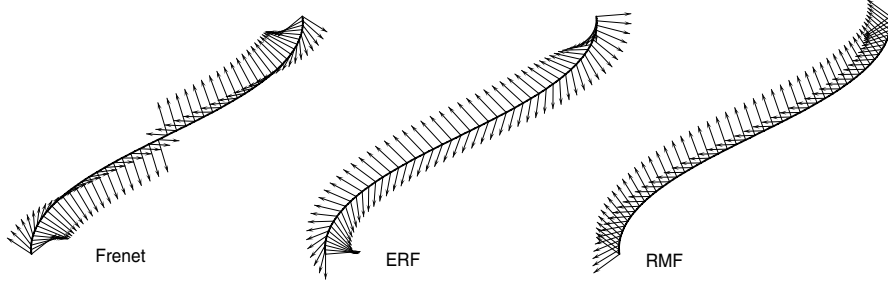


Fig. 30.10. Comparison of the Frenet frame (left), Euler–Rodrigues frame (center), and rational approximation of the rotation–minimizing frame (right) along the PH quintic of Example 30.5 (for clarity, the tangent is omitted in each case). Note the sudden “flip” in the normal and binormal of the Frenet frame at the inflection point.

rational approximants. Since the one–point Padé approximant of order (m, n) to a function $f(\xi)$ agrees with all terms in its Taylor series up to and including ξ^{m+n} , the approximant will have $O(|\xi/R|^{m+n+1})$ error for $|\xi| < R$, where R is the radius of convergence⁶ of the Taylor series [24]. The convergence rates for multi–point Padé approximants or rational Hermite interpolants have not been investigated as thoroughly, but it seems likely that they are equivalent to those of one–point Padé approximant of the same order.

30.8 Parameterization of Canal Surfaces

As stated in §24.6, a *canal surface* is the envelope of a one–parameter family of spheres, whose centers and radii are specified by a given “spine curve” $\mathbf{c}(t)$ and scalar function $r(t)$, respectively. To obtain a real envelope surface, the derivatives of the spine curve and radius function must satisfy

$$|\mathbf{c}'(t)|^2 \geq r'^2(t) \quad (30.39)$$

for all t . Clearly, this is satisfied for the simplest case with $r(t) = \text{constant}$, in which the envelope is sometimes called a *pipe surface* [314].

If condition (30.39) holds, we may regard the canal surface as comprising a one–parameter family of *characteristic circles* in \mathbb{R}^3 . Namely, if $\mathbf{p} = (x, y, z)$, the sphere corresponding to parameter value t has the implicit equation

$$F(t, \mathbf{p}) = |\mathbf{p} - \mathbf{c}(t)|^2 - r^2(t) = 0,$$

and setting its derivative with respect to t equal to zero,

$$F'(t, \mathbf{p}) = [\mathbf{p} - \mathbf{c}(t)] \cdot \mathbf{c}'(t) + r(t)r'(t) = 0,$$

⁶ Padé approximants may converge even outside the radius of convergence of the Taylor series (this is often used as a practical approach to analytic continuation).

defines a plane in \mathbb{R}^3 . The intersection of the sphere $F(t, \mathbf{p}) = 0$ with the plane $F'(t, \mathbf{p}) = 0$ defines the characteristic circle that this sphere contributes to the envelope. Note that, except for the case of a pipe surface with $r(t) = \text{constant}$, this circle is *not* in general a great circle on the sphere $F(t, \mathbf{p}) = 0$, since the plane $F'(t, \mathbf{p}) = 0$ does not pass through the center of that sphere.

Pipe surfaces are especially important for specifying *constant radius blends* in the design of load-bearing mechanical components [192, 243, 381, 457]. The presence of sharp edges on such parts typically incurs stress concentrations, that may cause a fatigue failure under cyclical loading. Hence, it is common practice to round out such edges with a blend or fillet of fixed radius r , defined by a pipe surface with the original sharp edge as spine curve. Such blends can be generated by machining the part with a spherical tool of appropriate radius.

The fact that taking a PH curve as the spine yields pipe surfaces amenable to rational parameterization was first noted in [188]. Such a parameterization has (for constant r) the form

$$\mathbf{r}(s, t) = \mathbf{c}(t) + r \frac{(1 - s^2) \mathbf{u}(t) + 2s \mathbf{v}(t)}{1 + s^2},$$

where $\mathbf{u}(t), \mathbf{v}(t)$ define an orthonormal basis for the normal plane at each point of the spine curve $\mathbf{c}(t)$, and have a rational dependence on the parameter t . It was observed in [188] that the principal normal and binormal $\mathbf{p}(t), \mathbf{b}(t)$ are not suitable for this purpose, since they are not both rational in t . However, a new basis $\mathbf{u}(t), \mathbf{v}(t)$ that is rational in t can always be defined by a rotation of $\mathbf{p}(t), \mathbf{b}(t)$ through an angle θ having an appropriate variation with t .

Actually, to obtain a rational parameterization of a pipe surface, it is not necessary for the spine to be a PH curve. Lü and Pottmann [314] showed that the pipe surfaces associated with *any* rational curve as spine admit rational parameterizations, and this result was extended by Peterzell and Pottmann [360] to show that superposing any rational radius function $r(t)$ on a rational spine curve $\mathbf{c}(t)$ yields canal surfaces with rational parameterizations when the condition (30.39) holds. Determining its rational parameterization requires an algorithm to write the non-negative rational function $|\mathbf{c}'(t)|^2 - r'^2(t)$ as a sum of squares — namely, if $\mathbf{c}(t) = (x(t), y(t), z(t))$ we must find rational functions $f(t), g(t)$ such that

$$x'^2(t) + y'^2(t) + z'^2(t) - r'^2(t) = f^2(t) + g^2(t). \quad (30.40)$$

Although such a decomposition always exists [360], it cannot be determined exactly except in very simple cases, since it requires numerical factorizations (i.e., root-solving) of polynomials. Moreover, the resulting parameterizations may be of rather poor quality — the isoparametric curves exhibit unnecessary rotation about the spine. Choi et al. [81, 88, 89] have interpreted (30.40) as the Pythagorean hodograph condition for the Minkowski space $\mathbb{R}^{3,1}$ with three space-like and one time-like coordinates, and note that it is satisfied for *any* rational (or polynomial) functions $x'(t), y'(t), z'(t), r'(t)$ — see also §24.6.

The most “natural” parameterizations of a canal surface are perhaps those based on employing an RMF to define local coordinates along the spine curve. Since the RMF is not ordinarily a rational frame, rational approximations of it must be invoked to obtain rational surface parameterizations. Several authors have described RMF approximation schemes for the spatial PH curves (which have the advantage of a rational tangents). Jüttler and Mäurer [268] proposed RMF approximations for spatial PH cubics. The method of [162], summarized in §30.7, focuses on Padé approximation for RMFs on PH quintics. Choi et al. [88] take a somewhat different approach, based upon the differential equations (30.9) and the Clifford algebra representation in the space $\mathbb{R}^{3,1}$. Another recent study based on the spatial PH quintics is described in [415]. For more complete details on these approximate rotation-minimizing parameterizations of canal surfaces, the reader may consult the original papers.

Closure

*How dull it is to pause, to make an end,
To rust unburnish'd, not to shine in use!*

Alfred, Lord Tennyson (1809–1892), *Ulysses*

It ain't over till it's over.

Yogi Berra

Since their inception [186] in 1990, a substantial volume of literature on Pythagorean–hodograph curves has accumulated — the bibliography includes over 80 papers concerned with elucidating the basic theory of PH curves, their extensions and generalizations, algorithms for their construction and analysis, and their applications in computer–aided design and manufacturing, robotics, motion control, graphics and animation, and related fields. Nevertheless, many problems merit further study, and research on PH curves remains very active. A forthcoming special issue of *Computer Aided Geometric Design* is devoted to the theme “Pythagorean–hodograph curves and related topics.”

The aim of this book was to present a comprehensive survey of the current state of knowledge concerning all the different PH curve incarnations proposed thus far (polynomial or rational, planar or spatial, Euclidean or Minkowski) — including their fundamental algebraic structures, development of geometrical algorithms for their construction, and the various practical applications that motivate their introduction. In preparation for the discussion of PH curves, a detailed summary of pertinent ideas and methods from algebra, geometry, and computer–aided geometric design was included. As observed in Chap. 1, the study of PH curves offers a natural setting in which to explore the deep–rooted and pervasive connections between classical algebra and geometry.

For planar PH curves, the complex–variable representation is indispensable in facilitating the development of basic algorithms for their construction and

analysis. Currently available methods for specifying and manipulating single Hermite interpolants or C^2 splines are comparable in efficiency and versatility to the standard (linear) Bézier/B-spline representation schemes of computer-aided geometric design. Certain features of the latter that are a consequence of their linear nature (e.g., the convex hull and variation-diminishing properties) are not available with the PH curves, but this is of little practical consequence in view of the typically superior shape properties of PH curves, compared with “ordinary” polynomial curves, as interpolants to discrete data. For spatial PH curves expressed in the quaternion formulation, on the other hand, further research is needed in elucidating the theoretical foundations and in developing algorithms to satisfy the needs of practical applications.

In §22.5, we noted that a one-to-one correspondence between “ordinary” polynomial space curves and spatial PH curves (analogous to that established for planar curves in Chap. 19, through the complex variable model) has yet to be determined. The Hopf map model [89] summarized in Remark 22.1, and the Clifford algebra geometric product model [358] mentioned in §22.4, are less well-developed alternatives to the quaternion representation, that may prove more fruitful in this context. Another interesting theoretical problem concerns the “double” PH curves [33] satisfying both (23.21) and (23.22) — see §23.5. As noted in [33], the double PH structure is sufficient and necessary for cubic and quintic space curves to be helical, but there exist non-helical double PH curves of degree 7. The geometrical properties, construction algorithms, and potential applications of such curves warrant further investigation.

As described in Chap. 30, one of the key attractions of spatial PH curves is the ability to compute rotation-minimizing frames (RMFs) on them, for 3D motion planning, whether through exact integrations that incur logarithmic terms or rational (Padé) approximation. Spatial PH curves with exact *rational* RMFs are particularly advantageous, but remain rather elusive. Choi and Han [85] showed that the only PH cubics and quintics for which a rational Euler–Rodrigues frame (ERF) may coincide with an RMF are planar, and that the simplest non-planar PH curves for which ERFs can be RMFs have degree 7. A characterization of such PH curves with rational RMFs is given in [85], but it does not readily lend itself to intuitive geometrical constructions. The study of rational RMFs on spatial PH curves deserves more attention.

Apart from these theoretical issues, there are a number of important open algorithmic difficulties that arise in the construction and analysis of spatial PH curves by means of the quaternion representation. Foremost among these is the issue of identifying optimal choices for the two free parameters that occur in Hermite interpolation by spatial PH quintics (see §28.2), and applying these choices in the formulation of spatial C^2 PH quintic splines (see §28.9). Some recent progress on this problem is reported in [160]. There is also scope for much further work on PH curves defined under the Minkowski metric of $\mathbb{R}^{(2,1)}$ — so as to provide practical algorithms for the approximation of medial axis transforms of planar domains, and the reconstruction of domain boundaries (and their offset curves) from the medial axis transform.

The question of how to extend the Pythagorean hodograph concept from curves to surfaces often arises. Some progress has been made (see §20.8) in the study of surfaces with rational offsets, although this is not yet a mature theory (especially with regard to the formulation of practical free-form surface design schemes). Rational offsets are only one of many advantageous properties of PH curves, however, and may be too restrictive as the sole basis for an extension to surfaces. For curves, there is a universal ideal of “natural parameterization”—namely, that for which the parameter corresponds to *distance* measured along the curve. Although we have seen in §16.1 that this ideal is incompatible with simple (polynomial or rational) forms, the PH curves provide a useful “bridge” to it, by ensuring that the curve arc length is simply a polynomial or rational function in the parameter. For surfaces, however, considerations of distance alone do not suffice to specify a “natural” parameterization: since a surface is a two-dimensional locus, one must also consider *direction* on the surface. The study of parameterizations that provide useful links to the intrinsic geometry of polynomial or rational surfaces is thus an important topic.

Examples of (local) “natural” surface parameterizations are the geodesic polar and geodesic parallel coordinates briefly mentioned in §8.5.9—for which the isoparametric curves remain orthogonal in some neighborhood of a chosen point. Another relevant idea, that of *isothermal parameters* on a surface, arises in the study [351] of minimal surfaces. These surface parameters are defined such that the coefficients (8.80) of the first fundamental form satisfy $F = 0$ and $E = G$, ensuring that the surface is a conformal image of the parameter domain. Identifying isothermal parameters (u, v) on a given surface $\mathbf{r}(u, v) = (x(u, v), y(u, v), z(u, v))$ is equivalent to satisfying $\phi_x^2(\zeta) + \phi_y^2(\zeta) + \phi_z^2(\zeta) = 0$, where $\zeta = u + i v$, $\phi_x = \partial x / \partial u - i \partial x / \partial v$, and likewise for ϕ_y , ϕ_z . Although, in general, we cannot expect to identify global natural parameterizations for free-form surfaces, a PH surface formulation that offers a useful “bridge” to them, expressed in terms of “simple” (polynomial or rational) functions, would nevertheless be extremely useful in a variety of contexts.

Because of the wealth of interesting problems they present, the emphasis in research on PH curves to date has been primarily on the basic mathematical theory and on algorithms for their construction and characterization. However, one must not lose sight of the motivations for studying PH curves—namely, the exactitude of many basic geometrical computations they provide, and the ability to take advantage of these computations for practical applications in geometric design, motion control, path planning, animation, and graphics. It is expected that the development of algorithms to exploit the unique properties of PH curves in these fields will suggest many interesting new problems.

*Read not to confute and contradict, nor to believe and take for granted,
nor to find talk and discourse, but to weigh and consider.*

Francis Bacon (1561–1626)

References

1. ANSI/IEEE Standard 754–1985 (1985), IEEE Standard for Binary Floating–Point Arithmetic, Institute of Electrical and Electronics Engineers, New York.
2. EIA Standard RS-274-D (1979), Interchangeable variable block data format for positioning, contouring, and contouring/positioning numerically controlled machines, Electronic Industries Association, Engineering Dept., Washington, D.C.
3. S. S. Abhyankar (1971), *Algebraic Space Curves*, University of Montreal Press.
4. ——— (1990), *Algebraic Geometry for Scientists and Engineers*, American Mathematical Society, Providence, RI.
5. S. S. Abhyankar and C. Bajaj (1987), Automatic parameterization of rational curves and surfaces I: conics and conicoids, *Comput. Aided Design* **19**, 11–14.
6. ——— (1987), Automatic parameterization of rational curves and surfaces II: cubics and cubicoids, *Comput. Aided Design* **19**, 499–502.
7. ——— (1988), Automatic parameterization of rational curves and surfaces III: algebraic plane curves, *Comput. Aided Geom. Design* **5**, 309–321.
8. ——— (1989), Automatic parameterization of rational curves and surfaces IV: algebraic space curves, *ACM Trans. Graphics* **8**, 325–334.
9. F. S. Acton (1970), *Numerical Methods that (Usually) Work*, Harper & Row, New York.
10. M-H. Ahn and G-I. Kim (2004), Characterization of Pythagorean curves and Pythagoreanization using a rational transform, *J. Symb. Comput.* **37**, 377–389.
11. M-H. Ahn, G-I. Kim, and C-N. Lee (2003), Geometry of root–related parameters of PH curves, *Appl. Math. Lett.* **16**, 49–57.
12. R. Ait Haddou and L. Biard (1995), G^2 approximation of an offset curve by Tschirnhausen quartics, in *Mathematical Methods for Curves and Surfaces* (M. Daehlen, T. Lyche, and L. L. Schumaker, eds.), Vanderbilt University Press, 1–10.
13. R. Ait Haddou, L. Biard, and M. A. Slawinsky (2000), Minkowski isoperimetric–hodograph curves, *Comput. Aided Geom. Design* **17**, 835–861.
14. R. Ait Haddou, W. Herzog, and L. Biard (2007), Pythagorean–hodograph ovals of constant width, preprint.
15. G. Albrecht and R. T. Farouki (1996), Construction of C^2 Pythagorean–hodograph interpolating splines by the homotopy method, *Adv. Comput. Math.* **5**, 417–442.

16. G. Alefeld and J. Herzberger (1983), *Introduction to Interval Computations*, Academic Press, New York.
17. E. L. Allgower and K. Georg (1990), *Numerical Continuation Methods: An Introduction*, Springer, Berlin.
18. ——— (1993), Continuation and path following, *Acta Numerica* **2**, 1–64.
19. H. Alt and O. Schwarzkopf (1995), The Voronoi diagram of curved objects, *Proceedings, 11th ACM Computational Geometry Symposium*, Vancouver, B.C., 89–97.
20. S. L. Altmann (1986), *Rotations, Quaternions, and Double Groups*, Clarendon Press, Oxford.
21. V. I. Arnol'd (1990), *Huygens and Barrow, Newton and Hooke* (translated by E. J. F. Primrose), Birkhäuser, Basel.
22. K. G. Baass (1984), The use of clothoid templates in highway design, *Transport. Forum* **1**, 47–52.
23. J. C. Baez (2002), The octonions, *Bull. Amer. Math. Soc.* **39**, 145–205.
24. G. A. Baker and P. Graves-Morris (1996), *Padé Approximants* (2nd edition), Cambridge University Press.
25. T. Banchoff, T. Gaffney, and C. McCrory (1982), *Cusps of Gauss Mappings*, Putnam, Boston.
26. C. Bangert and H. Prautzsch (1997), Circle and sphere as rational splines, *Neural Parallel Sci. Comput.* **5**, 153–161.
27. M. E. Baron (1969), *The Origins of the Infinitesimal Calculus*, Pergamon Press, Oxford (reprinted by Dover Publications, Mineola, NY).
28. A. Barr, B. Currin, S. Gabriel, and J. Hughes (1992), Smooth interpolation of orientations with angular velocity constraints using quaternions, *Computers & Graphics* **26** (2) (Proc. SIGGRAPH '92), 313–320.
29. B. J. Barsky (1988), *Computer Graphics and Geometric Modelling Using Beta-Splines*, Springer, New York.
30. E. Bayro Corrochano and G. Sobczyk, eds., (2001), *Geometric Algebra with Applications in Science and Engineering*, Birkhäuser, Boston.
31. E. F. Beckenbach and R. Bellman (1961), *Inequalities*, Springer, Berlin.
32. E. T. Bell (1937), *Men of Mathematics*, Simon and Schuster, New York.
33. J. V. Beltran and J. Monterde (2007), A characterization of quintic helices, *J. Comput. Appl. Math.* **206**, 116–121.
34. S. N. Bernstein (1912), On the best approximation of continuous functions by polynomials of a given degree (in Russian), *Comm. Kharkow Math. Soc.* (Series 2), **13**, 49–194.
35. P. Bézier (1966), Définition numérique des courbes et surfaces I, *Automatisme* **XI**, 625–632.
36. ——— (1967), Définition numérique des courbes et surfaces II, *Automatisme* **XII**, 17–21.
37. ——— (1971), Example of an existing system in the motor industry: the UNISURF system, *Proc. Royal Soc. London A* **321**, 207–218.
38. ——— (1972), *Numerical Control: Mathematics and Applications* (translated by A. R. Forrest and A. F. Pankhurst), Wiley, London.
39. ——— (1974), Mathematical and practical possibilities of UNISURF, *Computer Aided Geometric Design* (R. E. Barnhill and R. F. Riesenfeld, eds.), Academic Press, New York, 127–152.
40. ——— (1977), Essai de Définition Numérique des Courbes et des Surfaces Expérimentales, PhD Thesis, University of Paris VI.

41. ——— (1986), *The Mathematical Basis of the UNISURF CAD System*, Butterworths, London.
42. L. Bieberbach (1953), *Conformal Mapping* (translated by F. Steinhardt), Chelsea, New York.
43. G. Birkhoff and C. de Boor (1965), Piecewise polynomial interpolation and approximation, *Approximation of Functions* (H. L. Garabedian, ed.), Elsevier, Amsterdam, 164–190.
44. R. L. Bishop (1975), There is more than one way to frame a curve, *Amer. Math. Monthly* **82**, 246–251.
45. G. A. Bliss (1946), *Lectures on the Calculus of Variations*, University of Chicago Press, Chicago.
46. ——— (1946), *Algebraic Functions*, Dover Publications (reprint), New York.
47. H. Blum (1967), New algorithm for medial axis transform of plane domain, *Graph. Models Image Proc.* **59**, 463–483.
48. ——— (1973), Biological shape and visual science (Part I), *J. Theoret. Biol.* **38**, 205–287.
49. H. Blum and R. N. Nagel (1978), Shape description using weighted symmetric axis features, *Pattern Recog.* **10**, 167–180.
50. W. Boehm (1990), On cyclides in geometric modeling, *Comput. Aided Geom. Design* **7**, 243–255.
51. W. Boehm and H. Prautzsch (1994), *Geometric Concepts for Geometric Design*, AK Peters, Wellesley, MA.
52. V. G. Boltyanskii (1964), *Envelopes*, MacMillan, New York.
53. F. L. Bookstein (1979), The line–skeleton, *Comput. Graphics Image Proc.* **11**, 123–137.
54. A. M. Bork (1966), Vectors versus quaternions — the letters in *Nature*, *Amer. J. Phys.* **34**, 202–211.
55. O. Bottema and B. Roth (1979), *Theoretical Kinematics*, Dover Publications (reprint), New York.
56. C. B. Boyer and U. C. Merzbach (1991), *A History of Mathematics*, Wiley, New York.
57. J. W. Brandt, A. K. Jain, and V. R. Algazi (1991), Medial axis representation and encoding of scanned documents, *J. Visual Commun. Image Repres.* **2**, 151–165.
58. R. P. Brent (1973), *Algorithms for Minimization without Derivatives*, Prentice-Hall, Englewood Cliffs, NJ.
59. C. Brezinski and J. Van Iseghem (1994), Padé Approximations, *Handbook of Numerical Analysis III* (P. G. Ciarlet and J. L. Lions, eds.), Elsevier, 47–222.
60. T. J. I.’A. Bromwich (1906), *Quadratic Forms and Their Classification by Means of Invariant Factors*, Cambridge Tracts in Mathematics and Mathematical Physics No. 3, Cambridge University Press.
61. J. Bronowski (1973), *The Ascent of Man*, British Broadcasting Corporation, London.
62. J. W. Bruce and P. J. Giblin (1981), What is an envelope?, *Math. Gazette* **65**, 186–192.
63. ——— (1984), *Curves and Singularities*, Cambridge University Press.
64. A. M. Bruckstein and A. N. Netravali (1990), On minimal energy trajectories, *Comput. Vision, Graphics, Image Proc.* **49**, 283–296.

65. E. M. Bruins (1949), On Plimpton 322, Pythagorean numbers in Babylonian mathematics, *Koninklijke Nederlandse Akademie van Wetenschappen Proceedings* **52**, 629–632.
66. ——— (1955), Pythagorean triads in Babylonian mathematics: The errors in Plimpton 322, *Sumer* **11**, 117–121.
67. G. Brunnett (1992), A new characterization of plane elastica, in *Mathematical Methods in Computer Aided Geometric Design II* (T. Lyche and L. L. Schumaker, eds.), Academic Press, New York, 43–56.
68. ——— (1992), Properties of minimal energy splines, *Curve and Surface Design* (H. Hagen, ed.), SIAM, Philadelphia, 3–22.
69. G. Brunnett and J. Kiefer (1994), Interpolation with minimal energy splines, *Comput. Aided Design* **26**, 137–144.
70. H. Bruyninckx and D. Reynaerts (1997), Path planning for mobile and hyper-redundant robots using Pythagorean–hodograph curves. *Proceedings, International Conference on Advanced Robotics (ICAR 97)*, Monterey, CA, 595–600.
71. R. C. Buck (1978), *Advanced Calculus* (3rd edition), McGraw–Hill, New York.
72. ——— (1980), Sherlock Holmes in Babylon, *Amer. Math. Monthly* **87**, 335–345.
73. E. Buckingham (1949), *Analytical Mechanics of Gears*, McGraw–Hill, New York.
74. W. Burkert (1972), *Lore and Science in Ancient Pythagoreanism* (translated by E. L. Minar, Jr.), Harvard University Press, Cambridge, MA.
75. C. Burnett (1987), editor, *Adelard of Bath: An English Scientist and Arabist of the Early Twelfth Century*, The Warburg Institute, University of London.
76. M. F. Burnyeat (2007), Other lives, *London Review of Books* **29** (4).
77. W. S. Burnside and A. W. Panton (1960), *The Theory of Equations*, Volumes I & II, Dover Publications (reprint), New York.
78. F. Cajori (1980), *A History of Mathematics* (3rd edition), Chelsea, New York.
79. J. J. Callahan (2000), *The Geometry of Spacetime*, Springer, New York.
80. LL. G. Chambers (1969), *A Course in Vector Analysis*, Chapman and Hall, London.
81. H. C. Cho, H. I. Choi, S. H. Kwon, D. S. Lee, and N–S. Wee (2004), Clifford algebra, Lorentzian geometry, and rational parameterization of canal surfaces, *Comput. Aided Geom. Design* **21**, 327–339.
82. B. K. Choi and R. B. Gerard (1998), *Sculptured Surface Machining: Theory and Applications*, Kluwer Academic Publishers, Dordrecht.
83. H. I. Choi, S. W. Choi, C. Y. Han, and H. P. Moon (1997), Mathematical theory of medial axis transform, *Pacific J. Math.* **181**, 57–88.
84. H. I. Choi, R. T. Farouki, S. H. Kwon, and H. P. Moon (2007), Topological criterion for selection of quintic Pythagorean–hodograph Hermite interpolants, *Comput. Aided Geom. Design* to appear.
85. H. I. Choi and C. Y. Han (2002), Euler–Rodrigues frames on spatial Pythagorean–hodograph curves, *Comput. Aided Geom. Design* **19**, 603–620.
86. H. I. Choi, C. Y. Han, H. P. Moon, K. H. Roh, and N–S. Wee (1999), Medial axis transform and offset curves by Minkowski Pythagorean hodograph curves, *Comput. Aided Design* **31**, 59–72.
87. H. I. Choi, C. Y. Han, H. P. Moon, and N. S. Wee (1997), New algorithm for medial axis transform of plane domain, *Graph. Models Image Proc.* **59**, 463–483.

88. H. I. Choi, S-H. Kwon, and N-S. Wee (2004), Almost rotation-minimizing rational parameterization of canal surfaces, *Comput. Aided Geom. Design* **21**, 859–881.
89. H. I. Choi, D. S. Lee, and H. P. Moon (2002), Clifford algebra, spin representation, and rational parameterization of curves and surfaces, *Adv. Comput. Math.* **17**, 5–48.
90. J. J. Chou (1989), Numerical Control Milling Machine Toolpath Generation for Regions Bounded by Free Form Curves, PhD Thesis, University of Utah.
91. ——— (1995), Voronoi diagrams for planar shapes, *IEEE Comput. Graph. Appl.* **15** (3), 52–59.
92. ——— (1995), Higher order Bézier circles, *Comput. Aided Design* **27**, 303–309.
93. J. J. Chou and D. C. H. Yang (1991), Command axis generation for three-axis CNC machining, *ASME J. Eng. Indus.* **113**, 305–310.
94. ——— (1992), On the generation of coordinated motion of five-axis CNC/CMM machines, *ASME J. Eng. Indus.* **114**, 15–22.
95. G. Chrystal (1889), *Textbook Of Algebra*, Volumes I & II, Chelsea (reprint), New York.
96. J. E. Cobb (1989), Letter to the editor, *Comput. Aided Geom. Design* **6**, 85–86.
97. A. Coffman, A. J. Schwartz, and C. Stanton (1996), The algebra and geometry of Steiner and other quadratically parameterizable surfaces, *Comput. Aided Geom. Design* **13**, 257–286.
98. S. D. Conte and C. de Boor (1980), *Elementary Numerical Analysis: An Algorithmic Approach*, McGraw-Hill, New York.
99. J. H. Conway and D. A. Smith (2003), *On Quaternions and Octonions: Their Geometry, Arithmetic, and Symmetry*, A K Peters, Natick, MA.
100. J. L. Coolidge (1940), *A History of Geometrical Methods*, Oxford University Press (reprinted by Dover Publications, Mineola, NY).
101. ——— (1959), *A Treatise on Algebraic Plane Curves*, Dover Publications (reprint), New York.
102. P. Costantini (2000), Curve and surface construction using variable degree polynomial splines, *Comput. Aided Geom. Design* **17**, 419–446.
103. P. Costantini, R. T. Farouki, C. Manni, and A. Sestini (2001), Computation of optimal composite re-parameterizations, *Comput. Aided Geom. Design* **18**, 875–897.
104. P. Costantini and M. L. Sampoli (1998), Abstract schemes and constrained curve interpolation, *Creating Fair and Shape-Preserving Curves and Surfaces* (H. Nowacki and P. D. Kaklis, eds.), B. G. Teubner, Stuttgart, 121–130.
105. M. Cotlar and R. Cignoli (1974), *An Introduction to Functional Analysis*, North Holland, Amsterdam.
106. M. G. Cox (1972), The numerical evaluation of B-splines, *J. Inst. Maths. Applics.* **10**, 134–149.
107. H. S. M. Coxeter (1946), Quaternions and reflections, *Amer. Math. Monthly* **53**, 136–146.
108. M. J. Crowe (1967), *A History of Vector Analysis*, Dover Publications (reprint), New York.
109. A. Cuyt (1992), Rational Hermite interpolation in one and more variables, in *Approximation Theory, Spline Functions and Applications* (S. P. Singh, ed.), Kluwer Academic Publishers, 69–103.

110. G. Dahlquist and Å. Björck (1974), *Numerical Methods*, Prentice–Hall, Englewood Cliffs, NJ.
111. M. Daniel and J. C. Daubisse (1989), The numerical problem of using Bézier curves and surfaces in the power basis, *Comput. Aided Geom. Design* **6**, 121–128.
112. J. H. Davenport, Y. Siret, and E. Tournier (1988), *Computer Algebra*, Academic Press, London.
113. P. J. Davis (1975), *Interpolation and Approximation*, Dover Publications (reprint), New York.
114. C. A. Deavours (1973), The quaternion calculus, *Amer. Math. Monthly* **80**, 995–1008.
115. C. de Boor (1972), On calculating with B-splines, *J. Approx. Theory* **6**, 50–62.
116. ——— (1978), *A Practical Guide to Splines*, Springer, New York.
117. C. de Boor, K. Höllig, and M. Sabin (1987), High accuracy geometric Hermite interpolation, *Comput. Aided Geom. Design* **4**, 269–278.
118. P. de Casteljau (1963), *Courbes et Surfaces à Pôles*, Société Anonyme André Citroën, Internal Report.
119. ——— (1985), *Formes à Pôles*, Hermès, Paris.
120. ——— (1986), *Shape Mathematics and CAD*, Kogan–Page, London.
121. C. Decker (1975), *Edward FitzGerald's Rubaiyat of Omar Khayyam: A Critical Edition*, University of Virginia Press, Charlottesville, VA.
122. W. L. F. Degen (1993), High accurate rational approximation of parametric curves, *Comput. Aided Geom. Design* **10**, 293–313.
123. ——— (1996), The types of triangular Bézier surfaces, in *The Mathematics of Surfaces VI* (G. Mullineux, ed.), Oxford University Press, 153–170.
124. ——— (2004), Exploiting curvatures to compute the medial axis for domains with smooth boundary, *Comput. Aided Geom. Design* **21**, 641–660.
125. J. W. Demmel (1988), On condition numbers and the distance to the nearest ill-posed problem, *Numer. Math.* **51**, 251–289.
126. J. P. Den Hartog (1949), *Strength of Materials*, Dover Publications (reprint), New York.
127. R. Descartes (1637), *La Géométrie* (translated as *The Geometry of René Descartes* by D. E. Smith and M. L. Latham), Dover Publications, New York.
128. D. J. de Solla Price (1964), The Babylonian “Pythagorean triangle” table, *Centauros* **10**, 219–231.
129. L. E. Dickson (1952), *History of the Theory of Numbers*, Vol. II, Chelsea (reprint), New York.
130. R. Dietz, J. Hoschek, and B. Jüttler (1993), An algebraic approach to curves and surfaces on the sphere and on other quadrics, *Comput. Aided Geom. Design* **10**, 211–229.
131. E. H. Dill (1992), Kirchhoff theory of rods, *Arch. Hist. Exact Sci.* **44**, 1–23.
132. M. P. do Carmo (1976), *Differential Geometry of Curves and Surfaces*, Prentice–Hall, Englewood Cliffs, NJ.
133. C. Doran and A. Lasenby (2003), *Geometric Algebra for Physicists*, Cambridge University Press.
134. L. Dorst, C. Doran, and J. Lasenby, eds., (2002), *Applications of Geometric Algebra in Computer Science and Engineering*, Birkhäuser, Boston.
135. P. Du Val (1964), *Homographies, Quaternions, and Rotations*, Clarendon Press, Oxford.

136. ——— (1973), *Elliptic Functions and Elliptic Curves*, Cambridge University Press.
137. L. Eckhart (1929), *Four-Dimensional Space* (translated by A. L. Bigelow and S. M. Slaby), Indiana University Press, Bloomington.
138. N. V. Efimov and E. R. Rozendorn (1975), *Linear Algebra and Multi-Dimensional Geometry*, Mir Publishers, Moscow.
139. L. P. Eisenhart (1939), *Coordinate Geometry*, Dover Publications (reprint), New York.
140. G. Elber, I.-K. Lee, and M.-S. Kim (1997), Comparing offset curve approximation methods, *IEEE Comput. Graph. Appl.* **17**(3), 62–71.
141. J. F. Epperson (1987), On the Runge example, *Amer. Math. Monthly* **94**, 329–341.
142. G. Farin (1989), Curvature continuity and offsets for piecewise conics, *ACM Trans. Graphics* **8**, 89–99.
143. ——— (1995), *NURB Curves and Surfaces*, AK Peters, Wellesley, MA.
144. ——— (1997), *Curves and Surfaces for Computer Aided Geometric Design*, 4th edition, Academic Press, San Diego.
145. G. Farin, B. Piper, and A. Worsey (1987), The octant of a sphere as a non-degenerate triangular Bézier patch, *Comput. Aided Geom. Design* **4**, 329–332.
146. R. T. Farouki (1986), The approximation of non-degenerate offset surfaces, *Comput. Aided Geom. Design* **3**, 15–43.
147. ——— (1991), On the stability of transformations between power and Bernstein polynomial forms, *Comput. Aided Geom. Design* **8**, 29–36.
148. ——— (1992), Pythagorean-hodograph curves in practical use, in *Geometry Processing for Design and Manufacturing* (R. E. Barnhill, ed.), SIAM, Philadelphia, 3–33.
149. ——— (1994), The conformal map $z \rightarrow z^2$ of the hodograph plane, *Comput. Aided Geom. Design* **11**, 363–390.
150. ——— (1996), The elastic bending energy of Pythagorean-hodograph curves, *Comput. Aided Geom. Design* **13**, 227–241.
151. ——— (1997), Optimal parameterizations, *Comput. Aided Geom. Design* **14**, 153–168.
152. ——— (1997), Pythagorean-hodograph quintic transition curves of monotone curvature, *Comput. Aided Design* **29**, 601–606.
153. ——— (2000), Convergent inversion approximations for polynomials in Bernstein form, *Comput. Aided Geom. Design* **17**, 179–196.
154. ——— (2000), Legendre–Bernstein basis transformations, *J. Comput. Appl. Math.* **119**, 145–160.
155. ——— (2002), Exact rotation-minimizing frames for spatial Pythagorean-hodograph curves, *Graph. Models* **64**, 382–395.
156. ——— (2002), Pythagorean-hodograph curves, *Handbook of Computer Aided Geometric Design* (G. Farin, J. Hoschek, and M-S. Kim, eds.), Elsevier, 405–427.
157. R. T. Farouki, M. al-Kandari, and T. Sakkalis (2002), Structural invariance of spatial Pythagorean hodographs, *Comput. Aided Geom. Design* **19**, 395–407.
158. ——— (2002), Hermite interpolation by rotation-invariant spatial Pythagorean-hodograph curves, *Adv. Comput. Math.* **17**, 369–383.

159. R. T. Farouki and J-C. A. Chastang (1992), Curves and surfaces in geometrical optics, in *Mathematical Methods in Computer Aided Geometric Design II* (T. Lyche and L. L. Schumaker, eds.), Academic Press, Boston, 239–260.
160. R. T. Farouki, C. Giannelli, C. Manni, and A. Sestini (2007), Identification of spatial PH quintic Hermite interpolants with near-optimal shape measures, preprint.
161. R. T. Farouki and T. N. T. Goodman (1996), On the optimal stability of the Bernstein basis, *Math. Comp.* **65**, 1553–1566.
162. R. T. Farouki and C. Y. Han (2003), Rational approximation schemes for rotation-minimizing frames on Pythagorean-hodograph curves, *Comput. Aided Geom. Design* **20**, 435–454.
163. ——— (2006), Algorithms for spatial Pythagorean-hodograph curves, in *Geometric Properties for Incomplete Data* (R. Klette, R. Kozera, L. Noakes, and J. Weickert, eds.), Springer, 43–58.
164. R. T. Farouki, C. Y. Han, C. Manni, and A. Sestini (2004), Characterization and construction of helical polynomial space curves, *J. Comput. Appl. Math.* **162**, 365–392.
165. R. T. Farouki and J. K. Johnstone (1994), The bisector of a point and a plane parametric curve, *Comput. Aided Geom. Design* **11**, 117–151.
166. ——— (1994), Computing point/curve and curve/curve bisectors, in *Design and Application of Curves and Surfaces (The Mathematics of Surfaces V)* (R. B. Fisher, ed.), Oxford University Press, 327–354.
167. R. T. Farouki, B. K. Kuspa, C. Manni, and A. Sestini (2001), Efficient solution of the complex quadratic tridiagonal system for C^2 PH quintic splines, *Numer. Algor.* **27**, 35–60.
168. R. T. Farouki, J. Manjunathaiah, and S. Jee (1998), Design of rational cam profiles with Pythagorean-hodograph curves, *Mech. Mach. Theory* **33**, 669–682.
169. R. T. Farouki, J. Manjunathaiah, D. Nicholas, G-F. Yuan, and S. Jee (1998), Variable feedrate CNC interpolators for constant material removal rates along Pythagorean-hodograph curves, *Comput. Aided Design* **30**, 631–640.
170. R. T. Farouki, J. Manjunathaiah, and G-F. Yuan (1999), G codes for the specification of Pythagorean-hodograph tool paths and associated feedrate functions on open-architecture CNC machines, *Inter. J. Mach. Tools Manufac.* **39**, 123–142.
171. R. T. Farouki, C. Manni, and A. Sestini (2001), Real-time CNC interpolators for Bézier conics, *Comput. Aided Geom. Design* **18**, 639–655.
172. ——— (2003), Shape-preserving interpolation by G^1 and G^2 PH quintic splines, *IMA J. Numer. Anal.* **23**, 175–195.
173. ——— (2003), Spatial C^2 PH quintic splines, *Curve and Surface Design: Saint Malo 2002* (T. Lyche, M.-L. Mazure, and L. L. Schumaker, eds.), Nashboro Press, 147–156.
174. R. T. Farouki and C. A. Neff (1990), Analytic properties of plane offset curves, *Comput. Aided Geom. Design* **7**, 83–99.
175. ——— (1990), Algebraic properties of plane offset curves, *Comput. Aided Geom. Design* **7**, 101–127.
176. ——— (1990), On the numerical condition of Bernstein-Bézier subdivision processes, *Math. Comp.* **55**, 637–647.

177. ——— (1995), Hermite interpolation by Pythagorean–hodograph quintics, *Math. Comp.* **64**, 1589–1609.
178. R. T. Farouki, C. A. Neff, and M. A. O'Connor (1989), Automatic parsing of degenerate quadric surface intersections, *ACM Trans. Graphics* **8**, 174–203.
179. R. T. Farouki and J. Peters (1996), Smooth curve design with double–Tschirnhausen cubics, *Ann. Numer. Math.* **3**, 63–82.
180. R. T. Farouki and H. Pottmann (1996), Polynomial and rational Pythagorean–hodograph curves reconciled, *The Mathematics of Surfaces VI* (G. Mullineux, ed.), Oxford University Press, 355–378.
181. R. T. Farouki and V. T. Rajan (1987), On the numerical condition of polynomials in Bernstein form, *Comput. Aided Geom. Design* **4**, 191–216.
182. ——— (1988), Algorithms for polynomials in Bernstein form, *Comput. Aided Geom. Design* **5**, 1–26.
183. R. T. Farouki and R. Ramamurthy (1998), Specified–precision computation of curve/curve bisectors, *Int. J. Comput. Geom. Applic.* **8**, 599–617.
184. ——— (1998), Degenerate point/curve and curve/curve bisectors arising in medial axis computations for planar domains with curved boundaries, *Comput. Aided Geom. Design* **15**, 615–635.
185. R. T. Farouki, K. Saitou, and Y–F. Tsai (1998), Least–squares tool path approximation with Pythagorean–hodograph curves for high–speed CNC machining, *The Mathematics of Surfaces VIII* (R. Cripps, ed.), Information Geometers, Winchester, 245–264.
186. R. T. Farouki and T. Sakkalis (1990), Pythagorean hodographs, *IBM J. Res. Develop.* **34**, 736–752.
187. ——— (1991), Real rational curves are not “unit speed,” *Comput. Aided Geom. Design* **8**, 151–157.
188. ——— (1994), Pythagorean–hodograph space curves, *Adv. Comput. Math.* **2**, 41–66.
189. ——— (2007), Rational space curves are not “unit speed,” *Comput. Aided Geom. Design* **24**, 238–240.
190. R. T. Farouki and T. W. Sederberg (1995), Analysis of the offset to a parabola, *Comput. Aided Geom. Design* **12**, 639–645.
191. R. T. Farouki and S. Shah (1996), Real–time CNC interpolators for Pythagorean–hodograph curves, *Comput. Aided Geom. Design* **13**, 583–600.
192. R. T. Farouki and R. Svärrisson (1996), Approximation of rolling ball blends for free–form parametric surfaces, *Comput. Aided Design* **28**, 871–878.
193. R. T. Farouki and Y–F. Tsai (2001), Exact Taylor series coefficients for variable–feedrate CNC curve interpolators, *Comput. Aided Design* **33**, 155–165.
194. R. T. Farouki, Y–F. Tsai, and G–F. Yuan (1999), Contour machining of free–form surfaces with real–time PH curve CNC interpolators. *Comput. Aided Geom. Design* **16**, 61–76.
195. R. T. Farouki, Y–F. Tsai, and C. S. Wilson (2000), Physical constraints on feedrates and feed accelerations along curved tool paths. *Comput. Aided Geom. Design* **17**, 337–359.
196. A. Fässler (1991), Multiple Pythagorean number triples, *Amer. Math. Monthly* **98**, 505–517.
197. J. Fauvel, R. Flood, and R. Wilson, eds., (1993), *Möbius and His Band*, Oxford University Press.

198. W. Feller (1950), *An Introduction to Probability Theory and Its Applications*, Volume 1, Wiley, New York.
199. G. M. Fichtenholz (1971), *The Indefinite Integral*, Gordon and Breach, New York.
200. K. Fink (1900), *A Brief History of Mathematics* (translation of *Geschichte der Elementar-Mathematik* by W. W. Beman and D. E. Smith), Open Court Publishing Company, Chicago.
201. J.-C. Fiorot, P. Jeannin, and I. Cattiaux-Huillard (1997), The circle as a smoothly joined BR-curve on $[0, 1]$, *Comput. Aided Geom. Design* **14**, 313–323.
202. J. C. Fiorot and T. Gensane (1994), Characterizations of the set of rational parametric curves with rational offsets, *Curves and Surfaces in Geometric Design* (P. J. Laurent, A. Le Méhauté, and L. L. Schumaker, eds.), AK Peters, 153–160.
203. R. H. Fowler (1929), *The Elementary Differential Geometry of Plane Curves*, Cambridge University Press.
204. G. E. Forsythe (1970), Pitfalls in computation, or Why a math book isn't enough, *Amer. Math. Monthly* **77**, 931–956.
205. J. Friberg (1981), Methods and traditions of Babylonian mathematics I: Plimpton 322, Pythagorean triples, and the Babylonian triangle parameter equations, *Historia Math.* **8**, 277–318.
206. B. K. Fussel, C. Ersoy, and R. B. Jerard (1992), Computer generated CNC machining feed rates, *JAPAN/USA Symposium on Flexible Automation*, Vol. 1, ASME, 377–383.
207. G. Galilei, translated by S. Drake (1967), *Dialogue Concerning the Two Chief World Systems* (2nd ed.), University of California Press.
208. F. R. Gantmacher (1959), *The Theory of Matrices* Vol. 2, Chelsea, New York.
209. W. Gautschi (1973), On the condition of algebraic equations, *Numer. Math.* **21**, 405–424.
210. ——— (1984), Questions of numerical condition related to polynomials, *Studies in Numerical Analysis* (G. H. Golub, ed.), MAA Studies in Mathematics **24**, 140–177.
211. P. Goetgheluck (1987), Computing binomial coefficients, *Amer. Math. Monthly* **94**, 360–365.
212. R. N. Goldman, T. W. Sederberg, and D. C. Anderson (1984), Vector elimination: A technique for the implicitization, inversion, and intersection of planar parametric rational polynomial curves, *Comput. Aided Geom. Design* **1**, 327–356.
213. H. Goldstein (1980), *Classical Mechanics* (2nd Edition), Addison-Wesley, Reading, MA.
214. F. Gomes Teixeira (1908), *Traité des Courbes Spéciales Remarquables Planes et Gauches, Tome I-III*, Chelsea (reprint), New York.
215. T. N. T. Goodman (2002), Shape preserving interpolation by curves, *Algorithms for Approximation IV* (J. Levesley, I. J. Anderson, and J. C. Mason, eds.), University of Huddersfield, 24–35.
216. W. J. Gordon and R. F. Riesenfeld (1974), Bernstein-Bézier methods for the computer-aided design of free-form curves and surfaces, *J. Assoc. Comput. Mach.* **21**, 293–310.
217. I. S. Gradshteyn and I. M. Ryzhik (1980), *Table of Integrals, Series, and Products*, Academic Press, New York.

218. L. M. Gross (1995), Transfinite Surface Interpolation Over Voronoi Diagrams, PhD Thesis, Arizona State University.
219. I. Grattan-Guinness (1994), editor, *Companion Encyclopedia of the History and Philosophy of the Mathematical Sciences*, Volumes 1 and 2, Routledge, London.
220. H. Guggenheimer (1989), Computing frames along a trajectory, *Comput. Aided Geom. Design* **6**, 77–78.
221. H. N. Gursoy and N. M. Patrikalakis (1992), An automatic coarse and fine surface mesh generation scheme based on the medial axis transform, I: Algorithms, *Eng. Computers* **8**, 121–137.
222. Z. Habib and M. Sakai (2007), On PH quintic spirals joining two circles with one circle inside the other, *Comput. Aided Design* **39**, 125–132.
223. ——— (2007), G^2 Pythagorean hodograph quintic transition between two circles with shape control, *Comput. Aided Geom. Design* **24**, 252–266.
224. D. Hacon (1993), Jacobi's method for skew-symmetric matrices, *SIAM J. Matrix Anal. Appl.* **14**, 619–628.
225. C. Y. Han (2007), Nonexistence of rational rotation-minimizing frames on cubic curves, preprint.
226. E. Hansen, ed., (1969) *Topics in Interval Analysis*, Oxford University Press.
227. ——— (1978), A globally convergent interval method for computing and bounding real roots, *BIT* **18**, 415–424.
228. ——— (1978), Interval forms of Newton's method, *Computing* **20**, 153–163.
229. P. Hartman (1957), The highway spiral for combining curves of different radii, *Trans. Amer. Soc. Civil Eng.* **22**, 389–409.
230. F. Hausdorff (1957), *Set Theory* (translated by J. R. Aumann et al.), Chelsea, New York.
231. M. A. Heald (1985), Rational approximations for the Fresnel integrals, *Math. Comp.* **44**, 459–461.
232. M. Held (1991), *On the Computational Geometry of Pocket Machining*, Springer, Berlin.
233. A. Henderson (1911), *The Twenty-Seven Lines on a Cubic Surface*, Cambridge Tracts in Mathematics and Mathematical Physics No. 13, Cambridge University Press.
234. P. Henrici (1964), *Elements of Numerical Analysis*, Wiley, New York.
235. ——— (1974), *Applied and Computational Complex Analysis*, Vol. 1, Wiley, New York.
236. T. Hermann (1996), On the stability of polynomial transformations between Taylor, Bernstein, and Hermite forms, *Numer. Algor.* **13**, 307–320.
237. V. Hernandez-Mederos and J. Estrada-Sarlabous (2003), Sampling points on regular parametric curves with control of their distribution, *Comput. Aided Geom. Design* **20**, 363–382.
238. D. Hestenes and G. Sobczyk (1984), *Clifford Algebra to Geometric Calculus: A Unified Language for Mathematics and Physics*, D. Reidel, Dordrecht.
239. J. K. Hinds and L. P. Kuan (1978), Surfaces defined by curve transformations, Proceedings of the 15th Numerical Control Society Annual Meeting & Technical Conference, 325–340.
240. ——— (1979), Sculptured surface technology as a unified approach to geometric definition, Technical Paper MS79–146, Computer and Automated Systems Association of the Society of Manufacturing Engineers, Dearborn, MI (1979).

241. K. Hoffman and R. Kunze (1971), *Linear Algebra*, 2nd edition, Prentice-Hall, Englewood Cliffs, NJ.
242. J. E. Hofmann (1974), *Leibniz in Paris 1672–1676: His Growth to Mathematical Maturity*, Cambridge University Press.
243. C. Hoffmann and J. Hopcroft (1986), Quadratic blending surfaces, *Comput. Aided Design* **18**, 301–306.
244. K. Höllig and J. Koch (1995), Geometric Hermite interpolation, *Comput. Aided Geom. Design* **12**, 567–580.
245. R. A. Horn and C. R. Johnson (1988), *Matrix Analysis*, Cambridge University Press.
246. E. Horowitz (1969), Algorithm for Symbolic Integration of Rational Functions, PhD Thesis, University of Wisconsin.
247. ——— (1971), Algorithms for partial fraction decomposition and rational function integration, *Proceedings, Second ACM Symposium on Symbolic and Algebraic Manipulation*, 441–457.
248. J. Hoschek (1983), Dual Bézier curves and surfaces, in *Surfaces in Computer Aided Geometric Design* (R. E. Barnhill and W. Boehm, eds.), North Holland, 147–156.
249. ——— (1984), Detecting regions with undesirable curvature, *Comput. Aided Geom. Design* **1**, 183–192.
250. ——— (1985), Offset curves in the plane, *Comput. Aided Design* **17**, 77–82.
251. ——— (1988), Spline approximation of offset curves, *Comput. Aided Geom. Design* **5**, 33–40.
252. J. Hoschek and N. Wissel (1988), Optimal approximate conversion of spline curves and spline approximation of offset curves, *Comput. Aided Design* **20**, 475–483.
253. J.-T. Huang and D. C. H. Yang (1992), A generalized interpolator for command generation of parametric curves in computer-controlled machines, *Proceedings, Japan/USA Symposium on Flexible Automation*, Volume 1, ASME, 393–399.
254. C. Huygens (1673), *Horologium Oscillatorium sive De Motu Pendulorum ad Horologia Aptato Demonstrationes Geometricæ*, Paris, 1673; translated by R. J. Blackwell as *The Pendulum Clock, or Geometrical Demonstrations Concerning the Motion of Pendula as Applied to Clocks*, Iowa State University Press, Ames, IA, 1986.
255. ——— (1690), *Traité de la Lumière, Avec un Discours de la Cause de la Pesanteur*, Dawsons of Pall Mall (facsimile reprint 1966), London.
256. E. Isaacson and H. B. Keller (1994), *Analysis of Numerical Methods*, Dover Publications (reprint), New York.
257. J. Jerome (1975), Smooth interpolating curves of prescribed length and minimum curvature, *Proc. Amer. Math. Soc.* **51**, 62–66.
258. E. D. Jou and W. Han (1990), Minimal-energy splines: I. Plane curves with angle constraints, *Math. Methods Appl. Sci.* **13**, 351–372.
259. ——— (1991), Elastica and minimal-energy splines, *Curves and Surfaces* (P. J. Laurent, A. Le Méhauté, and L. L. Schumaker, eds.), Academic Press, Boston, 247–250.
260. C. M. Jessop (1916), *Quartic Surfaces*, Cambridge University Press.
261. B. Jowett, translator (1968), *Plato's Republic*, Airmont Publishing Company, New York.

262. B. Jüttler (1994), Visualization of moving objects using dual quaternion curves, *Computers & Graphics* **18**, 315–326.
263. ——— (1997), A vegetarian approach to optimal parameterizations, *Comput. Aided Geom. Design* **14**, 887–890.
264. ——— (1998), Generating rational frames of space curves via Hermite interpolation with Pythagorean hodograph cubic splines, *Geometric Modeling and Processing '98*, Bookplus Press, 83–106.
265. ——— (1998), Triangular Bézier surface patches with a linear normal vector field, *The Mathematics of Surfaces VIII* (R. Cripps, ed.), Information Geometers, Winchester, 431–446.
266. ——— (2001), Hermite interpolation by Pythagorean hodograph curves of degree seven, *Math. Comp.* **70**, 1089–1111.
267. B. Jüttler and C. Mäurer (1999), Cubic Pythagorean hodograph spline curves and applications to sweep surface modelling, *Comput. Aided Design* **31**, 73–83.
268. ——— (1999), Rational approximation of rotation minimizing frames using Pythagorean-hodograph cubics, *J. Geom. Graphics* **3**, 141–159.
269. B. Jüttler and M. L. Sampoli (2000), Hermite interpolation by piecewise polynomial surfaces with rational offsets, *Comput. Aided Geom. Design* **17**, 361–385.
270. B. Jüttler and W. Wang (2003), The shape of spherical quartics, *Comput. Aided Geom. Design* **20**, 621–636.
271. M. Kallay (1986), Plane curves of minimal energy, *ACM Trans. Math. Software* **12**, 219–222.
272. L. V. Kantorovich and G. P. Akilov (1982), *Functional Analysis* (2nd edition), Pergamon Press, Oxford.
273. L. C. Karpinski (1915), *Robert of Chester's Latin Translation of the Algebra of al-Khowarizmi*, Macmillan, New York.
274. D. S. Kasir (1931), *The Algebra of Omar Khayyam*, Bureau of Publications, Teachers College, Columbia University, New York (reprinted by AMS Press, New York, 1972).
275. K. Kendig (1977), *Elementary Algebraic Geometry*, Springer, New York.
276. B. H. Kim and C. N. Chu (1994), Effect of cutter mark on surface roughness and scallop height in sculptured surface machining, *Comput. Aided Design* **26**, 179–188.
277. G-I. Kim and M-H. Ahn (2003), C^1 Hermite interpolation using MPH quartic, *Comput. Aided Geom. Design* **20**, 469–492.
278. M.-S. Kim and K.-W. Nam (1995), Interpolating solid orientations with circular blending quaternion curves, *Comput. Aided Design* **27**, 385–398.
279. F. C. Kirwan (1992), *Complex Algebraic Curves*, Cambridge University Press.
280. R. Klass (1983), An offset spline approximation for plane cubic splines, *Comput. Aided Design* **15**, 297–299.
281. M. Kline (1972), *Mathematical Thought from Ancient to Modern Times* (3 volumes), Oxford University Press, New York.
282. ——— (1980), *Mathematics and the Loss of Certainty*, Oxford University Press.
283. F. Klok (1986), Two moving coordinate frames for sweeping along a 3D trajectory, *Comput. Aided Geom. Design* **3**, 217–229.
284. M. Kneser (1960), Über die Darstellung algebraischer Raumkurven als Durchschnitte von Flächen, *Arch. Math.* **11**, 157–158.

285. R. Komanduri, K. Subramanian, and B. F. von Turkovich, eds., (1984), *High Speed Machining*, PED–Vol. 12, ASME, New York.
286. P. A. Koparkar and S. P. Mudur (1983), A new class of algorithms for the processing of parametric curves, *Comput. Aided Design* **15**, 41–45.
287. J. Kosinka and B. Jüttler (2006), G^1 Hermite interpolation by Minkowski Pythagorean hodograph cubics, *Comput. Aided Geom. Design* **23**, 401–418.
288. ——— (2007), C^1 Hermite interpolation by Pythagorean hodograph quintics in Minkowski space, preprint.
289. M. Kracht and E. Kreyszig (1990), E. W. von Tschirnhaus: His role in early calculus and his work and impact on algebra, *Historia Math.* **17**, 16–35.
290. E. Kreyszig (1959), *Differential Geometry*, University of Toronto Press.
291. L. Kronecker (1882), Grundzüge einer arithmetischen Theorie der algebraischen Größen, *J. Reine Angew. Math.* **92**, 1–122.
292. K. K. Kubota (1972), Pythagorean triples in unique factorization domains, *Amer. Math. Monthly* **79**, 503–505.
293. J. B. Kuipers (1999), *Quaternions and Rotation Sequences*, Princeton University Press, Princeton, NJ.
294. B. I. Kvasov (2000), Algorithms for shape–preserving local approximation with automatic selection of tension parameters, *Comput. Aided Geom. Design* **17**, 17–37.
295. L. D. Landau and E. M. Lifshitz (1986), *Theory of Elasticity* (3rd edition), Pergamon Press, Oxford.
296. J. M. Lane and R. F. Riesenfeld (1981), Bounds on a polynomial, *BIT* **21**, 112–117.
297. S. Lang (1999), *Complex Analysis* (4th edition), Springer, New York.
298. M. Lávička and B. Bastl (2006), Rational hypersurfaces with rational convolutions, preprint.
299. D. F. Lawden (1989), *Elliptic Functions and Applications*, Springer, New York.
300. J. D. Lawrence (1972), *A Catalog of Special Plane Curves*, Dover Publications, New York.
301. D. T. Lee (1982), Medial axis transformation of a planar shape, *IEEE Trans. Pattern Anal. Mach. Intell.* **4**, 363–369.
302. E. T. Y. Lee (1987), The rational Bézier representation for conics, in *Geometric Modeling: Algorithms and New Trends* (G. Farin, ed.), SIAM, 1–19.
303. E. Lee and G. Forsythe (1973), Variational study of nonlinear spline curves, *SIAM Rev.* **15**, 120–133.
304. B–G. Lee, Y. Park, and J. Yoo (2002), Application of Legendre–Bernstein basis transformations to degree elevation and degree reduction, *Comput. Aided Geom. Design* **19**, 709–718.
305. M. Lembo (2001), On the free shapes of elastic rods, *Eur. J. Mech. A/Solids* **20**, 469–483.
306. R–S. Lin and Y. Koren (1996), Real–time interpolators for multi–axis CNC machine tools, *Manufac. Sys.* **25**, 145–149.
307. M. Lipschutz (1969), *Theory and Problems of Differential Geometry*, McGraw–Hill, New York.
308. E. H. Lockwood (1967), *A Book of Curves*, Cambridge University Press.
309. A. E. H. Love (1944), *A Treatise on the Mathematical Theory of Elasticity*, Dover Publications (reprint), New York.

310. P. Lounesto (1997), *Clifford Algebras and Spinors*, Cambridge University Press.
311. W. Lü (1994), Rationality of the offsets to algebraic curves and surfaces, *Applied Mathematics* **9** (Ser. B), 265–278.
312. ——— (1995), Offset-rational parametric plane curves, *Comput. Aided Geom. Design* **12**, 601–616.
313. ——— (1996), Rational parameterization of quadrics and their offsets, *Computing* **57**, 135–147.
314. W. Lü and H. Pottmann (1996), Pipe surfaces with rational spine curve are rational, *Comput. Aided Geom. Design* **13**, 621–628.
315. N. Mackey (1995), Hamilton and Jacobi meet again: quaternions and the eigenvalue problem, *SIAM J. Matrix Anal. Appl.* **16**, 421–435.
316. M. A. Malcolm (1977), On the computation of nonlinear spline functions, *SIAM J. Numer. Anal.* **14**, 254–282.
317. C. Manni (2001), On shape-preserving C^2 Hermite interpolation, *BIT* **41**, 127–148.
318. H. P. Manning (1910), editor, *The Fourth Dimension Simply Explained*, Dover Publications (reprint), New York.
319. ——— (1914), *Geometry of Four Dimensions*, Dover Publications (reprint), New York.
320. K. Marciniaik (1991), *Geometric Modelling for Numerically Controlled Machining*, Oxford University Press.
321. D. S. Meek and R. S. D. Thomas (1991), A guided clothoid spline, *Comput. Aided Geom. Design* **8**, 163–174.
322. D. S. Meek and D. J. Walton (1989), The use of Cornu spirals in drawing planar curves of controlled curvature, *J. Comput. Appl. Math.* **25**, 69–78.
323. ——— (1992), Clothoid spline transition spirals, *Math. Comp.* **59**, 117–133.
324. E. Mehlum (1974), Nonlinear splines, *Computer Aided Geometric Design* (R. E. Barnhill and R. F. Riesenfeld, eds.) Academic Press, New York, 173–207.
325. S. N. Meshkat and C. M. Sakkas (1987), Voronoi diagram for multiply-connected polygonal domains II: Implementation and application, *IBM J. Res. Develop.* **31**, 373–381.
326. R. S. Millman and G. D. Parker (1977), *Elements of Differential Geometry*, Prentice-Hall, Englewood Cliffs, NJ.
327. H. Minkowski (1908), Space and Time, translation of an address delivered at the 80th Assembly of German Natural Scientists and Physicians, September 21, 1908, Köln, in *The Principle of Relativity* (Dover, 1952).
328. H. P. Moon (1998), Computing rational offsets via medial axis transform using polynomial speed curves in $\mathbf{R}^{2,1}$, in *Geometric Modeling and Processing '98*, Bookplus Press, 187–203.
329. ——— (1999), Minkowski Pythagorean hodographs, *Comput. Aided Geom. Design* **16**, 739–753.
330. ——— (1999), Medial Axis Transform and Minkowski Geometry, PhD Thesis, Seoul National University.
331. H. P. Moon, R. T. Farouki, and H. I. Choi (2001), Construction and shape analysis of PH quintic Hermite interpolants, *Comput. Aided Geom. Design* **18**, 93–115.
332. R. E. Moore, *Interval Analysis*, Prentice-Hall, Englewood Cliffs, NJ (1966).

- 333. ———, *Methods and Applications of Interval Analysis*, SIAM, Philadelphia (1979).
- 334. R. Morandi and A. Sestini (1999), C^2 locally convexity-preserving interpolation through the control point form method, *The Visual Computer* **15**, 483–493.
- 335. A. P. Morgan (1987), *Solving Polynomial Systems Using Continuation for Engineering and Scientific Problems*, Prentice-Hall, Englewood Cliffs, NJ.
- 336. A. P. Morgan and A. Sommese (1987), A homotopy for solving general polynomial systems that respects m -homogeneous structures, *Appl. Math. Comp.* **24**, 101–113.
- 337. ——— (1987), Computing all solutions to polynomial systems using homotopy continuation, *Appl. Math. Comp.* **24**, 115–138.
- 338. S. P. Mudur and P. A. Koparkar (1984), Interval methods for processing geometric objects, *IEEE Comput. Graph. Appl.* **2**, 7–17.
- 339. P. J. Nahin (1998), *An Imaginary Tale: The Story of $\sqrt{-1}$* , Princeton University Press, Princeton, NJ.
- 340. S. Napajit, H. N. Phien, and D. B. Khang (1996), Pythagorean hodograph of planar cubic curves, *Ann. Numer. Math.* **3**, 285–296.
- 341. S. H. Nasr (1968), *Science and Civilization in Islam*, Harvard University Press, Cambridge, MA.
- 342. T. Needham (1997), *Visual Complex Analysis*, Oxford University Press.
- 343. O. Neugebauer (1957), *The Exact Sciences in Antiquity* (2nd edition), Brown University Press (reprinted by Dover Publications, New York).
- 344. O. Neugebauer and A. J. Sachs (1945), *Mathematical Cuneiform Texts*, American Oriental Series Vol. 29, American Oriental Society, New Haven.
- 345. P. M. Neumann, G. A. Stoy, and E. C. Thompson (1994), *Groups and Geometry*, Oxford University Press.
- 346. I. Newton (1730), *Opticks, or a Treatise of the Reflections, Refractions, Inflections & Colours of Light*, Dover Publications (reprint of 4th edition, London 1730), New York.
- 347. A. W. Nutbourne, P. M. McLellan, and R. M. L. Kensit (1972), Curvature profiles for plane curves, *Comput. Aided Design* **4**, 176–184.
- 348. B. H. Ong (1996), An extraction of almost arc length parameterization from parametric curves, *Ann. Numer. Math.* **3**, 305–316.
- 349. J. O'Rourke (1993), *Computational Geometry in C*, Cambridge University Press.
- 350. J. M. Ortega (1968), The Newton-Kantorovich theorem, *Amer. Math. Monthly* **75**, 658–660.
- 351. R. Osserman (1969), *A Survey of Minimal Surfaces*, Dover Publications (reprint) New York.
- 352. ——— (1985), The four-or-more vertex theorem, *Amer. Math. Monthly* **92**, 332–337.
- 353. R. R. Patterson (1988), Parameterizing and graphing non-singular cubic curves, *Comput. Aided Design* **20**, 615–623.
- 354. F. Pelosi, R. T. Farouki, C. Manni, and A. Sestini (2005), Geometric Hermite interpolation by spatial Pythagorean-hodograph cubics, *Adv. Comput. Math.* **22**, 325–352.
- 355. F. Pelosi, M. L. Sampoli, R. T. Farouki, and C. Manni (2007), A control polygon scheme for design of planar C^2 PH quintic spline curves, *Comput. Aided Geom. Design* **24**, 28–52.

356. O. Perron (1942), Über das Vahlensche Beispiel zu einem Satz von Kronecker, *Math. Z.* **47**, 318–324.
357. H. Persson (1978), NC machining of arbitrarily shaped pockets, *Comput. Aided Design* **10**, 169–174.
358. C. B. U. Perwass, R. T. Farouki, and L. Noakes (2007), A geometric product formulation for spatial Pythagorean–hodograph curves with applications to Hermite interpolation, *Comput. Aided Geom. Design* **24**, 220–237.
359. M. Peternell and H. Pottmann (1996), Designing rational surfaces with rational offsets, in *Advanced Topics in Multivariate Approximation* (F. Fontanella, K. Jetter, and P. J. Laurent, eds.), World Scientific Press, 275–286.
360. ——— (1997), Computing rational parameterizations of canal surfaces, *J. Symb. Comput.* **23**, 255–266.
361. ——— (1998) A Laguerre geometric approach to rational offsets, *Comput. Aided Geom. Design* **15**, 223–249.
362. B. Pham (1988), Offset approximation of uniform B–splines, *Comput. Aided Design* **20**, 471–483.
363. ——— (1992), Offset curves and surfaces: a brief survey, *Comput. Aided Design* **24**, 223–229.
364. G. M. Phillips and P. J. Taylor (1973), *Theory and Applications of Numerical Analysis*, Academic Press, London.
365. L. Piegl (1986), The sphere as a rational Bézier surface, *Comput. Aided Geom. Design* **3**, 45–52.
366. G. Polya (1954), *Mathematics and Plausible Reasoning, Volume 1: Induction and Analogy in Mathematics*, Princeton University Press, Princeton, NJ.
367. I. R. Porteous (1994), *Geometric Differentiation*, Cambridge University Press.
368. H. Pottmann (1994), Applications of the dual Bézier representation of rational curves and surfaces, *Curves and Surfaces in Geometric Design* (P. J. Laurent, A. Le Méhauté, and L. L. Schumaker, eds.), AK Peters, 377–384.
369. ——— (1995), Rational curves and surfaces with rational offsets, *Comput. Aided Geom. Design* **12**, 175–192.
370. ——— (1995), Curve design with rational Pythagorean–hodograph curves. *Adv. Comput. Math.* **3**, 147–170.
371. H. Pottmann and M. Peternell (1998), Applications of Laguerre geometry in CAGD, *Comput. Aided Geom. Design* **15**, 165–186.
372. M. J. Pratt (1990), Cyclides in computer aided geometric design, *Comput. Aided Geom. Design* **7**, 221–242.
373. F. P. Preparata (1977), The medial axis of a simple polygon, *Proceedings, 6th Symposium on Mathematical Foundations of Computer Science*, 443–450.
374. E. J. F. Primrose (1955), *Plane Algebraic Curves*, Macmillan, London.
375. R. Ramamurthy and R. T. Farouki (1999), Voronoi diagram and medial axis algorithm for planar domains with curved boundaries I. Theoretical foundations & II. Detailed algorithm description, *J. Comput. Appl. Math.* **102**, 119–141 & 253–277.
376. T. J. Rivlin (1990), *Chebyshev Polynomials: From Approximation Theory to Algebra and Number Theory*, Wiley, New York.
377. E. Robson (2001), Neither Sherlock Holmes nor Babylon: A reassessment of Plimpton 322, *Historia Math.* **28**, 167–206.

378. ——— (2002), Words and pictures: New light on Plimpton 322, *Amer. Math. Monthly* **109**, 105–120.
379. J. Roe (1993), *Elementary Geometry*, Oxford University Press.
380. F. Rosen (1986), *The Algebra of Mohammed ben Musa*, Georg Olms Verlag, Hildesheim (reprint).
381. J. R. Rossignac and A. A. G. Requicha (1984), Constant-radius blending in solid modeling, *Computers Mech. Engr.* **3**, 65–73.
382. M. Rothstein (1976), Aspects of Symbolic Integration and Simplification of Exponential and Primitive Functions, PhD Thesis, University of Wisconsin.
383. J. W. Rutter (2000), *Geometry of Curves*, Chapman & Hall/CRC, Boca Raton.
384. M. Sabin (1997), Rational speed pseudo-quadratic B-splines, in *Curves and Surfaces with Applications in CAGD* (A. Le Méhauté, C. Rabut, and L. L. Schumaker, eds.), Vanderbilt University Press, 395–402.
385. T. Sakkalis and R. T. Farouki (1993), Algebraically rectifiable parametric curves, *Comput. Aided Geom. Design* **10**, 551–569.
386. G. Salmon (1879), *A Treatise on the Higher Plane Curves*, 3rd edition, Chelsea (reprint), New York.
387. H. Samet (1982), Neighbor finding techniques for images represented by quadtrees, *Comput. Graphics Image Proc.* **18**, 37–57.
388. ——— (1988), Hierarchical data structures and algorithms for computer graphics. I. Fundamentals, *IEEE Comput. Graph. Appl.* **8** (3), 48–68.
389. M. L. Sampoli, M. Peternell, and B. Jüttler (2006), Rational surfaces with linear normals and their convolutions with rational surfaces, *Comput. Aided Geom. Design* **23**, 179–192.
390. G. M. Scarpello and A. Scimone (2005), The work of Tschirnhaus, La Hire and Leibniz on catacaustics and the birth of the envelopes of lines in the 17th century, *Arch. Hist. Exact Sci.* **59**, 223–250.
391. R. Schickentanz (1997), Interpolating G^1 splines with rational offsets, *Comput. Aided Geom. Design* **14**, 881–885.
392. ——— (1999), *Interpolation und Approximation durch rationale B-Spline Flächen mit rationalen Offsets*, Dissertation, Technische Universität Darmstadt.
393. O. Schmidt (1980), On Plimpton 322. Pythagorean numbers in Babylonian mathematics, *Centaurus* **24**, 4–13.
394. I. J. Schoenberg (1946), Contributions to the problem of approximation of equidistant data by analytic functions, Parts A & B, *Quart. Appl. Math.* **4**, 45–99 & 112–141.
395. ——— (1959), On variation-diminishing approximation methods, *On Numerical Approximation* (R. E. Langer, ed.), University of Wisconsin Press, 249–274.
396. O. Schreier and E. Sperner (1961), *Projective Geometry of n Dimensions*, Chelsea Publishing Co., New York.
397. H. Schwerdtfeger (1979), *Geometry of Complex Numbers*, Dover Publications (reprint), New York.
398. T. W. Sederberg (1986), Improperly parameterized rational curves, *Comput. Aided Geom. Design* **6**, 67–75.
399. T. W. Sederberg and D. C. Anderson (1985), Steiner surface patches, *IEEE Comput. Graph. Appl.* **5** (5), 23–36.

400. T. W. Sederberg, D. C. Anderson, and R. N. Goldman (1984), Implicit representation of parametric curves and surfaces, *Comput. Vision, Graphics, Image Proc.* **28**, 72–84.
401. ——— (1985), Implicitization, inversion, and intersection of planar rational cubic curves, *Comput. Vision, Graphics, Image Proc.* **31**, 89–102.
402. T. W. Sederberg and R. T. Farouki (1992), Approximation by interval Bézier curves, *IEEE Comput. Graph. Appl.* **12** (5), 87–95.
403. T. W. Sederberg, T. Saito, D. Qi, and K. S. Klimaszewski (1994), Curve implicitization using moving lines, *Comput. Aided Geom. Design* **11**, 687–706.
404. T. W. Sederberg and J. P. Snively (1986), Parameterization of cubic algebraic surfaces, in *The Mathematics of Surfaces II* (R. R. Martin, ed.), Oxford University Press, 299–319.
405. T. W. Sederberg and X. Wang (1987), Rational hodographs, *Comput. Aided Geom. Design* **4**, 333–335.
406. J. G. Semple and G. T. Kneebone (1959), *Algebraic Curves*, Oxford University Press.
407. J. G. Semple and L. Roth (1986), *Introduction to Algebraic Geometry*, Oxford University Press (reprint).
408. E. C. Sherbrooke, N. M. Patrikalakis, and F-E. Wolter (1996), Differential and topological properties of medial axis transforms, *Graph. Models Image Proc.* **58**, 574–592.
409. A. Shima, T. Sasaki, T. Ohtsuki, and Y. Wakimoto (1996), 64-bit RISC-based Series 15 NURBS interpolation, *FANUC Tech. Rev.* **9** (1), 23–28.
410. K. Shoemake (1985), Animating rotation with quaternion curves, *Computers & Graphics* **19** (3) (Proc. SIGGRAPH '85), 245–254.
411. M. Shpitalni, Y. Koren, and C. C. Lo (1994), Realtime curve interpolators, *Comput. Aided Design* **26**, 832–838.
412. C. C. Silva and R. de Andrade Martins (2002), Polar and axial vectors versus quaternions, *Amer. J. Phys.* **70**, 958–963.
413. Z. Šír and B. Jüttler (2005), Euclidean and Minkowski Pythagorean hodograph curves over planar cubics, *Comput. Aided Geom. Design* **22**, 753–770.
414. ——— (2005), Constructing acceleration continuous tool paths using Pythagorean hodograph curves, *Mech. Mach. Theory* **40**, 1258–1272.
415. ——— (2005), Spatial Pythagorean hodograph quintics and the approximation of pipe surfaces, in *The Mathematics of Surfaces XI* (R. Martin, H. Bez, and M. Sabin, eds.), Springer, Berlin, 364–380.
416. ——— (2007), C^2 Hermite interpolation by Pythagorean hodograph space curves, *Math. Comp.* **76**, 1373–1391.
417. Å. W. Sjöberg (1972), In praise of the scribal art, *Journal of Cuneiform Studies* **24**, 126–131.
418. T. S. Smith and R. T. Farouki (2001), Gauss map computation for free-form surfaces, *Comput. Aided Geom. Design* **18**, 831–850.
419. T. S. Smith, R. T. Farouki, M. al-Kandari, and H. Pottmann (2002), Optimal slicing of free-form surfaces, *Comput. Aided Geom. Design* **19**, 43–64.
420. D. E. Smith and L. C. Karpinski (1911), *The Hindu–Arabic Numerals*, Ginn & Company, Boston.
421. S. Smith and J. Tlusty (1997), Current trends in high-speed machining, *ASME J. Manufac. Sci. Eng.* **119**, 664–666.

422. V. Snyder and C. H. Sisam (1914), *Analytic Geometry of Space*, Henry Holt & Co., New York.
423. D. M. Y. Sommerville (1951), *Analytical Geometry of Three Dimensions*, Cambridge University Press.
424. V. Srinivasan and L. R. Nackman (1987), Voronoi diagram for multiply-connected polygonal domains I: Algorithm, *IBM J. Res. Develop.* **31**, 361–372.
425. V. Srinivasan, L. R. Nackman, J-M. Tang, and S. N. Meshkat (1992), Automatic mesh generation using the symmetric axis transform of polygonal domains, *IEEE Proc.* **80**, 1485–1501.
426. N. E. Steenrod (1951), *Topology of Fiber Bundles*, Princeton University Press, Princeton, NJ.
427. D. J. Steigmann and M. G. Faulkner (1993), Variational theory for spatial rods, *J. Elast.* **33**, 1–26.
428. R. J. Stephenson (1966), Development of vector analysis from quaternions, *Amer. J. Phys.* **34**, 194–201.
429. P. Sterbenz (1974), *Floating Point Computation*, Prentice-Hall, Englewood Cliffs, NJ.
430. G. W. Stewart (1973), *Introduction to Matrix Computations*, Academic Press, New York.
431. J. Stoer and R. Bulirsch (1992), *Introduction to Numerical Analysis* (2nd edition), Springer-Verlag, New York.
432. D. J. Struik (1986), editor, *A Source Book in Mathematics 1200–1800*, Princeton University Press, Princeton, NJ.
433. ——— (1961), *Lectures on Classical Differential Geometry*, Dover Publications (reprint), New York.
434. G. Szegö (1975), *Orthogonal Polynomials* (4th edition), American Mathematical Society, Providence, RI.
435. T. K. H. Tam and C. G. Armstrong (1991), 2D finite element mesh generation by medial axis subdivision, *Adv. Eng. Software* **13**, 313–324.
436. R. A. Tapia (1971), The Kantorovich theorem for Newton's method, *Amer. Math. Monthly* **78**, 389–392.
437. H. G. Telling (1936), *The Rational Quartic Curve in Space of Three and Four Dimensions*, Cambridge University Press.
438. W. P. Thurston (1997), *Three-Dimensional Geometry and Topology*, Volume 1, Princeton University Press, Princeton, NJ.
439. S. D. Timar, R. T. Farouki, T. S. Smith, and C. L. Boyadjieff (2005), Algorithms for time-optimal control of CNC machines along curved tool paths, *Robotics. Comput. Integ. Manufac.* **21**, 37–53.
440. S. P. Timoshenko (1953), *History of Strength of Materials*, Dover Publications (reprint), New York.
441. J. Tlusty (1993), High-speed machining, *CIRP Ann.* **42**, 733–738.
442. B. M. Trager (1976), Algebraic factoring and rational function integration, *Proceedings, ACM Symposium on Symbolic and Algebraic Computation*, 219–226.
443. C. Truesdell (1958), The new Bernoulli edition, *Isis* **49**, 54–62.
444. Y-F. Tsai and R. T. Farouki (2001), Algoriohm 812: BPOLY: An object-oriented library of numerical algorithms for polynomials in Bernstein form, *ACM Trans. Math. Software* **27**, 267–296.

445. Y.-F. Tsai, R. T. Farouki, and B. Feldman (2001), Performance analysis of CNC interpolators for time-dependent feedrates along PH curves, *Comput. Aided Geom. Design* **18**, 245–265.
446. E. W. von Tschirnhaus (1683), A method for removing all intermediate terms from a given equation, *ACM SIGSAM Bulletin* **73**, 1–3 (translated by R. F. Green from the Latin original in *Acta Eruditorum*, May 1683, 204–207)
447. K. Ueda (1997), Deformation of plane curves preserving Pythagorean hodographs, *Proceedings, 1997 IEEE Conference on Information Visualization*, IEEE Computer Society, 71–76.
448. ——— (1998), Spherical Pythagorean-hodograph curves, *Mathematical Methods for Curves and Surfaces II* (M. Daehlen, T. Lyche, and L. L. Schumaker, eds.), Vanderbilt University Press, 485–492.
449. ——— (1998), Pythagorean-hodograph curves on isothermal surfaces, in *The Mathematics of Surfaces VIII* (R. Cripps, ed.), Information Geometers, Winchester, 339–353.
450. ——— (1998), Helical curves over Pythagorean-hodograph curves, *Geometric Modeling and Processing '98*, Bookplus Press, 115–128.
451. ——— (1998), Pythagorean-hodograph space curves by quaternion calculus, preprint.
452. J. V. Uspensky (1948), *Theory of Equations*, McGraw-Hill, New York.
453. K. Th. Vahlen (1891), Bemerkung zur vollständigen Darstellung algebraischer Raumkurven, *J. Reine Angew. Math.* **108**, 346–347.
454. J. von zur Gathen and J. Gerhard (1999), *Modern Computer Algebra*, Cambridge University Press.
455. M. G. Wagner and B. Ravani (1997), Curves with rational Frenet–Serret motion, *Comput. Aided Geom. Design* **15**, 79–101.
456. R. J. Walker, *Algebraic Curves*, Dover Publications (reprint), New York (1950).
457. J. Wallner and H. Pottmann (1997), Rational blending surfaces between quadrics, *Comput. Aided Geom. Design* **14**, 407–419.
458. D. J. Walton and D. S. Meek (1996), A Pythagorean-hodograph quintic spiral, *Comput. Aided Design* **28**, 943–950.
459. ——— (1998), G^2 curves composed of planar cubic and Pythagorean hodograph quintic spirals, *Comput. Aided Geom. Design* **15**, 547–566.
460. ——— (2002), Planar G^2 transition with a fair Pythagorean hodograph quintic curve, *J. Comput. Appl. Math.* **138**, 109–126.
461. ——— (2004), A generalisation of the Pythagorean hodograph quintic spiral, *J. Comput. Appl. Math.* **172**, 271–287.
462. ——— (2007), G^2 curve design with a pair of Pythagorean hodograph quintic spiral segments, *Comput. Aided Geom. Design* **24**, 267–285.
463. W. Wang and B. Joe (1993), Orientation interpolation in quaternion space using spherical biarcs, *Proceedings, Graphics Interface '93*, 24–32.
464. ——— (1997), Robust computation of the rotation minimizing frame for sweep surface modelling, *Comput. Aided Design* **29**, 379–391.
465. Wessel, C. (1799), Om directionens analytiske betegning, et forsøg, anvendt fornemmelig til plane og sphaeriske polygoners oplosning, *Nye samling af det Kongelige Danske Videnskabernes Selskabs Skrifter*, 2nd ser., **5**, 496–518; translation of excerpts in D. E. Smith (1959), *A Source Book in Mathematics*, Dover Publications, New York, 55–66.

466. R. S. Westfall (1980), *Never at Rest: A Biography of Isaac Newton*, Cambridge University Press.
467. H. Whitney (1937), On regular closed curves in the plane, *Compositio Mathematica* **4**, 276–284.
468. J. H. Wilkinson (1959), The evaluation of the zeros of ill-conditioned polynomials, Parts I & II, *Numer. Math.* **1**, 150–166 & 167–180.
469. ——— (1963), *Rounding Errors in Algebraic Processes*, Prentice-Hall, Englewood Cliffs, NJ.
470. ——— (1984), The perfidious polynomial, *Studies in Numerical Analysis* (G. H. Golub, ed.) , MAA Studies in Mathematics, Vol. 24.
471. ——— (1988), *The Algebraic Eigenvalue Problem*, Clarendon Press, Oxford.
472. R. M. Winger (1962), *An Introduction to Projective Geometry*, Dover Publications (reprint), New York.
473. R. Woodhouse (1810), *A History of the Calculus of Variations in the Eighteenth Century*, Chelsea (reprint), New York.
474. W. Wunderlich (1973), Algebraische Böschungslinien dritter und vierter Ordnung, *Sitzungsberichte der Österreichischen Akademie der Wissenschaften* **181**, 353–376.
475. D. C. H. Yang and T. Kong (1994), Parametric interpolator versus linear interpolator for precision CNC machining, *Comput. Aided Design* **26**, 225–234.
476. C.-K. Yap (1987), An $O(n \log n)$ algorithm for the Voronoi diagram of a set of simple curve segments, *Discrete Comput. Geom.* **2**, 365–393.
477. S-S. Yeh and P-L. Hsu (1999), The speed-controlled interpolator for machining parametric curves, *Comput. Aided Design* **31**, 349–357.
478. A. P. Youschkevitch and B. A. Rosenfeld (1980), *Al-Khayyami, Dictionary of Scientific Biography* (C. C. Gillespie, ed.), Scribner, New York.
479. W. Zulehner (1988), A simple homotopy method for determining all isolated solutions to polynomial systems, *Math. Comp.* **181**, 167–177.
480. C. Zwikker (1963), *The Advanced Geometry of Plane Curves and Their Applications*, Dover Publications (reprint), New York.

Index

- 3–sphere, 66, 472
Abel, N. H., 395
absolute circle, 128
absolute differentiation, 243
absolute rotation index, 532, 566, 600
absolutely perpendicular, 75
acceleration/deceleration profiles, 632
acnode, 203
adapted frame (space curve), 665
Adelard of Bath, 23
affine point, 113
affine transformation, 119
algebraic curve, 92, 114, 197, 199–212
algebraic function, 378
algebraic geometry, 92
algebraic space curve, 197, 222–230
algebraic surface, 197, 219–222
algebraically–rectifiable curve, 378, 449
al–Khwarizmi, M. ibn M., 22
analytic function, 52, 251
angle in a surface, 185
anti–parallel tangents, 535
anticaustics, 440
approximation errors, 263
arc length, 137, 149, 154, 369–380, 386,
 439, 566, 600, 620, 627
Argand, J. R., 46
arithmetic errors, 263
arithmetic genus, 221
arithmetic–geometric mean, 623
associative law, 26
asymptotic directions, 189
asymptotic lines, 193
axial vectors, 82
axis (of helix), 456, 461, 486
B–spline basis, 346, 354
backward error analysis, 270, 290
barycentric coordinates, 94
 on interval, 94, 249
 on triangle, 95
 on d –dimensional simplex, 103
 un–normalized, 102
barycentric vector, 99
 dot product, 100
 norm, 100
base curve (of quadric pencil), 493
base point (of rational curve), 431
basic length unit (BLU), 647
basis conversion (for splines), 364
bending moment, 325
Bernoulli, Daniel, 323
Bernoulli, Jakob, 161, 325
Bernoulli, Johann, 131, 159, 325
Bernoulli–Euler theory, 543
Bernstein, S.N., 5
Bernstein, S. N., 250
Bernstein basis, 31, 95, 249–252, 274,
 295, 359
beta splines, 339
Bézier, P., 5, 295, 619
Bézier forms, 274
Bézout, E., 214
Bézout resultant, 39
Bézout’s theorem, 214, 560

- binormal (of space curve), 178
- birational correspondence, 205
- birational transformation, 106, 211
- bitangent, 213
- bivariate spline function, 348
- bivector, 80, 83
- blade, 83
- Bolyai, J., 231
- Böttger, J. F., 394
- brachistochrone, 160
- C^2 continuity, 329
- calculus of residues, 372
- calculus of variations, 159, 341
- cam profile, 537
 - dwell segment, 537
 - return segment, 537
 - rise segment, 537
- canal surface, 519, 653, 689
- cancellation (significant digits), 268, 540
- canonical rational cubic, 315
- Cardano, G., 45
- Cardano's method, 37
- cardinal basis, 346
- cardinality, 410
- Cartan connection matrix, 665
- Cartesian coordinates, 91
- Castelnuovo's theorem, 221
- Catalan, E., 398, 462
- Cauchy, A.-L., 52
- Cauchy index, 645
- Cauchy's residue theorem, 54
- Cauchy's theorem, 53
- Cauchy–Riemann relations, 52
- caustic curves, 396, 440
- Cayley, A., 122
- center of curvature, 135, 145
- center of mass, 297
- center of projection, 123
- central projection, 123, 306
- Cesàro, E., 539
- characteristic circle, 689
- Chebyshev basis, 34
- Chebyshev economization, 35
- Chebyshev nodes, 327
- chord-length parameterization, 338
- Christoffel symbols, 193, 241
- circle at infinity, 128
- circle of curvature, 145
- circular arc (Bézier form), 312
- circular points at infinity, 115, 214
- Clairaut, A.-C., 226
- class of a curve, 118, 148
- Clifford, W. K., 79
- Clifford algebra, 79–86, 516, 519, 604
- clothoid, 539
- CNC machines, 619
- coaxal system of circles, 74, 141
- codimension, 197
- commutative law, 26
- compact support, 354
- complete spline, 330
- complex derivative, 52
- complex numbers, 45–60, 81
- complex projective plane, 201
- components of a curve, 200
- composite polynomial, 446
- composite surface intersections, 223
- condition number, 272
 - linear map, 285
 - root of polynomial, 276
 - value of polynomial, 273
- cone of normals, 166
- cones, 221
- confocal ellipsoidal coordinates, 193
- conformal map, 51, 54, 408
- conformal transplant, 56
- conics, 120, 199, 309, 623
- connection coefficients, 241
- constant radius blend, 690
- contact loci (with surface), 651
- continuous transformation, 314
- contour machining, 651
- contraction, 317
- contraction mapping, 575
- contravariant components, 233
- control lines, 433
- control net
 - tensor–product patch, 313
 - triangular patch, 321
- control points, 295, 384, 464, 470, 558, 585, 607
- control polygon, 295, 354, 587
- convergence
 - Bernstein approximation, 251
 - Newton–Raphson method, 260
 - spline approximation, 336

- convex combination, 103, 296
- convex hull, 296, 308
- convolution, 355
- coordinate axes, 91
- coordinate transformation, 236
- Cornu, M. A., 539
- Cornu spiral, 539
- covariant components, 233
- covariant differentiation, 242
- Cox-de Boor algorithm, 361
- Cremona, L., 211
- Cremona transformation, 211
- critical set, 139
- cross product, 61, 82
- cross ratio, 59, 122
- crunode, 203, 402
- cubic curves, 125, 199, 203
- cubic end segments, 559
- cubic equation, 24, 37, 395
- cubic splines, 328
- curl (of vector field), 61, 65
- curvature
 - elastic beam, 325
 - implicit curve, 200
 - plane curve, 134
 - space curve, 178, 664
- curve lying on a surface, 185
- curve of constant slope, 439, 486
- curve/curve bisector, 511
- curvilinear coordinates, 51, 104
- cusp, 153, 163, 203, 302, 430, 432
- cuspidal ridge, 221
- cutting force, 650
- cycles, 444
- cyclic array, 332, 359
- cyclographic image, 445
- cyclographic map, 444
- cycloid, 157, 159, 198, 375
- cycloidal rise function, 537
- cylindrical polar coordinates, 112
- cylindrical tool, 651
- Darboux, J. G., 181
- Darboux vector, 181, 601, 664
- de Casteljau, P., 5
- de Casteljau algorithm, 256, 300, 321, 433
- degree elevation/reduction, 255
- degrees of freedom, 199
- del Ferro, S., 45
- de l'Hôpital, G. F. A., 131, 161, 398
- de Moivre's theorem, 48
- De Morgan, A., 62
- depth of cut, 643
- de Roberval, G. P., 198, 375
- Desargues, G., 121
- Descartes, R., 1, 29, 91, 199, 374
- Descartes' Law of Signs, 36, 253
- developable surface, 180, 189, 246, 445
- differential geometry, 92
- dilatation, 444
- direction in a surface, 185
- directional derivative, 100
- Dirichlet boundary conditions, 56
- discriminant, 40, 169
- distance function
 - curve/curve, 170
 - point/curve, 168
- distributive law, 26
- divergence (of vector field), 61, 65
- dot product, 61, 82
- double point, 203, 494
- double Pythagorean hodograph, 497, 504
- double rotation, 76, 478
- dual Bézier representation, 433
- dual bases, 234
- dual form, 397, 427, 538
- dual statements, 116, 127
- duality, 116
- ducks, 324
- dummy index, 236
- Dupin, C., 189, 193
- Dupin indicatrix, 189
- Dürer, A., 126
- dynamometer, 649
- eigenvalue, 236, 284, 480
- eigenvector, 236, 284, 480
- Einstein, A., 236
- elastica, 325, 341, 543
- elliptic curves, 219
- elliptic functions, 219, 369
- elliptic integral, 156, 343, 623
- elliptic point (of surface), 189
- end conditions, 330, 365, 558
- energy (framed space curve), 669

- energy integral, 325, 335, 341, 543, 566, 600, 668
- envelope, 139, 397
- epicycloid, 397
- Euclidean algorithm, 42, 672
- Euclidean norm, 281
- Euclidean space, 231
- Euler, L., 323, 325, 341, 540, 543
- Euler's theorem
 - homogeneous function, 100, 206
 - normal curvature, 188
- Euler–Lagrange equation, 159, 193, 240, 335, 342
- Euler–Rodrigues frame (PH curve), 666
- Euler–Rodrigues parameters, 666
- evolute, 135, 144, 146, 154, 164, 169, 396, 440
- exponent, 264
- extended complex plane, 49, 59
- face (of a simplex), 103
- family of plane curves, 138
- Farin points, 307
- feed acceleration, 649
- feedback controller, 619
- feedrate, 619
 - constant, 624
 - curvature-dependent, 625, 642
 - linear in arc length, 628
 - quadratic in arc length, 628
 - time-dependent, 622, 630
- Fermat, P., 91, 376
- ferocious formulae, 69
- Ferrari's method, 38, 610, 675, 681
- field, 26, 41
- fillet arcs, 166
- first fundamental form, 183
- first-order contact, 136
- floating-point
 - arithmetic, 93, 263
 - dynamic range, 264
 - IEEE standard, 265
 - number, 264
 - underflow/overflow, 264
- floor function, 288
- flux of a vector field, 56
- foci (of conics), 120
- folium of Descartes, 199
- Fontana, N., 45
- forward error analysis, 267
- four-dimensional rotation, 74, 478
- four-vertex theorem, 137
- free index, 236
- free lunch, 288
- Frenet frame, 179, 180, 466, 661, 664
- Frenet–Serret equations, 181, 486
- Fresnel integrals, 539
- function of a complex variable, 49
- functional iteration, 574
- Fundamental Theorem of Algebra, 36, 202, 214
- G^2 continuity, 339
- G codes, 620, 634
- Galileo, 160, 375
- Galois theory, 38
- Gauss, K. F., 46, 184, 231
- Gauss map (of curve), 531
- Gauss map (of surface), 190, 655
- Gaussian curvature, 187, 246, 655
- general helical PH quintic, 492, 500, 609
- generating function, 198
- genus
 - plane curve, 204–207, 212, 217
 - space curve, 227–228
 - surface, 221
- geodesic, 193, 240, 243
- geodesic curvature, 194, 246
- geodesic equations, 241
- geodesic parallel coordinates, 196
- geodesic polar coordinates, 196
- geometric algebra, 79
- geometric continuity, 145, 339
- geometric genus, 221
- geometric Hermite interpolation, 339
- geometric product, 83, 84, 604
- geometrical algebra, 92
- geometrical optics, 440
- Gibbs, J. W., 63
- gift-wrapping algorithm, 296
- global smoothness, 328, 334
- gnomonic projection, 114
- graded algebra, 80
- gradient, 109, 241
- gradient (of scalar field), 61
- Grassmann, H. G., 83
- great circle, 71, 86, 195, 472, 486, 602

- greatest common divisor, 42
- group, 28, 59, 66, 85, 86, 476, 666
- Hadamard, J., 407
- Hamilton, W. R., 61, 302, 469
- harmonic function, 56
- Hausdorff distance, 171
- Heaviside, O., 63
- helix, 456, 460, 485
- Hermite basis, 31, 328
- Hermite interpolation, 523, 595
- Hessian matrix, 578
- high-speed machining, 620
- hodograph, 302, 308, 381
- Hölder's inequality, 282
- holomorphic function, 52
- holonomy, 246
- homeomorphism, 207
- homogeneous coordinates, 113, 303, 314
- homogeneous equation, 114, 201
- homogeneous polynomial, 30
- homotopy method, 561
- homotopy variable, 561
- Hooke, R., 325, 375
- Hooke's Law, 325
- Hopf map, 471
- Horner's method, 30, 267, 291
- Horologium Oscillatorium, 154
- Huygens, C., 144, 154, 161, 376, 396
- Huygens' Principle, 396, 440
- hyperbolic point (of surface), 189
- ill-conditioned problem, 263, 271
- ill-posed problem, 289
- image plane, 123
- implicit representation, 198
- implicitization, 216
- improper parameterization, 446
- incidence relations, 122, 125
- indicatrix, 451
- inflection, 302, 423, 431, 533
 - PH curve, 385
 - plane curve, 135
 - space curve, 181, 661
 - inflectional tangent, 213
- initial system (homotopy method), 561
- inner product, 83
- interpolation integral, 621
- intersection multiplicity, 214
- intersections of quadrics, 225
- interval arithmetic, 27, 271
- intrinsic equations
 - plane curve, 138
 - space curve, 182
- invariants, 240
- inversion in a circle, 211, 656
- involute, 144, 149, 164, 396, 430, 440
- irreducible curve, 200
- isochronous pendulum, 155
- isophotes, 450
- isothermal coordinates, 188
- isothermal parameters (surface), 695
- isotropic lines, 115
- Jacobi, C. G. J., 105
- Jacobi polynomials, 35
- Jacobian, 105, 109, 111, 143
- Jacobian elliptic function, 155, 343
- Jacobian matrix, 236, 562, 575, 585
- Joukowski map, 58, 59
- Kantorovich theorem, 577
- Kepler, J., 120
- Khayyam, O., 11, 23
- knot vector, 356
- knots, 328
- Kronecker, L., 224
- Kronecker delta, 236
- Kummer, E. E., 83
- Lagrange basis, 326, 347
- Lagrange interpolant, 337
- Lagrange multiplier, 342
- Laguerre, E., 444
- Laguerre geometry, 444
- Laguerre transformations, 444
- Lambert, J. H., 374
- Lamé, G., 104
- Laplace equation, 56
- Laplacian, 56, 65
- least-squares approximation, 32
- Lebesgue, V. A., 462
- Legendre basis, 32
- Leibniz, G. W., 140, 160, 393, 397
- level curves, 50
- Levi-Civit  , T., 243
- l'H  pital's cubic, 398
- license to compute, 261

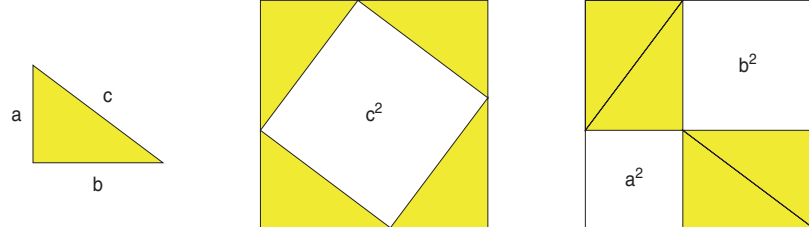
- light-like vector, 80, 445, 509
- line at infinity, 114
- line coordinates, 117, 429
- line equation, 117
- linear precision, 363, 590
- lines of curvature, 191
- Lipschitz constant, 578, 585
- Listing, J. B., 94
- local intrinsic shape, 131
- local shape modification, 354, 591
- local smoothness, 328, 334
- logarithmic spiral, 375
- Lorentz transformation, 514
- machine unit, 265, 569
- Maclaurin, C., 214
- magnification of errors, 268
- mantissa, 264
- material removal rate, 643
- matrix condition number, 286
- matrix norm, 282, 572
- Maxwell, J. C., 63
- mean curvature, 187
- mean value theorem, 575
- mechanical spline, 324
- medial axis, 510, 516
- medial axis transform, 507, 510, 657
- metric tensor, 107, 232
- minimal element, 275
- minimal surface, 188, 189
- Minkowski, H., 507
- Minkowski norm, 445
- Minkowski Pythagorean hodograph curve, 507
- Minkowski space, 508, 512, 514, 690
- Minkowski sum, 451
- Minkowski's inequality, 282
- Möbius, A. F., 58, 83, 94, 302
- Möbius band, 94
- Möbius transformation, 58, 305, 395
- Monge, G., 192, 397
- monoid, 218, 222
- monomial basis, 31
- monotone-helical PH quintic, 490, 503, 605
- Monte Carlo experiment, 551
- multinomial formula, 104
- multiple knots, 354, 357, 589
- multiple root, 36, 672
- multivector, 80
- natural parameterization, 370
- natural spline, 332
- negative pedal, 398
- Neil, W., 376
- nested multiplication, 30
- Neumann boundary conditions, 56
- Newton, I., 125, 158, 160, 198, 199, 325, 369, 396
- Newton–Raphson method, 260, 262, 388, 563, 576, 624, 630, 645
- Nicholas of Cusa, 158
- nodal points, 588
- nodes, 328
- Noether, M., 209, 212
- Noether's theorem, 209
- non-Euclidean geometry, 232
- non-Euclidean space, 231
- non-negative basis, 273
- non-uniform knots, 337, 582
- normal curvature, 186
- normal line, 134
- normal plane, 180
- normal section (of surface), 186
- normal vector (of plane curve), 134
- not-a-knot condition, 331, 558
- numerical stability, 261
- NURBS, 362
- object plane, 123
- oblique coordinates, 105
- octonions, 81
- offset curve, 144, 161, 377, 429, 435, 444, 451, 511, 514, 626, 651
- offset surface, 450
- Oldenburg, H., 393
- one-to-one correspondence, 105, 110, 346, 409, 483
- optical path length, 440
- order of a curve, 118
- oriented contact, 444
- oriented lines and circles, 444
- oriented planes and spheres, 444
- origin, 91
- orthogonal basis, 472
- orthogonal matrix, 119, 472, 476, 665
- orthogonality property, 33, 34

- osculating circle, 135, 136, 145, 173, 643
- osculating plane, 180
- outer product, 83
- Padé approximation, 677, 679
- parabola, 120, 304, 446
- parabola of safety, 142
- parabolic line (of surface), 191, 655
- parabolic point (of surface), 189
- parallel curve, 144, 161, 196
- parallel projection, 124
- parallel transport, 243
- parameterization
 - arc-length, 137, 370–374
 - natural, 137
 - of elliptic curve, 219
 - of rational curve, 217
 - proper, 217
 - rational, 201, 217
 - unit-speed, 137
- parametric continuity, 339
- parametric curve, 92, 334
- parametric representation, 198
- parametric speed, 133, 369, 386, 620
- partial fraction decomposition, 42, 371, 544, 547, 625, 672, 681
- partially-ordered set, 275
- partition of unity, 102, 252, 354
- Pascal, B., 157
- Peano G., 345
- pedal curve, 398
- pencil of curves, 140, 217
- pencil of quadrics, 223
- periodic end condition, 331, 559
- perspectivity, 120, 129
- perturbation regions, 281
- pipe surface, 689
- pitch angle, 456, 460
- planar section (of surface), 651
- plane algebraic curve, 199
- plane at infinity, 127
- Plimpton, G. A., 11
- Plimpton 322, 11–17
- Plücker, J., 213
- Plücker equations, 213
- Plücker line coordinates, 127
- p -norm (of vector), 281, 572
- point at infinity, 30, 103, 113, 201, 303, 431, 658
- point/curve bisector, 511
- Poisson's ratio, 669
- polar coordinates, 110
- polar vectors, 82
- polynomial, 29, 249
- polynomial basis, 31
- polynomial roots, 275
- Poncelet, J. V., 122
- Pope, A., 1
- porcelain, 394
- potential function, 56
- power basis, 31
- predicate function, 198
- predictor–corrector scheme, 563
- principal curvatures, 187
- principal directions, 187
- principal normal (of space curve), 178
- procedurally-defined loci, 198
- profile curve, 314
- projective geometry, 113
- projective line, 114
- projective plane, 103, 113
- projective transformation, 119, 314
- pseudo-Euclidean norm, 445
- pseudoscalar, 80
- pseudovectors, 82
- Pythagoras of Samos, 17
- Pythagorean quartuple, 373, 462
- Pythagorean theorem, 17–22, 91
- Pythagorean triple
 - integers, 14, 18, 412
 - polynomials, 21, 371, 382, 487
 - primitive, 383
- Pythagorean–hodograph curve, 369, 381
- quadratic end spans, 330
- quadratic equation, 37
- quadric surface, 193, 221, 223, 319, 451, 493
- quadtree, 653, 656
- quartic equation, 38, 610
- quaternions, 27, 61–77, 81
- radical axis, 141
- radius of curvature, 135, 145
- ramphoid cusp, 210
- rapid prototyping, 660
- rational curve, 205, 303, 315
- rational function, 29, 41, 370, 672

- rational normal curve, 315
- rational quartic (space curve), 493
- rays, 440
- real-time interpolator, 619
- reasonable sequence (point data), 573
- rectification of curves, 20, 374
- rectifying developable, 180
- rectifying plane, 180, 195
- reference points, 619
- reference triangle, 96, 208
- reflection, 69, 85, 119, 440, 481, 604
- regular curve, 133
- regular surface, 183
- relaxation methods, 575
- residue, 43, 54, 372
- resolution of singularities, 208
- resultant, 39
- reverse engineering, 660
- Riemann, G. F. B., 52
- Riemannian geometry, 232
- Riesz convexity theorem, 286
- ring, 26, 29
- robustness, 261
- Rodrigues, O., 69
- root at infinity, 36
- root condition number, 276
- rotation, 85, 119
- rotation index, 423, 531, 645
- rotation invariance, 414, 476, 598
- rotation-minimizing frame, 662, 667
- rotor, 86
- rounding, 265
- ruled surface, 189
- Runge example, 327
- sampling interval, 619
- scaling, 119, 125
- scallop height, 654
- scallops, 653
- Schoenberg, I. J., 324
- second fundamental form, 184
- second-order contact, 136
- Segre characteristic, 225
- selector matrix, 316
- self-intersection
 - curve, 203, 227, 402, 535
 - surface, 221
- untrimmed offset, 167
- semicubical parabola, 376
- sexagesimal numbers, 11
- shadows, 123–126
- shape parameters, 339
- shape-preserving splines, 586
- shear modulus, 669
- silhouette, 139
- simple root, 36
- simplex, 103
- singular curve, 221
- singular point, 201–204, 654
 - double point, 203
 - at infinity, 206
 - evolutes and involutes, 153
 - implicit, 208
 - infinitely near, 208
 - m -fold point, 204
 - multiplicity, 204
 - neighborhoods, 208
 - offset curves, 163
 - ordinary, 204
 - tangents, 204
- singular values (of matrix), 285
- small circle, 71, 486
- small-slope regime, 335, 543
- solid angle, 190
- solution by radicals, 37
- $\text{SO}(n)$, 28, 76, 476
- space-like vector, 80, 445, 509
- spatial motion, 661
- spatial rotation, 67, 71, 469, 477, 596, 666
- special orthogonal matrix, 28
- special theory of relativity, 80, 508
- spectral norm (of matrix), 285
- sphere, 196, 319
- spherical image (of surface), 190, 655
- spherical polar coordinates, 112
- spherical tool, 651
- Spinoza, B., 393
- spiral segment, 539
- spline, 323, 324, 543
- spline basis, 346
- spline curve, 336
- standard form (Hermite data), 528
- standard parameterization (of rational Bézier curve), 305
- standard quadratic transformation, 208
- stationary set, 76

- Steiner, J., 222
 Steiner surface, 222
 stereographic projection, 49, 656
 Stirling approximation, 299
 stochastic matrix, 255
 strain energy, 325, 543
 stress tensor, 235
 Sturm sequence, 42
 subdivision matrix, 289
 summation convention, 236
 support coordinates, 431
 support function, 431
 surface area, 184
 surface normal vector, 184, 652
 surface of revolution, 319
 surface patch
 bicubic, 313
 biquadratic, 313
 tensor-product, 312
 triangular, 321
 sweep curve, 314
 swept surfaces, 314
 Sylvester determinant, 39
 symmetric functions, 36
 symmetrized Gauss map, 656
 tachometer, 648
 tacnode, 210
 tangent cone, 220
 tangent indicatrix, 486
 tangent line, 117, 133, 145, 203, 434
 tangent line (implicit curve), 200
 tangent plane, 127, 184, 220
 tangent vector (of plane curve), 133
 Tartaglia, 45
 tautochrone, 161
 Taylor series, 621
 tension parameter, 343, 586
 tensor, 235
 tensor contractions, 240
 tensor transformations, 235
 theology, 157
 theorem of Weierstrass, 250
 three-leaved rose, 206
 time-like vector, 80, 445, 509
 tolerance zone, 162
 toothache, 157
 topologically rectangular, 351
 topology, 207
 Torricelli, E., 375
 torsion (space curve), 178, 664
 torus, 195, 319
 total curvature (space curve), 182, 665
 transcendental curve, 158, 198
 translation, 119
 triangle inequality, 171, 281
 tridiagonal system, 329, 332, 366, 564
 trimmed offset, 163, 167, 171
 trimming procedure, 163, 167, 176
 trinomial coefficient, 102
 trisectrix of Catalan, 398
 trivector, 83
 truncation, 265
 Tschirnhaus, E. W., 161, 393–399, 427
 Tschirnhaus transformations, 394
 Tschirnhausen's cubic, 398, 400–404,
 442, 545
 twist vectors, 352
 Uccello, P., 126
 umbilic, 188
 uniform knots, 337
 unimodality, 252
 unique factorization domain, 21, 488
 unit-speed approximation, 379
 unit-speed point, 422
 untrimmed offset, 162, 166
 Vancouver Stock Exchange, 264
 Vandermonde matrix, 326
 van Heuraet, H., 376
 vanishing line, 124
 variation-diminishing property, 253,
 298, 308
 vector analysis, 61
 vector fields, 109
 vector in a surface, 185
 vector norm, 281
 vertex (of a cone), 221
 vertex (of plane curve), 137, 146, 153,
 302, 424, 647
 visual continuity, 339
 volume of a simplex, 103
 Voronoi diagram, 510
 wavefront, 162, 440
 weight points, 307

- weights, 304
well-conditioned problem, 263, 271
Wessel, C., 45–48
Wilkinson, J. H., 270, 277
Wilkinson’s polynomial, 277–281
winding number, 535
Wren, C., 375
Young’s modulus, 669
zero divisors, 85



Beauty is truth, truth beauty, — that is all
Ye know on earth, and all ye need to know.

John Keats (1795–1821)

